PRE-ANDEAN TECTONIC EVENTS FROM ALBIAN TO EOCEN IN THE MIDDLE MAGDALENA VALLEY AND SITUATION OF THE WESTER PROTO-CORDILLERA ORIENTAL (COLOMBIA).

Jairo Guerrero Moreno

Communauté
UNIVERSITÉ Grenoble Alpes

Departamento de Geociencias
Facultad de Ciencias
Sede Bogotá

UNIVERSIDAD NACIONAL DE COLOMBIA

THÈSE

Pour Obtenir le grade de

DOCTEUR EN SCIENCES DE LA TERRE DE LA COMUNITE UNIVERSITE GRENOBLE ALPES ET LA UNIVERSIDAD NACIONAL DE COLOMBIA

Préparée dans le cadre d´une cotutella entre la Communauté Université Grenoble Alpes el l´Universidad Nacional de Colombia.

Spécialite**: Doctorat TUE/Sciences de la Terre el del´Univers, Enviroment.**

Arrêté ministériel: le 25 mai 2016

Présentée par

« Jairo Guillermo GUERRERO MORENO »

Thèse dirigée par **« Etienne JAILLARD», «Luis MONTES »**
Prêparêe au sein des Departament des Geosciences et Laboratoires ISTerre Dans les Universidad Nacional de Colombia et Écoles Doctorales de l´Université Grenoble Alpes

Evènements tectoniques pré-andins de l'Albien à l'Eocène dans la Moyenne-Vallée de la Magdalena et sur le flanc ouest de la proto-Cordillère Orientale de Colombie.

Thèse soutenue publiquement le **26 octobre 2018**
devant le jury composé de:

M. Mauricio BERMUDEZ
Dr., Univ. Pedagógica y Tecnológica, Colombie (Rapporteur Président)
M. Andres PARDO
Dr., Universidad de Caldas, Manizales, Colombie (Rapporteur)
Mme. Andrea RITTER
Dr., Universidade Federal do Rio Grande do Sul, Bresil (Examinateur)
M. Matthias BERNET
Dr., Université Grenoble Alpes, France (Examinateur)
M. Alejandro BELTRAN
Dr., Universidad EAFIT, Medellin, Colombie (Examinateur)
M. Etienne JAILLARD
DR1, IRD ISTerre, Université Grenoble Alpes, France (Directeur de thèse)
M. Luis MONTES
Dr., Univ. Nacional de Colombia, Bogotá, Colombie (Directeur de thèse)
M. Andreas KAMMER
Dr., Univ. Nacional de Colombia, Bogotá, Colombie (Co-directeur de thèse)

UNIVERSITE GRENOBLE -ALPES

UNIVERSIDAD NACIONAL DE COLOMBIA

Thesis

PRE-ANDEAN TECTONIC EVENTS FROM ALBIAN TO EOCENE IN THE MIDDLE MAGDALENA VALLEY AND SITUATION OF THE WESTERN FLANK OF THE PROTO-EASTERN CORDILLERA (COLOMBIA).

EVÈNEMENTS TECTONIQUES PRÉ-ANDINS DE L'ALBIEN À L'EOCÈNE DANS LA MOYENNE-VALLÉE DE LA MAGDALENA ET SUR LE FLANC OUEST DE LA PROTO-CORDILLÈRE ORIENTALE DE COLOMBIE.

EVENTOS TECTONICOS PRE-ANDINOS DEL ALBIANO AL EOCENO EN EL VALLE MEDIO DEL MAGDALENA Y SITUACION DEL COSTADO OCCIDENTAL DE LA PROTO-CORDILLERA ORIENTAL (COLOMBIA)

Submitted by

Jairo Guillermo GUERRERO MORENO

To receive the title of Doctor in Earth Sciences
Of the Université Grenoble - Alpes
And of the Universidad Nacional de Colombia
October 2018

EVENTOS TECTONICOS PRE-ANDINOS DEL ALBIANO AL EOCENO EN EL VALLE MEDIO DEL MAGDALENA Y SITUACION DEL COSTADO OCCIDENTAL DE LA PROTO-CORDILLERA ORIENTAL (COLOMBIA)

PRE-ANDEAN TECTONIC EVENTS FROM ALBIAN TO EOCENE IN THE MIDDLE MAGDALENA VALLEY AND SITUATION OF THE WESTERN FLANK OF THE PROTO-EASTERN CORDILLERA (COLOMBIA).

Jairo Guillermo Guerrero Moreno

Tesis presentada como requisito parcial para optar por el titulo Ph.D.

Doctor en Geociencias

Director:
Profesor Luis Montes
Co-Director:
Etienne Jaillard
Codirector:
Andreas Kammer

Línea de Investigación:
Estratigrafía, Tectonica y Geodinamica
Grupo de Geología estructural y Fracturas

Universidad Nacional de Colombia
Facultad de Ciencias
Departamento de Geociencias
Bogotá, Colombia

October 2018

EVÈNEMENTS TECTONIQUES PRÉ-ANDINS DE L'ALBIEN À L'EOCÈNE DANS LA MOYENNE-VALLÉE DE LA MAGDALENA ET SUR LE FLANC OUEST DE LA PROTO-CORDILLÈRE ORIENTALE DE COLOMBIE.

PRE-ANDEAN TECTONIC EVENTS FROM ALBIAN TO EOCENE IN THE MIDDLE MAGDALENA VALLEY AND SITUATION OF THE WESTERN FLANK OF THE PROTO-EASTERN CORDILLERA (COLOMBIA).

Thèse

Présentée par

Jairo Guillermo Guerrero Moreno

Pour l´obtention du grade de

Docteur ès Sciences

De l´université Grenoble Alpes

Encadrant:

Professeur Etienne Jaillard

Co-encadrant:

Professeur Luis Montes

Co-encadrant:

Professeur Andreas Kammer

Géologie structural, Tectonique et Geodynamique

Equipé de Recherche:

Tectonique, reliefs et bassins (TRB)

Université Grenoble Alpes

Ecole Doctorale TUE, Laboratoire ISTerre

Grenoble, France

October 2018

To my beautiful wife, Claudia Alexandra, who has always supported my projects, giving me her great love and decorating my live, to my son Julian and my daughter Salome, and my mother and my father who are always there.

Acknowledgments

To my great God for helping me in the difficult moments and giving me strength, the capacity and the opportunity to finish this important project in my life.

To my advisor in Grenoble, Etienne Jaillard, for believing in this project, for all the support and for finding the resources to make technical analysis and for the revision of all the chapters.

To my advisor in Colombia, Luis Montes, for his advice, for believing in this project, for all the support, the important observations and urging me to go forward.

To Matthias Bernet, for helping me with all the thermochrological aspects of this project, for the discussion and analysis of the samples, for his advice, important opinions and for being a great person.

To Andreas Kammer, for accepting to help me as a co-advisor, and for the observations and revision, in structural geology and also in other important topics of my thesis

To Ecopetrol and To Adriano Lobo, for allowing me to use their seismic data and technical information, for the year of internship that I was granted in ISTERRE to make important analyzes.

To Universidad Nacional de Colombia, for all the teachings during all my bachelor's degree, my MSc and my PhD.

To the University of Grenoble for receiving me in their classrooms, for the Laboratory support and helping me through the thesis director, administrative and technical staff that supported me during these years.

To my friend Alvaro Vargas, for his help in the field necessary in this project and the important discussions that were generated during our several field visits.

To Professor Jose Ma. Jaramillo and GMAS for the help in the separation of crystals for thermochronology and preparations of some thin sections for petrography.

To Ricardo Molano for the separation of some samples, and professor Juan Carlos Molano for his help, and for allowing the use of the laboratory in the separation of apatite and zircons. Also, to Professor Nadejda Tchegliakova for her help in the paleontological determination.

To my Family Mother and Father for supporting me and encouraging me throughout my life.

To my beautiful wife who has always given me words of strength and hope and has had the strength to fight by my side day by day and wait for me during my long absences writing this thesis, also to my son and my daughter who are my strength and inspiration, for their love and for joining me on several field trips.

To Halliburton, especially to Claudia for supporting me with the software Decision Space in France for the seismic interpretation.

And to all the people that contributed to finish this important project.

ABSTRACT

For years in Colombia research has been mainly centered on the knowledge of the most recent uplifting of the Eastern Cordillera, and on the evaluation of the Tertiary units in many basins to understand the recent deformation. Recently, due to the necessities of the oil industry to evaluate new targets, new information has been acquired on Cretaceous units form the Eastern Cordillera and Middle Magdalena Valley.

The aim of this work is to analyse the data which gives evidence of deformation in the basin of Middle Magdalena Valley during the Cretaceous.

The Cretaceous units are exposed in the Eastern Cordillera, but not in the Middle Magdalena Valley, where only a few outcrops are known. Instead a lot of seismic information is available on this area and some wells that have drilled the Cretaceous units. Using large seismic reflection sections and well information, I could identify important events, unconformities, and faults which were inverted in different stages during the Lower Cretaceous to the Eocene, prior to the Andean Orogeny.

For that, I will show some key seismic sections interpreted in the Middle Magdalena Valley (MMV). This interpretation will be validated with sections using surface field information and well information, and the structural styles will be discussed.

My results highlight the new proposed interpretation for the cretaceous sequence, showing more details especially in the MMV, due to the seismic coverage and well information, and in the Western Eastern Cordillera (WEC) with more difficulty using some surface information that was collected during this work as well as preexisting information from available literature, how there were multiple phases of deformation that include different states of uprising or relative sea level change during the Cretaceous period, which is important to understand the real process that affected the Cretaceous behavior and also to suggest that tectonics and sea level changes or their interaction could be more complex during this time.

Based on the construction and analysis of transgressive-regressive curves and Fischer relative accommodation space plots, I interpreted system tracts and sea-level variations and recognized major surface boundaries surface (unconformities or their correlative conformities) at the Barremian-Aptian, during the Late Albian-Early Cenomanianand

and Early Campanian times. Aditionally, based on tracts interpreted and surface boundaries, I built regional paleo-facies maps from Berriasian to Coniacian-Santonian, showing several periods of regression and transgression till early Campanian.

From seismic interpretation made in this work, using seismic stratigraphy and wheeler diagrams, five sequences (S) and five unconformities (SU) were identified as sequence boundaries: recognized at the Jurassic-Cretaceous, Late Barremian-Early Aptian (~125 Ma), and at the Albian-Cenomanian (~100 Ma), Santonian-Campanian (~ 80 Ma), and Paleocene-Eocene boundaries, these unconformities or their correlative conformities (SU) have a regional extension.

The thermochronological information collected, prepared, analyzed, interpreted and modeled in this work, helped me to recognized two events of heating and two events of cooling for samples deposited before 85 Ma. The heating events occurred from the sedimentation of the units till ~85– 80 Ma and from ~70 Ma to ~10 Ma and the cooling events occurred between ~80 Ma till ~70 Ma and from ~10-2 Ma. The paleo-geothermal gradient versus the present-day thermal gradient make it possible to identify the presence of unconformities.

The integration of the structural reconstructions made in this work through the Cretaceous, considering the sequences (S) and the discordances (SU) and the transgressive-regressive sequences (paleo-facies maps), shows the relation between deformation, deposition and erosion and when each of these events happened during the Cretaceous in these basins (MMV and WEC).

My tectonic and geodynamic reconstruction makes it possible to conclude that from the Jurassic to the Paleocene, repetitive tectonic extension and compression events produced by a cyclic subduction regime, explain the relative sea fluctuation and the deposition, exhumation and erosion phases observed in the MMV and WEC during the Cretaceous.

Finally, the presence of accreted blocks (for ex. Quebradagrande) is undeniable. However, the deformation of the upper plate in my model is not dependent on these accreted terranes, but rather on the subduction regime, for example changes in the plate subduction angle (steep or flat subduction), the convergence rate, the polarity of subduction, the age of the slab, etc.

CONTENTS

Pag

CHAPTER 4

Seismic interpretation of the Cretaceous unconformities and sequences in the Middle Magdalena Valley and western margin of the Eastern Cordillera, Colombia.

CHAPTER 5

Thermal Evolution of the Western Eastern Cordillera and MMV: Relationship with the Cretaceous Unconformities

CHAPTER 6

Late Jurassic to Early Eocene tectonic and sedimentary evolution in the Middle Magdalena Valley and western flank of the Eastern Cordillera, Colombia.

FIGURES LIST

***Figure 5.9**. The map on the left shows the central age of the ZFT, for the samples from the norther area of study, note that the ZFT age tends to decrease towards the central part of the Los Cobardes Anticline, where the Jurassic units are present. The section in figure 5.7 shows the same behavior. The map in the center shows the minimum age from ZFT, note that also towards the center of Los Cobardes Anticline the age tends to decrease; the same behavior is observed on the map on the right, mapping the minimum age from the AFT.*

***Figure 5.10**. Map showing the location of AFT ages in the Northern section Barichara- Bucaramanga.*

***Figure 5.11.** Structural sections (this work) in the northern area (figure 5.1), above is shown the section in the Sogamoso River and below is shown the Barichara- San Vicente de Chucuri section*

***Figure 5.12.** Map showing the location of the apatites and zircon samples in the Central section: Villa de Leyva - Chiquinquira.*

***Figure 5.13.** Structural section in the Northern section Villa de Leyva - Chiquinquira, showing the location of the zircon samples.*

***Figure 5.14.** Structural section in the Northern section Villa de Leyva - Chiquinquira, showing the location of the apatites samples.*

***Figure. 5.15.** Graph showing detrital thermochronological central age (tcc) on the x-axis versus stratigraphic age (td) on the y-axis.*

***Figure 5.16**. The map on the left shows central age of ZFT for the samples in the central area of study, note that the ZFT age tends to decrease towards the central part of the Arcabuco Anticline, where the Jurassic units are present (Figure 5.14 shows the same behavior). The map on the right shows the minimum age of DZFT, note that also at the center of the Arcabuco Anticline the age tends to decrease; however at the right and left side of the structure the central and minimum age also decrease.*

***Figure 5.17**. Map showing the location of the AFT and ZFT ages in the Southern section La Vega-Villeta.*

***Figure 5.18**. Structural section in the Northern section La Vega-Villeta, showing the location of the zircon samples.*

***Figure 5.19**. Structural section in the Northern section La Vega-Villeta, showing the location of the apatites samples.*

***Figure. 5.20.** Graph showing detrital thermochronological central age (tcc) on the x-axis versus stratigraphic age (td) on the y-axis.*

***Figure 5.21**. At the left is showing the map of the central age of the ZFT, for the samples from the Southern area of study, note that the ZFT age tends to decrease towards the core of the Villeta Anticline, where the Lower Cretaceous units are present (Trinchera/Utica), the section in Figure 5.18 shows the same behavior. At right is showing the map of the minimum age of the ZFT, note that the minimum age in the Villeta Anticline tends to decrease; however at the east of the map the central and minimum age also decrease, showing that thermochronological age values always tend to decrease in older units.*

***Figure 5.22**. Semilogarithmic plots of vitrinite reflectance and equivalent maximum temperature (left), and temperature vs age. The maximum temperatures were calculated using Eq. 1 shown in the text. Suite of vitrinite reflectance data collected by various researchers (Gomez, 2001; Caballero, 2013; Mora et al., 2013; Moreno et al., 2013).*

***Figure 5.23**. Semilogarithmic plots of vitrinite reflectance and equivalent maximum temperature (left), and temperature vs age. The maximum temperatures were calculated using Eq. 1 shown in the text. Suite of vitrinite reflectance data collected by the ICP, mainly from samples from the MMV.*

***Figure 5.24.** Vitrinite Reflectance (Ro) and temperature (Tmax) vs depth.*

***Figure 5.25**. Cross plot of Stratigraphic age Vs Tmax, organized by sectors to assess the behavior of different zones in the basin.*

***Figure 5.26.** Temperature vs depth plots for wells Infantas-1613(A), RW-1 (B) and Cascajales-1 (C). The Paleotemperatures were greater than the present-day temperatures, in general in A, B and C the paleogradient presents two tendencies that mark an Albian- Cenomianian or earlier unconformity.*

***Figure 5.27**. Map showing the distribution of Ro in all the area of study, the bubble colors correspond to Ro value samples from tables 5.8 and 5.9.*

***Figure 5.28**. Plots of DAFT, DZFT and Temperature versus stratigraphic age, by sector: for the south (right); for the central (center) and for the north (left).*

TABLES LIST

Tabla 5.8 *- Vitrinite reflectance (Ro) collected by several authors (Gomez, 2001; Caballero, 2013; Mora et al., 2013; Moreno et al., 2013), the maximum temperatures (Tmax*) were calculated using Equation-1, shown in the text (after Baker and Pawlewicz, 1994).*

Tabla 5.9 *- Vitrinite reflectance (Ro) collected by the ICP (Instituto Colombiano de Petróleo), the maximum temperatures (Tmax*) were calculated using Equation-1 shown in the text (after Baker and Pawlewicz, 1994).*

Table 5.10 *- Vitrinite reflectance (Ro) collected by the ICP (Instituto Colombiano del Petróleo), the maximum temperatures (Tmax*) were calculated using Equation-1 shown in the text (after Baker and Pawlewicz, 1994). The tables also have values related to the temperature. Compiled from well description in Gomez 2001 volume II.*

Table 5.11a *– Compiled fission-track data, analyzed with laser-ablation-inductively coupled plasma-mass spectrometry (LA-ICP-MS), from the areas of Guaduas, Villeta and the Armas Syncline.*

Table 5.11b *– Samples taken from other authors, analyzed with (U-Th)/He in zircons and apatite, from the Armas Syncline.*

Table 5.11c – *Fission-track age compilation from other author mainly from the north and south, and some from the central area studied in this work.*

LIST OF PETROGRAPHIC SECCIONS

Petrographic section 3.1. *Thin section of sample JG-P4-12, sandstone from the Trinchera Fm (Figure 3.19).*

Petrographic Section 3.2. *Sample JG-P4-13 corresponding to the conglomeratic sandstone in the Trinchera/Socota Fm*

Petrographic Section 3.3. *This sample JG-P1-02 corresponds to a Biomicrite (Folk, 1962) or Packstone (Dunham, 1962).*

Petrographic Section. 3.4. *Sandstone from the Upper Aptian-Lower Cenomanian Areniscas de Chiquiquira Fm.*

LIST OF PHOTOS

Photo 3.1. *Litharenite of Early Aptian age (Upper Trinchera Fm).*

Photo 3.2. *Siliceous sandstone (Upper Trinchera Fm, Early Aptian).*

Photo 3.3. *Conglomerate in the Trinchera/Socota Fm (Late Aptian – Early Albian).*

Photo 3.4*. Outcrop of yellow quartz sandstone (right red rectangle) and red layers interpreted as paleosoils (left red rectangle), of the Albian Lower San Gil Fm (Tablazo Fm).*

Photo 3.5. *Outcrop of the Churuvita Formation along the Sachica road, before the deviation towards Cucaita –Villa de Leyva town.*

Photo 3.6*. Detail of ichnofossils (burrows) at the base of a thick sandstone bed of the Churuvita Fm.*
Photo 3.7. *Contact between the Upper San Gil and Churuvita Fms along the Villa de Leyva –Cucaita road.*

Photo 3.8*. Expression of the La Paja Fm (Barremian-Aptian) in the area of study.*

Photo 3.9. *Showing the characteristic lithology from La Paja Formation with black to gray shales and a red level of claystones with nodels, sometimes with ammonites (right upper square).*

Photo 3.10. *Thick sandstone level in the Chiquinquira Sandstone (Late Albian to Early Cenomanian).*

Photo 3.11. *E-W panoramic view, showing from base to top, the contact between the Simití Fm and the Areniscas de Chiquinquira Fm, and the Conejo Fm at the top.*

PRE-ANDEAN TECTONIC EVENTS (ALBIAN TO EOCENE) IN THE MIDDLE MAGDALENA VALLEY AND SITUATION OF THE WESTERN PROTO-EASTERN CORDILERA (COLOMBIA).

The History of Science is an oscillation backward and forward between the empirical and the theoretical.

CHAPTER 1

General introduction and outline

1.1. Introduction

Tectonics describes the processes of mountain building and the behavior of rocks. It is defined as the processes that control the structures and properties of the Earth's crust and its evolution through time. It is also understood as the study of structural or deformational features, involving the origin, interaction and historical evolution of oceanic basins, continents, mountains etc. In that way, as shown by Williams (1993), it is difficult to separate tectonics from other factors (sea level changes and sedimentation supply), which together control the stratigraphy and architecture of sedimentary basins.

Our primary aim was to identify the tectonic events occurring during the Cretaceous (Late Jurassic-Early Cretaceous to Paleocene-Eocene). These can be deciphered using different techniques involving field observation, stratigraphy and sedimentology, geochronology, structural geology and thermocronology among others.

This tectonic analysis is important to understand the phenomena observed in the basins, which in turn, provides constraints to understand the evolution of tectonic regimes, and thus, the interactions between tectonic plates. This study is based on observations, which led us to suspect that the Cretaceous history of some Colombian sedimentary basins is more complex than thought today. Finally, because the petroleum industry is looking for new possible reservoirs of conventional and non-conventional hydrocarbons, this kind of study may be key to finding new opportunities in the Cretaceous sedimentary basins.

Although this work focuses on the Cretaceous period, the old history started with the Grenville Orogeny (Orinoco Collision Orogeny), which resulted from the collision of North-America with the Guiana shield (2.25 to 0.95 Ma) about 1200 Ma ago (Kroonenberg, 1984; Hoffman, 1991; Hartnady, 1991). From 480 to 416 Ma the continental crust underwent a regional continental-type orogeny (Quetama Orogeny), documented by the accretionary prism of Cajamarca-Valdivia, and by a regional lifting during Silurian-Devonian times (Cediel et al., 2003). From 360 to 125 Ma (Bolivar aulacogen) a taphrogenesis allowed the deposition of thick sequences, from Mississipian to Early-middle Cretaceous times, over extensive areas in the Central Continental Subplate (CODIGEM, 1993a; Litherland et al., 1994; Cediel, 2003). The

opening of the Central Atlantic Ocean occurred in the late Middle Jurassic (≈157 Ma, Klitgord and Schouten, 1986) and possibly as early as in the late Liassic (180 Ma, Scotese et al., 1988). Since around 157 Ma the central Atlantic just began opening (Klitgord and Schouthen, 1986) since they were together before this time (Biari et al., 2017) the Jurassic features suggest the development of symmetric rifting followed by asymmetric oceanic accretion, probably as is indicated by pre-break reconstruction, due to two possible situations 1) because Colombia was facing the continental block involved in the new oceanic crust of the Tethyan (Jaillard et al., 1990; Litherland et al., 1994) or 2) because Colombia is directly facing the oceanic paleo-pacific-plate (Jaillard, 2000). The Kimmeridgian-Berriasian period (156 to 140 Ma) is a transition period, marked in Colombia and Ecuador by accretions, compressional deformation and the end of magmatic activity (Aspden et al., 1987; Jaillard et al., 1990; 1995), resulting from global geodynamic changes. If a Tethyan-Colombian oceanic arm did exist, Tethys accretion would have induced a northeastward convergence between the Phoenix and South American plates (Duncan and Hargraves, 1984; Jaillard et al., 1990). In the Late Jurassic, extensive rifting was marked by the deposition of Giron, La Quinta and Noreán formations (Cediel and Cáceres, 2000). This regional extension culminated with a shift from an extensional to a compressional tectonic regime, which is recorded by a regional erosional gap observed in the lower Aptian (Cediel et al., 2003).

The opening of the South Atlantic Ocean is important to understand the evolution of western South America, since it controlled the westward drift of the South American Plate and thus, the changes in the convergence rate in the subduction zone of Western South America (Frutos, 1981; Sébrier and Soler, 1991; Jaillard et al., 2000). The definitive opening of the South Atlantic Ocean occurred in the Albian (Emery and Uchupi, 1984; Scotese et al., 1988), triggering the absolute westward drift of South America (Jaillard, 2000). This event coincides with the beginning of compressional deformation along the Peruvian-Ecuadorian-Colombian margin in the Late Albian (100-95 Ma) and with the onset of the trenchward motion of the upper plate (Uyeda and Kanamori, 1979; Cross and Pilger 1982: Jarrard, 1986). The Middle Cenomanian-Turonian period (95-89 Ma) recorded a major regional marine transgression.

The Albian-Turonian period is a period of high convergence, whereas the Coniacian-Late Paleocene interval is marked by a slowdown in the convergence rate (Late Santonian-Early Campanian (85-75 Ma). This period is also characterized by the beginning of the Cretaceous compressional events (Jaillard et al., 2000).

According to Gayet et al. (1991) and Jaillard et al. (1993), during the Late Campanian (75-70 Ma), a major contractional phase occurred in Peru, which was responsible for a 300 km-long overthrust.

1.2. Aims of this study

The aim of this PhD thesis is to decipher the tectonic evolution of the Cretaceous sequence in the Middle Magdalena Valley (MMV) basin and in the western flank of Eastern Cordillera (WEC), which bounds the MMV basin to the East. For this, we used stratigraphic, structural, chronostratigraphic and thermochronological data from this and other works to analyze the

Cretaceous tectonic events and to understand the mechanisms of basin formation from Cretaceous to Middle Eocene times. For this, what we did was:

1. Study the Pre-Eocene deformations (Albian to Eocene) in the MMV and WEC, and their relationship with tectonic events that generated them during the Cretaceous time, evaluating the unconformities occurring during the studied time-interval.

2. Interpret and evaluate three structural deformed sections and restore a key section for the Cretaceous interval (Albian to Eocene) through the MMV, using seismic reflection information, wells and surface information.

3. Perform tectonic evolution modeling based on the deformation and deposition observed in the MMV and WEC, illustrated by structural sections highlighting the tectonostratigraphic history.

4. Make tectonic considerations on the pre-Eocene deformational events that occurred in the MMV, and their effects on the WEC.

In this work, I used seismic information from the MMV, and outcrop evidences in the WEC to study the evolution of the Cretaceous sequences. I also included, structural analysis, biostratigraphic data and zircon and apatite thermochronological age determination from the WEC. Finally, the integration of data provided by paleofacies maps, seismic interpretation, seismic stratigraphy, termochronology and the geological context of the MMV and WEC, made it possible to propose a regional tectonic framework. Although biostratigraphic information is available in almost all the studied area, it is not accurate enough to support the hiatus or unconformities identified in this thesis. However, in spite of this uncertainty, the use of seismic information allowed to identify gaps and unconformities thanks to the chronostratigraphic framework provided by the seismic reflectors.

1.3. Thesis Outline

This thesis comprises an introductory chapter. The second chapter summarizes the regional conceptualization and the stratigraphic nomenclature used in this thesis. Chapter 3 provides a sequential stratigraphy analysis, interpretations of the relative sea level changes, local facies distribution maps generated for the northern, central and southern parts of the studied area, and the integration of these facies maps into regional maps to understand the facies changes and the shoreline migration (regression/transgression) during the Cretaceous.

Chapter 4 presents the seismic interpretation and the chronostratigraphic seismic interpretation based on chronostratigraphic charts constructed using Wheeler diagrams, which allowed the identification of five unconformities limiting sedimentary sequences.

Chapter 5 exposes the detrital zircon and apatite fission-track results of the analysis of apatites and zircons collected in the field, as well as their interpretation.

Chapter 6 shows schematic restored structural sections from the Jurassic-Berriasian to the Present, showing the step by step deformation and making the assessment of total shortening

possible. Block diagrams illustrating the evolution of paleo-facies deformation are also shown. Finally, paleo-plate reconstruction and the Cretaceous tectonic evolution of the MMV and WEC are presented.

Each chapter in this dissertation includes a geological context, results, discussions, and conclusions, with the idea of generating independent articles.

CHAPTER 2

Regional geological context

2.1. Tectonic framework of the Northern Andes (Colombia) and Caribbean

Northwestern South America (Western margin of Colombia) is comprised of a series of plates, tectonic blocks and features, including oceanic rifts, oceanic trenches, active subduction zones, accretionary prisms, deformed belts, transform fault zones, oceanic normal faults, continental plate faults and independent lithospheric blocks (figure 2.1). These tectonic terranes are limited to the east by the Guaicáramo fault (number 43 in the figure 2.1). The Andes of Colombia present three cordilleras (Western, Central and Eastern Cordilleras), separated by the Cauca and Magdalena valleys (Figure 2.1). The Middle Magdalena Valley (MMV) sedimentary basin is 560 km long and around 80 km wide (Figure 2.3). To the West, west-dipping thrust faults separate it from the central cordillera (CC), while to the East, east-dipping thrust faults separate it from the Eastern Cordillera (EC) (Butler and Schamel, 1988; Namson et al., 1994; Gomez et al., 2003).

Figure 2.2 is a generalized map of tectonic blocks of northwestern South America (Colombia and Ecuador). On the map the most important terranes that are present in the Andes of Colombia are highlighted. Cediel (2003) distinguishes lithotectonic units, deformed by tectonic processes, and Morphostructural Units, the topography of which is controlled by faults, folds or discordances. Blocks like Chicamocha (Chibcha terrane), Cajamarca-Valdivia (Tahamí), Quebradagrande, Arquia, Amaime and Dagua terranes constitute the Central and Western Cordillera.

The Guiana Shield, located east of the Guaicáramo Fault, is a lithotectonic unit made of Precambrian autochthonous rocks (Priem et al., 1982; pink in figure 2.2), which extends throughout eastern Colombia and southern Venezuela, and includes the Gazón massif. The Chicamocha or Chibcha Terrane (Ramos, 2008; Figure 2.2) is an allochthonous Proterozoic Terrane representing possibly a relict of the North American Plate, which was added to the Guiana Shield during the late Mesoproterozoic Orinoc orogeny (1300-900 Ma), this terrane is buried by sedimentary sequences of the Lower Paleozoic, Mesozoic and Cenozoic ages.

These terrane are represented principally in the east of Central Cordillera by fragments of granulite grade bodies of migmatite and quartz-feldspar gneiss. Cediel et al. (2003), consider that this wedge may be analogous to the Arequipa terrane exposed in Peru (Dalmayrac et al., 1977). The Chicamocha or Chibcha Terrane (Ramos, 2008; Figure 2.2 and 6.8) is an allochthonous Proterozoic Terrane, possibly a relict of the North American Plate, which was added to the Guiana Shield during the late Mesoproterozoic Orinoc orogeny (1300-900 Ma), this terrane is buried by sedimentary sequences of the Lower Paleozoic, Mesozoic and Cenozoic

ages (Hackley et al., 2007; Gray et al, 2010; Giunta and Orioli, 2011; Garcia-Casco et al., 2011). The Cajamarca-Valdivia terrane (Tahami terrane – Gomez et al., 2015, figure 6.8) was accreted to the Chicamocha terrane (Chibcha terrane) or directly to the Guiana shield to the south (Figure 2.2; Loja Terrane in Ecuador, Litherland et al., 1994), during a Middle Ordovician to Silurian cordilleran-type orogeny, it is composed of greenschist till lower amphibolite metamorphic facies, pelitic and graphite-bearing schists, amphibolites, intrusive rocks and ophiolites. According to Restrepo-Peace (1972), their affinity with the intra-oceanic arc and continental-margin rocks suggest the collision and docking of an intra-oceanic magmatic arc, forming an allochthonous to parautochthomous accretionary prism of Ordovician to Silurian age.

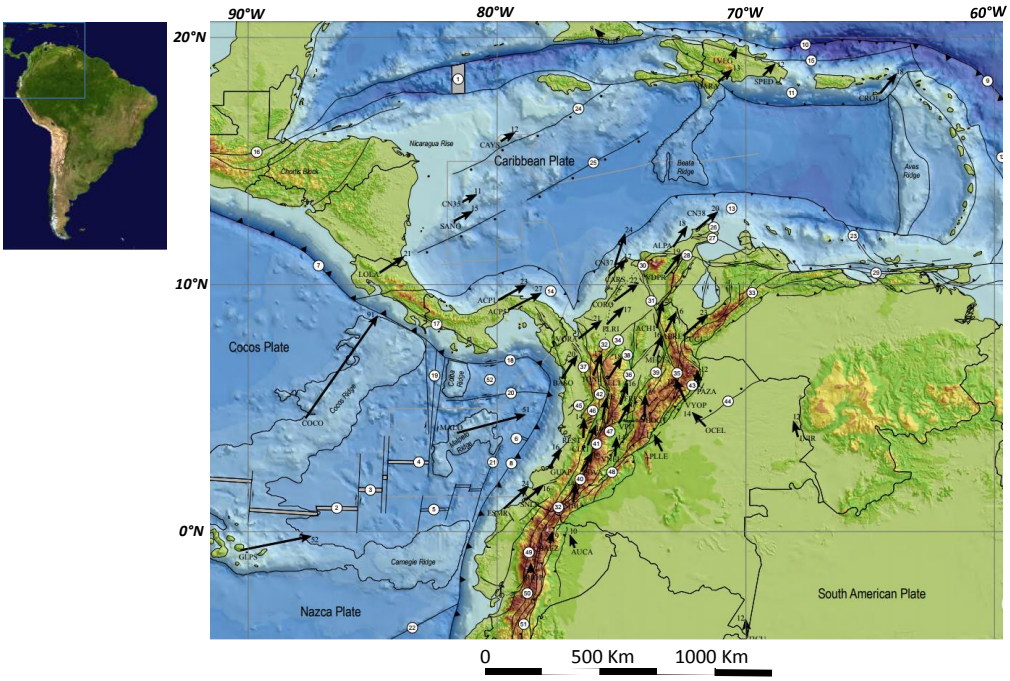

Figure 2.1. Tectonic Framework of Northwestern South America and the Caribbean (modified from Hey, 1977; Lonsdale and Klitgord, 1978; Case et al., 1984; Adamek et al., 1988; Hardy, 1991; Zamora and Litherland, 1993; Meschede et al., 1998; Gutscher et al. 1999; Audemard et al., 2000; Barckhausen et al., 2001; MacMillan et al., 2004; Giunta et al., 2006; and Escuder Viruete et al., 2006). Vector values of the relative plate movements were adapted from GPS data by Mora et al. (2014) and Protti et al. (2012). Active oceanic rifts: (1) Cayman, (2) Galápagos, (3) Ecuador, and (4) Costa Rica. Inactive oceanic rifts: (5) Malpelo and (6) Buenaventura. Oceanic trenches and active subduction zones: (7) Middle America, (8) Colomboecuatoriana, and (9) Caribbean. Oceanic trenches and inactive subduction zones: (10) Puerto Rico. Accretionary prisms-deformed belts: (11) Los Muertos, (12) Lesser Antilles, (13) Caribbean, and (14) Panamá. Transform fault zones: (15) Septentrional-Oriente, (16) Motagua-Swan, (17) Celmira-Ballena, (18) Jordan, (19) Panamá, (20) Hey, (21) Yaquina, (22) Grijalva, and (23) Los Roques. Oceanic normal faults: (24) Pedro Bank and (25) Hess. Continental plate faults: (26) Simarúa, (27) Cuisa, (28) Oca, (29) El Pilar, (30) Santa Marta, (31) Algarrobo, (32) Cauca-Almaguer, (33) Boconó, (34) Espíritu Santo, (35) Bucaramanga, (36) Palestina, (37) Murindó, (38) Otú, (39) La Salina, (40) Silvia-Pijao, (41) San Jerónimo, (42) Mistrató, (43) Guaicáramo, (44) Meta, (45) Istmina Fault Zone, (46) Garrapatas, (47) Ibagué, (48) Algeciras, (49) Pallatanga-Pujili, (50) Peltetec, and (51) Cosanga. Independent lithospheric blocks: (52) Coiba Microplate.

As is shown in figure 2.2, table 2.1 and in a more simple way in chapter 6 (figures 6.8 and 6.7) conciliating different terranes divisions in a simplified manner, Colombia is divided in six terranes that from the Eastern Cordillera towards the west are: Chibcha terrane (Chicamocha terrane), Tahamí Terrane (Cajamarca-Valdivia Terrane), and Quebradagrande, Arquia, Amaime and Dagua terranes (Kwedge in figure 6.7, Romeral terrane in figure 2.2.). These terranes are located between the Guiana Shield, the Maracaibo subplate and the western tectonic units (composed in figure 2.2 by Gorgona, Sinu, San Jacinto terranes, Cañas Gordas and Baudo Terranes).

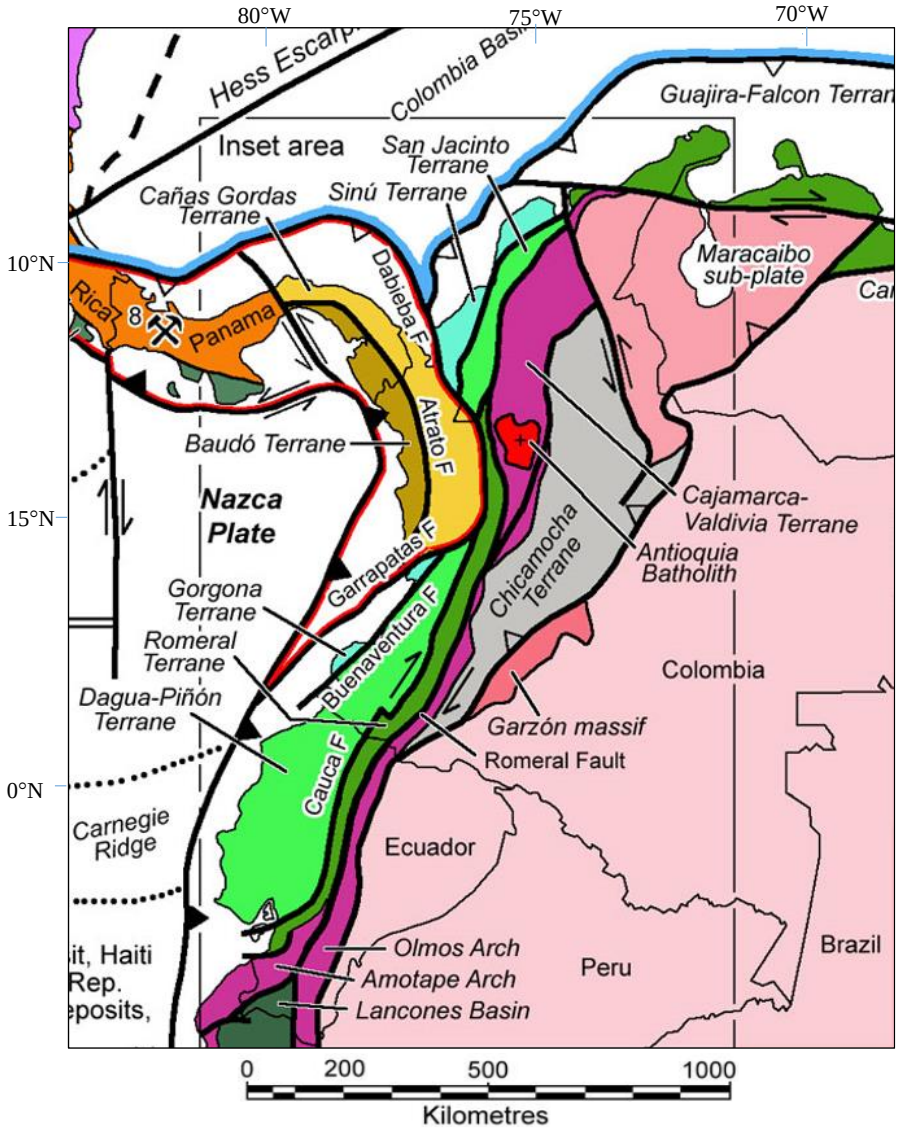

Figure 2.2 *Tectonic framework of the northern Andes of South America (after Cediel et al., 2003; Hackley et al., 2006; Gomez et al., 2007; Kennan and Pindell, 2009; Gray et al,,.2010; Giunta and Orioli, 2011; Garcia-Casco et al., 2011; Schutte et al., 2012).*

The Romeral, Dagua, San Jacinto and Sinu terranes correspond to the lithotectonic units recognized by Etayo et al. (1983). The Romeral Terrane was accreted to the Cajamarca-Valdivia Terrane 132-125 Ma ago (Litherland et al. 1994), based on radiometric dating of

phengite and glaucophane-bearing schists in the El Oro Arch (Ecuador, McCourt and Feininger, 1984) and in Jambaló (Colombia). The Dagua Terrane (Figure 2.2) was accreted after emplacement of the Romeral Terrane (Cediel et al, 2003), which is evidenced by a period of uplift and erosion around 56 Ma, resulting in a regional unconformity. This event would have resulted from the oblique convergence of the Dagua terrane, prior to the collision of the Dagua Oceanic Plateau around 49 Ma ago (Cediel et al. 2003).

Terrane	Terrane (2)	age	Accretion age	Orogeny	Tectonic Event
Chibcha Terrane	**Chicamocha T.**	Precambrian	1300-900 Ma Meso-Neo-Proterozoic	Grenville_orinoco Collision	Allochthonous, Collision North A. with Guiana
Tahami	**Cajamarca-Valdivia**	No Pre-Devonian radiometric dating	480-416 Ma Ordovician - Silurian	Cordilleran type orogeny	subsidence of the basement
Quebradagrande Complex **0**		140-130 Ma 77+/- 5, 75+/- 8, 67+/- 5 (K/Ar) Early Cretaceous Mid-Hauterivian – Early Albian	100 Ma ???	Mochica Phase	oceanic terranes accreted
Arquía complex	**K-Wedge or Romeral**	Cretaceous to Paleocene ??? K–Ar (55-58 +/- 1), Rb–Sr (53 – 57+/- 2 Ma) and Ar–Ar (45.8+/- 1.7) 91,1+/- 16,4, 97+/- 10, 131+/- 9, 127+/- 5, 77+/- 4	????	Middle Ordovician to Silurian Cordillera-type Orogeny	oceanic terranes accreted
Amaime Terane		Early Cretaceous ?? subject to controversy 113+/-4, 97+/-1067+/-2,81+/-5, 114+/-3, 70+/-14	??		oceanic terranes accreted
Dagua-Piñon Terrane		Coniacian–Campanian based of radiolarians and foraminifers	c, 58 Ma Late Paleocene	Inca Phase	oceanic terranes accreted

Terrane	Terrane (2)	Lithology	Author
Chibcha Terrane	**Chicamocha T.**	Granulites metamorphic rocks	Kroonenberg, 1984; Hoffman, 1991 and Hartnady, 1991; Cediel et al, 2003 Nivia et al. (2006); Ordóñez-Carmona et al., (2006)
Tahami	**Cajamarca-Valdivia**	extensive sequence of marine, greenschist till anphibolite methamorphic facies pelitic, graphite-bearing schist, amphibolite , intrusive rocks, ophiolitesand and epicontinental sediments	Cediel et al., 2003
Quebradagrande Complex	**K-Wedge or Romeral**	continental-derived sediments clast of basic and intermediate volcanic rocks Basalt basalt, andesites and volcanoclastic rocks, occasionally ophiol	Kennan and Pindell, 2009; Aspden and McCourt, 1986; Nivia et al., 2006 Gansser, 1973; Goossens and Rose, 1973 In Moreno-Sánchez and Pardo-Trujillo, 2003 (Restrepo et al. (1991) Maya and González (1995 Gonzáles, (1980)
Arquía complex		sediments interbedded with basalts metamorphic rocks of high a medium pressure Tonalita, Quarzodiorite, Diorite, schist, anphibolite.	Restrepo and Toussaint, 1976; McCourt et al., 1984 McCourt et al., 1984; Restrepo-Pace, 1995 Maya and González (1995), In Moreno and Pardo, 2003 (Globel and Stibane (1979), Gonzáles et al (1978) Tousand and Restrepo (1976)).
Amaime Terane		ophiolites, lavas and basaltic, affected by granitic intrusions Granite, Basalts, diabases, mudstones, Quarzodiorite, Gabbro	A. Nivia, 1989 In Moreno and Pardo, 2003 (Maya (1992), Brook(1984), Espinosa (1985) Tousand and Restrepo (1978)).
Dagua-Piñon Terrane		interpillow sediments	Etayo et al. 1983 Vanmelle et al. 2008 Jaillard E. (2009)

Table 2.1 Shows the most important accretion terranes related with figures 2.2, 6.7 and 6.8.

Unconformities in the Cretaceous sedimentary series have been proposed or observed by Mattson (1984), Khon et al. (1984), Hanq et al. (1987), Macellari (1988), Van der Wiel (1991), Pindell and Tabutt (1995), Rollon (1997), Ramos and Alleman (2000), Jaillard et al. (2000), Guerrero (2002), Jaimes et al. (2006), Cooney et al. (2009) and Patarrollo (2009). Additionally, uplift, erosion or igneous activity related to tectonic events were also shown. Using K-Ar from igneous rocks from the Cordillera de la Costa, Curaçao and Isla de Los Hermanos. Santamaria and Schubert (1974) mentioned igneous activity related to tectonic events of Cenomanian age, in the Central Cordillera, Rodríguez and Rojas (1985) suggested uplift or deformation during Late Cretaceous times. In Venezuela and in the Garzón Massif, Late Cretaceous zircon ages (85 to 113 Ma) suggest a tectonic-thermal event interpreted by Van der Wiel (1991) as an orogenic event. However, according to Van der Beek (1995) these data probably indicate local uplift of faulted blocks located at rift margins. In the Ecuadorian Andes, Rivadeneira (1999) suggested uplift or deformation during the Late Cretaceous time. Toro et al. (1990) and Gómez et al. (2005) using zircon fission track ages from the Central Cordillera of Colombia evidenced

uplift during the Jurassic (185 Ma) and Late Cretaceous (≤ 77 Ma). Apatite and zircon F-T ages from granites from the same Central Cordillera suggest a Cenomanian igneous activity related to a tectonic event (Villagomez et al., 2008). In the Upper Magdalena Valley (UMV) of Colombia and in the Maracaibo basin of Venezuela unconformities of the Campanian and Cenozoic ages were recognized (Jaimes and De Freitas, 2006; Cooney and Lorente, 2009). In Peru, Jaillard et al. (2000) suggest that the Late Albian Mochica tectonic event (≈ 100 Ma) was related to an increasing convergence rate, due to the opening of the Equatorial Atlantic Ocean.

2.2. General Settings

The scientific knowledge of the Cretaceous sediments in the Andes started with d'Orbigny (1840-1842), and Charles Darwin (1846). D'Orbigny showed a special interest in the Cretaceous strata of the Andes, which are found from Colombia to Patagonia, and identified some fossils of Neocomian age.

The Cretaceous sequence is important from both the academic and economic points of view and provides information about subduction, collision and rifting, since the latter control subsidence, sedimentation, unconformities and abundance of volcanic activity, either marine or continental (Pindell et al., 1994). The Cretaceous sequence is classically considered as deposited in an extensional basin, which was inverted during the Cenozoic. In Northwestern South America the interaction between the Nazca, Caribbean and South American Plates (figure 2.1) controls the tectonic evolution and the accretion of terranes against western Colombia (figure 2.2; Duque-Caro, 1990). The latter were responsible for the inversion of extensional basins during the Late Cretaceous and Late Miocene, respectively.

Marine deposition occurred in a wide rift system developed in the western part of Colombia (Aspden et al, 1987) during the whole Cretaceous period, and came to an end due to the accretion of oceanic terranes of the Western Cordillera, which created a Paleogene foreland basin (Cooper et al., 1995). The MMV basin includes Tertiary sediments that are thicker to the east, below the WEC (Figure 2.1). The middle Eocene regional unconformity represents the upper limit of Pre-Tertiary units.

Tectonics and deformation

The MMV and EC (Figure 2.3) are interpreted as Mesozoic extensional basins, the tectonic inversion of which remains poorly documented and understood (Sarmiento, 2001). Several hypotheses have been proposed to explain the uplift of the WEC (Figure 2.3). Van der Hammen (1958) suggested that the uplift of the EC took place during the Miocene to Pliocene, 6-4 Ma ago (see also Campbell and Burgl, 1965). In the model proposed by Colletta et al. (1990), a single inversion event occurred during the Miocene-Pliocene. Dengo and Covey (1993) proposed a two-step inversion process, in which thin-skinned deformation during the Miocene-Pliocene, was followed by the uplift of the basement in Pliocene-Holocene times. Other authors suggest that inversion tectonics began in the Paleogene (Van der Hammen, 1961; Roeder and Chamberlain, 1965; George et al., 1997; Gómez, 1999; Sarmiento, 2001). More recently it has been proposed that the Paleocene-Middle Eocene initial shortening in the MMV was associated

with the tectonic inversion of the Mesozoic rift (Restrepo-Pace et al., 2004; Cortés et al 2005; Moretti et al., 2004; Parra et al., 2012). Crustal shortening in the MMV occurred prior to the deposition of continental sediment of the Lower-Middle Eocene age (Parra et al. 2012), which gave way to the regional unconformity called the Late Cretaceous-Cenozoic Unconformity by Gómez et al. (2003).

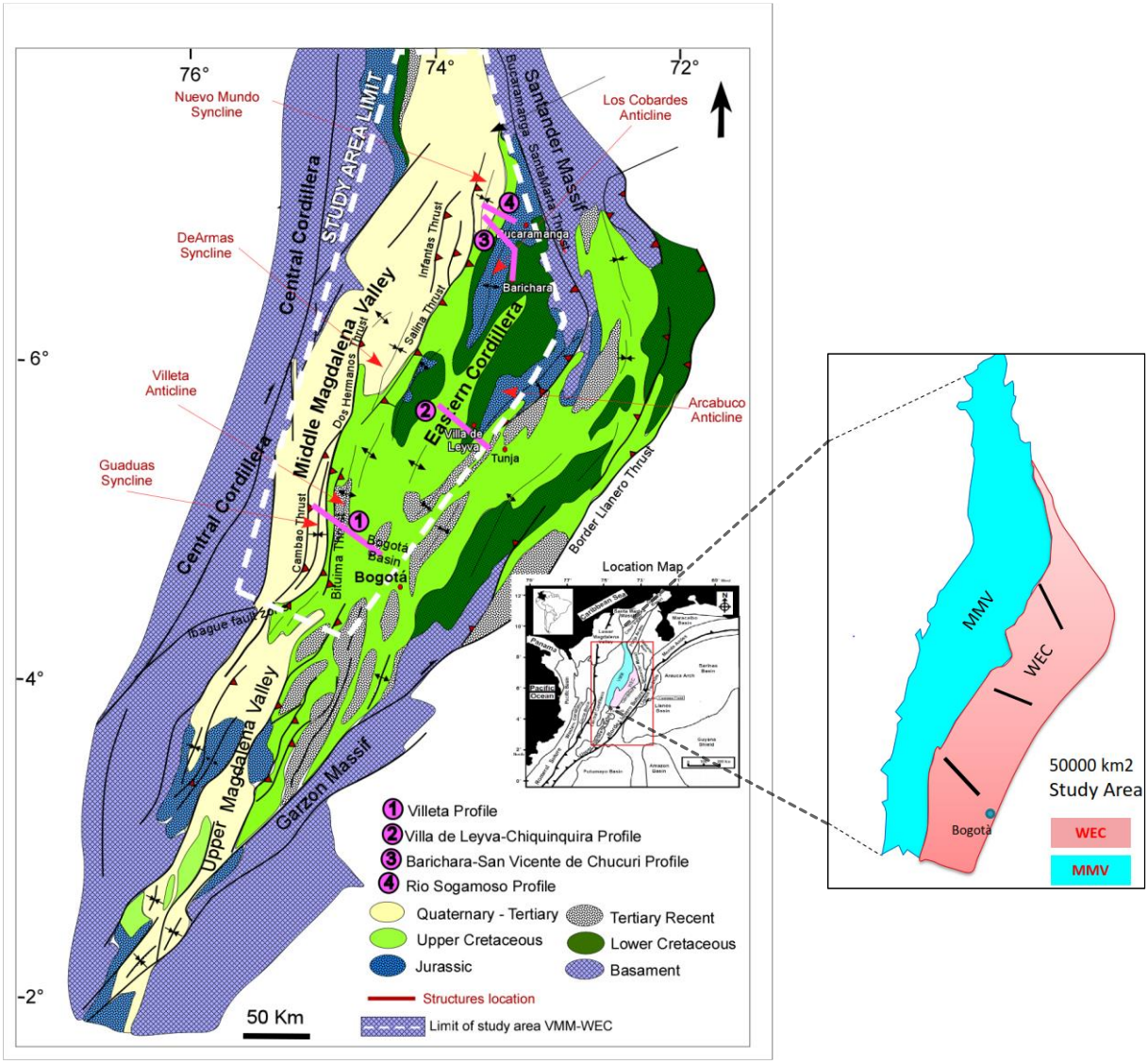

Figure 2.3 *Geological Map (left) (modified from Restrepo-Peace et al. (2004),) of the study area, showing the most important structural and geological features, the general stratigraphic units, the location of the section profiles analyzed in this work (pink lines); to the right is the location of the Middle Magdalena Valley (MMV, light blue) and Western flank of Eastern Cordillera (WEC, pink), representing the study area.*

The tectonic events are illustrated by the phases of subsidence in different sedimentary basins (Figure 2.4; Sarmiento, 2001). Rapid subsidence in the Triassic-Middle Jurassic would result from the stretching of the lithosphere (e.g. McKenzie, 1978; Ziegler, 1994), since sediments of this age were accumulated in wide rift basins (Macia, 1985; Bayona et al., 1994; Mojica et al., 1996), they locally and/or sporadically affected normal faulting (Saldaña Fm, Guillande, 1988).

Actually, the Triassic and Jurassic succession presents several unconformities separating various stratigraphic intervals (Cooper et al., 1995).

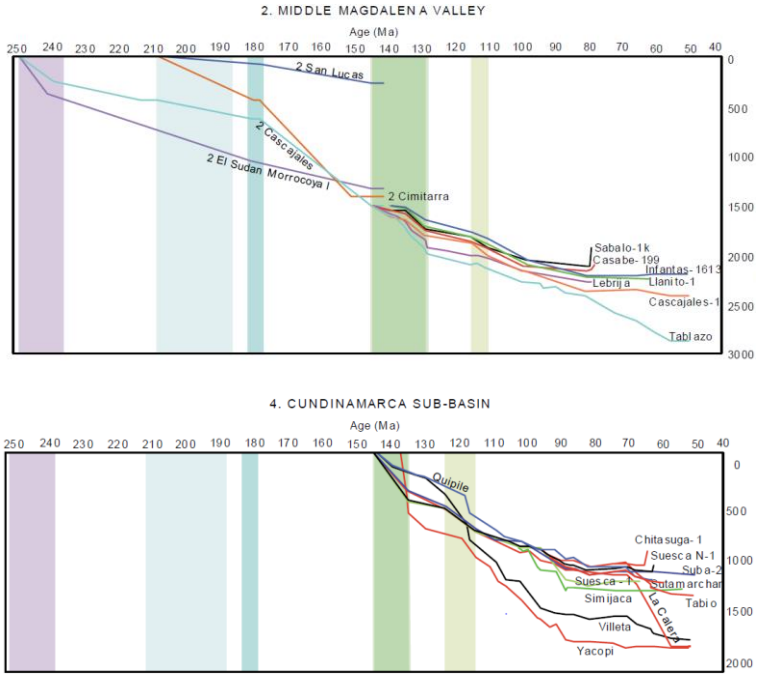

Figure 2.4 *Subsidence curves for the MMV and WEC basins (from Sarmiento, 2001).*

Sarmiento (2001) identified three periods of rapid subsidence during the Cretaceous (between 144 to 127 Ma) associated to the maximum tectonic subsidence produced by lithosphere stretching, with extensional tectonic movement; at 121-102 Ma (Aptian – Albian) other fast subsidence event occurred at the location of EC and MV; between 113 to 85 Ma Van der Wiel (1991) interpreted an orogenic event that in the area of extensional basin probably reflects cooling and uplifting of rift shoulders (*c.f.* Van der Beek, 1995). In the Cenomanian-Turonian (93-88 Ma) the subsidence increased during the global sea-level maximum (Haq *et al*., 1987; Villamil and Arango, 1998). At 80-65 Ma (Campanian – Maastrichtian) in the area of Suesca-1, Sabal-1k y Casabe-199, the onset of the uplift is insinuated.

Within the context typically accepted by the geological community is a history of deformation that begins in the Upper-Cretaceous to Paleocene, when a first deformation phase was generated (Cooper, et al., 1995) due to the accretion of the Western Cordillera as shown in Figure 2.5. According with Fabre (1985a, b) this was not notable in the EC, except in the Sierra Nevada del Cocuy, but that nevertheless determines the completion of marine sedimentation and gave rise to continental deposits. Another important deformation phase is that which occurred in the Middle Eocene known as pre-Andean orogeny (Duque-Caro, 1979, Villamil and Restrepo, 1997) and which marked the cessation of paleogene sedimentation. According to several authors, the maximum deformation occurred in the Miocene (Villamil, 1999) approximately 10.5 million years ago (Cooper, et al., 1995), producing a rapid uplift, erosion and molasic sedimentation towards the flanks of the mountain range; according to Acosta, 2002, this event is responsible for the generation of most of the EC structures.

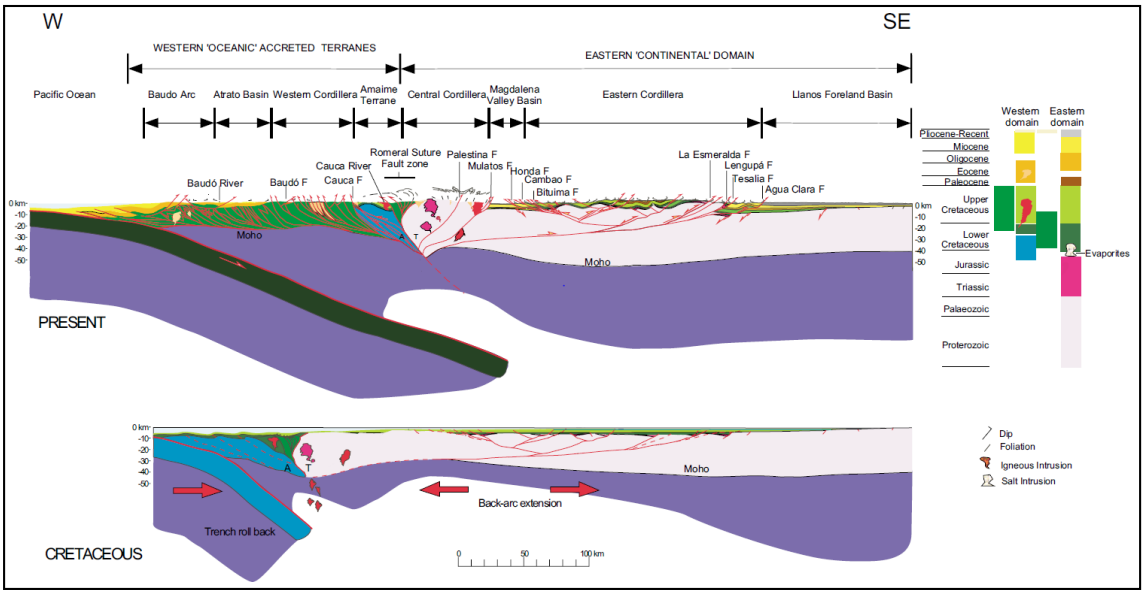

Figure 2.5 *Tectonic evolution of the Eastern Cordillera since the Cretaceous (Cooper et al., 1995).*

The first models of deformation of the EC were given by Colleta et al. (1990), Dengo and Covey (1993) and Roeder and Chamberlain (1994) (figure 2.6). These three models show a root depth of 36 km, the model showing a low angle of thrust, followed by the formation of the foreland basin; proposed by Dengo and Covey (1993) is the most documented of the three models, and has strong consistency with the Bouguer gravity model, although Roeder and Chamberlain proposed another model, due to its poor consistency between blocks of the crust and the position of Moho, assuming that the tilt of the Magdalena basin is due to the elastic flexure load.

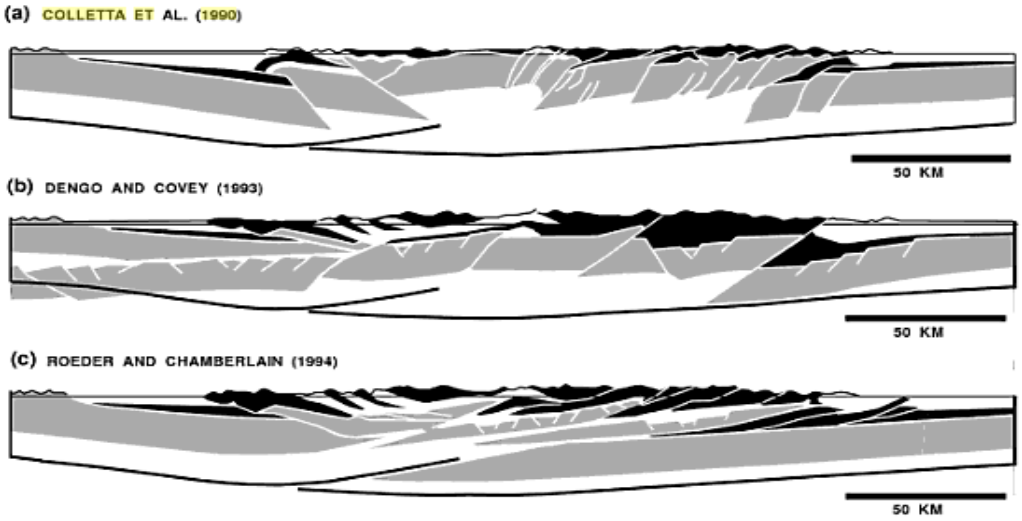

Figure 2.6 *Comparison of three deformation models of the Eastern Cordillera: a. Colleta et al. (1990); b. Dengo and Covey (1993); c. Roeder and Chamberlain (1994).*

Cooper et al. (1995), propose a hypothesis of development and tectonic history of the Llanos, EC and MMV basin that goes from the Triassic to the Middle Miocene (Figure 2.7). Development begins in the Triassic until the early Cretaceous with the formation of a Synrift

megasequence (Figure 2.7a and b), which continues in the Cretaceous in a Back-arc frame to the east of the Andean subduction zone, marine deposits were interrupted during the early Maastrichtian due to the accretion of the Western Cordillera (CW) (Figure 2.7b), which creates the megasequence of the pre-Andean Foreland basin (Late Masstrichtian - Early Eocene) dominated by fluvio-deltaic strata that covers the VMM, the EC and the Llanos basin (Figure 2.7b). Since the beginning of the Middle Miocene the deformation of the EC separates totally the MMV from the Llanos Basin as is observed in Figure 2.7c.

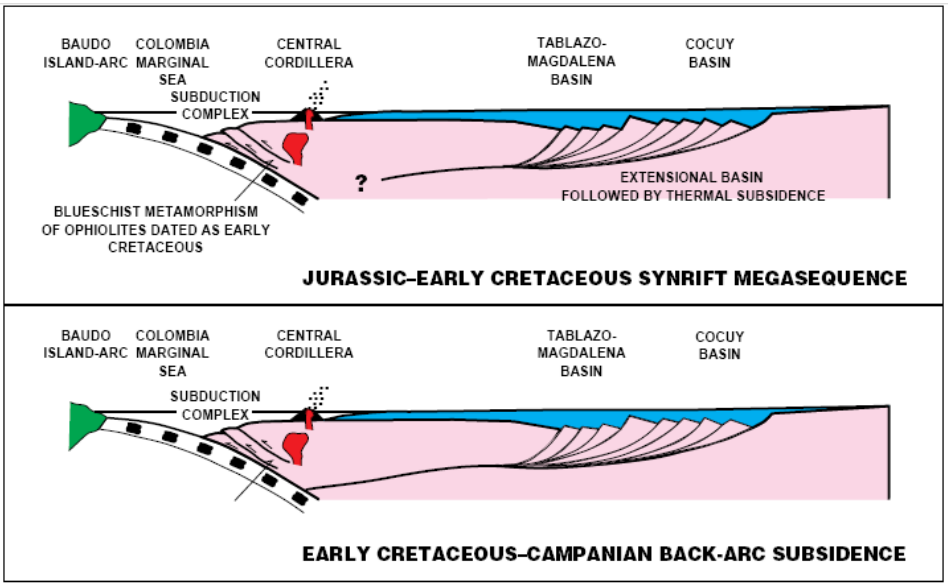

Figure 2.7a*Tectonic history from Jurassic to Campanian (from Cooper, 1995).*

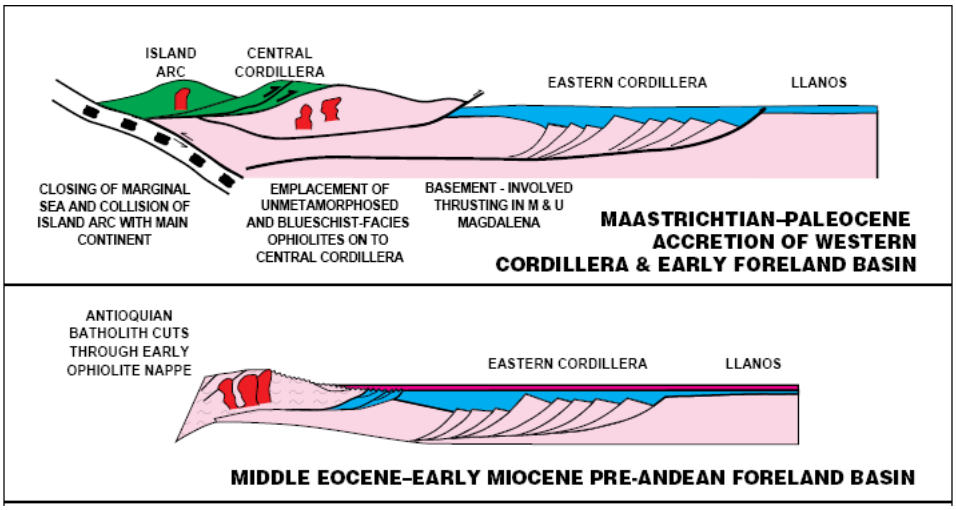

Figure 2.7b *Tectonic history related to the separation of North America from South America in the Proto-Caribbean from Maastrichtian to Miocene (from Cooper, 1995).*

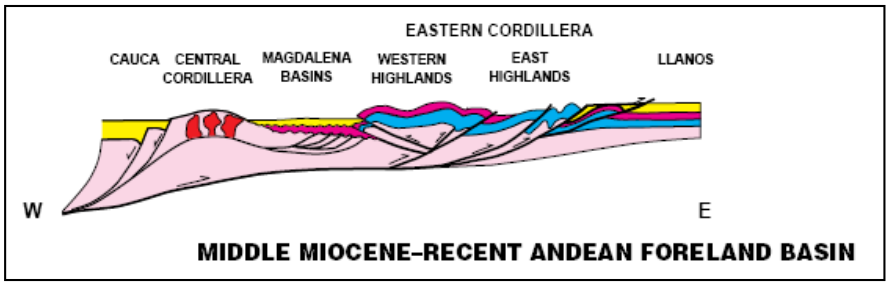

***Figure 2.7c**. Foreland Andean megasequence, showing the incipient Andean deformation in the EC, which separates the MMV from the Llanos basin (from Cooper, 1995).*

Sarmiento (2001), focuses his doctoral thesis on the tectonic formation of the basin and the inversion history of the EC of Colombia in terms of geodynamic processes. He compiles local data, analysis and quantitative models of tectonic subsidence and mechanisms of formation of the basin to test possible tectonic scenarios related to the Paleogenic tectonic history. The author argues that the accretion of oceanic lands of the EC during the Paleogene generates an incipient inversion of the Mesozoic extensional basin. For the author, the present discordances, lateral changes of facies, thickness, and the limited thermochronologic data suggest an incipient inversion of the extensional basin during the Paleocene and for the Mesozoic basin (Sarmiento, 2001 and Gomez et al., 1999), together with the local formation of topography in the area of the EC, a hypothesis that contrasts with that posed by Cooper et al., 1995 who suggests the existence of a foreland basin east of the CC for the Paleocene. According to Sarmiento (2001), during the Eocene the convergence of the Caribbean plate and South America increased (Daly, 1989), there was a lifting of the CC, folding and faulting in the VMM. This is an important point since there is a rift zone in the current position of the EC, it is difficult to think that the zones of weakness associated with the EC rift would not have been reactivated and inverted during this deformation that Sarmiento suggests (2001) and very possibly in previous shock and deformation events in times such as those proposed by Villagomez (2010).

In the Eocene- early Oligocene the convergence rate was reduced and was mainly driven by the movement from South America to the west, towards the stationary plate of the Caribbean. The Farallones plate was rotated between the plates of Coco and Nazca during the Oligocene, about 25 Ma ago (Wortel and Cloetingh, 1981; Duncan and Hardgraves, 1984). According to Cooper et al., (1995), changes in the movement of the tectonic plates (Pilger, 1984, Avraham and Nur, 1987) did not cause any deformation in the EC. The collision - accretion of the Cuna terrain (Serranía del Baudo) with the north of South America occurred during the middle Miocene (Duque and Caro, 1990). According to Cooper et al, 1995, the collision could contribute to the initial deformation of the EC. However, Kerr et al. (1997), based on the age of the Dabeiba magnetic arc, suggested that the obduction and accretion of the volcanic rocks of the Serrania del Baudo probably occurred during the late Eocene, similarly Feininger (1980, 1986) proposes a subduction towards the west.

Authors such as Gómez (2001, 2003, and 2005) propose explanations for the formation of the MMV and EC basin, indicating that numerous studies have tried to explain the discordance of the middle Eocene in the VMM (Figure 2.9), the inclination of the latter towards the East and

strata geometry as due to the deformation of the CC (Schamel, 1991; Cooper et al., 1995). The perception has been that the basins of the Llanos and VMM behaved like a single foreland basin of the CC until the EC uprising occurred (Dengo and Covey, 1993; Gomez, 2003). The same author also suggests that the relationship between strata is explained by a dual development of CC and EC. He establishes the relationship between sedimentary environments and the evolution of these two mountain ranges from stratigraphic and structural studies, integrated with provenance data, paleoflow, and geochronology of fission tracks and Ar-Ar on volcanic ash. This author presents a history of evolution of the CC and EC based on data from the south of the VMM (figure 2.8), evaluated from the Maastrichtian to the present, using the record of unconformities, strata and structures with which it extracts the history of exhumation of the CC and evolution of the EC.

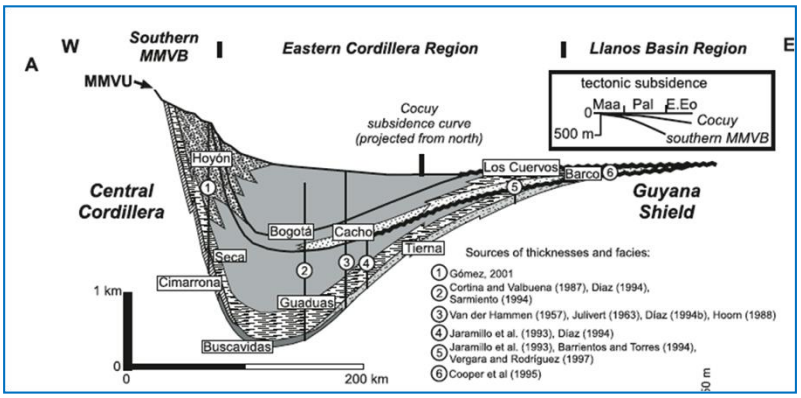

Figure 2.8 *Palinspastically restored section of the Maastrichtian foreland basin (MMV and EC) attached to the Central Cordillera (from Gomez, 2005).*

Gomez et al., (2005) indicates that for the Cretaceous-Cenozoic the MMV, the EC and the Llanos behaved as a single basin of foreland to the East of the CC (figure 2.8), interpreting and analyzing this configuration from the Maastrichtian to the Late Oligocene and evaluates the flexural response due to the lifting and tectonics of the CC. Additionally, the author analyzes the deposits on the Eocene discordance documenting the transformation of the MMV basin in to an inner basin due to the deformation of the EC, registered by growth strata and changes in the sediment origin during the Tertiary. He also establishes a thermal history using fission tracks in apatites and vitrinite reflectance showing two cooling events in the anticline of the Cowards, La Cira Infantas and the well Catalina-1, which began 5 Ma ago, the other event reports cooling data in sands of Tablazo and Umir in 80 and 30 Ma. The youngest event (30 Ma) correlates with the deformation of the EC during the Pliocene, but the oldest cooling event (80 Ma), it is attributed to the formation of the VMM during the Early Eocene, however this event allows to introduce the idea that old deformation events affected the VMM (Figure 2.9) and possibly the EC, facts that have not yet been sufficiently analyzed. This is possibly one of the most important deformations observable in the study area, evident in seismic data in the MMV and UMV.

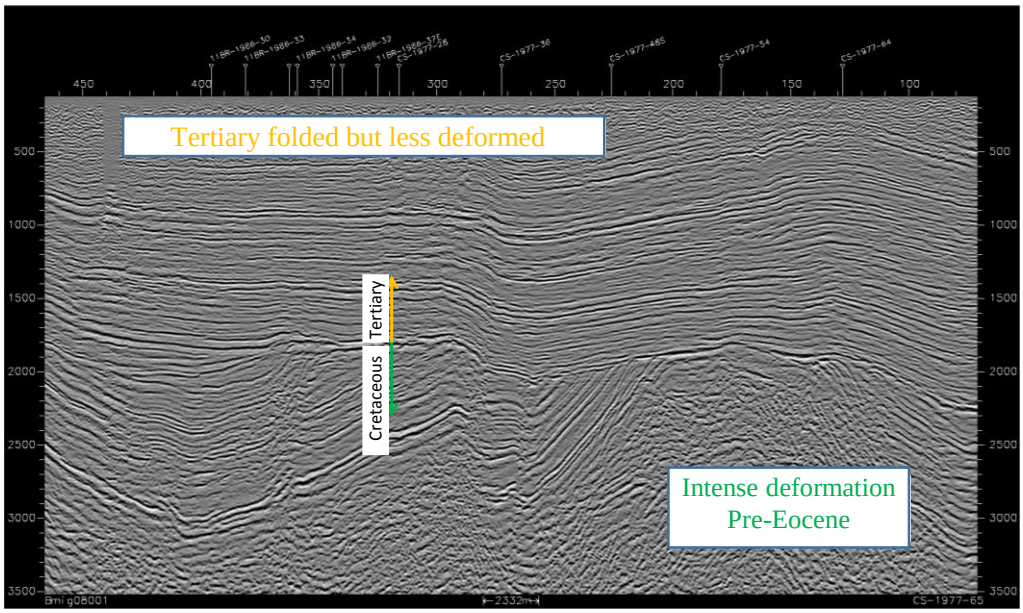

Figure. 2.9 *Seismic sections in the MMV area, where the intense deformation of the Cretaceous-Paleocene units is observed under the Eocene discordance (from Guerrero, 2010, unpublished report).*

Unconformities and sequence boundaries

Macerralli (1988) was the first author who recognized several unconformity-bounded depositional cycles in western South America, making a separation between Northern South America (Venezuela to Peru, including Colombia) and southern South America. In his extensive paleogeographical work, he recognized five cycles separated by regional unconformities in Northern South America (Figure 2.10). These cycles are comparable in magnitude to the second-order cycles of Haq et al. (1987), and result from the interaction between thermal and tectonic subsidence, variations in sedimentation and eustatic sea-level fluctuations. According to Maceralli (1988), a large portion of the continental margin was primarily covered by Early Cretaceous quartz sandstones derived from the Guayana Massif (Aguardiente, Une and Caballos formations), deposited in deltaic to shallow marine environments. These sandstones covered the Putumayo, Upper Magdalena, Santander Massif and the Merida Arch, and grade westward to a fine-grained deposits with carbonate intercalations (Villeta, Simiti and other units).

Morales (1958; 1965 *in* Barrio and Coffield, 1992) identified three unconformities or non-depositional surfaces in the MMV, which are from base to top: 1) between Paja and Tablazo Formation (Albian age), Late Cenomanian 2) Simiti-Salto/lower La Luna Fm. (Late Cenomanian) and 3) Umir Fm (Late Campanian age), respectively. Barrio and Coffield (1992) also identified an unconformity or no depositional surface at the Campanian time that could be followed from the MMV to the UMV (Upper Magdalena Valley) crossing the WEC (Villeta Apulo area) (Figure 2.11). According to these authors, another surface that probably corresponds to the same in the MMV in the Aptian time is at the base of Caballos Formation in the UMV and la Paja/Tablazo in the MMV (Figure 2.11).

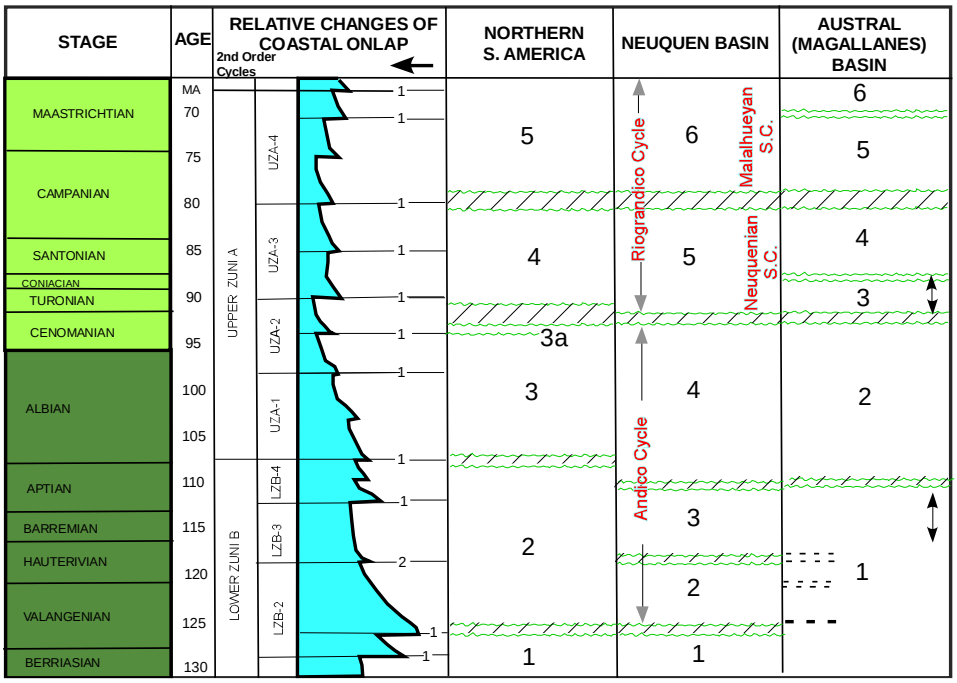

Figure 2.10 *Unconformities identified from Northern South America, Neuquén basin and Austral basin (modified from Macellari, 1988)*

Below the Caballos Formation in the UMV some authors have recognized the Yavi Formation as a continental unit (Macia and Mojica, 1981; Macia, 1985; Peñas and Vargas, 1989). The Yavi Fm is made of shallow marine to continental deposits, which were controlled by the paleotopography. Peñas and Vargas (1989) and Agudelo and Peñaloza (1990) recognized in the Quebrada Calambé that the Yavi Fm. was deposited in alluvial fans and braided river environments. The Yavi Fm correlate with the presence of an unconformity reported by Morales (1958) in the MMV, at the limit between the Paja and Tablazo fms (Figure 2.11).

Important changes in Villeta Fm. from western to eastern of Magdalena Basin, vary from 800 meters to 6000 in the area of Apulo-Villeta (Sarmiento, 1989). According to Barrio and Coffield (1992), clearly the subsidence rate was lower in the west than in the east. That could be interpreted as a positive relief in the Central Cordillera during this time, however the abundance of carbonates in this sequence implies minor clastic input (Tankard, 1986). These authors conclude that in the UMV, the first transgression took place during the Hauterivian –Barremian and was restricted to the North of the area, a second during the Aptian-Albian, and they finally indicated that regional flooding of northern of South America is recorded during the Cenomanian-Turonian deposition of Villeta Formation.

Plate reconstruction.

Pindell et al., (2009), presents an update of Yucatan rotation models and Pacific origin for the evolution of the Caribbean and the Gulf of Mexico. It presents Pre-Aptian, Aptian and younger maps with a surprising simplicity of Caribbean-America interaction. The oceanic lithosphere of the Caribbean has moved little relative to the hot spot in the Cenozoic, but moved northward at 50 km / Ma during the Cretaceous, while the plates of America have traveled west farther

and faster and thus they are responsible for the movement history of America with respect to the Caribbean plate.

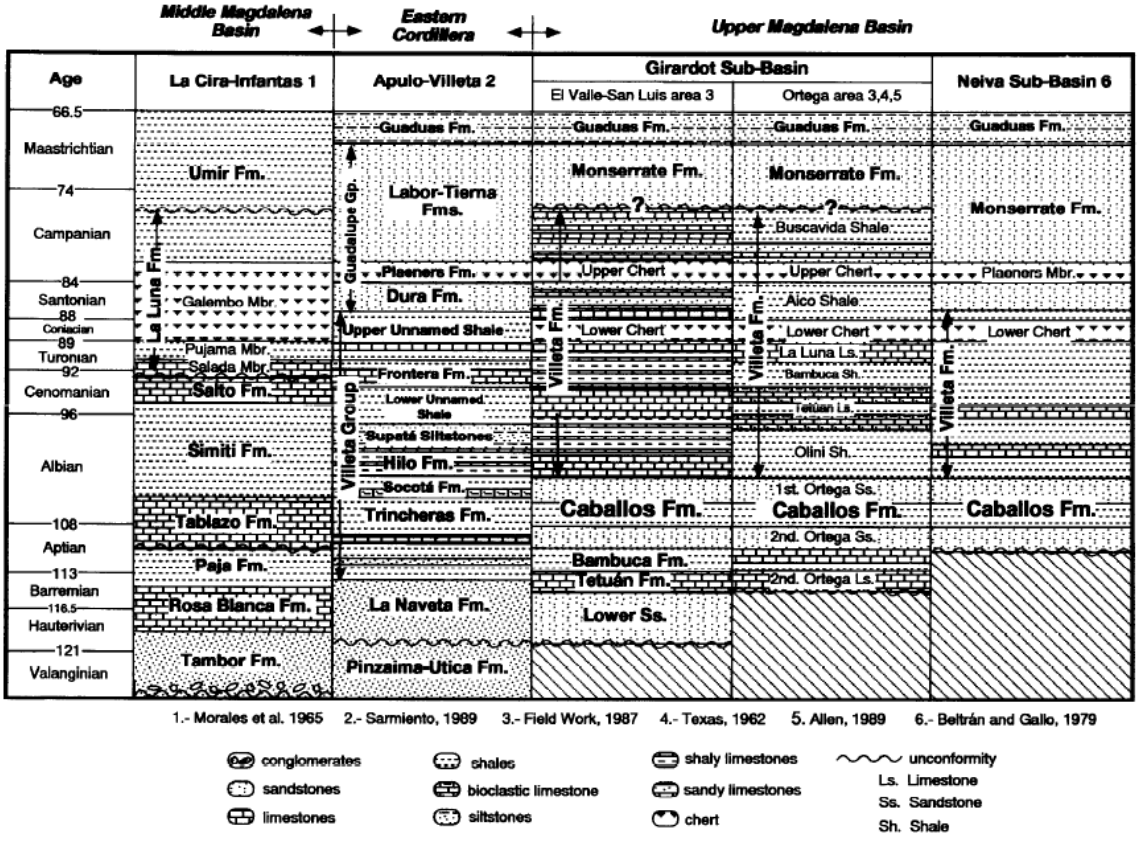

Figure 2.11 *Cretaceous stratigraphic correlation between the MMV, the Eastern Cordillera and the Upper Magdalena Valley (UMV - Girardot and Neiva sub-basins) (from Barrio and Coffield, 1992).*

Note that there is a great movement of the South America plate during the Cretaceous, an effect that is notorious in the maps shown by Pindell (2009) between about 84 to 70 Ma.

Pindell (2009) begins reconstruction in the Lower Jurassic of western Pangea, continuing with the opening of the Central Atlantic and the Gulf of Mexico and the early development of Mexico, the Northern Andes, and the Proto-Caribbean passive margin. He then continues with the evolution of the Caribbean lithosphere and its interaction with America, from the oldest to the newest and ends with the evaluation of the Neo-Caribbean phase of deformation over the last 10 Ma. Figures 2.12 show this reconstruction for 148, 125, 100 and 71 Ma.

The maps of Pindell (2009) show how the block north of South America moves towards the east until 120 and 100 Ma., When the movement changes direction towards the West, and probably at this time a compression process may have started, inverting existing areas using zones of weakness. Between 84 and 71 Ma., the great migration of South America to the west is remarkable, in Pindell's maps (2009) an area to be subducted under South America is

observed that could have generated a compression that affected Cretaceous units already deposited east of the CC in the position of the MMV till the Llanos.

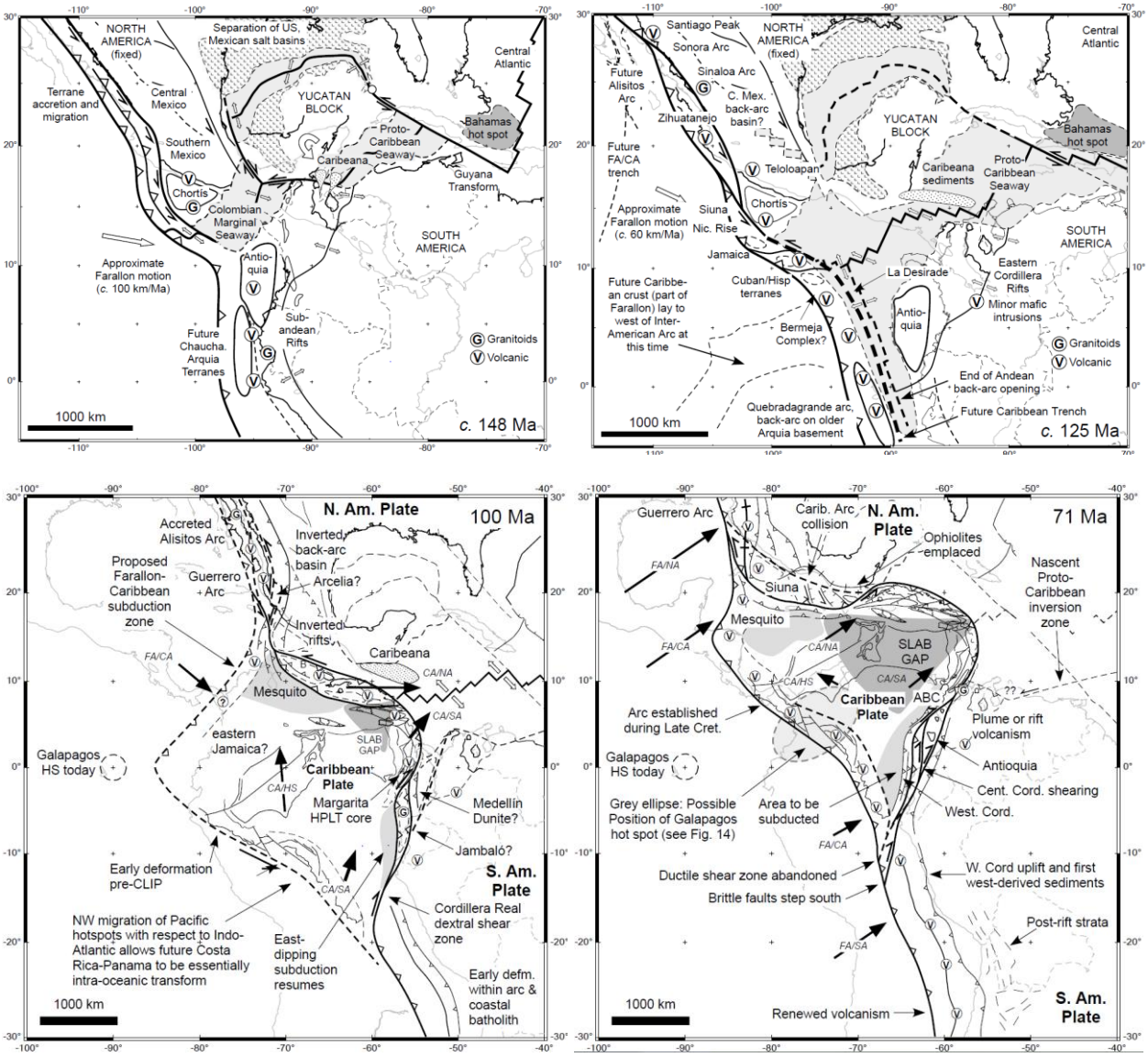

Figure 2.12 *Plate reconstruction for 148, 125, 100 and 71 Ma (from Pindell 2009).*

In contrast, examples of "flat slab" subduction (western Colombia, southern Mexico) show more uplift and erosion, perhaps as much as 5-7 km. in Colombia, and the generation of the regional discordance of the "Middle Eocene"(Figure 2.13).

According to Pindell (2009), the basement was extensively exposed and eroded during this time in the CC, providing clastic detritics from the Jurassic, Paleozoic and Precambrian during the Early Paleocene-Eocene to the VMM. This hypothesis of a lifting is also supported by the maps of Pindell and Kennan (2001), which show a possible start of uplifting at the south of EC about 100 Ma.

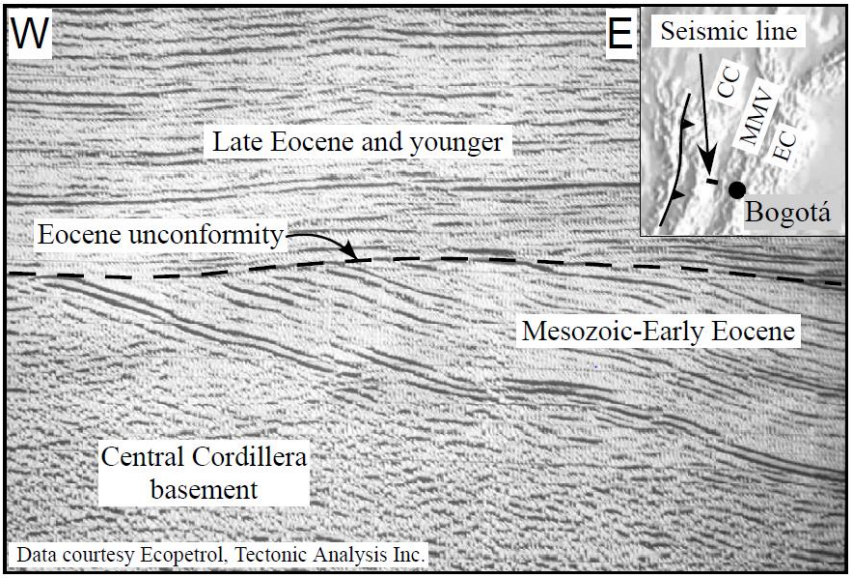

Figure 2.13 *E-W trending seismic section across the MMV, showing the Eocene unconformity (from Pindell 2009).*

Collision, accretion events and exhumation

For Villagomez (2010), northern South America is the only one among the Andean orogenic chain that was built by numerous land collisions and accretion events since the Early Cretaceous. The accretion of terranes has a lithological and geochemical character and are juxtaposed against the paleo-continental margin of the Romeral fault system. The time frame evolution of the Colombian Andes has been addressed by scarce data of zircon U-Pb [e.g. Cardona et al., 2006; Vinasco et al., 2006; Ordoñez-Carmona and Pimentel, 2002], K / Ar, Rb / Sr [see compilation in Aspden et al., 1987; Restrepo et al., 2009] and Apatito (U-Th) / He (Restrepo - Moreno et al., 2009), which have been interpreted to determine the time of intrusive magmatism and metamorphism in CC. New data taken by Villagomez (2010) from isotopes (16 zircon, 35 $^{40}Ar/^{39}Ar$, 76 data from apatite and zircon fission track, 21 from apatite and Zircon ((U-Th) / He) and 43 geochemical analyzes allowed him to characterize the tectonic origin of the geological units. Villagomez (2010) presents geochronological, thermochronological and geochemical data of different types of rock from the southern Ecuadorian border to the extension of the Western Cordillera (WC), CC, and Cauca Valley and up to the Sierra Nevada de Santa Marta. The peculiarity of the northern Andean zone (Ecuador, Colombia and Venezuela) compared to the southern Andean zone (Peru-Chile), is that it comprises a number of oceanic allochthonous and para-autochtonic blocks accreted mainly during the Cretaceous against the paleocontinental margin in the location of the Romeral fault.

The CC of Colombia is formed by autochthonous rocks that define the Pre-Cretaceous continental margin (Tahami Terrain) that is juxtaposed against tectonic blocks for-autochthonous, alloctonos, accreted during the Cretaceous, forming the Romeral fault system that extends towards Ecuador. According to Villagomez (2010), there were two (2) events of collision and accretion during the Pre-Eocene against the western margin of the current CC, that produced two tectonic deformation events at 115 Ma - 105 Ma (Aptian-Albian) and 75 Ma

- 70 Ma (Campanian – Maastrichtian) in the CC. The approach of Villagomez (2010) fits the hypothesis that during the Maastrichtian-Middle Paleocene significant deformations and uplifts of rocks had already been produced. This affected the VMM for the analyzed time, only due to the lifting of the CC and possibly to the proto-EC.

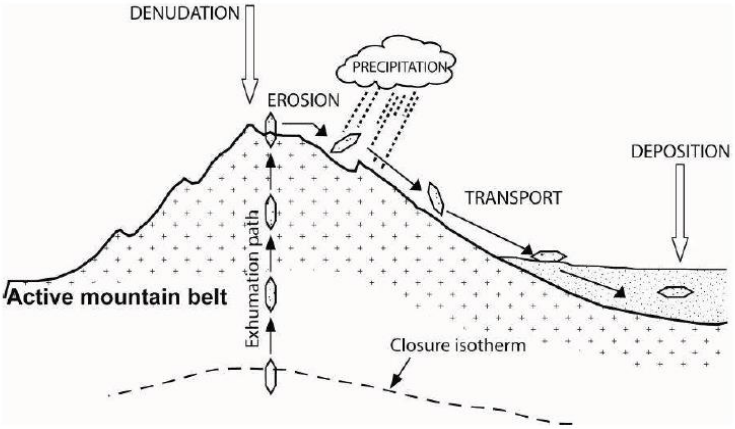

Figure 2.14 *Interaction between exhumation, denudation, erosion, transport and deposition through an active orogen (taken from Crowley et al., 1989 and modified by Bermúdez, 2010).*

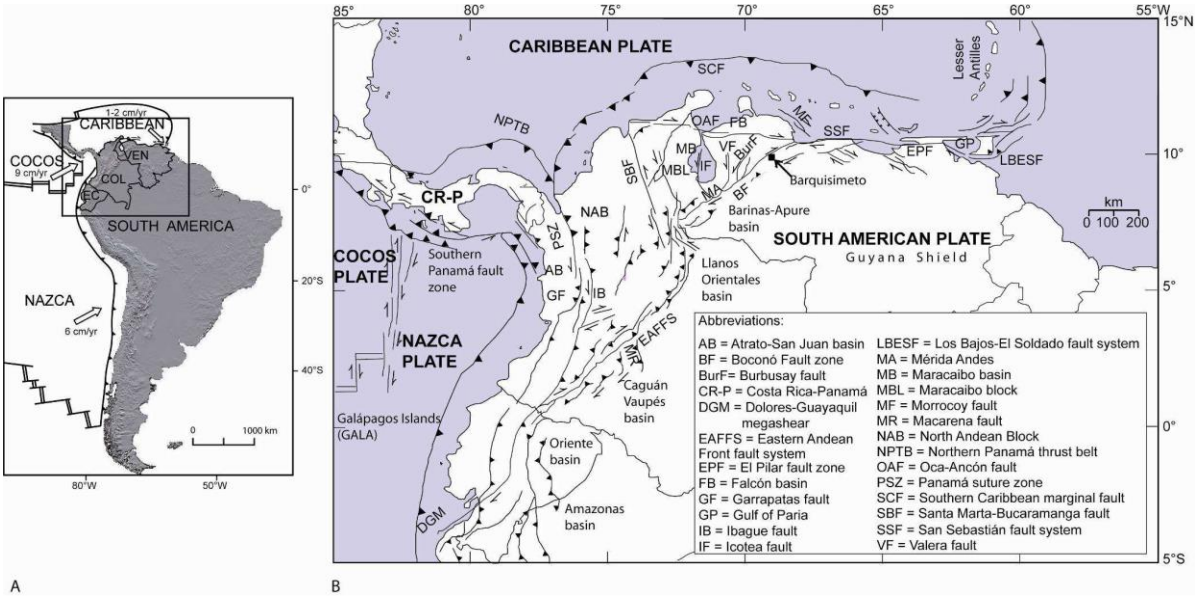

Figure 2.15 *Present-day configuration of the tectonic plates (taken from Colmenares and Zoback, 2003 and modified by Bermúdez, 2010).*

Bermudez (2010), presents the history of exhumation of the Venezuelan Andes during the Miocene to the present supported by thermochronological data of AFT, rock samples, detrital sediments and modern sediments, and the relationship between non-inherited structures and the development of the topography in response to tectonic and surface processes (Figure 2.14). These mountainous belts are the result of the transpression caused by the oblique convergence of the continental block of Maracaibo and the plate of South America, controlled on a large scale by the triple convergence between the South American, Caribbean and Nazca plates (Figure 2.15). The author presents data on the history of the exhumation of the Venezuelan Andes, but only analyzes exhumation events from the Miocene to the recent one, without

analyzing the oldest ones, as is intended for the case of the Colombian Andes in the present proposal

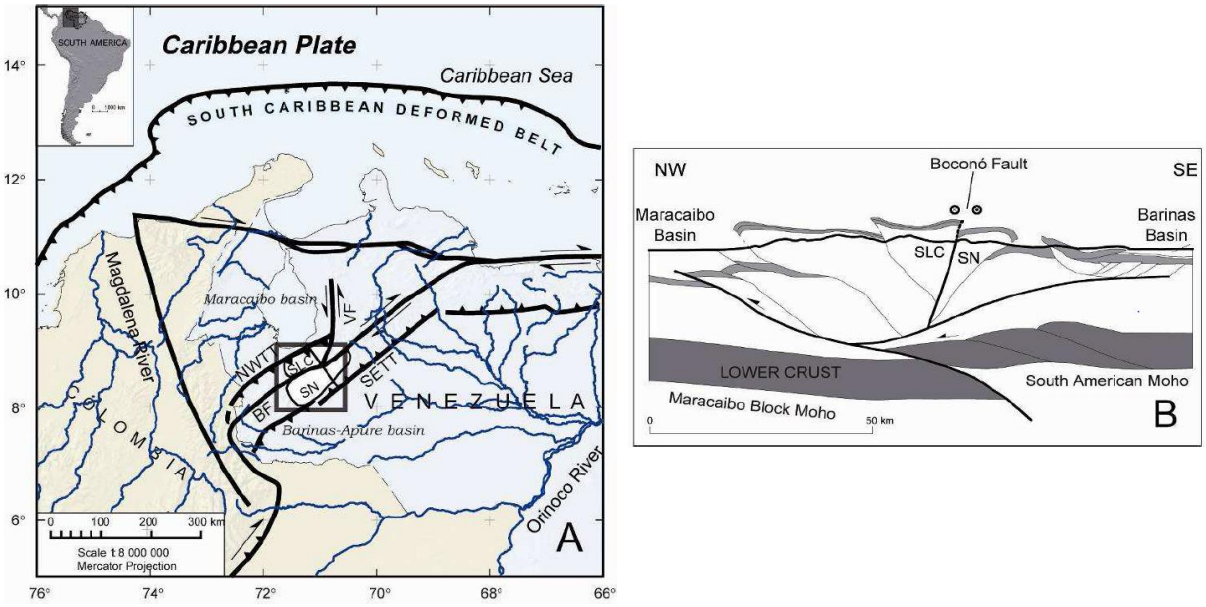

Figure 2.16 *Simplified structural section of the Venezuelan Andes and its surroundings (taken from Colleta et al., 1997 and modified by Bermúdez, 2010). Note the similarity (B) with the scheme for the Cordillera Oriental in Colombia (see figure 2.5).*

The tectonic implications of Bermudez's work (2010) are that the structures and development of the Venezuelan Andes have been controlled by the reactivation of faults and pre-existing structures and the inversion of Jurassic grabens and rift (Colleta, 1997; Kellogg and Bonini, 1982; Mora et al., 1993; Audemard and Audemard, 2002; Jacques, 2004), as also happened in the EC of Colombian (Corredor 2003, Cortes et al., 2006, Mora et al., 2009, Parra et al., 2009). (Figure 2.16).

Bermúdez (2010) also analyzes the relationship between exhumation and climate control (Figure 2.17). Establishing a lack of correlation between long-term exhumation rates and precipitation (Bermúdez et al., 2013) he suggests that precipitation is not the main factor that controls the exhumation and the development of the relief in the Venezuelan Andes.

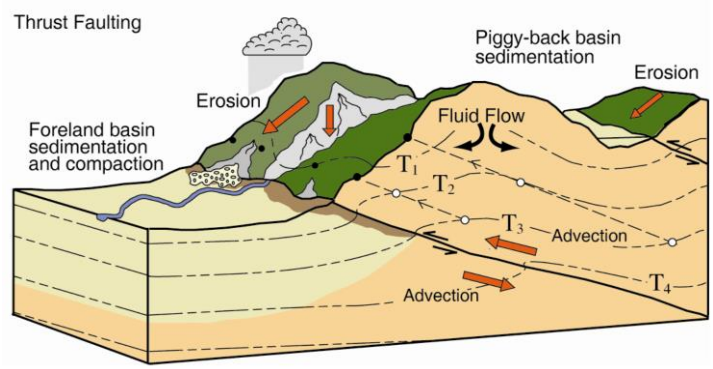

Figure 2.17 *Thermo-tectonic processes that influence thermochronometric interpretations (Ehlers, 2005).*

Mora et al., (2006) states that the main factors that condition extensional structural styles, such as compressional, are strongly related to the nature of the basement and the pre-existing zones of weakness (Figure 2.18). Indeed, the width of the deformation, the degree of shortening, the spatial development of structures, and the places of tectonic activity are fundamentally influenced by inherited structures in the basement rocks. In conclusion, Mora et al., (2006) and Bermudez (2010) works highlight the role of the inherites basement structures that influence mountain growth processes and guide the deformation and uplift of the interior continent.

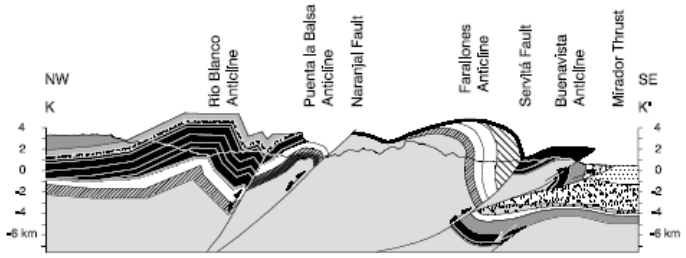

Figure 2.18 *Regional structural section across Rio Blanco – Buenavista Anticlines. Note the control exercised by the basement, and the reactivation of normal faults (taken from Mora, 2006).*

Although the observations of Mora et al., (2006) involve the analysis of Cretaceous rocks in a segment of the EC, he only analyzes the most recent deformations that produced the current landscape. Mora et al. (2009) proposes the complex interaction between the Cretaceous extension and the subsequent inversion of the Cretaceous paleo-rift of Guatiquía (Figure 2.19). Mapping of structures, analysis of the current topography and rocking of sections indicate that an inversion of extensional structures was focused along the boundary faults of the basin. In this way, areas of maximum subsidence accommodate maximum elevations in compression and form high topographies that remain as elevated areas.

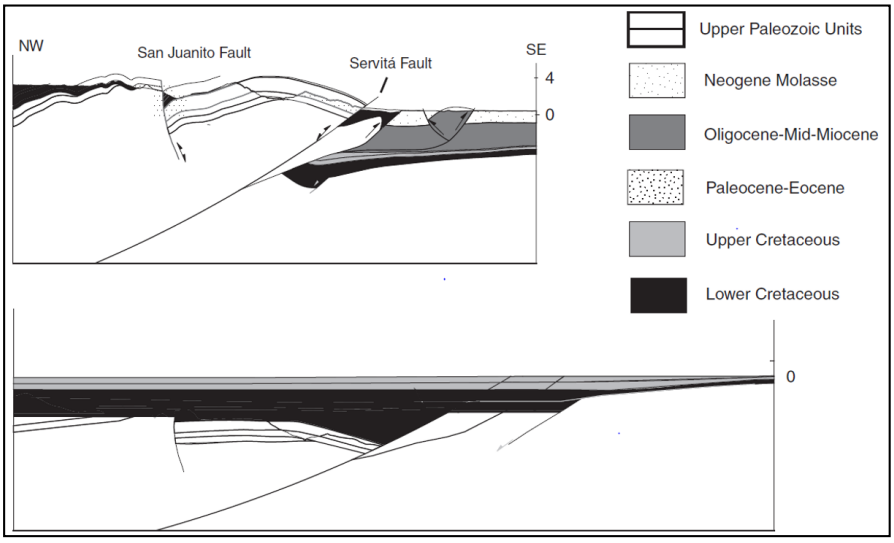

Figura 2.19 *Balanced sections across distinct segments of the studied area (taken from Mora et al., 2009).*

The structures of the Andes of the EC were analyzed by Cortes et al., (2006) based on field data, reflection seismic and biostratigraphic controls, with which a series of balanced structural

sections indicating two different structural styles were constructed (Figure 2.20). As a result of the deformation, a shortening of 70 km for the EC is calculated.

Bayona et al., (2008), based on geodynamic models, relates the evolution of the foreland basin through temporal and spatial variation of the lithosphere geometry (Figure 2.21) on the eastern side of the EC, generated by variations in the tectonic loads (orogen). Other efforts focused on the margins of the EC define histories of deformation locally from stratigraphic-structural relationships (Gómez et al., 2003, 2005; Toro et al., 2004; Sassi et al., 2007) and thermochronologic records (Parra et al., 2009). Advances in understanding the relationship between climate and orogenic evolution have been addressed by several authors (Koons, 1989, Molnar and England, 1990, Beaumont, et al., 1992, Masek et al., 1994, Willett, 1999; Montgomery et al., 2001; Molnar, 2004; Strecker et al., 2007; Herman et al., 2013; Schildgen et al., 2018).

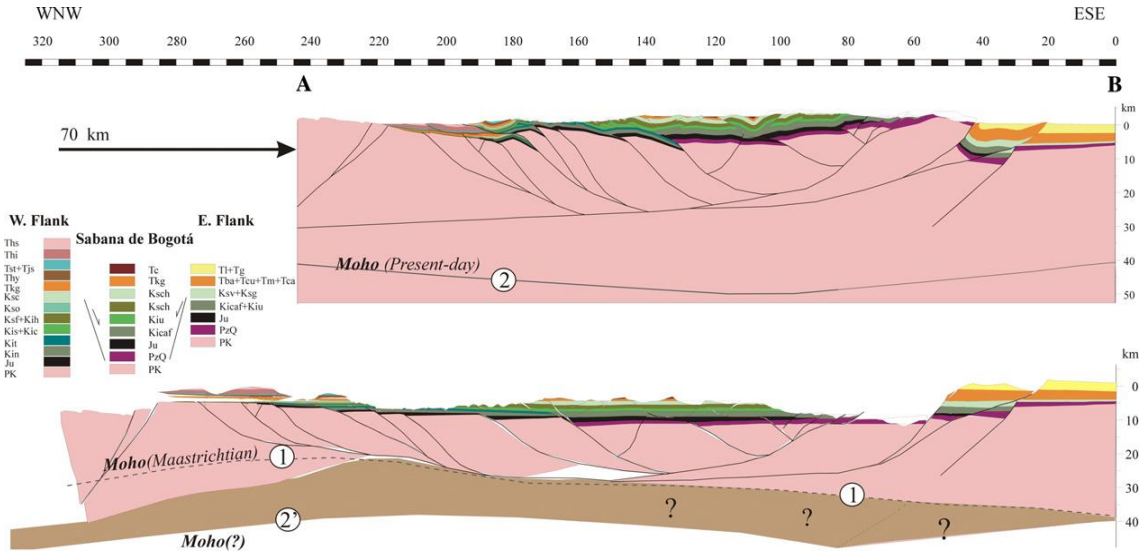

Figure 2.20 *Present-day and restored structural sections of the Eastern Cordillera (from Cortes et al., 2006).*

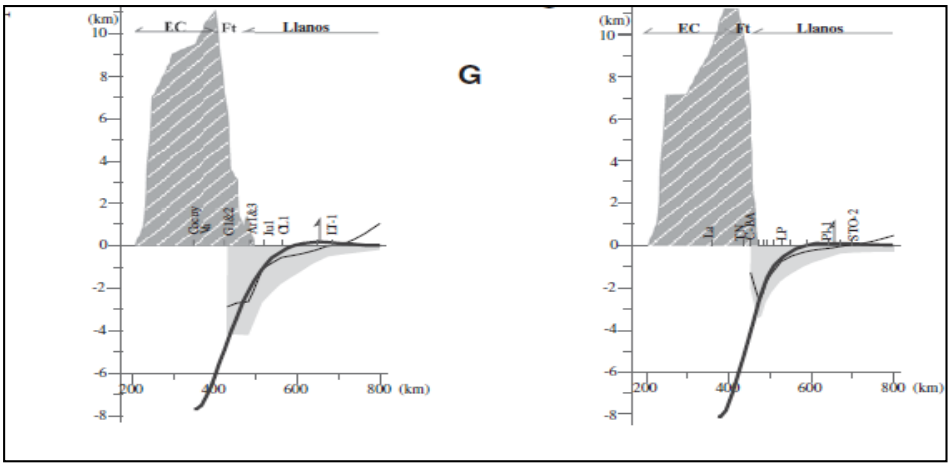

Figure 2.21. *Flexural behavior of the lithospheric plate generated by two different sections, with different loads up to the present (from Bayona, 2008).*

For the case of the EC, Mora et al., 2008 proposes an increase in the exhumation to the northernmost part of South America about 3 Ma. ago, when the EC forms an orographic barrier that intercepts the winds laden with moisture, producing great erosion and deformation to the east of the EC and dry zones towards the west of the EC with low rates of deformation and exhumation, as shown in Figure 2.22. Mora et. al., (2010), presents a study of thermochronology of low temperature with structural evidence that shows that the exhumation pattern has induced thrusts both along the two sides of the EC and between its axial segments (Figure 2.23).

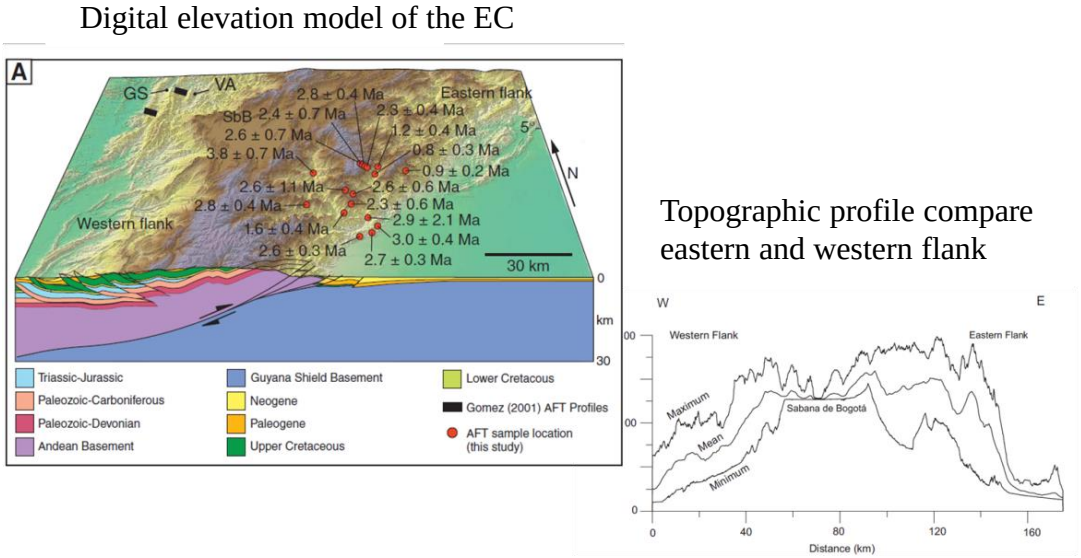

Figure 2.22. *Elevation model and topographic profile comparing the behavior of either sides of the EC, resulting from the erosion that differentially affected both flanks (modified from Mora, 2008).*

Parra (2008), in the Medina basin, eastern flank of the EC, integrates structural mapping, sedimentological data based on palynological data that links with the early-Oligocene-to-early-Miocene tectonic wedge in a tectonic episode that began 30 Ma. ago, which according to the author, evidences the generation of topographic load due to the advance of the EC west of the basin and therefore limits the beginning of mountain formation in this area. An exhumation assessment based on apatites and zircons and thermal modeling reveals the location of these riding charges along the compressional fault of Soapaga in the eastern sector of the EC.

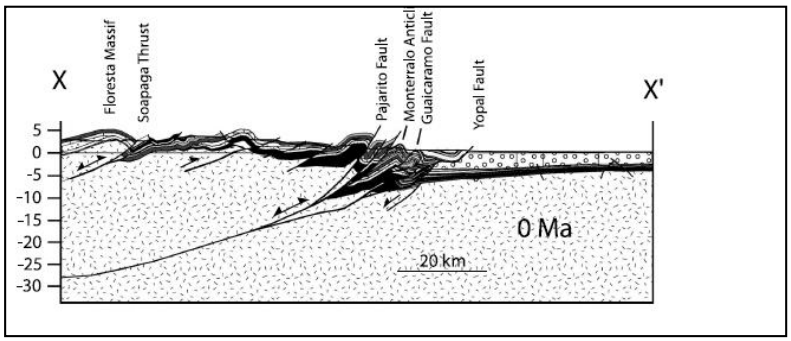

Figure 2.23. *Structural section of the eastern flank of the Eastern Cordillera, showing the migration of deformation, the same effect is observable on the western side of the mountain range (from Mora, 2010).*

Parra (2008), identifies three stages of propagation of the orogen. First, initiation of the mountainous uplift in the CC during the Late Cretaceous; the front propagates towards the east (0.5 - 3.1 mm / yr) until the Early Eocene. The second corresponds to a rapid orogenic advance (4.0 - 18 mm / yr) during the Late-Middle Eocene, and locally at least 100 mm / yr in the Middle Eocene, a result of the initial tectonic inversion of EC (Figure 2.25). The third corresponds to a stagnation along the Miocene deformation front, forming reactivated faults of the rift boundary on the east flank of the CO, which resulted in a decrease in the orogen's advance.

Further to the east, data from AFT and ZFT document the beginning of the exhumation, induced by the thrust associated with the compressional reactivation of the Servita Fault about 20 Ma ago (Figure 2.24). The author incorporated new thermochronology data with published data of AFT and chronological indicators of fragile deformation, with the idea of evaluating migration patterns of the orogenic front in the Andes of central Colombia (Figure 2.25). This spatio-temporal analysis reveals an episode of migration towards the East from the orogenic front, with an average ratio of 2.5 - 2.7 mm/yr during the Late Cretaceous-Cenozoic.

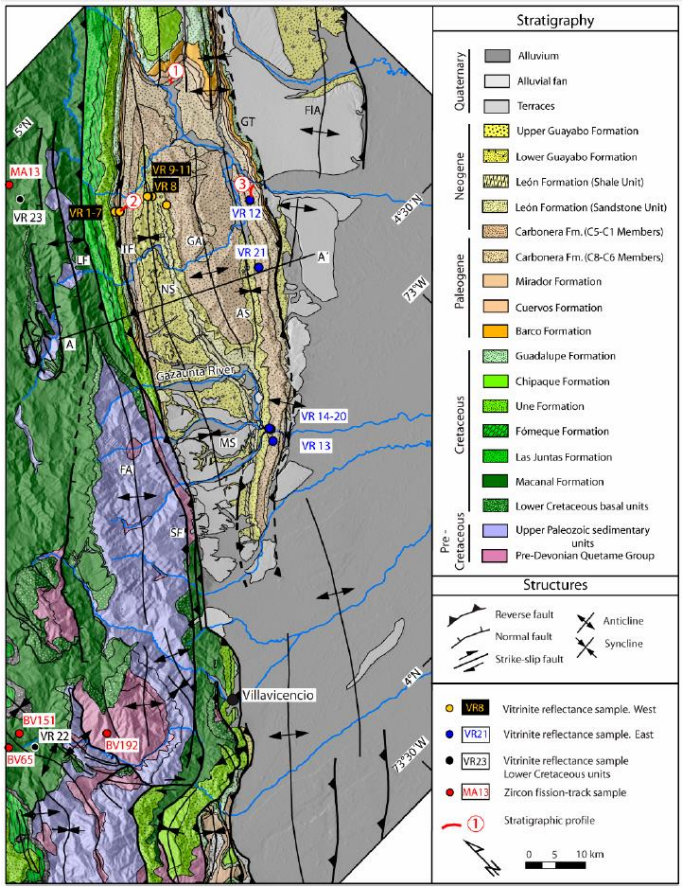

Figure 2.24 *Map of the location and geology of the Medina area, showing the most important structural features, the position of the samples for vitrinite reflectance and ZFT (From Parra, 2008).*

Basin Evolution

The sedimentological data evaluated by Parra (2008) in the Medina basin reveal a rapid accumulation of fluvial and lacustrine sediments at rates of up to ~ 0.5 mm /yr during the Miocene. Provenance data based on petrography and paleo-currents, reveal that Paleocene and

Upper Cretaceous sediments contributed to those fluvial systems exposed in the west of the EC. Many of the contributions to the Tertiary units possibly come from deposits of the Cretaceous age, already raised during the Pre-Eocene that contributed sediments to the adjacent basins.

According to Parra (2008), their data demonstrates anisotropy inherited from the crust, such as that of faults formed by the limit of the rift in the EC, favoring a non-systematic progression of deformation of the foreland basin through time by sliding accommodation and load by thrust (Figure 2.24, 2.25).

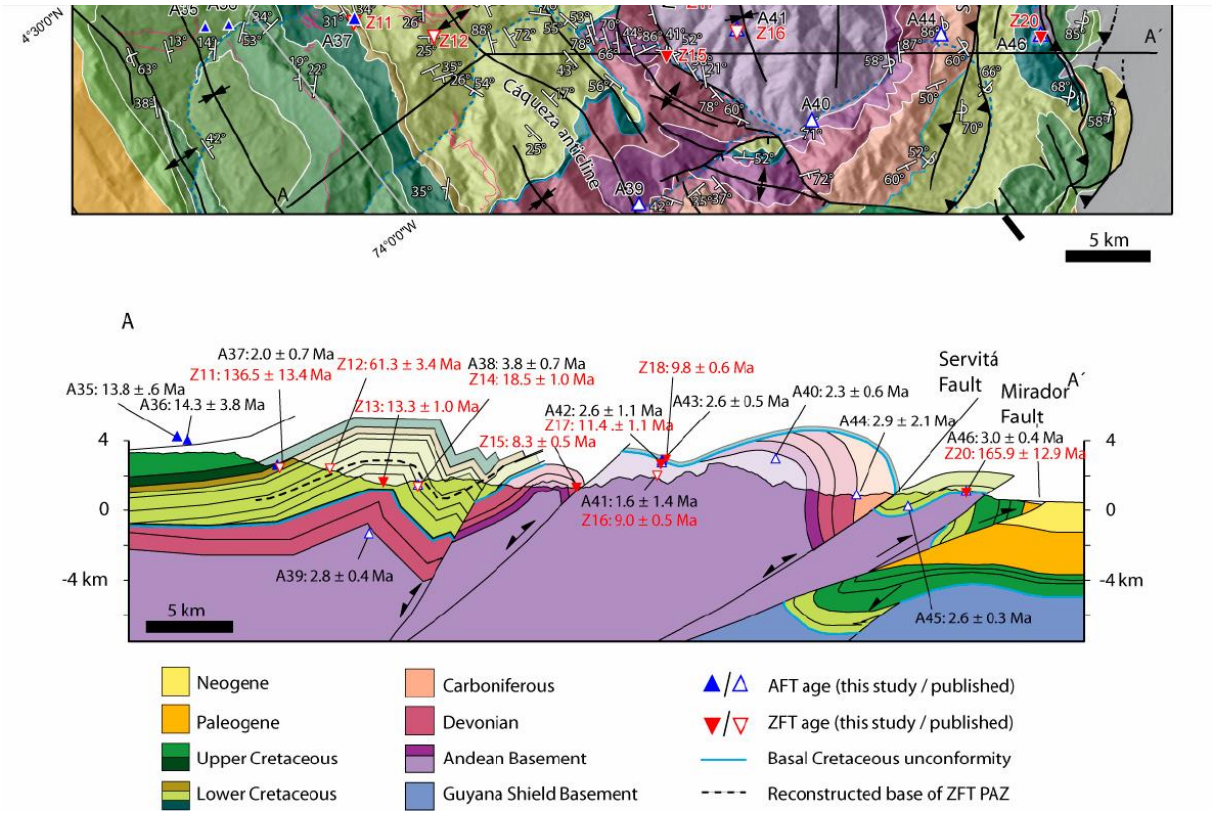

Figure 2.25 *Deformed structural section of the study area, showing the data of ZFT and AFT, sample Z20 from the Cretaceous age shows a modified age by re-cooking, and samples Z11-Z12 show an increase in ages towards shallower structural levels (From Parra, 2008).*

Horton et al., (2010), based on the analysis of 29 samples of EC, reveals the origin of the basement and sedimentation patterns during the Paleozoic subsidence, the Jurassic-Early Cretaceous extension, the post-rift subsidence, the Cenozoic shortening and the evolution of the foreland basin. According to the author, U-Pb geochronological data indicates that the Pre-Cambrian basement is the product of Paleozoic-early magmatism (520-420 Ma). Data from U-Pb zircons in Paleozoic strata from the Andean basement show non-depositional magmatic sources (420-380 Ma), and distal sources mainly from the Meso-Proterozoic basement (1650-900 Ma) present in the East Amazonian craton (Guyana) or in continental lands along the western margin of South America. Sedimentation during early Jurassic-Cretaceous rifting is expressed in the age of detrital zircons, with an Andean base source recycled from the Paleozoic and from igneous sources of the Carboniferous-Permian (310-250 Ma) and late Triassic-early Jurassic (220- 180 Ma).

At this point Horton's observations are valid in the sense that the contributions to the old rift must surely come from the higher parts of the Paleozoic craton that could have been lifted from both sides of the rift and even in some areas within it.

The provenance of detritic zircons during the cretaceous extension and post-rift thermal subsidence recorded the elimination of sources of the Andean basement and increases the influence of drainage systems derived from the Paleo-Proterozoic and Meso-Proterozoic craton (2050-950 Ma).

For Horton, even during the Eocene zircons from the Guyana massif dominated the detrital signal in the easternmost part of the EC, coetaneous deposits in the axial part of the EC show record of zircons from the Cretaceous-Paleocene (90-55 Ma), Jurassic (190-150 Ma), and the Permian-Triassic limit (280-220 Ma), recording the initial uplift and exhumation mainly of rocks of Mesozoic magmatic arcs to the west in the CC. Oligocene-Miocene sandstones of the Eastern Plains basin document uplift induced by exhumation of the folded and failed belt from the EC and the recycling of the Paleocene cover rich in detritus derived from arc (180-40 Ma) and craton derivatives (1850-950). Following these observations Horton shows some schematic sections of the evolution of the Colombian Andes beginning in the Fanerozoic until the late Oligocene-Miocene. For the author the beginning of the uplift of the EC occurs until the late Eocene-Early Oligocene and it's not until the Late Oligocene- Miocene that the EC separates the VMM from the Llanos basin (figure 2.28).

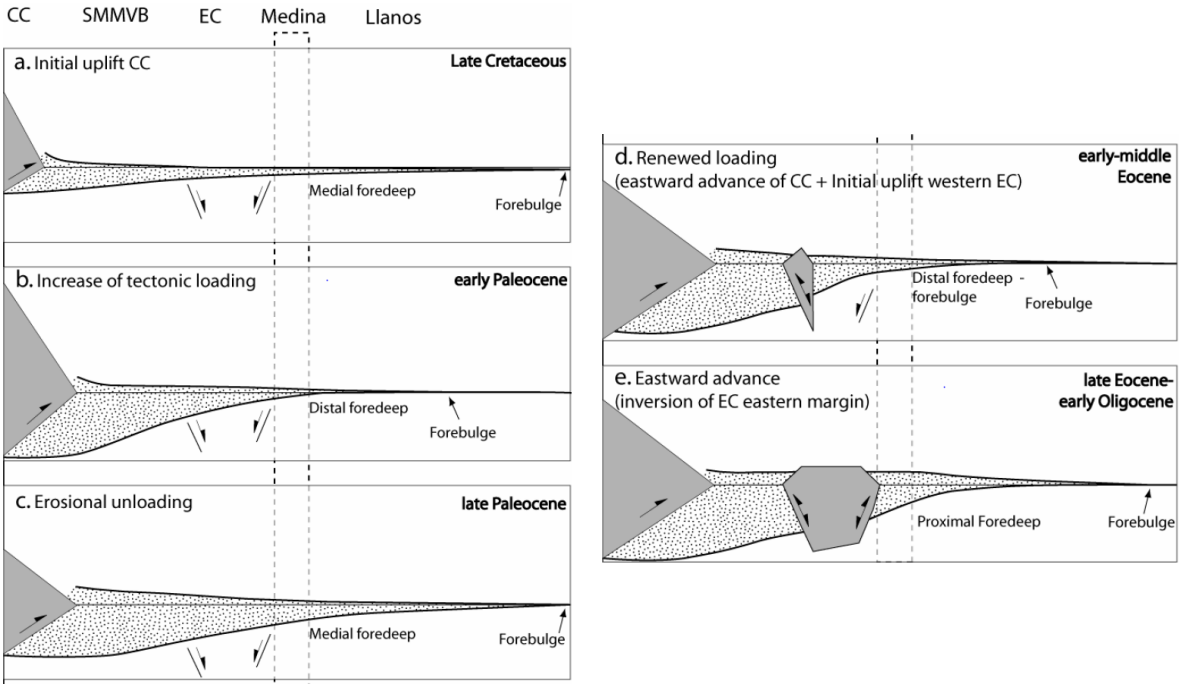

Figure 2.26 *Sketch illustrating the evolution of the foreland basin in response to the uplift of the Central and Eastern Cordillera (from Parra, 2008).*

Note that for Parra (2008) the time of the beginning of the EC rise corresponds to the early-middle Eocene, while for Horton (2010) it corresponds to the Early Eocene-Late Oligocene representing a difference of some 15 Ma. Additionally, at that time, the EC separated the valleys of the VMM and Llanos. For Parra (2008) this occurred in the Late Eocene-Early Oligocene

while for Horton (2010) this occurred only until the Late Oligocene-Miocene with a difference of 10 Ma.

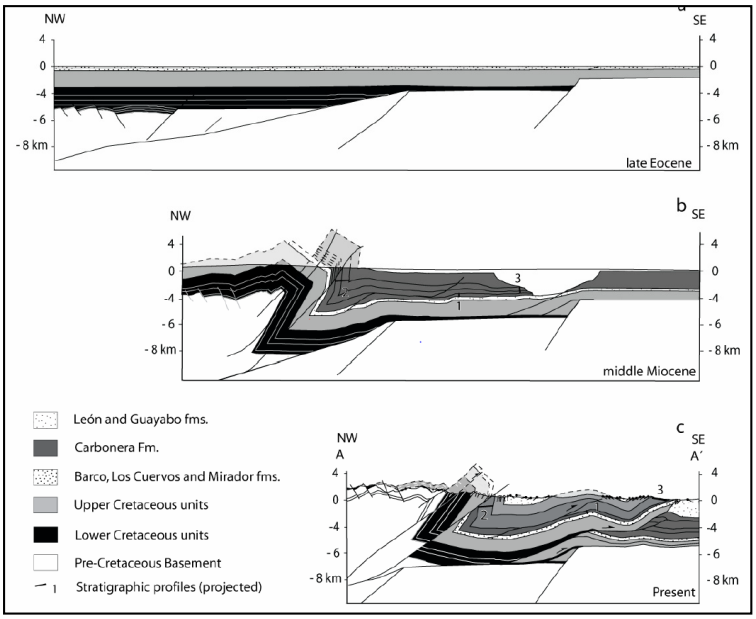

Figure 2.27 *Restored section through the Medina basin, the projected location of the stratigraphic sections and vitrinite samples and ZFT analysis are indicated for each time. Exhumation induced by thrusting along the Quetame massif during the early Miocene incorporated the western part of the syntectonic wedge of the Medina basin between the folded and faulted belt (from Parra, 2008).*

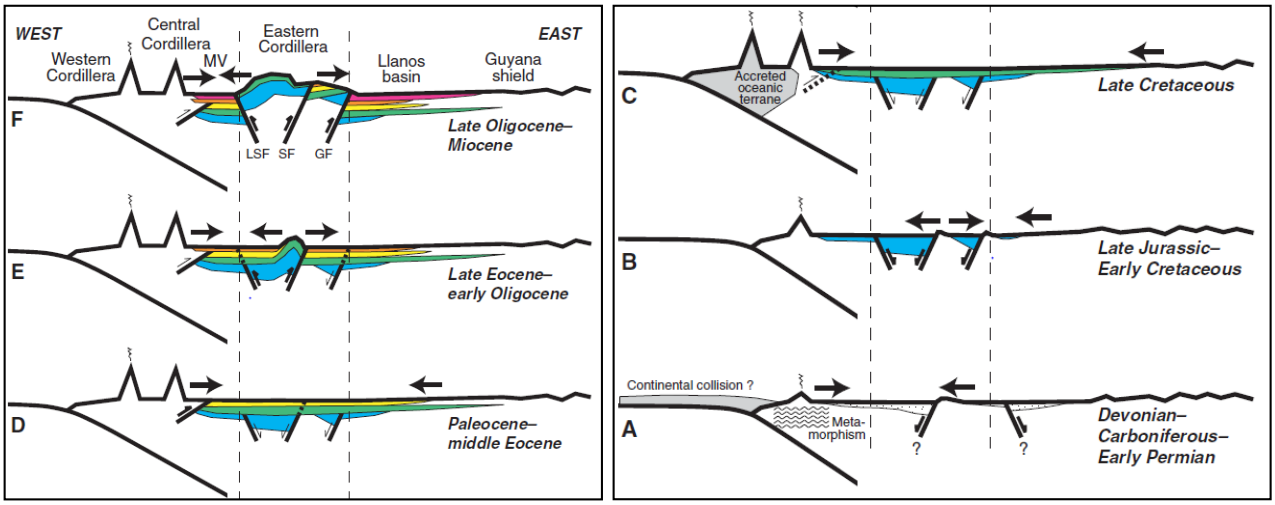

Figure 2.28 *Sketch illustrating of the evolution of the Colombian Andes (from Horton et al, 2010).*

Nie et al. (2010) indicate that the moment of the lifting of the northernmost part of the Andes is limited to ranges that go from the Cretaceous to the Pliocene (Figure 2.29). Ages from U-Pb detrital zircons from the VMM in Colombia reveal two changes in provenance during the Cenozoic, indicating that the first change occurred between the early and late Paleocene strata. Nie's results show a change from Proterozoic domain to Phanerozoic domain, the author attributes this change to the exhumation related to the lifting of the CC (a change of origin from the Craton to the CC). The second change occurred between the Late Eocene and Late

Oligocene strata, where the Grenville ages increased and the Mesozoic ages decreased, which may be related to the rise of the EC (change of origin from the Cordillera Central to the Eastern Cordillera), a probable source of zircons of the Grenville age is the Cretaceous section of the EC (Horton et al., 2010), which is consistent with the initial recycling of the coverture of the EC.

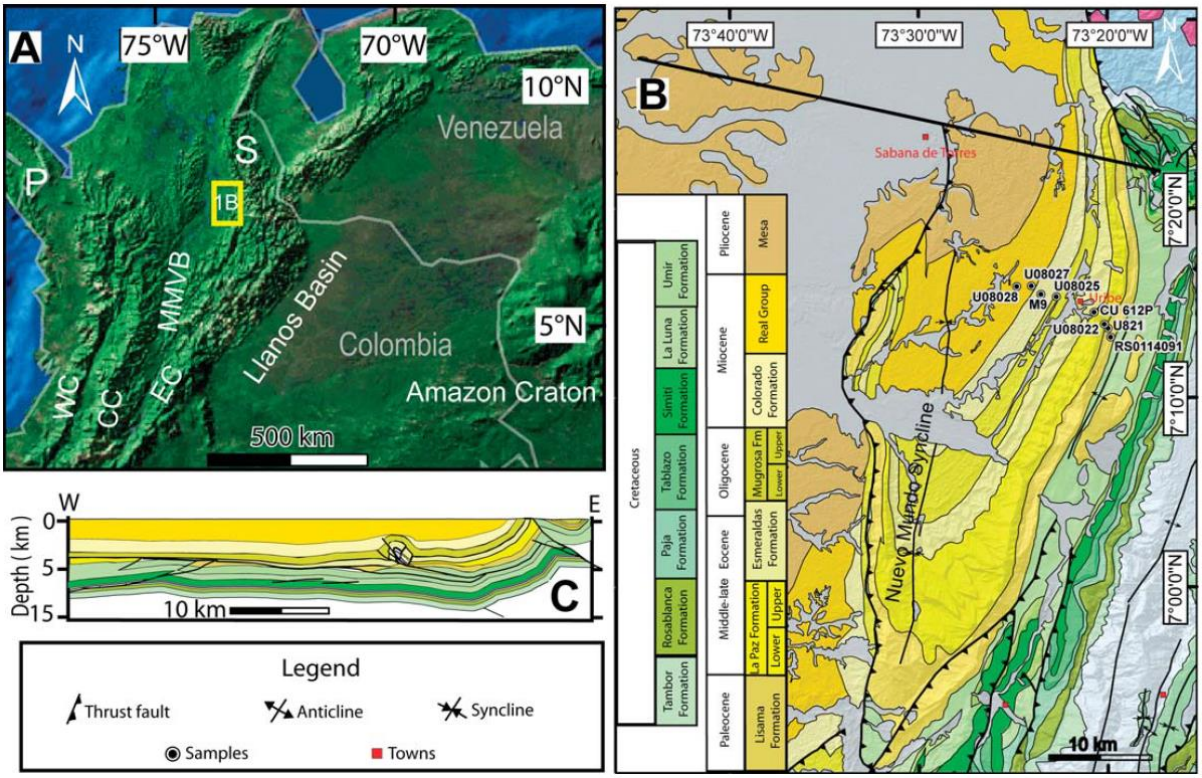

Figure 2.29. *Map showing the study area (Nuevo mundo syncline), and the different tectono-morphological provinces of the northernmost part of the Andes (from de Nie et al., 2010).*

Studies by Nie et al. (2010), in conjunction with previous studies (Horton et al., 2001; DeCelles and Horton, 2003; Horton, 2005) suggest that the Andes, almost to their full extent, were probably subject to shortening related to Paleocene uprising and exhumation. In summary, the observations of Nie (2010) suggest that the initial uplift of the CC was underway by the Middle Paleocene and that the initial EC lifting occurred between the Middle to Late Eocene and the Late Oligocene, highlighting the importance of this Andean uplift in the dynamics of the Paleogene climate. Nevertheless, there is a difference between the different time intervals proposed by various authors (Nie, 2010, Horton, 2010, etc.) that must be analyzed.

Bayona et al., (2012), reports ages of U/Pb in plutons that support the presence of a magmatic arc that extends 700 km along the northern margin of the Andes. Ages of 45-65 Ma in zircones of the Paleocene, from 19 localities of Colombia and Venezuela indicate that the volcanic detritus were supplied by a magmatic arc parallel to the subduction zone, which shows an intraplate magmatism that extends for more than 400 km. The distribution of this magmatism of the Early Paleogene age is related to the subduction of the Caribbean plate, the short time of magmatism and detachment of the subduction. According to the author this is related to the

difficulty of the thick plate to subduct and the lateral displacement towards the north of the Caribbean and South America plates.

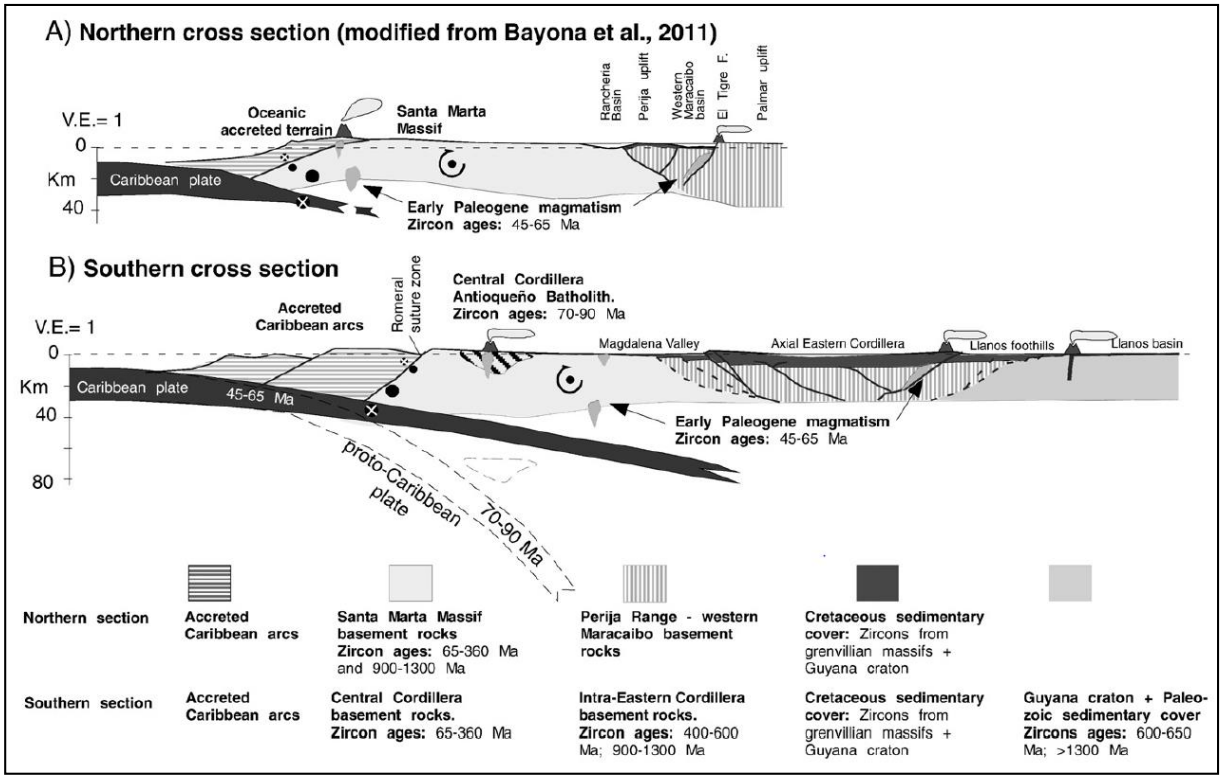

Figure 2.30. *Regional section, showing the relationship between subduction, magmatic activity and basin filling, in northern Colombia (A) and in the central zone (B) (from Bayona, 2011).*

The magmatic activity occurring predominantly between 54 and 59 Ma provides a new chronostratigraphic restriction of Paleocene-lower Eocene stratum correlation. The differences between the entire population of detritic zircons from the eastern and western locations, the presence of unstable fragments of rock in sandstones containing volcanic zircons, and the irregularity of volcanic deposits allowed the author to infer that volcanic activity reached up to 400 km from the area of the collision margin.

The short period of magmatism is related to the oblique and flat subduction of the oceanic plate against the continental one under the northwestern corner of South America. This magmatic activity reinforces the hypothesis that the subduction of the oceanic plates modifies the continental crust (Figure 2.30).

Evidences of Cretaceous deformation.

Although there are still groups looking for evidence of the lifting of the EC (ICP, ARES, Smithsonian, etc.), it is worth noting that efforts have already been made trying to find evidence of the history of the lifting of the EC. However, as this proposal indicates, few authors have focused their work on the possibility that there were old events, before 60 Ma and the existence of important old uplifts in the position of the VMM and the western side of the EC, only a few authors suggest that the configuration of EC is possibly due to a coeval rising of the CC and CO, (Gómez, 2005, Sarmiento, 2001, etc).

Authors like Jaimes and Defreitas (2006) using seismic and biostratigraphic at the level of the Villeta Formation in the area of the UMV (south of the MMV) showed evidences of the occurrence of an important unconformity during the Albia-Cenomanian age, which is totally opposite to the affirmation of Barrio and Coffield (1992).

An example of the seismic evidences exposed by Jaimes and De Freitas (2006) is shown in Figure 2.31. A Cenomanian deformation is observed, resulting from the compressional reactivation of faults, which is sealed by an erosional unconformity at the base of the La Luna Fm (Early Turonian-Late Santonian).

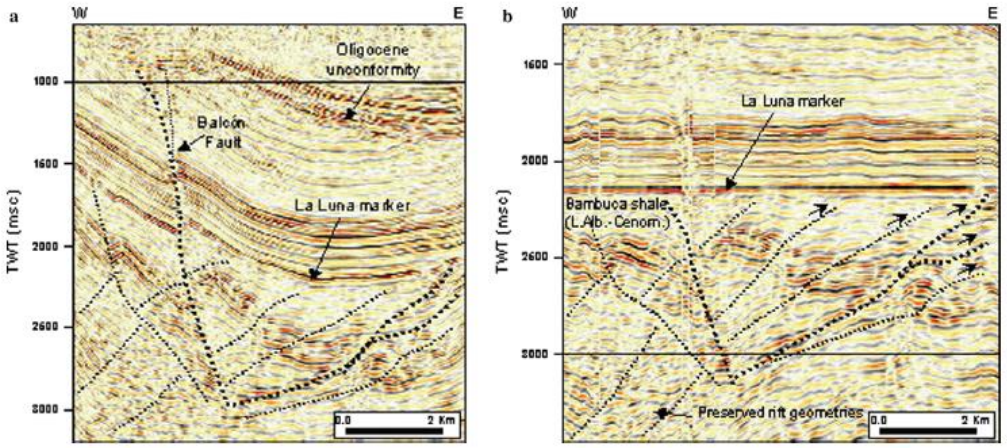

Figure.2.31 *Seismic profiles: a) Present-day deformation; b) flattened at the level of the La Luna marker (Cenomanian-Turonian) (Jaimes et al., 2006)*

Likewise, the studies of Jaillard et al. (1991) about what the author called "Early history of the Andes", makes some geodynamic considerations and show that in addition to the most recent uplift event of the Andes from 60 to 5 Ma and 40-35 Ma, other events of great importance occurred approximately 100 Ma ago which corresponds to a time of major changes and an abrupt acceleration of the movements of the plates worldwide and in particular in the area of Andean subduction (Figure 2.32).

Also, during this period South America separated from Africa and began its migration to the West, opening the Atlantic Ocean. Between 100 to 95 Ma a slowing down in the speed of the plates occurred (Figure 2.32), towards 90 Ma. there is a deceleration event of the plates, about 80 Ma., there is a period of stabilization, followed around 75 Ma. by a period of re-invasion of the basins. A major tectonic phase occurred around 60-55 Ma. which caused an intense deformation, an event that coincides with the abrupt change in the direction of the Pacific oceanic plate (without changing the convergence rate, Figure 2.32). Other important tectonic events occurred some 40-35 Ma ago, this epoch is coeval with abrupt deceleration of the plates in the subduction zone.

Jaillard (1991) studied the evolution of sedimentary basins in Ecuador between 110 to 40 Ma a period which corresponds to the incipient formation of the Andes, and which allows to date the layers and geological events, thanks to the occurrence of marine fossils. Comparing the evolution of the Ecuadorian sedimentary basins and the known geodynamic events, he recognized four tectonic-geodynamic events. The first one occurred around 100 Ma ago, a

period marked by an abrupt acceleration of the plates around the world and by the opening of the Equatorial Atlantic Ocean due to the separation of South America from Africa. Another event is placed at 100 – 95 Ma when a deceleration of the plates occurred, near 90 Ma, when a decrease in the velocity of convergence and in 80 Ma an important tectonic phase occurred, related with the occurrence of unconformities which is coincident with the plate velocity stabilization in the Andean zone. Finally, a major tectonic phase occurred between 60 and 50 Ma, which was coincident with the abrupt change in the direction of the Paleo-Pacific oceanic plate.

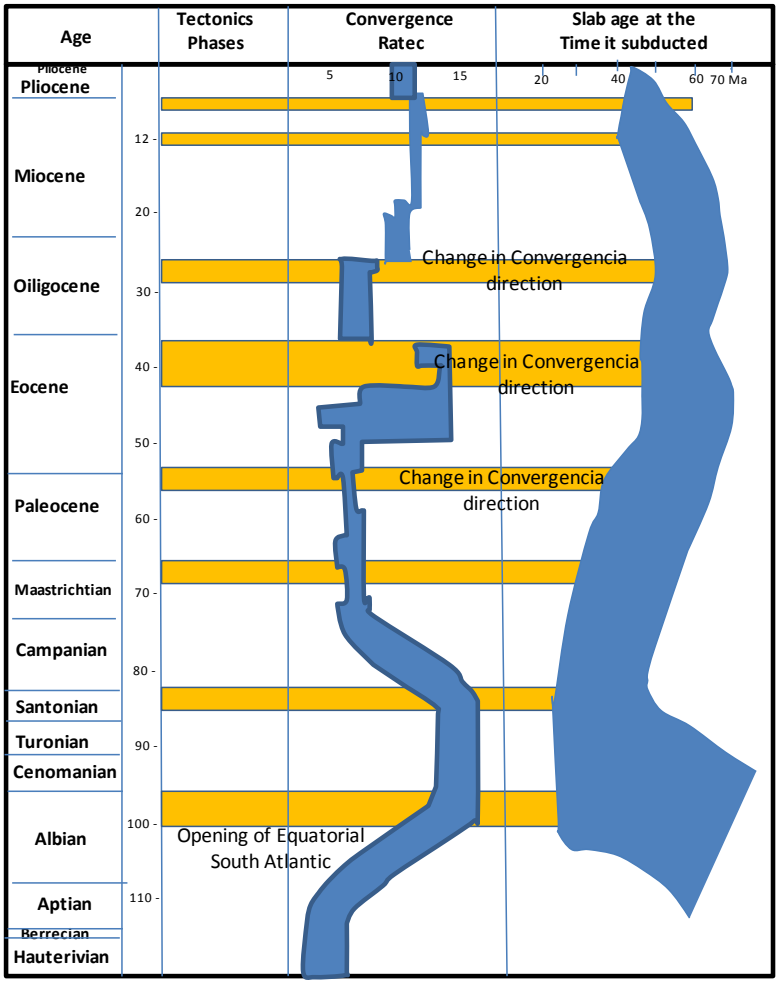

Figure 2.32 *Comparison between the early tectonic events of the Andes and the geodynamics of the plates in the subduction zone (modified from Jaillard, 1991).*

Meanwhile Jaillard et al. (2000) showed that some events are related to changes in the convergence rate (Figure 2.32) and suggested that a first important deformation was recorded in the Late Albian (Mochica Tectonic event), during a period of high convergence, coinciding with the opening of the Equatorial Atlantic. In the same way, Pindell and Tabbutt (1995) proposed that compressional deformation began during the Late Albian-Early Cenomanian (100-95 Ma), coeval with the westward movement of the South American plate.

These observations are consistent with what was observed by Van der Wiel, (1991); Van der Beek, (1995); Gomez, (2005); Villagomez, (2010), and the hypothesis proposed in this doctoral

work, where one thinks about the existence of ancient pre-Eocene events that generated the existence of important old lifting, prior to the generation of the current EC orogen.

In the Caribbean area, Mattson (1984) recognized six unconformities from 110 to 5 Ma, which he associated with important tectonic events at 110, 85 and 66 Ma. He suggested that during the Early Cretaceous (140-110 Ma) the Northern part of South America was largely emergent.

In an internal report of Ecopetrol, Rollon et al. (1997) using sequential stratigraphic analysis in the WEC, identified three regional sequences separated by unconformities at the level of the la Paja, Tablazo and Simiti Formations.

Guerrero et al. (2002) proposed a classification of system tracts for the Barremian to Maastrichtian sequence in the Cretaceous basin of Colombia. They made a division based on the recognition of regional sedimentary discontinuities which correspond to mainly transgressive and regressive surfaces. Based on their observations, these authors indicate that the second order sequences are of primary importance in Colombia, because they allow to make correlations through the basins, and that there are complex interactions between sedimentary supply, subsidence and eustacy, the latter being the dominant process.

In Venezuela, Cooney et al. (2009), using seismic and paleontological information identified an important unconformity of Campanian age over a structured La Luna Fm. and the complete absence of structuring in the Colon and Mito Juan units implies early structuration. In this case at the seismic Top of La Luna Fm, as proposed by Burke et al. (1984) and Pindell and Tabbutt (1995), structures like rollover, fold bend, but more common fold propagation fault at the level of La Luna Top (Cooney et al., 2009) may be produced by the subduction of the Caribbean Plate beneath South America or related to the uplift of the Central Cordillera of Colombia.

Stratigraphic nomenclature

The generalized stratigraphic column of the formations described in the MMV and WEC is shown in Figure 3.4 (chapter 3). The Triassic–Jurassic sedimentary record is made of continental deposits, mainly red beds, pyroclastic and volcanic effusive rocks, locally interbedded with marine deposits. These sediments were deposited in an extensional rift. According to Mojica et al. (1996), they are mainly located in the UMV-WEC and San Lucas region.

Girón Formation

The Girón Formation (Fm) was originally described by Hettner (1892), who stablished a new division for the Cretaceous, based on studies by Karsten (1858, 1886). The latter divided the Cretaceous into Neocom, Gault and Upper Cretaceous. However, Hettner (1892) considered the Neocom and Gault as lower Cretaceous, which corresponds to a thick set of shale, with thick beds of black and white limestones, levels of white quartz-sandstone, red or green limestones and siliceous layers.

Hubach (1931b, p. 98) extended the name Girón Fm to the whole Eastern Cordillera (EC). This interpretation, supported by Liddle (1928), was erroneous, since the "Girón facies" is not characteristic of the EC. The Girón Fm has also been mentioned in the Huila (Grosse, 1935b) and Bogotá areas (Hubach, 1931b; Scheibe, 1938).

Scheibe (1938) divided the Girón Fm into a lower Girón unit called the Lebrija conglomerate, and the upper Girón unit mainly made of grey, white, yellow or red sandstones, called the Arcabuco Sandstone. Based on the first description of an unconformity between the Girón and Cretaceous sequences by Notestein, Schuchert (1935, p. 670) dated the Girón Fm as pre-Cretaceous. Additionally, he noted that the poor definition of the limits of the Girón Fm was due to the similarity of the basal Cretaceous and the Girón sediments, since the base of the Cretaceous sequence reworks the Girón Formation. The age assignment by Notestein has been accepted by subsequent authors (Jullivert, 1958a, 1960, p 8; Langenheim, 1959). Then, Oppenheim (1940b, p. 1616) extracted the quartzites of the Cocuy from the Girón Fm, correlated the La Quinta Fm in Venezuela with the Girón Fm in Colombia, and ascribed them a Jurassic age. Since then, the name of Girón Fm is restricted to pre-Cretaceous, Jurassic-Triassic sediments. Nevertheless, Bruckner (1954) found ostracods and flora of Carboniferous age, thus making a Paleozoic age possible for part of the Girón Fm.

The upper limit of the Girón Fm is marked by a regional unconformity below the Cretaceous series. The exact identification of this boundary is difficult due to the lithologic similarity of the Girón Fm and the basal, transgressive Cretaceous beds (Tambor Fm), and to the low angle of the unconformity. Sedimentologic and petrographic studies (Lopez, unpubl.) allow to establish a difference between the Tambor Fm and Girón units, but their distinction remains difficult in outcrops, where they are superimposed. The lower limit of the Girón Formation is clear where it rests directly on the igneous-metamorphic basement, as can be observed to the east and west of the Santander Massif (Julivert, 1960, p. 8; 1963b).

In the type area, the Girón Fm. is constituted by red clastic deposits, deposited in a subaerial environment. Langenheim (1959) proposed to subdivide the Girón Fm into three members. In the area of Mesas, West and SW of Bucaramanga, Julivert (1958a) decribed a more complete, 2500 m thick stratigraphic sequence. Finally, Navas (1963) established a detailed stratigraphy of the Girón Fm in the same type section used by Langenheim and divided the Girón Fm into six units (Lower shaly unit, Lower arcosic unit, Upper shaly unit, Upper arcosic unit, Shaly red beds, and Upper coarse-grained unit).

Tambor Formation

According to Morales et al. (1958) the name Tambor Fm has been given by Hedberg (1931) to a succession that crops out in the Cañon of the Lebrija river, along the railway from Bucaramanga to Puerto Wilches, close to the hamlet El Tambor. South of Zapatoca, the Tambor Fm is composed of shales, red conglomerates and sandstones, similar to the Girón Fm (Morales et al., 1958, p. 644-645). The type section is 650 m thick, and the upper part includes some limestone beds. The Tambor Fm unconformably rests upon the Girón Fm and is covered by the Rosablanca Fm. According to Navas (1963) the conglomerates along the railway seem to be unconformably eroded by sandstones, which are ascribed to the Tambor Fm in the region of the

Mesas. He therefore concluded that these conglomerates must be related to the Girón Fm rather than to the Tambor Fm. The thickness of the Tambor Fm is more than 200 m in the area of La Mesa de Los Santos and 120 m to the East border, suggesting that the formation thins toward the Santander Massif.

Age. The uppermost part of the Tambor Fm is marked by few layers of limestones, which yielded *Choffatella decipiens* Schlumbergerer, *Nodosaria* sp. and *Robulus* sp., as well as pelecipods (*Pholadomya robinaldina buchiana*) and bryozoans (Morales et al., 1958; p. 644). In spite of the paleontological data, the age of the Tambor Fm remains uncertain, and it is ascribed to the Hauterivian-Valanginian interval. In the area of Mesas and Cuestas, a succession of hard sandstone is called the Arcabuco Fm. Although this unit is similar to the Tambor Fm, these sandstones are considered Valanginian in age (Bürgl, 1954)

Los Santos Formation

The Los Santos Formation conformably rests on the Girón Fm and corresponds to the Tambor Fm (Ward et al., 1969; Julivert et al., 1964; Tellez, 1964). According to Laverde and Clavijo (1985), the stratigraphic section called Tu y Yo, northwest of Zapatoca (Santander), could be the reference locality of the Los Santos Fm (Cediel, 1968). This formation was redefined by Laverde et al. (1985) and Mendoza (1985). Where the Tambor Fm rests on fine sediments of the Girón Fm it is easier to establish the limit. Its lower boundary is often difficult to define, as in the western border of the Santander Massif (Navas, 1963), type area of the Girón Fm.

Cumbre Formation

This unit was previously mapped without denomination by Hubach (1953) and Julivert (1958a, b). A regional geological survey allowed to recognize this unit around the Santander Massif (Ulloa and Rodriguez, 1979a; Pulido, 1979a, b). *Environment*. This unit was interpreted by Etayo (1978) as deposited in a mixed tidal flat with sediments deposited in a subaerial, delta front environment.

Age. Hubach (1953) assigned to this unit a Tithonian age, and Etayo (1972) assigned a Lower Valanginian

Rosablanca Formation.

According to Morales et al. (1958, unpublished report), the name of Rosablanca Fm was given by Wheeler (1929) to a succession located in the Rosablanca hill, located 5 km North of the northeastern corner of the Conseción De Mares. The type section was studied in the cañon of Rio Sogamoso, west of La Mesa de los Santos. Zamarreño (1953) indicated that the basal part is characterized by evaporite levels (gypsum), which suggest hypersaline and quiet conditions. The Rosablanca Fm was also mentioned by Groose (1930) in the area of Arcabuco-Moniquirá, Hubach (1931b, p. 90), Sheibe (1938) west of Vélez, and Dickey (1941). The latter mentions the occurrence of this formation, together with the la Paja Fm in the MMV. Bürgl (1954) described the Rosablanca Fm in the Villa de Leyva area, east of Loma la Yesera, and Chenevart (1963) interpreted the Rosablanca Fm as a facies change of the Tambor Fm.

Zamarreño (1963) divided the Rosablanca Fm into several units: (1) Lower unit of grey limestone and dolomite; (2) intercalation of brown limestone; (3) Lower marly unit; (4) Shaly

unit with beds of limestone; (5) Intercalations of limestone; (6) Upper marly unit; (7) Sandy unit; (8) Coquina horizon. According to Cardozo and Ramirez (1985), the Rosablanca Fm is constituted predominantly by irregularly bedded grey limestone and dolomite. The lower part presents dolomite and sparite with ooliths, intraclasts and ostracods, and sedimentary structures such as desiccation cracks and seaweed sheets; the middle part is marked by micrites and mottled biomocrites with thalassinoides, chondrites and bivalves; and the upper part presents calcareous mudstone, biomicrites and sandstones. In the area of Otache-Coscuez-Peñas Blancas (esmerald zone), Guerrero and Carrrillo (1998) described this formation as a monotonous sequence of dark grey to black, compact, fine grained limestone, with sporadic intercalations of sandy limestones with parallel-laminae and locally wavy contacts. Toward the top, limestone beds alternate with calcareous shale. The upper boundary is represented by the contact between the overlying limestones and the shales, which marks the lithological transition to the La Paja Fm. Etayo (1968) indicated that the Rosablanca Fm rests over the Cumbre Fm and underlies the Ritoque Fm. However, Hubert and Wiedmann (1985) considered that the Rosablanca Fm is an intercalation within the Ritoque Fm. According to Ulloa and Rodriguez (1979a), the Rosablanca Fm concordantly overlies the Cumbre Fm and its upper limit is net and concordant with the La Paja Fm. The Rosablanca Fm is interpreted as deposited in a shallow marine, neritic to coastal environment, based on the presence of thick-shelled molluscs (Ward et al. 1973, in Ulloa and Rodriguez, 1994).

Age. Along the Barrancabermeja-San Gil highway (Morales et al., 1958) and south of Villa de Leyva (Bürgl, 1954), the faunal content suggests a Valanginian to Barremian age. Following Cardozo and Ramirez (1985), Etayo (1968) assigned the Rosablanca Fm to the Late Valanginian-Early Hauterivian. More recently, fauna collected from this formation in the Otanche-Peñas Blancas area by Guerrero and Carrillo (1998) was analyzed by Tchegliakova (1997), who concluded an Upper Valangenian to Hauterivian age.

Utica Formation

The Utica Sandstone and the Murca Fm were first referred to as the Caqueza Sandstone, the upper part of which encompasses Tithonian to Hauterivian times (Champertier et al., 1961c; Bürgl, 1961; Campbell and Burgl, 1965; Thompson, 1966; Julivert, 1968; Gallo, 1977; Ulloa, 1988). The Utica Sandstone was initially considered the upper part of the Cáqueza Group (Champertier, 1961; Thomson, 1966; Gallo, 1977; Acosta and Obando, 1984; Ulloa, 1988; Moreno, 1990). Later, Sarmiento et al. (1985) present a synthesis of the Utica Fm. This unit was recognized in the railroad between Utica and Tobia, in the core of Utica anticline

The Utica Fm consists of coarse to fine sandstone with black shale interbeds. The lower part consists of black shales interlayered with yellow-gray arkosic wackestone, with some limestone beds at the top. The sandstone contains igneous and sedimentary lithic fragments (Moreno, 1989). According to Moreno (1989) on the road from Villeta to Utica, near La Magdalena, the Utica sandstone consists of interlayered beds of mudstone, with lenses of gastropods and oysters, and calcareous sandstones with plant fragments, coral fragments, and low angle cross-stratification with symmetrical ripple marks. According to Moreno (1989), the Utica sandstone was deposited in a shallow marine environment. The presence of plant remains and coral

fragments, reported by Garcia (1983) and Allen et al. (1988), support a shallow marine environment (Moreno, 1989)

Age. The basal part of the Utica Fm was assigned by Garcia (1983) to the Middle Jurassic, based on a specimen of *Nerinea decorate* Piette from an outcrop on the Rio Negro river, along the railroad between Utica and Tobia. Very close to this site, an ammonite was collected, determined by Etayo as Late Berriasian in age. Fossils collected by Burgl led Thompson (1966) and Gallo (1977) assign a Hauterivian age. Therefore, the age of this formation could encompass the Middle Jurassic to Hauterivian interval.

Murca Formation

The Murca Fm (Upper Valanginian) was informally called the Murca-Pinzaima Sandstone in the Middle Magdalena Basin by Allen et al. (1988). The name Murca Fm is used here for the Lower Cretaceous sandstones that crop out in the core of the Murca anticline (Moreno, 1989). At the type locality corresponds to coarse-grained, fining-upward sandstone with large pyrite crystals at the base, and intercalations of siltstones and shales.

Paleo-environment. According to Moreno (1989) a debris flow facies is suggested by the presence of siltstone intraclasts in a coarse-grained sandy matrix in the basal segment of the Murca Fm. The intraclasts show basal inverse grading and clast alignment. This segment may correspond to coarse inter-channel (Nelson and Kulm, 1973), or to channel turbidity currents of an upper submarine fan such as those proposed by Shanmugam and Moiola (1988). The lower and middle parts of the Murca Fm show a typical boom sequence starting with a rapid flow of deposits on erosive surfaces, deposited in a middle fan; the lower segment corresponds to a interlayered fine grained sandstone, black shale and black siltstone (Moreno, 1989), deposited in a distal turbidite (Mutti and Ricci Lucchi (1972, *in* Walker and Mutti, 1973). The upper part also was deposited in the border of the fan.

Age. Ammonites and plant-remains found along the Palma road and Villeta-Nimaima road in the black shale interbeds include *Berriasella colombiana* Haas; *Pseudoosterella ubalaensis* Haas; *Berriasella* sp.; *Santafecites santafecinus* (d'Orbigny); *Karakaschiceras?* cf. *bakeri* (Imlay); *Neohoploceras? magnifica* (Imlay); *Neocomites* sp.?, and *Cupressinocladus* sp. (terrestrial plant). This fauna suggests a Late Valanginian age.

Ritoque Formation

The name Ritoque Fm was initially proposed by Etayo (1968). The type section is located in the Ritoque river. It concordantly rests on the RosaBlanca and Arcabuco Fms and is concordantly overlain by the La Paja Fm. It is a monotonous sequence of quartz siltstone, and alternating mudstone and siltstone, with well-stratified barite lens with a reddish and gray weathering surface. According to Ballesteros et al. (1985), its mineral composition is given by equal parts of quartz, clay and heavy minerals (hematite, muscovite, zircon and tourmaline).

Paleo-environment. According to its facies, this unit was deposited in a lagoon of shallow, warm marine water with normal salinity, which episodically favored the development of bivalves, whose growth led to the formation of shallow submarine barriers. The iron oxides rich mud and the barite lenses suggest the development of muddy ponds in the lagoon. The presence

of carbonate and mixed facies allow the delineation of the barrier that isolated the lagoon from the offshore regions (Ballesteros et al., 1985).

Age. The Ritoque Fm is rich in ammonites, echinoderms and numerous lamelibranchs. Bürgl (1954a, p. 12) considered this unit as Valanginian, based on the presence of *Polyptychites polyptychus* Keyserling, *Toxaster roulini* Agassiz, etc. Haas (1960, p. 14) noted that the first mention by Bürgl really corresponds to *Subastieria* aff. *sulcosae* (Pavlow and Lamplugh) and indicated that the specimen from Leiva is believed to be Late Valanginian in age. Etayo (1968) concluded that "Although no abundant fauna is available, it seems that the representatives of *Subastieria* and *Favrella hahlasen* are in favor of the lower Hauterivian, as age assignable to these layers".

Paja Formation (Barremian to Late Aptian)

The name Paja Fm is derived from the valley of La Paja, a tributary of the Sogamoso river, between Bucaramanga and San Vicente. The name was given by Wheeler (1929; *in* Morales et al., 1958). It is a fine-grained lithostratigraphic unit that spans the Hauterivian to Aptian period. This unit was mapped by Julivert (1958a, b) in the region of the Mesa-Cuestas, where it is frequently gypsiferous.

The Paja Fm was described by Etayo-Serna (1968) in the area of Villa de Leyva as mudstone in the lower part, with scattered quartz-sandstone beds. The abundance of sandstone is an important feature in many places, like in Arcabuco where Renzoni (1983) first identified the sandstone member of the Paja Fm. Etayo-Serna (1968) also described a middle member composed of mudstone, with a level of micrite and biomicrite of Barremian-Aptian age. According to Patarroyo (2009), this level is marked by abundant fossils (ammonites, bivalves and marine vertebrates). Finally, the Aptian Upper member of the Paja Fm is made of black laminated mudstone, characterized by abundant, sometimes fossiliferous nodules (Etayo, 1968). Renzoni (1969) divided the Paja Fm into two members: a sandy basal member, made of sandstone and claystone, and an upper member made of shales with intercalations of limestone. The lower part of the middle member of the Paja Fm yielded micro- and macro-fossils (foraminifera shells, ammonite fragments), as well as wood remains (Patarroyo, 2004). Is important also mention the present of important levels of gypsum at this level.

At the base of the "lodolitas abigarradas" of the La Paja Fm (term introduced by Etayo, 1968a, 1968b), Patarroyo (2009) noticed a level of high energy deposits, already identified as a stratigraphic reference level, and a possible sequence limit that marks a transgressive surface (Forero and Sarmiento, 1982, 1985; Patarroyo, 2000, 2004). The faunal association would mark an age from Barremian to Late Aptian. At the base of the "lodolitas abigarradas" fragments of disordered molluscs, ammonites with the broken room chambers filled with foraminifera, foraminifera and trunks of plant remains can be observed. The base of the strata are irregular and may represent erosional surfaces, related to a sudden energy increase, representing a sequence boundary or a transgressive event. The presence of this erosive level from Villa de Leyva to Vélez (Boyacá) suggests that this event of Early Barremian age has a regional extension (Patarroyo, 2004) (Figure 2.33).

Following paleontological and lithological evidences, this formation was deposited in a restricted, shallow marine environment with little water circulation (Etayo-Serna, 1968). Paleo-environmental information from the Otanche - Peñas-Blancas area suggests an inner to middle shelf environment, maybe outer shelf, with oxygen depletion. The presence of siltstone and sandstone beds at the top of the sequence probably indicates a shallow environment and possible subaerial exposition and erosion (Guerrero and Carrillo, 1997).

Age. Bürgl (1954) first dated la Paja Fm as Hauterivian-Albian. In the San Gil-La Mesa area, Morales et al. (1958) using paleontological data, gave a Barremian-Aptian age to the Paja Fm, and indicated that its lower limit is older from North to South. Etayo-Serna (1968) assigned the Paja Fm to the Hauterivian-Late Aptian interval, while in the area of Villa De Leyva, Hubert and Wiedmann (1978) dated the lower part of the Paja Fm as Hauterivian. Based on fauna collected from this unit and dated by Nadejda Tchegliakova (1997), Guerrero and Carrillo (1998) assigned an age from Late Hauterivian to Late Aptian to the Paja Fm, without discarding an extension to the Early Albian. In the La Mesa de Los Santos area, Rollon and Carrero (1995) claimed that there is a shore-fall in the stratigraphic record during the Late Hauterivian. Finally, based on a paleontological study, Patarroyo (1997) concluded that the age of the Paja Fm is comprised between the Early Barremian and the Late Aptian. Details on the ammonites are given by Etayo-Serna (1979) and Patarroyo (2004).

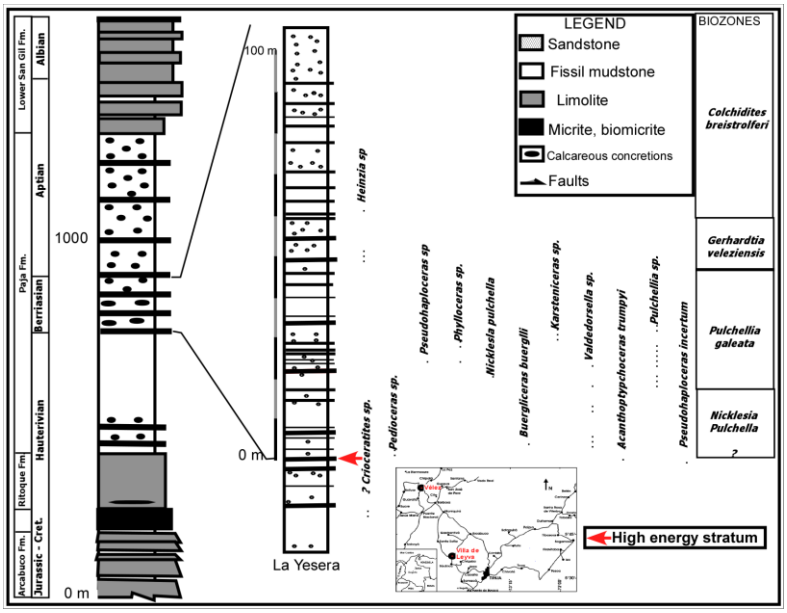

Figure 2.33. *Generalized stratigraphic section of Villa de Leyva (location in the map) with details of the Lodolitas Abigarradas level of the La Paja Fm. The stratigraphic position of the high energy deposits and the distribution of some species of ammonites are shown (Modified from Patarroyo et al., 2009).*

La Naveta Formation

Description. The La Naveta Fm consists of quartzitic sandstones and thin limestone levels with shells and some levels of pyritic schist. Burgl (1955a, p. 8) says that this level consists mostly of quartzitic sandstones, usually fine-grained, locally coarse. Frequently there are veins of calcite crosscutting the sandstones. There are also intercalations of clay schists, pyrite encrusted

with sulfur and iron oxide. Also, very thin veins of gypsum are often found. The thickness is 50-70 m according to Hubach (1931c) and 165 m according to Bürgl (1955a).

Age. Hubach (1931c) mentioned *Cyrena* sp. and *Paraglauconia* aff. *strombiformis* Schlotheim, apparently coming from the upper part, although found *ex situ*. Bürgl (1955a, p. 8-9) also quoted a Colombian *Nicklesia* (d'Orbigny), found by Intercol geologists. This fauna suggest a Hauterivian-Barremian age.

Tablazo Formation

This name was given by Wheeler (1929) in an unpublished report (Morales et al., 1958). This formation crops out on top of the first hills east of the town of Tablazo to the Rosablanca hill. It is composed of alternating blue-gray, very fossiliferous, hard limestones, and calcareous mudstone. According to Morales et al. (1958), the type locality of this formation is located in El Tablazo, where the Bucaramanga-San Vicente road crosses the Sogamoso River. The Tablazo Fm rests concordantly on the Paja Fm and usually forms an abrupt relief in comparison with the overlying and underlying units. In the area of Barichara, Moreno and Sarmiento (2002) divided the Tablazo Fm into five segments (A to E) and described each segment as follows: A (128 m): 30.9% of fossiliferous quartz-sandstone; 13.8% of fossiliferous quartz siltstones, 9.6% of quartz-sandstones, 15% of mudstones and 0.6% of quartz siltstones. B (57.2 m): 51.2% of quartz sandstone, 25.6% of fossiliferous quartz sandstone, 13.4% of mudstones, 5.2% of fossiliferous quartz-siltstone and 4.6% of biosparite. C (43.8 m): 49.9% of mudstones, 22.6% of fossiliferous quartz-sandstone, 14.1% of quartz sandstone, 10.6% of fossiliferous quartz-siltstones and 2.8% of biosparites. D (59.9 m): 48.2% of mudstones, 43.3% of fossiliferous quartz sandstone, 5.4% of fossiliferous quartz-siltstones and 3.1% of biosparite. E (70 m): 31.4% of mudstones, 27.2% of quartz-sandstones, 20.1% of fossiliferous quartz-sandstone, 13.7% of fossiliferous quartz-siltstones and 7.6% of quartz-siltstone.

The Tablazo Fm is 330 m thick in Barichara (Tellez, 1964), 480 m near Villa De Leiva (San Gil Inferior-Conjunto arenoso Calcáreo) (Etayo, 1968a), 277 m North of Bucaramanga (Ward et al., 1973), 239 m in Simacota, 239 m in Guadalupe, and 354 m in Suaita (Pulido, 1979a). According to Ulloa and Rodriguez (1978a) and Pulido (1979), and Moreno and Sarmiento (2002), the thickness progressively increases from north to south.

Environment. The Tablazo Fm was deposited in a shallow marine environment close to the coast (Hubach, 1957a, b), and is synchronous with the Lower San Gil Fm. According to Moreno and Sarmiento (2002), the transition from the Paja Fm to the Tablazo represents a shallow environment. The Tablazo Fm was deposited in an open marine environment of moderate to high energy, likely corresponding to a shoreface setting. The contact between the Tablazo Fm and the overlying Simití Fm corresponds to a deep environment or sea level rise, synchronous in the entire basin, the environment, however, remaining shallow.

Based on a detailed study of the Tablazo and Simiti formations, Moreno and Sarmiento (2002) established cycles in the sense of Wilkinson et al. (1996), i.e. a succession of layers occurring in a specific order and defining a pattern indicative of the energetic conditions. This pattern suggests an upward shallowing trend for these units.

Age. Morales (*in* Jullivert, 1968) dated the Tablazo Fm as Late Aptian to Lower Albian, based on the occurrence of the genera *Uhligella*, *Cheloniceras*, *Parahoplites* and *Douvilleiceras*, and on its stratigraphic position. In the area of Sáchica-Puente Samacá, Etayo (1968) identified *Colombiceras alexandrium* (d´Orbigny), *Colombiceras obliquum* (Riedel) and *Rhytidohoplithes* sp.; he considered the Tablazo Fm as Late Aptian-Early Albian, and the San Gil Fm as Late Aptian-Albian in age.

San Gil Inferior Formation

It is a succession named by Hubach (1953) to refer to a succession composed of limestones, calcareous sandstones, black shales and sandstones. Along the Sachica-Tunja highway, a 480 m thick succession of shales and siltstones with intercalations of variably calcareous sandstone and limestone, gray-green and micaceous fine-grained sandstones and dark gray sandy clays, sandy limestones and sandstones with remains of *echinoderms* is exposed.

Age. Both Julivert (1958a) and Hubach (1953) assigned an Albian age to this unit. However, Etayo assigns an Aptian age, based on the presence of *Colombiceras riedelii* and *Colombiceras alexandrium* in limestones with gastropods and lamelibranchs.

San Gil Superior Formation

Along the Sáchica-Tunja Highway, there is a 620 m thick succession of black shales with intercalations of sandy limestones with abundant lamelibranchs. This unit underlies the Churuvita Fm. originally called by Hubach (1953) “Conjunto San Gil Superior”, it has been later considered equivalent to the Simití Fm.

Age. The ammonites *Knemiceras semicostatum*, *Lyelliceras pseudolyelli*, cf. *Desmoceras chimuense*, *Prolyelliceras prorsocurvatum* allow dating this unit as late Early Albian. This formation underlies sandstones dated by Julivert and Hubach (1953) as Cenomanian. Etayo (does not indicate the year) included these sandstones within the Churuvuta Fm.

Trinchera Formation

The name was given by Cáceres and Etayo (1969) to describe a sequence of mudstone, with intercalation of limestone and sandstone in the lower part. It overlies the La Naveta Fm and underlies the Socotá Fm. The type location is located in the Trinchera gully (Quadrangle L-10). The Trinchera Fm. crops out from the town of Apulo to the South to the town of Utica to the North. North of the map 227 and on map 208, this unit is made of mudstone and its lower member cannot be distinguished (Ulloa and Acosta, 2001), while in the area of La Palma (Map 189), it is included in the La Palma group (La Paja, Tablazo and Simiti formations) (Rodriguez and Ulloa, 1994 a).

Ulloa and Acosta (2001) divided this formation into two members. The lower member comprises three units: Lower unit (20 m): non calcareous mudstone and micaceous claystone, with fine-grained quartzsandstone and volcanic fragments, medium-grained sub-litharenite, and finally biosparitic limestone with ostreids; Second unit (154 m): non calcareous claystone and mudstone with siliceous concretions, with beds of siltstone and thin layers with echinoderms and foraminiferas; Third unit (150 m): fine- to medium-grained quartz-sandstone in medium to

thick layers, with wavy to lenticular bedding, and very thin layers of claystone and siltstone, and two layers of sandy-shaly limestone (Figure 3.15).

Age. Caceres and Etayo (1969) collected *Heinzia* sp., *Pseudohaploceras* sp., *Heminautilus etheringtoni* and *Cheloniceras* sp., which indicate a Barremian to Early Aptian age.

Socota Formation

Description. The lower part of the Socota Fm is made up of laminated, black calcareous mudstone, with thin intercalations of calcareous quartz-siltstone, and fine-grained quartz-sandstone. The lamination evolves from parallel at the base to undulating to the top, due to the increasing sandstone content. At the base, thin layers of limestone sometimes lenticular and micrite concretions occur, and ammonites and fish remains may be found at the top of the coarsening- and thickening-upward sequences. The upper part is made of variably thick beds of fine- to medium-grained quartz-sandstone with calcareous cement and undulating lamination of mudstone and calcareous siltstone. This facies is organised in coarsening and thickening upward sequences. Ammonites and wood and leaf remains occasionally occur in the flaser-bedded mudstone. Calcareous concretions may reach 15 cm in diameter. Quartz-sandstone mainly includes angular monocrystalline quartz, corroded by the calcareous cement.

Age. Etayo (1979) determined the *Stoyanowiceras treffryanum-Dufrenoyia sanctorum* and *Parahoplites (?) hibachi-Acanthohoplites (?) leptoceratiforme* ammonite assemblage zones, which indicate an Early Aptian and Late Aptian age, respectively.

Simití Formation

The type locality of the Simití Fm is located along the left margin of the Ciénaga de Simití (Bolívar) (Morales et al., 1985). The unit is constituted by black laminated, carbonaceous claystones, with calcareous, often fossiliferous concretions, which become more abundant to the top where they are up to 3 m in diameter. In the area of Cienaga de Simití, this formation is 410 m thick (Morales et al., 1958), whereas in the area of Villa de Leyva, it could reach a thickness of 620 m. Moreno and Sarmiento (2002) quoted that in the Barichara area, the Simiti Fm is composed of mudstones with some levels of clean quartz-sandstone (50-55%), quartz-sandstone (24-38%), and fossiliferous quartz-sandstone (6.2-19%). In the area of Sachica (Boyacá), the Simití Fm in composed of mudstone (44-80%), fossiliferous quartz-sandstone (9.4-15%), quartz-sandstone (10-31%), biosparite (3-4%) and siltstone (3.5%) (Moreno and Sarmiento, 2002). The Tablazo and Simiti formations of the MMV and the Villa de Leyva areas, are correlated with the Socotá and Capote formations of the Tequendama area, and with the upper sandy member of the Caballos Fm and the Tetuán Fm of the Upper Magdalena Valley (Figure 2.11).

Environment. The transition from the Tablazo to the Simiti Fm is marked by the evolution from fossiliferous sandstone and biosparite (shoreface) to mudstone (offshore), which corresponds to a deepening upward trend. This change is ascribed to a sea level rise that began in the upper Albian (Villamil 1998; Guerrero et al., 2000). In the Sáchica section, the deposition in an offshore environment of the Simití Fm ended up with the deposition of quartz-sandstone beds of the Churuvita Fm (shoreface), showing a significant decrease of the deposition depth (Figure 2.34) (Moreno and Sarmiento, 2002). This limit corresponds to the Albian-Cenomanian

boundary and would be indicative of a sea level drop (Villamil 1998; Guerrero et al., 2000). The Fischer plot (Figure 2.34) of the Simiti and Tablazo formations evidences a decrease in the accommodation space for the Tablazo Fm. The transition from the Simití to the overlying Churuvita Fm in the MMV and Villa de Leyva areas is correlated with Tetuán-Hondita Fm transtion in the Upper Magdalena Valley.

Age. The age of the Simití Fm ranges from Middle to Upper Albian, based on the presence of the ammonite genera *Douvilleiceras*, *Parahoplites*, *Uhligella*, *Lyelliceras*, *Oxytropidoceras*, *Brancoceras* and *Pervinquieria* (Morales et al., 1958). In the area of Villa De Leyva, Etayo (1968a) stated an Early to Late Albian age for this formation, based on the occurrence of *Prolyelliceras prosocurvatum* (Gerhardt), which overlies *Desmoceras chimuense*, *Platiknemiceras* sp., *Knemiceras semicostatum* (Sommermeier), *Parengonoceras guadalupaeforme* (Sommermeier), *Engonoceras* sp., cf. *Desmoceras chimuense* and *Lyelliceras pseudolyelli sensu* Benavides Cáceres (non Par and Bon).

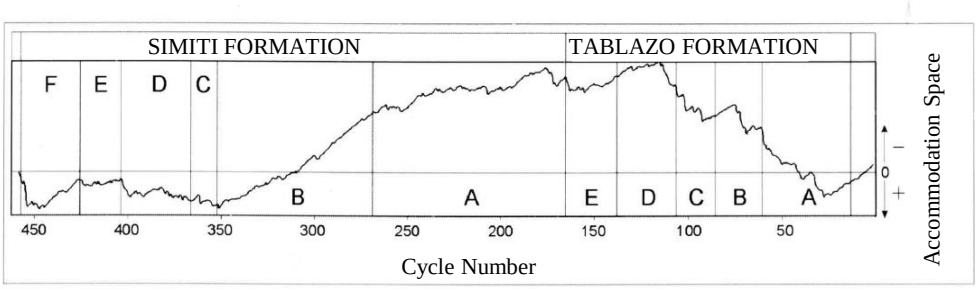

Fischer Diagram for Tablazo and Simiti Formations (Sachica Section)

Figure 2.34. *Fischer plot (relative accommodation space plot) for the Tablazo and Simití formations (Sachica section) (modified from Moreno and Sarmiento, 2002).*

Areniscas de Chiquinquira Formation

Description. This name was proposed by Ulloa and Rodriguez (1979) to refer to a series of lutitic sandy strata exposed along the Sutamarchan-Chiquinquira highway (Plate 190), where the type section is located. The base of this unit is defined at the first appearance of thick sandstone beds overlying conformably the black shales of the San Gil Fm. Its upper contact is concordant with the lower shales of the Chipaque Group is defined by the disappearance of sandstone beds. In the type section this unit is 337 m thick (Ulloa and Rodriguez, 1979). It comprises light grey to yellowish, micaceous, fine-grained quartz-sandstones, with thin intercalations of micaceous black shales (166 m); grey micaceous shales, with intercalations of white, fine-grained, muscovitic, massive quartz-sandstone (76 m); and grey shales with beds of micaceous siltstones and up to 3 m thick beds of quartz-sandstones (95 m) (Ulloa and Rodriguez, 1979).

Paleo-environment. Based on the homogeneous grain size, the fine lamination in some strata, the presence of muscovite and pyrite, Ulloa and Rodriguez (1979) suggest a quiet deposition environment, with little oxygenation and reducing conditions. According to Terraza (2012), the presence of bivalves and the facies of the Areniscas de Chiquinquira Fm reflect a shallow

marine environment dominated by tides, encompassing offshore bottom to muddy intertidal plain. The plant remains suggest the development of vegetation on the coast line.

Age. Based on its stratigraphic position, the Areniscas de Chiquinquira Fm is assumed to be of Cenomanian age (Ulloa and Rodriguez, 1979).

Salto Formation

This formation was first described by Morales et al. (1958). The name comes from the Salto river. It is constituted by dark grey, hard, shaly limestone, with thin beds of calcareous dark shale and local nodules. This unit is about 50 to 125 m thick. Its lower limit with the Simiti Fm is concordant and the upper limit is concordant with the Salada Fm. This formation is correlated with the Churuvita Fm of the Villa de Leyva area, since the Salto Fm is restricted to the North of the MMV, north of the Chucurí inflexion.

Age. The presence of the genera *Brancoceras*, *Knemiceras*, *Neoharpoceras* and *Turrilites* indicates an Albian age (Morales et al., 1958, p. 652). However, *Exogyra squamata* d´Orbigny found in the San Vicente area and *Calycoceras* sp. from the Cienaga of Simití indicate a Cenomanian age.

Churuvita Formation (Cenomaniano-Turoniano)

The name of this formation comes from the Quebrada Churuvita (on the Churuvita syncline), tributary of the Samaca river. This unit was first described and mapped in the Villa de Leyva area by Etayo (1965, 1968) to refer to a series of fine- to medium- grained, micaceous quartzite and sandstone. These exhibit intercalations of shales, siltstones, sandstones and limestones full of *Rhynchostreon squamatum* and *Ostrea* sp. (coquina) in the middle part, and of thick bedded sandstone (quartzite) and sandy limestones in the upper part. East of Chiquinquira, 50 to 100 m strata corresponding to this unit form crests. The Churuvita Group *sensu* Etayo (1965, 1968) corresponds to the Churuvita and San Rafael formations. Their lower contact corresponds to the appearance of shaly-silty levels. The lower contact with the San Gil Superior Fm may be abrupt or progressive (Etayo, 1978). In the type section, it is marked by a strong morphological and lithological contrast. The contact with the overlying formation is net and separated by rocks of quartz sandstones with intercalations of laminated mudstones.

Age. The Churuvita Fm is assumed to be of Cenomanian-Turonian age because it overlies units of Late Albian age and contains *Mammites afer* and cf. *Coilopoceras lesseli* of Early Turonian age. Although scarce and poorly preserved, the ammonites of the Churuvita Fm (Acanthoceratidae, *Venezoliceras*) suggest a Late Albian age (Etayo, 1968). The underlying San Gil Superior Fm yielded *Platiknemiceras colombiana*, *Rinconiceras rinconi*, *Lyelliceras pseudolyelliforme* and *Hysteroceras carinatum* (Etayo-Serna, 1979; Etayo *in* Caicedo, 2005) of Middle to Late Albian age. In the overlying San Rafael Fm, Etayo (1968, 1979) reports the Early Turonian. Therefore, the Churuvita Fm would encompass the Late Albian-Early Turonian interval.

Simijaca Formation/Pacho Formation

Ulloa and Rodríguez (1991) were the first to propose the name Simijaca Fm to describe a succession of dark grey mudstone and siltstone, with partly clayey quartz-sandstone beds,

which underlies the La Frontera Fm and overlies the Sandstones of Chiquinquirá. In its type locality, this unit reaches a thickness of 693 m. It consists mainly of black to dark grey laminated claystone. The lower and middle parts of this unit consist of claystones to laminated mudstones in which fish scales are frequent and, in smaller proportion, small bivalves and ammonites, as well as fragments of small crustaceans.

Paleoenvironment. The occurrence of planktic foraminifera at the base and of leaf remains, bivalves and bioturbation to the top suggests a shallow deposit. This unit may represent the prodelta area of the Une Fm sandstones known on the eastern side of the Eastern Cordillera (Acosta and Ulloa, 2001).

Age. Some bivalves determined as *Exogyra* sp., *Ostrea* sp. and *Pecten* aff. *tenouklensis*? Are associated with scarce planktic foraminifera of the genus *Hedbergella* (Acosta and Ulloa, 2001). The suggested age for this unit is Cenomanian (Etayo, 1979).

Hilo Formation

This siliceous unit was initially named the Hiló Horizon by Hubach (1931), after the name of the Hiló hamlet. Later, Cáceres and Etayo (1969) named it the Hiló Fm and proposed the Guayabal Bituima Acosta section as the type locality. Its lower limit is marked by the first appearance of siliceous siltstones (Etayo, 1979) and the upper boundary is defined by the appearance of black laminated mudstones on siliceous siltstones. The thickness of this section is approximately 450 m. The lower part consists of calcareous mudstones, sometimes slightly siliceous, with parallel lamination. *Inoceramus* sp. and impressions of ammonites occur towards the base. The middle part consists of parallel laminated calcareous mudstones, slightly to totally siliceous (cherts), with very thin to thin bedded chert layers, and undulating, non-parallel planes, medium to thick layers of biomicritic limestones, with lenticular stratification, with a concresional aspect, siliceous levels contain abundant planktic foraminifera filled with calcite or silica. The upper part consists of laminated calcareous mudstone, slightly siliceous at the base; they contain some micritic concretions and layers of lenticular limestone, with casts of ammonites.

The presence of *Oxytropidoceras* sp. *Paleoenvironment*. *Suggests* this sequence was deposited in deep water conditions (Hart, 1980, Brasier, 1980), under anoxic conditions (Demaison and Moore, 1980, Berner 1981).

Age. The presence of *Rotalipora reicheli*, *Praeglobotruncana stephani* and *Rotalipora mitcheli* support a late Albian (Vraconian) to early Cenomanian age. Bürgl (1957) suggests a Middle to Late Albian age.

Socotá Formation

The name Socotá Fm was given by Cáceres and Etayo (1969) to a series of calcareous sandstones (Socotá member), overlain by grey shales (middle member) and capped by shales and fossiliferous marls (Capotes member, "Horizonte de Esferitas" of Hubach, 1931). Acosta and Ulloa (2001) suggested to restrict the term Socotá Fm to the Socotá member.

The lower part consists of black laminated calcareous mudstones, with very thin intercalations of calcareous quartz-siltstones and fine-grained quartz-sandstones with calcareous cement. The

sandstone content increases upward, as well as the number of micritic concretions. Fossils (ammonites and fish remnants) are usually found at the top of coarsening- and thickening-upward sequences. The middle part consists of very thin- to thick-bedded, very fine- to medium-grained quartz-sandstones with calcareous cement, presenting wavy layers of mudstone and limestone siltstones. Occasional ammonite and plant remnants may be found. The upper part consists of black laminated calcareous mudstones with thin intercalations of fine-grained, calcareous quartzite. Beds of conglomerates with quartzose clasts and ammonite and mollusc fragments bound by calcareous cement, exhibit erosional lower surface.

Age. Etayo (1979) determined the *Stoyanowiceras treffryanus-Dufrenoyia sanctorum* and *Parahoplites (?) hubachi-Acanthohoplites (?) leptoceratiforme* assemblage zones, of Aptian age.

La Luna Formation

The term La Luna Limestone was introduced by Garner (1926) in Venezuela for a succession of fossiliferous, calcareous, black shale, with concretions of black limestone. The name La Luna comes from the La Luna river located NW of Perijá (Venezuela). Hedberg and Sass (1937) referred to this unit as the La Luna Fm, a term that was introduced in Colombia by geologists of the Caribbean Petroleum Company. Notestein et al. (1944) introduced the term in Colombia applying it to the Concession Barco. Renz (1956, 1960) applied the name La Luna Fm to the Peninsula of La Guajira and in the region of Punta Espada and divided it into two members. Morales et al. (1958) adopted the name in the MMV and subdivided the La Luna Fm into three members, which are the Salada, Pujamana and Galembo members.

The Salada Member

This member was first used in 1929 by Wheeler in an unpublished report. The type locality is located in the Salada valley, on the right margin of the Sogamoso river, NE of the Mares Concession in the MMV. The Salada Member is composed of hard and laminated, calcareous black shales, with intercalations of black micrite, concretions and pyrite. Notestein et al. (1944) cited *Inoceramus labiatus* Schloteim, which indicates an Early Turonian age, without excluding a Cenomanian and Coniacian age for part of the Salada. In the MMV, Morales et al. (1958) assigned a Turonian-Santonian age for this member.

Pujamana Member

Description. According to Morales et al. (1958, p. 654) this name was first reported by Wheeler, after the Quebrada Pujamana, tributary of the Sogamoso river, between Bucaramanga and San Vicente. It represents the 50 to 225 m thick Middle member of the La Luna Fm, made of gray shales or marls.

Age. Morales et al. (1958) cite *Amonia* sp. and *Inoceramus* sp. The age would be Late Turonian to Early Coniacian, with a diachronous upper limit.

Galembo Member (Upper Turonian – Coniacian Santonian?

Description. This member was original reported by Morales et al., (1958) as the upper member of La Luna Fm. The name comes from the Galembo edge (in the Sogamoso valley) between Bucaramanga and San Vicente the Chucurí. It is composed of a series of calcareous shales

alternating with thin layers of limestone and numerous discoidal nodules of limestones (ammonites) with several meters of ammonites. Layers of lidites are also common. The thickness of this member varies from 180 to 350 m.

Age. The Galembo Mb would be of Upper Turonian-Santonian? age (Morales et al., 1958, p. 655). The Turonian age is based on the presence of *Metoicoceras* (rather considered as Cenomanian), while *Peroniceras* and *Barroisiceras* support a Coniacian age. The Galembo Mb contains the following foraminifera zones: *Anomalina redmondi* subzone, *Bolivina explicate* horizon level and *Marginulina curviseta* Zone (Morales et al., 1958). The Santonian stage has not been defined paleontologically, which suggests a sedimentary hiatus of Santonian age.

La Frontera Formation

This name was given by Hubach (1931) for the sequence of limestone and siliceous layers outcropping in the La Frontera quarry, located near the railway station of the same name (Municipio de Albán). This series overlies and underlies thick shale deposits. A type section has been proposed by Cáceres and Etayo (1969) at "La Gran Vía", along the road between Alicachín and the El Colegio municipality. Because this site is quite covered, Acosta and Ulloa (2001) proposed the Rio Curi and Anolaima - La Florida sector to be the type section.

The base of this unit consists of black, laminated calcareous mudstone, locally cross-bedded. Lens-shaped, biomicritic limestone, laminated calcareous mudstone, calcareous-siliceous mudstones and giant or small-sized micritic concretions occur. The middle part is composed of black cherts in thin to very thin, undulating layers. The upper part is dominated by thin- to very thin-bedded, continuously laminated chert and calcareous-siliceous mudstones.

Environment. Acosta and Ulloa (2001) suggest a deep-water environment, below the photic zone, with anoxic conditions at the water-sediment interface. Parallel lamination, absence of benthic life and abundant pyrite support sulfidic, anoxic conditions (Berner, 1981).

Age. In the La Frontera Fm, Etayo (1979) proposed the *Mammites nodosoides appelatus-Franciscoites suarezi* ammonite assemblage zone, of Early Turonian age. The planktonic foraminifera *Whiteinella archeocretacea*, *Whiteinella aprica*, *Whiteinella baltica* and *Heterohelix reussi* support the Early Turonian age for the base of the formation (Acosta and Ulloa, 2001). In the upper part of the La Frontera Fm, casts of the bivalve *Didymotis roemeri variabilis* suggest a Middle Conianian (Bürgl, 1957).

Conejo Formation

The Conejo Fm is the name proposed by Renzoni (1967) to describe the succession of shales with sandstone and sporadic limestone beds, exposed along the road between the town of Pontezuela and the San Rafael Trail, close to the Alto El Conejo. The Conejo Fm overlies the Churuvita Group and underlies the Plaeners Fm. In the Sáchica-Tunja area, the upper part of the unit probably corresponds to the so-called Arenisca Dura Fm of the Sabana de Bogotá. Ulloa and Rodríguez (1991) use the term Conejo Fm to refer to the sequence of shales below the Guadalupe Group, which overlies the siliceous siltstones of the La Frontera Fm, and proposed a reference section along the Sutamarchán-Chiquinquirá road.

The lower part of this unit is characterized, by a succession of grey claystone and laminated mudstone, commonly calcareous, in which micritic concretions (< 20 cm) occur. These are overlain by non-calcareous laminated claystones, containing thin- to medium-bedded silicified quartz-siltstone. The lower part ends up with fine- to medium-grained quartzite, in which lamination is commonly wavy and discontinuous, and Thalassinoides sp. occur.

The middle part of the Conejo Fm is marked by medium- to very thick-bedded, nodular biomicritic limestone, which evolves upward into medium- to thick-bedded intercalations of medium- to fine-grained quartz-sandstone, and quartz-siltstones with phosphatic peloids. claystone and mudstone are locally calcareous. To the south of Plate 227, the terrigenous intercalations evolve upward from fine-grained sandstone to siltstone.

Paleoenvironment. Outershelf conditions are supported by the abundance of planktic foraminifera, especially keeled foraminifera (e.g. *Dicarinella* sp., Hart, 1980). Oxygenation of the seabed was fluctuating, with predominance of anoxy (littl or no benthic life) and sporadic incursions of aerobic conditions (Thalassinoides) related to the presence of sandstone beds. Occasional turbiditic flows and the increase of sandstones toward the top mark the transition to a shallow siliciclastic sea.

Age. In this unit, Etayo (1979) identified the *Gloriaceras correai-Protexanites cucaitaense-Codazziceras scheibei* ammonite assemblage zone, of early Conianian age. In the memoir of the geological sheet 227 (Ingeominas), the following foraminifera *Marginotruncana sinuosa*, *M.* aff. *schneegansi*, *Dicarinella concavata, Whiteinella archeocretacea, W. inornata* and *Whiteinella baltica*, support the Coniacian age.

Olini Group

The name Olini Group was introduced by Petters (1954, *in* De Porta, 1966) while describing some species of foraminifera, but without presenting a lithological description. The same author used the term for a lithostratigraphic unit composed of two siliceous levels called Lower Chert (Lidita Inferior) and Upper Chert (Lidita Superior), separated by the Shale Level. The locality is found along the road that leads from the Piedras Municipality to the Cuchilla La Tabla.

The Lidita Inferior Fm is constituted predominantly by very thin layers of chert and siliceous siltstone, containing poorly preserved foraminifera. The Shale Level is made of quartzite, siltstone and micaceous and slightly siliceous calcareous mudstone, with thick intercalations of fine- to medium-grained, black-brown quartz-arenite, locally slightly silicified. The Lidita Superior Fm, comprises calcareous cherts with parallel and undulating lamination, black cherts with parallel lamination, rarely slightly inclined. There are also horizons of yellow-orange claystone, whose origin is not clear, since they usually limit sets of layers showing angularity to each other (Acosta and Ulloa, 2001).

Age. (1) Lidita Inferior Fm. The foraminiferaand zone of *Globigerina cretacea*, the assemblage zone of *Inoceramus peruanus-Texanites* aff. *serratomarginatus*, and the occurrence of *Globotruncana fornicata* in the upper part of the unit indicate a late Conianian - early Santonian age (Bürgl and Dumit, 1954). (2) Shale Level. The zones of *Bulimina compressa - Dentalina lorneiana* and *Haplophragmoides excavata - Anomalina redmondi* indicate a Santonian age (Bürgl and Dumit, 1954), while Petters (1955) defines the *Anomalina redmondi* as indicative

of the Coniacian. (3) Lidita Superior Fm. Bürgl and Dumit (1954) quote the foraminifera zones of *Wheelerella, Sporobulimina* and *Siphogenerinoides plummeri*, of Campanian age. Based on the occurrence of *Globirinelloides prairiehillensis, Rugoglobigerina* sp., *Globotruncana ventricosa* (?) and *Globotruncana* aff. *insignis*?, Acosta and Ulloa (2001) confirmed a Campanian age (Caron, 1985).

Umir Formation

The type locality of this formation is the Quebrada Umir, located 3 km west of the Umir Hill in the MMV. It was first defined by Huntley (1917, unpubl. report), who included in this unit what is today known as the Lisama Fm (*in* Morales et al., 1958, p. 655). It was then redefined by Link (1925, unpubl. report), who gave it its present definition.

The first extensive description was given by Morales et al. (1958). The lower part of the Umir Fm corresponds to grey to bluish-black, thin-bedded shales, with micaceous and carbonaceous layers, and ferruginous concretions. Its upper part is constituted by grey to black, thin-bedded, soft shales, with thin beds of coal, iron minerals, fine-grained sandstone and siltstone. The thickness of this formation is around 1000 m. Due to its predominantly shaly lithology, the Umir Fm forms wide valleys. This formation overlies in slight discordance the Galembo Member of the La Luna Fm. Its upper boundary is concordant with the Lisama Fm.

Age. Based on the occurrence of the marine foraminifera *Siphogenerinoides cretacea*, *S. bramlettei* and *Ammobaculites colombianus* (Petters, 1955), the Umir Fm is ascribed to the Campanian-Maastrichtian.

Guadalupe Group

The name Guadalupe was used for the first time by Hettner (1892, *in* Hubach, 1957), who named Piso de Guadalupe the Upper Cretaceous sandstones, which crop out on the eastern hills of the Bogotá area.

In the sense of Renzoni (1962-1968), it was limited at the base by the last occurrence of the mudstone of the Villeta Group and at the top by the first occurrence mudstone beds of the Guaduas Fm. The Guadalupe Group is distinctly sandy and is divided from base to top into the Arenisca Dura, Plaeners and Labor and Tierna formations, which are described below for Plate 227

Arenisca Dura Formation

The name Arenisca Dura is due to Hubach (1931), who proposed as type locality the strait of the San Francisco de Bogotá river. Renzoni (1962) gave it the range of Dura Sandstone Fm and proposed as reference section the section of the Choachí-Bogotá highway. Pérez and Salazar (1971) proposed as a type section the section along the road to Cerro del Cable, east of the city of Bogotá.

Description. Arenisca Dura Fm consists of fine-grained, very thin- to very thick-bedded, parallel to lens-shaped quartzite layers, with intercalations of thin- to very thin-bedded, slightly siliceous-quartz siltstones. Laminations are usually undulated, locally discontinuous, and affected by bioturbation, but rare cross-bedding (hummocky type?) and ripples are observed.

Ondulating surfaces (erosive?) may represent nonconformities. Fish remains (casts), bivalves and phosphatic peloids occur toward the base.

Paleo-enviroment. The hummocky type of stratification suggests a shallower depositional environment than the underlying unit, which is marked by turbiditic layers (Walker, 1984b). On the other hand, upwelling currents may favor phosphate and silica precipitation, through the proliferation of radiolarians and fishes. The presence of *Siphogenerinoides* (Etayo, 1964) is consistent with the abundance of phosphorus, while *Inoceramus* (Etayo, 1964) is typical of highly reducing conditions.

Age. Etayo (1964) mentioned the ammonite *Peroniceras (Gauthiericeras) bujuvaricum* and the benthic foram *Siphogenerinoides ewaldi*, among others, which suggest a Santonian age.

Pleaners Formation

Hubach (1931) first used the term Plaeners, to refer to the argillosa-liditic sequence, which is located in the middle part of the Upper Guadalupe Fm. Renzoni (1968) defined it as Plaeners formation and proposes as reference sections the Bella Suiza quarry, near Usaquén and the Bogotá-Choachí highway, in the descent towards the headwaters of the Raizal gully, where the lithostratigraphic unit appears complete. Pérez and Salazar (1971) proposed as a type section the section that crops out on the hill between the Rosales and La Vieja rivers.

Age. Pérez and Salazar (1971) mention the presence of *Ostrea tecticosta*? and the benthic foraminifera *Orthokarstenia cretacea* and? *Orthokarstenia clarki*, to which a Campanian-Maastrichtian age is assigned.

Labor y Tierna Formation

Description. The term Labor y Tierna was used for the first time in a stratigraphic sense by Hubach (1931) to designate the upper sandy part of the Guadalupe Fm. Later (1957), the same author defined it as a member belonging to the Upper Guadalupe Fm. Then, Renzoni (1962, 1968) proposed the present-day name of this unit, which represent the upper part of the Guadalupe Group. They established as the type-section the outcrops along the Choachí-Bogotá highway, before arriving to the páramo, in the quebrada Rajadero.

Lithologically it is characterized by medium- to thick-bedded, lens-shaped, fine- to medium-grained quartz-sandstone. Intercalations of mudstones and quartz-siltstone sporadically occur. Bioturbation is abundant (*Thalassinoides* sp. and *Arenicolites* sp., Hernández, 1990).

Age. Pérez and Salazar (1971) mention for Labor y Tender Formation, among others, the following species: *Sphenodiscus* sp, *Cyprimeria* cf. *coonensis* and *Tellina equilateralis*, on the basis of which an early Maastrichtian age is assigned.

Lisama Formation (Paleocene)

The name of this unit comes from the Quebrada Lisama, NE of the Mares Concession (Santander Department). This formation was first defined together with the La Paz Fm (Stutzer, 1923; Huntley and Mason, 1923; Anderson, 1926, 1927a; Harrison, 1930). Link (1925, unpubl. report) gave it the name of Lisama Fm and defined the type section, which was then described by Wheeler (1935).

This unit is constituted by variegated shale (red, brown and grey), with intercalations of grey, massive, medium- to fine-grained sandstone beds, which become thicker upward. Coal layers occur in the upper part. This unit is 1225 m thick. Its lower limit with the Umir Fm is transitional, whereas the upper contact with the La Paz Fm is a regional unconformity. Van Der Hammen (1958) correlated the Lisama Fm with the Barco and Cuervos formations in the Barco Concesion, and with the Upper Guaduas and with the lower part of the Bogotá Fm.

Environment. The Lisama Fm was deposited in deltaic to lagoon environments (Wheeler, 1935).

Age. Based on its stratigraphic position between the Umir Fm and the Horizonte Mugrosa, both are considered as belonging to the Eocene, Wheeler (1935) ascribed this formation to the Eocene. However, palynological data led Van Der Hammen (1954) to date the Lisama Fm as Paleocene, an age that has been confirmed by subsequent authors.

Seca Formation

Description. The name of this unit derives from the Quebrada Seca that flows into the Magdalena river to the S of Cambao. The type and reference sections are located along the road from Cambao-San Juan de Río Seco to Honda Guaduas. The total thickness of the Seca Fm is about 300 m. De Porta (1965, 1966) described the Seca Fm as a succession of red sandstones and shale, with a clear predominance of red shales in the upper half of the formation. The sandstone beds of the lower part correspond to orthoquartzite and their composition is similar to the La Primavera Member of the underlying Cimarrona Fm. Still in the lower half of the formation the sandstones change from orthoquartzite to arkoses.

Age. The available paleontological data indicate a Maastrichtian age, as indicated by the fauna mentioned by Bürgl (1957) in the surroundings of El Dindal. The palynological association formed by *Leiotriletes guaduensis* (Van der Hammen, 1958), *Psilamonocolpites medius* (Van der Hammen, 1958), *Tricolpopollenites* and *Monocolpopollenites* associated with small *Angiosperms* from Quebrada Seca (Porta, 1966, p. 109), is rather similar to those of the Guaduas Fm, but a greater precision is not yet possible. Consequently, this formation may encompass part of the Paleocene.

Guaduas Formation

The name of this unit comes from the town of Guaduas located on the western edge of the Cordillera Oriental on the Bogotá-Honda highway. The wide geographic extension of some sandstone levels allowed Hubach to specify that the units the Guaduas Fm had been subdivided (Hubach, 1931, *in* Kehrer, 1933). Basal unit: mainly dark gray clays with some fossils at the base. Middle Unit: made of two levels of sandstones (Guide Sandstone and Lajosa Sandstone); separated by compact dark grey clays, sometimes carbonaceous and containing exploitable coal seams (productive part of the Guaduas Fm). Upper Unit: "reddish, bluish, greenish and purple clay, among which locally there are unexploitable coal seams and beds of unstable, more or less coarse-grained sandstones. Radelli (1967) defined the Guaduas Fm as a Group and each of its three parts as formations. Thus, the Guaduas Group would comprise from bottom to top the Lower Guaduas Fm, Middle Guaduas Fm and Upper Guaduas Fm.

Age. Hettner (1892) considered the Guaduas as Late Cretaceous. Leaving aside the Eocene age assigned by Berry (1924b) on the basis of *Saccoglotis cipaconense* and followed by Anderson (1926, 1927a), the age of the Guaduas Fm has been estimated as a lower Tertiary. Scheibe (1934a) first assigned a Late Cretaceous-Early Tertiary age to this unit, without specifying the position of the K-T boundary. Hubach (1957a) and Van der Hammen (1954) considered the age of this formation as Maastrichtian-Paleocene.

La Paz Formation (Paleocene-Middle Eocene)

The name La Paz Fm derives from the Cordillera La Paz, located between the Sogamoso and Lebrija rivers. The type section is located along the Lebrija river, near Puerto Wilches downstream of the city of Venegas.

The first description of this unit was made by Stutzer (1923) who wrote "the forms of the surface of this cordillera remember some of the Buntsandstein in Germany. This sand reveals discordant structures". According to this author the La Paz Fm is constituted by alternating gray-blue clay and yellow, micaceous hard sandstone. Stutzer (1923) ascribed to the La Paz Fm all the sediments between the Piso Guaduas and Piso Honda. Simultaneously, Huntley and Masson (1923) described this unit with the name of "La Paz Sandstone series", but without a precise definition, except for its lower limit. Then, Harrison (1930, p. 405) gave the La Paz Fm its presently accepted definition, placing it between the "coal group" and the "Chusoas beds". He described the following succession: (1) sandstones with shaly layers and carbonized tree trunk; (2) gritty sandstone with coarse pebbly beds, coal pebbles and hard, fine grained, ripple marked sandstones, with carbonized tree trunk, (3) coarse pebbly-beds and red mottled clays with pebbly interbeds.

Age. Paleocene-Middle Eocene.

Hoyon Formation

Description. The name Hoyón was first introduced by Hubach in a report of the Shell Company. Later, Raasveldt and Carvajal (1957) gave this name to sediments located between the Guaduas Fm and the Gualanday Fm, in the Jerusalem-Guaduas syncline. Van der Hammen (1958, p. 101), first described the Hoyon Fm, as made of conglomerates with quartz and cherts, greenish sandstones and red-purple clays and shales, with few dark grey shales and some silicified tree trunks. Van der Hammen measured a thickness of 600 m in the type section, located along the Chaguaní and Hoyón rivers, from which its name derives. Porta (1965, 1966, p. 122-141) divided the Hoyón Fm from base to top into three members: Cambao Mb (200 m): gravelly and sandy beds intercalated with red shales. Shales Level (130 m). Aguasclaras Mb (152 m): thick-bedded gravels and sandy gravels with few intercalated shales. Capira Mb (200 m): very thick-bedded gravels without stratification.

Age. The age of the Hoyón Fm is not precisely stated. If the age of the Hoyón Fm is Eocene, as Van der Hammen proposed, there is a strong discrepancy with the coeval palynological assemblages in Venezuela. If the Hoyón is Oligocene in age, there must be a significant stratigraphic gap between the Seca Fm and the Hoyón Fm.

CHAPTER 3
Sequence Stratigraphy of the Cretaceous units from the Middle Magdalena Valley and the Western Margin of the Eastern Cordillera.

3.1 Introduction

The cretaceous clastic sediments in Colombia are normally composed of sediments derived from the Guyana Shield to the East, and from the Central Cordillera to the West. Most of the units comprise mainly fine-grain sediments like claystones and shales and also limestone, especially at the base. However, the presence of sandstone levels in different localities of the Middle Magdalena Valley (MMV) and western slope of the Eastern Cordillera (WEC) has to be analyzed to distinguish between tectonic, eustatic and sedimentary processes, and to provide information about the changes occurring in the basin. These changes have been analyzed in several sections of the study area. Based on well information (cuttings, wireline) and stratigraphic field sections, I built stratigraphic correlations and reconstructed the Cretaceous paleo-environments.

In spite, that identify the stratigraphic boundaries in fine-grained facies is not an easy task. I use the sequence stratigraphy concepts to determine the sequence boundarys (SB). However, the presence of sandstones in shallower environment and their distribution was important to analyze to understand the facies changes and sea level variations. For Example, in the area of Villa de Leyva, Etayo (1979) indicated that the Churuvita Formation is thinner to the south and sandier to the west. In the region of Samacá-Candelaria, Ulloa and Rodriguez (1991) showed the Churuvita Formation to be less calcareous and sand-rich, so they introduced the name of Areniscas de Chiquinquira, considering this new unit as a facial change of the Churuvita Formation. Fabre (1985) considered this unit as the western extension of the Une Sandstone.

In the study area, sedimentation is generally continuous and fine-grained, so unconformities are represented by correlative conformities (BSFR) or forced regression, represented by relatively shallow-water deposits with conformable bases (Posamentier et al., 1990; 1992). However, in the area of the MMV and the WEC the definition of the sequence was possible thanks to the use of the Fischer plot which is a powerfull method for interpretation in shallow-water, allowing to distinguish the local tectonic and sedimentologic effect on relative sea levels, from global eustatic oscillations or large-scale tectonic movements. Accommodation space plots were also used to make intrabasinal correlation (Figures 3.24, 3.36 and 3.47) and to corroborate our TR curves estimated in all studied Cretaceous sections. The well information was used to support the paleo-environmental interpretation and recognition of important unconformities during the cretaceous that represent the sequence boundaries.

During this work, several sections have been interpreted in the MMV and part of the WEC (Chapter 4) and four field sections from the WEC have been studied (Figure 3.1, 3.2, 3.3 and 3.5). Nearly 100 control points were visited in the field (Figure 3.3), to find evidences of mountain uplift through the observation of changes in the depositional setting (e.g. grain size, paleosoils, etc), not easy to obtain in the field due to restricted outcrops. Field geology generally provides scarce data, which are interpreted by each geologist with his own criteria (Asch, 2001). Nevertheless, the field evidences obtained from this work in the WEC and MMV, from wells in the MMV and some taken from other works in the WEC (Ulloa and Acosta (2001), Hernandez (1990), Caicedo, 2005, Terraza (2012), Reyes et al. (2006), etc), support the hypothesis that the Cretaceous basin was tectonically active.

3.2 **Materials and Methods**

In the MMV due to the widespread Quaternary cover, we used wells and logs information. In the WEC, outcrop information has been obtained from four field sections which are from south to north: The La Vega-Villeta Section, the Villa de Leyva – Chiquinquira section (central part), and the Barichara - San Vicente de Chucuri and Rio Sogamoso – Lebrija (northern section) (Figures 3.1, 3.2, 3.3). More than 100 samples from different units were taken and analyzed (Figures 3.2, 3.3 and 3.5).

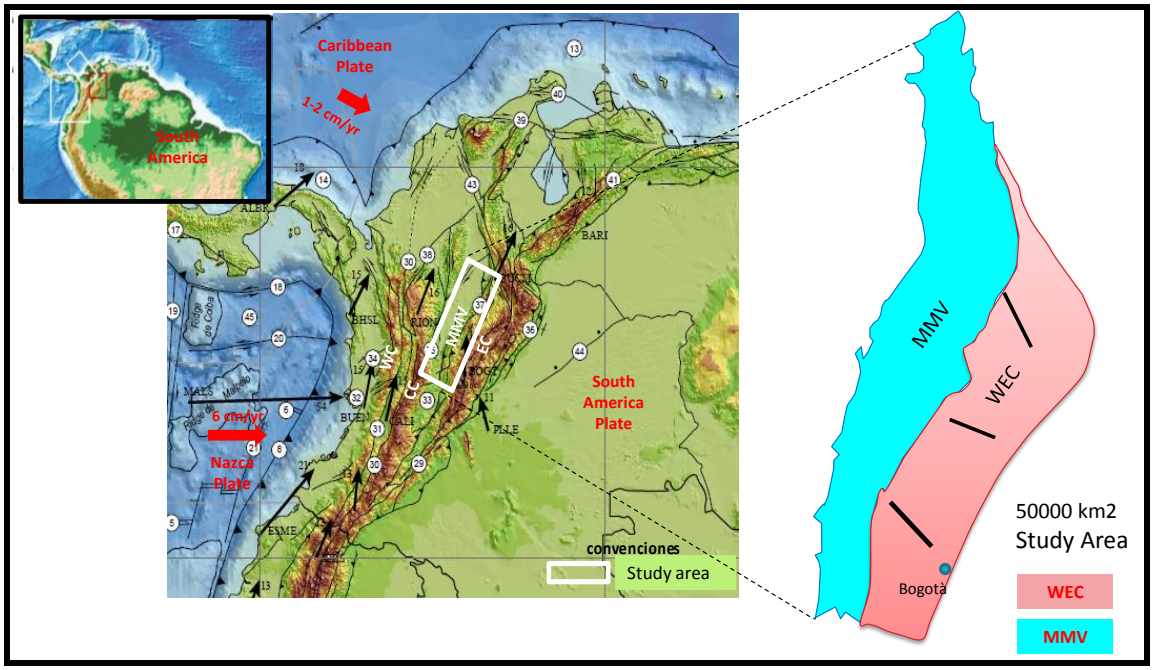

Figure 3.1 - Location map of the study area. MMV: Middle Magdalena Valley; WEC: Western flank of the Eastern Cordillera.

A general description of the stratigraphic units in the study area has been given in chapter 2 and its correlation is showed in the chart of Figure 3.4.

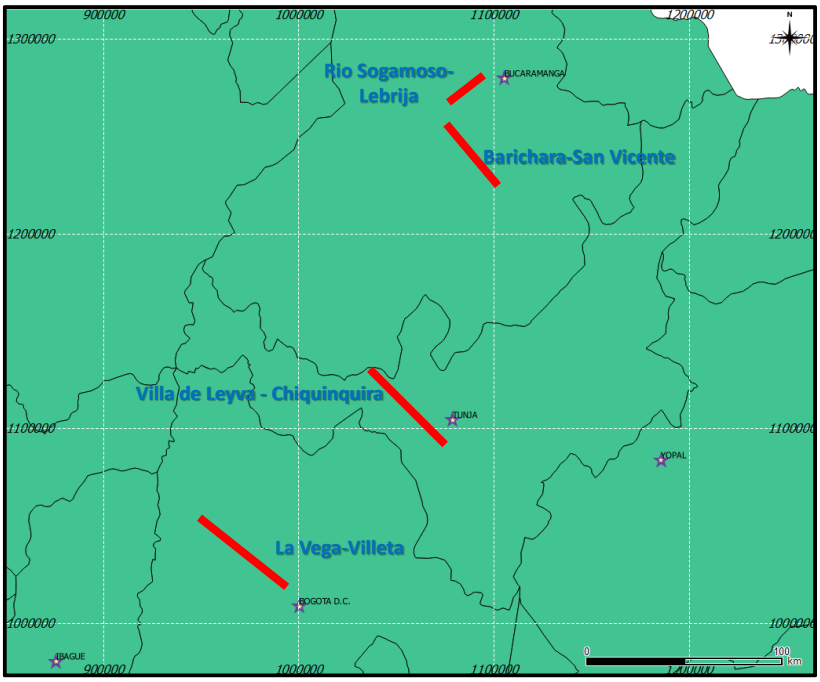

Figure 3.2 Field sections in the WEC.

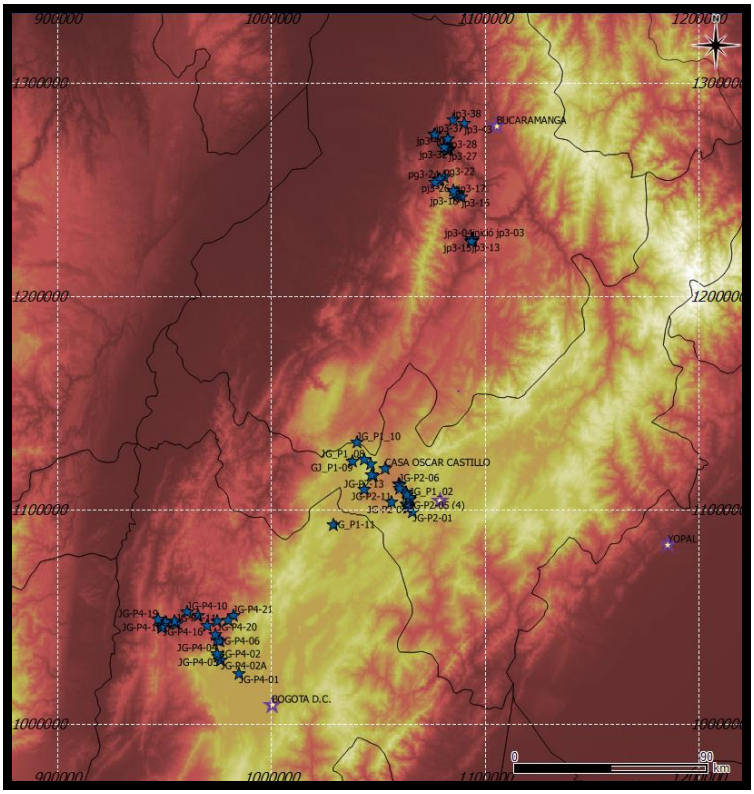

Figure 3.3 Location of field samples in the WEC.

Units of Jurassic to Recent age are present in the study area; however, the stratigraphic nomenclature changes from one area to another (Figure 3.4); in this chapter, we describe the units based on our observations (outcrops, drilling wells); complemented or modified with the information from others author. Stratigraphic sections are presented from South to North, with their lithological description, petrography, biostratigraphic

content and sedimentological interpretation. Then, the analysis and discussion of this information is presented.

For all regions, the sections containing biostratigraphic information are presented, to assign reliable ages to the units and, when was possible, to identify non-deposition or erosion events, and to specify the depositional environment and their changes with time. For each region a correlation was made, and facies changes and stratigraphic sequences were evaluated and interpreted. Stratigraphic sequence analysis was achieved through the Cretaceous stratigraphic succession to identify sea level fluctuation through time.

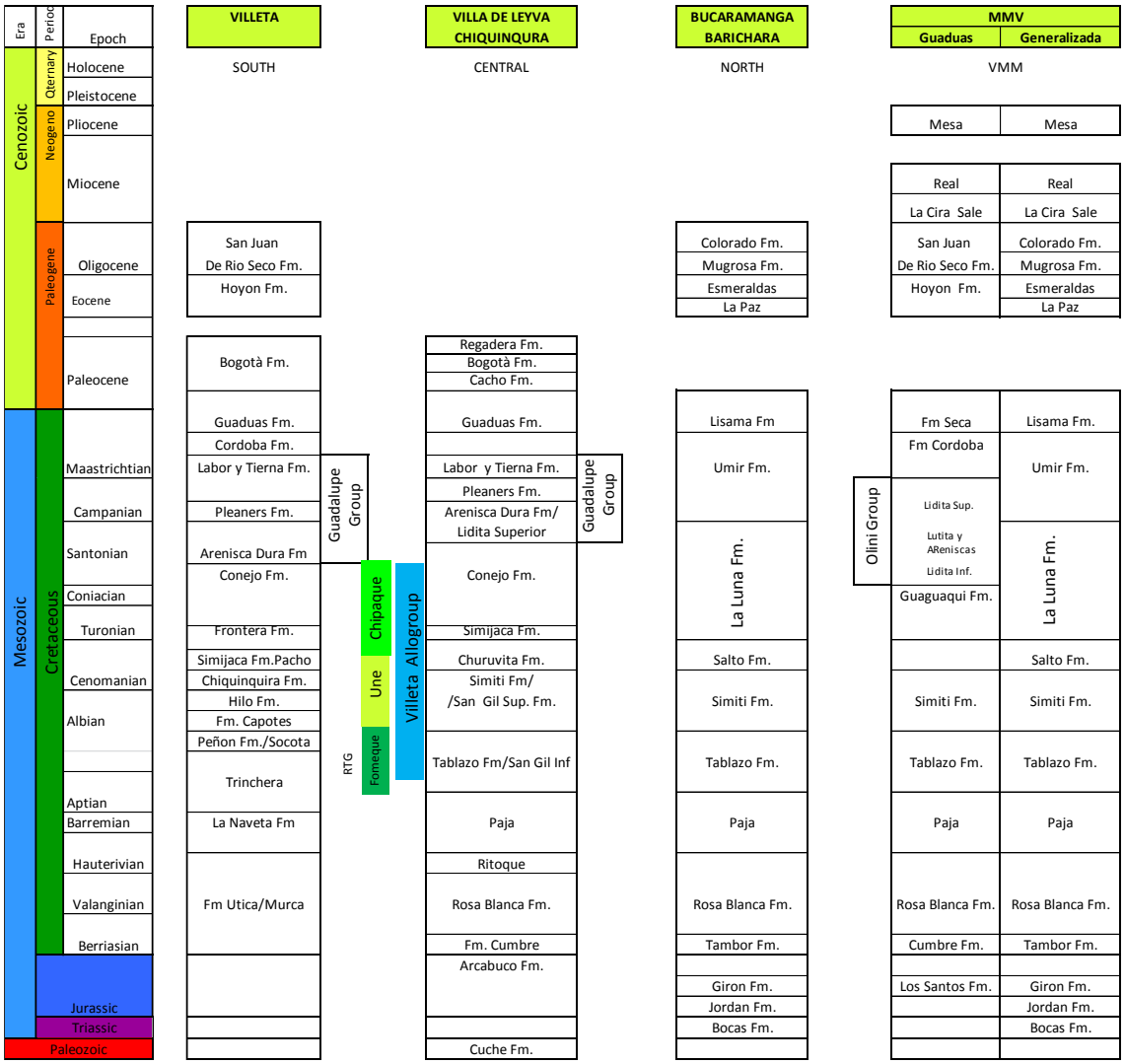

Figure 3.4. Correlation chart in the study area, showing the different nomenclatures used for different areas (compiled in this work).

Finally, facies distribution maps, taking into account the whole of the available information, were drawn for different ages, which show the sea level fluctuation. Several major transgressive-regressive cycles and depositional sequences were identified.

3.3 Key Terms and Definitions

Sequence stratigraphy is a method used to explain, describe or predict the occurrence, extension and geometry of the sedimentary facies, taking into account the fluctuations of sea level, subsidence rates, sediments input, climatic conditions and tectonic influences. For this purpose, we need to know the precise age of the units, and the depositional environment and geometry of the basin. However, part of this information is frequently not available. Well information, seismic models, biostratigraphy and geochemistry may offer additional information for the final interpretation.

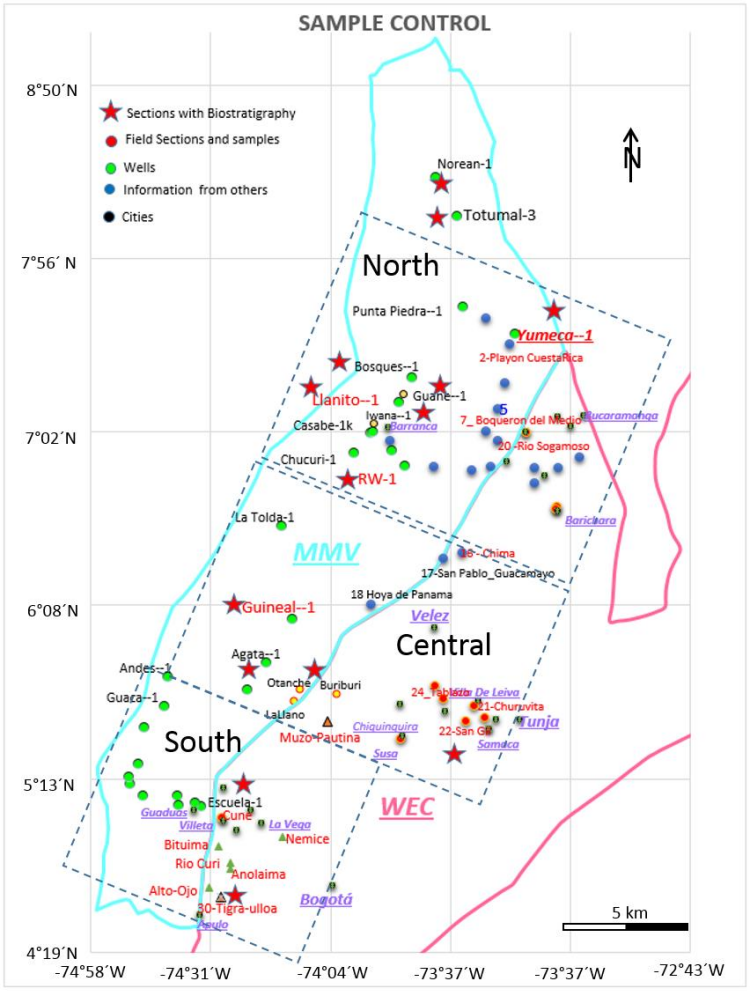

Figure 3.5 – *Location of wells and field sections. Green dots: wells; red dots: field sections and samples; blue dots: information from other authors; red stars: sections with biostratigraphy information; black dots: cities.*

Biostratigraphy is the age determination and correlation of rocks, based on their fossil content (Staines, 1985).

Chronostratigraphy is the branch of stratigraphy that studies rocks in terms of time (which includes system, series, epoch and sequential depositions) (Staines, 1985).

Lithostratigraphy is based only on the lithology of sedimentary units, regardless of biostratigraphy, paleomagnetism or any temporal relation (Staines, 1985).

Depositional system defines the sediment deposited during a specific segment of the sea level variation curve.

Seismic Stratigraphy is related to the lithology in the sub-surface and its stratigraphic relations based on the analysis of seismic reflectors.

Sequence stratigraphy is a multidisciplinary approach which uses available data (lithology, stratigraphy, seismic data and well logs) to identify the genetically related facies, located between key surfaces considered as time-lines. Units located between these regionally correlated key surfaces or regional unconformities are called depositional sequences (Vail, 1978). As the sequences tend to be cyclic, the relative positions of facies may be predicted. Therefore, the use of sequence stratigraphy generates a geologically sound and predictable stratigraphic framework.

Seismic data illustrates the regional framework and strata geometry; well logs provide precise information on lithology and depositional systems; biostratigraphy allows to identify condensed sections, chronostratigraphic surfaces, paleobathymetry and climatic conditions.

Sea level cycle is a complete period of rise and fall of the sea level. These cycles are controlled by events of different nature and have variable durations. A sea level cycle may be related to global, regional or local events. The stratigraphic record developed between two events of sea level fall is defined as a eustatic cycle (Vail et al., 1977). The latter comprises an initial period of sea level fall, followed by a period of sea level rise until the maximum immersion is reached, before a new period of sea level fall begins.

In many cases, age data is not accurate enough to know how much time is involved within a sequence, even in young and well explored basins (Catuneanu, 2006). Despite this, the hierarchy systems based on cycle duration are built on the assumption that the controls on cyclicity at specific hierarchical orders are predictable, repetitive, and unchanged during the evolution of the Earth. This means that the controls on stratigraphic cyclicity are governed by the law of uniformitarianism throughout the Earth´s history (Catuneanu, 2006).

Nevertheless, recent work on Precambrian geology (Catuneanu and Eriksson, 1999; Eriksson *et al*., 2004, 2005a, b) points to different conclusions (Catuneanu, 2006) emphasizing that the tectonic mechanisms controlling the formation and evolution of sedimentary basins, for the greater part of geological time, were far more diverse and erratic in terms of origin and process rates than originally inferred from the study of the Phanerozoic record. Similar conclusions have been reached studying the Milankovitch cycles, which demonstrate that the periods of precession and obliquity have changed significantly with time due to the continued evolution of the Earth-Moon system (Lambeck, 1980; Walker and Zahnle, 1986; Algeo and Wilkinson, 1988; Berger and Loutre, 1994).

Since the assessment of the duration of the cycles is sometimes problematic, a time-based hierarchy in the rock record is difficult (Algeo and Wilkinson, 1988; Carter *et al*., 1991; Drummond and Wilkinson, 1996), which is highlighted by the discrepancies in

the cycle duration established by different authors. For example, a third-order cycle has a periodicity of 1–10 Ma in the view of Vail *et al.* (1977), 0.5–3 Ma in the hierarchy of Mitchum and Van Wagoner (1991), 1–11 Ma according to Krapez (1996), and so on (Catuneanu, 2006).

To understand the changes around the basins, we use the hierarchy system based on cycle duration evaluated as follows:

First order cycles (> 50 Ma) are produced by plate tectonics. Eustatic cycles of higher frequency can be generated by variations in sea floor spreading, glacio-eustacy or astronomic factors (Milankovic theory). These cycles are labeled as follow:

Second order cycles (5 – 50 Ma) (Haq et al. 1987).

Third order cycles (0.5 – 5 Ma) are the fundamental units of sequence stratigraphy, as identified in outcrop or subsurface, and allowed to build the global sea level curve of Haq et al. (1987) (Figure 3.6).

Fourth order cycles (0.1 – 0.5 Ma) are present within third order sequences (Figure 3.6).

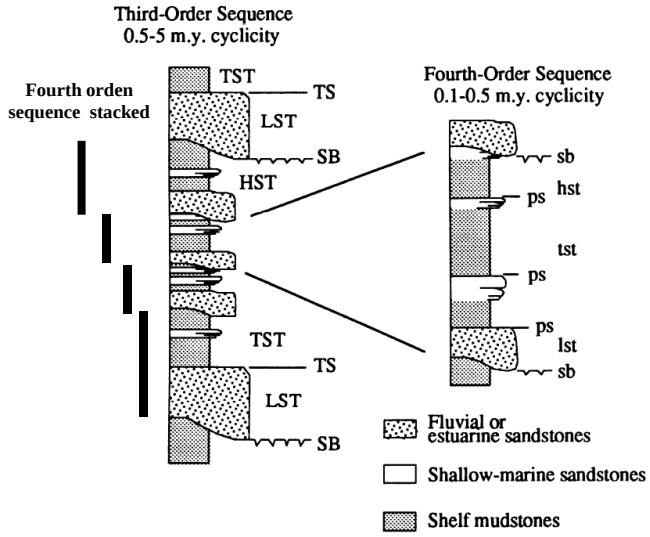

Figure 3.6 *- Stack of fourth order sequences and its correspondence with a third order sequence. Taken from Levy (1991).*

Fifth order cycle (0.01 – 0.1 Ma) are assumed to be controlled by orbital elements of the earth (Milankovitch).

Sixth order cycle (< 0.01 Ma).

Parasequence is a relative conformable succession of genetically related strata, bounded at the base and top by surface boundaries (SB) (Van Wagoner, 1985; Van Wagoner et al., 1988). In general, the parasequences are an upward-shallowing succession of facies (Figure 3.6, 3.7 and 3.8).

These parasequences can be (1) progradational (or forestepping), when the creation of accommodation space is lower than the sedimentation rate; (2) aggradational when the rate of accommodation space creation approximately matches the sedimentation rate;

and (3) retrogradional (or backstepping) when the creation of accommodation space is quicker than the sedimentation accumulation. (Van Wagoner, 1985).

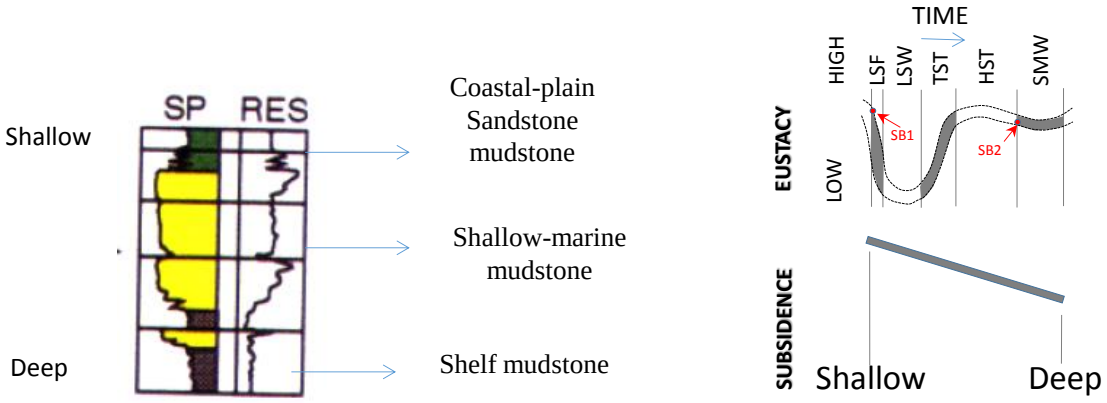

Figure 3.7 – Example of relation between a progradational parasequence set (right) modified from Wagoner et al. (1990) and a eustacy curve (left) modified from Hag et al (1987). HST = Highstand Systems track, TST = Transgressive systems track, LSW = Lowstand Wedge systems track, LSF= Lowstand fan system track SMW = Shelf margin wedge system tract.

Sequence model / Events	Depositional Sequence II	Depositional Sequence III	Depositional Sequence IV	Genetic Sequence	T-R Sequence
	HST	early HST	HST	HST	RST
end of transgression					
	TST	TST	TST	TST	TST
end of regression					
	late LST (wedge)	LST	LST	late LST (wedge)	RST
end of base-level fall					
	early LST (fan)	late HST (fan)	FSST	early LST (fan)	
onset of base-level fall					
	HST	early HST (wedge)	HST	HST	

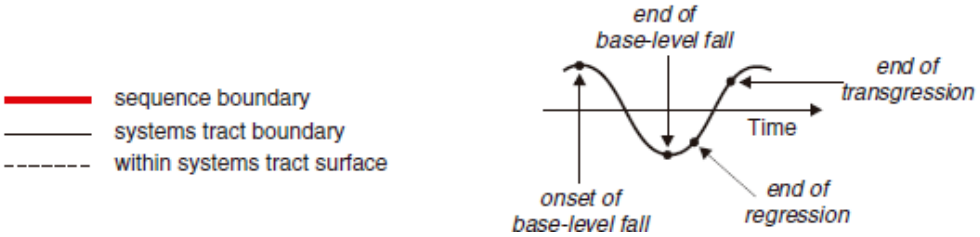

Figure 3.8 – Nomenclature of systems tracts and timing of sequence boundaries for the various stratigraphic sequences approached (modified from Catuneanu, 2002). In the graph: LST - lowstand systems tract; TST—transgressive systems tract; HST—highstand systems tract; FSST—falling-stage systems tract; RST—regressive systems tract; T–R— transgressive-regressive.

Lowstand System Track (LST) is deposited during a relative sea-level fall and the early phase of sea level rise. LST sediments often fill or partially fill incised valleys that were cut in earlier deposits by subaerial erosion during platform emergence. Incised valley fills (ivf) are the only deposits of the LST that are laid down on the emergent shelf. In seismic lines, they are expressed by the erosional truncation of the underlying sequence and internal onlap. The earlier term ´Shelf-margin Systems Tract (type 2 of Posamentier et al., 1988), is nowadays left out (Posamentier and Allen, 1999; catuneanu, 2006) because these deposits are now considered part of LST.

The Lowstand Prograding Wedge (lpw, or lowstand prograding) is overlain by the TST. The lpw varies from fluvial-coastal to shallow-marine environment at the base, to hemipelagic facies and, in some cases, overlapping turbidites at the top. In well logs, the lpw is funnel shaped (Figure 3.9). It may be recognized in seismic lines by offlap aggradational.

The Transgressive System Tract (TST) is an indicator of a transgressive regime, since it is deposited during relative sea-level rise. It is comprised between the transgressive surface at the top the LST, and the MFS at its top (Catuneanu et al. 2011). The TST is composed of retrogradational parasequences, which become thinner and deeper upward. As the TST overlaps the shelf, it fills the incised valleys. The TST usually overlies the SB landward of the shelf border. It presents a bell shape (fining upward) in well logs (Figure 3.9).

The Highstand System Tract (HST) is an indicator of a high sea-level and is widely distributed on the shelf. Its basal limit is the MFS and its top is the SB on the shelf and the shelf edge. In the HST parasequences grade upward from aggradational to progradational, and their depositional environment also becomes shallower. In the basin it is represented by a condensed section. The top of the HST downlaps seaward and is also marked by toplaps and erosional truncations below the upper SB. The HST is deposited during the last phase of relative sea-level rise and the early stage of relative sea- level fall. In well logs it is represented by a funnel shape.

In this analysis I used well log shapes and description lithology in wells. The log shapes typically show changes in the depositional regime. Funnel shapes suggests coarsening-upward, which means increasing-upward energy; bell shapes mean fining-upward grain and a decrease in current energy; and cylinder shapes mean relative constant grain size and depositional energy (Figure 3.9).

Figures 3.9, 3.10 and 3.11 show some examples of log shapes related to depositional environments.

As quoted by Catuneanu (2006), efforts are being made to clarify the meaning of “unconformity-bounded units” and “discontinuity-bounded units”. In this way, the term unconformity was refined by Bates and Jackson (1987), who distinguished unconformity, diastem and conformity (Figure 3.12).

Unconformity represents an important gap in the geological record; usually related to uplift and erosion, which possibly implies loss of previous deposits (due to subaerial or

subaqueous erosion, non-deposition or weathering). Hence, the term unconformity (Bates and Jackson, 1987) comprises (1) Disconformity, when the beds above and below the hiatus are essentially parallel; (2) Paraconformity, when the overlying and underlying beds are parallel and there is an uncertain erosional or hiatus unconformity;

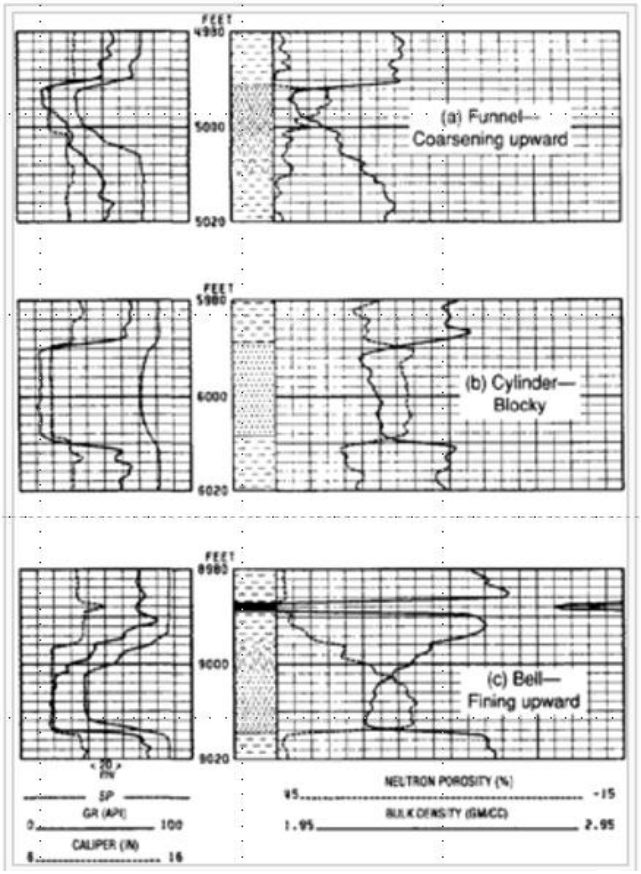

Figure 3.9 *– Types of log shapes; a) Funnel shape: coarsening upward; b) Cylinder shape – blocky; c) Bell shape: fining upward.*

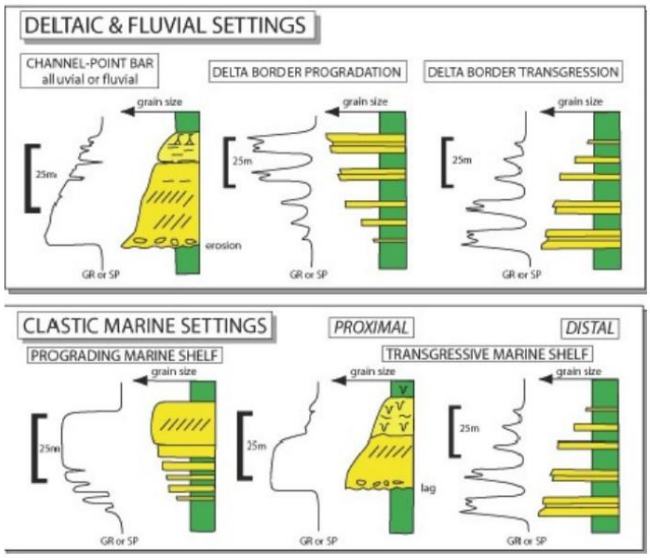

Figure 3.10 *- Examples of gamma Ray response to different depositional environments (from Tsai-Bao Kuo, 1986)*

(3) Angular unconformity, when the beds above and below the surface are not parallel, (Bates and Jackson, 1987)

(4) Nonconformity, when sediments are deposited over old basement rocks (Bates and Jackson, 1987 in Figure 3.12).

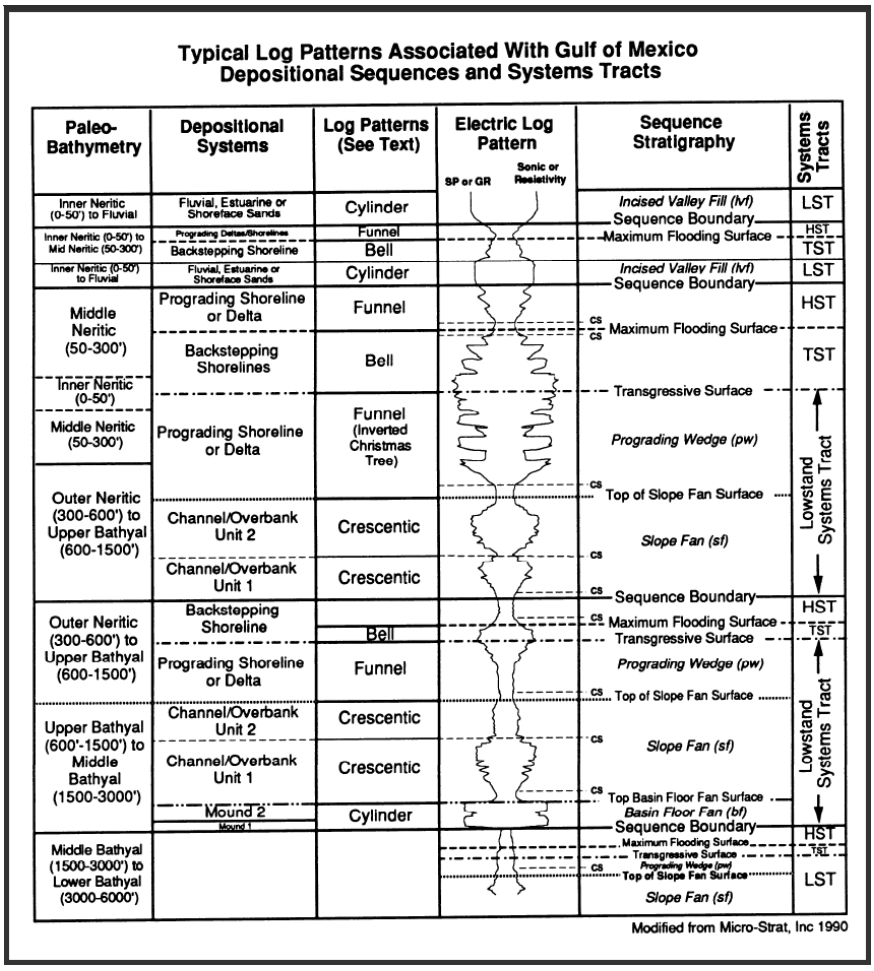

Figure 3.11- Example of curve patterns, their system tracks and their possible depositional environment in the Gulf of Mexico (taken from Micro-Strat, inc., 1990).

Diastem corresponds to a short interruption of sedimentation, where little or no erosion is present (Bates and Jackson, 1987).

Conformity marks the lack of hiatus and a stratigraphic continuity in the sequence. When sediments are laid down one above the other in uninterrupted succession, the so formed strata are said conformable (Bates and Jackson, 1987).

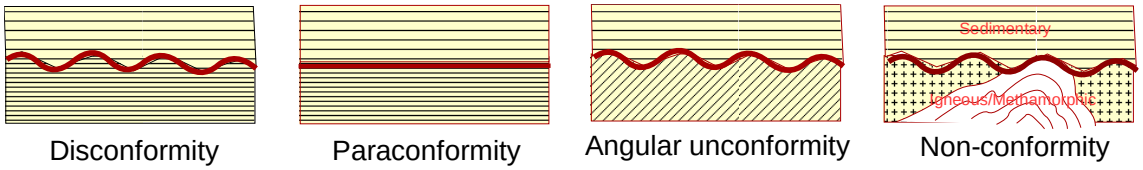

Figure 3.*12 – Types of stratigraphic contacts (modified from Bates and Jackson, 1987)*

In the early stages of sea level rise (after sea level drop), sedimentation rate is most likely to outpace the rate of creation of accommodation, leading to a *'normal' regression* of the shoreline, thus continuing the regressive trend. The end of shoreline regression, therefore, does not coincide with the end of base-level fall, but rather with an early stage of base level rise. Once the increasing rate of base-level rise outpaces the sedimentation rate, the *transgression* of the shoreline begins (Figure 3.13).

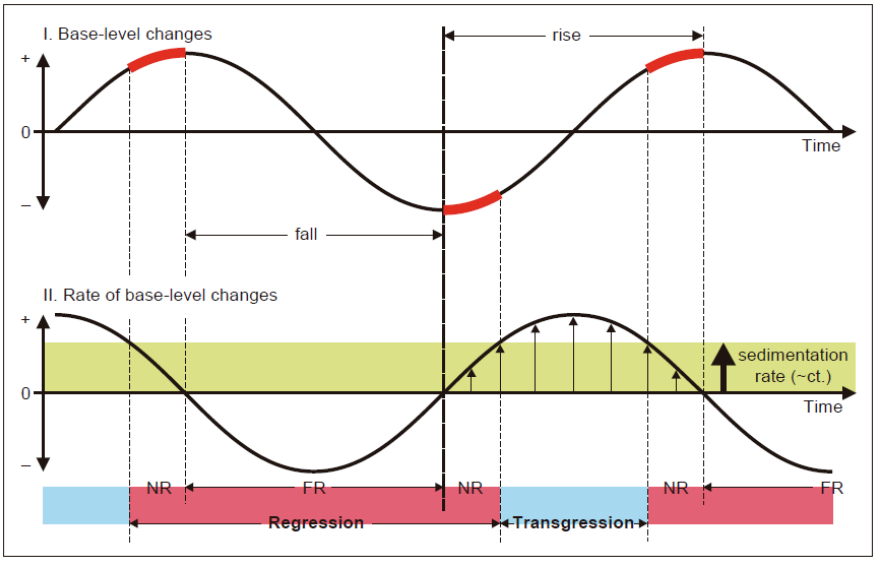

Figure 3.13 – Concept of transgression, normal regression and forced regression, showing the relation between base-level changes (blc) and sedimentation.
The upper sine curve shows the magnitude of base level changes through time; the red portions in this curve indicate early and late stages of base-level rise (increasing from zero and increasing to zero, respectively) are outpaced by sedimentation rates.
Below: The green area shows the constant sedimentation rate; the black curve shows the rate of base-level change, which equals zero at the end of base-level rise and base-level fall stages. Transgression occurs when the rate of base level rise outpaces the sedimentation rate, for simplicity the reference base-level curve is symmetrical but in the real case asymmetrical is more likely in the geological record.
Abbreviations: FR-forced regression; NR-normal regression (from Catuneanu, 2004a).

In the last stages of base-level rise, when sea-level rise rate is low (decreasing to zero), sedimentation takes over once again, triggering a second *'normal' regression* of the base-level cycle. Therefore, the end of shoreline transgression does not occur during the onset of base level fall, but rather during the late stages of base-level rise (Fig. 3.13). The curve shows that transgressive stages are shorter in time (less than half of a cycle), relative to the regressive stages (normal plus forced). However, the duration of transgressive and regressive periods changes according to the basin (Catuneanu, 2004a).

In Figure 3.13 above the black curve constant sedimentation rates are assumed, but the real function curve can be asymmetrical to represent the realistic fluctuations through time (Catuneanu, 2006).

Base level changes are idealized (symmetric sine curves) in Figures 3.13 and 3.14, but in reality, for example the tectonic control on base-level, may generate asymmetrical base-level curves. As a function between sedimentation and base-level fluctuations (Figures 3.13 and 3.14), four main events associated with changes in depositional trends

are recorded during a complete cycle of baselevel shifts, 1) onset of forced regression; 2) end of forced regression (end of base-level fall); 3) end of regression (marks the change from regression to transgression); end of transgression (base-level rise) marks the change in the direction from transgression to regression (Figure 3.14 and 3.15).

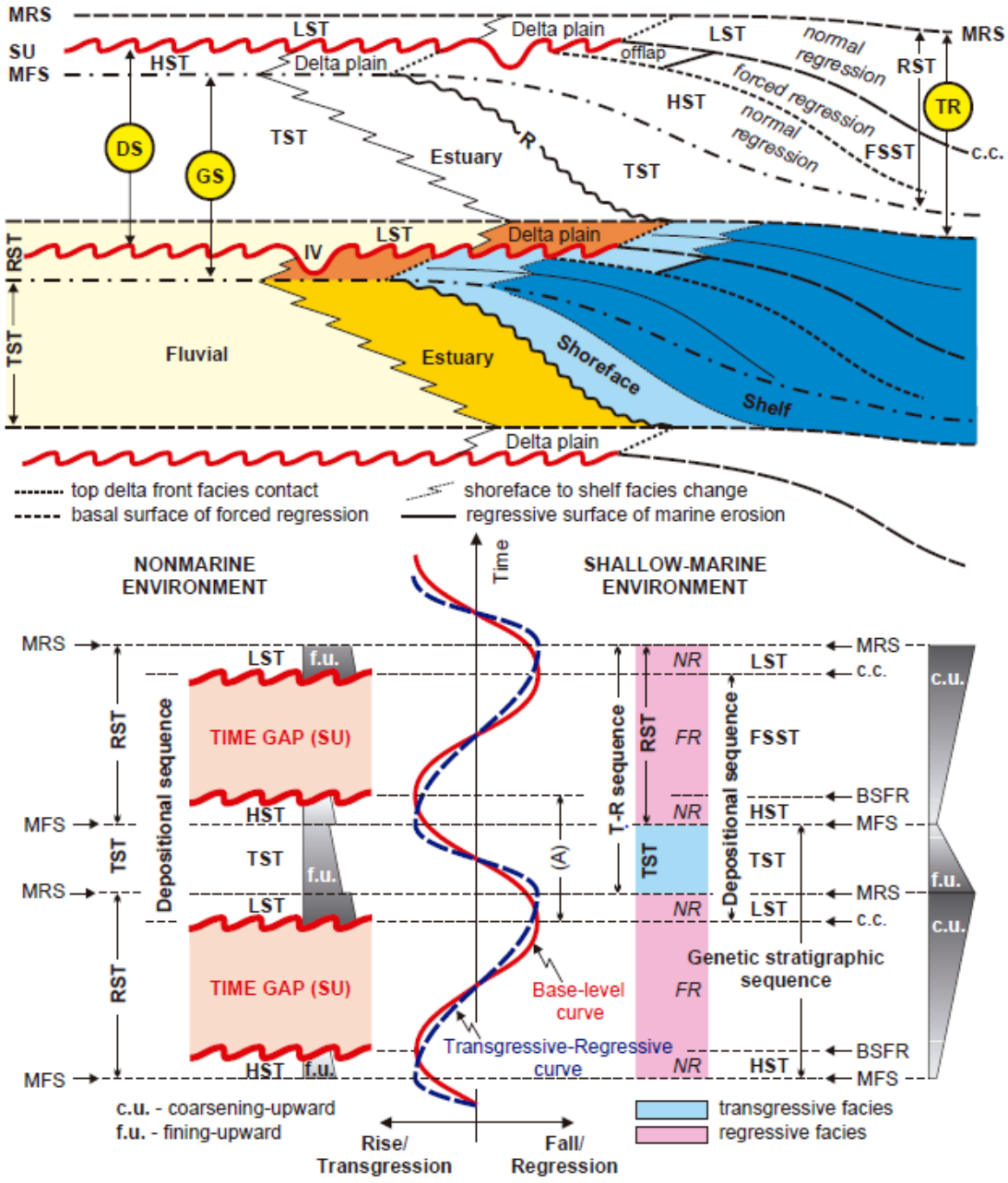

Figure 3.14 – Stratigraphic surfaces, sequence and system tracts defined based of sea-level and Transgressive-Regressive curves (in Catuneanu 2006*). MFS (Maximum flooding surface); MRS (Maximum Regression surface); BSFR - Basal surface of forced regression (correlative conformity sensu Posamentieretal., 1988); NR – Normal Regression; FR – Forced Regression; HST – highstand system track ; LST – lowstand system track (Hunt and Tucker, 1992); TST – transgressive system track; FSST – Falling-stage system track); DS – depositional sequence; GS – genetic stratigraphic sequence; TR – transgressive – regressive sequence ; NR –normal regression; FR – forced regression; R – transgressive wave-ravinement surface; IV –incised valley; A – positive accommodation (Base level rise).*

3.3.1 Transgressive – Regressive Curve

The onset or end of regression or transgression are shown in Figure 3.15. Each surface may be defined as a distinct stratigraphic contact that marks a specific event or stage of the base level cycle.

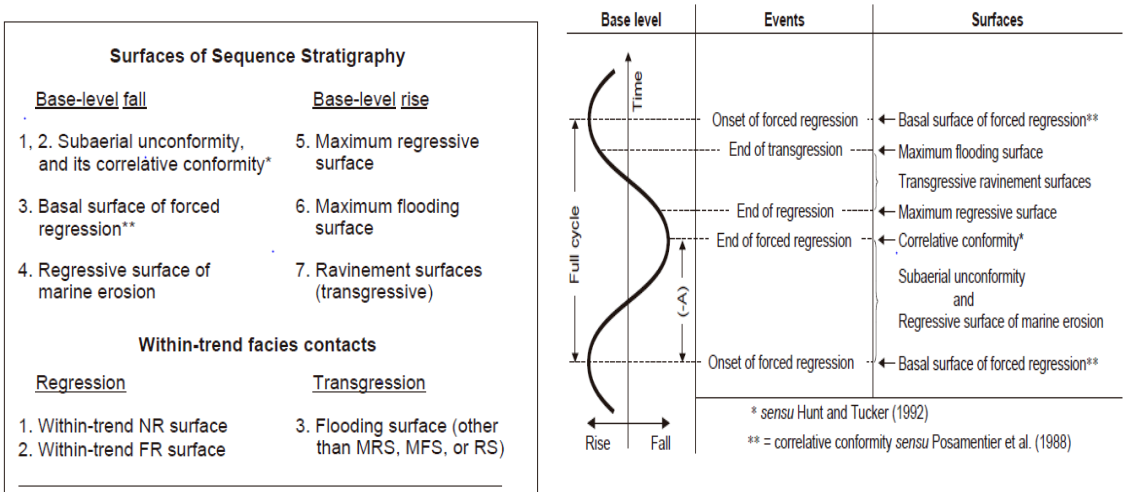

Figure 3.15. Transgressive –regression curve (base-level cycle) relative to the main events (Modified from Catuneanu et al., 1998b and Embry and Catuneanu, 2002. - In Catuneanu, 2006).

Seven surfaces of sequence stratigraphy are shown in Figure 3.15 during a full cycle (basal surface or forced regression, subaereal unconformity and correlative conformity, maximun regression surface, maximun flooding surface). The subaerial unconformities are surfaces of erosion or nondeposition created during base-level fall. Subaerial unconformities correspond to long-lasting stratigraphic hiatuses, which separate genetically unrelated strata (Figure 3.14; Catuneanu, 2006), and laterally grade to correlative marine conformity, whose age corresponds to the end of the base-level fall (*sensu* Hunt and Tucker, 1992).

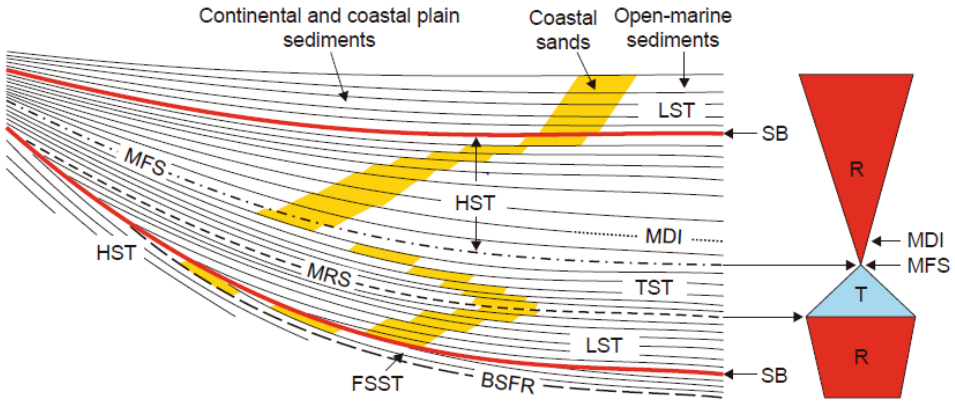

Figure-3.16. Sequence stratigraphic model for a low gradient ramp in an intracratonic basin (modified by Vecsei and Duringer, 2003). Abbreviations: HST—highstand systems tract; FSST—falling-stage systems tract; LST—lowstand systems tract; TST—transgressive systems tract; SB—depositional sequence boundary; BSFR—basal surface of forced regression; MRS—maximum regressive surface; MFS—maximum flooding surface; MDI—maximum depth interval; regression and coarsening upward (R); transgression and fining upward (T).

Sequence stratigraphy was interpreted using the information of each column, based on the identification of regressive, coarsening upward trends (R) and transgressive fining upward trends (T) (Figure 3.16). The water depth in any location depends on the interaction between subsidence, sea level changes and sedimentation. In this way, subsidence and sea-level rise produce water deepening, and sea-level fall and sedimentation produce water shallowing. Alternatively, sedimentation developed during transgressive and regressive shifts of the shoreline are controlled by sediment supply and depositional energy (Catuneanu, 2006).

3.4. Stratigraphic nomenclature

In the study area, a wide variety of nomenclature has been used by successive authors. Figure 3.4 shows the nomenclature used, from south to north, in the WEC and in the MMV. In the MMV and in the northern area of WEC (Bucaramanga-Barichara) the nomenclature is basically the same, as well as in the central area for the Valanginian to Cenomanian interval. Elsewhere, nomenclatures are different, especially in the Villeta area, where the nomenclature is shared only for the Turonian - Paleocene interval. Figure 3.4 shows the lithological units and their correlations from one region to others. The principal units and their equivalents were described in Chapter two.

3.5 Stratigraphic sections

Different stratigraphic sections will be described from South to North (area of Villeta, Villa de Leyva and Bucaramanga), in order to detect the changes along the basins.

The studied sections and their vertical evolution are shown in Figures 3.17 to 3.46; as well as regions presenting some biostratigraphic information (Figures 3.17 to 3.23 in the South; Figures 3.25-3.35 in the centre; Figures 3.37-3.46 in the North) to corroborate the age of the units and to obtain information, if available, about depositional environments.

The sections from these three zones (south, central and North) were used for correlations: The La Tigra to the Esculela -1 section to the South (Figure 3.24), from Villa de Leyva to Guineal in the centre (Figure 3.36) and from Barichara to the Chucuri-1 section to the North (Figure 3.47). For all sections the transgressive-regressive curves have been interpreted, and relative sea-level variations have been obtained from outcrops and wells, using the accommodation space plots or Fischer plots (Fischer, 1964). These curves do not provide the absolute magnitude of sea level fluctuation, they provide stacking patterns that can be interpreted in terms of relative sea level fall and rise, condensed intervals and sequence boundaries.

The Fischer plot is a powerfull method for basin analysis and geohistoric interpretation in shallow-water carbonate systems (Villamil, 1998). With this method, the sea-level history of different basins can be defined and compared, and it allows to distinguish local tectonic and sedimentologic effects on relative sea level, from global eustatic

oscillations or large-scale tectonic movements (Villamil, 1998). Our main aim is to identify the regional events (second order cyles from 5 – 50 My), which are assumed to be caused by eustatic or large-scale tectonics. Accommodation space plots were also used to make intrabasinal correlation (Figures 3.24, 3.36 and 3.47) and to corroborate our TR curves estimated in all studied Cretaceous sections. The well information was used to support the paleo-environmental interpretation.

3.5.1 Southern region

- **La Tigra section**

In the La Tigra section, the studied sequence corresponds to the Trinchera Formation (Fm) of Barremian-Early Aptian age. The name was given by Cáceres and Etayo (1969) to describe a sequence of mudstone with intercalation of limestone and sandstone in the lower part. For further description see chapter 2.

Caceres and Etayo (1969) collected *Heinzia, Pseudohaploceras, Heminautilus etheringtoni* and *Cheloniceras*, of Barremian to Early Aptian age.

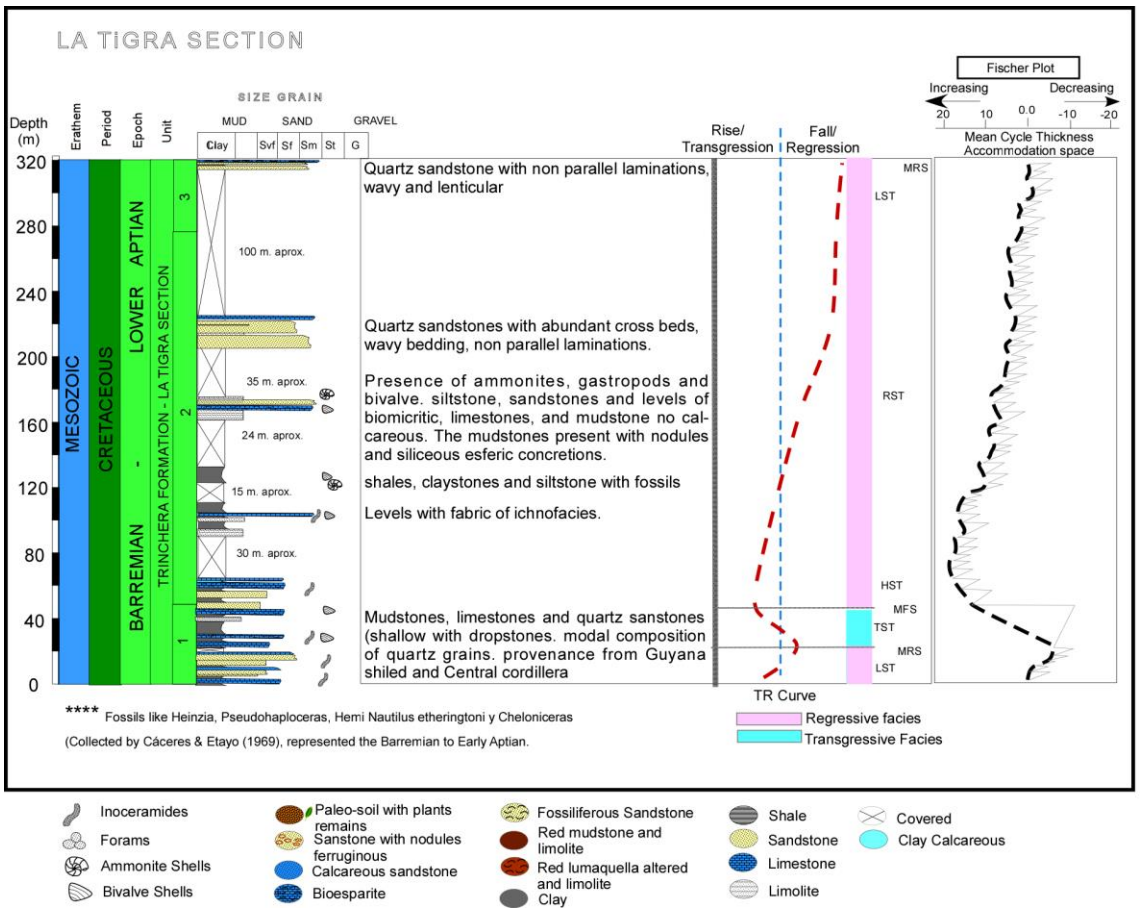

Figure 3.17. La Tigra stratigraphic section, near the town of Villeta, corresponding to the Trinchera Fm (Barremian - Early Aptian). Two successions of sandstones are shown at the base and top of the section. (Drawn after personal observations and from Ulloa and Acosta (2001), stratigraphic interpretation from this work.)

The abundance of benthonic foraminifera in the section suggests a shallow mixed siliciclastic-calcareous system, with well oxygenated water, while the accumulation of shells, crinoids and gastropods, and sedimentary structures like wavy lamination and dropstones, suggest episodes of high energy, especially in the lower segment.

The facies succession in the lower segment (mudstone, sandstone and limestone) is interpreted as a shallowing-upward sequence of autocyclic origin. However, Ulloa and Acosta (2001) reported the presence of dropstones of up to 20 cm of diameter and a possible unconformity (aggradational cycles of Anderson and Goodwin, 1980; in James, 1984), and they suggested the existence of a regional discordance for Barremian-Aptian or Upper Aptian as suggested by Maceralli (1988).

Ulloa and Acosta (2001) proposed a mixed provenance for the sandstone, suggested by monocrystalline quartz grains derived from a recycled orogen, and by volcanic fragments proceeding from a magmatic arc (Dickinson, 1988). This suggests that input came from the Guyana shield to the East and from the volcanic Cretaceous basement of the ancestral Central cordillera (Saldaña Fm) to the West (Cediel et al., 1980).

In this section (Figure 3.17) I interpreted the existence of cycles from TST-HST-RST-LST (retrogradational-aggradational-progradational and high aggradational). The second cycle lacks the RST (FSST), which probably represents an erosional unconformity as shown in Figure 3.14. This unconformity is of Late Barremian-Early Aptian age.

- **Alto-Ojo stratigraphic section**

South of the town of Villeta, the Alto-Ojo section allows to study the Upper Aptian to Lower Albian rocks of the Socota Fm (Figure 3.18).

The lower part is constituted by black, laminated, calcareous mudstone, with thin intercalations of quartz siltstone, and fine-grained quartz sandstone with calcareous cement. The lamination varies from parallel at the base to undulating at the top, with increasing sandstone content. At the base, thin layers of limestone, locally lenticular, and micritic concretions can be observed, as well as ammonites and fish-remains, usually at the top of the coarsening- and thickening-upward sequences.

In segment 2, thin to coarse layers of fine- to medium-grained quartz sandstone with calcareous cement dominate; they show undulating laminations of mudstone, quartz siltstones and calcareous siltstone. These facies are arranged in coarsening- and thickening-upward sequences. Occasionally, mudstone with flaser bedding yield ammonoids, carbonized wood-remains, leaves and calcareous concretions generally with diameters < 15 cm. Petrographically, the quartz-sandstone is mainly composed of angular monocrystalline quartz, corroded by calcareous cement.

Etayo (1979), determined the *Dufrenoyia sanctorum-Stoyanowiceras treffryanus*, and the *Parahoplites (?) hibachi - Acanthohoplites (?) leptoceratiforme* assemblage zones, which indicate a Late Aptian age.

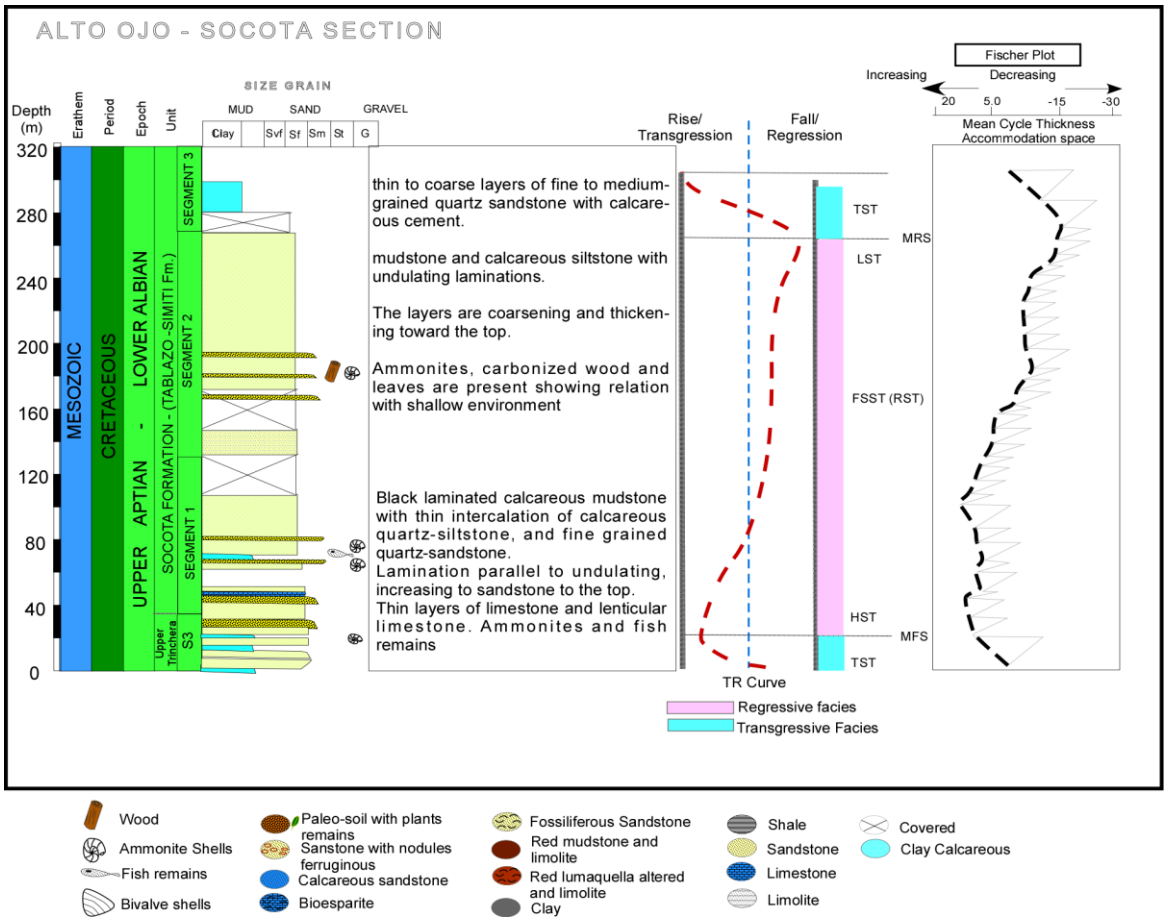

Figure 3.18 Alto-Ojo Stratigraphic section, near to Villeta town, corresponding to the Socotá Fm (Tablazo-Simiti Fm, Upper Aptian - Lower Albian). A thick succession of sandstone is capped by mudstone and calcareous siltstones (Drawn after personal observations and from Ulloa and Acosta (2001), stratigraphic interpretation from this work.)

- **<u>Quebrada Cune Section</u>** (Early Aptian-Late Aptian)

The Quebrada Cune section is located near the town of Villeta in the Cune creek. The sequence is composed at the base by 30 cm to 2 m thick beds of fine- to medium-grained sandstone, separated by thin (5 cm to 15 cm) interbeds of black to grey, siliceous shales and claystones (Figure 3.19; photo 3.1). Some layers are lens-shaped at the centimeter to meter scale (Figure 3.19; photo 3.2), which, according to field observations and comparison, corresponds to the Early Aptian Upper Trinchera Fm (Figure 3.19).

Sample JG-P4-12 was taken from a sandstone with planar lamination and internal cross-bedding (detail in photo 3.1). In thin section (Petrographic Section. 3.1) is composed of quartz crystal (43%), volcanic fragments (30%), plagioclase (17%), chert (6%), micas (4%), oxides (1.7%) and heavy minerals (0.4%).

This rock was classified as an immature feldspar litharenite (Folk, 1974). In sample JG-P4-12, grain size ranges from 100 to 300 µm. Sample JG-P4-12 is finer-grained than sample JG-P4-13.

At the same level as sample JG-P4-12 I observed lens shaped levels or lenticular beds within a fine lithology as shown in detail in photo 3.2.

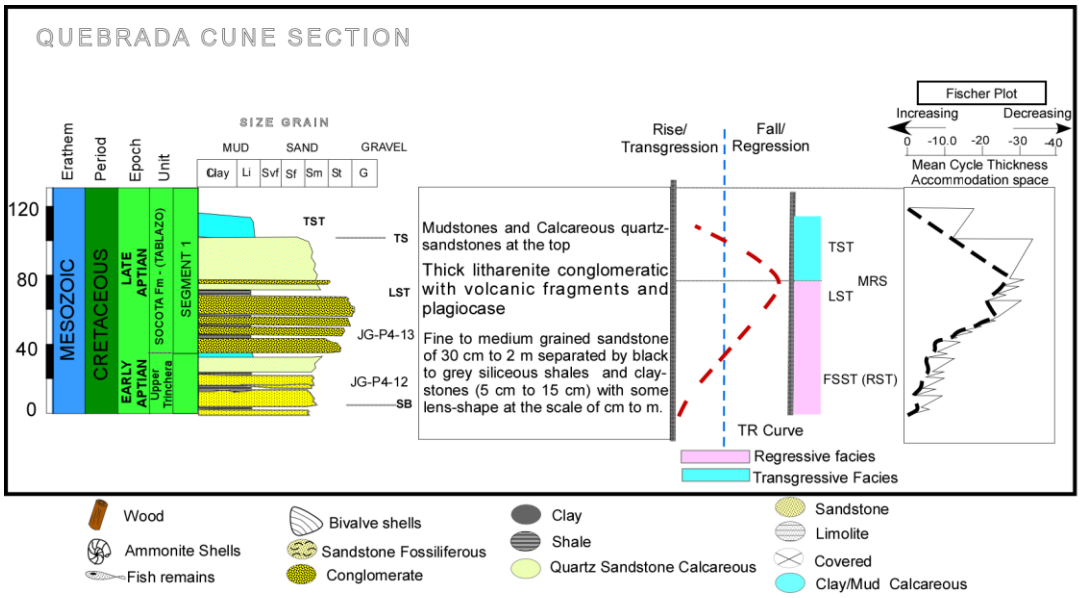

Figure 3.19 - Quebrada Cune stratigraphic section, near the Villeta town, corresponding to the Trinchera and Socotá Fms (Late Aptian). Thick beds of sandstones capped by thin shales are overlain by thick conglomerate levels; mudstone crops out at the top. Personal observations.

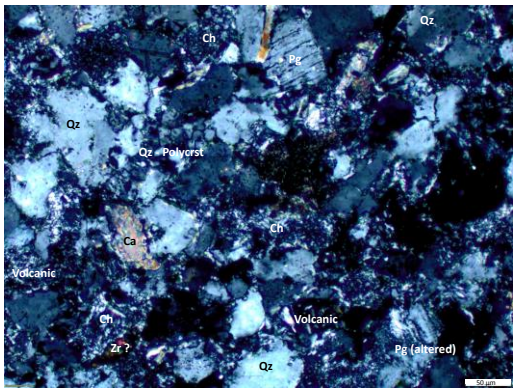

Petrographic section 3.1. Thin section of sample JG-P4-12, sandstone from the Trinchera Fm (Figure 3.19). Classified as litharenite (Folk 1974).

In sample JG-P4-13, grain size varies from 400 to around 1000 μm. The composition is: quartz grains (45%), plagioclase (38.5%), chert and volcanic fragments (14.5%), micas (1%) and oxides (1%). The plagioclase is altered to albite and probably to microcline. Quartz grains are made up of two or more crystals, they show undulating extinction and slight differences in color, which result from deformation and mostly characterize metamorphic sources. There are rock fragments made up of very-fine-grained quartz (micro-quartz), with appearance of chert. This rock may be classified as a medium- to coarse-grained litharenite (feldspathic litharenite).

Photo 3.1. Litharenite of Early Aptian age (Upper Trinchera Fm). Note the lens-shaped layers and cross laminations (upper red square).

Photo 3.2. Siliceous sandstone (Upper Trinchera Fm, Early Aptian). Note the lens-shaped layers (upper red square).

Photo 3.3. Conglomerate in the Trinchera/Socota Fm (Late Aptian – Early Albian).

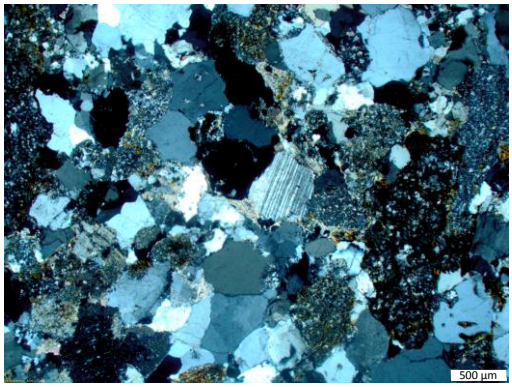

Petrographic Section 3.2. Sample JG-P4-13 corresponding to the conglomeratic sandstone in the Trinchera/Socota Fm shown in photo 3.1.

Based on the presence of *Heinzia*, *Pseudohaploceras*, *Heminautilus etheringtoni* and *Cheloniceras* (Caceres and Etayo, 1969) in the Trichera Fm and of the *Stoyanowiceras treffryanus*, *Dufrenoyia sanctorum* and *Parahoplites (?) hibachi – Acanthohoplites (?) leptoceratiforme* zones in the Socota Fm, the age of this section extends from Early Aptian to Late Aptian (Figure 3.19).

As shown in Figure 3.19, the Quebrada Cune section (Early to Late Aptian) shows a coarsening-upward evolution from the base to the middle part of the section, which may represent the last part of the RST reaching a maximun regression (MRS) at meter ≈ 80. Upward, the series is interpreted as a TST.

- **Bituima section** (Late Aptian-Late Cenomanian)

This sequence encompasses the Late Aptian to Late Cenomanian interval (Socota, Hilo and Simijaca Fms). Its lower part (Late Aptian, Socota Fm) comprises from base to top: 1) fossiliferous sandstones (Socota member), 2) gray shales, 3) lutites and fossiliferous marls, 4) "Horizon of Esferitas" of Hubach (1931b; Cáceres and Etayo, 1969) and clay and calcareous mud, with some levels of siliceous siltstones and few thin layers of limestones. It is overlain by Late Albian-Early Cenomanian units (Hilo Fm, correlated with the Areniscas de Chiquinquira), which correspond at the base to calcareous mudstones, sometimes slightly siliceous, with layers of micrite and casts of inoceramids and ammonites (Figure 3.20). The middle part of the Hilo Fm is made of black calcareous mudstone, locally siliceous layers of chert with wavy bedding, with thin to

thick beds of biomicritic limestones. Siliceous levels contain planktic foraminifera dissolved and filled with calcite or silica, in a matrix of amorphous silica and organic material (Figure 3.20). The upper part of the Hilo Fm is composed of calcareous mudstone, slightly siliceous, with some micritic concretions and layers of lenticular limestone with casts of ammonites.

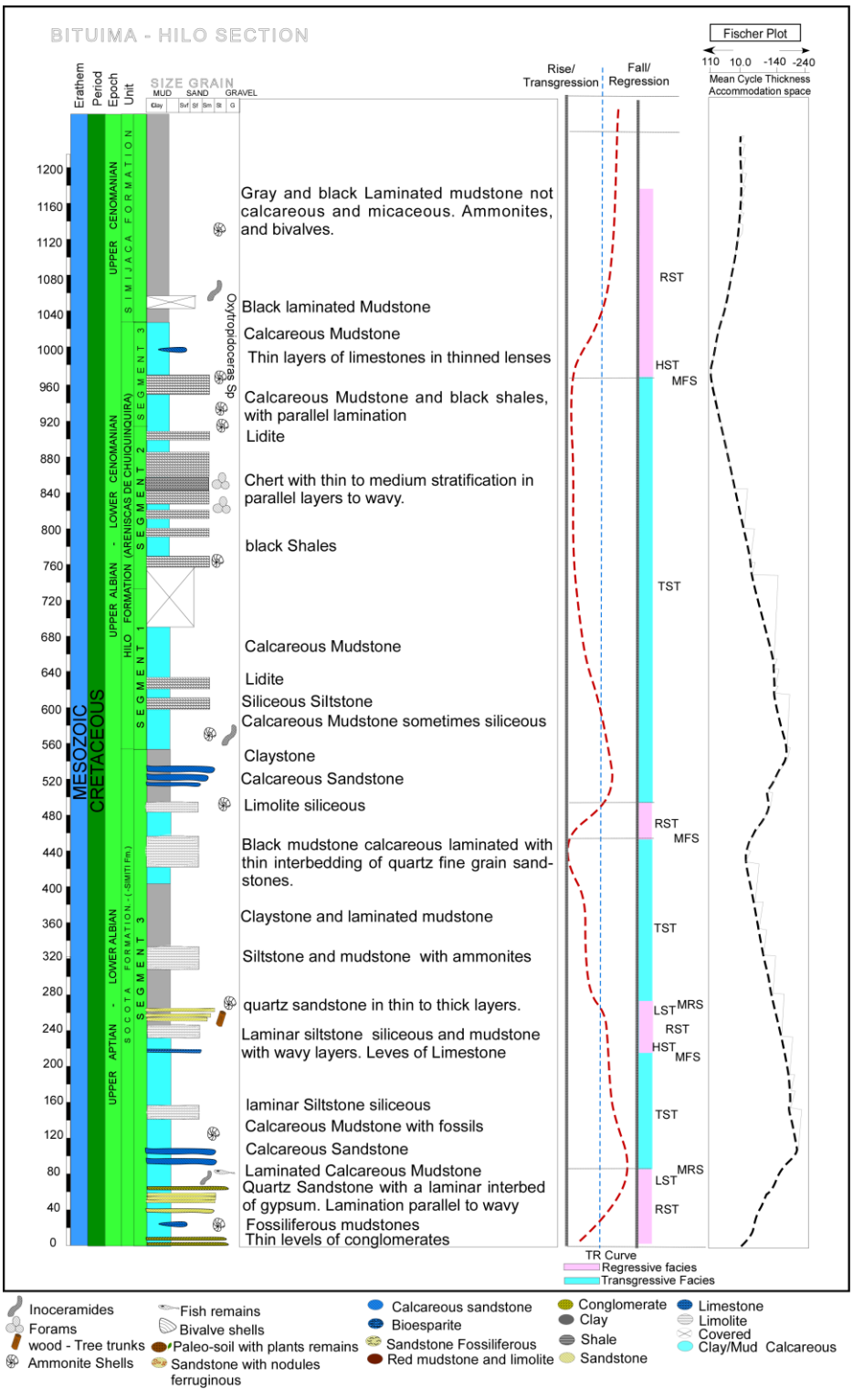

Figure 3.20. Bituima section of the Hilo Fm, showing Late Aptian – Late Cenomanian units. (Lithological description modified from Ulloa and Acosta (2001); stratigraphic interpretation from this work.)

The Upper part of the Bituima section is represented by the Simijaca Fm, which is composed basically of siliceous mudstone of Cenomanian age (Etayo, 1979).

The presence of *Rotalipora reicheli*, *Praeglobotruncana stephani* supports a Late Albian-Early Cenomanian age (Acosta and Ulloa, 2001). However, the occurrence of *Oxytropidoceras* sp. suggests a Middle Albian for part of the Hilo Fm (Burgl, 1957). In the Simijaca Fm, bivalves as *Exogyra* sp., *Ostrea* sp. and *Pecten* aff. *tenouklensis?* and planktic foraminifera like *Hedbergella* sp. suggest a Cenomanian age (Etayo, 1979).

The Socota Fm corresponds to a shallow marine deposit. The sandstone interbeds were interpreted by Polania and Rodriguez (1974) as a possible "variety of turbidites". However, Guerrero (2002) indicated that they are probably storm beds deposited in a shallow marine environment. Polania and Rodriguez (1974) also recognized a 30-77 m thick sandy sequence in the Socota Fm, and a marker sandstone bed that marks the interruption of the dominant sedimentation. These authors also reported at the base of the section two conglomeratic layers of 14 and 22 meters, and two, 7 and 15 cm thick conglomeratic sandstones at around ~55 m.

Near the La Mesa towm, Martinez and Vergara (1999) recognized a 270 m thick section of the Socota Fm. It included a series of 120 m of fossiliferous mudstones with very thin siltstone and fine-grained sandstone interbeds, overlain by 150 m of coarsening-upward cycles. These comprise from base to top, fossiliferous mudstone, siltstone/mudstone intercalations with ammonites, leaves and tree trunks, calcite-cemented quartz arenite, overlain by 30 m of mudstones with thin beds of fine-grained sandstone with quartz conglomerate.

The sandstones and conglomerates mark a brief incursion of coarse material in a succession dominated by fine sandstones. The marker sandstone bed reported by Polania and Rodriguez (1974) presents laminar intercalations of gypsum which are more frequence at the top. According to Polania and Rodriguez (1974), the fossils and the presence of gypsum support the idea of a shallow depositional environment. However, the increase of sandstones and conglomerates may have been controled by tectonic events (Kelling, 1964). The action of weak currents is suggested by occasional undulating and cross lamination. However, according to Walker (1965, *in* Polania and Rodriguez, 1974), parallel lamination may result from the reworking of sediment, which predominates in the Socota Fm.

In this work and according to other studies (Polania and Rodriguez, 1974; Martinez and Vergara, 1999; Guerrerro, 2002), the Bituima section involves a complete sequence cycle comprising TST, HST, RST and LST (Figure 3.20), related to sea level fluctuation and partly controlled by tectonic events as suggested by other authors.

- **Escuela -1 Section** (Figure 3.21)

The information gathered from cuttings samples from the Escuela-1 well allowed to date the units and evidenced three major stratigraphic breaks at 2500', 2750' and 3200'.

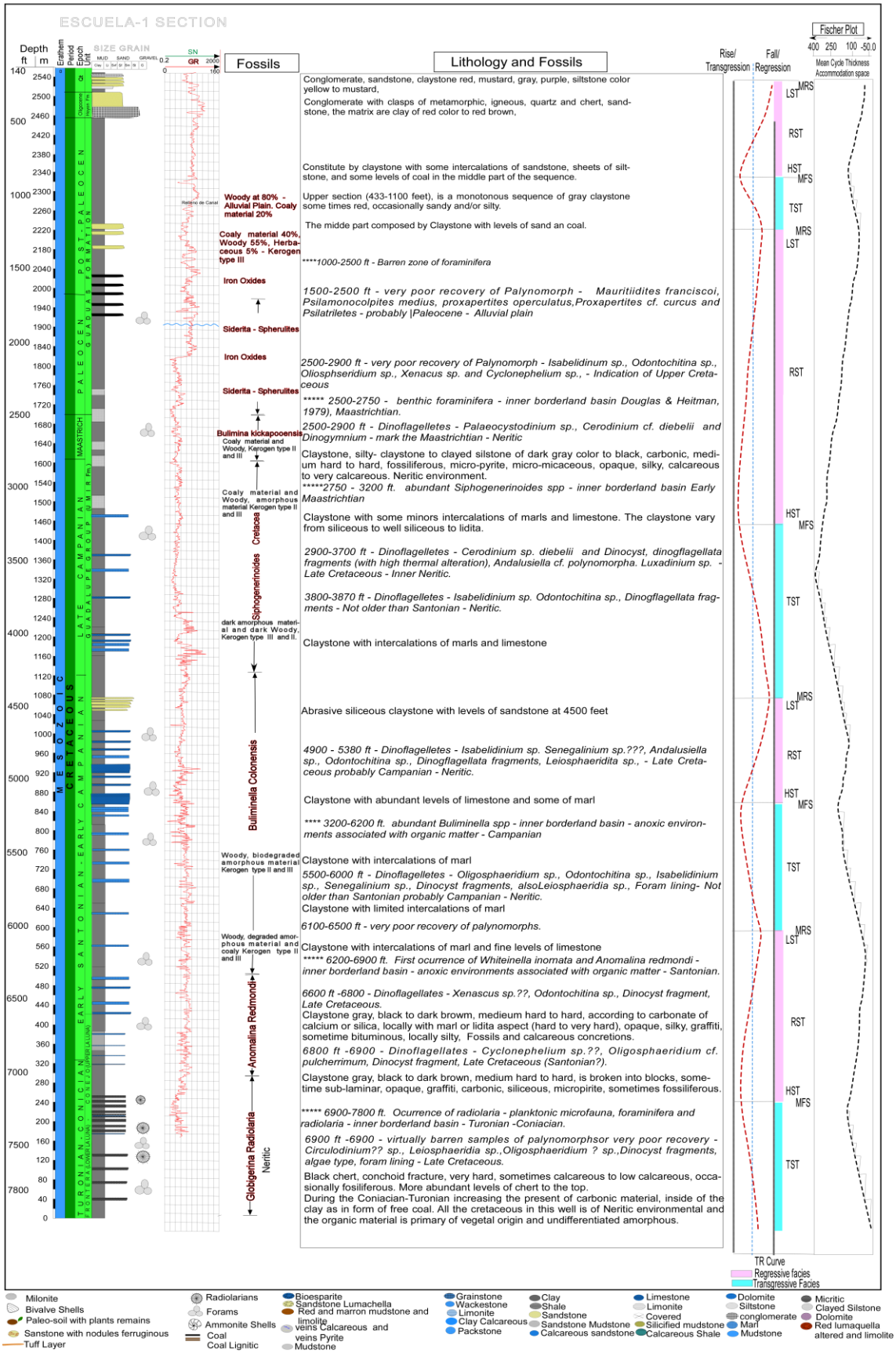

Figure 3.21. Stratigraphic section of Escuela-1 well, showing the sequence of the Turonian – Maastrichtian units to the present (reconstruction and interpretation from this work).

(1) 2500 ft. This hiatus is marked by the contrast between a Tertiary terrestrial sequence above and a Cretaceous sequence below. This abrupt change is interpreted as a regional and erosional unconformity between the Tertiary and Cretaceous sequences of the Middle Magdalena Basin, which is suggested by the absence of the latest Cretaceous *Ammobaculites columbianus* Zone.

(2) 2750 ft. The second break, marked also by a contrast both in microfaunal preservation and composition, marks the boundary between the *Bulimina kickapooensis* Zone (Maastrichtian) and the underlying *Siphogenerinoides bramlettei-S cretacea* mixed Zone. The *Bulimina kickapooensis* Zone (Early Campanian-Late Campanian, Gauger *in* Jones, 1953) corresponds to the upper portion of the *Siphogenerinoides bramlettei* Zone (Campanian), which directly overlies the *Siphogenerinoides bramlettei-Siphogenerinoides cretacea* Mixed Zone. This contrasting boundary and the mixed character of the underlying zone appears associated with tectonic phenomena.

(3) 3200 ft. This break marks the boundary between the *Siphogenerinoides bramlettei-Siphogenerinoides cretacea* Mixed Zone of early Maastrichtian age, and the underlying *Siphogenerinoides cretacea* Zone, which appears to mark the top of the Campanian to Turonian, apparently in normal sequence.

(4) 3200-6200 ft. *Buliminella* spp. (associated with anoxic environments and organic matter paleoenvironments) is of common occurrence within the latest Cretaceous biostratigraphy of the Upper Magdalena Basin (Petters, 1955), and particularly within the *Siphogenerinoides cretacea* Zone (peak abundances are typical in the Campanian). In the same way, the occurrence of *Sporobulimina perforata* within this zone (4300'-5300') also confirms its Campanian age.

(5) 6200 – 6900 ft. The occurrences of *Whiteinella inornata* and *Anomalina redmondi*, although scarce, place this zone within the Santonian.

(6) 6900 – 7800 ft. *Globigerina*-Radiolaria Zone. This is a typical biostratigraphic unit in other Upper Magdalena Basin localities, where it contains diagnostic Turonian and Coniacian planktonic markers.

In the Bituima section I identified four cycles (TST-LST). Three are of Cretaceous age: one in the Turonian to Santonian-Campanian, a second in the early Campanian, and a third in the Late Campanian to Paleocene-Eocene. These help to recognize surfaces or sedimentological discontinuities of transgressive or regressive surface.

- **Rio Curi - Anolaima – La Florida Section**.

Units cropping out in the Anolaima-La Florida section correspond to the base of the Simijaca Fm. Its base is marked by the appearance of laminated, micaceous, non-calcareous gray claystone that overlie the Upper Albian Areniscas de Chiquinquira. The top of the Simijaca Fm is marked by bioturbated quartz siltstone to medium-grained quartz sandstone beds, with wavy lamination and shells casts, which underly the

Turonian Frontera Fm (Figure 3.22). The Simijaca Fm can be followed from the Chiquinquira area to the Villeta zone, with similar characteristics. Meanwhile, the Upper Albian unit laterally grades from the Areniscas de Chiquinquira, to the Pacho Fm, and to the Hiló Fm.

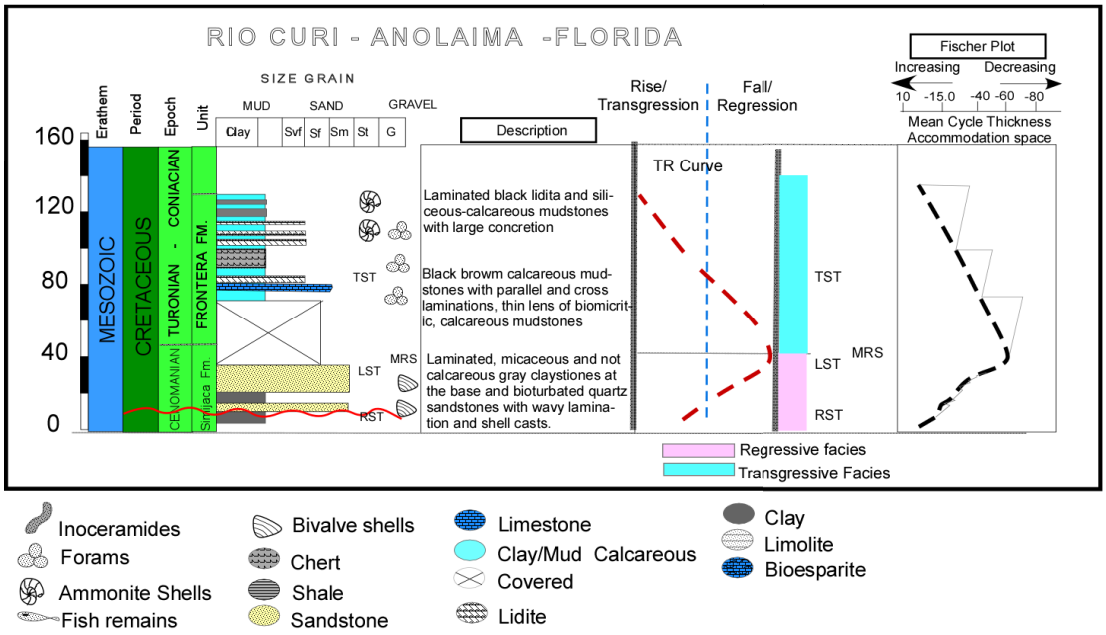

Figure 3.22. Rio Curi-Anolaima section, corresponding to the Simijaca (Cenomanian) and Frontera (Turonian-Middle Coniacian) Fm, showing the transgresive-regession curve and the Fischer plot. After personal observations and Ulloa and Acosta (2001).

Biostratigraphy: 50 meters below the Frontera Fm, Hubach (1957) quoted the occurrence of *Exogyra squamata*. Besides *Exogyra* sp. or *Ostrea* sp., *Pecten* aff. *tenouklensis ?* and planktonic foraminiferas such as *Hedbergella* sp. suggest a Cenomanian age (Etayo, 1979, *in* Acosta & Ulloa, 2001, Map La Mesa 227).

The micaceous clay, siltstone and sandstone of the Simijaca Fm suggest a terrigenous supply. The occurrence of planktic foraminifera, the fining upward trend at the base, and the presence of leave remains, bivalves and bioturbation, together with a coarsening upward evolution at the top, suggest a shallowing upward evolution.

In the overlying Turonian Frontera Fm, the lower and middle parts are made of black-brown calcareous mudstone presenting parallel and cross laminations, with thin lens-shaped beds of biomicritic limestone, calcareous mudstone with large concretions (1.2 m), micrite and siliceous mudstone. The middle part is composed of black chert in thin, wavy layers and occasional micritic concretions. The middle to upper parts are dominated by laminated black lidita and siliceous-calcareous mudstones, with layers of micritic limestone and very large concretions (Acosta and Ulloa, 2001). The upper part is made of calcareous mudstone, non-calcareous claystone and siliceous siltstone.

Predominant fossils are planktonic foraminiferas, ammonites and inoceramids. Etayo (1979) proposed the ammonite zone *Mammites nodosoides appelatus – Franciscoites suarezi*, of Early Turonian age. The planktic foraminiferas *Whiteinella archeocretacea*,

Whiteinella aprica, Whiteinella baltica and *Heterohelix reussi* support an Early Turonian age for the Lower Frontera Fm. The upper part yielded casts of *Didymotis roemeri variabilis* of middle Coniacian age (Burgl, 1957).

The scarcity of benthic life (crustaceans and echinoids) and the abundance of laminations, planktonic foraminifera and amorphous silica, suggest a pelagic to hemi-pelagic environment and dysoxic conditions below the photic zone, resulting from a sea level rise (Acosta and Ulloa, 2001).

- **Quebrada Nemice section**

In the area of Quebrada Nemicé, west of San Francisco, the 370 m thick, Coniacian Conejo Fm had been studied by Hernández (1990), who described a transitional lower contact with the Turonian Frontera Fm, and a transitional upper contact (Fig. 3.23).

This unit is characterized by grey claystone and laminated mudstone, usually calcareous, with micritic concretions, which grade to non-calcareous laminated claystone presenting thin intercalations of siliceous quartz-siltstone.

The upper part includes fine- to medium-grained quartz-sandstones arranged in medium to thick beds, with undulating, non-parallel, discontinuous laminae and *Thalassinoides* sp. bioturbations. They are overlain by medium to very thick beds of nodular biomicritic limestone. The top comprises quartz-siltstone, fine- to medium-grained quartz sandstone with peloids and phosphate, as well as claystone and mudstone, locally calcareous.

From a biostratigraphic point of view, Etayo (1979) identified the *Gloriceras correai* zone with *Protexanites cucaitaense, Codazziceras scheibei*, and assigned an Early Coniacian age. The foraminifera association includes *Marginotruncana sinuosa, M.* aff. *schneegansi, Dicarinella concavata, Whiteinella archeocretacea, W. inornata* and *Whiteinella baltica*.

Sedimentary facies show that the Conejo Fm evolves from a dis-aerobic (abundant planktonic foraminifera) outer shelf environment, as supported by the occurrence of keeled planktonic foraminiferas (*Dicarinella* sp., cf. Hard, 1980), to an oxygenated, shallow siliciclastic shelf marked by bioturbated sandstones (Thalassinoides).

Sandstone beds locally present graded bedding: erosive surface and reworked bioclasts are overlain by parallel and ondulating, bioturbated lamination.

In Quebrada Nemice, the series shows four sedimentary discontinuities corresponding to maximum regression surfaces (MRS) located at the top of regressive system (RST), and maximum flooding surfaces (MFS) at the top of the transgressive system (TST). In this section, two cycles (TST-HST-RST-LST) are identified. The transgression cycle ends in the Late Turonian and the regression starts at the Turonian/Coniacian limit, and extends through most of the Coniacian-Santonian.

The system tracts analyzed and the age indicated by biostratigraphic data (Figures 3.17-3.23) made a lateral correlation of sections of the southern studied area and to identify the regional sedimentary surfaces (Figure 3.24) possible.

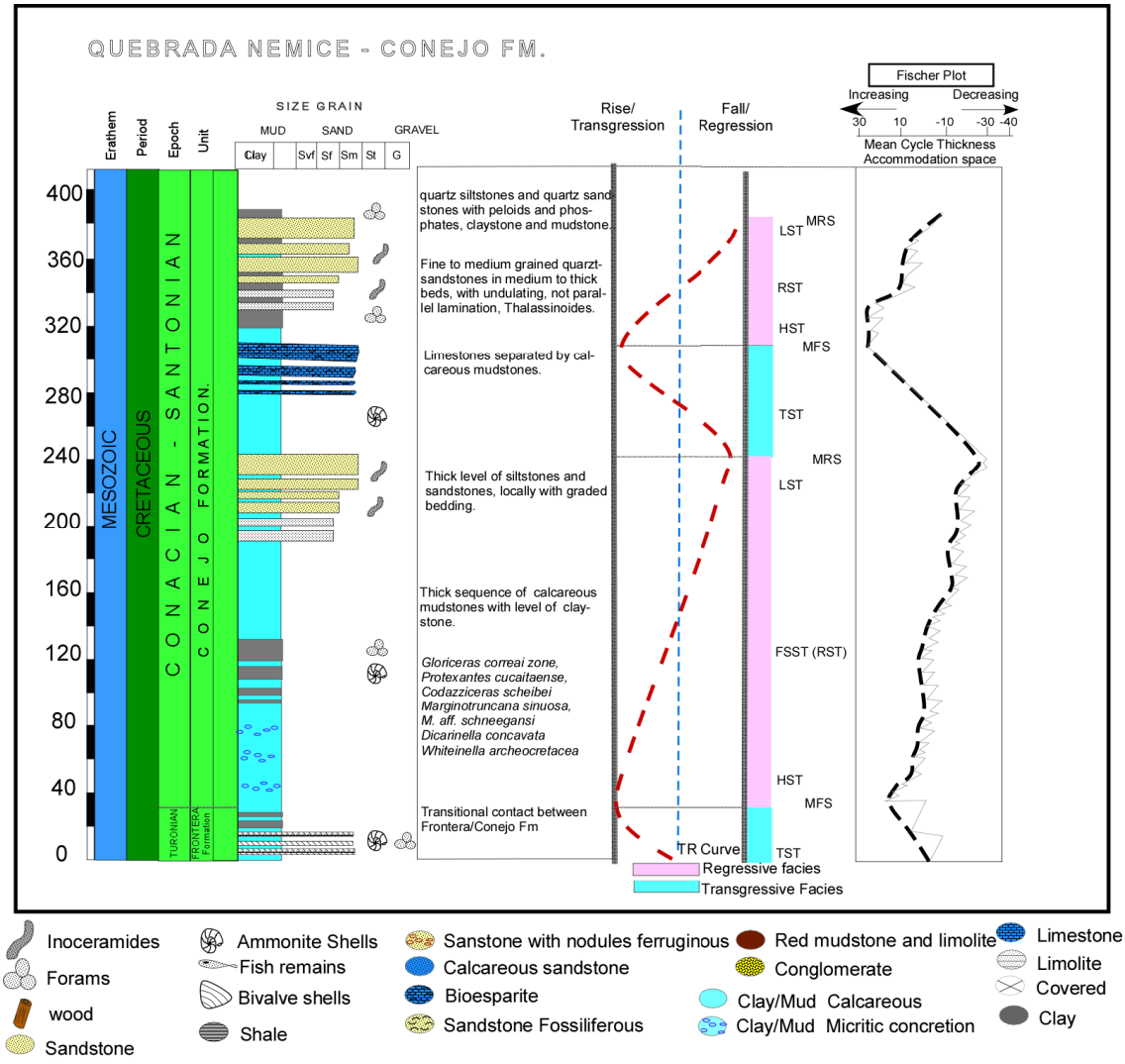

Figure 3.23. Quebrada Nemice section, describing the Lower Coniacian Conejo Fm. Section initially described by Hernandez (1990) and revised during this work.

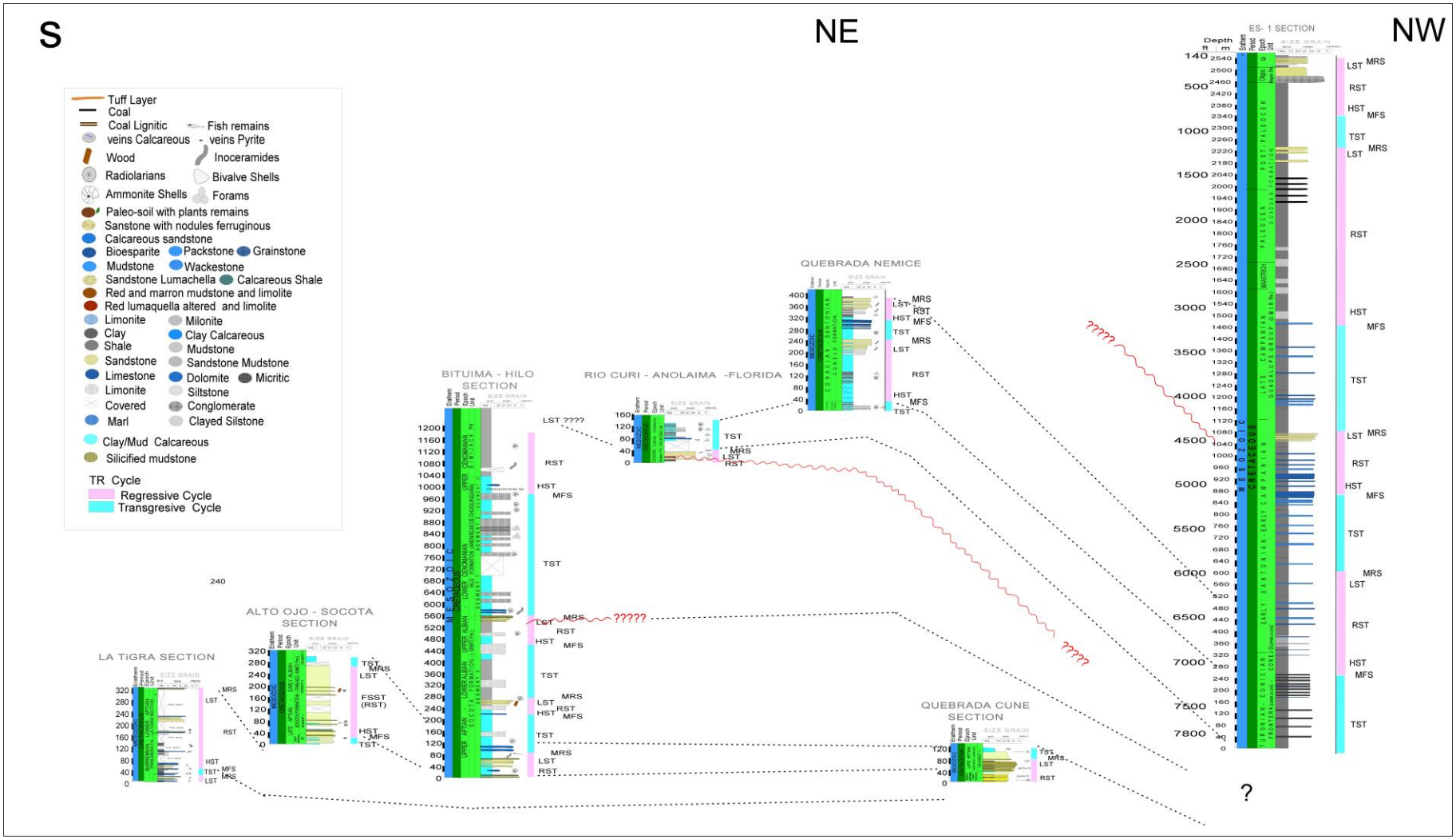

Figure 3.24. N-NE-NW correlation of the southern part of the study area.

3.5.2 Central Region

- **Sachica – Chiquinquira section**

This section allows the study of the Tablazo Fm (correlated with the Lower San Gil Fm). The San Gil Group has been defined by Hubach (1931) in the type locality of San Gil (Santander). In the Central area, the San Gil Group is divided into a Lower San Gil Formation and an Upper San Gil Formation. The term Upper San Gil Fm was used by Etayo (1968) near Villa De Leyva, to describe the laminated black mudstone, which is overlain by the Churuvita Fm. The latter corresponds to the Simiti Fm (Ulloa and Rodriguez, 1979; Moreno and Pérez, 2001). However, this unit presents different features in Villa De Leyva and Chiquinquira.

According to lithostratigraphic correlations, the part of the Tablazo Fm identified in this work corresponds to the Lower San Gil Formation (Figure 3.25). Its base is made of sparite and micrite with shale, siltstone, and some sandstones beds (Figure 3.25).

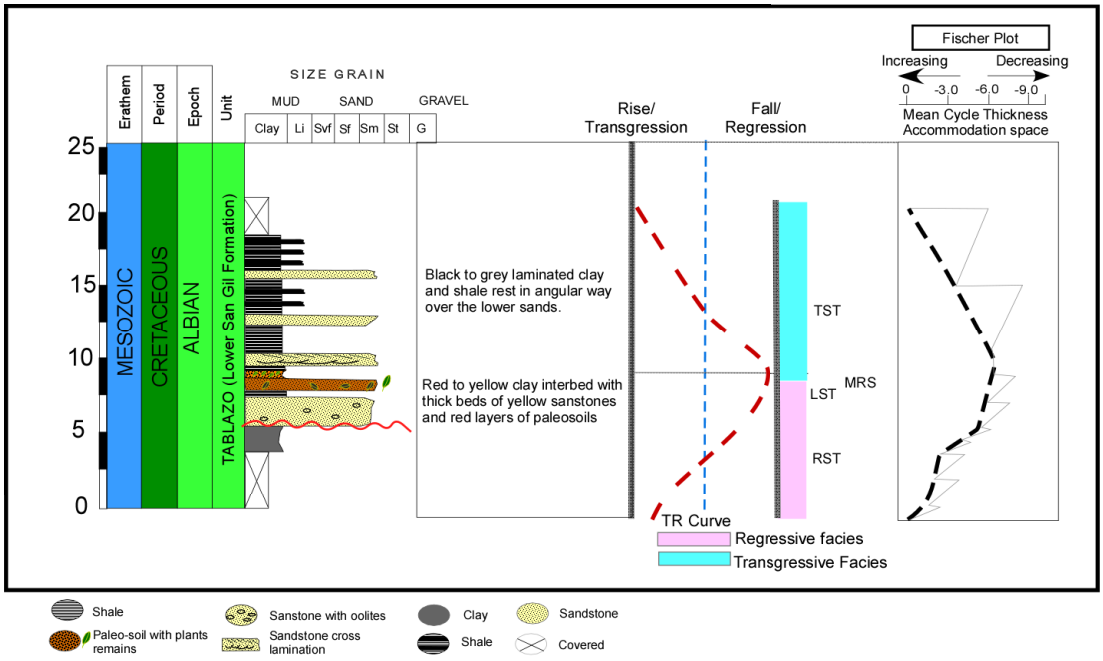

Figure 3.25. *Sachica – Chiquinquira road section, corresponding to the Tablazo Fm. Local coal mining has been reported for this formation in this area. This work.*

In the lower part, red to yellow clay is interbedded with thick beds of yellow sandstone and red layers interpreted as paleosols (Photo 3.4). The upper part consists of black to grey laminated clay and shale that rest in angular and abrupt contact on a sandstone bed (blue line in Photo 3.4), interpreted in this work as an unconformity.

- **Samaca–Villa de Leyva section** Lower San Gil Fm (Tablazo Fm).

The Lower San Gil Fm rests on the Lower Aptian Paja Fm. In the lower part, mudstone is interbedded with fine to medium-grained sandstone beds, muddy-sandstones and sandy-mudstone (Figure 3.26).

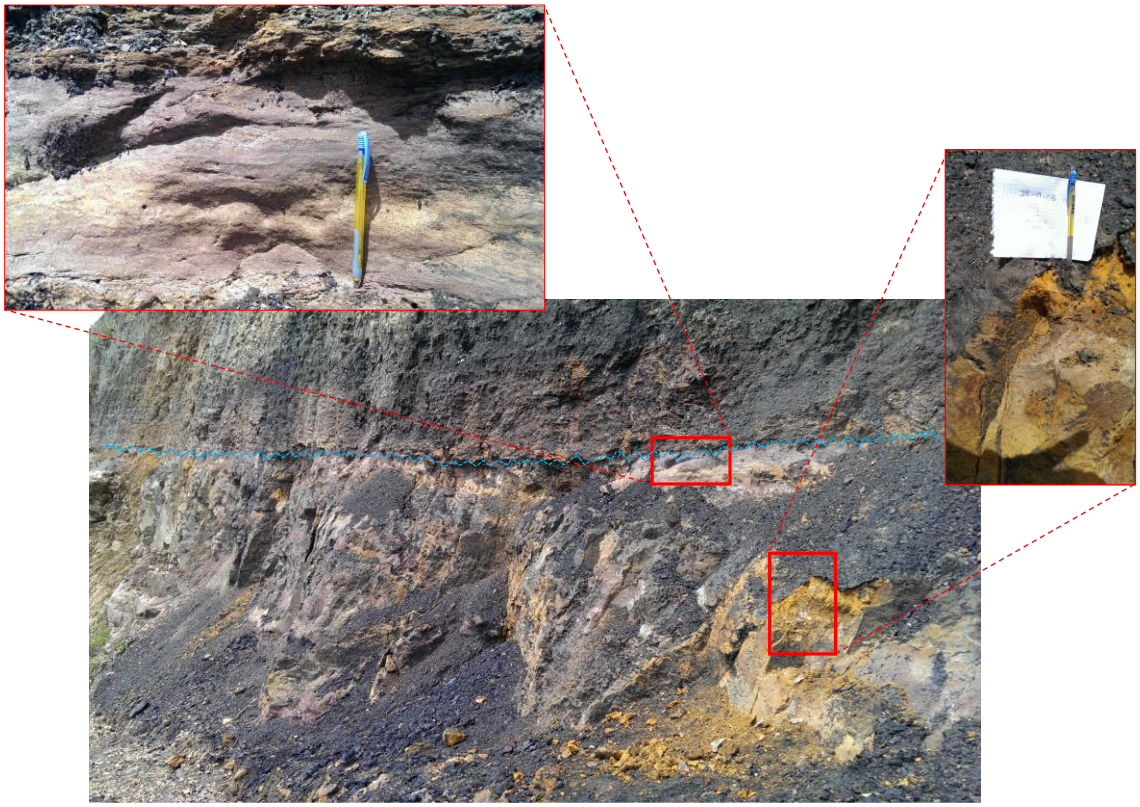

***Photo 3.4**. Outcrop of yellow quartz sandstone (right red rectangle) and red layers interpreted as paleosoils (left red rectangle) of the Albian Lower San Gil Fm (Tablazo Fm).*
Note the angular and abrupt contact with the overlying laminated clay (blue line).

Along the Samaca-Villa de Leyva road, the Lower San Gil Fm comprises from base to top: (1) siltstone increasingly abundant upward, interbedded with black to grey claystone, and scarce intercalations of thick sandstone beds, fossiliferous sandstones and biosparitic limestone (90 m); (2) grey to black claystone with levels of siltstones, sandstone, fossiliferous sandstone and biosparitic limestone (50 m); (3) a thickening upward succession (90 m) of siltstone, sandstone and some levels of biosparitic limestone and fossiliferous sandstone interbedded with claystone; (4) thick beds of sandstone, limestone and fossiliferous sandstone (90 m); and (5) yellow to white sandstone beds, associated with paleo-soils with plant remains, layers of red mudstone and siltstone, and some packages of crossbedded sandstone.

This succession (Figure 3.26) is interpreted as a shallowing upward sequence, from a middle clastic shelf environment at the base (Upper Aptian, base of Tablazo Fm) to a very shallow, sporadically emergent clastic shelf at the top (Lower Albian, top of Tablazo Fm). This shallow sequence is overlain by the Upper Albian Upper San Gil Fm (= Simiti Fm), which is mainly composed of 200 meters of dark grey shale and grey to black claystone (more than 90 % of the sequence) with scarce and thin beds of sandstone and siltstone, showing a deepening upward trend.

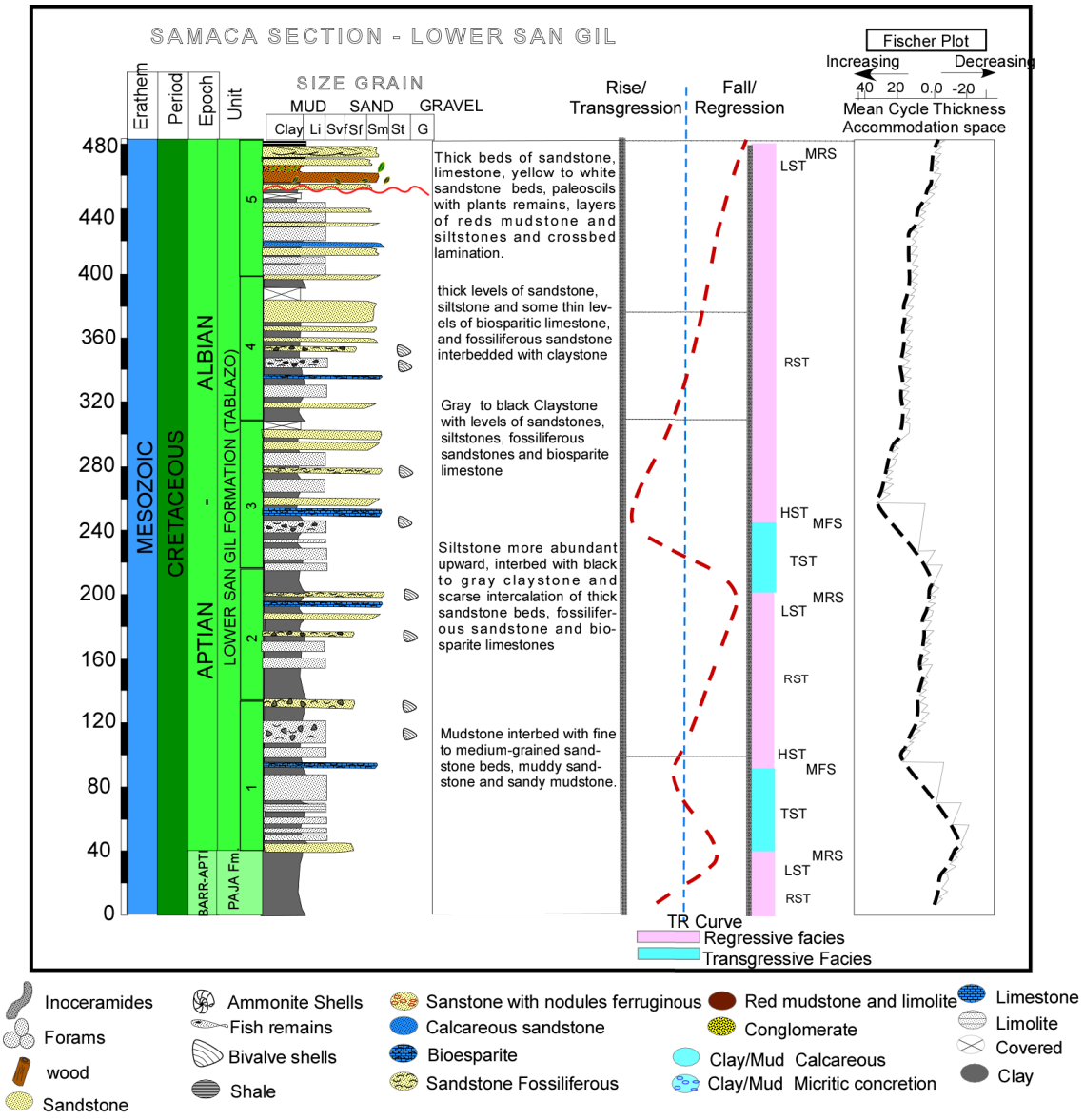

***Figure 3.26**. Section along the Samaca – Villa de Leyva road, showing the Lower San Gil Fm. Sandstone beds and paleosoils were observed in the upper part of the section.*

Samaca – Villa de Leyva section Upper San Gil Fm (Simiti Formation).

The shallow marine facies of the shore or nearshore sandstone of the Lower San Gil Fm contrast with the fining upward succession of the Upper San Gil Fm in the area of Villa de Leyva, as shown in Figures 3.26 to 3.27. According to Villamil (1998), the same evolution can be observed in the transition from the Caballos Fm to the Villeta Fm in the Upper Magdalena Valley (UMV) and in the Bogotá region between the Socotá and Hiló Fms. Villamil (1998) stated that the maximum flooding surface is of Middle Albian age (104 Ma). In the UMV, the Villeta Fm shows a deepening upward trend until reaching a first transgression maximum, coinciding with an "oceanic anoxic event" (Villamil, 1998).

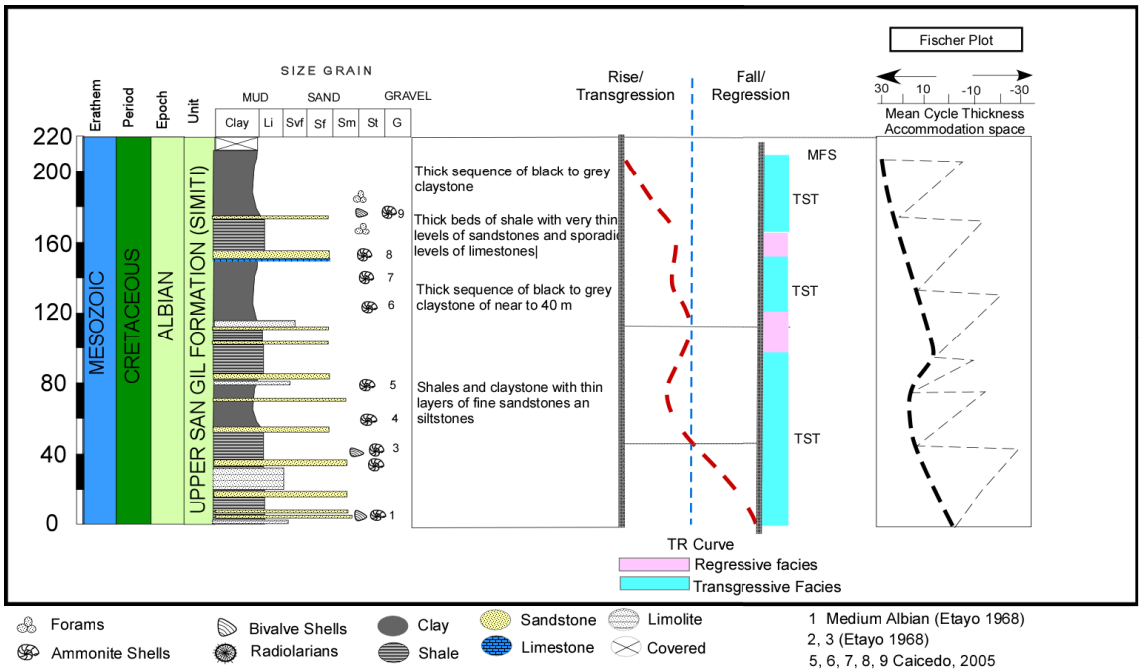

Figure 3.27*. Section along the Samaca – Villa de Leyva road, corresponding to the Upper San Gil Fm. From personal observations, and after Caicedo (2005).*

In the same area, the Middle Albian MFS is characterized by condensed limestone-shale cycles (phosphatic pebbles, pyritous concretions, fish debris), while it is marked by condensed chert-shale in the Bogotá region (Villamil, 1998), and by claystone in the Cocuy area (Etayo, 1985). The same observations can be made in the Upper San Gil Fm in the Villa de Leyva area, where the MFS is constituted by black, organic-rich shales.

The opposite situation occurs for the transition from the Upper San Gil Fm to Churuvita Fm, where the shallowing upward trend represents a regression, probably the same as described as a progradation in the UMV during Late Albian-Early Cenomanian times, interpreted as a HST by Villamil (1998). There, the latter is formed by fine grained facies, the same as in Villa de Leyva, where the Upper San Gil Fm is defined by the apparition of claystone and shales (90% of the composition in this section).

During the Early Cenomanian a regression is represented in the area of Villa de Leyva. This limit is evidenced by the Churuvita Sandstone Fm overlying the shales of the Upper San Gil Fm (Figures 3.27 and 3.28). In Villa de Leyva (MMV), this change is clearer than in the UMV, where it is marked by siltstone and claystone overlying calcareous shale and pelagic limestone (Villamil, 1998). Around Bogotá, the contact is marked by shales overlying cherts of the Hiló Fm, while in the Cocuy area it is difficult to identify (Villamil, 1998).

Biostratigraphy: Ammonites, bivalves and foraminiferas collected by Caicedo (2005) and information from other authors, allow to assign a Middle to Late Albian age to the Upper San Gil Fm. Etayo (1968) mentions *Platiknemiceras colombiana*, *Rinconiceras rinconi*, *Lyelliceras pseudolyelliforme* of Middle Albian age (Etayo, 1978) and

Hysteroceras carinatum of Late Albian age (Caicedo 2005). In the stratigraphic section (Figure 3.27) the presence of the following had been reported:

1. *Knemiceras semicostatum* Sommermeier, *Engonoceras* cf. *E.* gr. *gibbum*, cf. *Parengonoceras guadalupaeforme*, cf. *P. pernodosum, Lyelliceras pseudolyelli* sensu Benavides (non Par - Bon), cf. *Desmoceras chimuense* Benavides-Cáceres, and *Lyelliceras isaacleni*.

2. *Ralphimlayites* sp. indet., *Eubrancoceras* sp. aff. *aegoceratoides* (Steinmann), *Platiknemiceras* sp. indet.,

3. *Eubrancoceras aegoceratoides* (Steimann), *Oxytropidoceras (Mirapelia)* sp. aff. *mirapelianum* (d´Orbigny), *Knemiceras compressum* Hyatt, *Knemiceras laraense* Renz, *Parengonoceras* cf. *pernodosum* (Sommerneir).

4-5. *Knemiceras laraense* Renz, *Oxytropidoceras (Mirapelia)* sp. indet., *Ralphimlayites* sp. indet., *Ralphimlayites prorsocurvatum* (Gerhardt), *Dipoloceras* cf. *cristatum* (Brongniart).

6-7. *Knemiceras compressum* Hyatt, *Oxytropidoceras (Venezoliceras)* sp. cf. *acostae* (d´Orbigny), *Venezoliceras* n. sp., *Parengonoceras discoides* Renz, *Dipoloceras* cf. *cristatum* (Brongniart).

8-9. *Knemicera compressum* Hyatt, *Dipoloceras* cf. *cristatum* (Brongniart), *Oxytropidoceras (Benavidesites) karsteni* (Stieler), *Venezoliceras* n. sp. The bivalves *Syncyclonema inconspicua, Mediterraneotrigonia* aff. are reported from the Middle Albian; *Camptonectes striatopunctatus, Ceratostreon* cf. *flabellatum, Mediterraneotrigonia* aff. *hondana, Neithea syriaca, Pecten* cf. *sulcatocostatus, Pinna robinaldina, Inoperna flagellifera* and *Scabrotrigonia*? *ethra*, from the Late Albian (Caicedo, 2005).

Benthic foraminifera reported from the Upper San Gil Mb are *Haplophragmoides langsdalensis, H. arenatus, H. gigas, H. excavata, Ammobaculites subcretacea, Trochammina callima, T. orchardensis* and *Lenticulina exarata* subsp. *danubiana*, which correspond to the *Haplophragmoides langsdalensis* zone of Late Albian age (Caicedo, 2005). Plancktic foraminiferas from the Upper San Gíl Mb and San Rafael Fm are species present from the Early Aptian to the Turonian – Santonian times (*Hedbergella delrioensis, H. planispira, H. simplex*). *Rotalipora* cf. *cushmani* has been mentioned, which would be indicative of a Late Cenomanian age (Caron, 1985).

<u>Villa de Leyva - Cucaita - Churuvita section</u> (Upper part of the Chiquinquira Fm).

The Churuvita Fm was defined by Etayo (1968), who divided it into three members: a lower member made of fine- to medium-grained, micaceous quartz-sandstone, with interbeds of claystone and siltstone; a middle member composed of coquina with *Rhynchostreon squamatum* and *Ostrea* sp., interbedded with claystone, sitstone and quartzsandstone; and an upper member made of thick bedded, fine- to medium-grained quartz-sandstone and calcareous sandstone with silty-clayey interbeds.

In the studied section, the Churuvita Fm is composed of claystone with intercalations of black limestone, biomicritic limestone and yellow sandstone beds (Photo 3.5) that become more numerous and thicker upward. In the middle part of the section (Figure 3.28) thin layers of fossiliferous sandstone can be observed. Photo 3.5 shows thick packages of white to yellow, medium-grained sandstone of the Churuvita Fm. Two levels of paleosoils were identified: a red altered coquina bearing siltstone at the base of the section, and another at the top of the Churuvita Fm (Figure 3.28, photo 3.5). Note the presence of ichnofossils (burrows) at the base of some sandstone beds (Photo 3.6).

Whereas Etayo (1968) described a transitional contact between the Churivita Fm and the underlying San Gil Fm, according to Caicedo (2005) this contact is clear, and there is no fault as proposed by Patarroyo (1995) and Moreno and Pérez (2001).

Our observations show that thick, massive or crossbedded quartz-sandstone beds (> 1 m), locally conglomeratic, with shell casts of the Cenomanian Churuvita Fm (Photo 3.7), rest on black laminated mudstone of the Upper Albian of San Gil Fm (Figure 3.28). This contact suggests an abrupt change from offshore mudstones (San Gil Fm) to shoreface sandstone (Churuvita Fm), probably associated with erosion (blue line on Photo 3.7).

Photo 3.5. *Outcrop of the Churuvita Formation along the Sachica road, before the deviation towards Cucaita –Villa de Leyva town. Note the unconformity with a possible level of paleosoil at the base, overlaid by thick, to medium-grained, white to yellow sandstone beds.*

The contact between the Upper Albian and Lower Cenomanian strata is marked by the disappearance of laminated shales of the Upper San Gil Fm and the first appearance of sandstone and fossiliferous sandstone, locally conglomeratic, with shell casts of the Churuvita Fm (Figure 3.28). The middle member is marked by black laminated mudstone with intercalations of sandstone. The contact between the middle and upper members is marked by the sudden appearance of thick sandstone and conglomeratic sandstone with fossil casts (shells). This clearly marks an abrupt shallowing of the environment, apparently corresponding to an unconformity (Figure 3.28, Photo 3.5).

Photo 3.6. *Detail of ichnofossils (burrows) at the base of a thick sandstone bed of the Churuvita Fm. Same location as photo 3.5.*

The contact between the Churuvita Fm and the overlying San Rafael Fm is clear, as it separates the quartz-sandstone with an interbed of mudstone of the Churuvita Fm, from laminated mudstone with intercalated micritic limestone beds of the San Rafael Fm. The abrupt change at the boundary between the San Gil and Churuvita Fm, and the wavy and discontinuous aspect of this limit (Photo 3.7, central and upper right side) suggest an unconformity at this level (Photo 3.7 blue line).

Biostratigraphy: The Churuvita Fm is assigned with doubts to the Late Albian. Reported ammonites are a poorly preserved Acanthoceratidae (mostly Cenomanian) from the upper member, and a *Venezoliceras* (Late Albian) from the lower member (Etayo, 1968). Elsewhere, Burgl (1955) reported *Acanthoceras? ospinae* (Karsten) near the Ubaté town, which could be of Early Turonian age (Patarroyo, 2011). In general, the information from ammonites for the Churuvita Fm is not conclusive.

Bivalves reported by Caicedo (2005) in the Churuvita Fm are *Amphidonte* cf. *obliquata, Camptonectes striatopunctatus, Plicatula radiola ?, Rhynchostreon subsquamatum* of Late Albian-Early Cenomanian age; *Afrogyra africana, Camptonectes striatopunctatus, Ceratostreon* cf. *flabellata, Costagyra olisiponensis, Curvostrea rouvillei, Gyrostrea* cf. *delettrei, Mimachlamys* sp., *Oscillopha syphax, Pecten tenouklensis, Plicatula auressensis, Plicatula ferryi, P. radiola, P. fourneli, Rhynchostreon subsquamatum* (abundant), *Scabrotrigonia ? ethra* and *Gyrostrea ? tarfayensis* of Cenomanian age.

The base of the Simijaca Fm yielded early Turonian ammonites (Etayo, 1968, 1979). The Cenomanian-Turonian boundary would be located near the top of the Churuvita Fm (Villamil and Arango, 1998). According to Gaona (2004, in Caicedo, 2005), the Upper Cenomanian age of the Churuvita Fm-Simijaca Fm boundary is based on the abundance of *Afrogyra africana* (Lamarck).

Regarding benthic foraminifera, Caicedo (2005) established that, for the whole section of the San Gil to Simijaca fms, the San Gil-Churuvita boundary corresponds to the *Ammobaculites exertus* local zone assigned to the Upper Albian.

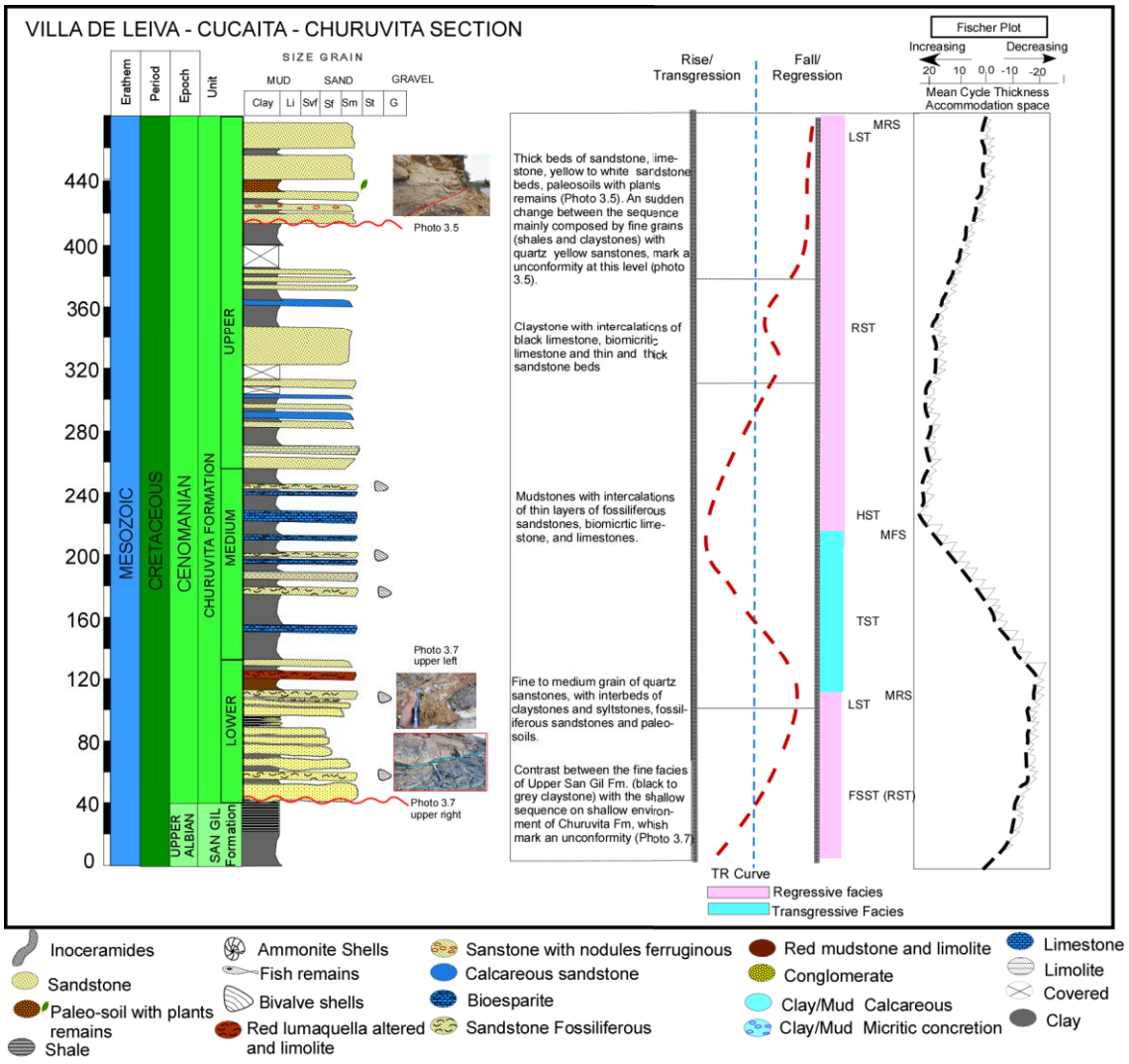

Figure 3.28. *Stratigraphic section in the Villa de Leyva-Cucaita road that corresponds to the Churuvita Formation, with an important content of sandstones which are increasing from the base to the top of the sequence (from this work).*

For the middle and lower part of the upper member of the Churuvita Fm, the *Ammobaculites subcretacea* local zone indicates a Late Albian to Early Cenomanian age. Finally, in the upper part of the Churuvita Fm and base of the Simijaca Fm, the benthic foraminifera *Ammobaculites arenata* suggests an Early to Late Cenomanian age for the Churuvita-Simijaca boundary.

The Upper San Gil Fm and Simijaca Fm yielded the planktonic foraminifera *Hedbergella delrioensis*, *H. planispira* and *H. simplex* and *Rotalipora* cf. *cushmani*. The latter species indicate a late Middle to early Late Cenomanian age (Caron, 1985).

Petrography: Sample JG-P1-02 is composed of calcareous grains, some quartz grains, large perforated shells filled by micrite (center of the photo), fish teeth, echinoids and oysters. Fish teeth suggest a shallow marine environment and borings indicate very shallow to intertidal environments. This bed is interpreted as a beach deposit.

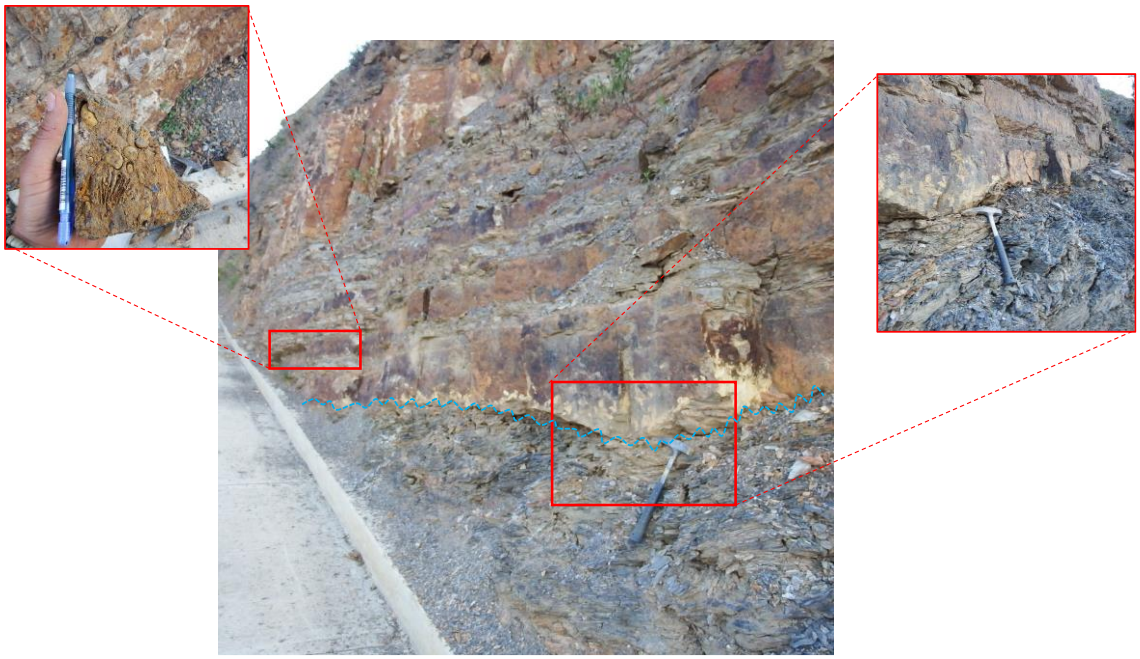

Photo 3.7. *Contact between the Upper San Gil and Churuvita Fms along the Villa de Leyva –Cucaita road. This contact is interpreted as an unconformity as shown in the central and upper right side.*

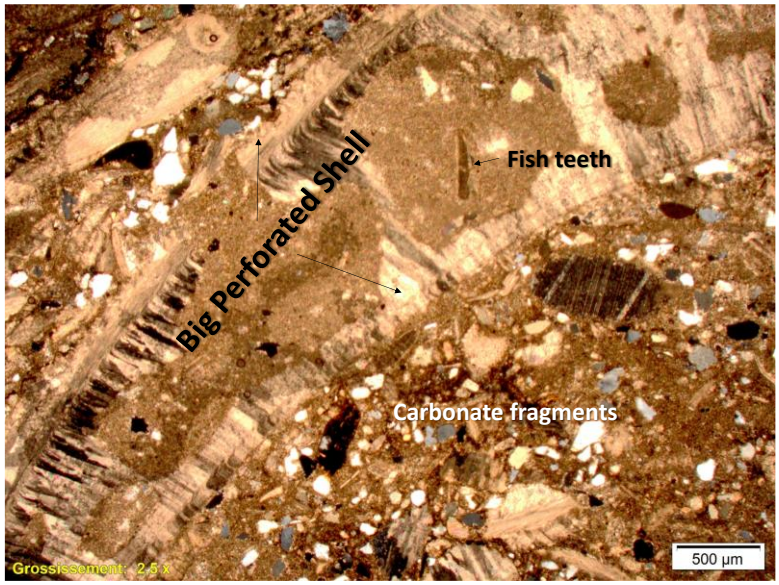

Petrographic Section 3.3. *This sample, JG-P1-02, corresponds to a Biomicrite (Folk, 1962) or Packstone (Dunham, 1962).*

The presence of planktonic foraminiferas in the San Gil Fm contrasts with the nearshore deposits of the Churuvita Fm (Figure 3.28, Photos 3.6 and 3.7) and suggests that an important discontinuity separates these two units.

This change between the shales of the San Gil Fm and the first package of beach sandsones of the Churuvita Fm, represents an increase of energy, with surface exposition and probably related to an unconformity (Figure 3.28, Photos 3.6 and 3.7).

From the Upper San Gil Fm to the Churuvita Fm, the environment changes from deep to shallow during the Late Albian to Early Cenomanian during the regressive sequence (HST-FSST).

- **Villa de Leyva – La Paja section**

A 160 m thick section of the La Paja Fm (Barremian-Aptian, Figure 3.29) has been studied along the Villa de Leyva-Sachica road. There, exposed from base to top (segment 1, Figure 3.29) are the following: intercalation of black and red shales with levels of red claystone, red nodules and oxide nodules in the first 30 to 40 meters. In the middle part, the content of laminated black shale increases, containing some levels of red claystone, red and black nodules (photo without numeration in Figure 3.29) and thin levels of gypsum. In the upper part of first segment, black shale containing nodules without fossils. The upper part of the section (segment 2, Figure 3.29) begins with ≈ 20 meters of grey claystone and black shales with levels of red claystone, with fossiliferous nodules (ammonites, photo 3.9), iron crusts and scarce thin levels of fine sandstone. At the top (≈ 30 m) a thick level of black shales and gray-red claystone contains abundant black nodules (Figure 3.29).

The La Paja Fm has been widely studied by many authors (Etayo, 1979; Forero and Sarmiento, 1985; Patarroyo, 1997; 1999; 2000; 2009; Hoedmaeker Ph, 2004; Patarroyo et al., 2009; Galvis and Valencia, 2009; Barbosa and Lopez, 2009; Pinto and Peña, 2013; Cadena and Parham, 2015). The La Paja Fm, is widely recognized as encompassing the Hauterivian to part of Aptian interval, and as deposited in a shallow marine environment.

In 1998 geologists from the Nationaal Natuurhistorisch Museum (NNM) in The Netherlands, collected many *in situ* ammonites from the Hauterivian and Barremian strata in the Villa de Leyva area. Patarroyo (1999, 2000a, b) wrote his dissertation on the biostratigraphy of Barremian ammonites, integrating Hoedemaeker's data. Philip (2004) combined the sequence stratigraphy analysis of Hoedemaeker (1997) with the Barremian biostratigraphy of Patarroyo, and followed Etayo´s subdivision of the Aptian, but added the occurrence of *Procheloniceras albrechtiaustriae* and *Cheloniceras cornuelianum* (lower Aptian assemblage-zone). Philip (2004) concluded that the Loma La Yesera section (photo 3.8) can be procesely correlated with the European Barremian stratotype. The presence of *Pseudocrioceras* in Colombia can be inferred at the top of the Barremian, which probably occupies the upper part of the last HST of the Barremian stage (Philip, 2004).

The description and facial analysis of the La Paja Fm in the Villa de Leyva area was first made by Etayo (1968) and then by Forero and Sarmiento (1985). They divided the Arcillolitas Abigarradas Member into 5 segments that they describe in detail. In segment one, the presence of sparse gypsum like crystals and veins of microsparite strata like trombolites mounts, crusts of fibrous calcite with cracked rough surface led

Forero and Sarmiento (1985) interpreted this part of the section as deposited in a salt tidal flat.

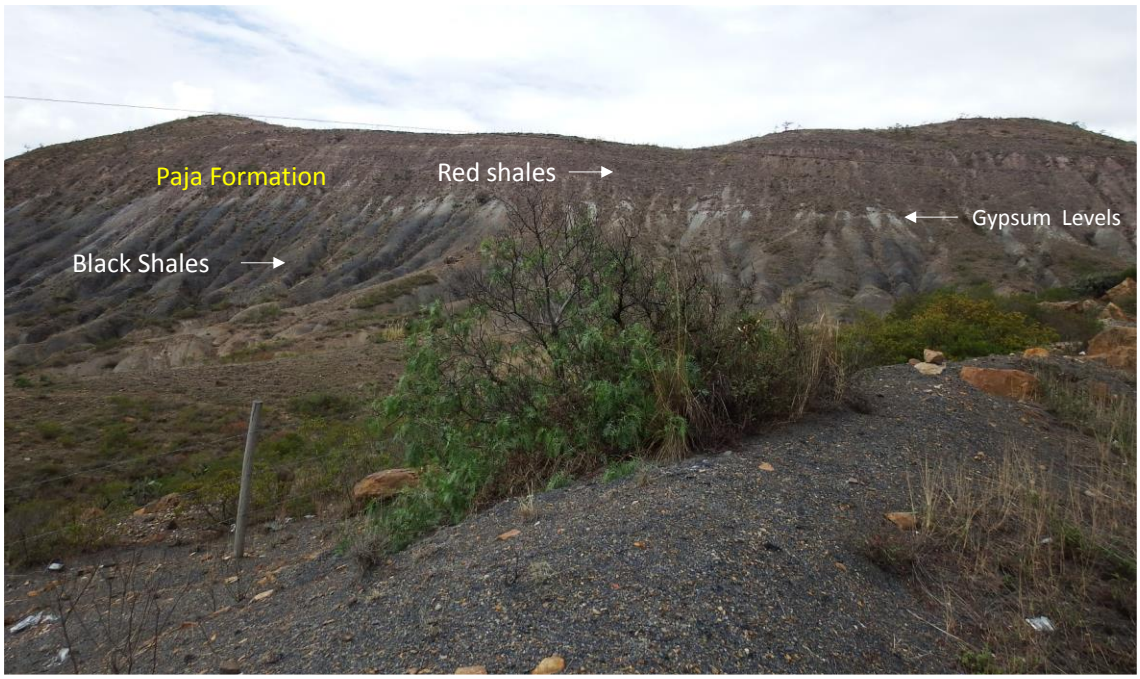

Photo 3.8. *Expression of the La Paja Fm (Barremian-Aptian) in the area of study. Note in the lower part the presence of black shales, separated by a gypsum level from the upper red shales.*

In the member of "arcillolitas abigarradas" the presence of desiccation cracks and algal mats suggests an intertidal to supratidal depositional environment (Forero and Sarmiento, 1985). The evolution from an intertidal to a supratidal flat environment shows a withdrawal of the sea towards the western side of the area. Toward the top, mechanical accumulations of marine fossils increase in quantity and variety, showing open sea communication, and representing the beginning of a transgression, which will continue in the lower part of the lower San Gil Fm (Late Aptian) (Forero and Sarmiento, 1985).

According to Forero and Sarmiento (1985), the fauna in this unit corresponds to concentrations of ammonites and bivalves shells, bone and fish remains, reptiles and foraminifers. The accumulation of different taxonomic groups, not dispersed, indicate mechanical accumulation. Etayo (1968, 1978, 1979, *in* Forero and Sarmiento, 1985) proposed that this accumulation, especially the fossils in nodules, correspond to transport by selective currents in tidal channels. Fragments of wood, branches, leaves of conifers and cycads (Huertas, 1969, 1970, 1971, *in* Forero and Sarmiento, 1985), and of plants growing in continental environments were transported from the continent to the sea, and eventually deposited at the flat. Subtle prints of leafs and little stems in black shales with or without gypsum are probably related to swamp vegetation, without any transport, which suggest a swamp environment.

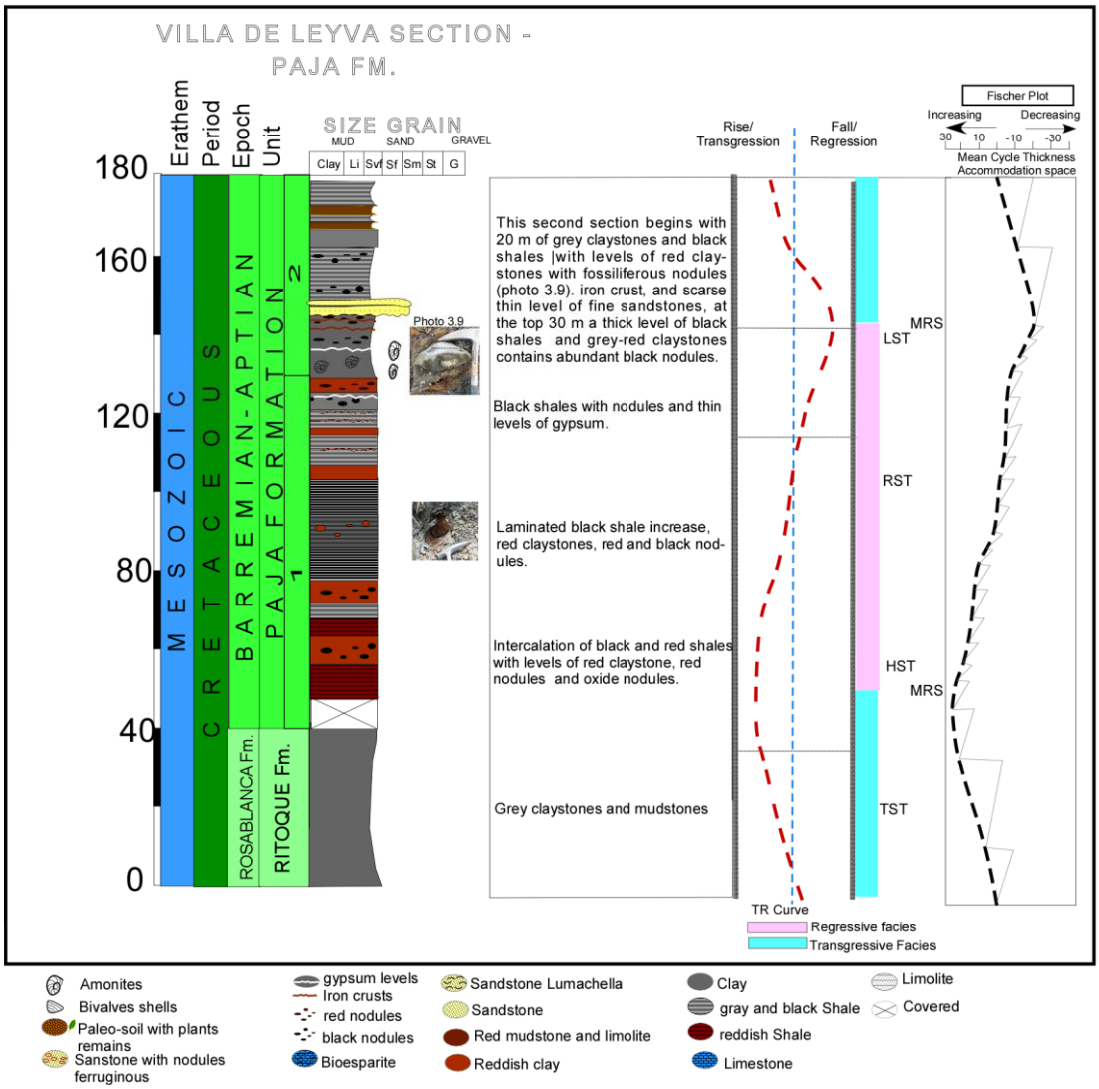

Figure. 3.29. *Section of the La Paja Fm (Barremian-Aptian age), measured and described along the Villa de Leyva-Sachica road (from this work).*

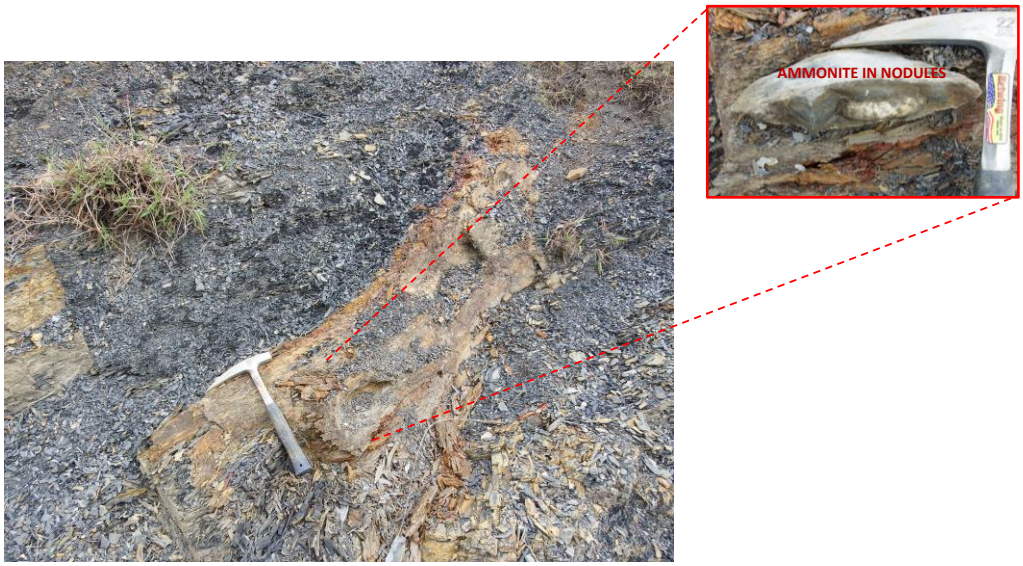

Photo 3.9*. Showing the characteristic lithology from La Paja Formation with black to gray shales and a red level of claystones with nodels, sometimes with ammonites (right upper square).*

Autochtonous fossils, like criptoalgaceas structures, burrows, trails, indicate a soft substratum. Burrows and footprints are not deformed, which suggests an early hardening of the rock before lithification of the sediment. Print of soft leaves, small stems within black claystones are associated with swamp vegetation.

- **Chiquinquira Section**

The name and age of the Upper Albian to Lower Cenomanian Chiquinquira Fm were proposed by Ulloa and Rodriguez (1979) (see chapter 2). The Chiquinquira Fm has been studied along the Sutamarchan-Chiquinquirá highway (Photo 3.10 and 3.11). There, an 800 m thick series is exposed, made of claystone and dark gray shale with thick intercalations of sandstone beds (Figure 3.30).

Photo 3.10*. Thick sandstone level in the Chiquinquira Sandstone (Late Albian to Early Cenomanian).*

The Areniscas de Chiquinquira is divided into 5 contrasted segments (Ulloa and Rodriguez, 1979, 1991). Segments 1, 3 and 5 in Figure 3.30 correspond to sandstone levels, while sequences 2 and 4 are fine-grained claystone, mudstone and shales. Sandstone is approximately made of quartzarenite (80%) and sublitharenite (20%).

The base of the Chiquinquira Fm is marked by the first appearance of thick sandstone beds above the shales of the Hilo Fm (Lower Simiti Fm). The sequence (1 to 5) shown in the left part of the column represents the division given originally by Terraza (2012). The sequence 1 shows an increase in the thickness and grain size of the sandstone beds. The sequence 2 is composed principally by clay and shale with few and thin beds of sandstone. The third sequence (Figure 3.30) is composed of claystone with few levels of siltstone, and important and thick beds of fine- to medium-grained sandstone (photo 3.10). Sequence 4 is almost totally covered but the topographic aspect suggests that much of the sequence is composed by claystone. Sequence 5 is made of claystone with several beds of white, fine- to medium-grained quartz-sandstone. (Figure 3.30).

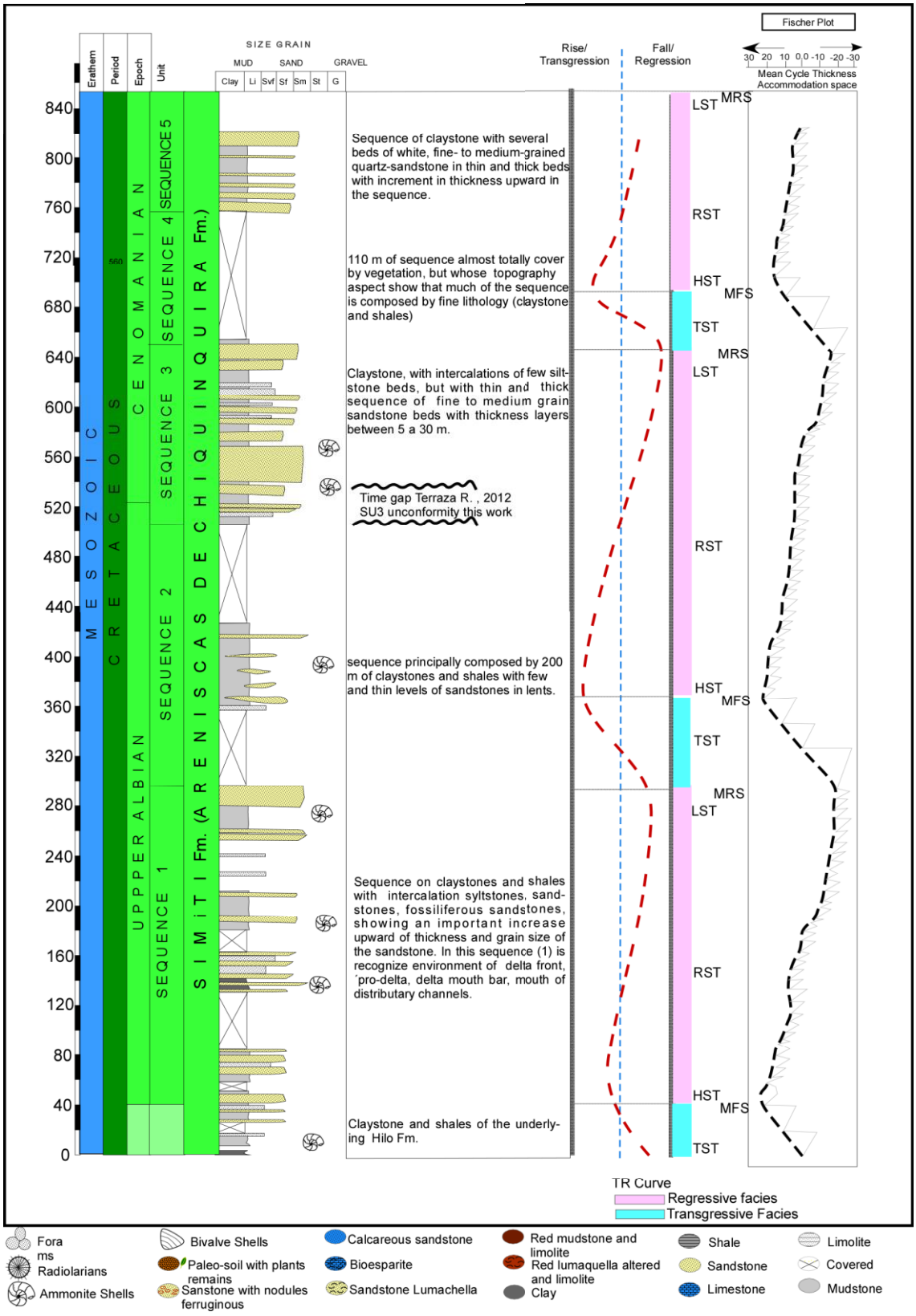

Figure 3.30. *Chiquinquira section, composed by observations made in this work and modified from Terraza (2012).*

These sandy segments (1, 3 and 5) represent prograding shallow marine, tidal-dominated environments, under low hydraulic regime (Terraza, 2012), while fine facies

represent a calm sea offshore bottom, interrupted by accumulation of sand and shell remains. Segments 1 and 2 are of Late Albian age and segments 3, 4 and 5 are Cenomanian in age.

In general, segments 1, 3 and 5, considered as sandy or with high sandy content, represent a prograding shallow marine environment, where shore facies prograde onto clayey offshore facies (segments 2 and 4). These shallow environment developed extensive sandy to sandy-muddy tidal flats, experiencing important periods of subaereal exposition (Terraza, 2012).

For example, in sequence (1) a deltaic environment is recognized, made of delta front, pro-delta, delta mouth bar, and mouth of distributary channels. Sequences 2 and 3 (in the sense of Terraza, 2012), composed primarily of claystones, mudstones and shales, represent an offshore marine environment with storm-deposited sand accumulation.

Photo 3.11. *E-W panoramic view, showing from base to top, the contact between the Simití Fm and the Areniscas de Chiquinquira Fm, and the Conejo Fm at the top.*

Terraza (2012) reported a stratigraphy hiatus at the base of sequence 3, probably in the Late Albian or Early Cenomanian, which is correlated with the sequence boundary of Villamil (1998) located at the base of the Churuvita Fm (top of the Upper San Gil Fm) as a consequence of a relative falling sea level (Villamil, 1998). This discontnuity was also identified by Guerrero (2002) at the boundary between the Middle Une (Late Albian) and Upper Une Allomembers (Cenomanian). This time gap, reported by Terraza (2012), coincides with one of the regional unconformities (SU) identified in this work.

Petrography: Thin sections from the Upper Albian to Lower Cenomanian Chiquinquira Fm (Petrographic section 3.4) show an increasing grain size from very fine in sample JG-P1-07 (a; lower part of sequence 1), to samples JG-P1-08 (b) and JG-P1-09 (c), where the grain size is fine to medium and sand is cleaner and better sorted. Grain size then decreases from sample JG-P1-09 (c) to the top of the section (d, sample JG-P1-10). At the base (a) and top (d), sandstone is more clayey, cleaner and better sorted.

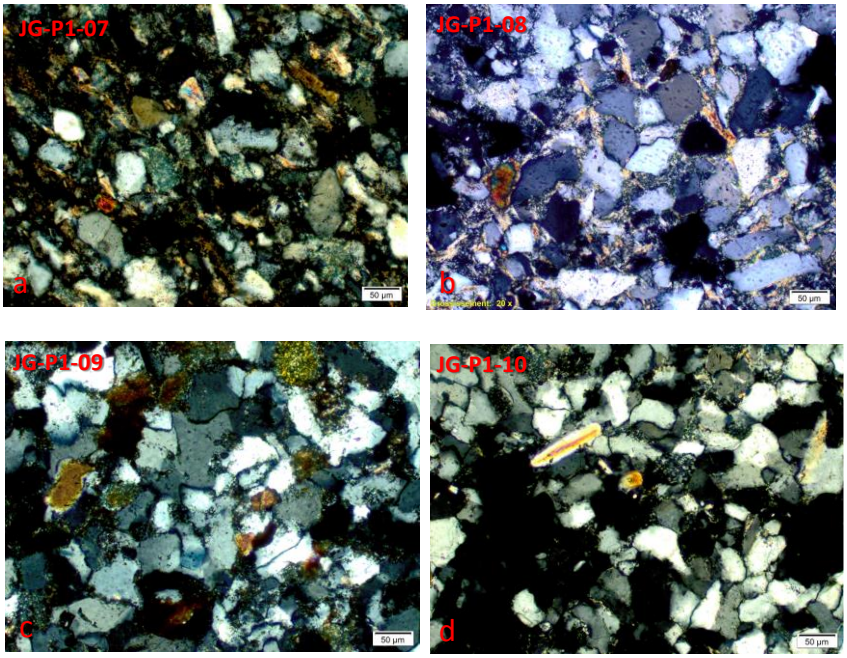

Petrographic Section. 3.4*. Sandstone from the Upper Aptian-Lower Cenomanian Areniscas de Chiquiquira Fm. a) Near the Simiti-Lower Areniscas de Chiquinquira limit; b) Upper part of sequence 1; c) Lower part of sequence 3; d) Near the top of the Arenicas de Chiquinquira Fm.*

Based on our interpretation (transgression – regression curve and Fisher plot) and on observations by other authors (Ulloa and Rodriguez, 1979; 1991; Villamil, 1998; Guerrero, 2002; Terraza, 2012), we propose the following schema of sequence stratigraphy for the Arenisca de Chiquinquira Fm (Figure 3.30): Three complete T-R sequences as is shown in Figure 3.14 (TST-HST-FSST-LST) are developed from the base to the top in the section of Figure 3.30. The lower T-R sequence coincides with the unit sequence 1 of Terraza (2012), the second T-R sequence covers the unit sequences 2 and 3 in the sense of Terraza (2012); and finally our third T-R sequence (at the top) covers the unit sequences 4 and 5 of Terraza (2012). In the description of the Areniscas de Chiquinquira, Terraza (2012) recognizes an unconformity at the Late Albian/Early Cenomanian boundary which probably corresponds to the unconformity SU3 recognized in this work (chapter 4).

- **Otanche section**

In the Otanche area (Puerto Boyaca), a compiled section of the Cretaceous succession (Figure 3.31) was recontructed from three stratigraphic sections (Guerrero et al., 1998). This area is principally devoted to the exploitation of emeralds from the La Paja Fm. Guerrero et al. (1998) collected samples for biostratigraphic purposes.

The section starts with 120 m of limestone and calcareous shales with some levels of sand of the Rosablanca Fm of Valanginian age. They are overlain by the 380 m thick la Paja Fm, composed of calcareous shales, siltstone and thick black to gray shales with foraminifera and ammonites.

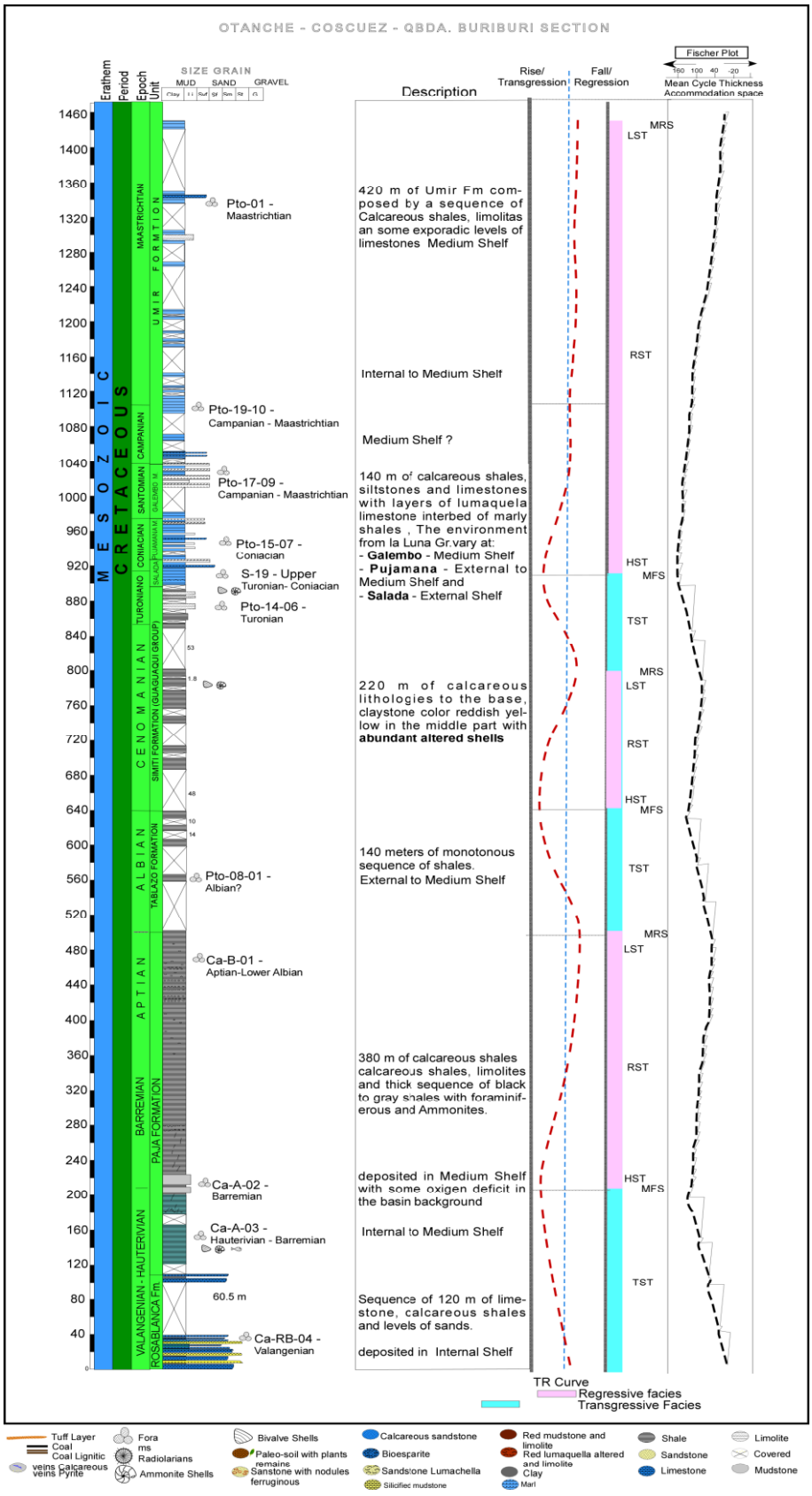

Figure 3.31. *Stratigraphic section in the area of Otanche, showing the La Rosablanca-Tablazo to Umir Fm succession. Modified from Guerrero et al. (1998).*

Then, the monotonous sequence of the 140 m thick Tablazo Fm, is covered by the 220 m thick Simiti Fm (Guaguaqui Group), made of calcareous lithologies at the base, reddish to yellow claystone with abundant altered shells. The Simiti Fm is overlain by 140 m thick series of calcareous shales, siltstones and limestones with coquina interbeds of the Salada, Pujama and Galembo Fms (La Luna Group). The section ends with the 420 m thick Umir Fm composed by calcareous shales, limolitas and sporadic levels of limestone, of Maastrichtian age.

Guerrero et al. (1998) collected 31 samples from the Cretaceous series of the Otanche section (WEC) and determined the age of the different formations as shown in Figure 3.31. Macrofossils collected by Guerrero et al. (1998) indicate ages corresponding to the Upper Hauterivian-Lower Valangenian (*Olcostephanus* sp.) to Aptian (*Gargasiceras* sp.??), and to the base of the Late Albian (*Laraiceras* sp. *Oxytropidoceras* sp., *Venezoliceras* sp.).

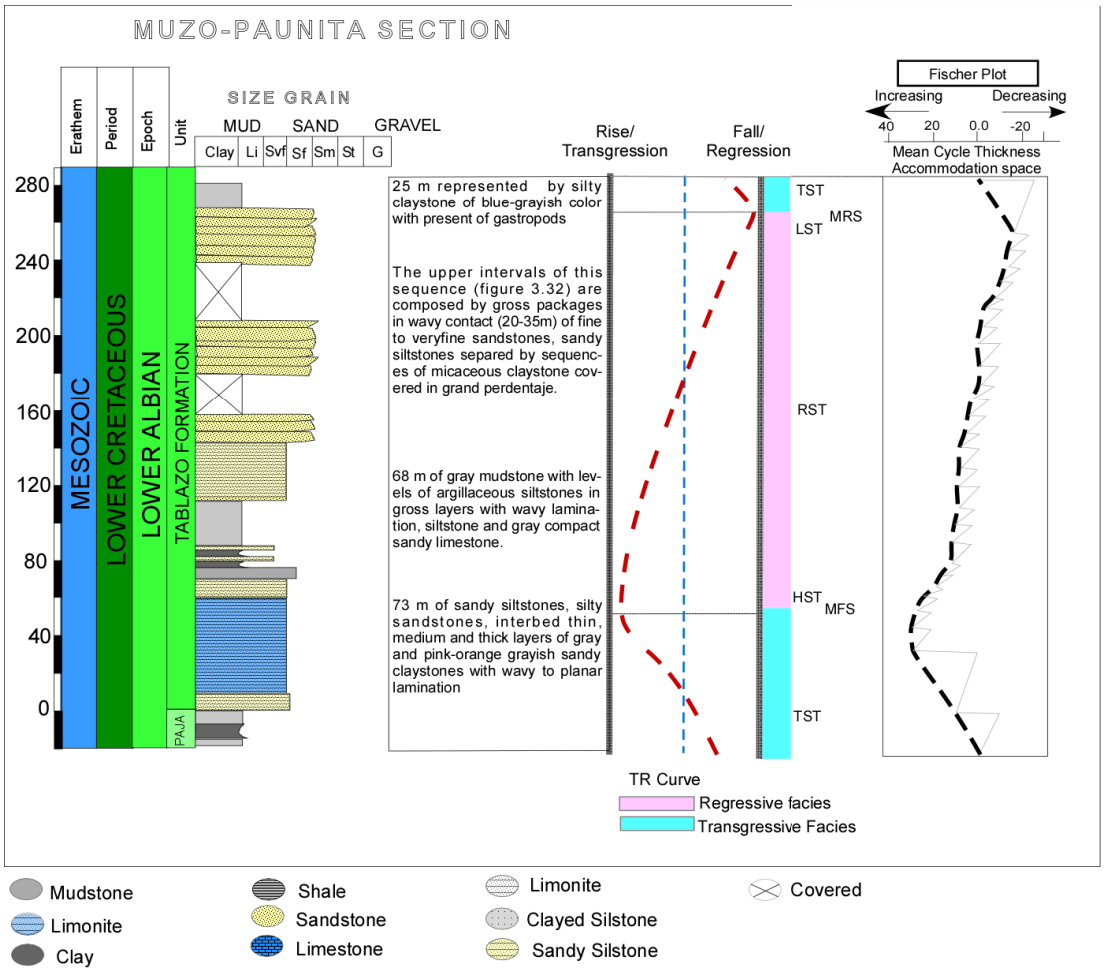

***Figure 3.32**. Muzo-Painita stratigraphic section, corresponding to the Tablazo Fm. Modified from Reyes et al. (2006).*

- **Muzo-Paunita section**

In the area of Muzo-carretera vieja-vereda Pautina, Reyes et al. (2006) studied a 273 m thick section of the Tablazo Fm resting on the La Paja Fm (Figure 3.31). According to its stratigraphic position, an Early Albian age is inferred for the Tablazo Fm (Reyes et al., 2006). From base to top this unit is composed of sandy siltstone, silty sandstones, with thin, medium and thick interbeds of gray to pink-orange grayish sandy claystones with wavy to planar lamination (73 m); gray mudstone with thick layers of argillaceous siltstone with wavy lamination, siltstone and gray compact sandy limestone (68 m); Thick sets of fine to very fine sandstone and sandy siltstone in wavy contact, separated by layers of micaceous claystone, mostly covered (20-35 m); and finally, blue-grayish silty claystone with gastropods (10 m) (Figure 3.32).

- **La Palma Otanche-Florian-Terraza section**

In the center of the study area (La Palma, Otanche, Florian, Terraza, Pauna, Borbur, Muzo, Coscuez, Yacopí), Terraza and Montoya (2011) compiled field sections of Valanginian to Lower Albian age (Figure 3.33). The exposed units are, from base to top: The Lower Valanginian Rosablanca Fm, the Upper Valanginian Ritoque/Furatena Fm, the Hauterivian-Barremian Lower Paja/Muzo Fm, the Late Aptian-Early Albian Upper Paja/Capotes Fm and the Early Albian Tablazo Fm. This highlights the lack of Early Aptian deposits, which is supported by the section by Guerrero et al. (1998), in which none of the collected fossils are of Early Aptian (Figure 3.31).

Samples collected by Guerrero et al. (1998) in the area of Otanche-Coscuez yielded foraminifera of Valanginian (*Globuligerina Caucasia* Gorb & Por., *Globuligerina* cf. *gulekhensis* Gorb & Por, *Marssonella* sp., *Trocholina aptica* Leup.) and Aptian to Lower Albian age (*Hedbergella aptica* (Agalarova), *Clavihedbergella bollii* (Longoria), *Hedbergella planispira* (Tappan), *Hedbergella infracretacea* (Glaessner), *Pleurostonella obtuse* Berth, *Globigerinelloides ultramicrus* (Subb.)).

- **Chima section**

In the area North of Velez and South of the Barichara town, Rollon and Carrero (1995) described a succession from the Arcabuco Fm (Jurassic) to the Areniscas de Chiquinquira Fm (Cenomanian), which shows an important sandstone content with thin intercalations of shales in almost the whole series.

The content of sandstones is more important at the base (Arcabuco and Cumbre Fms) and in the upper part of the section (upper la Paja, Tablazo and Simiti Fms). In the middle part of the section, is a ~700 m thick series of shales with sporadic thin layers of sandstone. The Berriasian-Early Hauterivian Rosablanca Fm is marked by the presence of thick level of limestones. The base of the section is interpreted as the upper part of a RST reaching a MRS, overlain by two complete sequence (TST-HST-RST-LST) of Early Hauterivian to Barremian/Early Aptian boundary, and Early-Aptian to Lower Cenomanian age, respectively (Figure 3.34).

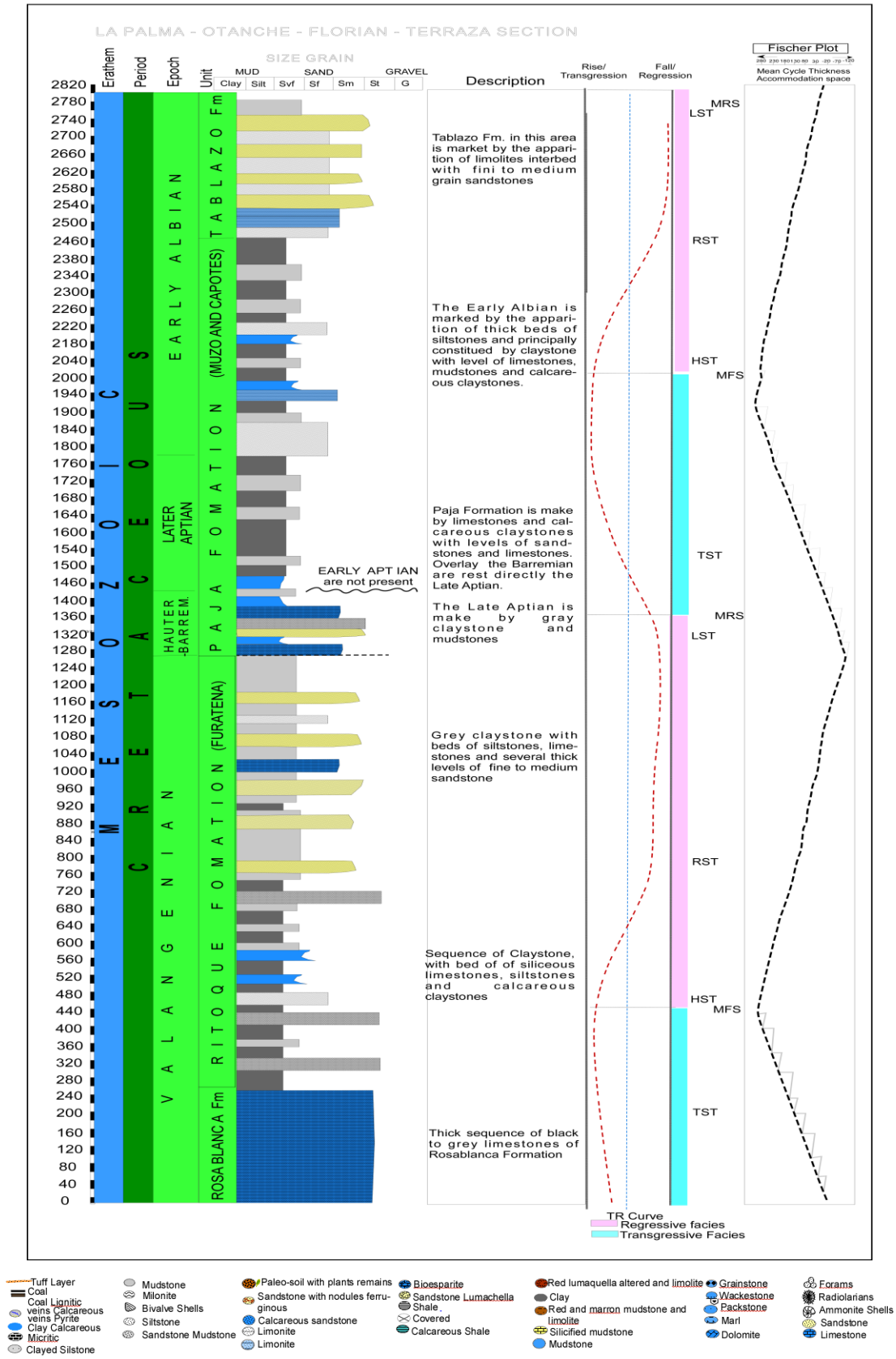

Figure 3.33. *Stratigraphic section in the Pauna – Muzo – Coscuez area, showing the Rosablanca to Tablazo Fm succession. Modified from Terraza and Montoya (2011) and interpreted in this work. Note the Early Aptian hiatus reported by Terraza and Montoya (2011).*

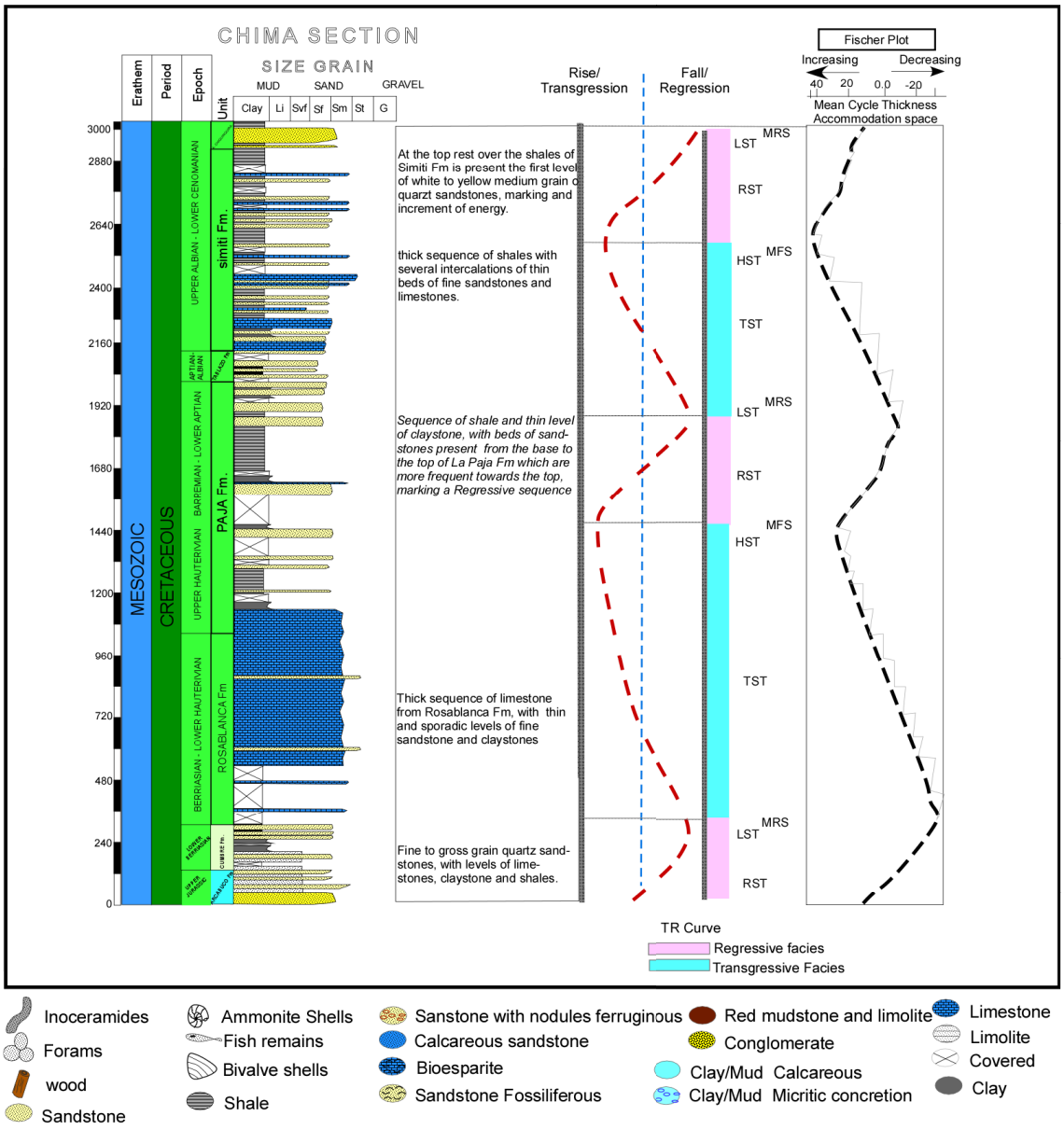

Figure 3.34. *Stratigraphic section of Chima, North of Velez town –southwest of Barichara town, showing the succession from the Arcabuco (Jurassic) to the Areniscas de Chiquinquira Fm (Cenomanian) (Modified from Rolón and Carrero, 1995).*

- Guineal well section

Figure 3.35 shows the Guineal well section (location in Figure 3.5). It comprises from top to base:

(1) Galembo Mb (Santonian-Coniacian): The upper half part consists of marl and claystone, with 20-50 ft thick beds of sandstone in lesser proportion. The lower half part is a calcareous series made of claystone, calcareous siltstone with an increase of calcareous detrital and of limestone beds; at the base, the unit presents massive, 40 ft thick limestone beds. Siltstone and claystone are black, locally dark brown, slightly to very calcareous, locally with sparse pyrite crystals, veins and siliceous to slightly calcareous nodules. Remains of cephalopods, fish scales, pelecypods and ichnofossil are

present, as well as few thin beds of friable sands. Planktonic microfossils (globigerina, radiolarian) indicate a Santonian-Coniacian age and an upper bathyal environment.

(2) Pujama Mb (Coniacian-Turonian): The Pujama Mb is the middle member of the La Luna Fm. It is mainly made of shale and in minor proportion of siltstone. Scattered, 1-20 ft thick levels of sandstone are present mostly in the lower part of the member. Claystone and siltstone are black to dark grey, hard to soft, finely laminated, tabular, bituminous, slightly calcareous and locally dolomitic. Pyrite is disseminated in small crystals or in veins. Ichnofossils are present. The upper part exhibits beds of medium-grained, consolidated sandstone formed of white to milky, angular, well sorted quartz grains and siliceous cement. The sandstone is poor in glauconite and has a low porosity. Massive limestone beds are greyish to black, hard, microcrystalline, occasionally with abundant pyrite and crystals of sparite, and grade locally to calcareous sandstone.

(3) Salada Mb (Turonian-Upper Cenomanian): The lower member of the La Luna Fm is dominantly made of calcareous shale, with thin limestone beds and occasional clastic intercalations. Shales are black to greyish black, bituminous to very bituminous, locally silty to sandy, and grade to clayey limestone. Limestone is black to greyish, very hard, occasionally slightly silty to sandy. Clastic intercalations are made of medium- to coarse-grained loose quartz, sub-angular to sub-rounded, poorly sorted, and contain sporadic grains of calcite and glauconite.

(4) Simiti Fm (Middle to Lower Albian): The upper part of the Simiti Fm is composed of black shale, in part silty or calcareous, with intercalations of thin layers of limestone and sandstone. These lithologies gradually change in the lower part to dark brown, silty shales with beds of limestone and marl. Sandstone is loose, made of medium- to coarse-grained, angular and moderately sorted translucent quartz. Occasionally, white, clean, well consolidated, fine-grained sandstone, present sub-angular to sub-rounded grains and a good porosity. No fauna is reported. The lack of fauna and the abundance of pyrite, siderite and carbonaceous remains indicate a low energy, dysoxic marine environment, with little circulation at the bottom.

(5) Tablazo Fm (Albian-Upper Aptian): The two upper thirds of this unit are constituted by massive, grey dark and dark brown, 20-40 ft thick limestone beds, with thin intercalations of dark brown to brown cream colored mudstone, of wackstone and occasionally packstone texture. The lower third (below 7450 ft) is made of calcareous shale and silty, calcareous claystone; limestones beds are more frequent. The base exhibits soft, brown to grey and black calcareous clay, locally silty, with abundant pyrite and limestone at the base.

(6) Paja Fm (Aptian-Barremian): The Paja Fm is mainly composed by hard to very hard calcareous claystone. It locally presents black to dark brown shales, levels of soft calcareous claystone, occasionally dolomitic, with micro-pyrite in veins, and abundant veins and fractures filled of calcite.

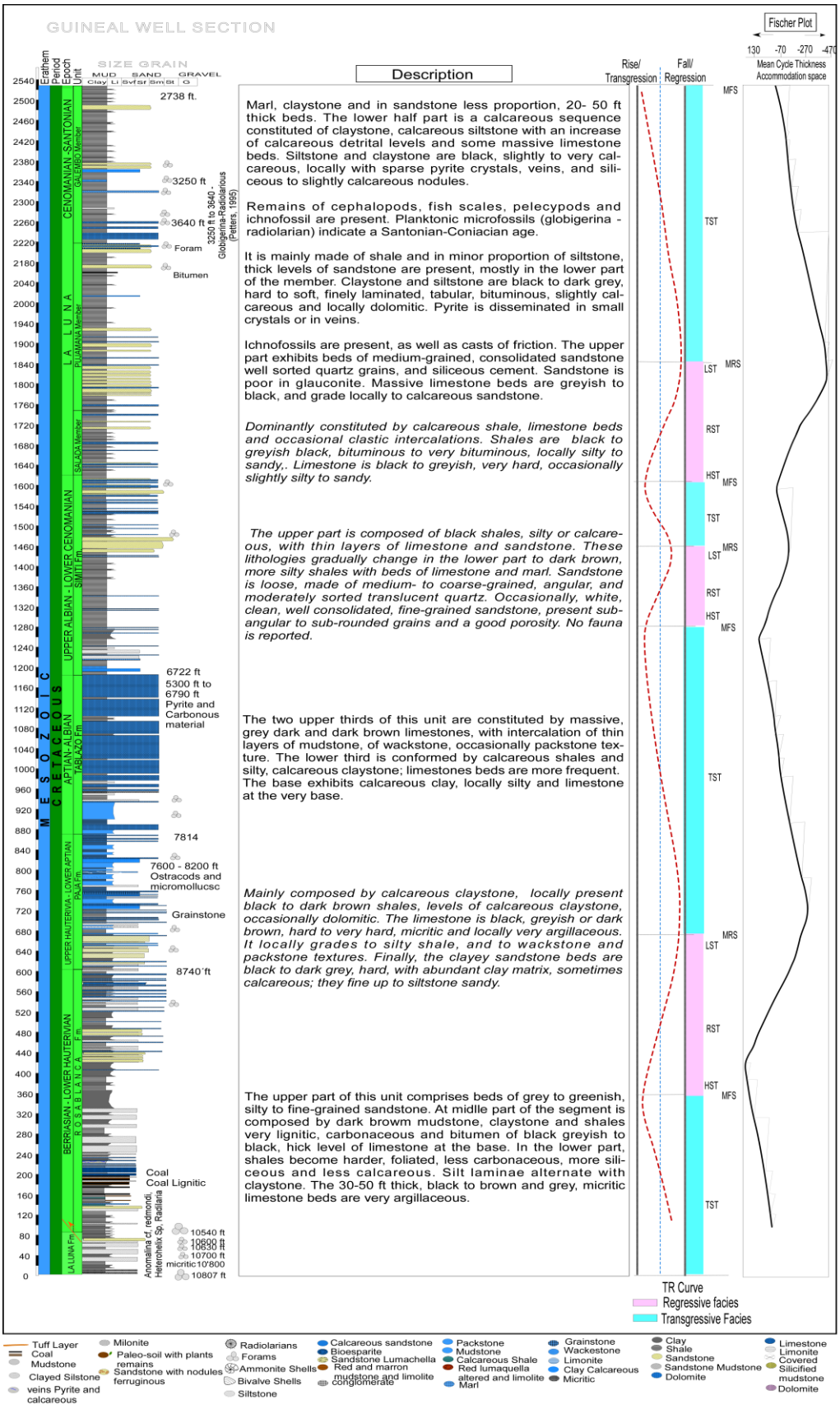

Figure 3.35. *Stratigraphic section of the Guineal well, showing all the sequences from the Berriasian – Santonian (Well data taken from Ecopetrol, reconstruction and interpretation from this work).*

The limestone is black, greyish or dark brown, hard to very hard, micritic and locally very argillaceous. It locally grades to silty shale, of wackstone and packstone textures. The clayey sandstone beds are black to dark grey, hard, with abundant clay matrix, sometimes calcareous; they vary from fine up to siltstone sandy.

(7) Rosa Blanca Fm (Hauterivian): The upper part of this unit comprises beds of grey to greenish, silty to fine-grained siliceous sandstone, well cemented (quartzite-like). Its midlle part is composed by a thick series of grey to dark brown, very lignitic, carbonaceous and bitumen-rich mudstone, claystone and black greyish to black shales, hard to soft, slightly to very calcareous and carbonaceous with thick levels of limestone at the base. In the lower part, shales become harder, foliated, less carbonaceous, more siliceous and less calcareous. Silt laminae alternate with claystone. The 30-50 ft thick, black to brown and grey, micritic limestone beds are very argillaceous, hard, with calcite veins.

Biostratigraphy and stratigraphy: 117 samples were analyzed from the the Guineal-1 well. Microfossils were identified from the Galembo and Pujama Mbs, while the other intervals were dated using ostracod and mollusk species. No microfossils were found in the Simiti Fm. In the Tablazo and La Paja Fms (Zone C), only ostracods and small mollusks were reported. Planktonic foraminiferas (*globigerinids, radiolarians*; Petters, 1995) were identified in the La Luna Fm, indicating a Coniacian age and an upper bathyal depositional environment.

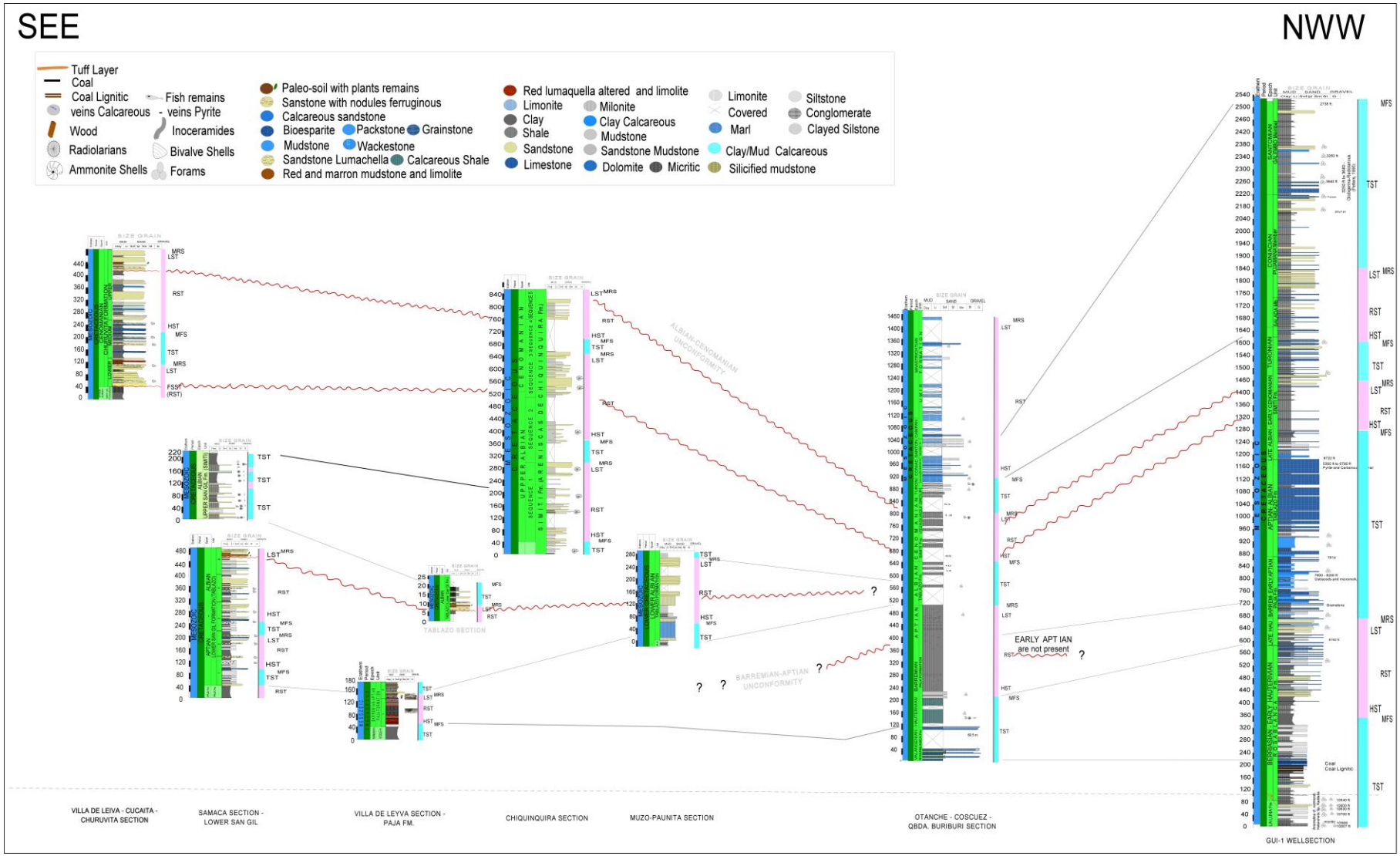

***Figure 3.36**. SEE-NWW correlation in the Centre of the study area, showing stratigraphic changes from the Berriasian to the Cenomanian. Note that the sandstone levels in the eastern and central parts become fine sediments to the West, and that units become thicker in the same direction.*

3.4.3 Northern Region

The units of the northern area of the WEC are the same as in the MMV (see chapter 2). These units are from base to top, the Girón, Arcabuco, Tambor-Cumbre, Rosablanca, Paja, Tablazo, Simiti, La Luna, Umir and Lisama Fms (Figure 3.4).

- Barichara section

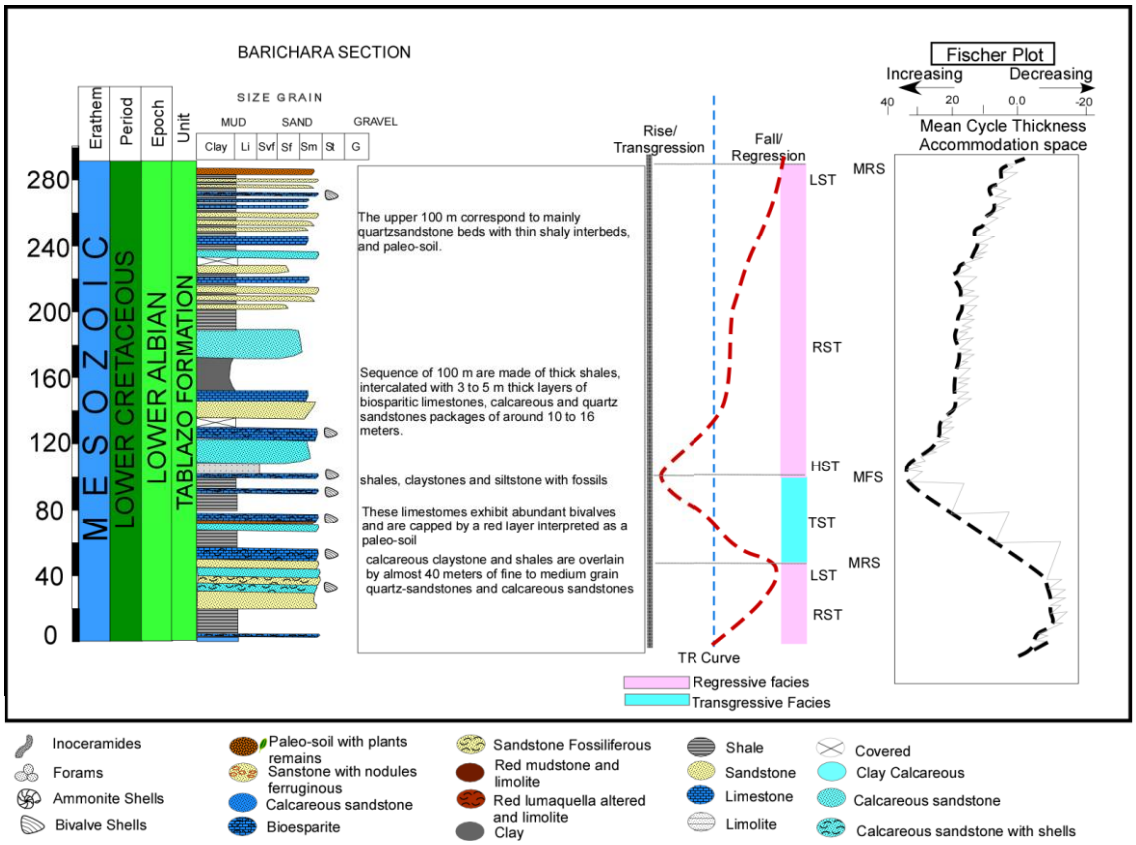

Figure 3.37*. Barichara section of the Tablazo Fm. Personal observations, reconstruction and interpretation from this work.*

A stratigraphic section of the Tablazo Fm has been studied in the area of Barichara (Figure 3.37). At the base, calcareous claystone and shales are overlain by almost 40 meters of fine- to medium-grained quartz-sandstones and calcareous sandstones. These exhibit abundant bivalves and are capped by a red layer interpreted as a paleo-soil. The overlying 100 m are made of thick shales, intercalated with 3 to 5 m thick layers of biosparitic limestones, calcareous and quartz sandstones packages of around 10 to 16 meters. The upper 100 m correspond to mainly sandstone beds with shaly interbeds. The thickening- and coarsening-upward trend suggests an increasing energy.

- Rio Sogamoso section

The Sogamoso succession starts with a 120 m thick series of medium- to coarse-grained white quartz sandstones with intercalations of claystones (Tambor Fm, Berriasian). This

is overlain by a 720 m thick set of monotonous gray limestones in variably thick layers (from 20 to 130 m) and intercalations of black shales and calcareous shales.

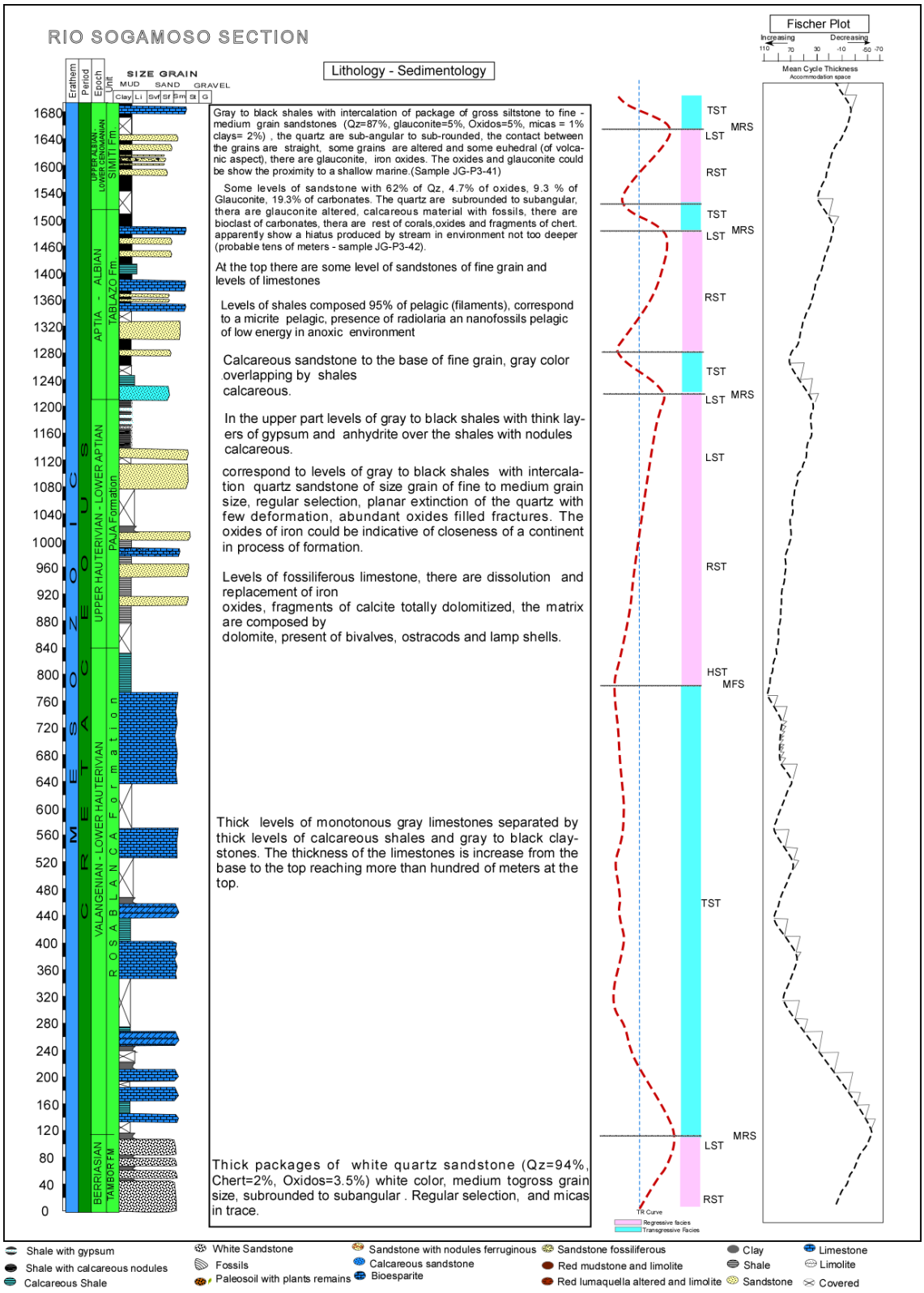

Figure 3.38*. Rio Sogamoso section, corresponding to the Berriasian-Lower Cenomanian interval. The column indicates the trangresive-regresive curve (dust red line) and the Fisher plot shows the variation in the accomodation space. Reconstruction and interpretation from this work.*

The Late Hauterivian is composed of shales. The Barremian is marked by the first appearance of thin layers of sandstone, which are present till the Early Albian, together with fossiliferous limestone beds (bivalves, ostracods and shells), dissolution and replacement of iron oxides. The Late Barremian-Early Aptian interval is marked by increasingly thick quartz sandstone beds, with abundant oxides filling the fractures, suggesting a close continent. The upper part of Early Aptian series is made of black shales with thin layers of gypsum and anhydrite. The succession continues upward with a thick series of black shales, calcareous sandstones, calcareous shales containing radiolarian and pelagic nannofossils, deposited in a low energy, anoxic environment during the Late Aptian-Early Albian (Tablazo Fm). The last 100 m comprise 20 meters of shales at the base, an increasing upward amount of sand layers in the next 60 m, showing an increase of the energy to the top and the last 20 m of limestone and shales. Some levels of limestone present a phosphate smell, red calcareous sandstones and dark limestone, some levels have thalassinoides and glauconitic sands. The boundary with the Simiti Fm is marked by the appearance of red levels of clayey sandstone. The thickness of this unit changes from 270 m in Bucaramanga, to around 280 m in Barichara, and to 440 m in Lower San Gil in the Villa de Leyva area (see Figure 3.24 from this work; Etayo 1968).

- Boqueron del Medio Section - Playon Cuesta Rica Section.

Figures 3.39 and 3.40 show successions of Jurassic to Cenomanian age (Los Santos to Simiti Fms). At the base, quartz sandstone and siltstone of Jurassic age correspond to the Los Santos Fm. Limestones of Berriasian-Lower Hauterivian age (Rosablanca Fm) are overlain by monotonous shales of Upper Hauterivian-Lower Aptian age (La Paja Fm). The Aptian-Albian interval is represented by sandstones and shales of the Tablazo Fm, in turn overlain by monotonous shales of Upper Albian-Lower Cenomanian age (Simiti Fm).

- Yumeca-1 Section

Figure 3.41 shows the lithologies described according to cuttings from the Yumeca-1 well (location on Figure 3.5). The main target of this 13664 ft deep well was to evaluate the reservoir potential of the Lower Cretaceous units (Los Santos-Cumbre and Rosablanca Fms). The Cretaceous units are described from top to base.

The *Umir Fm* (Campanian-Maastrichtian, not represented on Figure 3.41) is composed of thick levels of grey to dark grey, micaceous, highly carbonaceous claystone, with sporadic intercalations of sandstone, which are more frequent in the lower part.

The *La Luna Fm* (Cenomanian-Santonian) is mainly composed of limestone beds, claystone interbeds being more abundant in the middle and lower part of the sequence. Occasional intercalations of thin layers of sandstone and siltstone are observed. Siltstone is dark brown to white and may contain glauconitic grains. Claystone is slightly laminated. Sandstone is gray to greenish, fine- to very fine-grained, well sorted, with a clayey matrix and abundant siliceous cement, very calcareous locally. Some beds are coarse- to very coarse-grained with sub-rounded, poorly sorted grains.

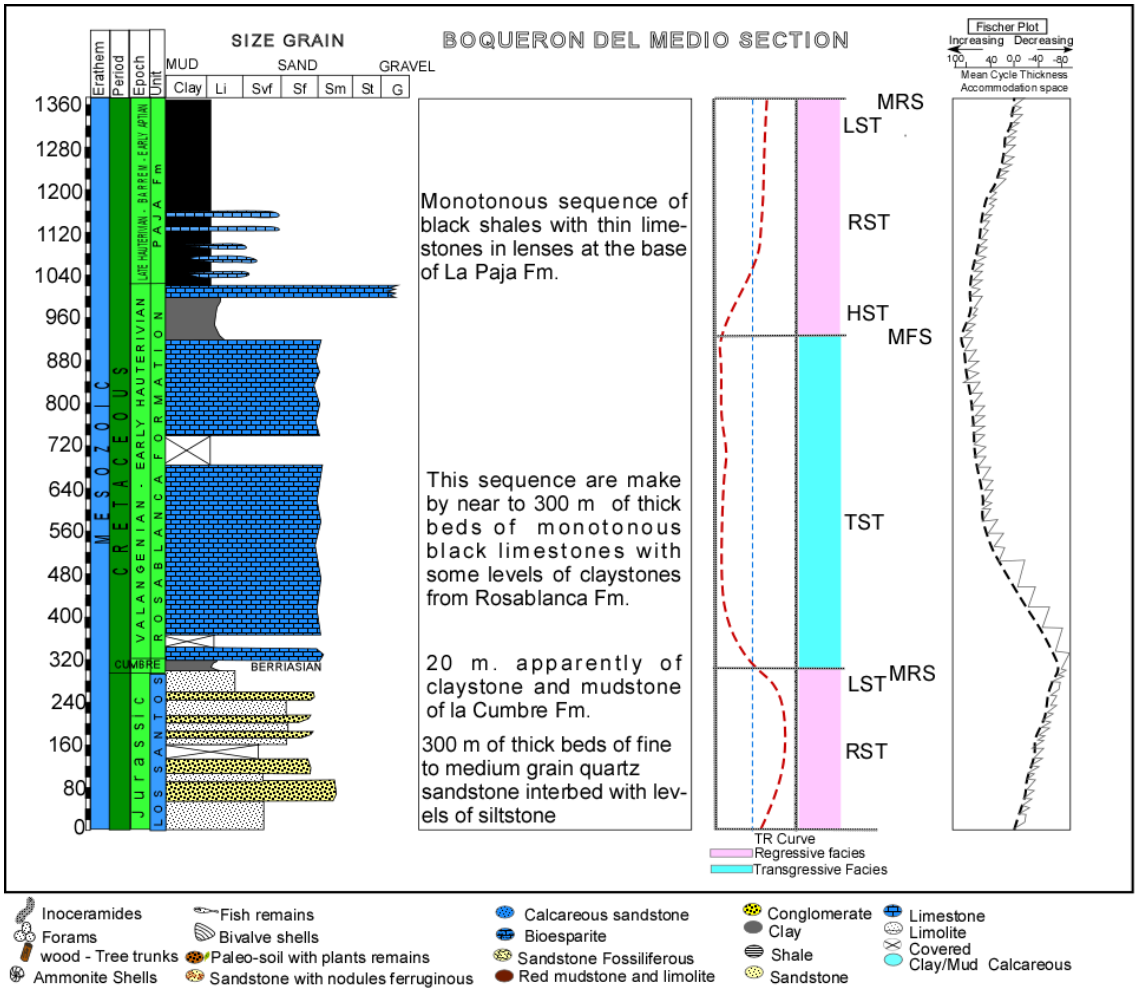

Figure 3.39. *Boqueron del Medio section, showing the Jurassic-Albian succession. Reconstruction and interpretation from this work.*

The *Simiti Fm* (Upper Albian-Lower Cenomanian) comprises grey to dark grey shale, although claystone is dominant in the upper 150 ft. The upper part shows sporadic thin beds of limestone and white to light grey, fine- to very fine-grained, slightly glauconitic sandstone. Sandstone is made of clean, sub-rounded to rounded, well-sorted quartz grains in an abundant siliceous, occasionally calcareous cement.

The upper 200 ft of the *Tablazo Fm* (Aptian-Albian) are made of sandstone, conglomeratic sandstone and limestone, with shale and claystone interbeds. The grey to dark grey sandstone contains very fine to fine, subangular, well sorted, translucent quartz grains in a clay matrix and calcareous cement. Limestone is light grey to white, massive, occasionally sandy. Grey claystone is present in the lower part of the unit.

The *Paja Fm* (Hauterivian-Lower Aptian) consists, in the lower part, of black shales and grey to dark, slightly calcareous shales, grey marls, dark grey, occasionally light grey limestone. In the upper part, thick beds of quartz sandstone and conglomeratic sandstone are present, marking the regional level “Paja Arenoso” (Barremian/Aptian).

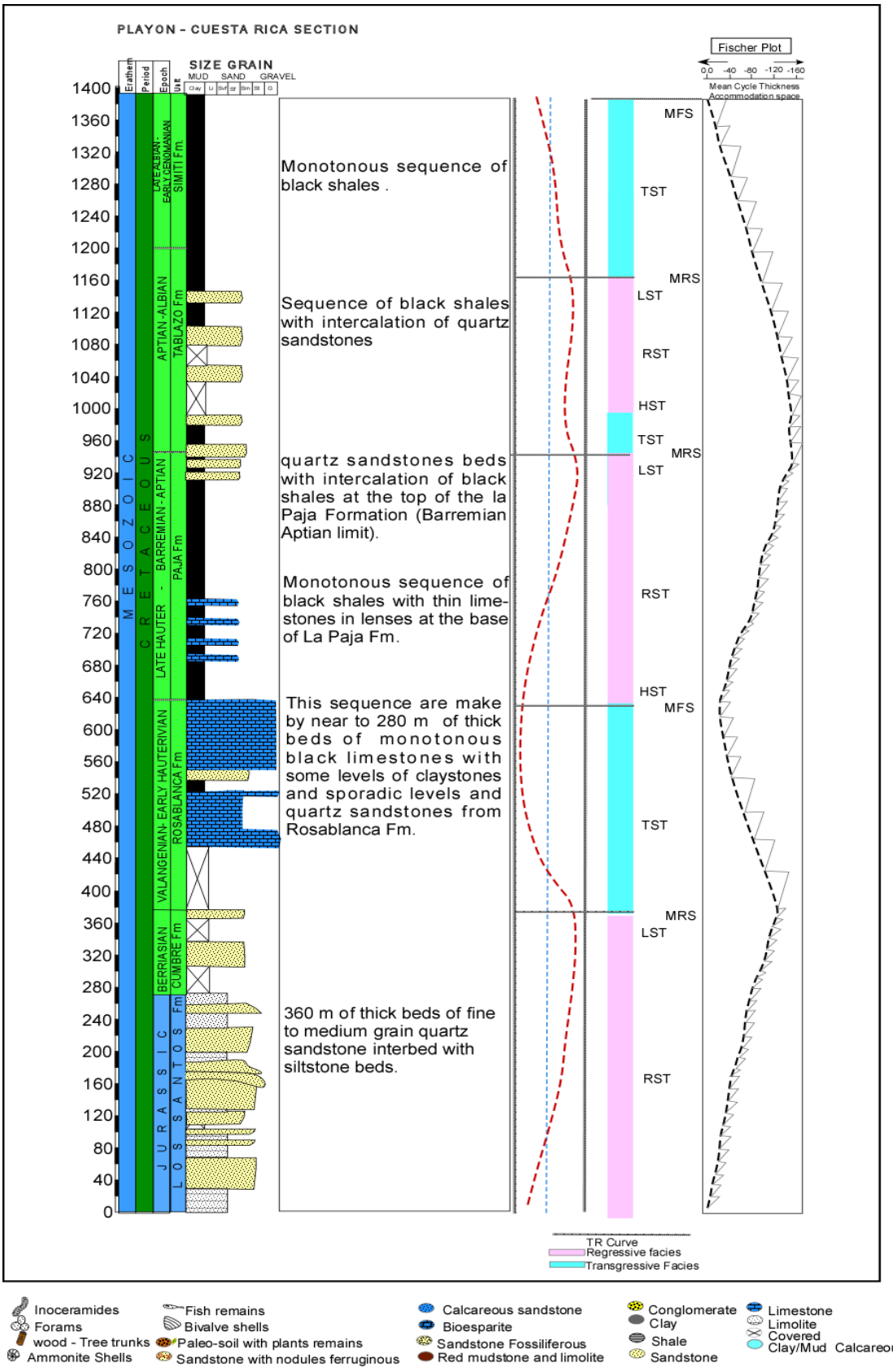

Figure 3.40. *Playon-Cuesta Rica section, showing the Jurassic-Albian succession. (Modified from Rolón and Carrero, 1995). Reconstruction and interpretation from this work.*

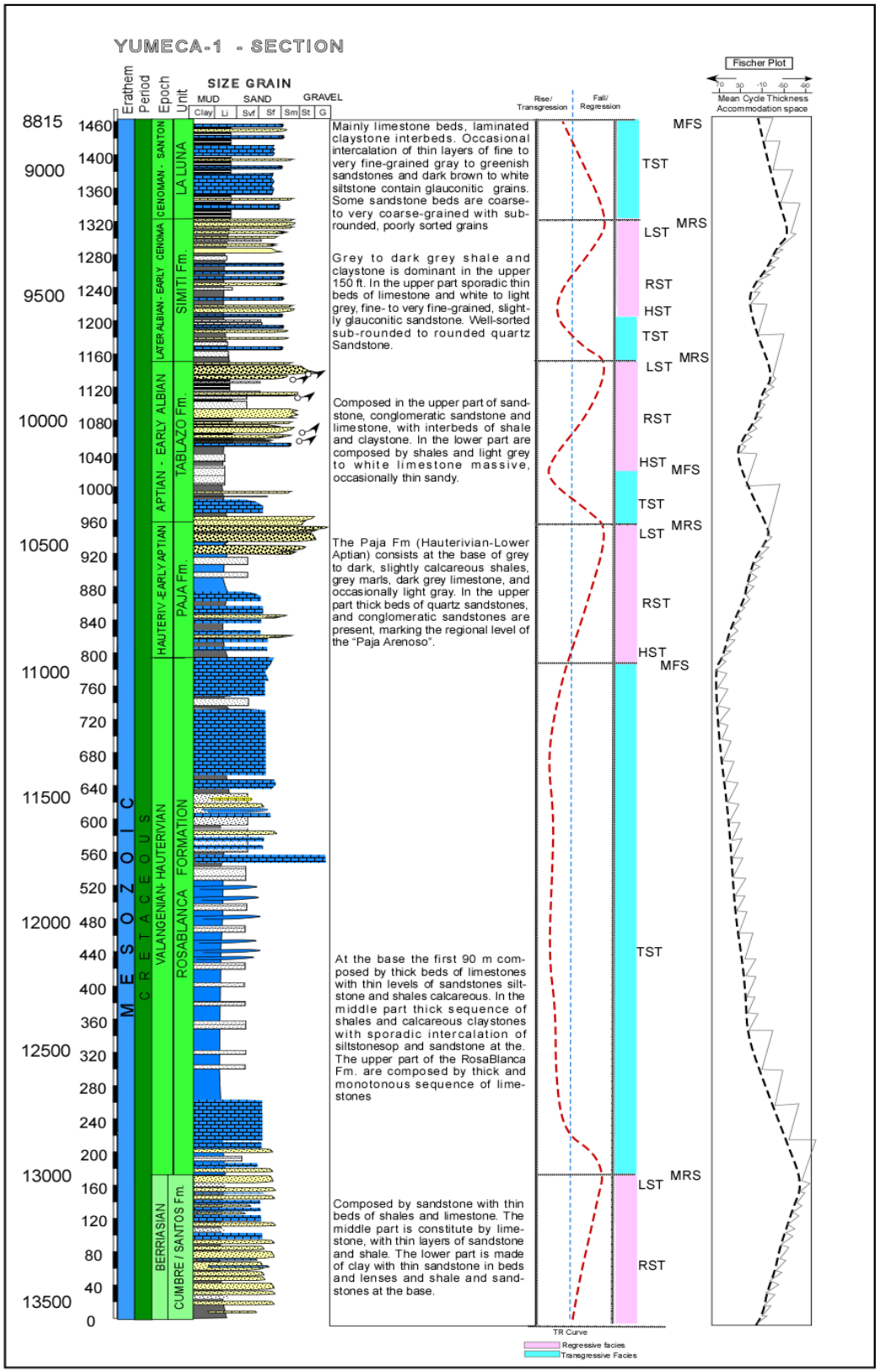

Figure. 3.41. *Yumeca 1 well section, showing a succession of Berriasian to Turonian age. Reconstruction and interpretation from this work.*

The *Rosablanca Fm* (Berriasian-Hauterivian) is mainly comprised of grey to dark grey limestone in the upper part, which is overlain by gray siltstone with thin lenses of limestone and sandstone, the grey shale becoming more abundant downward. The middle part is a thickening upward sequence of brown marl and shale with beds of light to dark limestone and calcareous lenses. The lower part is composed of light brown to yellow/cream limestone with shaly interbeds.

The *Cumbre/Santos Fm* (Berriasian) is composed, in its upper part, by sandstone with thin beds of shale and limestone. The middle part is constituted by limestone, with thin layers of sandstone and shale. The lower part is made of clay with thin sandstone in layers and lenses and shale at the base.

- Guane - 1 well

The Guane-1 well crosscuts a Jurassic-Tertiary succession. 39 samples of cuttings and cores were analyzed from the La Paja, Lower Tablazo, Rosablanca and Los Santos Fms.

Between 10510'-11330' (Upper La Paja-Lower Tablazo Fms), the laboratory Ecopetrol-ICP (2014) determined, besides gastropods, ostracods and possible radiolarians, the following groups and species. Planktonic foraminiferas: *Globigerinelloides* sp., *Hedbergella* sp., *Heterohelix* sp., *Ticinella* sp., *Ticinella* cf. *primula*, and fragments of *Rotaliporacea*; benthic foraminiferas: *Praebulimina wyomingensis*, *P.* cf. *wyomingensis*, *Praebulimina* sp. and Rotaliina. Common minerals are pyrite and siderite. The occurrence of *Ticinella* spp. and *P. wyomingensis* between 10560'-10860' indicates an Albian age.

In the 11341´ - 11781' interval (Rosablanca Fm), the following benthic foraminiferas were found: *Lenticulina* cf. *ouachensis*, *Lenticulina* cf *praegaultina*, *Choffatella* ssp. (maybe *C. decipiens*) with rest Rotaliina and Textularina. *L.* cf. *ouachensis*, *L.* cf. *praegaultina* and *Choffatella* spp. which suggest a Barremian-Early Aptian age, in the Early Cretaceous of Trinidad and the north of South America (Petters, 1954; Bartenstein and Bolli, 1977; Boli et al., 1994). Other fossils are gastropods, teeth fish, and remains of echinoids and ammonites. Between 11717' and 11750', ostracods, glauconite, pyrite and siderite are common. Ostracod species suggest a Valanginian age.

- Iwana - 1 section

In the Iwana-1 well (Figure 3.43), 36 core samples were analyzed in the Upper Tablazo-Lower Simiti Fms and from cuttings from the Rosablanca and Los Santos Fms.

- 9030'-9481' (Lower Simiti-Upper Tablazo): plancktonic foraminifera: *Hedbergella* sp., Heterohelicacea and Globigerinina; benthonic foraminiferas: *Lenticulina* sp., *Praebulimina* sp., *P. wyomingensis* and remains of Rotaliina and Textulariina; radiolarians: few *Dyctiomitra* sp. The Aptian-Albian age is based on the presence of Hedbergellids and radiolarians. Duque-Caro (2004, 2012) also quoted ammonites, while Patarroyo (2009) proposed an Early Albian age, based on bivalves and ammonites. The Simiti-Tablazo boundary is marked by the appearance of radiolarians reported in various wells: RW-1, Coyote-1, Iwuana-1, Punta Piedra-1, Torcoroma-1, Catalina-1,

Bosques-1, Prometeo-1 and Llanito-1 (Duque-Caro, 2004; Rodriguez et al., 2008; Patarroyo et al., 2013), which seems to be a significant regional event.

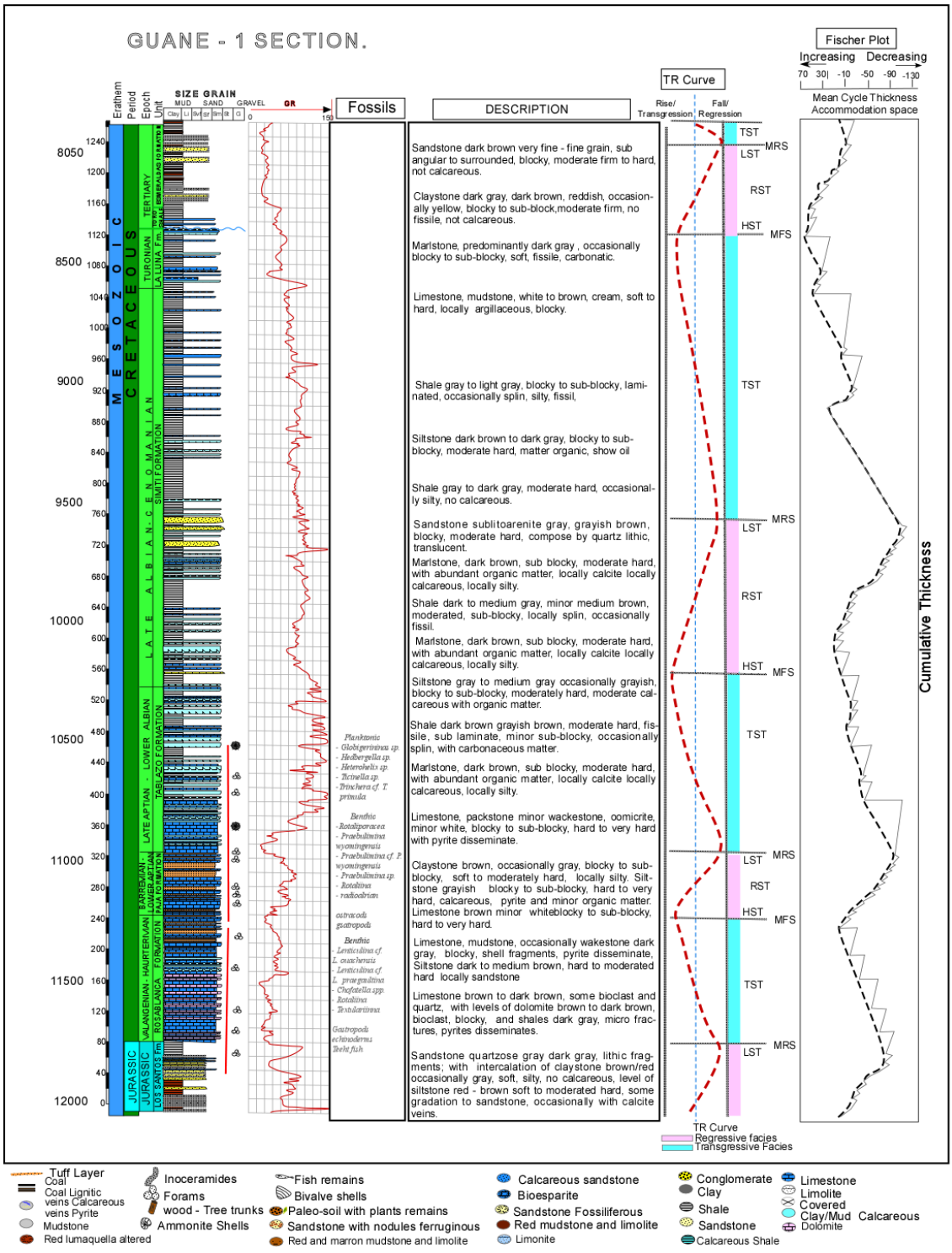

Figure 3.42*. Guane-1 Section, showing a Berriasian to Turonian succession. Reconstruction and interpretation from this work.*

- 11010'-11220' (Rosablanca-Arcabuco/Los Santos): only Globigerinina and abundant ostracods. At 11220': presence of shells, gastropods, phosphatic pellets, glauconite, amorphous pyrite and oxides.

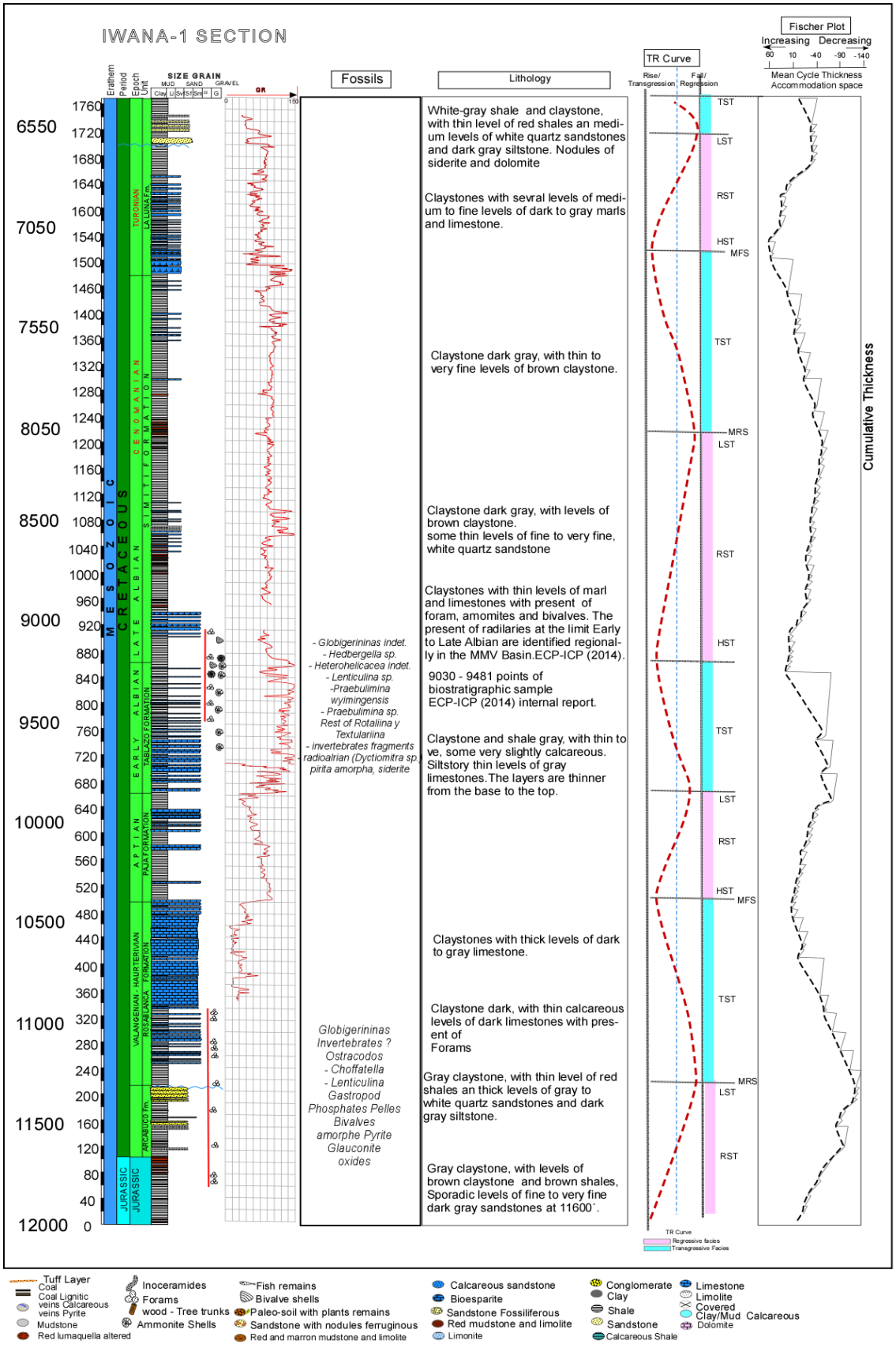

Figure 3.43. *Iwana-1 section, corresponding to a Jurassic to Paleocene-Eocene succession, Biostratigraphic analysis taken from ECP-ICP (2014). Reconstruction and interpretation from this work.*

With regards to the radiolarian event (Tablazo-Simiti boundary), the information from ammonites and bivalves in the wells RW-1, Prometeo-1 and Iwana-1 restricts this event from Early Albian to lower Late Albian (104-112 My, Gradstein et al. 2012). However, the absence of the genus *Ticinella* (specially *T. Primula*) dated by Leckie et al. (2002) as late Lower Albian to Middle Albian in age (109-105 My) suggests that this event is no younger than the Middle Albian.

The presence of ostracods, echinoderms, bivalves and benthonic foraminifera (Choffatella, Lenticulina), recognized from the Lower Rosablanca Fm in the wells Iwana-1, Prometeo-1, Bosques-1 and Catalina-1, and in outcrops in the Zapatoca region at the same level (Duque-Caro, 2004; Montenegro, 2012; Patarroyo et al., 2013), and the abundant appearance of ostracodes in the same interval suggests that this event at the level of the lower Rosablanca has a regional distribution in the basin of the MMV.

- RW-1 section

The RW-1 section (Figure 3.44), in the MMV, crosscut the Barremian-Campanian series. Three cores were taken in the Cretaceous section (ECP-2012). Biostratigraphic analysis have been made using cores and cutting in a total of 274 samples for palynology and 74 samples for micropaleontology. These data were complemented with macrofossil determinations in this section by Etayo (2012), a level of tuff dated at 10 176 ft by Cardona (2012), and with data from the La Sorda-1, Cascajales-1 (Brenac and Jaramillo, 2004), Prometeo-1 (Instituto Colombiano del Petroleo (ICP), 2013) and Catalina-1 wells, and from the la Sorda field section (Brenac and Jaramillo, 2004).

Palynological samples were analyzed in the Instituto Colombiano del Petroleo (ICP, 2013), where 200 individuals of pollen, spores and dinoflagellates were counted. The biostratigraphic study was supported by previous studies made in the ICP and by other authors in the wells Cascajales-1 (Brenac and Jaramillo, 2004), Prometeo-1 (ICP, 2013), Bosques-1, Punta Piedras-2, Catalina -1, Torcoronma-1, Llanito-1 (Figure 3.46), and in the la Sorda section (Brenac and Jaramillo, 2004).

Palynomorphs found in the RW-1 well were classified in 108 species of pollens, 45 of spores, 49 of dynoflagellate cysts, 15 of algae and copepod eggs, and 8 of acritarchs, which allowed to define the following zones.

1. *Callialasporites* sp. Zone. In this zone, the last occurrence of *Pseudoceratium* sp. is reported. Its top corresponds to the last occurrence of *Classopollis* sp. This biozone has been defined in the Simiti Fm (12273-14414 ft). In the Prometeo Well (9582'-11940') the assemblage *Classopollis* sp., *subtilisphaera* sp., *Callialasporites* sp., *Subtilisphaera* sp., *Callialasporites* sp. and *Pseudoceratium* sp. encompasses the Tablazo Fm and is correlated with the *Callialasporites* sp. biozone. In the La Sorda section and Cascajales-1 well, the last occurrence of *Classopollis* sp. together with the presence of *Afropollis* sp. and *Psilatriletes* sp., testify the presence of this biozone, which is restricted to the upper Simiti Fm and lower La Luna Fm.

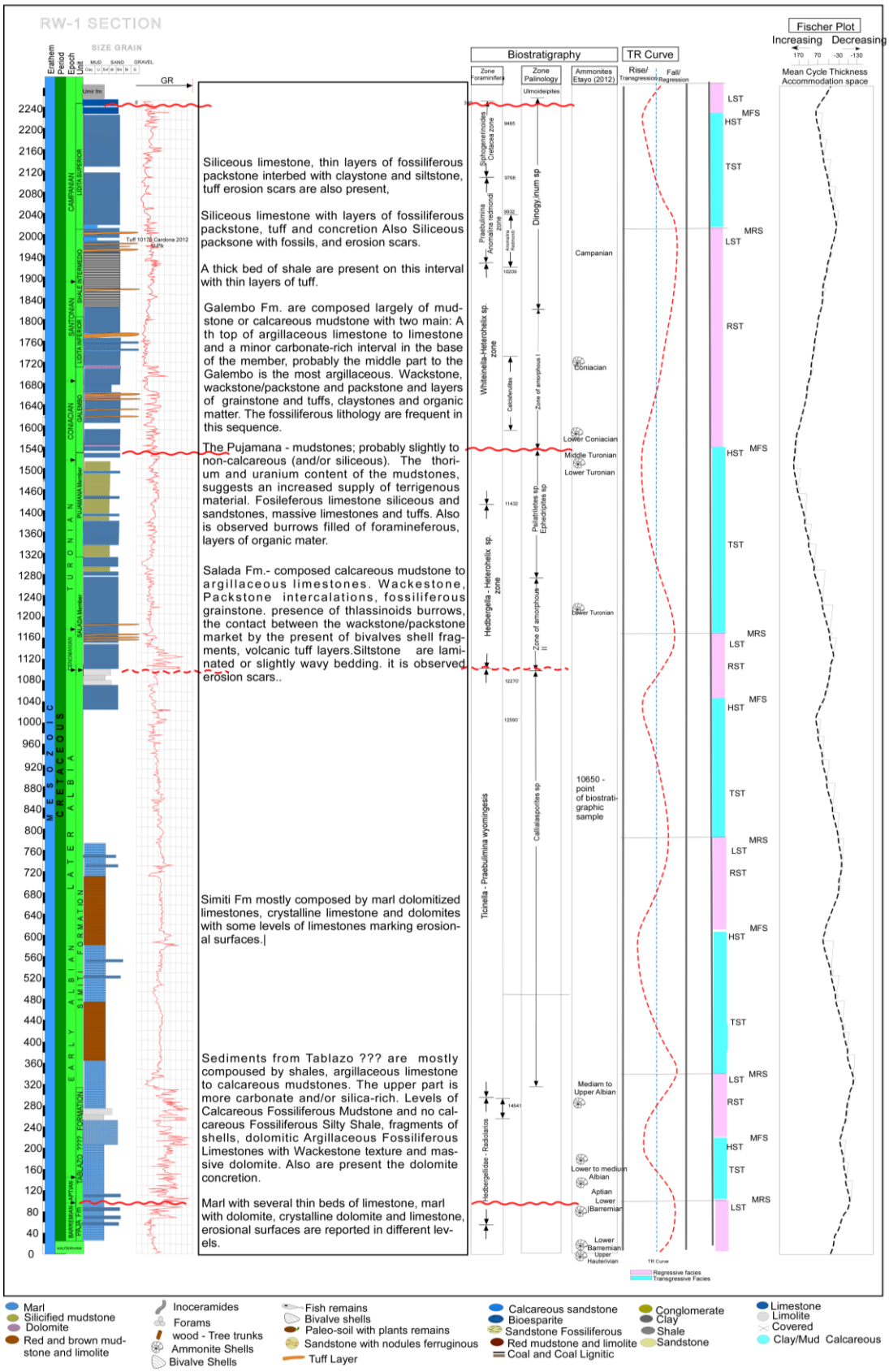

Figure 3.44. *RW-1 well, corresponding to a Barremian-Campanian succession and proposed interpretation. Data taken from Ecopetrol (unpublished data). Reconstruction and interpretation from this work.*

2. Amorphous Interval II. The base of this interval is difined by the appearance of the top of the *Callialasporites* sp. biozone, and the top of this interval by first occurrence of *Psilatriletes* sp. This interval is poor in palynomorphs and corresponds to the Salada Mb and the lower part of the Pujamana Mb (lower part of La Luna Fm). It had been recognized in the Cascajales-1 well above the *Classopollis* sp. zone, with occasional occurrence of *Psilatriletes* sp.; and also in the La Sorda section and in the Prometeo-1 well, from the upper part of the Simiti Fm/Upper Salada Mb to the lower part of the Pujamana Mb. Samples present abundant marine organic amorphous material, which increases upward, while phytoclasts decrease in number.

3. *Psilatriletes* sp. – *Ephedripites* sp. **Zone**. Its base is defined by the top of the Amorphous Interval II zone, and its top by the decreasing abundance of *Psilatriletes* sp. and *Ephedripites* sp. Other taxa are *Retitrescolpites "pujamanai"*, *Tetradites* sp., *Crasulina* sp., *Dicthyophyllidite* sp., *Striatricolpites* cf. *guzmanii* and *Subtilisphaera* sp. This biozone is present in the Pujamana Mb, and was identified in the La Sorda section, and in the Cascajales-1, Prometeo-1 and Catalina-1 wells, related to the Pujamana Mb.

4. Amorphous Interval I. Its base is defined by the top of the *Psilatriletes* sp. – *Ephedripites* sp. biozone, while the top is given by the first occurrence of *Dinogymnium* sp. It is characterized by a low palynological recovery, occurrence of dinoflagellate cysts and a high concentration of amorphous organic matter together with other phytoclasts. It corresponds to the Galembo Mb of the La Luna Fm. This zone has been recognized in the La Sorda section, and in the Cascajales-1, Prometeo-1 and Catalina-1 wells. Based on its palynological content and to the occurrence of *Dinogymnium* sp. (which appears around 90.8 My (ICP, 2012; Brinkhuis et al., 2009), it indicates a Turonian/Coniacian age.

5. *Dinogymnium* sp. Zone. The base of this zone is defined by the top of the Amorphous Interval I, and its top corresponds to an assemblage of land and marine palynomorphs. It is marked by the occurrence of *Odontochitina operculata*, *Alisogymnium* sp. and *Cerodinium* sp. It is found in the Umir Fm (= Olini Group in the Guaduas Syncline). This zone was only identified in the Prometeo-1 well, which may mean a time gap at the top of this biozone, which presents a change from predominantly marine to markedly continental palynomorph assemblages. This suggests non-deposition or erosion, the latter interpretation being supported by the absence of this biozone in the La Sorda section and Cascajales-1 well, and by thickness variations in the Pujamana Mb. The Lower to Middle Campanian age given by foraminiferas (ICP 2012; Petters, 1995) is supported by a U/Pb date of 80.3 ± 1.3 Ma (Cardona, 2012).

6. *Ulmoideipites krempii* Zone. Its base is defined by the first occurrence of *Ulmoideipites krempii*, and by the assemblage of *Andalusiella mauthei*, *Palaeocystodinium-Andalusiella* complex, *Spinizonocolpites baculatus*, *Buttinia andreevi*, *Echitriporites suescae*, *Echimonocolpites protofranciscoi*, *Echitriletes intercolensis, Gabonisporis vigorouxii* and *Scabratriletes granularis*. Its top is marked by the occurrence of *Proteacidites dehanni.* This biozone corresponds to the Umir Fm. In the Cascajales-1 well, the same zone was identified at the top of the interval with

marine influence and the presence of abundant continental palynoflora. According to Tchegliakova (1995) the lower part of the Umir Fm is of Middle to Upper Maastrichtian age.

- Chucuri well

The Chucuri-1 well, located in the northwestern part of the study area (Figure 3.5), is shown in Figure 3.45. This well shows, from base to top, the Rosablanca, Paja and Tablazo Fms.

The lowermost 80 m (Rosablanca Fm) are composed by siltstone overlain by very fine-, fine- to medium-grained siliceous sandstone beds, with grey to red siltstone beds. Sandstone is white, green or grey, with subangular quartz grains. Between 80 and 140 m, the amount of claystone increases, claystone is white, grey or brown, with intercalations of grey to dark grey siltstone beds and dark grey to black shale bearing macrofossil casts.

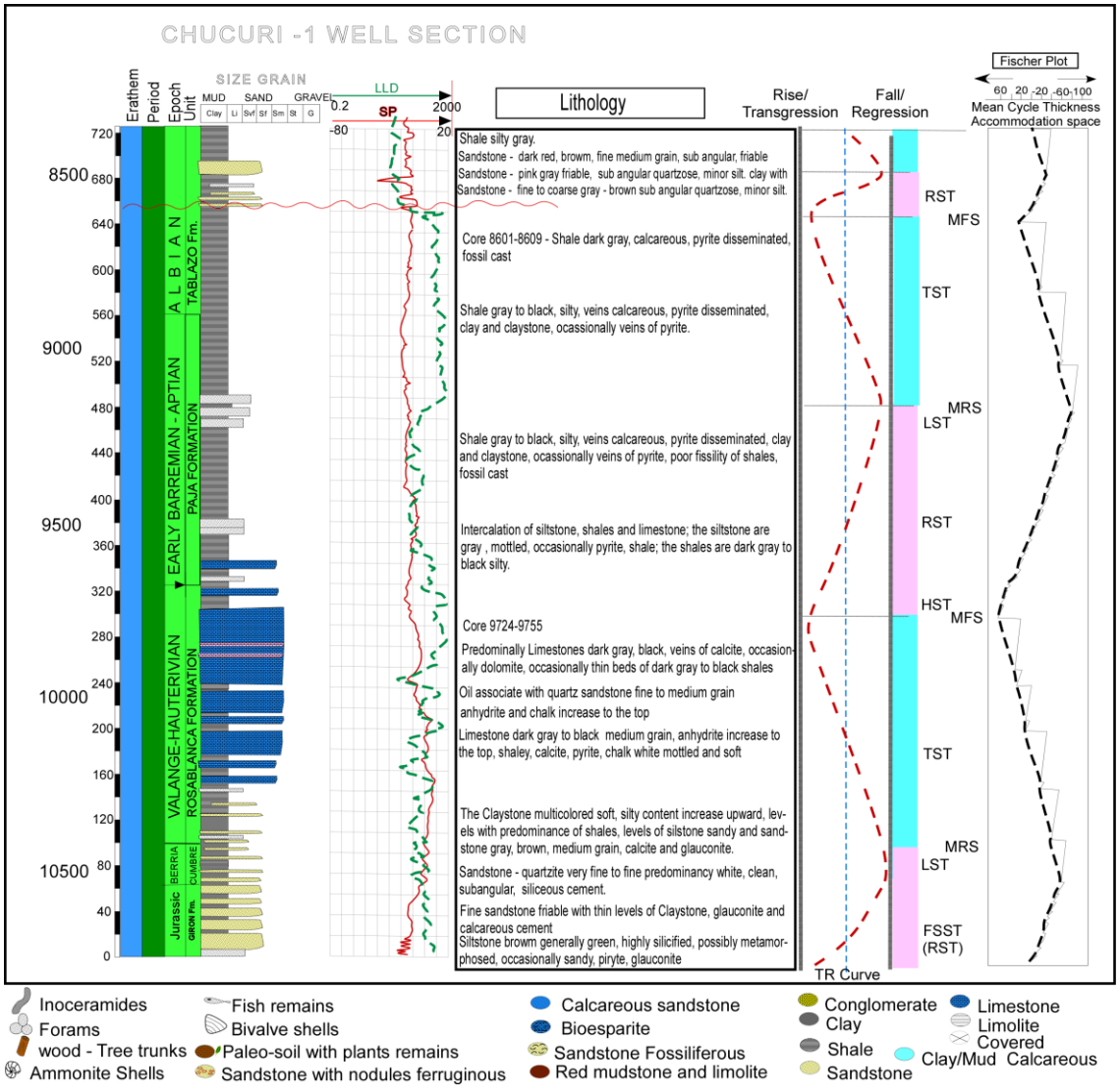

Figure 3.45. *Chucuri-1 well section, corresponding to a Hauterivian-Tertiary succession, and proposed interpretation. Reconstruction and interpretation from this work.*

Between 140 and 340 m, dark grey to black limestone beds become more and more frequent, oolitic, and are associated with pyrite and minor marly interbeds. White anhydrite increases from 10 125 to 10 100 ft.

From 340 to 650 m is a series of dark grey to black, silty shale (La Paja Fm). The shale contains pyrite, thin veinlets of calcite, multicolor claystone and few beds of limestone.

At 650 m, the appearance of Tertiary sandstone beds marks a sudden lithologic change over a regional unconformity. From East to West, the series shows an important erosion of the Late Cretaceous deposits (from Cenomanian to Maastichtian) below this unconformity.

- Llanito – 1 well

In the Llanito-1 well, the lithological change from predominantly dark grey shale and siltstone to varicolored shale, suggests that the contact between the Rosablanca and the underlying Girón Fm occurs at 13500 ft. The unfossiliferous grey quartzite, gray to green and red silt, shale and clay (core 13534'-13550') supports a continental environment for the Girón Fm.

The presence of *Chofatella sogamosa* at 12790' indicates a Hauterivian to lowermost Barremian age, and this level is ascribed to the lowermost Paja Fm or the uppermost Rosablanca Fm. The highest occurrence of Globigerinids between 9840'–10650' coincides with a lithological change. At 10650', *Pseudocyclammina rugosa* records abruptly its highest occurrence, which suggests an Early Cenomanian age (d'Orbigny, 1850). This species may be as young as Cenomanian but occurs most commonly in Barremian to Albian strata.

3.6. Stratigraphic correlations

The Berriasian to Coniacian-Santonian series of the VMM and WEC basins was divided into stratigraphic sequences of Berriassian, Valanginian-Early Hauterivian, Barremian-Early Aptian, Late Aptian-Late Albian, Albian-Cenomanian (Early Cenomanian), Late Cenomanian-Turonian and Coniacian-Santonian age. These divisions were based on the recognition of sedimentological discontinuities corresponding mainly to Regressive Surfaces (RS) located at the base or top of Regressive Systems tracts or between the Highstand systems track and Lowstand system track. These sequences were correlated across the whole basin of the MMV and WEC.

As previously shown, several sections of the study area were described from South to North, including their lithological, biostratigraphic, litological, sedimentological and sequence stratigraphic description and interpretation (see above). We then constructed three representative transects (Figures 3.24, 3.36 and 3.47) to observe the lateral facies variation from East to West.

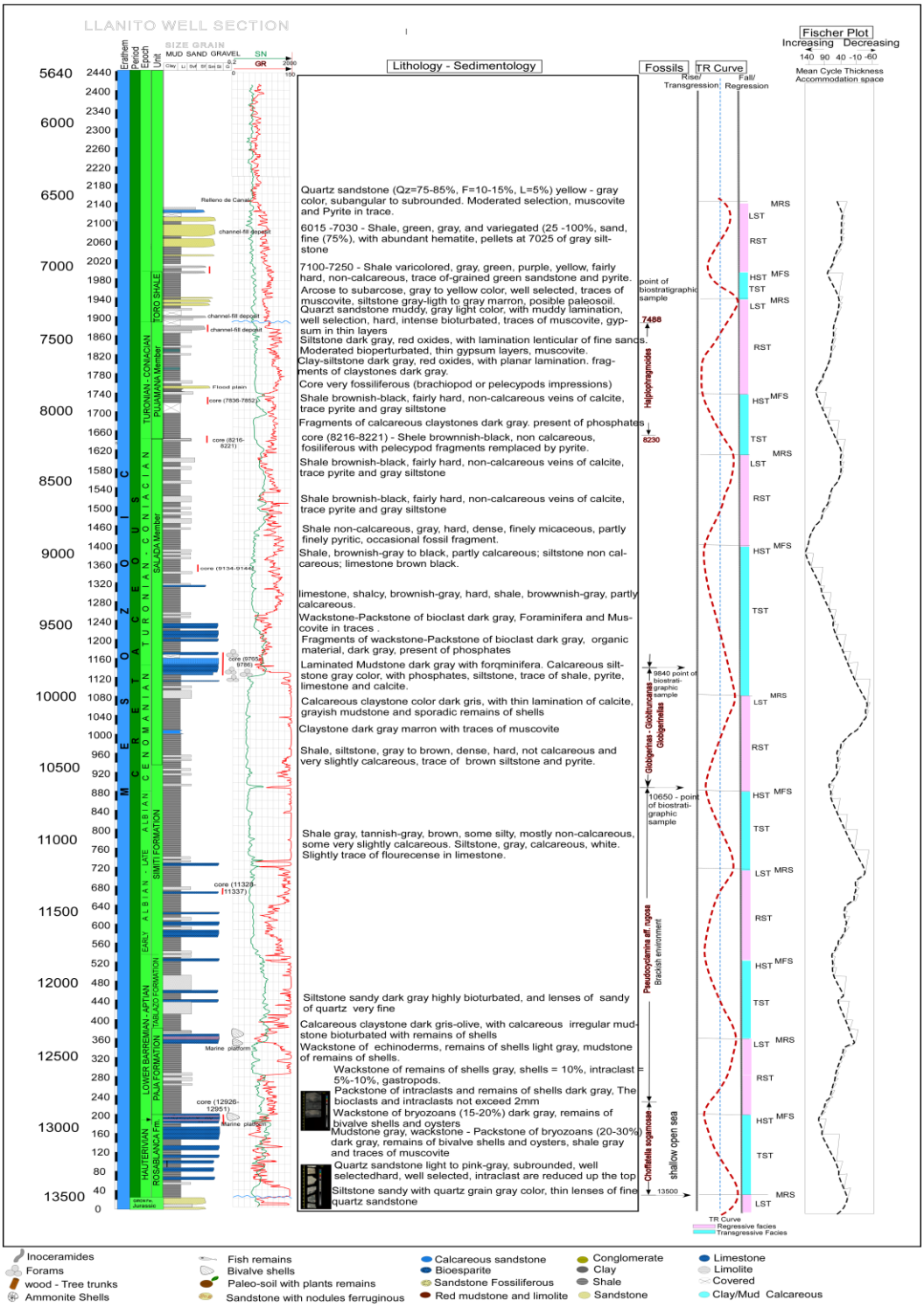

Figure. 3.46*. Stratigraphic section for Llanito-1 well; corresponds to a full sequence from Giron-La Luna. Descriptive lithostratigraphic and biostratigraphic information from Ecopetrol, section described and interpreted from this work.*

At the base of the succession, we observe a regressive sequence represented by medium- to coarse-grained quartz sandstone of Jurassic age (RST or FSST), which is more or less continuous toward the West and North. The overlying Berriasian deposits vary from quartz sandstone to the East to claystone, mudstone and shales to the West.

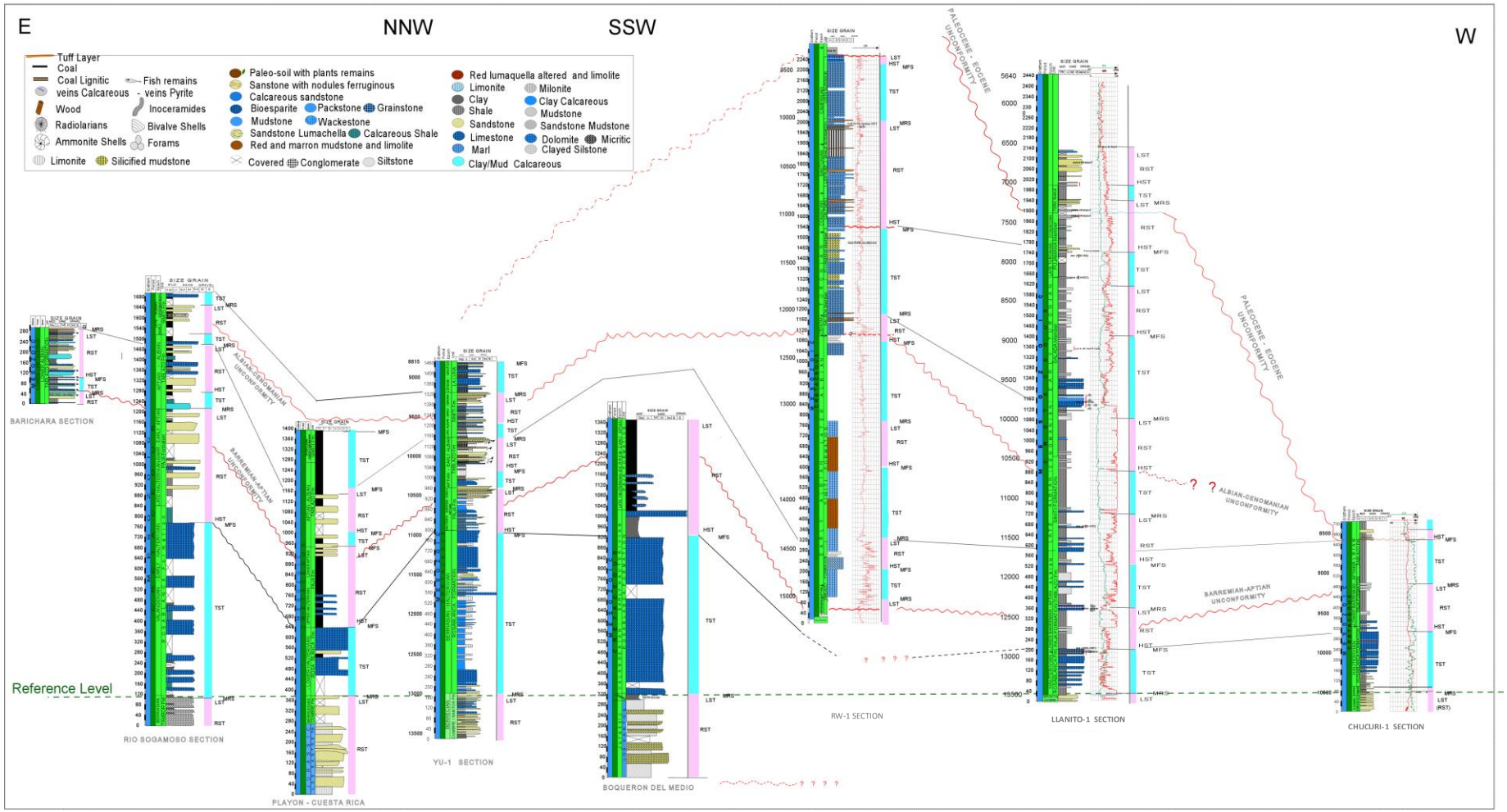

Figure 3.47. *Correlation SEE-NNW-SSW-W for the North Study area, showing stratigraphic changes from Berriasian to Cenomanian ages. Note that the levels of sandstones in the columns at the east and in the central part in the correlation tend to become fine sediments towards the west and thicker in the same direction.*

The Valanginian to Early Hauterivian interval is represented by a transgressive series (TST) represented by thick limestones, with some thin beds of claystone, calcareous claystone and siltstone. In Late Hauterivian to Early Aptian times, a regressive series (RST) is deposited, represented by fine-grained sediments (claystone, mudstone, shale, etc.) in an extensive area. These deposits are composed in the middle and upper parts by thin to thick beds of quartz sandstone marking the top of the regressive series (Paja Fm). The latter is overlain by a T-R sequence of Late Aptian – Early Albian age, marked by the increase of sandstone towards the top (ex. Yumeca section, Figure 3.41).

During the Late Aptian, a transgression occurred, followed by a regression of Early Albian age. The Late Aptian to Late Albian time-span is interpreted as a general regression (RST) from East to West. The latest Albian to Early Cenomanian also represents a complete T-R sequence, with apparition of sands marking possible erosion surfaces. Shallow deposits were migrating westward, expressing a regression and producing an erosion. During the Late Cenomanian-Turonian a general transgression (TST) occurred, expressed by fine deposits (claystone, mudstone, shale) of deep marine enviroment to the East and by limestone to the West. Finally, in the Coniacian to Santonian, a regression (RST) caused the shallow environments to move westward in the MMV and WEC.

3.7. Paleo-Facies Maps

The sections described previously and their correlation permit to analyze the vertical and horizontal facies changes and sea level fluctuations. These observations allow in turn to build different Cretaceous facies maps for the WEC and the MMV (Figures 3.48 to 3.56). These maps show the facies variation due to the sea level changes from Berriasian to Upper Coniacian times, using three base facies; sandstone, shale-claystone, and limestone.

The *Berriasian* is represented by a regressive sequence (RST) limited by a TS at the Early/Late Berriasian boundary (Figure 3.48). Its extension and areal distribution are shown in Figure 3.48. To the north the sandstone facies extends from the East to Llanito-1 and Chucuri-1 wells to the North, and to Buriburi in the centre. Fine facies are present in Boqueron del Medio and RW-1. In the Central area, Berriasian sandstones were deposited till 30 km to the west of the Chiquinquira section and about 5 km East of the Buriburi section (Figure 3.48). Shales and claystones were deposited to the West. This interval ends up with the transgressive surface (TS) at the top of the Early Berriasian when the TST started, which will last from Late Berriasian to Early Hauterivian times (deposition of the Rosablanca Fm.)

During the *Berriasian – Valanginian*, (Figure 3.49), a transgression (TST) started, showing a marine invasion and a sea level rise to the East, causing the migration of deep environments from West to East. This transgression continued until the deposition of the highstand systems tract in the *Hauterivian*, especially to the North when the

environment continued deepening to the East (Figure 3.50). Limestone facies covered all the northern area probably during the maximum flooding surface. In the central area, little environmental changes occurred in the Hauterivian.

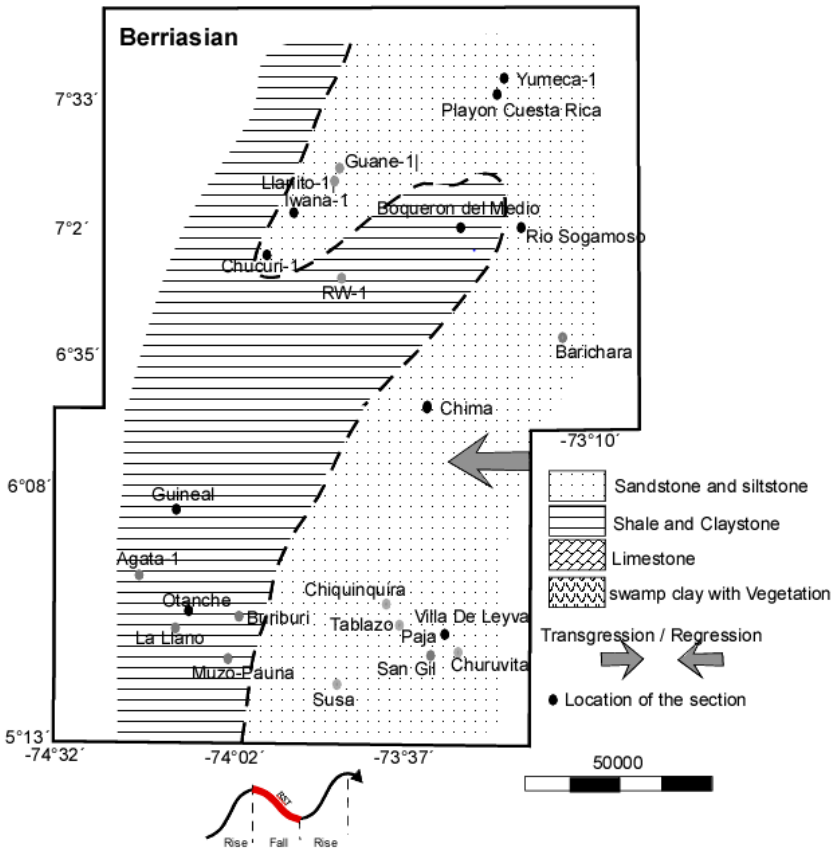

Figure 3.48. *Facies distribution map for the Berriasian (from this work).*

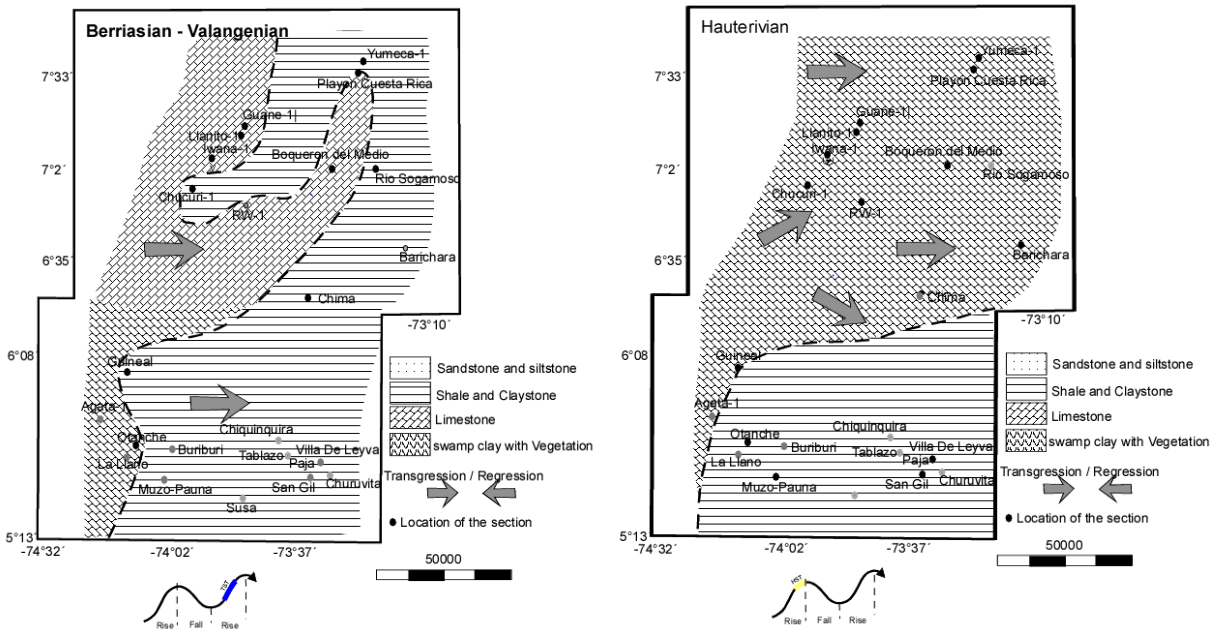

Figure 3.49. *Facies distribution map (left) for the Berriasian-Valanginian (from this work).*
Figure 3.50. *Facies distribution map (right) for the Hauterivian (from this work).*

During the Barremian, a period of regression (RST) or a fall stage system tract (FSST) occurred. Environments moved westward and shales and claystones were deposited in much of the basin. In the central area, depositions of gypsum and a lagoon environment with vegetation are observed (Paja Fm) in the Villa de Leyva region (location in Figure 3.51). To the north, the environment migrated northwestward, probably due to the geometry of the basin at that moment.

In the Barremian-Aptian (Figure 3.52) the environment migration continued toward the West. Sea level went on falling (LST) and a maximum regression surface (MRS) was reached. During this interval, the deposited units were probably partially or totally eroded.

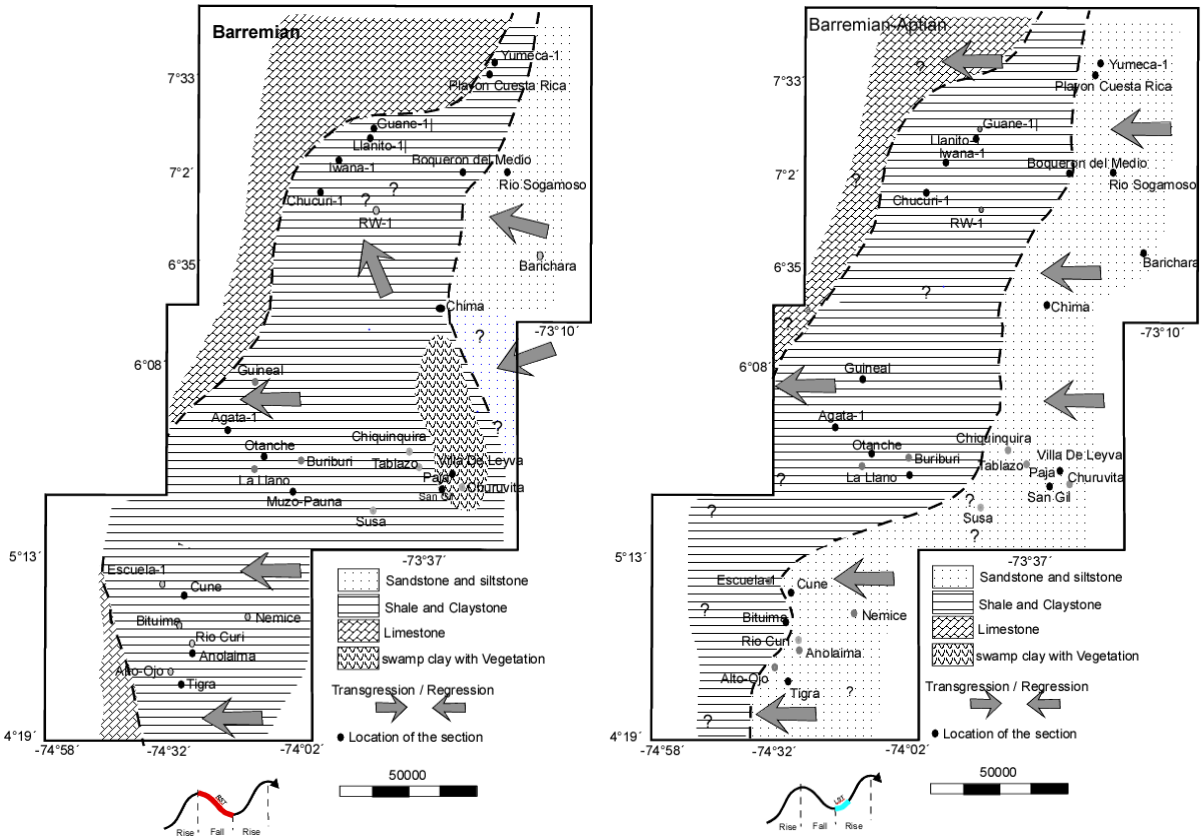

Figure 3.51. *Facies distribution map for the Barremian (left) (from this work).*
Figure 3.52. *Facies distribution map for the Barremian/Aptian (right) (from this work).*

The *Late Aptian-Albian* is a period of transgression, produced by a sea level rise. This period recorded deposition of a transgressive systems tract that generated a 5 to 25 km eastward migration of the environment belts.

During the *Early Cenomanian*, a sea level fall occurred producing a regression event. At that time, the environment was shallowing westward moving from a few km to the North (Yumeca-1) to more than 50 km to the West in the central area (shale deposited in the Aptian-Albian in the San Gil area moved westward to the Muzo-Pautina area). This regression created a sequence boundary and is represented in some sections by siltstone or sandstone overlying shales or calcareous beds (eg. Yumeca-1), or by an abrupt change from claystone to siltstones.

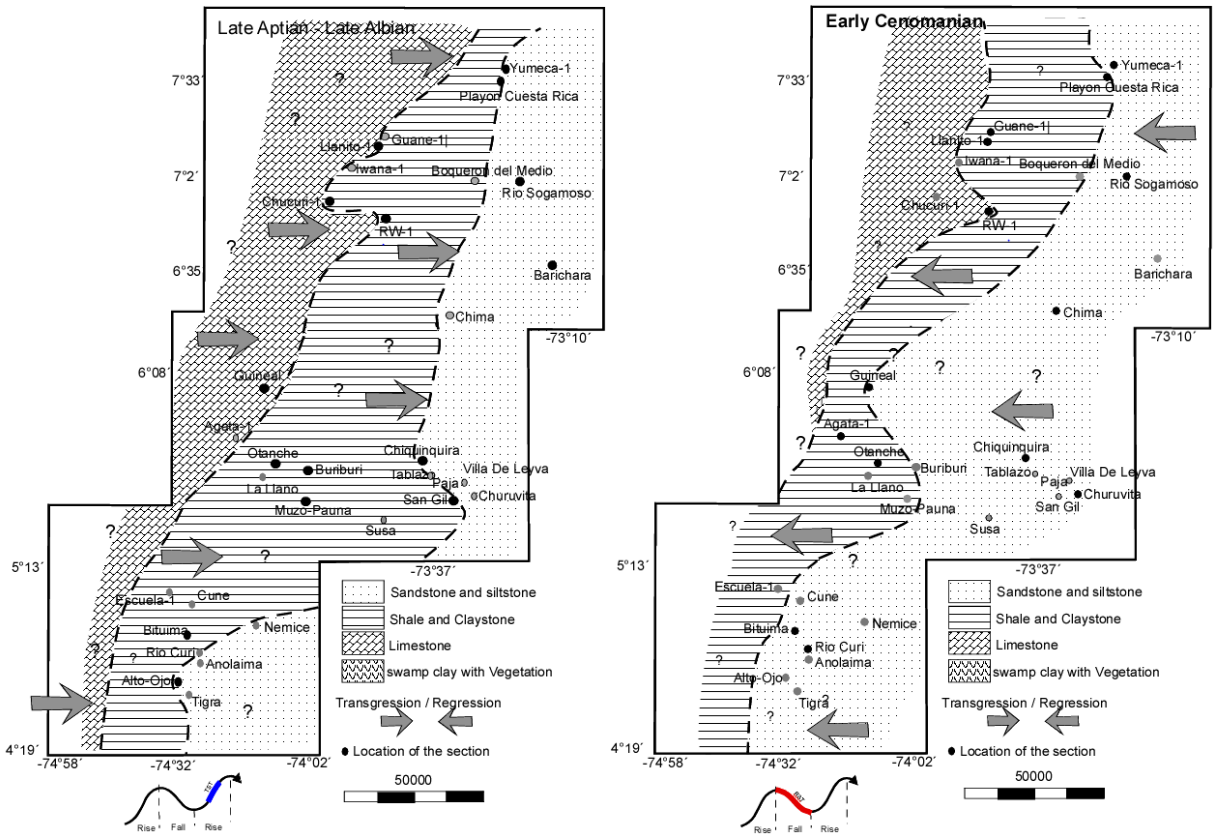

Figure 3.53*. Facies distribution map in North to South areas for the Late Aptian/Late Albian (left) (from this work).*
Figure 3.54*. Facies distribution map in North to South areas for the Early Cenomanian (right) (from this work).*

The *Late Cenomanian-Turonian* recorded the worldwide recognized eustatic transgression that flooded the shallow deposits to the East. During the Cenomanian-Turonian, the deep facies were moving eastward, where shales and limestones overlie sandstone beds of Early Cenomanian age (Figure 3.55).

During the *Coniacian-Santonian* the sea level withdrew to the west (sea level fall) producing a regression (Figure 3.56).

The stratigraphic sequences (Transgressive-Regressive) exposed in previous sections are independently illustrated in these maps. The Cretaceous evolution started with a regression and continued untill the Hauterivian with an important transgression (TST – Figures 3.49-3.50). During the Barremian to Barremian-Aptian time-span, the facies migrated to the West due to the eustatic regression (Figure 3.51; 3.52). Once again during the Late Albian-Aptian, a transgression occurred but its observation may be more complex to the North. During the Early Cenomanian, a general regression took place and finally, during the Coniacian-Santonian, a regression occurred, which probably continued during the Early Campanian.

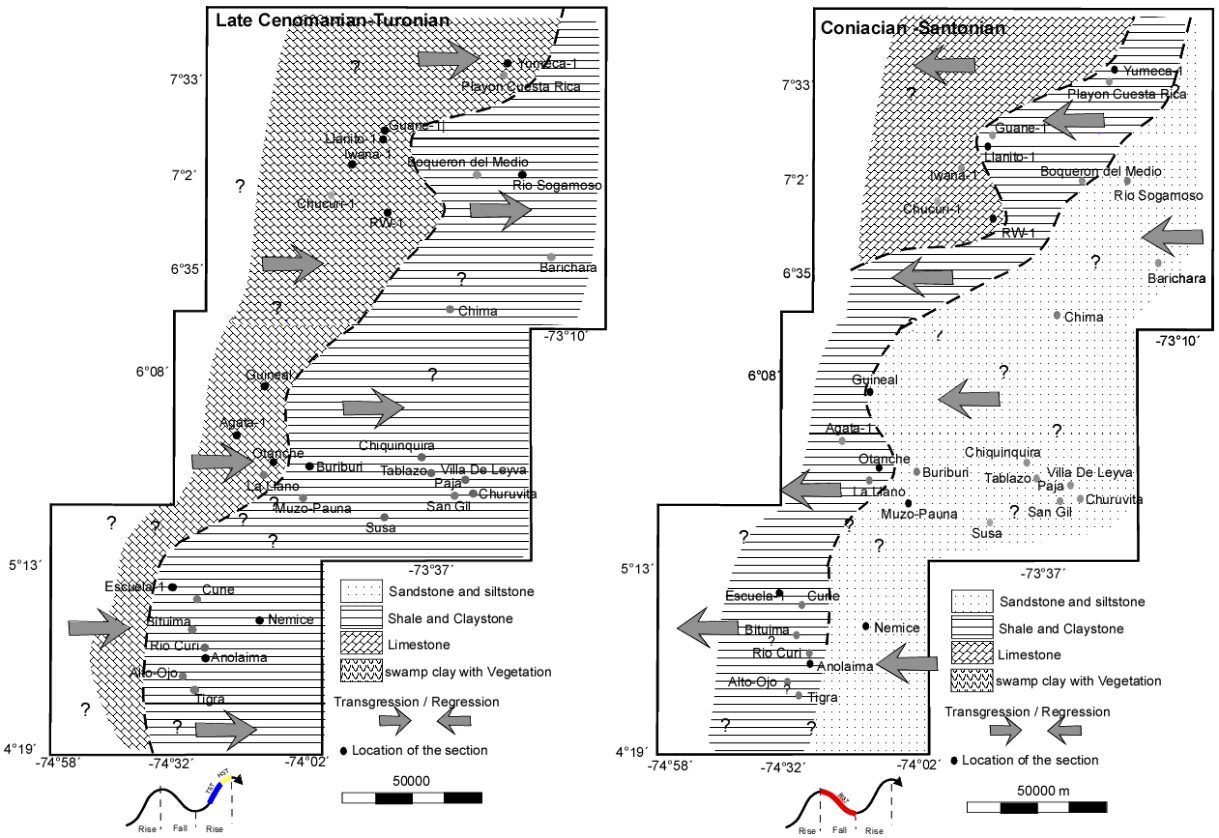

Figure 3.55. *Facies distribution map for the Late Cenomanian-Turonian (left) (from this work).*
Figure 3.56. *Facies distribution map for the Late Coniacian-Santonian (right) (from this work).*

3.8. Discussion

This section proposes a sequence stratigraphy interpretation related to relative sea level changes for the Cretaceous units. Only the Berriasian to Coniacian-Santonian interval has been considered due to sample distribution, and to the little information available for the Campanian-Maastrichtian and the Cretaceous-Tertiary boundary.

The detailed description is shown in the columns for the three sections (South, Central and North (locations in Figures 3.2 to 3.5), the interpretation of sea level fluctuation using transgression-regressive curves permits to propose an interpretation for vertical and lateral variations in the basin of predominantly fine-grained Cretaceous facies. Due to the distribution of the samples in the WEC and the MMV, and the regional controls were possible to interpret the facies maps from Cretaceous units in the basin when it was possible to observe the changes. Sequence stratigraphy represents an analytical approach to predict facies changes, also the correct understanding of sequence geometry in the basin for one or several ages could be helpful to understand the movement of the environment and the dynamics of the basin. This methodology for basin analysis, as said by Villamil (1998), requires detailed field work information but not high technology, and in this case, I added detailed well information to understand the changes from the WEC to the MMV. It is important to say that stacking patterns (Parasequences) are a representation of shallowing (coarsing upward) or deepening

upward (fining upward) and also changes in energy (the rate of clastic sediment supply has to decrease at specific points with transgression as coarse sediment are trapped shoreward (Villamil, 1998)) reflect changes in the vertical; In addition, a vertical distribution of the parasequence (A/S) reflects changes in the stratigraphic sequence (fine grain upward means transgression, coarse grain upward means regression); even more the analysis of the lateral distribution of these facies for the same age also shows the variation over time for all the basins (Figures 3.48 – 3.54).

Limited information from wells and outcrops in different localities support the existence of possible discordances, shallower conditions or subaerial exposition, relative sea level rise or sea level fall or events associated to tectonic phenomena. These evidences are shown zone by zone in this work as a part of the discussion (South to North):

In the southern area (Figures 3.5 and 3.19), one case is in the La Tigra section (Figure 3.17) of Barremian – Lower Aptian age, where, based on biostratigraphic data from the upper part of the section, two conditions support the idea of a paleo-environment of shallow waters with good oxygenation; and the accumulation of shells, crinoids, gastropods and dropstone structures support an episode of high energy in the lower segment strongly related with the cooling of the layers below (unconformity). Also in the Alto el Ojo section, supported by stratigraphy, the sequence shows an event of a shallow environment produced by a regressive event (RST) at the top of the sequence of Late Aptian – Lower Albian age, where there are remnants of woods possibly related to a shallow paleo- environment (flood plain?). In the Quebrada Cune section, the lithological description made in field shows a change from transgressive to regression conditions marked by the presence of conglomeratic sequences (Figure 3.19 and Photo 3.3), marking an increase of the energy from the base to the top (RST) and possibly associated to an unconformity likely near the limit of the Trinchera – Socota Fm. (Tablazo). In the Bituima section (Figure 3.20) of Late Albian – Early Cenomanian age (supported by biostratigraphy) the abundant content of organic material, the parallel lamination, the absence of benthonic life, the great abundance of planktonic quillado (for example Rotalipora reicheli) and the presence of radiolarians (nasselarides and espumelarides), suggest pelagic to hemipelagic sedimentation as a product of relative sea level rise. In the section **Escuela-1** three majors events were identified: The first one at 2500 ft. marked by the contrast between a Tertiary terrestrial sequence and a Cretaceous sequence below, suggested by the absence of the late Cretaceous Ammobaculites columbianus Zone; the second at 2750 ft. marked by a contrast in microfaunal preservation and composition, which also marks a mixed zone at the limit between the *Bulimina kickapooensis Zone* and the underlying *Siphogenerinoides bramlenei-Siphogenerinoides cretacea*, this mixed zone and the contrast appear associated with tectonic phenomena during the Campanian or Campanian – Maastrichtian. In the **Rio Curi section** (Figure 3.22), the lithology suggests a terrigenous supply, the presence of planktonic foraminifera, bivalves and bioturbation at the top suggest a sea level fall showing conditions for prodelta deposits. The lithology, structures, fossils and paleo-environmental suggest that a sea level rise (TST) are

coincident with global changes at the Cenomanian-Turonian limit. The **Quebrada Nemice section** (Coniacian age - Figure 3.23) shows variations of external platform conditions (abundance of planktonic) to shallow siliciclastic condition (aerobic conditions RST) related with the presence of sandstones (Thalassinoides), erosive surfaces and bioclasts, followed by parallel and ondulating-bioperturbed lamination.

In the central regional area (Figures 3.4 and 3.5): From field information from the **Sachica Chiquinquira section** (Figure 3.25- Albian age) an unconformity is recognized (Photo 3.4) in the sequence of the Tablazo Fm (Upper part of the Lower San Gil Fm). In the **Samaca section (Lower San Gil** – Figure 3.26) the same unconformity was recognized for the upper part of the column (Albian age). In the **Samaca section (Upper San Gil** – Figure 3.27) the maximum flooding surface is observed (MFS) at Middle Albian times (around 104 Ma). In the **Samaca – Villa de Leyva - Churuvita section** (Upper part of the Chiquinquira Fm. - Figure 3.28), field evidences of shallow conditions (Photo 3.6) like paleosoils, thalasinoids and angularity in erosive surfaces (unconformity – upper part of Figure 3.28 and Photo 3.6) show an event of subaerial conditions (RST). Also, at the base of the same section at the limit of the San Gil Fm/Churuvita Fm. an unconformity is recognizable in an outcropping (lower part of Figure 3.28) as an angular surface (Photo 3.7) showing the abrupt change from deep to a shallow environment during this limit (Late Albian/Early Cenomanian) conforming a change from a high stand system tract (HST) to a regression system tract (RST = FSST). In the **Villa de Leyva - La Paja section** (Figure 3.29 - Barremian-Aptian), the La Paja Fm. as is recognize by the geologists the presence of gypsum and anhydrite make it possible to interpret a salt tidal flat as the depositional environment for this unit, also the presence of cracking, desiccation marks and algal mats are signs of *subaerial conditions* (intertidal depositional environment), according to Huertas (1967, 1970, 1971) the fragments of wood, branches, plants, leafs, conifers and plants that grow in continental environments were transported from the continent to the sea and deposited finally at the flat. The subtle prints of leafs and little stems in black shales with or without gypsum are surely related with *swamp vegetation*. This, without any transport, suggests a *swamp environment*. In the Otache – Cozcuez Section (Figure 3.6), the fossils were dated from Valangenian to Maastrictian units (Rosablanca Fm. to Umir Fm in Guerrero J. et al., 1998) in environments that vary from internal to external shelf; In the area of Muzo-Paunita a sandy sequence of Albian age of the Tablazo Fm. (Capotes Fm.) was also described by Reyes et al. (2006); In the same area Muzo-Coscuez-Otanche-Yacopi, Terraza and Montoya (2011) compiled a section from Valanginian to Lower Albian for the whole area, which suggests the absence in this area of the Early Aptian (erosion or non-deposition).

In the north regional area (Figures 3.4 and 3.5); the **Barichara section** of the Tablazo Fm (Lower Albian - Figure 3.37) shows an important content of calcareous and siliceous sandstone. The increase of sandstone levels at the top insinuates the regression system towards the top, and the presence of paleo-soils insinuates shallow conditions for sediment deposition; In the **Yumeca 1 section** (Figure 3.41), the well crosses from

Berresian units at the base (Cumbre/Los Santos Fm.) to Maastrichtian (Umir Fm.) at the top. Interesting lithological changes can be observed in the sequence crossed. The changes from fine lithology to thick packages of sandstones at Berresian (Cumbre/Los Santos Fm.), Early Aptian (Paja Fm – Arenoso Mb), Early Albian (Top of Tablazo) and Early Cenomanian (Simiti Top) highlight the clear regressive events. Nevertheless the Lower Aptian is the point where the coarse grain as conglomerate lithology are present, which could represent the point of maximum regressive surface in all the sequence. In the **Guane-1 section** the Cretaceous sequence in more monotonous with scarse levels of sandstones. The majority of the sequence is represented from the base to the top by thick packages of limestone at the base from Valangenian to Lower Aptian, and then from Lower Albian to Turonian the fine grain content increases with sporadic levels of limestones, showing in general that for almost all the Cretaceous sequence the western part (of the MMV) shows a deeper environment (deeper facies) than those that could be observed at the east (towards the WEC). The same could be observed in the case of the **Iwana-1 section**. In the case of the **RW-1 section** (Barremian to Campanian), several zones were defined in the well to determine the age of the units present, however the *Zone of Dinogymnium sp*, that are present in the Umir Fm, are present in the well Prometeo-1 but apparently absent in the well Cascajales-1 and la Sorda section which means a lack of time towards the top of this biozone (it passes from a predominantly marine to a markedly continental sequence). This could be related to erosion or non-deposition; erosion supported by the absence of this biozone and dated as 80.3 ±1.3 Ma (Cardona, 2012) using U/Pb, and by foraminifera (In ICP 2012; Petters, 1995) locating this zone in the Early to medium Campanian. The Llanito-1 section is constituted by a monotonous sequence of shales different only during the Hauterivian and Cenomanian-Turonian boundary with important sequences of limestone, some levels of limestone and siltstone in the middle of Simiti Fm. From the middle Turonian to Coniacian it is a monotonous sequence of Shales, with some scarse and thin levels of sandstone, where the middle Turonian have been interpreted as deposited in a flood plain, finally covered by the Tertiary of Toro Shale.

The presence of the radiolarians event in different wells in the MMV, like RW-1, Coyote-1, and Iwuana-1 (Patarroyo et al., 2013), and Punta Piedra-1, Torcoroma-1, Catalina-1, Bosques-1, Prometeo-1 and Llanito-1 (Duque-Caro, 2004; Rodriguez et al., 2008; Patarroyo et al., 2013), shows that the radiolarians events (104-112 Ma. Based on ammonites and bivalves) present over and below of the Tablazo-Simiti contact, has a stratigraphic regional significance in the MMV for this limit.

Stratigraphic correlation from different sections shows the behavior of the units in the WEC to MMV in the orientation South to North and East to West. This allowed me to understand the variation in deposition using lithology, energy changes and possible sea level changes. The vertical variation and correlations permit me to analyze sea level variation and facies changes (Figures 3.48-3.56).

In this chapter I recognized six transgression events and five regression events occurred during the Berriasian to Campanian in the area of the MMV and the WEC. Authors like Maceralli C. (1988), Villamil T. (1998) and Guerrero J. (2001), have recognized cycles in the Cretaceous, some of Maceralli´s unconformities or boundary cycles correspond to the boundarie sequences recognized also by Villamil T, (1998) and Guerrero J. (2001) which are consistent with the unconformities or cycles recognized in this work. For example during the Late Cenomanian to Early Turonian all of us interpreted a transgressive cycle (TS o condensed section).

Villamil (1998), working in the UMV from Albian to Campanian recognized five sequence boundaries (SB) or unconformities and four transgressive surfaces (TS). Villamil´s sequence boundaries (SB) are located at the Albian/Cenomanian limit, Late Cenomanian, Late Turonian?, Early Santonian and Campanian, and his transgressive surfaces (TS) at the middle Albian, Early Cenomanian, Late Cenomanian to Cenomanian/Turonian and Late Santonian.

Guerrero (2001) recognized regional sedimentary discontinuities in Colombia, based on the recognition of transgressive surfaces (TS) located at the base of the TST and regressive surfaces (RS) located at the base of the Regresive system track (RST). He recognized RS at Berriasian/Valangenian, Early Hauterivian-Late Hauterivian, Aptian-Albian, Late Albian-Cenomanian, Santonian-Early Campanian, Late Campanian-Maastrichtian, and TS at Hauterivian-Barremian, Early-Middle Albian, Cenomanian-Turonian, Early Campanian-Late Campanian, and Early-Late Maastrichtian.

In our area of study (MMV and WEC) we recognized in the same sense of Villamil T. (1998) a sequence boundary SB (coincident with the MFS) and TS (coincident with the MRS). Our SB are located at Early Hauterivian/Late Hauterivian, Late Aptian/Early Albian, Late Albian/Early Cenomanian, Turonian/Coniacian, Late Campanian; and for the TS, we recognized Berriasian/Valangenian, Early Aptian/Late Aptian, Early Albian/ Late Albian, Early Cenomanian/Late Cenomanian, Cenomanian/Turonian, Early Campanian/Late Campanian. So, some of the SB and TS recognized in this work are consistent with those stablish by Villamil (1998) and Guerrero J. (2001). However, considering that the unconformities SU or time gaps are generated during the regression system track (RST), during a period between the HST and LST (Figure 3.14), our surface erosion surface (SU) are located in the Barremian-Aptian, Late Albian-Early Cenomanian and Early Campanian (Figures 3.24, 3.36 and 3.47).

3.9. Conclusions

1. Sequence stratigraphy of the Cretaceous units has been analyzed in an area of 50 000 km^2 that covers the MMV and the WEC, using outcrop information collected in the WEC and well information from the MMV. A total of 30 sections were described and analyzed to understand the facies distribution, sea level fluctuations and sedimentary changes occurring from Berriasian to Campanian times.

2. Interpretation of sea level fluctuation using Transgression-Regressive curves in each section permitted to propose an interpretation for vertical and lateral facies variation in the basin. For these analyses, third (0.5-5 Ma) to second order cycles (5 – 50 Ma) were identified in outcrops which allowed to build sea level curves. Transgressive-Regressive curves and relative sea-level variations have been obtained using relative accommodation space plots proposed by Fischer (1964).

3. From the interpreted TR curves and Fischer diagrams, we determined cycles based on the identification of maximum regression surfaces, transgressive surfaces at the base of transgressive systems tract, maximum flooding surfaces, and regressive surfaces (RS) or sequence boundaries (SB), located at the base of regressive system track (RST).

4. Consistent with Villamil (1998) and Guerrero (2001), we recognized a MFS at the Early/Late Hauterivian boundary, near the Late Aptian/Early Albian boundary, and in Late Albian/Early Cenomanian, Turonian/Coniacian and Late Campanian times. Considering that the unconformities (SU) or time gaps are generated during regression systems tracts (RST), between the HST and LST (Figure 3.14), we recognized major erosion surfaces (SU) close to the Barremian-Aptian boundary, and in Late Albian-Early Cenomanian and Early Campanian times (see Figures 3.24, 3.36 and 3.47).

5. Based on the above information, we built facies maps from Berriasian to Coniacian-Santonian times. 1) the Berriasian correspond to a period of regression, 2) followed during the Berriasian/Valangenian by an onset of transgression 3) that continues during the Hauterivian to the east, 4) the Barremian represents the onset of a new regression that 5) continues during the Barremian/Aptian where the MRS was reached, 6) during the Late Aptian/Late Albian a new period of transgression is recorded 7) followed during the Early Cenomanian by a period of regression; 8) during the Late Cenomanian/Turonian a regional period of transgression occurred, 9) followed by a period of regression that could continue during the Early Campanian where the MRS could be reached.

6. Shallow marine conditions associated with high energy were identified in the **Barremian-Early Aptian**, for example in la Tigra Section and RW-1. Also, a possible unconformity occurred at the Late Aptian – Early Albian as is insinuated in different sections such as Quebarada Cune, Samaca-lower San Gil, Barichara sections, and Yumeca -1. At the **Late Albian-Early Cenomanian** boundary and in the **Late Cenomanian**, shallow marine environments and erosive surfaces (unconformities) were identified in the Samaca-Churuvita, Chiquinquira section, RW-1. In the **Campanian**, an event of erosion or non-deposition surface is reported in the section
RW-1.

7. According to the regional facies maps, shallower facies are always present eastward towards the WEC, while deep facies are located westward in the MMV towards the CC. The variations in the Cretaceous deposits suggest that there was an uprising zone to the west that was always affected by sea level fluctuations.

CHAPTER 4

Seismic interpretation of the Cretaceous unconformities and sequences in the Middle Magdalena Valley and western margin of the Eastern Cordillera, Colombia.

Abstract

For years, geoscientists focused on the recent uplift of the Eastern Cordillera of Colombia, especially on Tertiary sedimentary units, to understand the recent deformation. However, Cretaceous series remained poorly known. Recently, due to the need of the oil industry to evaluate new targets, new information has been acquired, which has led to a better understanding of the Cretaceous units. While Cretaceous sedimentary units are exposed in the Eastern Cordillera, outcrops are scarce in the Middle Magdalena Valley. In the latter area however, a lot of seismic information is available and some wells have been drilled in the Cretaceous succession.

This chapter attempts to identify unconformities bounding seismic sequences and to decipher the structural deformation in the Cretaceous series in the Middle Magdalena Valley and Western Eastern Cordillera, based on the interpretation of large seismic reflection sections and well information. These led to define sedimentary sequences (S1 to S5) limited by hiatus or unconformity surfaces (SU1 to SU5) and to identify successive states of pre-Eocene deformation. Finally, correlations with unconformities recognized by other authors in the Upper Magdalena Valley, Venezuela and other places in South America, suggest that these unconformities represent regional tectonic events.

4.1. Introduction

The study area covers a large part of the Middle Magdalena Valley (MMV) and of the Western part of the Eastern Cordillera (WEC), with a special focus on the MMV, which is a Cretaceous basin located between the Central Cordillera (CC) and the Eastern Cordillera (EC) of Central Colombia (Fig 4.1). The MMV basin recorded several sea level changes and sedimentary unconformities related to the evolution of the north Andean active margin. The Cretaceous fine-grained marine succession of the MMV and WEC is classically considered deposited in a syn-rift basin related to an extensional regime, without major compression tectonic events (Cooper et al., 1995).

However, observations made in other Andean regions suggest that Cretaceous times were marked by some tectonic events, the nature of which needs to be specified. Jaillard et al. (2000) suggested that the Late Albian Mochica tectonic event is related to the high convergence rate along the Andean margin, due to the opening of the Atlantic Ocean at Equatorial latitude. Based on seismic information and biostratigraphy, sedimentary hiatuses in the Cretaceous sedimentary record have been recognized in the Cenomanian in the Upper Magdalena Valley (UMV) (James and de Freitas, 2006), and during the Campanian in the Maracaibo basin (Cooney and Lorente, 2009). Comparable time gaps were also reported by Macellari (1988) based on paleogeographic synthesis, and by Morales (1958) based on regional observations in the MMV. Dates on apatites and zircons from granites of the CC in Colombia (Villagómez, 2010), and K-Ar ages from igneous rocks from the Cordillera de la Costa, Curaçao and Isla de los Hermanos (Santamaria and Schubert, 1972) indicate Cenomanian igneous activity related to tectonic events (Cooney and Lorente, 2009).

These observations led us to analyze the Cretaceous sedimentary record of the MMV and WEC, based on seismic reflection profiles and information from wells (e.g. RW-1 in Figure 3.5) in the MMV, and from geological field sections in the WEC. These works allowed us to identify five regional unconformities of Jurassic/early Cetaceous to Paleocene/Eocene age, some of them being newly defined here.

4.2 Geological Setting

The tectonic evolution of northwestern South America is controlled by the interaction between the Nazca, Caribbean and South American plates. This led the western part of Colombia to behave as an active margin submitted to subduction processes and provoked the accretion of oceanic terranes (Western Cordillera, Baudó-Panamá block) against the western margin of Colombia (Duque-Caro, 1990). These accretionary events are assumed to be responsible for compressional tectonic events, especially the tectonic inversion of rift basins during Late Cretaceous and Late Miocene times (Gomez et al. 2003; Colmenares & Zobac 2003, Cortes et al, 2005; Sassi et al. 2007; Parra 2008; Parra et al. 2009; Horton et al. 2010 Moreno et al 2011).

The Andes of Colombia comprise three cordilleras (Western, Central and Eastern Cordilleras), separated by two valleys (Cauca Valley and Magdalena Valley, Figures 4.1, 4.2). The MMV basin is located between the Central Cordillera (CC) and Eastern Cordillera (EC) of Colombia (Figure 4.1). It is about 560 km long and 80 km wide, and is separated from the CC to the west by eastward thrust faults and from the EC to the east by a westward thrust belt (Butler and Schamel, 1988; Namson et al., 1994; Gómez et al., 2003).

The MMV and the EC are made of varied lithologie. The Grenvillian orogeny is responsible for high grade metamorphism of rocks of the EC (Forero, 1990), which were then intruded by plutonic rocks during the Cambrian and Ordovician (Horton et al. 2010a, b). The Grenvillian sequence is unconformably overlain by metamorphic rocks of Cambrian and Ordovician age and these unconformably overlain by sedimentary rocks of Devonian-Carboniferous age (Forero-Suárez 1990). Jurassic red beds unconformably overly the Paleozoic rocks, and are coeval with plutonic and volcanic activity in the MMV and CC, related to the creation of a Mesozoic rift. As a matter of fact, the MMV - WEC basin is considered a Mesozoic extensional basin, subsequently tectonically inverted during the Cenozoic.

Thick sequences of continental Triassic-Jurassic, and marine Cretaceous rocks were deposited in the extensional basins during the phases of rifting and thermal subsidence (Etayo et al., 1969; Sarmiento, 2001; Clavijo et al., 2008). According to Aspden et al. (1987), the deposition of marine sediments during the whole Cretaceous in a wide rift system related to the subduction of the Paleo-Pacific plate in western Colombia came to an end due to the accretion of oceanic terranes in the present-day Western Cordillera, which created a Paleogene foreland basin in the MMV (Cooper et al., 1995).

Van der Hammen (1957) and Campbell and Burgl (1965) suggested that uplift of the EC took place during the Late Miocene and Pliocene (6-4 Ma). Colletta et al. (1990) proposed that a single inversion event occurred in the Miocene-Pliocene, while Dengo and Covey (1993) proposed that thin-skinned deformation during Miocene – Pliocene times was followed by the uplift of the basement in the Pliocene-Holocene. Other authors suggest that incipient inversion occurred in Paleogene time (Roeder and Chamberlain, 1955; Van der Hammen, 1961; George et al., 1997; Restrepo-Pace et al., 1999; Gómez et al., 1999; Sarmiento, 2001). More recently, the initial shortening in the MMV has been related to the tectonic inversion of the Mesozoic rift in Paleocene-Middle Eocene times (Restrepo-Pace et al., 2004; Cortés et al., 2005; Moretti et al., 2010; Parra et al., 2012). Crustal shortening in the MMV occurred prior to the

deposition of the Lower to Middle Eocene continental units (Parra et al., 2012), which coincide with the regional unconformity called the Late Cretaceous-Cenozoic Unconformity by Gómez et al. (2003).

Subaerial deposition began in the MMV during the Maastrichtian (Cooper et al., 1995; Villamil, 1999; Gómez et al., 2003). Paleocene deposits consist of alluvial, fluvial and coastal strata (Gómez et al., 2003; Moreno et al., 2011; Bayona et al., 2013). In the MMV basin, Tertiary sediments thicken toward the East and toward the WEC. A Mid-Eocene regional unconformity represents the upper limit of the studied time-interval.

In the Santander Massif, the uplift began around 55-32 Ma (Eocene-early Oligocene) (Fabre, 1987). However, the initial uplift of the Garzon Massif probably occurred during the Early Cretaceous, ≈ 110 Ma ago (Van der Wiel and Andriessen, 1991; Andriessen, 1995). In the Bogotá and Cocuy areas, uplift would have begun around 5 Ma ago (Hooghiemstra Hooghiemstra, H., 1989), which could be coeval with the structural recent inversion of the basin (Restrepo, 2004).

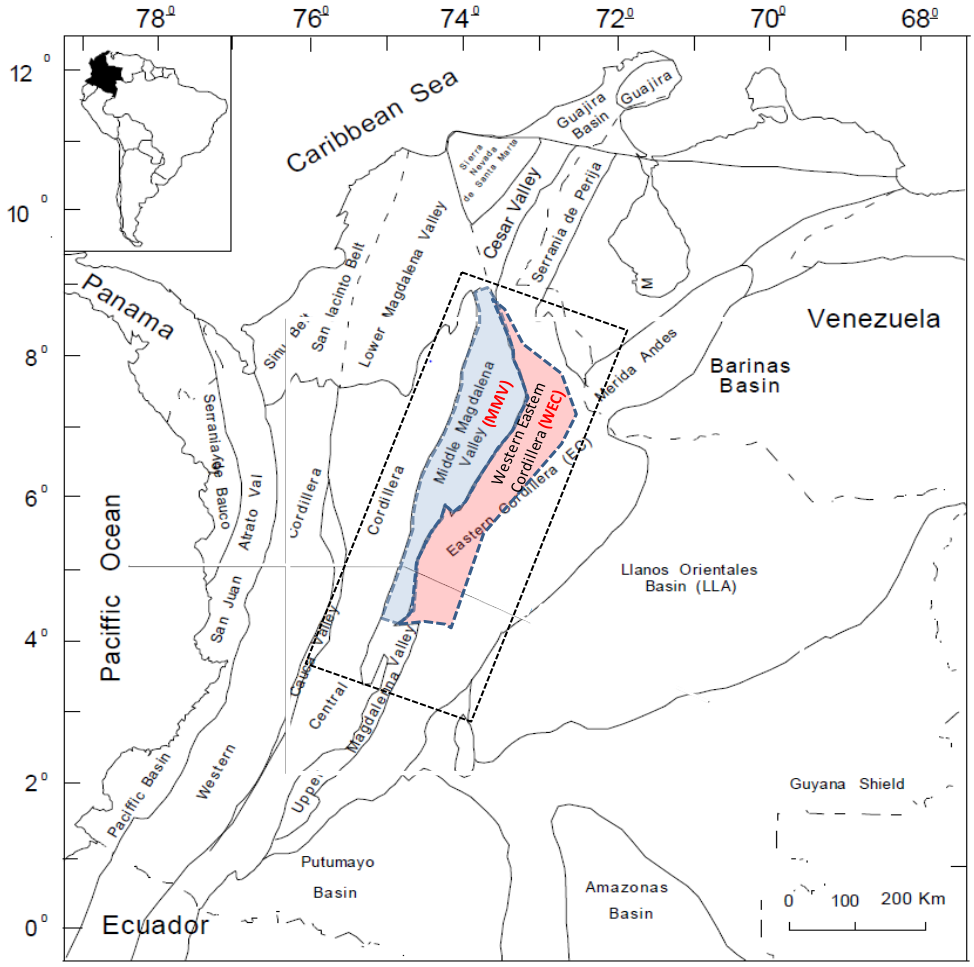

Figure 4.1. *Location map of the Middle Magdalena Valley (light blue) and the Western margin of Eastern Cordillera (pink), modified from Sarmiento (2001).*

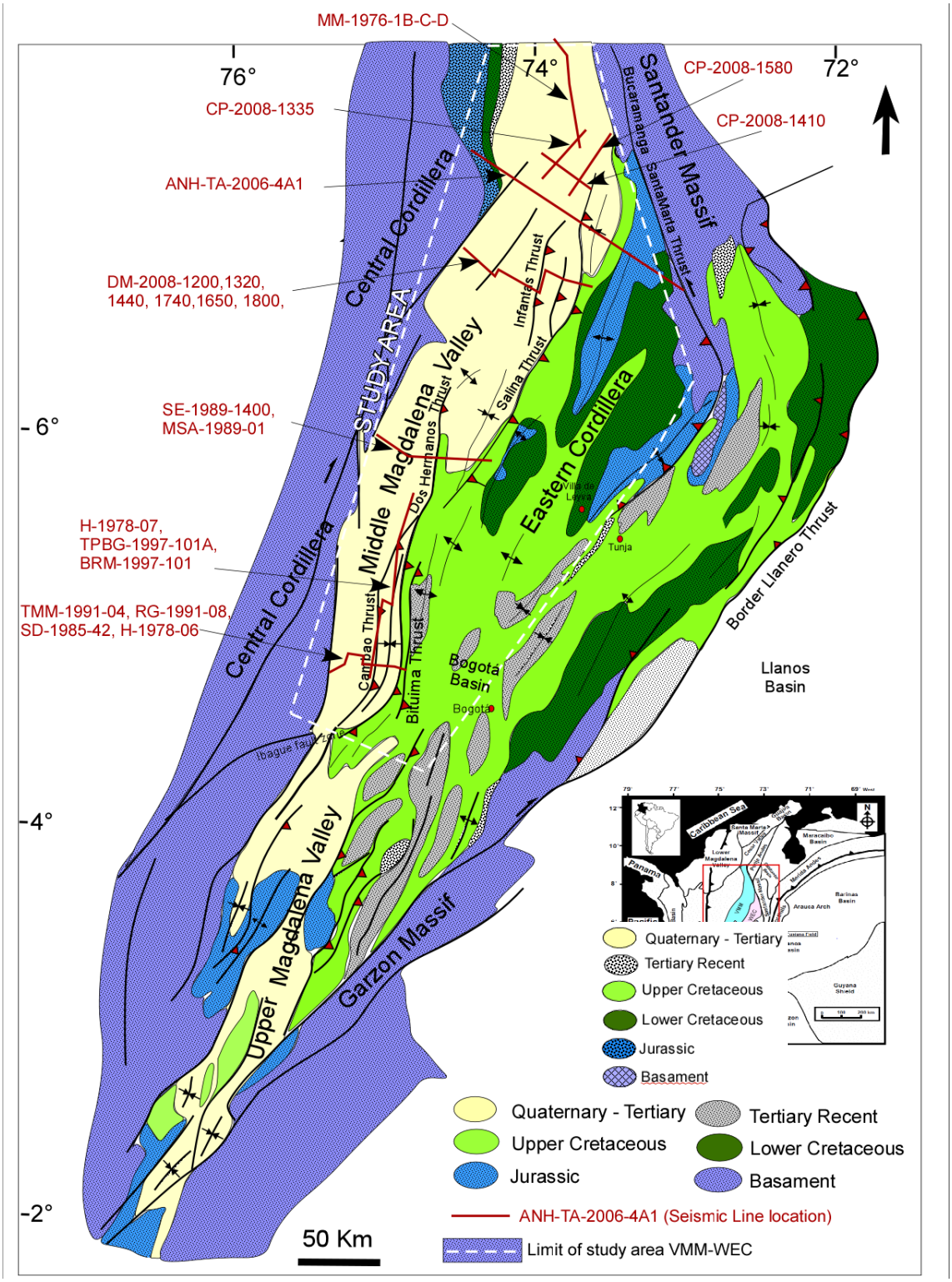

Figure 4.2. *Map showing of Cretaceous units and main structural features of the Middle Magdalena Valley, Eastern Cordillera and Upper Magdalena Valley. (Modified from Restrepo et al., 2004). Some seismic references lines location using in this work are shows in red lines in the map.*

4.3 Materials and methods

The MMV and WEC area is about 50.000 km^2 wide. 1559 seismic lines representing more than 50.000 km were made available for regional projects (Figure 4.7, light blue and black

lines). We selected the most representative and best quality lines to carry out the regional analysis in the MMV and WEC and to build structural sections. Detailed seismic interpretation using well logs, structural and stratigraphic information, allowed to regionally correlate the seismic units and to construct chronostratigraphic charts.

Thousands of wells have been drilled in the MMV and only a few wells in the WEC, the majority of which only crossed the Tertiary sequence. Only wells that crossed the Cretaceous sequence and have lithological and sedimentological information were taken in to account. The list of the wells used in this work is shown in Table 4.1, and some key wells are shown in Figure 3.5.

Information used for the structural description of the WEC has been collected during field work, or derives from published works and geological maps (Renzoni et al., 1967; Rodriguez and Ulloa, 1991; 1994; Acosta and Ulloa, 2001; Fuquen and Osorno, 2005).

4.3.1 Seismic reflection patterns and identification of unconformities.

Distinct types of stratal terminations like truncation, toplap, offlap, onlap, dowmlap have been defined by Ramsayer (1979) and Emery and Meyers (1996) as is shown ig Figures 4.3 and 4.4.

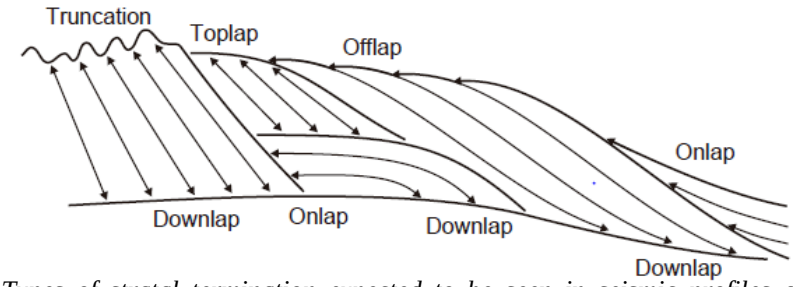

Figure 4.3 *– Types of stratal termination expected to be seen in seismic profiles and outcrops. Note that truncations are usually related to conformities or erosion surfaces (from Emery and Myers, 1996).*

Descriptor	Position	Code	Explanation	Expression
Top	A (Upper boundary character)	C	Concordant	
		Top	Toplap	
		Di	Divergent	
		Tr	Truncation	
Base	B (Lower boundary character)	C	Concordant	
		Dwn	Downlap	
		Di	Divergent	
		On	Onlap	
Internal	C (Reflection character)	P	Parallel	
		Ob	Oblique	
		Si	Sigmoidal	
		Md	Hummocky	
		Subp	Subparallel	
		GS	Growth Strata	
		Ch	Chaotic	

Figure 4.4 *– Types of stratal terminations as observed in seismic profiles. A and B defines the seismic facies unit (modified from Ramsayer, 1979) and C defines the reflection character based on types of stratal termination.*

The seismic expression of reflectors (Figure 4.5), their geometry, the relation between strata and stratigraphic surfaces (reflector surfaces) against which they terminate were important to define the sequences and their boundaries (unconformity). Our observations derive from 2D and 3D seismic analysis and from outcrops (Fig. 4.6a, 4.6b).

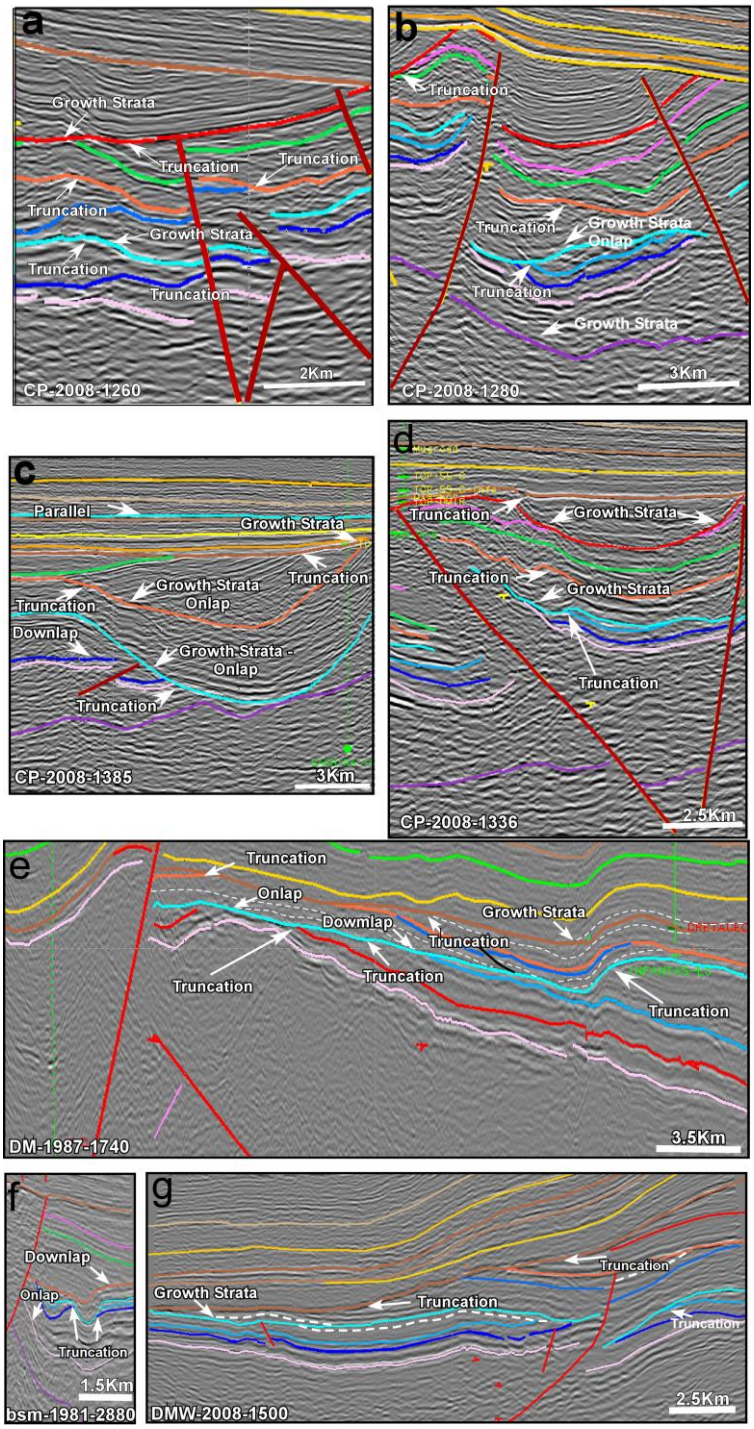

Figure 4.5 *- Seismic reflection patterns for the identification of unconformities. Truncation and growth strata are shown on different examples of seismic sections from this work. From base to top: SU1 in pink (Jurassic unconformity); SU2 in light blue (Barremian/Aptian unconformity); SU3 in Orange (Albian/Cenomanian unconformity); SU4 in red (Santonia/Campanian Unconformity); SU5 in brown (Paleocene/Eocene Unconformity or younger).*

Other terms have been introduced to define the architecture of seismic reflections (Mitchum et al., 1977; Mitchum and Vail, 1977), or to describe staking patterns, surfaces and system tracts (Posamentier et al., 1988; Van Wagoner et al., 1988; Christie-Blick, 1991).

Truncation represents the termination of strata against an overlying erosional surface. Truncation implies the development of an erosional relief or an angular unconformity. *Toplap* represents the termination of inclined strata (clinoform) against an overlying lower angle surface (mainly result of nondeposition or minor erosion). *Onlap* describes a low angle termination against a steeper stratigraphic surface; it may develop in marine, coastal and non marine settings. *Downlap* is a termination of inclined strata against a lower angle surface. *Offlap* results from the progressive offshore shift of the updip termination of sedimentary bodies within a conformable sequence; it usually results from a base level fall, and is therefore related to forced regression (Mitchum 1977; Galloway, 1989; Emery and Meyers, 1996). *Growth Strata* are stratigraphic intervals in which deposition occurred during deformation and are important to define unconformities or erosional surfaces. The age of growth strata define the timing of deformation.

These definitions were used to identify the seismic sequences and boundaries in the MMV-WEC Basin. Figures 4.5 (a to g) show truncations and growth strata (more examples in Shaw et al., 2005). We added examples where faults are sealed by an unconformity (Figure 4.5g). Truncations, growth strata and faults are good evidences of unconformities or erosion surfaces, and of tectonic-sedimentary events affecting the basin.

4.4 Seismic interpretation of the Cretaceous series in the MMV and WEC

4.4.1 Structural Cretaceous behavior

The WEC and MMV basin has been created as a rift basin associated to normal faulting. The rifting occurred during the Late Triassic-Middle Jurassic and gave way to the deposition of the Jordán and Girón Formations. Rifting continued during the Lower Cretaceous associated with a rapid subsidence, which allowed the deposition of a thick marine sedimentary pile (mudstone, limestone, sandstones, shales, chert, and phosphorites). Such deposition took place in the Eastern Cordillera in the Bogotá sub-basin, in the Cocuy sub-basin to the North, and in the Tablazo sub-basin to the west (Sarmiento, 2001), which were limited by normal faults, presently tectonically inverted (Sarmiento et al., 2006; Sarmiento, 2001; Fabre, 1983; Etayo, 1968).

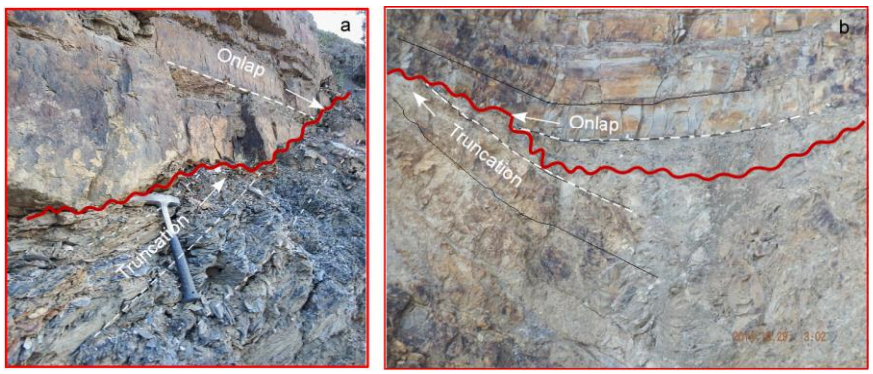

***Figure 4.6** – Unconformities identified in outcrops. Note the angularity between the units below and above the unconformities. a) The Late Albian (Upper San Gil) - Early Cenomanian (Churuvita Fm) limit along the Villa de Leyva-Cucaita road; b) The Cenomanian Simijaca/Frontera Fm south of the town of Susa town.*

It is usually believed that compressive deformation did not occur before the Maastrichtian to Paleocene, and was associated to the oblique accretion of the present-day Western Cordillera, which produced shortening and uplift of the Central Cordillera (Gómez, 2005; Cooper, 1995). This event occurred during the Paleocene-Eocene interval and produced an important erosion that affected the foreland basin.

According to Restrepo (2004), the EC would result from compressional deformation and uplift related to the Late Miocene-Pliocene orogeny. In contrast, based on their detailed mapping of the fold belt in the WEC, Restrepo-Pace et al. (2004) proposed that deformation and erosion actually began in the Late Paleocene-Early Eocene time, and that several structures related to this event are concealed by this Eocene unconformity.

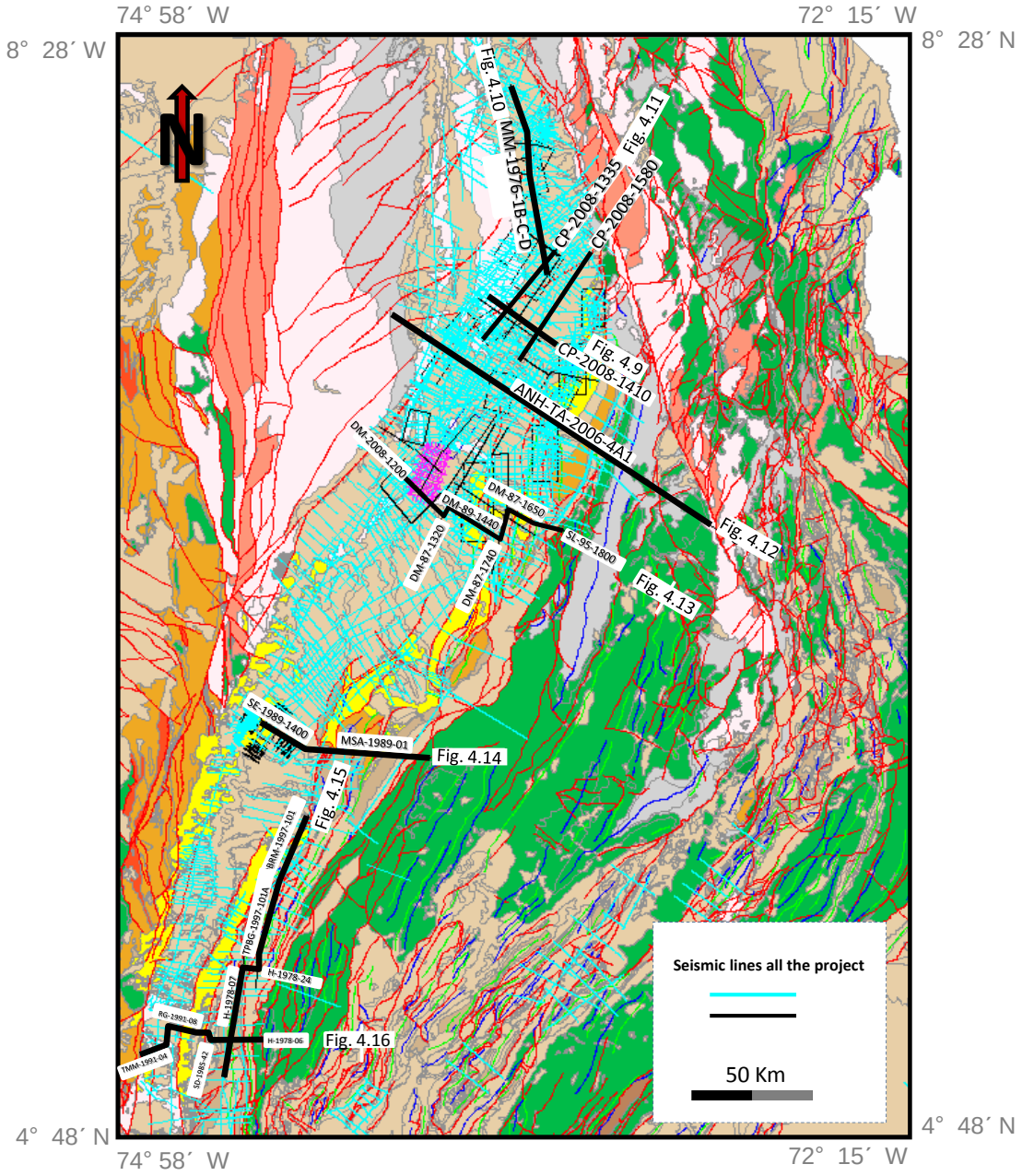

Figure 4.7- *Simplified geological map of the study area. Green: Cretaceous; Yellow and orange: Tertiary; Dark pink and light purple: Pre-Cretaceous. 2D seismic information available in the MMV (light blue). The central and western cordilleras bound the MMV.*

WELLS	Longitud (W)	Latitud (N)
AGATA-1 & ST	74° 19´ 18.7"	05° 49´ 49.0"
ANDES-1	74° 41´ 25.1"	05° 45´ 36.3"
BOSQUES-1	73° 46´ 09.4"	07° 19´ 11.4"
CACERES-1	74° 23´ 35.0"	05° 41´ 30.6"
CAÑO RICO-1	74° 46´ 39.1"	05° 29´ 32.5"
CASABE-199	73° 55´ 11.9"	07° 02´ 05.8"
CASABE-K-1	73° 55´ 36.9"	07° 01´ 41.4"
CASCAJALES-1	73° 41´ 30.8"	06° 51´ 34.4"
CATALINA-1	73° 41´ 40.0"	08° 16´ 04.5"
CHUCURI-1	73° 59´ 20.5"	06° 55´ 36.6"
COYOTE-1	73° 40´ 12.6"	06° 53´ 32.2"
ESCUELA-1	73° 33´ 48.6"	05° 05´ 00.8"
GUANE-1	73° 48´ 22.4"	07° 14´ 18.93"
GUINEAL-1	74° 13´ 27.5"	06° 03´ 28.19"
IGUANA-1	74° 13´ 27.5"	07° 37´ 43.6"
IWANA-1	74° 13´ 27.5"	07° 05´ 05.0"
JUAN PABLO-1	74° 39´ 03.1"	05° 05´ 25.0"
JUANITA-1	74° 39´ 18.8"	05° 08´ 13.3"
RW-1	73° 47´ 49.9"	06° 51´ 33.2"
LA TOLDA-1	74° 15´ 39.8"	06° 32´ 42.0"
LA TORA-1	73° 50´ 47.5"	06° 56´ 21.2"
LLANITO-1	73° 49´ 04.8"	07° 11´ 22.3"
NOREAN-1	73° 40´ 54.9"	08° 21´ 40.4"
PROMETEO-1	73° 50´ 23.1"	07° 10´ 13.7"
PUNTA PIEDRA-2	73° 34´ 44.4"	07° 40´ 58.2"
SEGUNDO-1	74° 35´ 12.6"	05° 06´ 16.2"
TOTUMAL-3	73° 36´ 05.7"	08° 09´ 28.9"
YAGUALI-1	74° 47´ 04.1"	05° 08´ 07.7"
YUMECA-1	73° 22´ 52.1"	07° 32´ 48.6"

Table 4.1 *– List of the wells used in this work. Location are shown in Figure 3.5. Some of these wells are described in Chapter 3.*

Based on detailed mapping of an area along of the western flank of the Eastern Cordillera, Restrepo-Pace et al. (2004) studied rocks varying in age from Barremian to Holocene, and determined an important hiatus (unconformity) in the late Paleocene-early Eocene, coeval with the uplift of the Central Cordillera. For these authors, the fold belt resulted from a series of compressional events that began in the WEC during the late Paleocene-early Eocene, and farther West, with the uplift of Central Cordillera (CC) during the late Campanian to Maastrichtian (Restrepo-Pace et al., 2004). Finally, during the Late Miocene structural reactivation and exhumation occurred in the break-back thrusting sequence.

Figure 4.8 shows a regional section from the Central Cordillera (CC) to the WEC crossing the MMV. Its upper part presents two interpretative structural sections from the WEC along the Rio Sogamoso. The interpretation details are shown using (1) only field information and geological maps (left), and (2) seismic information (right), which allow to interpret in more detail in order to identify unconformities (Figure 4.8).

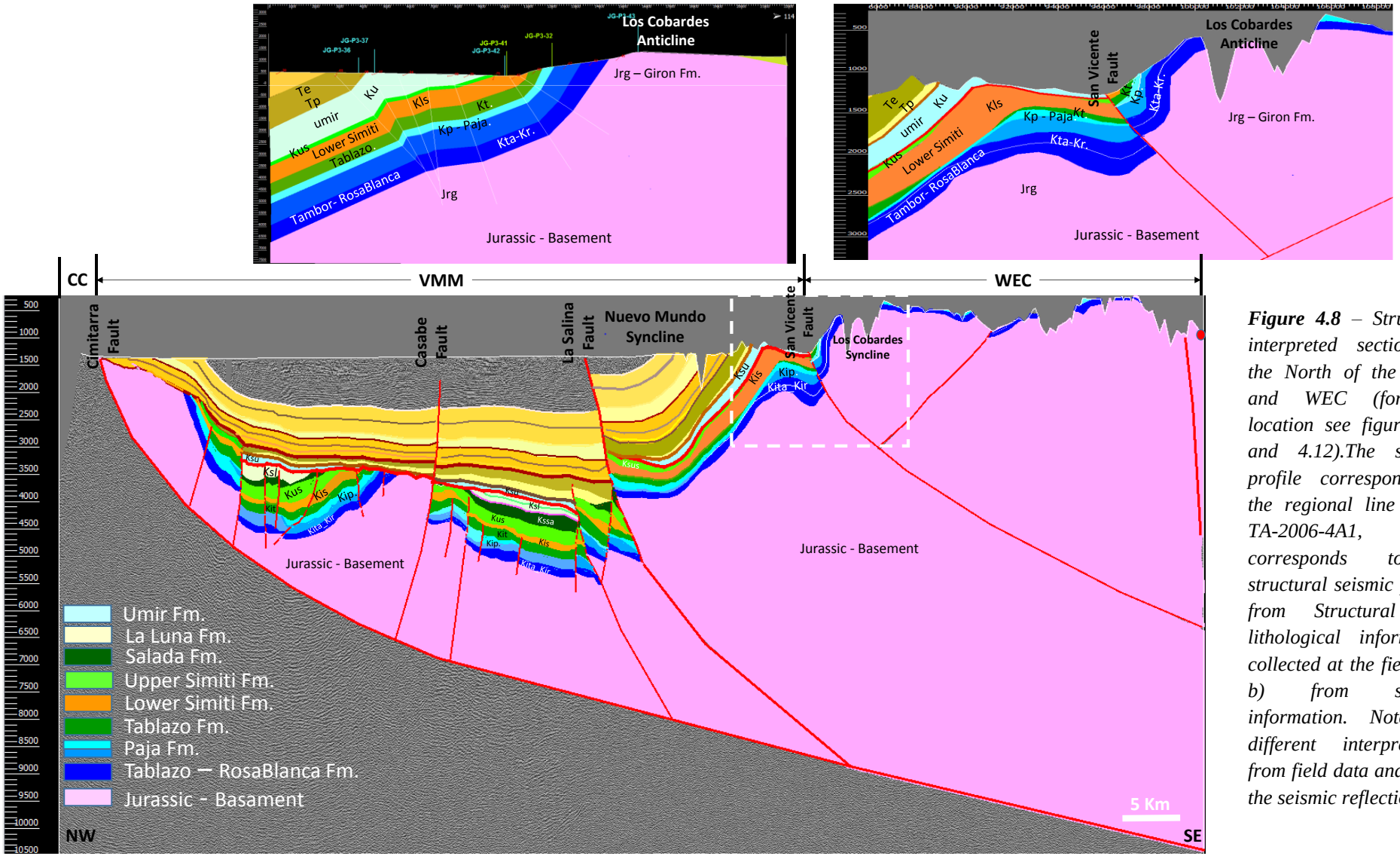

Figure 4.8 *– Structural interpreted section, at the North of the MMV and WEC (for the location see figures 4.7 and 4.12).The seismic profile corresponds to the regional line ANH-TA-2006-4A1, a) corresponds to a structural seismic profile from Structural and lithological information collected at the field and b) from seismic information. Note the different interpretation from field data and using the seismic reflection*

4.4.2 Seismic Sequences

Several seismic lines were interpreted from North to South (Figure 4.7) in the MMV and in the WEC, to understand the behavior of the basin during the Cretaceous. Based on the interpretation of wells and seismic lines, and on the few available biostratigraphic, we identified five Cretaceous sequences (S), bounded by five unconformity surfaces (SU). Seismic sequence boundaries were defined by the identification of discontinuity surfaces interpreted in the seismic lines as unconformities or their correlative conformities. These discontinuities were followed using seismic patterns (Figure 3.12, 4.4 and 4.5).

Figure 4.9 shows the interpretation of a NE-SW trending seismic line. As shown in figure 4.9, the Cretaceous sequence exhibits a complex structure and evolution, and most of it is locally eroded by pre-Andean unconformity surfaces (SU1 to SU5).

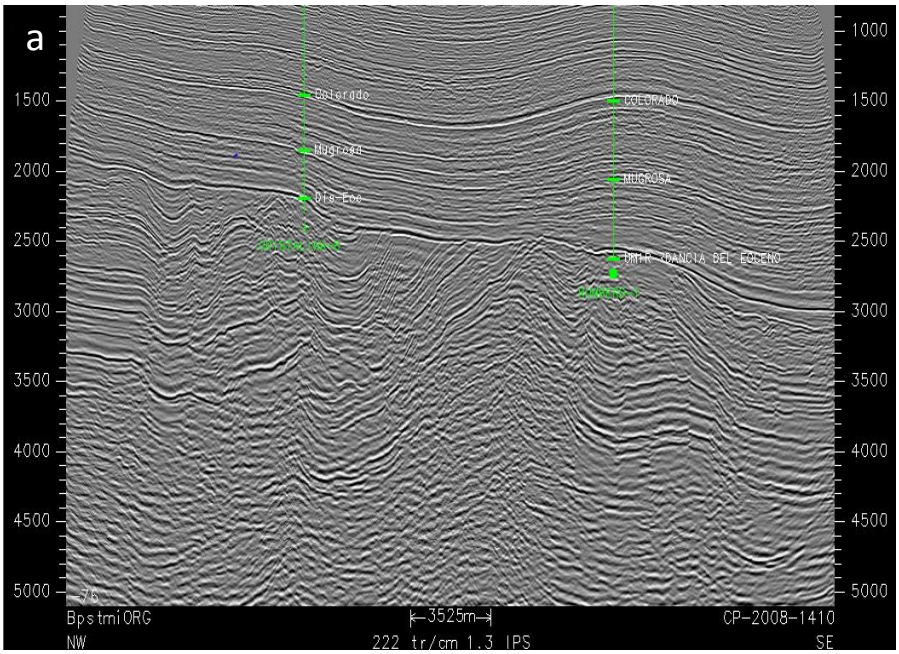

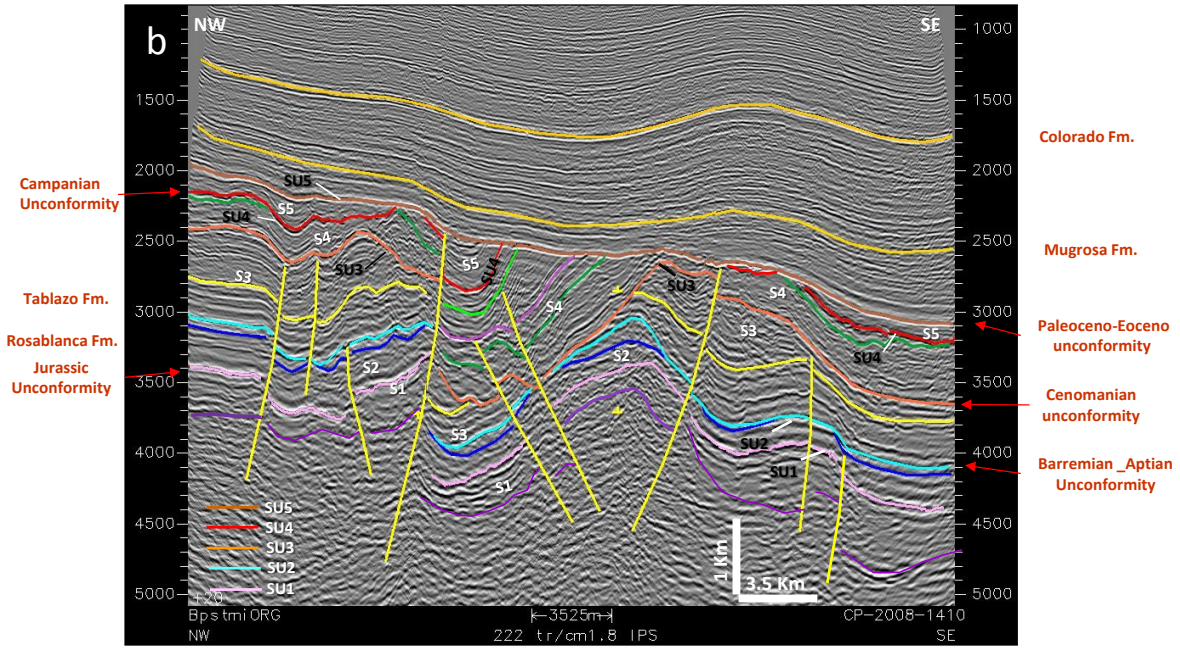

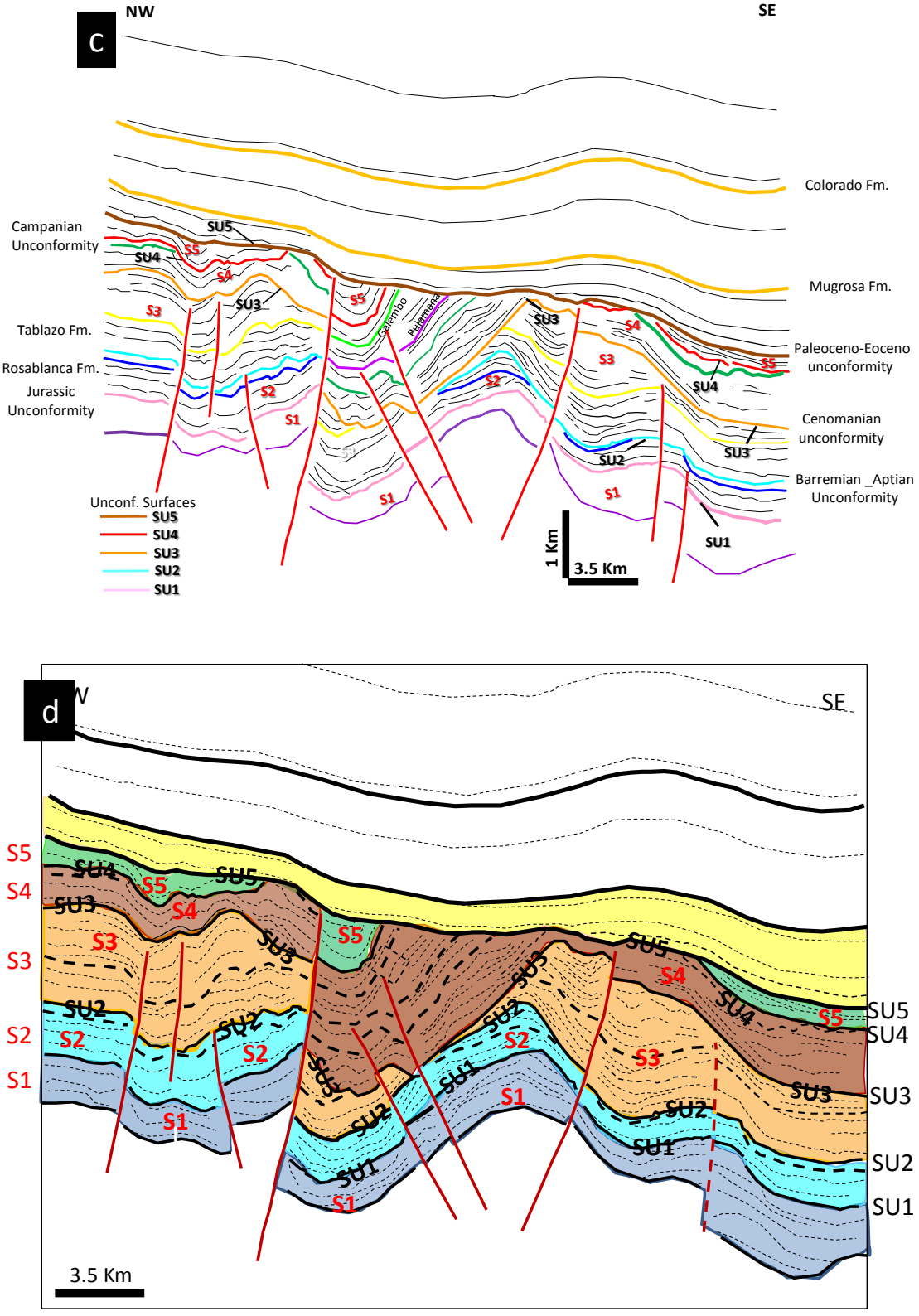

Figure 4.9. *Seismic reflection profile CP-2008-1410, orientated NW-SE, in the northern MMV (location on Figure 4.7). a - Seismic section; b - Seismic interpretation, showing unconformities or non-deposition surfaces below the Eocene unconformity; c - Sketch illustrating the seismic units and unconformities from Barremian to Paleocene times; d - Seismic stratigraphy sketch, showing the main sequences identified in the Cretaceous (S1 to S5) and surface unconformities (SU1 to SU5).*

In Figure 4.9c, all sequences are limited by unconformities or boundaries, which were only identified in some wells in the MMV (e.g. RW-1 well) and correlated during the seismic interpretation (Figures 4.9 to 4.22). These unconformities are labeled as follows: SU1 corresponds to a Jurassic/Cretaceous unconformity (pink), SU2 is of Barrremian/Aptian age (light blue), SU3 is the Cenomanian unconformity (orange), SU4 represents the Campanian unconformity (red), and SU5 the Tertiary unconformity (brown) (Figures 4.9 to 4.22). The Cretaceous deformation and the presence of several unconformities evidence that the Cretaceous history of the MMV-WEC basin is more complex than previously thought (Figures 4.17 to 4.22).

The five sequences (S1 to S5) are described below.

The complex Cretaceous tectonic-sedimentary evolution of the MMV-WEC (Figures 4.9 to 4.16) is not only due to tectonic deformation, but also to the erosion or non-deposition occurring in different time-spans during the Cretaceous. Reverse faults produced deformation in the basin as observed in different sections (Figures 4.9 – 4.16), where some faults affect only a part of the sequence and other faults other parts of the sequence (Figures 4.9 to 4.16). For example in Figure 4.9, some faults are propagated only till unconformity SU2 affecting only the Pre-Aptian sequence (S2), others affect Aptian-Albian deposits (sequence S3) till unconformity SU3 and others crosscut the pre-Campanian sequence (S4) till unconformity SU4, and the last one affects sequence S5 till the unconformity SU5. This indicates that various tectonic events occurred during the Cretaceous, which is supported by the folding observed in the pre-Tertiary unconformity surfaces (SU1 to SU5). The inversion started during the Barremian-Aptian times and continued till Cenomanian and Campanian times, being more and more intensive through time, and finally culminating with the pre-Tertiary erosions, in which the Campanian unconformity produced the most important erosion during the Cretaceous.

S1 Sequence (Jurassic prior to 145 Ma)

The S1 sequence (Figures 4.9 to 4.16) was deposited during Jurassic times. It corresponds to the Girón Fm or Los Santos Fm in the MMV and north of the WEC (Bucaramanga-Barichara area), and to the Arcabuco Fm in the central part of the WEC (Villa de Leyva-Chiquinquira, location on Figure 3.5). The regional facies distribution of this sequence has not been analyzed in chapter 3, but the sequences are shown in the seismic sections (Figures 4.9 to 4.16). In the MMV, no wells crosscut this sequence but it crops out in the in the northern part of the WEC (Los Cobardes syncline, Figure 3.5) and in the central part of the study area (Arcabuco syncline, Figure 3.5).

S2 Sequence (Early Berriasian-Late Barremian)

The S2 sequence is bounded by the regional unconformities SU1 at the base and SU2 at the top. It has been recognized in all the study area from North (Figure 4.9) to South (Figure 4.16), and is composed by units deposited from Early Berriasian to Late Barremian times, and partly eroded by the SU2 (Barremian-Aptian). This observation is consistent with the erosion and/or hiatus presented in Chapter 3, and with the marine regression highlighted by the analysis of the Barremian-Aptian facies (Figure 3.52). As a matter of fact, shallow marine facies apparently migrated from East to West through time, the observed facies being deeper to the west. In the RW-1well, the ammonite succession from the core section evidences the Late Barremian-Early Aptian hiatus in the La Paja Fm (Etayo, 2012, internal report).

S3 Sequence (Early Aptian - Late Albian)

The S3 sequence is bounded by the unconformities SU2 at the base and SU3 at the top and is

present in the whole study area (Figures 4.9 to 4.16). The duration of this sequence is about 25 Ma and it corresponds to the Upper La Paja, Tablazo and Simiti Fms (San Gil Central area) in the MMV and in the northern and central areas of the WEC (location in figure 3.5), and to the Trinchera, Peñon/Socota, Capotes e Hilo Fms in the southern part of the WEC (Figure 3.4). S3 sequence comprises the units deposited during the Early Aptian-Late Albian interval, which were partly eroded by SU3 as shown in Figures 4.9a to 4.9c and 4.17 to 4.22. The SU3 unconformity may encompass the Early Cenomanian as shown in Figure 3.54, where the unconformity interpreted on the seismic line would be coeval with the regression which eroded partially or totally units deposited in a period of marine transgression, probably due to a sea level rise during the Albian (Tablazo-Lower Simiti). The Early Cenomanian unconformity may be represented in the study area, by outcrops along the Villa de Leyva-Cucaita road (Figure 3.28). There, a possible unconformity marks the contact between fine-grained deposits of the San Gil Fm, and coarse sandstones and conglomeratic sandstones at the base of the Early Cenomanian Churuvita Fm (Figure 3.28, photo 3.7, Figures 4.17 to 4-18).

S4 Sequence (Early Cenomanian – Late Santonian)

The S4 sequence is defined between unconformities SU3 at the base and SU4 at the top. It is composed by the Simijaca, Pacho, Frontera, Conejo and Arenisca Dura stratigraphic units in the South; by the Churuvita (Figure 3.28), Simijaca, Conejo and Lidita Superior Fms in the center; by the Upper Simiti, Salto and La Luna Fms in the north of the WEC and in the MMV. The Campanian SU4 unconformity that bounds the S4 sequence has also been recognized in the well RW-1, and is a regional unconformity also present in Venezuela (Cooney, 2009).

In the RW-1and Cascajales-1 wells and in the Quebrada la Sorda, the SU4 unconformity (Lower Campanian) is marked by the lack of the Dynogymniun zone described in chapter 3, accompanied by a change in thickness for example between the Pujamana Top and base of Umir (Internal report ICP-Ecopetrol, 2013) marked in the seismic data by truncations, growth strata or onlap (figure 4.5). The top of this zone is marked by a change from mainly marine to mostly continental palynological assemblages at the base of Umir Formation (for more details see chapter 3).

S5 Sequence (Campanian - Paleocene)

S5 sequence is limited by SU4 at the base and by the Paleocene-Eocene hiatus (SU5) at the top. It is composed to the North by the Umir and Lisama Fms; in the central area by the Arenisca Dura, Pleaners, Labor y Tierna, Guaduas, Cacho, Bogotá and Regadera Fms; to the South by the Pleaners, Labor y Tierna, Cordoba and Guaduas Fms; and by the Umir and Lisama Fms in the MMV.

The base of this sequence is marked by the agglomeration of species (Andalusiella mauthei, *Andalusiella* complex, *Spinizonocolpites baculatus*, etc), with the first occurrence of the pollen *Ulmoidipites krempii*, and its top by the occurrence of the pollen *Proteacidites dehanni*. The base presents a marked continental influence. This sequence was eroded by the regional Eocene unconformity (SU5). The same interval has been recognized in the Cascajales-1 well, where deposits bearing continental palynoflora overlie a marine sequence.

4.4.3 Cretaceous unconformities

The unconformities identified in the MMV basin may be due to tectonic activity or to sea level fluctuations (Chapter 3). Unfortunately biostratigraphical information is usually not accurate enough to identify stratigraphic gaps, except in the RW-1well, which is exceptionally rich in ammonites (Etayo, 2012, internal report).

Some unconformities are supported by information from well log (i.e. biostratigraphy and palynology in RW-1and Cascajales-1), and from scarce outcrops (see chapter 3). These data, and above all the interpretation of seismic reflection sections allowed to identify and follow the unconformities in the whole MMV and in some areas of the WEC (e.g. the 147 km long seismic profile ANH-TA-2006-4A1, in Figure 4.12).

In the study area, five unconformities (SU1 to SU5) define the above described seismic sequences. Two of these unconformities were already recognized: around the Jurassic-Cretaceous (SU1) and the Cretaceous-Tertiary (SU5).

Unconformity SU1

This unconformity encompasses the Upper Jurassic-lower Cretaceous boundary, and may erode sequence S1 and even basement rocks. It is acknowledged as a regional unconformity that is locally an angular unconformity, suggesting compressional deformation in the latest Jurassic (Pulido et al., 1979a; 1979b; 1980). In the Los Cobardes range, SU1 is identifued in the Early Cretaceous units with angular unconformity upon the Jurassic units (see Figures 4.11 to 4.16). In the rest of the study area, SU1 is an erosional surface, which underlines the Cretaceous sequence (Figures 4.9 to 4.16, and 4.5).

Unconformity SU2

The second unconformity corresponds to the Late Barremian to Early Aptian unconformity (SU2 - light blue in Figures 4.9 to 4.22 and 4.5), which underlines the Tablazo Fm. It deeply erodes sequence S2, as shown in Figures 3.25, 3.26, 4.9 and 4.17, and may remove part of the Rosablanca Fm of Berriasian-Valanginian age (e.g. figure 4.20), or even Jurassic deposits (Figures 4.13 to 4.21). Figure 4.13 shows an angular truncation below SU2 (light blue) at the Infantas-E5 well. Growth strata are other evidences of this unconformity (Figures 4.14, 4.15, 4.26). It conrresponds to the Late Barremian-Early Aptian hiatus reported in the RW-1well (Chapter 3).

Few authors report comparable unconformities. Macellari (1988) identified various unconformities; one of them of Aptian age would be consistent with the unconformity SU2 recognized in this work. Morales (1958) identified an unconformity of Aptian age. In the UMV, Barrio et al. (1992) and Allen (1989) reported an unconformity of Barremian-Aptian age in the Payande-Chaparral area, and in the area of Ortega, respectively (Figure 4.26).

Unconformity SU3

An important unconformity (SU3) has been identified within the Simití Fm or at the San Gil-Churuvita boundary of Cenomanian age (orange line in Figures 4.9 to 4.16, 3.28 and 4.17 to 4.22). The SU3 unconformity erodes sequence S3 possibly till Jurassic rocks (Figures 4.19 to 4.22). Growth strata and onlap terminations are visible above and below the the SU3 surface. Angular truncation can be observed (probably divergent as shown in figure 4.4) (Figures 4.9, 4.11, 4.13, 4.14 and 4.15). Line dmw-2008-1500 (Figure 4.5) shows both an oblique truncation below the SU3 unconformity, and pre-Late Cenomanian deformation generated by faults sealed by SU3. This stratal termination shows a deformation that occurred in the MMV, previous to the erosion of SU3.

Such a Cenomanian unconformity has been reported by Morales (1958) in the MMV, and by Macellari (1988) in Maracaibo, Middle Magdalena Valley and western Peru (Figure 4.26), and by Jaimes and De Freitas (2006) in the UMV. The SU3 is responsible for an important erosion, which may have removed strata of Lower Cenomanian to Aptian age.

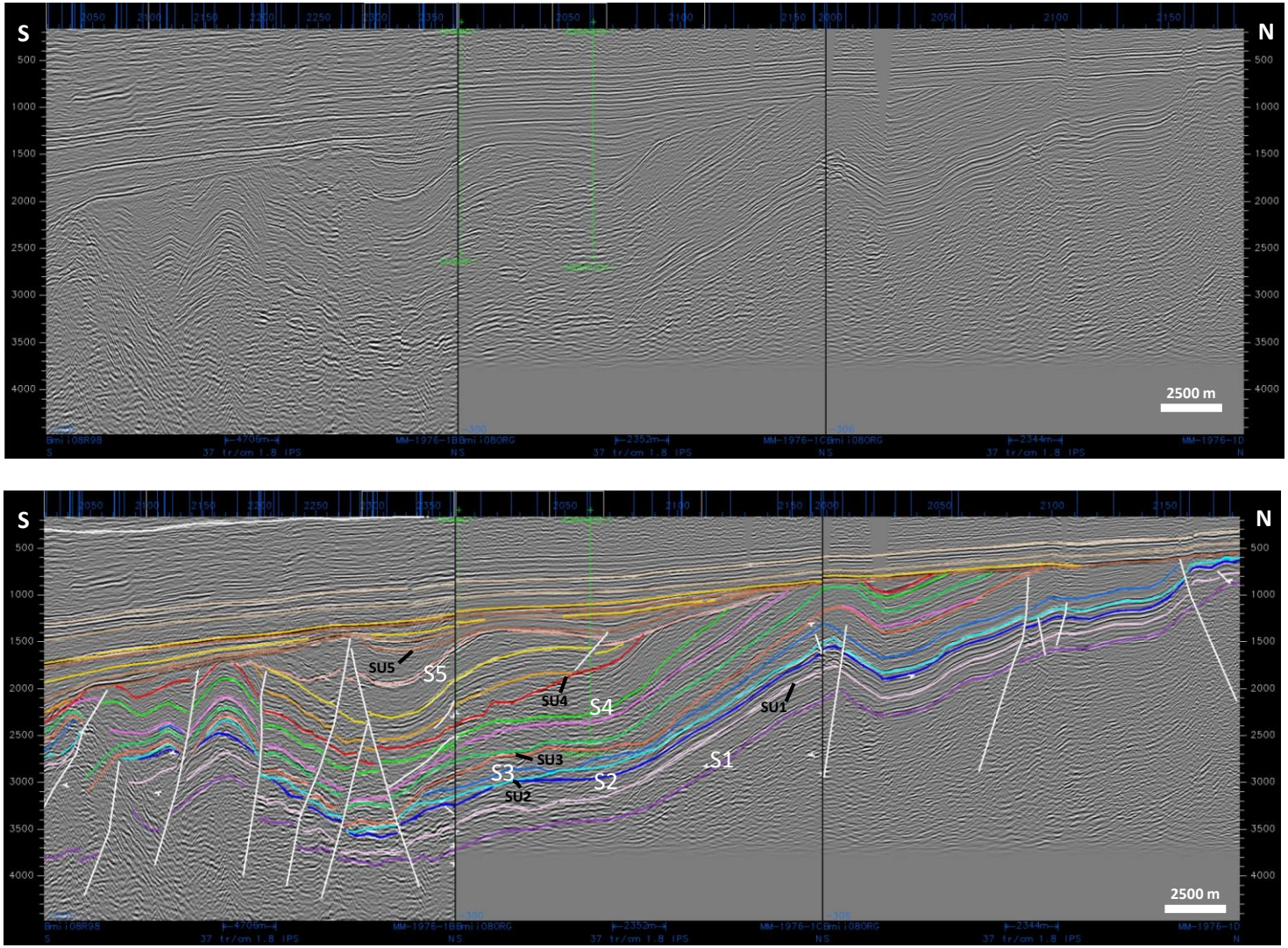

Figure 4.10. *S-N trending seismic reflection profile MM-1976-1B, 1C and 1D in the north of the MMV (location on Figure 4.7). Above: un-interpreted section; below: proposed interpretation. The main faults are presently reverse faults. Note the northward increasing erosion below the Mid-Eocene unconformity: to the North, the Albian unit is directly overlain by Tertiary units.*

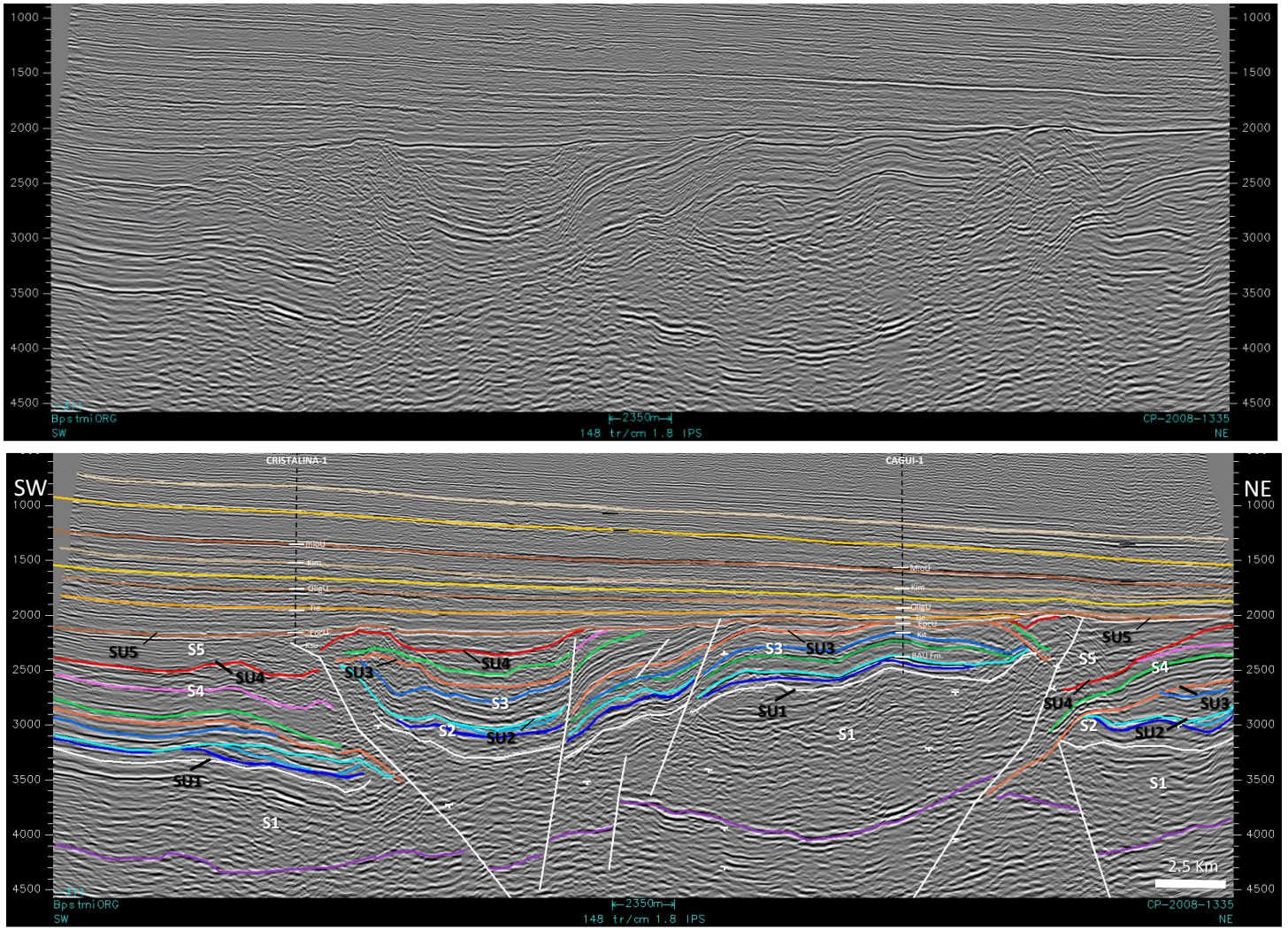

Figure 4.11. *S-N trending seismic reflection profile CP-2008-1335 in the northern part of the MMV (location on Figure 4.7). Above: un-interpreted section; below: proposed interpretation.*

Unconformity SU4

The SU4 unconformity of Campanian age (red line in Figure 4-5 to 4.16) underlies the Umir Fm or the Guadalupe Group. In the MMV, much of the SU4 surface has been removed by the Paleocene-Eocene erosion (SU5, Figure 4.9-4.16). In Figure 4.14, only patches of the S4 sequence may be observed to the East, near the surface, but S4 is widespread in other parts of the basin (e.g. Figure 4.10 and 4.19). Our analysis shows that the SU4 erosional unconformity removed deposits of sequence S4 (Early Campanian to Cenomanian), removing up to a ≈ 1500 m thick pile of sediments (Figure 4.9). Compared with the previous SU2 and SU3 unconformities, SU4 is the most important erosional event. This SU4 major event has been recognized by Balkwill et al. (1995), Jaillard (2000), Veloza et al. (2008) and Cooney and Lorente (2009), in Peru, Ecuador, Venezuela and Colombia.

Unconformity SU5

The SU5 unconformity is located at the top of the Cretaceous sequence, and represents the well known Mid-Eocene regional unconformity. It is easily seen in seismic profiles, where it is always represented by angular truncations.

The SU5 unconformity is well known in the MMV, but is frequently eroded by younger erosions (Oligocene and Miocene unconformities). In our study area, the Paleocene-Eocene SU5 unconformity is totally eroded North of the Cimitarra town (Armas syncline). This observation shows that the strong seismic reflector, with angular truncation, at the top of the Cretaceous sequence, which is usually interpreted as the Paleocene-Eocene unconformity, can be much younger.

A fundamental law in geology (Steno, 1669, later formulated by Hutton (1975) and Lyell (1830)) indicates that a feature that cuts another one is the younger of the two features. In the MMV, we clearly observe that younger unconformities cut and erode totally or partially the older ones. As an example, the Paleocene-Eocene or younger (Oligocene) unconformities cut the Campanian unconformity (SU4) or older unconformities (Figures 4.9 to 4.16, and 4.17 to 4.22). In the same way, the Early Campanian unconformity (SU3) may cut the Cenomanian, the Cenomanian may cut the Barremian-Aptian (SU2) and so on.

The more recent unconformities may have eroded the oldest sediments in the basin (Figures 4.9 to 4.16, and 4.17 to 4.22). In Figure 4.11, the SU3 unconformity in some places (ex. right side) locally eroded the whole Cretaceous sequence until reaching Jurassic deposits, leading to the disappearance of the SU1 and SU2 unconformities. In the same way, in some areas of the MMV, the Mid-Eocene SU5 unconformity eroded totally or partially older unconformities (Figure 4.17 to 4.22). This may lead to confusing interpretations, when several unconformities are amalgamated.

4.5 Chronostratigraphic seismic interpretation

3500 km of 2D seismic lines (Figures 4.7, and 4.9 to 4.16) as well as tie wells were used to construct the chronostratigraphic charts across the MMV and in some parts of the WEC, in order to identify the sequences and unconformities in the basins.

We first identified and constructed paleo-facies maps (Figures 3.48 to 3.56) from the well information to visualize the evolution of the basin during the Cretaceous time, from 145 to 85 Ma. In Chapter 3 we distinguished four facies (sandstone/siltstone, shale/claystone, limestone, and swamp clay with vegetation) to try to illustrate the facies migrations, the sea level variations, and to evidence the possible erosions.

In seismic sequence stratigraphy, the basic idea is that the seismic reflectors follow the geological time line, and are thus chronostratigraphic lines. Thus, seismic reflection profiles were used to build chronostratigraphic charts (Wheeler diagrams).

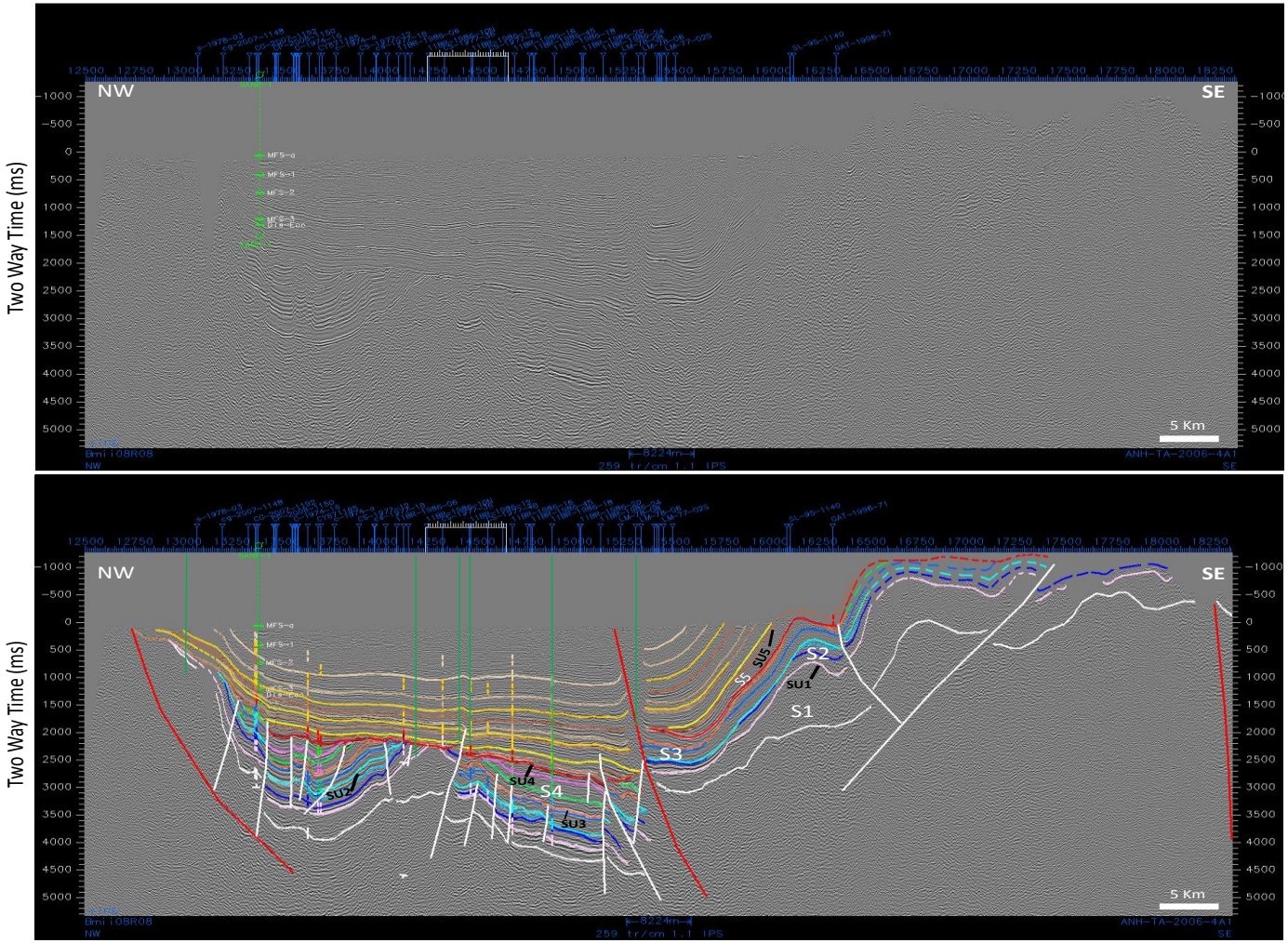

Figure 4.12 *– NW-SE trending seismic reflection profile ANH-TA-2006-4A1 in the north of the MMV (location on Figure 4.7). Above: un-interpreted section; below: proposed interpretation. Sequences and unconformities have been labeled as S1 to S5, and SU1 (pink), SU2 (light blue), SU3 (orange), SU4 (red) and SU5 (brown), respectively.*

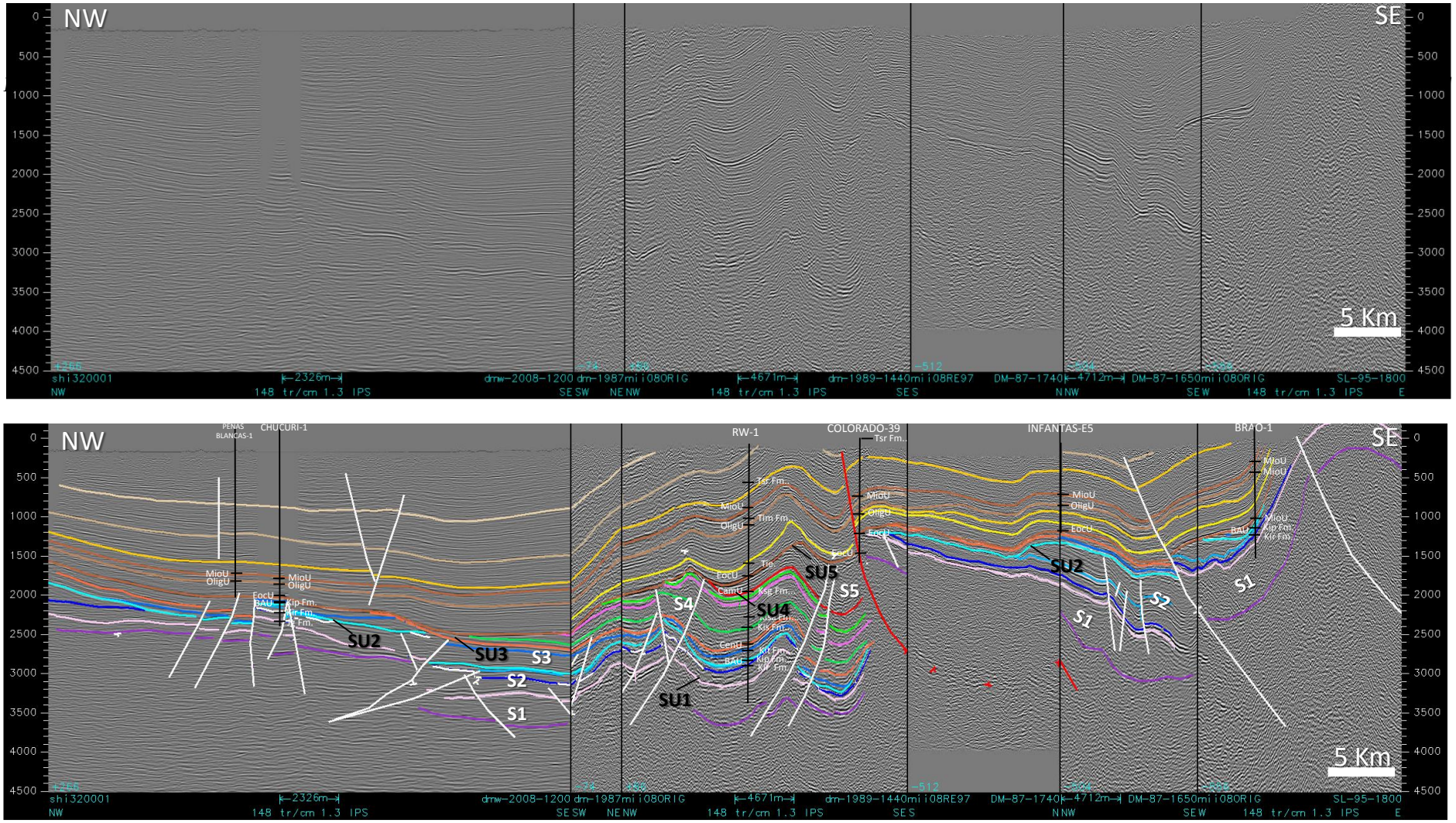

Figure 4.13 *a – Seismic section at the north of MMV. Above: un-interpreted section. Below: interpreted along the seismic reflection profile dmw-2008-1200, dm-1987-1320, dm-1989-1440, DM-87-1740, DM-87-1650, SL-951800, in direction NW-SE in the north of the MMV. (see Figure 4.7 for the location). Intense deformation in the Cretaceous sequence limited by faults that didn´t affect the Tertiary units which cover cretaceous unit at the central and western part, while at the East the Lower Cretaceous units are exposed in the surface. Seismic sequences observed in the section have been labeled as S1 to S5 and the sequence boundaries labeled in the section as SU1 (pink), SU2 (blue light), SU3 (orange), SU4 (red), SU5 (brown).*

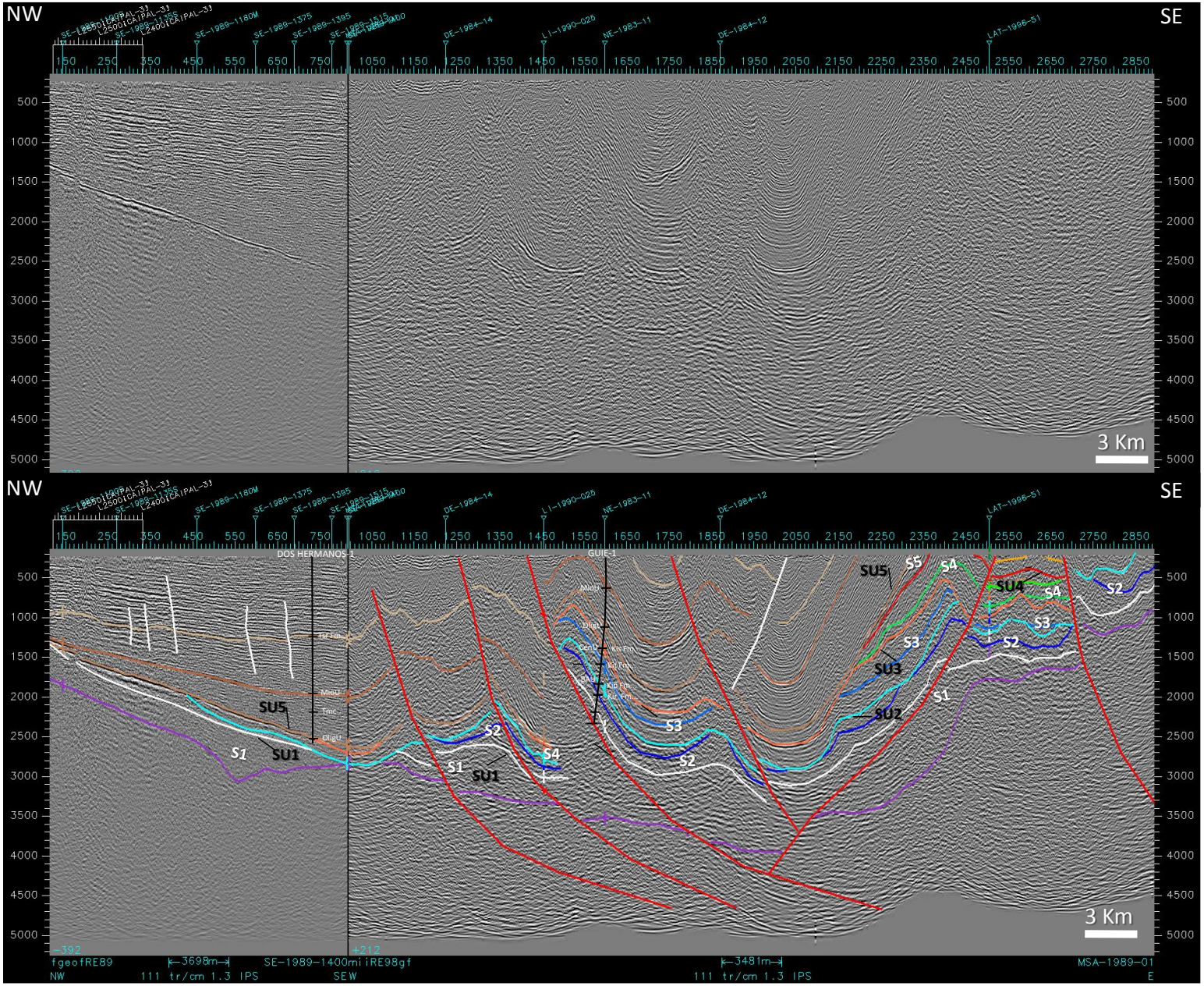

Figure 4.14 *– Seismic section at the north of MMV. Above: un-interpreted section. Below: section interpreted along the seismic reflection profile SE-1989-1400, MSA-1989-01, in direction NW-SE in the north of the MMV. (see figure 4.7 for the location). Intense deformation in the Cretaceous sequence limited by faults that didn´t affect the Tertiary units which cover cretaceous unit at the central and western part, while at the East the Lower Cretaceous unit are exposed in the surface. Seismic sequences observed in the section have been labeled as S1 to S5 and the sequence boundaries labeled in the section as SU1 (pink), SU2 (blue light), SU3 (orange), SU4 (red), SU5 (brown).*

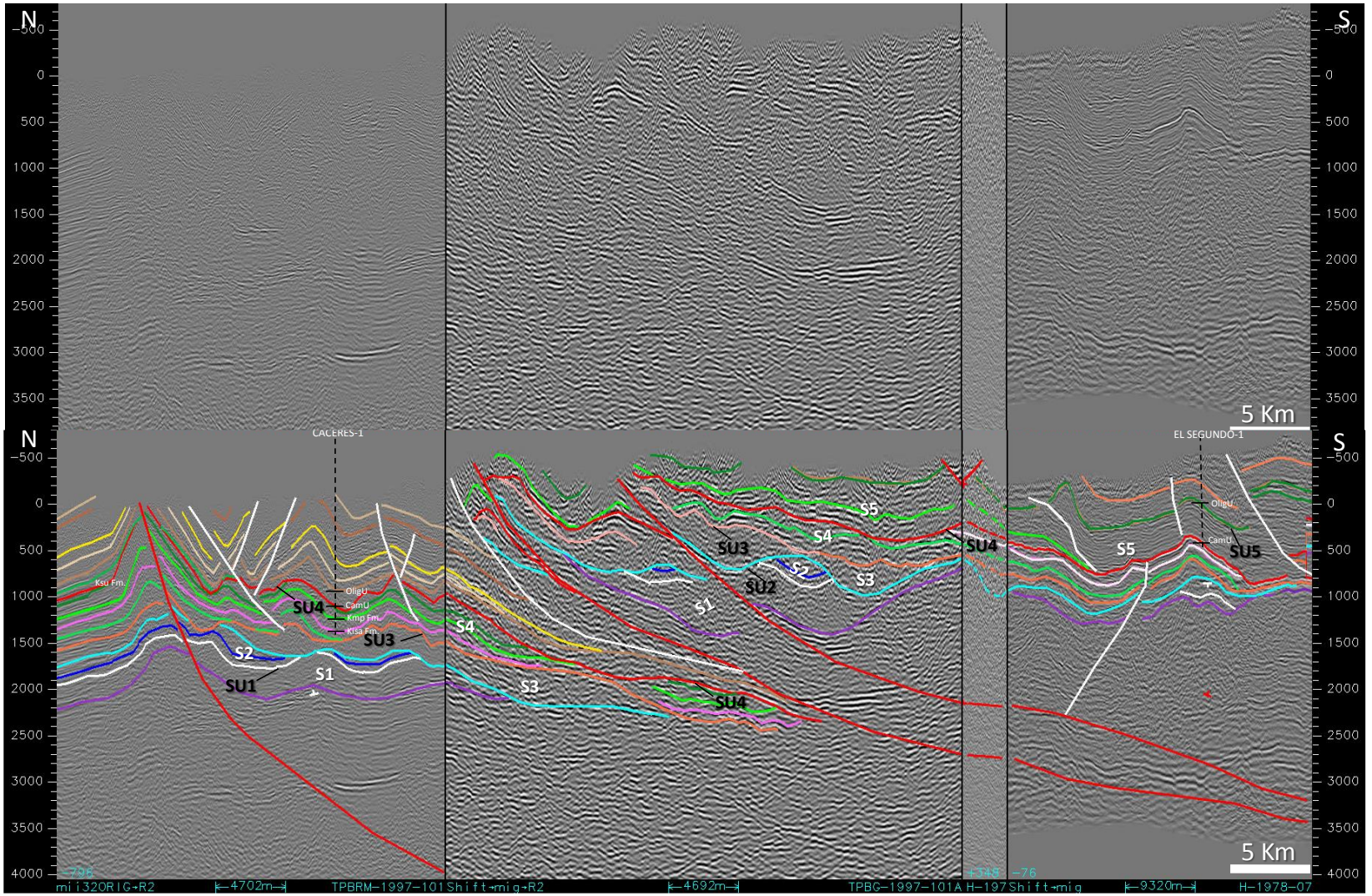

Figure 4.15 *– Seismic section at the north of the MMV. Above: un-interpreted section. Below: interpreted along the seismic reflection profile TPBRM-1997-101, TPBG-1997-101A, H-1978-07, in direction near N-S in the south of the MMV. (see Figure 4.7 for the location). Intense deformation in the Cretaceous sequence limited by faults that didn´t affect the Tertiary units which cover cretaceous unit at the central and western part, while at the East the Lower Cretaceous unit are exposed in the surface. Seismic sequences observed in the section have been labeled as S1 to S5 and the sequence boundaies labeled in the section as SU1 (pink), SU2 (blue light), SU3 (orange), SU4 (red), SU5 (brown).*

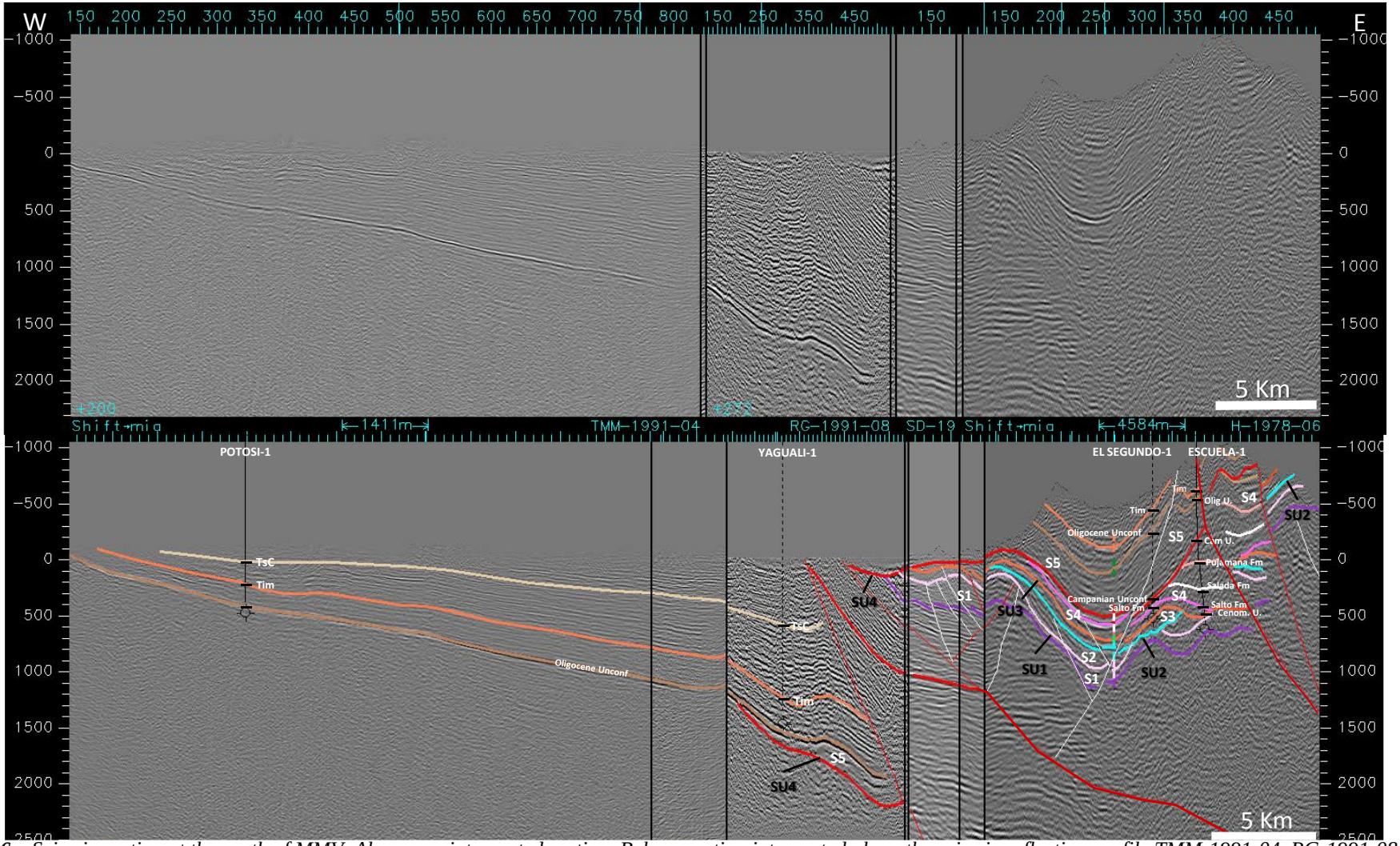

Figure 4.16 *– Seismic section at the north of MMV. Above: un-interpreted section. Below: section interpreted along the seismic reflection profile TMM-1991-04, RG-1991-08, SD-1985-42, H-1978-06 in approximate direction N-S in the south of the MMV. (see Figure 4.7 for the location). Intense deformation in the Cretaceous sequence limited by faults that did not affect the Tertiary units which cover cretaceous unit at the central and western part, while at the East the Lower Cretaceous unit are exposed in the surface. Seismic sequences observed in the section have been labeled as S1 to S5 and the sequence boundaries labeled in the section as SU1 (pink), SU2 (blue light), SU3 (orange), SU4 (red).*

The Wheeler diagram is one of the fundamental tools used by geologists to understand the spatio-temporal relationships of strata. This diagram displays the horizontal distribution of sequences and facies, and highlight the significant sedimentary hiatus. Theoretically, this diagram is used to show the time relationships of both the depositional system and system tracts, and their relationship to surfaces of erosion or non-deposition (Emery et al., 1996). In these charts the basic units are called "chronosomes", represented by horizontal ribbons representing sedimentary units bounded by time planes (called here unconformities). Chronostratigraphic charts are best constructed from interpreted seismic sections, because these images help to understand how sedimentary sections spatially develop through time. In chronostratigraphic charts, the horizontal axis matches the horizontal dimension of the seismic section and the vertical axis represents the time (Figures 4.17 to 4.22).

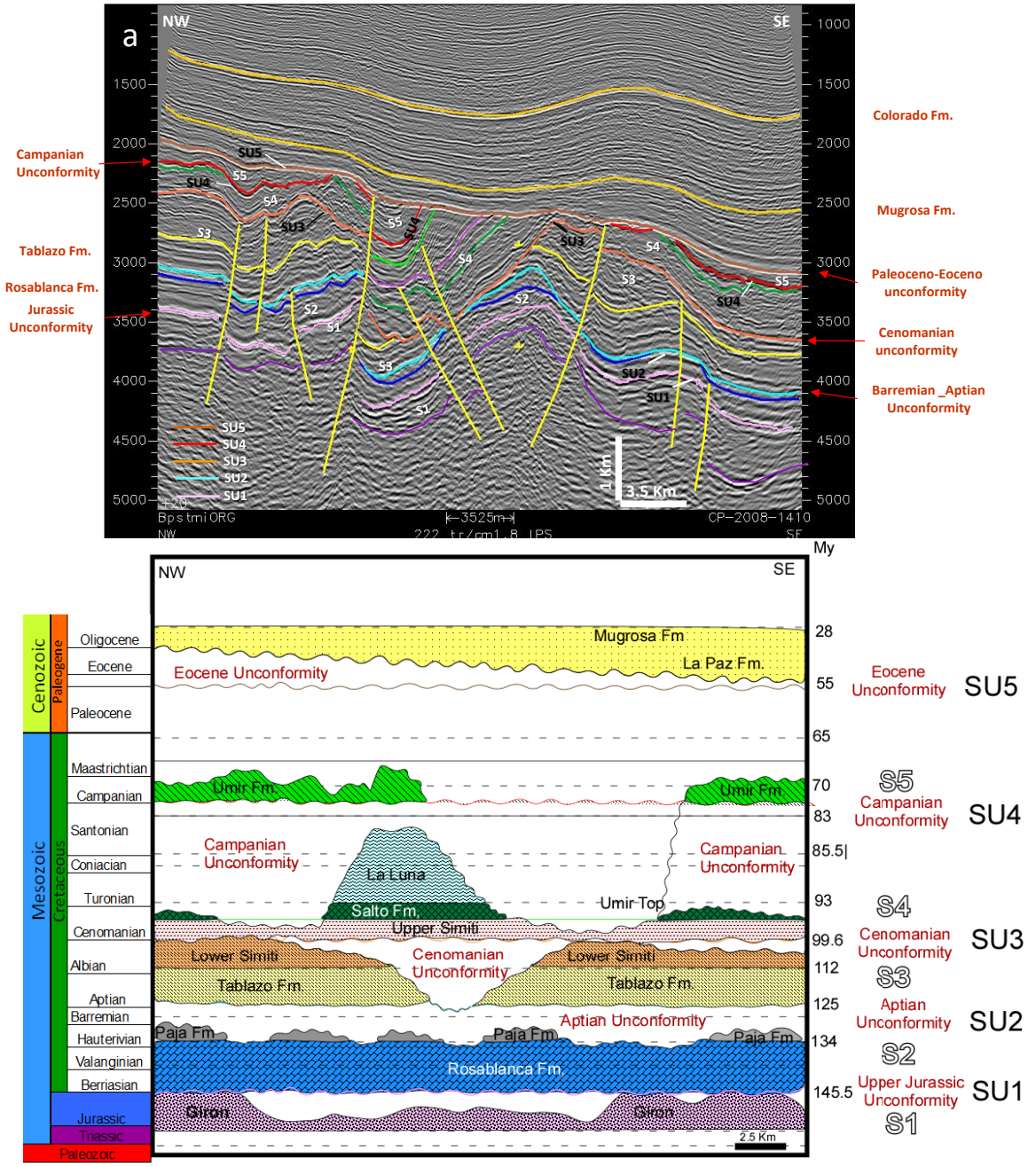

Figure 4.17 *– a- Seismic stratigraphic interpretation of inline CP-2008-1410; b- Chronostratigraphic chart after seismic stratigraphic interpretation using a Wheeler diagram. The Chart clearly shows the unconformities for Aptian (SU2), Cenomanian (SU3) and Campanian (SU4) times; and also for the Jurassic/Lower Cretaceous (SU1), Eocene and Oligocene (SU5) that bounded stratigraphic sequences from S1 to S5.*

Using Wheeler diagrams, we constructed seismic chronostratigraphic charts showing the identified sequences (S1 to S5) and the sequence boundaries or unconformities (SU1 to SU5). When a reflector truncates the seismic horizons and is related to a hiatus, it corresponds to an unconformity. Sediment present between sequence boundaries represents the deposit unit preserved during a particular geological time period. Seismically driven Wheeler diagram are constructed in relative geological time without additional well information.

Our constructed chronostratigraphic charts (Figures 4.17 to 4.22) show that the defined sequences (S1 to S5) and identified unconformities (SU1 to SU5) were observed in all the interpreted sections in the study area.

In Figure 4.17 (upper part), the surface defined as an unconformity cuts down previous deposits expressing erosion. This is notorious for all unconformities (SU1 to SU5). For example SU3 (orange in Figure 4.17) locally removes the Albian-Aptian units (Lower Simiti and Tablazo Fms), as is also observed in the NW part of profile CP-2008-1410 (Figure 4.17).

In the lower part of Figure 4.17, the chronostratigraphic chart expresses the time gap related to the unconformities. Unconformity SU1 (Jurassic-Cretaceous boundary) produced an important erosion, mainly in the central part of the section. SU2 (Barremian-Aptian boundary) affected the whole area crossed by the section, eroding ≈ 450 m to ≈ 700 m of deposits, and cutting part of the Barremian-Early Aptian sequence (Paja Fm) and reaching the Late Hauterivian sequence (Rosablanca Fm). SU3 (Albian-Cenomanian boundary) locally eroded the Early Cenomanian to Middle Aptian sequence (Lower Simití and Tablazo Fms), eroding up to ≈ 900 m of deposits. SU4 (Santonian-Campanian boundary) removed the Santonian to Late Cenomanian deposits (Upper Simiti, Salto and La Luna Fms), eroding 350 to 1500 m of sediments. Finally, the well-documented Paleocene-Eocene unconformity (SU5) eroded the Campanian to Paleocene units (S5, Umir and Lisama Fms). Considering that in the MMV, S5 may be 2500 m thick, around ~1700 m of sediment may have been eroded in this area.

Figure 4.18a shows two well marked and broad pre-Campanian synclines determined by the fact that SU4 is burying the underlying units and less deformation on the Umir Fm (overlying SU4) is in turn sealed by the unconformity of Mid-Eocene. In Figure 4.18, the SU1 unconformity erodes ~ 380 m of sediments of the Jurassic unit (probably Girón Fm). Unconformity SU2 (Barremian-Aptian boundary) erodes early Hauterivian-late Aptian deposits strongly and the Berriasian-Valanginian unit (Rosablanca Fm) partially, leaving a relic of the lower La Paja Fm. SU2 erodes up to ~ 750 m of the S2 sequence, probably due to the Late Barremian-Early Aptian low sea level period. SU3 (Albian-Cenomanian boundary) eroded the Albian sequence S3, but also part of the Aptian-Lower Albian Tablazo Fm, removing up to ~ 650 m. SU4 (Santonian-Campanian boundary) was responsible for the erosion of Early Cenomanian to Late Santonian deposits, eroding ~ 580 m to ~1150 m of sediments from sequence S4. SU5 (Mid-Eocene unconformity) only preserved part of the Campanian units (relict of the Umir Fm), removing units of Campanian to Lower Paleocene age (~1700 to ~ 2200 m of sediment removed).

In seismic section CP-2008-1335 (Figure 4.19), a series of anticlines and synclines are limited by faults, some of which cross cut the S1 to S5 sequences. Unconformities are marked by truncations below, or growth strata above the unconformity. The chronostratigraphic chart for section CP-2008-1335 (Figure 4.19) shows that SU1 eroded part (100 m to 1250 m) of the Jurassic sediments (Girón Fm). SU2 eroded partially or totally the Hauterivian-Barremian, and partially the Berriasian-Valanginian strata, eroding 500 to 728 m of S2. SU3 (Early Cenomanian unconformity) eroded sequence S3, i.e. ~50 to ~720 m of Late Aptian-Late Albian sediments. The SU4 unconformity removed Late Santonian to Early Cenomanian deposits (220 to 1150 m). Finally, considering that the sequence had been eroded by

unconformities SU2 to SU4 untill Late Santonian, the pre-Eocene erosion removed the Campanian to Paleocene sequence that could represent an erosion of 1100 to 2200 m.

The NW-SE trending seismic section of Figure 4.20 shows the erosion of almost the whole Upper Cretaceous sequence around the Infantas-E5 well and in the western part of the section (Chucuri-1 well). The Chucuri-1, RW-1, Colorado-39 and Brao-1 wells were used to tie stratigraphy with seismic sequences, and to identify and analyze the Cretaceous succession. The key well RW-1 cut almost the complete Cretaceous sequence and represents one of the best-documented sections of the Cretaceous series in the MMV (Figure 4.20, see Chapter 3). The biostratigraphic information from the RW-1well has been used to identify the unconformities, sequences and time-gaps (Aptian, Campanian, Figure 3.44). As shown in the resulting chronostratigraphic chart (Figure 4.20), the RW-1 well has been drilled in the middle part of the section, where most of the Cretaceous sequence is preserved

There, the seismic interpretation reveals that these two unconformities are present (Figure 4.20). In the RW-1 area, SU2 eroded Early Aptian to Late Barremian deposits (around 300 m), but in the rest of the section the erosion removed sediments down to the Hauterivian strata (i.e. 90 to 765 m). In the RW-1 well area, SU3 (Early Cenomanian) is not visible, and sequence S3 is ~570 m thick. Extrapolating this value, the SU3 unconformity may have eroded ~270 m to ~570 m of sediments. Around the RW-1 well, sequence S4 reaches a thickness of 1250 m, and SU4 eroded less than 320 m. Finally, erosion related to the Mid-Eocene unconformity SU5 removed the Lisama Fm. This latter erosion is sealed by Late Eocene deposits (Esmeraldas Fm).

Figure 4.21 shows a composite seismic section based on lines SE-1989-1400 and MSA-1989-01. To the West the erosion removed much of the Cretaceous sequence, making the analysis of Cretaceous discontinuities impossible, whereas to the East, Late Cenomanian to Maastrichtian units (Upper Simití to Umir Fms) are locally preserved. SU1 (Jurassic-Cretaceous boundary) locally eroded the Jurassic units (Girón Fm). Considering that this sequence may be up to ~2500 m thick, the erosion in this area may reach ~750 m to ~2250 m in thickness. The SU2 unconformity (Barremian-Early Aptian) eroded almost all the S2 sequence (Berriasian - Barremian) to the West (only part of the Early Berriasian was preserved). However, around the Guie-1 well and to the East, sequence S2 is better preserved; since its maximum thickness is ~ 1100 m, erosion may have removed up to ~750 m. In the same way, erosion of the middle Aptian-Late Albian sequence S3 by SU3 (Barremian-Cenomanian) is estimated at ~620 to ~120 m. SU4 eroded a great part of the sequence S4; removing a maximum of ~ 450 m. In this section, the SU5 Unconformity (Paleoce/Eocene) seems to have eroded sequence S5 in most parts, but to the East ~ 430 m were eroded. However, the Oligocene unconformity eroded the SU5 unconformity totally.

In the southern area of the MMV, because the Cretaceous sequence and evidences of Cretaceous unconformities have been totally removed by Miocene and post-Miocene erosions to the West, only the eastern part of the section will be analyzed (Figure 4.22). Jurassic sediments (sequence S1) were eroded by SU1. The Early Aptian unconformity (SU2) would have removed the Early Cretaceous deposits (Naveta, Lower Trinchera Fm) and only relics of Berriasian-Early Valangenian deposits (Utica and Murca Fms) are preserved. In the area of Villeta the Utica Fm is ~ 600 m thick, the La Naveta Fm is ~ 165 m thick (Bürgl and Julivert, 1968) and the Lower Trinchera Fm is 320 m thick (Ulloa and Acosta, 2001), which suggests that S2 was ~1100 m thick. Based on this thickness (figure 4.22), SU2 could have eroded ~750 to ~1100 m of the S2 sequence. In the Villeta area, sequence S3 is ~1550 m thick (620 m for upper Trinchera Fm, 380 m for El Peñon Fm and 550 m for Capotes Fm, see Fig. 3.4), so the Early Cenomanian SU3 may have eroded 1230 to 1550 m of sediment.

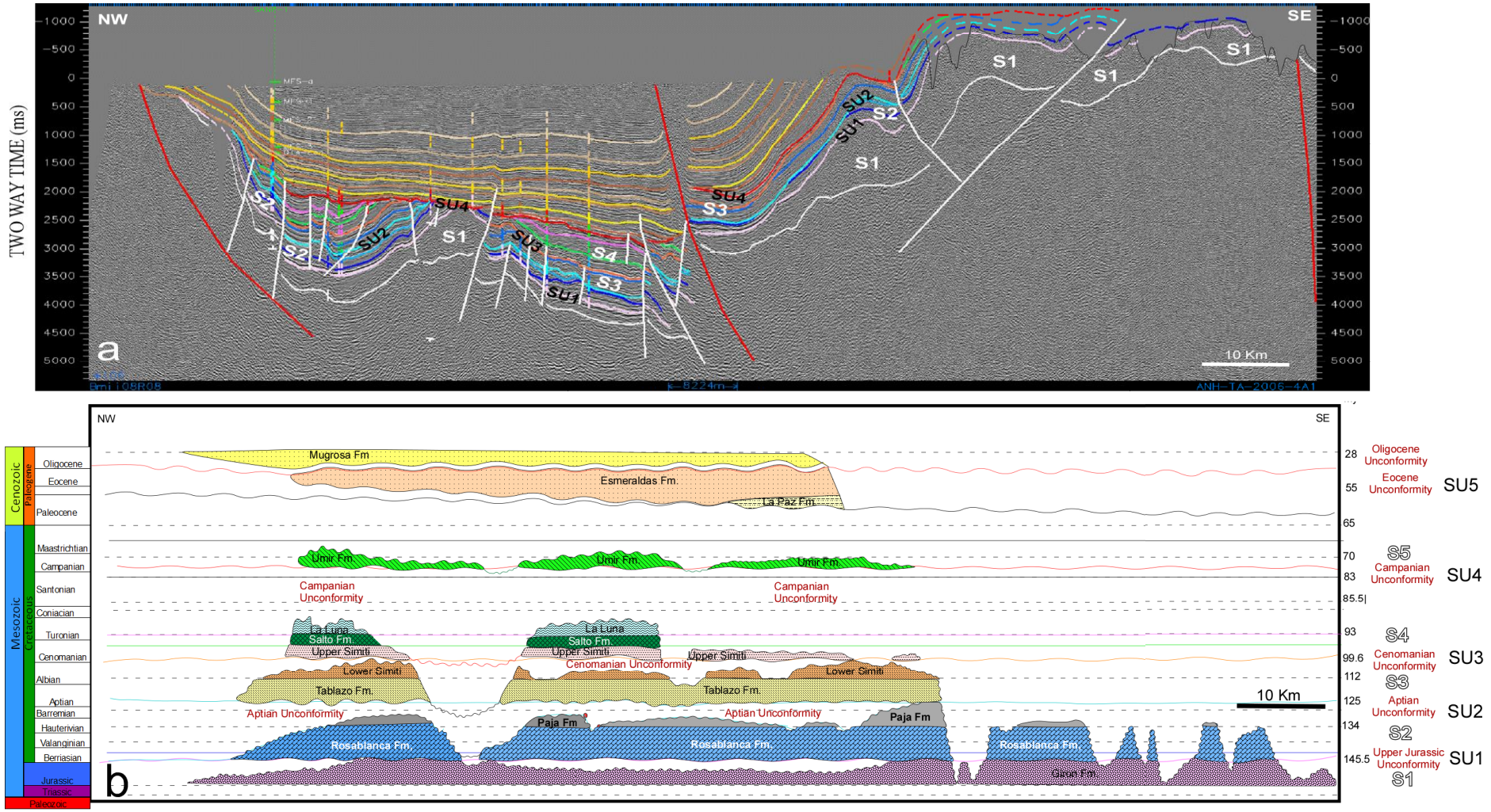

Figure 4.18 *a, b – Chronostratigraphic chart of the 147 km long profile ANH-1A-2006-4A1 (location on Figure 4.7). This section covers from the Central Cordillera to the WEC. Stratigraphic time-scale on the left, numerical ages on the right. Identified sequences are named S1 to S5 and unconformities labeled SU1 to SU5 (right).*

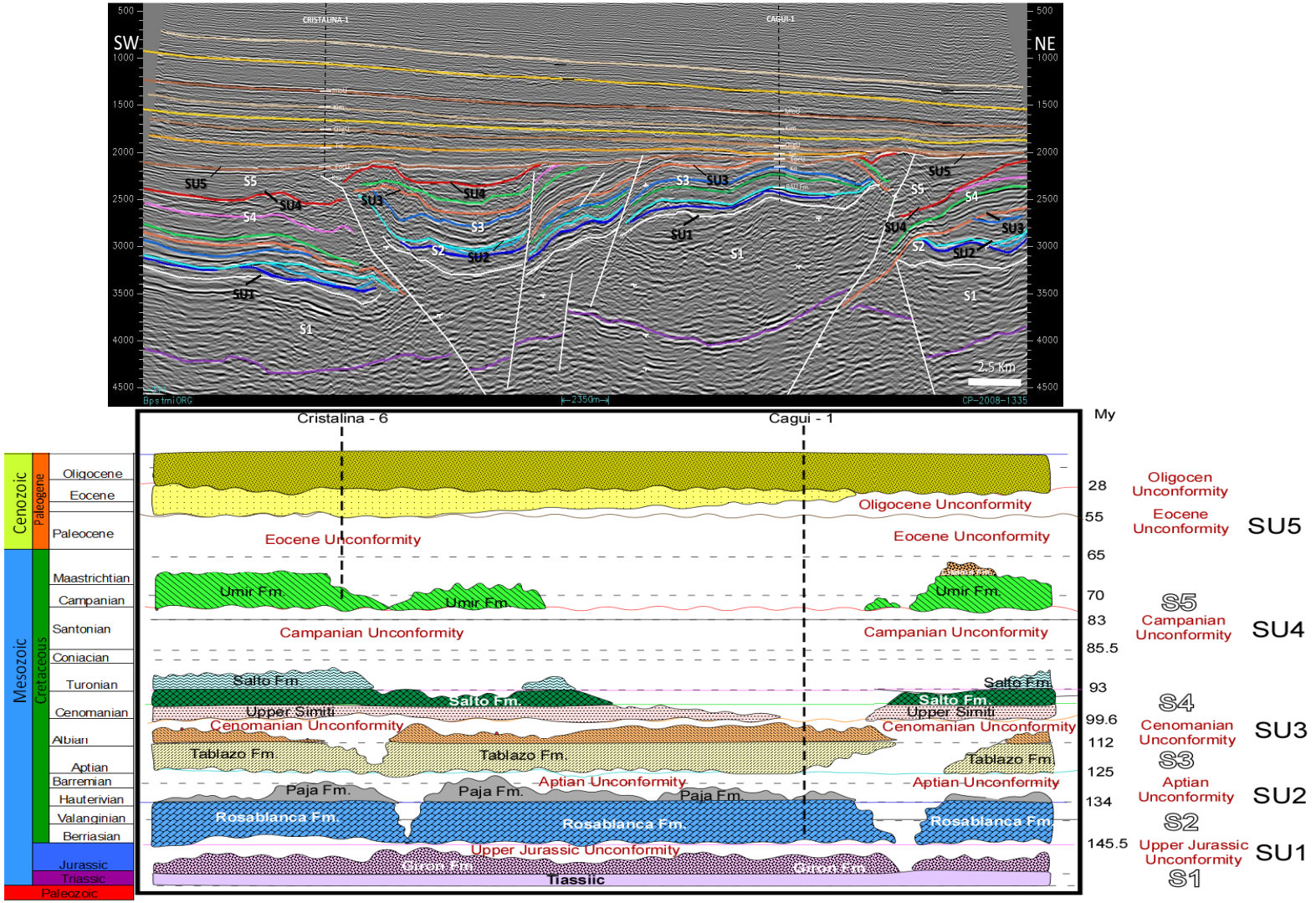

Figure 4.19 *– Chronostratigraphic chart generated from seismic reflection profile CP-2008-1335 (location on Figure 4.7). Five sequences (S1 to S5) are bounded by five unconformities (SU1 to SU5), responsible for hiatuses 5 to 25 Ma long.*

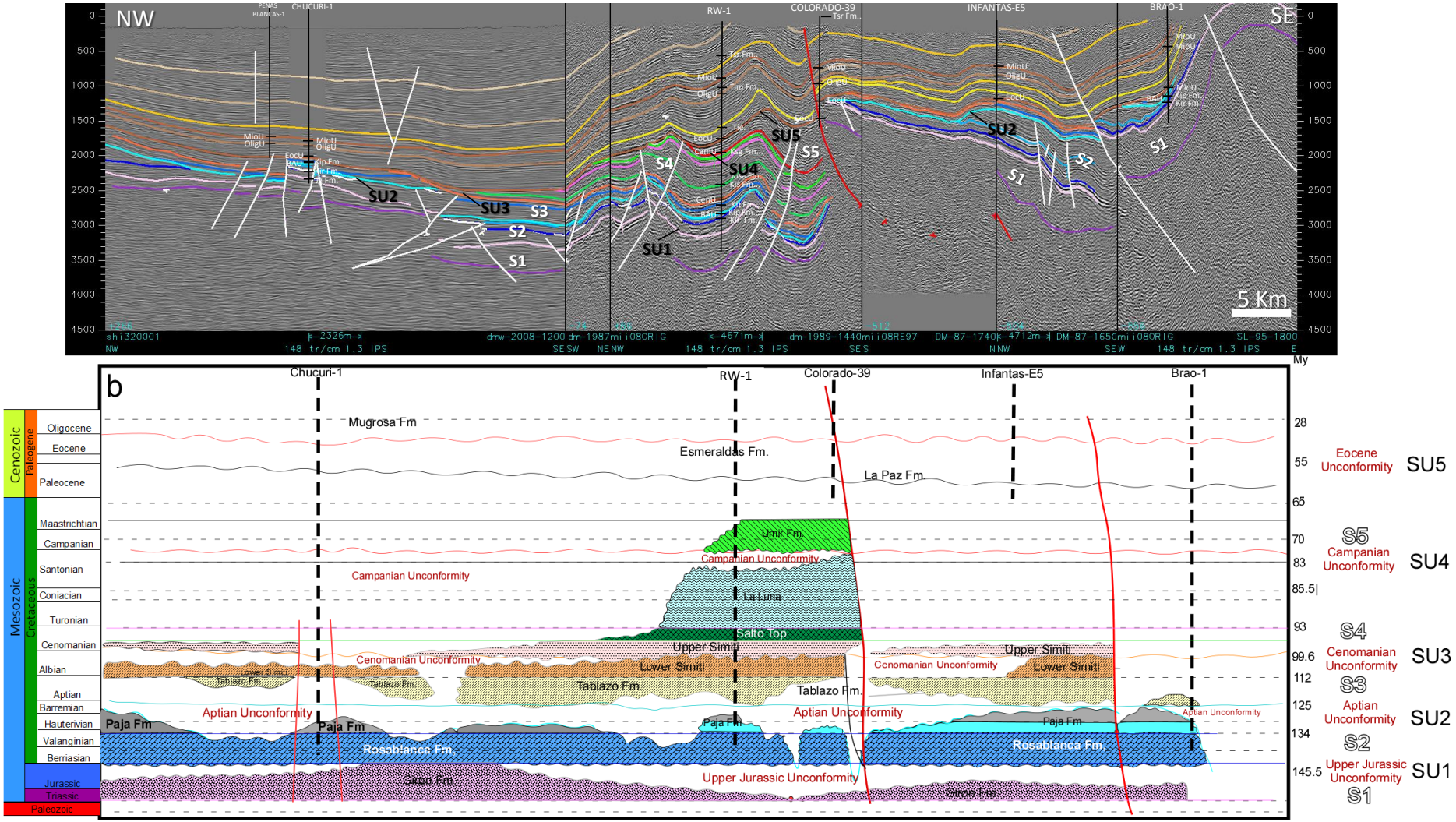

Figure 4.20. *(a,b) Composed seismic profile (dmw-2008-1200, dm-1987-1320, dm-1989-1440, DM-1987-1740, DM-1987-1650, SL-95-1800); (b) Chronostratigraphic chart for the section above (location on Figure 4.7). The stage ages are shown in the scale to the left and the age in Ma to the right. Five sequences (S1 to S5) are limited by five unconformities (SU1 to SU5). Three wells crosscut the Cretaceous sequence: the most complete succession has been found in the RW-1 well.*

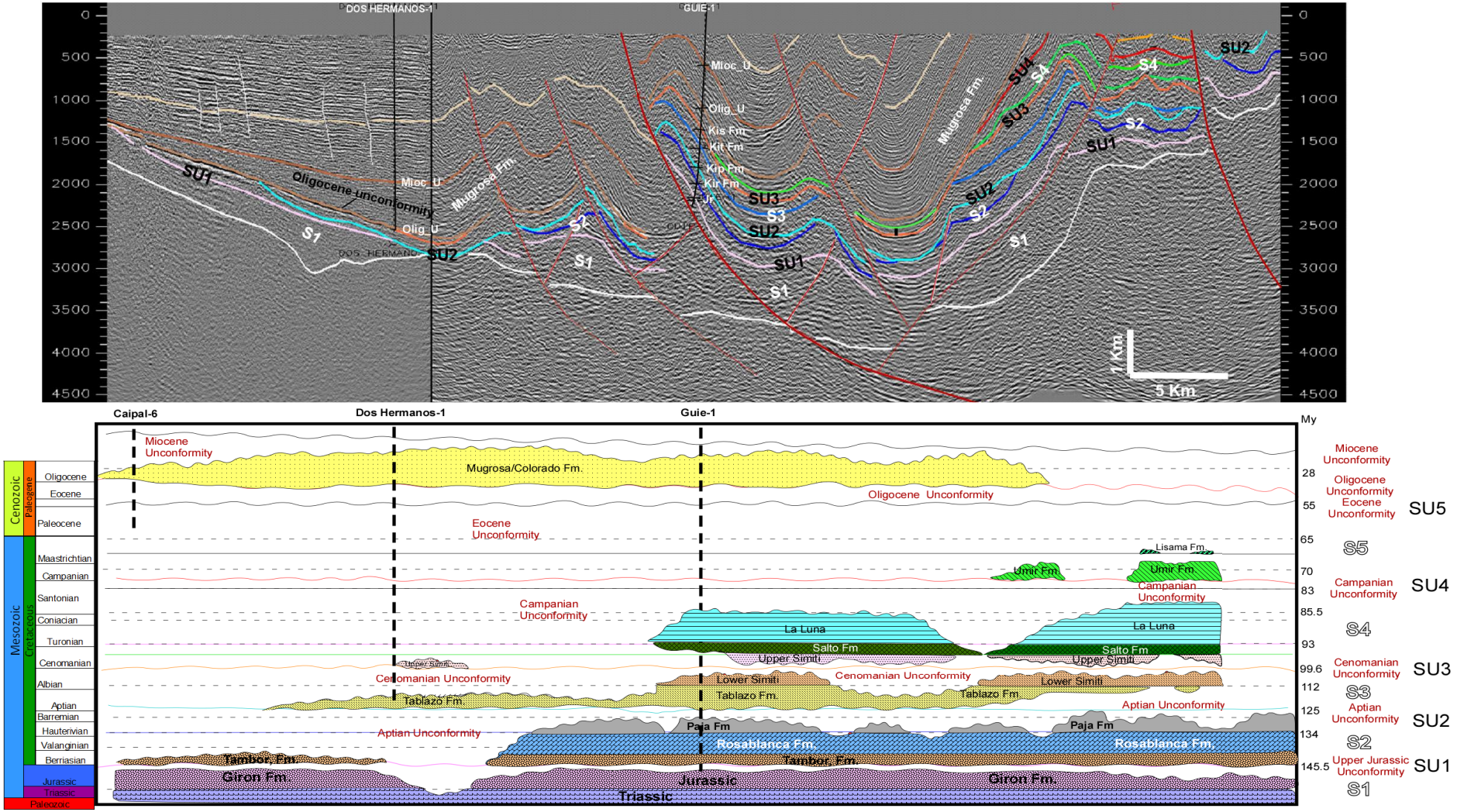

Figure 4.21 *– Seismic section and chronostratigraphic chart for the composite section SE-1989-1400 and MSA-1989-01 (location on Figure 4.7). Stratigraphic and numerical ages are shown on the left and right, respectively. The five identified sequences (S1 to S5) are bounded by five unconformities (SU1 to SU5). Hiatuses are in white.*

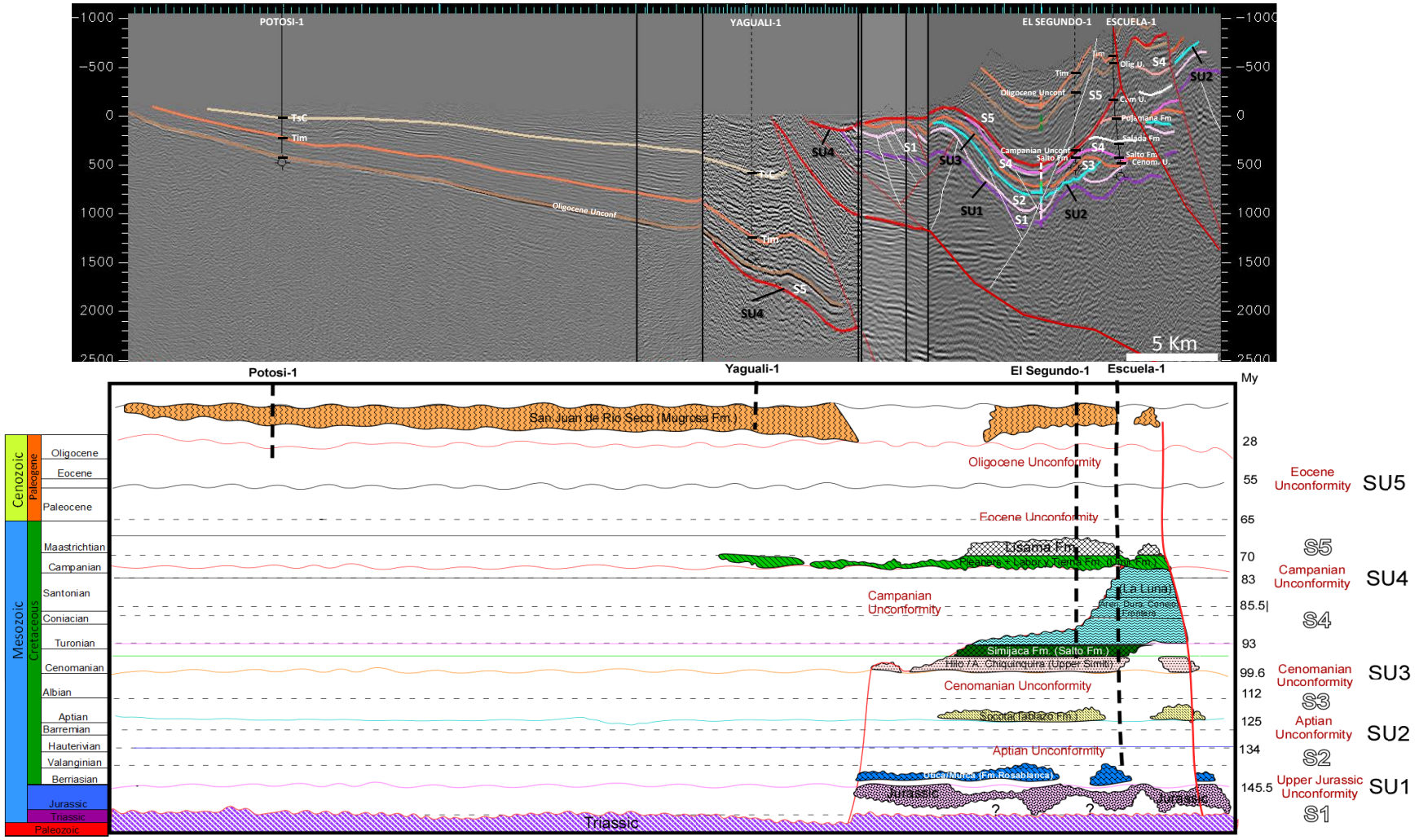

Figure 4.22 *– Seismic section and chronostratigraphic chart in the southern part of the study area (location on Figure 4.7). To the east, the Cretaceous series has been removed by pre-Miocene erosions. The Wells Potosi-1, Yaguali-1, El Segundo-1 and Escuela-1 were used to tie seismic interpretation and the horizons were also follow from other seismic sections.*

The S4 sequence may have reached a maximun of ~1500 m is this area, even though the type section of this unit reaches a total of ~2000 m. In this way, the Campanian unconformity SU4 may have eroded between ~ 500 and 2000 m of S4 sediments. Above the SU4 unconformity, deposits were eroded by pre-Oligocene erosions, which were sealed by the Mugrosa Fm.

4.6 Stratigraphic column based on new observations

Although outcrops are scarce in the MMV, synclines in the northern part of the valley (e.g. Nuevo Mundo syncline) exhibit Tertiary deposits and Cretaceous units in their flanks. Cretaceous units can also be studied in the western flank of the Eastern Cordillera. Using these observations, together with information from seismic reflection, wells from the MMV and WEC, and published data, we constructed a composite stratigraphic column of the MMV and WEC (Fig. 4.23).

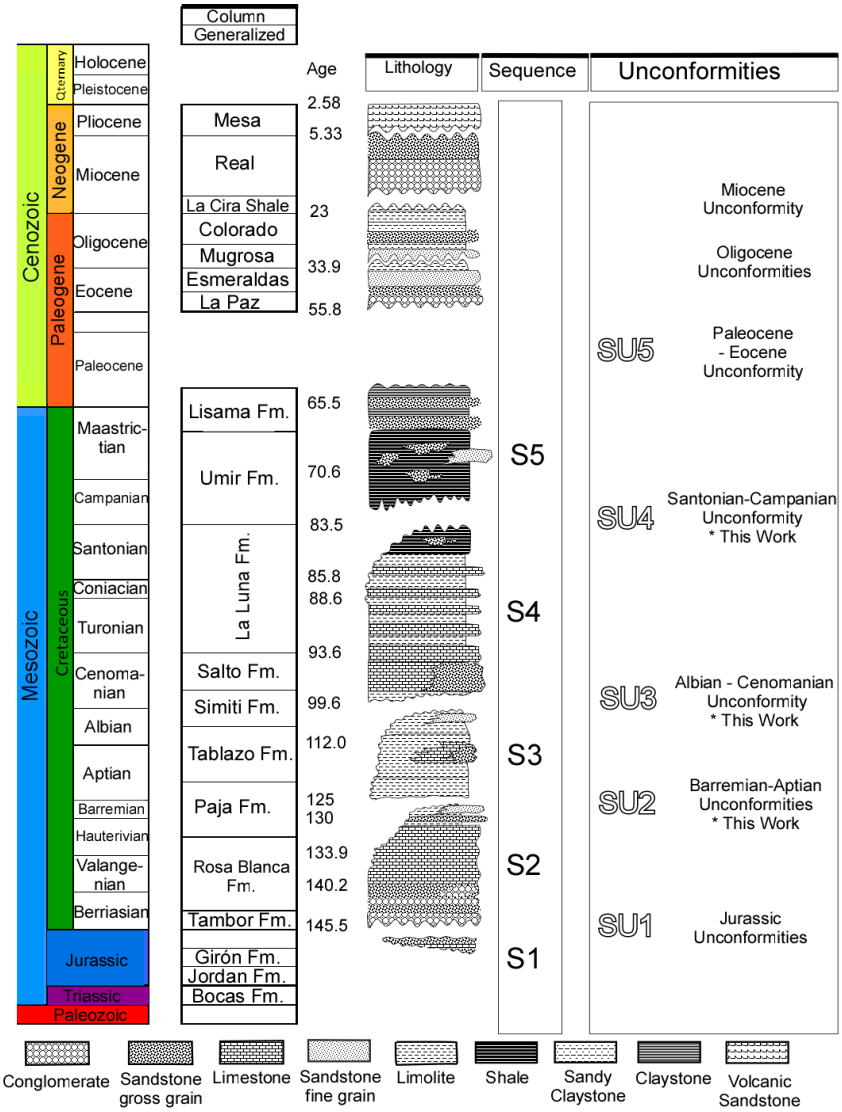

Figure 4.23 *- General stratigraphic column proposed for the MMV and WEC, showing the identified unconformities (SU1 to SU5) and sequences (S1 to S5).*

Sequence S1 overlies the Jurassic-Berriasian unconformity (SU1) that erodes previous deposits totally or partially. Sequence S2 (middle Berriasian-Late Barremian) is partially eroded by the SU2 discordance (Barremian-Aptian). Sequence S3 (Aptian to Late Albian) is

capped by unconformity SU3 (Albian-Cenomanian). Sequence S4 (Middle Cenomanian to the Late Santonian) is eroded by unconformity SU4 (Santonian-Campanian). Finally, sequence S5 (Campanian-Paleocene) is deeply eroded by the SU5 unconformity (Paleocene-Eocene).

4.7 Discussion

The seismic evidence (Figures 4.9 to 4.16) combined with information from wells and outcrops, show that the Cretaceous sequences of the MMV and WEC are controlled not only by sea level changes but also by deformations that occurred at different periods of the Cretaceous (Figures 4.5 to 4.12). Together with sea level variations, these movements triggered sedimentary hiatuses and erosion of deformed units, generating the unconformities SU1 to SU5 (Figure 4.17 to 4.22).

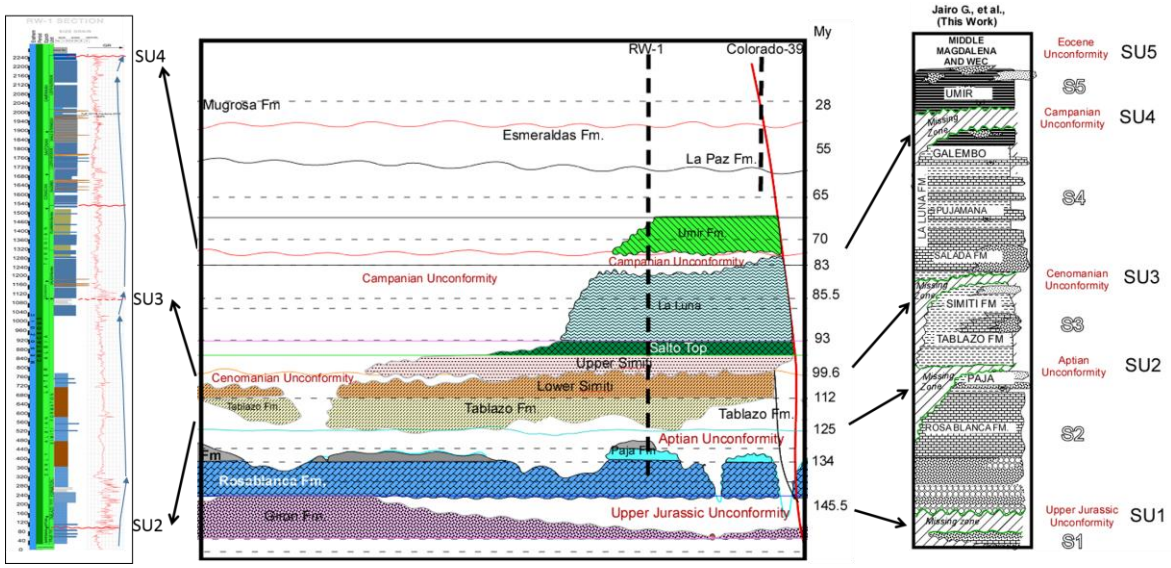

Figure 4.24. *Stratigraphic column of the RW-1 well reconstructed from the well log description and gamma ray data (left). Chronostratigraphic chart for the seismic profile, showing the sequences, unconformities and hiatuses, and the location of the RW-1 well (center). General stratigraphic column (this work).*

Five sequences (S1 to S5) and their bounding unconformities (SU1 to SU5) were identified (Figure 4.24). According to the description of the RW-1 well (Figure 4.24 left), three unconformities could be interpreted based on biostratigraphic information. Following the facies analysis (chapter 3), one may conclude that these event are of eustatic origin. However, seismic interpretation and chronostratigraphic chart analysis (Wheeler diagrams, Figures 4.17 to 4.22) allowed me to conclude that in addition to eustatic variations, tectonic activity played a role which resulted in a geometry of the MMV-WEC basin, in which Cretaceous unconformities seal deformed sedimentary sequences.

Other authors mentioned the existence of Cretaceous unconformities or identified Cretaceous regional sedimentary discontinuities in Andean basins (Etayo, 1974; Khon et al., 1984; Mattson, 1984; Hanq et al., 1987; Macellari, 1988; Van der Wiels, 1991; Pindell and Tabutt, 1995; Rollon, 1997; Jaillard et al., 2000; Ramos and Alleman, 2000; Guerrero, 2002; Duarte, 2003; Jaimes and de Freitas, 2006; Cooney et al., 2009; Patarrollo, 2009). In Figure 4.26, we compare the hiatuses (gaps) and unconformities reported by other authors with those stablished in this work. Macellari (1988) recognized several unconformity-bounded depositional cycles across the whole western margin of South America and in Venezuela, distinguishing northern of southern South America (Figure 4.25 and 4.26). The cycles stablished by Macellari (1988) are comparable in amplitude to the second-order cycles of Haq et al. (1987).

The cycles recognized by Macellari (1988) are interpreted as a result of eustactic variation. In chapter 3, analyzing facies changes (see facies maps), I identified four major regression cycles and three transgressive cycles during the Cretaceous. Sandy sediments dominated to the East of the basin, whereas the western, deeper part of the basin received limestones and fine-grained sediments with calcareous intercalations. These cycles can be described as follows:

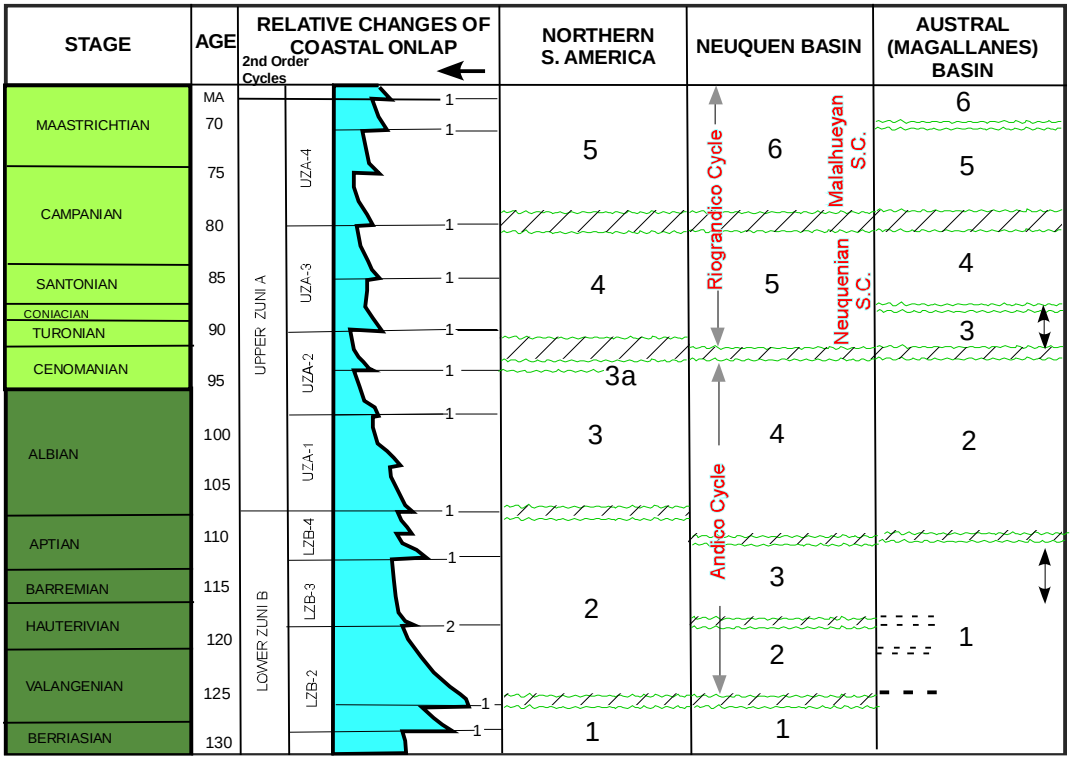

Figure 4.25 *- Comparison of Cretaceous cycles identified by Macellari (1988) in northern South America, and the Neuquén and Austral Basins with the global chart of coastal onlap (simplified from Haq et al., 1987).*

1. A regression occurred during the Early Berriasian (Figure 3.48). At this time sandstones are present in the Llanito-1, Guane-1, Iwana-1 and Chucuri-1 wells in the MMV (Figure 3.5), whereas shales and claystone were deposited in the RW-1 well (Figure 3.48).

2. During late Berriasian to Hauterivian times, a transgression produced a deepening of the depositional environments. Limestone facies reached the east of the study area (Figure 3.49, 3.50).

3. From Barremian to Aptian a general regression produced the shallowing of the basin and deposited sand, shales and claystone in a shallow environment, as shown in wells Guane-1, Chucuri-1, Guineal-1, Agata-1 Escuela-1, RW-1 and Butuima, while sandstones were laid down in Cune, Anolaima and Alto Ojo in the western part of the WEC (Figure 3.5 and Figure 3.51, 3.52)

4. Between Late Aptian and Late Albian times (Figure 3.53), a marked transgression occurred in the eastern and central parts of the basin, and to the west, resulting in a deepening of the depositional environments; shales and clays were deposited over the Barremian- Early Aptian sands.

5. During the early Cenomanian a regression took place in all the basin (Figure 3.54), while a subtle transgression occurred to the West.

6. In the Cenomanian-early Turonian (Figure 3.55), a general transgression occurred, flooding all the basin including the WEC, where shales and clays were deposited, while limestone deposits dominated to the West (Figure 3.55).

7. During the Coniacian-Santonian (Figure 3.56), a general regression occurred again from North to South, leading to shallower deposits.

In Figure 4.26 the correlations of sedimentary basins from Peru to Venezuela are shown. In northwestern South America, Macellari (1988) identified three unconformities of Late Aptian, middle Cenomanian and middle Campanian age, respectively. In Peru Macellari (1988) indentified an additional unconformity of Valanginian age, and the Late Cretaceous unconformity is ascribed to the Santonian/Campanian boundary. However, the valanginian unconformity of Peru does not appear in my analysis, while my Berriasian unconformity has not been recognized by Macellari (1988) in Peru.

In the Upper Magdalena Valley, Allen (1989) identified an unconformity of Barremian-Aptian age. In the same area, Barrios (1992) determined a diachronic Barremian-Aptian unconformity, and a Late Albian unconformity that eroded the Caballos Fm (Figure 4.26). In the same region, based on biostratigraphy and seismic interpretation, Jaimes and De Freitas (2006) recognized internal deformation and a Late Albian-Cenomanian unconformity in the Villeta Fm (Figure 4.26, 4.27).

In the MMV, Morales (1958) identified unconformities between the La Paja and Tablazo formations of Early Aptian age, in the Middle Cenomanian (Salto-Salada Fm boundary), and in the Campanian between the La Luna Fm and Umir Fms. These unconformities are almost coincident with those determined in this research.

In western Venezuela, Cooney and Lorente (2009) proposed that the age variation at the top of the La Luna Fm would be explained by an uplift and erosion event occurring during the Campanian (Figure 4.28 and 4.29), that can be correlated with a Caribbean Plate-wide event of Late Campanian-Early Maastrichtian age (74-68 Ma). This important event may correspond to my SU4 and is evidenced in the MMV and WEC at 80-70 Ma by our thermochronological analysis (see chapter 5). It represents, therefore, the most important Cretaceous tectonic event with a regional extension.

Guerrero (2002) divided the Cretaceous series of Colombia based on regional sedimentary discontinuities corresponding to mainly transgressive and regressive surfaces. He concluded that, in spite of complex interactions of eustacy, sedimentary supply and subsidence, sequences are mainly controlled by eustatic changes. He recognized second order regressive surfaces at the Early-Late Hauterivian, Late Aptian-Early Albian, Late Albian-Cenomanian, Santonian-Campanian and Campanian-Maastrichtian boundaries, which represent changes from deep to shallow depositional environments. The Santonian-Campanian and Albian-Cenomanian regressions are consistent with our SU4 (Santonian-Campanian) and SU3 (Late Albian-Cenomanian), respectively. However, our SU2 (regression surface and erosion at the Barremian-Aptian boundary), was interpreted as a transgressive event by Guerrero (2002).

In the Caribbean, Mattson (1984) recognized six unconformities related to important tectonic events between 110 and 5 Ma, among which those occurring at 110, 85 and 66 Ma are important. Using sequence stratigraphy analysis in the western foothills of the Eastern Cordillera, Rollon et al. (1997) defined 3 regional sequences separated by unconformities in the Paja, Tablazo and Simiti Fms.

Jaillard and Soler (1996) and Jaillard et al. (2000) recognized four Cretaceous tectonic events (Figure 4.30). The first one (~100 Ma) is coeval with an abrupt acceleration of the plates around the world and with the opening of the Atlantic Ocean at equatorial latitudes. Another event occurred at 100-95 Ma (Late Albian-Early Cenomanian), during a slowdown of the convergence rate. A Santonian event (≈ 85 Ma), coincides with a decrease in the convergence velocity, and in the mid-Campanian (≈ 80 Ma) a major tectonic event is coincident with the plate velocity stabilization in the Andean zone.

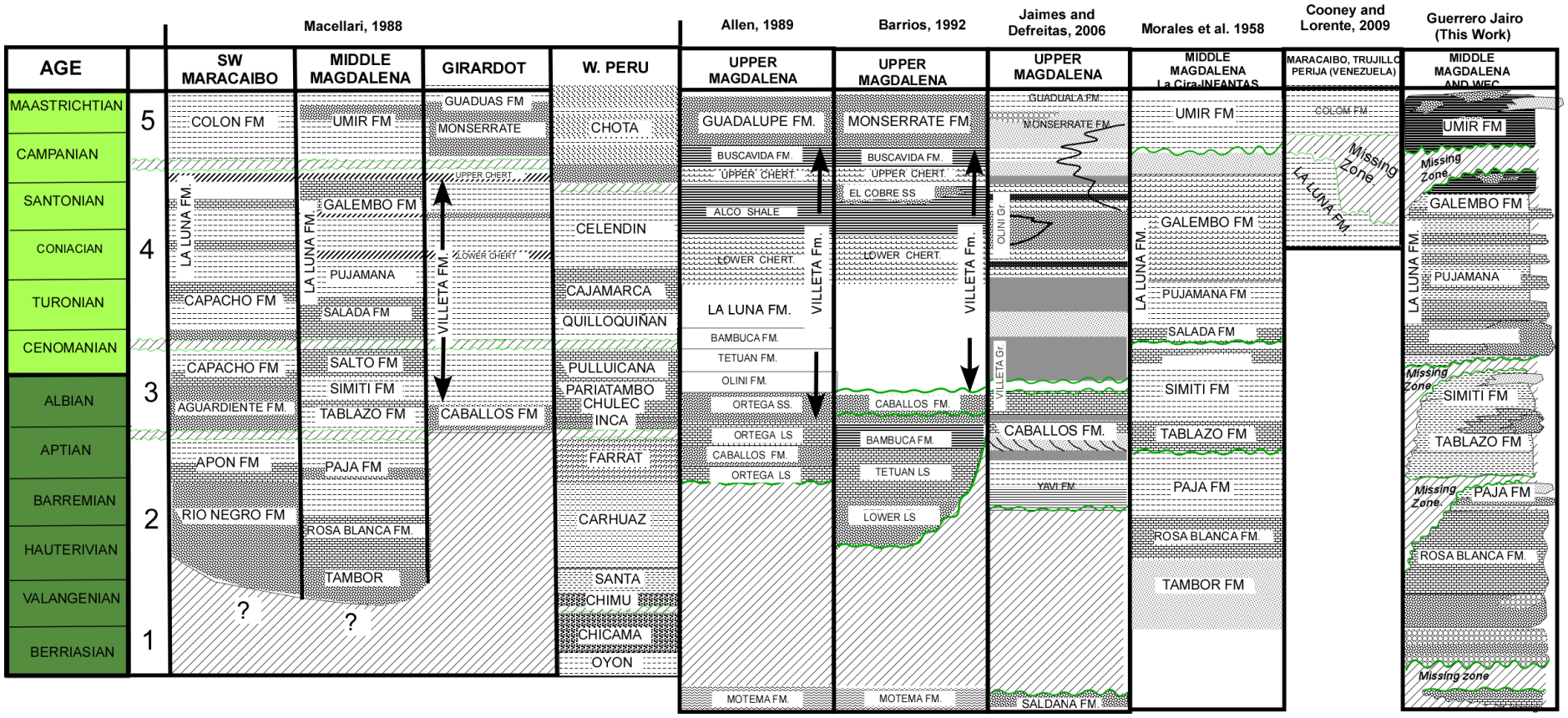

Figure 4.26. *Stratigraphic chart, correlation and comparison between sections from different localities from Peru to Venezuela.*

Stratigraphic series are from Western South America (Macellari, 1988), the Upper Magdalena Valley (Allen, 1988; Barrios, 1992; Jaimes and de Freitas, 2006), the Middle Magdalena Valley (Morales et al., 1985) and western Venezuela (Cooney and Lorente, 2009) and are compared with the column proposed in this work (right). The Late Aptian, mid-Cenomanian and mid-Campanian unconformities are identified in most basins.

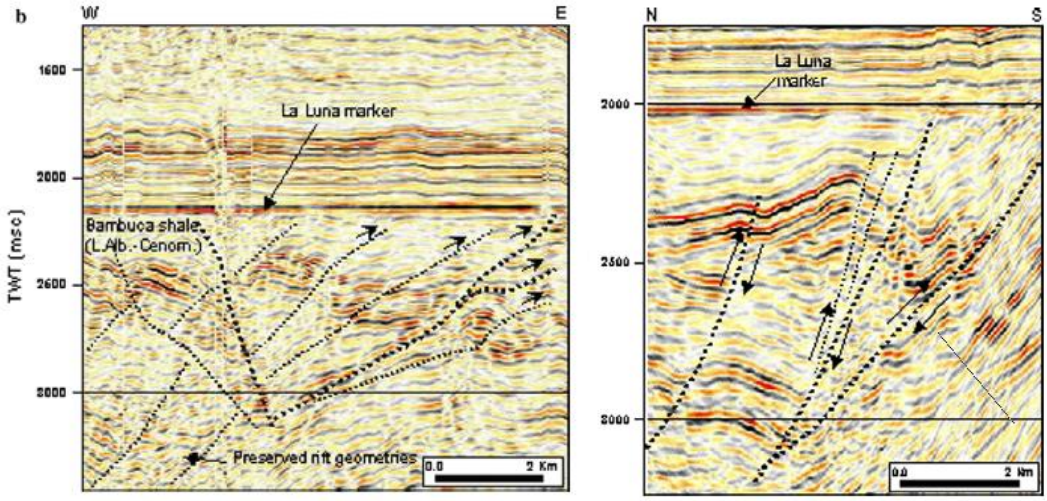

Figure 4.27*. Seismic profile from the Upper Magdalena Valley (flattened to La Luna marker (Cenomanian-Turonian boundary), showing the structures sealed by the La Luna Fm (Jaimes and de Freitas, 2006).*

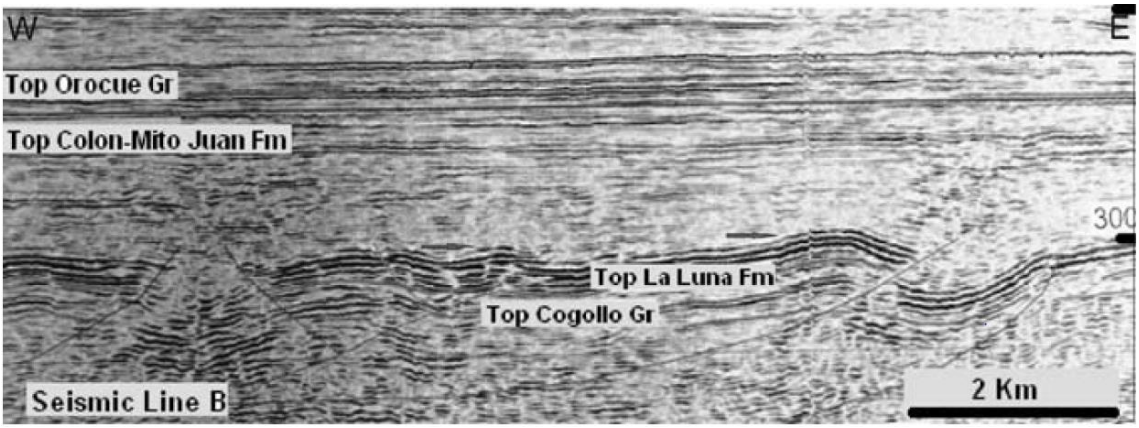

Figure 4.28. *Seismic profile in the Maracaibo Basin (Venezuela), flattened on the horizon "Colon-Mito Juan" units (Cooney and Lorente, 2012). Note the compressional deformation of pre-Late Campanian age.*

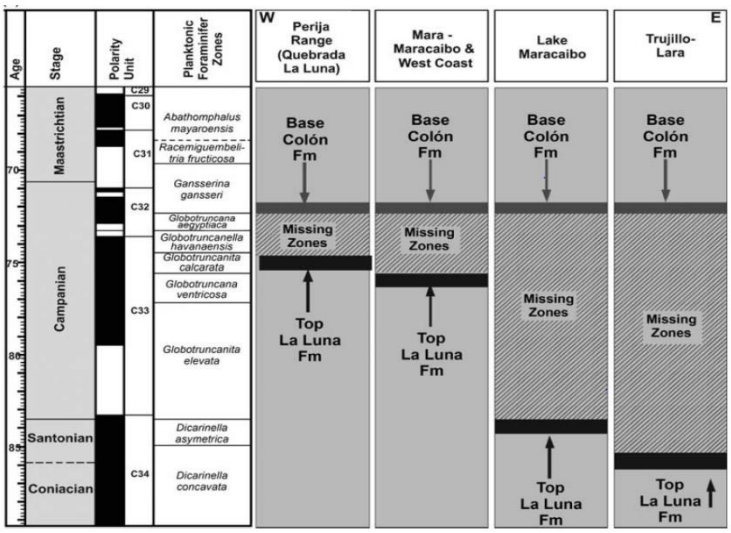

Figure 4.29. *Schematic chronostratigraphic section showing variations in the missing intervals for different areas studied by Cooney et al., 2009. Note the diachronous top of the la Luna Formation.*

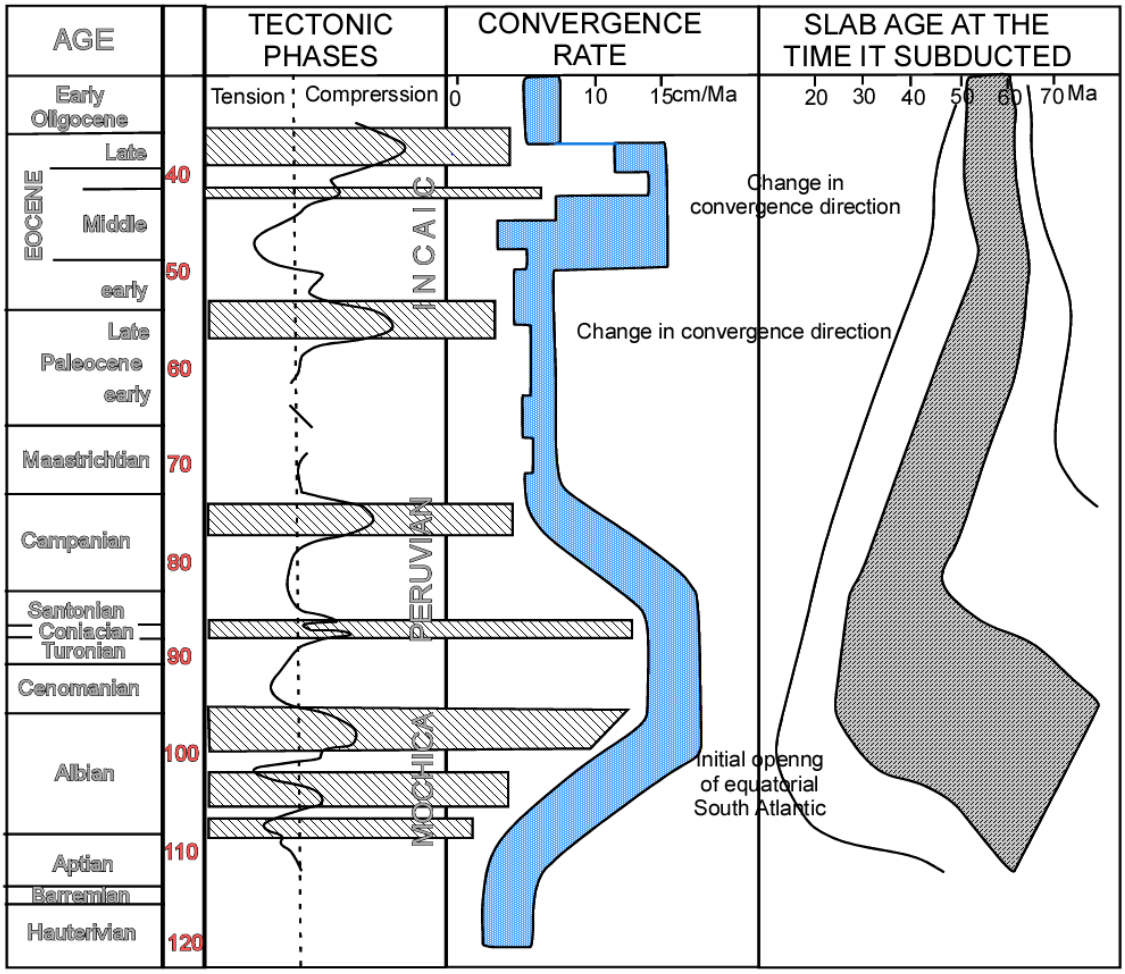

Figure 4.30. *Comparison between the early tectonic event (Precoz) in the Andes and the geodynamics of the plates in the subduction zone (modified from Jaillard, 1991).*

Jaillard et al. (2000), indicated that the change in the convergence direction that occurred between 60-50 Ma, may be responsible for the major tectonic event recorded in the Andean margin in the Late Paleocene. Jaillard and Soler (1996), observed that the beginning of contractional deformation in Albian times approximately coincides with the rejuvenation of the subducted oceanic plate, and that the Late Cretaceous and Paleocene shortening phase occurred during a continuous increase in the relative age of the subducted slab (Figure 4.30).

All of the authors cited above recognized erosions, non-depositional surfaces or unconformities during the Cretaceous. Some of these authors explained these events by sea level changes, others related them to the occurence of tectonic events related to plate movements. In this work, I propose that the Cretaceous erosional unconformities identified during this work resulted from significant tectonic events.

4.8 Conclusions

1. Structural and stratigraphic interpretations of 3500 km of seismic reflection profiles were carried out to understand the complex sedimentary and tectonic evolution of the MMV-WEC basin. Using well information, seismic reflection profiles from the MMV and partially from the WEC, and constructing Wheeler diagrams, we identified five sequences and unconformities interpreted as sequence boundaries. Cretaceous unconformities are dated at the Late Barremian-Early Aptian boundary (~125 Ma); at the Albian- Cenomanian boundary (~100 Ma), and at the Santonian-Campanian boundary (~ 80 Ma).

2. Our analysis suggests that the basin inversion may have started earlier than previously proposed by Cooper (1995), Restrepo-Pace et al. (2004), Cortés et al. (2005), Gómez (2005), Moretti et al. (2010) and Parra et al. (2012). The presence of faults sealed by unconformities, folds related to faults, truncation, deformation and growth strata are evidence that deformation started before the Late Cretaceous.

3. I suggest that the basin inversion began with an incipient initial inversion during the Barremian-Aptian (incipient deformation below the SU2 unconformity). A generalized composite stratigraphic column of the MMV and WEC is proposed, based on information from outcrops, seismic reflections, wells and published data.

4. The unconformities identified in this work are consistent with the early tectonic phases identified in Peru and Ecuador (Jaillard et al., 2000), in the Middle Magdalena Valley (Morales, 1958), in the Upper Magdalena Valley (Allen, 1989; Barrios, 1992; Jaimes and de Freitas, 2006) and in western Venezuela (Cooney and Lorente, 2009). These comparisons allow me to propose that at least three pulses of uplift, deformation and erosion occurred at the Barremian-Aptian, Albian-Cenomanian, Santonian-Campanian boundaries, and an additional one around the Paleocene-Eocene boundary, all of them are significant tectonic events of regional extension.

5. However more accurate biostratigraphic data are needed to support the proposed observations.

CHAPTER 5

Thermal Evolution of the Western Eastern Cordillera and MMV: Relationship with the Cretaceous Unconformities

5.1. Sampling

In general, for all the WEC and the eastern border of the MMV about 90 samples were collected from Cretaceous to Tertiary sedimentary rocks, of which 45 samples were selected for preparation and finally 39 samples were analyzed with the zircon (1842 zircons crystals of 21 samples) and apatite (409 apatite crystals of 17 samples) fission-track methods. The aim was to obtain information on basin thermal and tectonic evolution, and to improve our understanding on the evolution of the WEC and the eastern border of the MMV.

Section	Sample	Zr	Ap	Formation	Age	Elevation (m)	Longitude	Latitude	Lithology (from thin section)
							W	E	
Northern	JG-P3-36	x	x	Lisama	Maastrictian-Paleocene	410	73° 23´ 20.7"	07° 05` 32.22"	Quartz arenite
	JG-P3-41	x		Simiti	Albian	359	73° 19´ 51.2"	07° 04` 21.59"	wacke
	JG-P3-15	x	x	Tablazo	Aptian	1305	73°13` 53.87"	06° 38` 09.94"	Sandy-shale
	JG-P3-04	x	x	Tablazo	Aptian	1217	73° 13` 39.79"	06° 38` 56.79"	Quartz Arenite
	JG-P3-32	x	x	Paja	Barremian-Aptian	461	73° 14` 35.67"	07° 01` 51.10"	Quartz Arenite -fine grain
	JG-P3-19	x	x	Tambor	Berresian-Hauterivian	1809	73° 17` 38.02"	06° 50` 36.12"	Quartz arenite
	JG-P3-21	x	x	Giron	Upper Jurassic- Lower Berriasian	1932	73° 18` 31.59"	06° 51` 15.17"	Subfeldspatic (Quartz) arenite
	JG-P3-23	x		Tambor	Hauterivian-Berriasin	1195	73° 21` 55.39"	06° 53` 52.55"	Quartz arenite
	JG-P3-20	x		Giron	Upper Jurassic- Lower Berriasian	1937	73° 17` 58.44"	06°50` 34.10"	Subfeldspatic (Quartz) arenite
	JG-P3-22	x	x	Giron	Upper Jurassic- Lower Berriasian	1497	73° 20` 55.89"	06° 54` 30.69"	Feldspacthic - (Quartz arenite)
	JG-P3-42		x	Simiti	Albian	372	73° 19` 53.52"	07° 04` 19.54"	Quartz arenite - Calcareous Fosiliferous
	JG-P3-43	x		Giron	Upper Jurassic- Lower Berriasian	1153	73° 15` 44.87"	07° 08` 12.85"	Subfeldspatic (Quartz) arenite
	JG-P3-37		x	Umir	Maastrictian	444	73° 23` 02.09"	07° 05` 32.77"	wacke
Centtral	JG-P1-06	x	x	Tablazo	Aptian	2787	73° 39` 15.80"	05° 39` 00.05"	Quartz Arenite
	JG-P1-07	x		Simijaca	Turonian-Coniacian	3398	73° 39` 36.54"	05° 41` 40.21"	Greywacke
	JG-P2-05 (3)	x	x	Churuvita	Cenomanian-Turonian	2635	73° 29` 50.13"	05° 32` 48.79"	Quartz Arenite
	JG-P2-05 (4-2)	x		Churuvita	Cenomanian-Turonian	2635	73° 29` 50.13"	05° 32` 48.79"	Quartz Arenite
	JG-P1-08		x	Ar. Chiquinquira	Albian-Cenomanian	3177	73° 41` 07.51"	05° 42` 53.62"	Quartz Arenite
	JG-P2-01	x		Conejo	LowerCampanian	2628	73° 28` 56.59"	05° 29` 34.14"	fine sandstone
	JG-P5-03	x	x	Arcabuco	Upper Jurassic- Lower Berriasian	2407	73° 30` 29.36"	05° 38` 39.55"	Quartz Arenite
Southern	JG-P4-19	x		Guaduas	Lower to Middle Paleocene	1664	74° 33` 26.28"	05° 02` 18.58"	Non description
	JG-P4-02	x	x	Seca	Maastrictian-Lower Paleocene	2799	74° 17` 35.53"	04° 52` 04.88"	Quartz Arenite
	JG-P4-06	x	x	Labor & Tierna	Maastrictian	2114	74° 17` 48.99"	04° 56` 52.40"	wacke
	JG-P4-01	x		Pleaners	Campanian-Maastrictian	2590	74° 12` 54.11"	04° 48` 33.71"	Wacke
	JG-P4-10		x	Naveta/Murca	Valangenian-Hauterivian	838	74° 26` 01.91"	05° 04` 14.63"	Calcarenite (14% Qz)
	JG-P4-13	x	x	Trinchera	Barremian-Aptian	1035	74°47`9.11"	5°01` 76.10"	Subfeldspathic-lithic (Quartz) arenite

Table 5.1. *Information of the samples collected, prepared and used for the thermochronological analysis in this work, organized by areas, showing the name of the samples, formation, age, elevation, location coordinates, and a short description from the thin section.*

Samples used for fission track analysis in this project were collected from three different areas as shown in table 5.1and on the map of figure 5.1.

5.2. Methodology: Theory, concepts and laboratory processes.

Due to the complex history of the analyzed basins the fission-track data of detrital samples used in this project are usually more complex than data from other types of rocks such as metamorphic or igneous rocks. It is known that single-grain ages of detrital sediments provide information on landscape evolution, thermal history and exhumation or provenance (e.g., Hurford and Carter, 1991; Ireland, 1992; Gehrels et al. 1999; Carter, 1999; Gehrels, 2000). These applications are related to each other, but the

most common application is for provenance analysis. In active mountain belts the sediment source areas show different thermochronological patterns which allow to identify different areas by analyzing 50-100 grains or more per sample (Dodson et al., 1988 and Bernet et al., 2004; Vermeesch, 2012) if the grains were not partially or fully annealed during burial heating. From the attained single-age distributions, major age components are derived and compared with the source area age patterns. This works very well for modern river samples which allow a direct comparison, whereas detrital age spectra from ancient sandstone need to be carefully evaluated (Bernet and Garver, 2005). Another application is the use of thermo- and geochronological data for *landscape evolution*, invaluable help in the reconstruction of the dynamic evolution of orogens (Bernet and Spiegel, 2004).

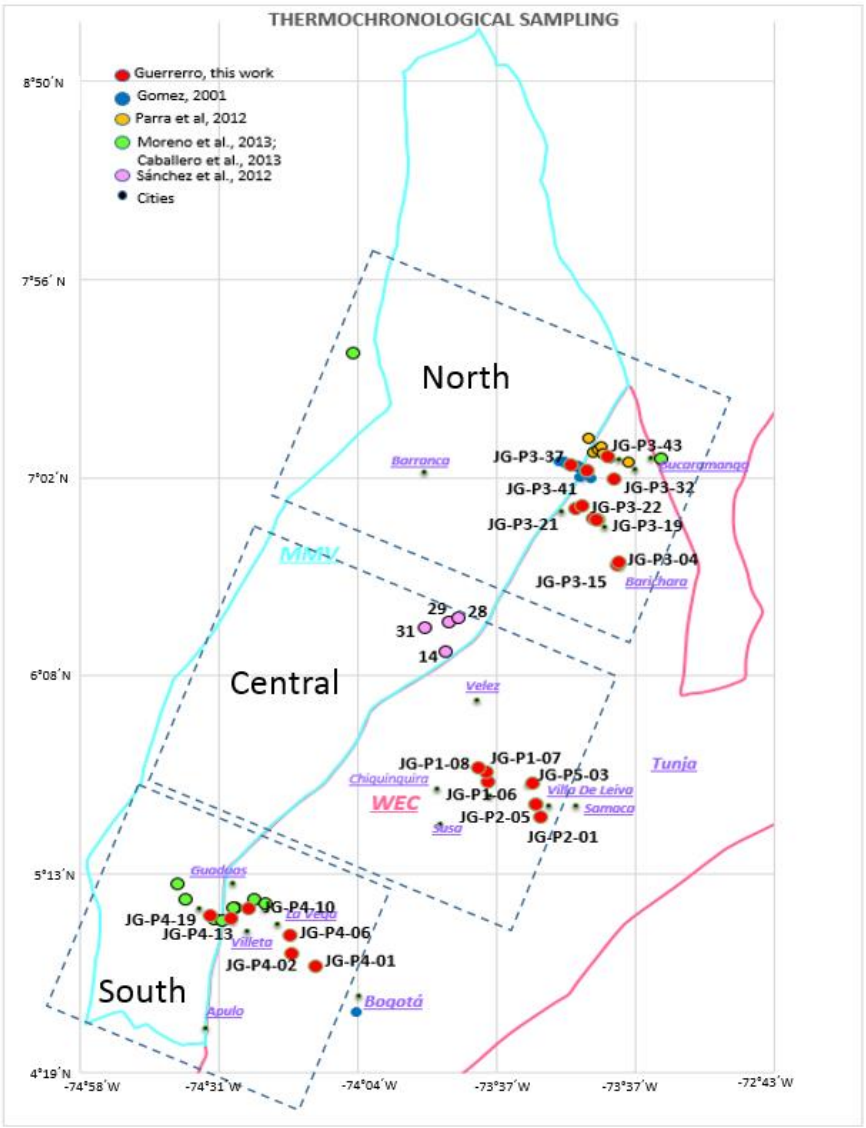

Figure 5.1. *Location map of thermochronological samples collected in this work (red points), and other authors (green, blue and yellow; the location of cities are marked as black dots).*

Several dating techniques exist for dating single grains. The most common is zircon U-Pb dating which provides general crystallization ages, whereas $^{40}Ar/^{39}Ar$ in white mica,

apatite and zircon fission-track analysis and apatite and zircon (U-Th)/He dating provide information for cooling ages (Bernet, et al., 2004), based on the closure temperature concept of Dodson (1973, 1979).

The thermochronological dating methods are based on the concept that decay-products (daughter isotopes or fission tracks) are lost while the crystal is above the so-called closure temperature. Decay-products are retained when the crystal cools below the closure temperature (Dodson, 1973). Cooling can be post-magmatic or caused by tectonic and erosional exhumation (Gallagher et al. 1998).

In this study only apatite and zircon fission-track analysis was used. Fission tracks are the damage produced in the crystal due to the spontaneous nuclear fission of ^{238}U and track densities are obtained by optical microscopy. Fission tracks may be partially or totally annealed if the crystals are exposed to elevated temperatures. The temperatures of the partial annealing zone (PAZ) of fission-tracks in apatite of average chemical composition are of about 80-110°C, and about 190-230°C for radiation damaged zircon, depending on hold time (Reiners and Brandon, 2006). The temperature for total annealing is around 110°C for apatite (Gleadow and Duddy, 1981) and for zircons around 240°C, depending on cooling rate during monotonic cooling (Hurford, 1986; Brandon et al., 1998; Bernet 2009).

The external detector method used for dating single detrital grains is explained in Fig. 5.2 (Gallagher et al., 1998)

In order to understand the exhumation history of the western Eastern Cordillera we used zircon (ZFT) and apatite fission-track (AFT) thermochronology. For better constraining the thermal history additional parameters are normally used in the case of apatite, such as track length measurements, which was not measured in this work, and etch pit size (Dpar) which were measured only when it was possible. Both are recommended because the annealing behavior of apatite depends on the chemical composition of the apatite (e.g. Gleadow et al., 1986; Donelick et al., 1999, Donelick et al., 2005, Ketcham et al., 1999). In rocks that have not been submitted to temperatures greater than 50°C since deposition, spontaneous fission tracks have characteristics of confined track lengths with a range of 14-15 μm and a deviation of 1 μm, in which case the FT age will be equal to the time over which the tracks have been accumulated (Gomez, 2001). In rocks subjected to temperatures greater than 50°C after deposition, the FT are shortened in a process known as annealing, in that way the final length of each tracks is determined by the maximum temperature reached. Temperature is the dominant factor in determining the final fission track parameters (Gomez, 2001), independent of when they were formed.

The track length can be related to the maximum temperature reached by the grain. The degree of shortening depends of time of heating and the composition of the apatites, this shortening produces a reduction in fission track age, however the age is highly dependent on the temperature reached being around 120°C due to the total annealing. Samples that were heated to the maximum paleo-temperature (~120°C) at some time in

the past and then cooled will probably contain two populations of tracks as happened with some samples here (figure 5.2 and 5.5), and contain a more complex distribution of length and ages. Tracks formed prior to the maximum temperature could be shortened to the same magnitude, so those formed during or after cooling will be longer (Gomez, 2001), the length distribution could consist of shorter and longer components. If the paleo-temperature was enough to shorten traces to 9 - 11 μm, and cooling was rapid up to temperatures of 50°C or less, traces could have a length of 14 - 15 μm; if the temperature was ~120°C all the pre-existing tracks will disappear and new traces will be formed after the onset cooling (related directly to the time of cooling).

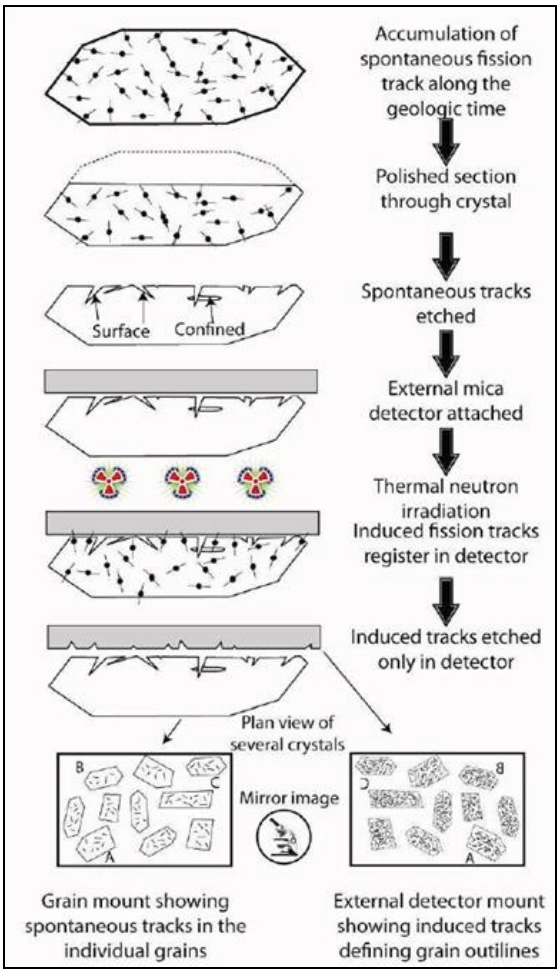

Figure 5.2. *The external detector method for fission-track dating is shown step by step: from top to base the formation of spontaneous fission tracks over geological time, polished grain mounts of zircon or apatite minerals; in the next step etching is used to reveal spontaneous tracks; grain mounts are covered with an uranium-free detector typically a muscovite mica, and the sample is irradiated in a nuclear reactor with low energy thermal neutrons, which induce fission in* ^{235}U*. After irradiation the mica detectors are etched to reveal the induced tracks on a mirror image of the original grain mount. Finally spontaneous and induced tracks are counted to determine the fission-track age on each grain (Gallagher et al., 1998).*

Thermal histories can be determined by forward and inverse modelling of time-temperature (t-T) paths based on grain age, track length and Dpar measurements (e.g., Ketcham, 2005), and additional information such as depositional age and vitrinite

reflectance (maximum burial temperature; e.g., Burnham and Sweeney, 1989) or ZFT data.

Detrital age spectra obtained from sedimentary rocks, are usually composed of more than one grain age population. To distinguish the possible presence of multiple age components the value P(χ^2) is used. When the value is less than 5% it is assumed that more than one population is present (Galbraith, 1981). Different age peaks can be determined using statistical techniques (Galbraith and Green, 1990; Sambridge and Compston, 1994; Brandon, 1992 and 1996). Normally P1 is the youngest age peak and Pn is the oldest (figure 5.3).

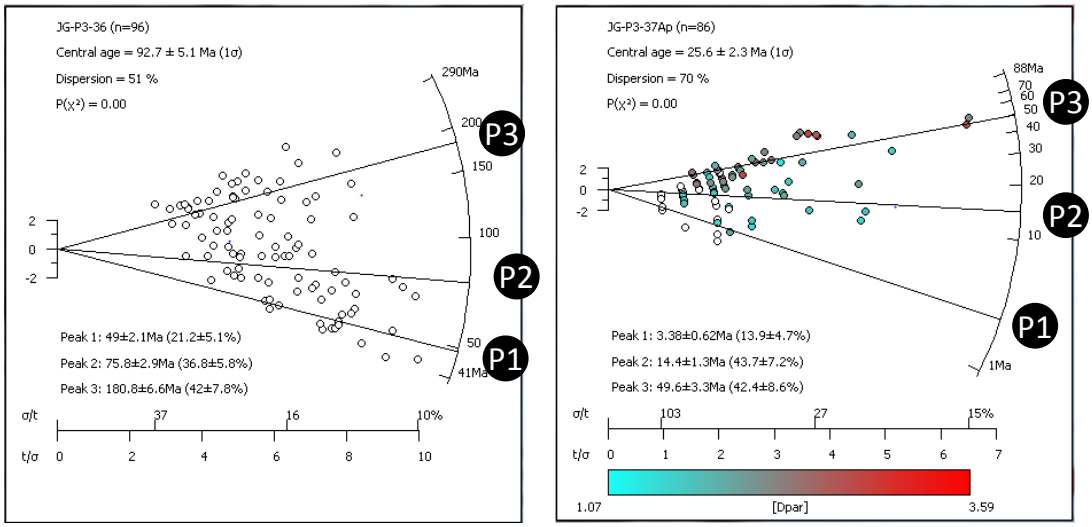

Figure 5.3. *Radial plot representation (Gailbraith, 1990) of ZFT (left) and AFT (right) of two different samples (using radialpltter aplication from Vermeesch, 2009) from the northern study zone of this work (for location see figure 5.5). The different ages, P1 to P3, were extracted from a raw dataset using statistical techniques (Galbraith and Green, 1990; Sambridge and Compston, 1994; Brandon, 1992 and 1996), the ages are indicated with a one sigma error (1σ); the number in parentheses is the number of grains beloning to each peak.*

Fission-track age equation:

The general equation of fission track age calculation is given by:

$$t = \frac{1}{\lambda} ln\left[1 + \frac{\lambda \zeta \rho_s c \rho_d}{\rho_i}\right] \quad \text{Eq. 5.1}$$

Where λ is the total decay constant of ^{238}U (1.55 x 10^{-10} yrs^{-1}); ρ_s, ρ_i in practical terms are the measured spontaneous and induced track density on internal crystal surfaces which are determined during the fission track counting of N_sN_i which are substituted by ρ_s, ρ_i, and ρ_d is the dosimeter track density. For more information see Wagner and Van den Haute (1992); *c* is a geometric factor (0.5). Where Ns/Ni is know as R.

The term ζ is called Z factor, which is a personal calibration factor (between 250 to 390 yr/cm^2) for apatite and zircon methods (Fleischer and Hart, 1972), this factor is

calculated and applied for the External Detector Method (Wagner and Van den Haute, 1992; Gallagher et al. 1998). This Z factor is calculated using the following equation.

$$\zeta = \frac{\varphi \sigma I}{\lambda_f \rho_d} \qquad \text{Eq. 5.2}$$

Where, φ is the neutron flux; σ is a cross section of neutron capture (580.2×10^{-24} cm^2); λ_f represents the fission decay constant of ^{238}U (8.5×10^{-17} y^{-1}); I is the ^{238}U/^{235}U ratio (7.2527×10^{-3}) and ρ_d is the track density of the glass monitor which is proportional to the fluence.

Pooled age is defined by:

The estimation of R is shown in the following equation (Burchart, 1981; in Bermudez, 2010):

$$\overline{R} = \overline{\left(\frac{N_s}{N_i}\right)_t} = \frac{\sum_{j=1}^{n} N_{sj}}{\sum_{j=1}^{n} N_{ij}} \qquad \text{Eq. 5.3}$$

Central age: This ages from many observations converge numerically to the maximum likelihood estimator for the ratio R, which allows this statistical estimation to be generally used as an age estimator, (Galbraith and Laslett, 1993; Galbtaith, 2005; in Bermudez, 2010).

$$\overline{R} = \frac{\eta}{1-\eta} \qquad \text{Where,} \qquad \eta = \frac{\sum_{j=1}^{n} w_j N_{sj}}{\sum_{j=1}^{n} w_j} \qquad \text{Eq. 5.4}$$

The expression N_{sj} and N_{ij} represent respectively the spontaneous and induced fission track counts for grains $j=1 \ldots \ldots n.$ and the sum is expressed by $N_s = \sum_{j=1}^{n} N_{sj}$ and $N_i = \sum_{j=1}^{n} N_{si}$

Minimum Age:

The term "minimum age" was introduced by Galbraith and Laslett (1993), and it can be expressed as the pooled age of the largest concordant fractions of young grains in a Fission track distribution. For the estimation of minimum age of a distribution the bimodal peak can also be used, which will be equal to the youngest component in the distribution. The minimum age from zircons is useful, for example, for a tuff can remove the contaminant effect of the older contaminant grains. For the rocks that have been reset it represents the time of closure for the fraction of grains with the lowest retention for fission tracks. Such radiation-damage zircons in ZFT dating (Brandon and Vance, 1992) or flourapatites in AFT (Brandon, et al. 1998).

Vitrinite Reflectance – Ro –Tmax

Vitrinite reflectance Ro is a measurement of maturity of organic matter. The vitrinite reflectance increases with increasing temperature (e.g., Bustin et al., 1990). The Ro measurement is related to heating in most cases associated to burial. The measure of Ro can provide the paleo-temperature reached during the burial history (sedimentation load). In this case, Vitrinita values were taken from existing literature. The range of vitrinite reflectance typically varies from 0.2 for temperatures <30°C to 6 for maximum paleo-temperature of >280°C. In the case of this study, Ro was used to estimate the paleo-temperature and determine the amount of overburden.

The maximum temperature (Tmax) can be estimated from the vitrinite reflectance (Ro) values, using empirical relations as indicated by Baker and Pawlewicz, (1994):

$$Tmax = \frac{\ln Ro + 1.68}{0.0124} \quad (3)$$

Where Tmax is the maximum temperature in Celsius degrees and Ro is vitrinite reflectance in %. It is know that there are other relationships to stablish the Tmax and other possibly more sophisticated methods (e.g., Sweeney and Burnham, 1990), however I decided to use this one (equation 3), because the possible refining in methodology would be small in comparison with other methods as is indicated by Lee Y. et al, (1999). The Tmax calculated using the equation (3) are shown in numeral 5.4.

t-T Thermal Modeling

In Figure 5.4 Ketcham et al. (2016), show us an interesting diagram that describes the paths t-T. In the figure solid boxes are used as a constrain and dashed boxes are implicit constrains from stratigraphic reasons. Lines linking cubes are in reality t-T paths, the dashed lines show paths controlled by samples and solid lines that are free to vary; A represents continuous deposition indicating what the lower sample is hosting between its deposition and the deposition of the upper section; B indicates unconformity, at least one episode of erosion (it means cooling between two consecutive episodes); C is independent where the upper and lower samples don't influence the others; and finally D represents the parallel where the upper sample has a history that is the inverse of the lower, while the lower sample is being buried.

Thermal history modeling is a more general and more comprehensive treatment of the thermo chronometric data (Ketcham et al., 2016). An advantage of thermo-kinematic models is that they stablish a spatial-structural relation between samples to evaluate structural scenarios (Erdos et al, 2014; Castellucio et al., 2015 and McQuarrie and Ehlers; in Ketcham et al., 2016). Information can predict the dates that corresponding to the exhumation of the source region and transport to the depocenter (Bernet & Garver, 2005).

Ketcham et al. (2016), showed that thermal history could be modeled using multiple samples simultaneously in HeFTy thermal history modeling software (Ketcham, 2005). In the case of QtQt modeling software one may try to determine the structure of the thermal history necessary to fit the data. In the case of HeFTy the application is written starting from the point of view that geological histories are more complex than the thermochronometers data could resolve (Ketcham et al., 2016). In HeFTy modeling software Ketcham et al. (2016) describe an extension that allows to explore questions that are inherent to sedimentary sequences and involve distinguishing different thermal histories for different strata, major unconformities, the amount of missing sections, and timing of burial. The new implementation works with a combination of a set of sample files that establish the stratigraphic and pre-depositional relationship with one another. Relations between the samples are defined in couples from bottom to top.

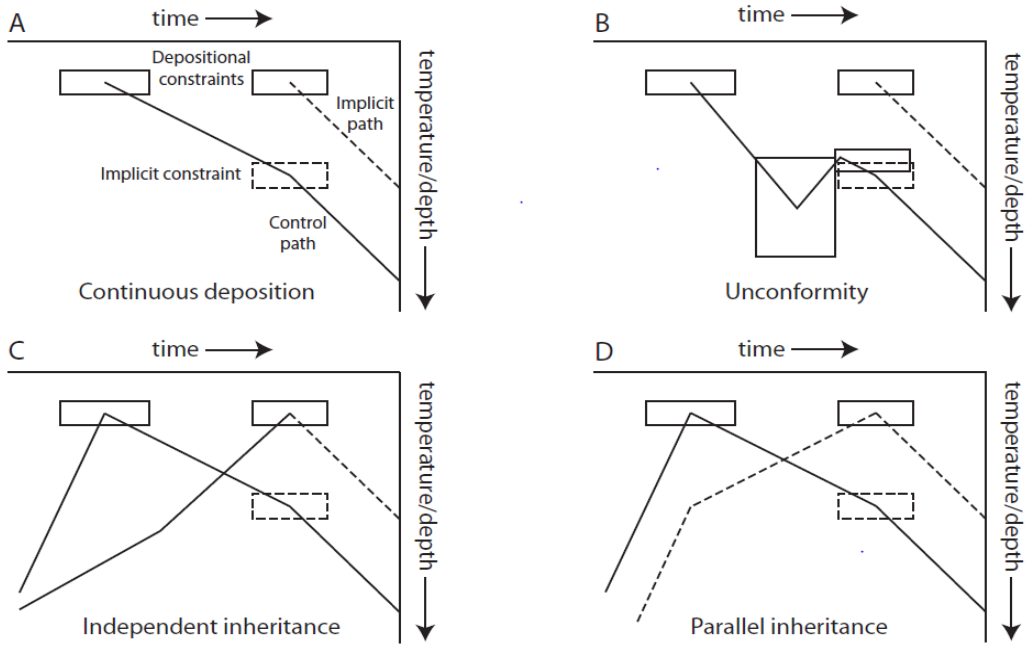

Figure 5.4 *– Shows schematic time-temperature (t-T) paths, solid boxes are used as imposed constrains and dashed boxes constrains are derived from stratigraphic relationships, lines represent t-T paths. Solid lines represent paths that are free to vary and dashed lines represent paths controlled by lower samples. A) Continuous deposition, B) An unconformity relationship, at least one episode of erosion and thus cooling, C) inheritance or pre-depositional history can be independent, D) parallel, not influenced by other sample (Taken from Ketcham et al., 2016).*

According to Ketcham et al. (2016), the burial history is defined by the relation between the adjacent samples, two relations were provided; continuous deposition where the thermal history of the lower sample is monotonically heating until deposition of the upper one; unconformity, where there is a missing section between the two samples, involving a period of exhumation and a later period of burial before the upper sample is deposited (its mean heating, cooling, heating again). The amount of missing section is determined using thermochronology (related to when the samples were at the maximum temperature; Corcoran & Doré, 2005). Independent, neighbor samples with entirely

independent thermal histories prior to deposition which are linked after deposition of the upper sample (C in figure 5.4); Parallel is the case where two samples behave similarly, cooling and exhumation at the same rate (after the lower sample is deposited the upper sample is forced to cool at the same rate as the lower sample is being heated or the source region is being eroded as fast as the sediment column is being buried (1D in figure 5.4). The thermal modeling (t-T thermal modeling) from samples in the three different areas in this work are shown in numeral 5.7.

5.3 Analytical procedure

In the lab the samples were crushed, pulverized and sieved, and from the 160 to 60 μm fraction heavy minerals were separated with standard magnetic and heavy liquid separation in three different laboratories (National University of Colombia at Bogotá, GMAS lab and ISTerre, University Grenoble Alpes). In the ISTerre thermochronology laboratory zircons were mounted in Teflon® sheets, polished and etched. For each zircon sample two mounts were prepared and etched for different lengths of time (10-30 h) at 228°C in a NaOH-KOH melt. Apatite grains were mounted in epoxy resin, polished and etched for 20s at 21°C in 5.5 molar HNO_3 (Figure 5.2).

Before sending the samples for irradiation to the FRM II reactor in Munich, Germany, the grain mounts were covered with muscovite sheets as external detectors. The samples were irradiated together with Fish Canyon Tuff and Buluk Tuff age standards and IRMM541 dosimeter glasses for zircons, and Durango Tuff and Fish Canyon Tuff age standards and IRMM540R dosimeter glasses for apatite. After irradiation the mica detectors were etched at 20°C for 18 minutes in 48% HF to reveal induced fission tracks (Figure 5.1). Zircon fission tracks were counted at 1250x with an Olympus BH2 microscope, whereas apatite fission tracks were counted at 1250x with an Olympus BX51 microscope at the ISTerre thermochronology laboratory in Grenoble, France.

The fission-track ages of single grains in addition to best-fit peak ages were first determined for each sample using BinomFit for Windows ver. 1.2. whereas minimum and central ages were calculated using the RadialPlotter software of Vermeesch (2009) (e.g., Figures 5.2 and 5.3).

5.4 Results

The results of the detrital ZFT and AFT analyses are shown in Tables 5.2, 5.4 and 5.6 for the zircons and 5.3, 5.5 and 5.7 for the apatites. The ZFT data show a large range of grain age distributions, with minimum age range varying from lower Eocene to Coniacian, and central age range varying from Turonian to Middle Jurassic.

Detrital zircon fission-track results, Northern section in WEC

Sample	Unit	n	P(χ^2) %	Stratigraphic Age (Ma)	ρ_s tracks/cm^2	Ns	ρ_i tracks/cm^2	Ni	ρ_d tracks/cm^2	P1 ±1σ Ma	P2 ±1σ Ma	P3 ±1σ Ma	P4 ±1σ	Central ±2σ age Ma.	Pooled ±2σ age Ma.	Minimun ±2σ Age Ma.	Age Dispersion %
JG-P3-36	Lisama	96	0	61±5	4.74 x 10^6	17933	1.34 x 10^6	5088	3.90 x 10^5	49 ±2.1 21,20%	75,8 ±2.9 36,80%	180 ±7.8 42%		92,7 ±10,2	93,4 ±4,4	48,3 ±4,2	51
JG-P3-41	Simiti Simiti	49	0	106 ± 6	1.01 x 10^7	6616	1.26 x 10^6	821	2.72 x 10^5	80 ±13 14%	166 ±10 86%			143,6 ±16,8	148,4 ±12	75,9 ±18	31
JG-P3-15	Tablazo	61	0	118 ± 6	9.85 x 10^6	8032	1.35 x 10^6	1097	2.73 x 10^5	76,3 ±8.2 12,70%	149 ±6.5 87,30%			133,1 ±12,6	.135.5 ±10	80 ±16	26
JG-P3-04	Tablazo	94	0	118 ± 6	6.31 x 10^6	13278	1.30 x 10^6	2747	3.84 x 10^5	50,4 ±3.8 7,40%	90 ±7.7 27,10%	166,9 ±6.7 68,50%		124,4 ±12,2	126 ±6,6	51,9 ±7,6	43
JG-P3-32	Paja	98	0	125 ± 3	6.83 x 10^6	14459	1.27 x 10^6	2690	3.88 x 10^5	91,9 ±4.5 24,80%	172,1 ±6 75,20%			142,2 ±10,4	141,4 ±7,4	88,1 ±11,2	28
JG-P3-19	Tambor	102	0	138 ± 8	8.85 x 10^6	29290	1.00 x 10^6	3318	2.73 x 10^5	46,3 ±7.4 1,80%	116,7 ±5.4 27,90%	196,5 ±6.9 70,20%		161,4 ±11,8	163 ±8,2	81 ±20	31
JG-P3-23	Tambor	90	0	139 ± 8	6.20 x 10^6	31165	9.93 x 10^6	4992	3.87 x 10^5	64,9 ±4.3 4,80%	100,1 ±5.6 11,20%	153,5 ±8.6 29,70%	226,3 ±7.6 54,30%	164,7 ±15	164 ±7,4	69,3 ±8	41
JG-P3-20	Giron	102	0	161 ± 15	8.84 x 10^6	26246	1.31 x 10^6	3899	2.72 x 10^5	75,2 ±4.8 11,10%	112,4 ±5.4 44,60%	167,4 ±7.7 44,30%		124,3 ±8,2	124,5 ±6,0	78,4 ±8,8	28
JG-P3-21	Giron	100	0	161 ± 15	5.96 x 10^6	21198	1.38 x 10^6	4907	3.85 x 10^5	70,1 ±3.9 21,20%	110,6 ±8.9 36%	147,5 ±7.6 43%		110,8 ±7,4	113 ±5,0	66 ±8	29
JG-P3-22	Giron	100	0	161 ± 15	5.32 x 10^6	16328	1.57 x 10^6	4805	3.86 x 10^5	44,8 ±3.4 6,20%	80,4 ±2.5 60%	129,9 ±5.8 33,90%		89,2 ±6	89,3 ±4,2	53,5 ±6,8	28
JG-P3-43	Giron	100		161 ± 15	5.83 x 10^6	22380	1.47 x 10^6	5622	3.90 x 10^5	55,3 ±6.6 3,50%	81,1 ±4.8 34%	106 ±10 25%	147,6 ±6.4 37%	104,5 ±7	105,6 ±4,8	72 ±9,4	29

Table 5.2 – Detrital ZFT results from the north region in the WEC. All the samples were analyzed and counted at 1250x using a BH2 Olympus microscope with digitalizing tablet by Jairo Guerrero with a zeta value of 137.14±1.57. ρ_S and ρ_i are the measured spontaneous and induced track densities; Ns and Ni are the number of spontaneous and induced tracks;P(χ^2) is the chi-square probability (Galbraith, 1981; Green, 1981) values like 0 represent multiple populations and greater than 5% represent a single populations age; ρ_d is the induced track density measured in the external mica detector, ND is the number of induced tracks counted in the mica to estimate RhoD; n represents the number of grains.

Detrital Apatite fission-track results, Northern section in WEC

Sample	Unit	n	P(χ^2) %	Stratigraphic Age (Ma)	ρ_s tracks/cm^2	Ns	ρ_i tracks/cm^2	Ni	ρ_d tracks/cm^2	P1 ±1σ Ma	P2 ±1σ Ma	P3 ±1σ Ma	Central ±2σ age Ma.	Pooled ±2σ age Ma.	Minimun ±2σ Age Ma.	Age Dispersion %	Dpar µm
JG-P3-36	Lisama	17	86	61±5	1.56 x 10^5	91	8.33 x 10^6	4858	1.29 x 10^6	3,41 ±0.37 100%			3,41 ±0.72	3,4 ±0.8	3,07 ±0.72	0,2	1,313
JG-P3-37	Umir	86	0		1.94 x 10^5	702	1.86 x 10^6	6722	1.30 x 10^6	3,38 ±0.62 14%	14,4 ±1.3 44%	49,6 ±3.3 42%	25,6 ±4,6	19,1 ±1,8	2,32 ±1,28	70	2,083
JG-P3-42	Simiti	24	0	106 ± 6	3.71 x 10^5	206	2.40 x 10^6	1332	1.30 x 10^6	5,9 ±1.7 17%	29,9 ±4.5 48%	54,5 ±9.7 35%	32,3 ±9,2	28,3 ±4,4	4,4 ±4,6	55	1,498
JG-P3-04	Tablazo	37	0	118 ± 6	1.58 x 10^5	237	4.43 x 10^6	6622	1.27x 10^6	3,23 ±0.39 64%	20,4 ±2.3 36%		9,4 ±3	6,4 ±0.8	3,33 ±1,36	88	1,549
JG-P3-15	Tablazo	27	2	118 ± 6	2.11 x 10^5	174	8.86 x 10^6	7308	1.23x 10^6	3,3 ±0.7 65%	5,9 ±1.6 35%		4,22 ±0.78	4,1 ±0.6	3,6 ±2,4	26	1,17
JG-P3-32	Paja	14	26	125 ± 3	1.83 x 10^5	77	1.13 x 107	4727	1.23x 10^6	2,82 ±0.33 100%			2,82 ±0.66	2,8 ±0.6	1,4 ±1,42	3,4	1,17
JG-P3-19	Tambor	34	63	138 ± 8	9.65 x 10^4	175	6.93 x 10^{-6}	12564	1.28x 10^6	2,5 ±0.2 100%			2,5 ±0.38	2,5 ±0.4	1,36 ±0.9	0	1,239
JG-P3-22	Giron	20	0	161 ± 15	3.61 x 10^4	373	2.29 x 10^{-6}	2366	1.28x 10^6	2,54 ±0.72 16%	19,2 ±3.3 16%	55,7 ±3.9 68%	40,4 ±12,8	28,5 ±3,4	1,48 ±1,44	64	1,658
JG-P3-21	Giron	18	0	161 ± 15	1.03 x 10^5	110	6.04 x 10^{-6}	6469	1.28x 10^6	1,9 ±0.43 61%	4,68 ±0.85 39%		3 ±0.84	3,1 ±0.6	0,9 ±0.8	43	1,639

Table 5.3 – Detrital AFT results from the north section of the WEC. All the samples were analyzed by Jairo Guerrero with a zeta value of 282.02±6.88.

Detrital zircon fission-track results, Central section in WEC

Sample	Unit	n	P(χ^2) %	Stratigraphic Age (Ma)	ρ_s tracks/cm^2	Ns	ρ_i tracks/cm^2	Ni	ρ_d tracks/cm^2	P1 ±1σ Ma	P2 ±1σ Ma	P3 ±1σ Ma	Central ±2σ age Ma.	Pooled ±2σ age Ma.	Minimun ±2σ Age Ma.	Age Dispersion %
JG-P2-01	Conejo	24	0	80± 3	5.72x 10^6	2260	1.58 x 10^6	623	3.82 x 10^5	49.9 ±4.3 26.50%	140.7 ±9.9 73.50%		97 ±22	94.3 ±9	46 ±9,2	52
JG-P1-07	Simijaca	85	0	90 ± 4	8.58x 10^6	9465	1.45 x 10^6	1600	2.74 x 10^5	59.9 ±4 12%	126.9 ±4.6 88%		111.6 ±9,4	110.1 ±6,8	60.6 ±10	28
JG-P2-05 (3)	Churuvita	84	0	95 ± 6	1.09x 10^6	11510	1.49 x 10^6	1574	2.74 x 10^5	59.2 ±7.2 5.60%	143.2 ±4.9 94.40%		133.4 ±10,4	135.7 ±8,6	72.3 ±13,6	25
JG-P2-05 (4-2)	Churuvita	100	0	95 ± 6	5.99x 10^6	18247	1.17 x 10^6	3572	3.83 x 10^5	59.9 ±3.3 12.00%	98 ±7.6 19.90%	172.4 ±5.7 68.10%	128.9 ±11,6	132.7 ±6,4	60.9 ±6,6	40
JG-P1-06	Tablazo	72	0	118 ± 3	6.94x 10^6	8482	1.05 x 10^6	1374	3.25 x 10^5	49.3 ±9.6 4%	103 ±14 25%	155.2 ±9.2 71%	130.6 ±11,2	131.1 ±9	69.5 ±14,4	26
JG-P5-03	Arcabuco	102	0	150 ± 10	4.77x 10^6	16033	2.01 x 10^6	6739	3.93 x 10^5	39.4 ±2 15.50%	59.6 ±1.8 60.80%	110.8 ±4.7 23.80%	63.7 ±5	63.8 ±3	41.4 ±4,6	33

Table 5.4 *–Detrital ZFT results from the central region in the WEC, for description see table 5.1.*

Detrital Apatite fission-track results, Central section in WEC

Sample	Unit	n	P(χ^2) %	Stratigraphic Age (Ma)	ρ_s tracks/cm^2	Ns	ρ_i tracks/cm^2	Ni	ρ_d tracks/cm^2	P1 ±1σ Ma	P2 ±1σ Ma	Central ±2σ age Ma.	Pooled ±2σ Age Ma.	Minimun ±2σ Age Ma.	Age Dispersion %	Dpar µm
JG-P2-05	Churuvita	21	0	95 ± 6	2.24x 10^5	182	7.5 x 10^6	6096	1.27 x 10^6	2,61 ±0.75 29%	6,54 ±0.73 71%	5,47 ±1,16	5,3 ±0.8	1,99 ±1,84	34	1,098
JG-P1-08	Ar. Chiquinquira	5	0	99 ± 2	2.70x 10^5	30	8.2 x 10^6	912	1.26 x 10^6	5,9 ±1.1 100%		9,3 ±8,2	5,9 ±2,4	4,8 ±2,8	88	0,93
JG-P1-06	Tablazo	24	0	118 ± 3	4.37x 10^5	343	1.17 x 10^7	9175	1.26 x 10^6	4,41 ±0.53 44%	9,21 ±0.91 56%	7,04 ±1,28	6,6 ±0.8	4,7 ±2	35	1,112
JG-P5-03	Arcabuco	10	0	150 ± 10	2.48x 10^5	150	8.63 x 10^6	945	1.32 x 10^6	3,87 ±0.48 61%	9,7 ±2.3 39%	5,88 ±1,9	5,4 ±0.8	3,43 ±1,26	44	1,26

Table 5.5 *– Detrital AFT results from the central section of the WEC. All the samples were analyzed by Jairo Guerrero with a zeta value of 282.02 ± 6.88, for description see table 5.1. For zeta value see table 5.2*

Detrital zircon fission-track results, South section in WEC

Sample	Unit	n	P(χ^2) %	Stratigraphic Age (Ma)	ρ_s tracks/cm^2	Ns	ρ_i tracks/cm^2	Ni	ρ_d tracks/cm^2	P1 ±1σ Ma	P2 ±1σ Ma	P3 ±1σ Ma	Central ±2σ age Ma.	Pooled age ±2σ Age Ma	Minimun ±2σ Age Ma.	Age Dispersion %
JG-P4-19	Guaduas	102	0	60± 3	4.91x 10^6	23743	1.05 x 10^6	5053	3.92 x 10^5	58,8 ±4.2 7%	102,1 ±4.7 33%	156,7 ±5.5 60%	123,8 ±8,8	125,8 ±5,8	79,9 ±9,2	32
JG-P4-02	Seca	44	0	65.5 ± 3	5.24x 10^6	4691	9.81 x 10^5	877	3.91 x 10^5	52 ±10 9%	93 ±9.6 30%	205 ±13 61%	131 ±22	141,8 ±11,4	67,7 ±16	48
JG-P4-06	Labor & Tierna	84	0	68± 2	1.04x 10^7	13992	1.23 x 10^6	1662	2.71 x 10^5	87,3 ±6.3 23,20%	182,8 ±7.4 76,80%		147,9 ±13,8	154,7 ±9,8	95,6 ±14	35
JG-P4-01	Pleaners	59	0	70.5± 6	9.31x 10^6	7812	2.15 x 10^6	1806	2.72x 10^5	37,7 ±3.2 12,50%	65,8 ±3.4 43,60%	162,7 ±9.8 44,00%	83,3 ±12,6	80,1 ±5	40,8 ±7	54
JG-P4-13	Trinchera	94	0	125± 3	8.22x 10^6	22542	1.31 x 10^6	3592	2.71 x 10^5	48,6 ±2.9 7,70%	84,3 ±3.6 38,70%	172,2 ±6.3 53,60%	110,9 ±11	115,5 ±6,0	57,3 ±6,8	44

Table 5.6- *Detrital ZFT results from the south region in the WEC, for description see table 5.1.*

Detrital Apatite fission-track results, South section in WEC

Sample	Unit	n	P(χ^2) %	Stratigraphic Age (Ma)	ρ_s tracks/cm^2	Ns	ρ_i tracks/cm^2	Ni	ρ_d tracks/cm^2	P1 ±1σ Ma	P2 ±1σ Ma	Central ±2σ age Ma.	Pooled ±2σ Age Ma.	Minimun ±2σ Age Ma.	Age Dispersion %	Dpar µm
JG-P4-02	Seca	7	61	65.5 ± 3	7.22x 10^4	24	7.0 x 10^6	2325	1.31 x 10^6	1,9 ±0.39 100%		1,9 ±0.78	1,9 ±0.8	1,62 ±0.76	0	1,486
JG-P4-06	Labor & Tierna	17	47	68 ± 2	1.32x 10^5	94	8.23 x 10^6	5851	1.31 x 10^6	2,97 ±0.32 100%		2,97 ±0.62	3 ±0.6	2,6 ±0.62	0	1,138
JG-P4-10	Naveta/Murca	9	1	133.9± 3	5.68x 10^5	28	3.71 x 10^6	1831	1.32 x 10^6	2,84 ±0.55 100%		3,11 ±01,4	2,9 ±1,2	2,07 ±1,40	26	1,51
JG-P4-13	Trinchera	39	0	125 ± 3	7.77x 10^4	173	2.92 x 10^6	6540	1.23 x 10^6	4,07 ±0.41 80%	13,2 ±4.1 20%	5,38 ±1,14	4,6 ±0.8	2,9 ±2,2	39	1,349

Table 5.7 *– Detrital AFT results from the south region in the WEC, for description see table 5.1. For zeta value see table 5.2*

5.5. Discussion

5.5.1 Northern Section

For the northern section eleven zircon and nine apatite samples were analyzed (Tables 5.2 and 5.3). Figure 5.5 shows a wide range of peak ages determined for the different samples and many of the peak ages are younger than the age of deposition, indicating partial annealing because of burial heating. For interpreting the detrital fission-track data, I separated the peaks into five different population ages (D1 to D5), showing that the ZFT ages for detrital tendencies D1 to D3 are in the partial resetting zone Lag-time < 0, whereas the samples D4 and D5 are older than the stratigraphic age. However D4 and D5 grain populations were also affected by partial annealing probably to a lesser degree than the other grains. Under these conditions the samples analyzed in this work do not provide a clear provenance signal, however, as we will see later, they could be useful to understand the thermal history of the area.

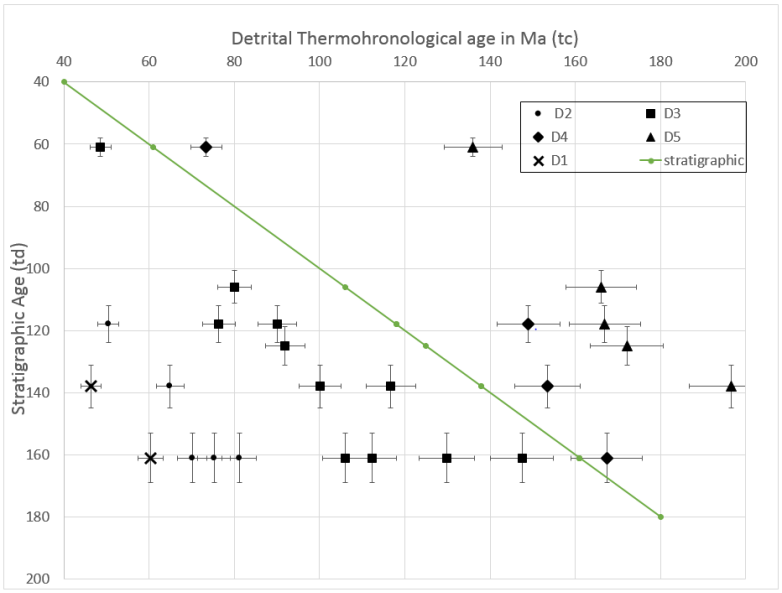

Figure 5.5 *- Graph showing detrital thermochronological age (tc) in x-axis versus stratigraphic age (td) in y-axis. Raw data, real example from the samples taken at the north area of this work. The measured ages showed five detrital population (D1 to D5). The area at the left below the stratigraphic line (tc=td) corresponds to the resetting zone (Lag Time=tc-td <0), which is a zone where grains (zircons in this case) had been heated after sedimentation to temperatures greater or in the range of temperature of closure (Tc) where there is a thermal overprint and reset the thermochronological clock. The samples over the stratigraphic age (D4 and D5) also present partial annealing even to a lesser degree.*

In the Rio Sogamoso section (Figures 5.6, 5.7 and 5.8) the ZFT ages are older on the western flank of the Los Cobardes anticline (samples JG-P3-32 at 142.2±5.2 Ma and sample JG-P3-41 with 143.6±8.4 Ma; figure 5.6 and 5.7). In the Girón Fm. in the core of the Los Cobardes anticline the ZFT ages are 104±3.5 Ma, somewhat younger (see Table 5.1 and Figure 3.4) where the stratigraphically younger units where cooled earlier than the stratigraphically older units during the exhumation. The same behavior is observed mapping minimum age from ZFT (Figures 5.6 and 5.9) and also mapping minimum age from AFT (Figures 5.9, 5.10 and 5.11), for the maps showing these tendencies see Figure 5.9.

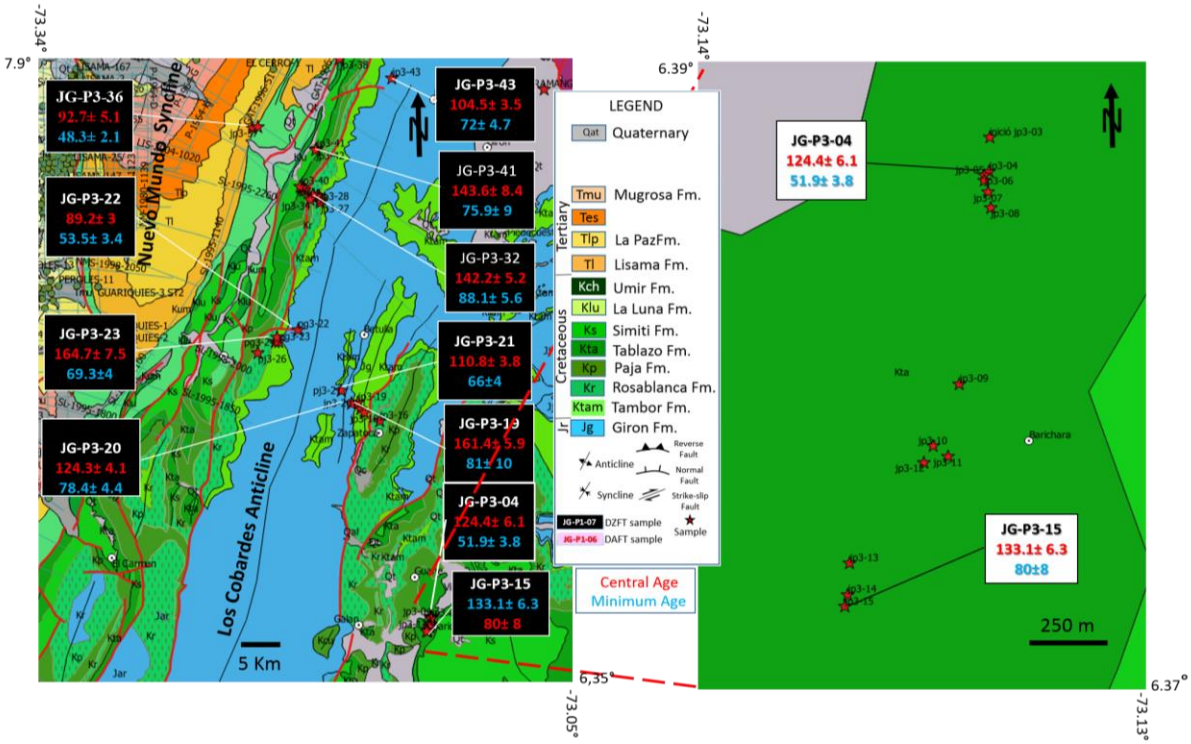

Figure 5.6*- Map showing the location of ZFT ages in the North area of study (for the location see figure 3.5). In the squares are the sample name, central and minimum age, at right a detail of the samples collected at SW is shown.*

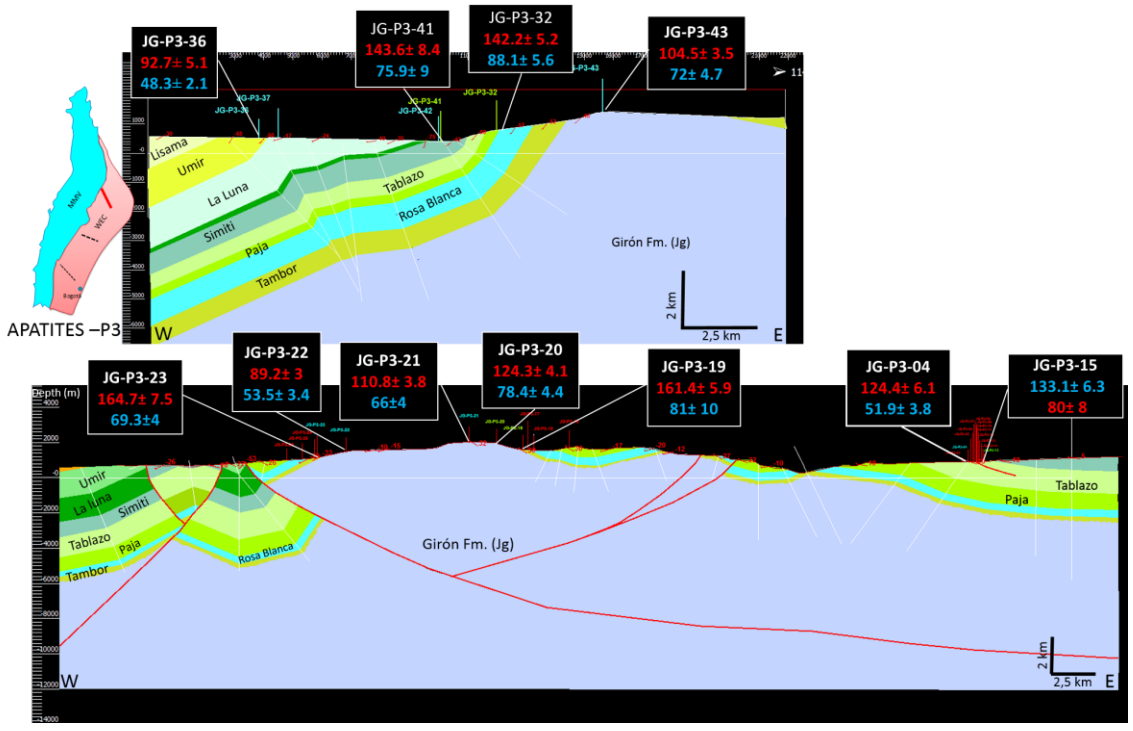

Figure 5.7*- Structural section in the Northern section above at the height of Rio Sogamoso and below at the Barichara- San Vicente de Chucuri road, showing of the location of the zircon samples, the peak age measured in laboratory, central and minimum age are also included in the squares with the ZFT age.*

The same is observed at the Barichara-San Vicente de Chucuri section (below in Figure 5.7) where at the core of Los Cobardes anticline (Giron Fm.) the ZFT ages are younger (samples JG-P3-21 at 110.8 ±3.8 Ma and JG-P3-22 with 89.2±3 Ma) than in the flanks (Tambor Fm) with ages of 161.4 ±5.9 Ma and 164.7±7.5 Ma (samples JG-P3-19 and JG-P3-23). From ZFT minimum age the same tendency is interpreted from samples JG-P3-19, JG-P3-20 to JG-P3-21 at the east flank of the anticline, and JG-P3-22, JG-P3-23 at the west (Figure 5.6, 5.7 and 5.9).

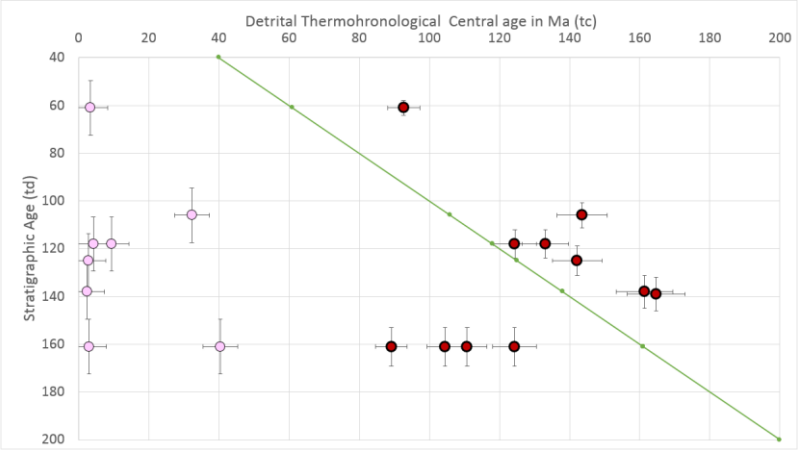

Figure. 5.8*- Graph showing detrital thermochronological central age (tcc) in x-axis versus stratigraphic age (td) in y-axis. About the raw data, note how the oldest Jurassic samples from ZFT (red points) are in the resetting zone, while the ZFT (red points) samples from Berriasian -Valangenian to Paleocene age are not reset. This probably shows that the Jurassic samples (Girón Fm.) had reached the partial annealing zone (PAZ). The Central ages from the AFT (pink points) are also plotted, which are all in the partial annealing zone PAZ.*

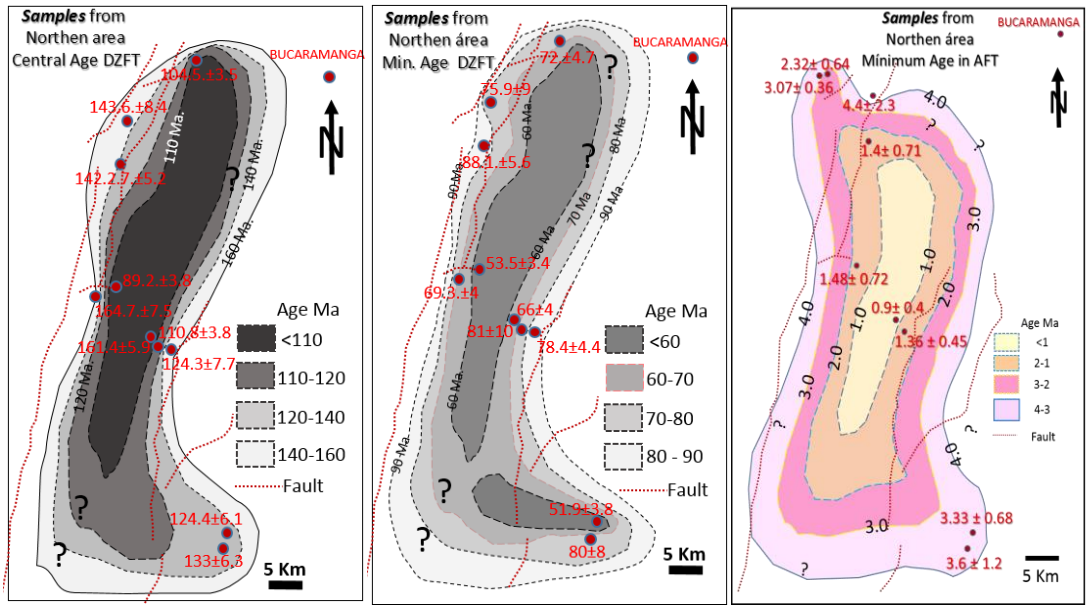

Figure 5.9 *- The map on the left shows the central age of the ZFT, for the samples from the norther area of study, note that the ZFT age tends to decrease towards the central part of the Los Cobardes Anticline, where the Jurassic units are present. The section in figure 5.7 shows the same behavior. The map in the center shows the minimum age from ZFT, note that also towards the center of Los Cobardes Anticline the age tends to decrease; the same behavior is observed on the map on the right, mapping the minimum age from the AFT.*

The same relation that is interpreted for the ZFT samples is observed for the minimum age of the AFT. The cooling age is younger at the core of the Los Cobardes anticline at the level of the Girón Fm., and successively older outwards (Figure 5.9). This indicates that the youngest stratigraphic units cooled first and the older units in the stratigraphic sequence (Girón Fm.) cooled after. The central age of the AFT does not show a clear tendency.

Also, what can be observed from the central age is that the only samples with a cooling age younger than the stratigraphy age are the units located in the core of the Los Cobardes anticline (Jurassic units) as is shown in Figures 5.6 and 5.7, which means that FT from the Jurassic units (Girón Fm.) were partially reset (more than the other younger units).

The location of the FT samples is shown in the structural sections of the Sogamoso River above and the Barichara- San Vicente de Chucuri section below (Figure 5.11).

On the left side the interpretation was made using only surface information and on the right it was constructed using seismic information and surface information, the latter allowed to observe in more detail. Two faults were identified and contrasting values of AFT can be observed on both sides of the fault: at the hanging wall (sample JG-P3-32) with a minimum age of 1.4±0.71 Ma (central age 2.8±0.33 Ma) and in the foot wall (sample JG-P3-42) with a minimum age of 4.4±2.3 Ma (central age 32.3±4.6 Ma), which I interpreted as the last movement of the hanging block with regards to the foot wall.

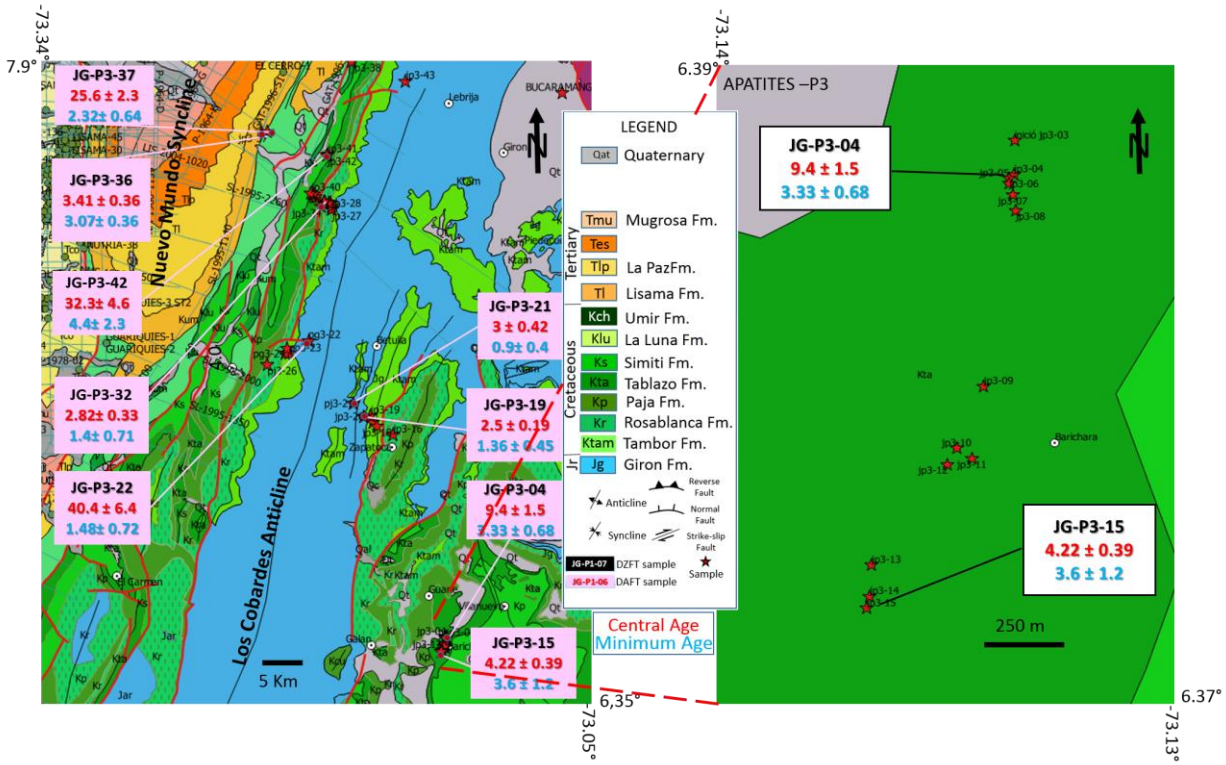

Figure 5.10*- Map showing the location of AFT ages in the Northern section Barichara- Bucaramanga.*

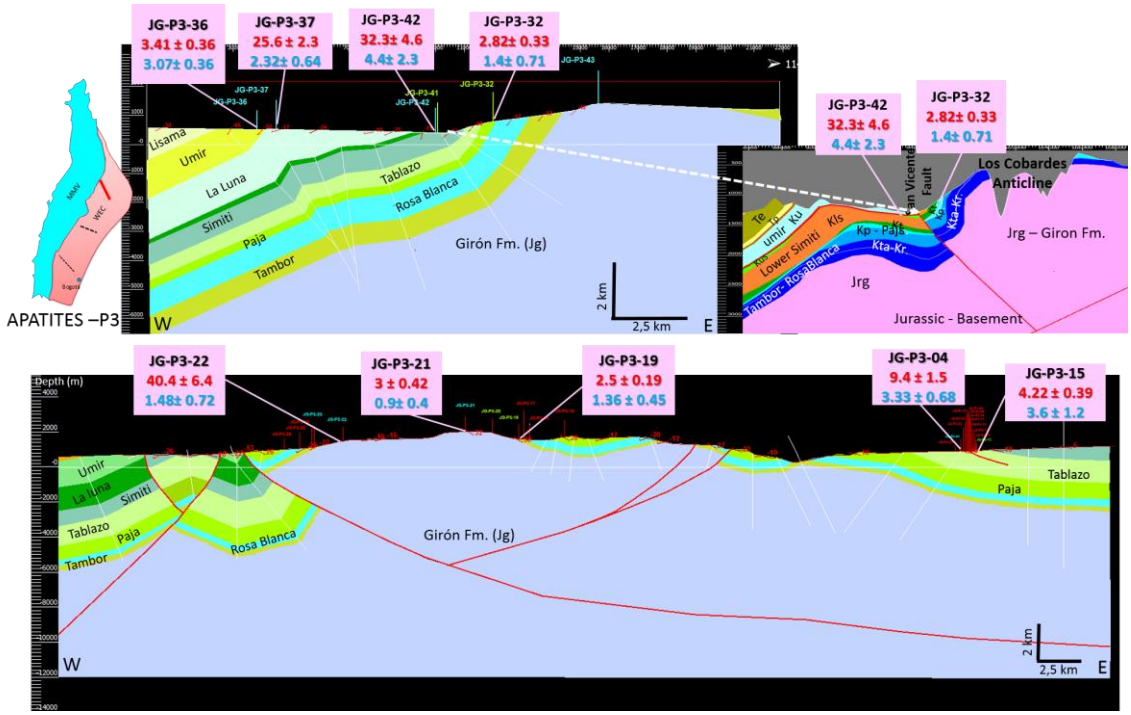

Figure 5.11- *Structural sections (this work) in the northern area (figure 5.1), above is shown the section in the Sogamoso River and below is shown the Barichara- San Vicente de Chucuri section, both sections were built using surface information, the structural section from the Sogamoso River is also shown above to the right, built using structural dips from surface and seismic information which allowed to interpret a subsurface structural section in detail, where one of the important fault is identified and its movement is consistent with the AFT ages (minimum and central) from samples JG-P3-32 and JG-P3-42.*

5.5.2 Central Section

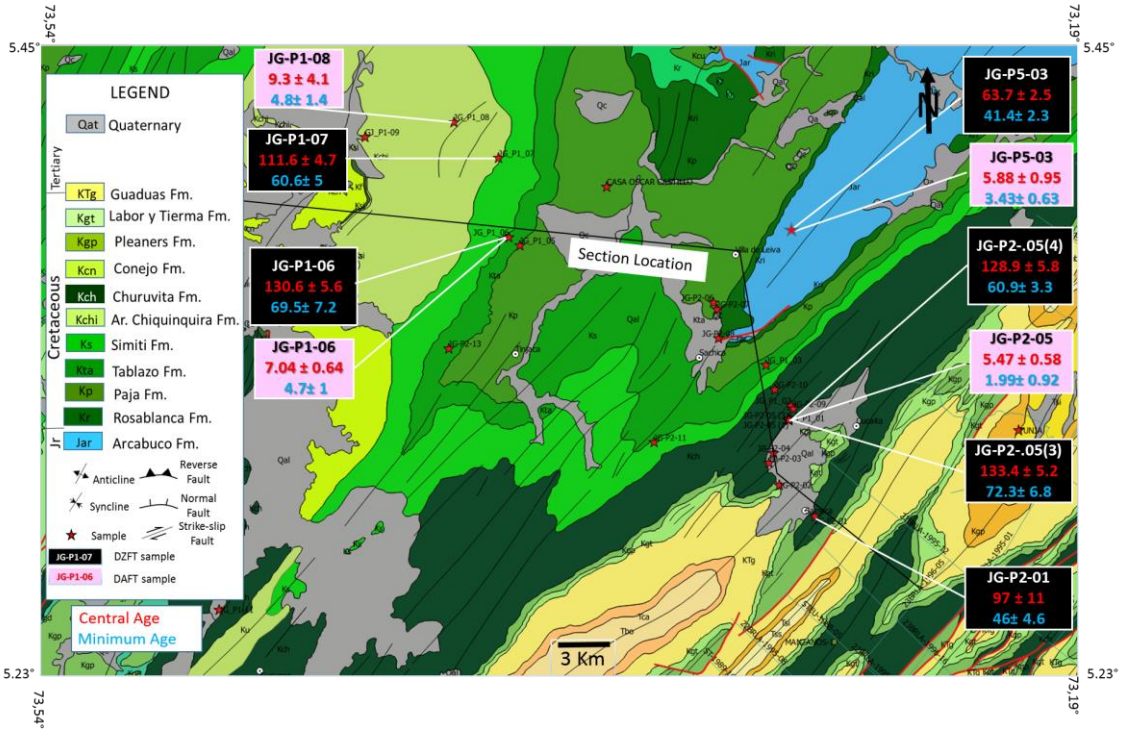

Figure 5.12- *Map showing the location of the apatites and zircon samples in the Central section: Villa de Leyva - Chiquinquira.*

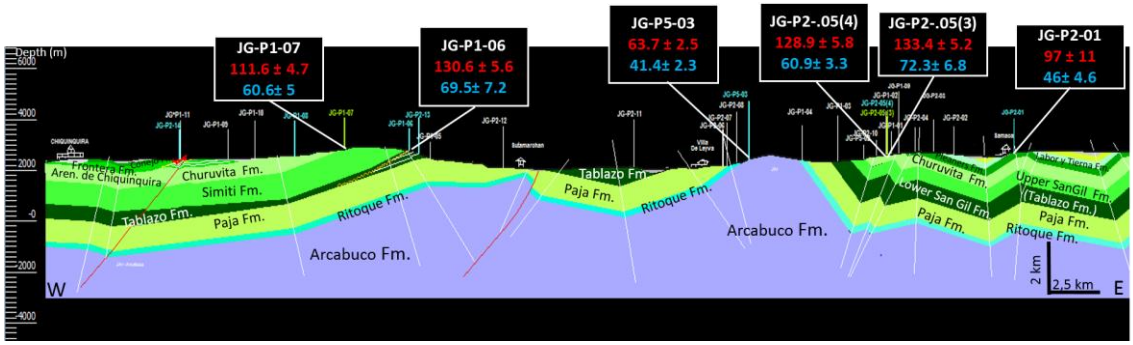

Figure 5.13*- Structural section in the Northern section Villa de Leyva - Chiquinquira, showing the location of the ZFT ages.*

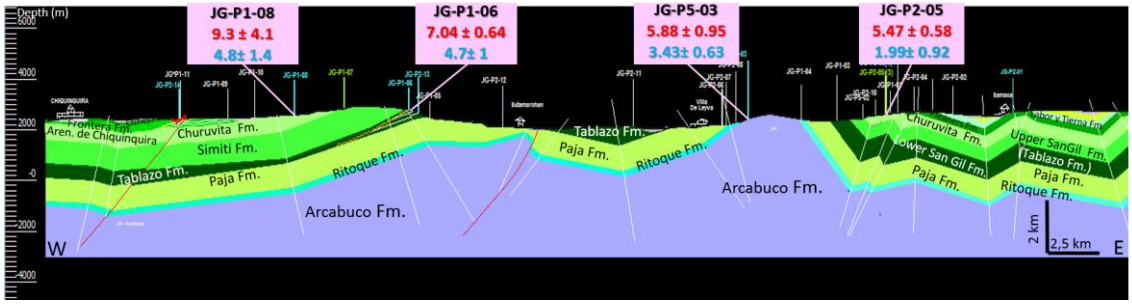

Figure 5.14*- Structural section in the Northern section Villa de Leyva - Chiquinquira, showing the location of the AFT samples.*

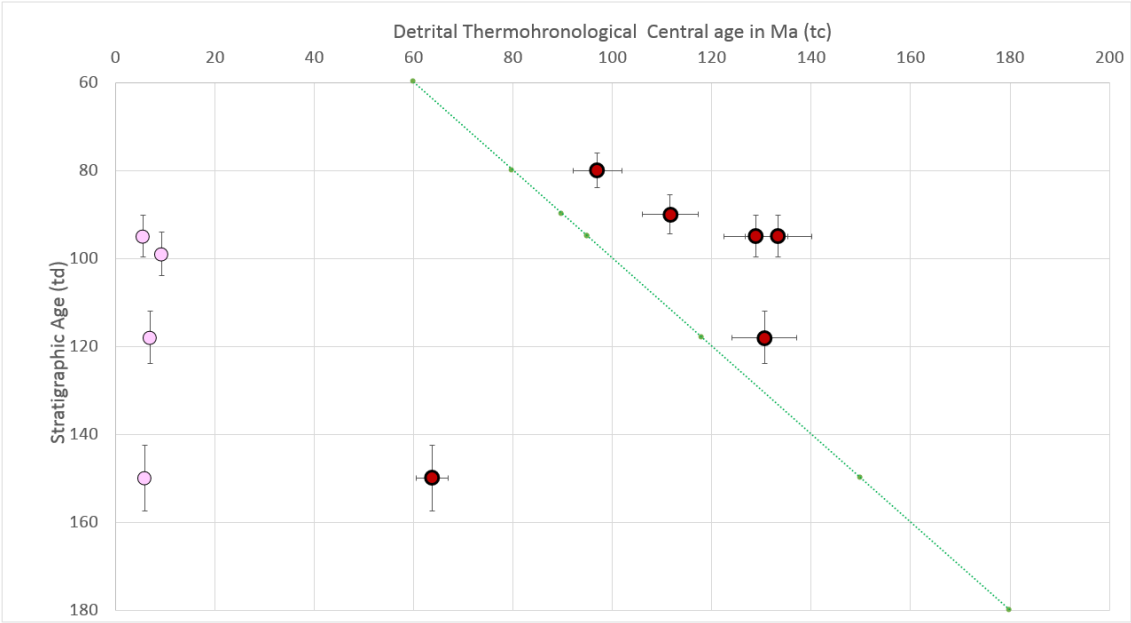

Figure. 5.15*- Graph showing detrital thermochronological central age (tcc) on the x-axis versus stratigraphic age (td) on the y-axis. Above raw data, note how the oldest Jurassic ages are in the partial annealing zone, while the samples from the lower Aptian to Paleocene units are not totally annealed. This probably shows that the Jurassic samples (Girón Fm.) had reached the partial annealing zone (PAZ).*

For the central section, six zircon and four apatite samples were analyzed. The ZFT data is shown on table 5.4 and the AFT data on Table 5.5.

In the Villa de Leyva-Chiquinquira structural section constructed from field data in this work, the ZFT ages are shown in Figure 5.13 and the AFT ages in Figure 5.14. The central and minimum ZFT ages show a clear tendency to younger ages from the flanks to the core of the Arcabuco anticline (Figure 5.16).

I suggest that the deformation associated to these ages very likely occurred during the cooling events, which will be discussed below with t-T models in this chapter. Nevertheless, the AFT central and minimum ages are increasing from the east to west, showing a different behavior than that of the ZFT ages. The behavior of the AFT ages seems to reflect a syn-deformation cooling.

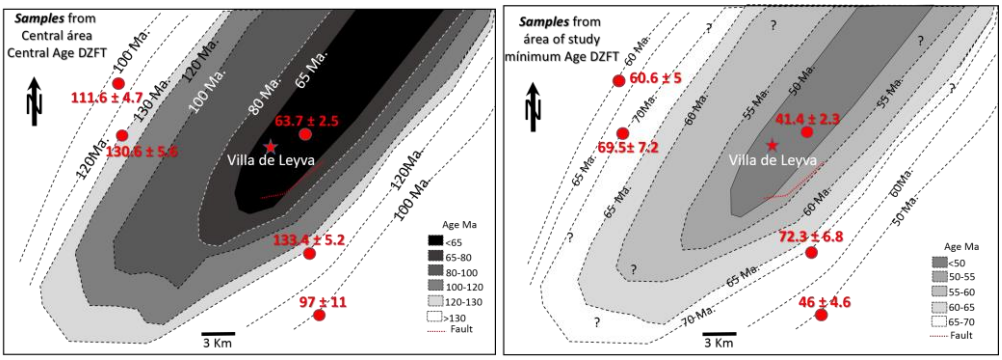

Figure 5.16 *- The map on the left shows central age of ZFT for the samples in the central area of study, note that the ZFT age tends to decrease towards the central part of the Arcabuco Anticline, where the Jurassic units are present (Figure 5.14 shows the same behavior). The map on the right shows the minimum age of DZFT, note that also at the center of the Arcabuco Anticline the age tends to decrease; however at the right and left side of the structure the central and minimum age also decrease.*

5.5.3 Southern Section

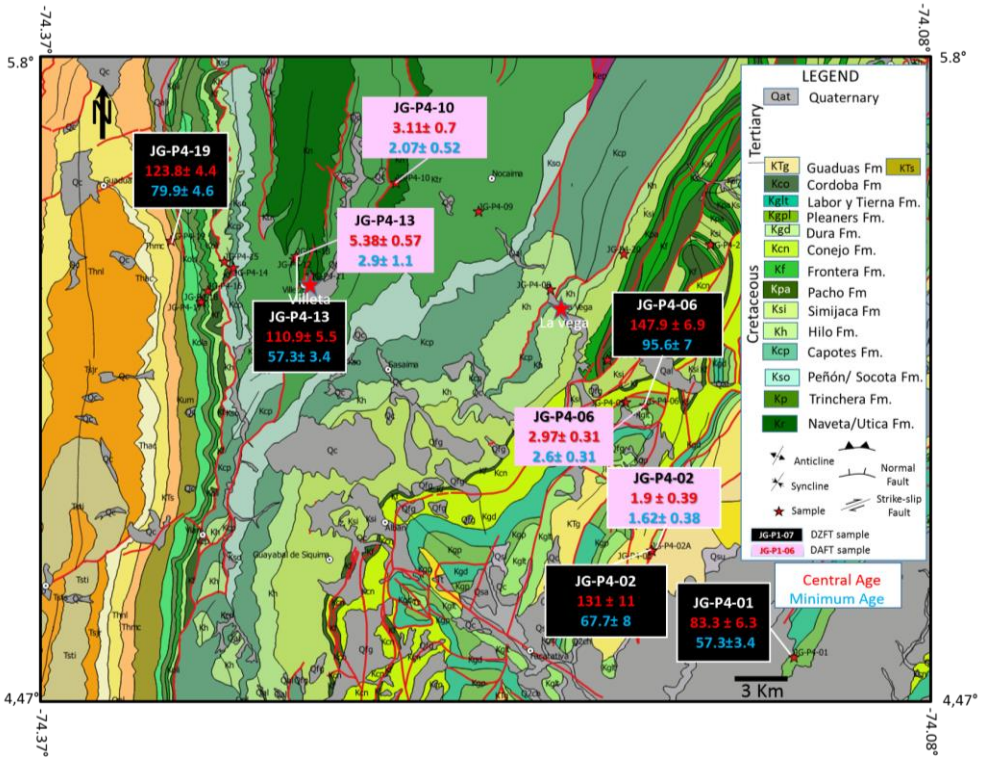

Figure 5.17*- Map showing the location of the AFT and ZFT ages in the Southern section La Vega-Villeta.*

For the southern section five zircon samples (Table 5.6) and four apatite samples (Table 5.7) were analyzed. The locations of the samples are shown in the maps of figures 5.1 and 5.17 and in the structural sections in figures 5.18 (zircons) and 5.19 (apatite).

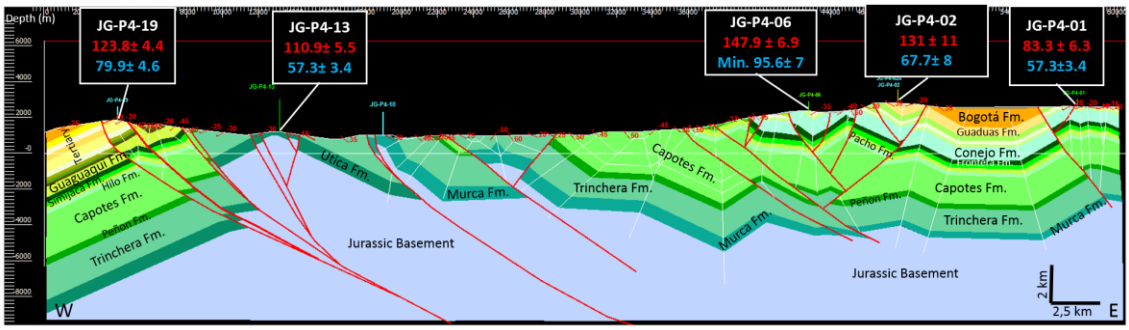

Figure 5.18*- Structural section in the Northern section La Vega-Villeta, showing the location of the ZFT ages.*

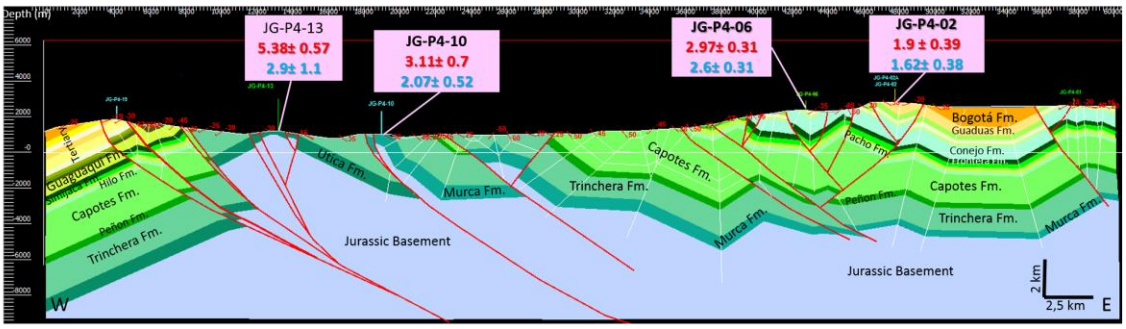

Figure 5.19*- Structural section in the Northern section La Vega-Villeta, showing the location of the AFT ages.*

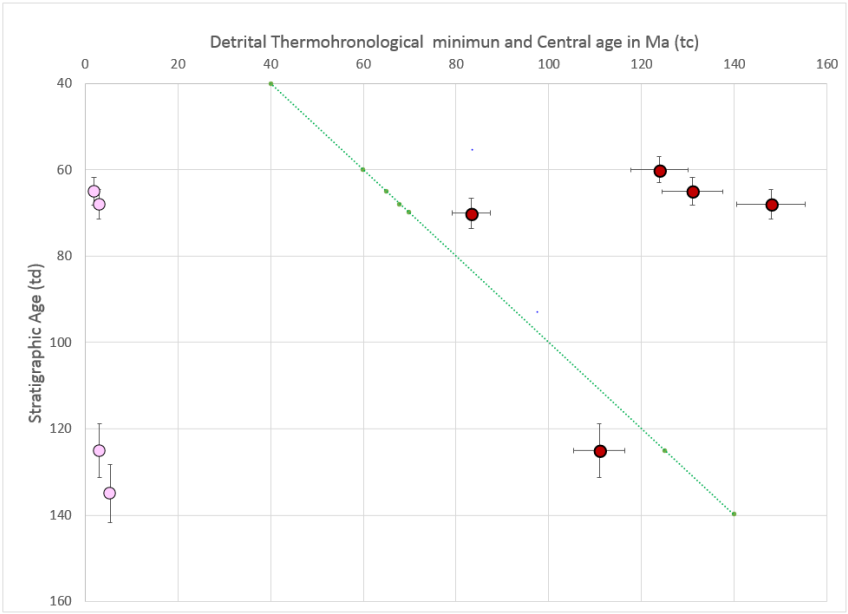

Figure. 5.20. *Graph showing detrital thermochronological central age (tcc) on the x-axis versus stratigraphic age (td) on the y-axis. Above raw data, note how the oldest DZFT (red point) from the lower Aptian age are in the resetting zone, while the samples from Campanian to Paleocene are not resetting. That probably shows that the Aptian samples (Giron Fm.) had reached the partial retention zone (PRZ) or partial annealing zone (PAZ).*

In the La Vega-Villeta section the behavior observed from ZFT ages is a little more complex than that observed in the central and northern sections, showing two different tendencies: One of these towards the Villeta anticline, where the Trinchera/Utica Formations of lower Cretaceous age are present (Figure 3.4 and 5.17). In this area central and minimum age from ZFT tends to decrease towards the core of the Villeta anticline; the second tendency is that the central and minimum ZFT age tends to decrease towards the east (to the right on the maps - Figure 5.21). In general, as is expected, the ZFT ages tend to decrease toward the core of the anticlines where older units of these folds are present (Figures 5.17 and 5.18). In the case of AFT, there is no clear trend that we can observe related with the core of the anticlines, nevertheless could be related with the recent displacement of local faults (Figure 5.19).

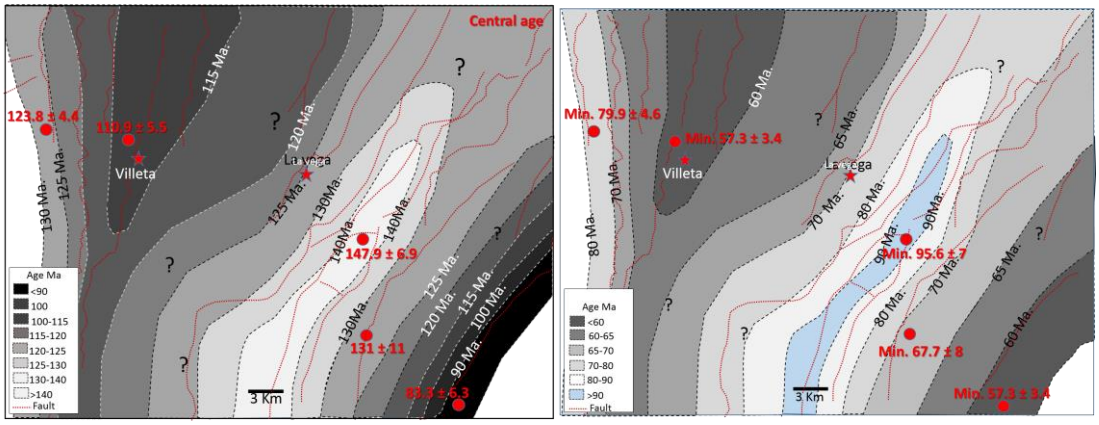

Figure 5.21 *- At the left is showing the map of the central age of the ZFT, for the samples from the Southern area of study, note that the ZFT age tends to decrease towards the core of the Villeta Anticline, where the Lower Cretaceous units are present (Trinchera/Utica), the section in Figure 5.18 shows the same behavior. At right is showing the map of the minimum age of the ZFT, note that the minimum age in the Villeta Anticline tends to decrease; however at the east of the map the central and minimum age also decrease, showing that thermochronological age values always tend to decrease in older units.*

From the northern (Figure 5.8), central (Figure 5.15) and southern (Figure 5.20) areas of the western Eastern Cordillera (WEC) I show lag-time plots of detrital ZFT of data collected from the three areas assessed. In the graphs showing detrital ZFT age versus stratigraphic age, it is noted that the oldest stratigraphic units in each section are partially or totally reset; in the northern and central area this corresponds to Jurassic units (Girón Formation and Arcabuco Formation respectively), and in the south to rocks from the Hauterivian (Murca Formation). However, on the other hand, the young units at the northern, central, and for the southern areas are from the Barremian-Valangenian to Paleocene and were also partially reset as is shown by the peak age in Figure 5.5 (Tables 5.2 -5.7).

In this way, since all the samples suffer from partial or total annealing, it is not possible to determine the exhumation rate of stratigraphic units during the basin inversion, because it is not possible to stablish a lag time. However, the totally annealing fission track ages from AFT could provide the timing of basin inversion and rates of exhumation but not the ZFT data.

5.6. Vitrinite Reflectance (Ro)

From Ro we can determine the maximum paleo-temperature and temperature gradient (Tables 5.8 and 5.9).

Sample	Stratigraphic Unit	Age Stage	Age (Ma)	Ro (%)	Tmax* °C	Source
RS-G26 - Nuevo Mundo	Esmeraldas Fm.	Upper Eocene	37	0.53	84.3	Gomez, 2001
RS-G13 - Nuevo Mundo	La Paz Fm.	Lower Eocene	51	0.55	87.3	Gomez, 2001
RS-PL1 - Nuevo Mundo	Lisama Fm.	Maastrihtian-Campanian	65.5	0.48	76.3	Gomez, 2003
N.D.† - Nuevo Mundo	Umir Fm.	Campanian_Maastrichtian	70	0.53	84.3	Rangel et al., 2002
CE-Umir - Nuevo Mundo	Umir Fm.	Campanian_Maastrichtian	70	0.61	95.6	Ecopetrol-ICP, 2003
CE-Luna - Nuevo Mundo	La Luna Fm.	Turonia-Santonian	87	0.77	114.4	Ecopetrol-ICP, 2003
CE-Simiti - Nuevo Mundo	Simiti Fm.	Albian-Cenomanian	99.6	0.82	119.5	Ecopetrol-ICP, 2003
726.28 - Villeta Anticlinorium	Supata/Frontera (Shale)	Turonian	90	4.52	257.1	Gomez, 2001
726.29 - Villeta Anticlinorium	Utica	Barremian	127	6.42	285.4	Gomez, 2001
726.30 - Villeta Anticlinorium	Frontera/Olini (Shale)	Turonian	90	1.36	160.3	Gomez, 2001
726.31 - Villeta Anticlinorium	Buscavidas/Cimarrona	Middle Maastrictian?	65	1.13	145.3	Gomez, 2001
660.57 - W. Guaduas Sync.	Base of San Juan de Rio s	Upper Eocene	15	0.58	91.6	Gomez, 2001
660.65 - W. Guaduas Sync.	Buscavidas	Middle Maastrictian?	67	0.60	94.3	Gomez, 2001
660.38 - Los Cobardes Ant.	Bocas	Triassic-Jurassic	199	5.52	273.3	Gomez, 2001
726.21 - Catalina -1				0.56	88.7	Gomez, 2001
730.3.1 - Infantas - 1613	Mugrosa.Colorado	Oligocen	29	0.44-2.14	196.8	Gomez, 2001
660.27 - La Cira-Infantas	Real Group	Middle Miocene	12	0.44	69.3	Gomez, 2001
660.24 - E. Nuevo Mundo	Top Colorado Formation	Oligocen	23	0.46	72.9	Gomez, 2001
660.37 - Nuevo Mundo	Umir ????	Campanian_Maastrichtian	70	0.6 - 1.53	169.8	Gomez, 2001
660.18 - Nuevo Mundo	Lower Mugrosa	lower Oligocen	30	0.50	79.6	Gomez, 2001
Ro210110-27 - Opon	Lower La Paz	Lower Eocene	51	0.66	102.0	Moreno et al (in Caballero 2013)
1072-123 -Guaduas Area	Umir	Campanian_Maastrichtian	70	1.4	162.6	Moreno et al (in Caballero 2013)
10GU65 -Guaduas Area	Socota	Albian-Cenomanian	106	5.38	271.2	Moreno et al (in Caballero 2013)
10GU48 -Guaduas Area	Trincheras	Aptian-Albian	112	1.27	154.8	Moreno et al (in Caballero 2013)
10GU57 -Guaduas Area	Trincheras	Aptian-Albian	112	1.98	190.6	Moreno et al (in Caballero 2013)
10GU46 -Guaduas Area	Naveta	Barremian	127	1.22	151.5	Moreno et al (in Caballero 2013)
10BY07 - Arcabuco Anticline	Tablazo	Aptian-Albian	112	3.5	236.5	Mora et al. (2013)
10BY10A - Arcabuco Anticline	Paja	Barremian	127	3.5	236.5	Mora et al. (2013)
10BY35 - Arcabuco Anticline	Paja	Barremian	127	4	247.3	Mora et al. (2013)
10BY34 - Arcabuco Anticline	Paja	Barremian	127	4.5	256.8	Mora et al. (2013)
GC1063-20 - Cagui-1	Colorado	Oligocen	23	0.43	67.4	Caballero et al. (2013)
GC1063-21 – Cagui	Esmeraldas	Upper Eocene	37	0.53	84.3	Caballero et al. (2013)
GC1063-25 ST - Cagui	Rosablanca	Valangenian	137	1.23	152.2	Caballero et al. (2013)

Tabla 5.8 *- Vitrinite reflectance (Ro) collected by several authors (Gomez, 2001; Caballero, 2013; Mora et al., 2013; Moreno et al., 2013), the maximum temperatures (Tmax*) were calculated using Equation 1, shown in the text (after Baker and Pawlewicz, 1994).*

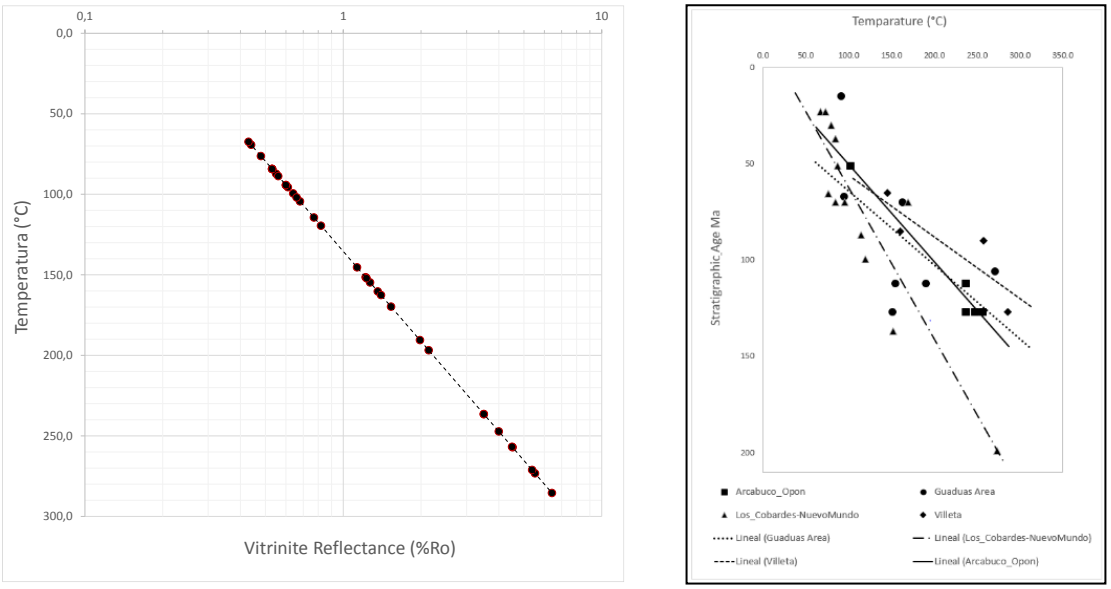

Figure 5.22 *- Semilogarithmic plots of vitrinite reflectance and equivalent maximum temperature (left), and temperature vs age. The maximum temperatures were calculated using Eq. 1 shown in the text. Suite of vitrinite reflectance data collected by various researchers (Gomez, 2001; Caballero, 2013; Mora et al., 2013; Moreno et al., 2013).*

Sample	Stratigraphic Unit	Age Stage	Age (Ma)	Ro (%)	Tmax* °C	Source
YUMECA-1	Umir	Campanian_Maastrichtian	70	0.41-0.91	63.6	Compilated ICP
YUMECA-1	Simiti Fm.	Albian-Cenomanian	99.6	0.81-0.97	118.5	Compilated ICP
YUMECA-1	Tablazo	Aptian-Albian	112	1.02	137.1	Compilated ICP
YUMECA-1	Paja	Barremian	127	1.07	140.9	Compilated ICP
YUMECA-1	Rosablanca	Valangenian	137	1.09-1.54	142.4	Compilated ICP
Norean-1	Rosablanca	Valangenian	137	0.7-1.52	106.7	Compilated ICP
Norean-1	Paja	Barremian	127	0.55	87.3	Compilated ICP
Norean-1	Tablazo	Aptian-Albian	112	0.54-0.9	85.8	Compilated ICP
Norean-1	Simiti Fm.	Albian-Cenomanian	99.6	0.38-0.99	57.5	Compilated ICP
Norean-1	La Luna Fm.	Turonia-Santonian	87	0.41-1.43	63.6	Compilated ICP
Norean-1	Umir	Campanian_Maastrichtian	70	0.52-0.98	82.7	Compilated ICP
Norean-1	Real Group	Middle Miocene	12	0.29-0.37	35.7	Compilated ICP
Infantas-1613	La Luna Fm.	Turonia-Santonian	87	0.53-1.38	84.3	Compilated ICP
Infantas-1613	Simiti Fm.	Albian-Cenomanian	99.6	0.93-1.10	129.6	Compilated ICP
Infantas-1613	Paja	Barremian	127	1.77	181.5	Compilated ICP
Infantas-1613	Rosablanca	Valangenian	137	2	191.4	Compilated ICP
Escuela-1	La Luna-1	Turonia-Santonian	87	0.38-1.18	57.5	Compilated ICP
Escuela-1	Villeta -Coniacian	Coniacian	87	2	191.4	Compilated ICP
Escuela-1	Villeta -Santonian	Santonian	84	2.07	194.2	Compilated ICP
Cordillera	La Luna	Turonia-Santonian	87	0.58-0.80	91.6	Compilated ICP
Cordillera	Guaduas	Maastrihtian-Paleocene	65.5	0.43-1.53	67.4	Compilated ICP
Cocuyo-1	La Luna	Turonia-Santonian	87	0.46-0.61	72.9	Compilated ICP
Cocuyo-1	Umir	Campanian_Maastrichtian	70	0.47	74.6	Compilated ICP
Cascajales-1	La Luna Fm.	Turonia-Santonian	87	0.93	129.6	Compilated ICP
Cascajales-1	Tablazo	Aptian-Albian	112	1.19	149.5	Compilated ICP
Cascajales-1	Paja	Barremian	127	1.24	152.8	Compilated ICP
Cascajales-1	Rosablanca	Valangenian	137	1.44	164.9	Compilated ICP
Casabe-199	Colorado	Oligocen	23	0.6	94.3	Compilated ICP
Casabe-199	La Luna	Turonia-Santonian	87	0.58-1.01	91.6	Compilated ICP
Casabe-199	Simiti	Albian-Cenomanian	99.6	0.81-1.37	118.5	Compilated ICP
Casabe-199	Tablazo	Aptian-Albian	112	0.94-1.74	130.5	Compilated ICP
Casabe-199	Paja	Barremian	127	1.05-1.59	139.4	Compilated ICP
Casabe-199	Rosablanca	Valangenian	137	1.16-2.08	147.5	Compilated ICP
Casabe-199	Tambor	Berriasian	143	1.12	144.6	Compilated ICP
Bosques-1	Real Group	Middle Miocene	12	0.25	23.7	Compilated ICP
Bosques-1	Colorado	Oligocen	23	0.44	69.3	Compilated ICP
Bosques-1	Simiti	Albian-Cenomanian	99.6	0.77-1.25	114.4	Compilated ICP
Bosques-1	Tablazo	Aptian-Albian	112	0.97-1.31	133.0	Compilated ICP
Bosques-1	Paja	Barremian	127	1.69	177.8	Compilated ICP
Bosques-1	Rosablanca	Valangenian	137	0.94	130.5	Compilated ICP
Bosques-1	Tambor	Berriasian	143	1.08	141.7	Compilated ICP

Tabla 5.9 *- Vitrinite reflectance (Ro) collected by the ICP (Instituto Colombiano de Petróleo), the maximum temperatures (Tmax*) were calculated using Equation-1 shown in the text (after Baker and Pawlewicz, 1994).*

Table 5.8 shows published vitrinite reflectance data ranging from 0.43 for temperatures <68°C to 6.42 for maximum paleo-temperature of >285°C (Gomez, 2001; Caballero, 2013; Mora et al., 2013; Moreno et al., 2013). In table 5.9, vitrine reflectance values from the ICP collection range from 0.25 for temperatures <24°C to 2.08 for maximum paleo-temperature of >194°C. Table 5.10, vitrinite reflectance values from the RW-1, Infantas-1613 and Catalina -1 drill holes vary from 0.3 (temperatures <40°C) to 2.08 for maximum paleo-temperatures of >194°C.

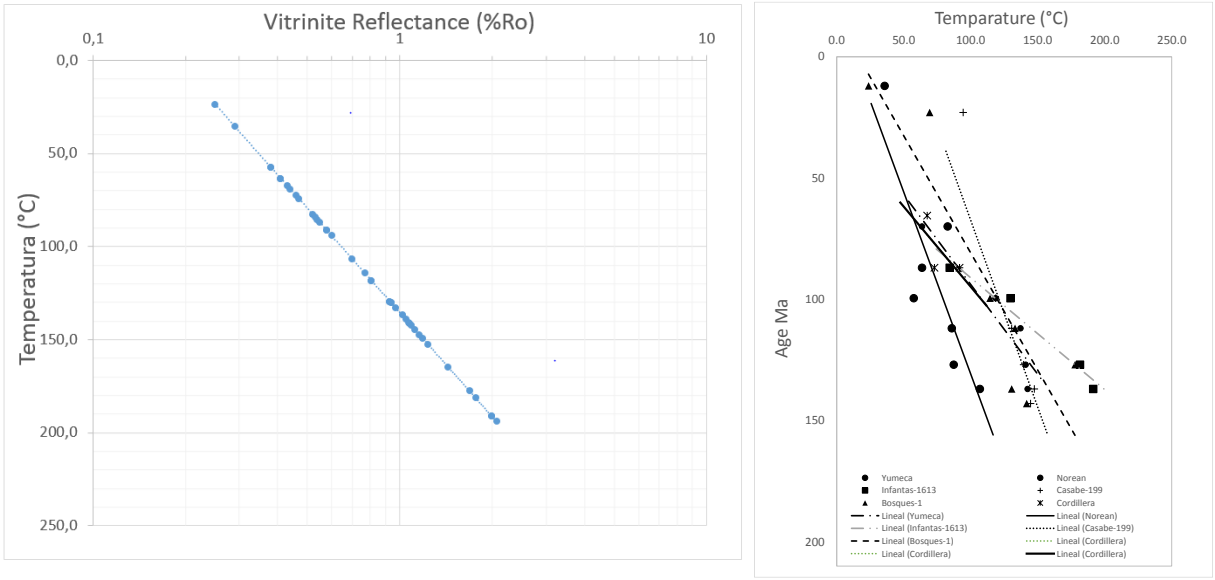

Figure 5.23 *- Semilogarithmic plots of vitrinite reflectance and equivalent maximum temperature (left), and temperature vs age. The maximum temperatures were calculated using Eq. 1 shown in the text. Suite of vitrinite reflectance data collected by the ICP, mainly from samples from the MMV.*

La Luna-1

Tope Depth ft	Form Name	Ro_ave %	Ro_min %	Ro_max %	Tmax °C
9406	LA LUNA	0.707	0.661	0.754	107.5
9545	LA LUNA	0.72	0.695	0.768	109.0
9675	LA LUNA	0.684	0.62	0.736	104.9
9910	LA LUNA	0.691	0.623	0.739	105.7
10041	LA LUNA	0.721	0.62	0.783	109.1
10253.83	LA LUNA	0.836	0.729	0.903	121.0
10505	LA LUNA	0.779	0.716	0.906	115.3
10733	LA LUNA	0.889	0.561	1.115	126.0
10846.7	LA LUNA	0.926	0.776	1.001	129.3
11130.5	LA LUNA	0.883	0.678	1.194	125.4
11522	LA LUNA	1	0.93	1.140	137.9
11714	LA LUNA	1	1	1.150	141.2

Infantas 1613

Tope Depth ft	Form Name	Ro_ave %	Ro_min %	Ro_max %	Tmax °C
4290	LA LUNA	0.44	0.3	0.58	69.3
4510	LA LUNA	0.51	0.41	0.62	81.2
5165	LA LUNA	0.61	0.46	0.74	95.6
5195	LA LUNA	0.68	0.54	0.88	104.4
6665	SIMITI	0.72	0.55	0.87	109.0
7720	SIMITI	0.77	0.74	0.83	114.4
9495	PAJA	1.72	1.68	1.76	179.2
10400	ROSABLANCA	1.86	1.68	2.02	185.5
10935	SANTOS	2.14	1.85	2.65	196.8

Catalina - 1

Tope Depth ft	Form Name	Ro_ave %	Ro_min %	Ro_max %	Tmax °C
2540	UMIR	0.56	0.4	0.71	88.7
3000	UMIR	0.55	0.44	0.66	87.3
3840	LA LUNA	0.55	0.41	0.69	87.3
4616	LA LUNA	0.52	0.37	0.71	82.7
5529	SIMITI	0.56	0.44	0.68	88.7
6082	LOS SANTOS *	1.32	0.88	2.04	157.9
6350	LOS SANTOS *	1.76	1.44	2.08	181.1

Table 5.10 *- Vitrinite reflectance (Ro) collected by the ICP (Instituto Colombiano del Petróleo), the maximum temperatures (Tmax*) were calculated using Equation-1 shown in the text (after Baker and Pawlewicz, 1994). The tables also have values related to the temperature. Compiled from well description in Gomez 2001 volume II.*

In all cases (figures 5.22 to 5.24), the temperature (Tmax) increases directly with the stratigraphic age (Figures 5.22 and 5.23). In figure 5.24 the relation between Ro or Tmax increases proportionally with depth, as is shown for the RW-1, Infantas-1613 and Catalina-1 wells.

Ro values of ~ 0.8 correspond to temperatures of about 117-120°C (Burnham and Sweeney, 1989). This Ro value is equivalent to the AFT total annealing temperature.

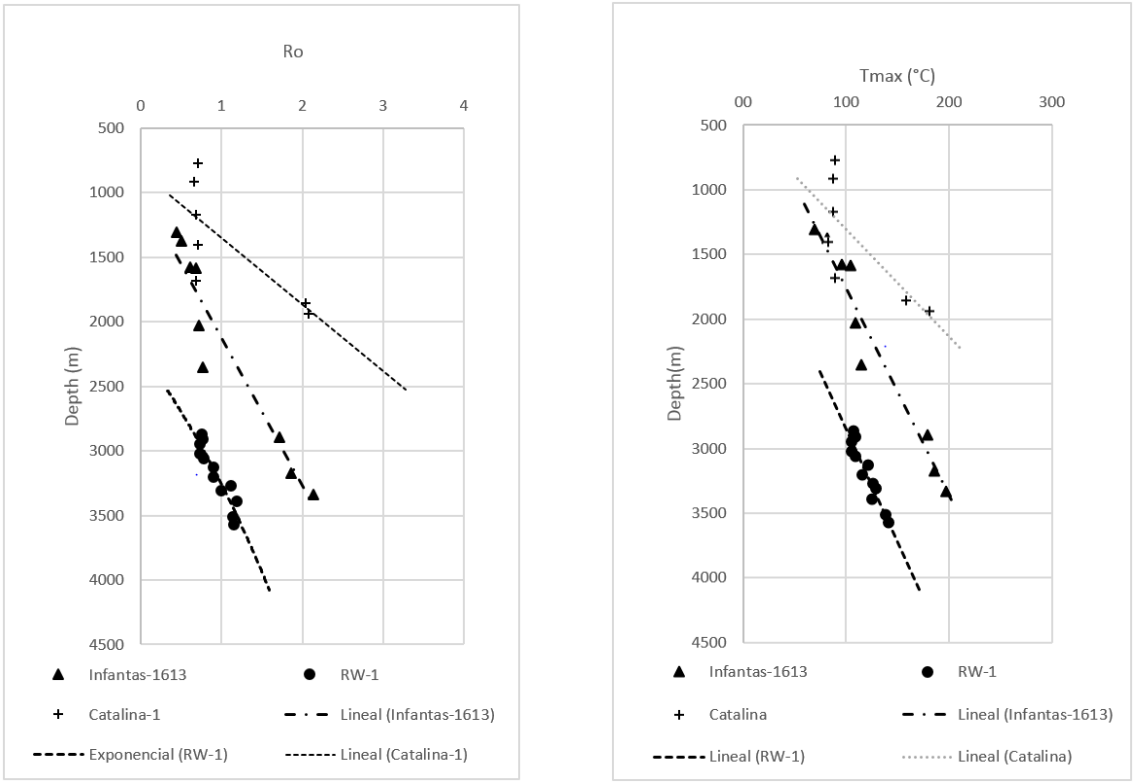

Figure 5.24 *Vitrinite Reflectance (Ro) and temperature (Tmax) vs depth. The maximum temperatures were calculated using Eq. 1 shown in the text. Suite of vitrinite reflectance data collected by the ICP, mainly from samples in the MMV from the wells RW-1, Infantas-1613 and Catalina-1.*

According to the data from the wells RW-1, Infantas-1613 and Catalina-1 and considering only one lineal tendency, the temperature gradient in the position of the wells RW-1 and Infantas-1613 is ~57.1°C/km to 57.4°C/km respectively and in the position of the well Catalina-1 is around ~121.5°C/km (Figure 5.24). However, the correlation coefficient (Temperature/Depth) from the wells RW-1 and Infantas-1613 is 0.95 to 0.90, while the coefficient for Catalina-1 is as low as 0.56. The location of the samples listed in tables 5.8, 5.9 and 5.10 are shown on the map of figure 5.27.

Figure 5.25 represents the Tmax °C calculated using Ro data collected from several sources (Tables 5.8 to 5.10) versus stratigraphic age. This figure shows the maximum paleo-temperature that different stratigraphic units experienced. In this figure I separated and ploted the Tmax from north to south to observe the paleo-temperature's behavior. It was observed that the lowest paleo-temperature was reached in the northernmost area (Norean-1) and this progressively rose towards the south zone where the highest paleo-temperature was reached. These high temperatures (central and south

zones) are probably due to one of the following reasons: 1) Sediment supply was enough to reach these paleo-temperatures. 2) The central and southern areas were affected by magmatic activity that increased the temperature till values as high as 285°C in rock.

An additional observation is that in the central and southern sections in the sediments deposited close to about 73-70 Ma, the paleo-temperature goes from 170 °C to 90 °C, and for the Villeta anticline area the paleo-temperatures behave in a more complex way in rocks deposited between 110 to 85 Ma.

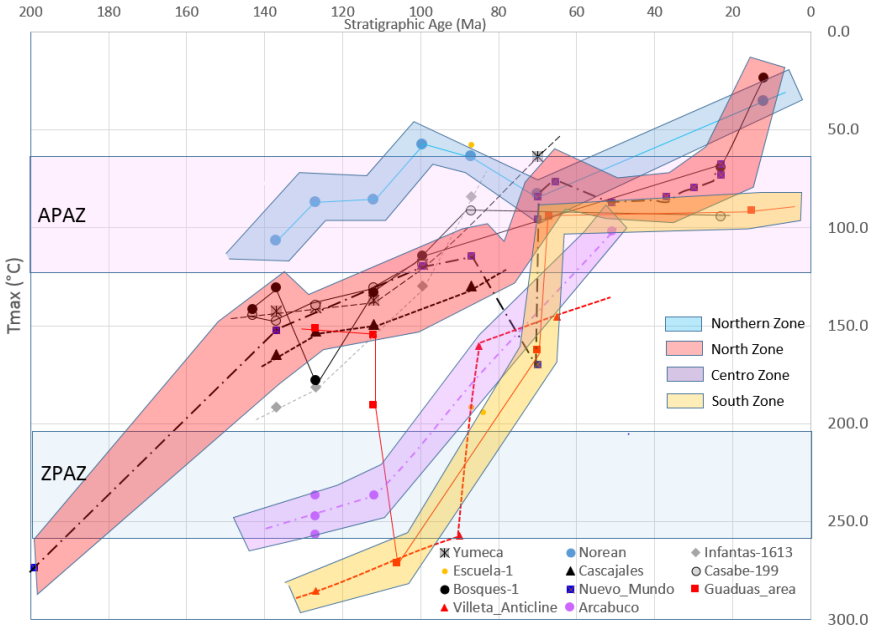

Figure 5.25 *- Cross plot of Stratigraphic age Vs Tmax, organized by sectors to assess the behavior of different zones in the basin: Yumeca well, Infantas 1613 well, Cascajales well, Bosques-1, Norean, Guaduas area, Arcabuco, Escuela-1; Casbe-199, Nuevo Mundo, and Villeta anticline. The APAZ (pink) and ZPAZ (light blue) are highlighted in the graph.*

The relation between paleo-temperatures and present-day temperatures is shown in Figure 5.26. The maximum paleo-temperatures are determined from samples from the wells (Tables 5.9 and 5.10). These maximum paleo-temperatures are also shown for the MMV in Figure 5.25 in which the maximum paleo-temperature in the central and southern zone can be observed. By comparing the paleo-geothermal gradient and present-day geothermal gradient, it is possible to interpret the cause of the high paleo-temperatures and the cause of the cooling to present temperature conditions.

In Figure 5.26, the presence of major unconformities during the Cretaceous in all the sections is shown (as is shown also in Dow W.G., 1976). The difference in paleo-thermal slopes probably suggests different thermal histories for the Cretaceous and Tertiary sections, reflecting (longer exposure time) a slower sedimentation rate in the Cretaceous (Dow W.G., 1976).

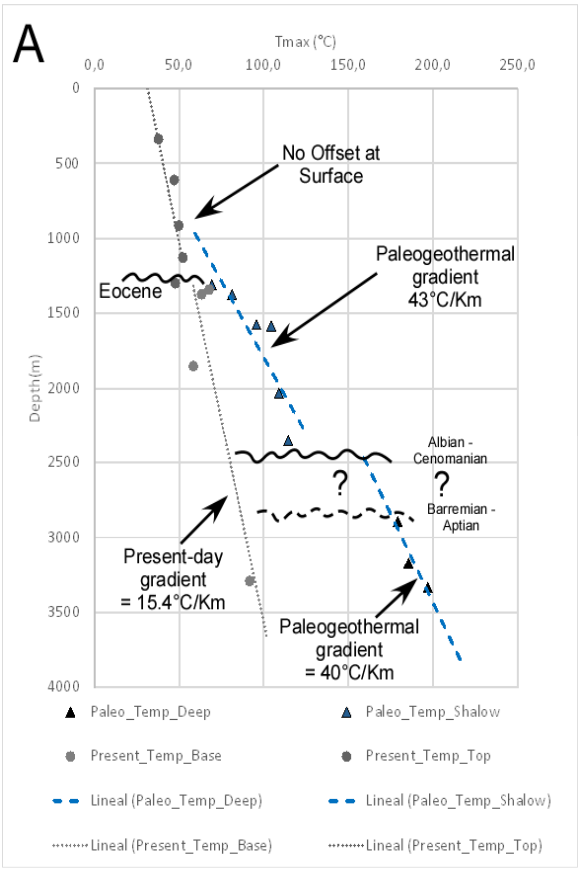

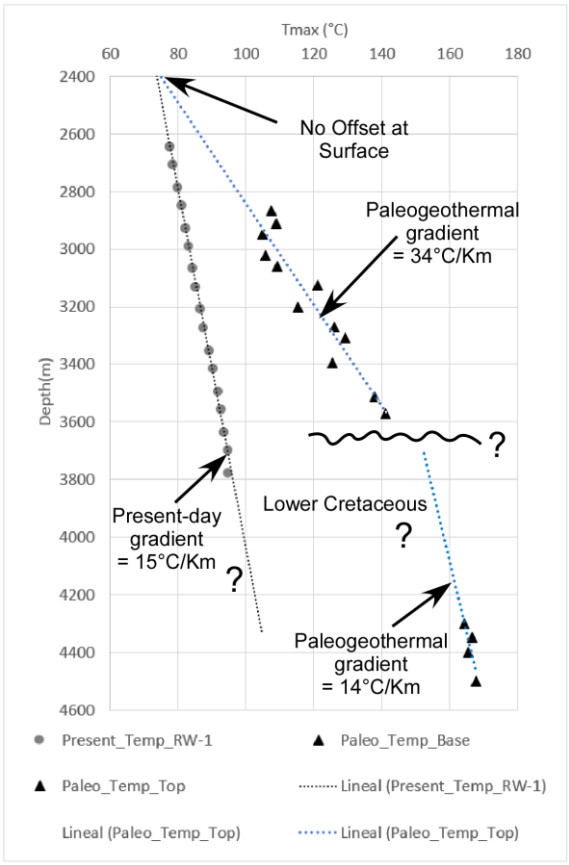

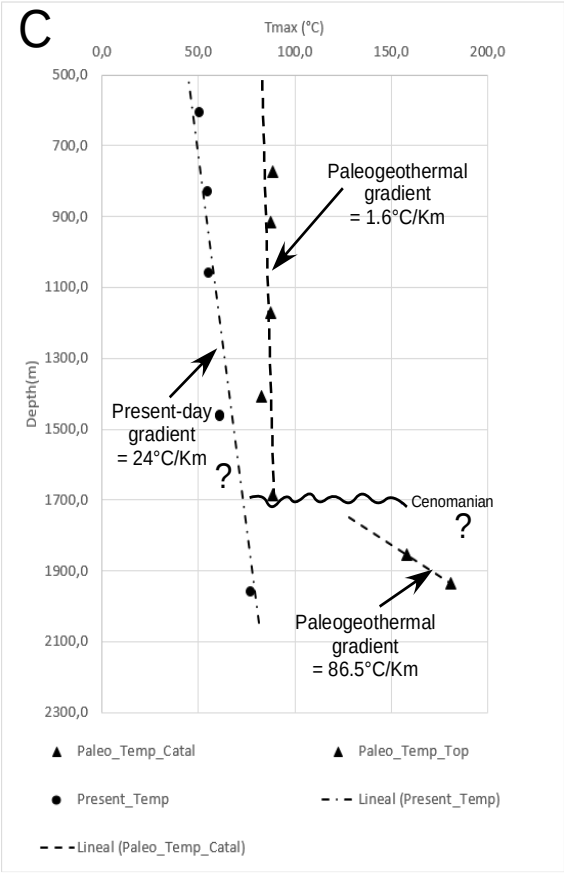

Figure 5.26. *Temperature vs depth plots for wells Infantas-1613 (A), RW-1 (B) and Cascajales-1 (C). The Paleotemperatures were greater than the present-day temperatures, in general in A, B and C the paleogradient presents two tendencies that mark an Albian-Cenomianian or earlier unconformity. The Paleogeothermal gradient line in A and B over the unconformity is greater than the present-day gradient and not offset at the surface. This indicates a drop in the geothermal gradient due to changes in heat flow which was responsible for cooling to the present temperature conditions. Two additional behavior differences between the paleogeothermal gradient and Present day gradient could indicate that the cooling must occur in response only to denudation (similar paleogeothermal gradient to the present-day gradient with an offset at the surface). A third possible case is if the cooling happens in response to both changes in the geothermal gradient and in denudation (O´Sullivan. 1999).*

As to the slope in the section over the Cenomanian in A and B (Figure 5.26), the paleo-gradients are higher than the present-day gradients with no offset at the surface. This probably means that the high temperatures are due to changes in the geothermal gradient, however in figure C this section showed a different behavior with a small paleo-gradient of 1.6°C/km while the preset-day gradient is of 24°C/km. In this case, cooling is probably a response to both factors (changes in geothermal gradient and denudation).

The plots shown in Figure 5.28 relate the central age for ZFT and AFT ages measured in this work with the Tmax calculated here from Ro. Also shown are samples for each region and the linear temperature tendencies region by region. The red reference lines show the lower limit of the PAZ (limit required to enter into a Total Annealing Zone-TAZ) and the blue reference lines show the upper limit of the PAZ.

In the northern zone (left in Figure 5.28), we observe that only older stratigraphic samples from the Girón Fm. (samples P3-43, 22, 21 and 20 in Table 5.2) suffered partial annealing because the heating was insufficient to produce complete annealing of pre-existing ZFT. For the northern area all samples were above red reference line of the TAZ (total annealing zone) which means that these samples were not totally reset.

The samples from the northern area, stratigraphically younger than ~140 Ma, corresponding to the Tambor, Paja, Tablazo, Simiti and Lisama formations, were never heated enough to suffer partial annealing in the ZPAZ. For sample JG-P3-36 from the Lisama Fm., heating was sufficient to fully anneal fission tracks in apatite before cooling during basin inversion. All apatite samples in this area were subjected to total or partial annealing as described above.

In the central zone, in the sample from the Arcabuco Fm, (JG-P5-03 in Table 5.4) the heating event was enough to anneal all pre-existing ZFT in this sample. In the sample from the Tablazo Fm. (JG-P1-06) the opposite happened: the heating was not enough to completely anneal all the pre-existing ZFT, as a result, in spite of the Tmax related with this sample (~240) that is shown in Figure 5.28, the ZFT age for this sample is probably older than the stratigraphic age. For the rest of the samples from Conejo, Churuvita and Simijaca formations (samples JG-P2-01, JG-P2-05, and JG-P2-07 see in Table 5.4) the heating was sufficient to completely anneal the AFT (samples in the TAZ).

The southern area probably has the most complex heating (Figure 5.28 – right); the sample form the Utica/Trinchera Fm (JG-P4-13 in Table 5.6) was probably totally annealed, as is shown in Figure 5.28 (right) located in the TAZ for zircons (below the red reference line). The rest of the samples (Table 5.6) stayed in the APAZ. In this zone the heating was also sufficient to completely anneal the AFT.

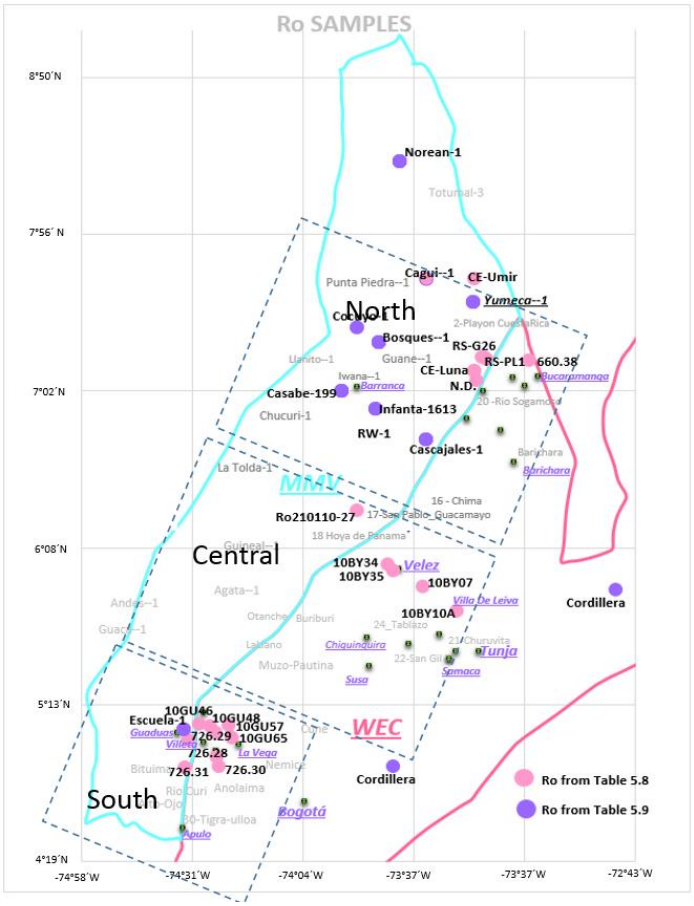

Figure 5.27 *- Map showing the distribution of Ro in all the area of study, the bubble colors correspond to Ro value samples from tables 5.8 and 5.9.*

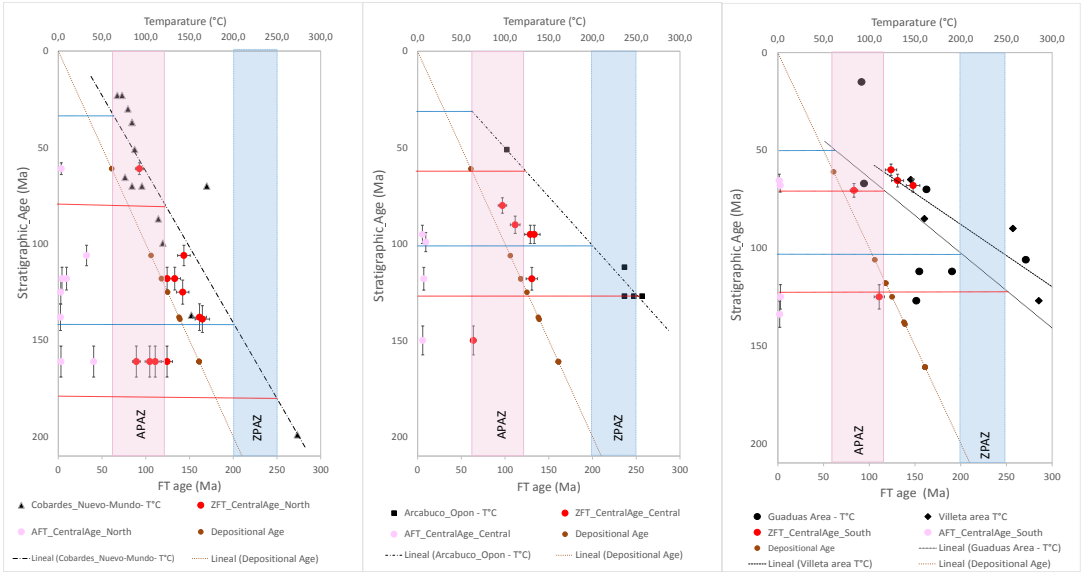

Figure 5.28 *– Plots of DAFT, DZFT and Temperature versus stratigraphic age, by sector: for the south (right); for the central (center) and for the north (left). The line of the stratigraphic age is shown in brown, and the linear tendency for temperature (T°C) is shown in a stippled black line. Also, shown is the Temperature from Ro.*

5.6.1 Discussion

Based on the previous plots (Figures 5.25 and 5.28) it is possible to conclude that the three thermal histories are different for the three sectors analyzed. Almost all samples are partially or totally annealed. Probably the southern section has the most complex history.

The partial or totally reset ZFT ages are probably due to one of these reasons: 1) According to our calculation of thermal gradients in the positions of the wells (from Ro data) RW-1 and Infantas-1613 (Figure 5.23), a burial at less between 3.5 to 4.5 km of sediment accumulation of Cretaceous deposits was necesary (4-6 km for Sanchez, 2012), and with regards to the AFT data, as much as 1.3 to 2 km of sediments or 2) Thermal anomalies due to magmatic activity as have been reported for example in the Villa de Leiva area (Bürgl, 1954) in the Paja Fm. (Forero and Sarmiento, 1982). In the Girón Fm. (Morales et al., 1968¸ Taborda, 1965), dacite porphyr cut the Tambor Fm. (Wards et al. 1973). In the south area of the study zone (Villeta zone) basic intrusions in the Cretaceous succession, that according to Fabre and Delayon (1983), and Moreno and Concha (1993) are small bodies (dikes and sills) of gabbroid, tholeite and alkalines with evidence of hydrothermal alteration in black shales of the lower Cretaceous (Fabre and Delaloye, 1983) indicating that these intrusions were located in the thinned lithosphere (Sarmiento, 2001), with incipient fusion of the mantle that permitted the intrusion.

Based on Tmax (Ro) different paleo-temperatures with less heating in the north (at the position of Norean-1) and stronger heating to the south, being higher in direction toward the south in Villeta-Guaduas area, are generally observed, (Figure 5.25).

The new AFT and ZFT data collected from Cretaceous to Paleocene sedimentary rocks are compared to the published data (Figure 5.27) from Gomez (2001), Gomez et al. (2003 and 2005), Parra et al. (2012), Sanchez et al. (2012) and Caballero et al. (2013), as is listed in tables 5.11a, 5.11b, 5.11c.

The comparison between paleo-geotemperatures and present-day temperatures gives an idea of the reason the presence of very high anomalous temperatures in some sectors in the MMV and WEC. It is observed that the paleo-temperatures were greater in all the wells (Infantas-1613 (A), RW-1 (B) and Cascajales (C)) than the present day temperatures. Two different tendencies are observed in all the cases shown in Figure 5.26; one at the Albian-Cenomanian limit or older and another over the Albian Cenomanian. These different tendencies marked the presence of unconformities at least at the Albian-Cenomanian time, in the Early-Albian/Cenomanian (Figure 5.26B) or Barremian – Aptian/Albian Cenomanian (Figure 5.26A) intervals. In Figures 5.26 A and B, below the unconformity the paleo-geothermal gradients are almost similar to what is observed in the present-day, contrary to what is observed in the well Cascajales-1 (Figure 5.26C). For the Paleo-geothermal gradients over the unconformity in Figure 5.26 (A, B) are higher than the present-day gradient and not offset at the surface, also in the well Cascajales-1 (Figure 5.26C) over the unconformity it is observed that the

paleo-thermal gradient is less than the present-day gradient or probably similar. The tendencies observed in Figures 5.26 A and B, probably indicate a drop in the geothermal gradient due to changes in heat flow. Finally the anomalous paleo-tendency observed in Cascajales-1 is a response to the change in the geothermal gradient and in denudation (O´Sullivan, 1999).

Apatite fission-track data from samples analysed with laser ablation-inductively coupled plasma -mass spectrometry (LA-ICP-MS)

Sample	Unit	Area Location	n	P(χ^2) %	Stratigraphic Age (Ma)		Ns*	∑(PΩ) (cm^2)	1σ∑(PΩ) (cm^2)	ζMS	1σ ζMS	^{43}Ca	^{238}U	Central age Ma.	±1σ	Dpar µm	Length µm	error µm	Author
1072-117	Hoyon	Guaduas	36	0	56	61	207	2.00E-04	6.83E-06	16.414	0.346	0.109	0.834	8.5	0.6	1.66	14.18	95	Caballero, 2013
1072-118	Seca	Guaduas	10	0	59	70	21	5.32E-03	1.84E-07	16.413	0.348	0.321	0.055	30.1	6.6	1.98	13.19	12	Caballero, 2013
1072-123	Umir	Guaduas	32	0.99	65	83	24	1.43E-05	7.12E-07	11.467	0.248	0.017	0.006	9.6	2	1.61	12.49	12	Moreno et al
1072-124	Socota	Guaduas	7	0.03	112	121	8	1.48E-05	2.11E-06	14.386	0.248	0.017	0.002	3.9	1.4	1.67	12.76	6	Moreno et al
1072-125	La Naveta	Villeta	14	0.02	130	140	12	2.30E-05	1.98E-06	14.464	0.286	0.027	0.003	3.8	1.1	1.52	14.27	11	Caballero, 2013
1072-126	La Naveta	Villeta	27	0.01	130	140	16	2.19E-05	2.30E-06	11.548	0.249	0.015	0.181	4.2	1.1	1.44	11.86	12	Moreno et al
1072-127	Trinchera	Villeta	18	0	121	130	8	3.25E-06	3.20E-07	14.588	0.289	0.021	0.242	17.69	6.4	1.42	12.44	3	Caballero, 2013
1072-128	Trinchera	Villeta	8	0.14	121	130	7	8.42E-06	1.22E-06	11.597	0.249	0.016	0.003	4.8	1.8	1.54	10.86	4	Caballero, 2013
29	Lisama?	The Armas Syncline	39		57	60	71	6.46E-01	1.99E-02	175.025	0.3486	0.0116	0.158	9.61	1.2	1.57	13.31	-----	Sanchez, 2012
31	Lisama?	The Armas Syncline	40		40	45	154	3.41E-01	5.99E-02	177.308	0.3536	0.119	0.207	39.9	3.4	2.16	11.8	-----	Sanchez, 2012
28	Umir	The Armas Syncline	40		65	79	50	3.24E-01	6.35E-02	173.823	0.346	0.945	0.231	13.4	1.9	1.81	13.96	-----	Sanchez, 2012
14	Umir	The Armas Syncline	36		65	79	63	9.03E-01	2.19E-02	156.245	0.2954	0.0227	0.772	5.45	0.7	1.85	13.41	-----	Sanchez, 2012
QA-0519	Umir	The Armas Syncline	20		65	79	170						0.305	14.1	1.2	1.92	9.6	-----	Mora, 2010
15	Umir	The Armas Syncline	25		69	73	8	1.03E-01	4.38E-03	157.438	0.2972	0.0213	0.439	6.12	2.2	1.73	11.44	-----	Sanchez, 2012
114	Arcabuco	The Armas Syncline	2	0.14	140	150	19					0.0201	0.000199	6.7	1.6	1.74	11.65	-----	Sanchez, 2012

Ns - number of spontaneous fission tracks counted. ∑(PΩ) Sum of R_i *W_i for all grains evaluated: R_i is (^{238}U/^{43}Ca) for apatite grain i; W_i, is the area over Ns and Ri are evaluated;

ζMS-calibration factor based on the LA-ICP-MS of fission-track age standards.

^{43}Ca is background corrected of Ca; 238U is background corrected of U; P(χ^2) is probability. Values greater than 5% are considered to pass this test a nd represent a single population of ages.

Table 5.11a *– Compiled fission-track data, analyzed with laser-ablation-inductively coupled plasma-mass spectrometry (LA-ICP-MS), from the areas of Guaduas, Villeta and the Armas Syncline. Data collected and analyzed by Caballero (2013), Sanchez (2012), etc.*

(U-Th)/He in Zircon (Zhe) thermocronology

Sample	Unit	Area Location	Stratigraphic Age (Ma)		Age (Ma)	±8% (Ma)	Author
29	Middle Lisama	The Armas Syncline	57	60	94,9	7,6	Sanchez, 2012
31	Upper Lisama	The Armas Syncline	40	45	78,4	6,3	Sanchez, 2013
28	Middle Umir	The Armas Syncline	65	79	192,8	15,4	Sanchez, 2014
14	Middle Umir	The Armas Syncline	65	79	175,5	14	Sanchez, 2015

(U-Th)/He in Apatite (Zhe) thermocronology

Sample	Unit	Area Location	Stratigraphic Age (Ma)		Age (Ma)	±8% (Ma)	Author
29	Middle Lisama	The Armas Syncline	57	60	6,6	0,4	Sanchez, 2012

Table 5.11b *– Samples taken from other authors, analyzed with (U-Th)/He in zircons and apatite, from the Armas Syncline. Data collected and analyzed by Sanchez (2012).*

Apatite fission-track analytical result - sample from Magdalena Valley (Geotrack Report # 660 and # 726

Sample	Unit	Area Location	n	P(χ^2) %	Stratigraphic Age (Ma)		ρ_s tracks/cm^2	Ns	ρ_i tracks/cm^2	N_i	ρ_d tracks/cm^2	N_d	Central * age Ma.	±1σ	Dpar µm	Length µm	error µm	Author
1082-12	Giron	Sonero Well	20	71,8	161	179	1,34	66	5,45	269	14,56	2357	70,4	9,85	ND	13,9		Caballero, 2013
1018-26	Giron	Central Cordilletra	8	63,4	161	179	3,58	29	15. 818	128	15,13	8201	59,8	12,4	1,34	ND		En Caballero, 2012
1063-25	Rosablanca	Cagui well	11	30,8	130	140	3,74	95	16,33	415	14,93	2357	66,7	7,8	ND	12,9		En Caballero, 2013
660-02	Lisama Fm.	Nuevo Mundo_Los Cobardes	20	1%	61	67	1,483	87	15,07	884	11,11	1707	22,3	4,2	ND	9,85	0,46	Gomez,2001
660-01	Lisama Fm.	Nuevo Mundo_Los Cobardes	25	1%	61	67	3,08	216	16,46	1156	11,19	1707	36,0	5,3	ND	10,3	0,39	Gomez,2001
1018-03	Lisama Fm.	Nuevo Mundo_Los Cobardes	3	20%	61	67	6,02	27	15,386	69	11,94	8201	81,4	18,6	1,29	NA	N.A.	Parra 2012
1018-04	Umir Fm.	Nuevo Mundo_Los Cobardes	20	66%	74	83	4,326	62	15,56	223	12,08	8201	58,6	8,5	2,29	12,4	0,22	Parra 2012
660-37	Umir Fm.	Nuevo Mundo_Los Cobardes	20	44%	74	83	3,497	169	17,38	840	14,72	2335	56,1	4,9	ND	12,7	0,40	Gomez,2001
1018-05	La Luna Fm.	Nuevo Mundo_Los Cobardes	14	32%	85	90	6,284	68	38,441	416	12,22	8201	34,9	4,6	1,66	10,1	1,23	Parra 2012
1018-06	Simiti Fm.	Nuevo Mundo_Los Cobardes	15	23%	106	99	8,091	198	33,877	829	12,36	8201	51,5	4,2	1,38	12,1	0,26	Parra 2012
660-36	Tablazo Fm.	Nuevo Mundo_Los Cobardes	21	0%	118	114	11,4	305	35,6	952	14,88	2335	65,5	17,1	ND	11,1	0,28	Gomez,2001
1018-07	Tablazo Fm.	Nuevo Mundo_Los Cobardes	21	92%	118	114	5,331	158	26,486	785	12,5	8201	43,9	3,9	1,48		N.A.	Parra 2012
1018-08	Tambor Fm.	Nuevo Mundo_Los Cobardes	1	N.A.	138	139	3,486	3	52,568	41	12,63	8201	16,2	6,9	1,24		N.A.	Parra 2012
1018-09	Giron Gr.	Nuevo Mundo_Los Cobardes	5	2%	161	150	8,411	41	36,105	176	12,77	8201	60,4	20,7	1,68		N.A.	Parra 2012
660-34	Giron Gr.	Nuevo Mundo_Los Cobardes	2	63%	161	150	1,673	6	25,65	92	15,12	1733	18,7	7,9	ND		N.A.	Gomez,2001
1018-10	Giron Gr.	Nuevo Mundo_Los Cobardes	2	35%	161	150	9,402	33	50,146	176	12,91	8201	42,3	8,1	1,07		N.A.	Parra 2012
GC660-1	Lisama	Nuevo Mundo _East-Sogamoso River	25	<1	65	56	0,308	216	1,646	1156	1,119	1707	40,9	± 3.3	ND	10,3	± 0.39	Gomez, 2001
GC660-2	Lisama	Nuevo Mundo _East-Sogamoso River	20	<1	65	56	0,131	77	1,506	883	1,11	1707	19	± 2.3	ND	9,85	± 0.46	Gomez, 2001
GC660-4	La Paz	Nuevo Mundo Syncline East	28	1	56	45	0,386	1,822	1,822	1496	1,104	1707	45,8	± 3.2	ND	10,5	± 0.24	Gomez, 2001
GC660-5	La Paz	Nortern Study-MMV	4	5	56	45	0,13	9	1,112	77	1,096	1707	25,1	± 8.9	ND			Gomez, 2001
GC660-6	La Paz	Nuevo Mundo Syncline - East	26	<1	56	45	0,689	319	3,208	1480	1,089	1707	45,8	± 3.2	ND	11,6	± 0.19	Gomez, 2001
													40,8	± 5.1				
GC660-7	La Paz	Nuevo Mundo Syncline - East	8	97	56	45	0,356	45	2,878	364	1,081	1707	26,2	± 4.2	ND	8,94	± 1.36	Gomez, 2001
GC660-8	La Paz	Nuevo Mundo Syncline - East	15	<1	56	45	0,401	125	2,103	655	1,074	1707	40,1	± 4.1	ND	11,6	±0.32	Gomez, 2001
													40,3	± 7.7				
GC660-12	Esmeraldas	Nuevo Mundo Syncline - East	4	2	45	35	0,633	47	1,966	146	1,066	1707	67,1	± 11.4	ND	9,74	± 0.74	Gomez, 2001
													73,5	± 20.2				
GC660-14	Esmeraldas	Nuevo Mundo Syncline - East	5	8	45	35	0,471	32	3,546	241	1,059	1707	27,6	± 5.3	ND	10,2	± 2.07	Gomez, 2001
GC660-15	Esmeraldas	Nuevo Mundo Syncline - East	9	<1	45	35	1,596	244	2,962	453	1,128	1733	118,2	± 10.1	ND	11,2	±0.53	Gomez, 2001
													65,8	± 30.1				
GC660-20	Colorado	Nuevo Mundo Syncline - East	3	41	35	29	0,268	14	2,221	116	1,121	1733	26,5	± 7.5	ND	12,2	± 0.55	Gomez, 2001
GC660-22	Real	Nuevo Mundo Syncline - East	9	1	29	23	0,262	46	1452	255	1,115	1733	39,4	± 6.4	ND	13	± 0.57	Gomez, 2001
													40,8	± 10.8				
GC660-27	Real	Nuevo Mundo Syncline - East	4	19	23	5	0,345	33	1401	134	1,108	1733	53,4	± 10.5	ND	10,2	± 2.25	Gomez, 2001
GC660-28	Real	Nuevo Mundo Syncline - East	26	<1	23	5	0,111	144	1485	1931	1,102	1733	16,1	± 1.5	ND	11,9	± 0.92	Gomez, 2001
													15	± 2.9				
GC660-29	Real	Nuevo Mundo Syncline - East	29	<1	23	5	0,297	384	2,709	3505	1,095	1733	23,5	± 1.5	ND	12,4	± 0.24	Gomez, 2001
													18,2	± 3.7				
GC660-30	Real	Nuevo Mundo Syncline - East	9	<1	23	5	0,184	31	1,109	187	1,082	1733	35,1	±6.9	ND	12,1	-	Gomez, 2001
													14,2	± 11.8				
GC660-34	Giron	Los Cobardes Anticline west	2	63	178	145	0,167	6	2,565	92	1,512	2335	18,7	± 7.9	ND			Gomez, 2001
GC660-35	iron - SS Santo	Los Cobardes Anticline-west	113	<1	145	135	1,534	278	1,959	355	1,504	2335	220,2	± 18.5	ND	12,1	± 0.28	Gomez, 2001
													234,1	±50.3				
GC660-36	Tablazo	Nuevo Mundo _East-Sogamoso River	21	<1	124	112	1,14	305	3,56	952	1,488	2335	90	±6.4	ND	11,1	0,28	Gomez, 2001
													65,5	±17.1				
GC660-37	Umir	Nuevo Mundo _East-Sogamoso River	20	44	83	65	0,35	840	1,738	840	1,472	2335	56,1	±4.9	ND	12,7	± 0.40	Gomez, 2001
GC726-24	Pinzaima Sst	Villeta **** JG-P4-10	18	72	134	135	0,036	7	1,152	224	1,289	2063	7,9	±3.0	ND	11,6		Gomez, 2001
GC726-25	Utica Sst	Villeta ***** JG-P4-13	20	<1	125	74	0,101	36	4,776	1698	1,296	2063	5,4	±0.9	ND	12,4	± 2.17	Gomez, 2001

Estándar external detector ρi and ρd measure in mica external detector; ρs measure in internal surface

* central age, used where sample contains a significant spread of single grain ages (P(χ^2) < 5%). Error quoted at ±1σ

Ages calculated using dosimeter glass CN5, Zeta of 380.4 ±5.7 Analyst C. O Brien for sample GC660-34 - 37 -42; CN5, Zeta of 392.9 ±5.7 Analyst M. Moore for samples GC-660 1-30, 40-41, 43-64, 21-27.

Table 5.11c – *Fission-track age compilation from other author mainly from the north and south, and some from the central area studied in this work. The apatite fission track (AFT) also includes measurements for Dpar and track length. Data collected and analyzed by Gomez (2001), Parra et al., (2012) and Caballero et al., (2013).*

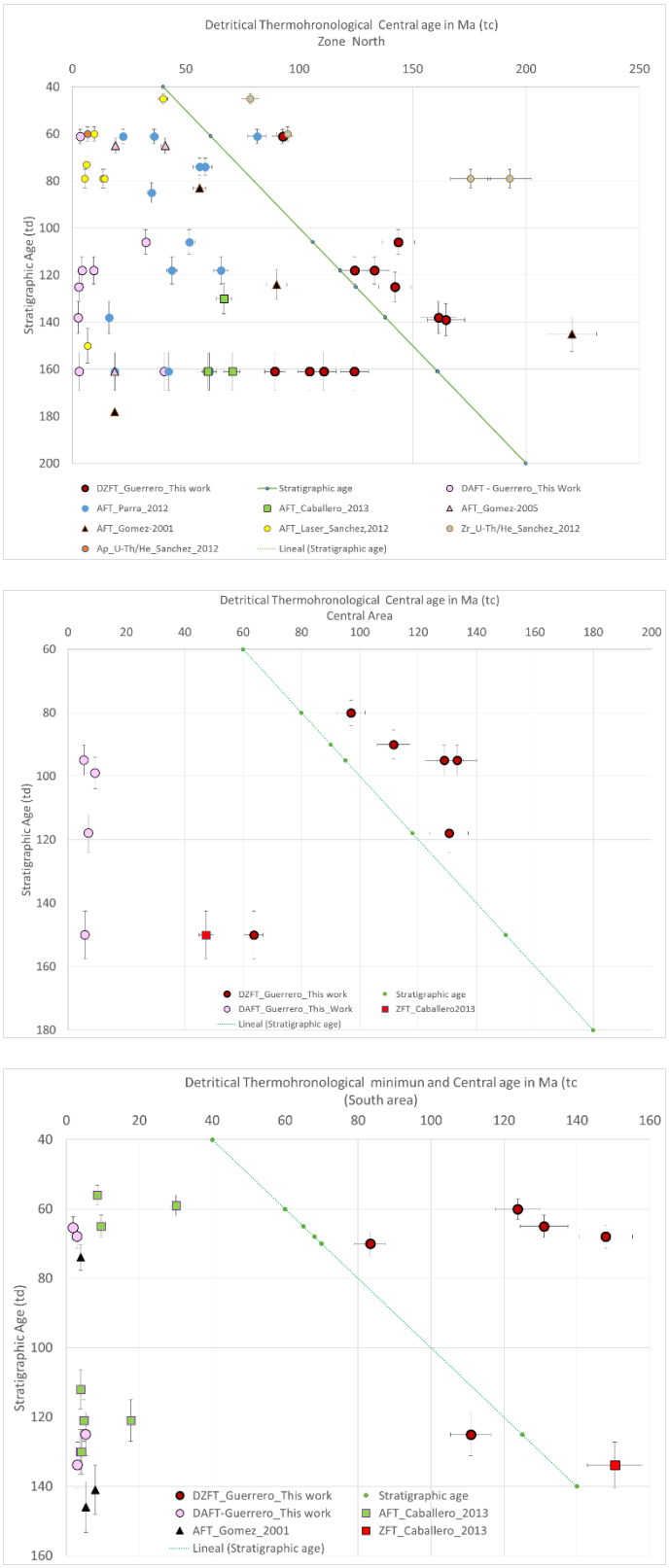

Figure 5.29. *Detrital fission track age collected and measured in this work compared with the FT age measured by other authors in the three areas studied in this work. North area (above), central area (center), and South area (below).*

5.7 Fission Track age comparison

5.7.1 Northern region

Figure 5.29 shows, the comparison of FT age from the north to the south areas of this work (location in Figure 5.1) and the data available from other authors (Table 5.11a), for the Cretaceous to Paleocene units. The samples shown in this work, have two characteristics related first with the P(χ2) which in the majority is <5, which means that there is a high probability for multiple age populations in the sample and that these samples were annealed differentially or there was different inheritance. Three samples for AFT in this area are the exception (JG-P3-19, JG-P3-32 and JG-P3-36) which have P(χ2) >5. Second, an important percentage of the grains have cooling ages younger than the depositional age (Figures 5.5 and 5.8, Tables 5.2 and 5.3). The majority of my samples have an AFT cooling age between 2.5±0.19 Ma to 9.4±0.19 Ma, related probably to a regional Neogene cooling episode, which is consistent with the data shown by Sanchez et al. (2012) in the area of the Armas Syncline as is illustrated in Figure 5.29 (north zone above). Three AFT samples with P(χ2)=0 from the Girón, Simiti and Umir formations (Table 5.3) show cooling ages between 40.4±6.4Ma to 25.6±2.3Ma, indicating partial or total resetting of the AFT, which is consistent with the Ro data (Figure 5.28, left). However, the younger ages could be related to a recent rapid cooling event, as we will see with the thermal modeling.

The ZFT cooling ages of the Girón Formation samples show partial annealing, which is also consistent with the Ro data (Figure 5.28). The ZFT cooling age calculated for units younger than the Girón Fm (<150Ma in Figure 5.28) are consistent with the ZFT dating by Sanchez et al (2012) for upper units of the Lisama Fm., and also for AFT of the Tambor Fm as shown by Gomez (2001) in Figure 5.29 (north zone), which are older than the stratigraphic age.

5.7.2 Central region.

In the central zone (Figures 3.5 and 5.1) I obtained ZFT and AFT cooling ages from Jurassic to Late Cretaceous units. As discussed for the north area, the characteristics related to P(χ2) <5 and to the cooling ages younger than the depositional age (Figure 5.15, Tables 5.4 and 5.5) are also present.

My new AFT data varies from 5.47±0.6Ma from the Churuvita Fm. to 9.3±8.2Ma from the Arenicas de Chiquinquira. These AFT ages are in general older than what we observed in the southern area, and as in the north, are related to the Neogene cooling episode.

I obtained ZFT cooling ages of 63.7±5 Ma for the Arcabuco Formation and 133.5±10.4 for the Churuvita Fm. According to the Ro (Tmax) data of the Arcabuco Fm. the ZFT must have been totally reset because the heating event was intense enough to anneal all the pre-existing ZFT of this sample (see the Tmax trend line in Figure 5.25 at the center). In the case of the Tablazo Fm., sample JG-P1-06 resided in the PAZ, and 71%

of the ZFT ages are older than the stratigraphic age (Table 5.4). For the rest of the samples from the Conejo, Churuvita, and Simijaca formations the samples remained in the TRZ for zircons (Figure 5.28 –center). An additional 47.3±7.6 Ma ZFT age of Caballero et al. (2013) for the Arcabuco Fm. is consistent with the age reported in this work (Figure 5.29).

5.7.3 Southern region.

In the southern zone (Figures 3.5 and 5.1) I obtained ZFT and AFT cooling ages from Early Hauterivian to Late Maastrichtian units. The P ($\chi 2$) <5 and cooling age younger than the depositional age (Figure 5.5 and Tables 5.6 and 5.7) show that almost all the samples had suffered partial annealing. According to the AFT data samples from the Labor and Tierna Formation JG-P4-06 and From Seca (JG-P4-02) have a P ($\chi 2$)>5 indicating one cooling age population. The age measured from the samples with P($\chi 2$)>5 varies from 3.11±0.7 from the La Naveta/Murca Fm to 1.9±0.4 from the Seca Fm., being the youngest ages measured in all the study area. This is related to a Pliocene-Pleistocene cooling episode. These age are consistent with some AFT data of Gomez (2001) and Caballero et al. (2013), as shown in Figure 5.29 and Tables 5.11a,c.

Not all the ZFT ages measured in this work for this area are younger than the depositional age (Figure 5.20). Two samples from the Labor and Tierna Fm. (JG-P4-06) and the Guaduas Fm. (JG-P4-19) with The P ($\chi 2$) <5 have a P1 age older or the same as the stratigraphic age (Table 5.6). This means that these samples were never heated enough to suffer annealing and always stayed in the TRZ.

5.7.4 Exhumation of the Eastern Cordillera

The AFT ages in this study provide new information on the exhumation of the western flank of the Eastern Cordillera. The new AFT ages from this study are younger than the AFT ages reported by Gomez (2001, 2003) and Caballero (2013) (Tables 5.11a and b). Our dates vary from AFT in the range of 1.9±0.39 Ma in the southern area to 3.41±0.36 Ma in the north (location in Figure 5.1). The AFT samples from the north and south compared with the central zone (5.47±0.58 to 9.3±4.1 AFT age) showed younger ages, which probably means an earlier age of exhumation at the central zone (Figure 5.1) than at the south and north. Additionally, the new AFT ages in the north and south of the WEC (1.9±0.39 to 3.41±0.36 Ma), are similar to AFT cooling age of 0.8±0.3 to 3.8±0.7 Ma of Mora et al. (2007, 2008) from the east flank of the EC. These new AFT values indicate that exhumation was almost simultaneous on both sides of the EC.

5. 8 t-T. THERMAL MODELING

Although I obtained the cooling age of ZFT and AFT with Dpar measure, the AFT samples in general have young cooling ages < 5 Ma with very low Uranium concentration. With these characteristics, even with 252Cf irradiation it is unlikely to obtain a significant number of track lengths, for that reason we could not get track lengths from our samples.

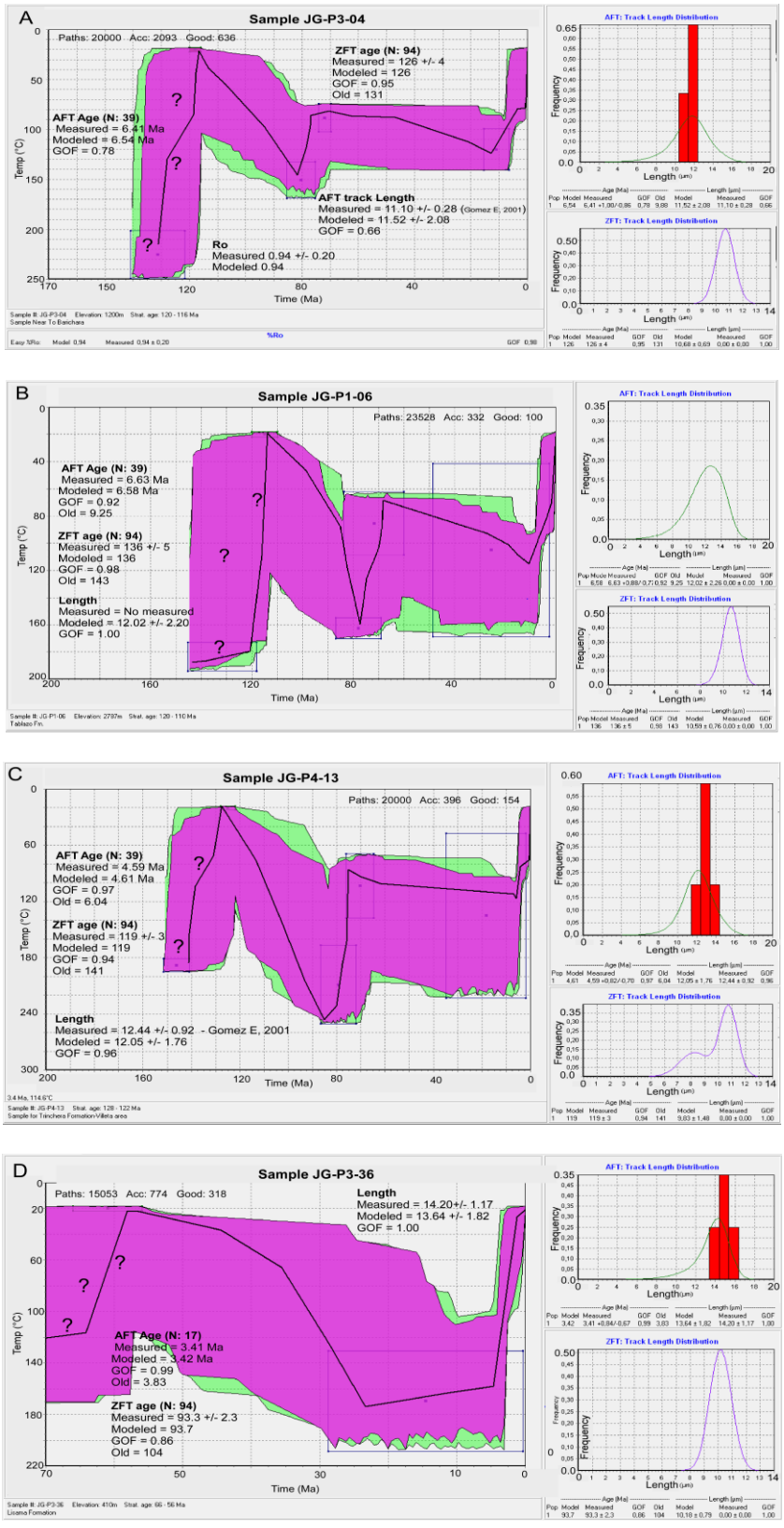

Figure 5.30– *Thermal modeling of samples from the northern (A) and central (B) area at the level of the Tablazo Formation and Trinchera at the southern area (C) in this study. Boxes define constraining events from Ro, unconformities determined from seismic chronostratigraphic interpretation, Cooling age from DAFT, DZFT, DPAR and Track length taken from others author. The Purple color represents good models and green acceptable models. Different model's (acceptable and good) paths are highlighted in each graph.*

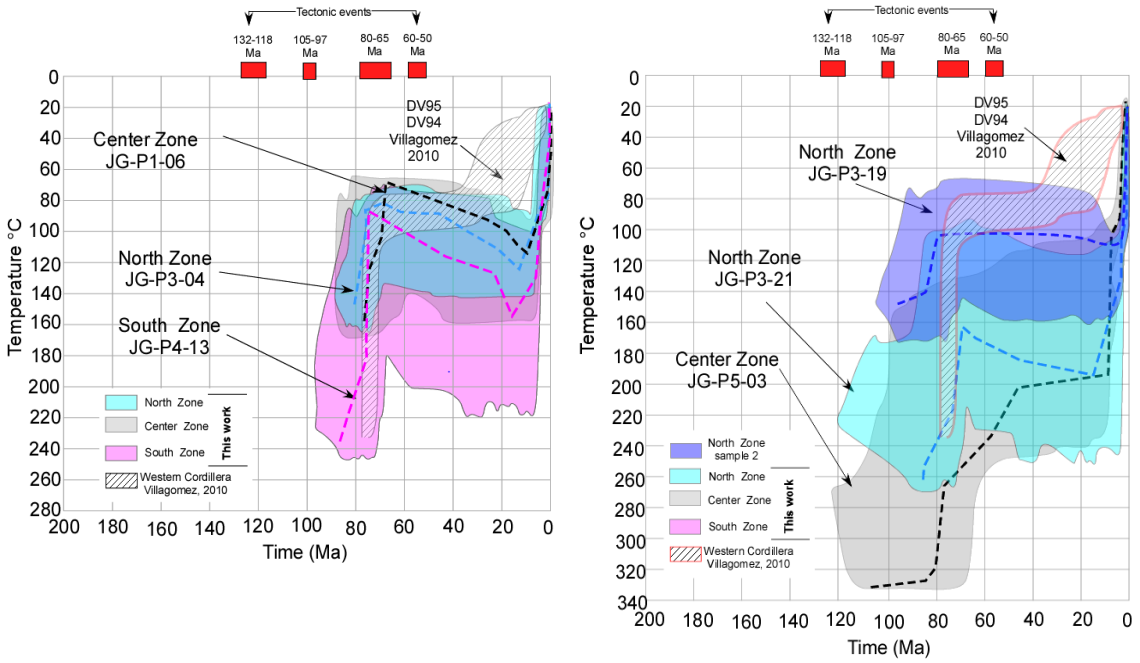

Figure 5.31 *Compendium of thermal modeling solutions for selected samples from the study area MMV and WEC (this work) for A: in Aptian-Albian units and B: older units in the northern and central zones from Jurassic and Berriasian and from Villagomez, 2010 in the western Cordillera. Red squares at the top, represent timing of major tectonic events in Colombia.*

Understanding the importance of the track lengths for modeling, we decided to try to construe the thermal modeling (t-T) with this limitation using whenever possible the track lengths reported from the same unit analyzed by other authors (Caballero et al. 2013, Gomez E. 2001 and Sanchez et al., 2012 in Tables 5.11a to 5.11c) to give more validity to our models. I then made a comparison with the models construed by other authors. From this exercise we obtained the result that is shown and discussed in the next paragraphs.

Eleven samples from all the areas were modeled integrating AFT and ZFT (ages, Dpar values), depositional age and whenever possible the Ro and track lengths reported by others authors (Figure 5.28). In general these thermal events correspond to: the first heating occurred from sedimentation age until ~ 85-80 Ma, followed by a fast steady-cooling which started at ~80Ma and finished at ~ 70Ma; the second heating occurred form ~70Ma till the onset of the second cooling in most cases from ~15-2Ma (recent event) until the present.

In general the thermal modeling from the north to the south indicates the occurrence of two events of heating and two events of cooling for units older than Campanian (Figure 5.30 A, B and C) and as is expected one event of heating and one event of cooling for units younger that ~70Ma (Figures 5.30D).

In Figure 5.30 (A, B, C), I show the representative samples for all the area analyzed, from Early Cretaceous Tablazo Formation samples from the northern and central areas

(JG-P3-04, JG-P1-06) and from the southern zone from the Trinchera Formation (sample JG-P4-13).

The sample JG-P3-04 (Figure 5.30-A), indicates a period of heating from deposition age till near to 80 Ma, from this time the sample indicates a period of cooling from depths below the apatite partial annealing zone (APAZ), reaching a temperature of ~145°C. This reset sample shows initial cooling at ~ 80 Ma till ~ 77 Ma and rapid cooling of 12°C/Myr, then a period of slow steady-heating while it spent a significant amount of time in the APAZ untill it reached a maximum temperature of ~ 122°C (0.57°C/Myr), finally a last period of cooling started at ~12 - ~2 Ma with a rapid cooling of 8.5-34 °C/Myr. Tablazo Fm sample JG-P1-06 (Figure 5.30-B) shows the first heating from deposition age till ~80 Ma when the first cooling started and extended till ~70 Ma with a rapid cooling of 10°C/Myr. The onset of a second period of heating occurred at ~70 Ma (at 65°C) untill it reached the temperature of 110°C at 10 Ma, staying in the APAZ with a slow heating rate of 0.75°C/Myr. The last event shown is a cooling onset at 10 Ma with a rate of 9°C/Myr. The Trinchera sample JG-P4-13 located at the south, shows the first onset of heating from the onset of the Trinchera deposition time till the ~85 Ma and a rapid heating rate of 5.4 °C/Myr, this event is followed by the first cooling which started at ~85 Ma till ~75 Ma with a rate of 16.5 °C/Myr. The second period of slow steady-heating of 85 – 115 °C occurred between ~75 Ma till ~5 Ma showing a heating rate of 0.43°C/Myr. The onset of the last cooling at ~5 Ma till the present shows a rapid cooling rate of 19°C/Myr.

t-T comparison from Figures 5.30 A,B and C with t-T tendency of Villagomez (2010) in the Western Cordillera, shows a similar behavior to what is observed in the MMV/WEC (left in Figure 5.31), consistent with the cooling event occurred at 80-70 Ma (Campanian) and with the fast exhumation in all the areas at ~12 - 2 Ma. Additionally, I made the same comparison with older units from the northern and central areas using the samples JG-P5-03, JG-P3-21 and JG-P3-19 (right in figure 5.31) from the Tambor and Girón (north area), and Arcabuco Fms (Central area), also showing a clear fast-cooling event at 80-70 Ma and the recent event at >5 Ma.

Similar thermal behavior is observed in all the samples collected and analyzed in this work, showing that in the MMV and WEC in general, two events of heating and two event of cooling occurred in Campanian rocks or older rocks.

5.8.1 Discussion

The thermal history obtained from younger units in this work (Late Cretaceous) are similar and consistent with those shown by Sanchez et al., (2012), (for comparison see Figure 5.32) where an event of heating from deposition age until ~20 Ma is observed, and both showing a cooling event that in my model starts later (~4 Ma) and with faster cooling than in the model presented by Sanchez et al. (2012).

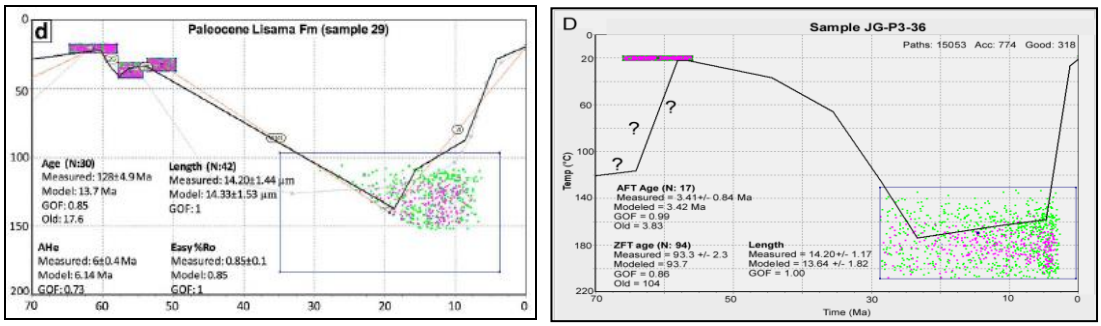

Figure 5.32– *Comparison between the Cooling histories obtained from the Lisama Fm. in this work (Upper Cretaceous) and from the same formation in Sanchez (2012). Observe that both models show cooling and heating episodes.*

As is shown in Figures 5.4A and B, the time-temperature paths (thermal model) may be interpreted in terms of heating (deposition and subsidence) or cooling (erosion and/or exhumation), applying this general concept in our t-T models, I can say that these events of heating and cooling probably indicate, at least for units older than ~80Ma, two events of deposition related to subsidence and two events of erosion related with the generation of unconformities (like the ones that were shown in chapter 4).

For units that showed high temperature values from Ro (>3.5) or during the modeling in which high-temperatures are observed in some levels in the central area and more intensely in the southern area where the temperature could exceed ~250°C, and where the thermal history could be more complex, it could be interpreted that those temperature excesses at the central and south areas were due to the presence of enough sediment supply in the cretaceous basin: at least between 3.5 to 4.5 km (this work) of sediment (4-6 km for Sanchez et al., 2012), or due to magmatic activity in the area of Villa de Leyva and basic intrusion in the southern area of this work in the Cretaceous succession, and in general for the southern area with evidences of hydrothermal alteration in black shales from the lower Cretaceous.

Due to the limit of the fission track resolution and the characteristics of the samples, the only event of erosion from the Cretaceous sequence that could be determinated from FT in this work corresponds to the ~80-70Ma, which is also supported by other data and other observations in this work like the Campanian unconformity recognized using seismic information (SU4 in Chapter 4), which have been recognized in the regional context. Caballero et al. (2013) in the Cagui area based on results from the Rosablanca Formation (Lower Cretaceous) documented that the cooling onset (inversion and thrusting) can be as early as Late Cretaceous (70-75 Ma) which is consistent with the first age of cooling determined by FT in this work (80-70 Ma) as was discussed in the previous paragraph. These new data suggest that one of the most important deformation and erosional-exhumation events occured at this time, this event is also documented by the preserved growth strata (this work).

Parra et al., (2012), suggest a Mesozoic reactivation, claiming that the initial age of deformation started in the MMV during the late Paleocene, as is documented farther

west in the CC where rapid cooling and erosion, including contractional reactivation of Mesozoic age that persists until Los Cobardes in the WEC (Gomez et al., 2005; Nie et al., 2010; and Caballero et al., 2012). With this idea, the onset of cooling proposed in this work occurred earlier than had been proposed previously.

Finally, in this work, based on different evidences, specially on seismic sections and also thermochronology data, a Campanian activity zone of deformation was identified and from the seismic data others as old as Lower Cretaceous. The evidences in this work shows that the initial deformation occurred in units beneath the MMV angular unconformity of Middle Eocene age, probably started during the Lower Cretaceous time.

5.9 Conclusions

1. In the WEC and MMV two events of heating an two events of cooling were identified: the first heating occurred from sedimentation age until ~ 85-80 Ma, followed by a fast steady-cooling which started at ~80Ma and finished at ~ 70Ma; the second heating occurred form ~70Ma till the onset of the second cooling which started at ~12-2Ma (recent event) until the present.

2. In general for all the areas (northern, central and southern) the AFT and ZFT central ages in Jurassic to Early Cretaceous units are younger than the depositional age because of post-deposition partial or total annealing. In contrast, in all samples from the Late Cretaceous and Tertiary units zircons conserved their source area cooling ages, whereas apatites have been partially annealed.

3. In the structural sections displacement blocks can be observed along faults, for example in the Rio Sogamoso section a displacement is detectable that could be explained using FT ages (Figure 5.11), where minimum and central age from AFT marked a movement of the block at around ~2.8 ±0.33 Ma (sample JG-P3-32) at the east with respect to the west block of ~32.3 ±4.6Ma (sample JG-P3-42). This shows that at the east of the fault the exhumation occurred more recently than at the west.

4. The zircon and apatite iso-age maps show in general that the younger ZFT central ages are located in the core of anticlines where the stratigraphically older units are exposed. In some cases a similar trend is observed in the AFT, but it is less pronounced.

5. The AFT age from this work showed that the cooling age at the north is younger than 2.5±0.19-3.41±0.36. This could be related with the most recent event of exhumation in the northern sector of the WEC; For the Central area the AFT ages vary from 5.47 ±0.58 to 9.3±4.1 which is older than in the northern and southern area; and in the southern area the younger age reached 1.9±0.39. The new dates of AFT at the south from this work show that the ages are younger than had been reported by other authors.

6. We observe from our new data of AFT, that the cooling age reported at the eastern flank of the East Cordillera by Mora (2007) is not substantially younger than the age reported in this work (Tables 5.3-5.7) at the western flank of the East Cordillera (northern and southern area), which probably means that the onset of rapid exhumation could be similar at both flanks of the Eastern Cordillera.

7. The time-temperature paths (thermal models) can be interpreted in general in terms of deposition (subsidence) or erosion (exhumation). I can say that these events of heating and cooling in the area of study generally indicate at least two events of deposition related to subsidence and two events of erosion related to the generation of unconformities. All of these are probably related to the tectonic inversion of the basin which occurred earlier than was previously suggested.

8. The paleo-geothermal gradient versus present-day thermal gradient plots permit to identify the presence of Late Abian/Early Cenomanian unconformities or older and insinuate that the excess of paleo-temperature (~250°C) is due to changes in the geothermal gradient because of changes in the heat flow (probably magmatic activity) or a combination of changes in the geothermal gradient, sediment charge and denudation.

CHAPTER 6

Late Jurassic to Early Eocene tectonic and sedimentary evolution in the Middle Magdalena Valley and western flank of the Eastern Cordillera, Colombia.

6.1 Introduction

Tectonics is the study of geometric or deformational features, and of their nature, origin and evolution. As an example, seismic interpretation allows to determine the total shortening of the Cretaceous sequence from the Late Jurassic-Berriasian to the Present.

Sedimentary tectonics refers to the analysis and interpretation of deformation as recorded by sedimentary rocks. Interpreting paleofacies maps allows to explore the distribution of sedimentary facies in a depositional basin during a given time interval and the process responsible for these patterns (see chapter 3). In this work, I used the paleofacies maps constructed in chapter 3, combined with the structural deformation observed in the field and seismic information, to draw 3D block diagrams to understand the relation between facies and deformation through time (from the Jurassic to the Coniacian-Santonian) (Figure 6.11). Finally, the tectonic paleo-reconstruction of northwestern South-America from the Jurassic to the Eocene, based on observations done in the MMV and the WEC, made it possible to propose a model to explain the relation between our local tectonic events and plate tectonic evolution during the analyzed period.

Tectonics is a key factor that controls stratigraphy in most basins, since it can change the base level, generate or reduce accommodation space (Figure 6.1), and controls surface rock-exposition and erosion (Figure 6.2).

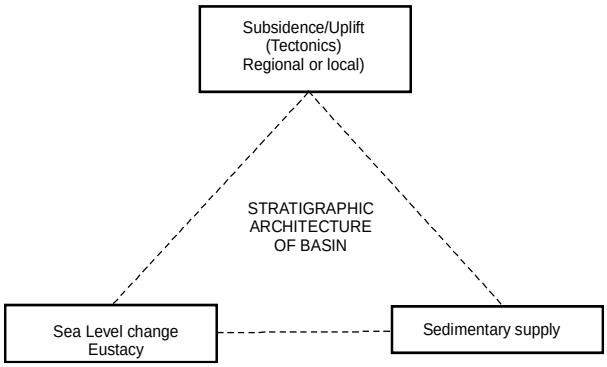

Figure 6.1 – Controls of stratigraphic architecture of a basin with a marine connection, also applicable to an intermountain lacustrine connection (modified from Williams, 1993).

The study of subsidence, regional and local uplift, climate, eustacy, sediment supply and erosion are key factors to understand the role of tectonics (Figure 6.1). As indicated

by Williams (1993), it is difficult to separate tectonics from other factors controlling the stratigraphic architecture in a basin.

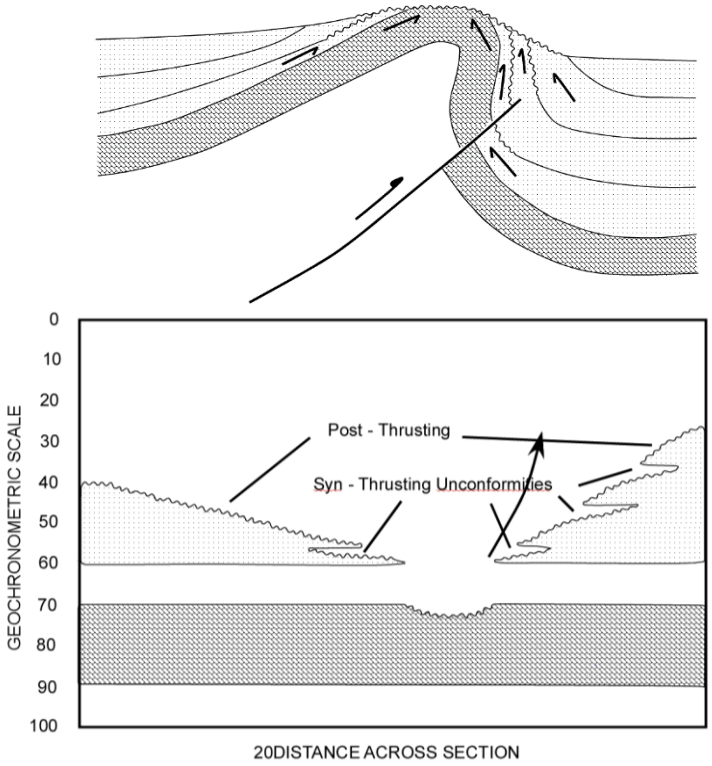

Figure 6.2 – Schematic stratigraphic cross-section (above) and corresponding chronostratigraphic chart (below), showing local tectonic control on the observed stratigraphy in a thrust-related fold (modified from Williams, 1993).

The eustatic sea-level changes may result from periods of glaciation and deglaciation, plate tectonic processes, or from a combination of both mechanisms. Regional subsidence rate interacts with the rate of sea level changes to generate accommodation space that may be filled by sediment, depending on sedimentation rate (Williams, 1993, Figure 6.1). Regional subsidence/uplift is controlled by the thinning/thickening of the lithosphere, isostatic balance (loading/unloading the lithosphere) and thermal anomalies of the lithosphere. Therefore, basin stratigraphy will result from the interaction of tectonics, eustacy, sediment supply (Figure 6.1) and contemporaneous system tracts (Allen and Allen, 1990). Local tectonic features may control stratigraphic sequences and megasequences at scales of hundreds of meters to kilometers (Figure 6.2), as is shown in several sections in the MMV, from seismic cross-sections to reconstructed chronostratigraphic charts (4.5 in chapter 4).

Steep subduction or flat subduction?

A simple subduction could generate thickening or thinning of the lithosphere, deposition, exhumation, deformation and erosion, however the variability of plate coupling modes depending on the geometry of the slab (shallowing, steepening) inferred from among other factors in the regional stress regimen, generating compression (coupled margin), not upper plate deformation (Neutral margin) or

extensional regimen (decoupled margin) and in fact the deformation depends on these regimes (Harabaglia and Doglioni, 1998; Figure 6.3).

Topography, structure and all the other geological features fall into what Doglioni et al. (1999) described as W-Class and E-Class. They show that the nature and age of the downgoing lithosphere is not the primary factor in determining the characteristics of these classes. With regards to the elevation, they propose that subduction with a high angle is related to low elevation and a deep trench of the hanging wall plate; and when the slab has a low angle, there is high elevation of the upper plate and trenches are shallower, whatever the nature, continental or oceanic, of the upper plate.

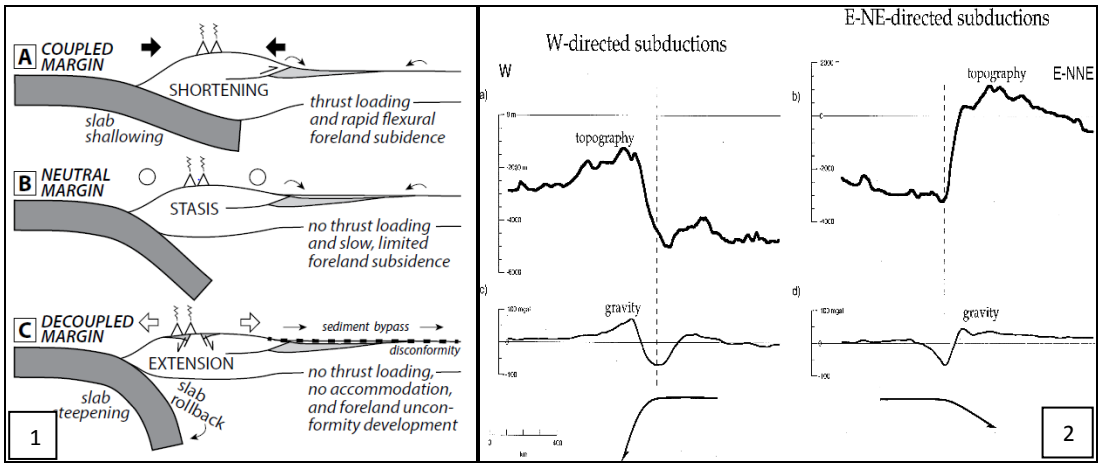

Figure 6.3. In 1) Schematic cross section showing models of variable plate coupling, variability of plate coupling (shallowing, steepening) inferred from among other factors in the regional stress regimen, generating compression (coupled margin), not upper plate deformation (Neutral margin) or extensional regimen (decoupled margin) and in fact the deformation depends on these regimens; 2) Average topographic profiles (a), (b), and free-air gravimetric profiles (c), (d) across the main subduction zones of the earth. These confirm the presence of two classes of subduction zones of which differences are related to the geographic polarity of the subduction zone (after Harabaglia and Doglioni, 1998).

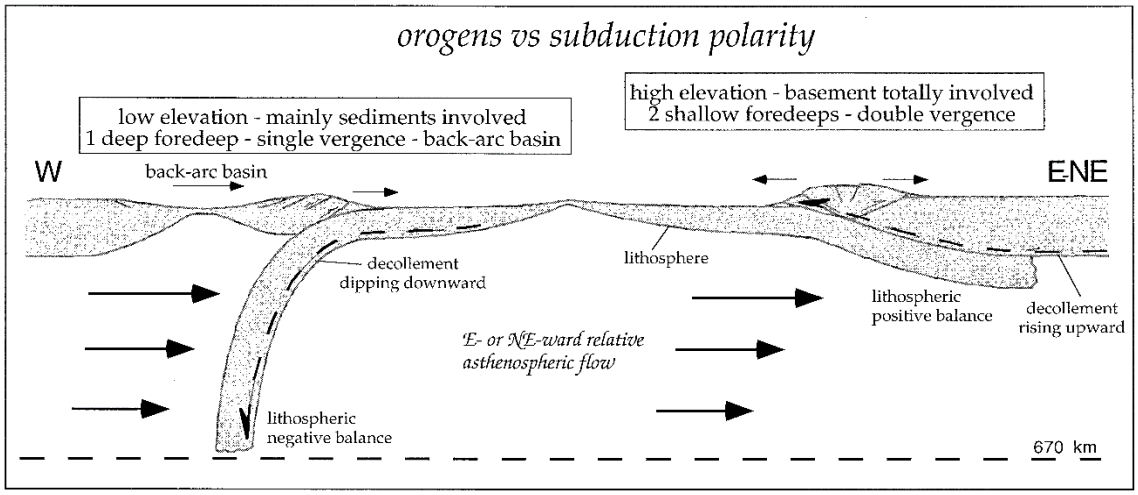

Figure 6.4. Schematic section showing a steeper and deeper slab to the W with regards to the ENE. The décollement plane to the East is deformed; the flat slab and ramp to the East provoke an uplift, while to the West, low elevation and even extension are observed (Taken from Doglioni C. et al., 1999).

Doglioni et al. (1999) also focused their analysis on the direction of subduction (Eastward or Westward). The geographic polarity of the subduction, more than any other parameter, constrains the different characters in the two classes. This analysis

finally poses the question of whether subduction can be ascribed only to slab pull or whether it is also influenced by the relative westward drift of the lithosphere with regards to the upper mantle, postulated by several authors (Le Pichon, 1968; O'Connell et al., 1991; Ricard et al., 1991). Although the contribution of Doglioni (1999) may be important, Colombia presents the interaction between at least three plates, and subduction occurs in ENE or ESE directions (Figure 6.5).

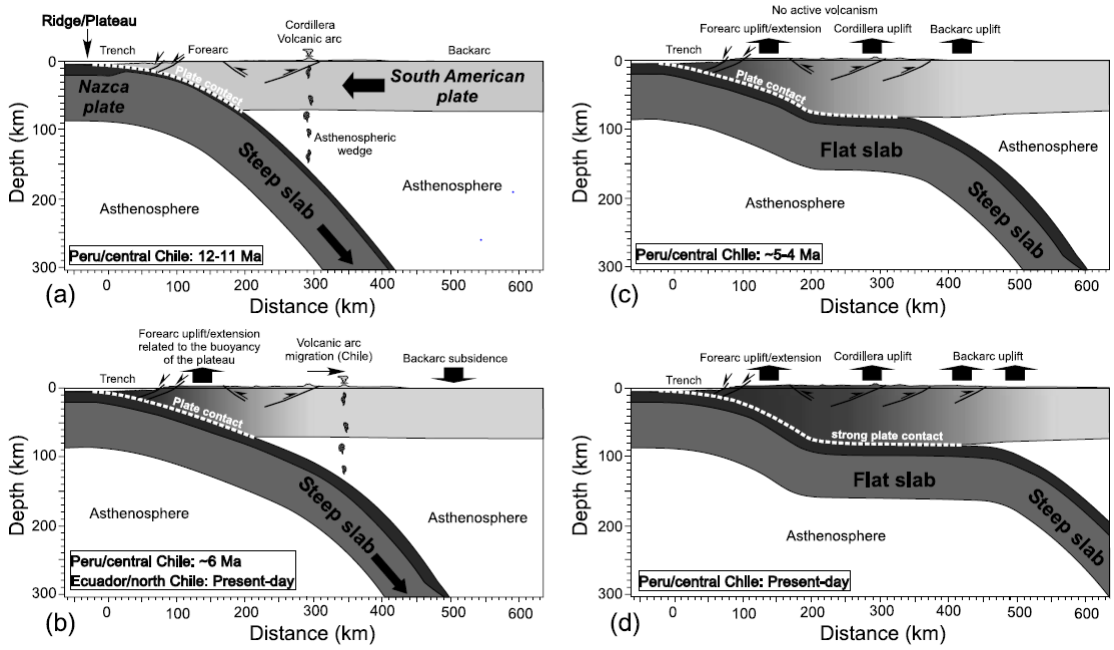

Figure 6.5 – Diagrams showing the evolution of the flat slab from analog models (after Gutscher et al. 2000a). a) Steep subduction of the dense Nazca plate; b) Subduction of buoyant and overthickened oceanic crust with uplift of the fore-arc area, the dip and slab decreases and volcanic arc migrate landward; c) The upper slab starts to underplate the overriding plate (flat slab) while the lower slab is steeper; d) The developed and Propagation of the flat slab continues beneath the overriding plate (experiments suggest that it is necessary to involve a large amount of buoyant plate to obtain a flat slab segment) (After Gutscher et al. 2000, in *Espurt et al., 2008).*

The models constructed following experiments (Gutscher et al., 2000b; van Huene et al., 2002a, 2002b) (Figure 6.5) suggest that the development of a flat slab results from large buoyance ridges/plateaus forced to subduct. The experiment shows that when a negatively buoyant slab subducts, the overriding plate motion does not modify the vertical component of the slab velocity. Thus, increasing the overriding plate motion results in a decrease of the dip of the slab, c) if the slab bears a 50 Ma old, 2 km high plateau, flat subduction occurs after approximately 700 km of buoyant plateau subduction. In northern Ecuador and northern Chile, the process of the slab flattening could be active but not completed, supporting the idea that the slab-flattening needs time to occur. Such a situation may have occurred in the Andes of Colombia (Figure 6.13).

6.2 Tectonic setting

The convergence of three lithospheric plates in the Northern Andes (South America, Nazca and Caribe) produces a complex tectonic area (Freymueller et al., 1993).

Subduction of the Nazca Plate at 70 mm/yr beneath the western margin of South America results in a seismically active area.

The North Andean system is bounded to the west by the Colombian-Ecuadorian trench and the Panamá block, at the north by the South Caribbean and Bocono and at the east by the Andean fault. Right-lateral transpressive movement is taking place along the Borde Llanero fault (Guaicaramo)(Pennington, 1981). To the East, the Eastern Cordillera is bounded by a west-dipping reverse fault and the North Andes is moving NNE-ward relative to the South American Plate at a velocity of 10 mm/yr (Kellogg et al., 1985). To the West, the Sinú and San Jacinto deformed belts result from the SE-ward subduction of the Caribbean plate beneath South America, at a rate of 17 mm/yr (Figure 6.6).

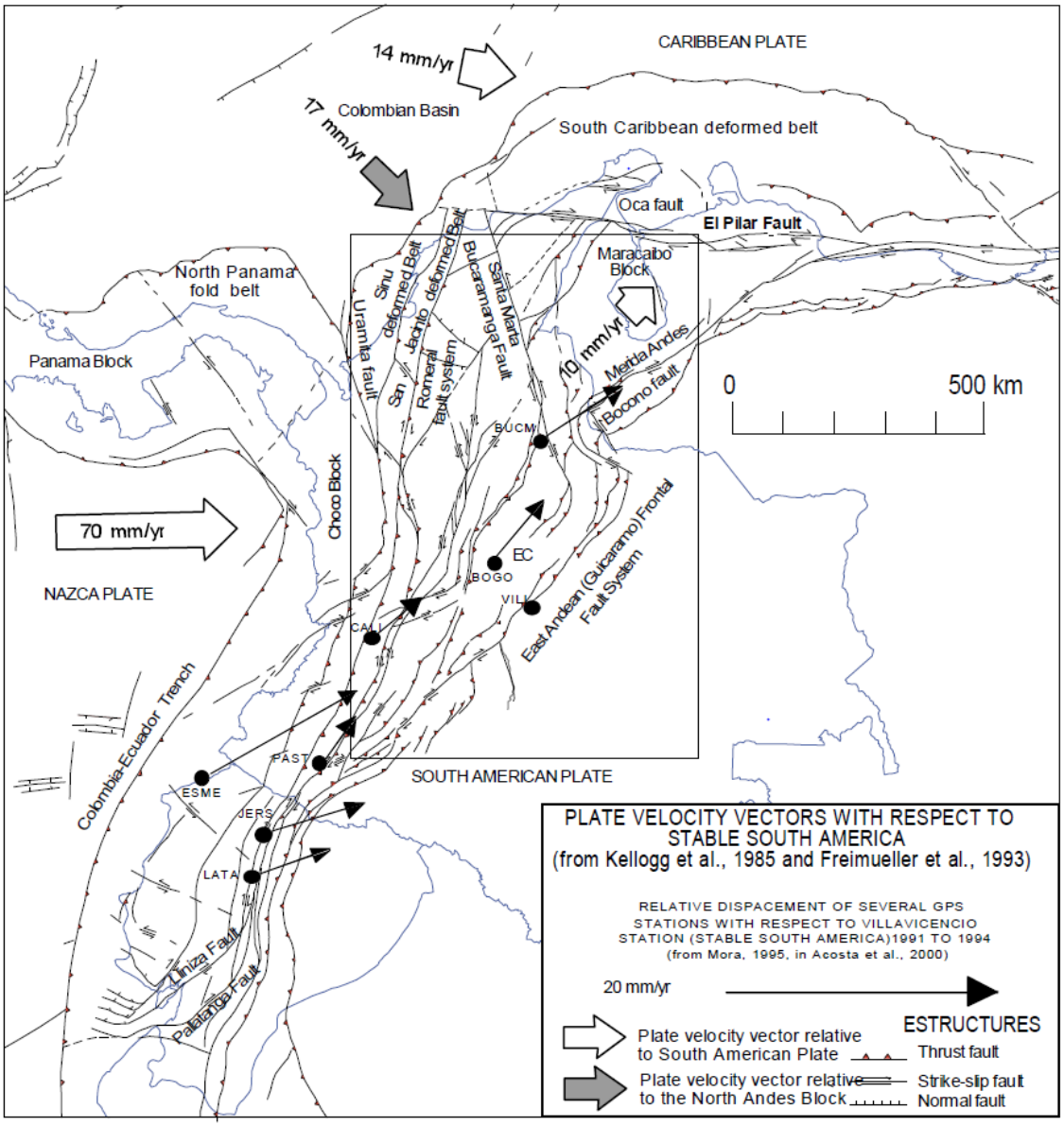

Figure 6.6. Tectonic-plate setting and major structures of the Northern Andes (from Sarmiento, 2001, modified from Mora, 1995 in Acosta et al 2000).

Cediel et al. (2003) divided Colombia into five tectono-stratigraphic zones: the Guyana Shield, the Maracaibo Sub-Plate, the Western Tectonic Realm, the Guajira Falcon

terrain and the Central Continental Sub-Plate. The Guayana shield extends beneath the eastern foreland of Colombia, through the Garzon Massif and under the Putumayo Basin.

The study area in this work is part of the Central Continental Sub-Plate (CCSP) (Figure 6.7), forming part of the South American Plate that contains the Proterozoic Chicamocha terrane, the Paleozoic Cajamarca-Valdivia terrane, the Mesozoic San Lucas and Ibague blocks (Cediel et al., 2003; Cediel and Shaw, 2019), the Magdalena Valley and the Eastern Cordillera.

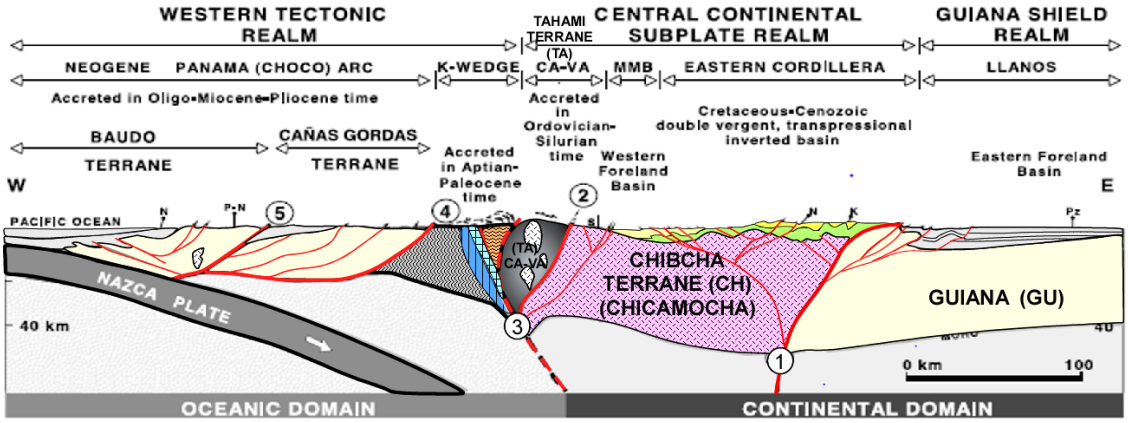

Figure 6.7. Section across the Colombian Andes. 1: Grenville (Orinoco) Santa Marta Bucaramanga – Suaza faults; 2: Ordovician-Silurian Palestina fault System; 3: Aptian Romeral-Peltetec fault system; 4: Oligocene-Miocene Garrapatas-Dabeiba fault system; 5: Late Miocene Atrato fault system. Abbreviations: K-wedge: Cretaceous wedge; CA-VA: Cajamarca-Valdivia terrane; MMB: Middle Magdalena Basin; sl: San Lucas Block; Pz: Paleozoic; K: Cretaceous; P: Paleogene; N: Neogene (Modified from Cediel et al, 2003).

A simplified terrane map of Colombia (Figure 6.8) shows the principal terranes identified in Colombia from the Eastern Cordillera to the Central Cordillera (Chibcha terrane = Chicamocha terrane, Tahamí Terrane = Cajamarca-Valdivia Terrane, and Kwedge = Quebradagrande, Arquia, Amaime and Dagua terranes).

The oldest allochthonous Precambrian component in the Central Continental Sub-Plate is the *Chicamocha terrane (Chibcha Terrane)*, which is considered a relic of the North American plate (Cediel et al., 2003; Cediel and Shaw, 2019), accreted to the Guiana Shield during the Grenville-Orinoco orogeny (1300-900 Ma, Cediel and Cáceres, 2000).

This belt is exposed in the Santander, Garzon and Sierra Nevada de Santa Marta massifs (granulites), and is bounded to the west by the Cajamarca-Valdivia terrane (CA-VA) = Tahamí Terrane(TA), intra-oceanic arc and continental margin accreted in the Ordovician-Silurian. This terrain collided the Chicamocha Terrane (Chibcha) to the North, and the Guyana shield to the South. The presently inverted sedimentary basin of the Eastern Cordillera and VMM overlies the Chicamocha Terrain (Cediel et al., 2003; Cediel and Shaw, 2019).

The separation of South America from North America and Africa during the Pangea break-up in the Early Jurassic (Wadge and Burke, 1983, Pindel and Kennan, 2001)

marks the start of the Caribbean evolution and generated different phases of extension, compression, plate convergence, subduction and obduction, which resulted in the current struture of the northwestern corner of South-America (Figure 6.7).

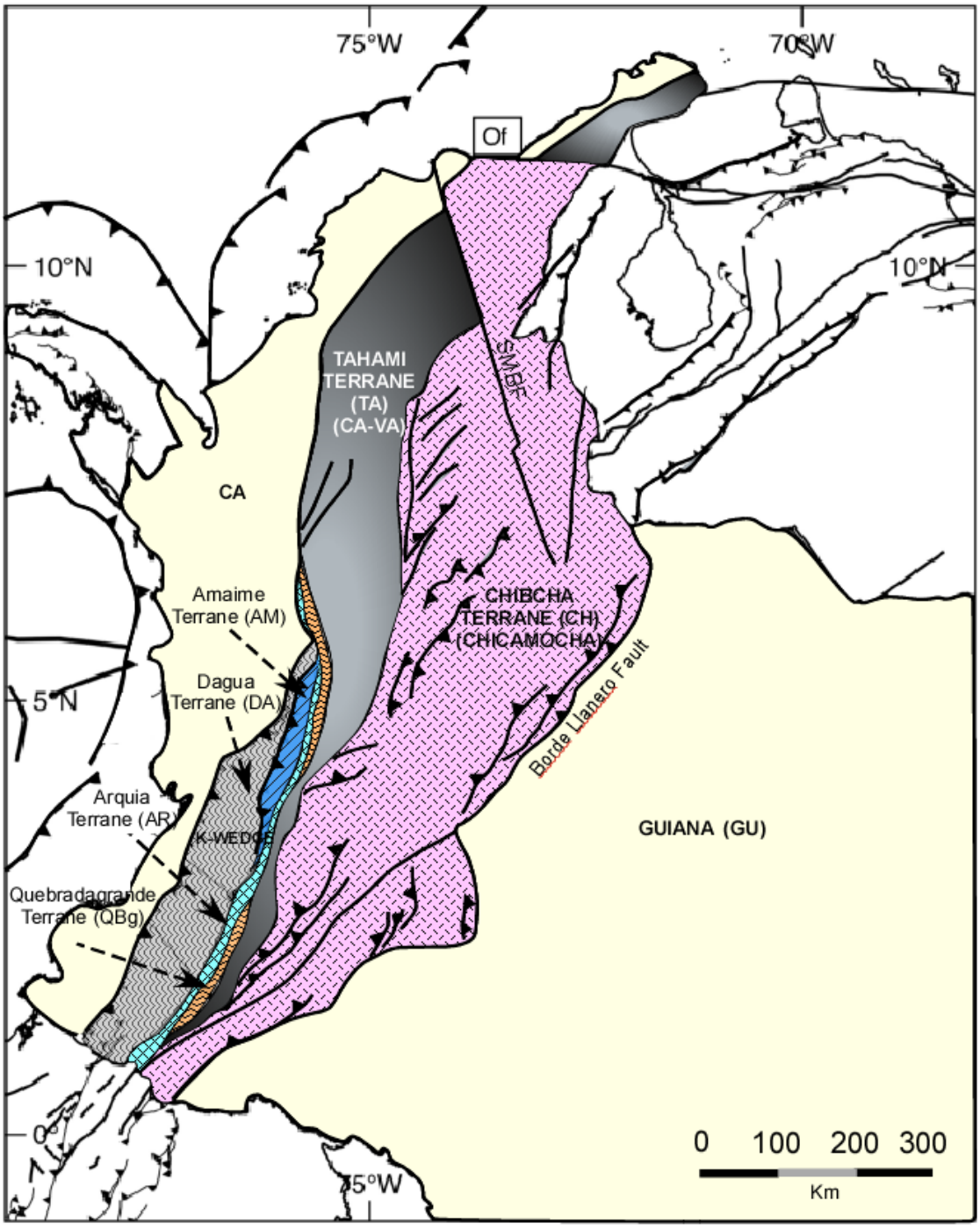

Figure 6.8.- Simplified map of northwestern South America showing the allochtonous terranes. TA: Tahamí terrane; AM: Amaime terrane; DA: Dagua terrane; AR: Arquia Terrane; QBg: Quebradagrande terrene; CA-VA: Cajamarca-Valdivia terrane = CH: Chibcha terrane; GU :Guiana; SMBF: Santa Martha – Bucaramanga Fault; CA:Caribe Terrane; Of: Oca fault. (Modified - after Colombian Geological Survey - Gomez et al., 2015).

Models summarizing the evolution of the deformation of northwestern South America were proposed by several authors. Mann (1995) proposed two hypotesis for the evolution of the Caribbean plate: 1) The Caribbean ocean results from the separation of North and South America between 130 and 80 Ma, and 2) The Caribbean plate is a result of the drift of an oceanic crust over the Galapagos hot spot.

The North Andean area extends from northwestern Peru to Colombia and eastern Costa Rica for about 2500 km, where Cretaceous allochthonous intra-oceanic arcs and oceanic terranes were accreted to the northwestern margin of South America.

The northern Andean zone has been subjected to different tectonic events for billions of years. At 1300-900 Ma the Grenville Orogeny (Orinoco Collision Orogeny) occurred as a result of the collision of the North American continental block with the Guiana Shield of South America (Kroonenberg, 1984; Hoffman, 1991 and Hartnady, 1991). High grade metamorphism occurred and the granulite belt of the Garzon Massif was exhumed at this time. At 480-416 Ma, a Cordilleran type orogeny took place, and subsidence of the basement allowed deposition of an extensive sequence of marine and epicontinental sediments during the Ordovician to Silurian. These supra-crustal levels underwent regional metamorphism and continental-type orogenic deformation (Quetame Orogeny in Colombia), evidenced by fragments of ophiolite and accretionary prism exposed in the Cajamarca-Valdivia (CA-VA) or Tahamí terrane (Figure 6.8), Loja and El Ori terranes (Cediel et al., 2003). The Tahamí terrane (or CA-VA) was added to western South America approximately along the Paleo-Palestina fault (Cediel et al., 2003; Cediel and Shaw, 2019). Between 360 and 125 Ma the Valle Alto rift opened (Bolivar Aulacogen), which allowed the invasion of a Cretaceous epicontinental seaway, marked by the deposition of variably thick sequences over extensive areas of the Central Continental Sub-Plate (CCSP), the Maracaibo Sub-plate, and part of the Guiana shield. Regional extension ended in the middle Cretaceous with the change of the compressional tectonic regime, as recorded by the lower Aptian regional erosional gap evidenced by stratigraphy (Cediel et al., 2003).

During the Late Jurassic (157 Ma), the separation of North America from northwest Africa is well documented, although still debated (Cinthia Labails, 2010). The pattern of volcanism, crustal thickness, geometry, and seismic velocities in the transition zone suggests symmetric rifting followed by asymmetric oceanic crustal accretion (Biari et al., 2017).

In general the tectonic style in the region is influenced by its interaction with the Caribbean plate (Pindell and Kennan, 2009). The northern Andean margin in Colombia comprises a series of accreted and autochthonous terranes juxtaposed to the continental plate during the Mesozoic (McCourt et al., 1984; Nivia et al., 2006; Villagómez et al., 2011).

The deformation at the western margin of South America may result from two tectonic regimes: extension with lithospheric thinning of the margin during the Late Jurassic to Early Cretaceous, and contraction from the Late Cretaceous to the Present. Then the igneous Quebradagrande Complex (140-130 Ma) onset to closed at 100 Ma (Kennan

and Pindell, 2009; Aspden and McCourt, 1986; Nivia et al., 2006). The northern Andes (Ecuador, Colombia) include oceanic terranes accreted to the western part of the continental northern South-America margin (Gansser, 1973; Goossens and Rose, 1973).

According to Nivia et al. (2006) metamorphic rocks of the Central Cordillera are Neoproterozoic in age, and are considered to be formed by at least two terranes separated by the Otú-Pericos fault (Etayo et al., 1986; Restrepo and Toussaint, 1988); the eastern terrane, named the Chibcha Terrane (or Chicamocha Terrane by Cediel et al, 2003), definitely has Proterozoic rocks (Ordóñez-Carmona et al., 2006) while in the western one, named the Tahamí Terrane (or Cajamarca-Valdivia (CA-VA) in Cediel et al, 2003; Cediel and Shaw, 2019), there are no reliable Pre-Devonian radiometric datings neither for the age of formation of the protoliths or for the age of metamorphism.

Three metamorphic events are reported: a Devo-Carboniferous one (Restrepo et al., 1991); a Permian-Triassic one (Restrepo et al., 1991; Ordóñez et al., 2001; Vinasco et al., 2006), and the Neoproterozoic age for the metamorphic basement is based on the Ordovician age of fossils of the Santa Teresa Formation (Nivia et al., 2006).

For the autochthonous Quebradagrande (QG) complex, Arquía blocks are located at the western edge of QG but are not clast of Arquia found in the sediments interbedded with basalts. Gómez-Cruz et al., (1995), show that the QG´s composition is bimodal, at the west composed by continental-derived sediments, while those composed of clast of basic and intermediate volcanic rocks and immature sediments, and metamorphic rocks are absent. The Quebradagrande complex (*sensu* Maya and González (1995), forms an elongated belt in N-S direction limited by the San Jerónimo fault at the east and Silvia–Pijao fault at the west, it is constituted by basalt, andesites and volcanoclastic rocks, occasionally ophiolites. The age of these units, based on fossils found in this formation, indicate Early Cretaceous (Moreno-Sánchez and Pardo-Trujillo, 2003). For Gonzáles (1980), the Mid-Hauterivian – Early Albian paleontological age of Quebradagrande is indicative that this terrane and all to the west were accreted after the Albian

The age of the Arquía metamorphic rocks corresponds to the Cretaceous to Paleocene ages (Restrepo and Toussaint, 1976; McCourt et al., 1984). The relation between Arquía and plutons is unknow, because the Arquia complex crops out in a very complex tectonic zone between the Romeral (San Jerónimo) and Cauca fault system ((Vinasco et al., 2006). The age of these blocks has been dated using K–Ar (55-58 +/- 1), Rb–Sr (53 – 57+/- 2 Ma) and Ar–Ar (45.8+/- 1.7), which indicates Paleocene ages (McCourt et al., 1984; Restrepo-Pace, 1995). For Maya and González (1995), the Arquía complex in general is formed by a belt of metamorphic rocks of high to medium pressure, limited at the west by the Cauca-Almaguer fault and to the east by the Sylvia-Pijao fault, the age of the metamorphic event based on dates is Early Cretaceous. This complex is the result of the union of several blocks of different ages and origins.

According to McCourt et al. (1984), the Amaime Formation is constituted by ophiolites, lavas and basaltic compositions affected by granitic intrusions (A. Nivia, 1989). Its age is subject to controversy, but the Early Cretaceous is suggested based on intrusions of

Buga Batholic. This unit groups the rocks of the Amaime Fm. between a block originated in an oceanic plateau, including the volcanic formation, located at west of the Cauca-Almaguer fault.

A stratigraphic gap is observed at 125-120 Ma (Barremian-Early Aptian) (Cediel et al., 2003), which supports the hiatus identified in this work using stratigraphic (Chapter 3) and geochronological information (chapter 4). During Late Aptian to early Albian times (115-105 Ma) an extensional regime prevailed (Jaillard, 1987). In Albian times (105-100 Ma), the Mochica phase records alternating extensional and contractional tectonic deformation (Cobbing et al., 1981; Mégard, 1984), responsible for the progradation of east-proceeding deltaic sandstones (Jaillard, 1987; 1994), while the western part of the margin recorded intense volcanic activity (Casma Group; Atherton et al., 1985; Soler, 1991). This event is interpreted as related to the opening of the Equatorial Atlantic Ocean, which provoked the westward drift of South America and an increased coupling along the subduction zone (Sébrier and Soler, 1990; Jaillard et al., 1996).

Around the Albian-Cenomanian boundary (≈100 Ma), flat subduction and metamorphism (K-Ar, high-pressure schist, eclogite) occurred in the northwest margin of South-America. Then, in Middle Cenomanian-Turonian times (95-89), a major marine transgression deposited shelf carbonates, while the volcanic arc front remained stable (Soler and Bonhomme, 1990; Jaillard 1991-1996).

Coniacian fine grained detrital (argillaceous) sediments overly, locally disconformably, Turonian limestones (Sempéré, 1994), and are probably related to the erosion of locally uplifted coastal areas (Jaillard, 1994). They are followed by coarser grained deposits of Santonian age and by a regional sedimentary hiatus (Jaillard et al., 2005), which represent the Peruvian phase of Steimann (1929). In the Late Campanian (75-70 Ma) a major contractional phase (Gayet et al., 1991; Jaillard et al., 1993) is responsible for a regional, widespread unconformity, and is followed by a new period of relative quiescence in the Maastrichtian. During the Maastrichtian-Paleocene times volcanic and plutonic rocks were emplaced along the Peruvian margin (Laughlin et al., 1968; Beckinsale et al., 1985; Clark et al., 1990). Later, widespread unconformities are observed between the fine-grained Paleocene and the coarse-grained Eocene continental deposits (Faucher and Savoyat, 1973; Maroco et al., 1987; Noble et al., 1990; Naeser et al,. 1991; Gayet et al., 1991), evidencing a major Late Paleocene tectonic phase. Then the Late Eocene shortening phase (Incaic phase) caused folding and reverse faulting (Dalmayrac et al., 1980).

The accretion of the Dagua terrane occurred in the Early Eocene (~49 Ma), and the accretion of the Gorgona terrane appears to be recorded in Middle Eocene-Oligocene times (40-28 Ma). Continued subduction and magmatism affected the Dagua-Piñon and Caribbean Mountain terrane. The Piñon in Ecuador typically was assigned to the Early Cretaceous (Goossens & Rose 1973; Jaillard et al. 1995a). However recently dated at the west of Guayaquil, the interpillow sediments are Coniacian–Campanian based on radiolarians and foraminifers (Vanmelle et al. 2008). The basalts, pillow basalts, dolerites and gabbroic intrusion are part of the Piñon Fm. According to Jaillard (2009),

this rock is geochemically very similar to Gorgona picrites, thus supporting the idea that some Colombian and Ecuadorian terranes belong to the same oceanic plateau (Jaillard E. 2009). As is indicated by Jaillard E. (2009), The Piñon terrane was accreted during the Late Paleocene (c, 58 Ma).

6.3 Tectonic evolution of the MMV and WEC

As indicated by Cooper et al. (1995), the MMV and EC were a major sedimentary area, which exhibits a complex history of evolution from Triassic to Recent times. The history started in the Jurassic as a synrift megasequence extending until the Early Cretaceous (Figures 6.6 and 6.11). Then the basin evolved as a back-arc basin located east of the subduction zone during the Cretaceous, and was dominated by shallow sedimentation until the Campanian. This sedimentation was suddenly interrupted by the collision of the Western Cordillera, which generated a foreland basin during the Maastrichtian (see also Etayo et al., 1969; Fabre, 1985; Cooper et al., 1995). Between Late Maastrichtian and Early Eocene times, this foreland basin received shallow marine sediments deposited in coastal plains and estuarine environments.

6.3.1. Cretaceous deformation and sedimentation in the MMV and WEC

The sequence of deformation and sedimentation in the MMV and WEC is illustrated on Figures 6.6 and 6.11. I used seismic information to understand and illustrate the evolution from Late Jurassic to Early Eocene times.

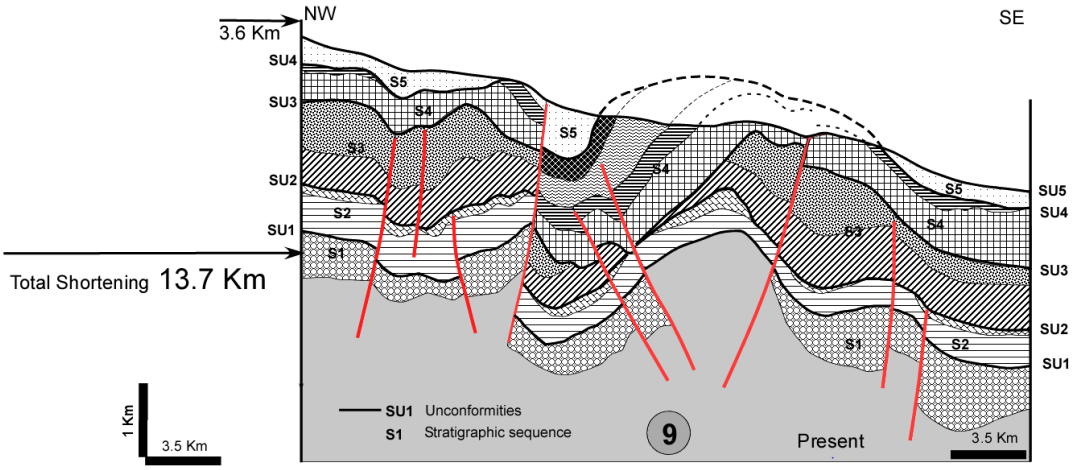

8 Late Campanian - Maastrichtian Deposition of S5 sequence

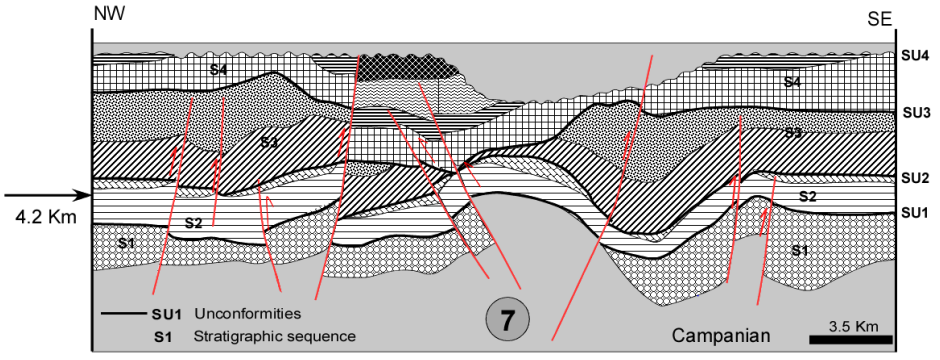

6 Late Cenomanian - Santonian Deposition of S4 sequence

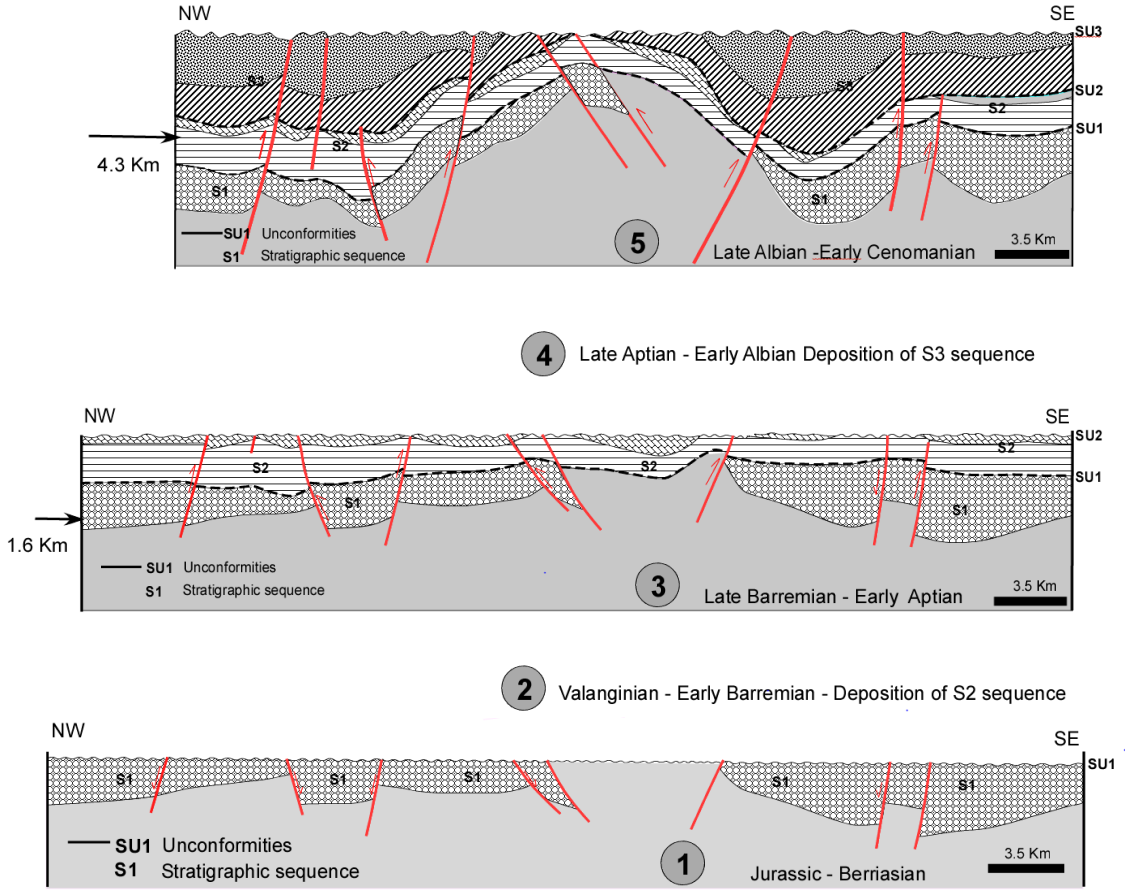

Figure 6.9 – Restored sections on profile CP-2008-1410 at different periods from Late Jurassic-Berriasian to the present times. SU1 to SU5, and S1 to S5 correspond to the unconformities and sequences identified in this work, respectively.

Jurassic syn-rift sediments (sequence S1) were partially eroded (SU1) during the Late Berriasian (Figure 6.9-1). Sequence S2 (6.9-2) was deposited during the Valanginian-Early Barremian, possibly during a sea level rise. In the Late Barremian-Early Aptian (Figure 6.9-3), a second emergence period eroded part of sequence S2 and generated the erosional surface SU2. A new marine transgression took place during the Late Aptian-Early Albian (Figure 6.9-4) and deposited sequence S3. A well-developed Late Albian to Early Cenomanian sequence was deposited (S3, Figure 6.9-5), which is subsequently deformed, generating a third unconformity (SU3) that deeply eroded sequence S3 and even locally reached sequence S2. The sequence S4, deposited during the Late Cenomanian-Santonian (Figure 6.9-6), was then eroded by unconformity SU4 during the Early Campanian (Figure 6.9-7). Finally, sequence S5 deposited from Late Campanian to Maastrichtian times (Figure 6.9-8) was deformed and eroded during the Paleocene-Early Eocene, generating unconformity SU5 (Figure 6.9-9).

The sections restored in Figure 6.9 show that several cycles of deposition and erosion occurred during the Cretaceous, which could result from the interaction between

subsidence, local or regional uplift, compressional events, climate, eustacy and sediment supply.

In the restored sections (Figures 6.9 and 6.10), I measured the shortening in each stage of deformation using length balancing (Figure 6.9). The total shortening, from late Jurassic to the present, is 13.7 km to the North (Figure 6.9) and 18.7 km to the South (Figure 6.10). The calculated shortening is almost 27% greater at the southern secion than at the northern section (Figure 6.9 and 6.10), which means that the total deformation was greater at the south along through the MMV and the WEC.

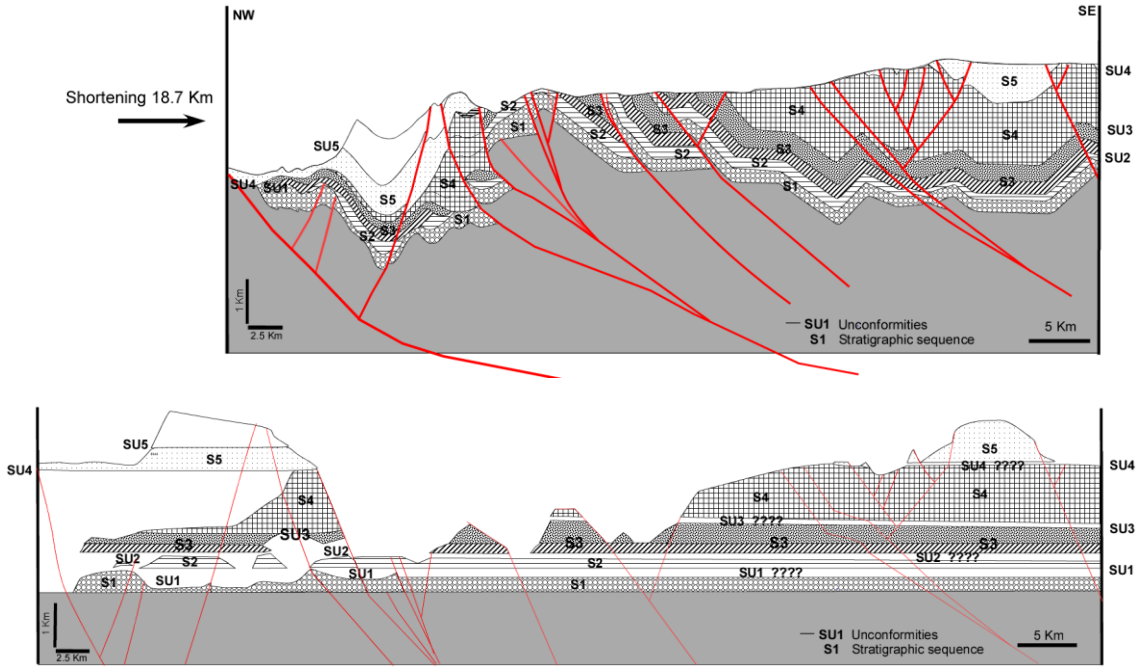

Figure 6.10 – Restored sections from the southern composed profile from seismic section RG-1991-08, SD-19, H-1978-06, and section from surface information. From non-deformed section during the Jurassic to the present. In these section the sequences deposited (S1 to S5), the unconformity surfaces (SU1 to SU5) and also the total shortening are shown (this work).

6.3.2. Geological evolution of the Middle Magdalena Basin and the Western Eastern Cordillera

Figure 6.11 shows schematic 3D-diagrams depicting the evolution of the MMV and WEC basins between Late Jurassic and Santonian times, taking into account the information obtained in chapters 3, 4 and the present chapter (Figure 6.6).

Paleofacies maps integrated in these diagrams show the vertical and lateral facies variations, the vertical distribution of parasequences (A/S) and the sea level fluctuations using transgressive-regression curves (chapter 3, Figure 3.5). Unconformities (sequence boundaries) have been identified, based on local information from wells, outcrops and chronostratigraphic analysis, using mainly seismic information.

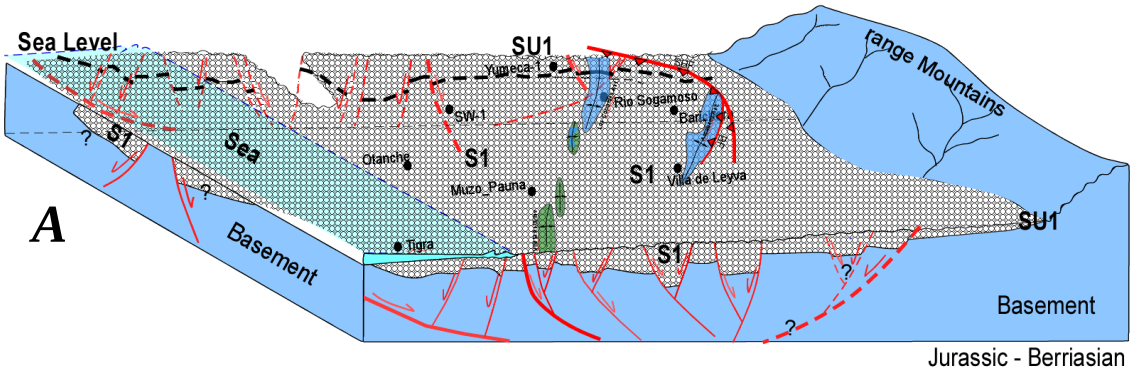
Sea Level
SU1
Yumeca-1
Rio Sogamoso
Barichara
range Mountains
SW-1
S1
Sea
Otanche
Muzo_Pauna
Villa de Leyva
A
Basement
Tigra
SU1
Basement
Jurassic - Berriasian

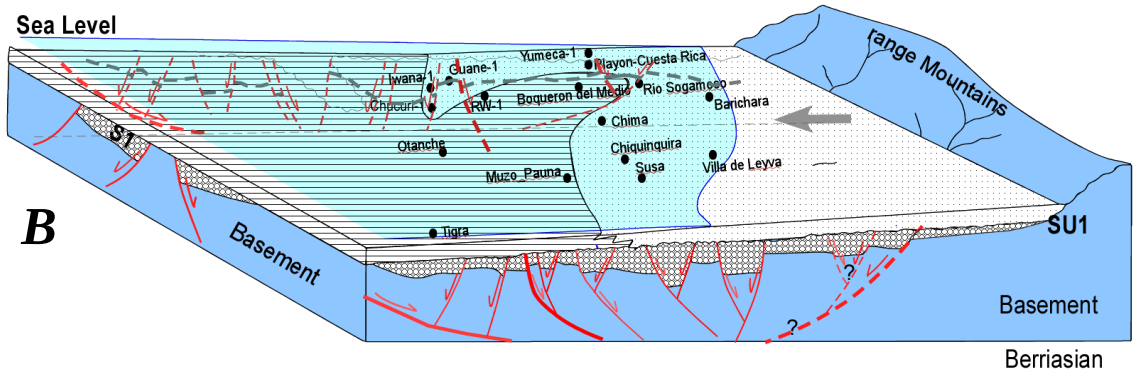
Sea Level
Yumeca-1
Playon-Cuesta Rica
Iwana-1
Guane-1
Rio Sogamoso
Chucuri-1
Boqueron del Medio
SW-1
Barichara
range Mountains
Chima
Otanche
Chiquinquira
Susa
Villa de Leyva
Muzo_Pauna
S1
B
Basement
Tigra
SU1
Basement
Berriasian

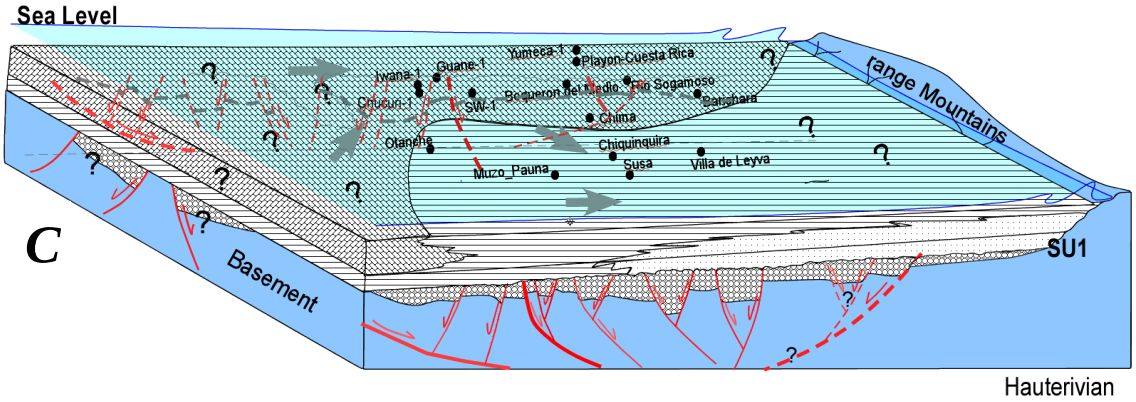
Sea Level
Yumeca-1
Playon-Cuesta Rica
Iwana-1
Guane-1
Rio Sogamoso
Chucuri-1
SW-1
Barichara
range Mountains
Chima
Otanche
Chiquinquira
Susa
Villa de Leyva
Muzo_Pauna
C
Basement
SU1
Hauterivian

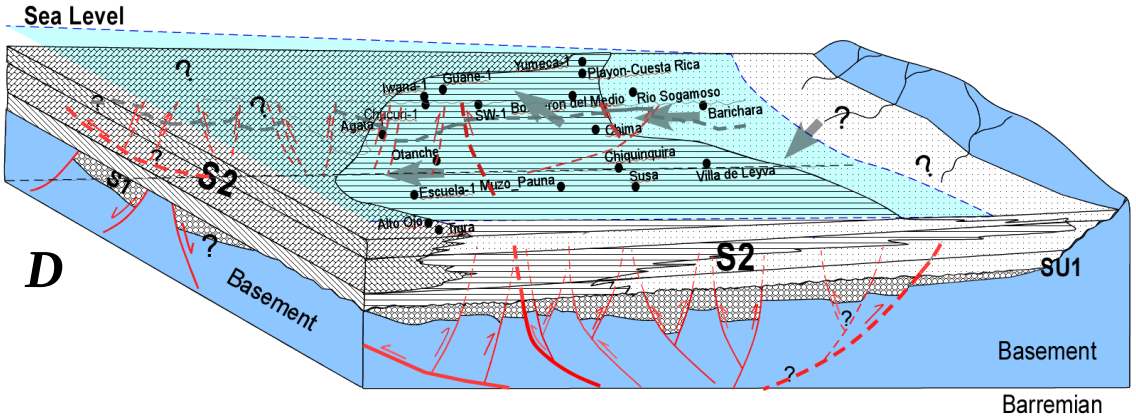
Sea Level
Yumeca-1
Playon-Cuesta Rica
Iwana-1
Guane-1
Rio Sogamoso
Chucuri-1
Agata
SW-1
Barichara
Chima
Otanche
Chiquinquira
Susa
Villa de Leyva
Escuela-1
Muzo_Pauna
Alto Cio
Tigra
S1
S2
D
Basement
S2
SU1
Basement
Barremian

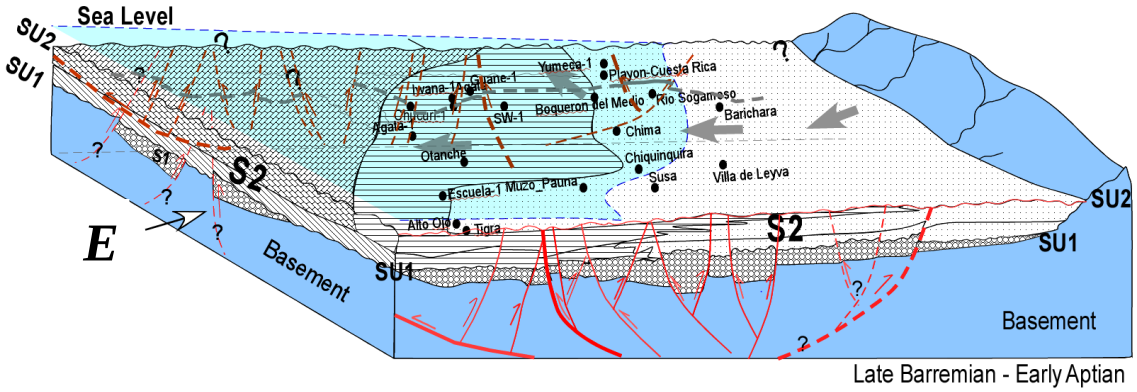

Late Barremian - Early Aptian

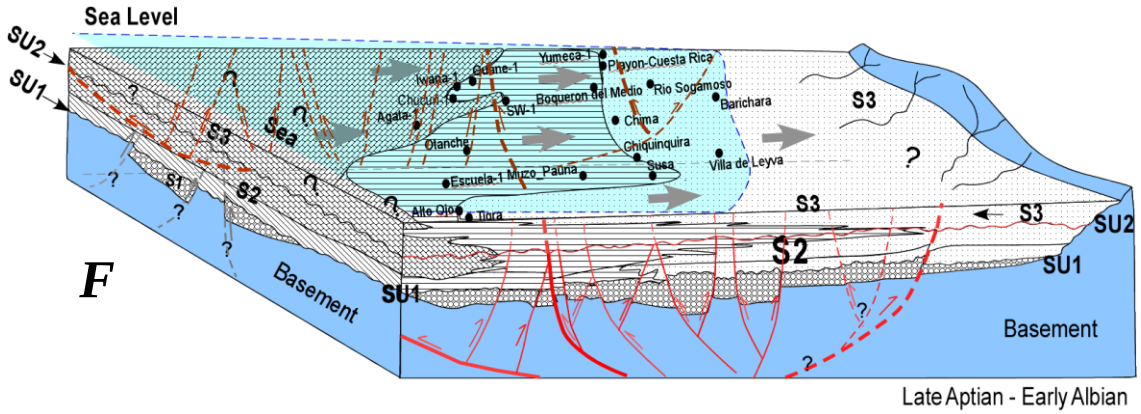

Late Aptian - Early Albian

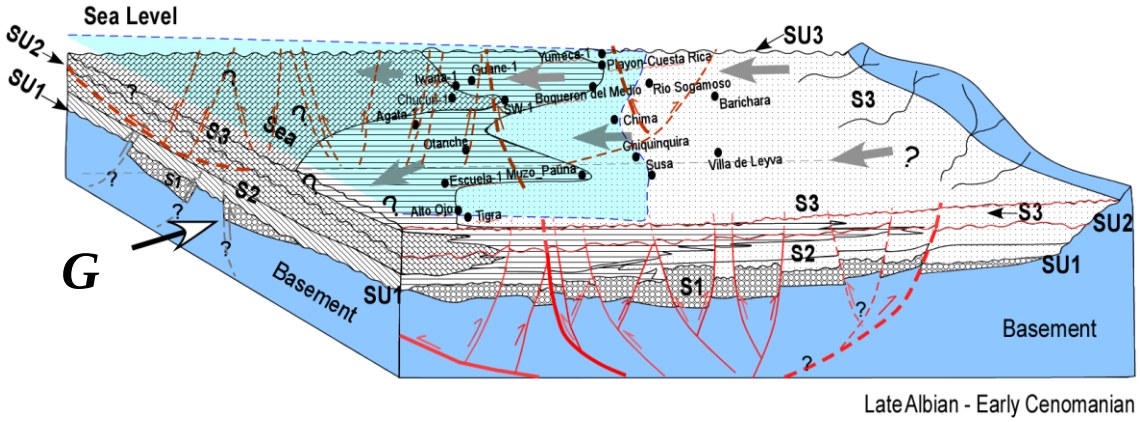

Late Albian - Early Cenomanian

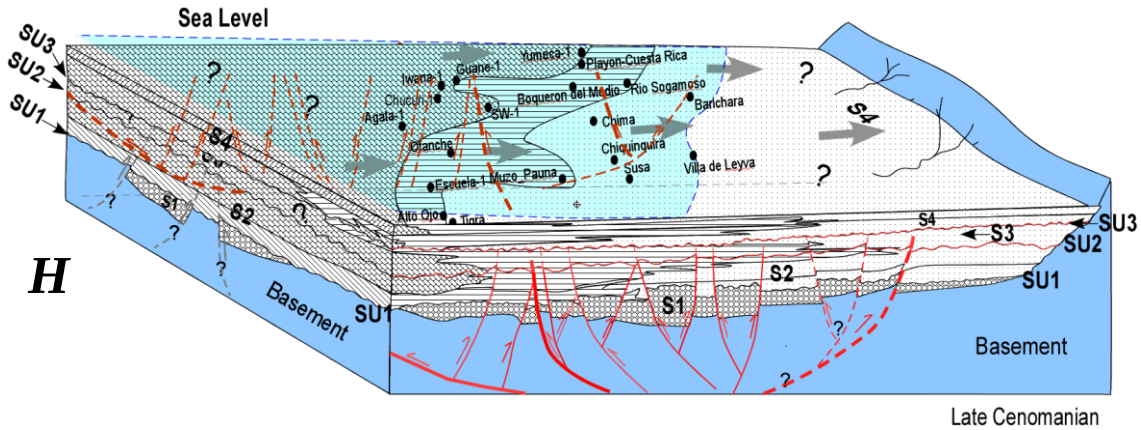

Late Cenomanian

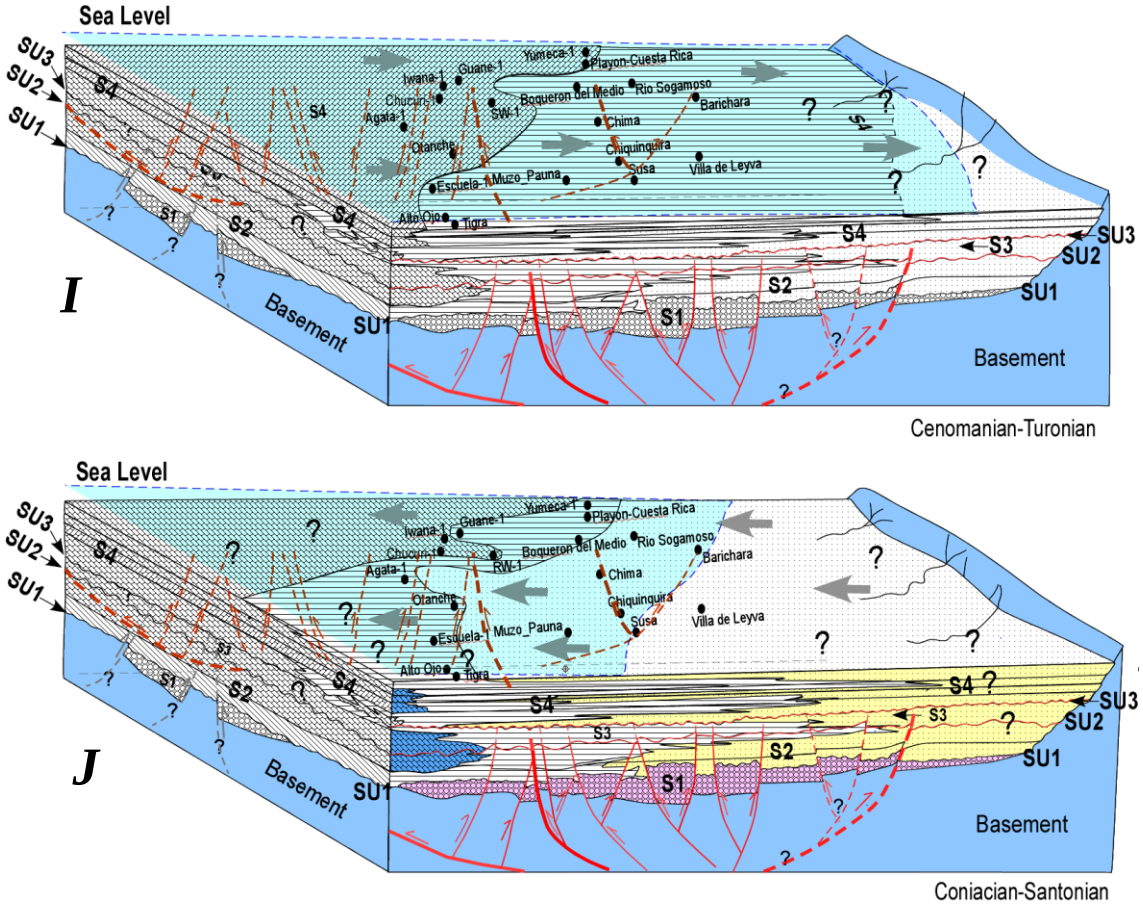

Figure 6.11 – Schematic 3D Diagrams, showing the evolution of the Middle Magdalena Basin from Late Jurassic (A) to Coniacian- Santonian times (J). Note that these sketches take into account depositional and erosion periods, as well as structural deformation.

During the Late Jurassic-Early Berriasian, red beds of sequence S1 were deposited in a rift basin (Figure 6.11-A) and partially eroded during the Late Berriasian (Figure 6.11-A). Deposition of sequence S2 started during the Late Berriasian regression (Figures 6.11-B and 3.48) and continued during the transgression occurred during the Hauterivian (Figures 6.11-C and 3.50). A new regression started during the Barremian (Figures 6.11D and 3.51), and the sequence S2 was partially eroded (Figures 6.11E and 3.52) during a major Late Barremian-Early Aptian regression. During the Late Aptian-Early Albian transgression (Figures 6.11F and 3.53), sequence S3 was deposited and subsequently partially eroded during a regression occurred in the Late Albian-Early Cenomanian (SU3; Figures 6.11G and 3.54). Sequence S4 began to be deposited during the Late Cenomanian transgression (Figure 6.11-H) that continued during the Late Cenomanian-Turonian, during an important regional marine transgression (Figures 6.11-I and 3.55) and ended with sandstone deposition during the Coniacian-Santonian regression (Figures 3.11J, 3.56). The Early Campanian erosion surface (SU4) partially or totally eroded the sequence S4, and older sequences locally. Sequence S5 was deposited discordantly over the eroded S4 sequence and is followed with the regional erosion surface of Paleocene-Early Eocene age (SU5). Note that deformation along through the 3D-diagrams in the northern areas is represented by dotted lines, while in the southern are represented by the continuous lines.

6.3.3. Ro and Thermal models

As was shown in chapter 5 the thermal modeling from the north to the south indicates the occurrence of two events of heating and two events of cooling for units older than Campanian (Figures 5.30 A, B and C) and as expected one event of heating and one event of cooling for units younger than ~70Ma (Figure 6.12).

As was discussed also in chapter 5, the higher temperatures in the southern area may be due to the sufficient sediment supply to the basin to reach a higher thickness, or magmatic activity in the central and southern areas that increased the temperature till values as high as 285°C (Gomez, 2001; Mora, et al., 2013) at 200 Ma (Gomez, 2001).

A comparable and similar behavior to what was determined in this work, was also observed by Villagómez et al. (2010) along the eastern margin of the Western Cordillera of Colombia (Figure 6.12). Also Villagómez et al. (2010) observed a slow cooling (< 2°C/Ma) between 65 Ma and 30 Ma, although our T-t tendency in this period is more similar to that observed by Sanchez (2012) in the WEC (Figure 5.32 in chapter 5). However, the last cooling event started at ~30 Ma in the WC for Villagómez et al. (2010) and at 20 Ma for Sanchez (2012), whereas I found that this event began at an age < 5 Ma in the WEC.

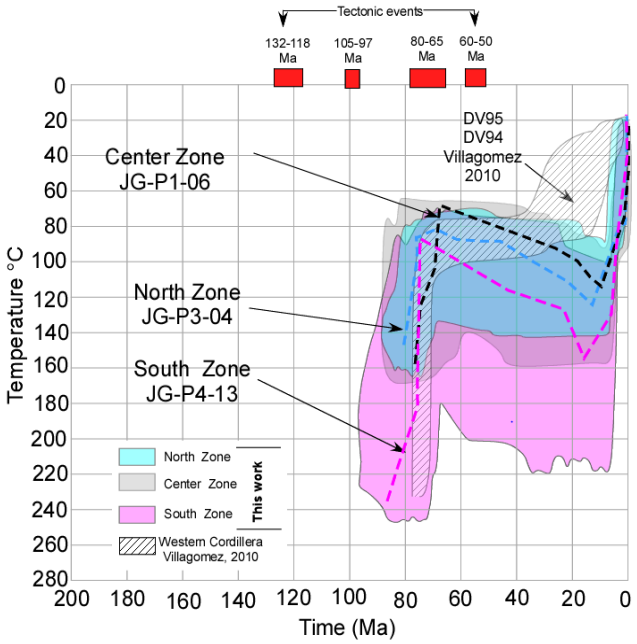

Figure 6.12 *- Compendium of thermal modeling solutions for selected samples in the study area for Aptian-Albian units., in the north, central and south zones. Data by Villagómez (2010) from the western Cordillera is also shown. Red squares at the top represent the timing of major tectonic events in Colombia.*

The thermal models from this work evidence a slow heating event between ~70 and ~5 Ma, and a rapid cooling event in the last 5 Ma or less. These last thermal observations from this work are consistent with that shown by Sanchez (2012) (see chapter 5, Figure 5.39) and differs from that evidenced by Villagómez et al. (2010) for the same period.

6.4 Model for the pre-Andean tectonic evolution of the MMV and WEC.

As is indicated by Jaillard et al. (1995), the onset of subduction in Colombia and Ecuador is poorly constrained, and may be subsequent to Triassic rifting and the opening of the western Tethys ocean. However, $^{40}Ar/^{39}Ar$ and U-Pb (Villagomez et al., 2010) and $K/^{39}Ar$ on horblend and biotite dates (Sillitoe et al., 1982; Brook, 1984) from granitoids of the Ibague Batholith suggest that subduction-related magmatism in Colombia occurred at 180 Ma, continued till 147 Ma and finalized around 145 Ma ago (Aspeden et al., 1987; Jaillard et al., 1990).

My tectonic reconstruction shows eight evolution stages for northwestern South America between 150 Ma (Late Jurassic, Figures 6.13-A-a) and 50 Ma (Early Eocene, Figure 6.13-G-g). In this interpretation I try to use simple concepts only related to the regime of subduction (Doglioni et al., 1998; Horton and Fuentes, 2016, Espurt et al., 2008) to explain the deformation observed in the MMV and WEC, taking into account our observations from the MMV-WEC and aiming to give a likely model explaining the evolution of the analyzed basin.

To the West, the Tahamí Terrane (CA-VA) was emplaced since the Ordovician-Silurian (Figure 6.13). Against this block, steep-dipping subduction of an oceanic plate below the proto-Central Cordillera occurred between 150 Ma-130 Ma (Figure 6.13-Aa), generating extension in the MMV and WEC paleo-basins and allowing the deposition of the sequences S1 and S2 in a rift basin. Between 132 to 125 Ma, no continental volcanic-arc activity is known (Jaillard et al., 2000). I propose that, during the Late Barremian – Early Aptian (125-118 Ma), the angle of subduction of the paleo-oceanic plate changed and flattened, probably till below the MMV, producing compression, elevation and shortening in the basin, thus generating partial or total erosion of the deposited sequences SU1 and SU2 (Figure 6.13 Bb).

During the Late Aptian – Early Albian (115-107 Ma), the slab continued subducting in a high angle (Figure 6.13C), inducing a period of extension and relaxation in the basin, generating acommodation space and depositing sequence S3 in the MMV–WEC.

The 150 to 110 Ma period is marked by the complete reorganization of the paleogeographic pattern, due to a drastic change in the convergence direction, which generated tectonic deformation and a magmatic arc reorganization, followed by a diachronous marine transgresion (Aspden et al., 1987; Jaillard et al., 1990; 1995; 2000).

In the Late Albian-Early Cenomanian (105-97 Ma), a flat subduction period induced a contractional tectonic regime, shortening, and erosion materialised in SU3 (Figure 6.13-Dd). At this time the Quebradagrande terrane was drifting toward the proto-Central Cordillera. This event was triggered by the openning of the equatorial Atlantic Ocean that forced South America to drift Westward (Jaillard, 1991; 1996; 2000). It can be correlated with the Mochica phase (Mégard, 1984), related to an increased convergence rate between the paleo-Pacific and South American plates (Jaillard, 1991; 1996; 2000), and provoking the progradation of deltaic sandstones proceeding from the east (Jaillard, 1987; 1994). This event is alternatively considered as extensional and contractional (Cobbing et al., 1981) and responsible for early deformation in Peru (Cobbing et al.,

1981) and for the incipient uplift of the Eastern Cordillera in Ecuador (Litherland et al., 1994),

Between 95 and 83 Ma (Late Cenomanian-Late Santonian), the slab continued sudducting with a high angle below the continent, generating a tectonic extension and enough space to deposit limestones and calcareous shales of the La Luna Formation (sequence S4, Figure 6.13 E). At this time a volcanic arc formed at the western edge of the paleo-Pacific Plate (Quebradagrande arc-Arquia), which drifted toward Northwestern South America.

The Piñon basement (Ecuador) was classically ascribed to the Early Cretaceous (Goossens and Rose 1973; Jaillard et al. 1995a). It has been recently dated west of Guayaquil, where interpillow sediments yielded Coniacian–Mid Campanian radiolarians and foraminifera (Vanmelle et al., 2008; Jaillard et al., 2009). The top of the Piñón Formation would be of Early Coniacian age, implying that the Piñón Formation is not Early Cretaceous, and represents a fragment of the Caribbean Colombian Oceanic Plateau (CCOP). This unit was also dated by Luzieux et al. (2007), who obtained a $^{40}Ar/^{39}Ar$ age of 88 Ma±1.6 on horblend, from oceanic plateau basement rock in coastal Ecuador.

Between 80-70 Ma, a new portion of the oceanic plate was subducted as a flat slab below the proto-CC and the proto-VMM (Figure 6.13 Ff), generating a tectonic compresion, shortening and deformation that triggered erosion. At that time, the Amaime terrane was drift toward the continent. This event is responsible for the erosion represented by surface SU4, which provoked the partial or total erosion of sequence S4, and locally down to sequence S2, and the rapid cooling evidenced by our fission track data (Figure 6.12), representing the most important Cretaceous unconformity. Gayet et al. (1991) and Jaillard et al. (1993) consider the Late Campanian event as a major contractional phase. According to Pindell et al. (1988, 2001), the spreading rate in the Proto-Caribbean plate decreased strongly in the Campanian, and the Caribbean boundary became compressional. This event triggered a significant uplift of the Central Cordillera of Colombia and Ecuador and accretion of oceanic terranes to the Ecuadorian and Colombian margin (Pindell et al., 2001; Jaillard et al., 2009) (Figure 6.13-Ff).

In the MMV and WEC of Colombia, Middle Campanian deposits (Umir Fm) directly rest upon Cenomanian (Simiti Fm, Figure 4.13), Turonian (Lower La Luna Fm), or even Jurassic strata (see Figure 4.14 in chapter 4). In Ecuador, Litherland et al. (1994) noted that this event is marked by a regional hiatus of Campanian age and by a significant thermal event recorded in the Eastern Cordillera around 80-70 Ma.

Santonian-Campanian times are known as a turning point in the Andean evolution (Steinmann, 1929). In Peru, diachronous Late Santonian to Middle Campanian transgressive shelf sediments overlie unconformably the deformed pre-Santonian turbidites (Jaillard et al., 1995. 1999). In the Talara basin of northern Peru, Albian deposits are unconformably overlain by Campanian trasngressive deposits (Gonzales, 1976; Macharé et al., 1986; Séranne, 1987; Morales, 1993); and in Paita (northern

Peru), Middle Campanian beds unconformably overly the Paleozoic basament (Jaillard et al., 1999; 2005).

In Early Maastrichtian-Early Paleocene times (70-60 Ma) a new oceanic plate subducted with a high angle (Figure 6.13 Gg), generating an extensional tectonics; accommodation space was created and sequence S5 was deposited. At that time, the Dagua terrane is migrating towards the proto-Central Cordillera.

Finally for the Late Paleocene-Early Eocene (60-50 Ma), the oceanic plate was subducted with a low angle (Figure 6.13 Hh) below the proto-Central-Cordillera (CC) and below the basin of the MMV and probably the WEC, generating a period of compression, shortening, uplift and erosion (SU5 unconformity).

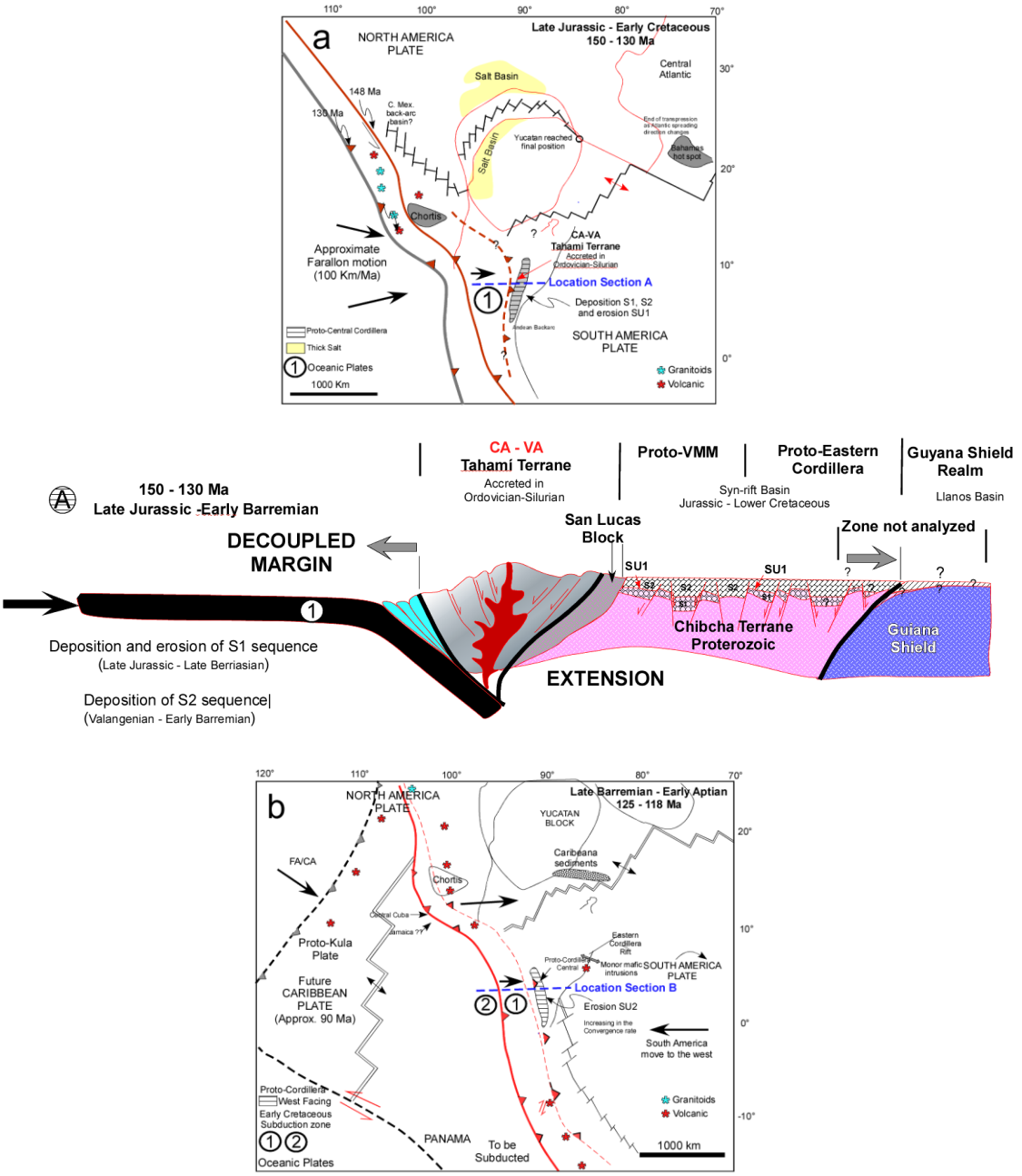

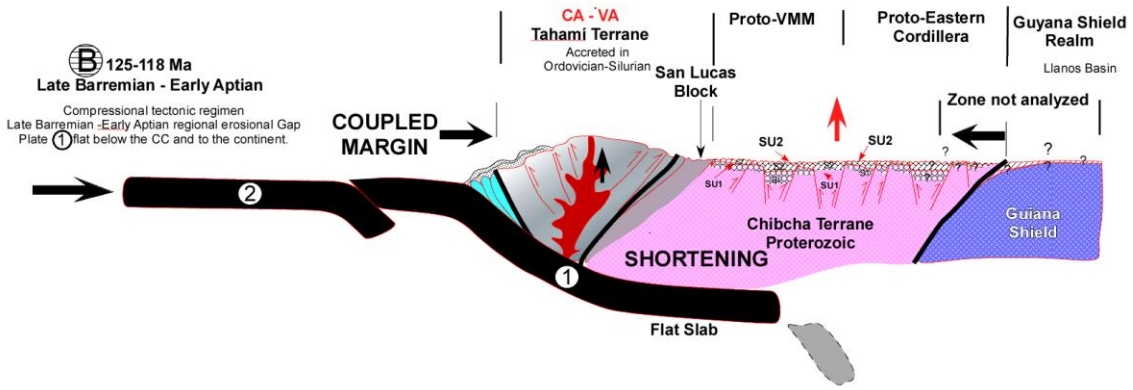
B
125-118 Ma
Late Barremian - Early Aptian
Compressional tectonic regimen
Late Barremian -Early Aptian regional erosional Gap
Plate 1 flat below the CC and to the continent.
CA - VA
Tahami Terrane
Accreted in
Ordovician-Silurian
Proto-VMM
Proto-Eastern
Cordillera
Guyana Shield
Realm
Llanos Basin
San Lucas
Block
Zone not analyzed
COUPLED
MARGIN
SU2
SU1
Chibcha Terrane
Proterozoic
Guiana
Shield
SHORTENING
Flat Slab

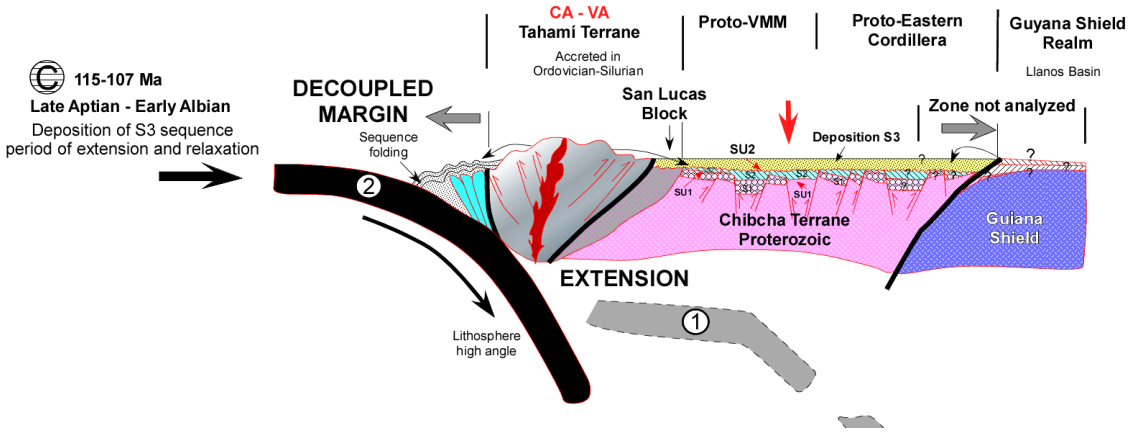
C
115-107 Ma
Late Aptian - Early Albian
Deposition of S3 sequence
period of extension and relaxation
CA - VA
Tahami Terrane
Accreted in
Ordovician-Silurian
Proto-VMM
Proto-Eastern
Cordillera
Guyana Shield
Realm
Llanos Basin
DECOUPLED
MARGIN
Sequence
folding
San Lucas
Block
Zone not analyzed
Deposition S3
SU2
SU1
Chibcha Terrane
Proterozoic
Guiana
Shield
EXTENSION
Lithosphere
high angle

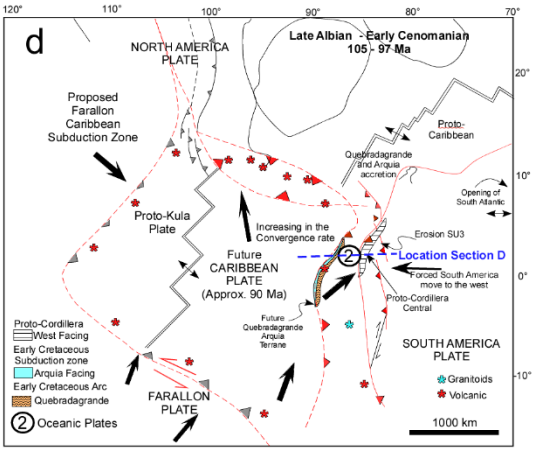
d
Late Albian - Early Cenomanian
105 - 97 Ma
NORTH AMERICA
PLATE
Proposed
Farallon
Caribbean
Subduction Zone
Proto-
Caribbean
Quebradagrande
and Arquia
accretion
Opening of
South Atlantic
Proto-Kula
Plate
Increasing in the
Convergence rate
Erosion SU3
Location Section D
Future
CARIBBEAN
PLATE
(Approx. 90 Ma)
Forced South America
move to the west
Proto-Cordillera
Central
Future
Quebradagrande
Arquia
Terrane
SOUTH AMERICA
PLATE
Granitoids
Volcanic
Proto-Cordillera
West Facing
Early Cretaceous
Subduction zone
Arquia Facing
Early Cretaceous Arc
Quebradagrande
Oceanic Plates
FARALLON
PLATE
1000 km

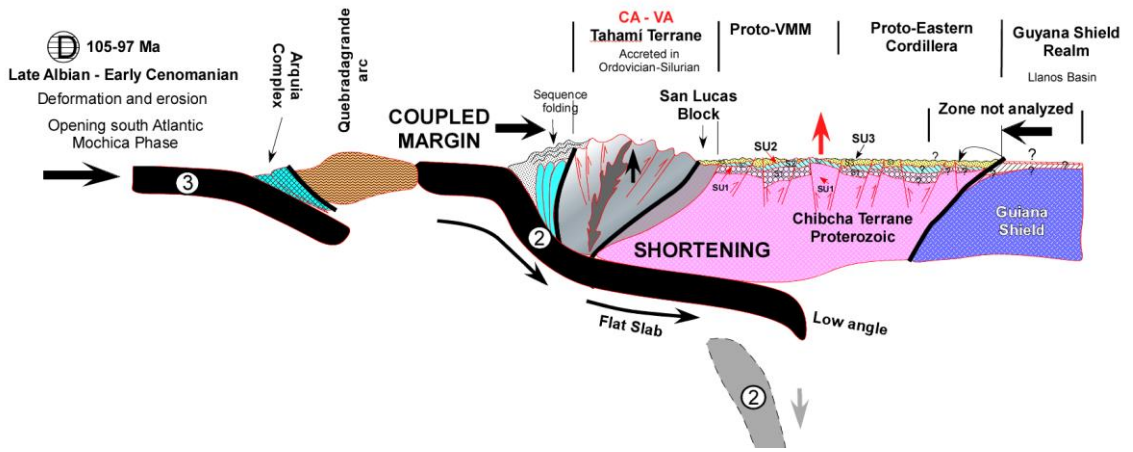
D
105-97 Ma
Late Albian - Early Cenomanian
Deformation and erosion
Opening south Atlantic
Mochica Phase
Arquia
Complex
Quebradagrande
arc
CA - VA
Tahami Terrane
Accreted in
Ordovician-Silurian
Proto-VMM
Proto-Eastern
Cordillera
Guyana Shield
Realm
Llanos Basin
COUPLED
MARGIN
Sequence
folding
San Lucas
Block
Zone not analyzed
SU2
SU3
SU1
Chibcha Terrane
Proterozoic
Guiana
Shield
SHORTENING
Flat Slab
Low angle

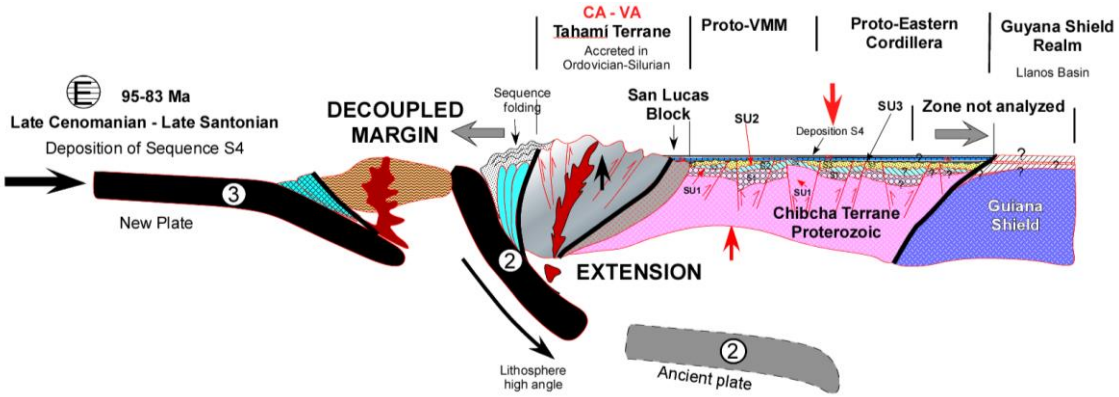
CA - VA
Tahamí Terrane
Accreted in
Ordovician-Silurian
Proto-VMM
Proto-Eastern
Cordillera
Guyana Shield
Realm
Llanos Basin
95-83 Ma
Late Cenomanian - Late Santonian
Deposition of Sequence S4
DECOUPLED
MARGIN
Sequence
folding
San Lucas
Block
SU2
SU3
Deposition S4
Zone not analyzed
New Plate
SU1
SU1
Chibcha Terrane
Proterozoic
Guiana
Shield
EXTENSION
Lithosphere
high angle
Ancient plate

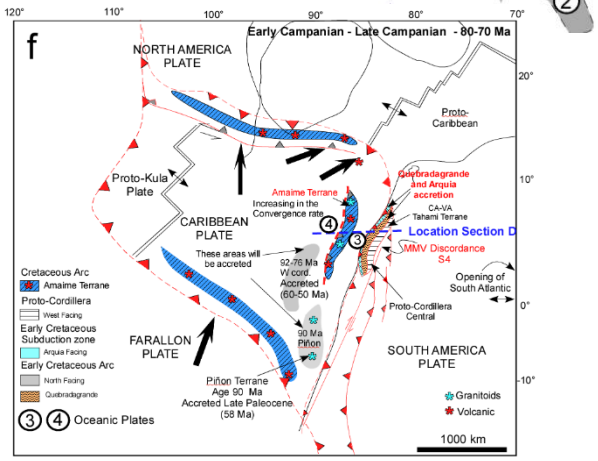
f
Early Campanian - Late Campanian - 80-70 Ma
NORTH AMERICA
PLATE
Proto-
Caribbean
Proto-Kula
Plate
Amaime Terrane
Increasing in the
Convergence rate
Quebradagrande
and Arquia
accretion
CA-VA
Tahami Terrane
CARIBBEAN
PLATE
Location Section D
MMV Discordance
S4
These areas will
be accreted
92-76 Ma
W cord
Accreted
(60-50 Ma)
Opening of
South Atlantic
Proto-Cordillera
Central
90 Ma
Piñon
FARALLON
PLATE
SOUTH AMERICA
PLATE
Piñon Terrane
Age 90 Ma
Accreted Late Paleocene
(58 Ma)
Granitoids
Volcanic
Cretaceous Arc
Amaime Terrane
Proto-Cordillera
West Facing
Early Cretaceous
Subduction zone
Arquia Facing
Early Cretaceous Arc
North Facing
Quebradagrande
3 4 Oceanic Plates
1000 km

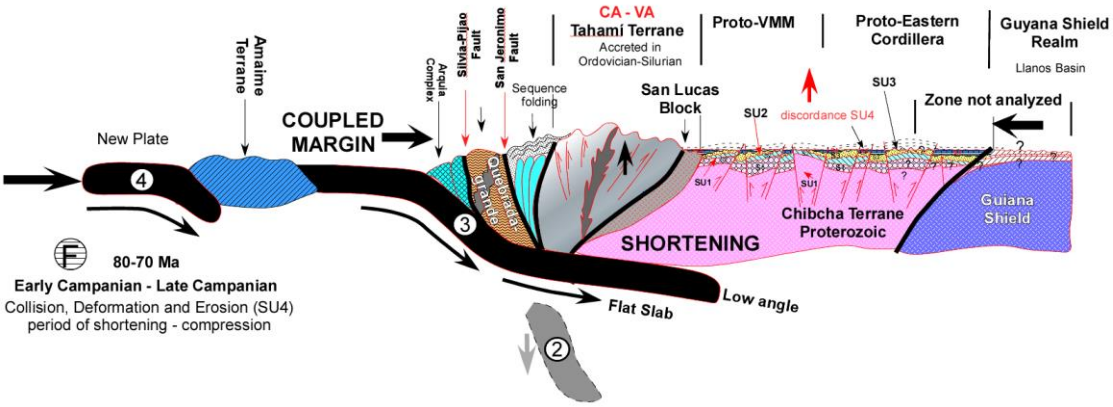
CA - VA
Tahamí Terrane
Accreted in
Ordovician-Silurian
Proto-VMM
Proto-Eastern
Cordillera
Guyana Shield
Realm
Llanos Basin
Amaime
Terrane
Arquia
Complex
Silvia-Pijao
Fault
San Jeronimo
Fault
Sequence
folding
San Lucas
Block
SU2
discordance SU4
SU3
Zone not analyzed
New Plate
COUPLED
MARGIN
Quebradagrande
SU1
SU1
Chibcha Terrane
Proterozoic
Guiana
Shield
SHORTENING
80-70 Ma
Early Campanian - Late Campanian
Collision, Deformation and Erosion (SU4)
period of shortening - compression
Flat Slab
Low angle

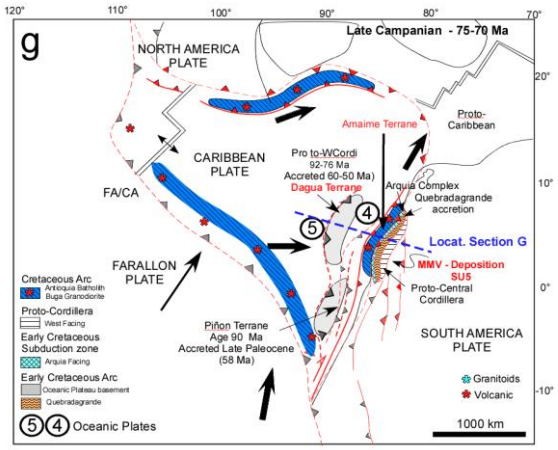
g
Late Campanian - 75-70 Ma
NORTH AMERICA
PLATE
Amaime Terrane
Proto-
Caribbean
CARIBBEAN
PLATE
Pro to-WCordi
92-76 Ma
Accreted 60-50 Ma)
Dagua Terrane
FA/CA
Arquia Complex
Quebradagrande
accretion
Locat. Section G
MMV - Deposition
SU5
FARALLON
PLATE
Proto-Central
Cordillera
SOUTH AMERICA
PLATE
Piñon Terrane
Age 90 Ma
Accreted Late Paleocene
(58 Ma)
Granitoids
Volcanic
Cretaceous Arc
Antioquia Batholith
Buga Granodiorite
Proto-Cordillera
West Facing
Early Cretaceous
Subduction zone
Arquia Facing
Early Cretaceous Arc
Oceanic Plateau basement
Quebradagrande
5 4 Oceanic Plates
1000 km

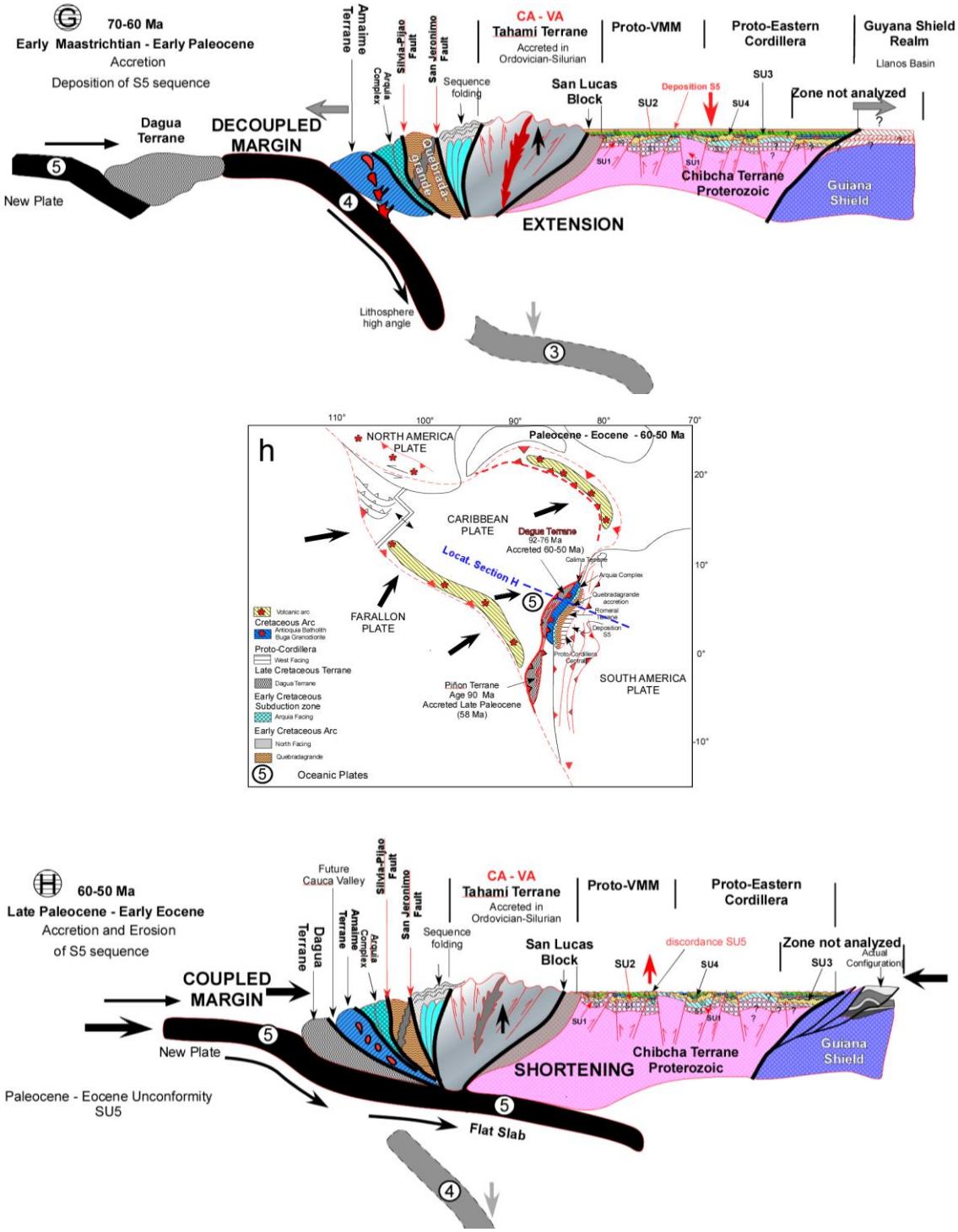

Figure 6.13. *Plate reconstruction (**a** to **h**) and sketchy tectonic evolution of northwestern South America (Western Colombia) (**A** to **H**) from Late Jurassic to Eocene times. Reconstruction based on this work and reconstructions proposed by Jaillard et al. (1996, 2000), Spiking et al. (2015), Villagómez (2010), Restrepo et al. (2004), Cediel et al. (2003). Relative positions of the plates and arcs are modified from Pindel and Kennan et al. (2001, 2009).*

Between 60-50 Ma, the Dagua Terrane, which correlated with the Piñon terrane in Ecuador, was accreted to the West of South America, probably at the same time that the Piñon was accreted in Ecuador. According to Jaillard et al. (2004, 2009), the Piñon

terrane, last fragment of the COP, was accreted to the Ecuadorian margin in the Late Paleocene (c. 58 Ma).

The Late Paleocene-Early Eocene interval corresponds to one of the most important unconformities (SU5) recorded in the MMV and WEC (11-Hh). The accretion of the Dagua terrane coincides with the abrupt change from Paleocene fine-grained deposits to Eocene coarse-grained continental deposits (Faucher and Savoyat, 1973; Marocco et al., 1987; Noble et al., 1990; Naeser et al., 1991; Gayet et al., 1991), as is also the case in Peru (Mégard et al., 1984; Noble et al., 1990; Jaillard et al., 1993; Contreras et al., 1996; Gil et al., 1996) and Ecuador (Dashwood and Abbots, 1990; Rivadeneira and Baby, 1999). The Paleocene or Early Eocene deposits rest unconformably on Cretaceous rocks in the MMV and WEC, and in other parts of Colombia (Cheilletz et al., 1997; this work).

6.5. Discussion

Contrary to Fabre (1987), according to the models proposed in this work, the Cretaceous-Early Paleocene deformation was not restricted to the Western Cordillera, Central Cordillera and Santander Massif, but also affected the MMV and WEC basins. Cooper et al. (1995) indicated that the Pre-Andean foreland basin developed in the Middle Magdalena Basin, Eastern Cordillera and Llanos Basin previous to the Early Miocene. Many tectonic plate interpretations have been published (Pindell and Dewey, 1982; Burke et al., 1984; Duncan and Hardgraves, 1984; Ross and Scotese, 1988; Pindell and Barret, 1990; Jaillard et al., 1990; 2000; 2009; Pindell, 1993; Pindell and Ericson, 1994; Meschede and Frisch, 1998; Pindell and Kennan, 2001; Cediel et al., 2003; Villagómez, 2010).

The tectonic evolution shown in Figure 6.13 is related to some key moments that mark changes in the subduction regimes (Figures 6.3, 6.4 and 6.5) that triggered the changes in the subduction slab, in the velocity of subduction, geometry, etc.

First of all, the onset of the Caribbean evolution is related to the separation of South America from North America and Africa during the Pangea break-up in the Early Jurassic (Wadge and Burke, 1983, Pindel and Kennan, 2001) generating different phases of extension, compression, plate convergence, subduction and obduction (Le Pichon, 1968; O'Connell et al., 1991; Ricard et al., 1991). This regional event may have generated the formation of an extensional basin that permitted the deposition of sequences S1 and S2 (Figure 6.13-Aa).

A stratigraphic gap is observed at 125-120 Ma (Barremian-Early Aptian) (Cediel et al., 2003), which is supported by the hiatus identified in this work using stratigraphic and geochronological information. This gap and hiatus evidence a tectonic compression that produced shortening and erosion of S2 (unconformity SU2) (Figure 6.13 Bb), which is related to the development of a flat slab as shown in Figure 6.5.

During Late Aptian to early Albian times (115-105 Ma) an extensional regime prevailed (Jaillard, 1987), which is consistent with the model shown in Figure 6.13C and modeled in Figures 6.5a and 6.3-1C.

During the Late Albian-Early Cenomanian (105 – 97 Ma), a tectonic compression was associated with shortening, related again to a new flat-slab period (Figures 6.3, 6.5), producing uplift and erosion of sequence S3 (unconformity SU3) (Figure 6.13D). This event was probably related to the opening of the Equatorial Atlantic Ocean, which provoked the westward drift of South America and an increased coupling along the subduction zone (Sébrier and Soler, 1990; Jaillard et al., 1996).

In the Late Cenomanian – Late Santonian (95-83 Ma), an extensional regime was established (Figure 6.13E) allowing the deposition of sequence S4 and a steep subduction was produced (Figure 6.3 and 6.5), allowing the establishment of an extensional regime (Figure 6.13E). This model is partly in agreement with the period determined by Soler and Bonhomme (1990), and Jaillard (1991, 1996), as a major marine transgression that deposited shelf carbonates, while the volcanic arc front was present.

During the Early Campanian – Late Campanian 80-70 Ma (Figure 6.13F), a compressive tectonic phase produced the shortening and deformation of all sequences, and the erosion of sequence S4 (discordance SU4). This compressional tectonic phase was due to the formation of a flat slab (Figures 6.3, 6.4, 6.5). This tectonic event is in agreement with a major contraction phase during the Late Campanian (75-70 Ma) (Gayet et al., 1991; Jaillard et al., 1993), which is responsible for a regional, widespread unconformity as shown in chapters 4 and 5.

In the Early Maastrichtian – Early Paleocene (70-60 Ma), an extensional context allowed the deposition of sequence S5 (Figure 6.13G), due to a steep subduction (Figure 6.3-1C and 6.5a). During this period the Amaime terrane was emplaced to the west of the Arquia complex, and plutonic and volcanic rock were emplaced in the Amaime terrane. This is consistent with the volcanic and plutonic emplacement observed by Laughlin et al. (1968), Beckinsale et al. (1985) and Clark et al. (1990) along the Peruvian margin.

Finally, during the Late Paleocene-Early Eocene (60-50 Ma), the shortening, deformation and erosion of sequences S5 and older, resulted from the flattening of the slab (Figures 6.3A, 6.4 and 6.5 c, d). During this period, the Dagua terrane was accreted to Colombia. The Piñon terrane was also accreted during the Late Paleocene (c, 58 Ma) (Jaillard et al., 2009), supporting the idea that Colombian and Ecuadorian terranes belong to the same oceanic plateau (Figure 6.13f, g and h) (Reynaud et al., 1999; Lapierre et al., 2000).

All of these subduction, exhumation, deformation and erosion events resulted from changes in the subduction regime (Figures 6.3, 6.4 and 6.5) that triggered changes in the subduction slab, in the subduction velocity, geometry, etc., as observed in the western side of South-America in Peru and Chile. Since, in the latter countries, these events are not dependent on accretions of oceanic terranes, our schematic model only shows

terrane accretions as reported by other authors. The schematic models shown on Figure 6.13 are based on the observations from this work in the MMV and WEC, and are independent of the postulated accretionary events.

6.6. Conclusions

1. The new information suggests that both sea level variations and tectonic events controlled the Cretaceous deposition and erosion periods in the MMV and WEC basins.
2. The Cretaceous sequence of the MMV underwent a total shortening of around 14.8 km to the South, and to 13.7 km to the North since the Late Barremian-Early Aptian. The calculated shortening is 1.6 km during the Barremian-Early Aptian; 4.3 km during the Late Albian-Early Cenomanian; 4.2 km during the Early Campanian, and 3.6 km from then on. The Late Barremian-Early Aptian shortening represents the first Cretaceous contractional event in the MMV and WEC.
3. Stratigraphic information from the WEC and the MMV allowed to identify several events of transgressions and regressions, controlled by sea level fluctuations.
4. Based on the seismic interpretation and the construction of chronostratigraphic charts, I identified five periods of erosion or non-deposition, which span the Late Jurassic-Early Berriasian (SU1), Late Barremian-Early Aptian (SU2), Late Albian-Early Cenomanian (SU3), Early Campanian (SU4), and Late Paleocene-Eocene (SU5). The latter represents one of the most important erosion periods in Colombia.
5. Thermal modelling showed that a fast cooling event occurred around 80-70 Ma in all the areas (Figure 6.12), with an average cooling rate of ≈ 13-15°C/Ma. This Campanian cooling event is interpreted as related to a major collisional event (80-70 Ma). Then a period of slow heating (65-5 Ma), followed by a new rapid cooling event is recorded since 5 Ma, with a mean rate of ≈ 9°C/Ma, recorded by AFT analyses in the WEC.
6. From the Jurassic to the Paleocene, repetitive tectonic extension and compression events produced by a cyclic subduction regime may explain the deposition, exhumation and erosion phases observed in the MMV and WEC during the Cretaceous. The presence in the northwestern corner of South America of accreted blocks from the Campanian, starting with the accretion of the blocks such as Quebradagrande is undeniable. However, the deformation of the upper plate in my model is not dependent on these terrane accretions (Figure 6.13), but rather on the subduction regime, for example changes in the plate subduction angle (steep or flat subduction), the convergence rate, the polarity of subduction, the slab age, etc.

CHAPTER 7
Synthesis and General Conclusions.

7.1 Synthesis

This dissertation has contributed with the following geological aspects for the understanding of the evolution and tectonics events of the Cretaceous sequences in Colombia based on the data from the entire basin of the Middle Magdalena Valley and the Western Eastern Cordillera:

- I contributed with newly acquired and collected data from an extensive area of 50.000 km2 in the Middle Magdalena Valley and Western Eastern Cordillera with a new focus, analysis and interpretation.
- I provided new structural, sedimentological, stratigraphic, petrographic and thermochronological information from different measurements, samples and descriptions made during the several field trips and laboratory phases.
- I made a regional-structural and stratigraphic-seismic interpretation along the MMV and part of the WEC, using more than 300 seismic reflection lines, and several wells in the basin were analyzed.
- I identified several stratigraphic sequences and unconformities based on sequence stratigraphy analysis made on stratigraphic columns described and measured in this work; I used sedimentological and lithological facts collected in this work, information from the wells and also reported by other authors. In general, the biostratigraphic information was compiled from information provided in other works.
- I presented new paleo-facies maps from the Berriasian to the Coniacian- Santonian, based on the periods of regression, transgression and sequence limits, to understand the cycle periodicity, sea level variation and facies distribution in the study area.
- Using seismic reflection data, I identified five sequences (S) and five unconformities (SU) corresponding to the sequence boundaries during the Cretaceous, three of which had not been identified before: at 125 Ma, 100 Ma and 80 Ma. Based on these new observations, I propose a new generalized composite stratigraphic column for the MMV and the WEC.
- Using the new thermochronological data from this work, I identified two events of heating and two events of cooling; the first of these occurred at 80-70 Ma, which corresponds to the unconformity of Campanian age identified from seismic information. The second cooling event occurred between 10 and 2 Ma.
- I proposed a new possible regional tectonic model, with repetitive tectonic extension and compression events during the Cretaceous, generated by a cyclic subduction regime that

explains the cyclicity in the deposition, exhumation and erosion phases and also the sea level variation.

7.2 General Conclusions

This thesis initially involved structural, lithological, sedimentological and stratigraphic information collected during this work in several field trips, in four different sections from the north to the south of the MMV and the WEC. Descriptive information from the wells was also used and I took into account descriptive information from other works. Based on these descriptive information, the information were totally analyzed and interpreted in this work.

1. With the information from 30 stratigraphic sections, sea level fluctuation analysis, transgressive regressive curves, and the Fisher plots constructed it was possible to conclude that:

- The analysis of third and second order cycles allowed to identify sea level curves and the vertical and lateral facies variation in the basin.
- Based on Genetic stratigraphic sequence-analysis composed by high-stand systems tract (HST), forced regression or falling-stage systems tract (FSST), low-stand systems tract (LST) and transgressive systems tract (TST); I identified cycles between the sequence boundaries (SB) occurred during the regression system, based on transgressive-regressive curves and the Fisher plots.
- Considering that the cycles are limited by the surface boundaries or unconformities (SU) represented by time gaps generated during regression systems tracts (RST), between the HST and LST; I recognized three new major erosion surfaces (SU) close to the Barremian-Aptian boundary, and in Late Albian-Early Cenomanian and Early Campanian times.
- The unconformities or sequence limits (SU) additionally to the description from field work and wells, were supported by some unconformities identified in outcrops and some biostratigraphic dates that insinuate some time gaps in sequences from the Albian-Cenomanian limit, Barremian-Aptian and Lower Campanian. The Fisher plots helped to identify the correlative conformities towards the basin center in the fine sequences.
- New paleo-facie maps from Berriasian to Coniacian-Santonian were interpreted in this work: The Berriasian correspond to a period of regression, Berriasian/Valangenian to the onset of transgression, Barremian represent the onset of new regression, the MRS was reached during Barremian/Aptian, a new period of transgression is recorded in the Late Aptian/Late Albian, Early Cenomanian features a period of regression, Late Cenomanian/Turonian a regional period of transgression, and finally a period of regression that could continuous during the Early Campanian.
- Shallow conditions related to high-energy events are interpreted at Barremian-Early Aptian (in the La Tigra Section, RW-1 well section); at the Late Albian-Early Cenomanian

boundary and in the Late Cenomanian (Samaca-Churuvita, Chiquinquira section, RW-1); and at the Campanian (reported in the RW-1 section).

2. In general, the facies from different system tracts shown in the regional maps interpreted in this work indicate that shallower facies are always present eastward while deep facies are located westward in the MMB towards the CC. Structural and Stratigraphic seismic interpretation of the Cretaceous sequence in the study area permit to conclude that:

- The regional presence of five sequences (S) limited by their corresponding unconformities (SU) interpreted as sequence boundaries at the Jurassic-Cretaceous unconformity (SU1), Late Barremian-Early Aptian unconformity (SU2), Albian-Cenomanian unconformity (SU3), Santonian-Campanian unconformity (SU4), and Paleocene-Eocene Unconformity (SU5).
- The chronostratigraphic charts construed along several seismic sections using Wheeler diagrams, permitted to stablish the regional extension across the MMV and WEC of the five stratigraphic sequences (S1 to S5) and their boundary surfaces (SU1 to SU5).
- Based on these interpretations and the extension of the surface boundaries or unconformity surfaces (SU), I proposed a generalized stratigraphic column for the whole region of this study that shows these five sequences and their boundaries.
- The presence of truncation, onlap, down-lap and growth strata, permitted to identify the major limit of the sequence with a regional extension.
- Comparison of the sequences and sequence boundaries interpreted in this work, with the regional sequences and the sequence boundaries interpreted in Peru, Magallanes, the Neuquén basin, Venezuela, the Upper Magdalena Valley, and in recent works done in the Catatumbo basin, show that these sequences and their limits have a regional extension.

3. Based on the new AFT and ZFT ages from this work, and my thermal modeling it was possible to conclude:

- Two events of heating and two events of cooling were identified; the events of heating for samples older than 85 Ma. occurred from the sedimentation age to ~80 Ma and from ~70 Ma to ~10 – 2 Ma. The cooling events occurred between~ 80-70 Ma. and from ~10-2 Ma to the present.
- The AFT age at the north area (2.5±0.2-3.41 ±0.37 Ma) and the age at the south area (1.9±0.39, 2.97±0.32Ma) are younger than in the center area (5.47 ±1.16 – 7.04±1.28) and younger than the ages that have been reported by other authors.
- According to the cooling age reported at the eastern flank of the Eastern Cordillera (EEC) by Mora (2007), the ages are not substantially younger than some ages reported in this work at the western flank of the East Cordillera (north and south area of the WEC), which probably means that the last exhumation could be similar on both flanks of the Eastern Cordillera.

- ZFT ages decrease from the flanks towards the core of the anticline, being younger in older units in each sequence like Giron, Arcabuco and Trinchera which present ZFT ages younger than stratigraphic ages evidencing total annealing. This behavior is confirmed with the Tmax data (Ro).

- Comparing the present-day thermal gradient versus the paleo-geothermal gradient permits to identify the presence of unconformities between Aptian-Barremian and Late Albian-Early Cenomanian ages.

- It is observed that the present temperature decrease compared with the paleotemperature, and also that the excess of paleo-temperature (~250°C), especially at the south, is due to changes in the geothermal gradient because of changes in heat flow (probably magmatic activity) or a combination of changes in the geothermal gradient, sediment charge and denudation.

- I used the criterion of comparison between the central age and the pooled age as a discrimination of age population to show that dispersion of age is only significant in the oldest samples in all the areas (Giron, Arcabuco and Trinchera Formations), where ZFT ages for the samples which underwent total annealing are younger than the stratigraphic ages. The other samples never were heated enough to suffer annealing.

4. A new regional tectonic model for the lower Cretaceous to Paleocene-Eocene ages is proposed in this work.

- The restoration shows a differential shortening in the basin, with a total shortening of around 18.7 km to the South, and 13.7 km to the North since the Early Berriasian to the present. Additionally, a section with the shortening calculated for each age from the Jurassic to the present is presented.

- I show the complete history of deformation and deposition in the basin, based on structural interpretations and the restoration of the section, taking into account the deposited sequences and erosion.

- The integration of the paleo-facies maps and structural restorations, shows that structural deformation in the basin and sea level fluctuation control deposition and erosion in the basin. The different stages of the basin's evolution (deformation, sea level fluctuation, deposition and erosion) are shown stage by stage from Jurassic/Berriasian to Coniacian/Santonian.

- The structural reconstruction through the Cretaceous considering the **sequences (S)**, the **discordances (SU)** and the transgressive-regressive sequences (paleo-facies maps), shows the relation between deformation, deposition and erosion and when each of these events happened during the Cretaceous in these basins (MMV and WEC).

- From the Jurassic to the Paleocene, **repetitive tectonic extension and compression events** produced by a **cyclic subduction regime,** explain the **deposition, exhumation and erosion phases** observed in the MMV and WEC during the Cretaceous.

- The presence of **accreted blocks** (for example Quebradagrande) is undeniable. However, in my model the deformation of the upper plate **is not dependent on these terrane accretions**, but rather on the subduction regime, for example changes in the plate subduction angle (steep or flat subduction), the convergence rate, the polarity of subduction, the slab age, etc.

7.3 Impact on the Petroleum Industry

- The results obtained in this work have several impacts on the Petroleum industry: the first one is to understand the tectonic history of the Cretaceous sequence which could impact the understanding of the petroleum system in several aspects such as presence of the seal rock, the tramp, reservoir and the source rocks, etc. These are important, because unlike classic models, the models in this work shows the presence of unconformities and missing sedimentary sequences or eroded sequences which in some cases cause the source rocks to not be present. Sometimes the reservoirs may have totally eroded, or the seal may not be present. This important difference with the previous models, affects all the basin history including the Tertiary sequence, but with a great impact over the Cretaceous sequence.
- The second impact is related to the unconventional oil industry which explores the Cretaceous sequence and the MMV is probably the best example in Colombia. The most important difference with the models that has been classically used, probably lies in the fact that these models considers a continuous sedimentation and in this way considers the presence of the complete sequence in all the basin. However, the model that I propose in this work considers that the sequences are not complete in the basin due to erosion which causes missing sections in the stratigraphic sequence, that have to be analyzed sector by sector during any new drilling well proposals or the new proposals for areas to explore. This understanding will reduce the uncertainty and the risk and allow to choose the best areas for future unconventional prospects.
- The understanding of the regional tectonic events suggested in this work and their relation with the deposition, exhumation and erosion phases observed in the MMV and WEC during the Cretaceous, have to be analyzed in conjunction with the synchronism necessary to have the accumulation of hydrocarbons in the basin.
- The knowledge of the thermal history is a key to understanding the maturity of organic matter. According to the Ro analysis made in this work, the temperature is progressively growing towards the south, reaching temperatures of up to 250°C. The excess of paleo-temperature is produced by changes in the geothermal gradient because of changes in the heat flow, which definitely helps define what kind of hydrocarbon will be expected to be accumulated in the trap.

- The understanding of when the heating and cooling events happened, and if those events happened over a short or long period of time is another important fact in order to know if the organic matter is mature or over-mature. For that (considering the thermal history in the valuation of the hydrocarbon) it is necessary to know the quality of the hydrocarbon and if the organic matter was exposed for a long time to high temperatures or if this came out quickly from the window of high temperature, probably of zircon total annealing zone.

7.4 Future Perspectives

- It is necessary to incorporate more detail in biostratigraphic analysis to determinate the gaps in the Cretaceous sequences. For these details it is important to acquire more dense and regional sampling from the basins.

- Increase the database for apatite and zircons in situ for the Cretaceous sequence, especially in the central area of this work, towards the syncline de Armas and Otanche area.

- Create future local projects that focus on corroborating the cretaceous unconformities in cretaceous sequence in the MMV and WEC.

- Future regional projects in other basins like the UMV, Putumayo basin, Catatumbo, etc, to corroborate the regional extension as is proposed in this work.

- Determine the AFT age in samples collected in field and wells using the Dpar and the track length measure to strengthen the model.

- Incorporate new and pre-existing data into 3D thermal modeling in conjunction with a structural deformation model, to test the model proposed and other possible models.

- Because this is a regional work, it is necessary to make several local studies in different areas to prove the existence of sequences and their surface boundaries, unconformities or correlative conformities that are suggested in this work.

- In future unconventional prospects (Shale gas), it is necessary to involve the models proposed in this work, and analyze the sections to know which parts of the sequence are still present, what was the deformation sequences, and also to know what was the thermal history.

References

Acosta, F.E. and Obando, E., 1984, Desarrollo estructural del extremo sur del Valle Medio del Magdalena: XXIII reconocimiento Geolegico. Colombian Society of Petroleum geologists and Geophysicists, Bogota, 14 p.

Acosta, J., Coward, M. P., Lonergan, L., 2000, Kinematics of the western foothills of the Colombian Eastern Cordillera and regional implications, London, 28 p.

Acosta, J. and Ulloa, E., 2001, Geología de las planchas 227 La Mesa, Colombia. Ingeominas Informe Explicativo.

Acosta, J., 2002, Structure, tectonics and 3D models of the western foothills of the Eastern Cordillera and Middle Magdalena Valley, Colombia. PhD. Thesis. Imperial College. London.

Acosta, J., Velandia, F., Osorio, J., Lonergan, L. and Mora, H., 2007, Strike-slip deformation within the Colombian Andes, *in* Ries, A.C., Butler, R.W.H., Graham, R.H., eds., Deformation of the Continental Crust: The Legacy of Mike Coward: Geological Society, London, Spec. Publ., 272, 303–319.

Agudelo, J. M. and Peñaloza, M del P., 1990, Cartografía y análisis estratigráfico de la Formación Caballos y la unidad Pre-Caballos en el área de Ortega (Tolima). Unpublished Thesis, Universidad de Caldas, Caldas, Colombia, 182 p.

Algeo, T. J., and Wilkinson, B. H., 1988, Periodicity of mesoscale Phanerozoic sedimentary cycles and the role of Milankovitch orbital modulation. *Journal of Geology*, Vol. **96**, pp. 313–322.

Allen, R. B., Resetar, R and Macellari, C., 1988, Magdalena study area: Final Report.- Earth Sciences and Resources Institute, University of South Carolina, 70 p.

Allen, G.D., 1989, *Structural Geology of the Ortega Region, Upper Magdalena Valley, Colombia.* Unpublished MS thesis, Baylor, University, Waco, TX, USA, 232 p.

Allen, P. A. and Allen, J. R., 1990, *Basin analysis, principles and applications.* Blackwell Scientific Publications, London, 451 p.

Anderson E.J. & Goodwin, P.W. 1980, Application of the PAC Hypothesis to limestones of the Helderberg Group: Society of Economic Paleontologist and Mineralogists (SEPM), Eastern section Field Trip Guidebook. 32p. (en James, N. P. 1984 - en Ulloa and Acosta 2001).

Andriessen, P.A.M., 1995, Fission-track analysis: principles, methodology and implications for tectono-thermal histories of sedimentary basins, orogenic belts, and continental margins. Geologie en Mijnbouw, 74, 1-12.

Asch, K., 2001, The IGME 5000: A means to pan-European Geological Standards? (or just another local and transient conventional?) IAMG Annual Conference (Camcum): http://www.kgs.ukans.edu/Conferences/IAMG/Sessions/I/asch2.html.

Aspden, J. A., W. J. McCourt, 1986, Low-K granitoids from the Western Cordillera of Colombia: Geología Norandina, 10, 19–27.

Aspden, J. A., McCourt, W. and Brook, M., 1987, Geometrical control of subduction-related magmatism: the Mesozoic and Cenozoic plutonic history of Western Colombia. Jour. Geol. Soc. London, 144: 893-905.

Atherton, M. P., Warden, V., Sanderson, L.M., 1985, The Mesozoic marginal basin of central Peru: A geochemical study of within-plate-edge volcanism. In: Pitcher, W.S., Atherton, M.P., Cobbing, E.J., Beckinsale, R.D. (eds.): Magmatism at a plate edge – The Peruvian Andes, 47-58; Glasgow (Blackkie).

Audemard, F.E., Audemard F.A., 2002, Structure of the Mérida Andes, Venezuela: relations with the South America-Caribbean geodynamic interaction. Tectonophysics, v. 345, p. 299-327.

Avraham, B. Z. and Nur, A., 1987, Effects of collisions at trenches on oceanic ridges and passive margins. In: J.W.H. Monger and J. Francheteau (eds.), *Circum-Pacific orogenic belts and evolution of the Pacific Ocean basin.* American Geophysical Union, Geodynamics Series, v.18, p. 9-18.

Balkwill, H.R., Rodrigue, G., Paredes, F.I. and Almeida, J.P., 1995, Northern part of Oriente basin, Ecuador: reflection seismic expression of structures, pp. 559-571. *En* Tankard, A. J., Suárez, R. and Welsink, H. J (eds), Petroleum basins of South America. AAPG Memoir 62. Houston, Texas, USA.

Ballesteros, I., and Nivia, A. 1985, La Formación Ritoque: Registro sedimentario de una albufera de comienzos del Cretácico, cp. XIV, p. 1-17. In Etayo-Serna F., and Laverde, F., (eds.), Proyecto Cretácico. Publicación Geológica Especial de Ingeominas, 16.

Barbosa, A., and Lopez A. P., 2009, Analisis facial de las secuencias del Cretacico Superior correspondientes a las Formaciones San Rafael, Conejo y Pleaners aflorantes en sectores aledaños a Villa de Leyva (Departamento de Boyaca, Colombia). Universidad de Caldas, Tesis de pregrado. Manizales. Pag. 1-93.

Barker, C.E., Pawlewicz, M.J., 1994, Calculation of vitrinite reflectance from thermal histories and peak temperatures: a comparison of methods. In: Mukhopadhyay, P.K., Dow, W.G. (Eds.), Vitrinite Reflectance as a Maturity Parameter: Applications and Limitations. American Chemical Society Symposium Series 570, pp. 216–229.

Barrio, C. A. and Coffield, D. Q., 1992, Late Cretaceous stratigraphy of the Upper Magdalena Basin in the Payandé-Chaparral segment (western Girardot Sub-Basin), Colombia. Jour. South Am. Earth Sci., 5(2): 132-139.

Bates, R. L., and Jackson, J. A. (Eds.), 1987, *Glossary of Geology* 3rd Ed. American Geological Institute, Alexandria, Virginia, p. 788.

Bayona et al., 2008, An integrated analysis of an orogen-sedimentary basin pair: Latest Cretaceous-Cenozoic evolution of the linked Eastern Cordillera orogen and the Llanos foreland basin of Colombia, Geological Society of America Bulletin; September/October; v. 120; no. 9/10; p. 1171-1197; doi: 10.1130/B26187.1; 15 figures; Data Repository item 2008078.

Bayona G., Cardona A., Jaramillo C., Mora A., Montes C., Valencia V., Ayala C., Montenegro O., Ibañez M., et al., 2012, Early Paleogene magmatism in the northern Andes: Insights on the effects of Oceanic Plateau.continent convergence, Earth and Planetary Science Letters, Elsevier, p 97-111, doi: 10.1016/j.epsl.2012.03.015.

Bayona, G., Cardona, A., Jaramillo, C., Mora. A., Montes, C., Caballero, V., Mahecha, H., Lamus, F., Montenegro, O., Jiménez, G., Mesa, A. and Valencia, V., 2013, Onset of fault reactivation in the Eastern Cordillera of Colombia and proximal Llanos Basin; response to Caribbean – South America collision in early Paleogene time. In: Thick-Skin-Dominated Orogens: From Initial Invertion to Full Accretion. (Nemcok, M., Mora. A. R., and Cosgrove, J.W. Eds.) Journal of the Geological Society of London, Special Publication, 377.

Bayona, G. A., García D. F. and Mora G., 1994, La Formación Saldaña: producto de la actividad de estratovolcanes continentales en un dominio de retroarco. In: F. Etayo Serna (ed.), Estudios geológicos del Valle Superior del Magdalena. Chapter I, Univ. Nacional de Colombia, Ecopetrol, Bogotá, 21 p.

Beaumont, C., Fullsack, P. and Hamilton, J., 1992, Erosional control of active compressional orogens, in Thrust Tectonics, pp. 19-31, ed. McClay, K.R., Chapman and Hall, London.

Beckinsale, R.D., Sánchez-Ftrnandez. A.W., Brook, M., Cobbing, E., Taylor, W.P. and Moore, N.D., 1985, Rb-Sr whole-rock isochron and K-Ar age determinations for the Coastal Batholith of Peru. In: Magmatism at a Plate Edge, the Peruvian Andes, eds. Pitcher, W.S., Atherton, M.P., Cobbing, E.J., Beckinsale, R.D., p. l77-202. Glasgow and Halsted Press, New York.

Bengtson, P., Jaillard, E., 1997, Stratigraphic revision of the Upper Cretaceous of the Peruvian-Ecuadorian border region: preliminary data and tectonic consequences. 18th I.A.S. Region. Europ. Meet. Sedimentology - 2nd Europ. Meet. Palaeont. Stratig. South America. *Gaea heidelbergemis, Heidelberg, 4, 71-72.*

Berger, A. L., and Loutre, M. F., 1994, Astronomical forcing through geological time. *In Orbital forcing and cyclic sequences* (P. L. de Boer and D. G. Smith, Eds.), pp. 15–24. International Association of Sedimentologists Special Publication **19**.

Bermúdez M., 2010, *Cenozoic exhumation patterns across the Venezuelan Andes: insights from fission-track thermochronology,* Université Joseph Fourier-Grenoble I, Docteur these, p5-314.

Bermúdez M., Van Der Beek P., Bernet M., 2013, Strong tectonic and weak climatic control on exhumation rates in the Venezuelan Andes. Lithosphere, Geological Society of America, 5 (1), pp.3-16.

Bernet, M., and Spiegel, C., 2004, Introduction: Detrital thermochronology, in Bernet, M., and Spiegel, C., eds., detrital thermochronology-provenance analysis, exhumation, and landscape evolution of mountain belts: Boulder, Colorado, Geological Society of America Special Paper 378, p. 1–00. For permission to copy, contact editing@geosociety.org. © 2004 Geological Society of America.

Bernet, M., Brandon, M.T., Garver, J.I., and Molitor, B., 2004, Fundamentals of detrital zircon fission-track analysis for provenance and exhumation studies with examples from the European Alps, in Bernet, M., and Spiegel, C., eds., detrital thermochronology Provenance analysis, exhumation, and landscape evolution of mountain belts: Geological Society of America Special Paper 378, p. 25–36 (this volume).

Bernet, M., Brandon, M.T., Garver, J.I. & Molitor, B.R., 2004 a. Downstream changes in Alpine detrital zircon FTages of the Rho"ne and Rhine Rivers. J. Sediment. Res., 74, 82-94. doi:10.1306/041003740082.

Bernet, M., Brandon, M.T., Garver, J.I. & Molitor, B.R., 2004 b, Fundamentals of detrital zircon FTanalysis for provenance and exhumation studies with examples from the European Alps. In: Detrital Thermochronology ^ Exhumation and Landscape Evolution of Mountain Belts (Ed. by M. Bernet & C. Spiegel), Geol. Soc. Am.Spec. Publ., 378, 25-36.

Bernet, M. & Garver, J. I., 2005, Fission-track analysis of detrital zircon. In: Low-Temperature Thermochronology (Ed. By P. Reiners & T. Ehlers), Rev.Mineral. Geochem. 58, 205-238.

Bernet, M., 2009, A field-based estimate of the zircon fission-track closure temperature, Chemical Geology 259 (2009) 181–189. Elsevier B.V. All rights reserved. doi:10.1016/j.chemgeo.2008.10.043.

Bernet, M., Brandon, M., Garver J., Balestieri, M., Venturas B., and Zattinz M., 2009, Exhuming the Alps through time: clues from detrital zircon fission-track thermochronology: Basin Research (2009) 21, 781–798, doi: 10.1111/j.1365-2117.2009.00400.x

Biari Y., Klingelhoefer F., Sahabi M., Funk T., Benabdellouahed M., Schnabel M., Reichert C., Bonner A., AustinJ. A. 2017, Opening of the central Atlantic Ocean: Implications for geometric rifting and asymmetric initial seafloor spreading after continental breakup. Volume 36, Issue 6, June, p 1129-1150.

Brandon, M.T., Roden-Tice, M.K., and Garver, J.I., 1998, Late Cenozoic exhumation of the Cascadia accretionary wedge in the Olympic Mountains, northwest Washington State: Geological Society of America Bulletin, v. 110, p. 985–1009.

Brandon, M.T., 1992, Decomposition of fission-track grain-age distributions: American Journal of Science, v. 292, p. 535–564.

Brandon, M.T., 1996, Probability density plot for fission track grain-age samples: Radiation Measurements, v. 26, p. 663–676.

Brandon, M.T. Roden-Tice, M., Garver, J., 1998, Late Cenozoic exhumation of the Cascadia accretionary wedge in the Olympic Mountains, northwest Washington State. *GSA Bulletin*; August 1998; v. 110; no. 8; p. 985–1009; 18 figures; 3 tables.

Branquet, Y., Laumonier, B., Cheilletz, A., and Giuliani, G., 1999, Emeralds in the Eastern Cordillera of Colombia: Two tectonic settings for one mineralization: Geology, v. 27, p. 597–600, doi: 10.1130/0091-7613(1999)027<0597:EITECO>2.3.CO;2.

Brasier, M.D. 1980, Microfossils. George Allen & Unwin, 193 p. London.

Brenac, P., and Jaramillo, C., 2004, Palinología Cascajales-1 y sección La Sorda (formaciones Umir-Simiti). Informe interno de Bioestratigrafía Instituto Colombiano del Petróleo. P.3.

Brook, M., 1984, New radiometric age data from SW Colombia. INGEOMINAS Mission Británica (British Geological Survey), Cali, Colombia, Report 10.

Burchart, J., 1981, Evaluation of uncertainties in fission track dating: Some statistical and geochemical problems. Nucl. Tracks, v. 5, p.87-92.

Bruckner, W.D., 1954, Note on some fossils from the Girón Group in the Río Lebrija valley, Department of Santander, Colombia. *Journ. Paleont.*, vol. 28, nº 1, pp. 112-113, Tulsa.

Bürgl, H., 1954. El Cretáceo Inferior en los alrededores de Villa de Leiva, Boyacá. Bol. Geol., Serv. Geol. Nal. Bogotá, Vol. 2(1), pp. 5-22.

Bürgl, H., 1955, Algunas amonitas interesantes de la colección Shell – Condor. Informe Servicio Geológico Nacional No 1082, Bogotá.

Bürgl L, H., 1957, Bioestratigrafía de la Sabana de Bogotá y sus alrededores. Boletín Geológico, Servicio Gológico Nacional. V. 15, No 2, ps. 113-185. Bogotá.

Burnham, A. K. and Sweeney, J.J. 1989, A chemical kinetic model of vitrinite reflectance maturation and reflectance: *Geochimica et Cosmochimica Acta*, 53, 2649–2657.

Burke, K., Cooper, C., Dewey, J.F., Mann, P. and Pindel, J.L. 1984, Caribbean tectonics and relative plate motions, in W. E. Bonini, R. B. Hargraves, and R. Shagam, eds., The Caribbean–South American Plate boundary and regional tectonics: Geological Society of America Memoir 162, p. 31–63.

Bürgl H., 1954, El Cretáceo inferior en los alrededores de Villa de Leiva (Boyacá). Bol. Geol., Inst. Geol. Nal., vol. 2, n° 1, pp. 5-22, 3 lám. (pl. I-IV), Bogotá.

Bürgl H., 1955a, El anticlinal de Apulo. *Ibid.*, vol. 3, nº 2, pp. 2-22, (pl. I-IV), Bogotá.

Bürgl H., 1957a, Biostratigrafía de la Sabana de Bogotá y sus alrededores, *Bol. Geol., Serv. Geol. Nal.*, vol. 5, nº 2, pp. 113-185, 1 mapa, 19 pl., Bogotá.

Bürgl H., 1961a, Historia Geológica de Colombia, *Rev. Acad. Col. Cien. Ex. Fis. Nat.*, vol. 1, nº 43, pp. 137-191, 41 fig., 4 tabl., Bogotá.

Bürgl H., 1961c, Sedimentacion cíclica en el Geosindinal Cretáceo de la Cordillera Oriental de Colombia. *Bol. Geol.*, Serv. Geol. Nal., vol. 7 (1959), nº 1-3, pp. 85-118, 9 fig., Bogotá.

Burke, K., C. Cooper, J. F. Dewey, P. Mann, and J. L. Pindell, 1984, Caribbean tectonics and relative plate motions, in W. E. Bonini, R. B. Hargraves, and R. Shagam, eds., The Caribbean–South American Plate boundary and regional tectonics: Geological Society of America Memoir 162, p. 31–63.

Burnham, A. K. and Sweeney, J.J. 1989, A chemical kinetic model of vitrinite reflectance maturation and reflectance: *Geochimica et Cosmochimica Acta*, 53, 2649–2657.

Bustin, R. M. Vellutini, D., and Goodarzi, F. 1990, Determining levels of organic diagenesis in sediments and fossil fuels. In: 1.A. Mcllеareath and D.W. Morrow (eds.), Diagenesis, Geoscience Canada Reprint 4th series, 205-226.

Butler, K. and Schamel, S., 1988, Structure along the eastern margin of the Central Cordillera, Upper Magdalena Valley, Colombia. Jour. South Am. Earth Sci., 1(1): 109-120.

Caballero, V., Parra, M. and Mora A., 2010, Levantamiento de la Cordillera Oriental de Colombia durante el Eocenio Tardio – Oligoceno Temprano: Proveniencia Sedimentaria en el Sinclinal de Nuevo Mundo, Cuenca Valle Medio del Magdalena. Boletín de Geología Vol. 32, N° 1, enero-junio de 2010. Pag. 45 -77.

Caballero, V., Parra, M., Mora A., López, C., Rojas, L., and Quintero, I., 2013, Factors Controlling Selective Abandonment and Reactivation in Thick-Skin Orogens: A Case Study in the Magdalena Valley, Colombia. In: *Thick-Skin-Dominated Orogens: From Initial Inversion to Full Accretion* (Ed. by M. Nemĉok, A. Mora & J. W. Cosgrove), *Special Publications*, **377**, 343-367. Geological Society, London. Publications published online March 8, as doi: 10.1144/SP377.4.

Caballero, V., Mora A., Quintero, I., Blanco, V., Parra, M., Rojas, L., López, C., Sánchez, N., Horton, B.K., Stockli, D.F. and Duddy, I.R. 2013, Tectonic Controls on Sedimentation in an Intermontane Hinterland Basin Adjacent to Inversion Structures: The Nuevo Mundo Syncline, Middle Magdalena Valley, Colombia. In: *Thick-Skin-Dominated Orogens: From Initial Inversion to Full Accretion* (Ed. by M. Nemĉok, A. Mora & J. W. Cosgrove), *Special Publications*, **377**, 315-342. Geological Society, London.

Cáceres, C., Etayo, F. 1969, Bosquejo geológico de la región del Tequendama. 1 Congr. Col. Geol., opúsculo guía, Exc. pre-congreso. 22 p. Bogotá.

Caicedo J. C., 2005, Significado Facial de la Formación Churuvita y su Respuesta Cartográfica, Tesis de Maestría, Universidad Nacional de Colombia. p 1-150.

Cadena, E.A., & Parham, J.F. 2015, Oldest known marine turtle? A new protostegid from the Lower Cretaceous of Colombia. PaleoBios 32: 1-42.

Campbell C. J., and Burgl H., 1965, Section through the Eastern Cordillera of Colombia, South America. Bull. Geol. Soc. Am., vol. 76, n° 5, pp 576-589, 7 fig., New York.

Cardona, A., Cordani, U. G. and MacDonald, W. D., 2006, Tectonic correlations of pre-Mesozoiccrust from the northern termination of the Colombian Andes, Caribbean region, Journal of South American Earth Sciences, 21(4), 337-354, doi: DOI: 10.1016/j.jsames.2006.07.009.

Cardona A., 2012, Informe de Geocronología de una toba de la cuenca del VMM. Informe interno Ecopetrol. P.6.

Cardozo E. and Ramírez C., 1985, Ambientes de depósito de la Formación Rosablanca: Área de Villa de Leiva. In: F. Etayo-Serna and F. Laverde-Montaño (eds.), Proyecto Cretácico, contribuciones. Chapter XIII, Ingeominas Publicación Geológica Especial 16, Bogotá, 13 p.

Caron, M., 1985, Cretaceous planktic foraminifera.- Bolli, H., Saunders, J. & Perch-Nielsen, K., eds., Plankton Stratigraphy, p. 17-86, Cambridge University Press, Cambridge.

Carter, R. M., Abbott, S.T., Fulthorpe, C. S., Haywick, D.W., Henderson, R. A., 1991, Application of global sea-level and sequence-stratigraphic models in southern hemisphere Neogene strata. In:

Macdonald, D. I. M. (ed.), Sedimentation, Tectonics and Eustasy: Sea-Level Changes at Active Margins. International Association of Sedimentologists, Special Publication **12**, 41–65.

Carter, A., 1999, Present status and future avenues of source region discrimination and characterization using fission-track analysis: Sedimentary Geology, v. 124, p. 31–45.

Catuneanu, O., Willis, A. J., and Miall, A. D. 1998b, Temporal significance of sequence boundaries. *Sedimentary Geology*, Vol. **121**, pp. 157–178.

Catuneanu, O. 2002, Sequence stratigraphy of clastic systems: concepts, merits, and pitfalls. *Journal of African Earth Sciences*, Vol. **35/1**, pp. 1–43. Catuneanu, O. (2003). Sequence Stratigraphy of Clastic Systems. *Geological Association of Canada, Short Course Notes*, Vol. **16**, p. 248.

Catuneanu, O. 2004, Retroarc foreland systems–evolution through time. *Journal of African Earth Sciences*, Vol. **38/3**, pp. 225–242.

Catuneanu, O. 2004, Basement control on flexural profiles and the distribution of foreland facies: the Dwyka Group of the Karoo Basin, South Africa. *Geology*, Vol. **32**, no. 6, pp. 517–520.

Catuneanu, O., 2006, Principles of Sequence Stratigraphy. Elsevier, Amsterdam, 375 pp.

Catuneanu, O., and Eriksson, P. G., 1999, The sequence stratigraphic concept and the Precambrian rock record: an example from the 2.7–2.1 Ga Transvaal Supergroup, Kaapvaal craton. *Precambrian Research*, Vol. **97**, pp. 215–251.

Cediel, F., 1968, El Grupo Girón, una molasa Mesozóica de la Cordillera Oriental. Servicio Geológico Nacional Boletín Geológico, Bogotá, 16(1-3): 5-96.

Cediel, F. Mojica, J. Macia, C. 1980, Definición estratigráfica del Triásico de Colombia, Suramerica. Formaciones Luisa, Payandé y Saldaña. Newslett. Stratigr. 9(2):73- 104.

Cediel, F., and C. Cáceres, 2000, Geological Map of Colombia, Third Edition: Geotec Ltd., Bogotá, digital format with legend and tectonostratigraphic chart.

Cediel, F., Shaw, R.P., Cáceres, C., 2003, Tectonic assembly of the Northern Andean Block, in C. Bartolini, R.T. Buffler, and J. Blickwede, eds., The Circum-Gulf of Mexico and the Caribbean: Hydrocarbon habitats, basin formation, and plate tectonics. Am. Assoc. Petrol. Geol., Memoir, v. 79, p. 815-848.

Cediel, F., Shaw R. P., 2019, Geology and Tectonics of Northwestern South America, Frontier in Earth Sciences, chapter 2, 97-112, doi:10.1007/978-3-319-76132-9_2.

Champertier de Ribes, G., Weeksteen, G., et al., 1961, Mapa Geológico de la plancha K-10, Villeta, esc. 1: 200 000, 1 lám., 46 x 71 cm, Bogotá.

Charles, D., 1846, South America: Geological observations on South America. Being the third part of the geology of the voyage of the Beagle, under the command of Capt. FitzRoy RN, during the years 1832 to 1836.By London: Smith, Elder and Co.

Cheilletz, A., Giuliani, G., Branquet, Y., Laumonier, B., Sánchez, M.A.J., Rueda, F., Féraud, G., Arhan, T., 1997, Datation K-Ar et $^{40}Ar/^{39}Ar$ à 65 M.a. des gisements d'émeraude du district Chivor-Macanal, argument en faveur d'une déformation précoce dans la Cordillère Orientale de Colombie. C.R. Acad. Sci., Séries II, Paris, 324(5): 369-377.

Chenevart Ch., 1963, Les dorsalis transverses anciennes de Colombie et leurs homologues d´Amérique latine. *Ecl. Geol. Helv*., vol. 56, n° 2, pp. 907-927, 7 fig., Basel.

Clark, A.H., Farrar, E., Kontak, D.J., Langridge, R.J., Arenas, M.J., France, LJ., McBride, S.L., Wlodrnan, P.L., Wasteneys, H.A., Sandeman, H.A., Douglas, D.A., 1990, Geologic and geochronologic constraints on the metallogenic evolution of the Andes of Southeastern Peru. *Economic Geology*, 85, 1520-1583.

Clavijo, J., Mantilla, L. C., J.E, P., Bernal, L. and Perez, A., 2008, Evolución geológica de la Serranía de San Lucas, Norte del Valle Medio del Magdalena y Noroeste de la Cordillera Oriental.: Boletín de Geología, Universidad Industrial de Santander, 30 (1): 45-62.

Cobbing, E.J., Pitcher, W.S., Wilson, J.J., Baldock, J.W., Taylor, W.P., McCourt, W., Snelling, N.J., 1981, The geology of the Westem Cordillera of Northern Peru. Institute of Geological Sciences London, *Overseas Memoir*, 5, 143 p.

CODIGEM, 1993a, Mapa Geológico de la República del Ecuador, Escala 1:1,000.000: Compilado por CODIGEM-BGS, Quito, Ecuador.

Colmenares, L., Zoback, M.D., 2003, Stress field and seismotectonics of northern South America. Geology, 31, 721-724.

Colleta, B., Hebrard, F., Letouzey, J., Werner, P., and Rudkiweicz, J.L., 1990, Tectonics style and crustal structure of the Eastern Cordillera (Colombia) from a balanced cross section, in Letouzey, J., ed., Petroleum and tectonics in mobile belts: Paris, Editions Technip, p. 81-100.

Colmenares, L., Zoback, M.D., 2003, Stress field and seismotectonics of northern South America. Geology, 31, 721-724.

Contreras, C., Jaillard, E., Paz, M., 1996, Subsidence history of the north peruvian Oriente (Marañón basin) since the Cretaceous. *3rd International Symposium on Andean Geodynamics-ISAG*, Saint-Malo, Orstom ed., París, 327-330.

Cooney, P. M. Lorente M.A., 2009, A structuring event of Campanian age in western Venezuela, interpreted from seismic and paleontological data. Geological Society, London, Special Publications. V. 328. P 628-703. Doi: 10.1144/SP328.27.

Cooper, M.R., 1982, Lower Cretaceous (Middle Albian) ammonites from Dombe Grande, Angola. Annals of the South African Museum 89, 265e314.

Cooper, M., Addison. F.T., Alvarez, R., Coral, M., Graham, R.H., Hayward, A.B., Howe, S, Martinez, J., Naar, J., Peñas, R., Pulham. A.J. & Taborda, A., 1995, Basin development and tectonic history of the Los Llanos Basin, Eastern Cordillera and Middle Magdalena Valley. Colombia.- Bulletin of the American Association of Petroleum Geologists, v. 79,10, p. 1421-1443, Tulsa.

Corcoran, D. V. & Doré, A. G., 2005, A Review of Techniques for the Estimation of Magnitude and Timing of Exhumation in Offshore Basins. *Earth Science Reviews*, 72, 129-168.

Corredor, F., 2003, Eastward extent of the Late Eocene-Early Oligocene onset of deformation across the northern Andes: constraints from the northern portion of the Eastern Cordillera fold belt, Colombia. Journal of South American Earth Sciences, v.16, p.445-457.

Cortés, M., Jacquest, A., Colleta, B., 2005, Paleostress evolution of the northern Andes (Eastern Cordillera Colombia): Implications on plate kinematics of South Caribbean region. Tectonics, Vol. 24, TC1008, doi: 10.1029/2003TC001551.

Cortes M., Colleta, B., Angelier, J., 2006, Structure and tectonics of central segment of Eastern Cordillera of Colombia, Journal of South American Earth Science 21, V.21, p. 437-465.

Christie-Blick, N. 1991, Onlap, offlap, and the origin of unconformity bounded depositional sequences. *Marine Geology*, Vol. **97**, pp. 35–56.

Cross, T.A., Pilger, R. H., 1982, Controls of subduction geometry, location of magmatic arcs, and tectonics of arc and back-arc regions. Geol. Soc. Am. Bull. 93: 545-562.

Crowley, K.D., Naeser, C.W., Naeser, N.D., 1989, Fission track analysis: Theory and applications. Short coursemanual. Geological Society of America Annual Meeting St. Louis, Missouri. USA.

Dahlen, F.A. and Barr, T.D., 1989, Brittle frictional mountain building 1. Deformation and mechanical energy budget, J. geophys. Res., 94, 3906– 3922.

Dalmayrac, B., G. Laubacher, and R. Marocco, 1977, Geologie des Andes Peruviennes: Caracteres generaux de l'evolution geologique des Andes Peruviennes: Doctoral Thesis, Universite des Sciences et Techniques du Languedoc, Academie de Montpellier, France, 361 p.

Dalmayrac, B., Laubacher, G., Marocco, R., Martfnez, C., Tomasi, P., 1980, La chaîne hercynienne d'Amérique du Sud: Structure et évolution d'un orogène intracratonique. *Geologische Rundschau, 69(I),* 1-21.

Daly, M. C., 1989, Correlations between Nazca/Farallon plate kinematics and forearc basin evolution in Ecuador. Tectonics, 8, 769-790.

Dashwood, M.F., Abbots, l.l., 1990, Aspects ofthe petroleum geology of the Oriente Basin, Ecuador. In: Classic Petroleum Provinces, ed. Brooks, J. *Geological Society of America, Special Publ.*, 50, 89-117.

Davis, D., Suppe, J. and Dahlen, F.A., 1983, Mechanics of fold and thrust belt and accretionary wedges, J. Geophys. Res., 94, 7278-7292.

DeCelles, P. G., and Horton B. K., 2003, Early to middle Tertiary foreland basin development and the history of Andean crustal shortening in Bolivia, Geol. Soc. Am. Bull., 115(1), 58–77, doi:10.1130/0016-7606(2003)1152.0.CO;2.

Dengo, C. A., and Covey M. C., 1993, Structure of the Eastern Cordillera of Colombia: Implications for trap styles and regional tectonics, AAPG Bull., 77, 1315 – 1337.

Dickey P. A., 1941, Pre-Cretaceous sediment in Cordillera Oriental of Colombia. Bull. Am. Ass. Petr. Geol., vol. 25, n°9, pp. 1789-1795, fig., Tulsa.

Dickinson, W.R. 1988, Provenance and sediment dispersal in relation to paleotectonics and paleogeography of sedimentary basins. En: Kleinspehn, K.L. y Paola, C. (eds), New Perspectives in Basin Analysis. Springer- Verlag,:3-25.

Dodson, M.H., Compston, W., Williams, I.S., J.F., 1988, A search for ancient detrital zircons in Zimbabwean sediments. J. Geol. Soc. 145, 977–983.

Doglioni, C., Mongelli, F., Pialli, G., 1998, Boudinage of the Alpine belt in the Apenninic back-arc. Mem. Soc. Geol. It. 52, 457–468.

Doglioni C., Doglioni C., Harabaglia P., Merlini S., Mongelli F. , Peccerillo A., Piromallo C., 1999, Orogens and slabs vs. their direction of subduction. Orogens and slabs vs. their direction of subduction. Earth-Science Reviews 45. 167–208.

Donelick, R. A., R. A. Ketcham, and W. D. Carlson, 1999, Variability of apatite fission-track annealing kinetics II: Crystallographic orientation effects, Am. Mineral., 84, 1224–1234.

Donelick, R.A., O'Sullivan, P.B., and Ketcham, R.A., 2005, Apatite fission-track analysis, in Reiners, P.W., and Ehlers, T.A., eds., Low temperature thermochronology: Techniques, interpretations, and applications: Mineralogical Society of America Reviews in Mineralogy and Geochemistry 58, p. 49–94, doi: 10.2138/ rmg.2005.58.3.

D'Orbigny A., 1840–1842, '*Paléontologie française; Terrains crétacés*. **1**, *Céphalopodes*, 1 120 (1840); 121–430 (1841); 431–662 (1842), 151 pls. Paris: Masson.

Dow, W.G., 1977, Kerogen studies and geological interpretations. *Journal of Geochemical Exploration*, 7 (1977) 79—99).

Drummond, C. N., Wilkinson, B. H., 1996, Stratal thickness frequencies and the prevalence of orderedness in stratigraphic sequences. Journal of Geology **104**, 1–18.

Duque-Caro, H., 1990, The Chocó block in the northwestern corner of South America: Structural, tectonostratigraphic, and paleogeographic implications. Jour. of South Am. Earth Sci., 3(1): 71-84.

Duque-Caro, H. 2004, Microestratigrafía y correlación de los pozos Bosques-1, Punta Piedras-2, Catalina-1 y Torcoroma-1, Valle Medio del Magdalena. Informe Interno para ECOPETROL-ICP.

Duque, N.E. 2008, Control petrográfico durante la perforación del pozo Guane-1, Valle Medio del Magdalena. Informe Final. Instituto Colombiano del Petróleo. Laboratorio de Petrología.

Duque-Caro, H. 2012, Análisis microestratigráfico de 40 muestras. Quebrada Aguadulce (Sector deLa Sorda, VMM). Informe Interno para GEMS S.A.

Duncan, R.A., Hargraves, R.B., 1984, Plate tectonic evolution of the Caribbean region in the mantle reference frame. In: The Caribbean–South American Plate Boundary and Regional Tectonics (W.E. Bonini, R.B. Hargraves and R. Shagam, eds), Geol. Soc. Am. Mem., 162, 81–93.

Dunham, R., 1962, Classification of carbonate rocks according to depositional texture.- American Association of PetroleumGeologists Memoir 1, p. 108-121, Tulsa.

Dumbar, J.A. and Sawyer, D.S., 1988, Continental rifting at pre-existing lithospheric weaknesses, Nature, 333, 450-452.

Dumbar, J.A. and Sawyer, D.S., 1989, How pre-existing weaknesses control the style of continental breading, J. Geophys, Res., 94, 7278-7292.

Duncan R. A. and Hargraves R. B., 1984, Plate tectonic evolution of the Caribbean region in the mantle reference frame. In: W.E. Bonini, R.B. Hargraves and R. Shagam (eds). The Caribbean-South American plate boundary and regional tectonics, Geol. Soc. Am., Mem., 162: 81-93.

Duque-Caro, H., 1979, Major structural elements and evolution of northwestern Colombia. In: J.S.Watkins, L. Montadert, and P.W. Dickerson. (Eds.), *Geological and geophysical investigations of continental margins*. A.A.P.G. Mem. 29: 329-351.

Duque-Caro, H., 1990, The Choco Block in the northwestern corner of South America: structural, tectonostratigraphic, and paleogeographic implications. Journal of South American Earth Sciences, v. 3(1), p. 71-84.

Ego, F., Sébrier, M., Lavenu, A., Yepes, H. and Egüez, A., 1996, Quaternary state of stress in the Northern Andes and the restraining model for the Ecuadorian Andes.- Tectonophysics, 259: 101-116.

Ellis, S., Schreurs G. and Panien, M., 2004, Comparisons between analogue and numerical models of thrust wedge development. Journal of Structural Geology, 26, 1659–1675.

Emery, K. O. and Uchupi, E., 1984, The Geology of Atlantic Ocean. Springer Verlag, New York, 1050 p.

Emery, D. and Myers, K.J., 1996, Sequence Stratigraphy, published by Blackwell Science Ltd., p. 297.

England, P. and McKenzie, D., 1982, A thin viscous sheet model for continental deformation, Geophys. J.R. astr. Soc., 70, 295-321.

England, P., Molnar, P., 1990, Surface uplift of rocks, and exhumation of rocks. Geology, v.18, p. 1173-1177.

Eriksson, P. G., Catuneanu, O., Nelson, D. R., and Popa, M., 2005a, Controls on Precambrian sea level change and sedimentarycyclicity. *Sedimentary Geology*, Vol. **176**, pp. 43–65.

Eriksson, P. G., Catuneanu, O., Els, B. G., Bumby, A. J., van Rooy, J. L., and Popa, M., 2005b, Kaapvaal craton: changing first- and second-order controls on sea level from c. 3.0 Ga to 2.0 Ga. *Sedimentary Geology*, Vol. **176**, pp. 121–148.

Eriksson, P. G., Altermann, W., Nelson, D., Mueller, W., and Catuneanu, O. (Eds.) 2004, *The Precambrian Earth: Tempos and Events*. Developments in Precambrian Geology **12,** Elsevier, Amsterdam, p. 941.

Etayo-Serna F., 1964, Posición de las faunas en los depósitos cretácicos colombianos y su valor en la subdivisión cronológica de los mismos. Bol. Geol., Univ. Ind. Santander, n° 16-17, pp. 5-141, 8 fig., Bucaramanga.

Etayo-Serna, F., 1968a, El sistema Cretáceo en la región de Villa de Leiva y zonas próximas. Geología Colombiana, Bogotá, 5: 5-74.

Etayo-Serna, F., 1968b, Sinopsis Estratigráfica de la Región de Villa de Leiva y Zonas Próximas.- Boletín de Geología UIS, N.21, p. 19 - 32, Bucaramanga.

Etayo, F., 1969, Lenticeras Baltai Lisson en Colombia y su probable posición zonal Santoniana. Geología Colombiana, n. 6, 1969· pp, 17·29, Igs, 4, Is.1·3.

Etayo-Serna, F., Renzoni, G. & Barrero, D. 1969, Contornos sucesivos del mar Cretáceo en Colombia. In: Primer Congreso Colombiano de Geología, Memorias. Imprenta Nacional de Colombia, Colombia, 217–252. Bogotá.

Etayo-Serna F. 1972, Cretaceous section: Villa de Leiva to Loma Piedra Gorda.- Colombian Society of Petroleum Geologists and Geophysicists. Thirteenth Annual Field Conference, p. 349 - 396, Bogotá.

Etayo, Serna F., 1978, Ideas para la reinterpretación de ambientes desimentarios del sistema cretácico en la región de Villa de Leiva (Departamento de Boyaca), Colombia. Segundo Congreso Colombiano de Geología. Excursión Pre-Congreso No. 3. 20p. Diciembre 2-3 de 1978.

Etayo, F., 1979, Zonation of the Cretaceous of Central Colombia by Ammonites. Publicaciones Especiales de Ingeominas, No. 2, p. 1-186. Bogotá.

Etayo-Serna, F., Barrero, D., Lozano, H., Espinosa, A., González, H., Orego, A., Zambrano, F., Duque, H., Vargas, R., Núñez, A., Álvarez, J., Ropaín, C., Ballesteros, I., Cardozo, E., Forero, H., Galvis, N., Ramírez, C. and Sarmiento, L., 1983, *Mapa de terrenos geológicos de Colombia*, Ingeominas Publicación Geológica Especial 14, Bogotá, 235 p.

Etayo-Serna, F., 1985, El límite Jurásico Cretácico en Colombia. In: F. Etayo-Serna and F. Laverde-Montaño (eds.), Proyecto Crétacico, contribuciones. Chapter XXII, Ingeominas Publicación Especial 16, Bogotá, 4 p.

Etayo et al., 1986, Mapa de terrenos geológicos de Colombia. Ingeominas Publicación Geológica Especial 14, 1–235.

Etayo, S., 2012, Informe del contenido paleontológico, en especial de amonjitas del pozo la Luna-1. Informe interno para Ecopetrol.

Emmerman S.H. and Turcote, D.L., 1983, A fluid model for the shape of accretionary wedges, Earth planet. Sci. Lett., 63, 379-384.

Engebretson, D. C., Cox, A. and Gordon, R. G. 1985, Relative motions between oceanic and continental plates in the Pacific Basin, Geological Society of America, Special Paper, 206.

Espurt N., Funiciello F., Martinod J., Guillaume B., Regard Vincent., Faccenna C., Brusset S., 2008, Flat subduction dynamics and deformation of the South American plate: Insights from analog modeling.Tectonics, Vol. 27, TC3011, doi: 10.1029/2007TC002175.

Fabre, A. and Delaloye, M., 1983, Intrusiones básicas Cretácicas de la Cordillera Oriental. Geología. Norandina, Bogotá, 6:19-28.

Fabre, A., 1983ª, La subsidencia de la Cuenca del Cocuy (Cordillera Oriental de Colombia) durante el Cretáceo y el Terciario Inferior. Primera parte: Estudio cuantitativo de la subsidencia. Geología Norandina, Bogotá, 8: 49-61.

Fabre, A., 1983b, La subsidencia de la Cuenca del Cocuy (Cordillera Oriental de Colombia) durante el Cretáceo y el Terciario Inferior. Segunda parte: Esquema de evolución tectónica. Geología Norandina, Bogotá, 8: 21-27.

Fabre A., 1985a, Dinámica de la sedimentación Cretácica en la región de la Sierra Nevada del Cocuy (Cordillera Oriental de Colombia). In: F. Etayo-Serna and F. Laverde-Montaño (eds.), *Proyecto Crétacico, contribuciones*. Chapter XIX, Ingeominas Publicación Geológica Especial 16, Bogotá, 20 p.

Fabre, A., 1985b, Subsidencia y maduración de la materia orgánica; un modelo de la evolución de la Cordillera Oriental y los Llanos durante el Cretácico y el Terciario (abstract). Mem. IV Congr. Latinoamericano de Geología., Bogotá, 2: 421-422.

Fabre, A., 1987, Tectonique et géneration d'hydrocarbures: Un modèle de l'évolution de la Cordillère Orientale de Colombie et du Bassin des Llanos pendant le Crétacé et le Tertiaire. Arch. Sc. Genève, 40 (Fasc. 2): 145-190.Feininger (1980, 1986).

Faucher. B., Savoyat. E., 1973, Esquisse géologique des Andes de l´equarteur: Revue de Géographie Physique et de Géologic Dynamique, v. 15 p. 115-142.

Feininger, T., 1980, Eclogite and related high-pressure regional metamorphic rocks from the Andes of Ecuador. Journal of Petrology 21, 107–140.

Feininger, T., Bristow, C.R., 1980, Cretaceous and Paleogene geologic history of coastal Ecuador. Geologische Rundschau 69, 849–874.

Feininger, T., Silberman, M.L., 1982, K-Ar geochronology of basement rocks on the northern flanks of the Huancabamba Deflection, Ecuador. Open File Report. United States Geological Survey, 82, p. 206.

Fischer, A. G., 1964, The Lofer cyclothcms of the Alpine Triassic: Kansas Geological Survey Bulletin, v. 169, p. 107- 149.

Fleischer, R.L., Hart, H. R., 1972, Fission-track dating techniques and problems. In Bishop, W., Miller, J., and Colle, S., (Eds.).Calibration of Hominoit Evolution. Scottish Academic Press, p.135-170.

Forero-Onofre, H., Sarmiento-Rojas, L. 1982, Ambiente de sedimentación del miembro arcillolitas abigarradas Formación Paja, área de Villa de Leiva. Trabajo de Grado, Univ, Nal. De Colombia, Bogotá, p. 187.

Forero O.H., Sarmiento R.L., 1982, Ambiente de sedimentación del miembro de arcillolitas abigarradas, Formacion Paja, área de Villa de Laiva, Trabajo Final. Depto. Geociencias . Univ. Nal. Colombia. 188 p, 36 figs, 13 lám. Bogotá.

Forero, H. and Sarmiento L., 1985, Las facies evaporítica de la Formación Paja en la región de Villa de Leiva. In: F. Etayo-Serna and F. Laverde-Montaño (eds.), *Proyecto Crétacico, contribuciones*. Chapter XVII, Ingeominas Publicación Geológica Especial 16, Bogotá, 16p.

Forero, A., 1990, The basement of the Eastern Cordillera, Colombia: an allocthonous terrane in nortwestern South America.: Journal of South American Earth Sciences, 3: 141-151.

Freymueller, J., J. Kellogg, V. Vega, **1993,** Plate motions in the North Andean Region, *J. Geophys. Res*., 98, 21, 853-21,863.

Frutos, J. 1981, Andean tectonics as a consequence of sea-floor spreading. Tectonophysics, 72, T21-T32.

Fuquen J. and Osorno J., 2005, Geología de la Plancha 190 Chiquinquirá. Ingeominas. Escala 1:100000. Version digital 2009.

Gabriele, P., Ballèvre, M., Jaillard, É., Henandez, J., 1999, Decompression at decreasing temperatures in edogite-facies metapelites (El Oro Metatmorphic Complex, SW Ecuador): A record of fast exhumation rates. *4th lnternational Symposium on Andean Geodynamics-ISAG*, Göttingen, IRD publ., París, 245-148.

Gallo, J. 1977, The environmental facies analysis of selected Tertiary and Cretaceous outcrops along the Villeta-Honda road, 1979 in Geological Field Trips, Colombia, 1958 1978.- Colombian Society of Petroleum Geologists and Gephysicists, p. 473-487, Bogota.

Galloway, W.E. 1989, Genetic stratigraphic sequences in basin analysis, I. Architecture and genesis of flooding-surface bounded depositional units. *American Association of Petroleum Geologists Bulletin*, Vol. **73**, pp. 125–142.

Galvis E. and Valencia L., 2009, Contribución en la determinación de los posibles paleoambientes de las rocas Cretácicas tempranas sobre la via Tunja – Villa de Leyva (entre alto del Arrayan – peaje Sáchica) y sectores aledaños, Departamento de Boyacá. Universidad de Caldas. Tesis pregrado.

Gansser, A., 1973, Facts and theories on the Andes. Journal of the Geological Society, London, 129, 93–131.

Gaona, T., 2004, Bivalvos del Albiano y del Cenomaniano de la Cordillera Oriental de Colombia, Bioestratigrafía y Paleoecología. Informe interno INGEOMINAS. 59 p. Bogotá.

Garcia, M. D., 1983, Estratigrafía de la unidad basal de la serie CretAC80 inferior en la región de Villeta. Tesis de grado, Universidad Nacional de Colombia, Departamento Geociencias, Bogota, 40 p.

Gayet, M., Marshall LG, Sempere T., 1991, The Mesozoic and Paleocene vertebrates of Bolivia and their stratigraphic context: A review in: Suarez-Suroco R (Ed) Fosiles y facies de Bolivia Vol. I Vertebrados. Santa Cruz-Bolivia, Revista Técnica de Ypfb. 12:393-433.

Gayet, M., Sempere, T., Cappena, H., jaillani, É. and Lévy, A., 1993, La présence de fossiles marins dans le Crétacé terminal des Andes centraleset ses conséquences paléogéographiques, *Palaeoclimatology, Palneoecology,* 102,183-319.

George, R. P., Pindell, J. L., and Cristancho, H., 1997, Eocene Paleosuture of Colombia and implications for history of generation and migration of hydrocarbons: VI simposio Bolivariano, exploración petrolera en las cuencas subandinas, Cartagena: Asociación Colombiana de Geólogos y Geofísicos del Petróleo, Tomo I, p. 133-140.

Gil, W., Baby, P., Paz, M., 1996, Continum tectonic during Cretaceous-Paleocene times in the north peruvian foreland Basin (Marañón Basin).3rd *lntern. Symp.And. Geodyn.-ISAG,* Saint-Malo, Orstom publ., Paris, 363-366.

Gómez-Cruz, A.D.J., Moreno-Sánchez, M., Pardo, A., 1995, Edad y origen del ‘‘Complejo metasedimentario Aranzazu-Manizales” en los alrededores de Manizales (Departamento de Caldas, Colombia). Geología Colombiana 19, 83–93.

Gómez, E., 1999, Geodinámica, tectonoestratigrafía, cronología y evolución termal de cuencas sedimentarias complejas y de sus áreas fuente. Métodos modernos de análisis cuantitativo y aplicaciones, implicaciones para exploración y producción de hidrocarburos. Curso-Taller con salida de campo. Santafé de Bogotá, Nov. 26 –30., 55 p.

Gomez, E., Jordan, T., Hegarty, K. and Kelley, S., 1999, Diachronous deformation of the Central and Eastern Andean cordilleras of Colombia and syntectonic sedimentation in the Middle Magdalena Valley Basin. Fourth ISAG, Gottingen, Germany, 4-6 October, p. 287-290.

Gómez, E., 2001, Tectonic controls on the Late Cretaceous to Cenozoic sedimentary fill of the middle Magdalena Valley Basin, Eastern Cordillera and Llanos Basin, Colombia: Ph.D. thesis, CornellUniversity, Ithaca, NewYork, 619 p.

Gomez E., Jordan T., Allmedinger W.R., Hegarty K., Kelley S., Heizler M., 2003, Controls on architecture of the Late Cretaceous to Cenozoic southern Middle Magdalena Valley Basin, Colombia: Geological Society of America Bulletin; February 2003; v. 115; no, 2; p. 131-147; 16 figures; 2 tables; Data Repository item 2003029.

Gomez E., Jordan T. E., Allmedinger W.R., Hegarty K., Kelley S., 2005, Syntectonics Cenozoic sedimentation in the Northern Middle Magdalena Valley Basin and implications for exhumation of the northern Andes: Geological Society of America Bulletin; v. 117, p. 547-569.

Gonzáles G., 1976, Ciclos de sedimentación en el Eoceno de la Cuenca de Talara. *Bol. Soc. geol. Perú,* 51, 73-80.

González de Juana, C., J. Iturralde, X. Picard, 1980, Geología de Venezuela y de sus Cuencas Petrolíferas: Caracas, Venezuela, Ediciones Fonives, 1031 p.

González, H. 1980, Geología de las planchas 167 (Sonsón) y 187 (Salamina). Boletín Geológico, Ingeominas, Vol. 23 (1): pp 1-174, Bogotá.

González, H., 1996, Mapa Geológico del Departamento de Antioquia: Memoria Explicativa, Ingeominas, Medellín, Colombia, 232 p.

Goossens, P. J. & Rose, W. I. 1973, Chemical composition and age determination of tholeitic rocks in the basic Cretaceous Complex, Ecuador. Geological Society of America Bulletin, 84, 1043–1052.

Gradstein et al. 2012, Geological Time Scale 2012 Publication.Newsletters on Stratigraphy, Vol. 45/2, 171-188, Stuttgard, July, p. 171-188.

Galbraith, R. F. 1981, On statistical models for fission tracks counts. Journal of Mathematical Geology. 13,471–478, doi: 10.1007/BF01034498.

Galbraith, R. F., and Green, P.F., 1990, Estimating the component ages in a finite mixture: Nuclear Tracks and Radiation Measurements, v. 17, p. 197–206.

Gallagher, K., Brown, R.W. and Jhonson, C.J., 1998, A novel method for constraining heat flow histories in sedimentary basins, in Basin Modeling: Practice and Progress, (Duppenbecker, S.J. and Illiffe J.E., Geological Soc. London Special Publication 141, 223-240.

Galbraith, R.F., 2005, Statistics for Fission Track Analysis: Boca Raton, Chapman and Hall/CRC, p.219

Galbraith R.F., Laslett, G.M., 1993, Statistical models for mixed fission track ages. Nuclear Tracks, v.21, p.459- 470.

Garver JI, Reiners PR, Walker LJ, Ramage JR, Perry S. E. 2005, Implications for timing of Andean uplift based on thermal resetting of radiation-damaged zircon in the Cordillera Huayhuash, northern Perú. J Geol. v. 113, n. 2, p. 117-138.

Gehrels, G.E., Johnsson, M.J., and Howell, D.G., 1999, Detrital zircon geochronology of the Adams Argillite and Nation River Formation, East-Central Alaska, USA: Journal of Sedimentary Research, v. 69, p. 135–144.

Gehrels, G.E., 2000, Introduction to detrital zircon studies of Paleozoic and Triassic strata in western Nevada and Northern California, in Soreghan, M.J., and Gehrels, G.E., eds., Paleozoic and Triassic paleogeography and tectonics of western Nevada and northern California: Geological Society of America Special Paper 347, p. 1–17.

Gleadow, A.J.W., and Duddy, I.R., 1981, A natural long-term annealing experiment for apatite: Nuclear Tracks and Radiation Measurements, v. 5, p. 169–174.

Gleadow, A. J. W., Duddy I. R., Green P. F., and Lovering J. F., 1986, Confined track lengths in apatite: A diagnostic tool for thermal history analysis, Contrib. Mineral. Petrol., 94, 405–415.

Gómez, E., 2001, Tectonic controls on the Late Cretaceous to Cenozoic sedimentary fill of the Middle Magdalena Valley Basin, Eastern Cordillera and Llanos Basin, Colombia [Ph.D. thesis]: Ithaca, New York, Cornell University, 619 p.

Gómez, E., T.E., J., Allmendiger, R. W., Hegarty, K., Kelley, S., and Heizler, M., 2003, Controls on architecture of the Late Cretaceous to Cenozoic southern Middle Magdalena Valley Basin, Colombia: Geological Society of America Bulletin, v. 115, p. 131-147.

Gómez, E., Jordan, T.E., Allmendinger, R.W., and Cardozo, N., 2005a, Development of the Colombian foreland-basin system as a consequence of diachronous exhumation of the northern Andes: Geological Society of America Bulletin, v. 117, p. 1272–1292, doi:10.1130/B25456.1.

Gómez, E., Jordan, T.E., Allmendinger, R.W., Hegarty, K., and Kelley, S., 2005b, Syntectonic Cenozoic sedimentation in the northern middle Magdalena Valley Basin of Colombia and implications for exhumation of the Northern Andes: Geological Society of America Bulletin, v. 117, p. 547–569, doi:10.1130/B25454.1.

Graveleau F., Malavieille, J., Dominguez, S., 2012, Experimental modelling of orogenic wedges: A review, Tectonophysics, 538-540, p. 2-66. doi:10.1016/j.tecto.2012.01.027.

Groose E., 1930, Informe Geológico preliminar sobre un viaje al Huila y Alto Caquetá. Bol. Min. Petr., t. 3, n° 17, pp. 387-398, 1 foto., Bogotá.

Guerrero J. and Carrillo G., 1998, Actualización Cartográfica de Unidades Litoestratigraficas Encajantes de Mineralizaciones Esmeraldiferas en el Cinturón Occidental de la Cordillera Oriental (Colombia). Tesis Pregrado. Universidad Nacional de Colombia.

Guerrero, J. 2002, A Proposal on the Classification of Systems Tracts: Application to the Allostratigraphy and Sequence Stratigraphy of the Cretaceous Colombian Basin. Part 2: Barremian to Maastrichtian. Geología Colombiana, 27, Pgs. 27 - 49, 2 Figs, 1 Table, Bogota.

Guerrero J., 2010, Informe de interpretación Campo Tisquirama y San Roque, superintendencia de Yacimientos, reporte interno de Ecopetrol, Marzo de 2010, pag 1- 28.

Guerrero J., Machado O., Osorio C., 2012, Campos Tisquirama y San Roque áreas que Vuelven a Renacer – Mediante la Caracterización de yacimientos. XI Simposio Bolivariano de las Cuencas Subandinas, p. 1-10.

Guerrero, J., and Sarmiento, G., 1996, Estratigrafía física, palinológica, sedimentológica y secuencial del Cretácico Superior y Paleoceno del Piedemonte Llanero: Implicaciones en exploración petrolera: Geologia Colombiana, v. 20, p. 3–66.

Guillande, M.R., 1988, Evolution Méso-Cénozoïque d'une vallée intercordilléraine andine: La Haute Vallée du Rio Magdalena (Colombie). Ph.D. Thesis Univer. Paris 6, Paris, 352p.

Gutscher, M.-A., Maury R., Eissen J. P., and Bourdon, 2000a, Can slab melting be caused by flat subduction?, Geology, 28, 535 – 538, doi:10.1130/0091-7613(2000)28<535:CSMBCB>2.0.CO;2.

Gutscher, M.-A., W. Spakman, H. Bijwaard, and E. R. Engdalh., 2000, Geodynamics of flat subduction: Seismicity and tomographic constraints from the Andean margin, Tectonics, 19, 814–833, doi:10.1029/1999TC001152.

Haq, B. U., Hardenbol, J. and Vail, P. R., 1987, Chronology of fluctuating sea levels since the Triassic (250 Myr ago to Present). Science, 235: 1156-1167.

Harabaglia, P., Doglioni, C., 1998, Topography and gravity across subduction zones. Geophys. Res. Lett. 25 (5)., 703–706.

Hartnady, C. J. H., 1991, About turn for supercontinents: Nature, v. 55, no. 1, p. 476–478.

Haas, O. 1960, Lower Cretaceous Ammonites from Colombia, South America. Amer. Mus. Novitates, 2005, 62 S., 145 Fig. New York.

Hart, M. 1980, A water depth model for the evolution of the planktonic Foraminiferida. Nature, 286 (5770): 252-254.

Hedberg, H.D., 1931, Cretaceous limestone as petroleum source rock in northwestern Venezuela. *Bull. Am. Ass. Petr. Geof,* vol. 15, nº 3, pp. 229-244, 8 fig., Tulsa.

Herman F, Seward D, Valla PG, Carter A, Kohn B, Willett SD, Ehlers TA., 2013, Worldwide acceleration of mountain erosion under a cooling climate. Nature 504(7480):423.

Hernández, H. 1990, Estratigrafía del Grupo Guadalupe al Occidente de La Sabana de Bogotá. Tesis de Grado, U. Nal., 142 p. Bogotá.

Hettner, A. 1892, Die Kordillere von Bogotá. *Peterm. Mitt.*, Erg-Bd. 22, Helft. nº 104, l31 pp., 9 fig., 2 Taf. (Kart., Prof.) Trad. Esp., Ed. Banco de la República, 351 pp., 9 fig., 2 taf., Bogotá

Hoedemaeker, Ph.J. 2004, On the Barremian-lower Albian stratigraphy of Colombia. Scripta Geologica, 128: 3-15, 3 Figs., Leiden, December 2004.

Hoffman, P., 1991, Did the breakup of Laurentina turn Gondwanaland inside-out?: Science, v. 252, p. 1409–1412.

Hooghiemstra, H., 1989, Quaternary and Upper-Pliocene glaciations and forest development in the tropical Andes: evidence from long high-resolution pollen record from the sedimentary basin of Bogotá, Colombia. Palaeogeography, Palaeoclimatology, Palaeoecology, 72: 11-26.

Horton, B.K., Hampton, B.A., and Waanders, G.L., 2001, Paleogene synorogenic sedimentation in the Altiplano plateau and implications for initial mountain building in the Central Andes: Geological Society of America Bulletin, v. 113, p. 1387–1400, doi: 10.1130/0016 -7606(2001)113<1387:PSSITA>2.0.CO;2.

Horton. B., 2005, Revised deformation history of the central Andes: Inferences from Cenozoic foredeep and intermontane basins of the Eastern Cordillera, Bolivia. Tectonics. DOI: 10.1029/2003TC001619.

Horton, B. K., Parra, M., Saylor, J. E., Nie, J., Mora, A., Torres, V., Stockli, D. F., and Strecker M. R., 2010, Resolving uplift of the northern Andes using detrital zircon age signatures, GSA Today, 20(7), 4-10, DOI: 10.1130/GSATG76A.1.

Horton, B.K, Saylor, J.E., Nie, J., Mora, A., Parra, M., Reyes-Harker, A. and Stockli, D., 2010b, Linking sedimentation in the northern Andes to basement conFiguration, Mesozoic extension, and Cenozoic shortening: Evidence from detrital zircon U-Pb ages, Eastern Cordillera, Colombia: *Geological Society of America Bulletin* 2010;122;1423-1442, doi: 10.1130/B30118.1.

Horton B. and Fuentes B., 2016, Sedimentary record of plate coupling and decoupling during growth of the Andes. Geology, August 2016; v. 44; no. 8; p. 647–650, Data Repository item 2016210, doi:10.1130/G37918.1.

Hubach, E., 1931a, El Valanginiano como sección del Piso de Girón en el Tablón (entre Cáqueza y Quetame) y la probabilidad del comienzo de la transgresión andina en Colombia durante el Portlandiano. Inf. Serv. Geol. Nal., (perdido). Resumen en ROYO y GÓMEZ 1945a, pp. 212-213.

Hubach, E., 1931b, Geología Petrolífera del Dpto de Norte de Santander. Serv. Geolo., Nal., informe n° 176 (inedito), parte A, pp. 1-218; parte B, pp 219-416; parte c (láminas), 26 lám., Bogotá. p. 90.

Hubach, E., 1931c, Exploración de la región de Apulo-San Antonio-Viotá. *Bol.. Min,. Petr.*, t. 4, nº 25-27, pp. 41-60, 1 lám., Bogotá.

Hubach, E., 1931d, Informe sobre las minas de carbón de Los Chorros, de propiedad del Ferrocarril del Pacífico, Dpto del Valle. Serv. Geol. Nal., informe 194 (inédito), 5 pp., Bogotá.

Hubach, E., 1953, Condiciones Geológicas de las variants de carretera en la región de Arcabuco- Barbosa-Oiba, Dptos Santander y Boyacá. Serv. Geol. Nal., informe n° 952 (inédito), 9 pp., 2 fig., Bogotá.

Hubach, E., 1957a (escrito en 1651), Estratigrafía de la Sabana de Bogotá y alrededores. Bol- Geol., Inst. Geol., Nal., vol.5, n°2, pp. 93-112, 2 lám., Bogotá.

Hubach E., 1957b, Contribución a las Unidades Estratigráficas de Colombia. Inst. Geol., Nal., informe n° 1212 (inédito), 166pp., Bogotá.

Huertas, G. G., 1969, Un nuevo género y especie fosil de las Lecitidaceas, Caldasia, vol. X, n. 48, pp. 365.369, 2 Figs., Bogotá.

Huertas, G. G., 1970, Disquisicion Paleohotanica, Mutisia, n. 23, pp. 21·28, 5 Figs. Bogotá.

Huertas, G. G., 1970, Sertum Floru1ae Fossilis Villae de Leiva, III, Caldasia, vol. X, n, 50, pp. 595·602, 4 Figs. Bogotá.

Huertas, G. G., 1971, Theobroma verum sp. nov., Mutisia, n. 34, pp. 10, 5 Figs. Bogotá.

Hubert, K., Wiedmann, J., 1985, El limite Jurásico-Cretácico en los alrededores de Villa de Leiva, Departamento de Boyacá. II congr. Colomb. Geol., Mem> 529-541 (En Imprenta). Bogotá.

Humphrey, C.G., 2010, In-situ U-Pb secondary ion mass spectrometry (INSIMS) geochronology from the Leeward Antilleos islands of Aruba, Curaçao, Bonaire, and Gran Roque: Implications for the temporal evolution of the Caribbean large igneous province (CLIP) and early arc magmatism [M.S. thesis]: Athens, University of Georgia, 86 p.

Hunt, D., and Tucker, M. E. 1992, Stranded parasequences and the forced regressive wedge systems tract: deposition during base level fall. *Sedimentary Geology*, Vol. **81**, pp. 1–9.

Huntley, L.G., 1923, Colombian oil Fiekds Trans. Am. Inst. Min. Met. Eng., vol. 68, pp 1014-1022, 5 fig., Pittsburgh.

Hurford, A.J. 1986, Cooling and uplift patterns in the Lepontine Alps, South Central Switzerland and an age of vertical movement on the Insubric fault line. Contribut.Mineral. Petrol., 92, 413^427.

Hurford, A.J. and Carter, A., 1991, The role of fission track dating in discrimination of provenance. In: *Developments in Sedimentary Provenance Studies* (Ed. by A.C. Morton, S.P.Todd & P.D.W. Haughton), Geol. Soc. Spec. Publ., 57, 67-78.

Hurford, A.J., 1986, Cooling and uplift patterns in the Lepontine Alps, South Central Switzerland and an age of vertical movement on the insubric fault line. Contribut.Mineral. Petrol., 92, 413-427.

Hutton, J., 1975, Theory of the Earth with proofs and illustrations. William creek edit, Edimburg.

Instituto Colombino del Petroleo Ecopetrol, 2013, Bioestratigrafía del pozo La Luna-1, Cuenca del Valle Medio del Magdalena. Informe Interno 07-13, Mayo.

Ireland, T.R., 1992, Crustal evolution of New Zealand: Evidence from age distributions of detrital zircons in Western Province paragneisses and Torlesse greywacke: Geochimica et Cosmochimica Acta, v. 56, p. 911–920.

Jacques, J.M., 2004, The influence of intraplate structural accommodation zones on delineating petroleum provinces of the Sub-Andean foreland basins. Petroleum Geoscience, v.10, p.1-19.

Jaillard, E. 1987, Sedimentary evolution of an active margin during middle and upper Cretaceous times: the North Peruvian margin from Late Aptian up to Senonian. *Geologische Rundschau*, 76, 677-697.

Jaillard, E. P., Solar, P., Carlier, G. and Mourier, T., 1990, Geodynamic evolution of the northern and central Andes during early to midle Mesozoic times: a Tethyan model. Jour. Geol. Soc., London, 147: 1009-1022.

Jaillard, E., Soler, P., Carlier, G., Mourier, T., 1990, Geodynamic evolution of the northern and central Andes during early to middle Mesozoic times: a Tethyan model. Journal of the Geological Society, London 147, 1009e1022.

Jaillard, E. P., Benitez, S., Berrones, G. Huaman, C., Ordonez, M, Rivadeneira, M., 1991, Analisis de Cuencas Sedimentaris e Historia Precoz de los Andes: marco de un convenio firmado por Petroproduccion (filial de Petroecuador) y el Orstom en el mes de Junio de 1991.

Jaillard, E., Cappetta, H., Ellenberger, F., Feist, M., Grambast-Fessard, N., Lefranc, J. P., Sigé, B., 1993, The Late Cretaceous Vilquechico Formation, Southern Peru. Sedimentology, Paleontology, Biostratigraphy, Correlations. *Cretaceous Research*, 14, 623-662.

Jaillard, E., 1994, Kimmeridgian to Paleocene tectonic and geodynamic evolution of the Peruvian (and Ecuadorian) margin. ln: J.A. Salfity (ed.). *Cretaceous tectonics in the Andes*, pp. l01-167. Earth Evolution Sciences, Fried. Vieweg and Sohn, Braunschweig/Wiesbaden.

Jaillard, E., Ordoñez, M., Benitez, S., Berrones, G., Jiménez, N., Montenegro, G., Zambrano I., 1995, Basin Development in an Accretionary, Oceanic-Floored Fore-Arc Setting: Southern Coastal Ecuador During Late Cretaceous-Late Eocene Time, in A. J. Tankard, R. Suárez s, and H. J. Welsink, Petroluem Basin Of South America> AAPG Memoir 62, p. 615-631.

Jaillard, E., Sempéré, T., Soler, P., Carlier, G., Marocco, R., 1995b, The role of Tethys in the evolution of the Northern Andes between Late Permian and Late Eocene times. In: Nairn, A.E.M., Ricou, L.-E., Vrielynk, B., Dercourt, J. (eds) The Tethys Ocean. Ocean Basins and Margins, 8. Plenum Press, New York, 463–492.

Jaillard, E., Ordoñez, M., Bengtson, P., Berrones, G., Bonhomme, M., Jiménez, N., Zambrano, l., 1996, Sedimentary and tectonic evolution of the arc zone of southwestern Ecuador during Late Cretaceous and Early Tertiary times. *Journal of South American Earth Sciences*, 9, 131-140.

Jaillard, E., 1997, Datos nuevos y discusion. In: Jaillard, E., Sintesis estratigráfica y sedimentológica del Cretáceo y Paleogeno de la Cuenca Oriental del Ecuador. Informe Final del Convenio Orstom-Petroproduccion, Orstom, Paris, 164 pp.

Jaillard, E., Laubacher, G., Bengtson, P., Dhondt, A., Bulot, L. 1999, Stratigraphy and evolution of the Cretaceous forearc "Celica-Lancones Basin" of Southwestern Ecuador. *Journal of South American Earth Sciences*, 12, 51-68.

Jaillard, E., Hérail, G., Monfret, T., Diaz-Martinez, E., Baby, P., Lavenu, A., Dumont, J.-F., 2000, Tectonic evolution of the Andes of Ecuador, Peru, Bolivia and northernmost Chile. In: Cordani, U.G., Milani, E.J., Thomaz, F., Campos, D.A. (eds) Tectonic Evolution of South America. Proceedings of the 31st International Geological Congress, Rio de Janeiro, 481–559.

Jaillard, E., Ordoñez,M., Suárez, J., Toro, J., Iza, D., Lugo,W., 2004, Stratigraphy of the late Cretaceous–Paleogene deposits of the cordillera occidental of central Ecuador: geodynamic implications. Journal of South American Earth **Sciences** 17, 49–58.

Jaillard, É., Bengtson, P., Dhondt, A., 2005, Late Cretaceous marine transgressions in Ecuador and northern Peru: a refined stratigraphic framework. *Journal of South American Earth Sciences*, **19**, 307-323.

Jaillard, E., Lapierre, H., Ordonez, M., Alava, J.T., Amortegui, A., Vanmelle, J., 2009, Accreted oceanic terranes in Ecuador: southern edge of the Caribbean Plate? Geological Society of London Special Publication 328, 469–485.

Jaimes, E., and de Freitas, M., 2006, An Albian-Cenomanian unconformity in the northern Andes: Evidence and tectonic signifi cance: Journal of South American Earth Sciences, v. 21, p. 466–492, doi: 10.1016/j.jsames.2006.07.011.

James, N. P. 1984, Shallowing – Upward sequences in Carbonates. En: Walker, R.G. (ed.), Facies Models (2nd. edition), Geoscience Canada, Reprint series 1:213-228.

Jaramillo, J.M., 1978, Determinación de las edades de algunas rocas de la Cordillera Central de Colombia por el método de huellas de fisión. II Congreso Internacional Geológico Colombiano. Resúmenes, Bogotá, p.19-20.

Jarrard, R. O., 1986, Relations among Subduction parameters. *Reviews of Geophysics*, 24, 217-284.

John H. Shaw, Christopher D. Connors, and John Suppe, 2005, Seismic Interpretation of Contractional Fault-Related Folds: An AAPG Seismic Atlas. Pages 1-59.

Julivert M., 1958a, La morfoestructura de la zona de mesas al SW de Bucaramanga (Colombia S.A.). Bol. Geol., Univ. Ind. De Sant., n°1, pp.7-43. 13 fig., Bucaramanga.

Julivert, M., 1958b, Geología de la zona tabular entre San Gil y Chiquinquirá, Cordillera Oriental, Colombia. Ibid., n° 2, pp. 33-45, 4 fig., Bucaramanga.

Julivert, M., 1960, Geología de la región occidental de García Rovira (Cordillera Oriental, Colombia). *Ibid.*, nº 5, pp. 5-32, 19 fig., Bucaramanga.

Julivert, M., 1963b, Nuevos datos sobre la dinámica del ámbito del Macizo de Santander durante el Secundario (Cordillera Oriental, Colombia). *Ibid.*, nº 12, pp. 45-49, 2 fig., Bucaramanga.

Julivert, M. and Barrero, D. Navas, J., 1964, Geología de la Mesa de Los Santos. Ibid, n° 18, pp. 5-11, 2 fig., 1 mapa f.t., Bucaramanga.

Julivert, M. 1968, Lexique Stratigraphique International. Colombie (primiere parte) Volumen 5, Fascicule 4a. Centre Nat. Rech. Sci. Paris.

Kammer, A., 1999, Observaciones acerca de un Origen Transpresivo de la Cordillera Oriental. Geología Colombiana No. 24, pgs. 29-53, 9 Figs., 2 Tablas, 2 Anexos, Santafé de Bogotá.

Kammer, A., Sanchez, J., 2006, Early Jurassic rift structures associated with the Soapaga and Boyaca faults of the Eastern Cordillera, Colombia: Sedimentological inferences and regional implications. J. South Am. Earth Sci., 21, 412–422. doi:10.1016/j.jsames.2006.07.006.

Karsten, H., 1858, Ueber die geognostischen Verhältnisse des westlichen Kolumbien, der heutigen Republiken Neu-Granada und Ecuador. Amtl. Ber. 32te vers. Deutseh. Naturf. Aerste z. Wien, 1856, pp. 80-117, 7 Taf. _ Trad. Esp., 1947, Rev. Acad. Colomb. Cienc. Ez. Fic. Nat., vol. 7, n° 27, pp. 361-381, 8 lam., Bogotá.

Karsten, H., 1886, Géologie de l´ancienne Colombie bolivarienne, Vénezuéla, Nouvelle-Grenade et Ecuador. 62 pp., 6 pl., 1 carte, 2 dépl. Coupes géol., Berlin (R. Friedlander and Sohn).

Kelling, G., 1964, The Turbidite concept in Britain. In: A. H. Bouma and A. Brouwer (Editors), Turbidites. Elsevier, Amsterdam, pp. 75·92.

Kellogg, J.N., Bonini, W.E., 1982, Subduction of the Caribbean Plate and basement uplifts in the overriding South American Plate. Tectonics, v.1, p.251-276.

Kellogg, J., Ogujiofor, I.J., Kansakar, D.R., 1985, Cenozoic tectonics of the Panama and North Andes blocks, Mem. Sixth Latin American Geological Congress. Bogotá, 1: 40-59.

Kerr, A.C., G.F. Marriner, J. Tarney, A. Nivia, A.D. Saunder, M. . Thirlwall, C.W. Sinton, 1997, Cretaceous basaltic terranes in Western Colombia: Elemental, Chronological and Sr-Nd isotopic constraints on petrogenesis: Journal of Petrology, v. 38, p. 677-702.

Kerr, A. C., Tarney J., Marriner, G. F., Nivia, A., Klaver, G. T. and Saunders A. D., 1996a, The geochemistry and tectonic setting of late Cretaceous Caribbean and Colombian volcanism: Journal of South American Earth Sciences, 9: 111 – 120.

Ketcham, R. A., R. A. Donelick, and W. D. Carlson, 1999, Variability of apatite fission-track annealing kinetics: III. Extrapolation to geological timescales, Am. Mineral., 84, 1235–1255.

Ketcham, R.A., 2005, Forward and inverse modeling of low-temperature thermochronometry data, *in* Reiners, P.W., and Ehlers, T.A., eds., Lowtemperature thermochronology: Techniques, interpretations, and applications: Mineralogical Society of America Reviews in Mineralogyand Geochemistry 58, p. 275–314.

Ketcham R., Mora A., Parra M., 2016, Deciphering exhumation and burial history with multi-sample down-well thermochronometric inverse modeling. Basin Research, DOI: 10.1111/bre.12207.

Klitgord, K. D. and Schouten, H., 1986, Plate kinematic of the central of thr central Atlantic. In Vogt, P. R. and Tucholke, B. E. (eds) The western North Atlantic Region. Geology of North America, M. Geological Society of America. M. Geological Society of America, Boulder CO, 351-378.

Koons, P. O., 1989, The topographic evolution of collisional mountain belts: A numerical look at the Southern Alps, New Zealand, *Am. J. Sci.*, **289**, 1041–1069.

Krapez, B., 1996, Sequence-stratigraphic concepts applied to the identification of basin-filling rhythms in Precambrian successions. Australian Journal of Earth Sciences **43**, 355–380.

Kroonenberg, S. B., 1984, A Grenvillian granulite belt in the Colombian Andes and its relation to the Guiana Shield: Geologie en Mijnbouw, v. 61, p. 325–333.

Kuslansky, G.H. 1982, Petrographic descriptions of samples from Cenozoic and Mesozoic Formations, Middle and Upper Magdalena Valley, Colombia. Exploration Memo. Pennzoil Exploration and Production Company, Houston, p. 45.

Labails, C., Olivet J.-L., Aslanian D., Roest WS., 2010, An alternative early opening for the Central Atlantic Ocean. Earth and Planetary Science letters. Vol 297 (3-4), p. 355 -368.

Lambeck, K., 1980, *The earth's variable rotation*. Cambridge University Press, Cambridge, p. 449.

Langenheim, J. H., 1959, Preliminary notes on plant fossils from Late Paleozoic and Early Mesozoic rocks in the Cordillera Oriental of Colombia. *Bol. Geol*., Univ. Ind. Santander, nº 3, pp. 51-53, Bucaramanga.

Laughlin, A.W., Damon, P.E., Watson, B.N., 1968, Potassium Argon Dates from Toquepala and Michiquillay, Peru. *Economic Geology*, 63, 166-168.

Laverde F. and Clavijo, J., 1985, Análisis facial de la Formación Los Santos, según el corte Yo y Tu (Zapatoca). In: F. Etayo-Serna and F. Laverde-Montaño (eds.), *Proyecto Crétacico, contribuciones*. Chapter VI, Ingeominas Publicación Geológica Especial 16, Bogotá, 9 p.

Lebrat, M., F. Mégard, C. Dupuis, J. Dostal, 1987, Geochemistry and tectonic setting of pre-collision Cretaceous and Paleogene rock of Ecuador: Geoloical Society of American Bulletin, 99, 569- 578.

Leckie, R.M., Bralower, T.J., Cashman, R. 2002, Oceanic anoxic events and plankton evolution: Biotic response to tectonic forcing during the mid-Cretaceous. Paleoceanography 17 (3), 10.1029/2001PA000623.

Lee Y. et al., 1999, Heat flow and thermal history of the Anadarko Basin and the western Oklahoma Platform. Tectonophysics 313 (1999) 399–410.

Le Pichon, X., 1968, Sea-floor spreading and continental drift. J. Geophys. Res. 73 (12), 3661–3697.

Liddle, R. A., 1928, The Geology of Venezuela and Trinidad, 1 vol., 552 pp., 21 fig., 83 pl., Fort Worth, Texas (J.P. Mac Gowan).

Litherland, M., J.A. Aspden, R.A. Jemielita, 1992, Terrane boundary reactivation: A control on the evolution of the northern Andes: Journal of South American Earth Sciences, 5, 71-76.

Litherland, M., J. A. Aspden, and R. A. Jemielita, 1994, The metamorphic belts of Ecuador: Overseas Memoir of the British Geological Survey No. 11, 147 p.

Luzieux, L.D.A., Heller, F., Spikings, R., Vallejo, C.F., Winkler, W., 2006, Origin and Cretaceous tectonic history of the coastal Ecuadorian forearc between 1°N and 3°S: paleomagnetic, radiometric and fossil evidence. Earth and Planetary Science Letters 249, 400–414.

Luzieux, L. 2007, Origin and Late Cretaceous-Tertiary evolution of the Ecuadorian forearc. PhD Thesis, ETH, Zurich

Lyell, Ch., 1830-1833, Principles of Geology, first edition. 1990-1991. University of Chicago Press, 584+330 pp.

Macia, C., Mojica, J. and Colmenares, F., 1985, Consideraciones sobre la importancia de la Paleogeografía y las áreas de aporte pre-cretácicas en la prospección de hidrocarburos en el Valle Superior del Magdalena, Colombia.- Geol. Colombiana 14, pp. 49-70, 11 Figs. Bogotá.

Macia, C. and Mojica, J., 1981, Nuevos puntos de vista sobre el magmatismo Triásico Superior (Fm. Saldaña), Valle Superior del Magdalena, Colombia.- Zbl. Geol. Palaontol. Teil I (3/4): 243-251, Stuttgart.

Macellari, C.E. and DeVries, T.J., 1987, Late Cretaceous upwelling and anoxic sedimentation in northwestern South America. ***Palaeogeography, Palaeoclimatology, and Palaeoecology 59,279-292.***

Macellari, C. E., 1988, Cretaceous Paleogeography and depositional cycles of western South America. *Journal of South American Earth Sciences*, Vol. 1 No. 4 pp. 373-418, Great Britain.

Macharé, J., Sébrier, M. Huamán, D., Mercier, J.-L., 1986, Tectónica cenozoica de la margen continental peruana. *Boletin de In Sociedad Geologica del Peru,* 76,45-77.

Malfere, J.-L., 1999, Géochimie et géochronologie du Complexe Métamorphique de Raspas (SW Equateur). *Mémoire DEA Dynamique de la lithosphère*, Univ. Grenoble 1, 29 p.

Manea, V.C., Manea, M., Kostoglodov, V., Sewell, G. 2006, Intraslab seismicity and thermal stress in the subducted Cocos plate beneath central Mexico, *Tectonophysics*, 420, 389-408.

Mann, P., ed., 1995, Geologic and Tectonic development of the Caribbean plate boundary in southern Central America: Geological Society of America, Special Paper 295, p. vii-xxxii (Preface).

Marocco, R., Baudino, R., Lavenu, A., 1995, The intermontane Neogene continental Basins of the Central Andes of Ecuador and Peru: Sedimentologic, tectonic and geodynamic implications. In: Petroleum Basins of South America, Tankard, A.J., Suárez, R., Welsink. H.J. eds., A*merican Association of Petroleum Geologists Memoir,62*, 597-613.

Marocco, R., Sempere, T., Cirbian, M., Oller, J., 1987, Mise en évidence d'une déformation paléocène en Bolivie du Sud. Sa place dans I'évolution géodynamique des Andes Centrals, C. R. Acad. Sci. Paris, sér. D, 3041 139-1 142.

Martínez, J.I. & Vergara, L.E., 1999, La Sucesión Paleoambiental del Cretácico de la Región de Tequendama y Oeste de la Sabana de Bogotá, Cordillera Oriental Colombiana.- Geología Colombiana 24, pgs. 107-147, 9 Figs., 1 Tabla, 6 Láminas, Santafé de Bogotá.

Masek, J.G., Isacks, B.L., Gubbels, T.L., and Fielding, E.J., 1994, Erosion and tectonics at the margins of continental plateaus: Journal of Geophysical Research, v. 99, p. 13,941–13,956, doi: 10.1029/94JB00461.

Mattson, P. H., 1984, Caribbean structural breaks and plate movements. Geological Society of America. Memoir 162. 1984. p. 131-152.

Maya, M., 1992, Catálogo de dataciones isotópicas de Colombia: Boletín Geológico, INGEOMINAS, v. 24, no. 1–3, p. 127–188.

Maya, M., González, H., 1995, Unidades litodémicas en la Cordillera Central de Colombia. Ingeominas Boletin Geológico 35 (2–3), 45–55.

McCourt, W.J., T. Feininger, 1984, High-pressure metamorphic rocks in the Central Cordillera of Colombia: British Geological Survey Report 84, no. 1, p. 28–35.

McCourt, W. J., Feininger, T. and Brook, M., 1984, New geological and geochronological data from the Colombian Andes: continental growth by multiple accretion. Jour. Geol. Soc. London, 141: 831-845.

Mégard, F. 1984, The Andean orogenic period and its major structures in Central and Northern Peru. Journal of the Geological Society of London, 141, 893–900.

Mendoza, H., 1985, La Formación Cumbre, modelo de transgresión marina rítmica, de comienzos del Cretácico. In: F. Etayo-Serna and F. Laverde-Montaño (eds.), *Proyecto Crétacico, contribuciones*. Chapter IX, Ingeominas Publicación Geológica Especial 16, Bogotá, 17 p.

Meschede, M., W. Frisch, 1998, A plate-tectonic model for the Mesozoic and Early Cenozoic history of the Caribbean Plate: Tectonophysics, v. 296, p. 269-291.

Mitchum, R.M.Jr., 1977, Seismic stratigraphy and global changes of sea level, part 11: glossary of terms used in seismic stratigraphy. *In Seismic Stratigraphy–Applications to Hydrocarbon Exploration* (C. E. Payton, Ed.), pp. 205–212. American Association of Petroleum Geologists Memoir **26**.

Mitchum, R.M.Jr. and Vail, P.R., 1977, Seismic stratigraphy and global changes of sea-level, part 7: stratigraphic interpretation of seismic reflection patterns in depositional sequences. *In Seismic Stratigraphy–Applications to Hydrocarbon Exploration* (C.E. Payton, Ed.), pp. 135–144. AAPG Memoir **26**.

Mitchum, R. M., Jr., Van Wagoner, J. C., 1991, High-frequency sequences and their stacking patterns: sequence stratigraphic evidence of high-frequency eustatic cycles. Sedimentary Geology **70**, 131–160.

Mojica, J., Kammer, A. and Ujueta, G., 1996, EI Jurásico del Sector Noroccidental de Suramérica y Guía de la Excursión al Valle Superior del Magdalena (Nov. 1-4/95), Regiones de Payandé y Prado, Departamento del Tolima, Colombia.- Geología Colombiana No. 21, p. 3-40, 18 Figs., 3 Laminas, Santafé de Bogota.

Mojica J, Macia C., 1983, Características Estratigráficas y Edad de la Formación Yaví, Mesozoico de la Región entre Prado y Dolores, Tolima, Colombia. Geología Colombiana 12: 7-32. Depto. de Geociencias, Universidad Nacional de Colombia, Bogotá.

Molnar, P., 2004, Late Cenozoic increase in accumulation rates of terrestrial sediment: How might climate change have affected erosion rates?: Annual Review of Earth and Planetary Sciences, v. 32, p. 67–89.

Molnar, P., England, P., 1990, Late Cenozoic uplift of mountain ranges and global climate change: chicken oregg?. Nature, 346, 29-34.

Montenegro, L.C. 2012, Análisis del componente micropaleontológico del segmento superior de la Formación Rosablanca, en el área de Zapatoca, Santander. Trabajo de Grado. Departamento de Geociencias, Universidad Nacional de Colombia. 43 p.

Montgomery, D.R., Balco, G., Willett, S.D., 2001, Climate, tectonics, and the morphology of the Andes. Geology, v. 29 (7), p. 579-582.

Mora, J., Loureiro, D., Ostos, M., 1993, Pre-Mesozoic rectangular network of crustal discontinuities: One of the main controlling factors of the tectonic evolution of northern South America. Abstract, AAPG/SVG International Congress and Exhibition, Caracas, 58.

Mora, A., Parra, M., Strecker, M.R., Kammer, A., Dimate, C., and Rodriguez, F., 2006, Cenozoic contractional reactivation of Mesozoic extensional structures in the Eastern Cordillera of Colombia: Tectonics, v. 25, p. TC2010, doi: 10.1029/2005TC001854.

Mora, A., 2007, Inversion tectonics and exhumation processes in the Eastern Cordillera of Colombia [PhD thesis]: Potsdam, Universität Potsdam, 133 p.

Mora, A., Parra M., Strecker M., Sobel E., Hooghiemstra H., Torres., Vallejo J. 2008, Climatic forcing of asymmetric orogenic evolution in the Eastern Cordillera of Colombia *GSA Bulletin*; July/August 2008; v. 120; no. 7/8; p. 930–949; doi: 10.1130/B26186.1; 13 figures; 3 tables.

Mora, A., T. Gaona, J. Kley, D. Montoya, M. Parra, L. I. Quiroz, G. Reyes, and M. Strecker, 2009, The role of inherited extensional fault segmentation and linkage in contractional orogenesis: A reconstruction of Lower Cretaceous inverted rift basin in the Eastern Cordillera of Colombia: Basin Research, v. 21, p. 111–137, doi:10 .1111/j.1365-2117.2008.00367.

Mora, A., Parra, M., Strecker, M.R., R. Sobel E. R., Zeilinger , G., Jaramillo, C., Da Silva, F.S., Blanco M. 2010, The eastern foothills of the Eastern Cordillera of Colombia: An example of multiple factors co ntrolling structural styles and active tectonics. *Geological Society of America Bulletin* 2010;122;1846-1864. doi: 10.1130/B30033.1

Mora, A., Reyes-Harker, A. et al. 2013, Inversion tectonics under increasing rates of shortening and sedimentation: Cenozoic example from the Eastern Cordillera of Colombia. In: Nemcˇok, M., Mora, A. R. & Cosgrove, J. W. (eds) Thick-Skin-Dominated Orogens: From Initial Inversion to Full Accretion. Geological Society, London, Special Publications. 377, first published online March 8, 2013, doi: org/10.1144/SP377.6.

Mora A., A. Reyes, G. Rodriguez, E. Tesón, J. C. Ramirez., M. Parra, V. Caballero, J.P. Mora, I. Quintero, V. Valencia, M. Ibañez, B.K. Horton, D.F. Stickli, 2013, Inversion tectonics under increasing rates of shortening and sedimentation: Cenozoic example from the Eastern Cordillera of Colombia: Geological Society, London Special Publ., 377, 411-442.

Morales, L. G. and the Colombian petroleum industry, 1958, General geology and oil occurrences of the Middle Magdalena Valley, Colombia. In: ***Habitat of Oil:*** A ***Symposium*** (edited by L.G. Weeks). American Association of Petroleum Geologists, Special Publication, 641-695.

Morales L. G., et al., 1958, General Geology and oil occurrences of Middle Magdalena Valley, Colombia. Habitat of Oil, Symposium Am. Ass. Petr. Geol. Pp. 641-695, 29 fig., Tulsa.

Morales, L.G., Podesta, D.J., Hatfield, W.C., Tanner, H., Jones, S.H., Barker, M.H., O'Donoghue, D.J., Mohler, C.E., Dubois, E.P., Jacobs, C., Goss, C.R., 1958, General geology and oil occurrences of the Middle Magdalena Valley, Colombia: Tulsa, Habitat of Oil Symposium, American Association of Petroleum Geologists, p. 641–695.

Morales, W., 1993, Reinterpretación geológica del area de Lagunitos (NW Perú) en base a sísmica reflexión. *3rd INGEPET*, INGP-055, Lima, 10 fig., 1-19.

Moreno, J.M. 1990, Stratigraphy of the Lower Cretaceous Rosablanca Formation, west flank, Eastern Cordillera, Colombia. Geología Colombiana, Bogotá, Vol. 17, pp. 65-86.

Moreno, C.J., Horton, B.K., Caballero, V., Mora, A., Parra, M. and Sierra, J., 2011, Depositional and provenance record of the Paleogene transition from foreland to hinterland basin evolution during Andean orogenesis, northern Middle Magdalena Valley Basin, Colombia. Journal of South American Earth Sciences 32.

Moreno, J. M., 1989, Petrography and Stratigraphy of the Lower Cretaceous Rosablanca and Cumbre Formations, Utica Sandstone and Murca Sandstone (Murca Formation), Cordillera Oriental, Colombia (M SC. Thesis).- 111 p, University 01 South Carolina, U.S.A.

Moreno, J. M., 1990, Stratigraphy of the Lower Cretaceous Rosablanca and Cumbre Formations, Utica Sandstone and Murca Formation, West Flank, Eastern Cordillera, Colombia.- Geol. Colombiana, 17, pp. 65 - 86,9 figs., Bogota.

Moreno, J.M. 1991, Provenance of the Lower Cretaceous sedimentary sequences, central part, Eastern Cordillera, Colombia. Revista Academia Colombiana Ciencias Exactas Físicas y Naturales, Vol. 18(69), p. 159-173.

Moreno, J. M. and Concha, A. E., 1993, Nuevas manifestaciones ígneas básicas en el flanco occidental de la Cordillera Oriental, Colombia.- Geología Colombiana, 18, pp. 143 - 150, 2 figs., 2 Tablas, Bogotá.

Moreno, G. and Pérez, A., 2001, Estratigrafía de las Formaciones Tablazo y Simití (Santander) y Grupo San Gil (Área de Villa de Leyva): Universidad Nacional de Colombia. Tesis pregrado.

Moreno, G., and Sarmiento, G., 2002, Estratigrafía Cuantitativa de las Formaciones Tablazo y Simiti en las localidades de Sáchica (Boyacá) y Barichara - San Gil (Santander), Colombia.- GEOLOGIA COLOMBIANA, 27, pp. 51-76, 21 Figs. , 2 Tablas, Bogotá.

Moreno-Sánchez, M. y Pardo-Trujillo, A., 2002, Historia geológica del Occidente Colombiano. Geo-Eco-Trop, Vol. 26 (2), pp.91-113.

Moreno-Sanchez, M., Pardo-Trujillo, A., 2003, Stratigraphical and sedimentological constraints on Western Colombia: implications on the evolution of the Caribbean Plate. In: Bartolini, C., Buffler, R.T., Blickwede, J. (Eds.), The Circum-Gulf of Mexico and the Caribbean: Hydrocarbon Habitats, Basin Formation, and Plate Tectonics: American Association of Petroleum Geologists Memoir, 79, pp. 891–924.

Moretti, I., Lykousis, V., Sakellariou, D., Reynaud, J.Y., Benziane, B. and Prinzhoffer, A., 2004, Sedimentation and subsidence rate in the Gulf of Corinth: what we learn from the Marion Dufresne's long-piston coring. *C.R. Geosci.*, **336**, 291–299.

Moretti, I., Rodriguez, G., Mayorca, M. and Mondragon, J. 2010, Integrated exploration workflow in the South Middle Magdalena Valley (Colombia). Journal of South America Earth Sciences, 29: 187-197.**Namson, J., Cunningham, R. and Wodcock, G., 1994.** Structural geology and hydrocarbon potential of the northern part of the Upper Magdalena Basin, Colombia. V Simposio Bolivariano Exploración Petrolera en las Cuencas Subandinas, Puerto La Cruz, Memoria: 356-364.

Mourier, T., 1988, La transition entre Andes marginales et Andes cordilléraines a ophiolites. Evolution sédimentaire, magmatique et structurale du relai de Huancabamba (3"-B"S, Nord Pérou-Sud Equateur). *Dr. Thesis, Université Paris* XI, 275 p. (unpublished).

Mutti, E. Y., Ricci Lucchi, F., 1972, Turbidities of the northern Apennines: Introduction to facies analysis (English translation by T. H. Nilsen, 1978): international Geology Review, v. 20, 125-166.

Naeser, C.W., Crochet, J. -Y., Jaillard, E., Laubacher, G., Mourier, T., Sigé, B. (1991). Tertiary Fission-Track ages from the Bagua syncline (Northern Peru).Stratigraphic and tectonic implications. *Journal of South American Earth Sciences*, 4, 61-71.

Navas, J., 1963, Estudio estratigráfico del Girón al W del Macizo de Santander. Ibid., n°12, pp. 19-33, 2 fig., Bucaramanga.

Namson, J., Cunningham, R. and Wodcock, G., 1994, Structural geology and hydrocarbon potential of the northern part of the Upper Magdalena Basin, Colombia. V Simposio Bolivariano Exploración Petrolera en las Cuencas Subandinas, Puerto La Cruz, Memoria: 356-364.

Nelson and Kulm, L. D., 1973, Submarine fans and deep-sea channels, in Middleton, G. V., and Bouma, A. H., co-chm., Turbidites and deep-water sedimentation: Pacific Sec., Soc. Econ. Paleontologists and Mineralogists, Lecture Notes for Short Course, May, p. 39-78.

Nie, J., Horton, B.K., Mora, A., Saylor, J.E., Housh, T.B., Rubiano, J., and Naranjo, J., 2010, Tracking exhumation of the Andean ranges bounding the Middle Magdalena Basin, Colombia: Geology, v. 38, p. 451–454, doi:10.1130/G30775.1.

Nivia, A., 1996, El Complejo Estructural Dagua, Registro de deformación de la Provincia Litósferica Oceánica Cretácica Occidental: Un prisma acrecionario: VII Congreso Colombiano de Geologı´a, Cali, Colombia, v. III, p. 54–67.

Nivia, A., 1989, El Terreno Amaime - Volcánico: Una Provincia Acrecionada de Basaltos de Meseta Oceánica. V Congreso Colombiano de Geología. pp. 1 - 30.

Nivia et al., 2006, Nivia, A., Marriner, G.F., Kerr, A.C., Tarney, J., 2006. The Quebradagrande Complex: A Lower Cretaceous ensialic marginal basin in the Central Cordillera of the Colombian Andes. Journal of South American Earth Sciences 21, 423–436.

Nivia et al., 2009, A COMMENT ON ‘‘The Quebradagrande Complex: A Lower Cretaceous ensialic marginal basin in the Central Cordillera of the Colombian Andes” Journal of South American Earth Sciences 28, 204–205.

Noble, D.C., McKee, E.H., Mourier, T., Mégard, F., 1990, Cenozoic stratigraphy, magmatic activity, compressive deformation, and uplift in Northern Peru. *Geological Society of America Bulletin*, 102, 1105-1113.

Norem, W.L, 1955, Pollen, spores and other organic Xicrofossils from the Eocene of Venezuela. *Micropaleontotogy,* vol. 1, nº 3, pp. 261-267, 1 fig. 2 pl., New York.

Notestein F. H., Hubman C. W., and Bowler j. W., 1944, Geology of the Barco Concession, Republic of Colombia, South America, Null. Geol. Soc. Amer., vol. 55, pp.1165-1215, 12 fig., 6 pl., New York.

O'Connell, R., Gable, C.G., Hager, B., 1991, Toroidal–poloidal partitioning of lithospheric plate motions. In: Sabadini, R., et al. (Eds)., Glacial Isostasy, Sea-Level and Mantle Rheology, Vol. 334. Kluwer Academic Publisher, pp. 535–551.

Ordóñez-Carmona, O., Martins P, M., Angel, C.P., 2001, Consideraciones Geocronólogicas e Isotópicas preliminares del Magmatismo Cretáceo–Paleoceno en el norte de la Cordillera Central. In proceedings of VIII Congresso Colombiano Geologia. 5p.

Ordóñez-Carmona, O., Restrepo Álvarez, J.J., Pimentel, M.M., 2006, Geochronological and isotopical review of pre-Devonian crustal basement of the Colombian Andes. Journal of South American Earth Sciences 21, 372–382.

Ordóñez-Carmona, O., Restrepo, J.J., Pimentel, M., 2006, Geochronological and isotopical review of pre-Devonian crustal basement of the Colombian Andes. Journal of South American Earth Sciences 21, 372–382.

Ordóñez, O., Pimentel, M., Correa, A.M., Martens, U., Restrepo, J.J., 2001, Edad Sm/Nd del metamorfismo de alto grado de El Retiro (Antioquia). VIII Congreso Colombiano de Geología, Manizales.

Ordóñez O., Pimentel, M., y De Moraes, R. 2002, Granulitas de Los Mangos, un Fragmento Grenvilliano en la Parte Oriental de la Sierra Nevada de Santa Marta. Revista de la Academia Colombiana de Ciencias Exactas, Físicas y Naturales (Separata). 26 (99): 169-179.

Oppenheim, V., 1940b, Jurassic-Cretaceous (Girón) beds in Colombia and Venezuela. *Bull. Am. Ass. Petr, Geol.,* vol. 24, nº 9, pp, 1611-1619, 5 fig., Tulsa.

Pardo-Casas, F., Molnar, P., 1987, Relative motion of the Nazca (Farallon) and South America plates since Late Cretaceous time. Tectonics, 6: 233-248

Parra, M., 2008, Cenozoic foreland-basin evolution in the northern Andes: insights from thermochronology and basin analysis in the Eastern Cordillera, Colombia. eingereicht an der Mathematisch-Naturwissenschaftlichen Fakultät der Universität Potsdam Dissertation.

Parra, M., Mora, A., Sobel, E.R., Strecker, M.R. and González, R., 2009, Episodic orogenic-front migration in the northern Andes: Constraints from low-temperature thermochronology in the Eastern Cordillera, Colombia: Tectonics, v. 28, p. TC4004, doi:10.1029/2008TC002423.

Parra, M., Mora, A., Lopez, C., Rojas, L. E. / Horton, B. K., 2012, Detecting earliest shortening and deformation advance in thrust-belt hinterlands. Example from Colombian Andes. Geology, 40, 175-178, http://dx.doi.org/10.1130/G32519.1.

Patarroyo, P., 1995, A propósito de la importancia paleogeográfica de la Falla de Boyacá. Geología Colombiana, N. 19, p. 187 - 188. Bogotá. (ISSN 0072-0992).

Patarroyo, P., 1997, Barremiano Inferior en la Base de la Formaci6n Paja, Barichara, Santander - Colombia.- GEOLOGIA COLOMBIANA, 22, pgs. 135-138,2 Figs., Santafé de Bogotá.

Patarroyo, P., 1999, Entwicklung der Ammoniten der Familie Pulchelliidae aus dem Barrême von ZentralKolumbien. Inaugural-Dissertation der Justus-Liebig-Universität, Giessen: 1-124.

Patarroyo, P. 2000a, Amonitas del Barremiano en Villa de Leyva-Boyacá (Colombia-Sur America): Datos bioestratigráficos preliminares. Zentralblatt der Geologie und Paläontologie, Teil 1,1999: 789-798.

Patarroyo, P., 2000, Distribución de amonitas del Barremiano de la Formación Paja en el sector de Villa de Leyva (Boyacá, Colombia). Bioestratigrafía. Geología Colombiana, 25, pp.149-162. Bogotá.

Patarroyo, P., 2004, Die Entwicklung der Ammoniten der Familie Pulchelliidae aus dem Barrême von Zentral-Kolumbien. Revue de Paléobiologie, 23 (1), pp. 1-65. Ginebra.

Patarroyo, P., 2009, Amonitas de un Nivel de Alta Energía del Barremiano Inferior en la Formación Paja de los Sectores de Villa de Leyva (Boyacá) y de Vélez (Santander). Boletín de Geología. Vol. 31, N° 2.

Patarroyo, P. & Vega, F., 2011, Albian ammonites and decapods of the Simití Formation near Vélez (Santander – Colombia. In Götz, S., Bengtson, P., Cueto Berciano, F.J., Sitinnesbeck, W. (Eds.) 2011: 22nd International Colloquium on Latin American Earth Sciences, Abstracts and Program. Gaea Heidelbergensis, 8, pp. 166.

Patarroyo, G., Torres, G. 2013, Reporte final de bioestratigrafía (Micropaleontología) Pozo La Luna-1, Cuenca del Valle Medio del Magdalena. Informe Interno 06-13. Instituto Colombiano del Petróleo. Grupo de Bioestratigrafía.

Pennington, W.D., 1981, Subduction of the Eastern Panama Basin and seismotectonics of northwestern South America. J. Geophys. Res. Solid Earth 86, 10753–10770. doi:10.1029/JB086iB11p10753.

Petters V., 1955, Development of Upper Cretaceous foraminiferal faunas in Colombia. *Journ. Paleont*., vol. 29, n° 2, pp. 212-225, 7 fig., Tulsa.

Pindell, J.L. and Dewey, J.F., 1982, Permo-Triassic reconstructionof western Pangea and the evolution of theGulf of Mexico/Caribbean region. *Tectonics,* **1**, 179-212.

Pilger, R. H. JR., 1984, Cenozoic plate kinematics, subduction and magmatism. Journal of the Geological Society of London, 141, 793–802.

Pindell, J. L., 1985a, Alleghenian reconstruction and thesubsequent evolution of the Gulf of Mexico, Bahamas and Proto-Caribbean Sea. *Tectonics,* **4**,1-39.

Pindell, J. L., 1985b, *Plate-tectonic evolution of the Gulf of Mexico and Caribbean Region.* Unpublished Ph.D. thesis, University of Durham, Durham.

Pindell, J.L., Cande, S.C., Pitman, W.C., III, Rowley, D.B., Dewey, J.F., LaBrecque, J.L., Haxby, W.F. 1988. A Plate kinematic framework for models of Caribbean evolution. *Tectonophysics,* 155, 121-138.

Pindell, J.L., Barret, S.F., 1990, Geological evolution of the Caribbean region: A plate tectonic perspective. In: G. Dengo, J. Case (eds.), The Caribbean region, vol. H, *The geology of North America*. Geol. Soc. Am. Boulder, Colo., p. 405-432.

Pindell, J.L., 1993, Regional synopsis of Gulf of Mexico and Caribbean evolution, *in* J.L. Pindell, B.F. Perkins, eds., Mesozoic and Early Cenozoic Development of the Gulf of Mexico and Caribbean Region: A Context for Hydrocarbon Exploration. Selected Papers Presented at the G.C.S.S.E.P.M Foundation Thirteenth Annual Research Conference, p. 251-274.

Pindell, J. L., 1994, Evolution of the Gulf of Mexico and the Caribbean. Caribbean geology: an introduction, redciencia.cu. U.W.I. Publishers' Association, Kingston, pag. 13-39.

Pindell, J.L., Erikson, J. P. 1994, Mesozoic passive margin of northern South America. *In*: Salfity, J. A. (ed.), *Cretaceous tectonics in the Andes*. Vieweg Publishing, Earth Evolution Sciences, Wiesbaden, Germany, International Monograph Series, 1-60.

Pindell, J.L., and Tabbutt, K. D., 1995, Mesozoic- Cenozoic Andean paleogeography and regional controls on hydrocarbon system, in Tankard, A.J., Suárez Soruco, R., and Welsink. H.J., eds., Petroleum Basins of South America: American Association of Petroleum Geologist. Memoir 62, P. 101-128.

Pindell, J., Kennan, L., 2001, Kinematic evolution of the Gulf of Mexico and Caribbean, in R.H. Fillon, N.C. Rosen, and P. Weimer (Eds.), Petroleum Systems of Deep-Water Basins: Global and Gulf of Mexico Experience: GCS-SEPM Foundation, XXI Annual Research Conference, Transactions, p.193-220.

Pindell, J.L., Kennan, L. 2001, Kinematic evolution of the Gulf of Mexico and Caribbean. In: Petroleum Systems of Deep-water Basins: Global and Gulf of Mexico Experience, SEPM Gulf Coast Section, Proceedings of the 21st Annual Research Conference. Society for Sedimentary Geology (SEPM), 193–220.

Pindell, J., Kennan, L., 2009, Tectonic evolution of the Gulf of Mexico, Caribbean and northern South America in the mantle reference frame: an update. In: The Origin and Evolution of the Caribbean Plate (K.H. James, M.A. Lorente and J. Pindell, eds), Geol.Soc. [Lond.] Spec. Publ., 328, 1–56. doi:10.1144/SP328.1

Pindell, J.L. and Kennan, L., 2009, Tectonic evolution of the Gulf of Mexico, Caribbean and northern South America in the mantle reference frame: an update.

Pinto, V. and Peña, C., 2013, Geología y estratigrafía del Corregimiento de Guane, (Departamento de Santander) y sectores aledaños. Universidad de Pamplona, Programa de Geología, Villa del Rosario, Norte de Santander. Tesis de grado.

Polania, H. and Rodriguez, G., 1978, Posibles Turbiditas del Cretaceo Inferior (Miembro Socota) en el area de Anapoima (Cundinamarca).- GeologiaColombiana 10, p. 87-116, Bogota.

Posamentier, H. W., Jervey, M. T., and Vail, P. R. 1988, Eustatic controls on clastic deposition I – conceptual framework. *In Sea Level Changes–An Integrated Approach* (C. K. Wilgus, B. S. Hastings, C. G. St. C. Kendall, H. W. Posamentier, C. A. Ross and J. C. Van Wagoner, Eds.), pp. 110–124. SEPM Special Publication **42**.

Posamentier, H. W., and Vail, P. R. 1988, Eustatic controls on clastic deposition II–sequence and systems tract models. *In Sea Level Changes–An Integrated Approach* C. K. Wilgus, B. S. Hastings, C. G. St.C. Kendall, H. W. Posamentier, C. A. Ross and J. C. Van Wagoner, Eds.), pp. 125–154. SEPM Special Publication **42**.

Posamentier, H.W., James, D.P., and Allen, G.P., 1990, Aspects of sequence stratigraphy: recent and ancient examples of forced regressions: American Association of Petroleum Geologists Bulletin, v. 74, p. 742.

Posamentier, H. W., Allen, G. P., and James, D. P., 1992a, High resolution sequence stratigraphy – the East Coulee Delta, Alberta. *Journal of Sedimentary Petrology*, Vol. **62**, no. 2, pp. 310–317.

Posamentier, H. W., Allen, G. P., James, D. P., and Tesson, M., 1992b, Forced regressions in a sequence stratigraphic framework: concepts, examples, and exploration significance. *American Association of Petroleum Geologists Bulletin*, Vol. **76**, pp. 1687–1709.

Priem, H. N., Andriessen, P., Boelrijk, N. A., De Boorder, H., Hebeda, E. H., Huguett, E., Verdumen, E., and Verschure, R., 1982, Precambrian Amazonas region of southeastern Colombia (western Guiana Shield): Geologie en Mijnbouw, v. 61, p. 229–242.

Porta, J. de., and Solé de Porta N., 1962, Discusión sobre las edades de las formaciones Hoyón, Gualanday y La Cira en la región de Honda-San Juan de Rioseco (Valle del Magdalena), *Ibid.,* nº 9, pp. 69-85, 1 fig., 1 lám., Bucaramanga.

Porta, J. de, 1965a, La Estratigrafía del Cretácico superior y Terciario en el extremo S del Valle Medio del Magdalena, *Bol. Geol.,* Univ. Ind. Sant., nº 19, pp. 5-30, 13 fig., Bucaramanga.

Porta, J. de, 1965b, Nota preliminar sobre la fauna de Vertebrados hallada en Curití (Depto. de Santander, Colombia), *Bol. Geol.,* Univ. Ind. Sant., nº 19, pp. 112-115, 2 fig., 2 fot., Bucaramanga.

Porta, J. de, 1966, Geología del extremo S del Valle Medio del Magdalena entre Honda y Guataquí (Colombia), *Bol. Geol.,* Univ. Ind. Sant., nº 22-23, 318 pp., 37 fig., 10 lám., 48 fot., 4 map. (1: 50000), Bucaramanga.

Pulido, O., 1979a, Geología de las planchas 135 Sa Gil y 151 Charalá. Departamento de Santander, Ingeominas, Boletín Geológico Ingeominas, Bogotá, 23(2): 42-78.

Pulido, O., 1979b, Mapa geológico preliminar de la plancha 135, San Gil. Scale 1:100.000, Ingeominas, Bogotá.

Pulido, O., 1980, Mapa geológico preliminar de la plancha 151, Charalá. Scale 1:100.000. Ingeominas, Bogotá.

Qayyum F., O., Catuneanu and Groot P., 2014, Historical developments in Wheeler diagrams and future directions. Basin Research, volume 26, pag 1-15, doi: 10.1111/bre.12077.

Raasveldt, H. C. and Carvajal J.M., 1957a, Mapa Geológico de la República de Colombia, Plancha K-9 "Armero", Esc. 1: 200000, *Serv. Geol. Nal.,* Bogotá. RAASVELDT (H.C.) and CARVAJAL (J.M.) *et al..*, 1957b. – Mapa geológico de la República de Colombia. Plancha M 8 (Ataco), Esc. 1: 200 000 Serv. Geol. Nal. 557 Bogotá.

Radelli, L. 1967, Géologie des Andes Colombiennes, *Thèse Fac. Sc. Univ. Grenoble*, pp. 1-455, B1-B12, 162 fig., Grenoble.

Ramón, J.C., 1998, Sequence stratigraphic framework of Tertiary strata and oil geochemical evaluation, Middle Magdalena Basin, Colombia [Ph.D. thesis]: Golden, Colorado, Colorado School of Mines, 270 p.

Ramos, V.A., Aleman, A., 2000, Tectonic evolution of the Andes. In: Cordani, U.G., Milani, E. J., Thomaz Filha, A., Campos, D.A. (Eds.), Tectonic Evolution of South America. 31st International Geological Congress, Rio de Janerio, pp. 635–685.

Ramsayer, G.R., 1979, Seismic stratigraphy, a fundamental exploration tool: 11th Annual. Offshore Technology Conference Proceedings, p. 101-109.

Reiners, P. W., Brandon, M.T., 2006, Using thermochronology to understand orogenic erosion, Annu. Rev. EarthPlanet. Sci., v.34, p.419-466, doi:10.1146/annurev.earth.34.031405.125202.

Restrepo, J.J., Toussaint, J.F., 1976, Modelos Orogénicos de tectónica de placas de los Andes colombianos. Boletín Ciencias de La Tierra, Universidad Nacional, Medellín 1, 1–47.

Restrepo, J.J., Toussaint, J.F., 1988, Terranes and Continental Accretion in the Colombian Andes. Episodes 11 (3), 189–193.

Restrepo, J.J., Toussaint, J.F., Gonzalez, H., Cordani, U., Kawashita, K., Linares, E.,Parica, C., 1991, Precisiones geocronológicas sobre el occidente Colombiano.Simposio sobre magmatismo Andino y su marco tectónico, Manizales, Memorias 1, 1–21.

Restrepo-Pace, A., 1995, Late Precambrian to Early Mesozoic tectonic evolution of the Colombian Andes, based on new geochronological, geochemical and isotopic data. Ph.D. Thesis, University of Arizona. p. 195.

Restrepo-Pace, P.A., Colmenares F., Higuera C., Mayorga M., 2004, A fold and-thrust belt along the western flank of the Eastern Cordillera of Colombia-Style, kinematics, and timing constraints derived from seismic data and detailed surface mapping, in Thrust Tectonics and HydrocarbonSystems, edited by K. R. McClay, AAPG Mem., 82, 598–613.

Renzoni, G., 1962, Apuntes acerca de la litología y tectónica de la zona al Este y Sureste de Bogotá. Bol. Geol., vol 10, n° 1-3, pp. 59-79, 1 map., Bogotá.

Renzoni, G., 1965, Geología del cuadrángulo L-11, Villavicencio, Serv. Geol. Nal. E Inventario Minero Nal., Map. Geol. Esc. 1:200000, Bogotá.

Renzoni, G., Rosas, H. and Etayo, F., 1967, Mapa geológico, plancha 191, Tunja, Map scale 1:100.000. Ingeominas, Bogotá. Publicado 1997.

Renzoni G., y Ospina, C., 1969, Geología del cuadrángulo J-12, Ingeominas, Informe No, 1546, 30 pp.

Renzoni G., 1983, Geología del cuadrángulo J-12, Tunja. Boletín Geológico 24(2):31-48.

Restrepo-Pace, P.A., Colmenares, F., Higuera, C. and Mayorga, M., 1999a, Fold and thrust belt along the western flank of the Eastern Cordillera of Colombia: style, kinematics and timing contraintsderived from seismic data and detailed surface mapping. In: K. McClay (ed.), A.A.P.G. Spec. Publ. In press. 25 p.

Restrepo-Pace P. A., Colmenares, F., Higuera, C., and Mayorga, M., et al., 2004, A fold and Thrust belt along the western flank of the Eastern Cordillera of Colombia. Style, Kinematics, and timing constrains derived from seismic data and detailed surface mapping. In: McClay, K. R. (ed.) Thrust Tectonics and Hydrocarbon Systems. American Association of Petroleum Geologists, Tulsa, OK, Memoirs, 82, 598-613.

Restrepo, J.J., Ordóñez-Carmona, O., Moreno-Sánchez, M., 2009, A comment on "The Quebradagrande Complex: a Lower Cretaceous ensialic marginal basin in the Central Cordillera of the Colombian Andes" by Nivia et al. Journal of South American Earth Sciences 28, 204–205.

Reyes G, Montoya D, Terraza R, et al., 2006, Geología del cinturon esmeraldifero occidental. Ingeominas 42.

Ricard, Y., Doglioni, C., Sabadini, R., 1991, Differential rotation between lithosphere and mantle: a consequence of lateral viscosity variations. J. Geophys. Res. 96, 8407–8415.

Rivadeneira, M. and Baby, P., 1999, La Cuenca Oriente: Estilo tectónico, etapas de deformación y caracttrfsticas geológicas de los principales campos de Petroproducción. Petroproducción-IRD pub., Quito, 88 p.

Robert, E., Bulot, L.G., Dhont, A., Jaillard, E., Villagómez, R., Rivadeinera, M., Paz, M., 1998, La transgresión del Cretáceo inferior en el margen andino (Perú y Ecuador): datos preliminares. Boletin de la Sociedad Geológica del Perú 88, 73-86.

Rodríguez, C., Rojas, R., 1985, Estratigrafía y tectónica de la serie InfraCretácica en los alrededores de San Félix, Cordillera Central de Colombia. In: Etayo-Serna, F., Laverde-Montaño, F. (Eds.), Proyecto Cretácico, contribuciones. Ingeominas Publ. Esp. 16, Bogotá, 21p. Chapter XXI. , Ingeominas Publicación Geológica Especial 16, Bogotá, p. 21.

Rodríguez, E. and Ulloa, C., 1994za, Mapa Geológico de la Plancha 169 de Puerto Boyacá: Ingeominas, Esc 1:100.000, Bogotá.

Roeder D., and Chamberlain, R. L., 1995, Eastern Cordillera of Colombia: Jurassic Neogene evolution. In: Tankard, A. J., Suarez-Soruco, R. and Welsink, H. J., (eds) Petroleum Basin of South America. American Association of Petroleum Geologist, Tulsa, OK, Memoirs, 62, 633-645.

Rolón, L. F. and Carrero, M., 1995, Análisis estratigráfico de la sección Cretácica aflorante al oriente del anticlinal de Los Cobardes entre los Municipios de Guadalupe-Chima-Contratación, Departamento de Santander. Tesis pregrado Geología, Univ. Nacional de Colombia, Bogotá, 80p.

Rollon et al., 1997, Analisis Estratigrafico Secuencial del Cretacico Inferior en el VMM sector Piedemonte Occidental de la Cordillera Oriental. Geosurvey Ltda. Reporte interno de Ecopetrol.

Ross, M., Scotese, C., 1988, A hierarchical tectonic model of the Gulf of Mexico and Caribbean region. Tectonophysics. Volume 155, Issues 1-4. December. Pages 139-168.

Rubiano, J. L., 1989, Petrography and stratigraphy of the Villeta Group, Cordillera Oriental, Colombia, South America. M.Sc. Thesis, Univ. South Carolina, Columbia, SC., p. 96.

Sambridge, M.S., Compston, W., 1994, Mixture modeling of multi-component data sets with application to ion-probe zircon ages. Earth Planet. Sci. Lett. 128, 373–390.

Sánchez, J., Horton, B., Teson E., Stockli, D.F., Mora A., Ketcham R.A., 2012, Kinematic evolution of Andean fold-thrust structures along the boundary between the Eastern Cordillera and Middle Magdalena Valley basin, Colombia, Tectonics, 31, TC3008, doi:10.1029/2011TC003089.

Santamaria, F., and Schubert, C., 1974, Geochemistry and geochronology of the Southern Caribbean-Northern Venezuela plate boundary. Geol. Soc. Am. Bull., v. 7, p. 185–198; En castellano (1975): Asoc. Ven. Geol., Min. y Petr., Bol. Informe, 18 (1):1-38.

Sarmiento, L.F., 1989, Stratigraphy of the Cordillera Oriental west of Bogotá, Colombia. M.Sc. Thesis University of South Carolina, Columbia, SC., p. 102.

Sarmiento, L., 2001, Mesozoic Rifting and Cenozoic Basin Inversion History of the Eastern Cordillera Colombian Andes-Inferences fron tectonic models. Vrije Universitteit Amtesdam. Tectonics Deparment . PhD thesis, 295p.

Sarmiento, L., Cardozo, E, Forero, H., and Ramirez, C., 1985, Importancia de la estratigrafía en la evaluaci6n de las anomalías geoquímicas: caso del área del rio Zumbe, Utica (Cundinamarca), in Etayo-Serna F. and Laverde, F. (eds.), Proyecto Cretácico.- Pub. Geol. Esp. Ingeominas No. 16, p. XXVIII-5 - XXVIII-l0, Bogotá.

Sarmiento-Rojas, L.F., Van Wess, J.D. and Cloetingh, S., 2006, Mesozoic transtensional basin history of the Eastern Cordillera, Colombian Andes: Inferences from tectonic models: Journal of South American Earth Sciences, v. 21, p. 383–411, doi: 10.1016/j.jsames.2006.07.003.

Sassi, W., Graham, R., Gillcrist, R., Adams, M., and Gomez, R., 2007, The impact of deformation timing on the prospectivity of the Middle Magdalena sub-thrust, Colombia, in A. C. Ries, R. W. H. Butler, and R. H. Graham, eds., Deformation of the continental crust: The legacy of Mike Coward: Geological Society (London) Special Publication 272, p. 473–498.

Scheibe, E. A., 1938, Estudios Geológicos sobre la Cordillera Oriental Est. Geol. Paleont. Cord. Orient. Col., 1a parte, 58 pp., 2 fig., 5 lám. Fotos, 1 lám. Cortes, 1 mapa 1: 1000000 f. t., Bogotá 4.

Schamel, S., 1991, Middle and Upper Magdalena Basins, in K. T. Biddle, ed., Active margin basins: AAPG Memoir 52, p. 283–301.

Scheibe, E. A., 1934a, Proyecto para explotar las carboneras de propiedad nacional en San Jorge y Llano de Animas, Municipio de Zipaquirá, y en Mongua, Municipio de Nemocón. *Comp. Est. Geol. Ofic. Col.*, t. 3, pp. 291-293, Bogotá.

Scheibe, E. A., 1934b, Informe sobre algunos trabajos de explotación emprendidos en las minas de carbón de San Jorge y Llano de Animas. *Ibid.*, t. 2, pp. 295-297.

Schildgen T. F., Hoke G., 2018, The Topographic Evolution of the central Andes. Elements, volume 14, Number 4: pp. 231-236.

Schuchert, Ch., 1935, Historical Geology of the Antillean- Caribbean Region. 1 vol., 811 pp., 123 fig., New York (John Wiley and Sons).

Scotese, C.R., Gahagan, L.M., Larson, R.L. et al., 1988, Plate tectonic reconstructions of the Cretaceous and Cenozoic ocean basins. In: Scotese, C. R., Sager, W. W. (eds) Mesozoic and Cenozoic Plate Reconstructions. Tectonophysics, 155: 27–48 Amsterdan.

Sébrier, M., Lavenu, A., Fornari, M., Soulas, J.-P., 1988, Tectonics and uplift in central Andes (Peru, Bolivia and northern Chile) from Eocene to present. Geodynamique, 3:85-106.

Sébrier, M. and Soler, P., 1991, Tectonics and magmatism in the Peruvian Andes from late Oligocene time to the present. In : R.S. HARMON & C.W. RAPELA Eds, Andean magmatism and its tectinic setting.- Geol. Soc. Am. Spec. Paper, 265, 259-278.

Sempere, T., 1990, Cuadros estratigráficos de Bolivia: Propuestas nuevas. Rev. Téc. Yacimientos Petrolíferos Fiscales Bolivianos, 11: 215-227.

Sempéré, T., 1994, Kimmeridgian (?) to Paleocene tectonic evolution of Bolivia. In: *Cretaceous tectonics in the Andes, ed.* Salfity, J.A., pp. 168-212, Earth Evolution Sciences, Fried. Vieweg and Sohn, Braunschweig/Wiesbaden.

Séranne, M., 1987, Evolution tectono-sédimentaire du bassin de Talara (nord-ouest du Pérou). *Bulletin de /'Jnstitut Franrais d'Etudes Andines,* 16, 103-115, Lima-París.

Shanmugam, G. and Moiola, R.J., 1988, Submarine fans: characteristics, models, classification, and reservoir potential. Earth-Sci. Rev., 24: 383-428.

Sillitoe, R. H., L. Jaramillo, P. E. Damon, M. Shafiqullah, and R. Escovar, 1982, Setting, characteristics and age of the Andean porphyry copper belt in Colombia: Economic Geology, v. 77, p. 1837–1850.

Sinton, C.W., Duncan, R.A., Storey, M., Lewis, J., and Estrada, J.J., 1998, An oceanic flood basalt province within the Caribbean plate: Earth and Planetary Science Letters, v. 155, p. 221–235.

Soler, P., 1991, Contribution a l'étude du magmatisme associé aux zones de subduction. Pétrographie, géochimie et géochimie isotopique des roches intrurives sur un transect des Andes du Pérou CentraL Jmplia~tions géodyMmiques el mitallogéniques. Dr Thesis, Univ. Paris VI, 950 p.

Soler, P., Bonhomme, M., 1990, Relations of magmatic activity to Plate dynamics in Central Peru from Late Cretaceous to Present In: Plutonism from Antarctica to Alaska, eds. Kay, S. and Rapela, C. *Geological Society* of *America Memoir,* 241. 173-191.

Steinmann, G. 1929, Geologie von Peru. Karl Winter, Heidelberg.

Steno, N., 1669, De Solido intra solidum naturaliter contento Dissertationis Prodromus, en: SCHERZ., edit. (1969). Steno. Geological Papers. Bibliotheca Universitatis Hauniense, Acta Historica Scienciarum Naturalium et Medicinalium. Copenhague, Volumen 20, páginas 133-217.

Stille, H., 1938, Estudios geológicos en la región del río Magdalena, *Comp. Est. Geol. Ofic. Col.,* t. 4, pp. 125-182, 8 fig., l lám., Bogotá.

Stoeckhert, B., W.V. Maresch, M. Brix, C. Kaiser, A. Toetz, R. Kluge, G. Krueckhans-Lueder, 1995, Crustalm history of Margarita Island (Venezuela) in detail: Constraint on the Caribbean plate-tectonic scenario: Geology, v. 23, no. 9, p. 787–790.

Strecker, M.R., Alonso, R.N., Bookhagen, B., Carrapa, B., Hilley, G.E., Sobel, E.R., Trauth, M.H ., 2007, Tectonics and climate of the southern central Andes. Ann. Rev. Earth Planet. Sci., v 35, p.747-787.

Stutzer O., 1927, Zur Geologie des mittleren Magdalenentales. Ibd., Beil.-Bd 57, Abt.B, pp. 342-363. 1 Kartenskizze

Stutzer O., 1934, (escrito en 1926). – Contribución a la Geología de la Cordillera Oriental, regiones ceca de Bogotá. Ibid., t. 2, pp. 141-182, fig. 38-44, Bogotá.

Sweeney, J., and Burnham, A., 1990, Evaluation of a simple model of vitrinite reflectance based on Chemical kinetics. American Association of Petroleum Geologist Bulletin · V.74. No. 10 (October 1990), p. 1559-1570, 8 Figs., 1 Table.

Sullivan P. B. 1999, Thermochronology, denudation and variations inpalaeosurface temperature: a case study from the North Slope foreland basin, Alaska. Basin Research Basin Research (1999) 11, 191–20411, 191–204.

Taboada, A.B. 1965, Guidebook to the geology of the Mares Concession. Field-trip 1965. Colomb. Soc. Petrol. Geol. Geoph., Bogotá, p. 25.

Taborda, A. B., 1965, Guidebook to the geology of the Mares Concession. Field-trip 1965. Colomb. Soc. Petrol. Geol. Geoph., Bogotá, p. 25.

Tankard. A J., 1986, On the depositional response to thrusting and lithospheeric and lithosphere flexure: example for Apalachian and Rocky Mountain basin. En P. A. Allen and P. Homewood (Eds.). – "Foreland Basins" IAS Spec. Publ., 8, 369-392.

Tarazona A. 1985, Palinología de la Formación Cushabatay del Pongo de Tiraco, Oriente Peruano. 1er Simposium Nacional del Carbón, 10-14 Junio, 20 p., Lima.

Tchegliakova, N., 1997, Análisis de 31 muestras provenientes de la secuencia cretácica aflorante en la región de Otanche-Coscuez-Peñas Blancas (Parte central de La Cordillera Oriental de Colombia). Informe interno Mineralco S.A. Santafé de Bogotá.

Tellez N., 1964, Geología de la Mesa de Barichara. Bol Geol., Univ. Ind. Sant., n° 18, pp. 12-21, 2 fig., 1 mapa f.t., Bucaramanga.

Terraza, R., Montoya, D. & Reyes, G., 2007, El Cretácico inferior en el Cinturón Esmeraldífero Occidental. Memorias XI Congreso Colombiano de Geología, Bucaramanga, Agosto 14 al 17 de 2007.

Terraza, R., & Montoya, D., 2011, Las Esmeraldas de Colombia en su ámbito Geologíco – Excursión Geológica a los Cinturones Esmeraldiferos de La Cordillera Oriental de Colombia en el marco del XIV Congreso Latinoamericano de Geología del 29 de Agosto al 2 de Septiembre de 2011. Servicio Geológico Colombiano. 94 paginas.

Terraza, R., 2012, Estratigrafía y Ambientes de Depósito de la Arenisca de Chiquinquirá en los Alrededores de la Localidad Tipo. Boletín de Geología, Vol. 34 núm. 2, Servicio Geológico Colombiano, p. 1-22.

Thompson, A. V., 1966, Guide Book of a geological section from Bogota to the Central Cordillera, Colombia, *Soc. Petr. Geol. Geoph.*, 20 p., 2 fig., 2 mapas, Bogotá.

Toro, J., 1990, The termination of the Bucaramanga Fault in the Cordillera Oriental, Colombia: Master,s thesis, University of Arizona, Arizona, 60 p.

Toro, J., Roure, F., Bordas-Le Floch, N., Le Cornec-Lance, S., and Sassi, W., 2004, Thermal and kinematic evolution of the Eastern Cordillera fold-and-thrust-belt, Colombia, *in* Swennen, R., Roure, F., and Granath, J.W., eds., Deformation, Fluid Flow, and Reservoir Appraisal in Foreland Fold and Thrust Belts: American Association of Petroleum Geologists Hedberg Series, v. 1, p. 79–115.

Treloar, P.J., Rex, D.C., Guise, P.G., Coward, M.P., Searle, M.P., Windley, B.F., Petterson, M.G., Jan, M.Q., and Luff, I.W., 1989, K-Ar and Ar-Ar geochronology of the Himalayan collision in NW Pakistan; constraints on the timing of suturing, deformation, metamorphism and uplift: Tectonics, v. 8, p. 881–909.

Tsai-Bao Kuo. 1986, Well log correlation using artificial intelligence (Rule-based, Expert System, Computer-assisted). PhD thesis.

Ulloa, C. and Roddríguez, E., 1979a, Geología de las planchas 170 velez y 190 Chiquinquirá, Colombia. Ingeominas Informe 1794, Sogamoso, 45 p.

Ulloa, C. and Rodríguez, E., 1979b, Geología del Cuadrángulo K-13, Tauramena. Boletin Geológico, Ingeominas, Bogotá, 24(2): 3-30.

Ulloa, C. 1988, Guía de la excursión Bogota-Honda: Anexo.- Geologia Colombiana No 16, Universidad Nacional de Colombia, Departamento de Geociencias, Bogotá.

Ulloa, C. y Rodríguez, E., 1978a, Mapa geológico preliminar de la Planche 170-Velez. Publicada en 1984. Escala 1:100.000 Ingeominas. Bogotá.

Ulloa, C.; Rodríguez, E., 1991, Mapa Geológico de Colombia, Plancha 190 Chiquinquirá, Memoria Explicativa. Ingeominas, 26 p. Bogotá.

Ulloa C. and Rodriguez, E., 1994, Geología de la Plancha 189 – La Palma. Escala 1:100.000 Memoria Resumida, Ingeominas.

Ulloa. C.E and Acosta J., 2001, Geología de la Plancha 227 – La Mesa, Memoria Explicativa, Ingeominas, p. 1-77.

Uyeda, S., Kanamori, H., 1979, Back-Arc Opening and the Mode of Subduction. Journal of Geophysical Research. Vol. 84 No. B3, March. 1049-1061.

Vail, P. R., Mitchum, R. M. Jr., Thompson, S., III, 1977, Seismic stratigraphy and global changes of sea level, part four: global cycles of relative changes of sea level. American Association of Petroleum Geologists Memoir **26**, 83–98.

Vail, P.R., Mitchum, R. M. J. and Thompson, S., 1977, Seismic stratigraphy and global changes of sea level, part 2. The depositional sequence as a basic unit for stratigraphic analysis. In; M26: Seismic Atratigraphy – Applications to Hydrocarbon Exploration (Ed. By C.E. Payton), pp. 53-62. American Association of Petroleum Geologist, Tulsa, OK, USA.

Vail, P. R., Mitchum, R. M. and Thompson, S., 1978, Seismic stratigraphy and global changes of sea levels, part 4: Global Cycles of relative changes of sea level. Amer. Assoc. Petrol. Geol. Mem. 26, 83-97.

Veloza, G., Mora, A., De Freitas, M. and Mantilla, M., 2008, Dislocación de facies en el tope de la secuencia Cretacica de la subcuenca de Neiva, Valle Superior del Magdalena y sus implicaciones en el modelo estratigráfico secuencial colombiano. *Boletín de Geología UIS*, volumen 30 (1), p. 29-44.

Vallejo, C., Winkler, W., Spikings, R.A., Luzieux, L., Heller, F., Bussy, F., 2009, Mode and timing of terrane accretion in the forearc of the Andes in Ecuador, *in* Kay, S.M., Ramos, V.A., Dickinson, W.R., eds., Backbone of the Americas, Geological Society of America Memoir 204, p.1-20, doi: 10.1130/2009.1204(09).

Vallejo, C., Spikings, R.A., Winkler, W., Luzieux, L., Chew, D., Page, L., 2006, The early interaction between the Caribbean Plateau and the NW South American plate: Terra Nova, v. 18, p. 264–269.

Van der Beek, P., 1995, Tectonic evolution of continental rifts, inferences from numerical modellingand fission track thermochronology. Ph.D. Thesis, Vrije Universitteit, Amsterdam, 232 p.

Van der Hammen Th., 1957b, Periodicidad climática y evolución de floras del Maestrichtiano y del Terciario, *Bol. Geol.* Inst. Geol. Nal., vol. 5, nº 2, pp. 5-48, 9 fig., 1 lám, Bogotá.

Van der Hammen, T., 1957, Estratigrafia palinologica de la Sabana de Bogotá, Cordillera Oriental de Colombia: Boletin Geologico del Instituto Geologico Nacional, v. 5, no. 2, p. 189–203

Van der Hammen Th., 1958a, Estratigrafía palinológica de la Sabana de Bogotá (Cordillera Oriental). Ibid., vol. 5 (1957), n° 2, pp. 187-203, 3 pl., Bogotá

Van der Hammen Th., 1958b, Estratigrafía del Terciario y Maestrichtiano continentales y tectogénesis de los Andes Colombianos. Ibid., vol. 6 n° 1-3, pp. 67-128, 7 pl. f.t., Bogotá.

Van der Hammen T. H., 1961. Late Cretaceous and Tertiary stratigraphy and tectogenesis of the Colombian Andes. Geologie en Mijnbouw, 40: 181-188.

Van der Wiel, A. M., 1991, Uplift and Volcanism of the SE Colombian Andes in Relation to Neogene Sedimentation of the Upper Magdalena Valley [Ph.D. thesis]: Wageningen, Free University, 208 p.

Van der Wiel, A.M. and Andriessen, P.A.M., 1991. Precambrian to recent thermotectonic history of the Garzón Massif (Eastern Cordillera of the Colombian Andes) as revealed by fission track analysis. In: A.M. Van der Wiel., Uplift and volcanism of the SE Colombian Andes in relation to Neogene sedimentation of the Upper Magdalena Valley. Ph.D. Thesis, Wageningen, 208 p.

Van Houtten F.B. and Travis R.B., 1968, Cenozoic Deposits, Upper Magdalena Valley, Colombia, *Bull. Am. Ass. Petr. Geol.*, vol. 52, nº 4, pp. 675-702, 13 fig., Tulsa.

Van Wagoner, J. C., Posamentier, H.W., Mitchum, R. M., Vail, P. R., Sarg, J. F., Loutit, T. S., Hardenbol, J., 1988, An overview of sequence stratigraphy and key definitions. In: Wilgus, C. K., Hastings, B. S., Kendall, C. G. St. C., Posamentier, H.W., Ross, C. A., Van Wagoner, J. C. (Eds.), Sea Level Changes – An Integrated ApproachSEPM Special Publication **42**, 39–45.

Vanmelle, J., Vilema, W. ET AL. 2008, Pre-collision evolution of the Piñon oceanic terrane of SW Ecuador: stratigraphy and geochemistry of the 'Calentura Formation'. Bulletin de la Socie´te´ Ge´ologique de France, 179, 433–444.

Vermeesch, P., 2009, RadialPlotter: A Java application for fission track, luminescence and other radial plots. *Radiat. Measur*, *44*, 409–410.

Vermeesch, 2012, On the visualitation of detrital age distributions. Chemical Geology, 312-313 190-194. Doi: 10.1016/j.chemgeo.2012.04.021.

Villagómez, D., Spikings, R., Seward, D., Magna, T., Winkler, W., 2008, New thermochronological constraints on the tectonic history of Western Colombia., In proceedings of the 11th International Conference on Thermochronometry. Anchorage – Alaska, USA. Extended Abstract 253-255.

Villagómez, D., 2010, Thermochronology, geochronology and geochemistry of the Western and Central cordilleras and Sierra Nevada de Santa Marta, Colombia: the tectonic evolution of NW South America., Département de Minéralogie, Université de Genève, Ph.D thesis, No 4277.

Villagómez, D., Spiking, R., 2013, Thermochronology and tectonics of the Central and Western Cordilleras of Colombia: Early Cretaceous–Tertiary evolution of the Northern Andes. Lithos 160–161 (2013) 228–249.

Villamil, T., 1994, High-resolultion stratigraphy, chronology and relaitve sea level of the Albiian- Santonian (Cretaceous) of Colombia. Ph.D. Thesis Univ. Of Colorado at Boulder, 446 p.

Villamil, T., and Restrepo P., 1997, Paleocene – Miocene Paleogeographic Evolution of Colombia. Memorias VI Simposio Bolivariano - Exploración Petrolera en las Cuencas Subandinas.

Villamil, T., 1998, Chronology, relative sea-level history and a new sequence stratigraphic model for basinal Cretaceous facies of Colombia. In: Pindell, J.L., Drake, C. (Eds.), Paleogeographic Evolution and Non-Glacial Eustasy, Northern South America, Society of Economic Paleontologists and Mineralogists Special Publication, 58, pp. 161-216.

Villamil, T., & Arango, C., 1998, Integrated stratigraphy of latest Cenomanian and early Turonian facies of Colombia. In: Pindell, J.L., Drake, C. (Eds.), Paleogeographic Evolution and Non-Glacial Eustasy, Northern South America, Society of Economic Paleontologists and Mineralogists Special Publication, 58, pp. 129-159.

Villamil, T., 1999, Campanian-Miocene tectonostratigraphy, depocenter evolution and basin development of Colombia and western Venezuela: Palaeogeography, Palaeoclimatology, Palaeoecology, v. 153, p. 239–275, doi: 10.1016/S0031-0182(99)00075-9.

Vinasco, C.J., Cordani, U.G., González, H., Weber, M., Pelaez, C., 2006, Geochronological, isotopic, and geochemical data from Permo-Triassic granitic gneisses and granitoids of the Colombian Central Andes. Journal of South American Earth Sciences 21(4), 355–371.

Wadge, G., Burke, K., 1983, Neogene Caribbean plate rotation and associated Central American tectonic evolution. Tectonics, v.2 (6), p. 633-643.

Wagner G, Van den Haute P., 1992, Fission-track dating: Netherlands: Solid Earth Sciences Library, Kluwer Academic Publishers, Amsterdam. p. 285

Walker, J. C. G., and Zahnle, K. J., 1986, Lunar nodal tide and distance to the moon during the Precambrian. *Nature*, Vol. **320**, p. 600–602.

Walker, R.G., 1965, The origin and significance of the internal sedimentary structures of turbidites. Proc. Yorkshire Geol. Soc; 35: 1·32.

Ward et al., 1969, D.E., *et al*., 1969, Mapa Geológico del Cuadrángulo H-12 "Bucaramanga", Colombia, *lnst. Nal. Inv. Geol. Min. and US. Geol. Surv.*, Bogotá.

Ward, D. E., Goldsmith, R., Cruz, J. and Restrepo, A., 1973, Geología de los cuadrángulos H-12 Bucaramanga y H-13 Pamplona, departamentos de Santander y Norte de Santander. Boletín Geológico Ingeominas, Bogotá, 21 (1-3): 1-132.

Washburne C. W., and White K. D., 1923, Oil possibilities of Colombia. *Trans. Amer. Inst. Min. Met. Eng.*, vol. 68, pp. 1023-1031, 2 fig., Pittsburgh.

Wheeler, H. E. 1958, Time stratigraphy. American Association of Petroleum Geologist Bulletin, 42, 1047-1063.

Wheeler O. C., 1929, Report on Palmira Series with notes on Stratigraphy of the Umir, Lisama, and La Paz formations near the Eastern part of De Mares Concession. Informe Emp. Petr, (inédito).

Willett, D., 1999, Orogeny and orography: The effects of erosion on the structure of mountain belts. Journal of Geophysical Research, Vol. 104, No. BI2, Pages 28, 957-28, 281, December 10.

Williams, G. D. and Dobb, A., (eds), 1993, Tectonics and Seismc" Sequence Stratigraphy. Geological Society Special Publication No. 71, 1-13.

Williams, G.D., 1993, Tectonics and seismic sequence stratigraphy: an introduction. Geological Society Special Publication No. 71, 1-13.

Wilkinson, B. H., Diedrich, N. W., Drummond, C.N., 1996, Facies succession in peritidal carbonate sequences. Journal of Sedimentary Research, 66: 1065-1078.

Wilson, J.J., 1963, Cretaceous stratigraphy of central Andes of Peru. American Association of Petroleum Geologists Bulletin 47, 1–34.

Wortel, R. and Cloetingh, S. 1981, On the origin of the Cocos_Nazca spreading center, Geology 9, 25-430.

Wright J, Wyld S., 2011, Late Cretaceous subduction initiation on the eastern margin of the Caribbean-Colombian Oceanic Plateau: One Great Arc of the Caribbean (?) *Geosphere*; April 2011; v. 7; no. 2; p. 468–493; doi: 10.1130/GES00577.1.

Zamarreño De Julivert I., 1963, Estudio petrográfico de las calizas de la formación Rosablanca de la región de la Mesa de los Santos (Cordillera Oriental, Colombia). Ibid., n° 15, pp 5-34, 4Fig., 4 lám., Bucaramanga.

Ziegler, P. A., 1994, Geodynamic processes governing development of rifted basins. In: Roure, F., Ellouz, N., Shein, V. S. and Skvortsov, I. (eds.), *Geodynamic evolution of sedimentary basins*. Institut Français du Pétrole, Technip, Paris, p. 16-97.

APPENDIX CHAPTER 5

Merged dataset:
C:\BH2\Jairo\Echantillon-IRR-10-2015\JG-P3-36Zr\JG-P3-36\JG-P3-36Zr.ftz
C:\BH2\Jairo\Echantillon-IRR-10-2015\JG-P3-36Zr\JG-P3-36aZr\JG-P3-36aZr.ftz

NEW PARAMETERS - ZETA METHOD

EFFECTIVE TRACK DENSITY FOR FLUENCE MONITOR (tracks/cm^2): 3,89E+05
RELATIVE ERROR (%): 1,26
EFFECTIVE URANIUM CONTENT OF MONITOR (ppm): 50,00
ZETA FACTOR AND STANDARD ERROR (yr cm^2): 137,14 1,57
SIZE OF COUNTER SQUARE (cm^2): 8,30E-07

GRAIN AGES IN ORIGINAL ORDER

Grain no.	RhoS (cm^-2)	(Ns)	RhoI (cm^-2)	(Ni)	Squares	U+/-2s	Grain Age (Ma) Age	--95% CI--	
1	5,78E+06	(168)	1,79E+06	(52)	35	230 64	85.4	62.4	119.1
2	4,63E+06	(123)	1,02E+06	(27)	32	131 50	119.9	79.1	189.2
3	3,43E+06	(199)	9,64E+05	(56)	70	124 33	93.9	69.7	128.8
4	9,46E+06	(377)	2,06E+06	(82)	48	264 59	120.8	95.2	153.3
5	2,38E+06	(138)	4,65E+05	(27)	70	60 23	134.3	89.1	211.0
6	4,89E+06	(73)	8,03E+05	(12)	18	103 58	158.5	86.9	320.5
7	2,56E+06	(85)	6,02E+05	(20)	40	77 34	111.7	68.6	192.2
8	4,37E+06	(116)	5,65E+05	(15)	32	73 37	201.2	118.9	369.9
9	4,14E+06	(206)	1,02E+06	(51)	60	132 37	106.6	78.4	147.9
10	4,28E+06	(142)	2,62E+06	(87)	40	337 72	43.2	33.0	56.4
11	8,68E+06	(346)	3,44E+06	(137)	48	442 76	66.8	54.7	81.5
12	2,17E+06	(72)	6,93E+05	(23)	40	89 37	82.6	51.4	138.6
13	4,24E+06	(88)	1,16E+06	(24)	25	149 60	96.6	61.4	158.9
14	5,62E+06	(112)	1,20E+06	(24)	24	155 63	122.7	79.0	199.4
15	5,96E+06	(89)	5,35E+05	(8)	18	69 47	285.0	142.6	672.7
16	6,73E+06	(201)	9,04E+05	(27)	36	116 44	194.6	131.1	302.0
17	5,57E+06	(111)	1,71E+06	(34)	24	219 75	86.2	58.5	130.7
18	5,36E+06	(178)	2,17E+06	(72)	40	279 66	65.2	49.6	85.7
19	4,72E+06	(196)	1,98E+06	(82)	50	254 56	63.1	48.7	81.7
20	5,66E+06	(94)	2,11E+06	(35)	20	271 91	71.1	47.9	108.1
21	7,59E+06	(252)	8,43E+05	(28)	40	108 41	234.6	160.0	358.8
22	9,47E+06	(110)	1,12E+06	(13)	14	144 78	219.5	125.4	423.5
23	4,66E+06	(232)	1,77E+06	(88)	60	227 49	69.6	54.4	88.9
24	5,60E+06	(186)	3,46E+06	(115)	40	445 84	42.8	33.9	54.1
25	4,37E+06	(145)	2,53E+06	(84)	40	325 71	45.6	34.9	59.7
26	2,64E+06	(105)	7,28E+05	(29)	48	94 35	95.5	63.2	149.6
27	9,48E+06	(118)	1,45E+06	(18)	15	186 87	171.3	105.1	298.5
28	4,31E+06	(179)	1,73E+06	(72)	50	223 53	65.6	49.9	86.2
29	8,57E+06	(128)	1,47E+06	(22)	18	189 80	152.5	97.4	251.6
30	5,79E+06	(101)	1,78E+06	(31)	21	229 82	86.0	57.3	133.3
31	3,92E+06	(52)	1,28E+06	(17)	16	164 79	80.6	46.2	148.9
32	6,82E+06	(198)	9,64E+05	(28)	35	124 47	185.0	125.3	285.1
33	5,82E+06	(87)	2,48E+06	(37)	18	318 104	62.3	42.1	94.2
34	4,88E+06	(162)	1,87E+06	(62)	40	240 61	68.8	51.4	92.1
35	4,96E+06	(144)	2,20E+06	(64)	35	283 71	59.7	44.2	81.5
36	5,82E+06	(169)	2,44E+06	(71)	35	314 75	62.8	47.6	82.8
37	3,58E+06	(95)	1,92E+06	(51)	32	247 69	49.4	34.9	71.0
38	7,03E+06	(140)	8,53E+05	(17)	24	110 53	214.3	131.0	376.9
39	2,46E+06	(102)	1,28E+06	(53)	50	164 45	51.1	36.4	72.6
40	3,77E+06	(250)	1,97E+06	(131)	80	254 45	50.5	40.8	62.5
41	3,90E+06	(291)	4,02E+05	(30)	90	52 19	252.5	174.9	379.5
42	2,38E+06	(79)	9,34E+05	(31)	40	120 43	67.4	44.2	105.8
43	3,15E+06	(157)	1,85E+06	(92)	60	237 50	45.1	34.9	58.4
44	8,11E+06	(175)	2,50E+06	(54)	26	322 87	85.7	63.0	118.6
45	5,99E+06	(154)	1,87E+06	(48)	31	240 69	84.8	61.2	120.0
46	3,98E+06	(198)	7,43E+05	(37)	60	95 31	140.7	99.2	205.6
47	4,53E+06	(188)	5,30E+05	(22)	50	68 29	222.6	144.5	362.5
48	4,60E+06	(107)	1,46E+06	(34)	28	188 64	83.2	56.3	126.3
49	4,50E+06	(112)	6,02E+05	(15)	30	77 39	194.4	114.7	357.9
50	4,29E+06	(210)	2,80E+06	(137)	59	360 62	40.6	32.7	50.5
51	3,73E+06	(186)	1,89E+06	(94)	60	243 50	52.3	40.8	67.1
52	4,23E+06	(172)	2,31E+06	(94)	49	297 62	48.4	37.6	62.3

Merged dataset:
C:\BH2\Jairo\Echantillon-IRR-10-2015\JG-P3-36Zr\JG-P3-36\JG-P3-36Zr.ftz
C:\BH2\Jairo\Echantillon-IRR-10-2015\JG-P3-36Zr\JG-P3-36aZr\JG-P3-36aZr.ftz

Grain no.	RhoS (cm^-2)	(Ns)	RhoI (cm^-2)	(Ni)	Squares	U+/-2s	Grain Age (Ma) Age	--95% CI--	
53	3,65E+06	(212)	1,72E+06	(100)	70	221 44	56.1	44.1	71.1
54	9,76E+06	(162)	2,35E+06	(39)	20	302 96	109.5	77.2	159.7
55	4,82E+06	(212)	9,55E+05	(42)	53	123 38	132.9	95.5	189.7
56	4,58E+06	(57)	2,17E+06	(27)	15	279 107	55.9	34.9	92.0
57	8,13E+06	(135)	2,53E+06	(42)	20	325 100	85.0	59.9	123.3
58	3,28E+06	(234)	1,36E+06	(97)	86	175 36	63.7	50.3	80.8
59	6,59E+06	(82)	2,73E+06	(34)	15	351 120	63.9	42.5	98.3
60	8,14E+06	(473)	1,33E+06	(77)	70	170 39	160.8	126.5	204.3
61	2,86E+06	(95)	1,66E+06	(55)	40	213 57	45.9	32.6	65.2
62	7,55E+06	(94)	8,84E+05	(11)	15	114 67	221.2	120.6	456.0
63	7,50E+06	(112)	1,14E+06	(17)	18	146 70	172.0	104.1	305.3

Merged dataset:
C:\BH2\Jairo\Echantillon-IRR-10-2015\JG-P3-36Zr\JG-P3-36\JG-P3-36Zr.ftz
C:\BH2\Jairo\Echantillon-IRR-10-2015\JG-P3-36Zr\JG-P3-36aZr\JG-P3-36aZr.ftz

NEW PARAMETERS - ZETA METHOD

EFFECTIVE TRACK DENSITY FOR FLUENCE MONITOR (tracks/cm^2): 3,90E+05
RELATIVE ERROR (%): 1,28
EFFECTIVE URANIUM CONTENT OF MONITOR (ppm): 50,00
ZETA FACTOR AND STANDARD ERROR (yr cm^2): 137,14 1,57
SIZE OF COUNTER SQUARE (cm^2): 8,30E-07

Grain no.	RhoS (cm^-2)	(Ns)	RhoI (cm^-2)	(Ni)	Squares	U+/-2s	Grain Age (Ma) Age	--95% CI--	
64	3,23E+06	(161)	1,89E+06	(94)	60	242 50	45.4	35.1	58.5
65	5,66E+06	(282)	1,20E+06	(60)	60	155 40	123.4	93.5	162.7
66	9,66E+06	(561)	1,15E+06	(67)	70	148 36	218.3	169.9	280.3
67	5,85E+06	(170)	3,27E+06	(95)	35	420 87	47.4	36.8	61.0
68	3,73E+06	(217)	1,12E+06	(65)	70	144 36	87.9	66.7	115.9
69	4,04E+06	(335)	1,52E+06	(126)	100	195 35	70.4	57.3	86.5
70	3,92E+06	(228)	1,38E+06	(80)	70	177 40	75.2	58.3	97.1
71	6,38E+06	(429)	7,44E+05	(50)	81	95 27	223.1	167.1	297.4
72	3,46E+06	(115)	1,48E+06	(49)	40	189 54	62.3	44.3	89.0
73	4,96E+06	(247)	4,62E+05	(23)	60	59 25	278.9	184.1	445.7
74	2,27E+06	(151)	4,22E+05	(28)	80	54 20	141.8	95.0	220.4
75	8,73E+06	(290)	1,05E+06	(35)	40	135 46	216.8	153.5	316.5
76	2,52E+06	(209)	6,87E+05	(57)	100	88 23	96.4	72.0	129.0
77	3,25E+06	(108)	1,75E+06	(58)	40	224 59	49.5	35.7	69.4
78	7,03E+06	(350)	1,20E+06	(60)	60	155 40	152.7	116.4	200.3
79	3,41E+06	(198)	1,41E+06	(82)	70	181 40	63.8	49.3	82.6
80	7,75E+06	(315)	1,38E+06	(56)	49	177 47	147.3	111.0	195.1
81	6,53E+06	(325)	8,63E+05	(43)	60	111 34	198.2	144.8	278.6
82	5,72E+06	(475)	5,30E+05	(44)	100	68 20	281.2	207.9	390.6
83	2,04E+06	(169)	9,40E+05	(78)	100	121 27	57.3	43.8	74.9
84	3,44E+06	(200)	1,70E+06	(99)	70	219 44	53.5	42.0	68.1
85	3,16E+06	(262)	1,94E+06	(161)	100	249 40	43.2	35.4	52.7
86	8,13E+06	(270)	1,17E+06	(39)	40	151 48	181.7	130.4	260.8
87	7,83E+06	(117)	9,37E+05	(14)	18	120 63	217.3	126.6	408.1
88	5,61E+06	(233)	6,27E+05	(26)	50	80 31	233.8	157.2	364.1
89	4,94E+06	(328)	1,76E+06	(117)	80	226 42	74.2	60.0	91.7
90	6,67E+06	(238)	8,69E+05	(31)	43	111 40	201.0	139.1	301.8
91	2,45E+06	(197)	3,35E+05	(27)	97	43 16	191.1	128.6	296.6
92	2,50E+06	(83)	4,52E+05	(15)	40	58 29	144.9	84.1	270.4
93	3,22E+06	(107)	1,33E+06	(44)	40	170 51	64.5	45.1	93.9
94	2,89E+06	(168)	8,09E+05	(47)	70	104 30	94.6	68.3	133.7
95	8,22E+06	(273)	1,36E+06	(45)	40	174 52	159.6	116.7	223.7
96	4,70E+06	(156)	6,02E+05	(20)	40	77 34	203.7	129.0	341.6
POOLED	4,74E+06	(17933)	1,34E+06	(5088)	4559	173 7	93.4	89.2	97.7

CHI^2 PROBABILITY (%): 0.0

POOLED AGE W/ 68% CONF. INTERVAL(Ma): 93.4, 91.2 -- 95.5 (-2.1 +2.2)
95% CONF. INTERVAL(Ma): 89.2 -- 97.7 (-4.1 +4.3)

CENTRAL AGE W/ 68% CONF. INTERVAL(Ma): 92.8, 87.6 -- 98.2 (-5.1 +5.4)
95% CONF. INTERVAL(Ma): 83.0 -- 103.7 (-9.8 +11.0)
AGE DISPERSION (%): 51.0

Merged dataset:
C:\BH2\Jairo\Echantillon-IRR-10-2015\JG-P3-36Zr\JG-P3-36\JG-P3-36Zr.ftz
C:\BH2\Jairo\Echantillon-IRR-10-2015\JG-P3-36Zr\JG-P3-36aZr\JG-P3-36aZr.ftz

FIT OPTION: Best-fit peaks using the binomial model of Galbraith and Green

INITIAL GUESS FOR MODEL PARAMETERS (number of peaks to fit = 3)

Peak #.	Peak Age	Theta	Fraction(%)	Count
1.	43.50	0.621	18.8	18.02
2.	93.30	0.779	19.1	18.36
3.	216.00	0.892	20.9	20.10

Total range for grain ages: 40,7 to 279,3 Ma
Number of active grains (Num. used for fit): 96
Number of removed grains: 0
Degrees of freedom for fit: 91
Average of the SE(Z)'s for the grains: 0,19
Estimated width of peaks in PD plot in Z units: 0,22

PARAMETERS FOR BEST-FIT PEAKS

* *Standard error for peak age includes group error*
* *Peak width is for PD plot assuming a kernel factor = 0.60*

#.	Peak Age(Ma)	68%CI	95%CI	W(Z)	Frac(%)	SE,%	Count
1.	49.2	-2,1 ...+2,2	-4,0 ...+4,3	0.16	21.6	5.2	20.8
2.	76.4	-3,0 ...+3,2	-5,9 ...+6,3	0.18	36.9	5.8	35.4
3.	181.8	-6,6 ...+6,8	-12,7 ...+13,6	0.22	41.5	5.2	39.9

Log-likelihood for best fit: -415,798
Chi-squared value for best fit: 94,299
Reduced chi-squared value: 1,036
Probability for F test: 0%
Condition number for COVAR matrix: 6,37
Number of iterations: 19

Merged dataset:
C:\BH2\Jairo\Echantillon-IRR-10-2015\JG-P3-36Zr\JG-P3-36\JG-P3-36Zr.ftz
C:\BH2\Jairo\Echantillon-IRR-10-2015\JG-P3-36Zr\JG-P3-36aZr\JG-P3-36aZr.ftz

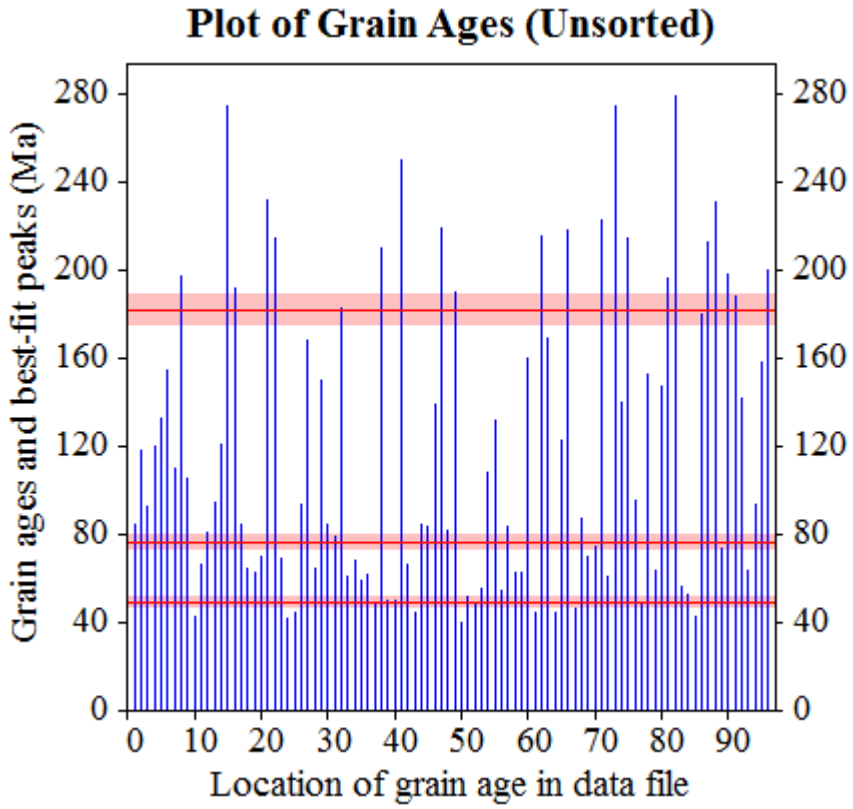

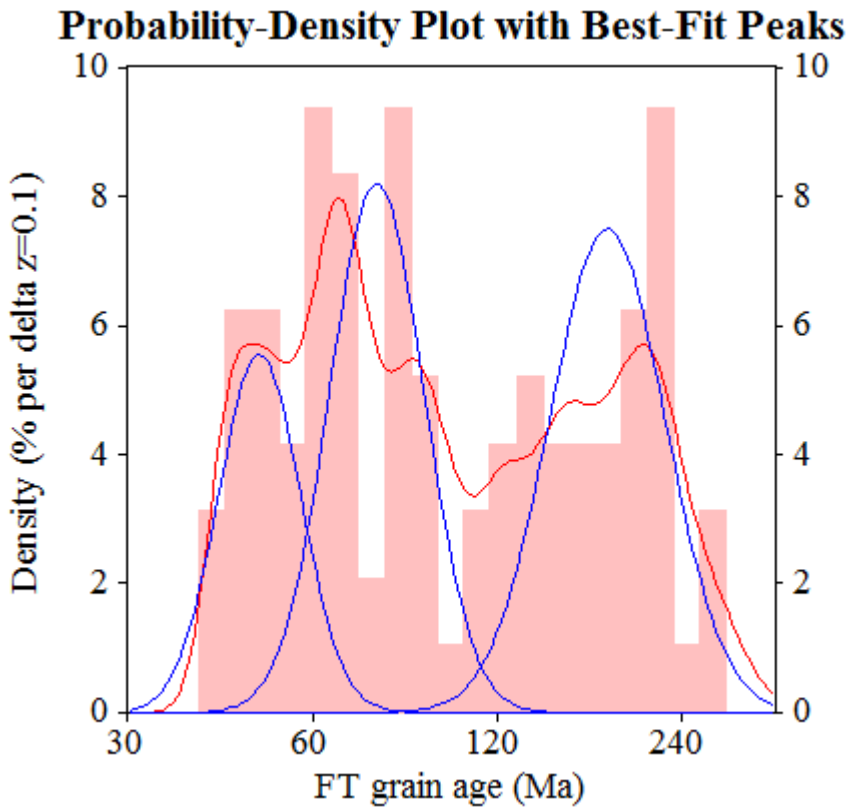

Merged dataset:
C:\BH2\Jairo\Echantillon-IRR-10-2015\JG-P3-36Zr\JG-P3-36\JG-P3-36Zr.ftz
C:\BH2\Jairo\Echantillon-IRR-10-2015\JG-P3-36Zr\JG-P3-36aZr\JG-P3-36aZr.ftz

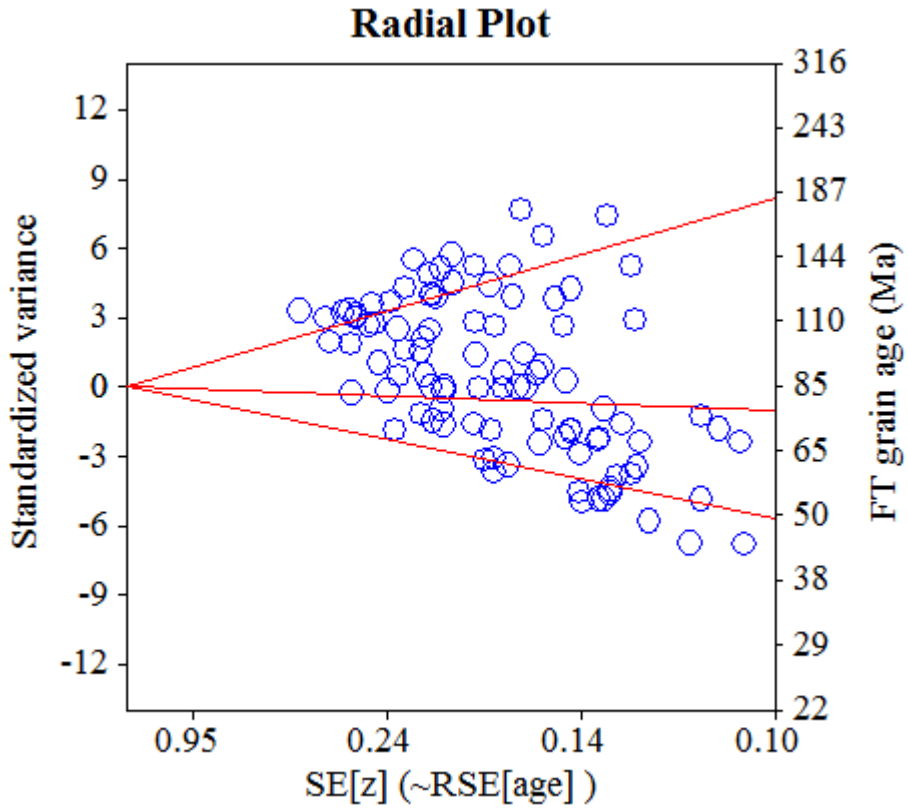

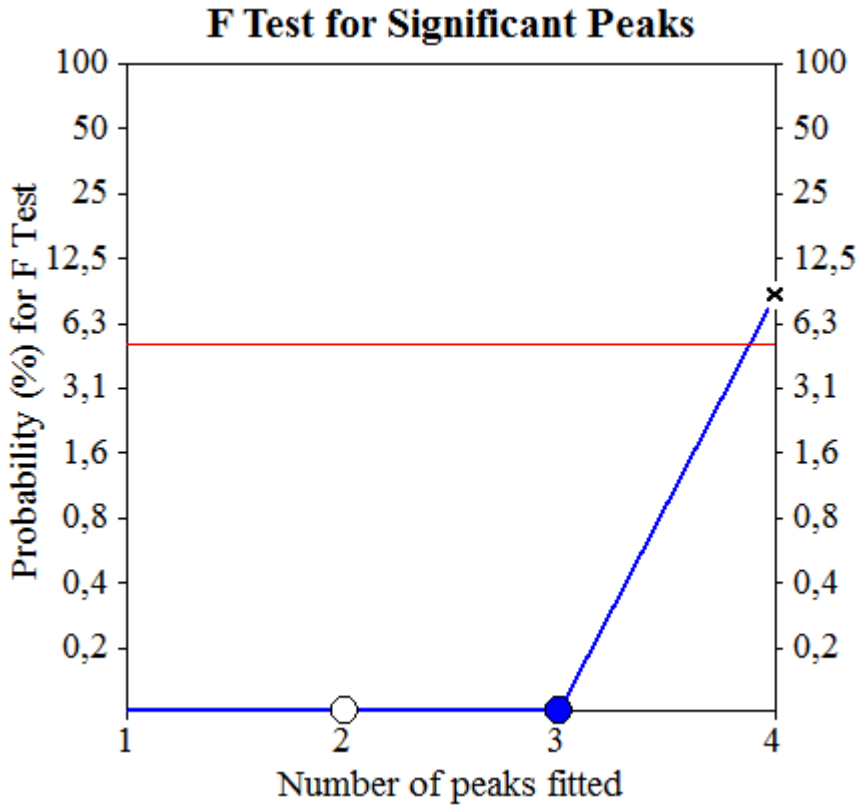

Merged dataset:
C:\BH2\Jairo\Samples-IRR-6-2015\JG-P3-41\JG-P3-41.ftz
C:\BH2\Jairo\Samples-IRR-6-2015\JG-P3-41\JG-P3-41a.ftz

NEW PARAMETERS - ZETA METHOD

EFFECTIVE TRACK DENSITY FOR FLUENCE MONITOR (tracks/cm^2): 2,72E+05
RELATIVE ERROR (%): 1,34
EFFECTIVE URANIUM CONTENT OF MONITOR (ppm): 50,00
ZETA FACTOR AND STANDARD ERROR (yr cm^2): 137,95 4,04
SIZE OF COUNTER SQUARE (cm^2): 8,30E-07

GRAIN AGES IN ORIGINAL ORDER

Grain no.	RhoS (cm^-2)	(Ns)	RhoI (cm^-2)	(Ni)	Squares	U+/-2s	Grain Age (Ma) Age	--95% CI--	
1	7,43E+06	(74)	1,20E+06	(12)	12	221 125	113.4	62.1	230.0
2	1,25E+07	(145)	6,02E+05	(7)	14	111 81	369.4	181.2	916.0
3	8,67E+06	(108)	1,20E+06	(15)	15	221 113	132.4	77.8	245.1
4	9,71E+06	(145)	9,37E+05	(14)	18	172 91	189.5	111.1	354.6
5	6,95E+06	(75)	1,20E+06	(13)	13	221 121	106.2	59.3	209.3
6	8,84E+06	(88)	9,04E+05	(9)	12	166 108	178.0	91.6	401.8
7	5,82E+06	(87)	6,69E+05	(10)	18	123 76	158.9	84.0	343.2
8	9,77E+06	(73)	1,74E+06	(13)	9	320 174	103.4	57.6	204.1
9	1,18E+07	(98)	2,41E+06	(20)	10	443 196	90.7	56.1	155.3
10	1,16E+07	(87)	1,61E+06	(12)	9	295 167	133.1	73.6	267.9
11	5,00E+06	(83)	9,04E+05	(15)	20	166 84	102.1	59.1	191.0
12	8,34E+06	(256)	1,01E+06	(31)	37	186 66	152.4	105.5	228.9
13	1,13E+07	(178)	1,40E+06	(22)	19	256 108	149.1	96.4	243.9
14	8,25E+06	(137)	6,63E+05	(11)	20	122 72	226.5	125.2	462.4
15	1,37E+07	(159)	2,15E+06	(25)	14	395 157	117.6	77.4	187.3
16	1,61E+07	(134)	1,45E+06	(12)	10	266 151	203.7	114.9	403.0
17	1,29E+07	(128)	1,00E+06	(10)	12	185 114	232.3	125.1	493.7
18	1,19E+07	(187)	1,40E+06	(22)	19	256 108	156.5	101.4	255.7
19	1,40E+07	(139)	1,10E+06	(11)	12	203 120	229.7	127.1	468.7
20	1,02E+07	(144)	7,09E+05	(10)	17	130 80	260.8	141.1	551.4
21	6,96E+06	(231)	5,72E+05	(19)	40	105 48	222.4	141.1	375.0
22	1,02E+07	(76)	2,28E+06	(17)	9	418 200	82.7	48.9	149.8
23	1,26E+07	(157)	1,69E+06	(21)	15	310 134	137.8	88.0	229.0
24	1,47E+07	(146)	1,41E+06	(14)	12	258 136	190.7	111.9	356.9
25	9,54E+06	(95)	1,61E+06	(16)	12	295 146	109.5	64.8	199.8
26	1,31E+07	(402)	8,47E+05	(26)	37	156 61	282.1	192.0	434.9
27	1,41E+07	(211)	1,47E+06	(22)	18	271 114	176.3	114.6	287.0
28	1,05E+07	(105)	2,01E+06	(20)	12	369 163	97.1	60.3	165.8

Merged dataset:
C:\BH2\Jairo\Samples-IRR-6-2015\JG-P3-41\JG-P3-41.ftz
C:\BH2\Jairo\Samples-IRR-6-2015\JG-P3-41\JG-P3-41a.ftz

NEW PARAMETERS - ZETA METHOD

EFFECTIVE TRACK DENSITY FOR FLUENCE MONITOR (tracks/cm^2): 2,72E+05
RELATIVE ERROR (%): 1,36
EFFECTIVE URANIUM CONTENT OF MONITOR (ppm): 50,00
ZETA FACTOR AND STANDARD ERROR (yr cm^2): 137,95 4,04
SIZE OF COUNTER SQUARE (cm^2): 8,30E-07

Grain no.	RhoS (cm^-2)	(Ns)	RhoI (cm^-2)	(Ni)	Squares	U+/-2s	Grain Age (Ma) Age	--95% CI--	
29	4,90E+06	(61)	6,43E+05	(8)	15	118 81	139.0	67.8	337.2
30	8,01E+06	(133)	1,08E+06	(18)	20	199 93	136.0	83.7	236.7
31	1,14E+07	(85)	1,34E+06	(10)	9	246 152	155.2	82.0	335.6
32	7,83E+06	(104)	8,28E+05	(11)	16	152 90	172.6	94.3	356.2
33	5,00E+06	(83)	6,02E+05	(10)	20	111 68	151.6	80.0	328.2
34	1,11E+07	(120)	2,50E+06	(27)	13	460 176	82.4	54.2	130.4
35	1,25E+07	(104)	1,81E+06	(15)	10	332 169	127.5	74.8	236.4
36	6,93E+06	(161)	2,41E+06	(56)	28	443 119	53.6	39.4	74.1
37	9,88E+06	(82)	2,05E+06	(17)	10	377 180	89.1	52.9	160.8
38	9,75E+06	(89)	1,97E+06	(18)	11	363 169	91.4	55.1	161.6
39	1,11E+07	(211)	1,15E+06	(22)	23	212 90	176.2	114.6	286.9
40	1,20E+07	(90)	2,14E+06	(16)	9	394 194	103.7	61.2	189.7
41	1,21E+07	(241)	1,31E+06	(26)	24	240 94	170.5	114.6	266.2
42	1,45E+07	(325)	1,38E+06	(31)	27	254 91	192.7	134.2	287.9
43	1,07E+07	(80)	1,20E+06	(9)	9	222 144	162.0	82.9	367.2
44	1,22E+07	(91)	1,07E+06	(8)	9	197 135	206.0	102.9	490.0
45	1,26E+07	(125)	1,81E+06	(18)	12	332 155	127.9	78.5	223.1
46	6,53E+06	(65)	7,03E+05	(7)	12	129 94	168.3	79.3	435.3
47	1,02E+07	(178)	1,15E+06	(20)	21	211 93	163.6	103.9	274.1
48	1,29E+07	(107)	1,57E+06	(13)	10	288 157	150.8	85.9	292.7
49	1,23E+07	(133)	1,11E+06	(12)	13	205 116	202.0	114.0	399.9
POOLED	1,01E+07	(6616)	1,26E+06	(821)	786	231 17	149.3	135.8	164.2

CHI^2 PROBABILITY (%): 0.0

POOLED AGE W/ 68% CONF. INTERVAL(Ma): 149.3, 142.2 -- 156.7 (-7.1 +7.4)
95% CONF. INTERVAL(Ma): 135.8 -- 164.2 (-13.5 +14.9)

CENTRAL AGE W/ 68% CONF. INTERVAL(Ma): 144.4, 135.2 -- 154.2 (-9.2 +9.8)
95% CONF. INTERVAL(Ma): 126.9 -- 164.2 (-17.5 +19.8)
AGE DISPERSION (%): 30.7

Merged dataset:
C:\BH2\Jairo\Samples-IRR-6-2015\JG-P3-41\JG-P3-41.ftz
C:\BH2\Jairo\Samples-IRR-6-2015\JG-P3-41\JG-P3-41a.ftz

FIT OPTION: Best-fit peaks using the binomial model of Galbraith and Green

INITIAL GUESS FOR MODEL PARAMETERS (number of peaks to fit = 2)

Peak #.	Peak Age	Theta	Fraction(%)	Count
1.	87.90	0.825	19.2	9.41
2.	149.40	0.890	39.1	19.15

Total range for grain ages: 53,4 to 354,1 Ma
Number of active grains (Num. used for fit): 49
Number of removed grains: 0
Degrees of freedom for fit: 46
Average of the SE(Z)'s for the grains: 0,28
Estimated width of peaks in PD plot in Z units: 0,32

PARAMETERS FOR BEST-FIT PEAKS

* *Standard error for peak age includes group error*
* *Peak width is for PD plot assuming a kernel factor = 0.60*

#.	Peak Age(Ma)	68%CI	95%CI	W(Z)	Frac(%)	SE,%	Count
1.	81.7	-11,2 ...+13,0	-20,6 ...+27,5	0.27	15.3	9.7	7.5
2.	167.8	-10,4 ...+11,1	-19,8 ...+22,4	0.31	84.7	9.7	41.5

Log-likelihood for best fit: -151,620
Chi-squared value for best fit: 45,840
Reduced chi-squared value: 0,997
Probability for F test: 0%
Condition number for COVAR matrix: 14,57
Number of iterations: 16

Merged dataset:
C:\BH2\Jairo\Samples-IRR-6-2015\JG-P3-41\JG-P3-41.ftz
C:\BH2\Jairo\Samples-IRR-6-2015\JG-P3-41\JG-P3-41a.ftz

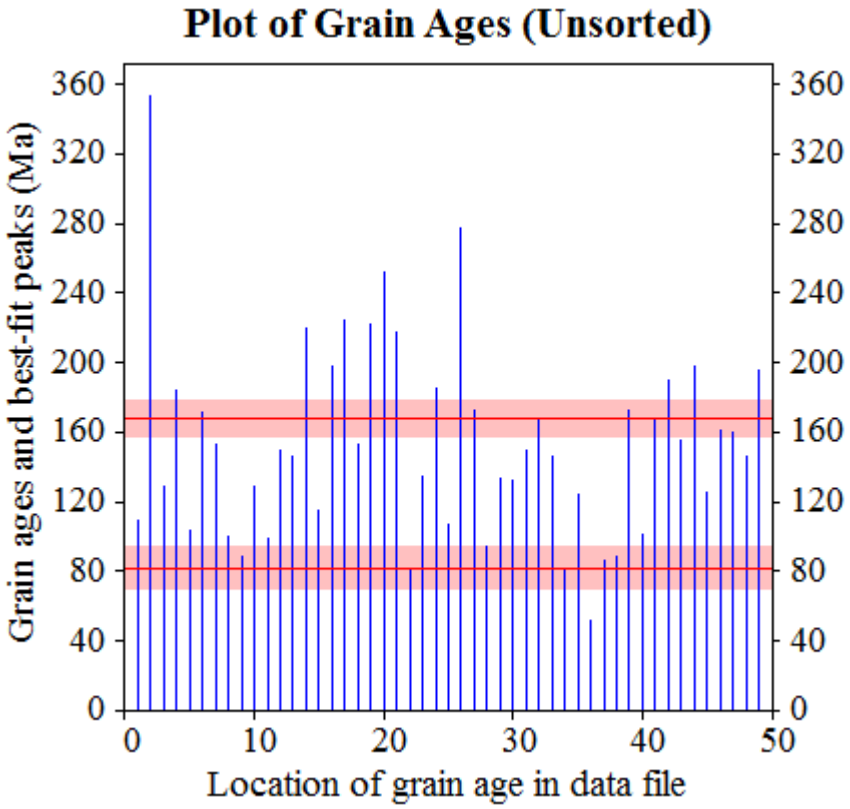

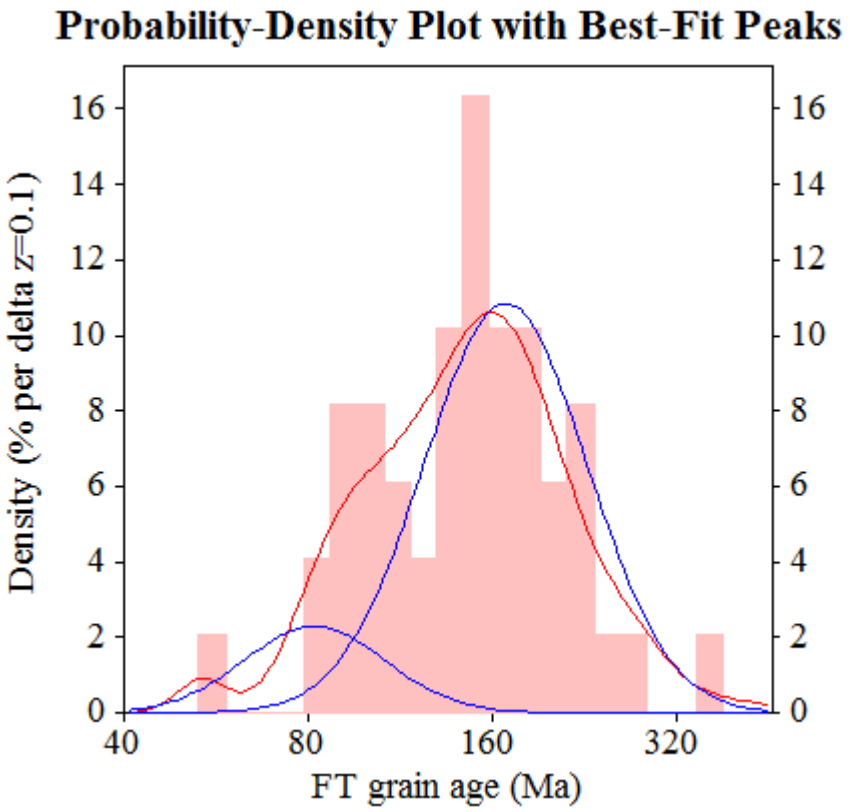

Merged dataset:
C:\BH2\Jairo\Samples-IRR-6-2015\JG-P3-41\JG-P3-41.ftz
C:\BH2\Jairo\Samples-IRR-6-2015\JG-P3-41\JG-P3-41a.ftz

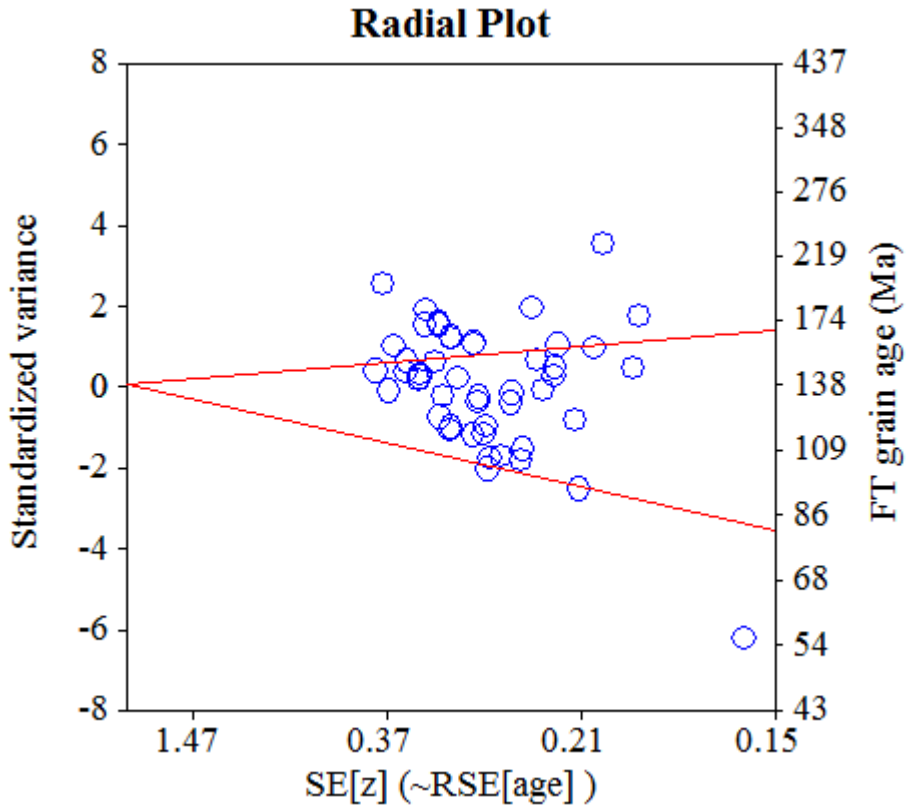

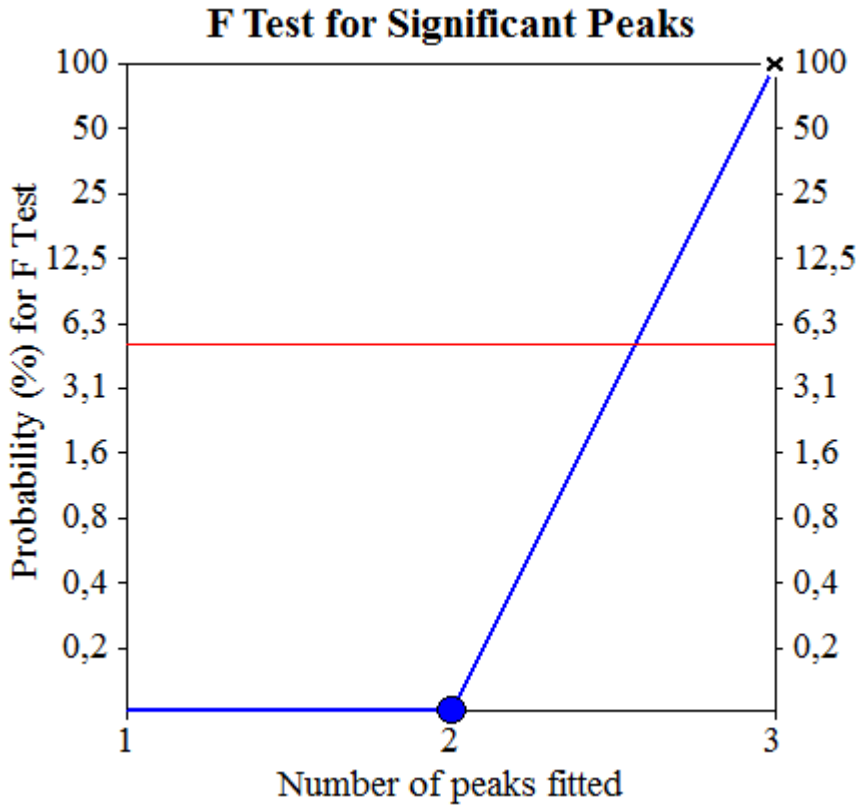

Merged dataset:
C:\BH2\Jairo\Samples-IRR-6-2015\JG-P3-15\JG-P3-15.ftz
C:\BH2\Jairo\Samples-IRR-6-2015\JG-P3-15\JG-P3-15a.ftz

NEW PARAMETERS - ZETA METHOD

EFFECTIVE TRACK DENSITY FOR FLUENCE MONITOR (tracks/cm^2): 2,73E+05
RELATIVE ERROR (%): 1,22
EFFECTIVE URANIUM CONTENT OF MONITOR (ppm): 50,00
ZETA FACTOR AND STANDARD ERROR (yr cm^2): 137,95 4,04
SIZE OF COUNTER SQUARE (cm^2): 8,30E-07

GRAIN AGES IN ORIGINAL ORDER

Grain no.	RhoS (cm^-2)	(Ns)	RhoI (cm^-2)	(Ni)	Squares	U+/-2s	Grain Age (Ma) Age	--95% CI--	
1	1,11E+07	(101)	1,53E+06	(14)	11	281 148	133.2	76.9	252.7
2	9,20E+06	(84)	1,53E+06	(14)	11	281 148	111.0	63.4	212.2
3	6,91E+06	(109)	1,52E+06	(24)	19	279 113	84.6	54.4	137.9
4	9,74E+06	(97)	2,71E+06	(27)	12	496 190	67.1	43.6	107.1
5	1,55E+07	(116)	2,41E+06	(18)	9	441 205	119.4	73.1	208.8
6	6,43E+06	(80)	9,64E+05	(12)	15	176 100	123.0	67.7	248.5
7	1,21E+07	(171)	1,56E+06	(22)	17	285 121	143.9	92.9	235.7
8	8,37E+06	(125)	1,14E+06	(17)	18	208 100	136.0	82.6	241.0
9	7,53E+06	(100)	1,13E+06	(15)	16	207 105	123.3	72.2	228.8
10	1,45E+07	(132)	2,41E+06	(22)	11	441 186	111.4	71.2	184.0
11	1,28E+07	(127)	1,51E+06	(15)	12	276 140	156.1	92.4	287.1
12	7,61E+06	(101)	1,20E+06	(16)	16	221 109	116.9	69.4	212.6
13	3,37E+06	(84)	6,83E+05	(17)	30	125 60	91.7	54.6	165.3
14	9,10E+06	(68)	1,47E+06	(11)	9	270 159	114.0	60.9	239.9
15	4,34E+06	(54)	1,61E+06	(20)	15	294 130	50.4	29.9	89.2
16	1,50E+07	(249)	2,05E+06	(34)	20	375 128	136.0	95.4	200.8
17	1,13E+07	(299)	1,28E+06	(34)	32	234 80	162.9	114.9	239.5
18	6,69E+06	(100)	1,54E+06	(23)	18	282 116	81.0	51.4	133.8
19	8,43E+06	(70)	2,77E+06	(23)	10	507 210	56.8	35.2	95.6
20	1,28E+07	(106)	1,93E+06	(16)	10	353 174	122.6	73.0	222.6
21	1,17E+07	(97)	1,81E+06	(15)	10	331 168	119.6	69.9	222.3
22	1,51E+07	(125)	2,05E+06	(17)	10	375 179	136.0	82.6	241.0
23	8,11E+06	(101)	1,37E+06	(17)	15	250 120	110.1	66.2	196.8
24	1,28E+07	(106)	1,69E+06	(14)	10	309 162	139.7	80.8	264.5
25	8,43E+06	(105)	1,20E+06	(15)	15	221 112	129.4	75.9	239.7
26	1,38E+07	(137)	1,71E+06	(17)	12	312 150	148.9	90.7	263.0
27	1,32E+07	(131)	1,20E+06	(12)	12	221 125	200.1	112.8	396.1

Merged dataset:
C:\BH2\Jairo\Samples-IRR-6-2015\JG-P3-15\JG-P3-15.ftz
C:\BH2\Jairo\Samples-IRR-6-2015\JG-P3-15\JG-P3-15a.ftz

NEW PARAMETERS - ZETA METHOD

EFFECTIVE TRACK DENSITY FOR FLUENCE MONITOR (tracks/cm^2): 2,73E+05
RELATIVE ERROR (%): 1,24
EFFECTIVE URANIUM CONTENT OF MONITOR (ppm): 50,00
ZETA FACTOR AND STANDARD ERROR (yr cm^2): 137,95 4,04
SIZE OF COUNTER SQUARE (cm^2): 8,30E-07

Grain no.	RhoS (cm^-2)	(Ns)	RhoI (cm^-2)	(Ni)	Squares	U+/-2s	Grain Age (Ma) Age	--95% CI--	
28	8,20E+06	(143)	5,16E+05	(9)	21	95 61	287.9	151.5	636.1
29	1,23E+07	(184)	8,03E+05	(12)	18	147 83	279.2	159.4	546.0
30	1,26E+07	(94)	1,74E+06	(13)	9	319 174	133.4	75.5	260.2
31	8,06E+06	(107)	1,05E+06	(14)	16	193 101	141.0	81.6	266.9
32	1,18E+07	(167)	1,28E+06	(18)	17	233 109	171.1	106.3	295.6
33	7,56E+06	(138)	1,48E+06	(27)	22	271 103	95.1	63.1	149.8
34	1,05E+07	(87)	8,43E+05	(7)	10	154 113	225.3	108.0	573.7
35	9,54E+06	(95)	1,51E+06	(15)	12	276 140	117.2	68.4	218.0
36	1,11E+07	(92)	1,57E+06	(13)	10	287 156	130.6	73.8	255.0
37	1,37E+07	(193)	7,80E+05	(11)	17	143 84	318.1	178.1	640.8
38	1,25E+07	(83)	1,66E+06	(11)	8	303 179	138.9	75.0	289.4
39	1,04E+07	(241)	9,47E+05	(22)	28	173 73	201.9	131.8	327.4
40	8,50E+06	(127)	1,07E+06	(16)	18	196 97	146.6	88.0	264.3
41	6,59E+06	(82)	9,64E+05	(12)	15	176 100	126.1	69.5	254.4
42	8,73E+06	(87)	7,03E+05	(7)	12	129 94	225.3	108.0	573.7
43	9,52E+06	(79)	1,45E+06	(12)	10	265 150	121.5	66.8	245.6
44	8,89E+06	(155)	1,09E+06	(19)	21	200 90	150.8	94.4	257.2
45	9,47E+06	(110)	6,88E+05	(8)	14	126 86	249.4	125.7	587.8
46	8,52E+06	(99)	1,29E+06	(15)	14	236 120	122.1	71.4	226.7
47	1,32E+07	(131)	2,01E+06	(20)	12	368 163	121.4	76.2	205.5
48	1,51E+07	(250)	1,27E+06	(21)	20	232 100	219.0	141.9	358.9
49	8,84E+06	(110)	8,03E+05	(10)	15	147 91	201.1	107.6	429.9
50	1,05E+07	(113)	1,48E+06	(16)	13	271 134	130.6	78.0	236.5
51	6,67E+06	(277)	1,64E+06	(68)	50	300 73	75.8	57.8	99.2
52	8,56E+06	(199)	1,29E+06	(30)	28	236 86	123.2	84.2	187.6
53	1,16E+07	(116)	1,10E+06	(11)	12	202 119	193.2	106.1	396.9
54	1,42E+07	(189)	1,51E+06	(20)	16	276 122	174.4	111.0	291.7
55	1,10E+07	(220)	1,46E+06	(29)	24	266 98	140.7	96.0	215.0
56	1,01E+07	(101)	1,41E+06	(14)	12	257 135	133.2	76.9	252.7
57	1,30E+07	(151)	1,29E+06	(15)	14	236 120	185.2	110.4	338.5
58	6,78E+06	(90)	1,51E+06	(20)	16	276 122	83.7	51.6	143.9
59	1,47E+07	(219)	1,14E+06	(17)	18	208 100	236.2	146.4	411.2
60	1,15E+07	(143)	1,61E+06	(20)	15	294 130	132.4	83.5	223.5
61	7,43E+06	(185)	1,00E+06	(25)	30	184 73	137.2	90.8	217.5
POOLED	9,85E+06	(8032)	1,35E+06	(1098)	982	247 16	136.3	124.9	148.8

CHI^2 PROBABILITY (%): 0.0

POOLED AGE W/ 68% CONF. INTERVAL(Ma): 136.3, 130.4 -- 142.6 (-6.0 +6.2)
95% CONF. INTERVAL(Ma): 124.9 -- 148.8 (-11.4 +12.5)

CENTRAL AGE W/ 68% CONF. INTERVAL(Ma): 134.0, 126.7 -- 141.8 (-7.3 +7.8)
95% CONF. INTERVAL(Ma): 120.0 -- 149.6 (-14.0 +15.6)
AGE DISPERSION (%): 26.4

Merged dataset:
C:\BH2\Jairo\Samples-IRR-6-2015\JG-P3-15\JG-P3-15.ftz
C:\BH2\Jairo\Samples-IRR-6-2015\JG-P3-15\JG-P3-15a.ftz

FIT OPTION: Best-fit peaks using the binomial model of Galbraith and Green

INITIAL GUESS FOR MODEL PARAMETERS (number of peaks to fit = 2)

Peak #.	Peak Age	Theta	Fraction(%)	Count
1.	136.30	0.880	49.0	29.91
2.	221.70	0.923	14.1	8.59

Total range for grain ages: 49,9 to 309,5 Ma
Number of active grains (Num. used for fit): 61
Number of removed grains: 0
Degrees of freedom for fit: 58
Average of the SE(Z)'s for the grains: 0,27
Estimated width of peaks in PD plot in Z units: 0,31

PARAMETERS FOR BEST-FIT PEAKS

* *Standard error for peak age includes group error*
* *Peak width is for PD plot assuming a kernel factor = 0.60*

#.	Peak Age(Ma)	68%CI	95%CI	W(Z)	Frac(%)	SE,%	Count
1.	77.5	-8,0 ...+8,9	-14,9 ...+18,4	0.25	13.4	5.8	8.2
2.	151.4	-7,4 ...+7,8	-14,2 ...+15,7	0.30	86.6	5.8	52.8

Log-likelihood for best fit: -187,110
Chi-squared value for best fit: 61,232
Reduced chi-squared value: 1,056
Probability for F test: 0%
Condition number for COVAR matrix: 8,62
Number of iterations: 44

Merged dataset:
C:\BH2\Jairo\Samples-IRR-6-2015\JG-P3-15\JG-P3-15.ftz
C:\BH2\Jairo\Samples-IRR-6-2015\JG-P3-15\JG-P3-15a.ftz

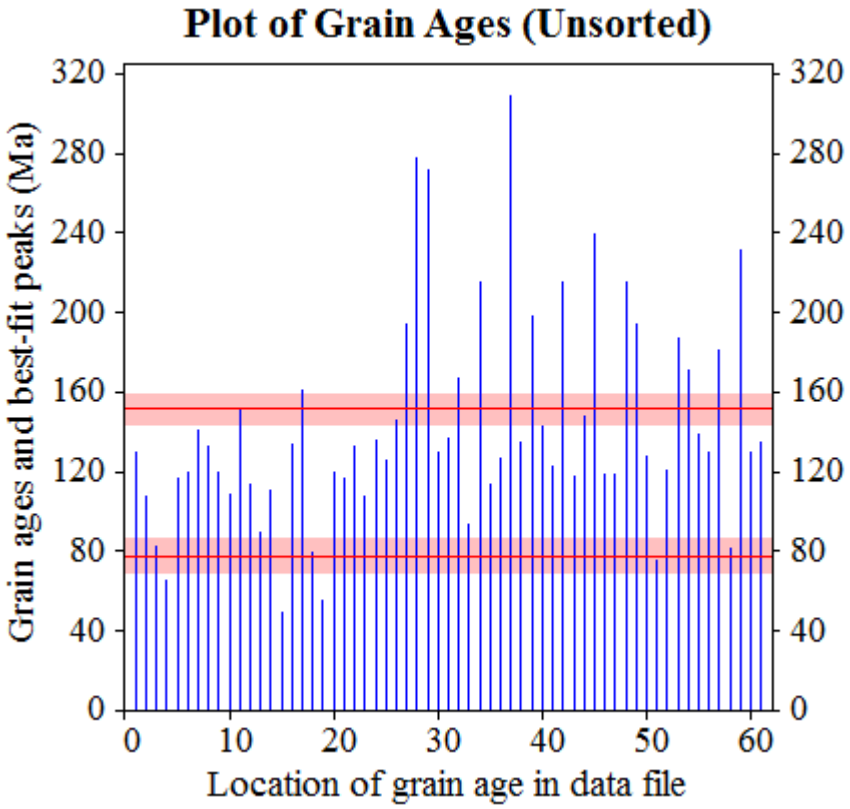

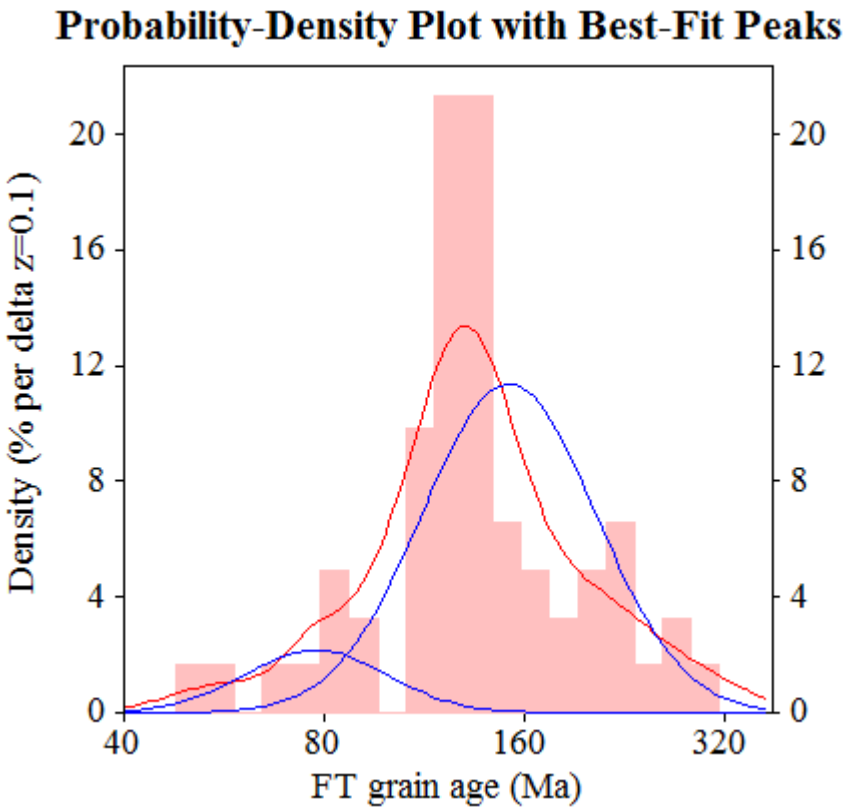

Merged dataset:
C:\BH2\Jairo\Samples-IRR-6-2015\JG-P3-15\JG-P3-15.ftz
C:\BH2\Jairo\Samples-IRR-6-2015\JG-P3-15\JG-P3-15a.ftz

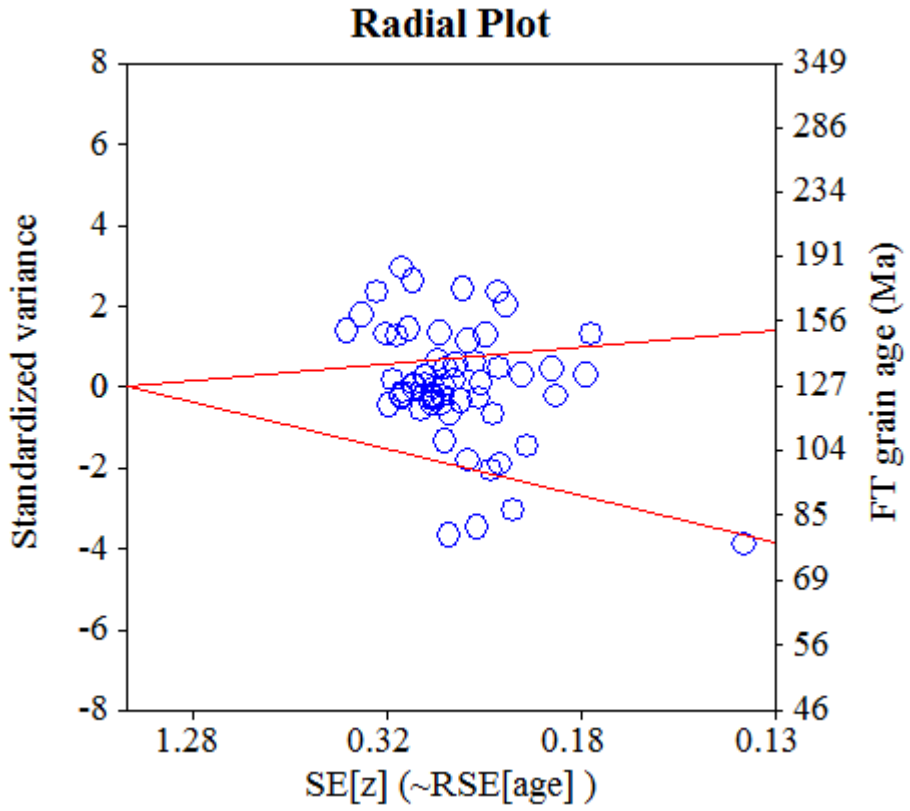

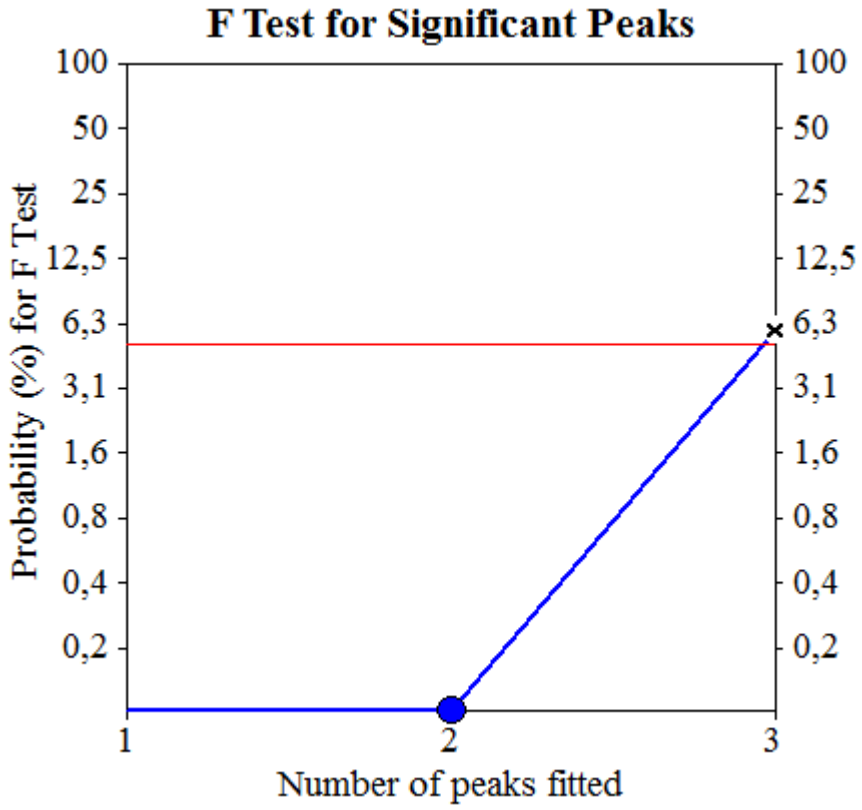

Merged dataset:
C:\BH2\Jairo\Echantillon-IRR-10-2015\JG-P3-04-Zr\JG-P3-04.ftz
C:\BH2\Jairo\Echantillon-IRR-10-2015\JG-P3-04-Zr\JG-P3-04a.ftz

NEW PARAMETERS - ZETA METHOD

EFFECTIVE TRACK DENSITY FOR FLUENCE MONITOR (tracks/cm^2): 3,84E+05
RELATIVE ERROR (%): 1,14
EFFECTIVE URANIUM CONTENT OF MONITOR (ppm): 50,00
ZETA FACTOR AND STANDARD ERROR (yr cm^2): 137,14 1,57
SIZE OF COUNTER SQUARE (cm^2): 8,30E-07

GRAIN AGES IN ORIGINAL ORDER

Grain no.	RhoS (cm^-2)	(Ns)	RhoI (cm^-2)	(Ni)	Squares	U+/-2s		Grain Age (Ma) Age	--95% CI--	
1	6,69E+06	(111)	1,27E+06	(21)	20	165	71	136.8	86.1	229.6
2	7,41E+06	(123)	1,75E+06	(29)	20	228	84	110.2	73.5	171.4
3	5,93E+06	(123)	2,75E+06	(57)	25	358	95	56.5	41.0	78.8
4	6,63E+06	(121)	2,19E+06	(40)	22	285	90	78.9	55.0	115.9
5	5,27E+06	(175)	1,60E+06	(53)	40	208	57	86.2	63.2	119.5
6	4,79E+06	(167)	1,61E+06	(56)	42	209	56	77.9	57.4	107.4
7	6,88E+06	(120)	1,72E+06	(30)	21	224	81	104.0	69.7	160.9
8	1,00E+07	(200)	1,36E+06	(27)	24	177	67	191.1	128.7	296.6
9	9,50E+06	(276)	2,13E+06	(62)	35	278	71	115.2	87.6	151.5
10	5,68E+06	(212)	1,18E+06	(44)	45	153	46	125.2	90.6	177.4
11	3,21E+06	(112)	1,49E+06	(52)	42	194	54	56.4	40.3	79.9
12	8,54E+06	(163)	1,57E+06	(30)	23	205	74	140.8	95.7	215.3
13	5,59E+06	(232)	7,23E+05	(30)	50	94	34	199.5	137.2	301.6
14	7,47E+06	(124)	1,81E+06	(30)	20	235	85	107.5	72.1	166.0
15	9,64E+06	(280)	1,79E+06	(52)	35	233	65	139.9	104.2	191.7
16	1,14E+07	(133)	1,64E+06	(19)	14	213	97	180.4	112.4	308.4
17	4,59E+06	(61)	1,51E+06	(20)	16	196	87	79.4	47.6	139.1
18	6,61E+06	(181)	6,94E+05	(19)	33	90	41	244.2	154.1	413.0
19	7,58E+06	(151)	1,51E+06	(30)	24	196	71	130.6	88.4	200.2
20	6,63E+06	(88)	1,05E+06	(14)	16	137	72	161.8	92.9	307.7
21	8,65E+06	(79)	1,20E+06	(11)	11	157	93	184.0	99.3	382.6
22	8,12E+06	(128)	9,51E+05	(15)	19	124	63	218.7	129.8	400.6
23	9,73E+06	(105)	1,76E+06	(19)	13	229	104	142.9	88.0	246.6
24	6,10E+06	(76)	2,01E+06	(25)	15	262	104	79.2	50.1	130.0
25	1,20E+07	(120)	1,51E+06	(15)	12	196	100	205.3	121.5	376.9
26	9,90E+06	(115)	1,38E+06	(16)	14	179	88	184.9	110.7	333.5
27	4,42E+06	(132)	7,36E+05	(22)	36	96	40	155.1	99.2	255.6
28	4,06E+06	(101)	7,23E+05	(18)	30	94	44	145.0	88.2	254.3
29	5,94E+06	(138)	1,08E+06	(25)	28	140	56	142.9	93.7	228.4
30	4,42E+06	(132)	2,95E+06	(88)	36	384	82	39.2	29.9	51.3
31	7,97E+06	(172)	8,80E+05	(19)	26	115	52	232.3	146.3	393.5
32	3,55E+06	(118)	1,99E+06	(66)	40	259	64	46.8	34.4	64.4
33	3,82E+06	(130)	1,12E+06	(38)	41	145	47	89.2	62.0	131.7
34	7,85E+06	(176)	2,01E+06	(45)	27	262	78	101.9	73.4	144.7
35	6,22E+06	(62)	1,00E+06	(10)	12	131	81	159.0	82.5	347.7
36	1,03E+07	(94)	1,75E+06	(16)	11	228	113	151.6	89.8	275.8
37	5,70E+06	(142)	8,03E+05	(20)	30	105	46	183.0	115.5	308.0
38	7,72E+06	(173)	8,48E+05	(19)	27	110	50	233.6	147.1	395.6
39	5,00E+06	(112)	1,74E+06	(39)	27	227	72	75.0	51.8	110.9
40	5,30E+06	(154)	9,64E+05	(28)	35	126	47	142.5	95.6	221.3
41	5,69E+06	(85)	1,07E+06	(16)	18	139	69	137.2	80.8	250.9
42	6,37E+06	(317)	6,63E+05	(33)	60	86	30	247.0	173.9	363.6
43	4,31E+06	(143)	5,42E+05	(18)	40	71	33	204.2	126.4	353.3
44	5,12E+06	(102)	6,02E+05	(12)	24	78	44	217.4	121.5	432.6
45	2,79E+06	(139)	7,63E+05	(38)	60	99	32	95.3	66.4	140.3
46	5,02E+06	(125)	1,93E+06	(48)	30	251	72	68.1	48.6	97.1

Merged dataset:
C:\BH2\Jairo\Echantillon-IRR-10-2015\JG-P3-04-Zr\JG-P3-04.ftz
C:\BH2\Jairo\Echantillon-IRR-10-2015\JG-P3-04-Zr\JG-P3-04a.ftz

NEW PARAMETERS - ZETA METHOD

EFFECTIVE TRACK DENSITY FOR FLUENCE MONITOR (tracks/cm^2): 3,84E+05
RELATIVE ERROR (%): 1,14
EFFECTIVE URANIUM CONTENT OF MONITOR (ppm): 50,00
ZETA FACTOR AND STANDARD ERROR (yr cm^2): 137,14 1,57
SIZE OF COUNTER SQUARE (cm^2): 8,30E-07

Grain no.	RhoS (cm^-2)	(Ns)	RhoI (cm^-2)	(Ni)	Squares	U+/-2s	Grain Age (Ma) Age	--95% CI--	
47	5,75E+06	(167)	3,41E+06	(99)	35	443 89	44.1	34.4	56.6
48	1,10E+07	(146)	1,58E+06	(21)	16	206 89	179.5	114.4	298.2
49	7,12E+06	(65)	1,64E+06	(15)	11	214 109	112.3	64.1	212.2
50	8,43E+06	(84)	1,51E+06	(15)	12	196 100	144.7	84.0	269.8
51	9,24E+06	(161)	1,78E+06	(31)	21	231 83	134.9	92.0	205.0
52	1,20E+07	(120)	1,51E+06	(15)	12	196 100	205.6	121.6	377.4
53	9,64E+06	(128)	1,58E+06	(21)	16	206 89	157.7	99.9	263.2
54	8,02E+06	(213)	1,32E+06	(35)	32	171 58	157.8	110.8	232.4
55	4,75E+06	(142)	8,37E+05	(25)	36	109 43	147.2	96.6	235.0
56	7,21E+06	(323)	8,03E+05	(36)	54	104 35	231.3	165.0	335.1
57	7,80E+06	(233)	9,71E+05	(29)	36	126 47	207.4	141.9	315.6
58	1,08E+07	(171)	1,90E+06	(30)	19	247 90	147.9	100.6	225.7
59	8,15E+06	(142)	1,32E+06	(23)	21	172 71	159.8	103.4	259.9
60	4,16E+06	(145)	1,86E+06	(65)	42	243 60	58.1	43.4	77.8
61	5,05E+06	(155)	8,14E+05	(25)	37	106 42	160.5	105.7	255.4
62	1,13E+07	(150)	2,64E+06	(35)	16	343 115	111.6	77.2	166.2
63	6,77E+06	(236)	9,75E+05	(34)	42	127 43	179.7	126.0	265.1
64	7,44E+06	(173)	8,61E+05	(20)	28	112 50	222.5	141.5	371.9
65	9,44E+06	(94)	1,31E+06	(13)	12	170 92	185.8	105.3	361.1
66	4,82E+06	(144)	9,04E+05	(27)	36	118 45	138.4	92.0	217.1
67	6,87E+06	(228)	7,53E+05	(25)	40	98 39	234.7	156.7	368.8
68	1,02E+07	(135)	2,03E+06	(27)	16	264 101	129.8	86.1	204.2
69	5,98E+06	(149)	1,12E+06	(28)	30	146 55	138.1	92.5	214.8
70	6,15E+06	(143)	7,31E+05	(17)	28	95 46	216.2	132.3	380.0
71	6,73E+06	(134)	1,00E+06	(20)	24	131 58	173.0	108.9	291.9
72	8,65E+06	(280)	1,30E+06	(42)	39	169 52	172.8	125.4	244.7
73	6,22E+06	(62)	1,31E+06	(13)	12	170 92	123.3	68.0	244.6
74	5,69E+06	(151)	1,20E+06	(32)	32	157 55	122.7	83.9	185.7
75	9,64E+06	(120)	1,69E+06	(21)	15	219 95	147.9	93.5	247.6
76	8,20E+06	(143)	1,20E+06	(21)	21	157 68	175.9	112.0	292.3
77	3,10E+06	(90)	8,61E+05	(25)	35	112 44	93.8	60.0	152.6
78	6,10E+06	(152)	7,23E+05	(18)	30	94 44	217.1	134.7	374.8
79	7,86E+06	(150)	1,47E+06	(28)	23	191 72	139.0	93.1	216.1
80	5,86E+06	(175)	8,03E+05	(24)	36	104 42	188.3	123.7	301.1
81	4,37E+06	(127)	1,31E+06	(38)	35	170 55	87.2	60.6	128.9
82	8,10E+06	(121)	1,54E+06	(23)	18	200 83	136.4	87.6	223.3
83	1,19E+07	(138)	1,89E+06	(22)	14	246 104	162.3	104.0	267.0
84	6,22E+06	(93)	2,01E+06	(30)	18	261 95	80.9	53.4	126.6
85	5,62E+06	(56)	1,81E+06	(18)	12	235 109	81.0	47.3	146.6
86	5,06E+06	(63)	2,09E+06	(26)	15	272 106	63.3	39.7	104.3
87	2,76E+06	(94)	6,17E+05	(21)	41	80 35	116.2	72.5	196.5
88	5,69E+06	(85)	1,41E+06	(21)	18	183 79	105.2	65.2	178.8
89	5,35E+06	(80)	1,61E+06	(24)	18	209 85	86.9	54.8	143.5
90	4,63E+06	(96)	1,93E+06	(40)	25	251 79	62.8	43.1	93.3
91	4,37E+06	(116)	1,47E+06	(39)	32	191 61	77.7	53.9	114.8
92	5,90E+06	(98)	7,83E+05	(13)	20	102 55	193.6	110.0	375.5
93	6,11E+06	(137)	8,92E+05	(20)	27	116 51	176.9	111.4	298.0
94	4,43E+06	(147)	7,53E+05	(25)	40	98 39	152.3	100.1	242.8
POOLED	6,31E+06	(13278)	1,30E+06	(2747)	2537	170 8	126.0	119.7	132.6

Merged dataset:
C:\BH2\Jairo\Echantillon-IRR-10-2015\JG-P3-04-Zr\JG-P3-04.ftz
C:\BH2\Jairo\Echantillon-IRR-10-2015\JG-P3-04-Zr\JG-P3-04a.ftz

```
CHI^2 PROBABILITY (%):  0.0

 POOLED AGE W/  68% CONF. INTERVAL(Ma):  126.0, 122.7 -- 129.3 ( -3.3  +3.3)
                95% CONF. INTERVAL(Ma):         119.7 -- 132.6 ( -6.3  +6.6)

CENTRAL AGE W/  68% CONF. INTERVAL(Ma):  124.5, 118.3 -- 131.0 ( -6.2  +6.5)
                95% CONF. INTERVAL(Ma):         112.6 -- 137.6 (-11.9 +13.1)
                    AGE DISPERSION (%):   42.7
```

Merged dataset:
C:\BH2\Jairo\Echantillon-IRR-10-2015\JG-P3-04-Zr\JG-P3-04.ftz
C:\BH2\Jairo\Echantillon-IRR-10-2015\JG-P3-04-Zr\JG-P3-04a.ftz

FIT OPTION: Best-fit peaks using the binomial model of Galbraith and Green

INITIAL GUESS FOR MODEL PARAMETERS (number of peaks to fit = 3)

Peak #.	Peak Age	Theta	Fraction(%)	Count
1.	43.90	0.626	4.4	4.18
2.	125.90	0.828	31.3	29.39
3.	175.00	0.871	34.2	32.11

Total range for grain ages:	39,3 to 244,8 Ma
Number of active grains (Num. used for fit):	94
Number of removed grains:	0
Degrees of freedom for fit:	89
Average of the SE(Z)'s for the grains:	0,22
Estimated width of peaks in PD plot in Z units:	0,26

PARAMETERS FOR BEST-FIT PEAKS

* *Standard error for peak age includes group error*
* *Peak width is for PD plot assuming a kernel factor = 0.60*

#.	Peak Age(Ma)	68%CI	95%CI	W(Z)	Frac(%)	SE,%	Count
1.	50.9	-3,6 ...+3,8	-6,8 ...+7,8	0.18	7.9	3.3	7.4
2.	92.2	-6,8 ...+7,4	-12,9 ...+15,0	0.23	25.2	6.1	23.7
3.	168.3	-6,4 ...+6,6	-12,3 ...+13,2	0.26	66.9	6.5	62.9

Log-likelihood for best fit:	-338,780
Chi-squared value for best fit:	90,577
Reduced chi-squared value:	1,018
Probability for F test:	1%
Condition number for COVAR matrix:	9,71
Number of iterations:	20

Merged dataset:
C:\BH2\Jairo\Echantillon-IRR-10-2015\JG-P3-04-Zr\JG-P3-04.ftz
C:\BH2\Jairo\Echantillon-IRR-10-2015\JG-P3-04-Zr\JG-P3-04a.ftz

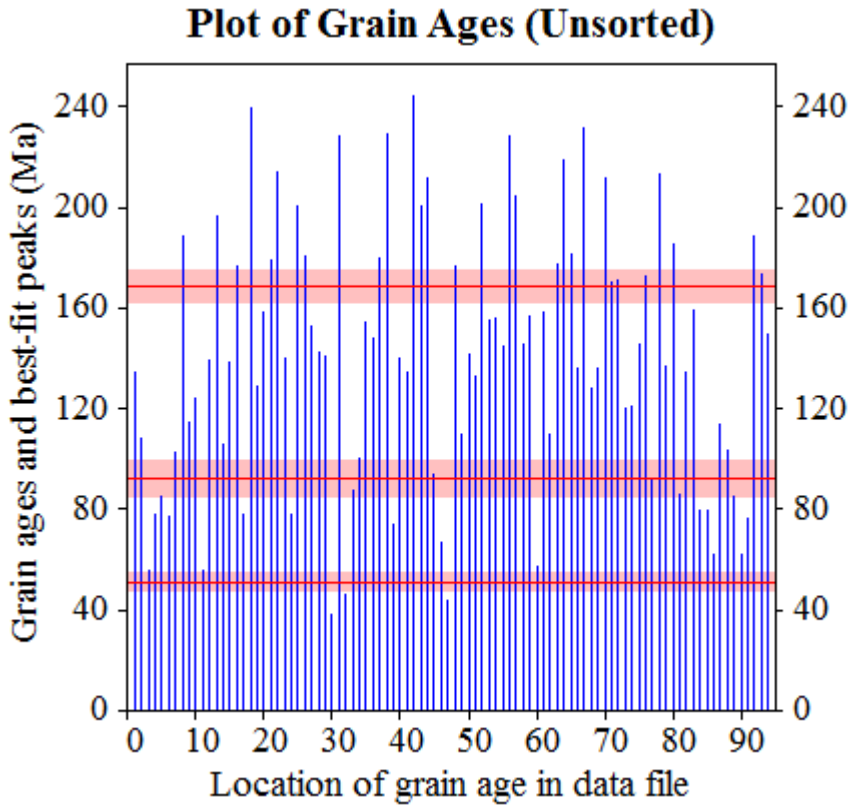

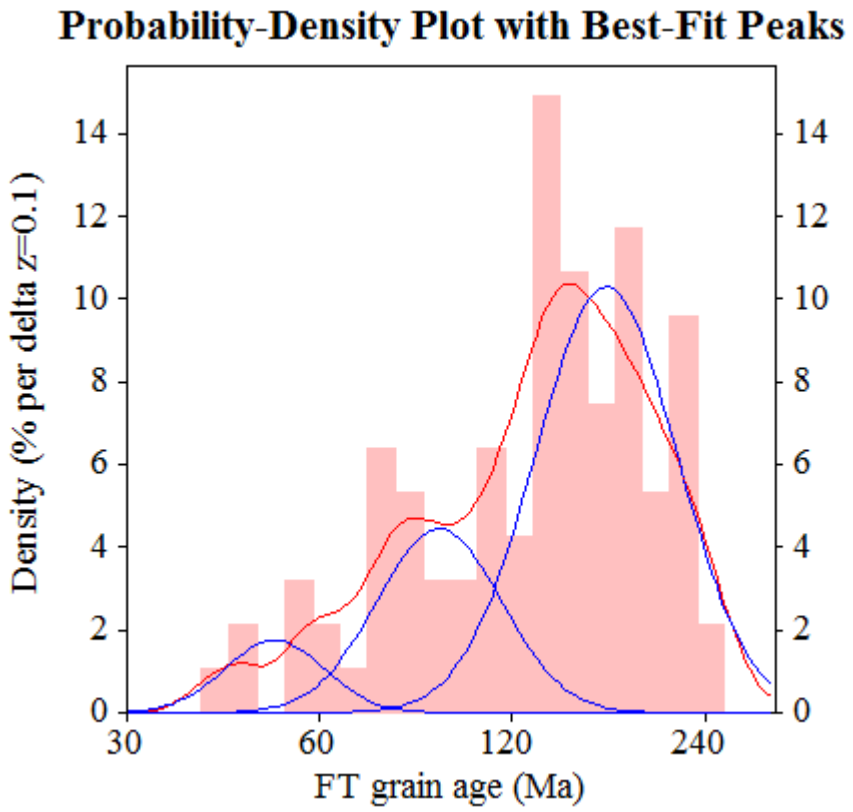

Merged dataset:
C:\BH2\Jairo\Echantillon-IRR-10-2015\JG-P3-04-Zr\JG-P3-04.ftz
C:\BH2\Jairo\Echantillon-IRR-10-2015\JG-P3-04-Zr\JG-P3-04a.ftz

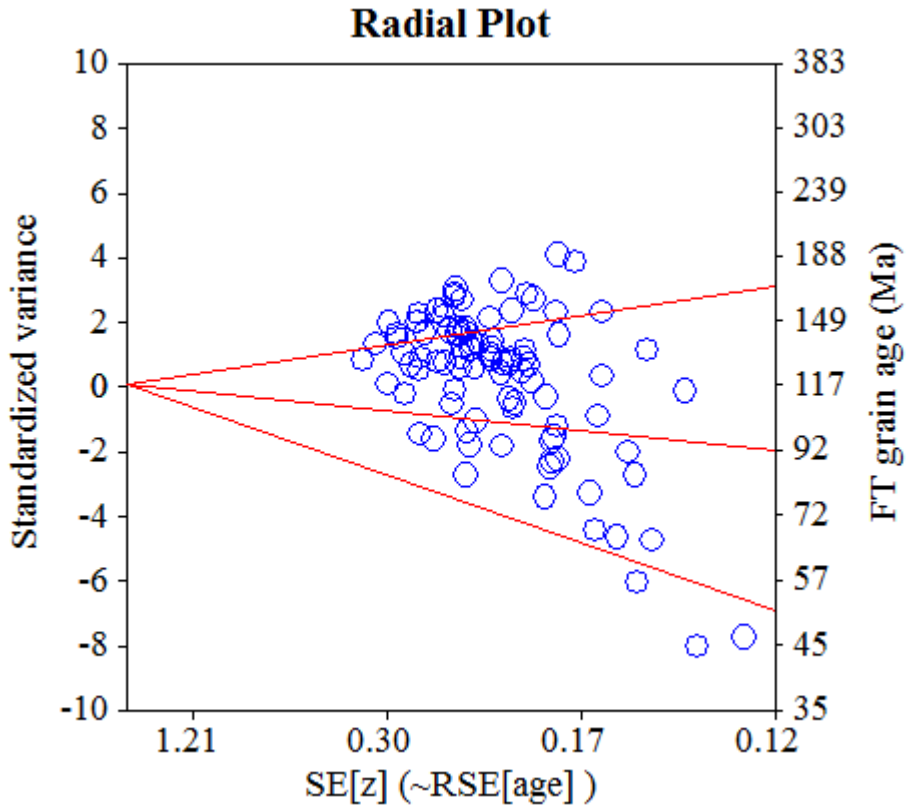

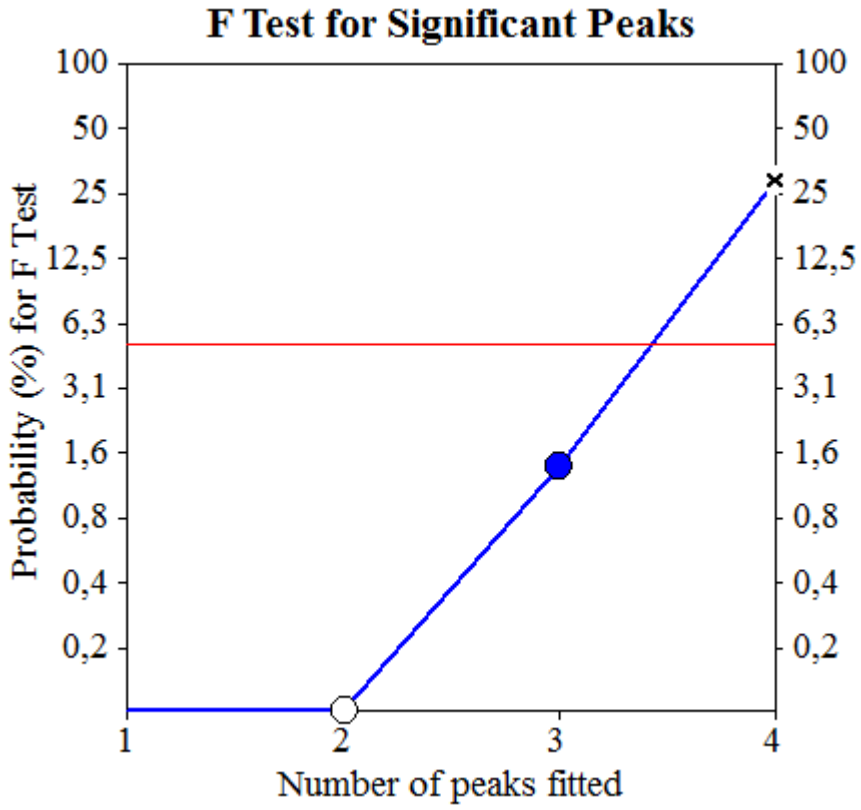

Merged dataset:
C:\BH2\Jairo\Echantillon-IRR-10-2015\JG-P3-32-Zr\JG-P3-32\JG-P3-32.ftz
C:\BH2\Jairo\Echantillon-IRR-10-2015\JG-P3-32-Zr\JG-P3-32a\JG-P3-32a.ftz

NEW PARAMETERS - ZETA METHOD

EFFECTIVE TRACK DENSITY FOR FLUENCE MONITOR (tracks/cm^2): 3,88E+05
RELATIVE ERROR (%): 1,23
EFFECTIVE URANIUM CONTENT OF MONITOR (ppm): 50,00
ZETA FACTOR AND STANDARD ERROR (yr cm^2): 137,14 1,57
SIZE OF COUNTER SQUARE (cm^2): 8,30E-07

GRAIN AGES IN ORIGINAL ORDER

Grain no.	RhoS (cm^-2)	(Ns)	RhoI (cm^-2)	(Ni)	Squares	U+/-2s	Grain Age (Ma) Age	--95% CI--	
1	1,33E+07	(154)	2,24E+06	(26)	14	288 112	154.9	102.7	244.4
2	6,16E+06	(92)	1,07E+06	(16)	18	138 68	150.0	88.7	273.2
3	1,28E+07	(138)	1,76E+06	(19)	13	227 103	189.1	118.0	322.8
4	9,77E+06	(227)	1,38E+06	(32)	28	177 62	185.3	128.6	276.8
5	5,98E+06	(144)	7,89E+05	(19)	29	102 46	197.1	123.3	336.1
6	9,56E+06	(119)	2,65E+06	(33)	15	341 118	94.9	64.4	144.2
7	8,18E+06	(129)	1,20E+06	(19)	19	155 70	176.9	110.1	302.8
8	9,84E+06	(245)	2,93E+06	(73)	30	378 89	88.1	67.9	114.4
9	7,15E+06	(285)	9,29E+05	(37)	48	120 39	201.0	143.5	290.7
10	4,45E+06	(85)	7,33E+05	(14)	23	94 50	158.1	90.5	301.1
11	9,37E+06	(140)	2,28E+06	(34)	18	293 100	108.3	74.4	162.5
12	1,13E+07	(226)	2,16E+06	(43)	24	278 85	138.0	99.7	195.8
13	1,00E+07	(158)	1,71E+06	(27)	19	221 84	153.1	102.2	239.4
14	9,41E+06	(164)	1,49E+06	(26)	21	192 75	164.9	109.5	259.5
15	7,86E+06	(261)	7,23E+05	(24)	40	93 38	281.4	187.4	444.6
16	4,42E+06	(55)	5,62E+05	(7)	15	72 53	201.8	94.2	522.7
17	6,02E+06	(240)	7,53E+05	(30)	48	97 35	208.5	143.6	314.9
18	8,17E+06	(305)	1,39E+06	(52)	45	179 50	153.8	114.9	210.5
19	8,03E+06	(80)	1,10E+06	(11)	12	142 84	188.3	101.7	391.3
20	9,24E+06	(138)	3,01E+06	(45)	18	388 115	80.9	57.6	116.0
21	8,02E+06	(193)	2,58E+06	(62)	29	332 84	81.7	61.4	108.6
22	1,01E+07	(219)	1,30E+06	(28)	26	167 63	203.8	138.5	313.0
23	1,08E+07	(162)	2,01E+06	(30)	18	259 94	141.5	96.1	216.4
24	1,00E+07	(150)	2,34E+06	(35)	18	302 102	112.7	78.0	167.8
25	8,89E+06	(354)	1,13E+06	(45)	48	146 43	205.4	151.3	286.1
26	8,53E+06	(425)	2,65E+06	(132)	60	341 60	84.8	69.7	103.2
27	6,59E+06	(82)	7,23E+05	(9)	15	93 60	234.3	120.5	527.1
28	6,67E+06	(83)	2,01E+06	(25)	15	259 103	87.4	55.6	142.8
29	2,59E+06	(73)	8,86E+05	(25)	34	114 45	76.9	48.5	126.6
30	5,08E+06	(118)	9,47E+05	(22)	28	122 52	140.3	89.3	232.3
31	9,29E+06	(185)	1,15E+06	(23)	24	149 61	209.3	136.8	337.4
32	5,91E+06	(108)	1,10E+06	(20)	22	141 62	141.2	88.0	240.2
33	3,48E+06	(52)	1,07E+06	(16)	18	138 68	85.3	48.4	160.4
34	4,50E+06	(142)	5,07E+05	(16)	38	65 32	229.9	138.9	411.3
35	6,32E+06	(194)	8,14E+05	(25)	37	105 42	202.1	134.3	319.2
36	5,98E+06	(139)	1,72E+06	(40)	28	222 70	91.6	64.3	133.7
37	7,13E+06	(296)	8,92E+05	(37)	50	115 38	208.7	149.1	301.5
38	5,46E+06	(145)	9,41E+05	(25)	32	121 48	151.7	99.6	242.0
39	6,31E+06	(157)	1,69E+06	(42)	30	217 67	98.4	69.9	141.9
40	7,53E+06	(75)	1,31E+06	(13)	12	168 92	150.2	84.0	295.0
41	8,33E+06	(83)	2,51E+06	(25)	12	323 128	87.4	55.6	142.8
42	6,14E+06	(102)	6,63E+05	(11)	20	85 50	239.0	130.9	491.0
43	6,68E+06	(122)	1,10E+06	(20)	22	141 62	159.2	99.8	269.6
44	3,94E+06	(36)	8,76E+05	(8)	11	113 77	116.8	54.5	291.7
45	5,18E+06	(86)	8,43E+05	(14)	20	109 57	159.9	91.6	304.4
46	4,97E+06	(198)	6,53E+05	(26)	48	84 33	198.5	132.8	310.6
47	9,48E+06	(118)	1,20E+06	(15)	15	155 79	204.1	120.7	375.0
48	6,12E+06	(132)	8,80E+05	(19)	26	113 51	181.0	112.7	309.5
49	9,19E+06	(183)	1,61E+06	(32)	24	207 73	149.8	103.2	225.3
50	2,61E+06	(65)	3,61E+05	(9)	30	47 30	186.5	94.5	424.9
51	5,87E+06	(117)	8,03E+05	(16)	24	103 51	190.1	113.9	342.6
52	5,32E+06	(106)	1,05E+06	(21)	24	136 59	132.1	82.9	222.2

Merged dataset:
C:\BH2\Jairo\Echantillon-IRR-10-2015\JG-P3-32-Zr\JG-P3-32\JG-P3-32.ftz
C:\BH2\Jairo\Echantillon-IRR-10-2015\JG-P3-32-Zr\JG-P3-32a\JG-P3-32a.ftz

Grain no.	RhoS (cm^-2)	(Ns)	RhoI (cm^-2)	(Ni)	Squares	U+/-2s	Grain Age (Ma) Age	--95% CI--	
53	4,56E+06	(106)	9,04E+05	(21)	28	116 50	132.1	82.9	222.2

Merged dataset:
C:\BH2\Jairo\Echantillon-IRR-10-2015\JG-P3-32-Zr\JG-P3-32\JG-P3-32.ftz
C:\BH2\Jairo\Echantillon-IRR-10-2015\JG-P3-32-Zr\JG-P3-32a\JG-P3-32a.ftz

NEW PARAMETERS - ZETA METHOD

EFFECTIVE TRACK DENSITY FOR FLUENCE MONITOR (tracks/cm^2): 3,89E+05
RELATIVE ERROR (%): 1,24
EFFECTIVE URANIUM CONTENT OF MONITOR (ppm): 50,00
ZETA FACTOR AND STANDARD ERROR (yr cm^2): 137,14 1,57
SIZE OF COUNTER SQUARE (cm^2): 8,30E-07

Grain no.	RhoS (cm^-2)	(Ns)	RhoI (cm^-2)	(Ni)	Squares	U+/-2s	Grain Age (Ma) Age	--95% CI--	
54	5,48E+06	(91)	7,83E+05	(13)	20	101 55	181.9	102.9	354.0
55	8,43E+06	(210)	1,12E+06	(28)	30	145 54	195.8	132.8	301.1
56	7,33E+06	(152)	1,06E+06	(22)	25	136 58	180.4	116.1	295.8
57	9,56E+06	(119)	2,01E+06	(25)	15	258 103	125.0	81.3	200.8
58	3,46E+06	(46)	4,52E+05	(6)	16	58 46	196.6	86.4	560.5
59	9,98E+06	(406)	1,20E+06	(49)	49	155 44	216.5	161.6	296.8
60	4,98E+06	(124)	6,83E+05	(17)	30	88 42	189.9	115.5	335.7
61	5,58E+06	(190)	5,88E+05	(20)	41	76 33	246.5	157.3	410.8
62	3,87E+06	(77)	5,52E+05	(11)	24	71 42	181.6	97.9	378.1
63	9,00E+06	(112)	1,12E+06	(14)	15	145 76	207.6	120.7	390.7
64	5,03E+06	(146)	8,26E+05	(24)	35	106 43	159.2	103.9	256.2
65	6,83E+06	(102)	8,70E+05	(13)	18	112 61	203.6	115.8	394.0
66	3,36E+06	(67)	4,52E+05	(9)	24	58 38	192.4	97.7	437.6
67	6,48E+06	(215)	2,26E+06	(75)	40	291 67	75.5	58.0	98.1
68	8,55E+06	(142)	2,29E+06	(38)	20	295 95	98.5	68.8	144.9
69	4,73E+06	(110)	8,61E+05	(20)	28	111 49	144.0	89.8	244.7
70	7,08E+06	(188)	1,39E+06	(37)	32	179 59	133.5	94.0	195.4
71	7,59E+06	(126)	1,45E+06	(24)	20	186 75	137.7	89.2	222.7
72	5,18E+06	(43)	7,23E+05	(6)	10	93 73	184.0	80.4	527.1
73	8,11E+06	(101)	1,37E+06	(17)	15	176 84	155.2	93.4	276.6
74	5,98E+06	(124)	1,69E+06	(35)	25	217 73	93.4	64.0	140.2
75	3,92E+06	(78)	1,51E+06	(30)	24	194 70	68.7	44.8	108.5
76	5,54E+06	(69)	1,37E+06	(17)	15	176 84	106.5	62.6	193.4
77	3,27E+06	(57)	1,15E+06	(20)	21	148 65	75.1	44.8	132.2
78	7,95E+06	(132)	1,27E+06	(21)	20	163 70	164.3	104.3	273.9
79	3,16E+06	(105)	6,33E+05	(21)	40	81 35	131.1	82.2	220.5
80	7,34E+06	(128)	1,03E+06	(18)	21	133 62	185.3	114.1	322.0
81	7,20E+06	(233)	1,36E+06	(44)	39	175 53	139.2	101.0	196.6
82	7,48E+06	(149)	9,54E+05	(19)	24	123 56	204.1	127.8	347.6
83	1,11E+07	(147)	2,18E+06	(29)	16	281 104	133.1	89.5	205.6
84	7,23E+06	(246)	1,56E+06	(53)	41	200 55	122.2	90.9	167.7
85	4,57E+06	(91)	9,04E+05	(18)	24	116 54	132.4	80.1	233.3
86	8,12E+06	(182)	1,61E+06	(36)	27	207 69	132.9	93.1	195.6
87	5,66E+06	(141)	8,03E+05	(20)	30	103 46	183.9	116.0	309.6
88	8,59E+06	(107)	2,25E+06	(28)	15	289 109	100.6	66.3	158.6
89	8,24E+06	(260)	1,08E+06	(34)	38	139 47	199.8	140.5	294.0
90	9,74E+06	(97)	1,91E+06	(19)	12	245 111	133.7	82.0	231.6
91	6,57E+06	(267)	2,02E+06	(82)	49	259 57	85.7	66.9	109.7
92	7,78E+06	(155)	2,46E+06	(49)	24	317 90	83.6	60.4	117.8
93	4,28E+06	(71)	8,43E+05	(14)	20	109 57	132.5	75.0	254.7
94	7,16E+06	(107)	1,47E+06	(22)	18	189 80	127.6	80.8	212.1
95	5,00E+06	(170)	6,46E+05	(22)	41	83 35	201.4	130.2	329.0
96	3,92E+06	(91)	6,45E+05	(15)	28	83 42	158.2	92.3	294.0
97	7,73E+06	(231)	1,84E+06	(55)	36	237 64	110.7	82.5	151.4
98	5,42E+06	(63)	7,75E+05	(9)	14	100 65	181.1	91.6	413.3
POOLED	6,83E+06	(14459)	1,27E+06	(2690)	2552	164 7	141.4	134.2	149.0

Merged dataset:
C:\BH2\Jairo\Echantillon-IRR-10-2015\JG-P3-32-Zr\JG-P3-32\JG-P3-32.ftz
C:\BH2\Jairo\Echantillon-IRR-10-2015\JG-P3-32-Zr\JG-P3-32a\JG-P3-32a.ftz

```
CHI^2 PROBABILITY (%):  0.0

 POOLED AGE W/  68% CONF. INTERVAL(Ma):  141.4, 137.7 -- 145.2 ( -3.7  +3.8)
                95% CONF. INTERVAL(Ma):         134.2 -- 149.0 ( -7.2  +7.6)

CENTRAL AGE W/  68% CONF. INTERVAL(Ma):  142.3, 136.8 -- 148.0 ( -5.5  +5.7)
                95% CONF. INTERVAL(Ma):         131.7 -- 153.7 (-10.6 +11.5)
                    AGE DISPERSION (%):   28.2
```

Merged dataset:
C:\BH2\Jairo\Echantillon-IRR-10-2015\JG-P3-32-Zr\JG-P3-32\JG-P3-32.ftz
C:\BH2\Jairo\Echantillon-IRR-10-2015\JG-P3-32-Zr\JG-P3-32a\JG-P3-32a.ftz

FIT OPTION: Best-fit peaks using the binomial model of Galbraith and Green

INITIAL GUESS FOR MODEL PARAMETERS (number of peaks to fit = 2)

Peak #.	Peak Age	Theta	Fraction(%)	Count
1.	141.30	0.843	39.2	38.37
2.	201.90	0.885	38.7	37.93

Total range for grain ages: 68,2 to 278,0 Ma
Number of active grains (Num. used for fit): 98
Number of removed grains: 0
Degrees of freedom for fit: 95
Average of the SE(Z)'s for the grains: 0,24
Estimated width of peaks in PD plot in Z units: 0,28

PARAMETERS FOR BEST-FIT PEAKS

** Standard error for peak age includes group error*
** Peak width is for PD plot assuming a kernel factor = 0.60*

#.	Peak Age(Ma)	68%CI	95%CI	W(Z)	Frac(%)	SE,%	Count
1.	92.3	-4,3 ...+4,5	-8,3 ...+9,1	0.20	25.3	5.3	24.8
2.	172.7	-5,8 ...+6,0	-11,1 ...+11,9	0.26	74.7	5.3	73.2

Log-likelihood for best fit: -319,893
Chi-squared value for best fit: 86,796
Reduced chi-squared value: 0,914
Probability for F test: 0%
Condition number for COVAR matrix: 4,36
Number of iterations: 14

Merged dataset:
C:\BH2\Jairo\Echantillon-IRR-10-2015\JG-P3-32-Zr\JG-P3-32\JG-P3-32.ftz
C:\BH2\Jairo\Echantillon-IRR-10-2015\JG-P3-32-Zr\JG-P3-32a\JG-P3-32a.ftz

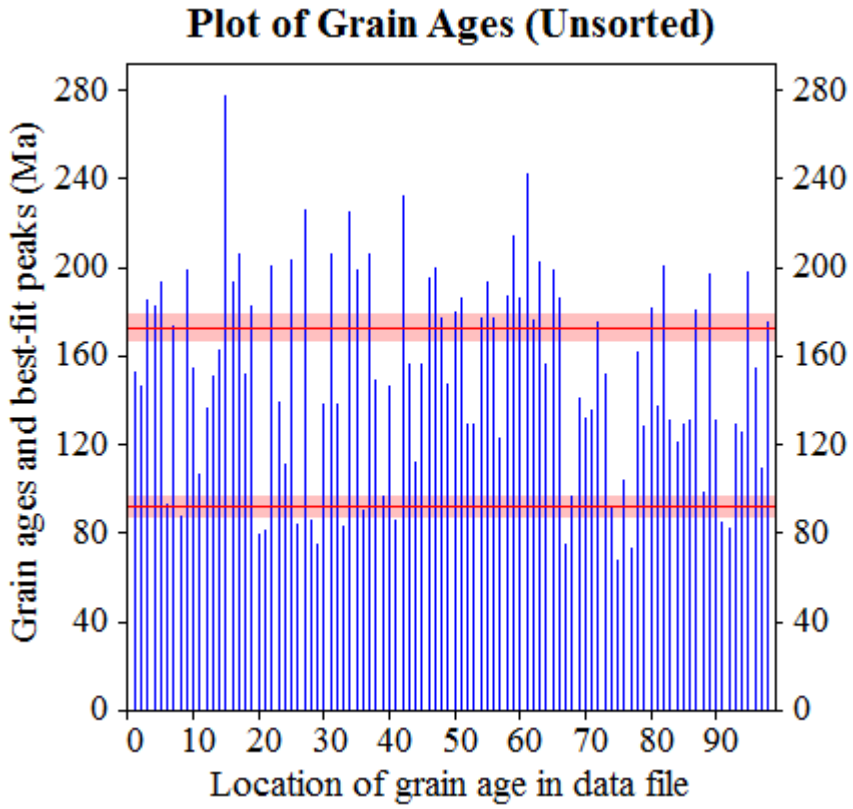

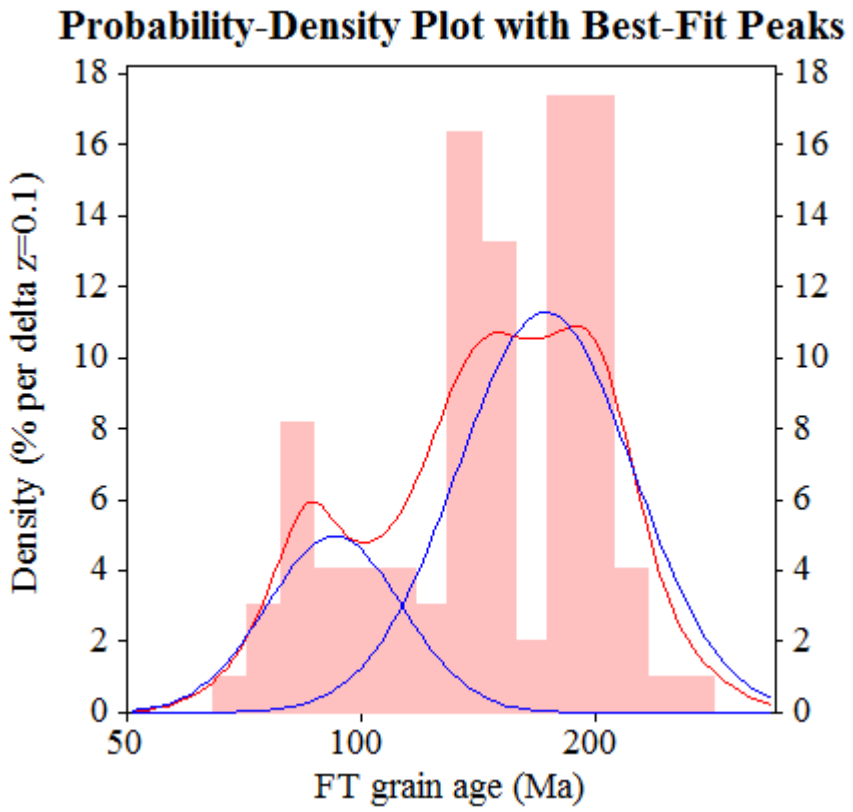

Merged dataset:
C:\BH2\Jairo\Echantillon-IRR-10-2015\JG-P3-32-Zr\JG-P3-32\JG-P3-32.ftz
C:\BH2\Jairo\Echantillon-IRR-10-2015\JG-P3-32-Zr\JG-P3-32a\JG-P3-32a.ftz

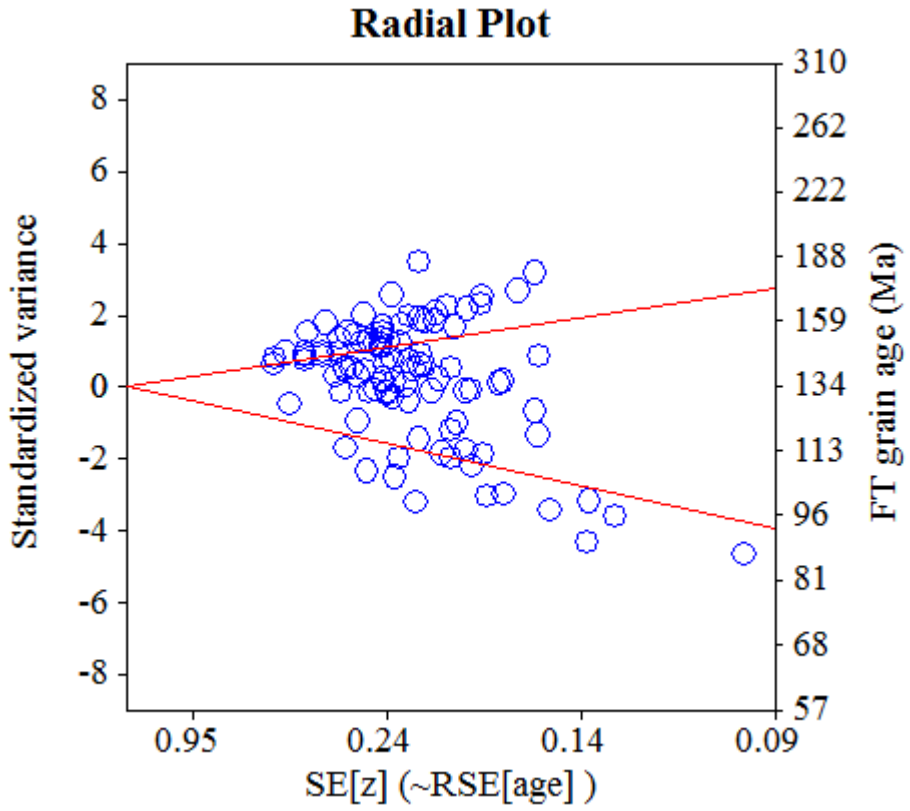

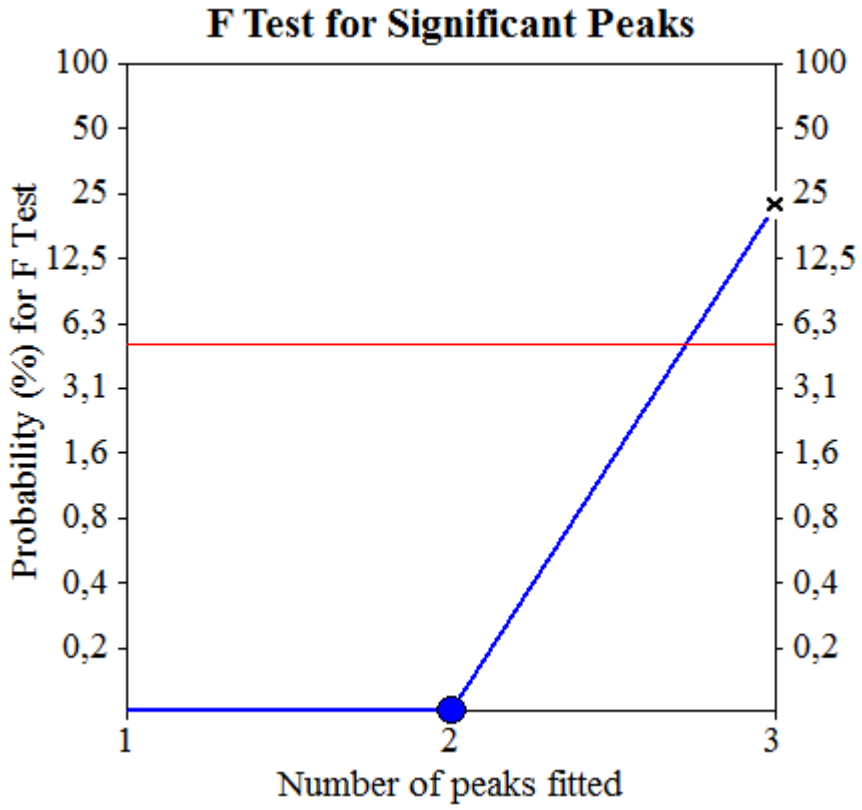

Merged dataset:
C:\BH2\Jairo\Samples-IRR-6-2015\JG-P3-19\JG-P3-19a.ftz
C:\BH2\Jairo\Samples-IRR-6-2015\JG-P3-19\JG-P3-19.ftz

NEW PARAMETERS - ZETA METHOD

EFFECTIVE TRACK DENSITY FOR FLUENCE MONITOR (tracks/cm^2): 2,73E+05
RELATIVE ERROR (%): 1,28
EFFECTIVE URANIUM CONTENT OF MONITOR (ppm): 50,00
ZETA FACTOR AND STANDARD ERROR (yr cm^2): 137,95 4,04
SIZE OF COUNTER SQUARE (cm^2): 8,30E-07

GRAIN AGES IN ORIGINAL ORDER

Grain no.	RhoS (cm^-2)	(Ns)	RhoI (cm^-2)	(Ni)	Squares	U+/-2s		Grain Age (Ma) Age	--95% CI--	
1	7,05E+06	(234)	7,23E+05	(24)	40	133	54	179.7	119.0	285.7
2	8,51E+06	(226)	6,40E+05	(17)	32	117	56	243.1	150.8	422.8
3	7,72E+06	(205)	5,65E+05	(15)	32	104	53	249.5	150.3	451.7
4	1,34E+07	(266)	1,00E+06	(20)	24	184	81	243.5	156.6	403.5
5	1,01E+07	(502)	8,23E+05	(41)	60	151	47	225.4	165.0	317.2
6	1,12E+07	(278)	1,12E+06	(28)	30	206	77	183.1	125.0	280.2
7	8,96E+06	(357)	6,02E+05	(24)	48	110	45	272.1	182.2	428.2
8	8,66E+06	(503)	5,16E+05	(30)	70	95	34	306.3	214.3	456.1
9	1,36E+07	(293)	1,11E+06	(24)	26	204	83	224.2	149.4	354.5
10	9,51E+06	(300)	9,83E+05	(31)	38	180	64	178.6	124.2	267.2
11	4,95E+06	(115)	4,73E+05	(11)	28	87	51	191.1	104.9	392.8
12	1,09E+07	(253)	7,31E+05	(17)	28	134	64	271.5	169.0	470.7
13	5,72E+06	(95)	5,42E+05	(9)	20	99	65	192.4	99.4	432.7
14	1,14E+07	(228)	7,53E+05	(15)	24	138	70	276.9	167.4	499.6
15	1,26E+07	(220)	1,09E+06	(19)	21	200	91	212.5	134.6	358.7
16	1,10E+07	(366)	8,73E+05	(29)	40	160	59	231.9	160.3	350.0
17	9,37E+06	(311)	9,64E+05	(32)	40	177	62	179.4	125.4	266.5
18	6,04E+06	(351)	7,75E+05	(45)	70	142	42	144.6	106.3	201.8
19	1,16E+07	(231)	9,04E+05	(18)	24	166	77	235.0	147.5	401.9
20	5,66E+06	(235)	5,78E+05	(24)	50	106	43	180.4	119.5	286.9
21	1,01E+07	(335)	1,05E+06	(35)	40	193	65	176.8	125.5	257.8
22	7,69E+06	(319)	5,30E+05	(22)	50	97	41	265.2	174.4	427.1
23	9,22E+06	(459)	1,71E+06	(85)	60	313	68	100.2	79.0	127.0
24	1,09E+07	(902)	1,11E+06	(92)	100	203	43	180.8	145.1	225.2
25	6,41E+06	(266)	6,51E+05	(27)	50	119	46	181.7	123.2	280.5
26	1,29E+07	(321)	1,37E+06	(34)	30	250	86	174.4	123.1	255.9
27	9,58E+06	(318)	1,27E+06	(42)	40	232	71	140.4	102.0	198.5
28	8,78E+06	(488)	7,91E+05	(44)	67	145	44	204.6	151.1	284.7
29	9,78E+06	(406)	1,37E+06	(57)	50	252	67	131.4	99.3	173.9
30	9,97E+06	(331)	1,30E+06	(43)	40	238	72	142.7	104.2	200.9
31	8,27E+06	(412)	1,51E+06	(75)	60	276	64	101.8	79.2	130.9
32	6,67E+06	(332)	1,18E+06	(59)	60	217	57	104.1	78.6	137.8
33	7,21E+06	(359)	1,12E+06	(56)	60	206	55	118.4	89.0	157.3
34	1,14E+07	(228)	2,11E+06	(42)	24	387	119	101.0	72.7	144.0
35	4,95E+06	(329)	5,12E+05	(34)	80	94	32	178.7	126.2	262.1
36	8,49E+06	(282)	1,14E+06	(38)	40	210	68	137.5	98.4	198.4
37	7,95E+06	(396)	9,04E+05	(45)	60	166	49	162.9	120.1	226.8
38	9,70E+06	(169)	9,75E+05	(17)	21	179	86	182.7	112.3	320.6
39	1,10E+07	(291)	1,05E+06	(28)	32	193	73	191.5	130.9	292.8
40	1,07E+07	(249)	1,08E+06	(25)	28	197	78	183.5	122.6	288.7

Merged dataset:
C:\BH2\Jairo\Samples-IRR-6-2015\JG-P3-19\JG-P3-19a.ftz
C:\BH2\Jairo\Samples-IRR-6-2015\JG-P3-19\JG-P3-19.ftz

NEW PARAMETERS - ZETA METHOD

EFFECTIVE TRACK DENSITY FOR FLUENCE MONITOR (tracks/cm^2): 2,73E+05
RELATIVE ERROR (%): 1,26
EFFECTIVE URANIUM CONTENT OF MONITOR (ppm): 50,00
ZETA FACTOR AND STANDARD ERROR (yr cm^2): 137,95 4,04
SIZE OF COUNTER SQUARE (cm^2): 8,30E-07

Grain no.	RhoS (cm^-2)	(Ns)	RhoI (cm^-2)	(Ni)	Squares	U+/-2s	Grain Age (Ma) Age	--95% CI--	
41	1,02E+07	(152)	1,54E+06	(23)	18	282 117	122.4	79.3	199.1
42	7,17E+06	(125)	1,09E+06	(19)	21	200 91	121.7	75.5	209.2
43	1,22E+07	(507)	9,64E+05	(40)	50	177 56	233.3	170.3	329.6
44	1,33E+07	(199)	1,27E+06	(19)	18	233 106	192.6	121.7	326.1
45	8,07E+06	(134)	1,27E+06	(21)	20	232 100	118.2	75.0	197.4
46	9,94E+06	(495)	1,02E+06	(51)	60	188 53	178.4	133.5	238.2
47	9,79E+06	(325)	7,83E+05	(26)	40	144 56	229.7	155.6	355.8
48	7,77E+06	(387)	6,43E+05	(32)	60	118 41	222.6	156.5	329.2
49	1,07E+07	(187)	8,03E+05	(14)	21	147 77	244.0	144.4	452.7
50	9,87E+06	(303)	8,14E+05	(25)	37	149 59	222.8	149.6	348.7
51	8,63E+06	(172)	1,20E+06	(24)	24	221 89	132.7	87.0	212.8
52	9,60E+06	(470)	9,60E+05	(47)	59	176 51	184.9	137.6	254.9
53	4,97E+06	(132)	9,41E+05	(25)	32	173 68	98.1	64.1	157.3
54	9,19E+06	(305)	7,53E+05	(25)	40	138 55	224.2	150.6	350.9
55	6,29E+06	(256)	4,67E+05	(19)	49	86 39	246.7	157.0	414.7
56	1,11E+07	(370)	1,60E+06	(53)	40	293 80	128.9	96.3	172.2
57	1,30E+07	(433)	1,96E+06	(65)	40	359 89	123.2	94.5	160.5
58	7,83E+06	(325)	1,01E+06	(42)	50	185 57	143.5	104.4	202.9
59	1,40E+07	(395)	9,21E+05	(26)	34	169 66	278.1	189.2	428.9
60	1,14E+07	(151)	9,04E+05	(12)	16	166 94	229.7	130.2	452.4
61	8,47E+06	(225)	7,15E+05	(19)	32	131 59	217.4	137.8	366.7
62	9,35E+06	(194)	1,30E+06	(27)	25	238 91	133.1	89.4	207.2
63	1,23E+07	(245)	1,51E+06	(30)	24	276 100	151.1	104.0	228.8
64	1,22E+07	(325)	7,53E+05	(20)	32	138 61	296.5	191.7	488.6
65	1,19E+07	(277)	1,16E+06	(27)	28	213 81	189.2	128.4	291.8
66	1,13E+07	(187)	1,02E+06	(17)	20	188 90	202.0	124.5	353.3
67	1,13E+07	(234)	1,35E+06	(28)	25	247 93	154.6	105.1	237.6
68	9,91E+06	(329)	6,02E+05	(20)	40	110 49	300.1	194.1	494.4
69	9,34E+06	(186)	1,41E+06	(28)	24	258 97	123.2	83.1	190.6
70	1,25E+07	(208)	1,33E+06	(22)	20	243 103	174.3	113.3	283.9
71	8,11E+06	(202)	1,12E+06	(28)	30	206 77	133.7	90.4	206.3
72	8,12E+06	(337)	9,16E+05	(38)	50	168 54	164.1	117.9	235.8
73	9,44E+06	(94)	1,51E+06	(15)	12	276 140	115.8	67.6	215.5
74	6,61E+06	(192)	9,29E+05	(27)	35	170 65	131.8	88.5	205.2
75	7,53E+06	(200)	9,04E+05	(24)	32	166 67	154.0	101.5	246.0
76	1,04E+07	(233)	1,07E+06	(24)	27	196 79	179.1	118.6	284.7
77	8,17E+06	(217)	1,17E+06	(31)	32	214 76	129.8	89.4	195.8
78	7,44E+06	(247)	5,72E+05	(19)	40	105 48	238.2	151.4	400.8
79	9,79E+06	(195)	1,10E+06	(22)	24	202 86	163.6	106.1	266.9
80	1,05E+07	(348)	9,64E+05	(32)	40	177 62	200.5	140.6	297.2
81	1,02E+07	(339)	2,17E+06	(72)	40	397 94	87.4	67.4	113.3
82	7,14E+06	(166)	6,45E+05	(15)	28	118 60	203.0	121.4	369.9
83	7,80E+06	(259)	9,04E+05	(30)	40	166 60	159.7	110.0	241.3
84	7,01E+06	(262)	1,07E+06	(40)	45	196 62	121.7	87.4	174.3
85	9,44E+06	(470)	1,67E+06	(83)	60	305 67	105.1	82.7	133.4
86	1,17E+07	(273)	1,38E+06	(32)	28	252 89	157.9	110.0	235.2
87	6,25E+06	(254)	4,67E+05	(19)	49	86 39	244.8	155.8	411.6
88	8,84E+06	(433)	1,39E+06	(68)	59	255 62	117.9	90.9	152.8
89	1,07E+07	(266)	1,08E+06	(27)	30	199 76	181.8	123.3	280.6
90	7,47E+06	(248)	9,34E+05	(31)	40	171 61	148.1	102.5	222.6
91	8,08E+06	(181)	7,59E+05	(17)	27	139 67	195.6	120.5	342.5
92	4,23E+06	(274)	6,95E+05	(45)	78	127 38	113.2	82.7	158.9
93	8,70E+06	(361)	6,99E+05	(29)	50	128 47	228.9	158.2	345.7
94	1,01E+07	(334)	1,27E+06	(42)	40	232 71	147.4	107.3	208.3

Merged dataset:
C:\BH2\Jairo\Samples-IRR-6-2015\JG-P3-19\JG-P3-19a.ftz
C:\BH2\Jairo\Samples-IRR-6-2015\JG-P3-19\JG-P3-19.ftz

Grain no.	RhoS (cm^-2)	(Ns)	RhoI (cm^-2)	(Ni)	Squares	U+/-2s		Grain Age (Ma) Age	--95% CI--	
95	9,40E+06	(234)	1,00E+06	(25)	30	184	73	172.8	115.2	272.2
96	7,47E+06	(310)	1,57E+06	(65)	50	287	71	88.5	67.4	116.1
97	8,21E+06	(327)	8,03E+05	(32)	48	147	52	188.6	132.1	279.9
98	9,85E+06	(327)	7,83E+05	(26)	40	144	56	231.1	156.5	357.9
99	7,43E+06	(370)	8,23E+05	(41)	60	151	47	167.0	121.5	236.4
100	4,82E+06	(80)	2,17E+06	(36)	20	397	132	41.6	27.8	63.6
101	6,19E+06	(190)	1,24E+06	(38)	37	227	73	93.1	65.7	135.7
102	2,75E+06	(73)	9,41E+05	(25)	32	173	68	54.5	34.4	89.8
POOLED	8,85E+06	(29290)	1,00E+06	(3316)	3989	184	8	164.0	152.7	176.1

CHI^2 PROBABILITY (%): 0.0

POOLED AGE W/ 68% CONF. INTERVAL(Ma): 164.0, 158.1 -- 170.0 (-5.9 +6.1)
95% CONF. INTERVAL(Ma): 152.7 -- 176.1 (-11.3 +12.1)

CENTRAL AGE W/ 68% CONF. INTERVAL(Ma): 162.3, 154.7 -- 170.3 (-7.6 +7.9)
95% CONF. INTERVAL(Ma): 147.8 -- 178.3 (-14.5 +15.9)
AGE DISPERSION (%): 31.2

Merged dataset:
C:\BH2\Jairo\Samples-IRR-6-2015\JG-P3-19\JG-P3-19a.ftz
C:\BH2\Jairo\Samples-IRR-6-2015\JG-P3-19\JG-P3-19.ftz

FIT OPTION: Best-fit peaks using the binomial model of Galbraith and Green

INITIAL GUESS FOR MODEL PARAMETERS (number of peaks to fit = 3)

Peak #.	Peak Age	Theta	Fraction(%)	Count
1.	41.40	0.688	1.4	1.42
2.	163.90	0.898	40.0	40.85
3.	231.00	0.926	32.4	33.04

Total range for grain ages:	41,4 to 303,2 Ma
Number of active grains (Num. used for fit):	102
Number of removed grains:	0
Degrees of freedom for fit:	97
Average of the SE(Z)'s for the grains:	0,2
Estimated width of peaks in PD plot in Z units:	0,24

PARAMETERS FOR BEST-FIT PEAKS

* *Standard error for peak age includes group error*
* *Peak width is for PD plot assuming a kernel factor = 0.60*

#.	Peak Age(Ma)	68%CI	95%CI	W(Z)	Frac(%)	SE,%	Count
1.	46.5	-6,9 ...+8,1	-12,6 ...+17,3	0.25	1.8	1.4	1.9
2.	117.9	-6,0 ...+6,4	-11,5 ...+12,8	0.19	28.8	6.3	29.4
3.	198.3	-8,4 ...+8,8	-16,2 ...+17,6	0.23	69.3	6.3	70.7

Log-likelihood for best fit:	-366,878
Chi-squared value for best fit:	89,307
Reduced chi-squared value:	0,921
Probability for F test:	0%
Condition number for COVAR matrix:	135,35
Number of iterations:	17

Merged dataset:
C:\BH2\Jairo\Samples-IRR-6-2015\JG-P3-19\JG-P3-19a.ftz
C:\BH2\Jairo\Samples-IRR-6-2015\JG-P3-19\JG-P3-19.ftz

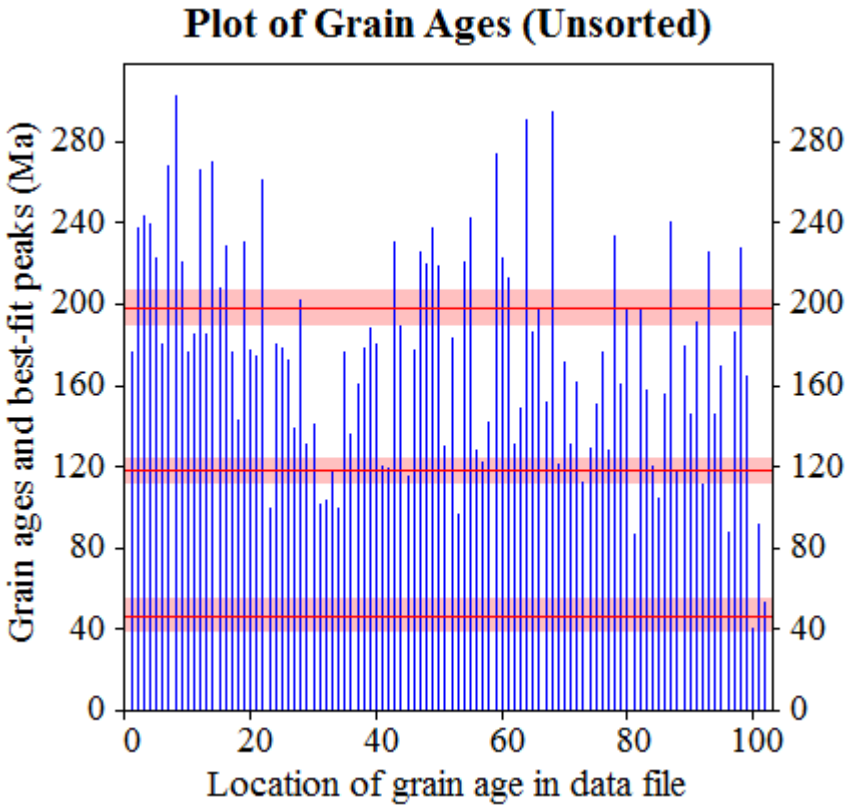

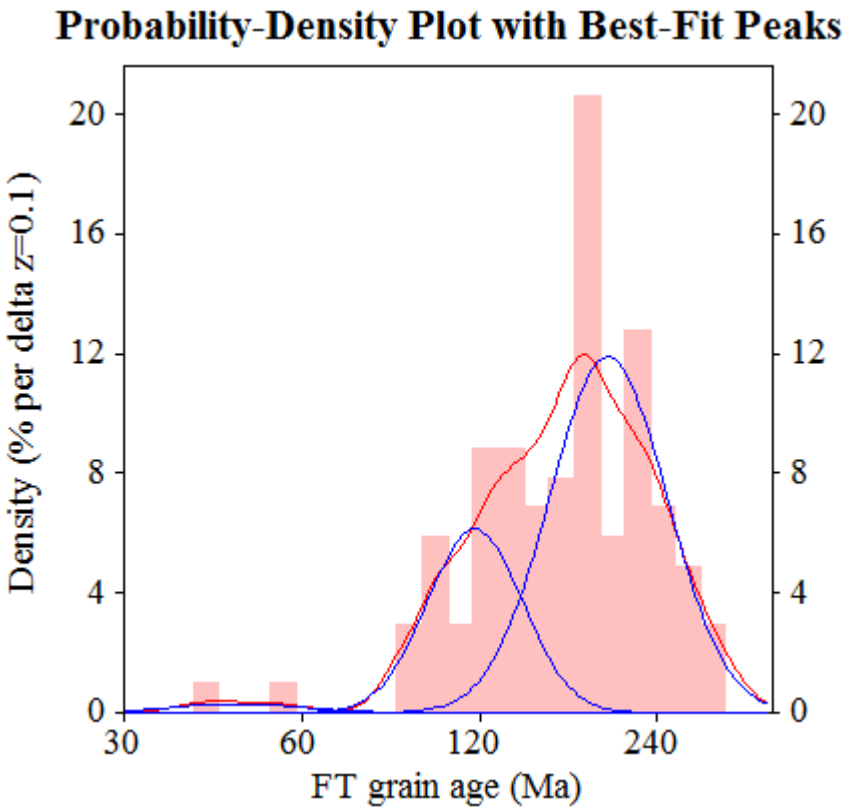

Merged dataset:
C:\BH2\Jairo\Samples-IRR-6-2015\JG-P3-19\JG-P3-19a.ftz
C:\BH2\Jairo\Samples-IRR-6-2015\JG-P3-19\JG-P3-19.ftz

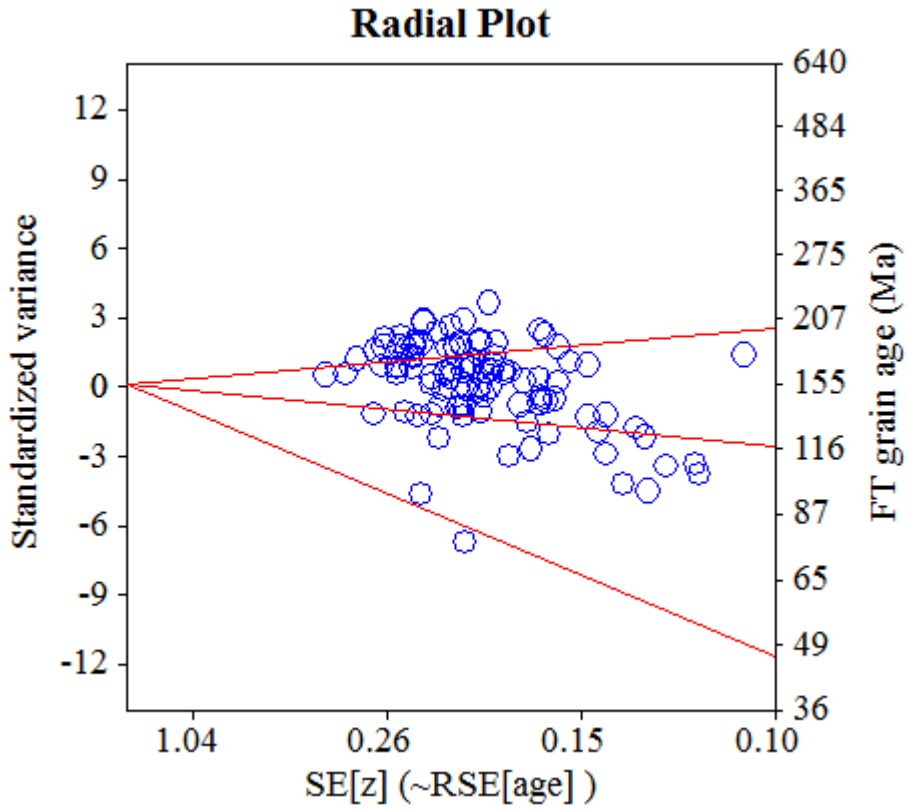

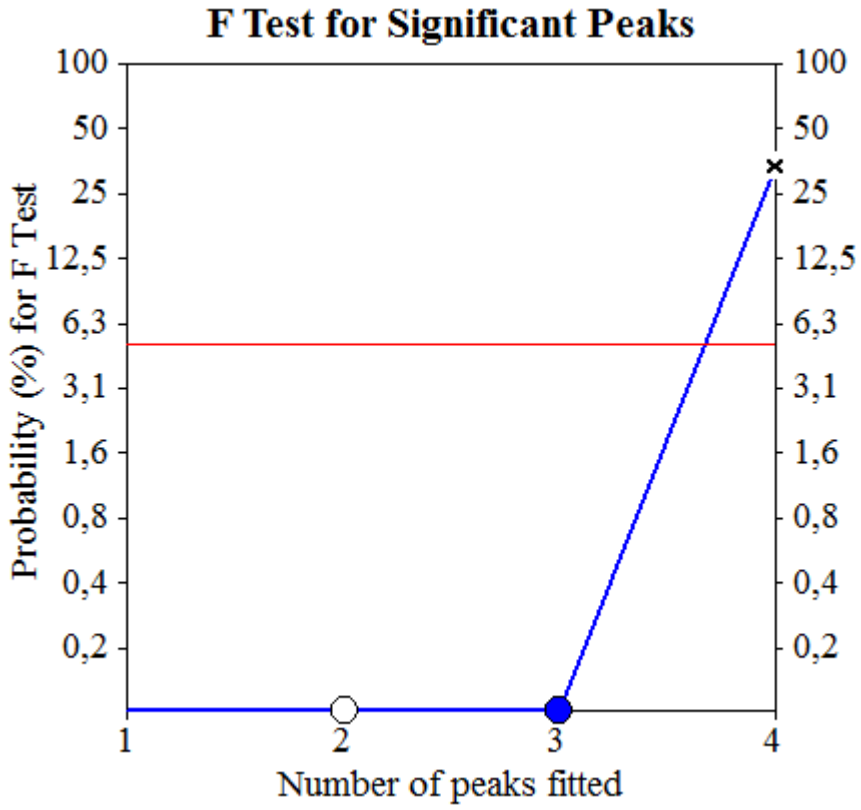

Datafile: C:\BH2\Jairo\Echantillon-IRR-10-2015\JG-P3-23-Zr\JG-P3-23.ftz
Title: Sample No. JG P3 23 Irr 10-2015-41

NEW PARAMETERS - ZETA METHOD

EFFECTIVE TRACK DENSITY FOR FLUENCE MONITOR (tracks/cm^2): 3,87E+05
RELATIVE ERROR (%): 1,20
EFFECTIVE URANIUM CONTENT OF MONITOR (ppm): 50,00
ZETA FACTOR AND STANDARD ERROR (yr cm^2): 137,14 1,57
SIZE OF COUNTER SQUARE (cm^2): 8,30E-07

GRAIN AGES IN ORIGINAL ORDER

Grain no.	RhoS (cm^-2)	(Ns)	RhoI (cm^-2)	(Ni)	Squares	U+/-2s		Grain Age (Ma) Age	--95% CI--	
1	7,13E+06	(142)	8,53E+05	(17)	24	110	53	216.1	132.2	379.9
2	8,39E+06	(418)	9,64E+05	(48)	60	125	36	226.4	168.7	311.1
3	5,71E+06	(237)	7,47E+05	(31)	50	97	34	198.8	137.6	298.5
4	3,89E+06	(323)	6,14E+05	(51)	100	79	22	165.5	123.5	226.7
5	6,87E+06	(342)	7,23E+05	(36)	60	93	31	246.3	175.9	356.3
6	7,55E+06	(188)	1,20E+06	(30)	30	156	56	163.4	111.6	248.7
7	6,49E+06	(539)	6,39E+05	(53)	100	83	23	262.0	198.4	345.3
8	5,53E+06	(459)	8,92E+05	(74)	100	115	27	161.5	126.5	206.0
9	4,60E+06	(382)	1,18E+06	(98)	100	153	31	102.1	81.8	127.5
10	5,90E+06	(490)	1,71E+06	(142)	100	221	37	90.6	75.1	109.3
11	7,86E+06	(326)	1,69E+06	(70)	50	218	52	121.6	94.0	157.1
12	6,23E+06	(362)	1,45E+06	(84)	70	187	41	112.7	88.9	142.8
13	5,92E+06	(295)	6,43E+05	(32)	60	83	29	239.0	167.2	354.6
14	8,09E+06	(235)	1,45E+06	(42)	35	187	57	146.3	105.6	208.2
15	8,17E+06	(339)	8,92E+05	(37)	50	115	38	237.7	170.4	342.3
16	4,47E+06	(371)	3,61E+05	(30)	100	47	17	318.5	221.9	475.7
17	5,30E+06	(176)	8,13E+05	(27)	40	105	40	169.8	113.8	264.6
18	8,83E+06	(293)	8,73E+05	(29)	40	113	42	261.4	180.1	395.3
19	8,36E+06	(694)	8,92E+05	(74)	100	115	27	242.6	191.4	307.2
20	6,99E+06	(174)	1,41E+06	(35)	30	182	61	130.1	90.6	192.8
21	5,82E+06	(338)	5,85E+05	(34)	70	76	26	257.4	182.3	376.4
22	1,04E+07	(344)	9,04E+05	(30)	40	117	42	295.9	205.8	442.7
23	6,89E+06	(572)	7,35E+05	(61)	100	95	24	242.2	186.6	314.0
24	4,25E+06	(141)	2,56E+06	(85)	40	331	72	43.6	33.3	57.1
25	5,97E+06	(347)	6,20E+05	(36)	70	80	27	249.8	178.5	361.3
26	5,61E+06	(466)	9,40E+05	(78)	100	121	28	155.7	122.6	197.5
27	7,92E+06	(460)	8,78E+05	(51)	70	113	32	232.8	175.0	309.2
28	1,01E+07	(251)	1,12E+06	(28)	30	145	55	232.4	158.5	355.5
29	5,49E+06	(456)	7,71E+05	(64)	100	100	25	184.9	142.7	239.5
30	8,02E+06	(333)	1,40E+06	(58)	50	181	47	149.3	113.2	196.8
31	7,86E+06	(652)	8,43E+05	(70)	100	109	26	240.9	188.8	307.0
32	1,01E+07	(234)	2,11E+06	(49)	28	272	78	125.2	92.0	173.9
33	7,83E+06	(273)	1,15E+06	(40)	42	148	47	178.0	128.2	254.3
34	3,81E+06	(316)	9,04E+05	(75)	100	117	27	110.1	85.7	141.5
35	4,47E+06	(371)	1,06E+06	(88)	100	137	29	110.3	87.4	139.1
36	9,72E+06	(242)	1,53E+06	(38)	30	197	64	166.2	118.5	240.3
37	4,54E+06	(264)	8,61E+05	(50)	70	111	31	138.2	102.3	190.9
38	6,42E+06	(373)	1,12E+06	(65)	70	145	36	149.4	115.0	194.0
39	7,31E+06	(364)	6,43E+05	(32)	60	83	29	293.6	206.5	433.4
40	1,03E+07	(180)	1,89E+06	(33)	21	245	85	142.6	98.6	213.3
41	8,11E+06	(471)	9,81E+05	(57)	70	127	34	213.8	162.9	280.2
42	8,38E+06	(487)	1,41E+06	(82)	70	182	40	154.8	122.6	195.3
43	1,88E+06	(156)	2,53E+05	(21)	100	33	14	192.9	123.3	319.6
44	2,75E+06	(228)	5,66E+05	(47)	100	73	21	127.1	92.9	177.9
45	7,28E+06	(604)	8,67E+05	(72)	100	112	26	217.4	170.6	276.7
46	2,67E+06	(222)	5,78E+05	(48)	100	75	22	121.2	88.8	169.3
47	6,12E+06	(508)	2,49E+06	(207)	100	322	45	64.6	54.9	76.2
48	9,37E+06	(389)	1,54E+06	(64)	50	199	50	158.1	121.6	205.4
49	5,78E+06	(480)	6,75E+05	(56)	100	87	23	221.6	168.6	290.9
50	5,92E+06	(491)	7,23E+05	(60)	100	93	24	211.9	162.5	275.9
51	8,53E+06	(354)	1,01E+06	(42)	50	131	40	219.1	160.0	308.6
52	5,29E+06	(439)	6,51E+05	(54)	100	84	23	210.3	159.1	277.7
53	7,39E+06	(613)	2,19E+06	(182)	100	283	42	88.5	74.9	104.6

Grain no.	RhoS (cm^-2)	(Ns)	RhoI (cm^-2)	(Ni)	Squares	U+/-2s		Grain Age (Ma) Age	--95% CI--	
54	7,77E+06	(361)	1,57E+06	(73)	56	203	48	129.1	100.4	165.7
55	8,81E+06	(731)	9,88E+05	(82)	100	128	28	231.0	184.2	289.3
56	6,63E+06	(550)	5,66E+05	(47)	100	73	21	302.3	226.0	414.5
57	1,94E+06	(161)	2,65E+05	(22)	100	34	14	190.1	122.7	311.1
58	9,94E+06	(231)	1,16E+06	(27)	28	150	57	221.9	150.1	342.9
59	7,87E+06	(653)	1,29E+06	(107)	100	167	32	159.2	129.8	195.2
60	9,04E+06	(345)	9,95E+05	(38)	46	129	42	235.6	169.6	337.6
61	5,20E+06	(432)	6,14E+05	(51)	100	79	22	218.9	164.3	291.1
62	4,52E+06	(150)	4,52E+05	(15)	40	58	30	257.5	153.9	468.7
63	8,19E+06	(544)	1,07E+06	(71)	80	138	33	198.8	155.6	253.9
64	6,69E+06	(333)	6,83E+05	(34)	60	88	30	253.7	179.6	371.0
65	8,01E+06	(266)	9,94E+05	(33)	40	128	44	209.5	146.8	309.9
66	2,78E+06	(136)	1,31E+06	(64)	59	169	42	56.1	41.4	76.8
67	5,71E+06	(474)	6,27E+05	(52)	100	81	22	235.3	177.4	311.6
68	3,66E+06	(304)	3,37E+05	(28)	100	44	16	280.4	192.3	426.7
69	4,58E+06	(380)	1,33E+06	(110)	100	171	33	90.6	73.2	112.1
70	6,45E+06	(375)	2,13E+06	(124)	70	276	50	79.4	64.8	97.4
71	9,34E+06	(310)	1,51E+06	(50)	40	195	55	162.0	120.5	222.8
72	8,19E+06	(340)	1,45E+06	(60)	50	187	48	147.5	112.3	193.5
73	8,16E+06	(474)	1,03E+06	(60)	70	133	34	204.6	156.9	266.7
74	3,04E+06	(252)	1,28E+06	(106)	100	165	32	62.5	49.8	78.5
75	7,95E+06	(396)	1,89E+06	(94)	60	244	51	110.3	88.1	138.0
76	9,28E+06	(154)	1,27E+06	(21)	20	163	71	190.4	121.7	315.7
77	8,92E+06	(370)	1,20E+06	(50)	50	156	44	192.9	144.1	264.2
78	7,17E+06	(357)	1,04E+06	(52)	60	135	37	178.0	133.4	237.1
79	6,85E+06	(273)	1,00E+06	(40)	48	130	41	178.0	128.2	254.3
80	3,43E+06	(285)	1,37E+06	(114)	100	177	33	65.7	52.8	81.7
81	2,92E+06	(242)	3,98E+05	(33)	100	51	18	190.9	133.4	283.1
82	7,42E+06	(431)	1,02E+06	(59)	70	131	34	189.4	144.7	247.8
83	8,26E+06	(240)	1,27E+06	(37)	35	165	54	169.2	120.2	245.8
84	1,02E+07	(254)	1,49E+06	(37)	30	192	63	179.0	127.3	259.6
85	7,83E+06	(156)	1,56E+06	(31)	24	201	72	131.6	89.7	200.2
86	4,52E+06	(105)	6,02E+05	(14)	28	78	41	194.1	112.4	366.1
87	3,37E+06	(112)	3,01E+05	(10)	40	39	24	286.4	153.8	607.5
88	6,77E+06	(281)	7,95E+05	(33)	50	103	36	221.1	155.2	326.6
89	9,40E+06	(312)	1,20E+06	(40)	40	156	49	203.0	146.8	289.0
90	7,63E+06	(190)	1,69E+06	(42)	30	218	67	118.6	84.9	169.8
91	4,28E+06	(142)	5,72E+05	(19)	40	74	34	193.9	121.2	330.7
POOLED	6,19E+06	(31306)	1,00E+06	(5077)	6094	130	5	161.6	154.7	168.7

CHI^2 PROBABILITY (%): 0.0

POOLED AGE W/ 68% CONF. INTERVAL(Ma): 161.6, 158.0 -- 165.2 (-3.5 +3.6)
95% CONF. INTERVAL(Ma): 154.7 -- 168.7 (-6.9 +7.2)

CENTRAL AGE W/ 68% CONF. INTERVAL(Ma): 161.4, 153.3 -- 169.8 (-8.0 +8.5)
95% CONF. INTERVAL(Ma): 146.0 -- 178.4 (-15.4 +17.0)
AGE DISPERSION (%): 44.2

FIT OPTION: Best-fit peaks using the binomial model of Galbraith and Green

INITIAL GUESS FOR MODEL PARAMETERS (number of peaks to fit = 4)

Peak #.	Peak Age	Theta	Fraction(%)	Count
1.	43.80	0.623	2.1	1.87
2.	53.20	0.668	1.9	1.68
3.	77.70	0.747	2.9	2.65
4.	161.60	0.860	36.0	32.77

Total range for grain ages: 43,8 to 315,4 Ma
Number of active grains (Num. used for fit): 91
Number of removed grains: 0
Degrees of freedom for fit: 84
Average of the SE(Z)'s for the grains: 0,17
Estimated width of peaks in PD plot in Z units: 0,19

PARAMETERS FOR BEST-FIT PEAKS

* *Standard error for peak age includes group error*
* *Peak width is for PD plot assuming a kernel factor = 0.60*

#.	Peak Age(Ma)	68%CI	95%CI	W(Z)	Frac(%)	SE,%	Count
1.	45.0	-6,5 ...+7,6	-11,9 ...+16,2	0.16	1.2	1.3	1.1
2.	66.9	-4,0 ...+4,2	-7,5 ...+8,5	0.12	5.4	2.5	4.9
3.	111.0	-5,3 ...+5,6	-10,2 ...+11,2	0.15	19.6	4.9	17.8
4.	206.7	-5,6 ...+5,8	-10,8 ...+11,4	0.18	73.8	5.3	67.2

Log-likelihood for best fit: -386,875
Chi-squared value for best fit: 91,053
Reduced chi-squared value: 1,084
Probability for F test: 1%
Condition number for COVAR matrix: 165,63
Number of iterations: 10

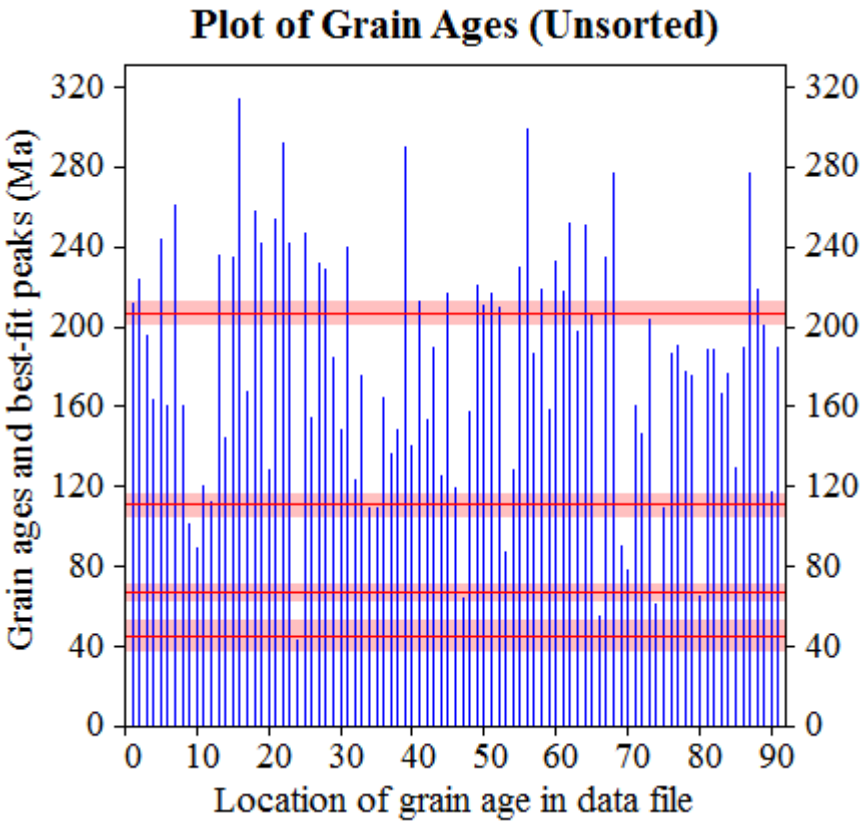
Plot of Grain Ages (Unsorted)
Grain ages and best-fit peaks (Ma)
0
40
80
120
160
200
240
280
320
0 10 20 30 40 50 60 70 80 90
Location of grain age in data file

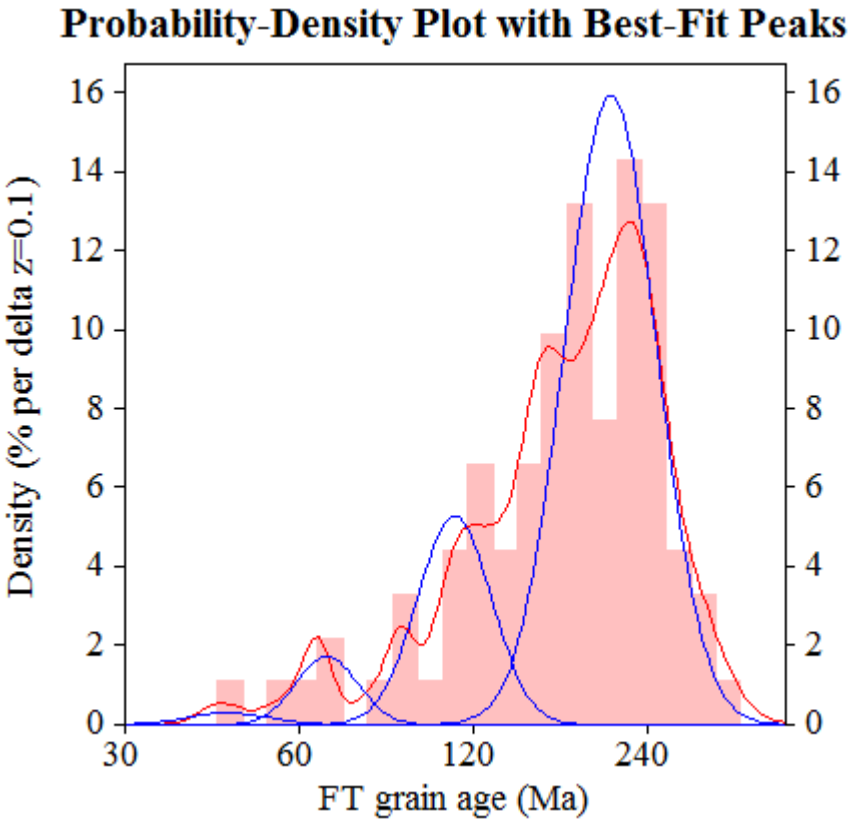
Probability-Density Plot with Best-Fit Peaks
Density (% per delta z=0.1)
0
2
4
6
8
10
12
14
16
30 60 120 240
FT grain age (Ma)

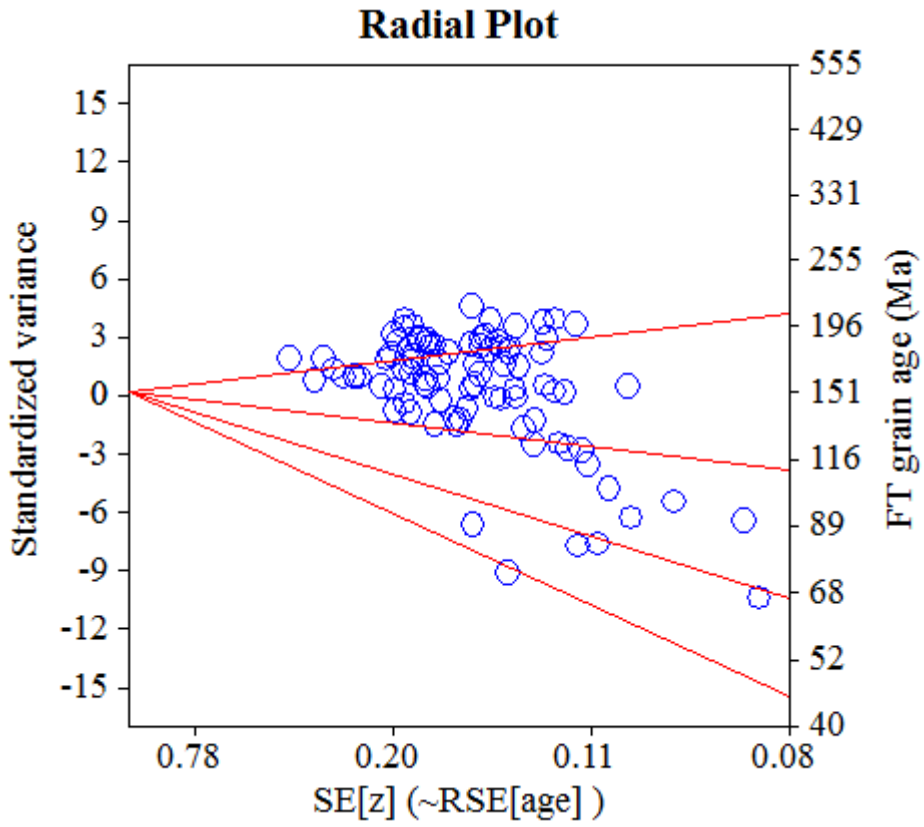
Radial Plot
Standardized variance
15
12
9
6
3
0
-3
-6
-9
-12
-15
555
429
331
255
196
151
116
89
68
52
40
FT grain age (Ma)
0.78
0.20
0.11
0.08
SE[z] (~RSE[age])

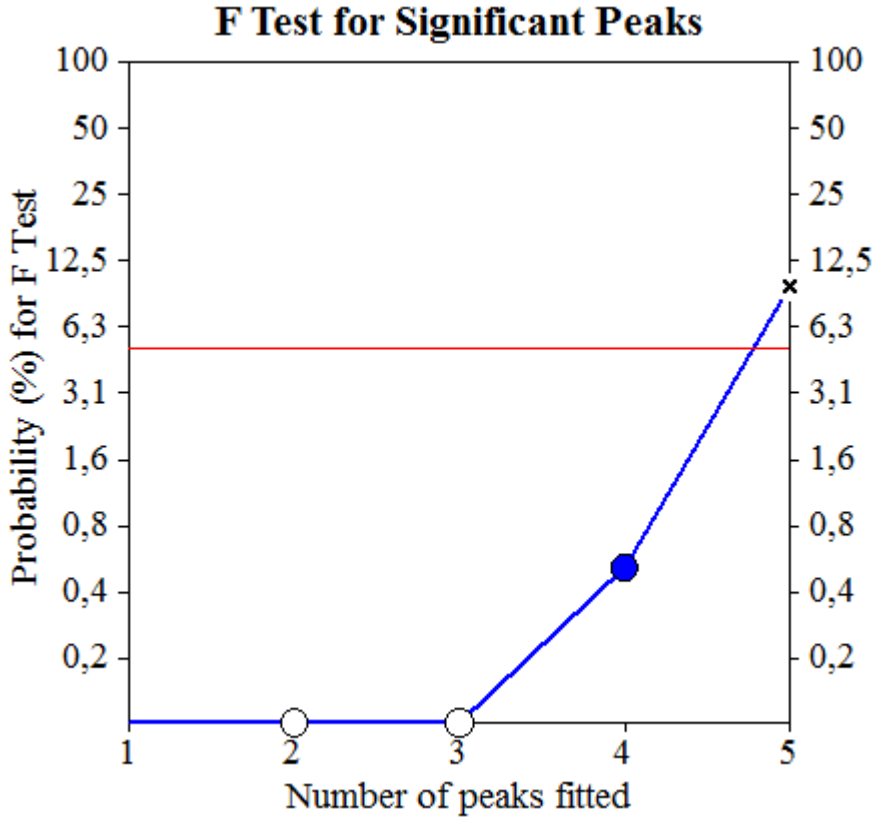
F Test for Significant Peaks
Probability (%) for F Test
100
50
25
12,5
6,3
3,1
1,6
0,8
0,4
0,2
1
2
3
4
5
Number of peaks fitted

Merged dataset:
C:\BH2\Jairo\Samples-IRR-6-2015\JG-P3-20\JG-P3-20a.ftz
C:\BH2\Jairo\Samples-IRR-6-2015\JG-P3-20\JG-P3-20.ftz

NEW PARAMETERS - ZETA METHOD

EFFECTIVE TRACK DENSITY FOR FLUENCE MONITOR (tracks/cm^2): 2,72E+05
RELATIVE ERROR (%): 1,32
EFFECTIVE URANIUM CONTENT OF MONITOR (ppm): 50,00
ZETA FACTOR AND STANDARD ERROR (yr cm^2): 137,95 4,04
SIZE OF COUNTER SQUARE (cm^2): 8,30E-07

GRAIN AGES IN ORIGINAL ORDER

Grain no.	RhoS (cm^-2)	(Ns)	RhoI (cm^-2)	(Ni)	Squares	U+/-2s		Grain Age (Ma) Age	--95% CI--	
1	8,59E+06	(164)	7,86E+05	(15)	23	144	73	200.1	119.7	364.9
2	6,40E+06	(223)	9,75E+05	(34)	42	179	61	121.5	84.9	179.9
3	6,29E+06	(94)	8,70E+05	(13)	18	160	87	132.9	75.2	259.3
4	1,04E+07	(241)	1,46E+06	(34)	28	269	92	131.2	91.9	193.9
5	5,85E+06	(102)	8,03E+05	(14)	21	148	78	134.0	77.4	254.1
6	9,98E+06	(232)	2,37E+06	(55)	28	435	117	78.5	58.5	107.5
7	1,13E+07	(328)	1,65E+06	(48)	35	304	88	126.7	93.7	175.3
8	7,07E+06	(352)	1,22E+06	(61)	60	225	58	106.6	80.9	140.4
9	1,24E+07	(144)	1,55E+06	(18)	14	285	133	147.3	91.0	255.7
10	9,40E+06	(312)	2,11E+06	(70)	40	387	93	82.6	63.4	107.5
11	9,04E+06	(180)	9,54E+05	(19)	24	175	79	174.1	109.6	295.7
12	9,45E+06	(251)	1,51E+06	(40)	32	277	87	116.3	83.5	166.9
13	9,16E+06	(304)	1,11E+06	(37)	40	205	67	151.9	108.4	219.7
14	1,06E+07	(440)	1,13E+06	(47)	50	208	61	172.9	128.5	238.6
15	1,05E+07	(348)	1,93E+06	(64)	40	354	89	100.5	76.6	131.8
16	7,50E+06	(249)	6,02E+05	(20)	40	111	49	227.9	146.3	378.3
17	6,66E+06	(221)	8,13E+05	(27)	40	149	57	151.1	101.9	234.4
18	8,91E+06	(466)	1,74E+06	(91)	63	320	67	94.9	75.3	119.6
19	1,12E+07	(364)	1,36E+06	(44)	39	250	75	153.0	112.3	214.1
20	1,41E+07	(187)	1,66E+06	(22)	16	304	129	156.6	101.4	255.9
21	1,18E+07	(392)	1,54E+06	(51)	40	282	79	142.3	106.6	194.5
22	1,18E+07	(549)	1,87E+06	(87)	56	344	74	116.7	92.5	147.2
23	5,21E+06	(242)	6,02E+05	(28)	56	111	42	159.4	108.5	244.8
24	1,04E+07	(516)	1,06E+06	(53)	60	195	54	178.6	134.3	237.2
25	1,39E+07	(427)	1,92E+06	(59)	37	353	92	133.4	101.2	175.6
26	1,72E+07	(343)	2,11E+06	(42)	24	387	119	151.0	110.0	213.3
27	1,19E+07	(238)	2,01E+06	(40)	24	369	116	110.4	79.1	158.5
28	9,17E+06	(137)	1,41E+06	(21)	18	258	112	120.5	76.5	201.2
29	1,01E+07	(160)	1,78E+06	(28)	19	326	122	105.9	71.0	164.6
30	8,82E+06	(205)	1,33E+06	(31)	28	245	88	122.4	84.2	185.0
31	1,07E+07	(124)	1,12E+06	(13)	14	206	112	174.7	100.1	337.0
32	8,11E+06	(202)	1,00E+06	(25)	30	184	73	149.1	99.0	235.8
33	1,24E+07	(308)	1,45E+06	(36)	30	266	88	158.0	112.4	229.7
34	5,18E+06	(258)	6,02E+05	(30)	60	111	40	158.7	109.3	239.9
35	8,31E+06	(469)	7,44E+05	(42)	68	137	42	205.6	150.8	288.5
36	1,12E+07	(364)	1,11E+06	(36)	39	204	68	186.3	133.1	269.9
37	4,94E+06	(328)	1,16E+06	(77)	80	213	49	79.0	61.3	101.8
38	8,78E+06	(204)	2,24E+06	(52)	28	411	114	73.1	53.8	101.2
39	7,29E+06	(242)	1,08E+06	(36)	40	199	66	124.5	88.0	182.1
40	1,07E+07	(178)	2,35E+06	(39)	20	432	138	84.8	60.0	123.4
41	1,12E+07	(298)	1,05E+06	(28)	32	194	73	195.8	133.9	299.1
42	8,23E+06	(164)	1,76E+06	(35)	24	323	109	87.1	60.4	129.4
43	5,22E+06	(104)	1,26E+06	(25)	24	231	92	77.2	49.8	125.1
44	1,27E+07	(294)	1,29E+06	(30)	28	237	86	180.5	124.8	272.0
45	1,08E+07	(270)	1,65E+06	(41)	30	302	94	122.1	88.1	174.0
46	6,31E+06	(157)	6,83E+05	(17)	30	125	60	169.7	104.0	298.4
47	6,65E+06	(276)	9,16E+05	(38)	50	168	54	134.4	96.1	194.1
48	1,03E+07	(682)	1,51E+06	(100)	80	277	56	126.2	101.6	156.6
49	1,33E+07	(442)	1,30E+06	(43)	40	238	72	189.5	139.2	265.2
50	7,68E+06	(357)	6,88E+05	(32)	56	126	44	205.2	143.9	303.9

Merged dataset:
C:\BH2\Jairo\Samples-IRR-6-2015\JG-P3-20\JG-P3-20a.ftz
C:\BH2\Jairo\Samples-IRR-6-2015\JG-P3-20\JG-P3-20.ftz

NEW PARAMETERS - ZETA METHOD

EFFECTIVE TRACK DENSITY FOR FLUENCE MONITOR (tracks/cm^2): 2,72E+05
RELATIVE ERROR (%): 1,30
EFFECTIVE URANIUM CONTENT OF MONITOR (ppm): 50,00
ZETA FACTOR AND STANDARD ERROR (yr cm^2): 137,95 4,04
SIZE OF COUNTER SQUARE (cm^2): 8,30E-07

Grain	RhoS	(Ns)	RhoI	(Ni)	Squares	U+/-2s	Grain Age (Ma)		
no.	(cm^-2)		(cm^-2)				Age	--95% CI--	
51	1,03E+07	(179)	1,15E+06	(20)	21	211 93	164.8	104.7	276.1
52	8,45E+06	(421)	1,43E+06	(71)	60	262 62	109.7	84.9	141.7
53	4,38E+06	(120)	1,61E+06	(44)	33	295 89	50.9	35.9	73.8
54	6,54E+06	(217)	6,33E+05	(21)	40	116 50	190.0	122.6	312.6
55	7,77E+06	(516)	1,33E+06	(88)	80	243 52	108.6	86.1	137.0
56	1,23E+07	(215)	2,29E+06	(40)	21	421 133	99.9	71.3	143.8
57	6,68E+06	(194)	8,61E+05	(25)	35	158 63	143.4	95.1	227.0
58	9,10E+06	(151)	1,27E+06	(21)	20	232 100	132.8	84.6	221.0
59	4,12E+06	(154)	5,89E+05	(22)	45	108 46	129.4	83.2	212.6
60	6,29E+06	(188)	1,94E+06	(58)	36	356 94	60.5	44.9	82.8
61	6,15E+06	(240)	6,41E+05	(25)	47	118 47	176.9	118.1	278.5
62	8,97E+06	(134)	1,41E+06	(21)	18	258 111	118.0	74.8	197.1
63	1,03E+07	(196)	1,31E+06	(25)	23	240 95	144.8	96.1	229.3
64	1,47E+07	(183)	2,01E+06	(25)	15	369 146	135.3	89.6	214.7
65	1,08E+07	(180)	2,23E+06	(37)	20	409 134	90.4	63.5	132.7
66	9,96E+06	(496)	1,75E+06	(87)	60	321 69	105.6	83.6	133.4
67	1,04E+07	(276)	2,07E+06	(55)	32	380 103	93.4	69.9	127.2
68	9,24E+06	(253)	8,03E+05	(22)	33	147 62	211.1	138.0	342.0
69	8,73E+06	(290)	9,04E+05	(30)	40	166 60	178.2	123.2	268.7
70	1,25E+07	(207)	1,51E+06	(25)	20	276 110	152.8	101.6	241.6
71	6,53E+06	(130)	1,26E+06	(25)	24	230 91	96.5	63.0	154.8
72	1,12E+07	(130)	2,15E+06	(25)	14	395 157	96.5	63.0	154.8
73	7,87E+06	(98)	8,03E+05	(10)	15	147 91	179.0	95.2	384.5
74	1,12E+07	(223)	2,11E+06	(42)	24	387 119	98.7	71.0	140.8
75	5,18E+06	(129)	4,82E+05	(12)	30	88 50	196.5	110.7	389.3
76	8,90E+06	(288)	2,07E+06	(67)	39	380 93	79.7	60.8	104.4
77	8,59E+06	(428)	9,64E+05	(48)	60	177 51	164.9	122.8	227.0
78	9,34E+06	(310)	1,42E+06	(47)	40	260 76	122.4	90.2	170.1
79	8,11E+06	(101)	1,20E+06	(15)	15	221 112	124.1	72.7	230.4
80	8,86E+06	(618)	2,28E+06	(159)	84	419 67	72.4	60.2	87.0
81	9,95E+06	(223)	1,65E+06	(37)	27	303 99	111.8	79.1	163.1
82	1,05E+07	(365)	8,32E+05	(29)	42	153 56	231.1	159.7	348.8
83	7,12E+06	(189)	1,05E+06	(28)	32	194 73	125.0	84.3	193.2
84	7,79E+06	(207)	1,32E+06	(35)	32	242 81	109.7	76.8	162.0
85	7,73E+06	(154)	6,02E+05	(12)	24	111 63	233.8	132.7	460.3
86	7,80E+06	(233)	1,37E+06	(41)	36	252 78	105.6	75.8	151.1
87	8,95E+06	(520)	8,61E+05	(50)	70	158 45	191.9	144.2	261.6
88	6,39E+06	(159)	1,24E+06	(31)	30	229 82	95.3	64.9	145.0
89	1,02E+07	(178)	9,75E+05	(17)	21	179 86	192.1	118.3	336.6
90	8,92E+06	(148)	8,43E+05	(14)	20	155 81	193.6	113.6	362.1
91	8,84E+06	(330)	9,64E+05	(36)	45	177 59	169.3	120.6	245.7
92	6,53E+06	(195)	1,24E+06	(37)	36	227 74	97.9	69.0	143.3
93	8,96E+06	(186)	2,46E+06	(51)	25	451 126	68.0	49.8	94.7
94	1,14E+07	(228)	1,31E+06	(26)	24	240 93	161.8	108.5	252.8
95	7,31E+06	(170)	1,20E+06	(28)	28	221 83	112.5	75.7	174.5
96	8,96E+06	(238)	1,05E+06	(28)	32	194 73	157.0	106.7	241.1
97	1,38E+07	(206)	2,48E+06	(37)	18	455 149	103.4	72.9	151.1
98	7,03E+06	(175)	1,08E+06	(27)	30	199 76	120.0	80.3	187.5
99	1,09E+07	(290)	2,15E+06	(57)	32	394 104	94.1	70.5	125.4
100	9,96E+06	(124)	2,25E+06	(28)	15	413 155	82.3	54.6	129.1
101	6,76E+06	(101)	1,14E+06	(17)	18	209 100	109.8	66.0	196.2
102	7,29E+06	(230)	1,01E+06	(32)	38	186 66	133.1	92.3	199.2
POOLED	8,84E+06	(26246)	1,31E+06	(3897)	3577	241 10	125.2	116.7	134.4

Merged dataset:
C:\BH2\Jairo\Samples-IRR-6-2015\JG-P3-20\JG-P3-20a.ftz
C:\BH2\Jairo\Samples-IRR-6-2015\JG-P3-20\JG-P3-20.ftz

```
CHI^2 PROBABILITY (%):  0.0

 POOLED AGE W/  68% CONF. INTERVAL(Ma):  125.2, 120.8 -- 129.8 ( -4.4  +4.6)
                95% CONF. INTERVAL(Ma):         116.7 -- 134.4 ( -8.6  +9.2)

CENTRAL AGE W/  68% CONF. INTERVAL(Ma):  125.1, 119.5 -- 130.9 ( -5.6  +5.8)
                95% CONF. INTERVAL(Ma):         114.4 -- 136.8 (-10.7 +11.7)
                    AGE DISPERSION (%):   27.6
```

Merged dataset:
C:\BH2\Jairo\Samples-IRR-6-2015\JG-P3-20\JG-P3-20a.ftz
C:\BH2\Jairo\Samples-IRR-6-2015\JG-P3-20\JG-P3-20.ftz

FIT OPTION: Best-fit peaks using the binomial model of Galbraith and Green

INITIAL GUESS FOR MODEL PARAMETERS (number of peaks to fit = 3)

Peak #.	Peak Age	Theta	Fraction(%)	Count
1.	107.30	0.852	39.3	40.10
2.	125.20	0.871	40.4	41.22
3.	179.40	0.906	32.6	33.21

Total range for grain ages:	50,7 to 228,7 Ma
Number of active grains (Num. used for fit):	102
Number of removed grains:	0
Degrees of freedom for fit:	97
Average of the SE(Z)'s for the grains:	0,2
Estimated width of peaks in PD plot in Z units:	0,23

PARAMETERS FOR BEST-FIT PEAKS

* *Standard error for peak age includes group error*
* *Peak width is for PD plot assuming a kernel factor = 0.60*

#.	Peak Age(Ma)	68%CI	95%CI	W(Z)	Frac(%)	SE,%	Count
1.	76.0	-5,0 ...+5,4	-9,5 ...+10,9	0.17	11.5	4.6	11.8
2.	113.5	-6,0 ...+6,3	-11,4 ...+12,7	0.20	44.4	8.4	45.3
3.	168.6	-8,5 ...+8,9	-16,2 ...+17,9	0.23	44.1	8.3	45.0

Log-likelihood for best fit:	-370,862
Chi-squared value for best fit:	99,865
Reduced chi-squared value:	1,030
Probability for F test:	0%
Condition number for COVAR matrix:	10,09
Number of iterations:	22

Merged dataset:
C:\BH2\Jairo\Samples-IRR-6-2015\JG-P3-20\JG-P3-20a.ftz
C:\BH2\Jairo\Samples-IRR-6-2015\JG-P3-20\JG-P3-20.ftz

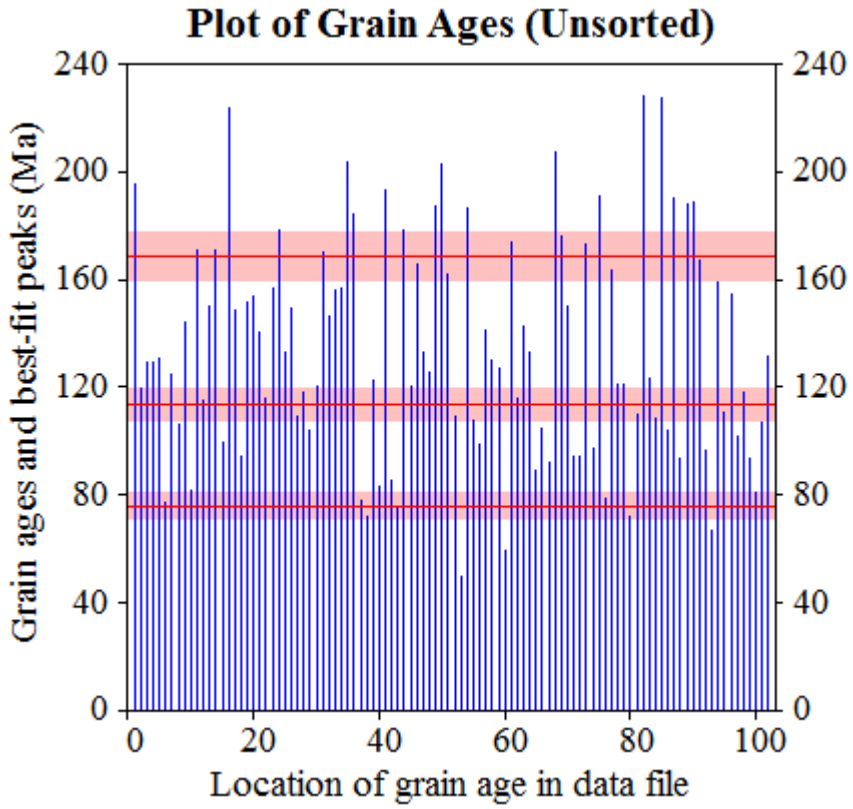

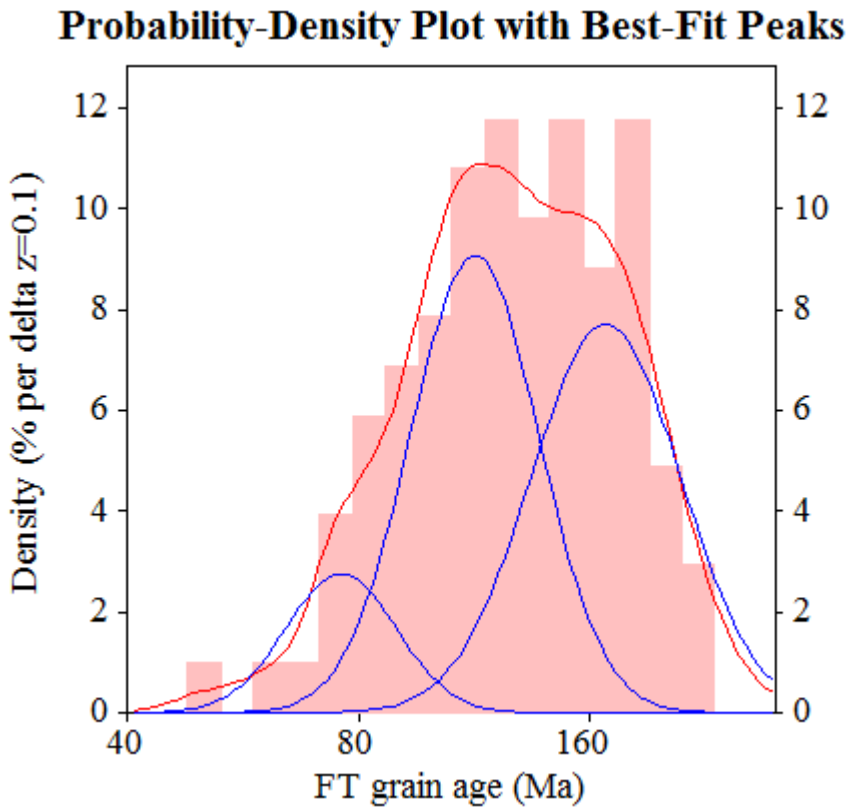

Merged dataset:
C:\BH2\Jairo\Samples-IRR-6-2015\JG-P3-20\JG-P3-20a.ftz
C:\BH2\Jairo\Samples-IRR-6-2015\JG-P3-20\JG-P3-20.ftz

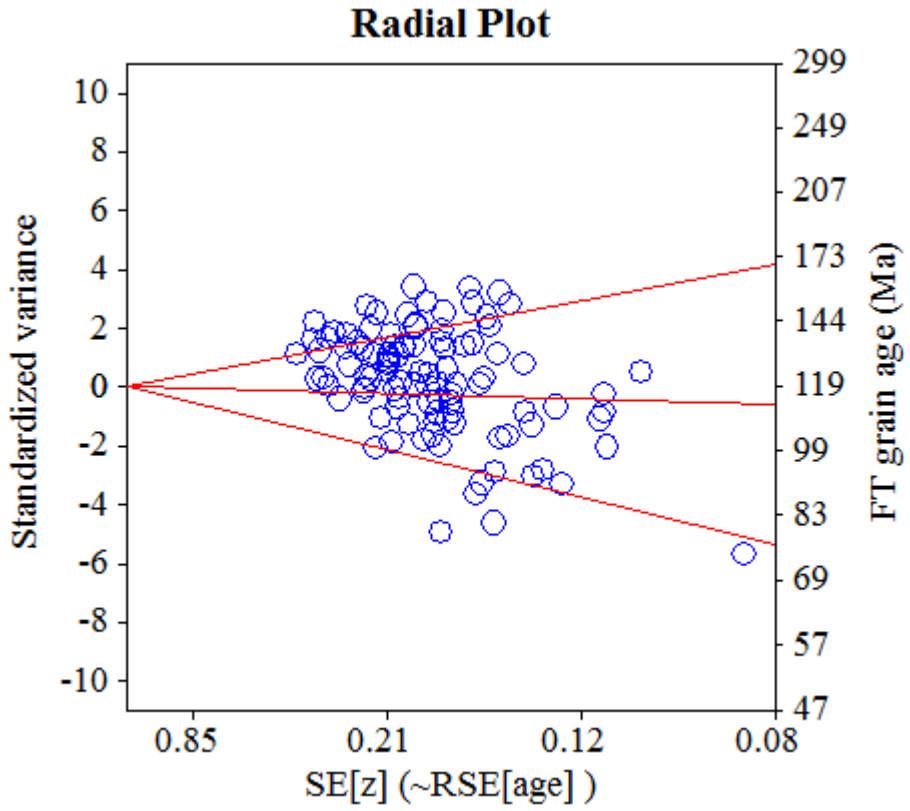

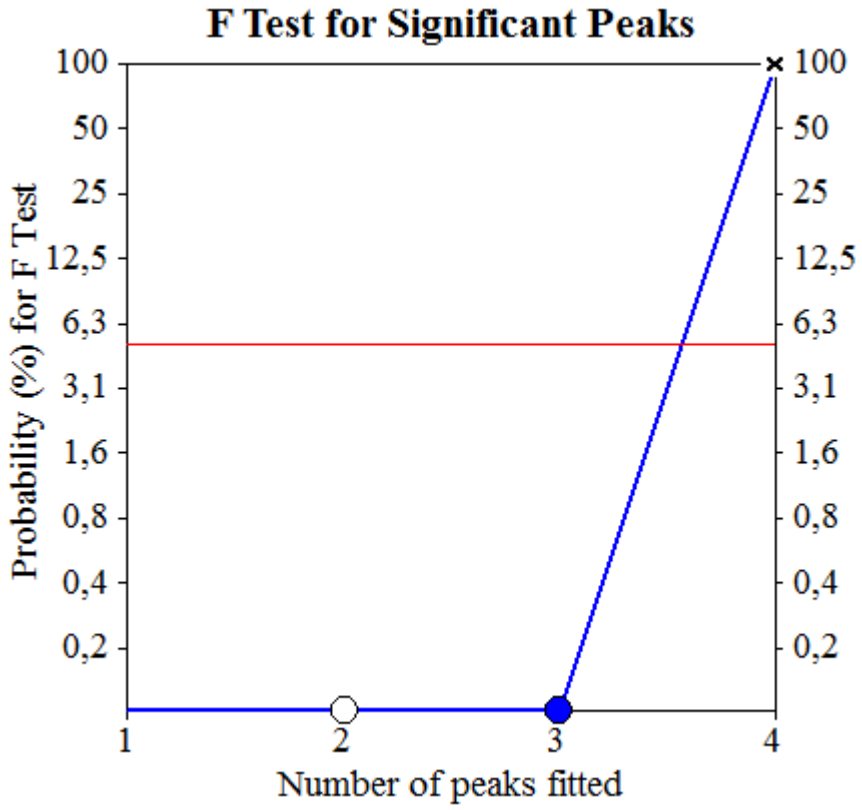

Datafile: C:\BH2\Jairo\Echantillon-IRR-10-2015\JG-P3-21-Zr\JG-P3-21-Zr.ftz
Title: Sample No. JG P3 214 Irr 10-2015-37

NEW PARAMETERS - ZETA METHOD

EFFECTIVE TRACK DENSITY FOR FLUENCE MONITOR (tracks/cm^2): 3,85E+05
RELATIVE ERROR (%): 1,15
EFFECTIVE URANIUM CONTENT OF MONITOR (ppm): 50,00
ZETA FACTOR AND STANDARD ERROR (yr cm^2): 137,14 1,57
SIZE OF COUNTER SQUARE (cm^2): 8,30E-07

GRAIN AGES IN ORIGINAL ORDER

Grain no.	RhoS (cm^-2)	(Ns)	RhoI (cm^-2)	(Ni)	Squares	U+/-2s	Grain Age (Ma) Age	--95% CI--	
1	3,05E+06	(81)	1,39E+06	(37)	32	181 59	57.4	38.6	87.2
2	7,71E+06	(96)	3,78E+06	(47)	15	490 143	53.6	37.5	77.7
3	7,38E+06	(147)	3,21E+06	(64)	24	417 104	60.2	44.7	82.2
4	5,16E+06	(210)	1,03E+06	(42)	49	134 41	130.2	93.6	185.9
5	7,29E+06	(121)	2,65E+06	(44)	20	344 104	72.0	50.8	104.2
6	7,71E+06	(256)	1,42E+06	(47)	40	184 54	141.8	104.0	197.7
7	7,29E+06	(121)	1,27E+06	(21)	20	164 71	149.3	94.4	249.8
8	3,53E+06	(88)	1,53E+06	(38)	30	198 64	60.7	41.2	91.3
9	7,69E+06	(447)	1,50E+06	(87)	70	195 42	133.5	106.1	167.7
10	7,29E+06	(363)	1,61E+06	(80)	60	209 47	117.9	92.6	150.1
11	7,17E+06	(238)	1,96E+06	(65)	40	254 63	95.2	72.4	125.1
12	1,01E+07	(167)	2,41E+06	(40)	20	313 99	108.9	77.1	157.9
13	1,08E+07	(189)	2,58E+06	(45)	21	335 100	109.6	79.2	155.3
14	6,93E+06	(207)	1,20E+06	(36)	36	157 52	149.4	105.2	219.1
15	4,25E+06	(134)	8,24E+05	(26)	38	107 42	133.9	88.2	212.4
16	3,98E+06	(119)	1,34E+06	(40)	36	174 55	77.8	54.2	114.4
17	6,42E+06	(426)	9,34E+05	(62)	80	121 31	177.4	136.3	230.9
18	6,67E+06	(166)	2,25E+06	(56)	30	292 78	77.6	57.2	107.1
19	3,16E+06	(105)	5,12E+05	(17)	40	67 32	159.7	96.3	284.2
20	8,63E+06	(86)	1,71E+06	(17)	12	222 106	131.1	78.2	235.5
21	6,41E+06	(149)	1,51E+06	(35)	28	196 66	111.0	76.8	165.3
22	7,28E+06	(145)	1,36E+06	(27)	24	176 67	139.5	92.8	218.8
23	6,02E+06	(90)	1,14E+06	(17)	18	148 71	137.2	82.0	245.7
24	8,31E+06	(138)	1,51E+06	(25)	20	196 78	143.3	93.9	228.9
25	6,44E+06	(155)	1,37E+06	(33)	29	178 62	122.3	84.1	183.9
26	3,08E+06	(92)	4,69E+05	(14)	36	61 32	169.5	97.5	321.6
27	7,35E+06	(183)	2,73E+06	(68)	30	355 86	70.1	53.1	92.6
28	9,20E+06	(229)	1,29E+06	(32)	30	167 59	185.3	128.7	276.8
29	7,13E+06	(278)	1,03E+06	(40)	47	133 42	180.2	129.9	257.3
30	5,21E+06	(173)	2,74E+06	(91)	40	356 75	49.7	38.6	64.1
31	2,23E+06	(111)	9,04E+05	(45)	60	117 35	64.6	45.5	93.6
32	1,03E+07	(94)	2,08E+06	(19)	11	270 123	128.4	78.6	222.7
33	7,39E+06	(233)	2,85E+06	(90)	38	371 78	67.6	53.0	86.2
34	2,32E+06	(154)	5,87E+05	(39)	80	76 24	103.1	72.5	150.5
35	7,37E+06	(306)	1,78E+06	(74)	50	232 54	107.5	83.5	138.4
36	6,29E+06	(141)	2,41E+06	(54)	27	313 85	68.4	49.8	95.5
37	6,63E+06	(435)	1,22E+06	(80)	79	158 36	141.1	111.2	178.8
38	1,02E+07	(177)	1,66E+06	(29)	21	216 80	158.4	107.4	243.0
39	6,52E+06	(433)	1,43E+06	(95)	80	186 38	118.6	95.0	148.0
40	7,15E+06	(356)	1,75E+06	(87)	60	227 49	106.5	84.3	134.6
41	5,76E+06	(287)	1,22E+06	(61)	60	159 41	122.0	92.7	160.5
42	6,69E+06	(333)	1,83E+06	(91)	60	237 50	95.4	75.6	120.2
43	5,23E+06	(243)	1,64E+06	(76)	56	212 49	83.3	64.4	107.7
44	9,91E+06	(148)	2,41E+06	(36)	18	313 104	107.2	74.5	159.0
45	4,42E+06	(367)	8,43E+05	(70)	100	110 26	136.0	105.4	175.2
46	5,82E+06	(145)	2,17E+06	(54)	30	282 77	70.3	51.3	98.1
47	6,75E+06	(336)	1,61E+06	(80)	60	209 47	109.2	85.6	139.3
48	6,54E+06	(217)	2,80E+06	(93)	40	364 76	61.0	47.8	77.8
49	6,24E+06	(518)	1,04E+06	(86)	100	135 29	156.2	124.4	195.9
50	3,25E+06	(270)	7,59E+05	(63)	100	99 25	111.3	84.7	146.1
51	4,91E+06	(106)	1,48E+06	(32)	26	193 68	86.5	58.1	132.9
52	6,22E+06	(155)	1,16E+06	(29)	30	151 56	138.9	93.7	214.1
53	7,71E+06	(384)	1,85E+06	(92)	60	240 50	108.7	86.6	136.4

Grain no.	RhoS (cm^-2)	(Ns)	RhoI (cm^-2)	(Ni)	Squares	U+/-2s	Grain Age (Ma) Age	--95% CI--	
54	4,82E+06	(168)	8,32E+05	(29)	42	108 40	150.4	101.8	231.2
55	7,91E+06	(197)	1,69E+06	(42)	30	219 67	122.2	87.7	174.9
56	4,82E+06	(120)	1,20E+06	(30)	30	157 57	104.3	69.8	161.3
57	4,60E+06	(370)	1,42E+06	(114)	97	184 35	84.7	68.6	104.6
58	7,85E+06	(202)	1,13E+06	(29)	31	146 54	180.4	122.9	275.7
59	2,95E+06	(98)	6,33E+05	(21)	40	82 35	121.3	75.8	204.6
60	4,48E+06	(156)	1,00E+06	(35)	42	130 44	116.1	80.5	172.7
61	2,18E+06	(145)	6,48E+05	(43)	80	84 26	88.2	62.6	127.0
62	5,16E+06	(257)	1,89E+06	(94)	60	245 51	71.4	56.3	90.4
63	4,82E+06	(112)	9,90E+05	(23)	28	129 53	126.5	80.9	207.7
64	6,31E+06	(157)	1,20E+06	(30)	30	157 57	136.1	92.3	208.3
65	3,58E+06	(104)	5,85E+05	(17)	35	76 36	158.2	95.4	281.6
66	3,83E+06	(127)	1,27E+06	(42)	40	164 51	79.1	55.6	115.0
67	6,55E+06	(163)	1,00E+06	(25)	30	130 52	168.9	111.5	268.2
68	4,84E+06	(225)	1,01E+06	(47)	56	131 38	124.8	91.2	174.7
69	9,98E+06	(174)	2,70E+06	(47)	21	350 102	96.7	70.0	136.5
70	6,24E+06	(290)	1,83E+06	(85)	56	238 52	88.9	69.8	113.2
71	8,11E+06	(101)	1,93E+06	(24)	15	250 101	109.6	70.2	178.9
72	8,49E+06	(282)	2,08E+06	(69)	40	270 65	106.2	81.7	138.0
73	4,99E+06	(207)	1,25E+06	(52)	50	163 45	104.0	76.7	143.8
74	2,93E+06	(85)	9,98E+05	(29)	35	130 48	76.6	50.0	121.3
75	5,66E+06	(329)	1,15E+06	(67)	70	150 37	127.4	98.1	165.4
76	6,55E+06	(272)	1,04E+06	(43)	50	135 41	164.3	119.5	232.0
77	7,20E+06	(215)	1,57E+06	(47)	36	204 59	119.3	87.0	167.2
78	4,51E+06	(374)	7,95E+05	(66)	100	103 25	146.8	113.2	190.2
79	7,23E+06	(294)	2,31E+06	(94)	49	300 62	81.6	64.7	102.9
80	4,46E+06	(74)	1,75E+06	(29)	20	227 84	66.8	43.1	106.5
81	5,44E+06	(158)	1,17E+06	(34)	35	152 52	121.0	83.6	180.9
82	3,58E+06	(119)	6,02E+05	(20)	40	78 35	154.1	96.5	261.1
83	9,24E+06	(161)	1,61E+06	(28)	21	209 78	149.3	100.3	231.5
84	9,24E+06	(115)	2,33E+06	(29)	15	303 112	103.4	68.7	161.3
85	6,50E+06	(151)	9,47E+05	(22)	28	123 52	177.5	114.3	291.2
86	8,09E+06	(188)	1,29E+06	(30)	28	168 61	162.6	111.0	247.3
87	5,45E+06	(362)	7,98E+05	(53)	80	104 28	176.2	132.4	234.1
88	7,69E+06	(217)	1,45E+06	(41)	34	189 59	137.7	98.8	197.2
89	9,87E+06	(172)	1,38E+06	(24)	21	179 72	185.3	121.7	296.5
90	9,17E+06	(213)	1,68E+06	(39)	28	218 70	142.1	101.2	205.2
91	7,33E+06	(365)	9,04E+05	(45)	60	117 35	209.9	154.7	292.2
92	7,67E+06	(191)	3,01E+06	(75)	30	391 91	66.4	50.9	86.7
93	7,65E+06	(165)	1,58E+06	(34)	26	205 70	126.3	87.4	188.5
94	7,95E+06	(231)	1,55E+06	(45)	35	201 60	133.7	97.3	188.2
95	5,98E+06	(283)	1,01E+06	(48)	57	132 38	153.3	113.2	212.6
96	4,53E+06	(376)	1,13E+06	(94)	100	147 30	104.2	83.1	130.6
97	8,99E+06	(179)	2,26E+06	(45)	24	293 87	103.9	74.8	147.4
98	9,07E+06	(414)	1,64E+06	(75)	55	213 49	143.1	112.0	182.7
99	5,40E+06	(287)	8,47E+05	(45)	64	110 33	165.7	121.3	231.9
100	8,23E+06	(205)	1,61E+06	(40)	30	209 66	133.4	95.2	192.1
POOLED	5,96E+06	(21198)	1,38E+06	(4907)	4285	179 7	113.0	108.1	118.1

CHI^2 PROBABILITY (%): 0.0

POOLED AGE W/ 68% CONF. INTERVAL(Ma): 113.0, 110.5 -- 115.6 (-2.5 +2.6)
95% CONF. INTERVAL(Ma): 108.1 -- 118.1 (-4.9 +5.1)

CENTRAL AGE W/ 68% CONF. INTERVAL(Ma): 110.8, 106.8 -- 115.0 (-4.1 +4.2)
95% CONF. INTERVAL(Ma): 103.0 -- 119.2 (-7.8 +8.4)
AGE DISPERSION (%): 29.4

FIT OPTION: Best-fit peaks using the binomial model of Galbraith and Green

INITIAL GUESS FOR MODEL PARAMETERS (number of peaks to fit = 3)

Peak #.	Peak Age	Theta	Fraction(%)	Count
1.	49.90	0.655	4.5	4.49
2.	83.60	0.761	19.2	19.24
3.	113.00	0.812	44.5	44.48

Total range for grain ages:	49,9 to 208,6 Ma
Number of active grains (Num. used for fit):	100
Number of removed grains:	0
Degrees of freedom for fit:	95
Average of the SE(Z)'s for the grains:	0,18
Estimated width of peaks in PD plot in Z units:	0,21

PARAMETERS FOR BEST-FIT PEAKS

* *Standard error for peak age includes group error*
* *Peak width is for PD plot assuming a kernel factor = 0.60*

#.	Peak Age(Ma)	68%CI	95%CI	W(Z)	Frac(%)	SE,%	Count
1.	69.4	-4,1 ...+4,4	-7,8 ...+8,8	0.17	20.4	5.8	20.4
2.	107.6	-8,6 ...+9,3	-16,2 ...+19,0	0.18	31.5	10.7	31.5
3.	145.3	-6,5 ...+6,8	-12,5 ...+13,7	0.20	48.1	12.3	48.1

Log-likelihood for best fit:	-382,896
Chi-squared value for best fit:	98,475
Reduced chi-squared value:	1,037
Probability for F test:	0%
Condition number for COVAR matrix:	20,30
Number of iterations:	52

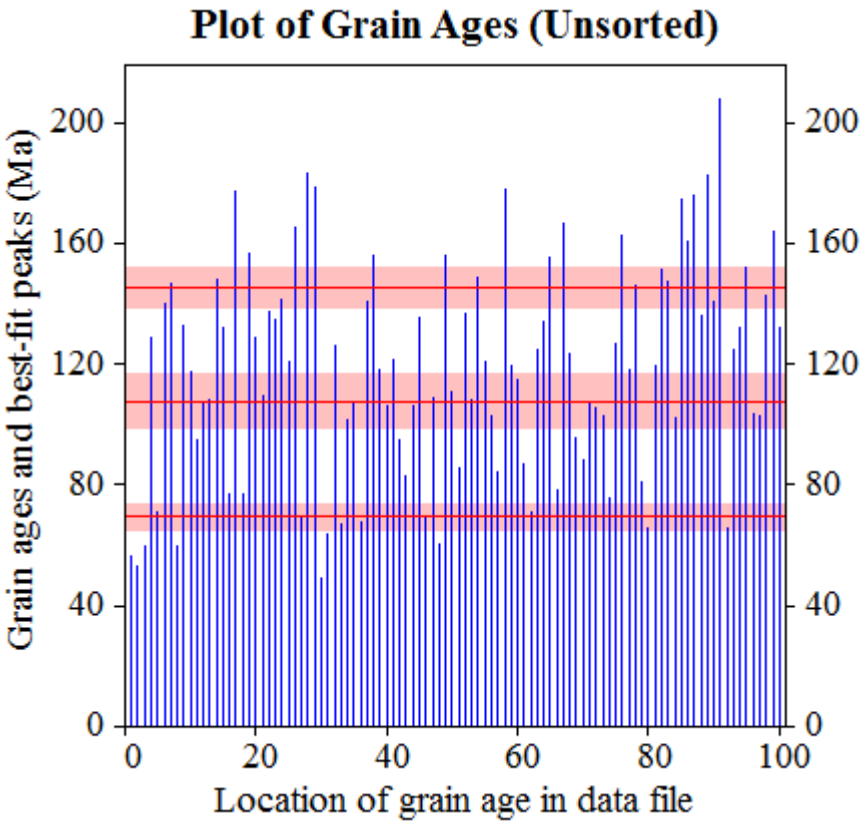
Plot of Grain Ages (Unsorted)
Grain ages and best-fit peaks (Ma)
0
40
80
120
160
200
0
20
40
60
80
100
Location of grain age in data file

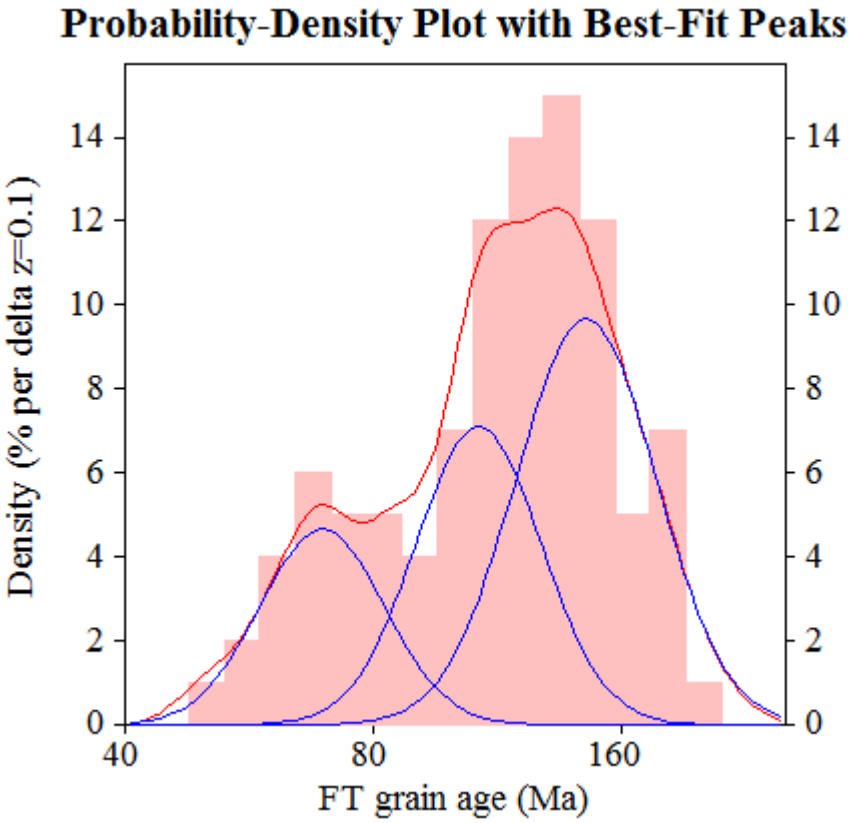
Probability-Density Plot with Best-Fit Peaks
Density (% per delta z=0.1)
0
2
4
6
8
10
12
14
40
80
160
FT grain age (Ma)

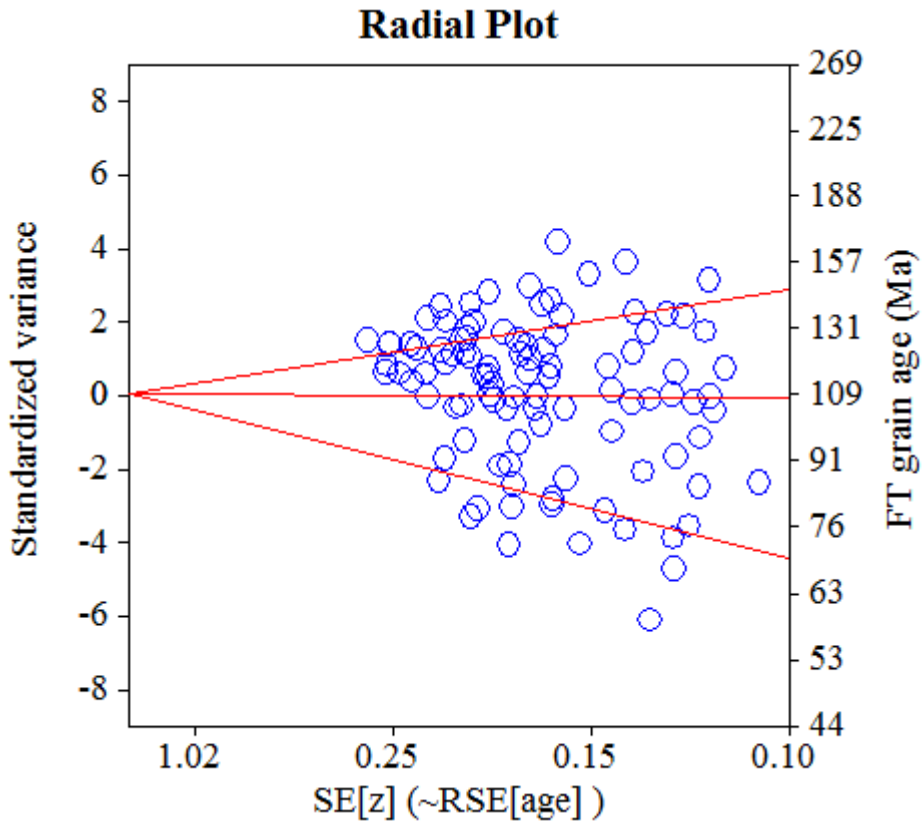
Radial Plot
Standardized variance
8
6
4
2
0
-2
-4
-6
-8
269
225
188
157
131
109
91
76
63
53
44
FT grain age (Ma)
1.02
0.25
0.15
0.10
SE[z] (~RSE[age])

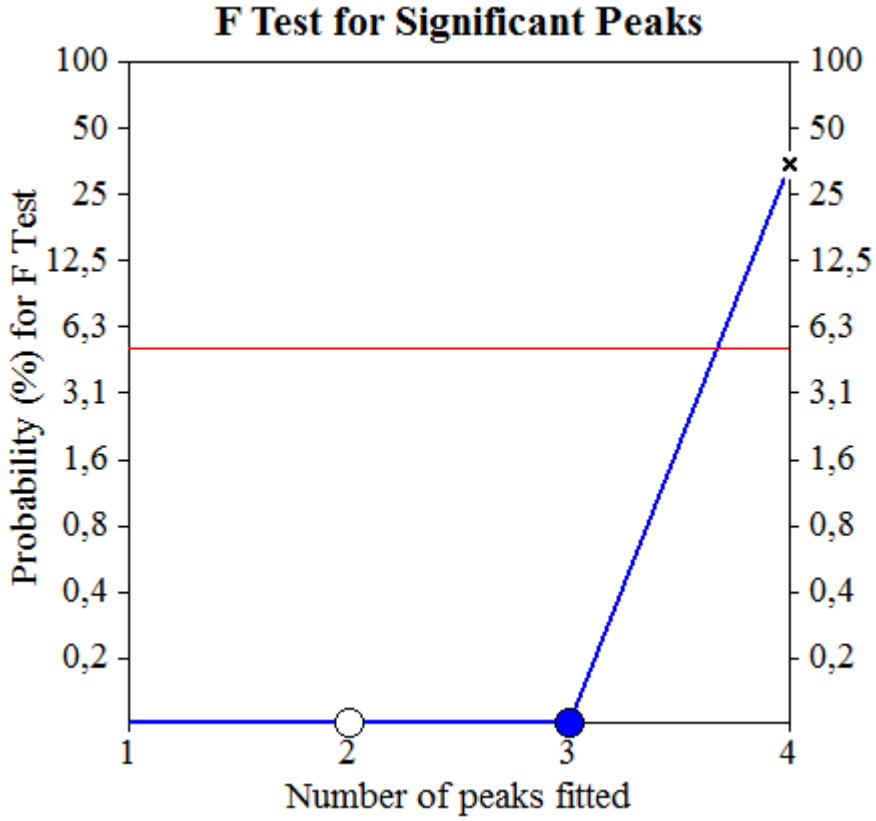
F Test for Significant Peaks
Probability (%) for F Test
100
50
25
12,5
6,3
3,1
1,6
0,8
0,4
0,2
1
2
3
4
Number of peaks fitted

Merged dataset:
C:\BH2\Jairo\Echantillon-IRR-10-2015\JG-P3-22-Zr\JG-P3-22-Zr.ftz
C:\BH2\Jairo\Echantillon-IRR-10-2015\JG-P3-22-Zr\JG-P3-22a-Zr.ftz

NEW PARAMETERS - ZETA METHOD

EFFECTIVE TRACK DENSITY FOR FLUENCE MONITOR (tracks/cm^2): 3,86E+05
RELATIVE ERROR (%): 1,17
EFFECTIVE URANIUM CONTENT OF MONITOR (ppm): 50,00
ZETA FACTOR AND STANDARD ERROR (yr cm^2): 137,14 1,57
SIZE OF COUNTER SQUARE (cm^2): 8,30E-07

GRAIN AGES IN ORIGINAL ORDER

Grain no.	RhoS (cm^-2)	(Ns)	RhoI (cm^-2)	(Ni)	Squares	U+/-2s	Grain Age (Ma) Age	--95% CI--	
1	8,86E+06	(103)	1,98E+06	(23)	14	256 106	116.8	74.4	192.5
2	4,77E+06	(95)	1,86E+06	(37)	24	241 79	67.4	45.8	101.5
3	4,49E+06	(108)	1,25E+06	(30)	29	161 59	94.2	62.7	146.4
4	6,70E+06	(178)	2,26E+06	(60)	32	293 76	77.4	57.8	103.6
5	4,32E+06	(86)	1,86E+06	(37)	24	241 79	61.1	41.2	92.5
6	3,29E+06	(131)	1,08E+06	(43)	48	140 43	79.9	56.4	115.7
7	6,08E+06	(338)	1,98E+06	(110)	67	256 49	80.5	64.8	99.8
8	3,94E+06	(98)	1,00E+06	(25)	30	130 52	102.4	65.9	166.0
9	5,82E+06	(145)	2,33E+06	(58)	30	302 79	65.7	48.3	90.8
10	5,34E+06	(155)	2,20E+06	(64)	35	285 71	63.3	47.3	84.6
11	5,57E+06	(194)	3,59E+06	(125)	42	464 84	40.8	32.5	51.1
12	7,08E+06	(141)	2,46E+06	(49)	24	319 91	75.6	54.4	106.9
13	2,11E+06	(70)	5,12E+05	(17)	40	66 32	107.3	63.1	194.7
14	5,46E+06	(272)	1,63E+06	(81)	60	211 47	87.8	68.5	112.4
15	4,34E+06	(119)	1,79E+06	(49)	33	232 66	63.8	45.5	91.0
16	4,70E+06	(78)	1,14E+06	(19)	20	148 67	107.1	64.8	187.4
17	3,82E+06	(95)	2,49E+06	(62)	30	323 82	40.4	29.1	56.6
18	4,94E+06	(82)	1,27E+06	(21)	20	164 71	101.9	63.0	173.5
19	4,94E+06	(164)	1,14E+06	(38)	40	148 48	112.9	79.3	165.2
20	3,92E+06	(130)	1,63E+06	(54)	40	211 57	63.3	45.9	88.7
21	3,82E+06	(152)	1,18E+06	(47)	48	153 44	84.8	61.0	120.4
22	3,70E+06	(123)	6,33E+05	(21)	40	82 35	152.2	96.3	254.4
23	8,32E+06	(435)	2,85E+06	(149)	63	369 61	76.6	63.5	92.3
24	7,11E+06	(118)	3,86E+06	(64)	20	499 125	48.6	35.6	66.9
25	6,16E+06	(92)	1,94E+06	(29)	18	251 93	83.1	54.5	131.0
26	4,46E+06	(100)	1,52E+06	(34)	27	197 67	77.1	52.0	117.5
27	5,90E+06	(196)	1,81E+06	(60)	40	234 60	85.2	63.9	113.6
28	4,42E+06	(154)	8,03E+05	(28)	42	104 39	143.3	96.1	222.5
29	8,96E+06	(223)	2,81E+06	(70)	30	364 87	83.2	63.6	108.7
30	4,85E+06	(153)	1,40E+06	(44)	38	181 54	91.1	65.0	130.6
31	3,80E+06	(101)	2,30E+06	(61)	32	297 76	43.6	31.5	61.0
32	5,56E+06	(83)	2,74E+06	(41)	18	355 111	53.3	36.3	79.5
33	7,47E+06	(248)	1,72E+06	(57)	40	222 59	113.2	85.0	150.6
34	6,73E+06	(67)	2,81E+06	(28)	12	364 137	62.8	40.0	101.5
35	6,06E+06	(352)	1,94E+06	(113)	70	252 48	81.6	65.9	100.9
36	5,66E+06	(235)	1,98E+06	(82)	50	256 57	75.0	58.3	96.4
37	2,98E+06	(247)	6,02E+05	(50)	100	78 22	129.1	95.4	178.6
38	1,59E+06	(74)	3,44E+05	(16)	56	45 22	120.3	70.2	221.5
39	4,75E+06	(130)	8,76E+05	(24)	33	114 46	141.0	91.5	227.9
40	5,69E+06	(302)	2,05E+06	(109)	64	266 51	72.6	58.3	90.4
41	5,60E+06	(93)	1,81E+06	(30)	20	234 85	81.2	53.6	127.1
42	4,39E+06	(51)	2,24E+06	(26)	14	290 113	51.6	31.7	86.2
43	3,96E+06	(92)	6,45E+05	(15)	28	84 43	158.9	92.8	295.1
44	8,07E+06	(67)	1,93E+06	(16)	10	250 123	109.0	63.2	201.8
45	9,17E+06	(137)	1,87E+06	(28)	18	243 91	127.6	85.1	199.1
46	1,40E+07	(116)	4,22E+06	(35)	10	546 184	86.8	59.3	130.7
47	2,59E+06	(129)	8,23E+05	(41)	60	107 33	82.5	57.9	120.4
48	6,99E+06	(116)	2,65E+06	(44)	20	343 103	69.2	48.7	100.4
49	8,49E+06	(282)	1,42E+06	(47)	40	183 53	156.4	115.1	217.6
50	4,44E+06	(70)	6,34E+05	(10)	19	82 51	180.2	94.3	391.2
51	7,07E+06	(176)	1,33E+06	(33)	30	172 59	139.1	96.1	208.2
52	6,43E+06	(96)	2,68E+06	(40)	18	347 109	63.1	43.3	93.7

Merged dataset:
C:\BH2\Jairo\Echantillon-IRR-10-2015\JG-P3-22-Zr\JG-P3-22-Zr.ftz
C:\BH2\Jairo\Echantillon-IRR-10-2015\JG-P3-22-Zr\JG-P3-22a-Zr.ftz

Grain no.	RhoS (cm^-2)	(Ns)	RhoI (cm^-2)	(Ni)	Squares	U+/-2s	Grain Age (Ma) Age	--95% CI--	
53	3,55E+06	(177)	1,16E+06	(58)	60	151 40	80.1	59.4	109.8
54	5,15E+06	(154)	1,84E+06	(55)	36	238 64	73.5	53.9	102.0
55	6,17E+06	(82)	3,69E+06	(49)	16	478 136	44.1	30.6	64.2
56	6,14E+06	(255)	2,05E+06	(85)	50	265 58	78.5	61.4	100.3
57	9,77E+06	(146)	1,81E+06	(27)	18	234 89	140.9	93.7	220.9
58	5,56E+06	(83)	8,03E+05	(12)	18	104 59	178.5	98.6	358.5
59	8,09E+06	(430)	1,15E+06	(61)	64	149 38	182.5	139.9	237.8
60	3,52E+06	(108)	7,82E+05	(24)	37	101 41	117.4	75.5	191.2
61	6,12E+06	(305)	1,75E+06	(87)	60	226 49	91.6	72.2	116.2
62	5,42E+06	(135)	1,16E+06	(29)	30	151 56	121.5	81.4	188.3
63	5,19E+06	(168)	9,89E+05	(32)	39	128 45	136.9	94.0	206.5
64	6,31E+06	(220)	2,01E+06	(70)	42	260 62	82.1	62.8	107.3
65	9,16E+06	(76)	2,53E+06	(21)	10	328 142	94.6	58.1	161.6
66	6,99E+06	(209)	1,77E+06	(53)	36	230 63	103.3	76.4	142.4
67	4,34E+06	(72)	1,33E+06	(22)	20	172 72	85.6	52.9	145.1
68	5,78E+06	(48)	1,81E+06	(15)	10	234 119	83.5	46.4	160.9
69	6,02E+06	(120)	2,16E+06	(43)	24	280 85	73.3	51.5	106.4
70	7,76E+06	(219)	1,70E+06	(48)	34	220 63	119.3	87.3	166.7
71	2,25E+06	(112)	1,08E+06	(54)	60	140 38	54.6	39.2	77.0
72	4,47E+06	(178)	1,46E+06	(58)	48	189 50	80.6	59.7	110.4
73	3,21E+06	(80)	6,83E+05	(17)	30	88 42	122.4	72.7	220.6
74	5,98E+06	(149)	1,93E+06	(48)	30	250 72	81.5	58.7	115.3
75	6,33E+06	(105)	1,33E+06	(22)	20	172 72	124.4	78.7	206.9
76	5,41E+06	(166)	1,14E+06	(35)	37	148 50	123.9	86.1	183.8

Merged dataset:
C:\BH2\Jairo\Echantillon-IRR-10-2015\JG-P3-22-Zr\JG-P3-22-Zr.ftz
C:\BH2\Jairo\Echantillon-IRR-10-2015\JG-P3-22-Zr\JG-P3-22a-Zr.ftz

NEW PARAMETERS - ZETA METHOD

EFFECTIVE TRACK DENSITY FOR FLUENCE MONITOR (tracks/cm^2): 3,87E+05
RELATIVE ERROR (%): 1,18
EFFECTIVE URANIUM CONTENT OF MONITOR (ppm): 50,00
ZETA FACTOR AND STANDARD ERROR (yr cm^2): 137,14 1,57
SIZE OF COUNTER SQUARE (cm^2): 8,30E-07

Grain no.	RhoS (cm^-2)	(Ns)	RhoI (cm^-2)	(Ni)	Squares	U+/-2s		Grain Age (Ma) Age	--95% CI--	
77	3,84E+06	(172)	1,29E+06	(58)	54	167	44	78.0	57.7	107.0
78	6,63E+06	(220)	1,36E+06	(45)	40	175	52	127.9	92.9	180.4
79	4,95E+06	(115)	1,46E+06	(34)	28	189	65	88.7	60.3	134.3
80	5,03E+06	(167)	1,23E+06	(41)	40	160	50	106.7	75.8	154.1
81	3,88E+06	(193)	9,64E+05	(48)	60	125	36	105.4	76.8	147.8
82	6,43E+06	(128)	1,81E+06	(36)	24	234	78	93.2	64.3	139.1
83	3,01E+06	(100)	9,64E+05	(32)	40	125	44	82.0	54.9	126.3
84	4,70E+06	(78)	1,33E+06	(22)	20	171	72	92.8	57.6	156.6
85	3,70E+06	(172)	1,36E+06	(63)	56	175	44	71.4	53.5	95.2
86	4,17E+06	(277)	1,10E+06	(73)	80	142	33	99.1	76.6	128.2
87	6,46E+06	(268)	1,88E+06	(78)	50	243	55	89.9	69.8	115.6
88	7,18E+06	(268)	1,39E+06	(52)	45	180	50	134.8	100.3	185.1
89	3,59E+06	(134)	1,34E+06	(50)	45	173	49	70.5	50.7	99.7
90	5,07E+06	(206)	7,38E+05	(30)	49	95	35	178.6	122.4	271.0
91	6,49E+06	(167)	1,75E+06	(45)	31	226	67	97.4	69.9	138.6
92	6,30E+06	(209)	2,26E+06	(75)	40	292	68	73.0	56.1	95.0
93	6,54E+06	(179)	2,08E+06	(57)	33	269	71	82.5	61.1	113.3
94	3,49E+06	(116)	7,23E+05	(24)	40	94	38	126.2	81.4	204.8
95	6,37E+06	(222)	1,95E+06	(68)	42	252	61	85.3	65.1	111.9
96	7,15E+06	(356)	2,87E+06	(143)	60	371	63	65.4	53.8	79.5
97	6,06E+06	(151)	1,57E+06	(39)	30	203	65	101.5	71.3	148.3
98	6,61E+06	(225)	1,18E+06	(40)	41	152	48	146.9	105.2	211.0
99	6,45E+06	(375)	1,46E+06	(85)	70	189	41	115.2	91.1	145.7
100	7,26E+06	(241)	1,51E+06	(50)	40	195	55	126.2	93.1	174.7
POOLED	5,32E+06	(16328)	1,57E+06	(4805)	3697	203	8	89.3	85.4	93.4

CHI^2 PROBABILITY (%): 0.0

POOLED AGE W/ 68% CONF. INTERVAL(Ma): 89.3, 87.3 -- 91.4 (-2.0 +2.1)
95% CONF. INTERVAL(Ma): 85.4 -- 93.4 (-3.9 +4.1)

CENTRAL AGE W/ 68% CONF. INTERVAL(Ma): 89.0, 85.8 -- 92.3 (-3.2 +3.3)
95% CONF. INTERVAL(Ma): 82.8 -- 95.7 (-6.2 +6.7)
AGE DISPERSION (%): 28.2

Merged dataset:
C:\BH2\Jairo\Echantillon-IRR-10-2015\JG-P3-22-Zr\JG-P3-22-Zr.ftz
C:\BH2\Jairo\Echantillon-IRR-10-2015\JG-P3-22-Zr\JG-P3-22a-Zr.ftz

FIT OPTION: Best-fit peaks using the binomial model of Galbraith and Green

INITIAL GUESS FOR MODEL PARAMETERS (number of peaks to fit = 3)

Peak #.	Peak Age	Theta	Fraction(%)	Count
1.	41.10	0.609	6.9	6.93
2.	47.90	0.645	7.0	7.00
3.	89.30	0.773	43.6	43.63

Total range for grain ages: 40,3 to 182,7 Ma
Number of active grains (Num. used for fit): 100
Number of removed grains: 0
Degrees of freedom for fit: 95
Average of the SE(Z)'s for the grains: 0,19
Estimated width of peaks in PD plot in Z units: 0,22

PARAMETERS FOR BEST-FIT PEAKS

* *Standard error for peak age includes group error*
* *Peak width is for PD plot assuming a kernel factor = 0.60*

#.	Peak Age(Ma)	68%CI	95%CI	W(Z)	Frac(%)	SE,%	Count
1.	44.8	-3,2 ...+3,5	-6,1 ...+7,0	0.18	6.3	2.8	6.3
2.	80.3	-2,4 ...+2,5	-4,6 ...+4,9	0.18	60.0	6.4	60.0
3.	129.7	-5,5 ...+5,8	-10,6 ...+11,5	0.22	33.7	6.2	33.7

Log-likelihood for best fit: -374,143
Chi-squared value for best fit: 93,987
Reduced chi-squared value: 0,989
Probability for F test: 0%
Condition number for COVAR matrix: 11,40
Number of iterations: 21

Merged dataset:
C:\BH2\Jairo\Echantillon-IRR-10-2015\JG-P3-22-Zr\JG-P3-22-Zr.ftz
C:\BH2\Jairo\Echantillon-IRR-10-2015\JG-P3-22-Zr\JG-P3-22a-Zr.ftz

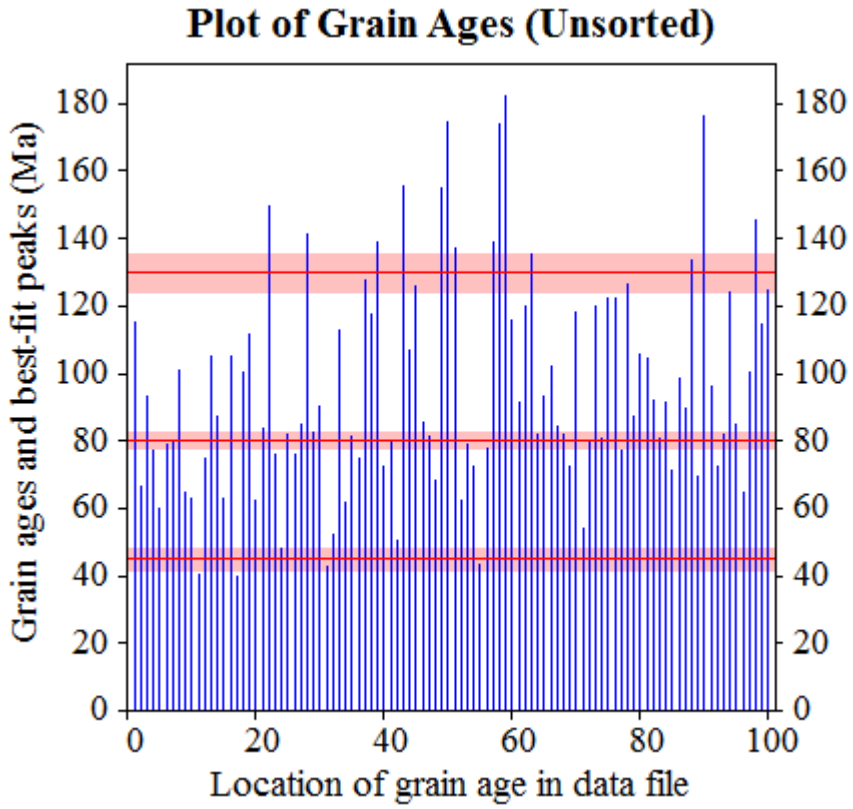

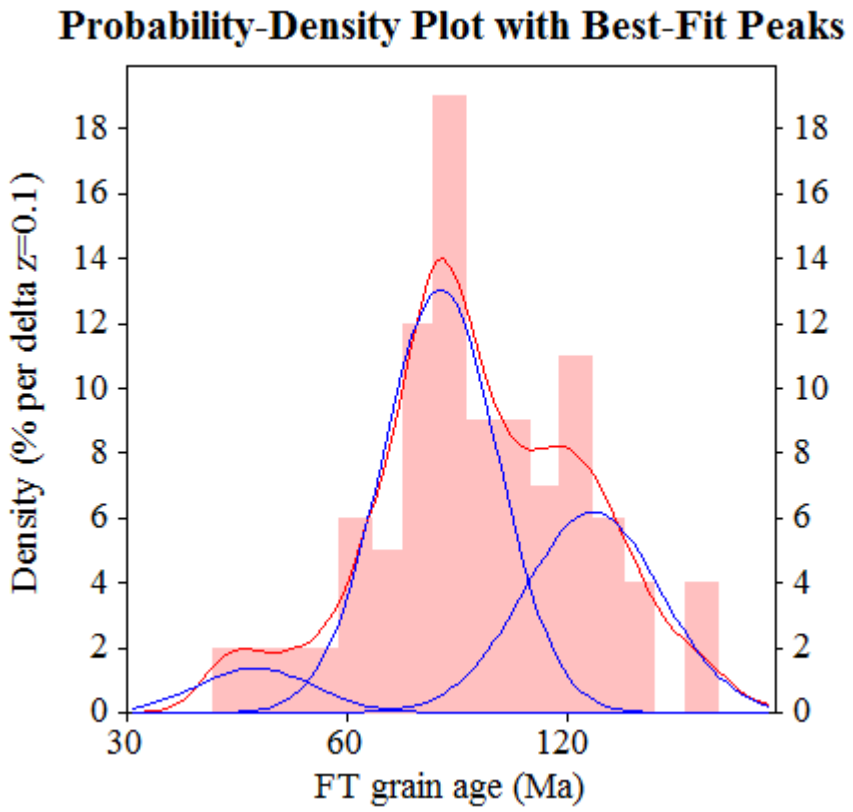

Merged dataset:
C:\BH2\Jairo\Echantillon-IRR-10-2015\JG-P3-22-Zr\JG-P3-22-Zr.ftz
C:\BH2\Jairo\Echantillon-IRR-10-2015\JG-P3-22-Zr\JG-P3-22a-Zr.ftz

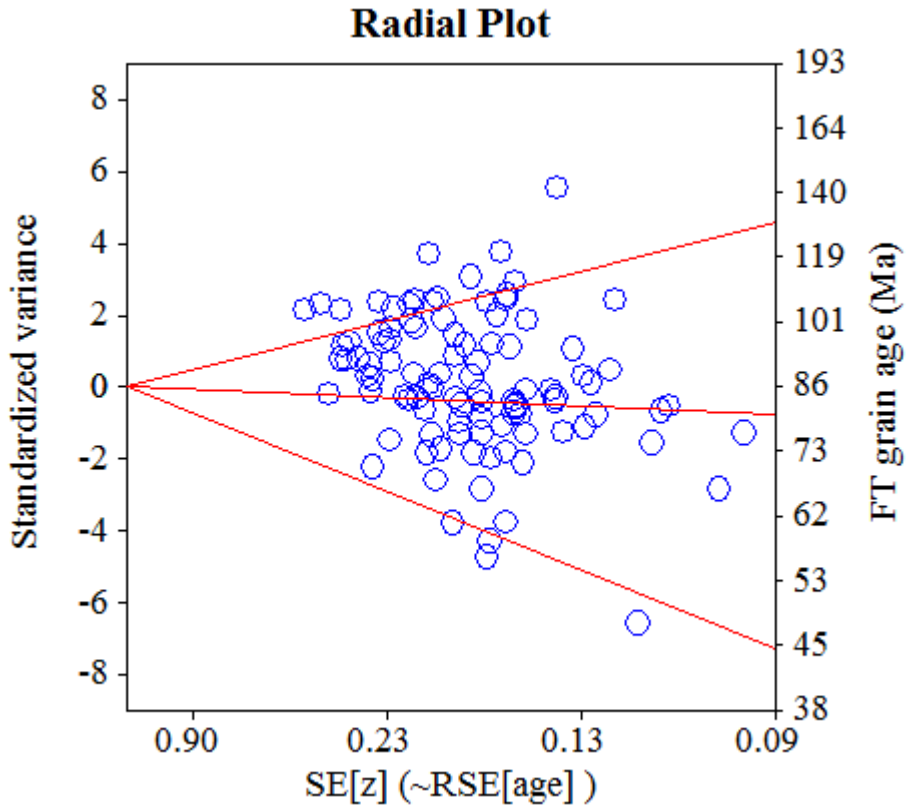

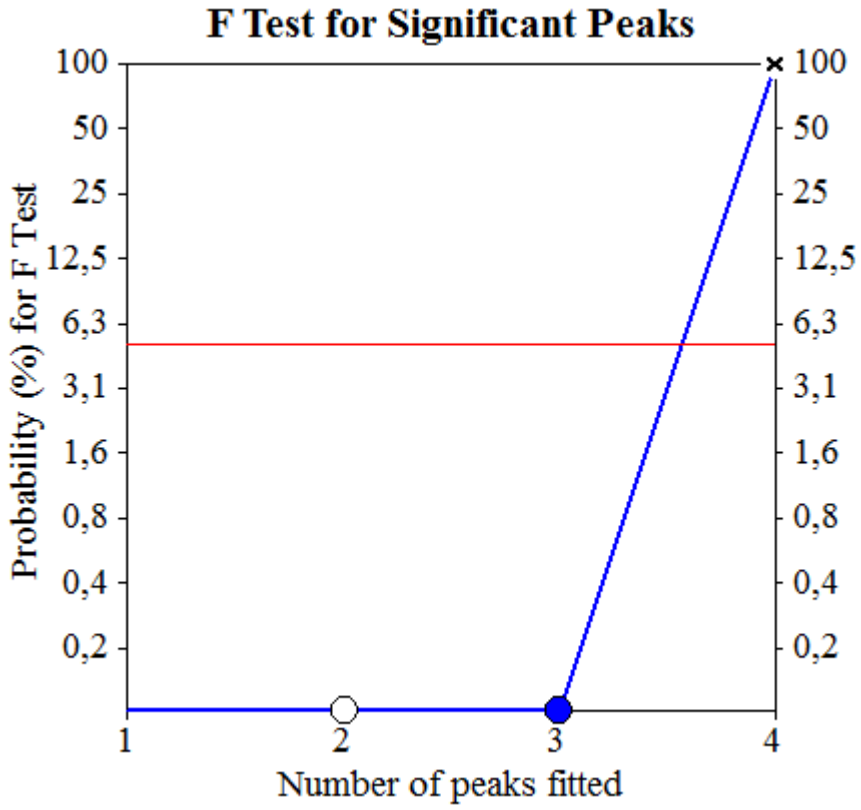

Datafile: C:\BH2\Jairo\Echantillon-IRR-10-2015\JG-P3-43Zr\JG-P3-43Zr.ftz
Title: Sample No. JG P3 43 Irr 10-2015-47

NEW PARAMETERS - ZETA METHOD

EFFECTIVE TRACK DENSITY FOR FLUENCE MONITOR (tracks/cm^2): 3,90E+05
RELATIVE ERROR (%): 1,29
EFFECTIVE URANIUM CONTENT OF MONITOR (ppm): 50,00
ZETA FACTOR AND STANDARD ERROR (yr cm^2): 137,14 1,57
SIZE OF COUNTER SQUARE (cm^2): 8,30E-07

GRAIN AGES IN ORIGINAL ORDER

Grain no.	RhoS (cm^-2)	(Ns)	RhoI (cm^-2)	(Ni)	Squares	U+/-2s		Grain Age (Ma) Age	--95% CI--	
1	8,65E+06	(237)	2,30E+06	(63)	33	295	74	99.1	75.1	130.7
2	6,94E+06	(219)	1,20E+06	(38)	38	154	50	151.8	107.9	220.2
3	5,16E+06	(214)	1,06E+06	(44)	50	136	41	128.5	92.9	182.0
4	5,04E+06	(226)	2,52E+06	(113)	54	323	61	53.1	42.3	66.6
5	3,67E+06	(213)	1,34E+06	(78)	70	172	39	72.2	55.7	93.6
6	4,65E+06	(162)	1,58E+06	(55)	42	202	55	78.2	57.4	108.3
7	8,35E+06	(208)	2,53E+06	(63)	30	324	82	87.1	65.7	115.3
8	5,50E+06	(137)	1,57E+06	(39)	30	201	64	93.0	65.0	136.5
9	3,88E+06	(174)	1,70E+06	(76)	54	217	50	60.6	46.3	79.3
10	4,97E+06	(165)	2,08E+06	(69)	40	266	64	63.2	47.7	83.7
11	3,86E+06	(128)	1,17E+06	(39)	40	151	48	87.0	60.6	128.0
12	3,13E+06	(83)	7,53E+05	(20)	32	96	43	109.4	67.1	188.4
13	6,16E+06	(179)	2,24E+06	(65)	35	287	71	72.7	54.8	96.5
14	5,35E+06	(120)	3,03E+06	(68)	27	389	94	47.0	34.6	64.3
15	4,71E+06	(313)	1,28E+06	(85)	80	164	36	97.2	76.5	123.5
16	5,62E+06	(140)	2,41E+06	(60)	30	309	80	62.0	45.6	85.5
17	7,20E+06	(538)	1,33E+06	(99)	90	170	34	143.1	115.5	177.2
18	5,06E+06	(210)	1,11E+06	(46)	50	142	42	120.7	87.7	169.9
19	6,29E+06	(261)	8,92E+05	(37)	50	114	37	185.3	131.9	268.6
20	5,16E+06	(120)	8,61E+05	(20)	28	110	49	157.5	98.6	266.8
21	3,98E+06	(198)	4,62E+05	(23)	60	59	24	224.9	147.4	361.8
22	4,52E+06	(150)	9,64E+05	(32)	40	124	43	123.7	84.5	187.3
23	6,70E+06	(278)	1,13E+06	(47)	50	145	42	155.9	114.7	217.0
24	4,82E+06	(240)	1,71E+06	(85)	60	219	48	74.7	58.3	95.7
25	5,50E+06	(274)	1,89E+06	(94)	60	242	50	77.1	61.0	97.5
26	5,69E+06	(189)	1,63E+06	(54)	40	208	57	92.8	68.4	128.0
27	5,54E+06	(193)	1,35E+06	(47)	42	173	50	108.7	78.9	152.9
28	4,19E+06	(139)	7,83E+05	(26)	40	100	39	140.8	92.8	222.9
29	5,46E+06	(317)	1,10E+06	(64)	70	141	35	130.2	99.6	170.0
30	8,17E+06	(407)	1,55E+06	(77)	60	198	45	139.0	109.0	177.1
31	6,95E+06	(173)	1,16E+06	(29)	30	149	55	156.9	106.3	241.1
32	5,51E+06	(160)	1,24E+06	(36)	35	159	53	117.4	81.8	173.6
33	6,57E+06	(229)	1,55E+06	(54)	42	198	54	112.2	83.4	153.9
34	7,90E+06	(367)	1,59E+06	(74)	56	204	48	130.5	101.7	167.3
35	6,05E+06	(261)	1,81E+06	(78)	52	232	53	88.4	68.6	113.8
36	3,09E+06	(218)	9,78E+05	(69)	85	125	30	83.4	63.6	109.3
37	7,79E+06	(194)	1,24E+06	(31)	30	160	57	164.6	113.1	248.6
38	5,52E+06	(275)	1,29E+06	(64)	60	165	41	113.1	86.2	148.2
39	6,46E+06	(193)	2,14E+06	(64)	36	274	69	79.6	60.0	105.5
40	4,96E+06	(247)	1,49E+06	(74)	60	190	44	88.1	68.0	114.2
41	7,17E+06	(232)	1,79E+06	(58)	39	230	60	105.3	79.0	140.1
42	5,54E+06	(161)	1,41E+06	(41)	35	181	56	103.9	73.7	150.3
43	4,04E+06	(228)	1,12E+06	(63)	68	143	36	95.4	72.2	125.9
44	7,75E+06	(90)	1,98E+06	(23)	14	254	105	103.3	65.3	171.3
45	7,27E+06	(193)	2,60E+06	(69)	32	333	80	73.9	56.1	97.2
46	8,98E+06	(298)	2,86E+06	(95)	40	367	76	83.0	65.8	104.6
47	3,69E+06	(92)	8,84E+05	(22)	30	113	48	110.3	69.2	184.6
48	6,29E+06	(120)	1,20E+06	(23)	23	154	64	137.3	88.1	224.8
49	1,15E+07	(249)	1,71E+06	(37)	26	220	72	176.9	125.7	256.8
50	3,43E+06	(91)	1,13E+06	(30)	32	145	53	80.4	52.9	125.9
51	4,54E+06	(230)	1,58E+06	(80)	61	202	45	76.0	58.9	98.0
52	3,48E+06	(101)	7,92E+05	(23)	35	101	42	115.8	73.6	191.0
53	7,80E+06	(272)	2,35E+06	(82)	42	301	67	87.6	68.4	112.2

Datafile: C:\BH2\Jairo\Echantillon-IRR-10-2015\JG-P3-43Zr\JG-P3-43Zr.ftz
Title: Sample No. JG P3 43 Irr 10-2015-47

Grain no.	RhoS (cm^-2)	(Ns)	RhoI (cm^-2)	(Ni)	Squares	U+/-2s	Grain Age (Ma) Age	--95% CI--	
54	6,81E+06	(164)	2,53E+06	(61)	29	325 83	71.4	53.0	97.5
55	7,23E+06	(144)	2,51E+06	(50)	24	322 91	76.4	55.2	107.8
56	6,23E+06	(207)	1,42E+06	(47)	40	181 53	116.5	84.8	163.5
57	6,09E+06	(480)	1,51E+06	(119)	95	193 36	106.6	87.1	130.4
58	8,61E+06	(143)	3,19E+06	(53)	20	409 112	71.7	52.1	100.2
59	6,93E+06	(345)	1,81E+06	(90)	60	232 49	101.2	80.2	127.6
60	4,94E+06	(82)	7,23E+05	(12)	20	93 52	178.2	98.4	358.3
61	6,73E+06	(559)	1,58E+06	(131)	100	202 36	112.8	93.1	136.5
62	9,31E+06	(170)	1,15E+06	(21)	22	147 64	211.6	135.7	349.6
63	8,59E+06	(214)	1,61E+06	(40)	30	206 65	141.1	100.8	203.0
64	4,46E+06	(126)	5,67E+05	(16)	34	73 36	205.5	123.5	369.4
65	7,19E+06	(179)	1,45E+06	(36)	30	185 62	131.2	91.8	193.2
66	6,45E+06	(214)	1,36E+06	(45)	40	174 52	125.6	91.1	177.3
67	7,47E+06	(124)	1,93E+06	(32)	20	247 87	102.5	69.4	156.3
68	6,78E+06	(270)	1,93E+06	(77)	48	248 57	92.6	71.9	119.2
69	5,56E+06	(369)	9,34E+05	(62)	80	120 30	156.1	119.5	203.7
70	5,53E+06	(459)	1,64E+06	(136)	100	210 36	89.4	73.7	108.3
71	7,04E+06	(292)	1,86E+06	(77)	50	238 54	100.0	77.8	128.5
72	9,28E+06	(231)	3,69E+06	(92)	30	473 99	66.5	52.2	84.7
73	4,50E+06	(112)	2,09E+06	(52)	30	268 74	57.3	40.9	81.3
74	6,37E+06	(317)	1,71E+06	(85)	60	219 48	98.5	77.5	125.1
75	4,36E+06	(217)	1,49E+06	(74)	60	190 44	77.5	59.5	100.8
76	8,43E+06	(168)	2,41E+06	(48)	24	309 89	92.7	67.2	130.7
77	4,58E+06	(357)	7,82E+05	(61)	94	100 26	153.5	117.2	200.9
78	6,12E+06	(305)	1,35E+06	(67)	60	172 42	119.8	92.0	155.8
79	5,45E+06	(181)	9,64E+05	(32)	40	124 43	149.0	102.6	224.1
80	6,31E+06	(157)	1,97E+06	(49)	30	252 72	85.0	61.5	119.7
81	7,03E+06	(350)	1,61E+06	(80)	60	206 46	115.3	90.5	146.9
82	9,77E+06	(227)	3,27E+06	(76)	28	419 96	78.9	60.9	102.3
83	6,52E+06	(265)	1,16E+06	(47)	49	148 43	148.7	109.2	207.2
84	3,05E+06	(152)	5,62E+05	(28)	60	72 27	143.0	95.8	222.1
85	7,42E+06	(277)	8,57E+05	(32)	45	110 39	226.5	158.2	336.6
86	6,45E+06	(107)	1,87E+06	(31)	20	239 85	91.4	61.1	141.1
87	8,61E+06	(500)	1,62E+06	(94)	70	207 43	140.0	112.4	174.5
88	6,27E+06	(312)	1,04E+06	(52)	60	134 37	158.2	118.1	216.3
89	6,99E+06	(174)	1,08E+06	(27)	30	139 53	169.3	113.4	263.9
90	2,02E+06	(84)	4,34E+05	(18)	50	56 26	122.8	73.9	217.3
91	4,73E+06	(157)	1,33E+06	(44)	40	170 51	94.5	67.5	135.3
92	7,48E+06	(503)	1,49E+06	(100)	81	191 38	132.6	106.9	164.2
93	3,81E+06	(158)	1,16E+06	(48)	50	148 43	87.3	63.0	123.3
94	4,51E+06	(262)	1,55E+06	(90)	70	198 42	77.0	60.6	97.9
95	6,60E+06	(115)	2,35E+06	(41)	21	301 94	74.4	51.9	109.2
96	4,43E+06	(147)	6,33E+05	(21)	40	81 35	183.4	116.9	304.5
97	4,02E+06	(167)	7,71E+05	(32)	50	99 35	137.6	94.4	207.5
98	5,23E+06	(304)	1,07E+06	(62)	70	137 35	128.9	98.2	169.0
99	7,17E+06	(119)	2,65E+06	(44)	20	340 102	71.8	50.6	104.0
100	7,42E+06	(308)	1,08E+06	(45)	50	139 41	180.0	132.1	251.6
POOLED	5,83E+06	(22380)	1,47E+06	(5622)	4622	188 7	105.6	101.0	110.4

CHI^2 PROBABILITY (%): 0.0

POOLED AGE W/ 68% CONF. INTERVAL(Ma): 105.6, 103.3 -- 108.0 (-2.4 +2.4)
95% CONF. INTERVAL(Ma): 101.0 -- 110.4 (-4.6 +4.8)

CENTRAL AGE W/ 68% CONF. INTERVAL(Ma): 104.5, 100.7 -- 108.4 (-3.8 +3.9)
95% CONF. INTERVAL(Ma): 97.1 -- 112.3 (-7.3 +7.8)
AGE DISPERSION (%): 29.0

FIT OPTION: Best-fit peaks using the binomial model of Galbraith and Green

INITIAL GUESS FOR MODEL PARAMETERS (number of peaks to fit = 4)

Peak #.	Peak Age	Theta	Fraction(%)	Count
1.	46.90	0.638	2.3	2.31
2.	52.60	0.664	4.9	4.91
3.	105.60	0.799	35.8	35.76
4.	224.50	0.895	5.3	5.34

Total range for grain ages: 46,9 to 224,5 Ma
Number of active grains (Num. used for fit): 100
Number of removed grains: 0
Degrees of freedom for fit: 93
Average of the SE(Z)'s for the grains: 0,17
Estimated width of peaks in PD plot in Z units: 0,2

PARAMETERS FOR BEST-FIT PEAKS

* *Standard error for peak age includes group error*
* *Peak width is for PD plot assuming a kernel factor = 0.60*

#.	Peak Age(Ma)	68%CI	95%CI	W(Z)	Frac(%)	SE,%	Count
1.	55.0	-6,2 ...+7,0	-11,5 ...+14,5	0.16	3.4	2.8	3.4
2.	80.0	-5,1 ...+5,5	-9,8 ...+11,1	0.17	30.8	12.9	30.8
3.	103.0	-9,0 ...+9,8	-16,8 ...+20,1	0.17	27.6	12.2	27.6
4.	147.0	-5,8 ...+6,1	-11,2 ...+12,1	0.19	38.3	7.4	38.3

Log-likelihood for best fit: -398,991
Chi-squared value for best fit: 102,098
Reduced chi-squared value: 1,098
Probability for F test: 3%
Condition number for COVAR matrix: 87,43
Number of iterations: 23

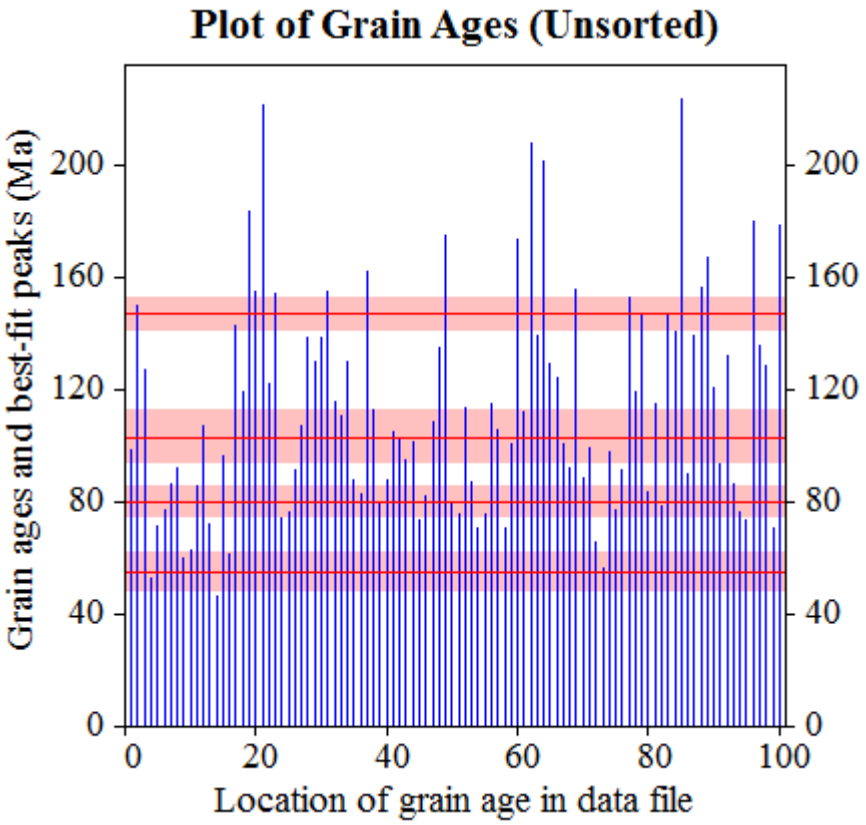
Plot of Grain Ages (Unsorted)
Grain ages and best-fit peaks (Ma)
0
40
80
120
160
200
0
20
40
60
80
100
Location of grain age in data file

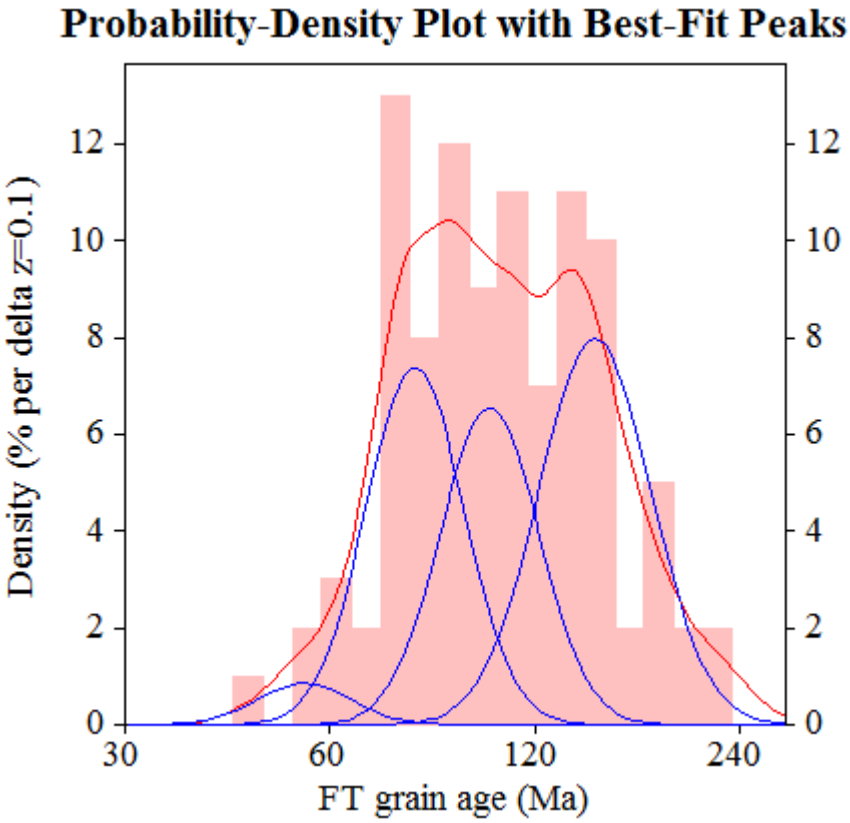
Probability-Density Plot with Best-Fit Peaks
Density (% per delta z=0.1)
0
2
4
6
8
10
12
30
60
120
240
FT grain age (Ma)

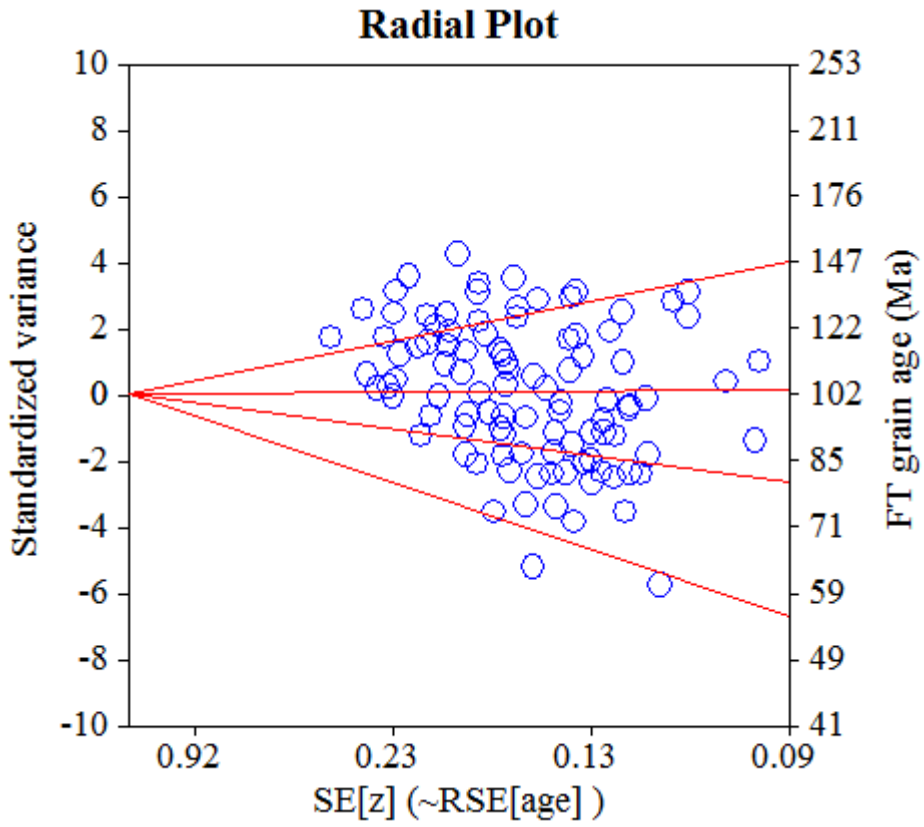
Radial Plot
Standardized variance
FT grain age (Ma)
10
8
6
4
2
0
-2
-4
-6
-8
-10
253
211
176
147
122
102
85
71
59
49
41
0.92
0.23
0.13
0.09
SE[z] (~RSE[age])

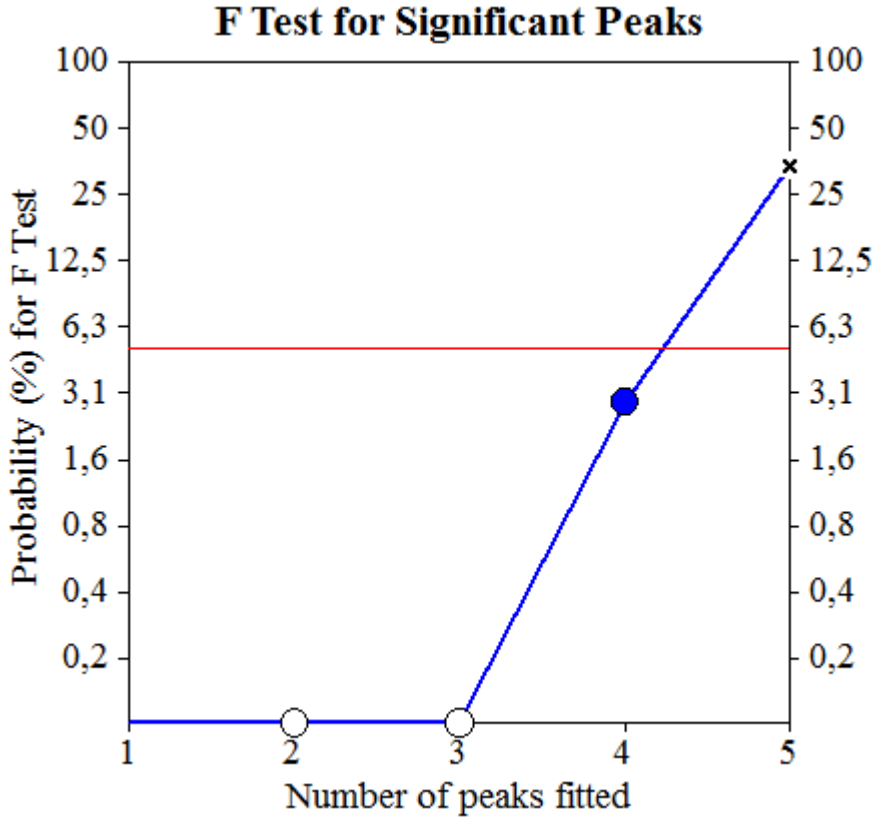
F Test for Significant Peaks
Probability (%) for F Test
100
50
25
12,5
6,3
3,1
1,6
0,8
0,4
0,2
1
2
3
4
5
Number of peaks fitted

Datafile: C:\BH2\Jairo\Echantillon-IRR082015\JG-P3-36\JG-P3-36Ap.fta
Title: JG-P3-36 Irr 8-2015-18

NEW PARAMETERS - ZETA METHOD

EFFECTIVE TRACK DENSITY FOR FLUENCE MONITOR (tracks/cm^2): 1,29E+06
RELATIVE ERROR (%): 1,18
EFFECTIVE URANIUM CONTENT OF MONITOR (ppm): 15,00
ZETA FACTOR AND STANDARD ERROR (yr cm^2): 282,02 6,88
SIZE OF COUNTER SQUARE (cm^2): 6,39E-07

GRAIN AGES IN ORIGINAL ORDER

Grain no.	RhoS (cm^-2)	(Ns)	RhoI (cm^-2)	(Ni)	Squares	U+/-2s		Grain Age (Ma) Age	--95% CI--	
1	1,81E+05	(6)	7,58E+06	(252)	52	88	11	4.5	1.6	9.6
2	2,74E+05	(7)	1,23E+07	(315)	40	143	16	4.1	1.6	8.4
3	1,37E+05	(7)	4,75E+06	(243)	80	55	7	5.4	2.1	11.0
4	2,09E+05	(4)	1,24E+07	(237)	30	144	19	3.2	0.8	8.0
5	2,01E+05	(5)	1,31E+07	(327)	39	152	17	2.9	0.9	6.6
6	2,09E+05	(4)	8,09E+06	(155)	30	94	15	4.9	1.3	12.3
7	1,25E+05	(8)	6,74E+06	(431)	100	78	8	3.4	1.5	6.7
8	1,66E+05	(7)	1,13E+07	(477)	66	131	12	2.7	1.1	5.6
9	1,04E+05	(2)	1,06E+07	(204)	30	124	18	1.9	0.2	6.5
10	1,13E+05	(5)	8,16E+06	(360)	69	95	10	2.6	0.8	6.0
11	1,17E+05	(6)	7,75E+06	(396)	80	90	9	2.8	1.0	6.1
12	1,79E+05	(8)	6,93E+06	(310)	70	80	9	4.8	2.0	9.4
13	1,84E+05	(2)	1,22E+07	(132)	17	141	25	3.0	0.3	10.2
14	3,13E+05	(6)	8,24E+06	(158)	30	96	15	7.1	2.5	15.4
15	1,12E+05	(5)	8,58E+06	(384)	70	100	10	2.4	0.8	5.6
16	1,88E+05	(6)	7,32E+06	(234)	50	85	11	4.8	1.7	10.3
17	7,82E+04	(3)	6,34E+06	(243)	60	74	10	2.4	0.5	6.7
POOLED	1,56E+05	(91)	8,33E+06	(4858)	913	97	4	3.4	2.8	4.2

CHI^2 PROBABILITY (%): 86.0
>>> Beware: possible upward bias in Chi^2 probability due to low counts <<<

POOLED AGE W/ 68% CONF. INTERVAL(Ma): 3.4, 3.1 -- 3.8 (-0.4 +0.4)
95% CONF. INTERVAL(Ma): 2.8 -- 4.2 (-0.7 +0.8)

CENTRAL AGE W/ 68% CONF. INTERVAL(Ma): 3.4, 3.1 -- 3.8 (-0.4 +0.4)
95% CONF. INTERVAL(Ma): 2.8 -- 4.2 (-0.7 +0.8)
AGE DISPERSION (%): 0.2

FIT OPTION: Best-fit peaks using the binomial model of Galbraith and Green

INITIAL GUESS FOR MODEL PARAMETERS (number of peaks to fit = 1)

Peak #.	Peak Age	Theta	Fraction(%)	Count
1.	3.40	0.018	33.2	5.65

Total range for grain ages:	2,2 to 7,5 Ma
Number of active grains (Num. used for fit):	17
Number of removed grains:	0
Degrees of freedom for fit:	16
Average of the SE(Z)'s for the grains:	0,45
Estimated width of peaks in PD plot in Z units:	0,52

PARAMETERS FOR BEST-FIT PEAKS

* *Standard error for peak age includes group error*
* *Peak width is for PD plot assuming a kernel factor = 0.60*

#.	Peak Age(Ma)	68%CI	95%CI	W(Z)	Frac(%)	SE,%	Count
1.	3.4	-0,4 ...+0,4	-0,7 ...+0,8	0.51	100.0	0.0	17.0

Log-likelihood for best fit:	-34,145
Chi-squared value for best fit:	10,124
Reduced chi-squared value:	0,633
Probability for F test:	0%
Condition number for COVAR matrix:	1,00
Number of iterations:	5

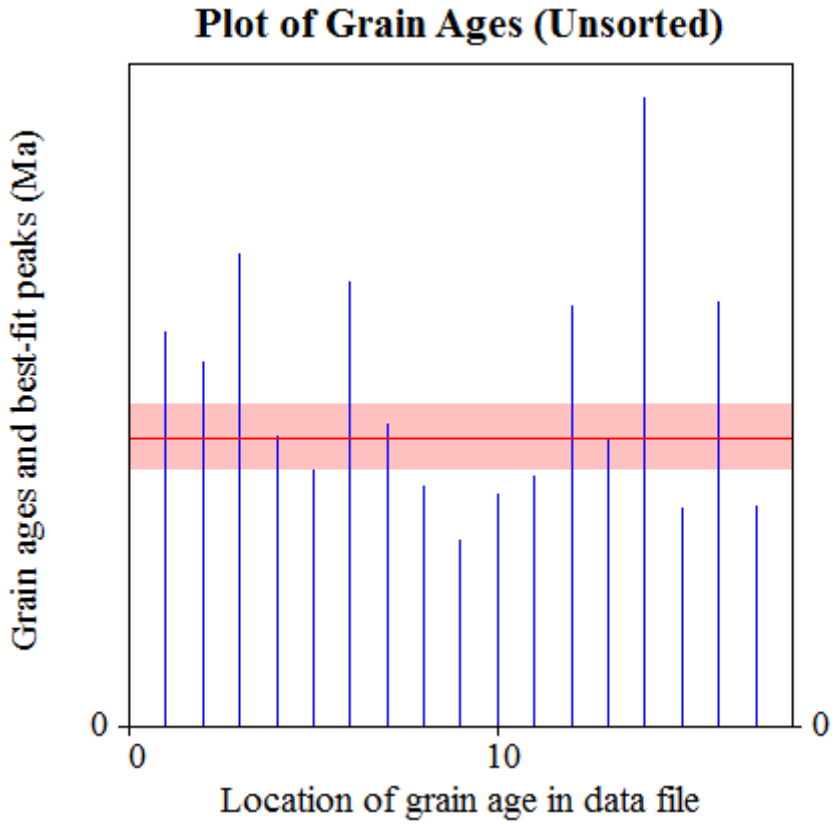
Plot of Grain Ages (Unsorted)
Grain ages and best-fit peaks (Ma)
0
0
10
0
Location of grain age in data file

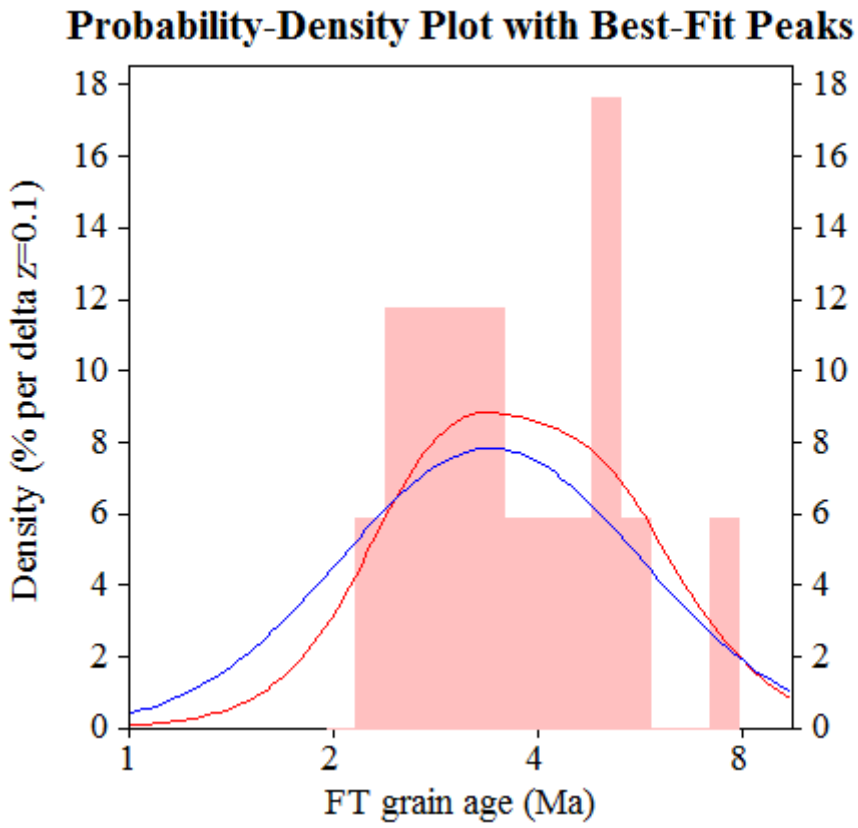
Probability-Density Plot with Best-Fit Peaks
Density (% per delta z=0.1)
18
16
14
12
10
8
6
4
2
0
1
2
4
8
FT grain age (Ma)

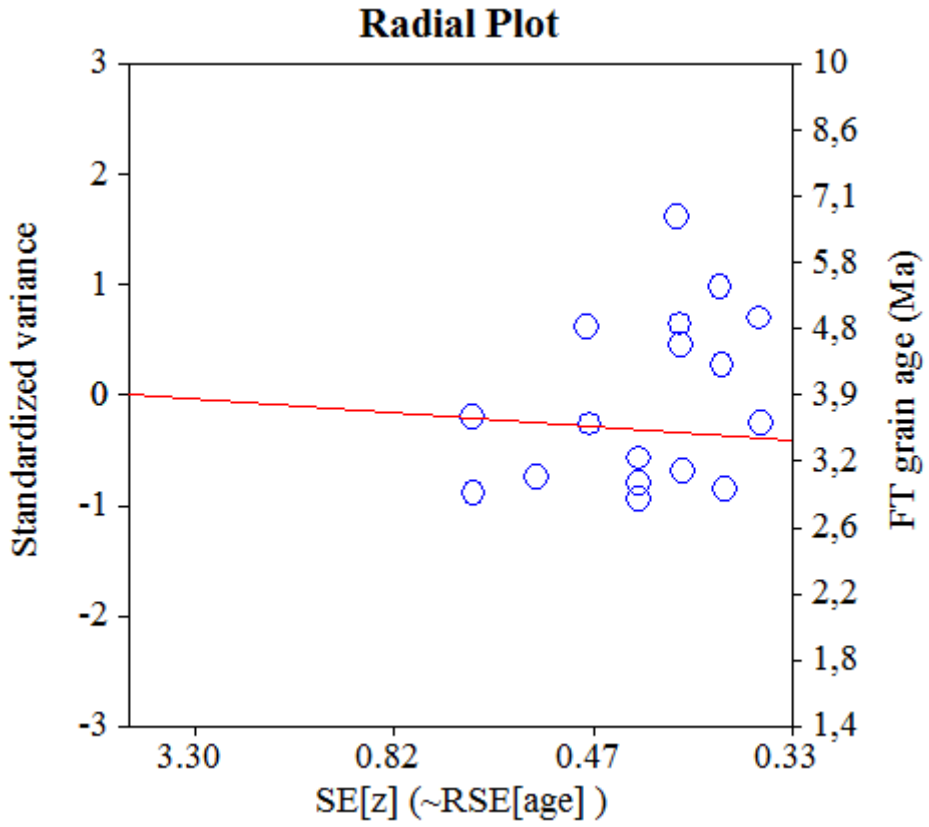
Radial Plot
Standardized variance
FT grain age (Ma)
SE[z] (~RSE[age])
3
2
1
0
-1
-2
-3
10
8,6
7,1
5,8
4,8
3,9
3,2
2,6
2,2
1,8
1,4
3.30
0.82
0.47
0.33

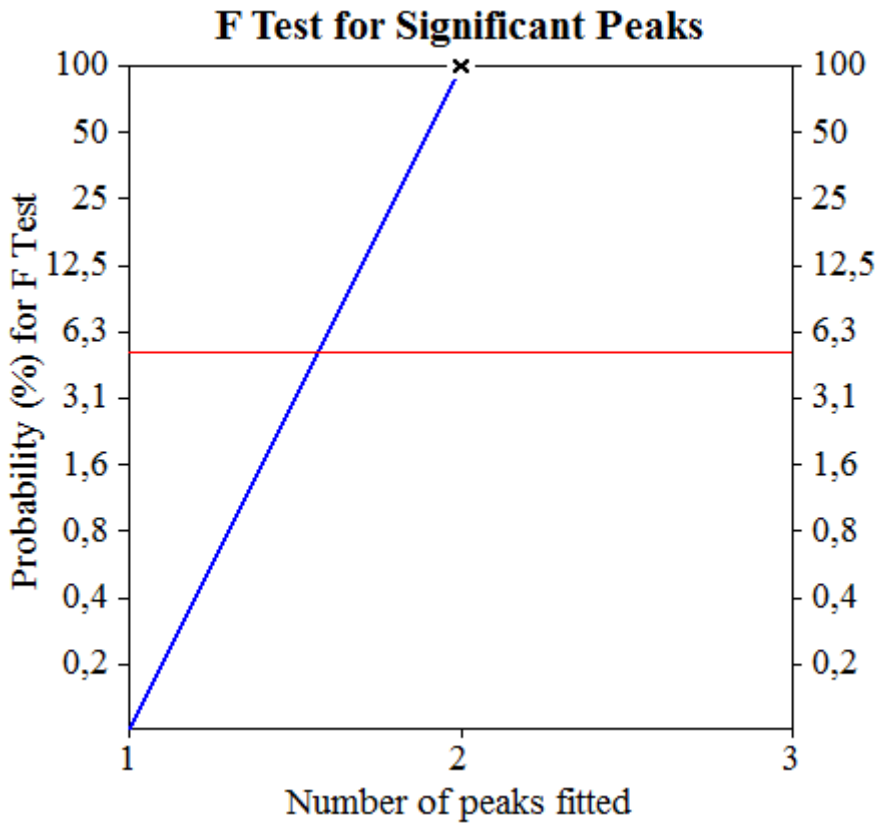
F Test for Significant Peaks
Probability (%) for F Test
Number of peaks fitted
100
50
25
12,5
6,3
3,1
1,6
0,8
0,4
0,2
1
2
3

Datafile: C:\BH2\Jairo\Echantillon-IRR082015\JG-P3-37\JG-P3-37Ap.fta
Title: JG-P3-37 Irr 8-2015-19

NEW PARAMETERS - ZETA METHOD

EFFECTIVE TRACK DENSITY FOR FLUENCE MONITOR (tracks/cm^2): 1,30E+06
RELATIVE ERROR (%): 1,21
EFFECTIVE URANIUM CONTENT OF MONITOR (ppm): 15,00
ZETA FACTOR AND STANDARD ERROR (yr cm^2): 282,02 6,88
SIZE OF COUNTER SQUARE (cm^2): 6,39E-07

GRAIN AGES IN ORIGINAL ORDER

Grain	RhoS	(Ns)	RhoI	(Ni)	Squares	U+/-2s		Grain Age (Ma)		
no.	(cm^-2)		(cm^-2)					Age	--95% CI--	
1	3,86E+04	(2)	6,18E+05	(32)	81	7	3	12.2	1.3	44.6
2	3,73E+04	(2)	3,73E+05	(20)	84	4	2	19.5	2.1	74.8
3	6,71E+04	(3)	6,26E+05	(28)	70	7	3	20.5	3.8	63.1
4	1,10E+05	(7)	1,31E+06	(84)	100	15	3	15.5	5.9	32.7
5	1,39E+05	(7)	6,34E+05	(32)	79	7	3	40.6	14.9	91.6
6	1,34E+06	(55)	4,55E+06	(186)	64	53	8	53.9	39.1	73.0
7	5,38E+05	(22)	9,88E+06	(404)	64	114	12	10.0	6.2	15.3
8	8,94E+04	(4)	3,58E+05	(16)	70	4	2	46.9	11.1	140.2
9	9,78E+04	(5)	8,22E+05	(42)	80	10	3	22.3	6.7	54.7
10	3,52E+05	(18)	7,24E+05	(37)	80	8	3	88.7	47.5	158.3
11	6,26E+04	(4)	5,32E+05	(34)	100	6	2	22.2	5.5	60.0
12	1,12E+05	(5)	4,02E+05	(18)	70	5	2	51.7	14.7	140.4
13	1,56E+05	(7)	6,71E+05	(30)	70	8	3	43.3	15.8	98.4
14	1,37E+05	(7)	1,31E+06	(67)	80	15	4	19.5	7.4	41.4
15	5,59E+04	(1)	1,12E+06	(20)	28	13	6	10.4	0.2	56.9
16	1,56E+05	(4)	6,38E+06	(163)	40	74	12	4.7	1.2	11.7
17	1,44E+05	(7)	5,56E+05	(27)	76	6	2	48.0	17.4	110.6
18	1,72E+05	(11)	6,42E+05	(41)	100	7	2	49.4	22.7	96.5
19	6,96E+04	(4)	3,39E+06	(195)	90	39	6	3.9	1.0	9.8
20	1,12E+05	(5)	2,28E+06	(102)	70	26	5	9.2	2.8	21.6
21	6,26E+04	(4)	6,73E+05	(43)	100	8	2	17.6	4.4	46.6
22	2,24E+05	(11)	6,10E+05	(30)	77	7	3	67.3	30.2	136.2
23	8,94E+04	(4)	1,05E+06	(47)	70	12	4	16.1	4.1	42.4
24	5,22E+05	(20)	1,30E+06	(50)	60	15	4	73.1	41.1	123.9
25	3,09E+05	(17)	6,73E+05	(37)	86	8	3	83.9	44.2	151.2
26	2,61E+04	(1)	3,91E+05	(15)	60	5	2	13.8	0.3	78.7
27	1,37E+05	(5)	8,13E+06	(296)	57	94	11	3.2	1.0	7.3
28	9,90E+04	(5)	5,74E+05	(29)	79	7	2	32.3	9.5	81.8
29	3,13E+05	(7)	1,13E+07	(252)	35	130	17	5.2	2.0	10.6
30	1,25E+05	(4)	1,05E+07	(335)	50	121	14	2.3	0.6	5.6
31	5,09E+05	(26)	1,51E+06	(77)	80	17	4	61.7	37.8	96.7
32	5,69E+04	(2)	6,54E+05	(23)	55	8	3	17.0	1.8	64.0
33	1,79E+05	(4)	3,76E+06	(84)	35	43	10	9.0	2.3	23.1
34	2,57E+04	(1)	4,62E+05	(18)	61	5	2	11.5	0.2	64.0
35	2,61E+04	(1)	5,74E+05	(22)	60	7	3	9.4	0.2	51.2
36	2,28E+05	(7)	1,01E+06	(31)	48	12	4	41.9	15.3	94.9
37	5,87E+04	(3)	5,67E+05	(29)	80	7	2	19.8	3.7	60.7
38	2,75E+04	(1)	4,39E+05	(16)	57	5	3	13.0	0.3	73.1
39	1,30E+05	(5)	8,87E+05	(34)	60	10	4	27.6	8.2	68.7
40	2,01E+05	(9)	7,38E+05	(33)	70	9	3	50.3	20.9	105.7
41	9,78E+04	(5)	4,50E+05	(23)	80	5	2	40.6	11.8	106.0
42	9,78E+04	(5)	4,30E+05	(22)	80	5	2	42.4	12.3	111.5
43	1,16E+05	(6)	5,99E+05	(31)	81	7	2	36.0	12.0	85.5
44	7,20E+04	(4)	3,78E+05	(21)	87	4	2	35.8	8.7	102.4
45	5,62E+05	(23)	4,79E+06	(196)	64	55	8	21.5	13.3	33.1
46	3,86E+04	(2)	5,60E+05	(29)	81	6	2	13.5	1.5	49.7
47	1,94E+05	(12)	8,07E+05	(50)	97	9	3	44.2	21.2	83.0
48	1,01E+05	(4)	1,11E+07	(441)	62	129	13	1.7	0.4	4.3
49	1,96E+05	(6)	1,11E+06	(34)	48	13	4	32.9	11.1	77.3
50	1,63E+05	(5)	4,89E+05	(15)	48	6	3	61.9	17.3	174.0
51	5,40E+04	(2)	7,55E+05	(28)	58	9	3	14.0	1.5	51.6
52	5,76E+05	(32)	2,70E+06	(150)	87	31	5	39.0	25.7	57.2
53	2,79E+04	(1)	1,98E+06	(71)	56	23	5	2.9	0.1	14.8
54	2,74E+05	(14)	4,58E+06	(234)	80	53	7	11.0	5.9	18.7

Grain no.	RhoS (cm^-2)	(Ns)	RhoI (cm^-2)	(Ni)	Squares	U+/-2s		Grain Age (Ma) Age	--95% CI--	
55	3,40E+04	(1)	7,48E+05	(22)	46	9	4	9.4	0.2	51.2
56	2,90E+05	(10)	2,78E+06	(96)	54	32	7	19.3	8.8	36.5
57	5,22E+05	(19)	1,15E+06	(42)	57	13	4	82.5	45.2	143.8
58	1,66E+06	(53)	6,20E+06	(198)	50	72	10	48.8	35.3	66.3
59	2,61E+05	(10)	9,91E+05	(38)	60	11	4	48.5	21.3	97.7
60	1,51E+05	(3)	6,06E+05	(12)	31	7	4	47.3	8.3	167.2
61	3,48E+04	(1)	5,22E+05	(15)	45	6	3	13.8	0.3	78.7
62	9,78E+04	(5)	3,52E+05	(18)	80	4	2	51.7	14.7	140.4
63	1,30E+05	(5)	4,96E+05	(19)	60	6	3	49.0	14.0	131.9
64	6,26E+04	(3)	2,09E+05	(10)	75	2	1	56.6	9.7	209.6
65	4,89E+05	(15)	2,25E+06	(69)	48	26	6	39.9	21.1	69.8
66	1,17E+05	(5)	1,10E+06	(47)	67	13	4	20.0	6.0	48.5
67	8,24E+04	(3)	5,49E+05	(20)	57	6	3	28.6	5.2	91.8
68	2,11E+05	(7)	6,41E+06	(213)	52	74	10	6.1	2.4	12.6
69	4,47E+04	(2)	8,94E+05	(40)	70	10	3	9.8	1.1	35.2
70	2,30E+05	(11)	2,44E+06	(117)	75	28	5	17.4	8.3	31.8
71	1,56E+05	(7)	8,72E+05	(39)	70	10	3	33.3	12.4	73.8
72	1,12E+05	(4)	7,55E+05	(27)	56	9	3	27.9	6.9	77.3
73	2,07E+05	(9)	6,44E+05	(28)	68	7	3	59.2	24.3	126.9
74	2,24E+04	(1)	1,16E+06	(52)	70	13	4	4.0	0.1	20.4
75	2,24E+05	(5)	5,14E+06	(115)	35	60	11	8.2	2.5	19.1
76	6,26E+04	(4)	1,06E+06	(68)	100	12	3	11.1	2.8	28.8
77	2,21E+05	(12)	1,71E+06	(93)	85	20	4	23.8	11.7	43.1
78	1,04E+05	(2)	1,31E+07	(251)	30	152	19	1.6	0.2	5.3
79	8,38E+04	(3)	5,87E+05	(21)	56	7	3	27.2	5.0	86.9
80	5,91E+04	(2)	1,54E+06	(52)	53	18	5	7.5	0.8	26.7
81	3,91E+05	(20)	9,39E+05	(48)	80	11	3	76.1	42.6	129.5
82	4,67E+05	(23)	7,07E+06	(348)	77	82	9	12.1	7.5	18.4
83	2,97E+05	(11)	3,43E+06	(127)	58	40	7	16.0	7.7	29.2
84	1,12E+05	(2)	8,38E+05	(15)	28	10	5	25.9	2.7	104.0
85	2,45E+04	(1)	5,62E+05	(23)	64	7	3	9.0	0.2	48.8
86	3,26E+05	(5)	9,78E+05	(15)	24	11	6	61.9	17.3	174.0
POOLED	1,94E+05	(702)	1,86E+06	(6722)	5666	21	1	19.1	17.3	20.9

CHI^2 PROBABILITY (%): 0.0
>>> Beware: possible upward bias in Chi^2 probability due to low counts <<<

POOLED AGE W/ 68% CONF. INTERVAL(Ma): 19.1, 18.2 -- 20.0 (-0.9 +0.9)
95% CONF. INTERVAL(Ma): 17.3 -- 20.9 (-1.7 +1.9)

CENTRAL AGE W/ 68% CONF. INTERVAL(Ma): 25.6, 23.3 -- 28.1 (-2.3 +2.5)
95% CONF. INTERVAL(Ma): 21.4 -- 30.7 (-4.3 +5.1)
AGE DISPERSION (%): 69.9

FIT OPTION: Best-fit peaks using the binomial model of Galbraith and Green

INITIAL GUESS FOR MODEL PARAMETERS (number of peaks to fit = 3)

Peak #.	Peak Age	Theta	Fraction(%)	Count
1.	19.10	0.095	14.5	12.50
2.	38.90	0.176	16.7	14.34
3.	51.40	0.220	18.3	15.71

Total range for grain ages:	1,8 to 89,5 Ma
Number of active grains (Num. used for fit):	86
Number of removed grains:	0
Degrees of freedom for fit:	81
Average of the SE(Z)'s for the grains:	0,51
Estimated width of peaks in PD plot in Z units:	0,6

PARAMETERS FOR BEST-FIT PEAKS

* *Standard error for peak age includes group error*
* *Peak width is for PD plot assuming a kernel factor = 0.60*

#.	Peak Age(Ma)	68%CI	95%CI	W(Z)	Frac(%)	SE,%	Count
1.	3.3	-0,6 ...+0,7	-1,0 ...+1,5	0.63	13.6	4.9	11.7
2.	14.2	-1,3 ...+1,5	-2,5 ...+3,0	0.50	43.8	7.3	37.7
3.	49.5	-3,2 ...+3,4	-6,1 ...+7,0	0.38	42.6	6.7	36.6

Log-likelihood for best fit:	-245,778
Chi-squared value for best fit:	75,584
Reduced chi-squared value:	0,933
Probability for F test:	0%
Condition number for COVAR matrix:	26,93
Number of iterations:	18

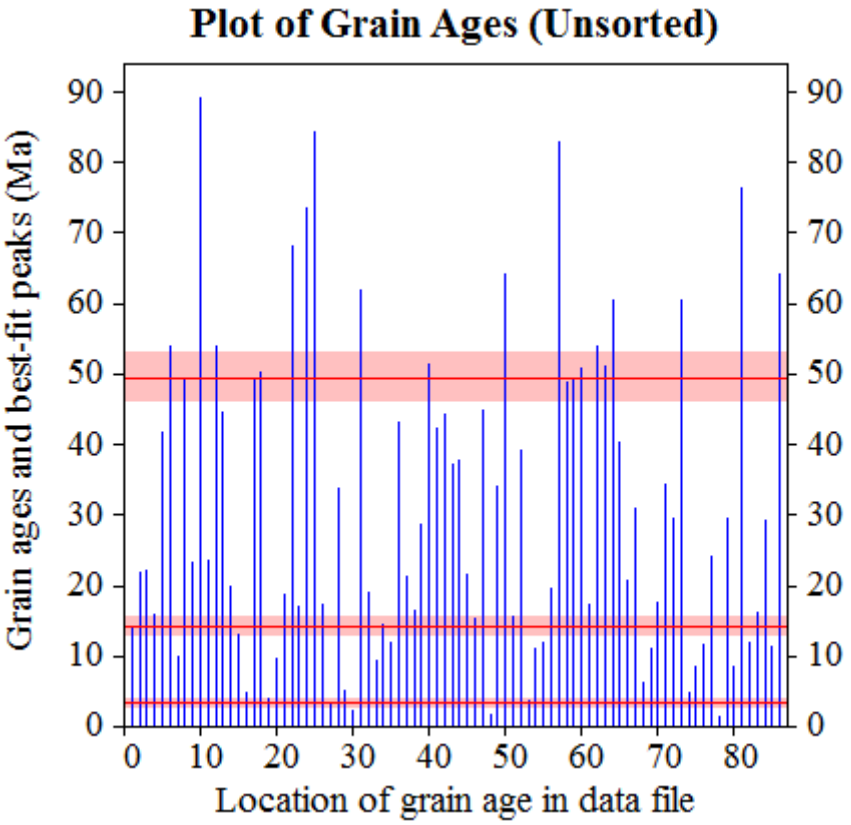
Plot of Grain Ages (Unsorted)
Grain ages and best-fit peaks (Ma)
0
10
20
30
40
50
60
70
80
90
Location of grain age in data file

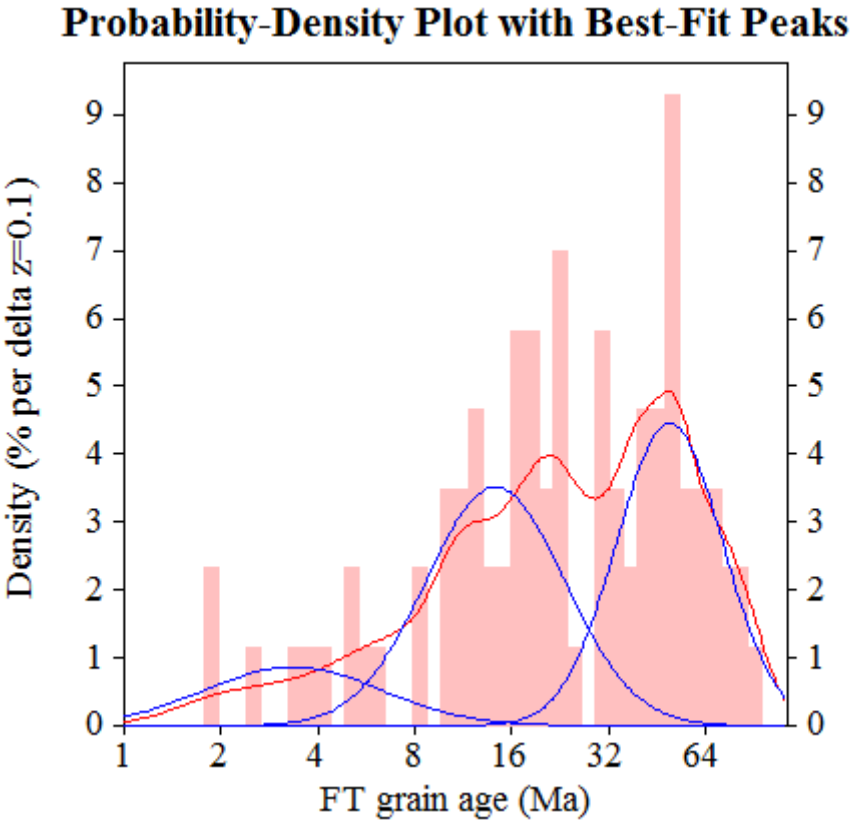
Probability-Density Plot with Best-Fit Peaks
Density (% per delta z=0.1)
0
1
2
3
4
5
6
7
8
9
1
2
4
8
16
32
64
FT grain age (Ma)

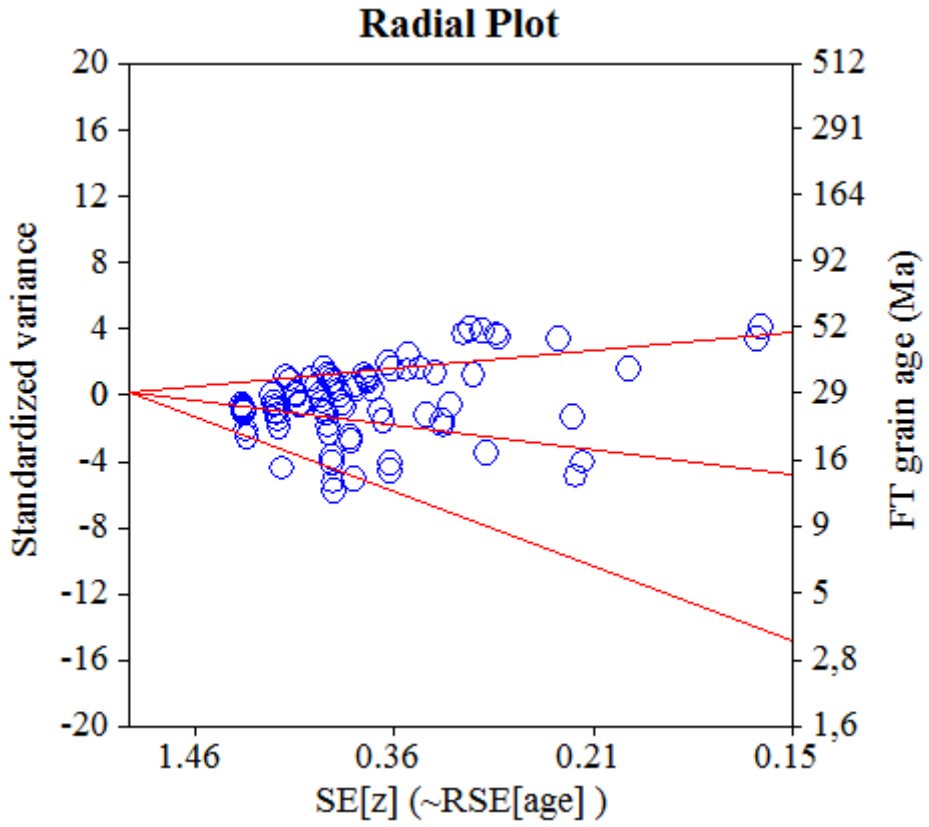
Radial Plot
Standardized variance
20
16
12
8
4
0
-4
-8
-12
-16
-20
512
291
164
92
52
29
16
9
5
2,8
1,6
FT grain age (Ma)
1.46
0.36
0.21
0.15
SE[z] (~RSE[age])

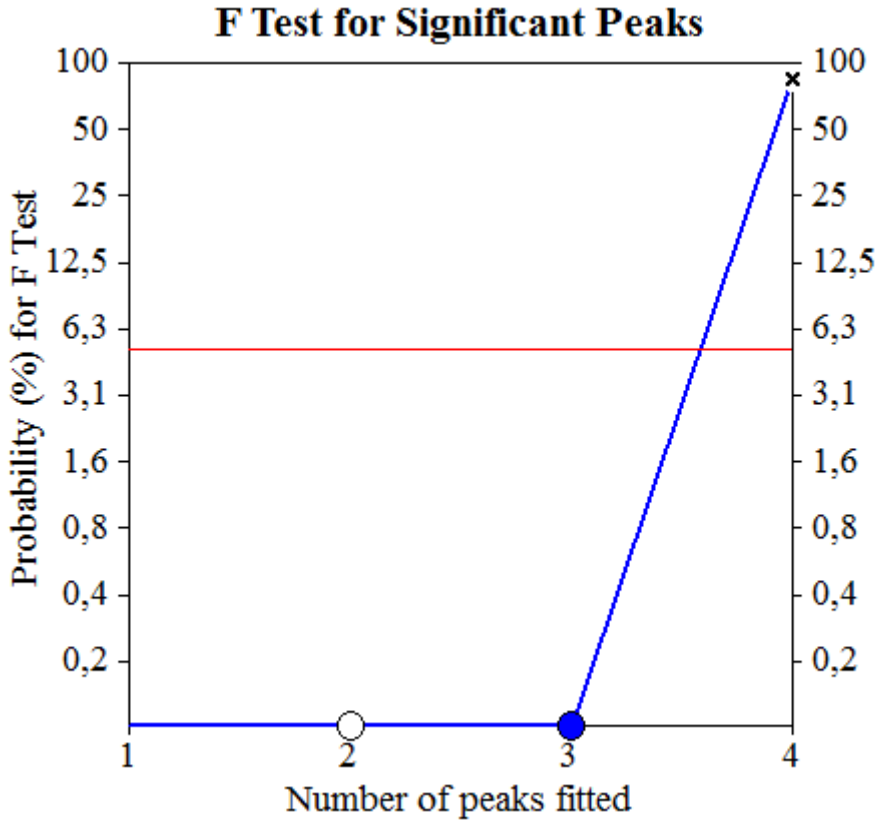
F Test for Significant Peaks
Probability (%) for F Test
100
50
25
12,5
6,3
3,1
1,6
0,8
0,4
0,2
1
2
3
4
Number of peaks fitted

Datafile: C:\BH2\Jairo\Echantillon-IRR082015\JG-P3-42\test.ftz
Title: JG-P3-42 Irr 8-2015-20

NEW PARAMETERS - ZETA METHOD

EFFECTIVE TRACK DENSITY FOR FLUENCE MONITOR (tracks/cm^2): 1,30E+06
RELATIVE ERROR (%): 1,25
EFFECTIVE URANIUM CONTENT OF MONITOR (ppm): 15,00
ZETA FACTOR AND STANDARD ERROR (yr cm^2): 282,02 6,88
SIZE OF COUNTER SQUARE (cm^2): 6,39E-07

GRAIN AGES IN ORIGINAL ORDER

Grain no.	RhoS (cm^-2)	(Ns)	RhoI (cm^-2)	(Ni)	Squares	U+/-2s		Grain Age (Ma) Age	--95% CI--	
1	2,01E+05	(5)	1,08E+06	(27)	39	13	5	34.7	10.2	88.9
2	5,59E+04	(1)	6,71E+05	(12)	28	8	4	17.3	0.4	102.5
3	1,27E+05	(3)	6,43E+06	(152)	37	74	12	3.8	0.7	10.8
4	5,63E+05	(9)	3,26E+06	(52)	25	38	10	32.1	13.7	64.7
5	1,04E+05	(2)	1,67E+06	(32)	30	19	7	12.3	1.3	44.8
6	4,04E+05	(8)	1,82E+06	(36)	31	21	7	41.3	16.3	88.6
7	4,37E+05	(12)	1,49E+06	(41)	43	17	5	54.0	25.6	103.3
8	2,96E+05	(7)	6,56E+06	(155)	37	76	12	8.5	3.3	17.5
9	2,61E+05	(4)	6,52E+05	(10)	24	8	5	74.6	16.8	249.4
10	1,89E+06	(29)	6,52E+06	(100)	24	75	15	53.2	33.8	80.6
11	3,85E+05	(15)	2,41E+06	(94)	61	28	6	29.5	15.7	50.6
12	8,03E+05	(20)	2,17E+06	(54)	39	25	7	67.9	38.4	114.4
13	1,84E+05	(6)	1,32E+06	(43)	51	15	5	26.1	8.9	60.1
14	2,00E+05	(6)	1,17E+06	(35)	47	13	5	32.1	10.8	75.1
15	3,48E+05	(8)	7,39E+05	(17)	36	9	4	86.6	32.1	207.6
16	3,74E+05	(11)	9,19E+05	(27)	46	11	4	74.9	33.3	153.8
17	6,89E+05	(11)	2,07E+06	(33)	25	24	8	61.4	27.8	122.8
18	1,74E+05	(2)	8,17E+06	(94)	18	94	20	4.2	0.5	14.5
19	3,73E+04	(1)	6,71E+05	(18)	42	8	4	11.6	0.2	64.2
20	3,77E+05	(13)	3,33E+06	(115)	54	38	7	20.9	10.7	36.8
21	1,49E+05	(2)	5,96E+05	(8)	21	7	5	48.2	4.7	225.7
22	1,04E+05	(2)	8,87E+05	(17)	30	10	5	23.0	2.4	90.3
23	9,00E+05	(23)	4,73E+06	(121)	40	55	10	35.0	21.2	54.6
24	2,35E+05	(6)	1,53E+06	(39)	40	18	6	28.8	9.7	66.8
POOLED	3,71E+05	(206)	2,40E+06	(1332)	868	28	2	28.3	24.2	33.1

CHI^2 PROBABILITY (%): 0.0
>>> Beware: possible upward bias in Chi^2 probability due to low counts <<<

POOLED AGE W/ 68% CONF. INTERVAL(Ma): 28.3, 26.1 -- 30.6 (-2.2 +2.3)
95% CONF. INTERVAL(Ma): 24.2 -- 33.1 (-4.1 +4.8)

CENTRAL AGE W/ 68% CONF. INTERVAL(Ma): 32.3, 28.0 -- 37.3 (-4.3 +5.0)
95% CONF. INTERVAL(Ma): 24.4 -- 42.8 (-7.9 +10.5)
AGE DISPERSION (%): 55.2

FIT OPTION: Best-fit peaks using the binomial model of Galbraith and Green

INITIAL GUESS FOR MODEL PARAMETERS (number of peaks to fit = 3)

Peak #.	Peak Age	Theta	Fraction(%)	Count
1.	4.20	0.022	3.5	0.85
2.	28.30	0.134	20.7	4.98
3.	54.70	0.231	19.4	4.65

Total range for grain ages:	4,2 to 88,4 Ma
Number of active grains (Num. used for fit):	24
Number of removed grains:	0
Degrees of freedom for fit:	19
Average of the SE(Z)'s for the grains:	0,5
Estimated width of peaks in PD plot in Z units:	0,58

PARAMETERS FOR BEST-FIT PEAKS

* *Standard error for peak age includes group error*
* *Peak width is for PD plot assuming a kernel factor = 0.60*

#.	Peak Age(Ma)	68%CI	95%CI	W(Z)	Frac(%)	SE,%	Count
1.	5.9	-1,5 ...+2,0	-2,6 ...+4,5	0.65	17.3	8.9	4.1
2.	29.6	-4,2 ...+4,8	-7,6 ...+10,2	0.44	46.6	19.0	11.2
3.	53.9	-9,1 ...+10,9	-16,4 ...+23,5	0.39	36.1	18.3	8.7

Log-likelihood for best fit:	-65,224
Chi-squared value for best fit:	23,538
Reduced chi-squared value:	1,239
Probability for F test:	1%
Condition number for COVAR matrix:	14,51
Number of iterations:	7

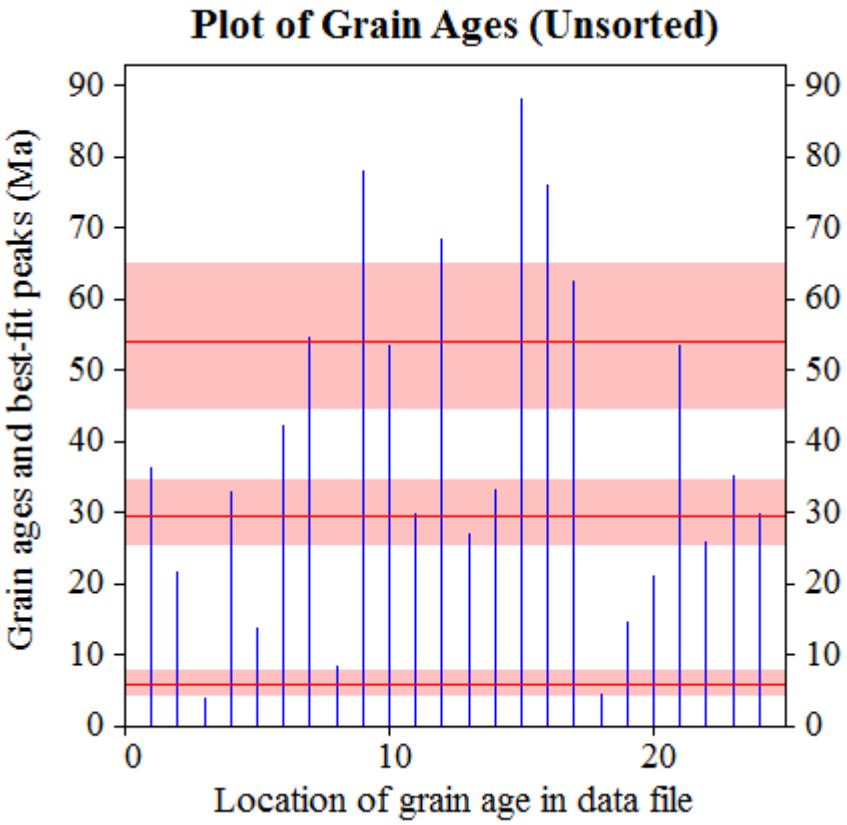
Plot of Grain Ages (Unsorted)
Grain ages and best-fit peaks (Ma)
0
10
20
30
40
50
60
70
80
90
Location of grain age in data file

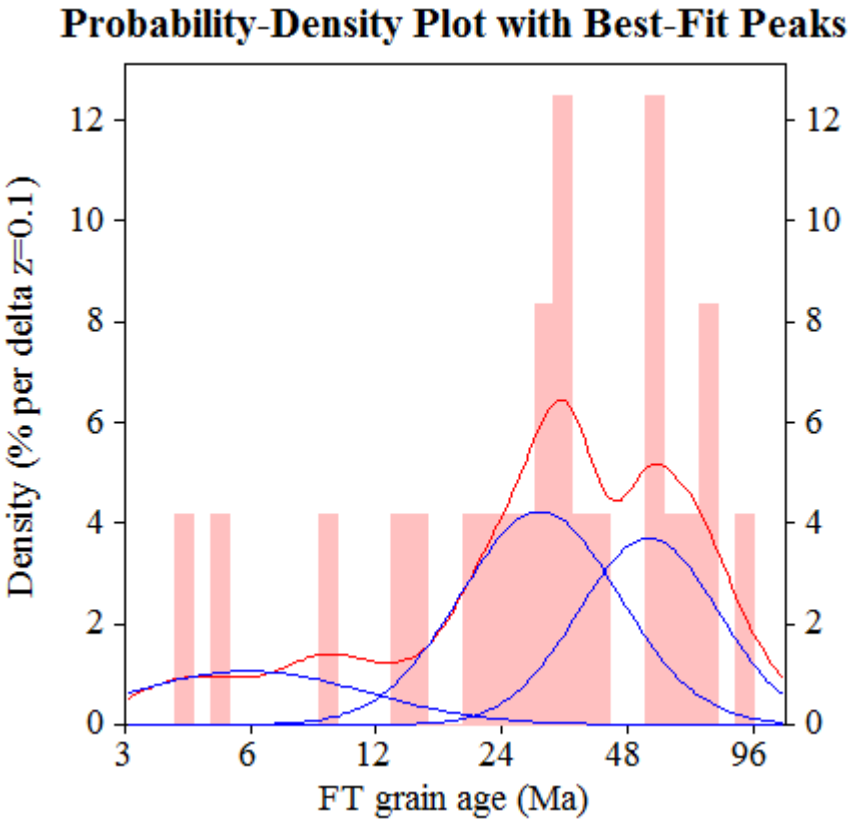
Probability-Density Plot with Best-Fit Peaks
Density (% per delta z=0.1)
0
2
4
6
8
10
12
3
6
12
24
48
96
FT grain age (Ma)

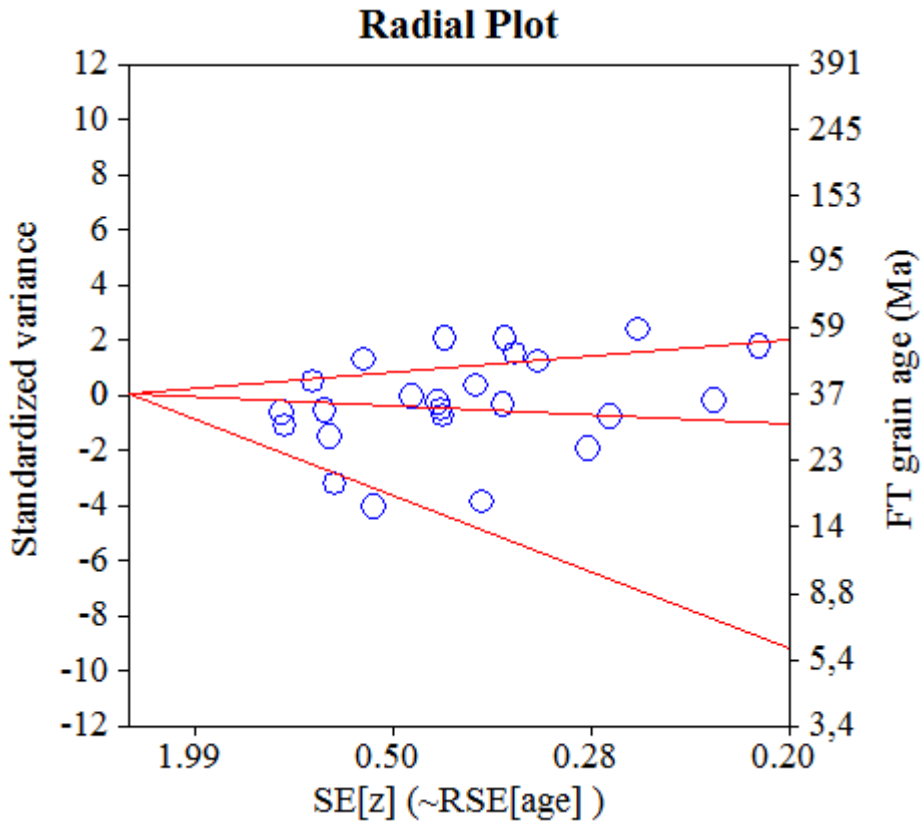
Radial Plot
Standardized variance
12
10
8
6
4
2
0
-2
-4
-6
-8
-10
-12
391
245
153
95
59
37
23
14
8,8
5,4
3,4
FT grain age (Ma)
1.99
0.50
0.28
0.20
SE[z] (~RSE[age])

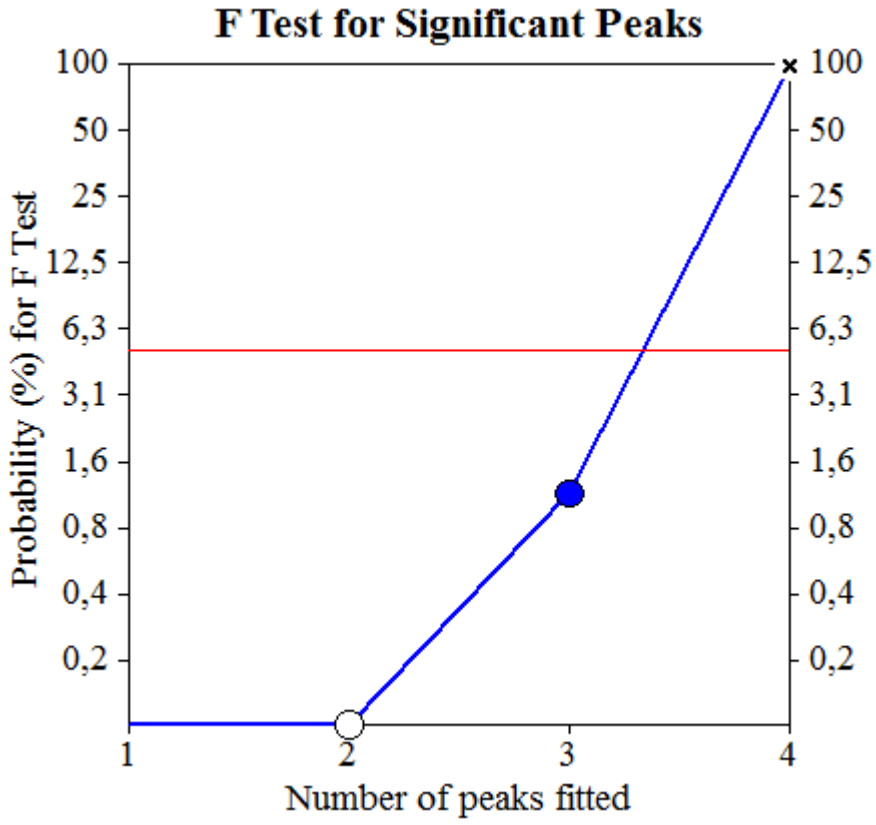
F Test for Significant Peaks
Probability (%) for F Test
100
50
25
12,5
6,3
3,1
1,6
0,8
0,4
0,2
1
2
3
4
Number of peaks fitted

NEW PARAMETERS - ZETA METHOD

EFFECTIVE TRACK DENSITY FOR FLUENCE MONITOR (tracks/cm^2): 1,27E+06
RELATIVE ERROR (%): 1,11
EFFECTIVE URANIUM CONTENT OF MONITOR (ppm): 15,00
ZETA FACTOR AND STANDARD ERROR (yr cm^2): 282,02 6,88
SIZE OF COUNTER SQUARE (cm^2): 6,39E-07

GRAIN AGES IN ORIGINAL ORDER

Grain no.	RhoS (cm^-2)	(Ns)	RhoI (cm^-2)	(Ni)	Squares	U+/-2s		Grain Age (Ma) Age	--95% CI--	
1	2,04E+05	(3)	7,89E+06	(116)	23	93	17	4.9	0.9	13.9
2	1,96E+05	(4)	1,22E+07	(249)	32	144	18	3.0	0.8	7.5
3	8,46E+04	(2)	1,21E+07	(287)	37	143	17	1.3	0.2	4.6
4	2,74E+05	(7)	1,37E+06	(35)	40	16	5	36.4	13.4	81.4
5	1,91E+05	(11)	9,39E+05	(54)	90	11	3	36.8	17.2	70.3
6	8,94E+04	(4)	6,22E+06	(278)	70	73	9	2.7	0.7	6.7
7	1,88E+05	(6)	5,04E+06	(161)	50	59	9	6.9	2.4	14.8
8	1,15E+05	(5)	5,75E+06	(250)	68	68	9	3.7	1.2	8.5
9	1,42E+05	(2)	5,90E+06	(83)	22	70	15	4.6	0.5	16.1
10	9,48E+04	(4)	7,04E+06	(297)	66	83	10	2.5	0.7	6.2
11	6,26E+04	(2)	1,19E+06	(38)	50	14	5	10.1	1.1	36.4
12	1,88E+05	(12)	1,97E+06	(126)	100	23	4	17.3	8.6	30.8
13	1,04E+05	(4)	1,51E+06	(58)	60	18	5	12.8	3.3	33.3
14	5,22E+04	(1)	8,82E+06	(169)	30	104	16	1.2	0.0	6.0
15	1,74E+05	(5)	1,04E+07	(299)	45	123	14	3.1	1.0	7.1
16	2,31E+05	(13)	1,49E+06	(84)	88	18	4	28.0	14.2	49.9
17	2,15E+05	(7)	1,20E+07	(392)	51	142	15	3.3	1.3	6.7
18	4,69E+04	(3)	8,65E+06	(553)	100	102	9	1.0	0.2	2.9
19	1,22E+05	(7)	1,90E+06	(109)	90	22	4	11.8	4.5	24.5
20	6,26E+05	(14)	3,44E+06	(77)	35	41	9	32.8	17.0	57.8
21	1,10E+05	(7)	1,31E+06	(84)	100	16	3	15.2	5.8	32.1
22	3,91E+04	(2)	5,30E+06	(271)	80	63	8	1.4	0.2	4.8
23	2,74E+05	(7)	7,20E+06	(184)	40	85	13	7.0	2.7	14.3
24	2,76E+05	(6)	7,04E+06	(153)	34	83	14	7.2	2.5	15.6
25	2,50E+05	(4)	5,38E+06	(86)	25	64	14	8.7	2.2	22.1
26	8,69E+04	(4)	1,35E+06	(62)	72	16	4	12.0	3.1	31.1
27	9,39E+04	(3)	1,00E+07	(320)	50	118	13	1.8	0.3	5.0
28	2,66E+05	(17)	1,74E+06	(111)	100	21	4	27.6	15.4	45.8
29	4,12E+04	(2)	1,13E+06	(55)	76	13	4	7.0	0.8	24.7
30	2,11E+05	(5)	1,08E+07	(255)	37	127	16	3.6	1.1	8.3
31	3,13E+05	(20)	2,57E+06	(164)	100	30	5	22.0	13.0	34.8
32	7,82E+04	(5)	1,71E+06	(109)	100	20	4	8.5	2.6	19.8
33	3,91E+04	(2)	7,43E+05	(38)	80	9	3	10.1	1.1	36.4
34	1,83E+05	(7)	3,10E+06	(119)	60	37	7	10.8	4.1	22.4
35	1,04E+05	(4)	9,68E+06	(371)	60	114	12	2.0	0.5	5.0
36	1,56E+05	(8)	7,51E+06	(384)	80	89	9	3.8	1.6	7.4
37	2,82E+05	(18)	2,21E+06	(141)	100	26	4	23.0	13.2	37.4
POOLED	1,58E+05	(237)	4,43E+06	(6622)	2341	52	2	6.4	5.6	7.4

CHI^2 PROBABILITY (%): 0.0
>>> Beware: possible upward bias in Chi^2 probability due to low counts <<<

POOLED AGE W/ 68% CONF. INTERVAL(Ma): 6.4, 6.0 -- 6.9 (-0.4 +0.5)
95% CONF. INTERVAL(Ma): 5.6 -- 7.4 (-0.8 +1.0)

CENTRAL AGE W/ 68% CONF. INTERVAL(Ma): 9.4, 8.0 -- 11.0 (-1.4 +1.6)
95% CONF. INTERVAL(Ma): 6.8 -- 12.8 (-2.5 +3.5)
AGE DISPERSION (%): 88.0

FIT OPTION: Best-fit peaks using the binomial model of Galbraith and Green

INITIAL GUESS FOR MODEL PARAMETERS (number of peaks to fit = 2)

Peak #.	Peak Age	Theta	Fraction(%)	Count
1.	6.40	0.035	10.3	3.81
2.	23.20	0.115	10.5	3.90

Total range for grain ages:	1,1 to 37,8 Ma
Number of active grains (Num. used for fit):	37
Number of removed grains:	0
Degrees of freedom for fit:	34
Average of the SE(Z)'s for the grains:	0,47
Estimated width of peaks in PD plot in Z units:	0,55

PARAMETERS FOR BEST-FIT PEAKS

* *Standard error for peak age includes group error*
* *Peak width is for PD plot assuming a kernel factor = 0.60*

#.	Peak Age(Ma)	68%CI	95%CI	W(Z)	Frac(%)	SE,%	Count
1.	3.2	-0,4 ...+0,4	-0,7 ...+0,9	0.58	63.6	9.6	23.5
2.	20.3	-2,3 ...+2,6	-4,2 ...+5,4	0.38	36.4	9.6	13.5

Log-likelihood for best fit:	-111,998
Chi-squared value for best fit:	40,163
Reduced chi-squared value:	1,181
Probability for F test:	0%
Condition number for COVAR matrix:	3,03
Number of iterations:	9

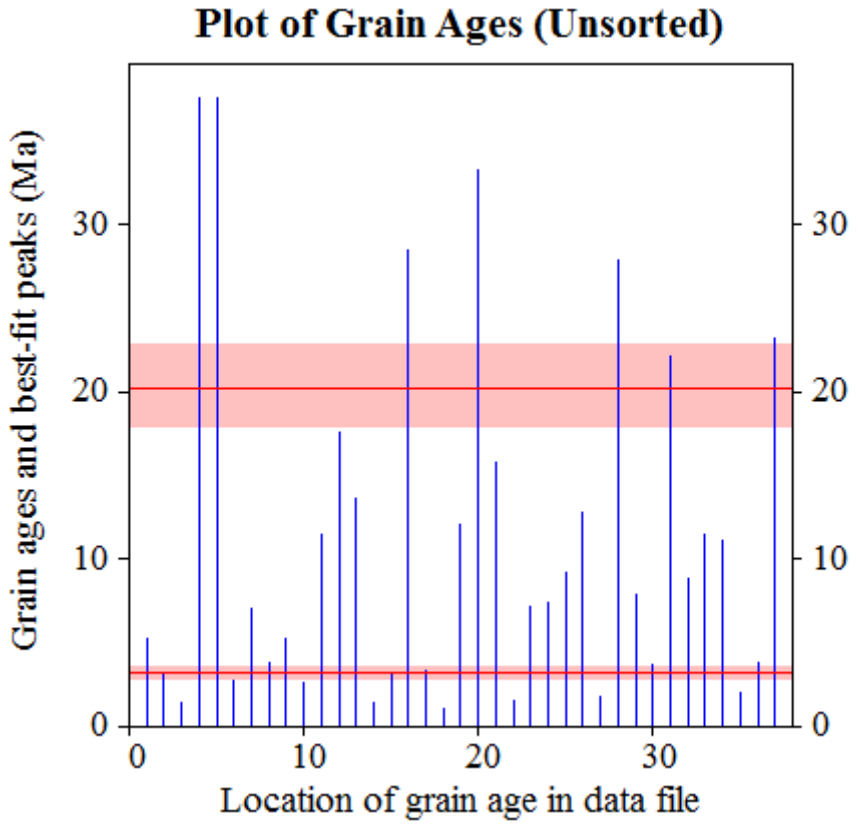
Plot of Grain Ages (Unsorted)
Grain ages and best-fit peaks (Ma)
0
10
20
30
Location of grain age in data file

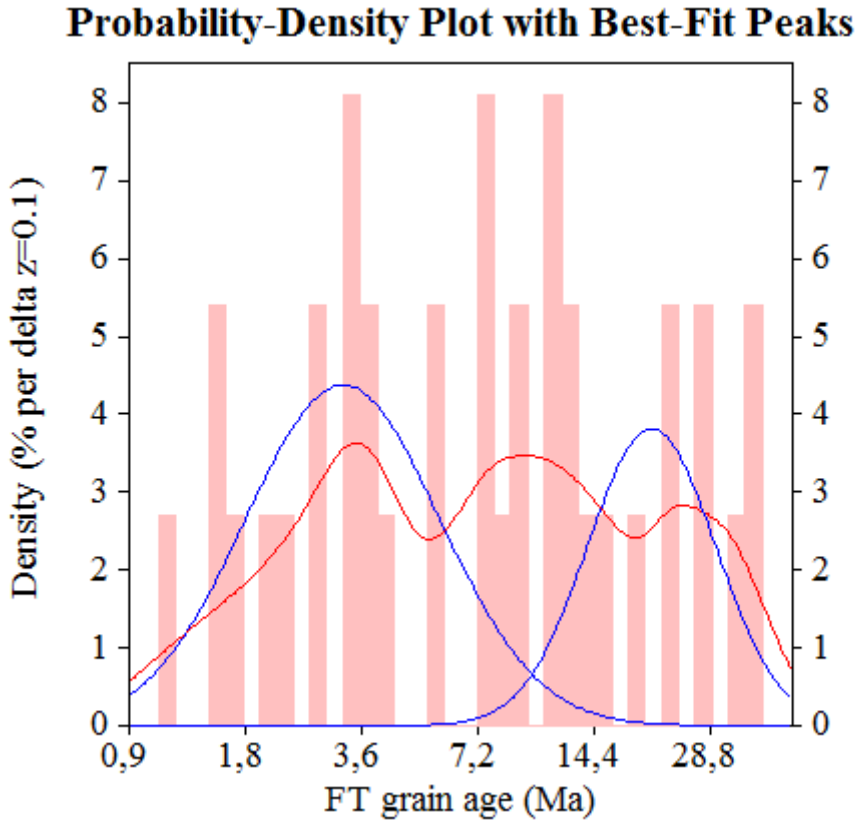
Probability-Density Plot with Best-Fit Peaks
Density (% per delta z=0.1)
0
1
2
3
4
5
6
7
8
0,9
1,8
3,6
7,2
14,4
28,8
FT grain age (Ma)

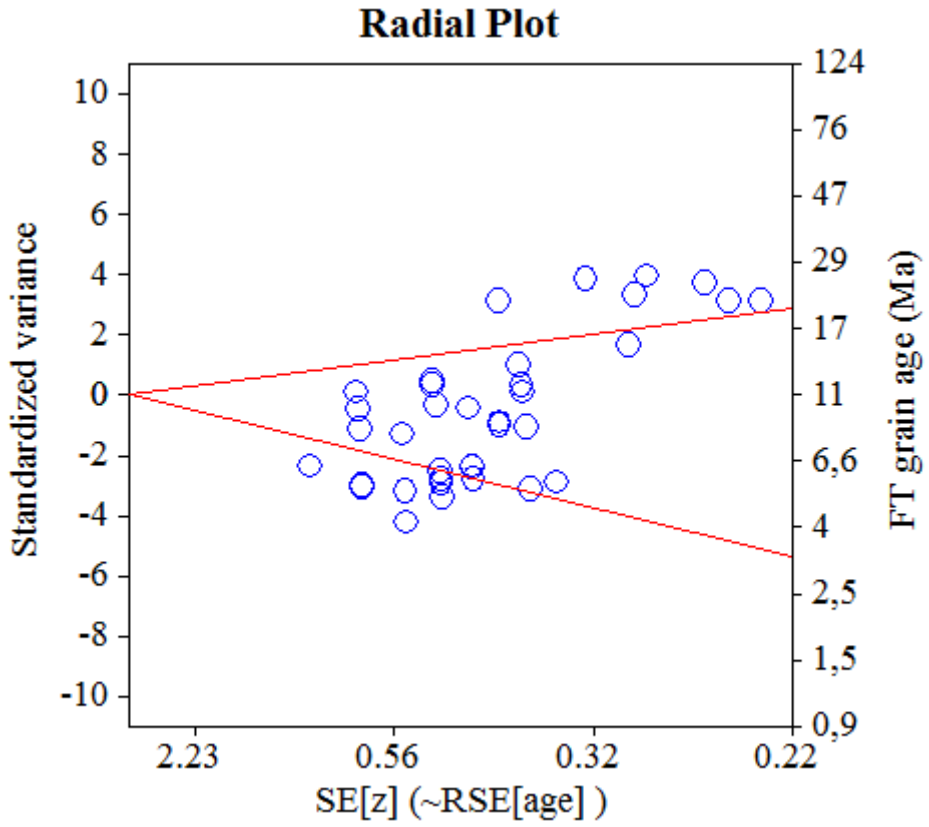
Radial Plot
Standardized variance
10
8
6
4
2
0
-2
-4
-6
-8
-10
124
76
47
29
17
11
6,6
4
2,5
1,5
0,9
FT grain age (Ma)
2.23
0.56
0.32
0.22
SE[z] (~RSE[age])

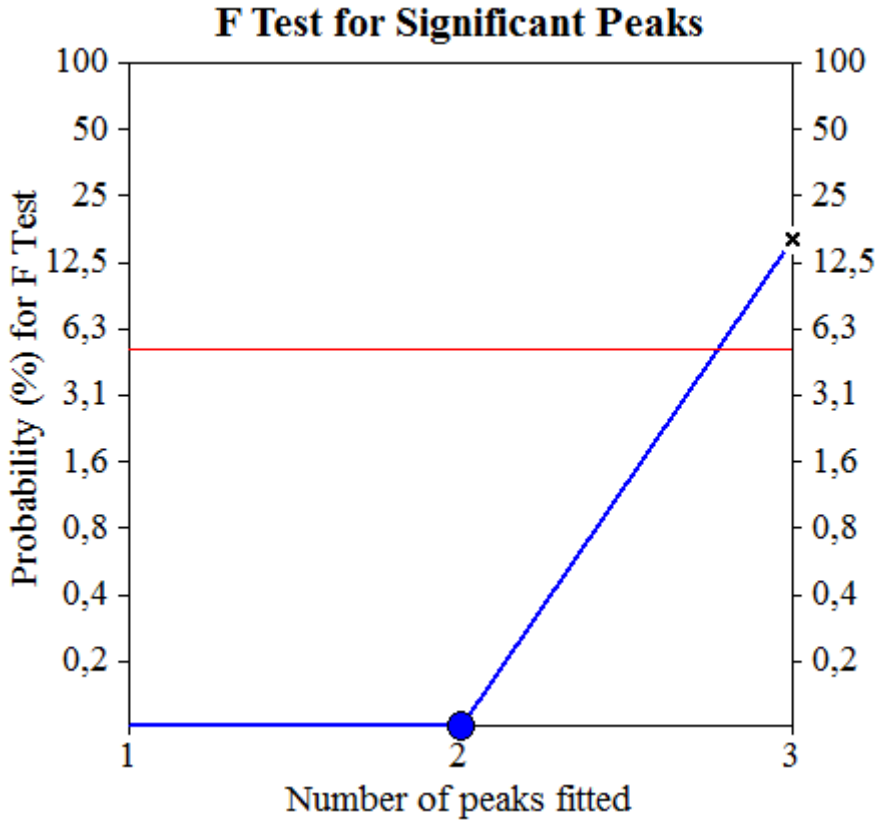
F Test for Significant Peaks
Probability (%) for F Test
100
50
25
12,5
6,3
3,1
1,6
0,8
0,4
0,2
1
2
3
Number of peaks fitted

Datafile: F:\Termo_Lab_Grenoble\Jairo\Apatites\Echantillon-IRR052015\JG-P3-15\JG-P3-15-Ap.ftz
Title: JG-P3-15 Irr 5-2015-24

NEW PARAMETERS - ZETA METHOD

EFFECTIVE TRACK DENSITY FOR FLUENCE MONITOR (tracks/cm^2): 1,23E+06
RELATIVE ERROR (%): 1,41
EFFECTIVE URANIUM CONTENT OF MONITOR (ppm): 15,00
ZETA FACTOR AND STANDARD ERROR (yr cm^2): 282,02 6,88
SIZE OF COUNTER SQUARE (cm^2): 6,39E-07

GRAIN AGES IN ORIGINAL ORDER

Grain no.	RhoS (cm^-2)	(Ns)	RhoI (cm^-2)	(Ni)	Squares	U+/-2s		Grain Age (Ma) Age	--95% CI--	
1	4,06E+05	(7)	1,05E+07	(182)	27	129	19	6.8	2.6	14.0
2	2,24E+05	(3)	8,42E+06	(113)	21	103	20	4.8	0.9	13.8
3	1,04E+05	(4)	6,16E+06	(236)	60	75	10	3.1	0.8	7.6
4	1,68E+05	(3)	9,84E+06	(176)	28	120	18	3.1	0.6	8.8
5	7,82E+04	(4)	4,91E+06	(251)	80	60	8	2.9	0.7	7.2
6	2,74E+05	(7)	1,10E+07	(281)	40	134	16	4.4	1.7	9.0
7	2,72E+05	(8)	1,06E+07	(312)	46	130	15	4.5	1.9	8.9
8	1,74E+05	(6)	1,15E+07	(397)	54	140	15	2.7	1.0	5.8
9	2,61E+05	(10)	7,41E+06	(284)	60	90	11	6.2	2.9	11.4
10	3,19E+05	(11)	7,65E+06	(264)	54	93	12	7.3	3.6	13.1
11	2,27E+05	(9)	1,13E+07	(449)	62	138	14	3.5	1.6	6.7
12	1,30E+05	(6)	8,37E+06	(385)	72	102	11	2.8	1.0	5.9
13	5,87E+05	(3)	1,23E+07	(63)	8	150	38	8.7	1.7	25.2
14	2,43E+05	(7)	9,39E+06	(270)	45	115	14	4.6	1.8	9.4
15	1,49E+05	(4)	4,99E+06	(134)	42	61	11	5.4	1.4	13.6
16	9,07E+04	(4)	7,39E+06	(326)	69	90	10	2.2	0.6	5.5
17	2,38E+05	(7)	7,72E+06	(227)	46	94	13	5.5	2.1	11.2
18	2,09E+05	(2)	7,41E+06	(71)	15	90	22	5.2	0.6	18.3
19	1,96E+05	(4)	1,30E+07	(266)	32	159	20	2.7	0.7	6.8
20	7,82E+04	(3)	1,07E+07	(409)	60	130	13	1.3	0.3	3.7
21	4,43E+05	(17)	1,01E+07	(388)	60	124	13	7.7	4.4	12.3
22	2,82E+05	(9)	1,14E+07	(364)	50	139	15	4.4	1.9	8.2
23	4,07E+05	(13)	1,26E+07	(402)	50	154	16	5.7	3.0	9.7
24	2,74E+05	(7)	3,25E+06	(83)	40	40	9	14.9	5.7	31.4
25	2,28E+05	(7)	1,04E+07	(319)	48	127	15	3.9	1.5	7.9
26	1,07E+05	(5)	9,99E+06	(466)	73	122	12	1.9	0.6	4.4
27	1,28E+05	(4)	6,07E+06	(190)	49	74	11	3.8	1.0	9.5
POOLED	2,11E+05	(174)	8,86E+06	(7308)	1291	108	4	4.1	3.5	4.8

CHI^2 PROBABILITY (%): 2.1
>>> Beware: possible upward bias in Chi^2 probability due to low counts <<<

POOLED AGE W/ 68% CONF. INTERVAL(Ma): 4.1, 3.8 -- 4.5 (-0.3 +0.4)
95% CONF. INTERVAL(Ma): 3.5 -- 4.8 (-0.6 +0.7)

CENTRAL AGE W/ 68% CONF. INTERVAL(Ma): 4.2, 3.8 -- 4.7 (-0.4 +0.4)
95% CONF. INTERVAL(Ma): 3.5 -- 5.1 (-0.7 +0.9)
AGE DISPERSION (%): 26.5

FIT OPTION: Best-fit peaks using the binomial model of Galbraith and Green

INITIAL GUESS FOR MODEL PARAMETERS (number of peaks to fit = 2)

Peak #.	Peak Age	Theta	Fraction(%)	Count
1.	4.10	0.023	27.3	7.37
2.	15.50	0.082	3.1	0.83

Total range for grain ages:	1,5 to 15,5 Ma
Number of active grains (Num. used for fit):	27
Number of removed grains:	0
Degrees of freedom for fit:	24
Average of the SE(Z)'s for the grains:	0,43
Estimated width of peaks in PD plot in Z units:	0,5

PARAMETERS FOR BEST-FIT PEAKS

* *Standard error for peak age includes group error*
* *Peak width is for PD plot assuming a kernel factor = 0.60*

#.	Peak Age(Ma)	68%CI	95%CI	W(Z)	Frac(%)	SE,%	Count
1.	3.4	-0,6 ...+0,8	-1,1 ...+1,7	0.50	66.6	34.6	18.0
2.	5.9	-1,4 ...+1,8	-2,4 ...+4,2	0.41	33.4	34.6	9.0

Log-likelihood for best fit:	-66,468
Chi-squared value for best fit:	28,317
Reduced chi-squared value:	1,180
Probability for F test:	0%
Condition number for COVAR matrix:	19,56
Number of iterations:	43

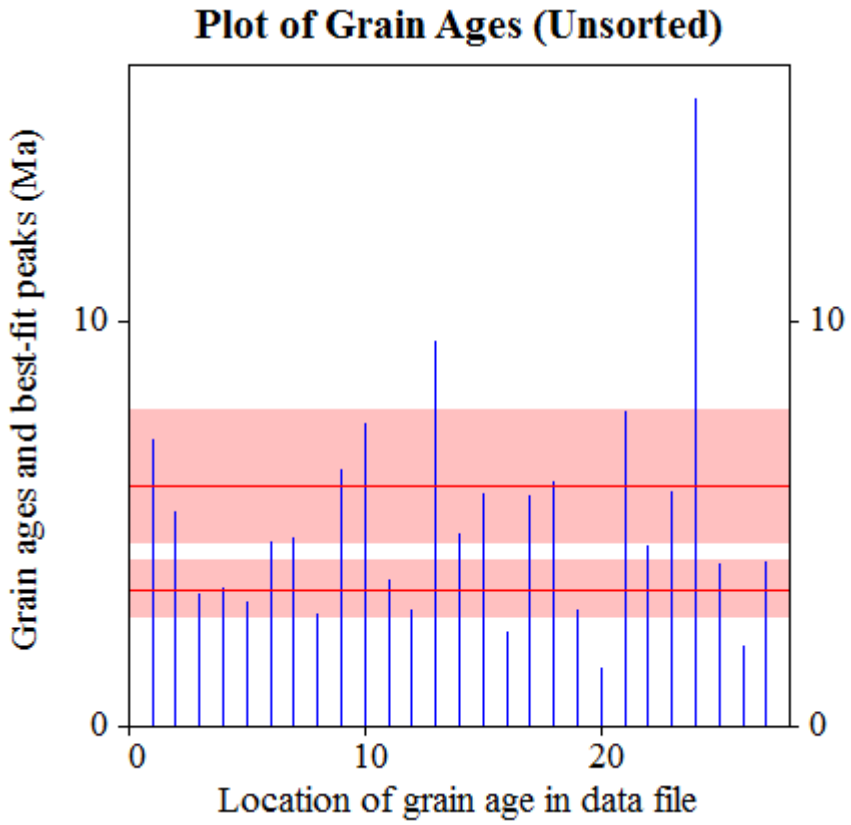
Plot of Grain Ages (Unsorted)
Grain ages and best-fit peaks (Ma)
10
0
0
10
20
Location of grain age in data file

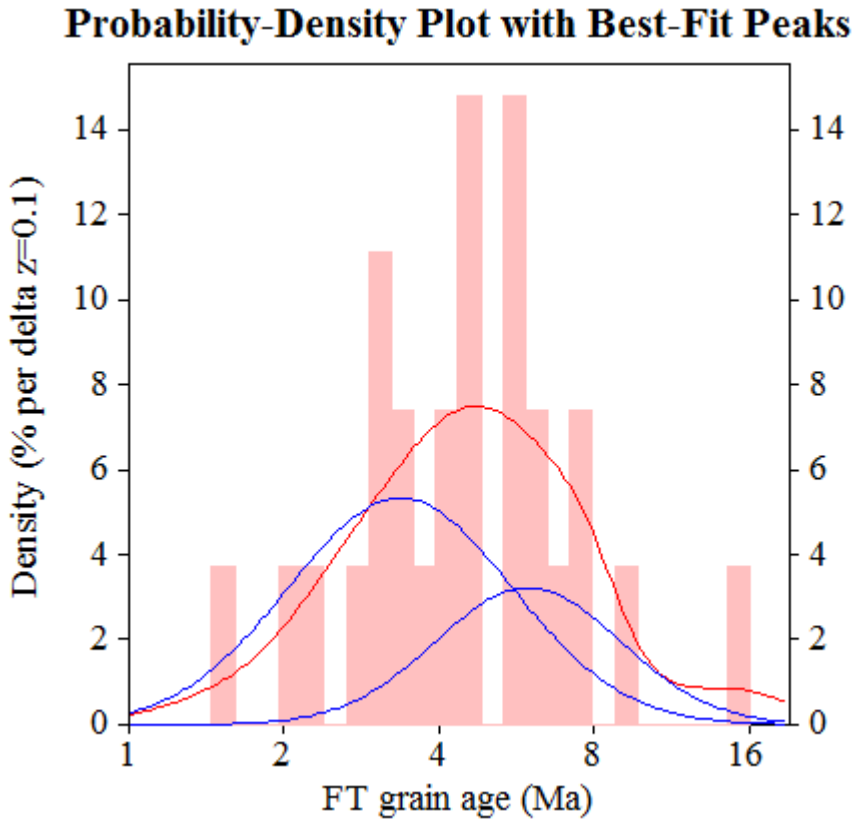
Probability-Density Plot with Best-Fit Peaks
Density (% per delta z=0.1)
14
12
10
8
6
4
2
0
1
2
4
8
16
FT grain age (Ma)

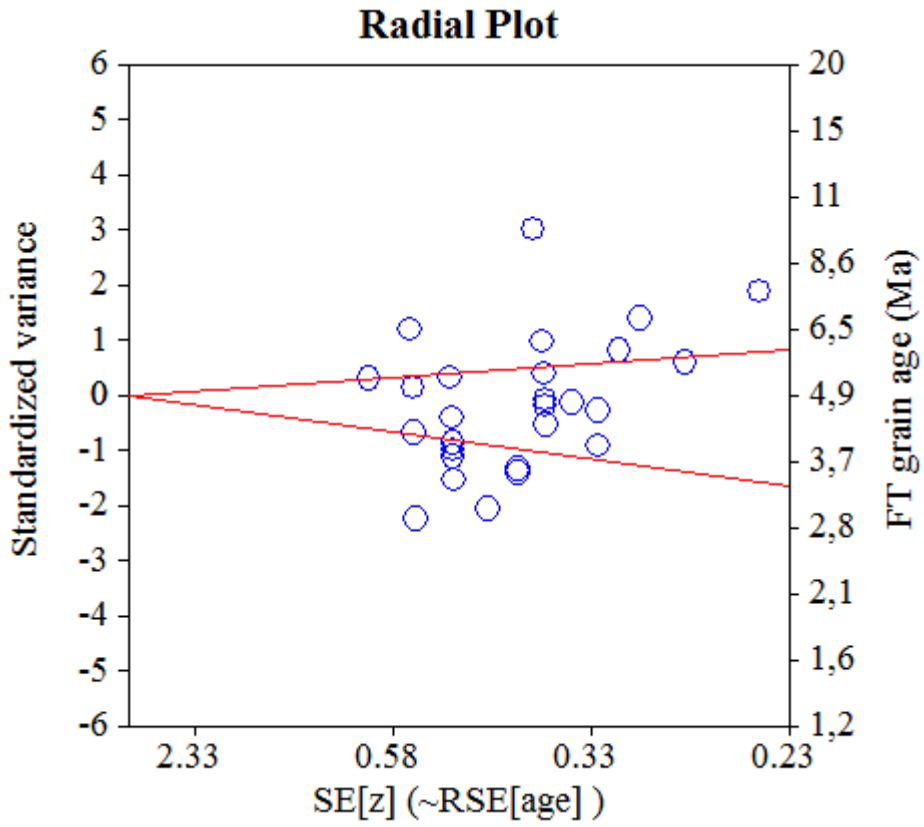
Radial Plot
Standardized variance
6
5
4
3
2
1
0
-1
-2
-3
-4
-5
-6
20
15
11
8,6
6,5
4,9
3,7
2,8
2,1
1,6
1,2
FT grain age (Ma)
2.33
0.58
0.33
0.23
SE[z] (~RSE[age])

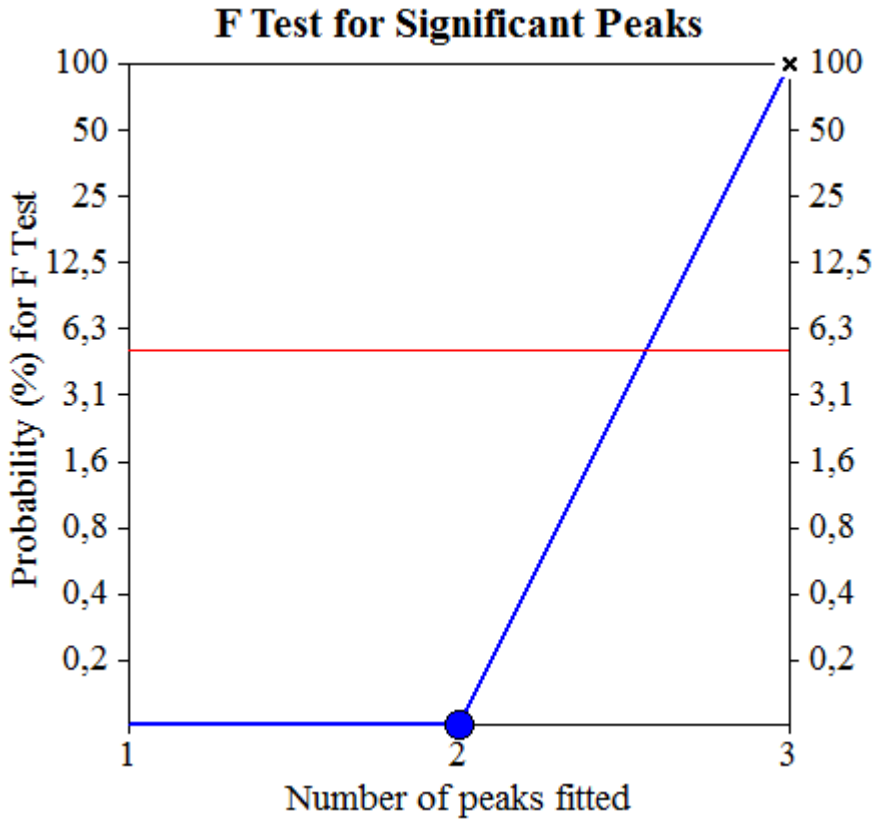
F Test for Significant Peaks
Probability (%) for F Test
100
50
25
12,5
6,3
3,1
1,6
0,8
0,4
0,2
1
2
3
Number of peaks fitted

Datafile: F:\Termo_Lab_Grenoble\Jairo\Apatites\Echantillon-IRR052015\JG-P3-32\JG-P3-32-Ap.ftz
Title: JG-P3-32 Irr 5-2015-23

NEW PARAMETERS - ZETA METHOD

EFFECTIVE TRACK DENSITY FOR FLUENCE MONITOR (tracks/cm^2): 1,23E+06
RELATIVE ERROR (%): 1,36
EFFECTIVE URANIUM CONTENT OF MONITOR (ppm): 15,00
ZETA FACTOR AND STANDARD ERROR (yr cm^2): 282,02 6,88
SIZE OF COUNTER SQUARE (cm^2): 6,39E-07

GRAIN AGES IN ORIGINAL ORDER

Grain no.	RhoS (cm^-2)	(Ns)	RhoI (cm^-2)	(Ni)	Squares	U+/-2s		Grain Age (Ma) Age	--95% CI--	
1	2,24E+04	(1)	6,73E+06	(301)	70	82	10	0.7	0.0	3.2
2	2,45E+05	(5)	6,90E+06	(141)	32	84	14	6.3	2.0	14.7
3	1,74E+05	(2)	1,87E+07	(215)	18	228	32	1.7	0.2	5.9
4	1,25E+05	(4)	1,17E+07	(375)	50	143	15	1.9	0.5	4.8
5	5,22E+04	(1)	9,02E+06	(173)	30	110	17	1.1	0.0	5.7
6	2,24E+05	(10)	1,34E+07	(598)	70	163	14	2.9	1.4	5.4
7	2,74E+05	(7)	1,68E+07	(430)	40	205	21	2.9	1.1	5.9
8	4,24E+05	(16)	1,63E+07	(613)	59	199	17	4.6	2.6	7.4
9	1,04E+05	(4)	9,57E+06	(367)	60	117	13	2.0	0.5	4.9
10	2,29E+05	(13)	1,27E+07	(720)	89	155	12	3.2	1.7	5.4
11	1,56E+05	(4)	9,55E+06	(244)	40	117	15	3.0	0.8	7.4
12	1,04E+05	(4)	8,14E+06	(312)	60	99	12	2.3	0.6	5.7
13	2,04E+05	(3)	1,11E+07	(163)	23	135	22	3.4	0.7	9.5
14	2,93E+05	(3)	7,34E+06	(75)	16	90	21	7.3	1.4	21.0
POOLED	1,83E+05	(77)	1,13E+07	(4727)	657	138	5	2.8	2.2	3.6

CHI^2 PROBABILITY (%): 26.1
>>> Beware: possible upward bias in Chi^2 probability due to low counts <<<

POOLED AGE W/ 68% CONF. INTERVAL(Ma): 2.8, 2.5 -- 3.2 (-0.3 +0.4)
95% CONF. INTERVAL(Ma): 2.2 -- 3.6 (-0.6 +0.7)

CENTRAL AGE W/ 68% CONF. INTERVAL(Ma): 2.8, 2.5 -- 3.2 (-0.3 +0.4)
95% CONF. INTERVAL(Ma): 2.2 -- 3.6 (-0.6 +0.7)
AGE DISPERSION (%): 7.4

FIT OPTION: Best-fit peaks using the binomial model of Galbraith and Green

INITIAL GUESS FOR MODEL PARAMETERS (number of peaks to fit = 1)

Peak #.	Peak Age	Theta	Fraction(%)	Count
1.	2.80	0.016	31.0	4.35

Total range for grain ages: 0,9 to 8,0 Ma
Number of active grains (Num. used for fit): 14
Number of removed grains: 0
Degrees of freedom for fit: 13
Average of the SE(Z)'s for the grains: 0,52
Estimated width of peaks in PD plot in Z units: 0,61

PARAMETERS FOR BEST-FIT PEAKS

* *Standard error for peak age includes group error*
* *Peak width is for PD plot assuming a kernel factor = 0.60*

#.	Peak Age(Ma)	68%CI	95%CI	W(Z)	Frac(%)	SE,%	Count
1.	2.8	-0,3 ...+0,4	-0,6 ...+0,7	0.50	100.0	0.0	14.0

Log-likelihood for best fit: -30,934
Chi-squared value for best fit: 15,775
Reduced chi-squared value: 1,213
Probability for F test: 0%
Condition number for COVAR matrix: 1,00
Number of iterations: 5

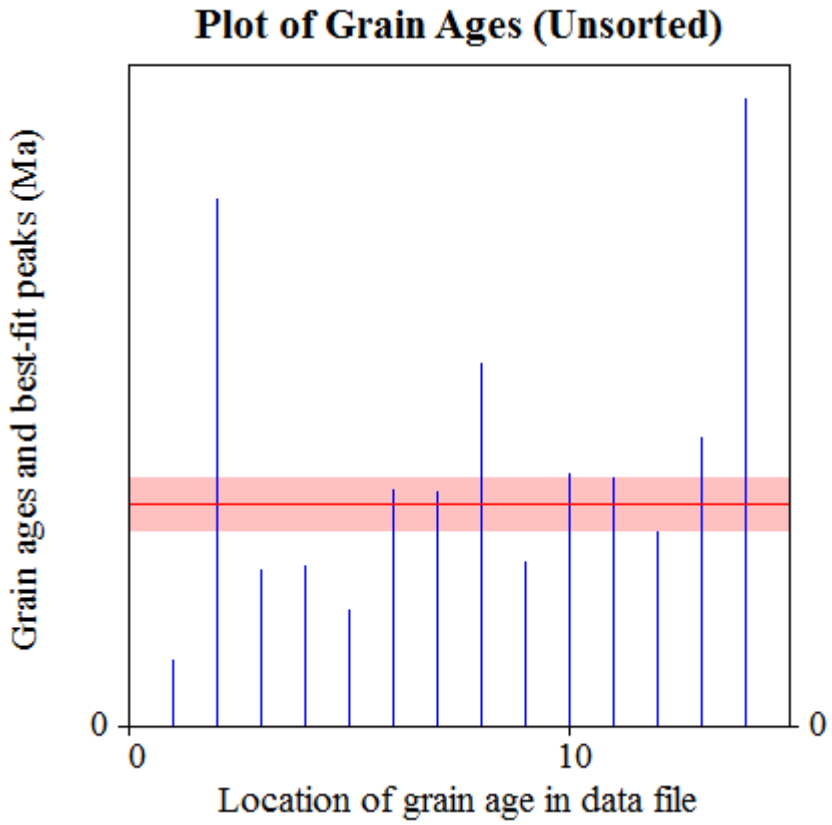
Plot of Grain Ages (Unsorted)
Grain ages and best-fit peaks (Ma)
0
0
10
0
Location of grain age in data file

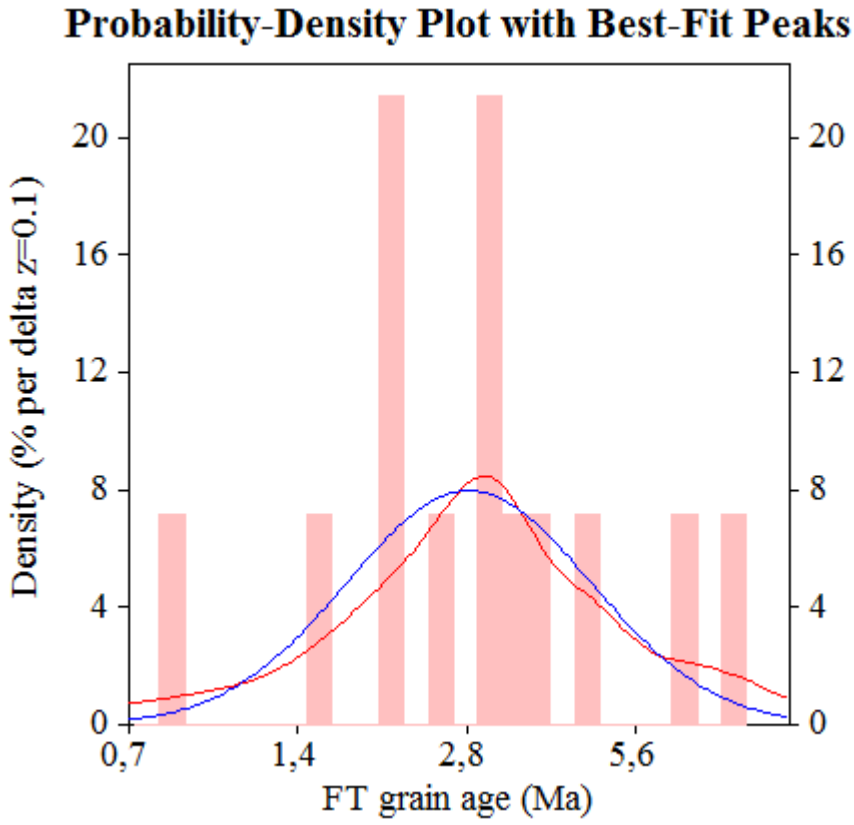
Probability-Density Plot with Best-Fit Peaks
Density (% per delta z=0.1)
20
16
12
8
4
0
0,7
1,4
2,8
5,6
FT grain age (Ma)

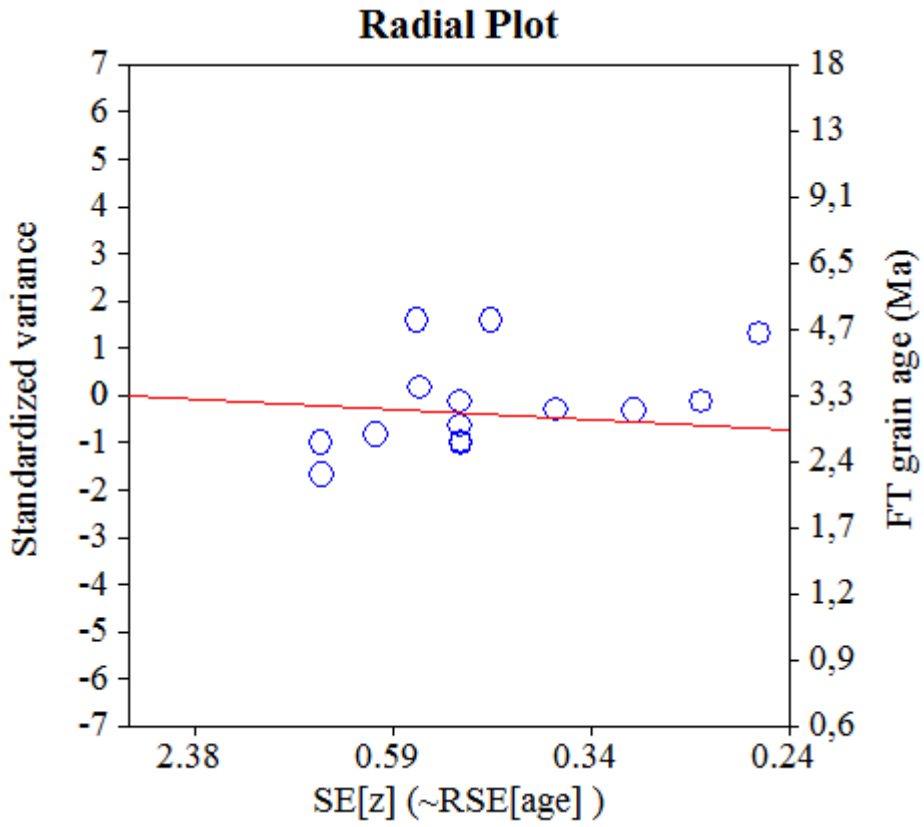
Radial Plot
Standardized variance
FT grain age (Ma)
7
6
5
4
3
2
1
0
-1
-2
-3
-4
-5
-6
-7
18
13
9,1
6,5
4,7
3,3
2,4
1,7
1,2
0,9
0,6
2.38
0.59
0.34
0.24
SE[z] (~RSE[age])

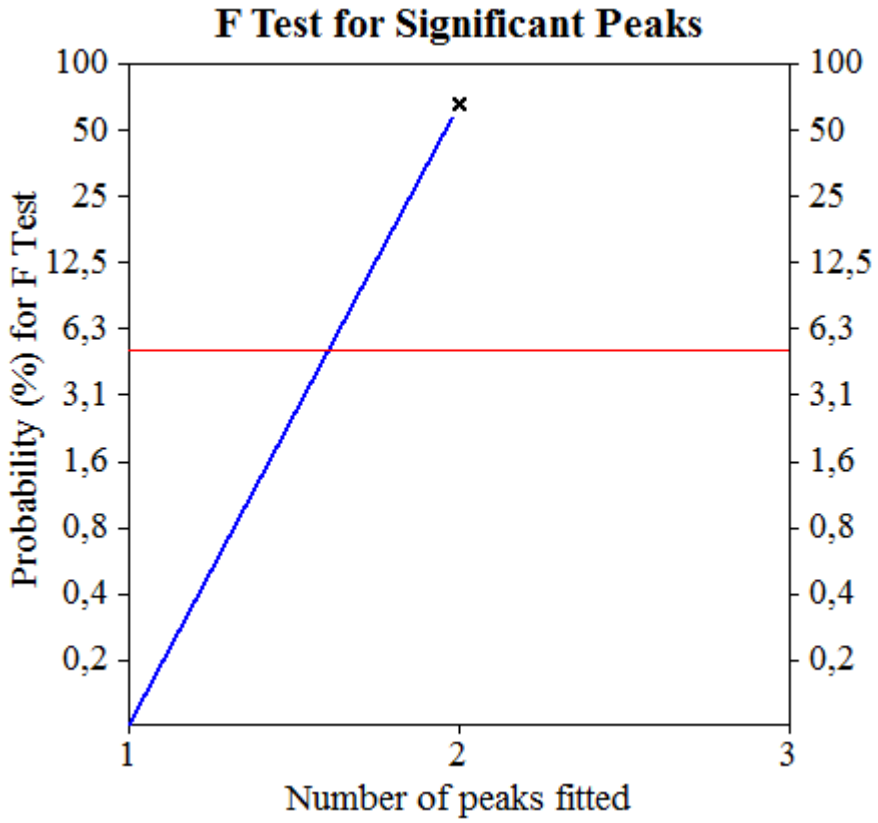
F Test for Significant Peaks
Probability (%) for F Test
100
50
25
12,5
6,3
3,1
1,6
0,8
0,4
0,2
1
2
3
Number of peaks fitted

Datafile: C:\BH2\Jairo\Echantillon-IRR082015\JG-P3-19\JG-P3-19Ap.fta
Title: JG-P3-19 Irr 8-2015-14

NEW PARAMETERS - ZETA METHOD

EFFECTIVE TRACK DENSITY FOR FLUENCE MONITOR (tracks/cm^2): 1,28E+06
RELATIVE ERROR (%): 1,11
EFFECTIVE URANIUM CONTENT OF MONITOR (ppm): 15,00
ZETA FACTOR AND STANDARD ERROR (yr cm^2): 282,02 6,88
SIZE OF COUNTER SQUARE (cm^2): 6,39E-07

GRAIN AGES IN ORIGINAL ORDER

Grain no.	RhoS (cm^-2)	(Ns)	RhoI (cm^-2)	(Ni)	Squares	U+/-2s		Grain Age (Ma) Age	--95% CI--	
1	6,26E+04	(4)	6,34E+06	(405)	100	75	8	1.8	0.5	4.6
2	1,41E+05	(9)	8,34E+06	(533)	100	98	9	3.1	1.4	5.8
3	9,39E+04	(6)	5,40E+06	(345)	100	64	7	3.2	1.1	6.9
4	2,61E+05	(5)	1,14E+07	(219)	30	134	18	4.2	1.3	9.7
5	7,82E+04	(5)	7,25E+06	(463)	100	85	8	2.0	0.6	4.6
6	1,25E+05	(8)	8,95E+06	(572)	100	105	9	2.6	1.1	5.0
7	1,17E+05	(3)	7,55E+06	(193)	40	89	13	2.9	0.6	8.3
8	8,69E+04	(5)	5,03E+06	(289)	90	59	7	3.2	1.0	7.3
9	5,87E+04	(3)	2,39E+06	(122)	80	28	5	4.6	0.9	13.2
10	7,82E+04	(5)	7,79E+06	(498)	100	92	8	1.9	0.6	4.2
11	9,94E+04	(4)	6,93E+06	(279)	63	82	10	2.7	0.7	6.7
12	1,10E+05	(7)	5,29E+06	(338)	100	62	7	3.8	1.5	7.8
13	9,78E+04	(5)	4,50E+06	(230)	80	53	7	4.0	1.3	9.3
14	1,17E+05	(6)	7,24E+06	(370)	80	85	9	3.0	1.1	6.4
15	1,10E+05	(7)	6,65E+06	(425)	100	78	8	3.0	1.2	6.2
16	3,91E+04	(2)	5,22E+06	(267)	80	61	8	1.5	0.2	4.9
17	6,26E+04	(4)	8,81E+06	(563)	100	104	9	1.3	0.3	3.3
18	7,82E+04	(5)	5,87E+06	(375)	100	69	7	2.5	0.8	5.6
19	7,82E+04	(5)	2,57E+06	(164)	100	30	5	5.7	1.8	13.0
20	1,25E+05	(4)	4,95E+06	(158)	50	58	9	4.7	1.2	11.9
21	1,28E+05	(4)	7,28E+06	(228)	49	86	11	3.3	0.9	8.2
22	7,82E+04	(5)	5,43E+06	(347)	100	64	7	2.7	0.8	6.1
23	6,26E+04	(4)	6,79E+06	(434)	100	80	8	1.7	0.4	4.3
24	1,42E+05	(7)	8,23E+06	(405)	77	97	10	3.2	1.2	6.5
25	1,83E+05	(7)	1,01E+07	(386)	60	118	12	3.3	1.3	6.8
26	1,25E+05	(8)	5,96E+06	(381)	100	70	7	3.8	1.6	7.5
27	1,74E+05	(10)	8,36E+06	(481)	90	98	9	3.8	1.8	6.9
28	1,37E+05	(7)	7,45E+06	(381)	80	88	9	3.4	1.3	6.9
29	5,22E+04	(3)	7,76E+06	(446)	90	91	9	1.3	0.2	3.6
30	3,48E+04	(2)	9,09E+06	(523)	90	107	10	0.7	0.1	2.5
31	5,87E+04	(3)	7,86E+06	(402)	80	93	9	1.4	0.3	3.9
32	3,13E+04	(2)	8,15E+06	(521)	100	96	9	0.7	0.1	2.5
33	1,04E+05	(4)	8,53E+06	(327)	60	100	11	2.3	0.6	5.7
34	1,56E+05	(7)	1,10E+07	(494)	70	130	12	2.6	1.0	5.3
POOLED	9,65E+04	(175)	6,93E+06	(12564)	2839	81	2	2.5	2.1	2.9

CHI^2 PROBABILITY (%): 63.0
>>> Beware: possible upward bias in Chi^2 probability due to low counts <<<

POOLED AGE W/ 68% CONF. INTERVAL(Ma): 2.5, 2.3 -- 2.7 (-0.2 +0.2)
95% CONF. INTERVAL(Ma): 2.1 -- 2.9 (-0.4 +0.4)

CENTRAL AGE W/ 68% CONF. INTERVAL(Ma): 2.5, 2.3 -- 2.7 (-0.2 +0.2)
95% CONF. INTERVAL(Ma): 2.1 -- 2.9 (-0.4 +0.4)
AGE DISPERSION (%): 1.9

FIT OPTION: Best-fit peaks using the binomial model of Galbraith and Green

INITIAL GUESS FOR MODEL PARAMETERS (number of peaks to fit = 1)

Peak #.	Peak Age	Theta	Fraction(%)	Count
1.	2.50	0.014	26.1	8.88

Total range for grain ages: 0,9 to 6,0 Ma
Number of active grains (Num. used for fit): 34
Number of removed grains: 0
Degrees of freedom for fit: 33
Average of the SE(Z)'s for the grains: 0,45
Estimated width of peaks in PD plot in Z units: 0,53

PARAMETERS FOR BEST-FIT PEAKS

* *Standard error for peak age includes group error*
* *Peak width is for PD plot assuming a kernel factor = 0.60*

#.	Peak Age(Ma)	68%CI	95%CI	W(Z)	Frac(%)	SE,%	Count
1.	2.5	-0,2 ...+0,2	-0,4 ...+0,4	0.52	100.0	0.0	34.0

Log-likelihood for best fit: -74,086
Chi-squared value for best fit: 29,752
Reduced chi-squared value: 0,902
Probability for F test: 0%
Condition number for COVAR matrix: 1,00
Number of iterations: 5

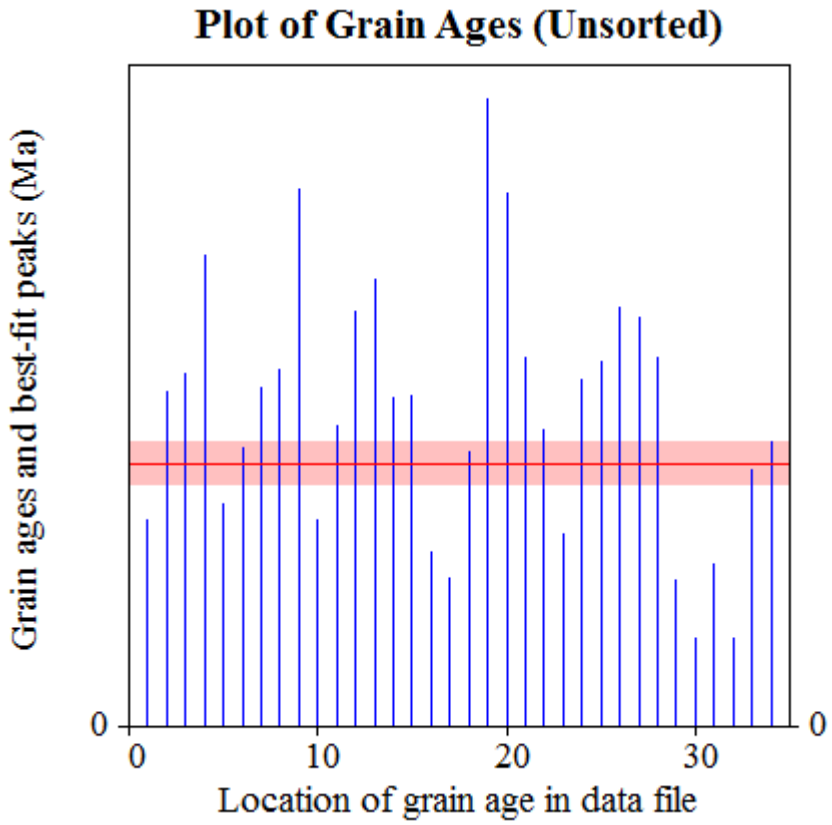
Plot of Grain Ages (Unsorted)
Grain ages and best-fit peaks (Ma)
0
0
10
20
30
0
Location of grain age in data file

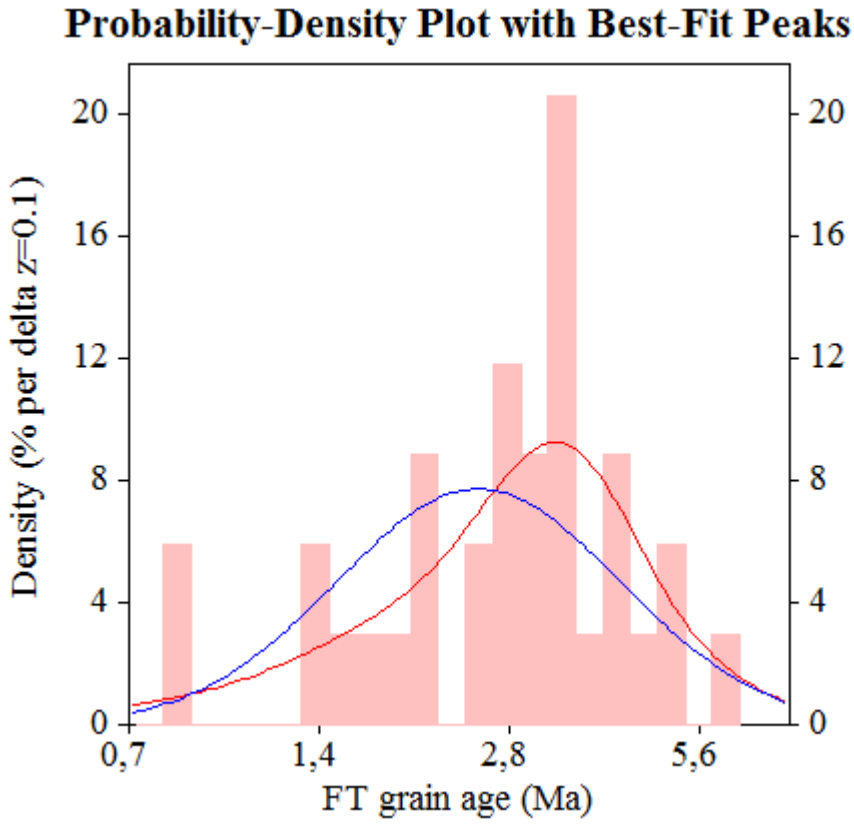
Probability-Density Plot with Best-Fit Peaks
Density (% per delta z=0.1)
20
16
12
8
4
0
0,7
1,4
2,8
5,6
FT grain age (Ma)

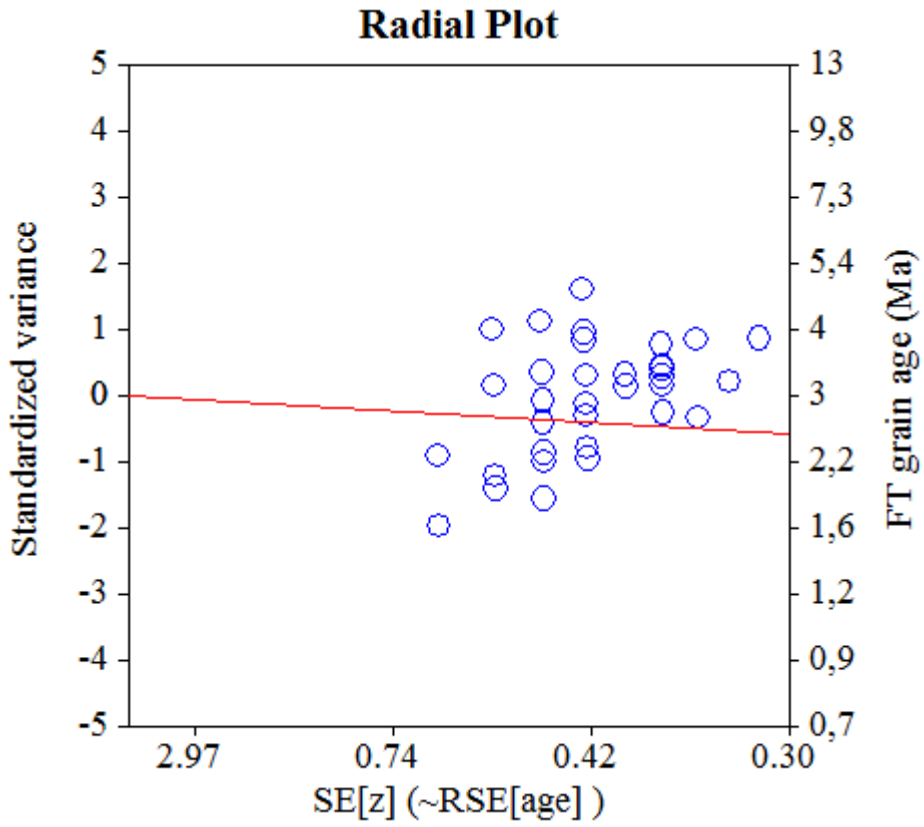
Radial Plot
Standardized variance
5
4
3
2
1
0
-1
-2
-3
-4
-5
FT grain age (Ma)
13
9,8
7,3
5,4
4
3
2,2
1,6
1,2
0,9
0,7
2.97
0.74
0.42
0.30
SE[z] (~RSE[age])

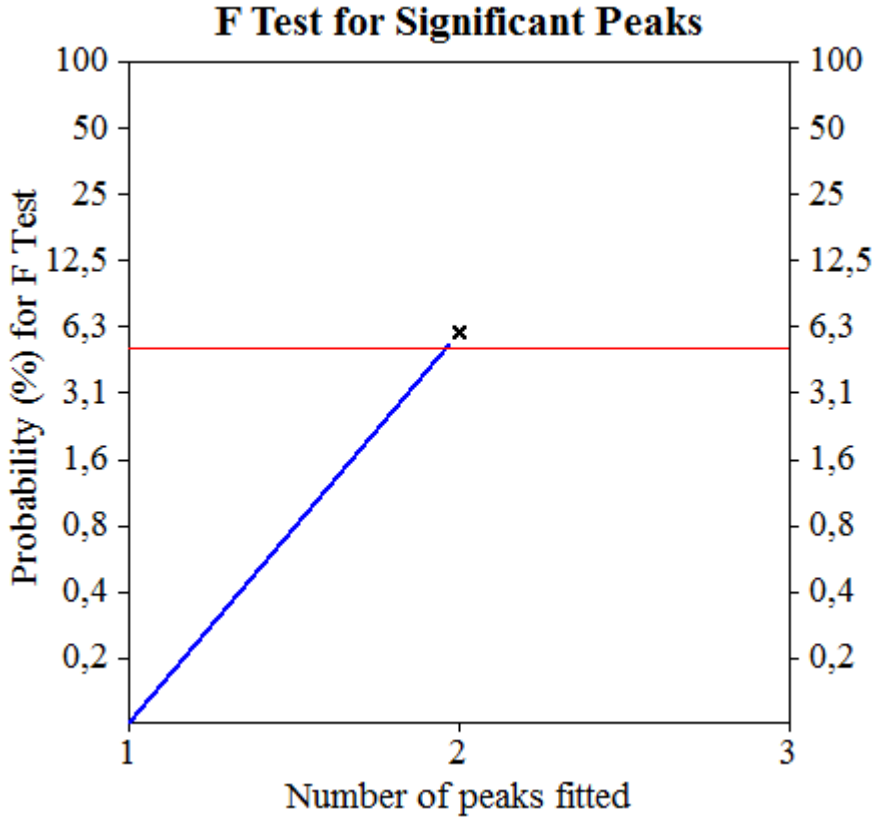
F Test for Significant Peaks
Probability (%) for F Test
100
50
25
12,5
6,3
3,1
1,6
0,8
0,4
0,2
1
2
3
Number of peaks fitted

Datafile: C:\BH2\Jairo\Echantillon-IRR082015\JG-P3-22\JG-P3-22Ap.fta
Title: JG-P3-22 Irr 8-2015-16

NEW PARAMETERS - ZETA METHOD

EFFECTIVE TRACK DENSITY FOR FLUENCE MONITOR (tracks/cm^2): 1,28E+06
RELATIVE ERROR (%): 1,14
EFFECTIVE URANIUM CONTENT OF MONITOR (ppm): 15,00
ZETA FACTOR AND STANDARD ERROR (yr cm^2): 282,02 6,88
SIZE OF COUNTER SQUARE (cm^2): 6,39E-07

GRAIN AGES IN ORIGINAL ORDER

Grain no.	RhoS (cm^-2)	(Ns)	RhoI (cm^-2)	(Ni)	Squares	U+/-2s		Grain Age (Ma) Age	--95% CI--	
1	5,28E+05	(27)	1,56E+06	(80)	80	18	4	61.0	37.8	94.9
2	1,41E+05	(9)	5,01E+05	(32)	100	6	2	51.3	21.3	108.2
3	6,71E+04	(3)	7,62E+06	(341)	70	89	10	1.7	0.3	4.7
4	6,71E+04	(3)	8,20E+06	(367)	70	96	10	1.6	0.3	4.4
5	3,72E+05	(19)	1,72E+06	(88)	80	20	4	39.2	22.4	64.4
6	7,44E+05	(29)	2,31E+06	(90)	61	27	6	58.3	36.8	88.9
7	8,76E+05	(56)	2,33E+06	(149)	100	27	5	67.8	48.9	92.5
8	1,41E+05	(9)	3,60E+05	(23)	100	4	2	71.2	28.8	157.0
9	2,91E+05	(16)	3,02E+06	(166)	86	35	6	17.6	9.7	29.1
10	1,17E+06	(45)	4,67E+06	(179)	60	55	8	45.5	31.9	63.1
11	2,19E+05	(14)	4,85E+05	(31)	100	6	2	81.7	40.0	156.4
12	2,66E+05	(17)	2,22E+06	(142)	100	26	4	21.8	12.3	35.8
13	6,10E+05	(39)	2,66E+06	(170)	100	31	5	41.5	28.4	58.9
14	3,84E+05	(14)	9,33E+05	(34)	57	11	4	74.6	36.8	141.0
15	1,25E+05	(8)	1,25E+06	(80)	100	15	3	18.4	7.5	37.3
16	3,13E+05	(10)	9,08E+05	(29)	50	11	4	62.8	27.1	130.4
17	4,76E+05	(7)	1,46E+07	(215)	23	171	24	6.0	2.3	12.3
18	2,97E+05	(19)	8,61E+05	(55)	100	10	3	62.6	34.9	106.2
19	2,97E+05	(19)	6,10E+05	(39)	100	7	2	87.9	47.9	154.5
20	2,01E+05	(10)	1,12E+06	(56)	78	13	4	32.7	14.7	63.6
POOLED	3,61E+05	(373)	2,29E+06	(2366)	1615	27	1	28.5	25.2	32.1

CHI^2 PROBABILITY (%): 0.0
>>> Beware: possible upward bias in Chi^2 probability due to low counts <<<

POOLED AGE W/ 68% CONF. INTERVAL(Ma): 28.5, 26.8 -- 30.3 (-1.7 +1.8)
95% CONF. INTERVAL(Ma): 25.2 -- 32.1 (-3.2 +3.7)

CENTRAL AGE W/ 68% CONF. INTERVAL(Ma): 39.9, 34.2 -- 46.6 (-5.7 +6.7)
95% CONF. INTERVAL(Ma): 29.5 -- 54.1 (-10.5 +14.2)
AGE DISPERSION (%): 63.0

FIT OPTION: Best-fit peaks using the binomial model of Galbraith and Green

INITIAL GUESS FOR MODEL PARAMETERS (number of peaks to fit = 3)

Peak #.	Peak Age	Theta	Fraction(%)	Count
1.	1.80	0.010	4.6	0.92
2.	28.50	0.136	5.1	1.02
3.	43.20	0.193	23.0	4.61

Total range for grain ages:	1,7 to 88,7 Ma
Number of active grains (Num. used for fit):	20
Number of removed grains:	0
Degrees of freedom for fit:	15
Average of the SE(Z)'s for the grains:	0,32
Estimated width of peaks in PD plot in Z units:	0,38

PARAMETERS FOR BEST-FIT PEAKS

* *Standard error for peak age includes group error*
* *Peak width is for PD plot assuming a kernel factor = 0.60*

#.	Peak Age(Ma)	68%CI	95%CI	W(Z)	Frac(%)	SE,%	Count
1.	2.5	-0,6 ...+0,8	-1,1 ...+1,9	0.57	14.9	8.0	3.0
2.	19.6	-3,2 ...+3,9	-5,8 ...+8,3	0.34	16.6	8.8	3.3
3.	54.8	-3,7 ...+4,0	-7,1 ...+8,1	0.28	68.5	10.8	13.7

Log-likelihood for best fit:	-70,184
Chi-squared value for best fit:	23,048
Reduced chi-squared value:	1,537
Probability for F test:	1%
Condition number for COVAR matrix:	18,93
Number of iterations:	7

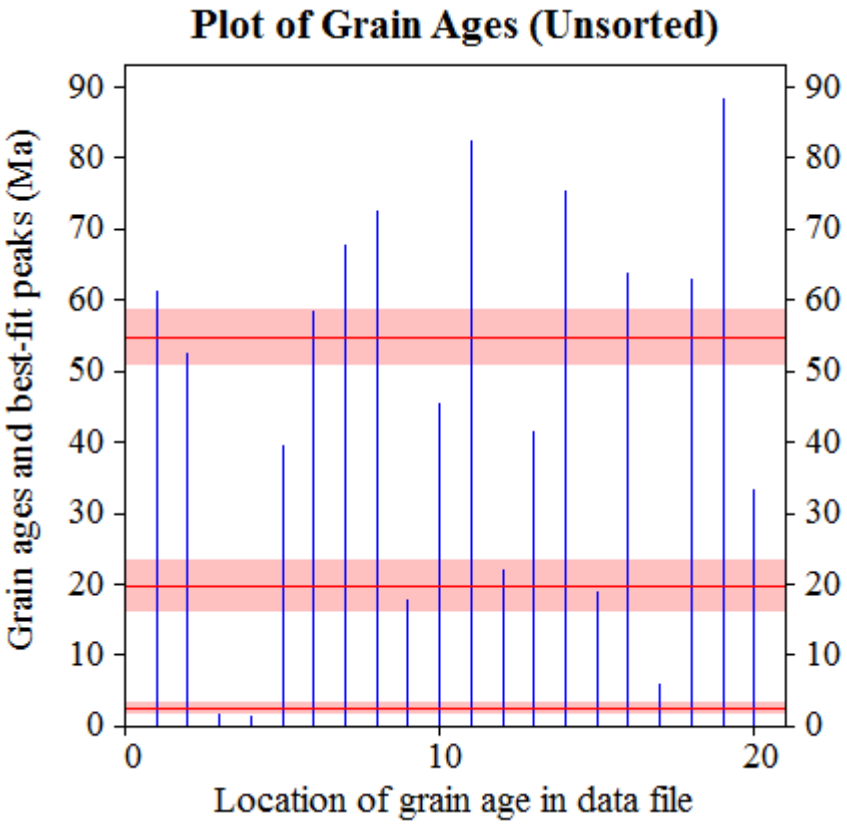
Plot of Grain Ages (Unsorted)
Grain ages and best-fit peaks (Ma)
0
10
20
30
40
50
60
70
80
90
0
10
20
Location of grain age in data file

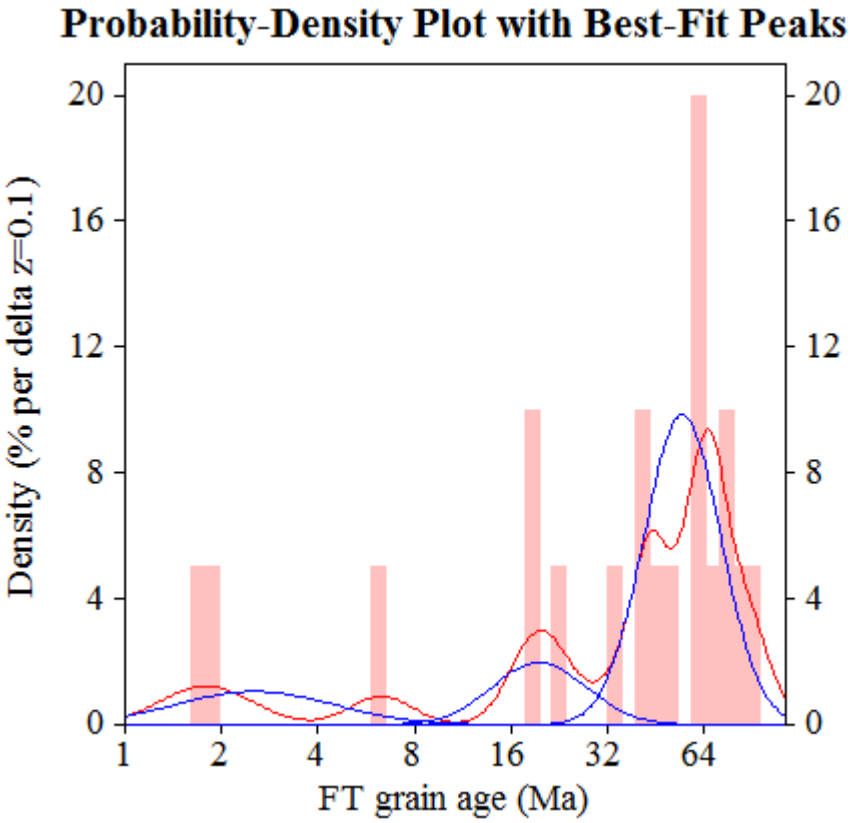
Probability-Density Plot with Best-Fit Peaks
Density (% per delta z=0.1)
0
4
8
12
16
20
1
2
4
8
16
32
64
FT grain age (Ma)

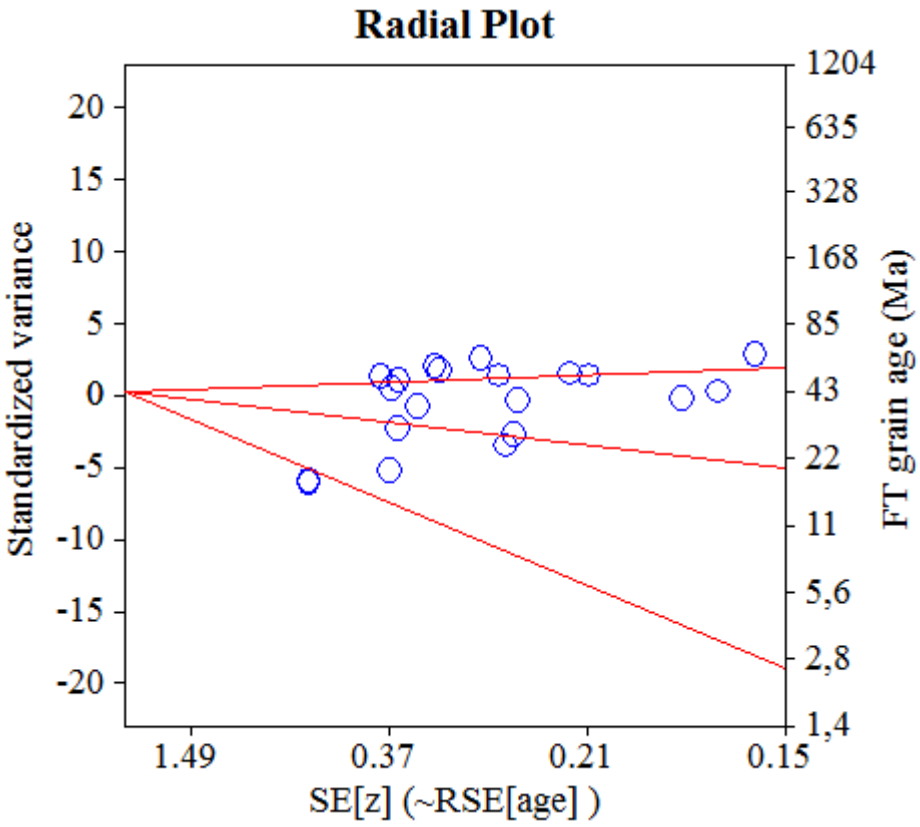
Radial Plot
Standardized variance
20
15
10
5
0
-5
-10
-15
-20
1204
635
328
168
85
43
22
11
5,6
2,8
1,4
FT grain age (Ma)
1.49
0.37
0.21
0.15
SE[z] (~RSE[age])

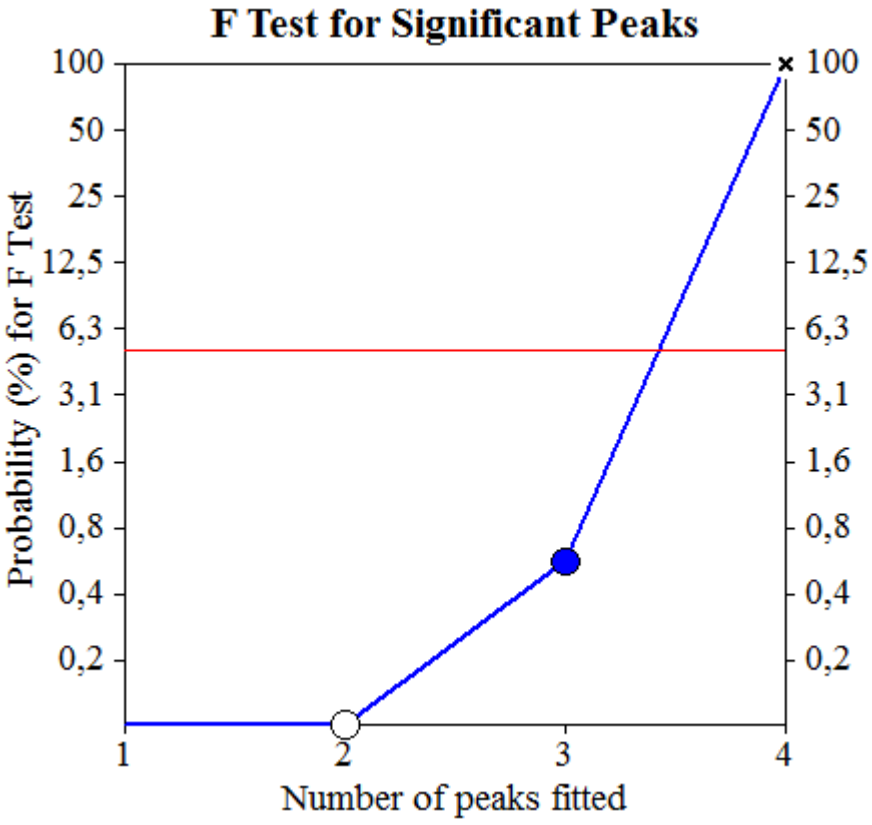
F Test for Significant Peaks
Probability (%) for F Test
100
50
25
12,5
6,3
3,1
1,6
0,8
0,4
0,2
1
2
3
4
Number of peaks fitted

Datafile: C:\BH2\Jairo\Echantillon-IRR082015\JG-P3-21\JG-P3-21Ap.fta
Title: JG-P3-21 Irr 8-2015-15

NEW PARAMETERS - ZETA METHOD

EFFECTIVE TRACK DENSITY FOR FLUENCE MONITOR (tracks/cm^2): 1,28E+06
RELATIVE ERROR (%): 1,12
EFFECTIVE URANIUM CONTENT OF MONITOR (ppm): 15,00
ZETA FACTOR AND STANDARD ERROR (yr cm^2): 282,02 6,88
SIZE OF COUNTER SQUARE (cm^2): 6,39E-07

GRAIN AGES IN ORIGINAL ORDER

Grain no.	RhoS (cm^-2)	(Ns)	RhoI (cm^-2)	(Ni)	Squares	U+/-2s		Grain Age (Ma) Age	--95% CI--	
1	1,25E+05	(8)	6,92E+06	(442)	100	81	8	3.3	1.4	6.5
2	3,44E+05	(22)	1,28E+07	(820)	100	150	11	4.9	3.0	7.4
3	7,82E+04	(4)	5,52E+06	(282)	80	65	8	2.7	0.7	6.6
4	4,69E+04	(3)	4,54E+06	(290)	100	53	6	2.0	0.4	5.5
5	1,10E+05	(7)	6,64E+06	(424)	100	78	8	3.0	1.2	6.2
6	3,23E+04	(2)	3,82E+06	(237)	97	45	6	1.6	0.2	5.6
7	1,96E+05	(10)	5,03E+06	(257)	80	59	7	7.1	3.3	13.1
8	7,82E+04	(5)	8,28E+06	(529)	100	97	9	1.8	0.6	4.0
9	1,88E+05	(12)	5,37E+06	(343)	100	63	7	6.4	3.2	11.2
10	2,15E+05	(11)	7,73E+06	(395)	80	91	9	5.1	2.5	9.1
11	7,82E+04	(5)	3,35E+06	(214)	100	39	5	4.3	1.4	10.0
12	5,87E+04	(3)	7,82E+06	(400)	80	92	9	1.4	0.3	4.0
13	3,13E+04	(2)	4,84E+06	(309)	100	57	7	1.3	0.1	4.3
14	7,82E+04	(5)	5,43E+06	(347)	100	64	7	2.7	0.8	6.1
15	7,82E+04	(3)	7,04E+06	(270)	60	83	10	2.1	0.4	5.9
16	1,56E+04	(1)	5,96E+06	(381)	100	70	7	0.5	0.0	2.7
17	7,82E+04	(5)	3,52E+06	(225)	100	41	6	4.1	1.3	9.5
18	3,13E+04	(2)	4,76E+06	(304)	100	56	7	1.3	0.1	4.3
POOLED	1,03E+05	(110)	6,04E+06	(6469)	1677	71	2	3.1	2.5	3.7

CHI^2 PROBABILITY (%): 0.4
>>> Beware: possible upward bias in Chi^2 probability due to low counts <<<

POOLED AGE W/ 68% CONF. INTERVAL(Ma): 3.1, 2.8 -- 3.4 (-0.3 +0.3)
95% CONF. INTERVAL(Ma): 2.5 -- 3.7 (-0.5 +0.7)

CENTRAL AGE W/ 68% CONF. INTERVAL(Ma): 3.0, 2.6 -- 3.5 (-0.4 +0.5)
95% CONF. INTERVAL(Ma): 2.3 -- 4.0 (-0.7 +1.0)
AGE DISPERSION (%): 42.5

FIT OPTION: Best-fit peaks using the binomial model of Galbraith and Green

INITIAL GUESS FOR MODEL PARAMETERS (number of peaks to fit = 2)

Peak #.	Peak Age	Theta	Fraction(%)	Count
1.	1.70	0.010	17.1	3.07
2.	3.10	0.017	21.0	3.78

Total range for grain ages:	0,7 to 7,3 Ma
Number of active grains (Num. used for fit):	18
Number of removed grains:	0
Degrees of freedom for fit:	15
Average of the SE(Z)'s for the grains:	0,49
Estimated width of peaks in PD plot in Z units:	0,57

PARAMETERS FOR BEST-FIT PEAKS

* *Standard error for peak age includes group error*
* *Peak width is for PD plot assuming a kernel factor = 0.60*

#.	Peak Age(Ma)	68%CI	95%CI	W(Z)	Frac(%)	SE,%	Count
1.	1.9	-0,4 ...+0,5	-0,7 ...+1,1	0.62	60.8	19.8	11.0
2.	4.7	-0,8 ...+0,9	-1,4 ...+2,0	0.37	39.2	19.8	7.0

Log-likelihood for best fit:	-44,878
Chi-squared value for best fit:	16,861
Reduced chi-squared value:	1,124
Probability for F test:	0%
Condition number for COVAR matrix:	5,61
Number of iterations:	18

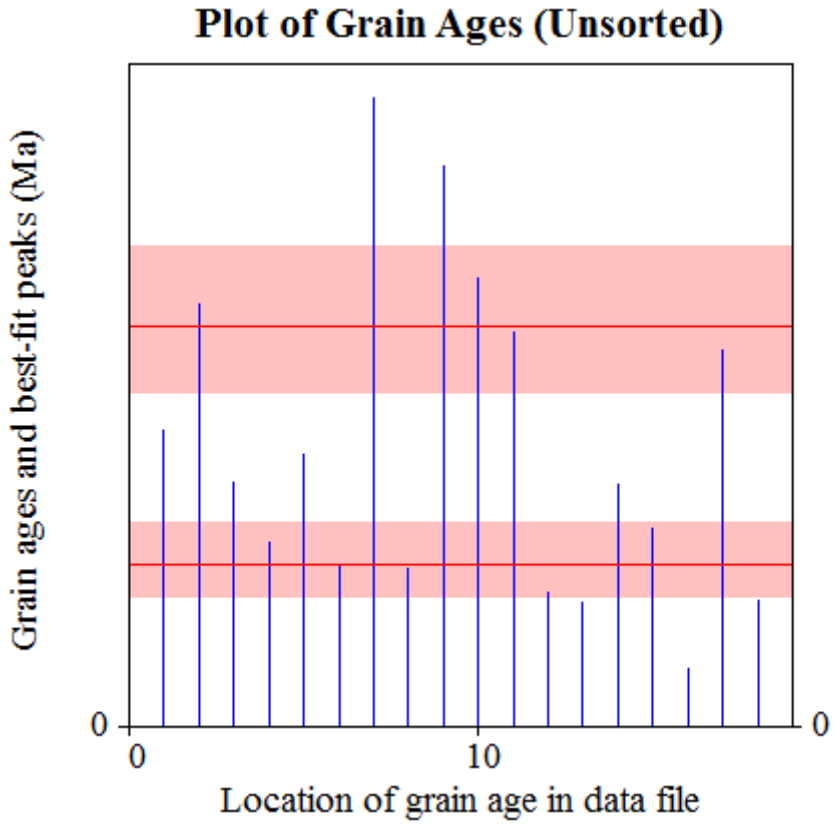
Plot of Grain Ages (Unsorted)
Grain ages and best-fit peaks (Ma)
0
0
10
0
Location of grain age in data file

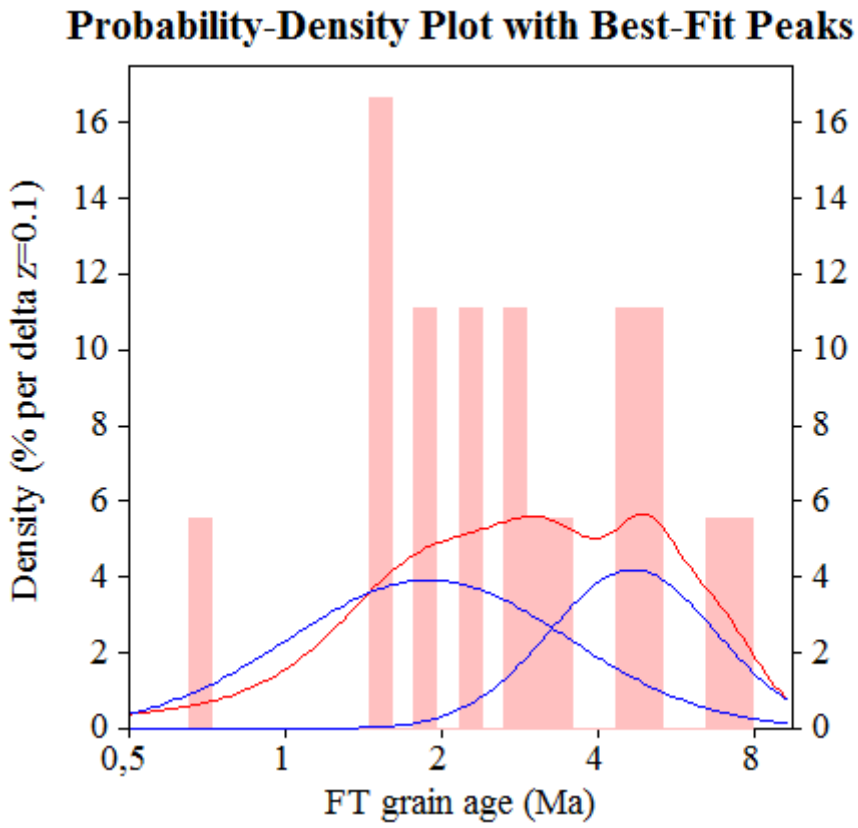
Probability-Density Plot with Best-Fit Peaks
Density (% per delta z=0.1)
16
14
12
10
8
6
4
2
0
0,5
1
2
4
8
FT grain age (Ma)

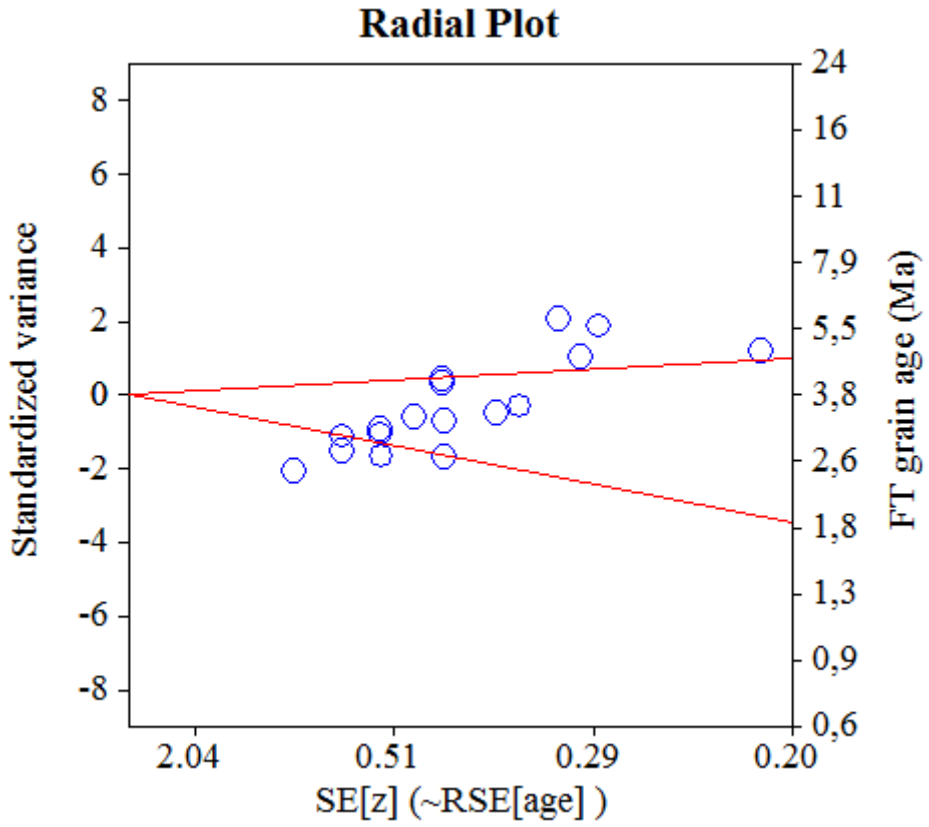
Radial Plot
Standardized variance
8
6
4
2
0
-2
-4
-6
-8
24
16
11
7,9
5,5
3,8
2,6
1,8
1,3
0,9
0,6
FT grain age (Ma)
2.04
0.51
0.29
0.20
SE[z] (~RSE[age])

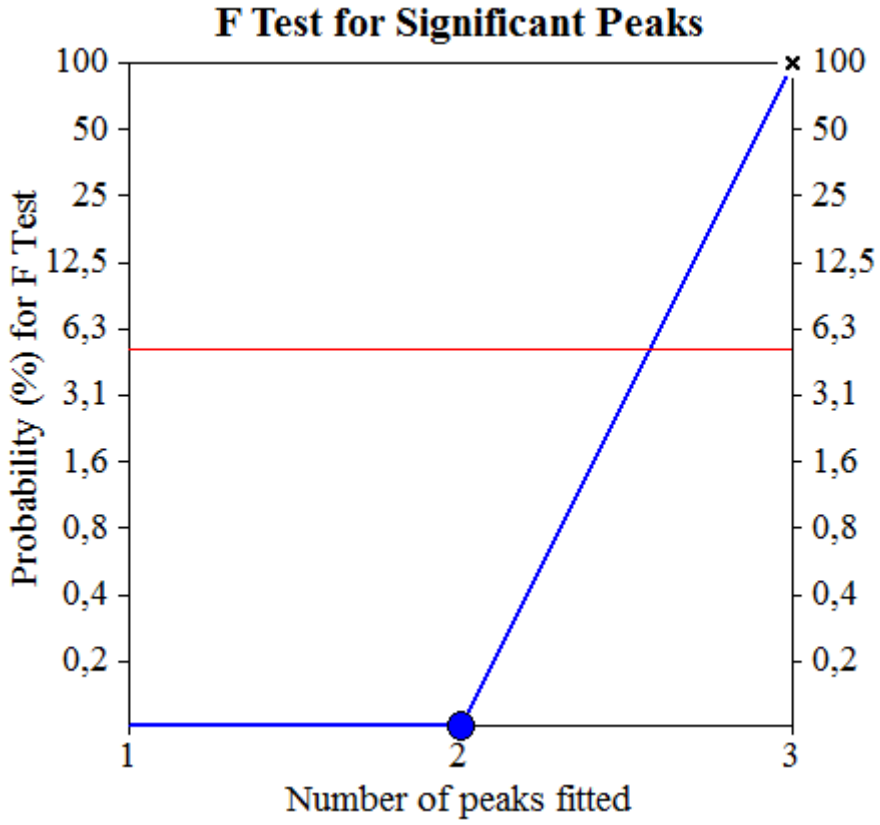
F Test for Significant Peaks
Probability (%) for F Test
100
50
25
12,5
6,3
3,1
1,6
0,8
0,4
0,2
1
2
3
Number of peaks fitted

Datafile: C:\BH2\Jairo\Echantillon-IRR-10-2015\JG-P2-01Zr\JG-P2-01-Zr.ftz
Title: Sample No. JG P2 01 Irr 10-2015-32

NEW PARAMETERS - ZETA METHOD

EFFECTIVE TRACK DENSITY FOR FLUENCE MONITOR (tracks/cm^2): 3,82E+05
RELATIVE ERROR (%): 1,12
EFFECTIVE URANIUM CONTENT OF MONITOR (ppm): 50,00
ZETA FACTOR AND STANDARD ERROR (yr cm^2): 137,14 1,57
SIZE OF COUNTER SQUARE (cm^2): 8,30E-07

GRAIN AGES IN ORIGINAL ORDER

Grain no.	RhoS (cm^-2)	(Ns)	RhoI (cm^-2)	(Ni)	Squares	U+/-2s	Grain Age (Ma) Age	--95% CI--	
1	2,15E+06	(57)	1,32E+06	(35)	32	172 58	42.5	27.5	66.7
2	3,13E+06	(52)	8,43E+05	(14)	20	110 58	95.8	52.9	187.6
3	6,33E+06	(63)	1,61E+06	(16)	12	210 104	101.6	58.6	188.8
4	3,06E+06	(61)	1,96E+06	(39)	24	256 82	40.8	26.9	62.7
5	8,43E+06	(84)	1,10E+06	(11)	12	144 85	194.7	105.4	403.6
6	4,65E+06	(54)	1,20E+06	(14)	14	158 83	99.5	55.1	194.2
7	6,11E+06	(71)	1,12E+06	(13)	14	146 80	140.2	78.1	276.1
8	3,44E+06	(80)	2,24E+06	(52)	28	293 81	40.2	28.0	58.1
9	8,96E+06	(305)	1,06E+06	(36)	41	138 46	217.5	154.9	315.5
10	5,42E+06	(108)	2,46E+06	(49)	24	322 92	57.4	40.7	82.3
11	6,76E+06	(157)	3,74E+06	(87)	28	490 105	46.9	36.1	60.9
12	5,49E+06	(114)	2,27E+06	(47)	25	296 86	63.1	44.7	90.8
13	7,44E+06	(105)	9,92E+05	(14)	17	130 68	191.7	111.1	361.8
14	2,01E+06	(20)	4,02E+05	(4)	12	53 50	125.8	43.7	507.0
15	4,92E+06	(49)	8,03E+05	(8)	12	105 72	156.0	74.9	381.2
16	6,27E+06	(52)	1,08E+06	(9)	10	142 92	147.5	73.5	340.6
17	7,95E+06	(99)	1,77E+06	(22)	15	231 98	116.2	73.3	193.9
18	5,34E+06	(124)	1,68E+06	(39)	28	219 70	82.6	57.4	121.7
19	9,56E+06	(127)	1,05E+06	(14)	16	138 72	231.2	135.1	432.7
20	3,29E+06	(41)	7,23E+05	(9)	15	95 61	116.7	56.9	273.7
21	8,23E+06	(82)	1,00E+06	(10)	12	131 81	208.5	110.2	449.1
22	9,92E+06	(107)	2,22E+06	(24)	13	291 118	115.2	74.1	187.7
23	5,42E+06	(180)	1,39E+06	(46)	40	181 53	101.5	73.4	143.6
24	6,83E+06	(68)	1,10E+06	(11)	12	144 85	158.1	84.5	331.3
POOLED	5,72E+06	(2260)	1,58E+06	(623)	476	206 17	94.3	85.9	103.6

CHI^2 PROBABILITY (%): 0.0

POOLED AGE W/ 68% CONF. INTERVAL(Ma): 94.3, 89.9 -- 98.9 (-4.4 +4.6)
95% CONF. INTERVAL(Ma): 85.9 -- 103.6 (-8.4 +9.2)

CENTRAL AGE W/ 68% CONF. INTERVAL(Ma): 96.8, 86.1 -- 108.9 (-10.8 +12.1)
95% CONF. INTERVAL(Ma): 76.9 -- 122.0 (-20.0 +25.1)
AGE DISPERSION (%): 52.1

FIT OPTION: Best-fit peaks using the binomial model of Galbraith and Green

INITIAL GUESS FOR MODEL PARAMETERS (number of peaks to fit = 2)

Peak #.	Peak Age	Theta	Fraction(%)	Count
1.	60.40	0.698	11.7	2.80
2.	94.30	0.784	26.0	6.25

Total range for grain ages: 40,1 to 226,5 Ma
Number of active grains (Num. used for fit): 24
Number of removed grains: 0
Degrees of freedom for fit: 21
Average of the SE(Z)'s for the grains: 0,28
Estimated width of peaks in PD plot in Z units: 0,32

PARAMETERS FOR BEST-FIT PEAKS

* *Standard error for peak age includes group error*
* *Peak width is for PD plot assuming a kernel factor = 0.60*

#.	Peak Age(Ma)	68%CI	95%CI	W(Z)	Frac(%)	SE,%	Count
1.	50.8	-4,6 ...+5,1	-8,6 ...+10,4	0.20	27.5	10.0	6.6
2.	142.2	-10,6 ...+11,5	-20,1 ...+23,4	0.31	72.5	10.0	17.4

Log-likelihood for best fit: -87,369
Chi-squared value for best fit: 25,319
Reduced chi-squared value: 1,206
Probability for F test: 0%
Condition number for COVAR matrix: 3,22
Number of iterations: 10

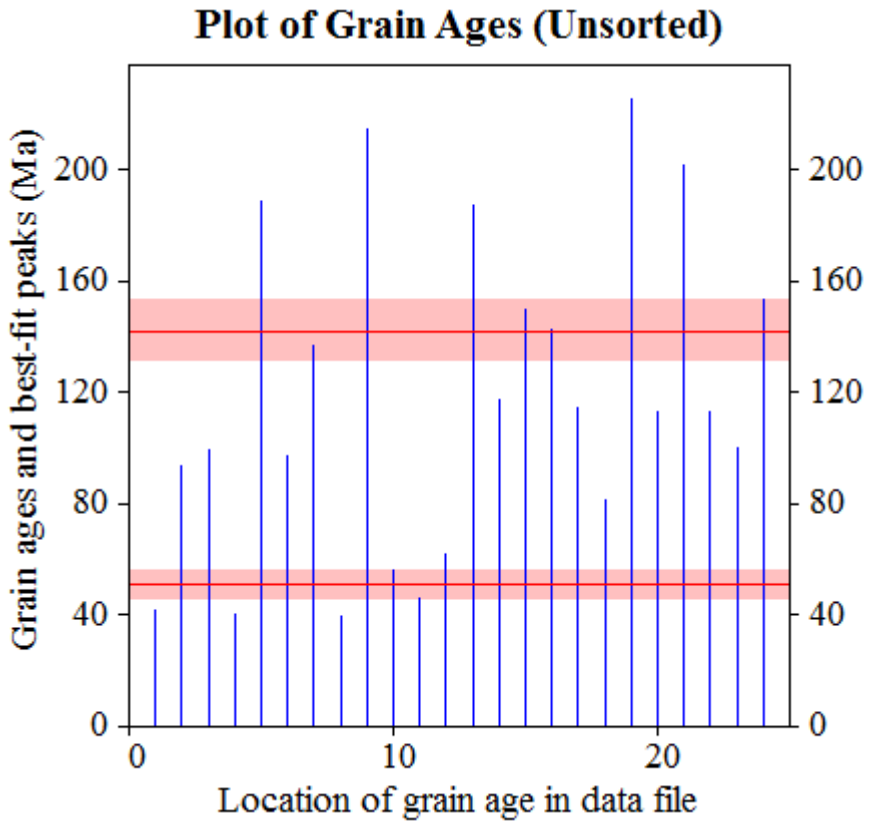
Plot of Grain Ages (Unsorted)
Grain ages and best-fit peaks (Ma)
0
40
80
120
160
200
0
10
20
Location of grain age in data file

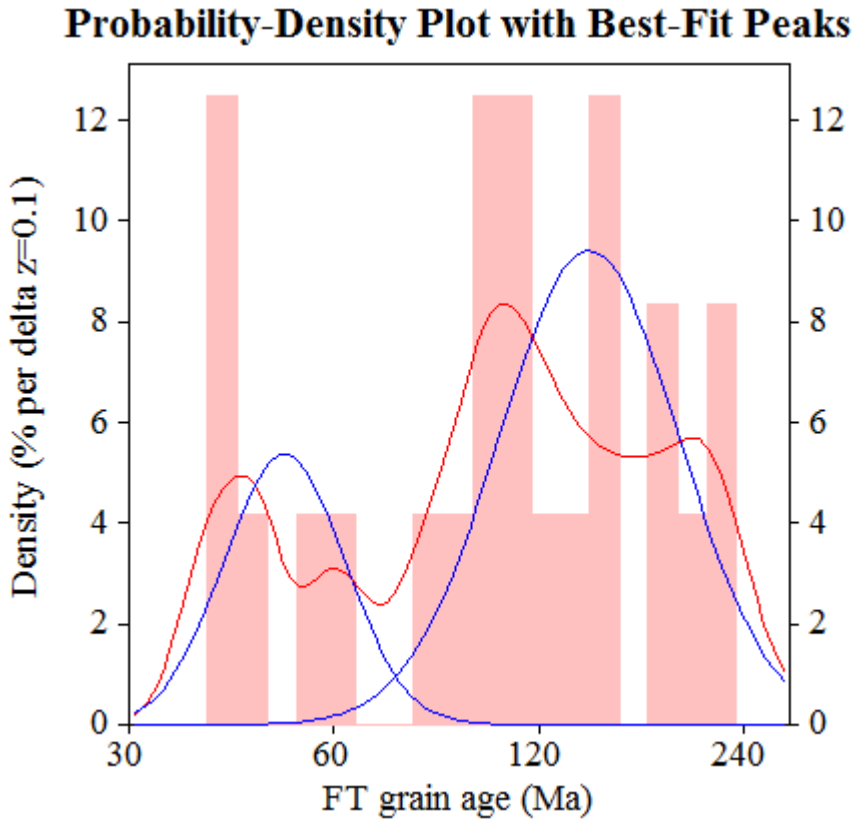
Probability-Density Plot with Best-Fit Peaks
Density (% per delta z=0.1)
0
2
4
6
8
10
12
30
60
120
240
FT grain age (Ma)

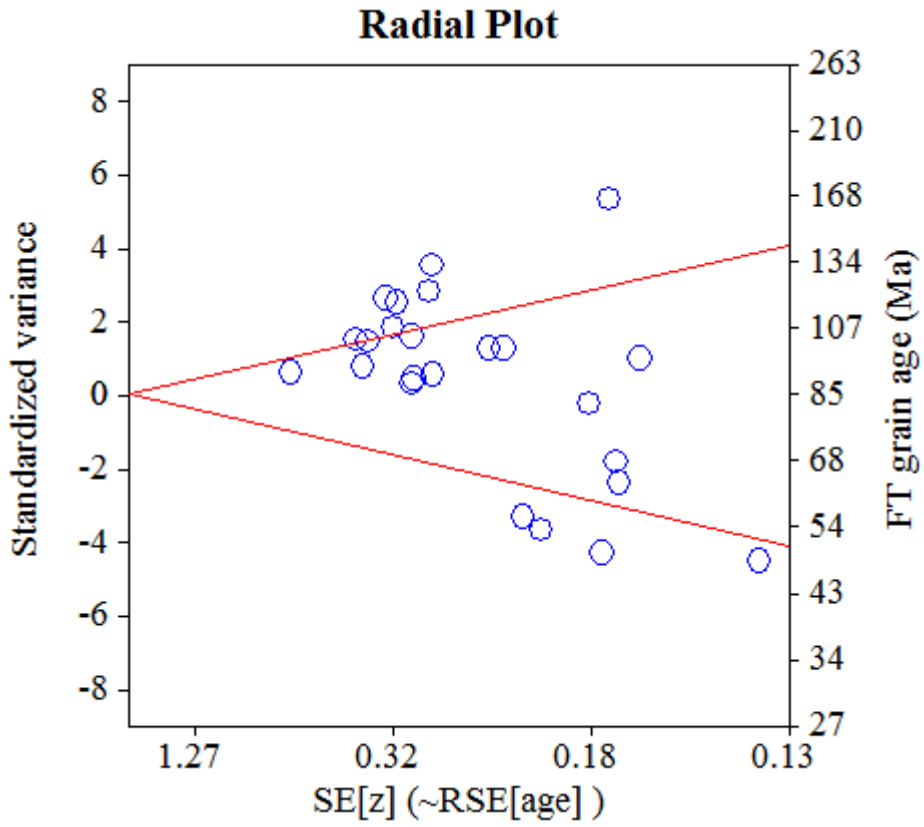
Radial Plot
Standardized variance
8
6
4
2
0
-2
-4
-6
-8
263
210
168
134
107
85
68
54
43
34
27
FT grain age (Ma)
1.27
0.32
0.18
0.13
SE[z] (~RSE[age])

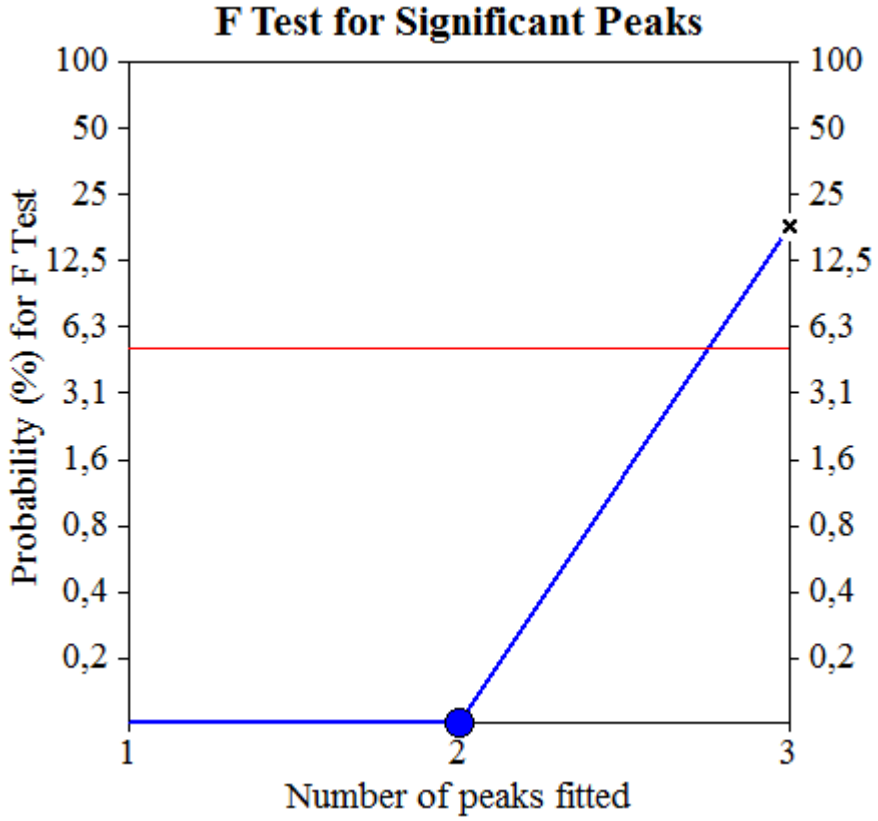
F Test for Significant Peaks
Probability (%) for F Test
100
50
25
12,5
6,3
3,1
1,6
0,8
0,4
0,2
1
2
3
Number of peaks fitted

Merged dataset:
C:\BH2\Jairo\Samples-IRR-6-2015\JG-P1-07\JG-P1-07a.ftz
C:\BH2\Jairo\Samples-IRR-6-2015\JG-P1-07\JG-P1-07.ftz

NEW PARAMETERS - ZETA METHOD

EFFECTIVE TRACK DENSITY FOR FLUENCE MONITOR (tracks/cm^2): 2,74E+05
RELATIVE ERROR (%): 1,18
EFFECTIVE URANIUM CONTENT OF MONITOR (ppm): 50,00
ZETA FACTOR AND STANDARD ERROR (yr cm^2): 137,95 4,04
SIZE OF COUNTER SQUARE (cm^2): 8,30E-07

GRAIN AGES IN ORIGINAL ORDER

Grain no.	RhoS (cm^-2)	(Ns)	RhoI (cm^-2)	(Ni)	Squares	U+/-2s	Grain Age (Ma) Age	--95% CI--	
1	6,87E+06	(114)	1,08E+06	(18)	20	198 92	117.6	71.9	205.8
2	7,35E+06	(61)	6,02E+05	(5)	10	110 94	220.0	92.8	696.1
3	6,73E+06	(67)	5,02E+05	(5)	12	92 78	241.2	102.4	758.5
4	1,41E+07	(70)	2,01E+06	(10)	6	367 226	129.1	67.4	281.6
5	5,30E+06	(44)	8,43E+05	(7)	10	154 113	115.4	52.8	305.1
6	4,82E+06	(36)	8,03E+05	(6)	9	147 115	109.9	47.1	321.0
7	6,75E+06	(84)	1,04E+06	(13)	15	191 104	119.6	67.2	234.4
8	6,88E+06	(80)	9,47E+05	(11)	14	173 102	134.2	72.3	280.1
9	6,51E+06	(54)	8,43E+05	(7)	10	154 113	141.2	65.7	368.9
10	4,57E+06	(91)	7,53E+05	(15)	24	138 70	112.5	65.6	209.7
11	6,51E+06	(54)	9,64E+05	(8)	10	176 121	124.1	60.0	303.1
12	5,72E+06	(76)	9,04E+05	(12)	16	165 93	117.2	64.3	237.3
13	8,73E+06	(87)	1,71E+06	(17)	12	312 149	95.2	56.7	171.2
14	9,04E+06	(135)	1,20E+06	(18)	18	220 102	139.0	85.7	241.8
15	8,11E+06	(101)	1,12E+06	(14)	15	205 108	133.5	77.1	253.2
16	6,35E+06	(58)	8,76E+05	(8)	11	160 110	133.2	64.7	323.9
17	4,58E+06	(76)	7,23E+05	(12)	20	132 75	117.2	64.3	237.3
18	8,73E+06	(116)	1,13E+06	(15)	16	206 105	143.1	84.4	264.0
19	6,18E+06	(77)	8,03E+05	(10)	15	147 91	141.8	74.5	307.9
20	2,11E+06	(35)	3,01E+05	(5)	20	55 47	127.4	51.4	418.5
21	6,71E+06	(117)	5,16E+05	(9)	21	94 61	237.1	123.7	528.3
22	5,12E+06	(85)	7,23E+05	(12)	20	132 75	130.9	72.3	263.7
23	9,00E+06	(112)	1,20E+06	(15)	15	220 112	138.2	81.4	255.4
24	8,03E+06	(60)	1,20E+06	(9)	9	220 143	122.8	61.8	282.5
25	6,57E+06	(109)	1,39E+06	(23)	20	253 105	88.4	56.4	145.5
26	6,21E+06	(98)	1,08E+06	(17)	19	197 94	107.1	64.3	191.7
27	9,56E+06	(119)	1,12E+06	(14)	15	205 108	157.0	91.3	295.8
28	1,33E+07	(88)	1,66E+06	(11)	8	303 179	147.4	79.9	306.4
29	9,29E+06	(108)	1,20E+06	(14)	14	220 116	142.6	82.6	269.8
30	6,80E+06	(79)	9,47E+05	(11)	14	173 102	132.5	71.4	276.8
31	1,26E+07	(125)	1,71E+06	(17)	12	312 149	136.3	82.8	241.5
32	9,17E+06	(137)	1,47E+06	(22)	18	269 114	115.8	74.1	191.1
33	7,23E+06	(108)	1,27E+06	(19)	18	232 105	105.7	65.2	182.7
34	1,20E+07	(100)	1,69E+06	(14)	10	308 162	132.2	76.3	250.8
35	9,84E+06	(98)	1,41E+06	(14)	12	257 135	129.6	74.7	246.1
36	9,56E+06	(119)	1,04E+06	(13)	15	191 104	168.7	96.5	326.0
37	1,08E+07	(144)	1,28E+06	(17)	16	234 112	156.7	95.7	276.4
38	8,43E+06	(112)	9,79E+05	(13)	16	179 97	158.9	90.7	307.8
39	1,05E+07	(87)	1,45E+06	(12)	10	264 149	133.9	74.1	269.6
40	5,92E+06	(59)	1,61E+06	(16)	12	293 145	68.8	39.4	128.4
41	1,02E+07	(136)	9,79E+05	(13)	16	179 97	192.4	110.7	370.0
42	8,01E+06	(133)	1,27E+06	(21)	20	231 100	117.7	74.7	196.7
43	1,39E+07	(162)	1,72E+06	(20)	14	314 139	150.1	95.1	252.3

Merged dataset:
C:\BH2\Jairo\Samples-IRR-6-2015\JG-P1-07\JG-P1-07a.ftz
C:\BH2\Jairo\Samples-IRR-6-2015\JG-P1-07\JG-P1-07.ftz

NEW PARAMETERS - ZETA METHOD

EFFECTIVE TRACK DENSITY FOR FLUENCE MONITOR (tracks/cm^2): 2,74E+05
RELATIVE ERROR (%): 1,17
EFFECTIVE URANIUM CONTENT OF MONITOR (ppm): 50,00
ZETA FACTOR AND STANDARD ERROR (yr cm^2): 137,95 4,04
SIZE OF COUNTER SQUARE (cm^2): 8,30E-07

Grain no.	RhoS (cm^-2)	(Ns)	RhoI (cm^-2)	(Ni)	Squares	U+/-2s	Grain Age (Ma) Age	--95% CI--	
44	1,36E+07	(90)	2,86E+06	(19)	8	522 237	88.3	53.9	153.8
45	1,22E+07	(202)	3,55E+06	(59)	20	649 169	64.3	48.0	87.5
46	6,16E+06	(92)	7,36E+05	(11)	18	134 79	154.2	83.8	319.7
47	1,11E+07	(222)	3,51E+06	(70)	24	641 153	59.3	45.1	77.9
48	1,49E+07	(223)	2,14E+06	(32)	18	391 137	129.8	89.9	194.4
49	1,34E+07	(200)	2,01E+06	(30)	18	366 133	124.2	84.9	189.0
50	1,24E+07	(124)	3,51E+06	(35)	12	641 216	66.4	45.5	99.7
51	8,43E+06	(70)	1,08E+06	(9)	10	198 128	143.1	72.7	326.5
52	1,12E+07	(335)	1,81E+06	(54)	36	330 90	115.2	86.1	153.9
53	9,28E+06	(154)	1,69E+06	(28)	20	308 116	102.6	68.7	159.7
54	1,34E+07	(100)	1,34E+06	(10)	9	244 151	183.6	97.8	394.1
55	1,17E+07	(97)	2,05E+06	(17)	10	374 179	106.1	63.6	189.9
56	1,20E+07	(200)	3,37E+06	(56)	20	616 164	67.0	49.7	91.9
57	6,48E+06	(43)	2,26E+06	(15)	8	412 210	53.6	29.4	104.2
58	8,19E+06	(170)	3,23E+06	(67)	25	589 144	47.4	35.6	63.2
59	1,12E+07	(139)	1,93E+06	(24)	15	352 142	107.9	70.2	174.3
60	1,31E+07	(152)	1,89E+06	(22)	14	345 146	128.5	82.6	211.2
61	8,67E+06	(108)	1,04E+06	(13)	15	191 104	153.4	87.4	297.5
62	7,16E+06	(107)	1,41E+06	(21)	18	257 111	95.0	59.6	160.0
63	6,22E+06	(62)	9,04E+05	(9)	12	165 107	126.9	64.0	291.4
64	9,04E+06	(120)	1,58E+06	(21)	16	289 125	106.4	67.2	178.4
65	4,74E+06	(59)	1,45E+06	(18)	15	264 123	61.3	35.9	110.7
66	5,57E+06	(74)	1,43E+06	(19)	16	261 118	72.7	43.8	127.9
67	7,43E+06	(111)	1,00E+06	(15)	18	183 93	137.1	80.7	253.4
68	3,74E+06	(87)	1,51E+06	(35)	28	275 92	46.7	31.3	71.3
69	4,42E+06	(44)	8,03E+05	(8)	12	147 101	101.4	48.2	250.8
70	6,75E+06	(56)	7,23E+05	(6)	10	132 104	170.0	75.7	482.7
71	9,87E+06	(172)	1,26E+06	(22)	21	230 97	145.2	93.8	237.7
72	9,44E+06	(329)	1,03E+06	(36)	42	188 63	169.8	121.0	246.4
73	8,25E+06	(137)	1,20E+06	(20)	20	220 97	127.3	80.1	215.1
74	8,06E+06	(107)	1,66E+06	(22)	16	302 128	90.7	57.4	151.1
75	1,08E+07	(90)	2,05E+06	(17)	10	374 179	98.5	58.8	176.9
76	6,87E+06	(57)	9,64E+05	(8)	10	176 121	131.0	63.6	318.9
77	1,08E+07	(287)	1,66E+06	(44)	32	302 91	121.7	88.8	171.3
78	7,23E+06	(84)	1,20E+06	(14)	14	220 116	111.3	63.6	212.8
79	1,11E+07	(83)	2,01E+06	(15)	9	366 186	102.8	59.6	192.4
80	6,63E+06	(44)	1,51E+06	(10)	8	275 170	81.6	41.1	182.8
81	1,39E+07	(115)	1,69E+06	(14)	10	308 162	151.9	88.2	286.6
82	1,11E+07	(257)	1,38E+06	(32)	28	251 88	149.4	103.9	222.9
83	7,83E+06	(65)	2,77E+06	(23)	10	506 209	52.9	32.6	89.5
84	8,97E+06	(67)	1,74E+06	(13)	9	318 173	95.7	53.0	189.6
85	7,97E+06	(119)	1,67E+06	(25)	18	305 121	88.9	57.8	143.1
POOLED	8,58E+06	(9465)	1,45E+06	(1599)	1329	265 15	110.8	102.2	120.1

CHI^2 PROBABILITY (%): 0.0

POOLED AGE W/ 68% CONF. INTERVAL(Ma): 110.8, 106.3 -- 115.4 (-4.5 +4.7)
95% CONF. INTERVAL(Ma): 102.2 -- 120.1 (-8.6 +9.3)

CENTRAL AGE W/ 68% CONF. INTERVAL(Ma): 112.2, 106.5 -- 118.2 (-5.7 +6.0)
95% CONF. INTERVAL(Ma): 101.3 -- 124.3 (-10.9 +12.1)
AGE DISPERSION (%): 28.3

Merged dataset:
C:\BH2\Jairo\Samples-IRR-6-2015\JG-P1-07\JG-P1-07a.ftz
C:\BH2\Jairo\Samples-IRR-6-2015\JG-P1-07\JG-P1-07.ftz

FIT OPTION: Best-fit peaks using the binomial model of Galbraith and Green

INITIAL GUESS FOR MODEL PARAMETERS (number of peaks to fit = 2)

Peak #.	Peak Age	Theta	Fraction(%)	Count
1.	62.90	0.770	11.9	10.14
2.	110.70	0.855	44.8	38.05

Total range for grain ages: 46,4 to 229,4 Ma
Number of active grains (Num. used for fit): 85
Number of removed grains: 0
Degrees of freedom for fit: 82
Average of the SE(Z)'s for the grains: 0,29
Estimated width of peaks in PD plot in Z units: 0,33

PARAMETERS FOR BEST-FIT PEAKS

* *Standard error for peak age includes group error*
* *Peak width is for PD plot assuming a kernel factor = 0.60*

#.	Peak Age(Ma)	68%CI	95%CI	W(Z)	Frac(%)	SE,%	Count
1.	60.2	-4,2 ...+4,5	-7,9 ...+9,1	0.22	12.4	4.1	10.5
2.	127.6	-5,6 ...+5,8	-10,7 ...+11,7	0.31	87.6	4.1	74.5

Log-likelihood for best fit: -244,326
Chi-squared value for best fit: 75,113
Reduced chi-squared value: 0,916
Probability for F test: 0%
Condition number for COVAR matrix: 4,29
Number of iterations: 6

Merged dataset:
C:\BH2\Jairo\Samples-IRR-6-2015\JG-P1-07\JG-P1-07a.ftz
C:\BH2\Jairo\Samples-IRR-6-2015\JG-P1-07\JG-P1-07.ftz

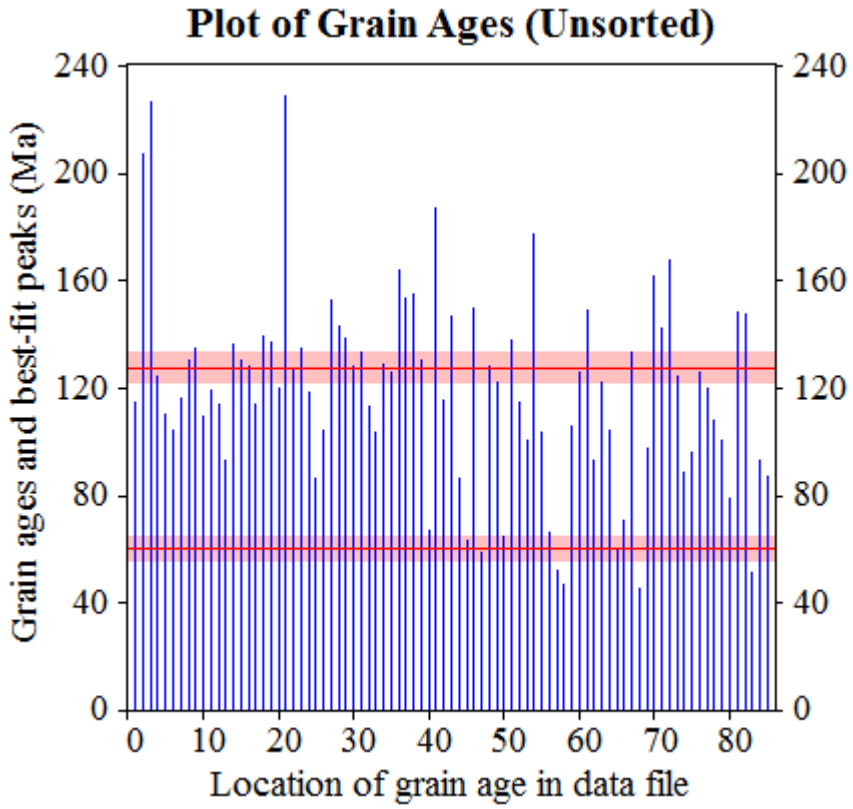

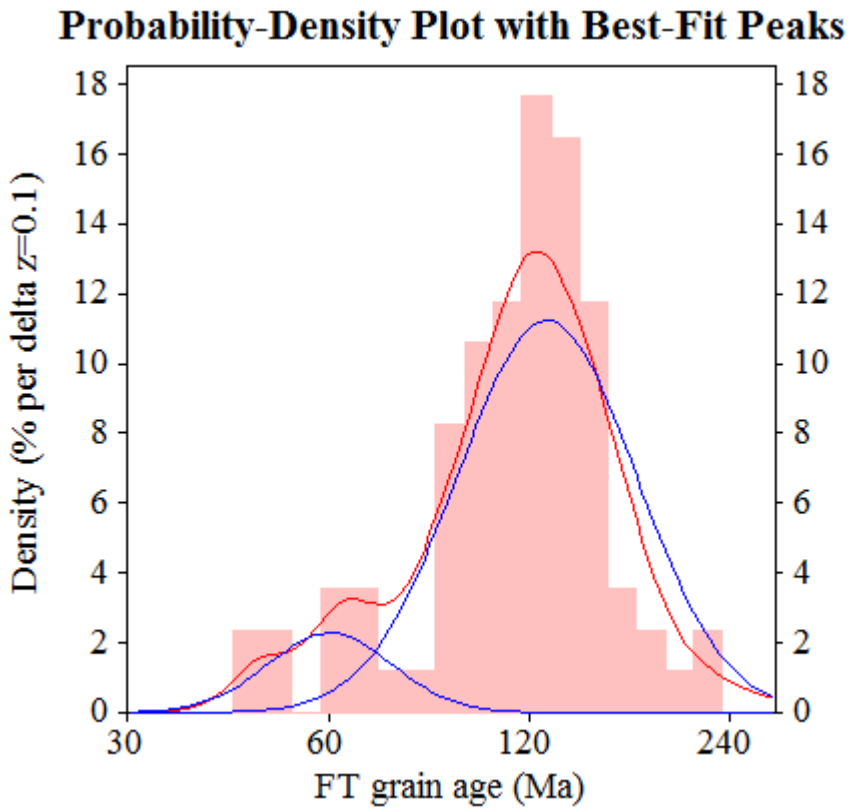

Merged dataset:
C:\BH2\Jairo\Samples-IRR-6-2015\JG-P1-07\JG-P1-07a.ftz
C:\BH2\Jairo\Samples-IRR-6-2015\JG-P1-07\JG-P1-07.ftz

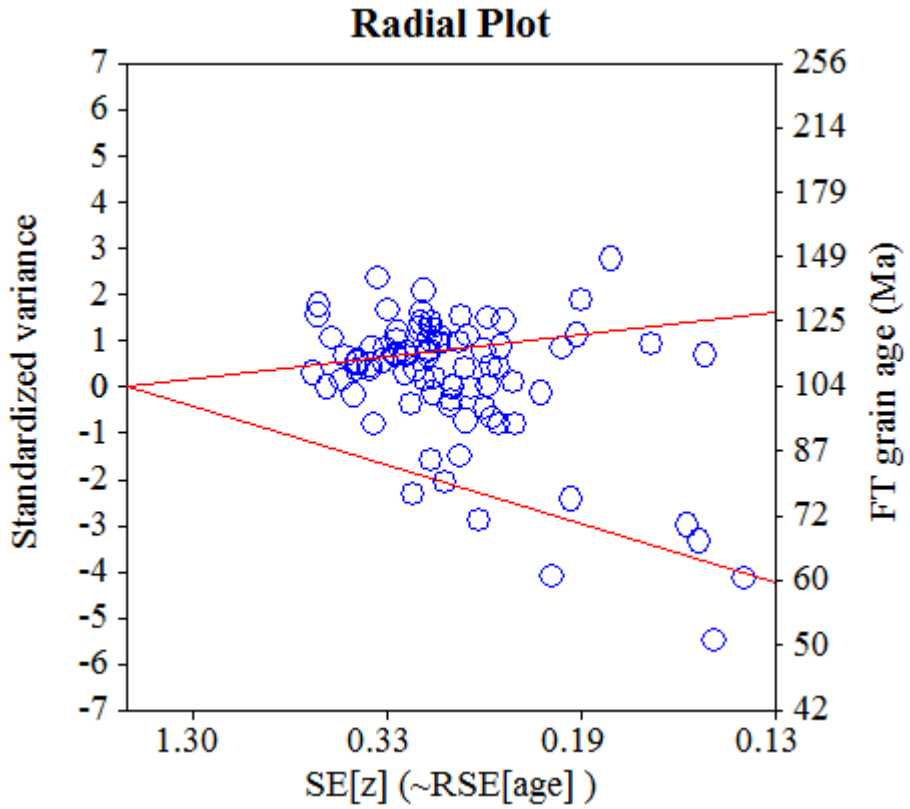

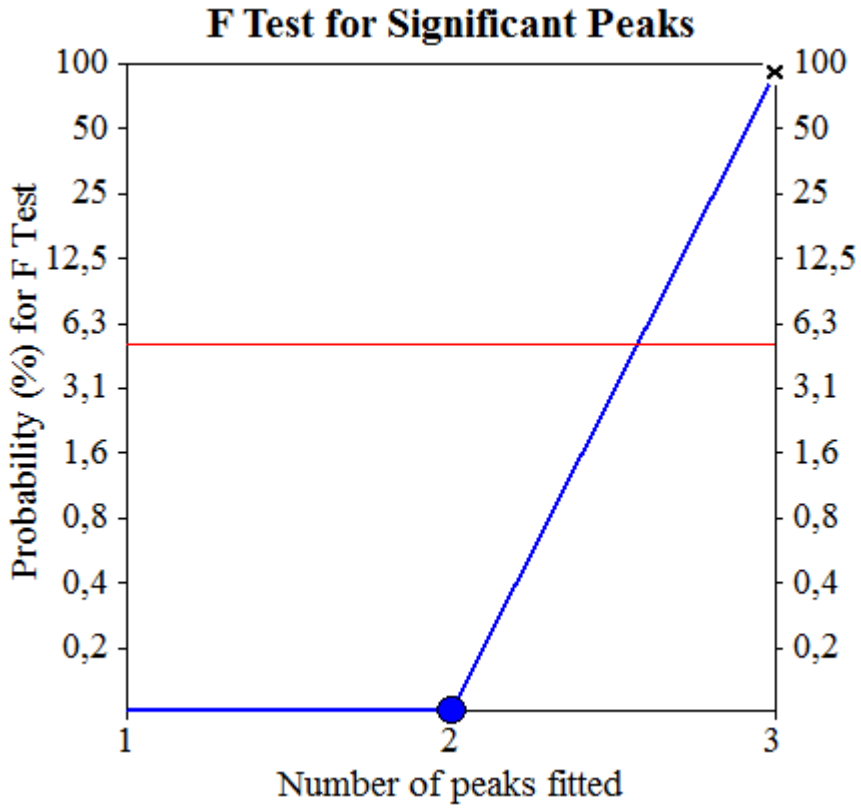

Merged dataset:
C:\BH2\Jairo\Samples-IRR-6-2015\JG-P2-05-3\JG-P2-05-3a.ftz
C:\BH2\Jairo\Samples-IRR-6-2015\JG-P2-05-3\JG-P2-05-3.ftz

NEW PARAMETERS - ZETA METHOD

EFFECTIVE TRACK DENSITY FOR FLUENCE MONITOR (tracks/cm^2): 2,73E+05
RELATIVE ERROR (%): 1,21
EFFECTIVE URANIUM CONTENT OF MONITOR (ppm): 50,00
ZETA FACTOR AND STANDARD ERROR (yr cm^2): 137,95 4,04
SIZE OF COUNTER SQUARE (cm^2): 8,30E-07

GRAIN AGES IN ORIGINAL ORDER

Grain no.	RhoS (cm^-2)	(Ns)	RhoI (cm^-2)	(Ni)	Squares	U+/-2s	Grain Age (Ma) Age	--95% CI--	
1	1,14E+07	(85)	1,34E+06	(10)	9	245 151	156.1	82.5	337.4
2	1,00E+07	(83)	1,57E+06	(13)	10	286 156	118.0	66.3	231.5
3	1,54E+07	(128)	2,05E+06	(17)	10	375 179	139.3	84.7	246.7
4	1,18E+07	(147)	1,37E+06	(17)	15	250 120	159.7	97.6	281.4
5	5,46E+06	(68)	8,03E+05	(10)	15	147 91	125.2	65.3	273.6
6	8,73E+06	(87)	2,51E+06	(25)	12	459 182	65.0	41.5	106.1
7	1,15E+07	(191)	1,87E+06	(31)	20	342 122	114.6	78.6	173.5
8	1,68E+07	(167)	1,61E+06	(16)	12	294 145	192.1	116.6	343.2
9	8,92E+06	(74)	1,20E+06	(10)	10	220 136	136.2	71.3	296.2
10	1,64E+07	(150)	2,63E+06	(24)	11	481 195	116.1	75.8	187.1
11	1,45E+07	(181)	1,53E+06	(19)	15	279 127	175.8	110.7	298.5
12	1,47E+07	(146)	1,71E+06	(17)	12	312 149	158.6	96.9	279.6
13	1,24E+07	(93)	2,01E+06	(15)	9	367 187	114.8	67.0	213.8
14	1,39E+07	(104)	2,68E+06	(20)	9	490 217	96.7	60.0	165.1
15	1,46E+07	(133)	1,75E+06	(16)	11	320 158	153.5	92.3	276.4
16	1,64E+07	(285)	1,66E+06	(29)	21	304 112	181.8	124.9	276.0
17	1,31E+07	(98)	1,87E+06	(14)	9	343 180	129.4	74.6	245.7
18	1,94E+07	(145)	2,95E+06	(22)	9	539 227	122.3	78.5	201.4
19	9,74E+06	(194)	1,15E+06	(23)	24	211 87	156.2	102.1	252.1
20	1,72E+07	(157)	1,64E+06	(15)	11	300 153	192.5	115.0	351.5
21	1,16E+07	(231)	1,51E+06	(30)	24	275 100	142.9	98.2	216.6
22	1,00E+07	(83)	1,45E+06	(12)	10	264 150	127.7	70.4	257.5
23	1,36E+07	(135)	2,11E+06	(21)	12	386 167	119.3	75.7	199.2
24	1,09E+07	(118)	1,30E+06	(14)	13	237 125	155.4	90.4	293.0
25	1,41E+07	(140)	2,31E+06	(23)	12	422 175	113.1	73.0	184.5
26	6,88E+06	(80)	1,29E+06	(15)	14	236 120	98.9	57.2	185.4
27	1,06E+07	(264)	1,45E+06	(36)	30	264 88	136.3	96.6	198.8
28	1,56E+07	(155)	2,31E+06	(23)	12	422 175	125.1	81.1	203.3
29	9,72E+06	(113)	1,72E+06	(20)	14	315 139	105.0	65.5	178.6
30	9,40E+06	(117)	1,12E+06	(14)	15	206 108	154.1	89.6	290.7
31	1,26E+07	(125)	1,81E+06	(18)	12	331 154	128.6	79.0	224.4
32	1,05E+07	(105)	1,91E+06	(19)	12	349 158	102.7	63.2	177.6
33	8,53E+06	(85)	1,51E+06	(15)	12	275 140	105.0	61.0	196.3
34	1,47E+07	(195)	1,73E+06	(23)	16	317 131	156.9	102.6	253.3
35	1,43E+07	(131)	1,20E+06	(11)	11	220 130	217.8	120.3	445.4
36	4,52E+06	(45)	1,41E+06	(14)	12	257 135	59.9	32.6	118.5
37	8,03E+06	(80)	2,01E+06	(20)	12	367 162	74.5	45.6	128.8
38	1,04E+07	(190)	1,53E+06	(28)	22	280 105	126.1	85.1	194.9
39	1,10E+07	(137)	1,04E+06	(13)	15	191 104	193.5	111.4	372.0
40	1,55E+07	(231)	2,01E+06	(30)	18	367 133	142.9	98.2	216.6

Merged dataset:
C:\BH2\Jairo\Samples-IRR-6-2015\JG-P2-05-3\JG-P2-05-3a.ftz
C:\BH2\Jairo\Samples-IRR-6-2015\JG-P2-05-3\JG-P2-05-3.ftz

NEW PARAMETERS - ZETA METHOD

EFFECTIVE TRACK DENSITY FOR FLUENCE MONITOR (tracks/cm^2): 2,74E+05
RELATIVE ERROR (%): 1,19
EFFECTIVE URANIUM CONTENT OF MONITOR (ppm): 50,00
ZETA FACTOR AND STANDARD ERROR (yr cm^2): 137,95 4,04
SIZE OF COUNTER SQUARE (cm^2): 8,30E-07

Grain no.	RhoS (cm^-2)	(Ns)	RhoI (cm^-2)	(Ni)	Squares	U+/-2s	Grain Age (Ma) Age	--95% CI--	
41	4,95E+06	(37)	5,35E+05	(4)	9	98 92	166.4	62.4	641.5
42	1,60E+07	(173)	1,76E+06	(19)	13	322 146	168.3	105.8	286.1
43	8,84E+06	(132)	1,47E+06	(22)	18	269 114	111.6	71.3	184.3
44	1,01E+07	(168)	1,45E+06	(24)	20	264 107	130.0	85.2	208.7
45	1,03E+07	(205)	1,41E+06	(28)	24	257 96	136.0	92.1	209.8
46	1,50E+07	(149)	9,04E+05	(9)	12	165 107	300.1	158.2	661.8
47	8,70E+06	(130)	1,20E+06	(18)	18	220 103	133.8	82.3	233.1
48	8,98E+06	(149)	1,14E+06	(19)	20	209 95	145.2	90.8	248.1
49	1,36E+07	(135)	1,71E+06	(17)	12	312 149	146.9	89.5	259.7
50	9,52E+06	(158)	1,51E+06	(25)	20	275 109	117.5	77.4	187.3
51	1,36E+07	(181)	1,66E+06	(22)	16	303 128	152.4	98.6	249.2
52	1,36E+07	(135)	1,31E+06	(13)	12	239 130	190.9	109.8	367.1
53	1,69E+07	(168)	1,20E+06	(12)	12	220 125	255.8	145.6	501.8
54	1,67E+07	(360)	1,34E+06	(29)	26	246 91	228.9	158.2	345.7
55	1,25E+07	(208)	2,11E+06	(35)	20	385 130	110.8	77.6	163.4
56	1,28E+07	(298)	1,16E+06	(27)	28	212 81	203.9	138.7	313.9
57	1,38E+07	(137)	1,71E+06	(17)	12	312 149	149.1	90.9	263.4
58	8,91E+06	(207)	9,90E+05	(23)	28	181 75	166.6	109.1	268.4
59	9,64E+06	(80)	1,57E+06	(13)	10	286 156	113.9	63.9	223.7
60	1,51E+07	(176)	1,98E+06	(23)	14	362 149	141.9	92.5	229.8
61	3,65E+06	(97)	1,02E+06	(27)	32	186 71	67.2	43.7	107.3
62	6,02E+06	(50)	4,82E+05	(4)	10	88 83	223.6	86.0	842.2
63	8,92E+06	(74)	8,43E+05	(7)	10	154 113	192.5	91.5	494.2
64	9,90E+06	(115)	2,41E+06	(28)	14	440 165	76.7	50.7	120.7
65	1,35E+07	(101)	8,03E+05	(6)	9	147 115	302.6	139.4	830.5
66	9,24E+06	(92)	7,03E+05	(7)	12	128 94	238.4	114.6	605.1
67	8,92E+06	(111)	8,84E+05	(11)	15	161 95	185.2	101.6	381.2
68	5,35E+06	(40)	9,37E+05	(7)	9	171 125	105.0	47.6	279.3
69	8,09E+06	(94)	6,02E+05	(7)	14	110 80	243.4	117.2	617.3
70	8,73E+06	(87)	1,20E+06	(12)	12	220 125	133.8	74.0	269.4
71	1,10E+07	(182)	1,33E+06	(22)	20	242 102	153.3	99.2	250.5
72	8,33E+06	(242)	1,14E+06	(33)	35	208 72	136.4	95.1	202.6
73	7,55E+06	(94)	1,61E+06	(20)	15	294 130	87.5	54.1	150.1
74	8,94E+06	(89)	1,41E+06	(14)	12	257 135	117.7	67.5	224.5
75	8,80E+06	(73)	1,20E+06	(10)	10	220 136	134.4	70.4	292.7
76	9,38E+06	(109)	1,72E+06	(20)	14	315 139	101.4	63.1	172.8
77	1,05E+07	(105)	1,41E+06	(14)	12	257 135	138.6	80.2	262.5
78	1,22E+07	(91)	1,61E+06	(12)	9	294 166	139.9	77.6	281.1
79	9,04E+06	(150)	1,33E+06	(22)	20	242 102	126.6	81.4	208.2
80	1,32E+07	(175)	1,88E+06	(25)	16	344 137	130.0	85.9	206.5
81	5,46E+06	(127)	2,37E+06	(55)	28	432 117	43.4	31.4	60.7
82	1,02E+07	(127)	1,45E+06	(18)	15	264 123	130.8	80.4	228.0
83	1,20E+07	(100)	1,69E+06	(14)	10	308 162	132.1	76.2	250.7
84	7,06E+06	(123)	9,75E+05	(17)	21	178 85	134.0	81.3	237.7
POOLED	1,09E+07	(11510)	1,49E+06	(1572)	1270	273 15	136.5	126.0	148.0

Merged dataset:
C:\BH2\Jairo\Samples-IRR-6-2015\JG-P2-05-3\JG-P2-05-3a.ftz
C:\BH2\Jairo\Samples-IRR-6-2015\JG-P2-05-3\JG-P2-05-3.ftz

```
CHI^2 PROBABILITY (%):  0.0

 POOLED AGE W/  68% CONF. INTERVAL(Ma):  136.5, 131.0 -- 142.3 ( -5.5  +5.7)
                95% CONF. INTERVAL(Ma):         126.0 -- 148.0 (-10.6 +11.5)

CENTRAL AGE W/  68% CONF. INTERVAL(Ma):  134.3, 127.8 -- 141.1 ( -6.5  +6.8)
                95% CONF. INTERVAL(Ma):         121.8 -- 147.9 (-12.4 +13.7)
                    AGE DISPERSION (%):   24.8
```

Merged dataset:
C:\BH2\Jairo\Samples-IRR-6-2015\JG-P2-05-3\JG-P2-05-3a.ftz
C:\BH2\Jairo\Samples-IRR-6-2015\JG-P2-05-3\JG-P2-05-3.ftz

FIT OPTION: Best-fit peaks using the binomial model of Galbraith and Green

INITIAL GUESS FOR MODEL PARAMETERS (number of peaks to fit = 2)

Peak #.	Peak Age	Theta	Fraction(%)	Count
1.	136.50	0.880	52.1	43.73
2.	290.30	0.940	4.2	3.57

Total range for grain ages: 43,2 to 290,3 Ma
Number of active grains (Num. used for fit): 84
Number of removed grains: 0
Degrees of freedom for fit: 81
Average of the SE(Z)'s for the grains: 0,27
Estimated width of peaks in PD plot in Z units: 0,32

PARAMETERS FOR BEST-FIT PEAKS

* *Standard error for peak age includes group error*
* *Peak width is for PD plot assuming a kernel factor = 0.60*

#.	Peak Age(Ma)	68%CI	95%CI	W(Z)	Frac(%)	SE,%	Count
1.	60.6	-6,7 ...+7,5	-12,4 ...+15,5	0.25	6.1	3.0	5.1
2.	144.5	-6,1 ...+6,3	-11,6 ...+12,6	0.29	93.9	3.0	78.9

Log-likelihood for best fit: -249,328
Chi-squared value for best fit: 77,067
Reduced chi-squared value: 0,951
Probability for F test: 0%
Condition number for COVAR matrix: 16,86
Number of iterations: 53

Merged dataset:
C:\BH2\Jairo\Samples-IRR-6-2015\JG-P2-05-3\JG-P2-05-3a.ftz
C:\BH2\Jairo\Samples-IRR-6-2015\JG-P2-05-3\JG-P2-05-3.ftz

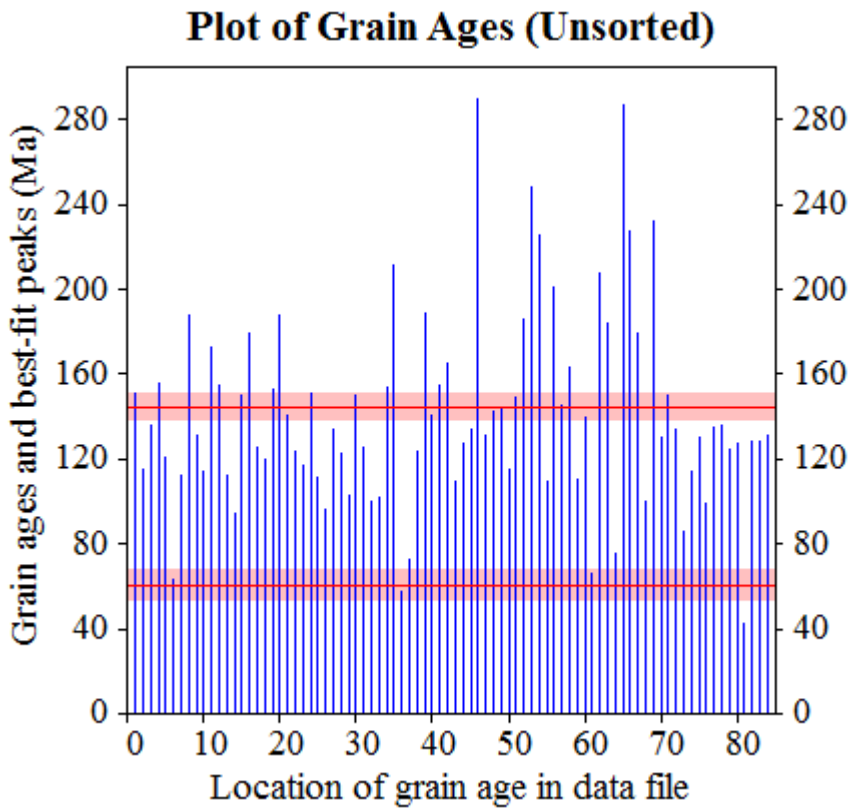

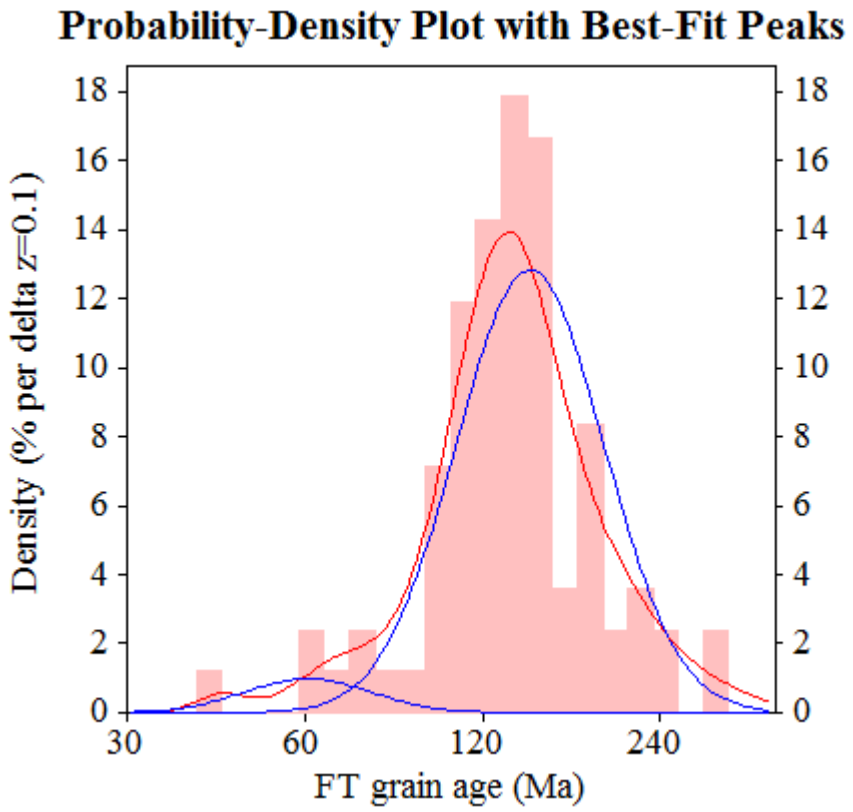

Merged dataset:
C:\BH2\Jairo\Samples-IRR-6-2015\JG-P2-05-3\JG-P2-05-3a.ftz
C:\BH2\Jairo\Samples-IRR-6-2015\JG-P2-05-3\JG-P2-05-3.ftz

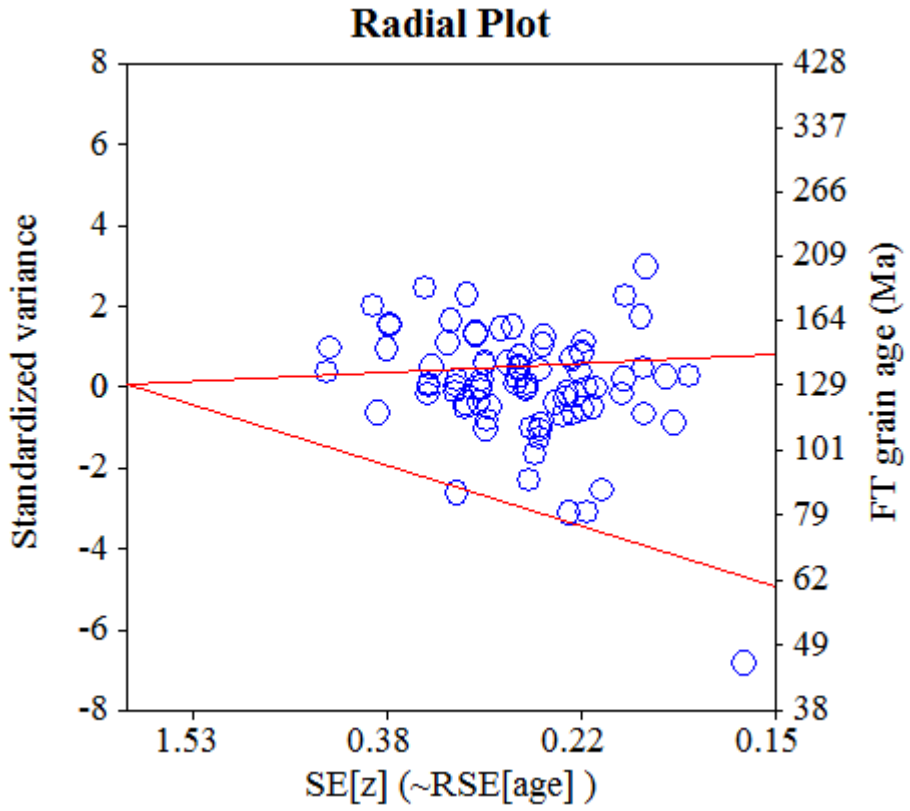

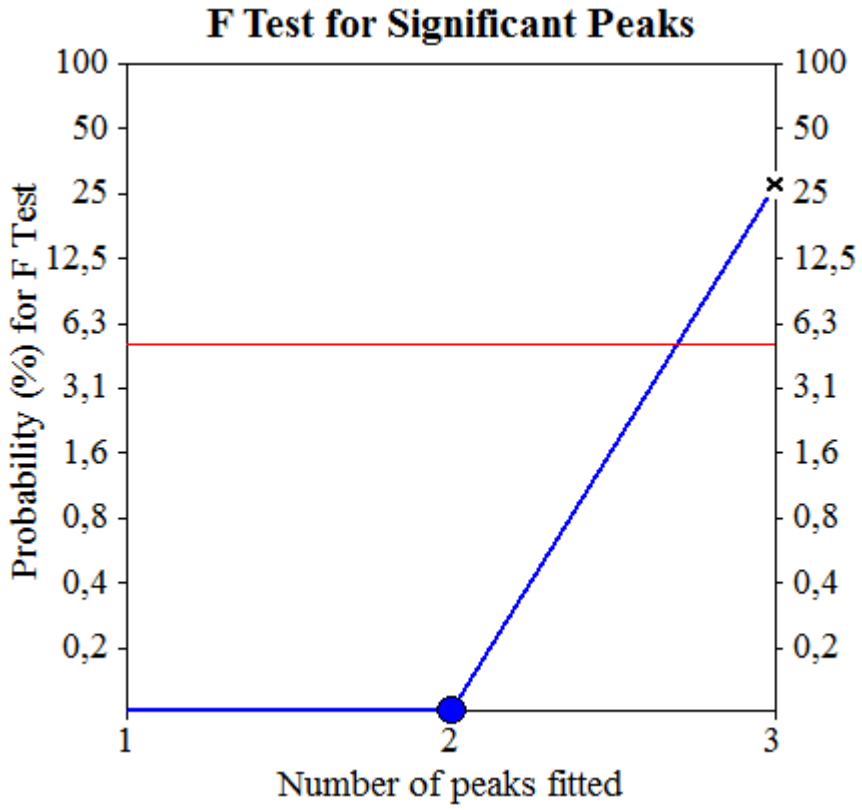

Datafile: C:\BH2\Jairo\Echantillon-IRR-10-2015\JG-P2-05-Zr\JG-P2-05-4-Zr.ftz
Title: Sample No. JG P2 05 Irr 10-2015-33

NEW PARAMETERS - ZETA METHOD

EFFECTIVE TRACK DENSITY FOR FLUENCE MONITOR (tracks/cm^2): 3,83E+05
RELATIVE ERROR (%): 1,12
EFFECTIVE URANIUM CONTENT OF MONITOR (ppm): 50,00
ZETA FACTOR AND STANDARD ERROR (yr cm^2): 137,14 1,57
SIZE OF COUNTER SQUARE (cm^2): 8,30E-07

GRAIN AGES IN ORIGINAL ORDER

Grain no.	RhoS (cm^-2)	(Ns)	RhoI (cm^-2)	(Ni)	Squares	U+/-2s	Grain Age (Ma) Age	--95% CI--	
1	4,79E+06	(143)	9,71E+05	(29)	36	127 47	127.6	85.7	197.3
2	9,84E+06	(98)	1,51E+06	(15)	12	197 100	167.7	98.3	310.6
3	7,65E+06	(254)	1,20E+06	(40)	40	157 50	164.0	117.9	234.7
4	4,75E+06	(197)	7,95E+05	(33)	50	104 36	154.2	107.0	230.0
5	8,59E+06	(214)	1,49E+06	(37)	30	194 64	149.5	105.8	217.9
6	4,32E+06	(251)	1,98E+06	(115)	70	259 48	56.8	45.5	70.9
7	4,57E+06	(167)	1,18E+06	(43)	44	154 47	100.9	72.1	144.5
8	3,40E+06	(158)	6,45E+05	(30)	56	84 31	136.2	92.4	208.4
9	3,35E+06	(139)	1,45E+06	(60)	50	189 49	60.4	44.4	83.3
10	8,33E+06	(83)	1,41E+06	(14)	12	184 97	152.3	87.1	290.5
11	7,13E+06	(355)	8,63E+05	(43)	60	113 34	212.4	155.6	298.0
12	8,07E+06	(268)	1,36E+06	(45)	40	177 53	154.0	112.6	216.0
13	3,96E+06	(263)	6,02E+05	(40)	80	79 25	169.7	122.1	242.7
14	6,96E+06	(289)	8,67E+05	(36)	50	113 38	206.5	146.9	300.0
15	7,29E+06	(121)	1,33E+06	(22)	20	173 73	141.9	90.4	234.7
16	8,06E+06	(107)	1,96E+06	(26)	16	256 100	106.6	69.4	170.7
17	8,43E+06	(112)	1,36E+06	(18)	16	177 82	160.1	98.0	279.6
18	5,59E+06	(195)	1,78E+06	(62)	42	232 59	81.4	61.2	108.2
19	5,24E+06	(100)	1,05E+06	(20)	23	137 61	129.1	80.1	220.3
20	1,03E+07	(256)	1,81E+06	(45)	30	236 70	147.2	107.4	206.7
21	8,39E+06	(209)	1,24E+06	(31)	30	163 58	173.8	119.8	261.9
22	3,88E+06	(103)	1,05E+06	(28)	32	138 52	95.4	62.7	150.7
23	8,47E+06	(422)	1,12E+06	(56)	60	147 39	193.2	146.6	254.2
24	2,86E+06	(190)	1,46E+06	(97)	80	191 39	51.0	39.9	65.1
25	6,08E+06	(116)	1,26E+06	(24)	23	164 66	125.0	80.7	202.9
26	7,26E+06	(422)	1,08E+06	(63)	70	142 36	172.1	132.4	223.6
27	7,23E+06	(144)	1,15E+06	(23)	24	151 62	161.3	104.4	262.3
28	3,04E+06	(101)	1,14E+06	(38)	40	150 48	69.2	47.4	103.4
29	7,37E+06	(318)	1,14E+06	(49)	52	148 42	167.7	124.5	231.1
30	9,50E+06	(142)	1,20E+06	(18)	18	157 73	202.2	125.1	350.0
31	9,71E+06	(137)	1,63E+06	(23)	17	213 88	153.6	99.2	250.1
32	2,58E+06	(214)	1,29E+06	(107)	100	168 33	52.1	41.2	65.7
33	4,36E+06	(217)	8,43E+05	(42)	60	110 34	133.8	96.3	190.8
34	5,90E+06	(294)	6,63E+05	(33)	60	87 30	228.7	160.7	337.4
35	4,44E+06	(236)	1,98E+06	(105)	64	258 51	58.5	46.4	73.6
36	9,01E+06	(157)	1,20E+06	(21)	21	157 68	192.0	122.8	318.1
37	9,32E+06	(116)	1,85E+06	(23)	15	241 100	130.3	83.5	213.6
38	3,42E+06	(108)	1,59E+06	(50)	38	207 58	56.4	40.0	80.5
39	6,95E+06	(173)	1,08E+06	(27)	30	142 54	165.2	110.6	257.5
40	7,26E+06	(271)	9,37E+05	(35)	45	122 41	199.3	140.9	291.4
41	6,42E+06	(213)	8,13E+05	(27)	40	106 41	202.8	136.8	314.0
42	5,12E+06	(51)	1,81E+06	(18)	12	236 110	73.5	42.6	133.9
43	7,43E+06	(370)	1,57E+06	(78)	60	205 46	122.6	96.1	156.3
44	6,27E+06	(78)	2,09E+06	(26)	15	273 106	77.9	49.7	126.7
45	7,85E+06	(176)	1,25E+06	(28)	27	163 61	162.1	109.3	250.7
46	5,34E+06	(124)	9,47E+05	(22)	28	124 52	145.4	92.8	240.2
47	5,77E+06	(115)	7,53E+05	(15)	24	98 50	196.3	115.9	361.1
48	7,56E+06	(113)	9,37E+05	(14)	18	122 64	206.4	120.0	388.2
49	9,54E+06	(190)	1,36E+06	(27)	24	177 68	181.2	121.8	281.6
50	8,31E+06	(207)	1,33E+06	(33)	30	173 60	161.9	112.6	241.1
51	6,97E+06	(81)	1,98E+06	(23)	14	259 107	91.3	57.3	152.2
52	7,57E+06	(314)	1,30E+06	(54)	50	170 46	149.5	112.3	198.9
53	5,62E+06	(280)	8,43E+05	(42)	60	110 34	172.1	124.9	243.7

Grain no.	RhoS (cm^-2)	(Ns)	RhoI (cm^-2)	(Ni)	Squares	U+/-2s		Grain Age (Ma) Age	--95% CI--	
54	4,42E+06	(110)	6,83E+05	(17)	30	89	43	166.3	100.5	295.3
55	6,91E+06	(258)	7,50E+05	(28)	45	98	37	236.2	161.3	361.1
56	4,96E+06	(103)	2,12E+06	(44)	25	277	83	61.0	42.6	89.0
57	6,12E+06	(305)	7,63E+05	(38)	60	100	32	206.5	148.2	296.8
58	4,89E+06	(134)	1,17E+06	(32)	33	153	54	108.6	73.8	165.1
59	6,75E+06	(112)	9,04E+05	(15)	20	118	60	191.3	112.8	352.2
60	7,36E+06	(220)	1,94E+06	(58)	36	254	67	98.0	73.5	130.6
61	3,08E+06	(174)	4,08E+05	(23)	68	53	22	194.4	126.8	314.0
62	4,29E+06	(57)	1,36E+06	(18)	16	177	82	82.1	48.0	148.4
63	8,63E+06	(172)	1,26E+06	(25)	24	164	65	177.1	117.1	280.8
64	6,02E+06	(120)	1,46E+06	(29)	24	190	70	107.3	71.5	167.0
65	3,75E+06	(168)	1,54E+06	(69)	54	201	48	63.2	47.7	83.5
66	7,03E+06	(175)	1,08E+06	(27)	30	142	54	167.1	112.0	260.3
67	6,63E+06	(77)	1,89E+06	(22)	14	247	104	90.7	56.3	153.3
68	5,90E+06	(245)	6,27E+05	(26)	50	82	32	241.4	162.6	375.4
69	8,48E+06	(197)	1,16E+06	(27)	28	152	58	187.8	126.4	291.5
70	3,58E+06	(95)	1,28E+06	(34)	32	167	57	72.7	48.9	111.1
71	3,43E+06	(114)	1,36E+06	(45)	40	177	53	66.0	46.5	95.5
72	8,35E+06	(104)	1,37E+06	(17)	15	178	85	157.4	94.9	280.1
73	7,61E+06	(202)	1,09E+06	(29)	32	143	53	179.4	122.2	274.3
74	3,97E+06	(89)	1,38E+06	(31)	27	181	65	74.7	49.3	116.4
75	9,14E+06	(182)	2,56E+06	(51)	24	334	93	92.8	67.9	129.2
76	8,11E+06	(202)	1,00E+06	(25)	30	131	52	207.5	138.0	327.3
77	5,72E+06	(114)	1,66E+06	(33)	24	216	75	89.7	60.8	136.6
78	6,93E+06	(92)	1,13E+06	(15)	16	148	75	157.6	92.0	292.7
79	7,36E+06	(171)	1,98E+06	(46)	28	259	76	96.6	69.7	136.9
80	4,99E+06	(145)	8,95E+05	(26)	35	117	45	144.0	95.2	227.7
81	4,78E+06	(238)	7,63E+05	(38)	60	100	32	161.8	115.2	233.9
82	1,16E+07	(135)	2,75E+06	(32)	14	360	126	109.4	74.4	166.3
83	5,85E+06	(136)	7,31E+05	(17)	28	96	46	204.9	125.1	360.9
84	6,93E+06	(115)	1,14E+06	(19)	20	150	68	155.8	96.5	268.0
85	7,87E+06	(209)	8,28E+05	(22)	32	108	46	243.1	158.3	394.4
86	5,21E+06	(173)	8,13E+05	(27)	40	106	41	165.2	110.6	257.5
87	7,71E+06	(384)	9,44E+05	(47)	60	123	36	210.3	156.1	290.5
88	7,62E+06	(253)	1,17E+06	(39)	40	153	49	167.5	120.0	240.7
89	5,98E+06	(278)	1,08E+06	(50)	56	141	40	143.9	106.7	198.5
90	7,88E+06	(157)	2,26E+06	(45)	24	295	88	90.7	65.0	129.4
91	5,98E+06	(298)	7,83E+05	(39)	60	102	33	196.8	141.6	281.7
92	6,17E+06	(123)	1,05E+06	(21)	24	138	59	151.0	95.5	252.4
93	7,87E+06	(196)	1,20E+06	(30)	30	157	57	168.5	115.3	256.0
94	4,52E+06	(180)	1,03E+06	(41)	48	134	42	113.9	81.1	164.0
95	5,15E+06	(205)	1,03E+06	(41)	48	134	42	129.5	92.7	185.8
96	5,29E+06	(123)	6,45E+05	(15)	28	84	43	209.7	124.3	384.7
97	7,43E+06	(111)	1,14E+06	(17)	18	149	71	167.8	101.5	297.9
98	3,73E+06	(124)	1,23E+06	(41)	40	161	50	78.7	55.1	115.0
99	7,44E+06	(383)	9,13E+05	(47)	62	119	35	209.8	155.7	289.8
100	7,83E+06	(117)	1,41E+06	(21)	18	184	79	143.7	90.7	240.7
POOLED	5,99E+06	(18247)	1,17E+06	(3572)	3668	153	6	132.7	126.6	139.1

CHI^2 PROBABILITY (%): 0.0

POOLED AGE W/ 68% CONF. INTERVAL(Ma): 132.7, 129.5 -- 135.9 (-3.2 +3.2)
95% CONF. INTERVAL(Ma): 126.6 -- 139.1 (-6.1 +6.4)

CENTRAL AGE W/ 68% CONF. INTERVAL(Ma): 128.9, 123.0 -- 135.1 (-5.9 +6.2)
95% CONF. INTERVAL(Ma): 117.6 -- 141.3 (-11.3 +12.4)
AGE DISPERSION (%): 40.3

FIT OPTION: Best-fit peaks using the binomial model of Galbraith and Green

INITIAL GUESS FOR MODEL PARAMETERS (number of peaks to fit = 3)

Peak #.	Peak Age	Theta	Fraction(%)	Count
1.	95.50	0.786	17.4	17.44
2.	132.70	0.836	28.5	28.55
3.	161.10	0.861	47.6	47.56

Total range for grain ages:	51,1 to 239,9 Ma
Number of active grains (Num. used for fit):	100
Number of removed grains:	0
Degrees of freedom for fit:	95
Average of the SE(Z)'s for the grains:	0,2
Estimated width of peaks in PD plot in Z units:	0,24

PARAMETERS FOR BEST-FIT PEAKS

* *Standard error for peak age includes group error*
* *Peak width is for PD plot assuming a kernel factor = 0.60*

#.	Peak Age(Ma)	68%CI	95%CI	W(Z)	Frac(%)	SE,%	Count
1.	60.0	-3,2 ...+3,4	-6,1 ...+6,8	0.17	12.3	4.0	12.3
2.	99.5	-6,9 ...+7,4	-13,1 ...+15,1	0.22	20.5	5.4	20.5
3.	173.3	-5,4 ...+5,6	-10,4 ...+11,1	0.23	67.2	5.7	67.2

Log-likelihood for best fit:	-363,343
Chi-squared value for best fit:	90,171
Reduced chi-squared value:	0,949
Probability for F test:	3%
Condition number for COVAR matrix:	8,83
Number of iterations:	19

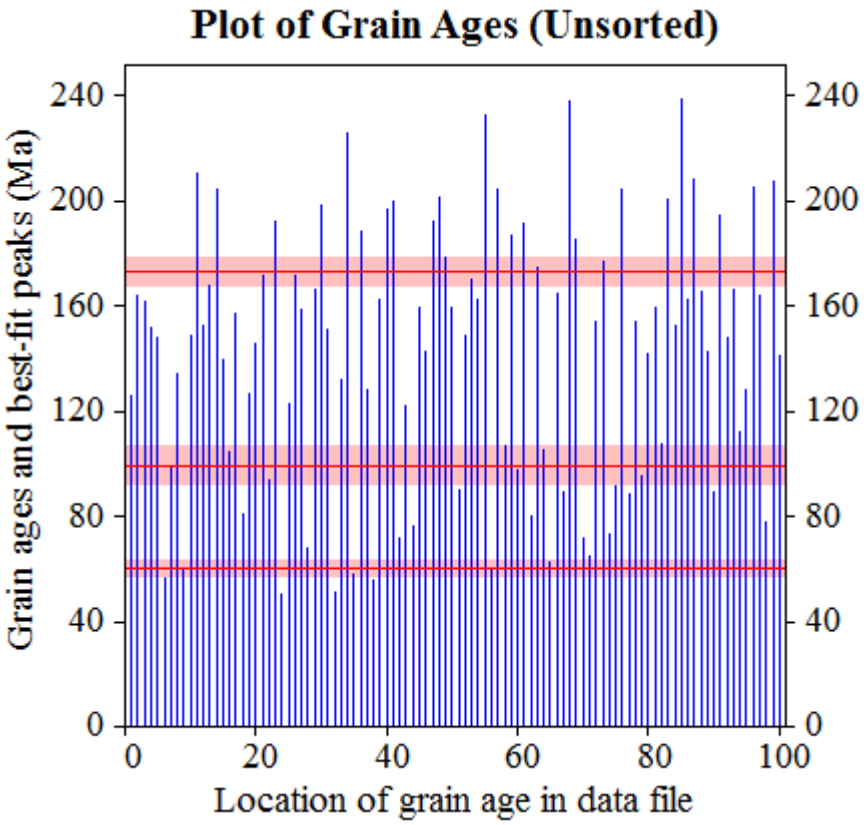
Plot of Grain Ages (Unsorted)
Grain ages and best-fit peaks (Ma)
0
40
80
120
160
200
240
0
20
40
60
80
100
Location of grain age in data file

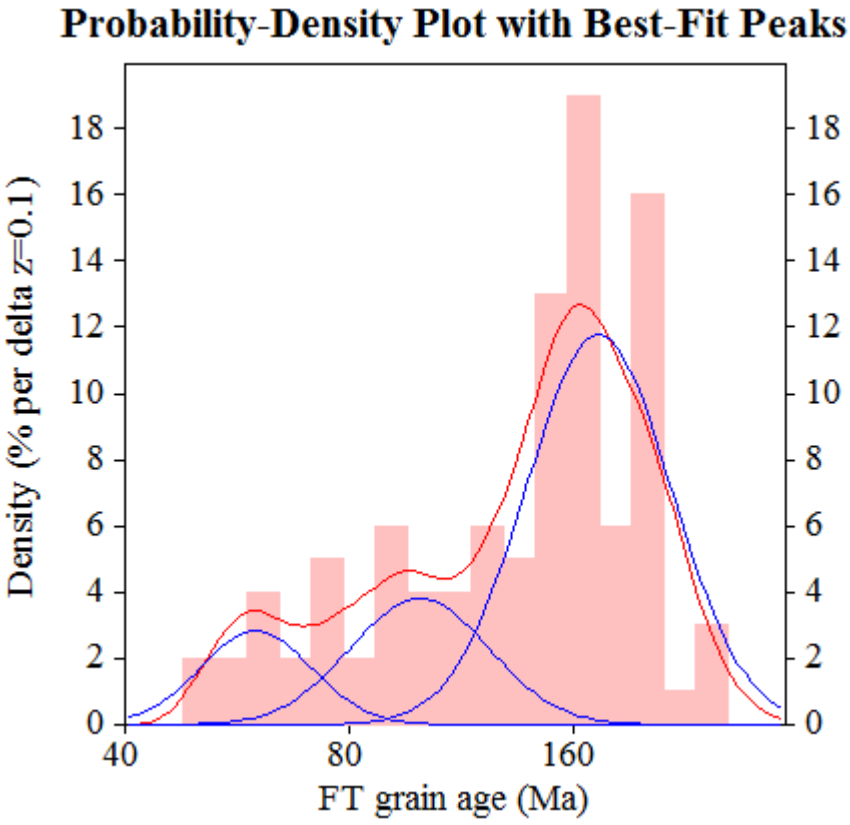
Probability-Density Plot with Best-Fit Peaks
Density (% per delta z=0.1)
0
2
4
6
8
10
12
14
16
18
40
80
160
FT grain age (Ma)

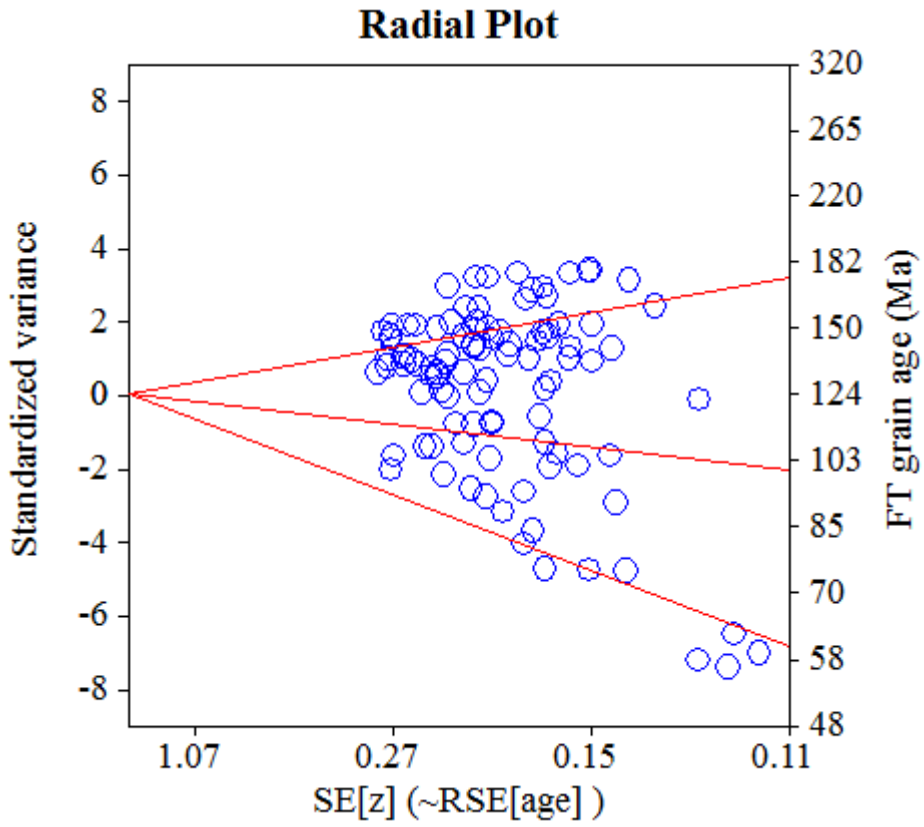
Radial Plot
Standardized variance
8
6
4
2
0
-2
-4
-6
-8
320
265
220
182
150
124
103
85
70
58
48
FT grain age (Ma)
1.07
0.27
0.15
0.11
SE[z] (~RSE[age])

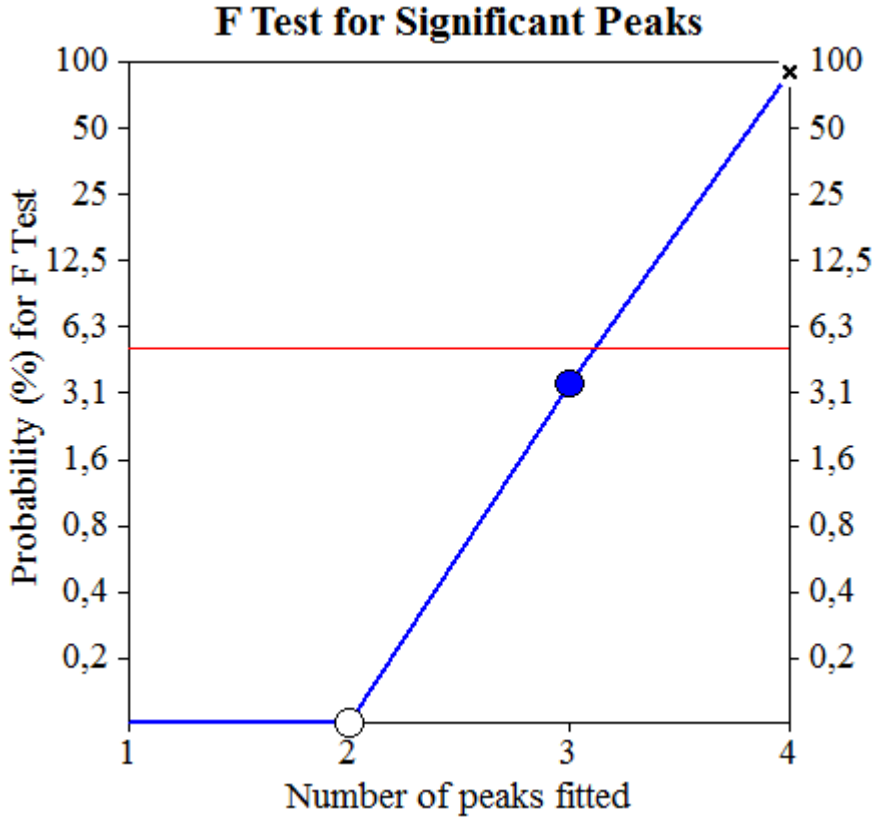
F Test for Significant Peaks
Probability (%) for F Test
100
50
25
12,5
6,3
3,1
1,6
0,8
0,4
0,2
1
2
3
4
Number of peaks fitted

Merged dataset:
C:\BH2\Jairo\Echentillon-IRR-12-2015\JG-P1-06Zr\JG-P1-06a-Zr.ftz
C:\BH2\Jairo\Echentillon-IRR-12-2015\JG-P1-06Zr\JG-P1-06Zr.ft40
C:\BH2\Jairo\Echentillon-IRR-12-2015\JG-P1-06Zr\JG-P1-06-Zr.ftz

NEW PARAMETERS - ZETA METHOD

EFFECTIVE TRACK DENSITY FOR FLUENCE MONITOR (tracks/cm^2): 3,82E+05
RELATIVE ERROR (%): 1,12
EFFECTIVE URANIUM CONTENT OF MONITOR (ppm): 50,00
ZETA FACTOR AND STANDARD ERROR (yr cm^2): 137,14 1,57
SIZE OF COUNTER SQUARE (cm^2): 8,30E-07

GRAIN AGES IN ORIGINAL ORDER

Grain no.	RhoS (cm^-2)	(Ns)	RhoI (cm^-2)	(Ni)	Squares	U+/-2s	Grain Age (Ma) Age	--95% CI--	
1	3,03E+06	(88)	6,54E+05	(19)	35	86 39	119.5	72.9	207.9
2	7,71E+06	(224)	9,98E+05	(29)	35	131 48	198.4	135.6	302.3
3	6,33E+06	(105)	7,23E+05	(12)	20	95 54	222.7	124.6	442.7
4	8,96E+06	(119)	1,28E+06	(17)	16	167 80	179.5	108.9	317.7
5	4,42E+06	(88)	7,03E+05	(14)	24	92 48	161.1	92.5	306.5
6	5,54E+06	(138)	6,02E+05	(15)	30	79 40	234.5	139.6	428.3
7	8,07E+06	(201)	1,49E+06	(37)	30	194 64	140.4	99.1	204.9
8	1,04E+07	(129)	1,12E+06	(14)	15	147 77	234.7	137.3	439.1
9	5,00E+06	(83)	8,43E+05	(14)	20	110 58	152.1	87.0	290.1
10	4,59E+06	(198)	6,95E+05	(30)	52	91 33	170.0	116.3	258.2
11	5,77E+06	(91)	9,51E+05	(15)	19	124 63	155.7	90.8	289.3
12	3,19E+06	(172)	6,86E+05	(37)	65	90 29	120.3	84.4	176.6
13	4,86E+06	(121)	8,84E+05	(22)	30	116 49	141.7	90.3	234.4
14	2,85E+06	(45)	1,59E+06	(25)	19	207 82	46.9	28.2	79.8
15	2,82E+06	(82)	6,20E+05	(18)	35	81 38	117.5	70.6	208.1
16	6,91E+06	(172)	8,03E+05	(20)	30	105 46	220.0	139.9	367.8
17	6,63E+06	(55)	1,33E+06	(11)	10	173 102	128.2	67.5	272.0
18	5,94E+06	(148)	8,03E+05	(20)	30	105 46	189.8	120.0	319.0
19	8,73E+06	(87)	1,20E+06	(12)	12	158 89	185.2	102.6	371.2
20	8,38E+06	(167)	1,10E+06	(22)	24	144 61	194.7	125.8	318.3
21	9,16E+06	(114)	1,37E+06	(17)	15	179 85	172.0	104.2	305.1
22	8,11E+06	(202)	8,84E+05	(22)	30	116 49	234.8	152.8	381.4
23	9,90E+06	(115)	1,20E+06	(14)	14	158 83	209.7	122.0	394.1
24	5,66E+06	(94)	1,27E+06	(21)	20	165 71	115.6	72.1	195.5
25	8,79E+06	(416)	9,93E+05	(47)	57	130 38	227.3	168.9	313.3
26	6,79E+06	(124)	1,53E+06	(28)	22	201 75	114.5	76.0	179.4
27	5,62E+06	(84)	1,27E+06	(19)	18	166 75	114.1	69.4	199.0
28	7,03E+06	(70)	1,00E+06	(10)	12	131 81	178.5	93.4	387.6
29	7,59E+06	(126)	8,43E+05	(14)	20	110 58	229.4	134.0	429.5
30	5,21E+06	(225)	7,41E+05	(32)	52	97 34	180.9	125.6	270.4
31	5,39E+06	(94)	9,18E+05	(16)	21	120 59	150.9	89.4	274.6
32	6,24E+06	(88)	1,13E+06	(16)	17	148 73	141.4	83.4	258.1
33	6,35E+06	(79)	8,03E+05	(10)	15	105 65	201.0	106.0	433.8
34	8,61E+06	(200)	9,90E+05	(23)	28	129 53	222.6	145.9	358.0
35	8,17E+06	(61)	1,20E+06	(9)	9	158 102	172.6	87.1	394.8
36	5,72E+06	(133)	6,45E+05	(15)	28	84 43	226.2	134.5	413.6
37	5,54E+06	(170)	6,19E+05	(19)	37	81 37	228.7	143.9	387.5
38	7,18E+06	(268)	1,26E+06	(47)	45	165 48	147.4	108.3	205.3
39	5,71E+06	(128)	8,48E+05	(19)	27	111 50	173.0	107.6	296.2
40	5,22E+06	(65)	6,43E+05	(8)	15	84 58	205.9	101.1	494.8
41	8,06E+06	(107)	1,20E+06	(16)	16	158 78	171.5	102.3	310.3
42	9,75E+06	(178)	1,04E+06	(19)	22	136 62	239.2	150.8	404.8
43	7,83E+06	(117)	1,14E+06	(17)	18	149 71	176.5	107.0	312.7
44	8,82E+06	(205)	2,02E+06	(47)	28	265 77	113.0	82.3	158.7
45	4,98E+06	(62)	1,20E+06	(15)	15	158 80	106.6	60.6	202.0
46	5,04E+06	(46)	8,76E+05	(8)	11	115 79	146.6	70.0	359.7
47	5,56E+06	(83)	8,03E+05	(12)	18	105 59	176.8	97.7	355.2

Merged dataset:
C:\BH2\Jairo\Echentillon-IRR-12-2015\JG-P1-06Zr\JG-P1-06a-Zr.ftz
C:\BH2\Jairo\Echentillon-IRR-12-2015\JG-P1-06Zr\JG-P1-06Zr.ft40
C:\BH2\Jairo\Echentillon-IRR-12-2015\JG-P1-06Zr\JG-P1-06-Zr.ftz

NEW PARAMETERS - ZETA METHOD

EFFECTIVE TRACK DENSITY FOR FLUENCE MONITOR (tracks/cm^2): 3,82E+05
RELATIVE ERROR (%): 1,12
EFFECTIVE URANIUM CONTENT OF MONITOR (ppm): 50,00
ZETA FACTOR AND STANDARD ERROR (yr cm^2): 137,14 1,57
SIZE OF COUNTER SQUARE (cm^2): 8,30E-07

Grain no.	RhoS (cm^-2)	(Ns)	RhoI (cm^-2)	(Ni)	Squares	U+/-2s	Grain Age (Ma) Age	--95% CI--	
48	5,59E+06	(65)	1,12E+06	(13)	14	146 80	128.5	71.1	254.3
49	4,17E+06	(83)	1,86E+06	(37)	24	243 80	58.4	39.3	88.6
50	7,67E+06	(70)	1,10E+06	(10)	11	143 88	178.5	93.4	387.6
51	5,36E+06	(89)	8,43E+05	(14)	20	110 58	162.9	93.6	309.7
52	9,48E+06	(118)	1,29E+06	(16)	15	168 83	188.8	113.2	340.3
53	8,77E+06	(131)	1,54E+06	(23)	18	201 83	146.8	94.6	239.4
54	1,67E+07	(194)	1,89E+06	(22)	14	248 105	225.6	146.6	367.0
55	1,03E+07	(77)	2,81E+06	(21)	9	368 159	94.9	58.4	162.0
56	5,56E+06	(83)	8,70E+05	(13)	18	114 62	163.5	92.0	319.6
57	3,38E+06	(59)	1,03E+06	(18)	21	135 63	84.8	49.8	153.0
58	1,19E+07	(148)	1,45E+06	(18)	15	189 88	210.4	130.3	363.5
59	3,67E+06	(64)	8,61E+05	(15)	21	113 57	110.0	62.7	208.1
60	6,69E+06	(50)	2,14E+06	(16)	9	280 138	80.8	45.7	152.4
61	5,79E+06	(101)	1,61E+06	(28)	21	210 79	93.5	61.4	147.7
62	5,22E+06	(104)	1,05E+06	(21)	24	138 60	127.7	80.1	215.0
63	7,71E+06	(64)	9,64E+05	(8)	10	126 87	202.8	99.5	487.8
64	9,12E+06	(106)	1,46E+06	(17)	14	191 92	160.1	96.6	284.8
65	9,14E+06	(91)	1,00E+06	(10)	12	131 81	230.9	122.7	494.9
66	7,73E+06	(77)	1,00E+06	(10)	12	131 81	196.0	103.2	423.6
67	4,74E+06	(59)	1,53E+06	(19)	15	200 91	80.4	47.6	143.1
68	6,99E+06	(58)	2,29E+06	(19)	10	299 136	79.1	46.8	140.8
69	5,35E+06	(80)	1,07E+06	(16)	18	140 69	128.7	75.5	236.0
70	7,65E+06	(146)	1,15E+06	(22)	23	151 64	170.6	109.6	280.1
71	8,21E+06	(109)	1,36E+06	(18)	16	177 83	155.6	95.1	272.2
72	1,07E+07	(89)	1,45E+06	(12)	10	189 107	189.3	105.0	379.2
POOLED	6,49E+06	(8482)	1,05E+06	(1379)	1575	138 8	159.2	149.3	169.7

CHI^2 PROBABILITY (%): 0.0

POOLED AGE W/ 68% CONF. INTERVAL(Ma): 159.2, 154.1 -- 164.5 (-5.1 +5.3)
95% CONF. INTERVAL(Ma): 149.3 -- 169.7 (-9.9 +10.5)

CENTRAL AGE W/ 68% CONF. INTERVAL(Ma): 154.0, 147.2 -- 161.2 (-6.8 +7.1)
95% CONF. INTERVAL(Ma): 140.9 -- 168.4 (-13.1 +14.3)
AGE DISPERSION (%): 26.2

Merged dataset:
C:\BH2\Jairo\Echentillon-IRR-12-2015\JG-P1-06Zr\JG-P1-06a-Zr.ftz
C:\BH2\Jairo\Echentillon-IRR-12-2015\JG-P1-06Zr\JG-P1-06Zr.ft40
C:\BH2\Jairo\Echentillon-IRR-12-2015\JG-P1-06Zr\JG-P1-06-Zr.ftz

FIT OPTION: Best-fit peaks using the binomial model of Galbraith and Green

INITIAL GUESS FOR MODEL PARAMETERS (number of peaks to fit = 3)

Peak #.	Peak Age	Theta	Fraction(%)	Count
1.	56.30	0.683	2.8	2.01
2.	81.00	0.757	8.2	5.92
3.	159.20	0.860	41.2	29.65

Total range for grain ages: 46,6 to 235,6 Ma
Number of active grains (Num. used for fit): 72
Number of removed grains: 0
Degrees of freedom for fit: 67
Average of the SE(Z)'s for the grains: 0,26
Estimated width of peaks in PD plot in Z units: 0,31

PARAMETERS FOR BEST-FIT PEAKS

* *Standard error for peak age includes group error*
* *Peak width is for PD plot assuming a kernel factor = 0.60*

#.	Peak Age(Ma)	68%CI	95%CI	W(Z)	Frac(%)	SE,%	Count
1.	58.2	-10,3 ...+12,5	-18,5 ...+27,0	0.26	3.5	2.7	2.5
2.	118.3	-14,5 ...+16,5	-26,8 ...+34,5	0.28	22.1	12.4	15.9
3.	181.3	-9,2 ...+9,7	-17,6 ...+19,5	0.29	74.3	12.5	53.5

Log-likelihood for best fit: -217,626
Chi-squared value for best fit: 63,905
Reduced chi-squared value: 0,954
Probability for F test: 0%
Condition number for COVAR matrix: 66,50
Number of iterations: 23

Merged dataset:
C:\BH2\Jairo\Echentillon-IRR-12-2015\JG-P1-06Zr\JG-P1-06a-Zr.ftz
C:\BH2\Jairo\Echentillon-IRR-12-2015\JG-P1-06Zr\JG-P1-06Zr.ft40
C:\BH2\Jairo\Echentillon-IRR-12-2015\JG-P1-06Zr\JG-P1-06-Zr.ftz

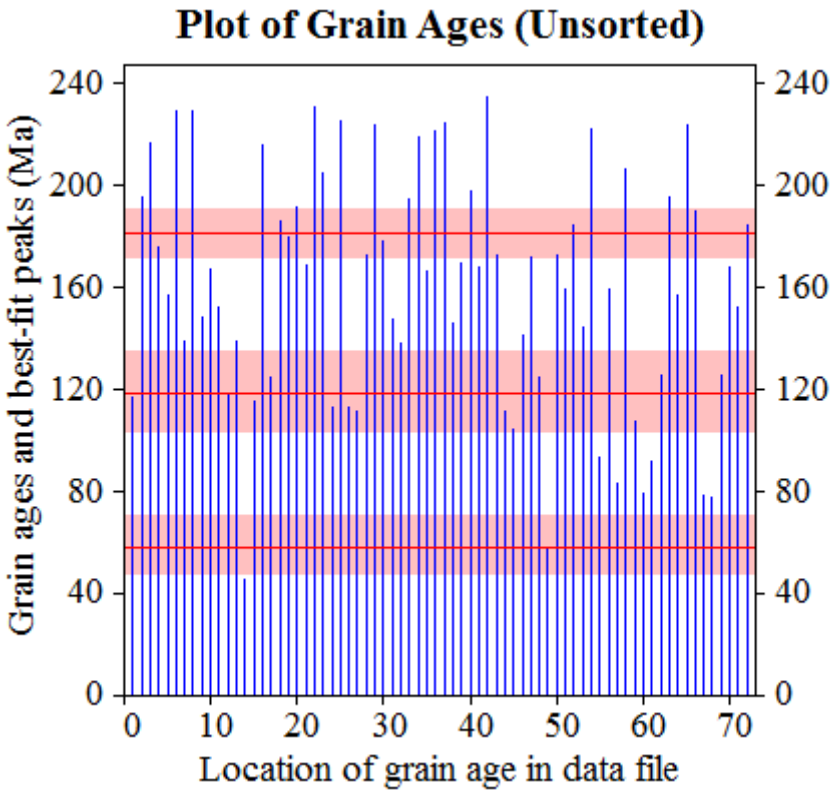

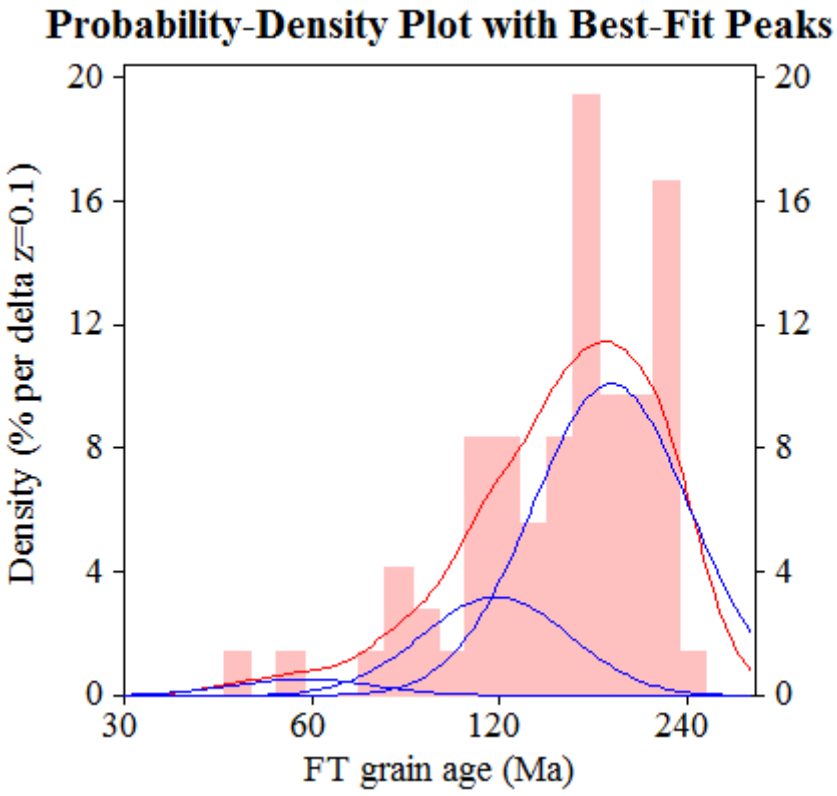

Merged dataset:
C:\BH2\Jairo\Echentillon-IRR-12-2015\JG-P1-06Zr\JG-P1-06a-Zr.ftz
C:\BH2\Jairo\Echentillon-IRR-12-2015\JG-P1-06Zr\JG-P1-06Zr.ft40
C:\BH2\Jairo\Echentillon-IRR-12-2015\JG-P1-06Zr\JG-P1-06-Zr.ftz

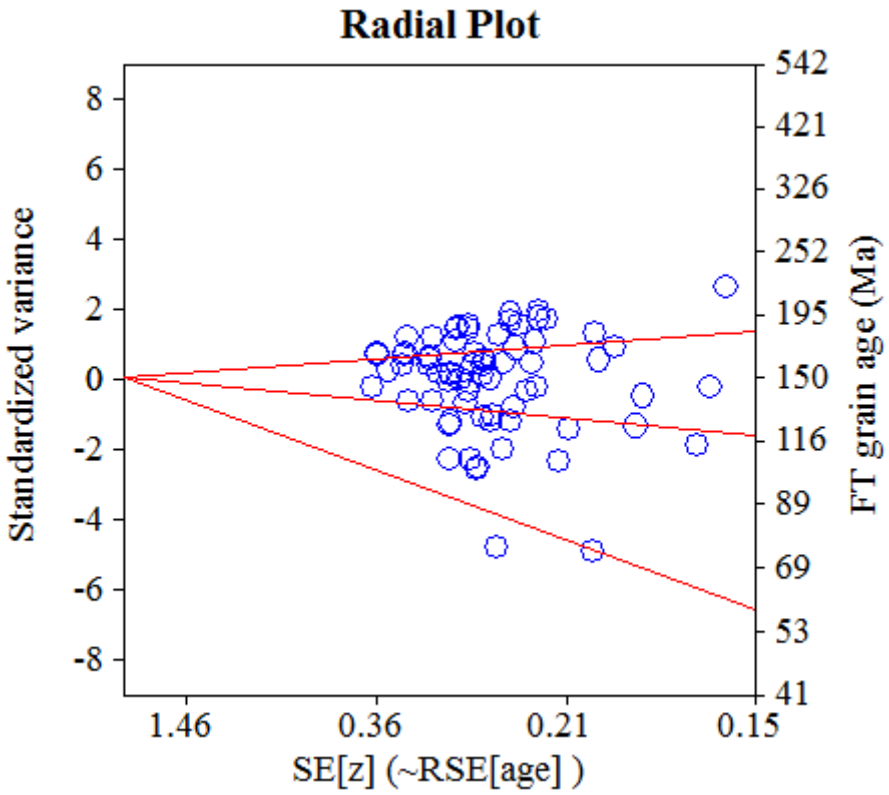

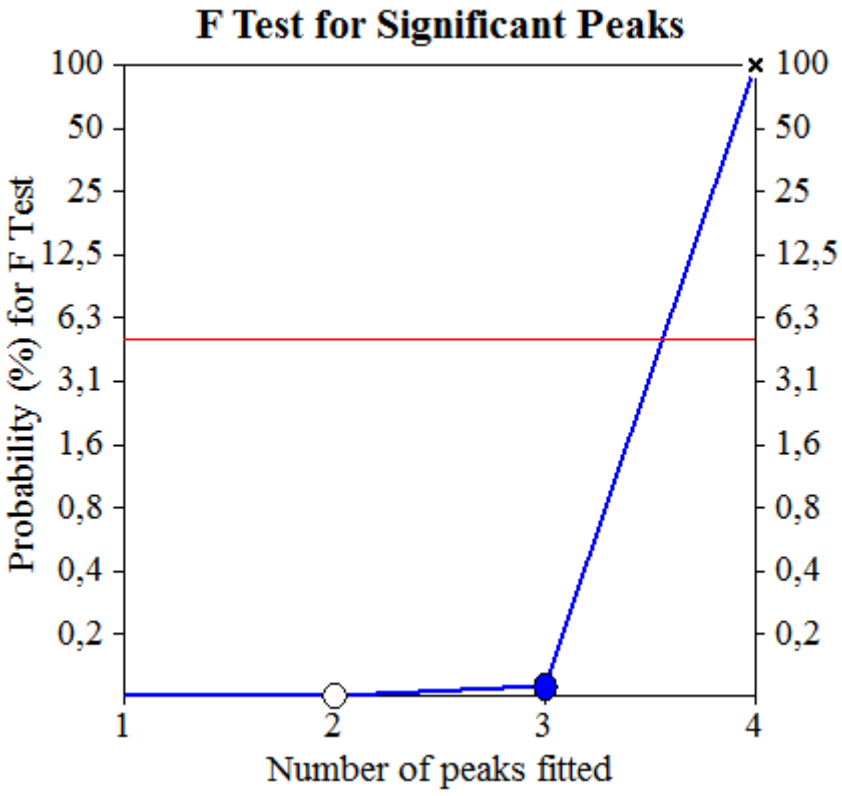

Datafile: C:\BH2\Jairo\Echantillon-IRR-10-2015\JG-P5-03a-Zr\JG-P5-03a.ftz
Title: Sample No. JG P5 03a Irr 10-2015-40

NEW PARAMETERS - ZETA METHOD

EFFECTIVE TRACK DENSITY FOR FLUENCE MONITOR (tracks/cm^2): 3,93E+05
RELATIVE ERROR (%): 1,41
EFFECTIVE URANIUM CONTENT OF MONITOR (ppm): 50,00
ZETA FACTOR AND STANDARD ERROR (yr cm^2): 137,14 1,57
SIZE OF COUNTER SQUARE (cm^2): 8,30E-07

GRAIN AGES IN ORIGINAL ORDER

Grain no.	RhoS (cm^-2)	(Ns)	RhoI (cm^-2)	(Ni)	Squares	U+/-2s		Grain Age (Ma) Age	--95% CI--	
1	3,37E+06	(140)	1,59E+06	(66)	50	202	50	56.5	42.2	75.8
2	4,82E+06	(200)	3,61E+06	(150)	50	460	76	35.7	28.9	44.3
3	4,40E+06	(219)	1,91E+06	(95)	60	243	50	61.6	48.3	78.4
4	5,38E+06	(219)	6,39E+05	(26)	49	81	32	222.0	149.0	346.4
5	6,43E+06	(192)	1,91E+06	(57)	36	243	64	90.0	66.8	123.3
6	5,38E+06	(268)	1,59E+06	(79)	60	202	46	90.3	70.2	116.0
7	9,20E+06	(229)	6,27E+06	(156)	30	796	129	39.4	32.0	48.3
8	6,99E+06	(174)	2,81E+06	(70)	30	357	86	66.2	50.2	87.4
9	5,46E+06	(290)	2,18E+06	(116)	64	278	52	66.8	53.8	83.0
10	6,43E+06	(320)	1,75E+06	(87)	60	222	48	97.9	77.2	124.1
11	3,54E+06	(147)	1,54E+06	(64)	50	196	49	61.6	45.7	84.0
12	5,26E+06	(131)	3,86E+06	(96)	30	490	101	36.5	28.0	47.6
13	4,35E+06	(253)	1,69E+06	(98)	70	214	44	68.9	54.5	87.1
14	3,77E+06	(125)	2,11E+06	(70)	40	268	64	47.7	35.6	63.9
15	3,92E+06	(130)	1,96E+06	(65)	40	249	62	53.6	39.6	73.5
16	1,12E+07	(297)	2,15E+06	(57)	32	273	72	137.8	104.0	182.6
17	5,54E+06	(184)	2,83E+06	(94)	40	360	75	52.3	40.8	67.1
18	2,47E+06	(164)	6,63E+05	(44)	80	84	25	99.5	71.2	142.2
19	4,08E+06	(264)	1,68E+06	(109)	78	214	41	64.7	51.7	81.0
20	6,79E+06	(547)	1,47E+06	(118)	97	186	35	123.3	101.0	150.6
21	2,70E+06	(157)	1,15E+06	(67)	70	147	36	62.4	46.9	83.1
22	6,59E+06	(164)	1,29E+06	(32)	30	163	58	136.2	93.4	205.6
23	7,78E+06	(452)	1,79E+06	(104)	70	228	45	115.6	93.3	143.1
24	4,24E+06	(176)	2,29E+06	(95)	50	291	60	49.5	38.5	63.6
25	4,48E+06	(223)	1,18E+06	(59)	60	151	39	100.3	75.3	133.5
26	5,11E+06	(339)	2,29E+06	(152)	80	291	48	59.7	49.2	72.4
27	7,50E+06	(112)	3,21E+06	(48)	18	408	118	62.5	44.3	89.7
28	3,48E+06	(260)	1,66E+06	(124)	90	211	38	56.1	45.2	69.6
29	4,97E+06	(371)	2,03E+06	(152)	90	259	43	65.3	53.9	79.0
30	3,94E+06	(196)	1,29E+06	(64)	60	163	41	81.5	61.4	107.9
31	4,47E+06	(141)	2,98E+06	(94)	38	379	79	40.1	30.9	52.1
32	3,15E+06	(235)	1,47E+06	(110)	90	187	36	57.1	45.5	71.7
33	5,35E+06	(142)	3,88E+06	(103)	32	493	98	36.9	28.6	47.6
34	5,11E+06	(123)	1,95E+06	(47)	29	248	72	70.0	49.8	100.3
35	4,37E+06	(145)	2,20E+06	(73)	40	280	66	53.0	40.0	70.2
36	4,57E+06	(360)	2,45E+06	(193)	95	311	46	50.0	41.9	59.7
37	6,36E+06	(285)	3,26E+06	(146)	54	414	69	52.3	42.7	63.9
38	4,64E+06	(77)	1,81E+06	(30)	20	230	83	68.6	44.7	108.5
39	7,11E+06	(118)	4,16E+06	(69)	20	528	128	45.9	33.8	62.8
40	3,43E+06	(114)	1,57E+06	(52)	40	199	55	58.8	42.0	83.3
41	7,45E+06	(235)	1,46E+06	(46)	38	185	55	135.9	99.2	190.7
42	8,31E+06	(138)	3,19E+06	(53)	20	406	112	69.7	50.5	97.7
43	7,68E+06	(255)	2,86E+06	(95)	40	364	75	71.6	56.5	90.7
44	6,02E+06	(235)	2,13E+06	(83)	47	270	60	75.5	58.7	97.0
45	2,83E+06	(108)	1,57E+06	(60)	46	200	52	48.3	34.9	67.5
46	3,76E+06	(156)	1,90E+06	(79)	50	242	55	52.7	40.2	69.1
47	5,56E+06	(277)	3,01E+06	(150)	60	383	63	49.5	40.5	60.4
48	5,84E+06	(194)	3,10E+06	(103)	40	394	78	50.4	39.6	64.0
49	5,49E+06	(310)	8,68E+05	(49)	68	110	32	167.9	124.5	231.7
50	7,83E+05	(26)	1,51E+05	(5)	40	19	16	135.3	52.7	451.7
51	2,82E+06	(164)	1,20E+06	(70)	70	153	37	62.5	47.2	82.6
52	8,88E+06	(442)	2,65E+06	(132)	60	337	59	89.4	73.4	108.7
53	2,41E+06	(54)	1,12E+06	(25)	27	142	56	57.8	35.5	97.0

Grain no.	RhoS (cm^-2)	(Ns)	RhoI (cm^-2)	(Ni)	Squares	U+/-2s	Grain Age (Ma) Age	--95% CI--	
54	3,58E+06	(104)	2,24E+06	(65)	35	284 71	43.0	31.2	59.6
55	6,47E+06	(188)	1,76E+06	(51)	35	223 63	98.4	72.1	137.0
56	5,34E+06	(266)	2,73E+06	(136)	60	347 60	52.4	42.5	64.5
57	3,33E+06	(174)	1,70E+06	(89)	63	216 46	52.2	40.4	67.5
58	3,37E+06	(252)	1,65E+06	(123)	90	209 38	54.8	44.1	68.1
59	5,42E+06	(144)	1,02E+06	(27)	32	129 49	141.6	94.1	222.1
60	3,27E+06	(217)	1,23E+06	(82)	80	157 35	70.6	54.7	91.0
61	8,19E+06	(204)	2,41E+06	(60)	30	306 79	90.3	67.8	120.3
62	5,58E+06	(139)	2,81E+06	(70)	30	357 86	53.0	39.7	70.6
63	3,53E+06	(170)	1,31E+06	(63)	58	166 42	71.8	53.8	95.8
64	6,75E+06	(112)	2,11E+06	(35)	20	268 90	85.5	58.2	128.9
65	1,89E+06	(94)	1,43E+06	(71)	60	181 43	35.6	25.9	49.2
66	2,41E+06	(100)	1,66E+06	(69)	50	211 51	38.9	28.4	53.8
67	4,78E+06	(127)	2,37E+06	(63)	32	302 76	54.1	39.7	74.4
68	5,01E+06	(187)	1,87E+06	(70)	45	238 57	71.2	54.1	93.6
69	3,64E+06	(151)	1,61E+06	(67)	50	205 50	60.1	45.0	80.1
70	5,59E+06	(102)	2,96E+06	(54)	22	376 102	50.7	36.1	71.9
71	4,62E+06	(188)	2,16E+06	(88)	49	275 59	57.1	44.3	73.5
72	6,63E+06	(77)	2,50E+06	(29)	14	317 117	71.0	46.0	113.0
73	6,55E+06	(261)	2,26E+06	(90)	48	287 61	77.3	60.8	98.3
74	5,27E+06	(394)	4,04E+06	(302)	90	514 61	35.0	30.0	40.8
75	3,94E+06	(206)	2,66E+06	(139)	63	338 58	39.7	32.0	49.3
76	3,00E+06	(224)	1,77E+06	(132)	90	225 40	45.4	36.6	56.4
77	5,16E+06	(210)	3,05E+06	(124)	49	388 70	45.3	36.3	56.7
78	5,22E+06	(130)	1,53E+06	(38)	30	194 63	91.3	63.5	134.9
79	5,27E+06	(175)	2,11E+06	(70)	40	268 64	66.6	50.5	87.9
80	3,44E+06	(160)	1,10E+06	(51)	56	139 39	83.9	61.0	117.4
POOLED	4,77E+06	(16033)	2,01E+06	(6739)	4049	255 10	63.8	61.0	66.8

CHI^2 PROBABILITY (%): 0.0

POOLED AGE W/ 68% CONF. INTERVAL(Ma): 63.8, 62.4 -- 65.3 (-1.5 +1.5)
95% CONF. INTERVAL(Ma): 61.0 -- 66.8 (-2.8 +3.0)

CENTRAL AGE W/ 68% CONF. INTERVAL(Ma): 63.7, 61.0 -- 66.6 (-2.7 +2.8)
95% CONF. INTERVAL(Ma): 58.5 -- 69.4 (-5.2 +5.7)
AGE DISPERSION (%): 32.9

FIT OPTION: Best-fit peaks using the binomial model of Galbraith and Green

INITIAL GUESS FOR MODEL PARAMETERS (number of peaks to fit = 3)

Peak #.	Peak Age	Theta	Fraction(%)	Count
1.	39.10	0.592	18.7	14.95
2.	63.80	0.704	42.7	34.20
3.	91.30	0.773	21.5	17.21

Total range for grain ages: 35,1 to 219,6 Ma
Number of active grains (Num. used for fit): 80
Number of removed grains: 0
Degrees of freedom for fit: 75
Average of the SE(Z)'s for the grains: 0,15
Estimated width of peaks in PD plot in Z units: 0,18

PARAMETERS FOR BEST-FIT PEAKS

* *Standard error for peak age includes group error*
* *Peak width is for PD plot assuming a kernel factor = 0.60*

#.	Peak Age(Ma)	68%CI	95%CI	W(Z)	Frac(%)	SE,%	Count
1.	39.6	-2,0 ...+2,1	-3,8 ...+4,2	0.14	15.9	5.2	12.7
2.	59.9	-1,8 ...+1,9	-3,5 ...+3,7	0.15	60.6	6.5	48.5
3.	111.2	-4,5 ...+4,7	-8,7 ...+9,5	0.17	23.5	5.1	18.8

Log-likelihood for best fit: -357,023
Chi-squared value for best fit: 83,423
Reduced chi-squared value: 1,112
Probability for F test: 0%
Condition number for COVAR matrix: 13,77
Number of iterations: 9

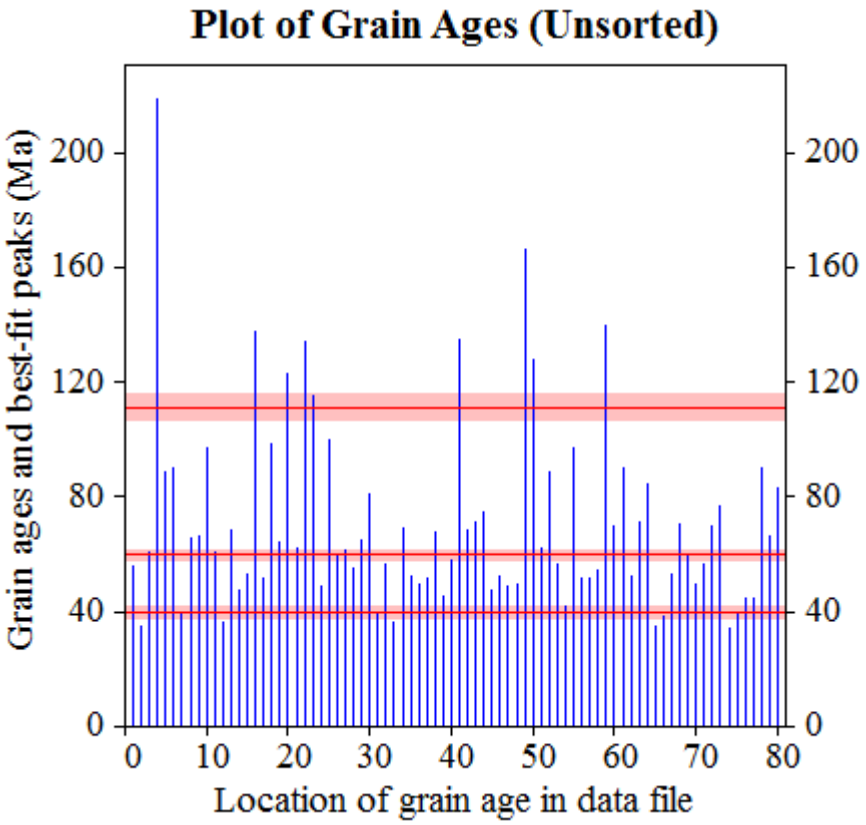
Plot of Grain Ages (Unsorted)
Grain ages and best-fit peaks (Ma)
0
40
80
120
160
200
0
10
20
30
40
50
60
70
80
Location of grain age in data file

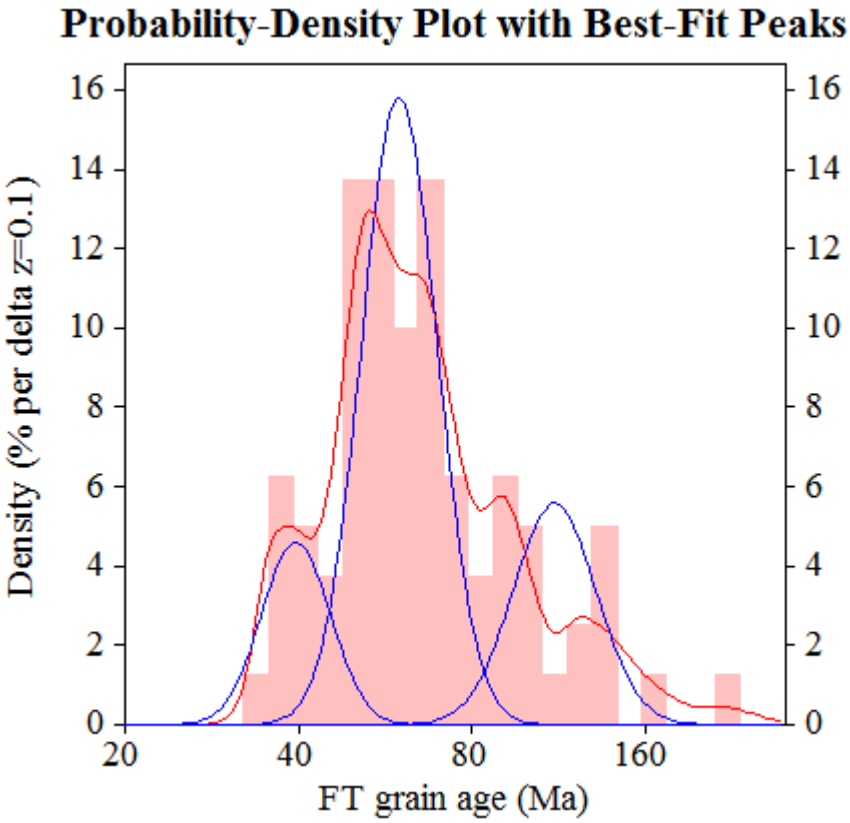
Probability-Density Plot with Best-Fit Peaks
Density (% per delta z=0.1)
0
2
4
6
8
10
12
14
16
20
40
80
160
FT grain age (Ma)

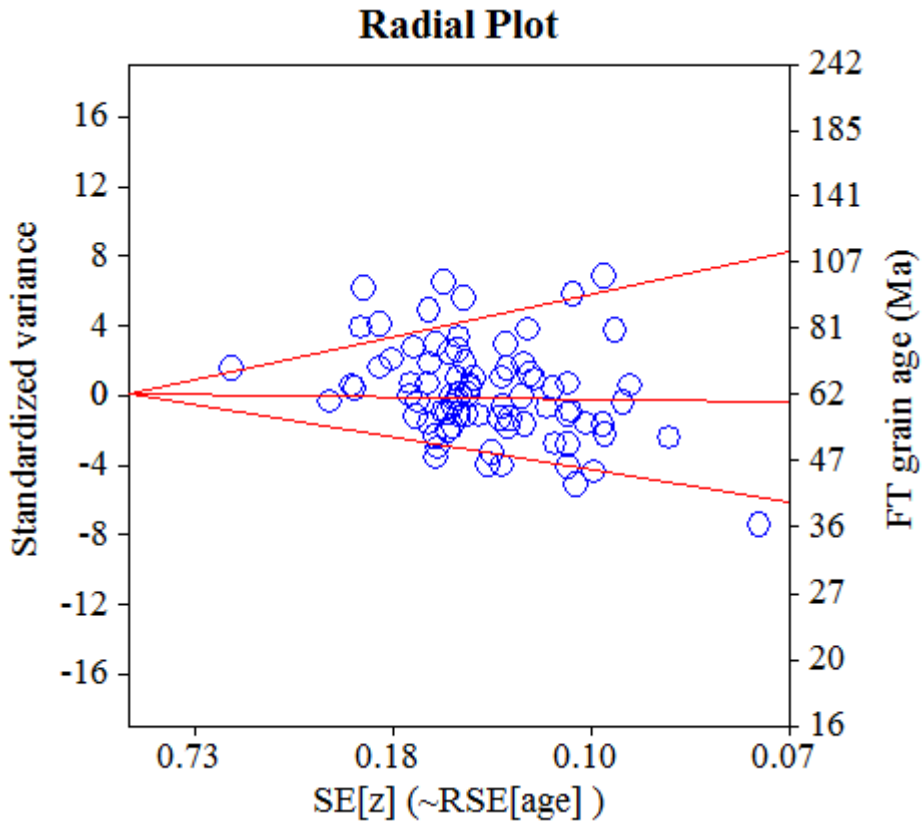
Radial Plot
Standardized variance
16
12
8
4
0
-4
-8
-12
-16
242
185
141
107
81
62
47
36
27
20
16
FT grain age (Ma)
0.73
0.18
0.10
0.07
SE[z] (~RSE[age])

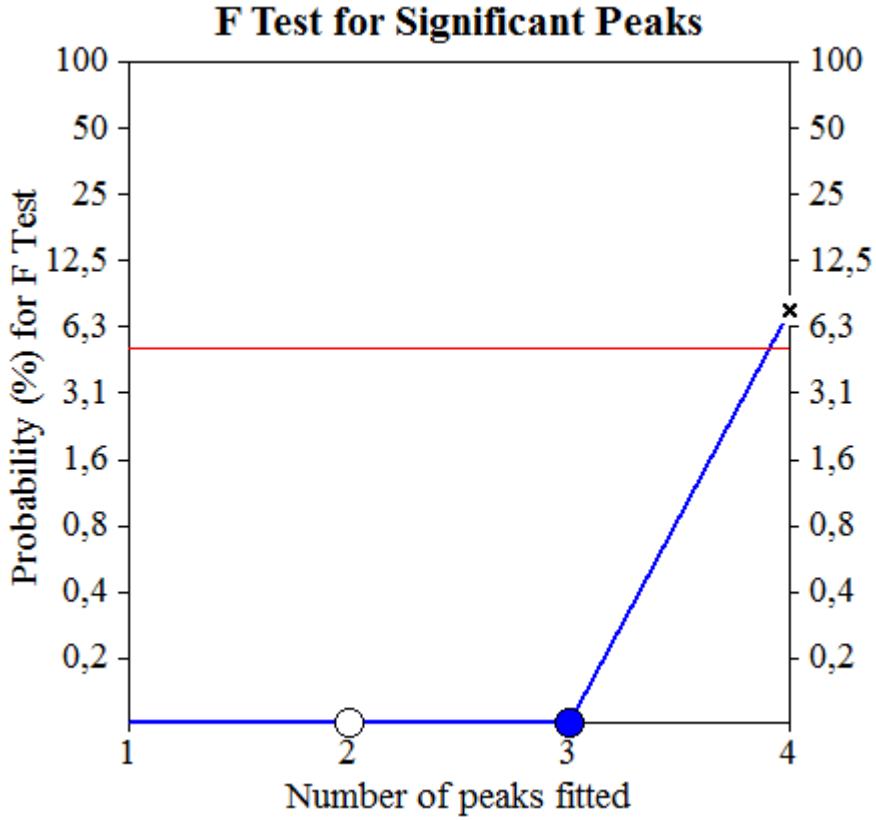
F Test for Significant Peaks
Probability (%) for F Test
100
50
25
12,5
6,3
3,1
1,6
0,8
0,4
0,2
1
2
3
4
Number of peaks fitted

NEW PARAMETERS - ZETA METHOD

EFFECTIVE TRACK DENSITY FOR FLUENCE MONITOR (tracks/cm^2): 1,27E+06
RELATIVE ERROR (%): 1,12
EFFECTIVE URANIUM CONTENT OF MONITOR (ppm): 15,00
ZETA FACTOR AND STANDARD ERROR (yr cm^2): 282,02 6,88
SIZE OF COUNTER SQUARE (cm^2): 6,39E-07

GRAIN AGES IN ORIGINAL ORDER

Grain no.	RhoS (cm^-2)	(Ns)	RhoI (cm^-2)	(Ni)	Squares	U+/-2s		Grain Age (Ma) Age	--95% CI--	
1	1,25E+05	(4)	6,54E+06	(209)	50	77	11	3.6	0.9	8.9
2	1,13E+05	(6)	5,60E+06	(297)	83	66	8	3.7	1.3	7.9
3	3,26E+05	(10)	8,22E+06	(252)	48	97	12	7.2	3.4	13.3
4	6,71E+05	(12)	1,17E+07	(210)	28	139	19	10.3	5.2	18.2
5	2,24E+05	(8)	2,54E+06	(91)	56	30	6	16.0	6.6	32.2
6	1,17E+05	(3)	5,16E+06	(132)	40	61	11	4.3	0.8	12.1
7	2,85E+05	(4)	1,20E+07	(169)	22	142	22	4.4	1.1	11.0
8	3,48E+04	(2)	5,58E+06	(321)	90	66	8	1.2	0.1	4.1
9	8,94E+04	(4)	8,90E+06	(398)	70	105	11	1.9	0.5	4.6
10	1,83E+05	(7)	8,95E+06	(343)	60	106	12	3.7	1.5	7.6
11	2,39E+05	(11)	8,46E+06	(389)	72	100	10	5.1	2.5	9.1
12	1,30E+05	(5)	9,99E+06	(383)	60	118	12	2.4	0.8	5.5
13	2,30E+05	(5)	1,33E+07	(289)	34	157	19	3.2	1.0	7.3
14	4,12E+05	(10)	7,82E+06	(190)	38	93	14	9.5	4.4	17.7
15	4,17E+05	(16)	1,06E+07	(405)	60	125	13	7.1	4.0	11.6
16	2,01E+05	(9)	4,25E+06	(190)	70	50	7	8.6	3.8	16.4
17	3,83E+05	(22)	9,88E+06	(568)	90	117	10	7.0	4.3	10.6
18	2,71E+05	(13)	7,55E+06	(362)	75	89	10	6.5	3.4	11.1
19	3,07E+05	(11)	1,07E+07	(382)	56	126	13	5.2	2.5	9.3
20	2,35E+05	(12)	5,93E+06	(303)	80	70	8	7.2	3.6	12.5
21	1,39E+05	(8)	3,70E+06	(213)	90	44	6	6.8	2.9	13.5
POOLED	2,24E+05	(182)	7,50E+06	(6096)	1272	89	3	5.3	4.6	6.2

CHI^2 PROBABILITY (%): 0.2
>>> Beware: possible upward bias in Chi^2 probability due to low counts <<<

POOLED AGE W/ 68% CONF. INTERVAL(Ma): 5.3, 4.9 -- 5.8 (-0.4 +0.4)
95% CONF. INTERVAL(Ma): 4.6 -- 6.2 (-0.8 +0.9)

CENTRAL AGE W/ 68% CONF. INTERVAL(Ma): 5.5, 4.9 -- 6.1 (-0.6 +0.6)
95% CONF. INTERVAL(Ma): 4.4 -- 6.8 (-1.1 +1.3)
AGE DISPERSION (%): 33.8

FIT OPTION: Best-fit peaks using the binomial model of Galbraith and Green

INITIAL GUESS FOR MODEL PARAMETERS (number of peaks to fit = 2)

Peak #.	Peak Age	Theta	Fraction(%)	Count
1.	5.30	0.029	22.6	4.74
2.	7.10	0.038	33.0	6.92

Total range for grain ages:	1,4 to 16,6 Ma
Number of active grains (Num. used for fit):	21
Number of removed grains:	0
Degrees of freedom for fit:	18
Average of the SE(Z)'s for the grains:	0,39
Estimated width of peaks in PD plot in Z units:	0,45

PARAMETERS FOR BEST-FIT PEAKS

* *Standard error for peak age includes group error*
* *Peak width is for PD plot assuming a kernel factor = 0.60*

#.	Peak Age(Ma)	68%CI	95%CI	W(Z)	Frac(%)	SE,%	Count
1.	2.6	-0,7 ...+0,9	-1,1 ...+2,0	0.55	28.8	16.2	6.1
2.	6.6	-0,7 ...+0,8	-1,3 ...+1,6	0.37	71.2	16.2	14.9

Log-likelihood for best fit:	-58,234
Chi-squared value for best fit:	24,547
Reduced chi-squared value:	1,364
Probability for F test:	0%
Condition number for COVAR matrix:	12,31
Number of iterations:	17

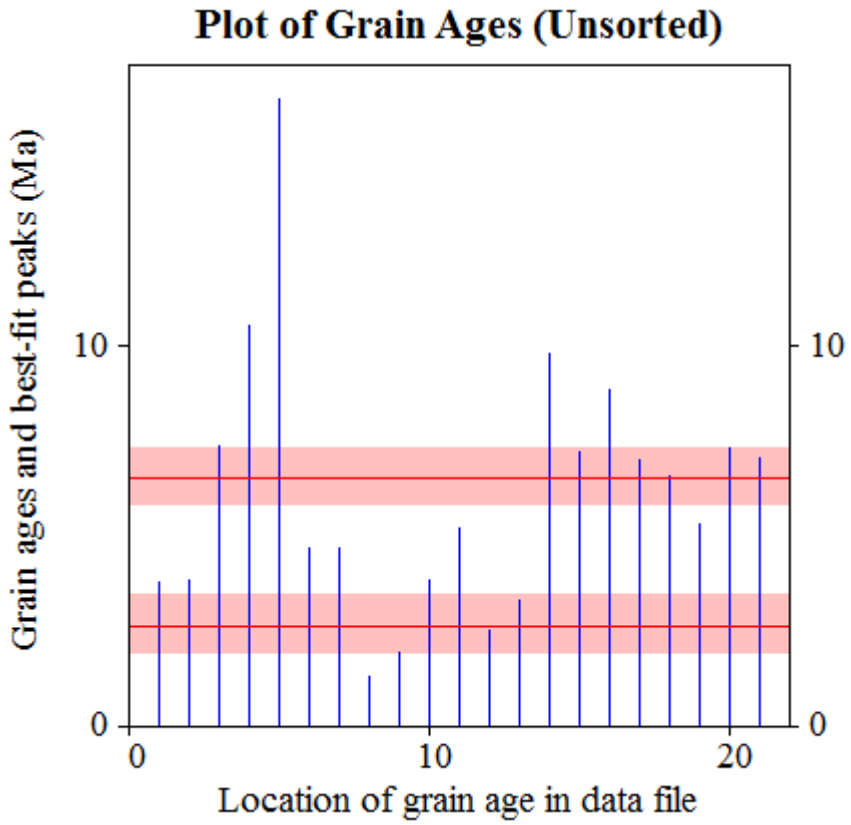
Plot of Grain Ages (Unsorted)
Grain ages and best-fit peaks (Ma)
0
10
0
10
20
Location of grain age in data file

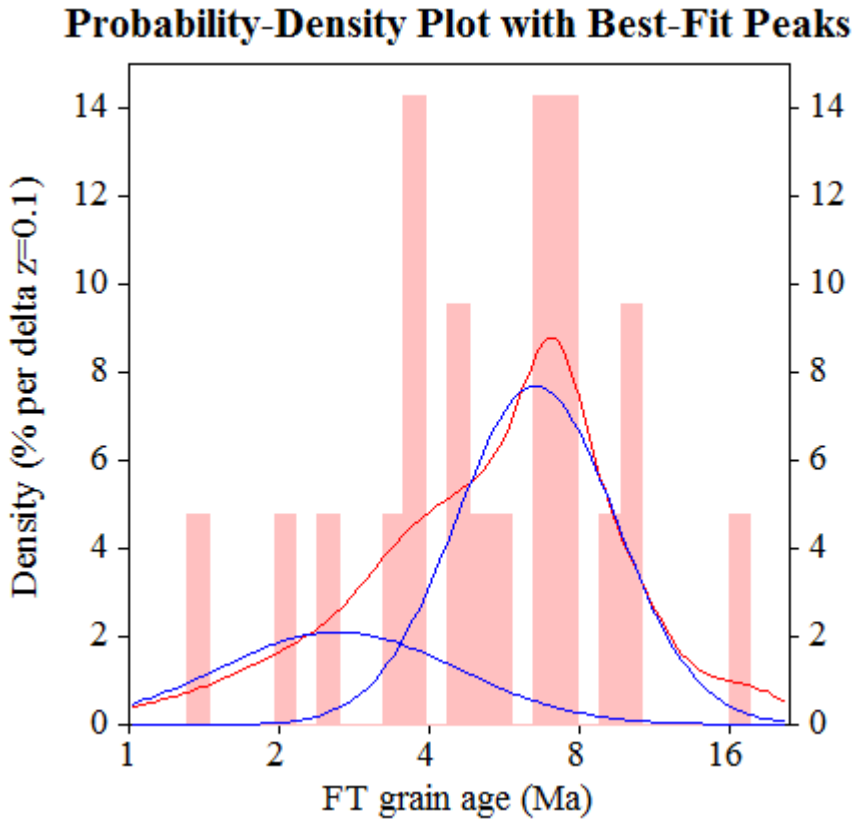
Probability-Density Plot with Best-Fit Peaks
Density (% per delta z=0.1)
0
2
4
6
8
10
12
14
1
2
4
8
16
FT grain age (Ma)

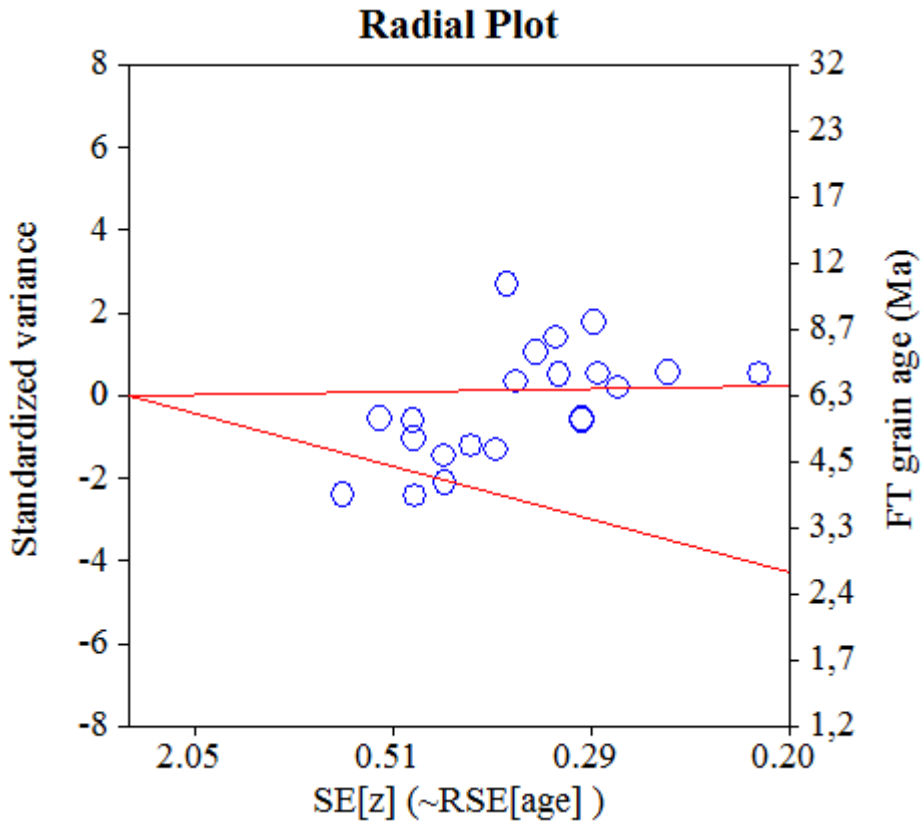
Radial Plot
Standardized variance
8
6
4
2
0
-2
-4
-6
-8
2.05
0.51
0.29
0.20
SE[z] (~RSE[age])
32
23
17
12
8,7
6,3
4,5
3,3
2,4
1,7
1,2
FT grain age (Ma)

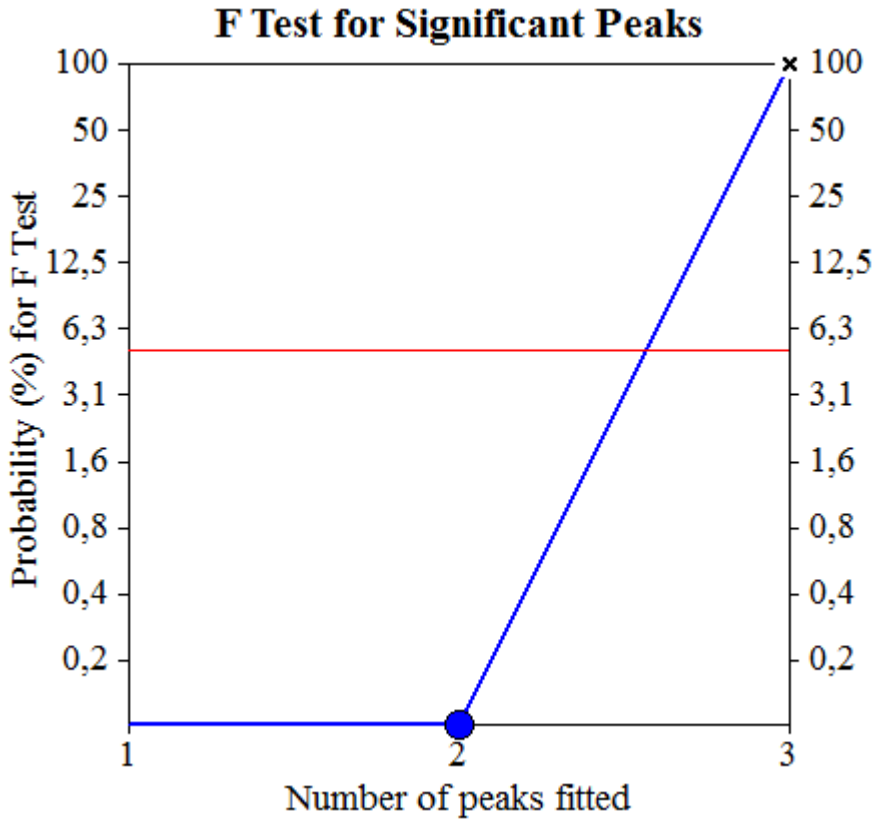
F Test for Significant Peaks
Probability (%) for F Test
100
50
25
12,5
6,3
3,1
1,6
0,8
0,4
0,2
1
2
3
Number of peaks fitted

NEW PARAMETERS - ZETA METHOD

EFFECTIVE TRACK DENSITY FOR FLUENCE MONITOR (tracks/cm^2): 1,26E+06
RELATIVE ERROR (%): 1,13
EFFECTIVE URANIUM CONTENT OF MONITOR (ppm): 15,00
ZETA FACTOR AND STANDARD ERROR (yr cm^2): 282,02 6,88
SIZE OF COUNTER SQUARE (cm^2): 6,39E-07

GRAIN AGES IN ORIGINAL ORDER

Grain no.	RhoS (cm^-2)	(Ns)	RhoI (cm^-2)	(Ni)	Squares	U+/-2s		Grain Age (Ma) Age	--95% CI--	
1	1,45E+05	(5)	8,98E+06	(310)	54	107	12	3.0	0.9	6.8
2	2,85E+05	(8)	1,09E+07	(306)	44	129	15	4.7	2.0	9.3
3	4,35E+05	(5)	9,13E+06	(105)	18	109	21	8.7	2.7	20.4
4	2,74E+05	(7)	1,33E+06	(34)	40	16	5	37.2	13.7	83.5
5	4,35E+05	(5)	1,36E+07	(157)	18	162	26	5.8	1.8	13.5
POOLED	2,70E+05	(30)	8,20E+06	(912)	174	97	7	5.9	3.9	8.4

CHI^2 PROBABILITY (%): 0.0
>>> Beware: possible upward bias in Chi^2 probability due to low counts <<<

POOLED AGE W/ 68% CONF. INTERVAL(Ma): 5.9, 4.8 -- 7.1 (-1.1 +1.3)
95% CONF. INTERVAL(Ma): 3.9 -- 8.4 (-2.0 +2.5)

CENTRAL AGE W/ 68% CONF. INTERVAL(Ma): 9.3, 6.0 -- 14.4 (-3.3 +5.1)
95% CONF. INTERVAL(Ma): 4.0 -- 21.9 (-5.4 +12.5)
AGE DISPERSION (%): 88.3

FIT OPTION: Best-fit peaks using the binomial model of Galbraith and Green

INITIAL GUESS FOR MODEL PARAMETERS (number of peaks to fit = 1)

Peak #.	Peak Age	Theta	Fraction(%)	Count
1.	5.90	0.032	24.5	1.23

Total range for grain ages: 3,2 to 38,6 Ma
Number of active grains (Num. used for fit): 5
Number of removed grains: 0
Degrees of freedom for fit: 4
Average of the SE(Z)'s for the grains: 0,41
Estimated width of peaks in PD plot in Z units: 0,48

PARAMETERS FOR BEST-FIT PEAKS

* *Standard error for peak age includes group error*
* *Peak width is for PD plot assuming a kernel factor = 0.60*

#.	Peak Age(Ma)	68%CI	95%CI	W(Z)	Frac(%)	SE,%	Count
1.	5.9	-1,0 ...+1,2	-1,8 ...+2,6	0.48	100.0	0.0	5.0

Log-likelihood for best fit: -17,538
Chi-squared value for best fit: 29,335
Reduced chi-squared value: 7,334
Probability for F test: 0%
Condition number for COVAR matrix: 1,00
Number of iterations: 5

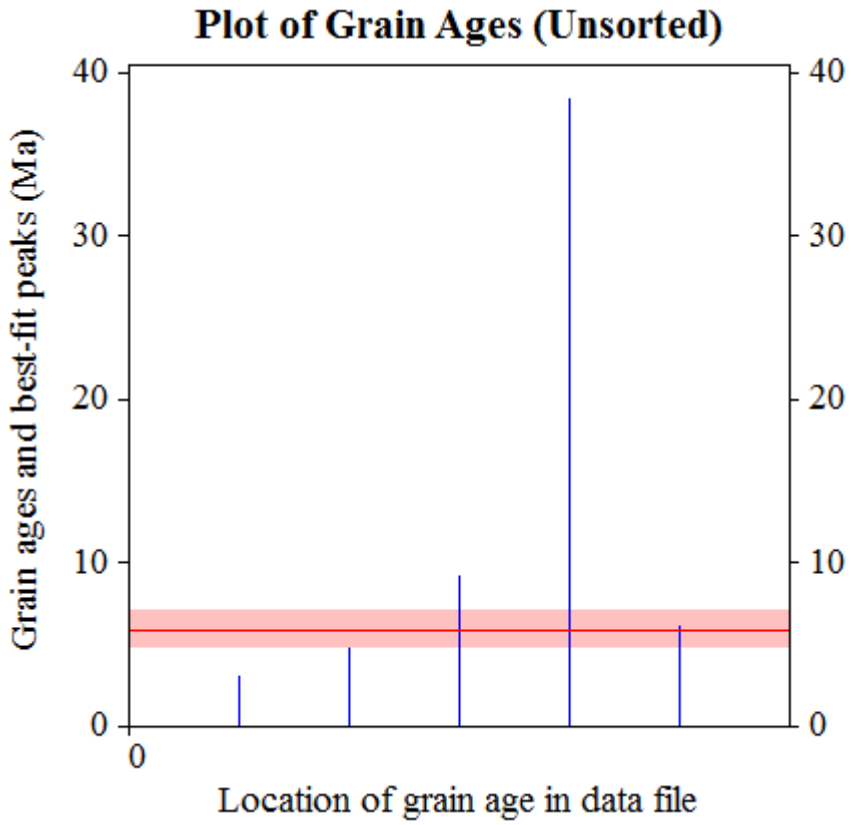
Plot of Grain Ages (Unsorted)
Grain ages and best-fit peaks (Ma)
40
30
20
10
0
0
Location of grain age in data file

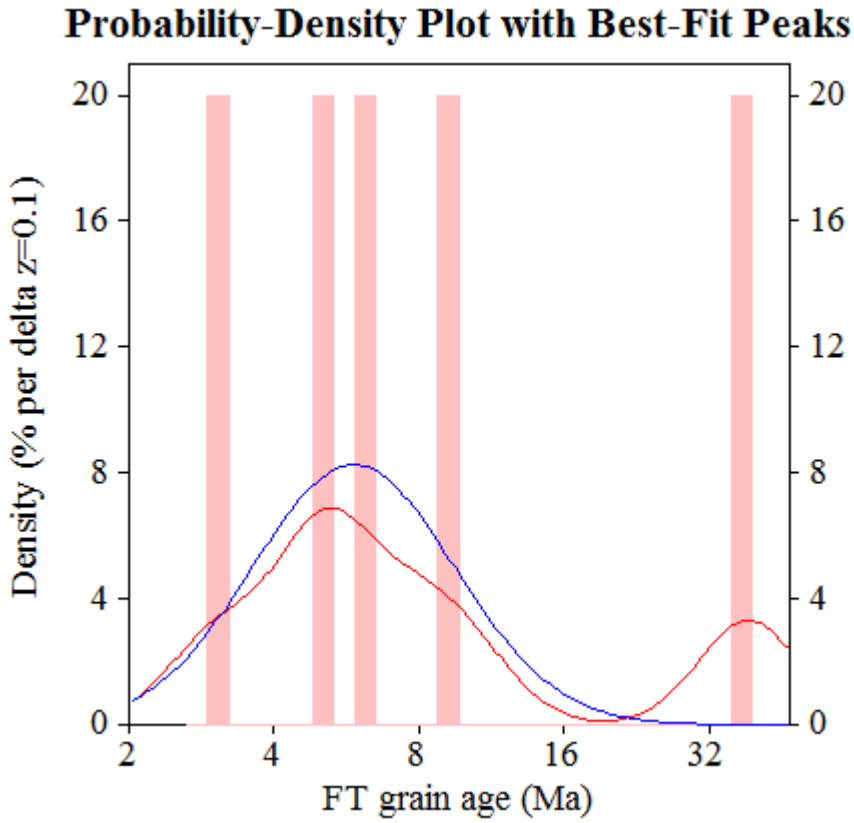
Probability-Density Plot with Best-Fit Peaks
Density (% per delta z=0.1)
20
16
12
8
4
0
2
4
8
16
32
FT grain age (Ma)

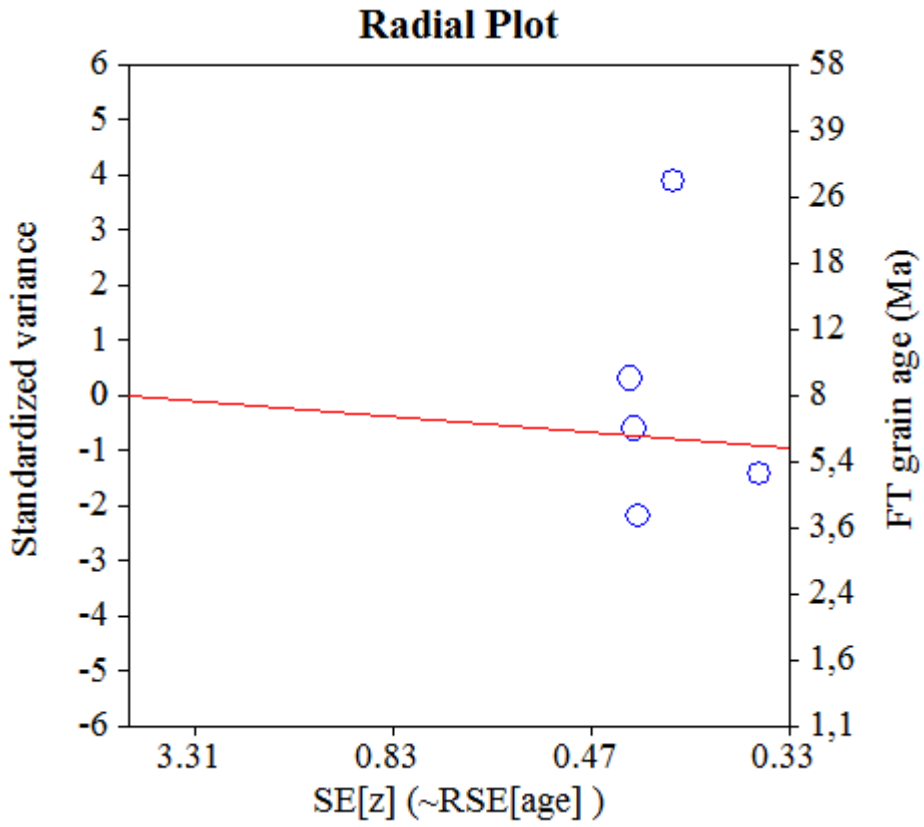
Radial Plot
Standardized variance
6
5
4
3
2
1
0
-1
-2
-3
-4
-5
-6
FT grain age (Ma)
58
39
26
18
12
8
5,4
3,6
2,4
1,6
1,1
3.31
0.83
0.47
0.33
SE[z] (~RSE[age])

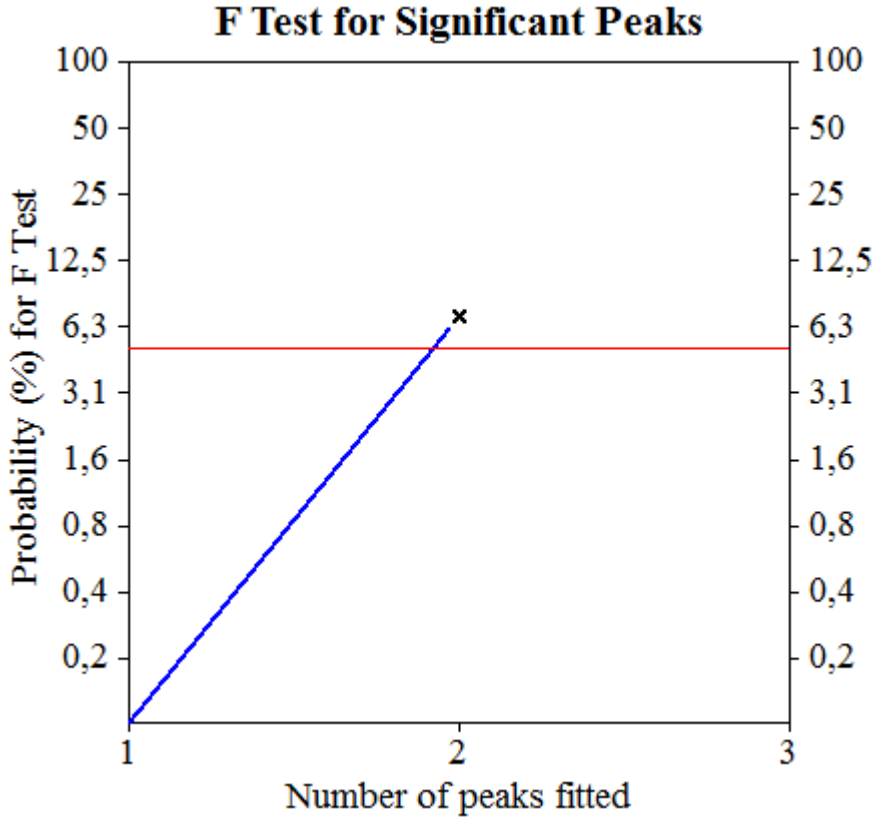
F Test for Significant Peaks
Probability (%) for F Test
100
50
25
12,5
6,3
3,1
1,6
0,8
0,4
0,2
1
2
3
Number of peaks fitted

NEW PARAMETERS - ZETA METHOD

EFFECTIVE TRACK DENSITY FOR FLUENCE MONITOR (tracks/cm^2): 1,26E+06
RELATIVE ERROR (%): 1,15
EFFECTIVE URANIUM CONTENT OF MONITOR (ppm): 15,00
ZETA FACTOR AND STANDARD ERROR (yr cm^2): 282,02 6,88
SIZE OF COUNTER SQUARE (cm^2): 6,39E-07

GRAIN AGES IN ORIGINAL ORDER

Grain no.	RhoS (cm^-2)	(Ns)	RhoI (cm^-2)	(Ni)	Squares	U+/-2s		Grain Age (Ma) Age	--95% CI--	
1	3,80E+05	(17)	1,35E+07	(602)	70	160	14	5.1	2.9	8.1
2	3,35E+05	(15)	1,15E+07	(513)	70	137	12	5.2	2.9	8.6
3	9,27E+05	(16)	1,68E+07	(289)	27	200	24	9.9	5.5	16.2
4	6,99E+05	(21)	1,54E+07	(462)	47	183	18	8.1	4.9	12.5
5	3,56E+05	(15)	1,23E+07	(519)	66	147	13	5.2	2.8	8.5
6	5,87E+05	(15)	1,26E+07	(321)	40	150	17	8.4	4.6	13.9
7	9,91E+05	(19)	1,32E+07	(253)	30	157	20	13.4	7.9	21.2
8	3,39E+05	(13)	1,67E+07	(642)	60	200	16	3.6	1.9	6.2
9	5,32E+05	(17)	1,35E+07	(431)	50	161	16	7.1	4.0	11.3
10	2,35E+05	(9)	6,96E+06	(267)	60	83	10	6.1	2.7	11.5
11	7,04E+05	(27)	1,35E+07	(517)	60	161	15	9.3	6.0	13.6
12	3,13E+05	(12)	6,68E+06	(256)	60	80	10	8.4	4.2	14.8
13	4,69E+05	(15)	1,76E+07	(563)	50	210	18	4.8	2.6	7.9
14	4,30E+05	(11)	1,12E+07	(285)	40	133	16	6.9	3.4	12.4
15	2,01E+05	(5)	1,80E+07	(448)	39	214	21	2.0	0.6	4.7
16	3,65E+05	(14)	6,29E+06	(241)	60	75	10	10.4	5.5	17.6
17	1,96E+05	(5)	2,07E+07	(529)	40	247	22	1.7	0.5	3.9
18	5,48E+05	(14)	7,82E+06	(200)	40	93	13	12.5	6.7	21.3
19	5,01E+05	(16)	1,52E+07	(486)	50	181	17	5.9	3.3	9.6
20	2,91E+05	(13)	3,98E+06	(178)	70	47	7	13.1	6.8	22.7
21	6,57E+05	(21)	1,20E+07	(384)	50	143	15	9.8	5.9	15.0
22	7,82E+05	(20)	1,19E+07	(303)	40	141	17	11.8	7.0	18.4
23	1,56E+05	(4)	6,22E+06	(159)	40	74	12	4.6	1.2	11.6
24	2,04E+05	(9)	7,42E+06	(327)	69	88	10	5.0	2.2	9.4
POOLED	4,37E+05	(343)	1,17E+07	(9175)	1228	139	4	6.6	5.9	7.5

CHI^2 PROBABILITY (%): 0.0

POOLED AGE W/ 68% CONF. INTERVAL(Ma): 6.6, 6.2 -- 7.0 (-0.4 +0.4)
95% CONF. INTERVAL(Ma): 5.9 -- 7.5 (-0.7 +0.8)

CENTRAL AGE W/ 68% CONF. INTERVAL(Ma): 7.0, 6.4 -- 7.7 (-0.6 +0.7)
95% CONF. INTERVAL(Ma): 5.8 -- 8.5 (-1.2 +1.4)
AGE DISPERSION (%): 35.3

FIT OPTION: Best-fit peaks using the binomial model of Galbraith and Green

INITIAL GUESS FOR MODEL PARAMETERS (number of peaks to fit = 2)

Peak #.	Peak Age	Theta	Fraction(%)	Count
1.	6.60	0.036	24.1	5.79
2.	13.20	0.069	18.7	4.48

Total range for grain ages:	1,8 to 13,6 Ma
Number of active grains (Num. used for fit):	24
Number of removed grains:	0
Degrees of freedom for fit:	21
Average of the SE(Z)'s for the grains:	0,29
Estimated width of peaks in PD plot in Z units:	0,34

PARAMETERS FOR BEST-FIT PEAKS

* *Standard error for peak age includes group error*
* *Peak width is for PD plot assuming a kernel factor = 0.60*

#.	Peak Age(Ma)	68%CI	95%CI	W(Z)	Frac(%)	SE,%	Count
1.	4.4	-0,5 ...+0,6	-0,9 ...+1,2	0.35	44.6	13.8	10.7
2.	9.2	-0,9 ...+1,0	-1,6 ...+2,0	0.29	55.4	13.8	13.3

Log-likelihood for best fit:	-78,160
Chi-squared value for best fit:	25,525
Reduced chi-squared value:	1,215
Probability for F test:	0%
Condition number for COVAR matrix:	4,25
Number of iterations:	14

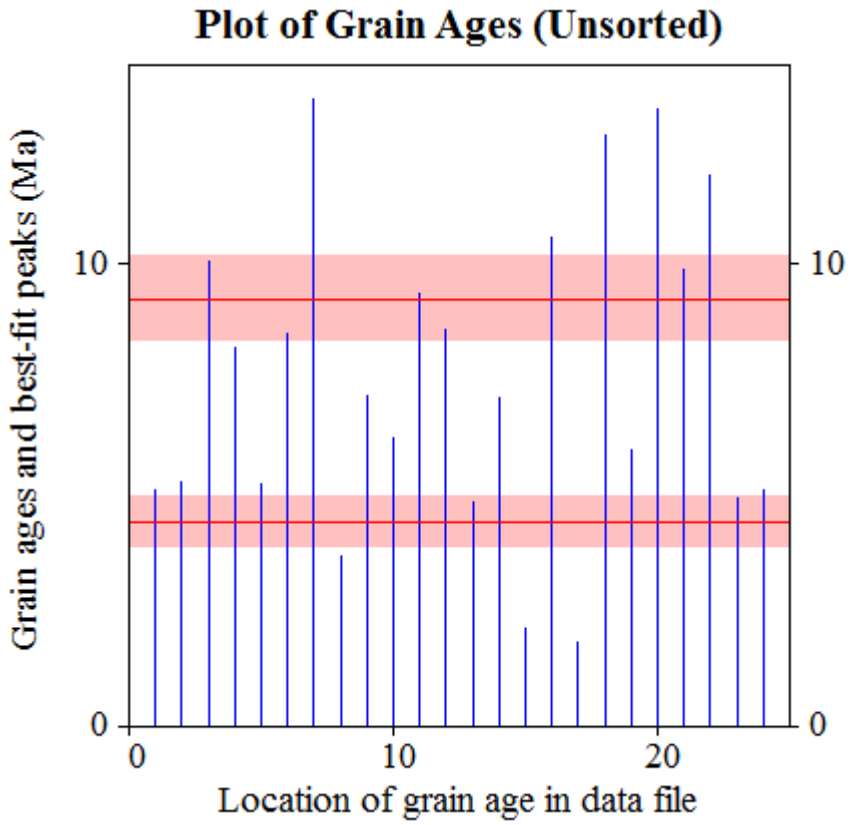
Plot of Grain Ages (Unsorted)
Grain ages and best-fit peaks (Ma)
10
0
0
10
20
Location of grain age in data file

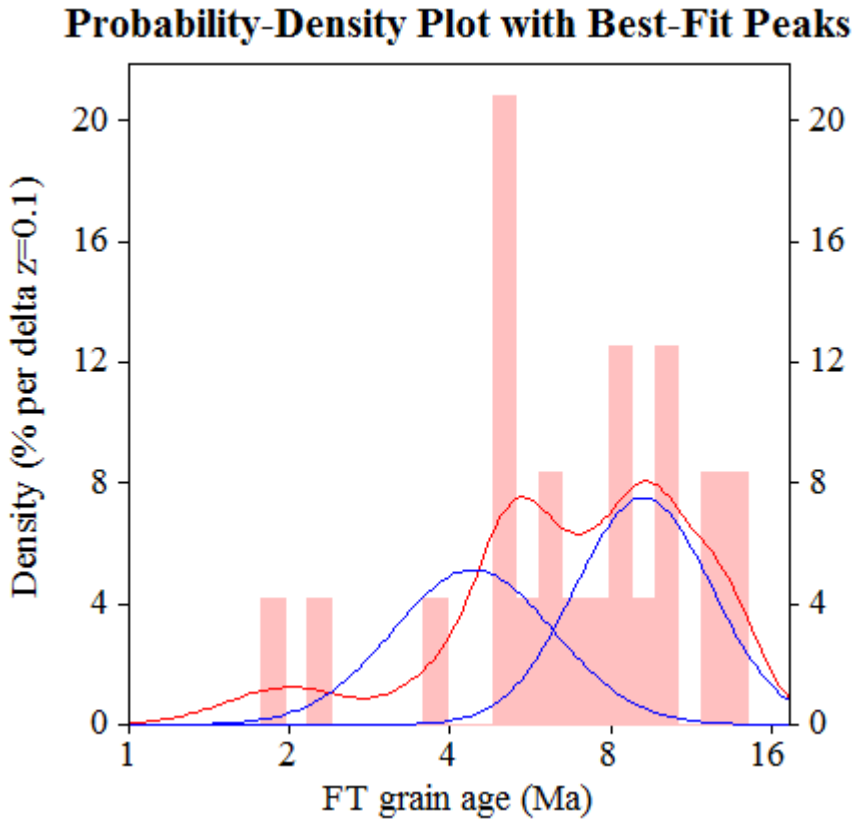
Probability-Density Plot with Best-Fit Peaks
Density (% per delta z=0.1)
20
16
12
8
4
0
1
2
4
8
16
FT grain age (Ma)

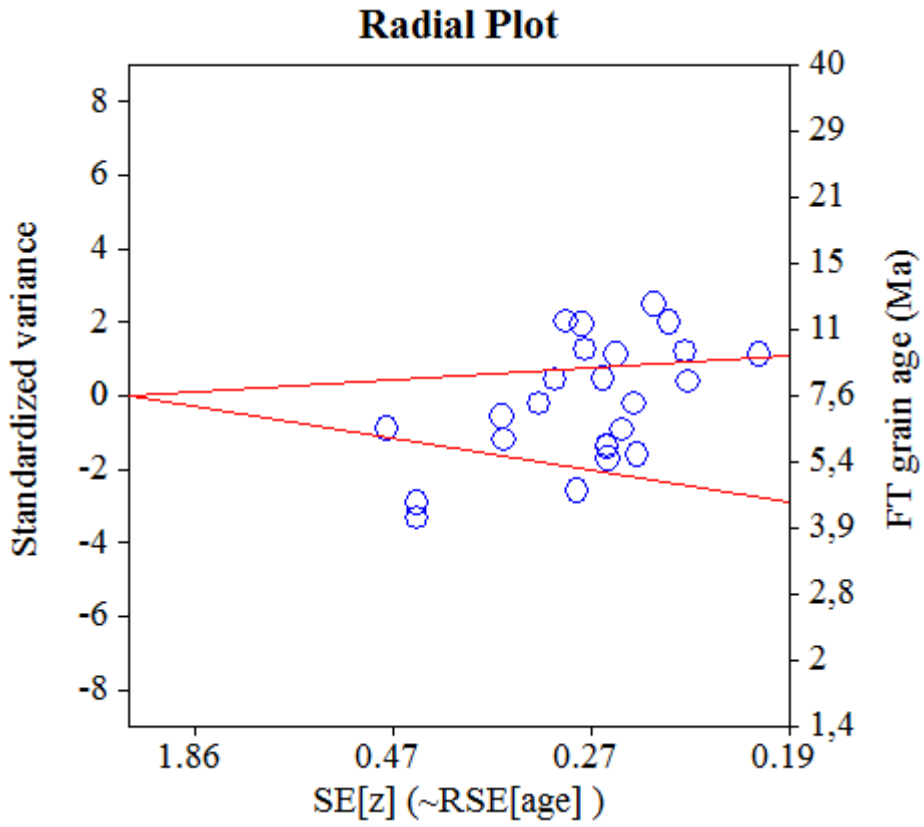
Radial Plot
Standardized variance
8
6
4
2
0
-2
-4
-6
-8
40
29
21
15
11
7,6
5,4
3,9
2,8
2
1,4
FT grain age (Ma)
1.86
0.47
0.27
0.19
SE[z] (~RSE[age])

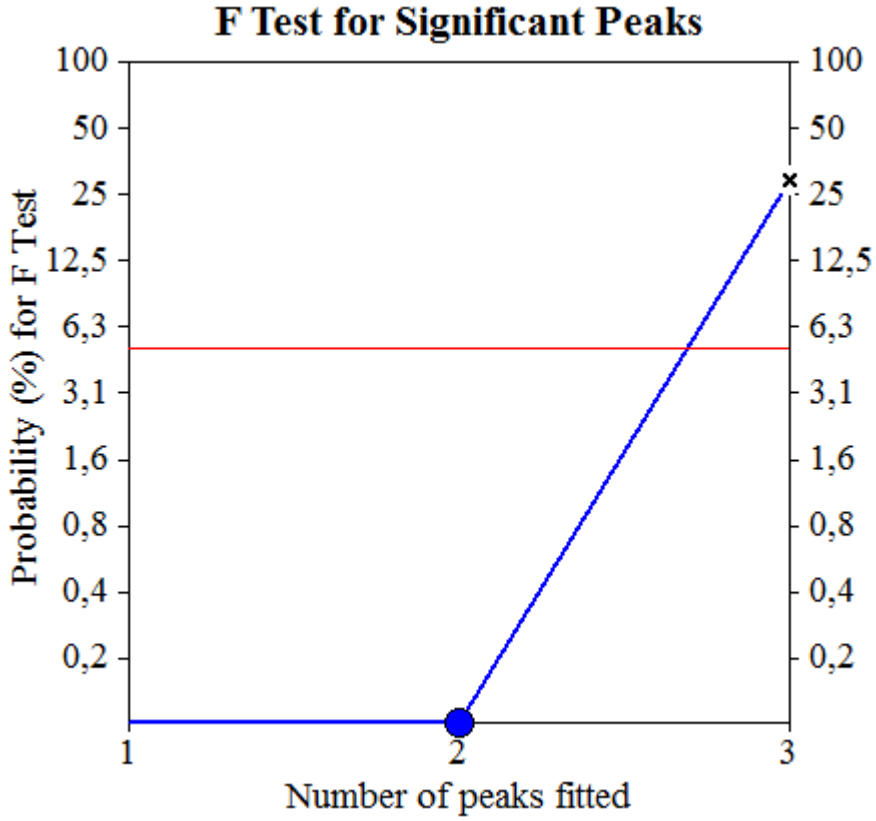
F Test for Significant Peaks
Probability (%) for F Test
100
50
25
12,5
6,3
3,1
1,6
0,8
0,4
0,2
1
2
3
Number of peaks fitted

Datafile: C:\BH2\Jairo\Echantillon-IRR082015\JG-P5-03\JG-P5-03-Ap.ftz
Title: JG-P5-03 Irr 8-2015-25

NEW PARAMETERS - ZETA METHOD

EFFECTIVE TRACK DENSITY FOR FLUENCE MONITOR (tracks/cm^2): 1,32E+06
RELATIVE ERROR (%): 1,47
EFFECTIVE URANIUM CONTENT OF MONITOR (ppm): 15,00
ZETA FACTOR AND STANDARD ERROR (yr cm^2): 282,02 6,88
SIZE OF COUNTER SQUARE (cm^2): 6,39E-07

GRAIN AGES IN ORIGINAL ORDER

Grain no.	RhoS (cm^-2)	(Ns)	RhoI (cm^-2)	(Ni)	Squares	U+/-2s		Grain Age (Ma) Age	--95% CI--	
1	2,97E+05	(19)	1,19E+07	(763)	100	135	11	4.7	2.8	7.3
2	1,25E+05	(8)	2,50E+06	(160)	100	28	5	9.5	4.0	18.8
3	2,66E+05	(17)	5,52E+06	(353)	100	63	7	9.1	5.2	14.6
4	4,23E+05	(27)	6,38E+06	(408)	100	72	7	12.4	8.0	18.2
5	2,97E+05	(19)	6,84E+06	(437)	100	78	8	8.2	4.8	12.8
6	2,35E+05	(15)	8,23E+06	(526)	100	93	9	5.4	3.0	8.9
7	2,36E+05	(14)	9,88E+06	(587)	93	112	10	4.5	2.4	7.5
8	3,25E+05	(11)	1,80E+07	(609)	53	204	18	3.4	1.7	6.1
9	1,41E+05	(9)	1,03E+07	(657)	100	117	10	2.6	1.2	4.9
10	1,74E+05	(11)	1,12E+07	(709)	99	127	10	2.9	1.4	5.2
POOLED	2,48E+05	(150)	8,63E+06	(5209)	945	98	4	5.4	4.5	6.4

CHI^2 PROBABILITY (%): 0.0
>>> Beware: possible upward bias in Chi^2 probability due to low counts <<<

POOLED AGE W/ 68% CONF. INTERVAL(Ma): 5.4, 4.9 -- 5.9 (-0.4 +0.5)
95% CONF. INTERVAL(Ma): 4.5 -- 6.4 (-0.8 +1.0)

CENTRAL AGE W/ 68% CONF. INTERVAL(Ma): 5.9, 5.0 -- 6.9 (-0.9 +1.1)
95% CONF. INTERVAL(Ma): 4.3 -- 8.1 (-1.6 +2.2)
AGE DISPERSION (%): 43.9

FIT OPTION: Best-fit peaks using the binomial model of Galbraith and Green

INITIAL GUESS FOR MODEL PARAMETERS (number of peaks to fit = 2)

Peak #.	Peak Age	Theta	Fraction(%)	Count
1.	2.70	0.014	17.3	1.73
2.	5.40	0.028	23.7	2.37

Total range for grain ages: 2,7 to 12,5 Ma
Number of active grains (Num. used for fit): 10
Number of removed grains: 0
Degrees of freedom for fit: 7
Average of the SE(Z)'s for the grains: 0,27
Estimated width of peaks in PD plot in Z units: 0,32

PARAMETERS FOR BEST-FIT PEAKS

* *Standard error for peak age includes group error*
* *Peak width is for PD plot assuming a kernel factor = 0.60*

#.	Peak Age(Ma)	68%CI	95%CI	W(Z)	Frac(%)	SE,%	Count
1.	3.9	-0,4 ...+0,5	-0,8 ...+1,1	0.33	61.4	16.3	6.1
2.	9.7	-1,2 ...+1,4	-2,2 ...+2,9	0.28	38.6	16.3	3.9

Log-likelihood for best fit: -32,410
Chi-squared value for best fit: 8,998
Reduced chi-squared value: 1,285
Probability for F test: 0%
Condition number for COVAR matrix: 1,97
Number of iterations: 11

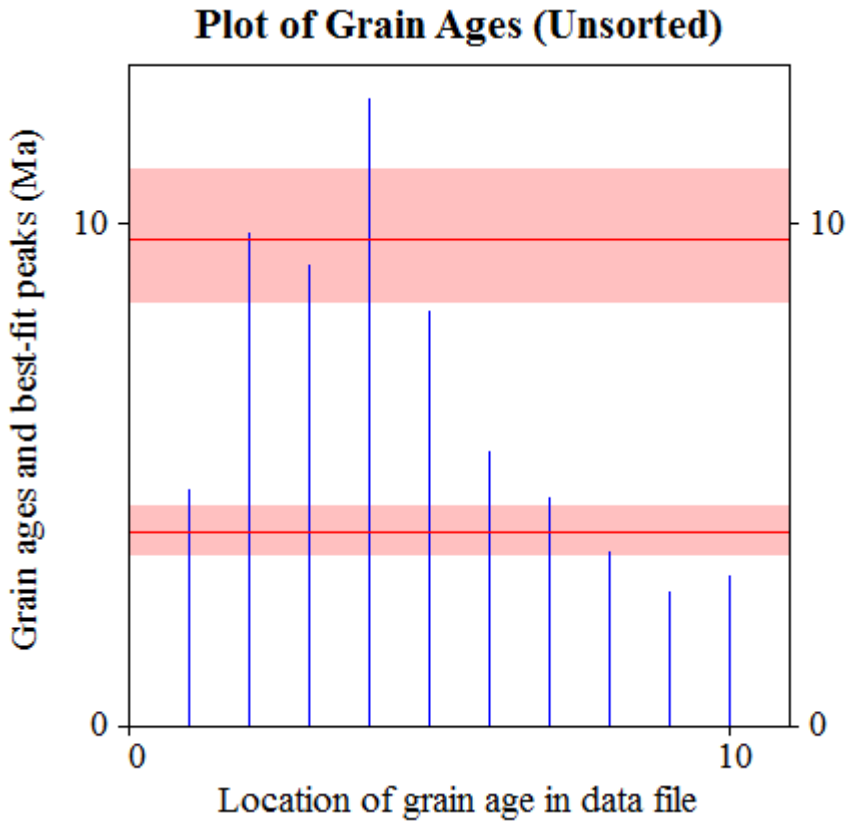
Plot of Grain Ages (Unsorted)
Grain ages and best-fit peaks (Ma)
10
0
0
10
Location of grain age in data file

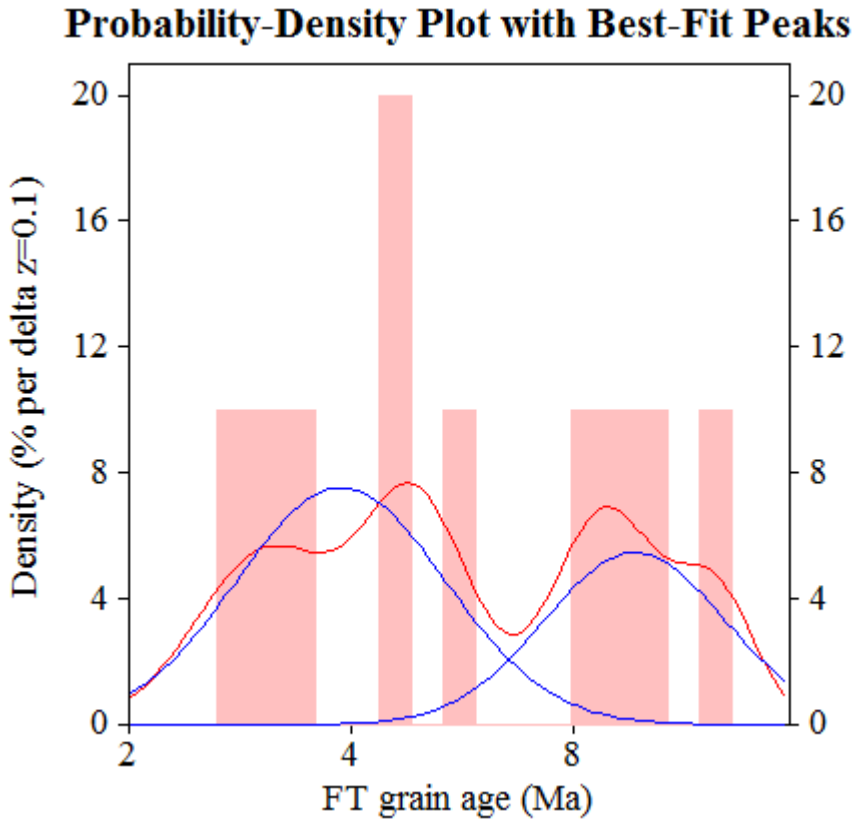
Probability-Density Plot with Best-Fit Peaks
Density (% per delta z=0.1)
20
16
12
8
4
0
2
4
8
FT grain age (Ma)

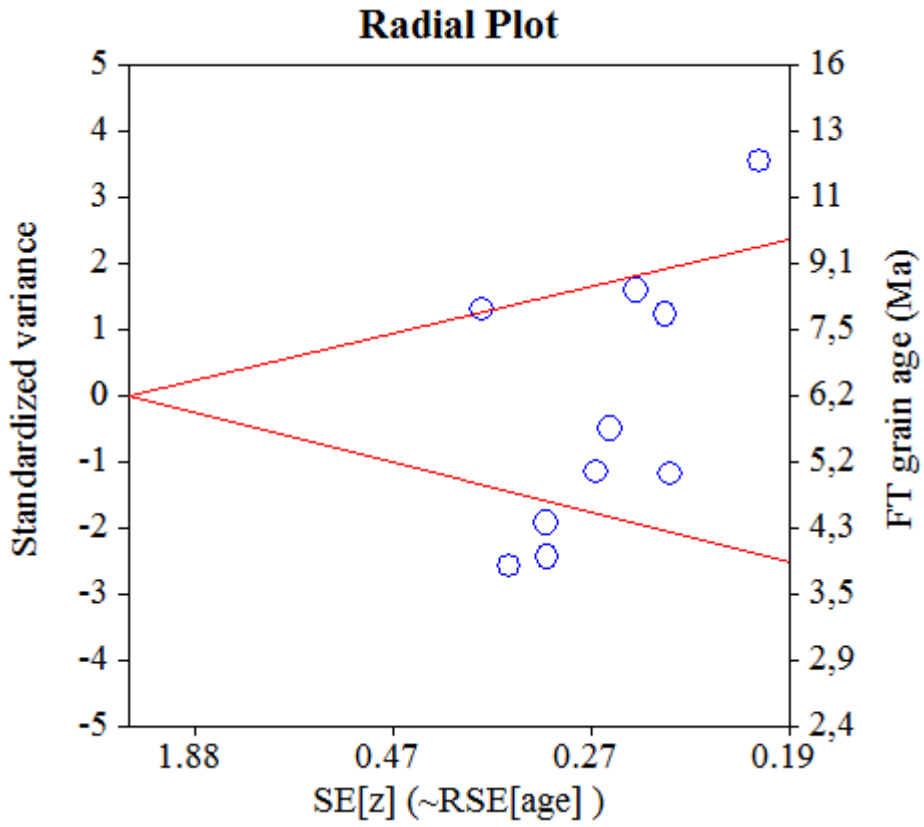
Radial Plot
Standardized variance
5
4
3
2
1
0
-1
-2
-3
-4
-5
16
13
11
9,1
7,5
6,2
5,2
4,3
3,5
2,9
2,4
FT grain age (Ma)
1.88
0.47
0.27
0.19
SE[z] (~RSE[age])

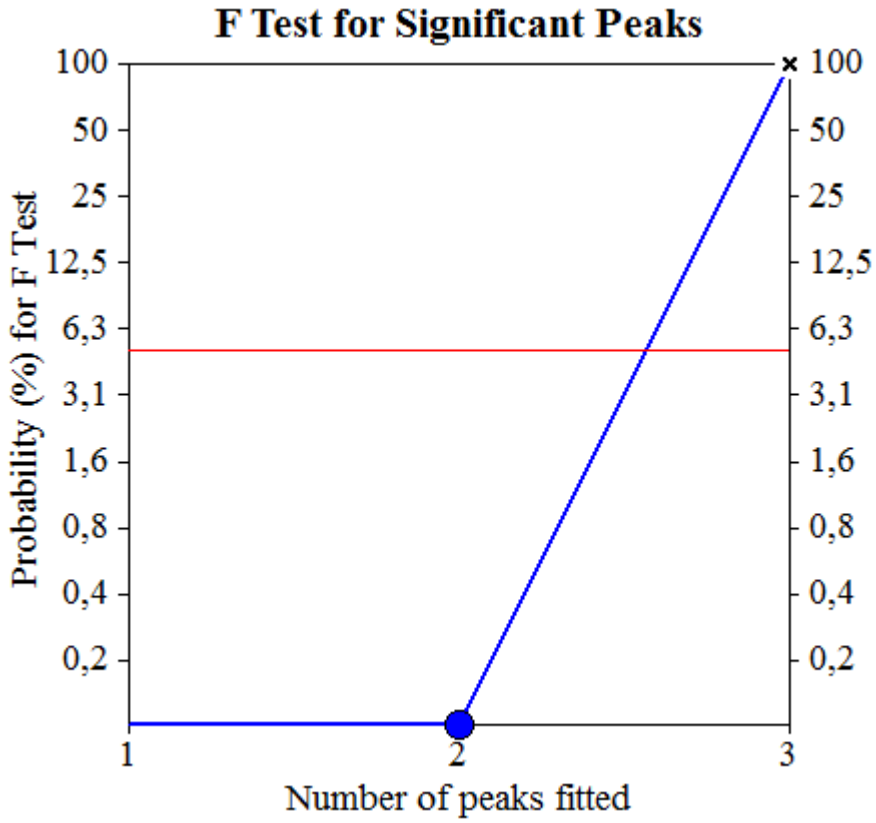
F Test for Significant Peaks
Probability (%) for F Test
100
50
25
12,5
6,3
3,1
1,6
0,8
0,4
0,2
1
2
3
Number of peaks fitted

Datafile: C:\BH2\Jairo\Echantillon-IRR-10-2015\JG-P4-19Zr\JG-P3-19.ftz
Title: Sample No. JG P3 19 Irr 10-2015-50

NEW PARAMETERS - ZETA METHOD

EFFECTIVE TRACK DENSITY FOR FLUENCE MONITOR (tracks/cm^2): 3,92E+05
RELATIVE ERROR (%): 1,35
EFFECTIVE URANIUM CONTENT OF MONITOR (ppm): 50,00
ZETA FACTOR AND STANDARD ERROR (yr cm^2): 137,14 1,57
SIZE OF COUNTER SQUARE (cm^2): 8,30E-07

GRAIN AGES IN ORIGINAL ORDER

Grain no.	RhoS (cm^-2)	(Ns)	RhoI (cm^-2)	(Ni)	Squares	U+/-2s		Grain Age (Ma) Age	--95% CI--	
1	3,83E+06	(140)	1,37E+06	(50)	44	175	49	74.6	53.8	105.3
2	3,98E+06	(198)	7,43E+05	(37)	60	95	31	141.6	99.9	207.0
3	3,86E+06	(128)	7,23E+05	(24)	40	92	37	140.9	91.4	227.9
4	1,95E+06	(115)	8,31E+05	(49)	71	106	30	62.6	44.5	89.4
5	3,55E+06	(295)	5,78E+05	(48)	100	74	21	162.5	120.1	225.2
6	2,89E+06	(144)	5,22E+05	(26)	60	67	26	146.3	96.7	231.4
7	3,93E+06	(326)	5,90E+05	(49)	100	75	22	175.8	130.5	242.2
8	4,16E+06	(276)	6,48E+05	(43)	80	83	25	169.6	123.3	239.4
9	1,73E+06	(115)	3,31E+05	(22)	80	42	18	138.1	87.8	228.8
10	3,55E+06	(206)	8,61E+05	(50)	70	110	31	109.5	80.3	152.3
11	5,55E+06	(461)	1,11E+06	(92)	100	141	30	132.5	105.9	165.7
12	5,23E+06	(217)	1,20E+06	(50)	50	154	43	115.2	84.7	160.1
13	6,43E+06	(267)	2,02E+06	(84)	50	258	57	84.3	66.0	107.8
14	7,56E+06	(251)	1,57E+06	(52)	40	200	55	128.0	95.0	176.1
15	7,83E+06	(455)	1,33E+06	(77)	70	169	39	155.8	122.5	198.1
16	3,27E+06	(163)	3,82E+05	(19)	60	49	22	224.7	141.2	381.4
17	5,77E+06	(115)	1,36E+06	(27)	24	173	66	112.9	74.2	178.7
18	5,08E+06	(135)	7,53E+05	(20)	32	96	43	177.6	111.8	299.4
19	4,00E+06	(199)	7,43E+05	(37)	60	95	31	142.4	100.4	208.0
20	1,30E+07	(140)	1,76E+06	(19)	13	225	102	193.5	120.9	330.2
21	7,81E+06	(227)	1,41E+06	(41)	35	180	56	146.5	105.3	209.6
22	7,68E+06	(204)	1,28E+06	(34)	32	163	56	158.5	110.6	235.0
23	4,60E+06	(206)	1,12E+06	(50)	54	142	40	109.5	80.3	152.3
24	3,96E+06	(329)	9,16E+05	(76)	100	117	27	114.5	89.2	146.8
25	4,38E+06	(291)	5,27E+05	(35)	80	67	23	218.6	154.9	319.2
26	7,06E+06	(293)	1,25E+06	(52)	50	160	44	149.2	111.3	204.4
27	4,98E+06	(331)	9,49E+05	(63)	80	121	31	138.5	105.9	181.0
28	5,98E+06	(248)	1,30E+06	(54)	50	166	45	121.9	90.8	166.8
29	5,16E+06	(257)	9,04E+05	(45)	60	115	34	151.2	110.3	212.2
30	5,99E+06	(179)	5,69E+05	(17)	36	73	35	274.4	169.4	478.5
31	4,94E+06	(164)	1,02E+06	(34)	40	131	45	127.8	88.4	190.7
32	7,69E+06	(383)	1,73E+06	(86)	60	220	48	117.9	93.3	148.8
33	6,49E+06	(323)	1,16E+06	(58)	60	149	39	146.6	111.1	193.4
34	4,28E+06	(284)	7,53E+05	(50)	80	96	27	150.4	111.5	207.3
35	2,50E+06	(54)	4,17E+05	(9)	26	53	35	156.8	78.4	361.2
36	4,24E+06	(211)	1,85E+06	(92)	60	236	49	61.0	47.7	78.0
37	5,56E+06	(166)	2,18E+06	(65)	36	278	69	67.7	50.9	90.2
38	5,55E+06	(129)	1,12E+06	(26)	28	143	56	131.2	86.3	208.5
39	4,71E+06	(313)	1,10E+06	(73)	80	140	33	113.4	87.9	146.2
40	2,49E+06	(124)	6,22E+05	(31)	60	79	28	106.1	71.5	162.9
41	1,06E+07	(247)	1,76E+06	(41)	28	225	70	159.3	114.7	227.3
42	5,25E+06	(183)	1,06E+06	(37)	42	135	44	131.0	92.1	191.9
43	4,44E+06	(258)	8,95E+05	(52)	70	114	32	131.6	97.7	180.8
44	5,18E+06	(301)	9,29E+05	(54)	70	119	32	146.7	110.0	195.4
45	3,20E+06	(133)	5,54E+05	(23)	50	71	29	152.6	98.4	248.8
46	9,94E+05	(33)	2,41E+05	(8)	40	31	21	108.2	50.0	272.0
47	4,46E+06	(185)	7,23E+05	(30)	50	92	34	162.8	111.1	247.9
48	3,45E+06	(286)	3,98E+05	(33)	100	51	18	227.7	159.8	336.1
49	3,99E+06	(159)	6,53E+05	(26)	48	83	32	161.4	107.0	254.3
50	7,35E+06	(610)	8,07E+05	(67)	100	103	25	238.3	185.6	305.5
51	4,79E+06	(171)	9,81E+05	(35)	43	125	42	129.4	90.1	191.9
52	5,12E+06	(153)	1,27E+06	(38)	36	162	53	106.9	74.9	156.9
53	4,63E+06	(192)	8,19E+05	(34)	50	105	36	149.3	104.0	221.7

Datafile: C:\BH2\Jairo\Echantillon-IRR-10-2015\JG-P4-19Zr\JG-P3-19.ftz
Title: Sample No. JG P3 19 Irr 10-2015-50

Grain no.	RhoS (cm^-2)	(Ns)	RhoI (cm^-2)	(Ni)	Squares	U+/-2s		Grain Age (Ma) Age	--95% CI--	
54	2,84E+06	(118)	1,08E+06	(45)	50	138	41	69.9	49.3	100.9
55	3,64E+06	(121)	6,63E+05	(22)	40	85	36	145.2	92.5	240.1
56	4,94E+06	(123)	8,43E+05	(21)	30	108	47	154.4	97.7	258.2
57	5,94E+06	(276)	1,74E+06	(81)	56	222	50	90.3	70.5	115.7
58	3,73E+06	(248)	1,25E+06	(83)	80	160	35	79.3	61.8	101.7
59	5,47E+06	(454)	7,83E+05	(65)	100	100	25	183.5	141.8	237.4
60	7,17E+06	(238)	1,30E+06	(43)	40	165	50	146.5	106.1	207.7
61	5,62E+06	(280)	1,55E+06	(77)	60	197	45	96.3	74.9	123.9
62	5,83E+06	(266)	1,27E+06	(58)	55	162	43	121.0	91.2	160.4
63	5,22E+06	(390)	1,45E+06	(108)	90	185	36	95.8	77.4	118.7
64	1,91E+06	(95)	2,81E+05	(14)	60	36	19	178.0	102.6	337.3
65	2,68E+06	(89)	1,11E+06	(37)	40	142	47	64.1	43.4	96.9
66	3,25E+06	(162)	7,63E+05	(38)	60	97	32	113.1	79.4	165.7
67	5,03E+06	(167)	9,64E+05	(32)	40	123	43	138.1	94.8	208.3
68	6,51E+06	(324)	1,22E+06	(61)	60	156	40	140.0	106.6	183.6
69	5,02E+06	(200)	8,03E+05	(32)	48	103	36	165.0	114.0	247.5
70	5,40E+06	(251)	7,53E+05	(35)	56	96	32	189.0	133.3	277.0
71	2,89E+06	(120)	6,27E+05	(26)	50	80	31	122.2	80.0	194.6
72	5,88E+06	(293)	1,41E+06	(70)	60	179	43	110.7	85.3	143.5
73	5,18E+06	(172)	8,73E+05	(29)	40	112	41	156.6	106.1	240.7
74	6,33E+06	(368)	1,86E+06	(108)	70	237	46	90.5	72.9	112.2
75	6,27E+06	(260)	9,88E+05	(41)	50	126	39	167.6	120.9	238.7
76	5,36E+06	(267)	1,61E+06	(80)	60	205	46	88.5	68.9	113.6
77	2,79E+06	(81)	2,41E+05	(7)	35	31	22	297.4	142.5	752.3
78	4,67E+05	(31)	3,31E+05	(22)	80	42	18	37.7	21.2	68.3
79	5,35E+06	(213)	1,33E+06	(53)	48	170	47	106.8	79.0	147.2
80	4,08E+06	(339)	1,13E+06	(94)	100	145	30	95.7	76.1	120.2
81	4,73E+06	(314)	2,58E+06	(171)	80	329	51	49.0	40.6	59.2
82	5,58E+06	(139)	1,73E+06	(43)	30	220	67	86.0	60.9	124.2
83	3,82E+06	(111)	1,07E+06	(31)	35	136	49	95.1	63.7	146.7
84	5,46E+06	(317)	1,62E+06	(94)	70	207	43	89.5	71.0	112.7
85	4,40E+06	(146)	6,93E+05	(23)	40	88	37	167.3	108.3	271.8
86	2,95E+06	(98)	1,27E+06	(42)	40	161	50	62.2	43.1	91.7
87	3,21E+06	(160)	7,03E+05	(35)	60	90	30	121.2	84.1	180.1
88	6,31E+06	(314)	1,57E+06	(78)	60	200	45	106.6	83.2	136.5
89	7,44E+06	(216)	9,64E+05	(28)	35	123	46	202.9	137.8	311.8
90	6,55E+06	(272)	1,30E+06	(54)	50	166	45	132.7	99.3	177.2
91	7,83E+06	(455)	1,46E+06	(85)	70	187	41	141.4	112.2	178.1
92	7,69E+06	(319)	1,49E+06	(62)	50	191	49	135.7	103.5	177.7
93	8,52E+06	(283)	1,48E+06	(49)	40	188	54	152.9	113.1	211.4
94	6,77E+06	(281)	1,01E+06	(42)	50	129	40	176.7	128.2	250.2
95	5,98E+06	(298)	1,29E+06	(64)	60	164	41	122.9	93.9	160.8
96	3,11E+06	(129)	1,06E+06	(44)	50	135	41	78.1	55.2	112.7
97	4,46E+06	(259)	1,15E+06	(67)	70	147	36	102.3	78.2	133.6
98	4,58E+06	(228)	5,62E+05	(28)	60	72	27	214.0	145.5	328.3
99	6,65E+06	(524)	1,51E+06	(119)	95	193	36	116.7	95.6	142.5
100	7,43E+06	(370)	1,16E+06	(58)	60	149	39	167.7	127.4	220.5
101	7,14E+06	(474)	1,07E+06	(71)	80	136	32	175.7	137.1	224.9
102	3,20E+06	(117)	1,07E+06	(39)	44	136	44	79.9	55.4	118.0
POOLED	4,91E+06	(23743)	1,05E+06	(5053)	5825	133	5	125.0	119.4	130.8

CHI^2 PROBABILITY (%): 0.0

POOLED AGE W/ 68% CONF. INTERVAL(Ma): 125.0, 122.1 -- 127.9 (-2.9 +2.9)
95% CONF. INTERVAL(Ma): 119.4 -- 130.8 (-5.6 +5.8)

CENTRAL AGE W/ 68% CONF. INTERVAL(Ma): 123.8, 119.0 -- 128.7 (-4.8 +5.0)
95% CONF. INTERVAL(Ma): 114.6 -- 133.7 (-9.2 +9.9)
AGE DISPERSION (%): 31.7

FIT OPTION: Best-fit peaks using the binomial model of Galbraith and Green

INITIAL GUESS FOR MODEL PARAMETERS (number of peaks to fit = 3)

Peak #.	Peak Age	Theta	Fraction(%)	Count
1.	37.50	0.583	0.9	0.91
2.	125.00	0.825	42.3	43.16
3.	235.90	0.899	8.4	8.53

Total range for grain ages: 37,5 to 285,5 Ma
Number of active grains (Num. used for fit): 102
Number of removed grains: 0
Degrees of freedom for fit: 97
Average of the SE(Z)'s for the grains: 0,18
Estimated width of peaks in PD plot in Z units: 0,21

PARAMETERS FOR BEST-FIT PEAKS

* *Standard error for peak age includes group error*
* *Peak width is for PD plot assuming a kernel factor = 0.60*

#.	Peak Age(Ma)	68%CI	95%CI	W(Z)	Frac(%)	SE,%	Count
1.	59.2	-4,0 ...+4,3	-7,6 ...+8,7	0.17	7.7	3.1	7.9
2.	102.8	-4,5 ...+4,7	-8,6 ...+9,4	0.17	32.9	6.8	33.6
3.	157.3	-5,3 ...+5,4	-10,2 ...+10,8	0.20	59.4	7.0	60.6

Log-likelihood for best fit: -403,138
Chi-squared value for best fit: 101,115
Reduced chi-squared value: 1,042
Probability for F test: 0%
Condition number for COVAR matrix: 9,17
Number of iterations: 30

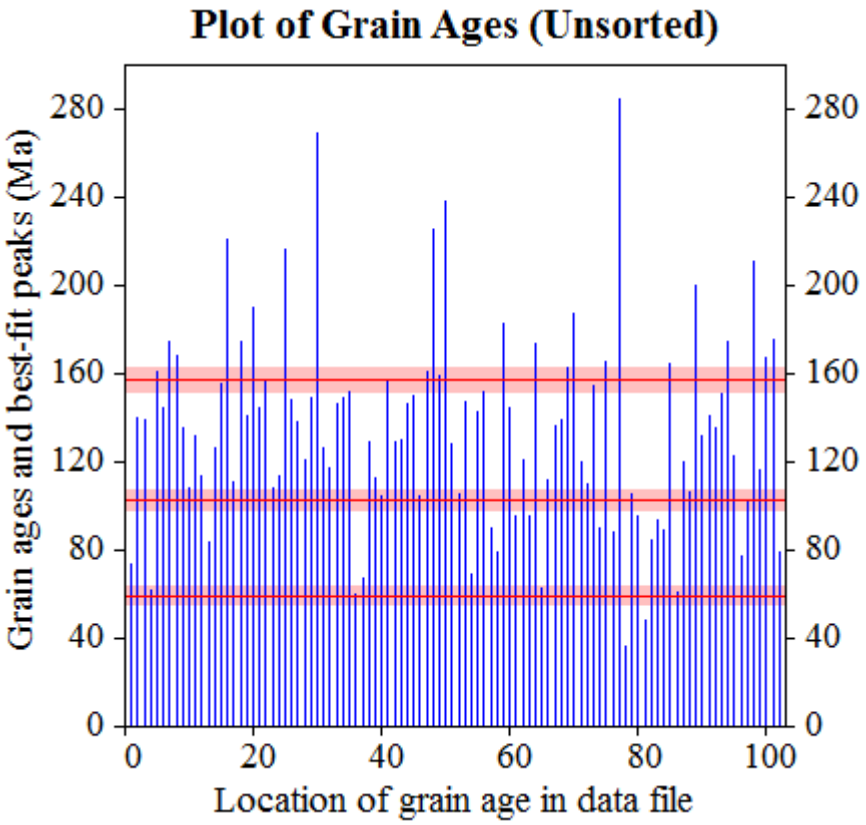
Plot of Grain Ages (Unsorted)
Grain ages and best-fit peaks (Ma)
0
40
80
120
160
200
240
280
0
20
40
60
80
100
Location of grain age in data file

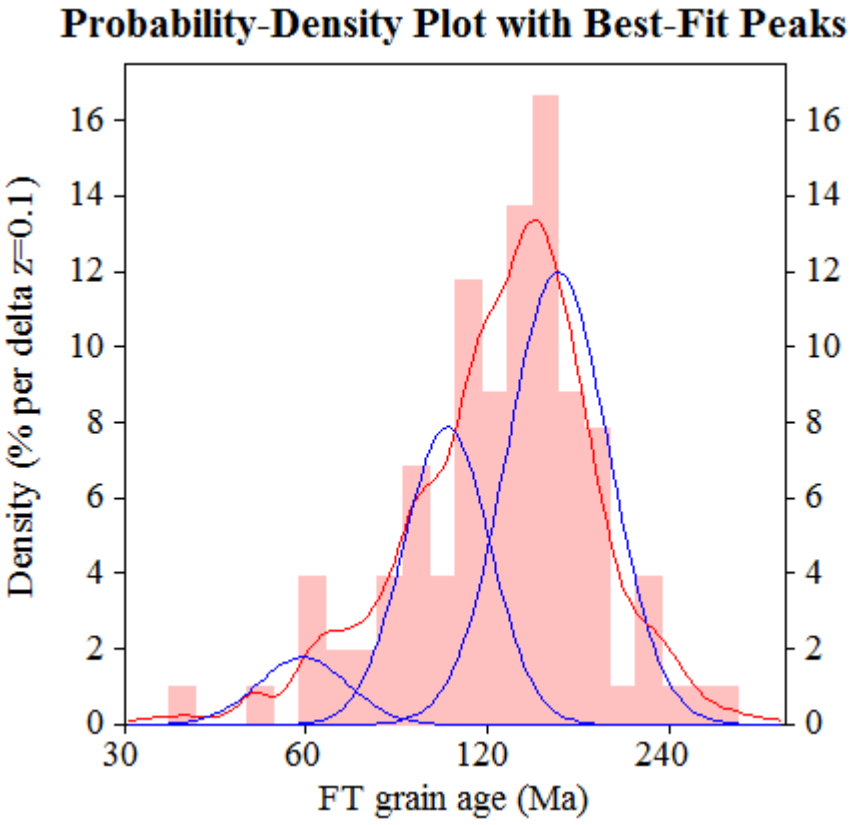
Probability-Density Plot with Best-Fit Peaks
Density (% per delta z=0.1)
0
2
4
6
8
10
12
14
16
30
60
120
240
FT grain age (Ma)

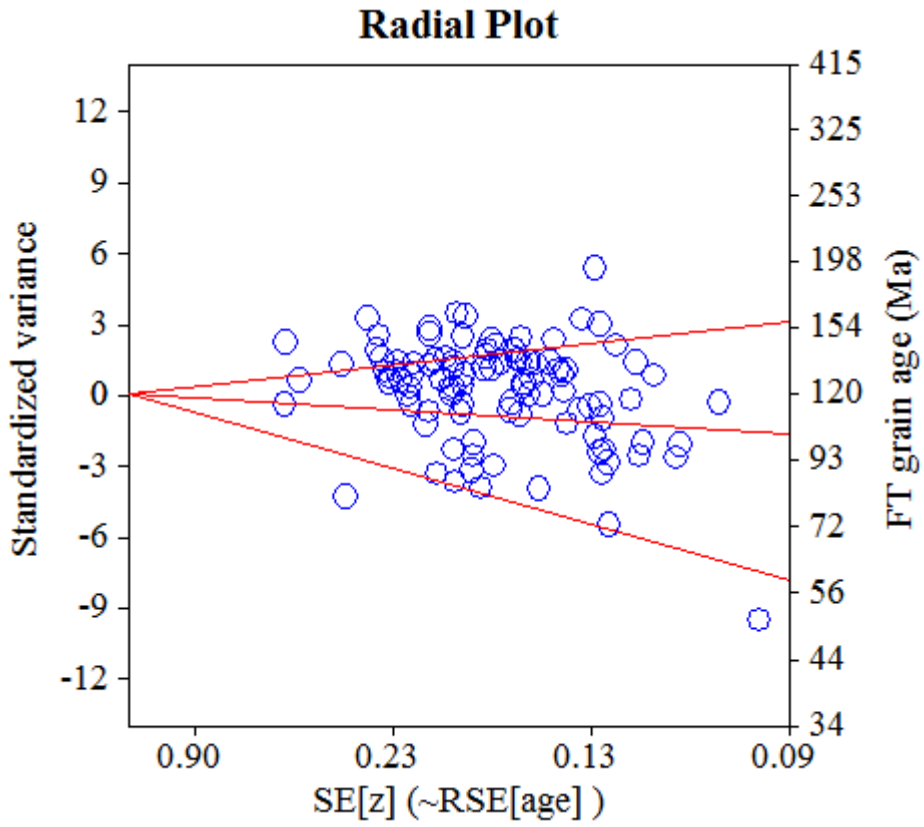
Radial Plot
Standardized variance
12
9
6
3
0
-3
-6
-9
-12
415
325
253
198
154
120
93
72
56
44
34
FT grain age (Ma)
0.90
0.23
0.13
0.09
SE[z] (~RSE[age])

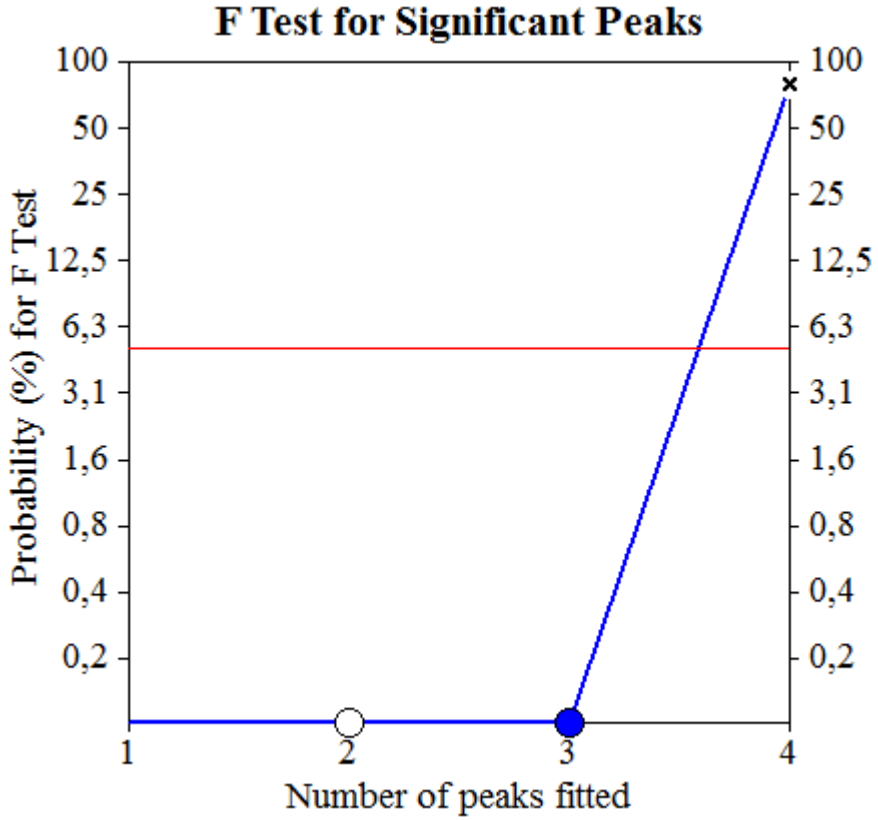
F Test for Significant Peaks
Probability (%) for F Test
100
50
25
12,5
6,3
3,1
1,6
0,8
0,4
0,2
1
2
3
4
Number of peaks fitted

Datafile: C:\BH2\Jairo\Echantillon-IRR-10-2015\JG-P4-02Zr\JG-P4-02-Zr.ftz
Title: Sample No. JG P4 19 Irr 10-2015-49

NEW PARAMETERS - ZETA METHOD

EFFECTIVE TRACK DENSITY FOR FLUENCE MONITOR (tracks/cm^2): 3,91E+05
RELATIVE ERROR (%): 1,33
EFFECTIVE URANIUM CONTENT OF MONITOR (ppm): 50,00
ZETA FACTOR AND STANDARD ERROR (yr cm^2): 137,14 1,57
SIZE OF COUNTER SQUARE (cm^2): 8,30E-07

GRAIN AGES IN ORIGINAL ORDER

Grain no.	RhoS (cm^-2)	(Ns)	RhoI (cm^-2)	(Ni)	Squares	U+/-2s		Grain Age (Ma) Age	--95% CI--	
1	6,37E+06	(74)	1,20E+06	(14)	14	154	81	138.9	78.9	266.5
2	6,85E+06	(91)	1,66E+06	(22)	16	212	89	109.4	68.6	183.2
3	2,68E+06	(100)	6,43E+05	(24)	45	82	33	110.2	70.6	180.1
4	9,14E+06	(91)	2,91E+06	(29)	12	372	137	83.3	54.6	131.4
5	6,72E+06	(223)	6,93E+05	(23)	40	89	37	253.4	166.7	406.1
6	8,65E+06	(366)	8,98E+05	(38)	51	115	37	252.4	181.9	361.1
7	9,34E+06	(93)	1,31E+06	(13)	12	167	91	187.1	105.9	363.6
8	4,56E+06	(87)	6,29E+05	(12)	23	80	45	189.4	104.9	379.6
9	8,26E+06	(144)	1,15E+06	(20)	21	147	65	189.0	119.3	317.9
10	8,78E+06	(102)	1,20E+06	(14)	14	154	81	190.6	110.3	360.1
11	5,75E+06	(167)	6,20E+05	(18)	35	79	37	242.2	150.8	416.8
12	3,99E+06	(106)	5,27E+05	(14)	32	67	35	198.0	114.7	373.3
13	4,10E+06	(102)	2,17E+06	(54)	30	277	75	50.4	35.9	71.5
14	8,73E+06	(174)	1,00E+06	(20)	24	128	57	227.6	144.8	380.4
15	6,49E+06	(97)	2,28E+06	(34)	18	291	99	75.8	51.0	115.7
16	6,41E+06	(117)	7,67E+05	(14)	22	98	52	218.1	127.0	409.7
17	3,28E+06	(87)	1,28E+06	(34)	32	164	56	68.1	45.5	104.5
18	1,05E+07	(140)	1,36E+06	(18)	16	173	81	203.7	125.9	352.7
19	3,61E+06	(27)	1,87E+06	(14)	9	240	126	51.2	26.1	105.9
20	4,08E+06	(61)	2,61E+06	(39)	18	334	107	41.8	27.5	64.2
21	3,28E+06	(87)	1,24E+06	(33)	32	159	55	70.1	46.7	108.2
22	3,06E+06	(71)	1,16E+06	(27)	28	148	57	69.9	44.5	113.4
23	4,70E+06	(78)	1,20E+06	(20)	20	154	68	103.1	63.0	178.2
24	4,69E+06	(105)	7,14E+05	(16)	27	91	45	172.2	102.6	311.8
25	5,46E+06	(127)	6,45E+05	(15)	28	82	42	221.1	131.2	405.0
26	4,70E+06	(78)	1,27E+06	(21)	20	162	70	98.3	60.6	167.8
27	6,18E+06	(77)	8,84E+05	(11)	15	113	67	182.8	98.5	380.5
28	2,71E+06	(54)	5,02E+05	(10)	24	64	40	141.4	72.6	311.6
29	7,50E+06	(112)	9,37E+05	(14)	18	120	63	209.0	121.5	393.2
30	1,00E+07	(133)	2,11E+06	(28)	16	269	101	125.6	83.6	196.2
31	2,11E+06	(49)	4,30E+05	(10)	28	55	34	128.5	65.4	284.8
32	7,29E+06	(242)	7,53E+05	(25)	40	96	38	253.1	169.3	397.1
33	4,22E+06	(105)	6,83E+05	(17)	30	87	42	162.3	97.9	288.8
34	6,02E+06	(100)	1,57E+06	(26)	20	200	78	101.9	66.1	163.6
35	2,48E+06	(37)	1,14E+06	(17)	18	145	70	57.8	32.0	109.7
36	8,13E+06	(81)	8,03E+05	(8)	12	103	70	261.3	130.1	619.9
37	3,16E+06	(105)	8,13E+05	(27)	40	104	40	103.0	67.4	163.7
38	1,49E+06	(31)	2,41E+05	(5)	25	31	26	159.9	63.8	526.0
39	3,05E+06	(152)	4,22E+05	(21)	60	54	23	190.0	121.3	315.2
40	5,27E+06	(70)	7,53E+05	(10)	16	96	59	182.6	95.5	396.4
41	9,22E+06	(153)	1,02E+06	(17)	20	131	63	235.0	144.2	412.1
42	3,24E+06	(43)	6,78E+05	(9)	16	87	56	125.1	61.3	292.4
43	3,44E+06	(60)	4,02E+05	(7)	21	51	38	221.4	104.1	570.5
44	5,54E+06	(92)	9,04E+05	(15)	20	115	59	161.0	94.0	299.0
POOLED	5,24E+06	(4691)	9,80E+05	(877)	1078	125	9	141.8	131.1	153.5

```
CHI^2 PROBABILITY (%):  0.0

 POOLED AGE W/  68% CONF. INTERVAL(Ma):  141.8, 136.2 -- 147.7 ( -5.6  +5.8)
                95% CONF. INTERVAL(Ma):         131.1 -- 153.5 (-10.8 +11.7)

CENTRAL AGE W/  68% CONF. INTERVAL(Ma):  131.1, 120.6 -- 142.5 (-10.5 +11.4)
                95% CONF. INTERVAL(Ma):         111.4 -- 154.4 (-19.8 +23.3)
                    AGE DISPERSION (%):   48.5
```

FIT OPTION: Best-fit peaks using the binomial model of Galbraith and Green

INITIAL GUESS FOR MODEL PARAMETERS (number of peaks to fit = 3)

Peak #.	Peak Age	Theta	Fraction(%)	Count
1.	41.60	0.609	4.8	2.10
2.	141.80	0.842	19.9	8.76
3.	187.50	0.876	33.9	14.93

Total range for grain ages: 41,6 to 252,2 Ma
Number of active grains (Num. used for fit): 44
Number of removed grains: 0
Degrees of freedom for fit: 39
Average of the SE(Z)'s for the grains: 0,27
Estimated width of peaks in PD plot in Z units: 0,32

PARAMETERS FOR BEST-FIT PEAKS

* *Standard error for peak age includes group error*
* *Peak width is for PD plot assuming a kernel factor = 0.60*

#.	Peak Age(Ma)	68%CI	95%CI	W(Z)	Frac(%)	SE,%	Count
1.	53.8	-11,5 ...+14,7	-20,3 ...+32,5	0.24	9.8	9.9	4.3
2.	95.1	-11,9 ...+13,7	-22,0 ...+28,6	0.27	30.0	10.9	13.2
3.	206.7	-12,0 ...+12,8	-22,9 ...+25,7	0.31	60.2	8.7	26.5

Log-likelihood for best fit: -145,925
Chi-squared value for best fit: 40,401
Reduced chi-squared value: 1,036
Probability for F test: 1%
Condition number for COVAR matrix: 36,01
Number of iterations: 28

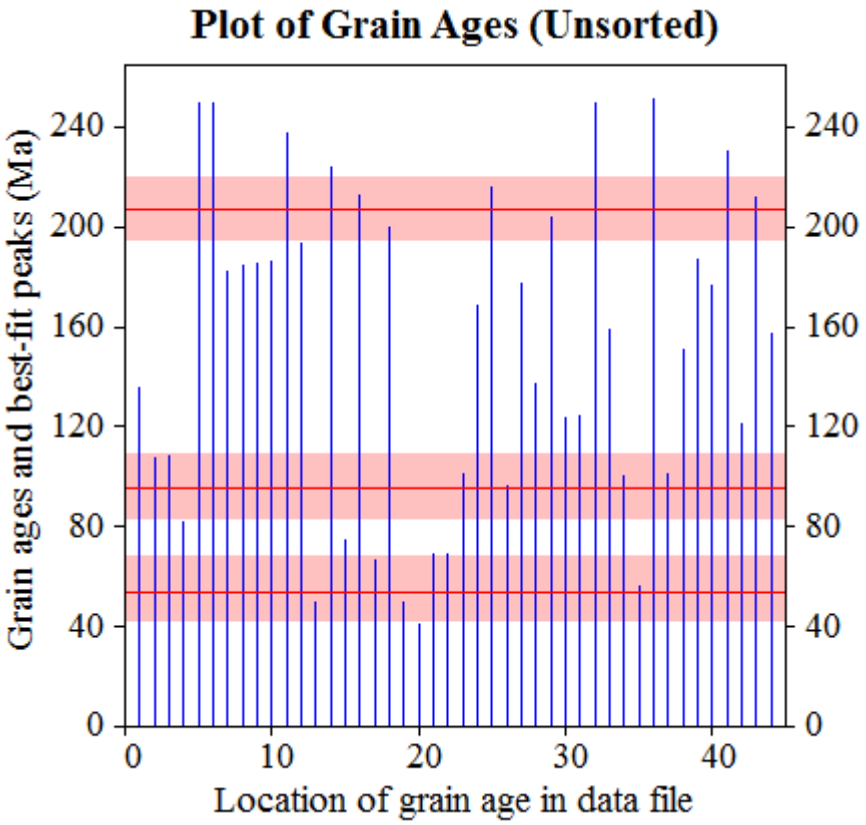
Plot of Grain Ages (Unsorted)
Grain ages and best-fit peaks (Ma)
0
40
80
120
160
200
240
0
10
20
30
40
Location of grain age in data file

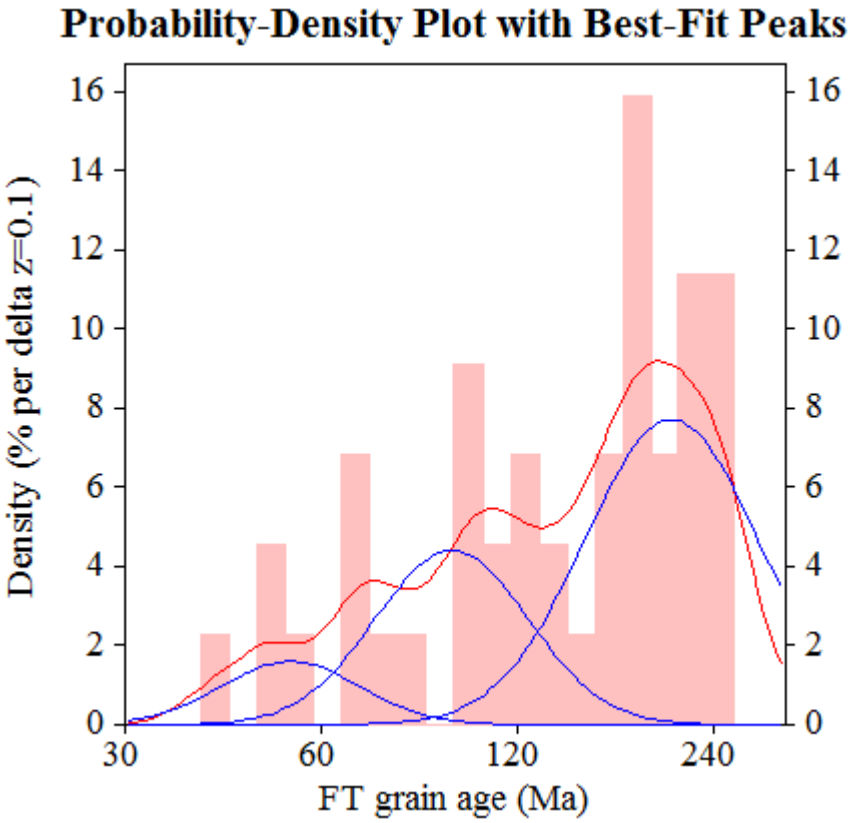
Probability-Density Plot with Best-Fit Peaks
Density (% per delta z=0.1)
0
2
4
6
8
10
12
14
16
30
60
120
240
FT grain age (Ma)

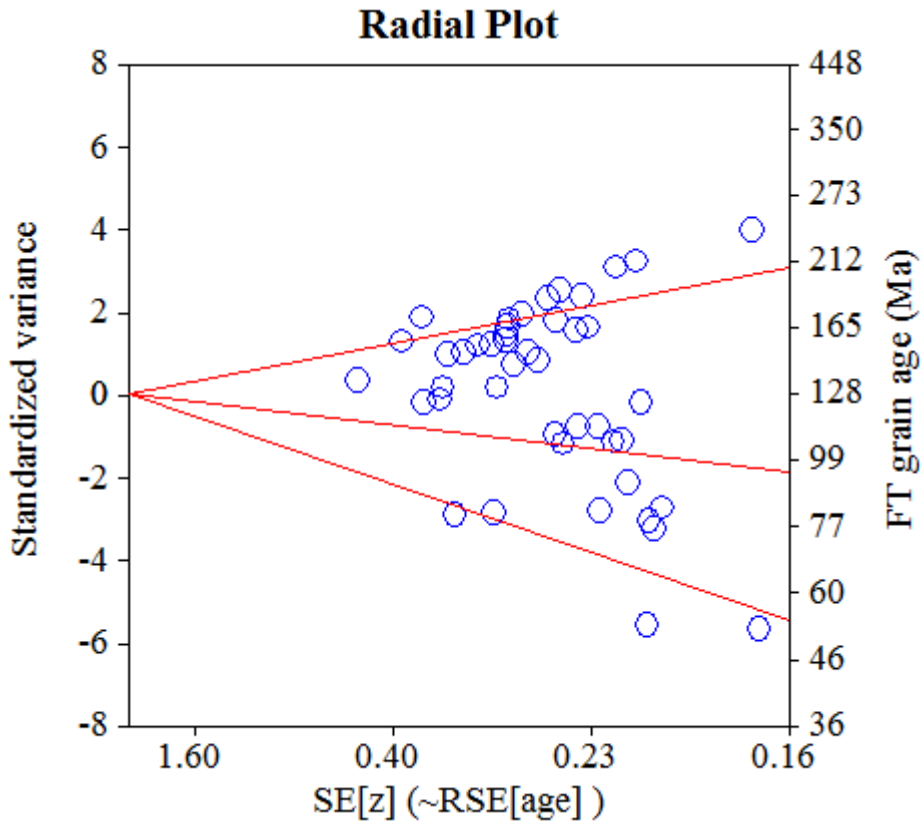
Radial Plot
Standardized variance
8
6
4
2
0
-2
-4
-6
-8
448
350
273
212
165
128
99
77
60
46
36
FT grain age (Ma)
1.60
0.40
0.23
0.16
SE[z] (~RSE[age])

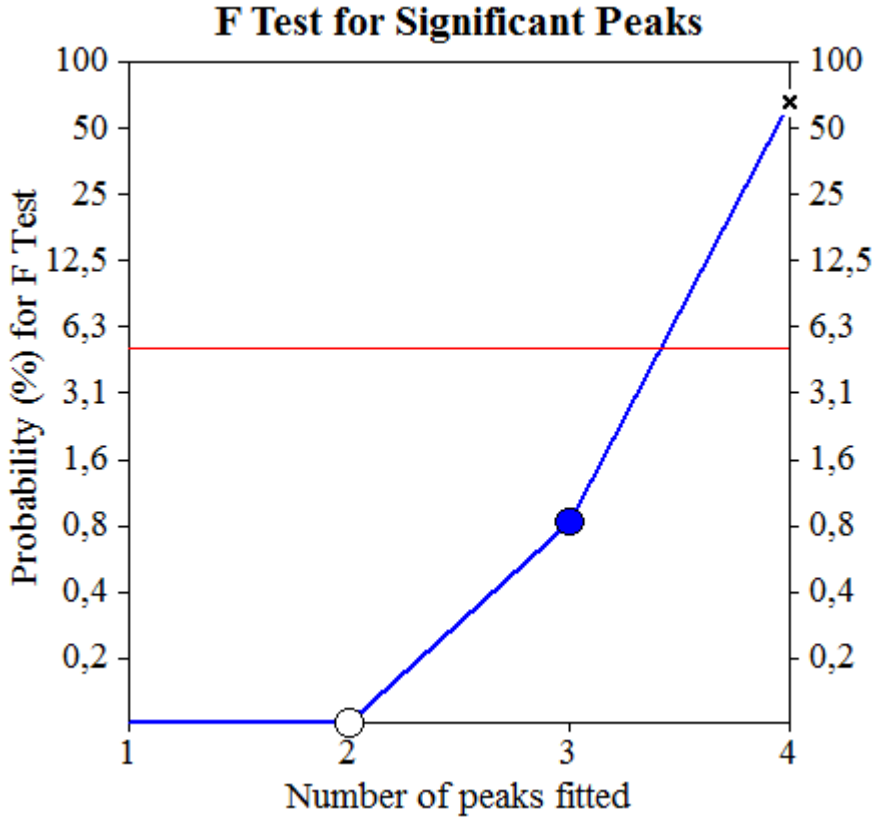
F Test for Significant Peaks
Probability (%) for F Test
100
50
25
12,5
6,3
3,1
1,6
0,8
0,4
0,2
1
2
3
4
Number of peaks fitted

Merged dataset:
C:\BH2\Jairo\Samples-IRR-6-2015\JG-P4-06\JG-P4-06.ftz
C:\BH2\Jairo\Samples-IRR-6-2015\JG-P4-06\JG-P4-06b.ftz

NEW PARAMETERS - ZETA METHOD

EFFECTIVE TRACK DENSITY FOR FLUENCE MONITOR (tracks/cm^2): 2,71E+05
RELATIVE ERROR (%): 1,44
EFFECTIVE URANIUM CONTENT OF MONITOR (ppm): 50,00
ZETA FACTOR AND STANDARD ERROR (yr cm^2): 137,95 4,04
SIZE OF COUNTER SQUARE (cm^2): 8,30E-07

GRAIN AGES IN ORIGINAL ORDER

Grain no.	RhoS (cm^-2)	(Ns)	RhoI (cm^-2)	(Ni)	Squares	U+/-2s	Grain Age (Ma) Age	--95% CI--	
1	1,29E+07	(193)	1,34E+06	(20)	18	247 109	176.8	112.6	295.6
2	1,66E+07	(165)	1,41E+06	(14)	12	259 136	214.5	126.4	399.8
3	1,91E+07	(190)	2,11E+06	(21)	12	389 168	165.9	106.6	274.1
4	1,71E+07	(170)	2,01E+06	(20)	12	370 164	156.0	98.9	261.8
5	1,82E+07	(151)	1,20E+06	(10)	10	222 137	272.4	147.6	575.0
6	8,61E+06	(100)	1,29E+06	(15)	14	238 121	122.4	71.6	227.3
7	1,14E+07	(152)	1,58E+06	(21)	16	292 126	133.1	84.8	221.5
8	2,18E+07	(235)	2,41E+06	(26)	13	444 173	166.0	111.4	259.3
9	9,24E+06	(230)	1,37E+06	(34)	30	252 86	124.8	87.3	184.7
10	8,97E+06	(67)	9,37E+05	(7)	9	173 126	173.1	81.7	446.8
11	3,45E+06	(43)	7,23E+05	(9)	15	133 87	87.5	42.8	205.4
12	9,24E+06	(92)	1,31E+06	(13)	12	241 131	129.7	73.2	253.2
13	8,73E+06	(87)	1,10E+06	(11)	12	204 120	144.4	78.2	300.4
14	9,97E+06	(149)	2,01E+06	(30)	18	370 134	91.9	62.1	141.1
15	7,03E+06	(70)	1,41E+06	(14)	12	259 136	92.0	52.0	177.5
16	7,93E+06	(79)	7,03E+05	(7)	12	130 95	203.5	97.0	520.9
17	9,37E+06	(140)	1,00E+06	(15)	18	185 94	170.6	101.4	312.8
18	9,37E+06	(70)	2,41E+06	(18)	9	444 207	71.9	42.7	128.6
19	1,51E+07	(150)	1,00E+06	(10)	12	185 114	270.6	146.6	571.5
20	1,94E+07	(145)	1,61E+06	(12)	9	296 168	219.5	124.2	433.1
21	8,95E+06	(156)	1,66E+06	(29)	21	307 113	99.4	67.0	153.5
22	7,63E+06	(76)	2,21E+06	(22)	12	407 172	64.0	39.6	108.3
23	1,12E+07	(168)	2,21E+06	(33)	18	407 141	94.2	64.9	141.5
24	1,31E+07	(261)	1,36E+06	(27)	24	250 96	177.4	120.2	274.1
25	1,44E+07	(167)	8,61E+05	(10)	14	159 98	300.6	163.5	631.9
26	7,40E+06	(86)	1,03E+06	(12)	14	190 108	131.2	72.5	264.2
27	7,05E+06	(117)	7,23E+05	(12)	20	133 75	177.7	99.7	353.5
28	1,54E+07	(256)	1,14E+06	(19)	20	211 96	245.3	156.1	412.5
29	1,80E+07	(179)	1,61E+06	(16)	12	296 146	204.1	124.1	363.9
30	9,74E+06	(194)	8,53E+05	(17)	24	157 75	208.2	128.5	363.9
31	6,98E+06	(110)	1,14E+06	(18)	19	210 98	112.5	68.6	197.2
32	1,43E+07	(142)	1,20E+06	(12)	12	222 126	215.0	121.6	424.6
33	6,45E+06	(107)	1,69E+06	(28)	20	311 117	70.8	46.6	111.7
34	1,06E+07	(247)	5,59E+05	(13)	28	103 56	342.0	200.7	644.3
35	1,89E+07	(188)	1,71E+06	(17)	12	315 151	201.9	124.5	353.1
36	1,09E+07	(181)	1,02E+06	(17)	20	189 90	194.5	119.8	340.6
37	1,04E+07	(129)	2,49E+06	(31)	15	459 164	77.1	52.0	118.3
38	1,81E+07	(180)	1,10E+06	(11)	12	204 120	295.0	164.8	596.2
39	1,22E+07	(243)	1,31E+06	(26)	24	241 94	171.6	115.3	267.7
40	1,08E+07	(215)	1,20E+06	(24)	24	222 90	164.5	108.6	262.2
41	7,70E+06	(179)	1,12E+06	(26)	28	206 80	126.8	84.4	199.6
42	1,52E+07	(467)	1,30E+06	(40)	37	240 76	214.0	155.9	302.9
43	1,02E+07	(127)	1,61E+06	(20)	15	296 131	116.9	73.3	198.2
44	1,07E+07	(80)	1,87E+06	(14)	9	346 182	105.0	59.8	201.3
45	1,12E+07	(130)	1,64E+06	(19)	14	301 137	125.8	78.2	216.0
46	1,39E+07	(115)	1,33E+06	(11)	10	244 144	190.2	104.4	390.9
47	1,61E+07	(240)	1,94E+06	(29)	18	358 132	152.2	104.1	232.2

Merged dataset:
C:\BH2\Jairo\Samples-IRR-6-2015\JG-P4-06\JG-P4-06.ftz
C:\BH2\Jairo\Samples-IRR-6-2015\JG-P4-06\JG-P4-06b.ftz

NEW PARAMETERS - ZETA METHOD

EFFECTIVE TRACK DENSITY FOR FLUENCE MONITOR (tracks/cm^2): 2,71E+05
RELATIVE ERROR (%): 1,47
EFFECTIVE URANIUM CONTENT OF MONITOR (ppm): 50,00
ZETA FACTOR AND STANDARD ERROR (yr cm^2): 137,95 4,04
SIZE OF COUNTER SQUARE (cm^2): 8,30E-07

Grain no.	RhoS (cm^-2)	(Ns)	RhoI (cm^-2)	(Ni)	Squares	U+/-2s	Grain Age (Ma) Age	--95% CI--	
48	1,02E+07	(288)	6,73E+05	(19)	34	124 56	275.1	175.6	461.1
49	9,04E+06	(135)	1,47E+06	(22)	18	272 115	113.0	72.3	186.6
50	1,22E+07	(303)	9,24E+05	(23)	30	170 70	240.1	158.9	383.2
51	7,98E+06	(106)	9,04E+05	(12)	16	167 94	161.1	90.0	321.7
52	5,42E+06	(108)	1,00E+06	(20)	24	185 82	99.5	61.9	169.7
53	1,37E+07	(205)	1,47E+06	(22)	18	272 115	170.8	110.9	278.3
54	7,19E+06	(167)	1,29E+06	(30)	28	238 87	102.8	69.8	157.3
55	5,06E+06	(84)	1,57E+06	(26)	20	289 113	59.9	38.3	97.1
56	1,03E+07	(94)	1,10E+06	(10)	11	202 125	170.9	90.7	367.9
57	8,53E+06	(255)	1,20E+06	(36)	36	222 74	130.6	92.4	190.7
58	1,05E+07	(348)	1,14E+06	(38)	40	211 68	168.3	121.0	241.8
59	1,06E+07	(88)	1,08E+06	(9)	10	200 130	177.4	91.3	400.5
60	7,83E+06	(65)	8,43E+05	(7)	10	156 114	167.9	79.1	434.1
61	1,36E+07	(270)	1,36E+06	(27)	24	250 96	183.3	124.3	282.9
62	1,61E+07	(107)	1,36E+06	(9)	8	250 162	215.0	111.7	481.2
63	8,30E+06	(193)	8,61E+05	(20)	28	159 70	176.6	112.5	295.4
64	1,07E+07	(80)	1,20E+06	(9)	9	222 144	161.5	82.7	366.2
65	9,28E+06	(77)	1,69E+06	(14)	10	311 164	101.0	57.4	194.0
66	9,06E+06	(158)	5,74E+05	(10)	21	106 65	284.5	154.4	599.6
67	4,46E+06	(74)	1,39E+06	(23)	20	256 106	59.6	37.1	100.0
68	1,46E+07	(242)	1,02E+06	(17)	20	189 91	258.5	160.6	448.8
69	7,14E+06	(83)	9,47E+05	(11)	14	175 103	137.8	74.4	287.2
70	7,77E+06	(258)	8,43E+05	(28)	40	156 58	169.1	115.2	259.3
71	1,09E+07	(227)	5,78E+05	(12)	25	107 60	340.0	195.3	660.1
72	5,69E+06	(85)	6,69E+05	(10)	18	123 76	154.8	81.7	334.7
73	1,17E+07	(387)	1,23E+06	(41)	40	228 71	173.5	126.3	245.4
74	7,03E+06	(105)	8,03E+05	(12)	18	148 84	159.6	89.1	318.9
75	9,16E+06	(228)	8,03E+05	(20)	30	148 66	208.1	133.2	346.4
76	7,71E+06	(64)	6,02E+05	(5)	10	111 95	228.3	96.6	720.5
77	1,26E+07	(146)	9,47E+05	(11)	14	175 103	240.2	133.2	489.3
78	1,20E+07	(240)	1,36E+06	(27)	24	250 96	163.2	110.3	252.7
79	6,11E+06	(137)	1,56E+06	(35)	27	288 97	72.5	49.9	108.5
80	9,98E+06	(116)	7,75E+05	(9)	14	143 93	232.7	121.4	519.0
81	5,42E+06	(117)	1,25E+06	(27)	26	231 88	80.1	52.7	127.0
82	1,53E+07	(445)	1,55E+06	(45)	35	286 85	181.7	134.2	252.5
83	6,19E+06	(257)	7,71E+05	(32)	50	142 50	147.8	102.8	220.6
84	9,32E+06	(232)	2,13E+06	(53)	30	393 108	81.1	60.1	111.7
POOLED	1,04E+07	(13992)	1,23E+06	(1662)	1621	228 13	155.6	143.5	168.7

CHI^2 PROBABILITY (%): 0.0

POOLED AGE W/ 68% CONF. INTERVAL(Ma): 155.6, 149.3 -- 162.1 (-6.3 +6.5)
95% CONF. INTERVAL(Ma): 143.5 -- 168.7 (-12.1 +13.1)

CENTRAL AGE W/ 68% CONF. INTERVAL(Ma): 148.7, 140.5 -- 157.3 (-8.2 +8.6)
95% CONF. INTERVAL(Ma): 133.1 -- 166.1 (-15.6 +17.4)
AGE DISPERSION (%): 35.1

Merged dataset:
C:\BH2\Jairo\Samples-IRR-6-2015\JG-P4-06\JG-P4-06.ftz
C:\BH2\Jairo\Samples-IRR-6-2015\JG-P4-06\JG-P4-06b.ftz

FIT OPTION: Best-fit peaks using the binomial model of Galbraith and Green

INITIAL GUESS FOR MODEL PARAMETERS (number of peaks to fit = 2)

Peak #.	Peak Age	Theta	Fraction(%)	Count
1.	77.60	0.807	12.7	10.65
2.	155.60	0.894	37.1	31.14

Total range for grain ages:	59,0 to 334,1 Ma
Number of active grains (Num. used for fit):	84
Number of removed grains:	0
Degrees of freedom for fit:	81
Average of the SE(Z)'s for the grains:	0,26
Estimated width of peaks in PD plot in Z units:	0,31

PARAMETERS FOR BEST-FIT PEAKS

* *Standard error for peak age includes group error*
* *Peak width is for PD plot assuming a kernel factor = 0.60*

#.	Peak Age(Ma)	68%CI	95%CI	W(Z)	Frac(%)	SE,%	Count
1.	88.2	-6,6 ...+7,1	-12,5 ...+14,5	0.26	23.5	6.0	19.8
2.	184.3	-8,6 ...+9,0	-16,5 ...+18,1	0.29	76.5	6.0	64.2

Log-likelihood for best fit:	-273,265
Chi-squared value for best fit:	84,662
Reduced chi-squared value:	1,045
Probability for F test:	0%
Condition number for COVAR matrix:	6,16
Number of iterations:	9

Merged dataset:
C:\BH2\Jairo\Samples-IRR-6-2015\JG-P4-06\JG-P4-06.ftz
C:\BH2\Jairo\Samples-IRR-6-2015\JG-P4-06\JG-P4-06b.ftz

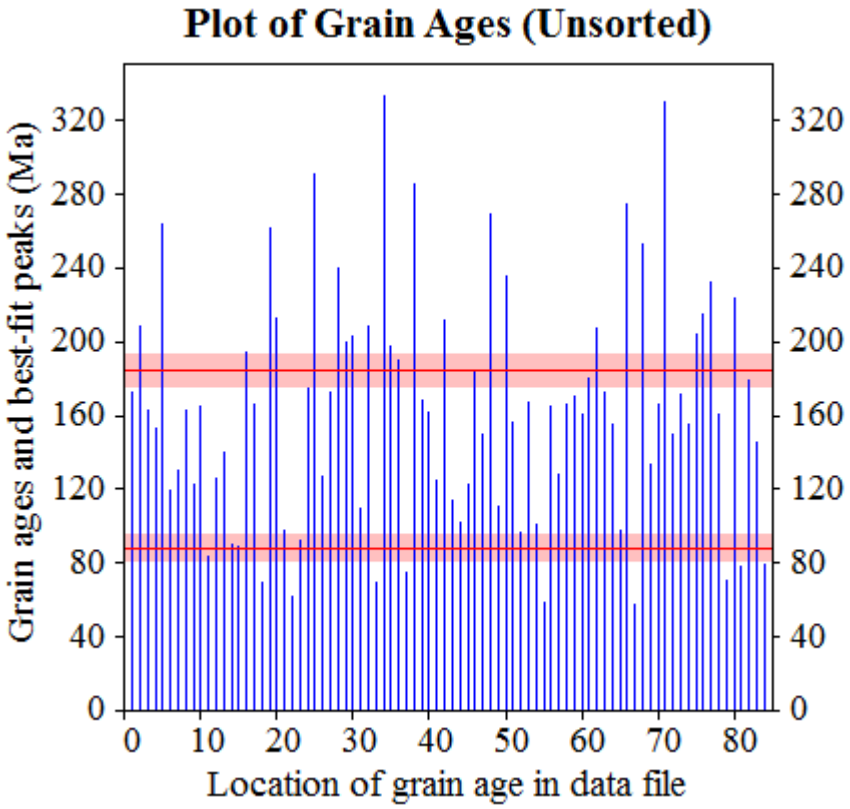

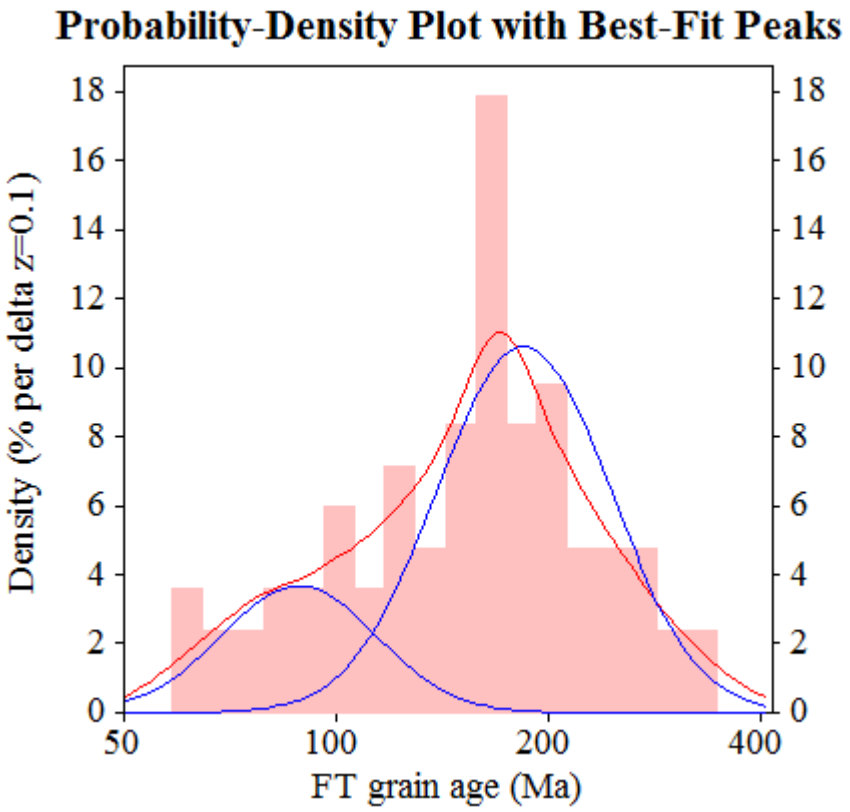

Merged dataset:
C:\BH2\Jairo\Samples-IRR-6-2015\JG-P4-06\JG-P4-06.ftz
C:\BH2\Jairo\Samples-IRR-6-2015\JG-P4-06\JG-P4-06b.ftz

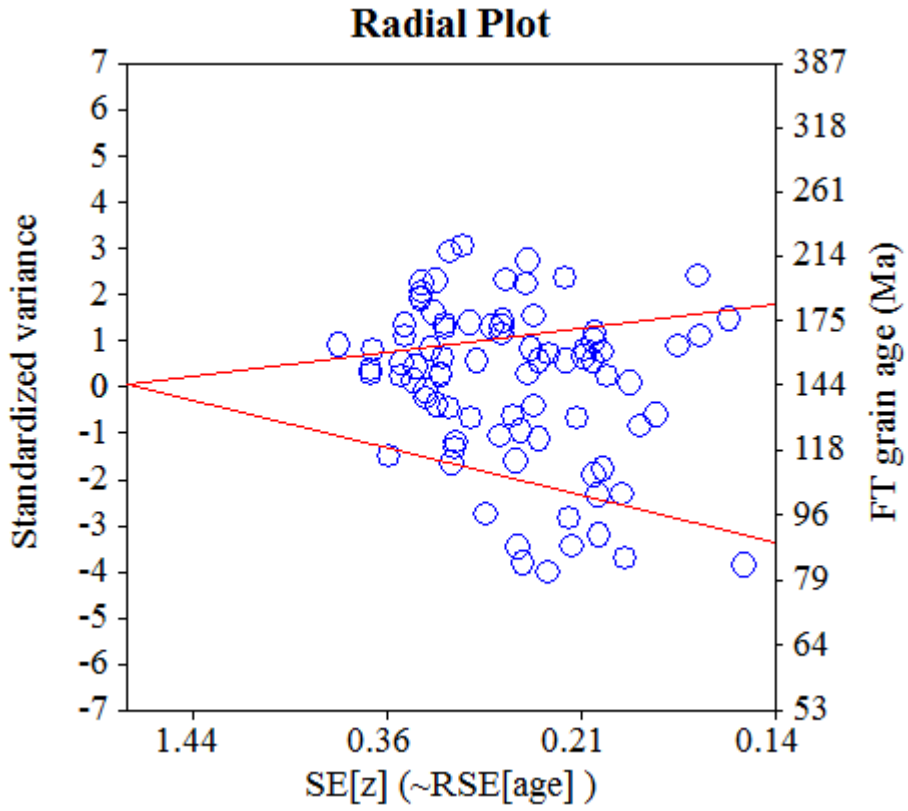

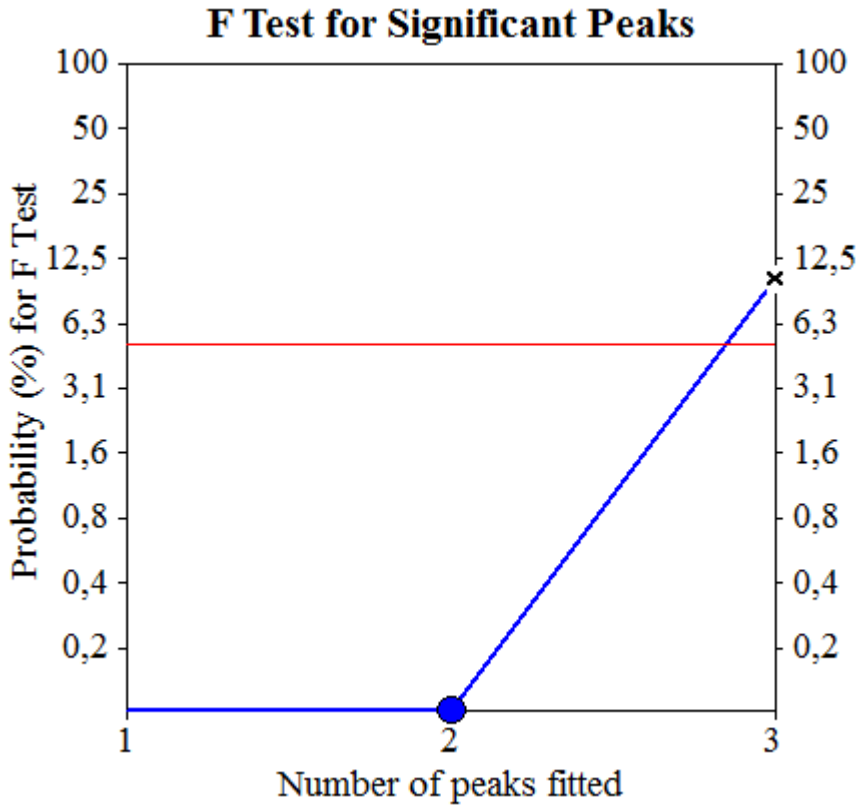

Merged dataset:
C:\BH2\Jairo\Samples-IRR-6-2015\JG-P4-01\JG-P4-01b.ftz
C:\BH2\Jairo\Samples-IRR-6-2015\JG-P4-01\JG-P4-01.ftz

NEW PARAMETERS - ZETA METHOD

EFFECTIVE TRACK DENSITY FOR FLUENCE MONITOR (tracks/cm^2): 2,71E+05
RELATIVE ERROR (%): 1,41
EFFECTIVE URANIUM CONTENT OF MONITOR (ppm): 50,00
ZETA FACTOR AND STANDARD ERROR (yr cm^2): 137,95 4,04
SIZE OF COUNTER SQUARE (cm^2): 8,30E-07

GRAIN AGES IN ORIGINAL ORDER

Grain no.	RhoS (cm^-2)	(Ns)	RhoI (cm^-2)	(Ni)	Squares	U+/-2s	Grain Age (Ma) Age	--95% CI--	
1	7,68E+06	(255)	9,94E+05	(33)	40	183 63	142.4	99.5	211.4
2	1,14E+07	(170)	1,14E+06	(17)	18	210 100	183.0	112.4	321.0
3	1,14E+07	(114)	9,04E+05	(9)	12	166 108	229.1	119.4	511.3
4	1,13E+07	(103)	1,64E+06	(15)	11	303 154	126.1	73.9	233.9
5	1,20E+07	(149)	6,43E+05	(8)	15	118 81	333.3	170.0	774.5
6	6,39E+06	(53)	2,29E+06	(19)	10	422 191	51.7	30.3	92.8
7	9,96E+06	(248)	2,61E+06	(65)	30	481 120	70.5	53.4	93.1
8	1,45E+07	(108)	9,37E+05	(7)	9	173 126	276.7	134.0	696.8
9	5,02E+06	(100)	1,86E+06	(37)	24	342 112	50.3	34.3	75.6
10	1,47E+07	(110)	1,20E+06	(9)	9	222 144	221.2	115.1	494.5
11	1,06E+07	(79)	3,08E+06	(23)	9	567 235	63.7	39.8	106.4
12	1,27E+07	(158)	1,20E+06	(15)	15	222 113	192.4	114.9	351.2
13	9,56E+06	(127)	2,86E+06	(38)	16	527 171	62.1	43.0	91.9
14	7,23E+06	(60)	1,08E+06	(9)	10	200 130	121.8	61.2	280.1
15	5,80E+06	(77)	2,41E+06	(32)	16	444 156	44.8	29.4	70.0
16	8,05E+06	(147)	2,85E+06	(52)	22	525 146	52.6	38.2	73.8
17	7,83E+06	(104)	9,79E+05	(13)	16	180 98	146.5	83.2	284.5
18	8,71E+06	(94)	1,95E+06	(21)	13	359 155	82.8	51.5	140.2
19	1,26E+07	(94)	9,37E+05	(7)	9	173 126	241.5	116.2	612.6
20	7,97E+06	(119)	3,08E+06	(46)	18	567 167	48.1	34.1	69.3
21	9,52E+06	(79)	3,61E+06	(30)	10	666 242	48.9	31.9	77.4
22	6,63E+06	(110)	2,83E+06	(47)	20	522 152	43.6	30.8	62.8
23	1,04E+07	(104)	2,61E+06	(26)	12	481 187	74.1	48.1	119.0
24	1,18E+07	(293)	2,73E+06	(68)	30	503 122	79.6	60.8	104.1
25	5,44E+06	(122)	2,77E+06	(62)	27	510 130	36.7	26.8	50.7
26	1,54E+07	(166)	1,67E+06	(18)	13	307 143	169.0	105.0	292.0
27	1,37E+07	(182)	1,36E+06	(18)	16	250 116	185.1	115.3	318.8
28	1,37E+07	(114)	2,05E+06	(17)	10	377 181	123.3	74.6	219.4
29	1,33E+07	(110)	1,69E+06	(14)	10	311 163	144.0	83.4	272.2
30	1,28E+07	(202)	5,90E+06	(93)	19	1086 227	40.3	31.3	51.9
31	1,14E+07	(171)	6,69E+05	(10)	18	123 76	307.8	167.6	646.5
32	1,12E+07	(242)	2,64E+06	(57)	26	487 129	78.8	59.0	107.3

Merged dataset:
C:\BH2\Jairo\Samples-IRR-6-2015\JG-P4-01\JG-P4-01b.ftz
C:\BH2\Jairo\Samples-IRR-6-2015\JG-P4-01\JG-P4-01.ftz

NEW PARAMETERS - ZETA METHOD

EFFECTIVE TRACK DENSITY FOR FLUENCE MONITOR (tracks/cm^2): 2,72E+05
RELATIVE ERROR (%): 1,39
EFFECTIVE URANIUM CONTENT OF MONITOR (ppm): 50,00
ZETA FACTOR AND STANDARD ERROR (yr cm^2): 137,95 4,04
SIZE OF COUNTER SQUARE (cm^2): 8,30E-07

Grain no.	RhoS (cm^-2)	(Ns)	RhoI (cm^-2)	(Ni)	Squares	U+/-2s	Grain Age (Ma) Age	--95% CI--	
33	6,83E+06	(68)	2,91E+06	(29)	12	536 198	43.6	28.0	70.1
34	1,28E+07	(340)	1,81E+06	(48)	32	333 96	131.0	97.0	181.2
35	5,50E+06	(137)	3,53E+06	(88)	30	651 139	28.9	22.0	38.1
36	7,30E+06	(212)	1,89E+06	(55)	35	349 94	71.7	53.2	98.4
37	5,99E+06	(194)	1,39E+06	(45)	39	256 76	80.0	57.8	113.5
38	7,34E+06	(67)	1,86E+06	(17)	11	343 164	72.9	42.7	132.9
39	6,43E+06	(64)	5,02E+05	(5)	12	92 79	228.8	96.8	722.0
40	5,90E+06	(49)	8,43E+05	(7)	10	155 113	127.3	58.8	334.5
41	1,12E+07	(140)	1,20E+06	(15)	15	222 113	170.9	101.6	313.3
42	8,21E+06	(109)	1,88E+06	(25)	16	347 138	80.8	52.2	130.5
43	7,33E+06	(73)	2,11E+06	(21)	12	388 168	64.4	39.5	110.6
44	9,18E+06	(160)	2,70E+06	(47)	21	496 145	63.3	45.6	89.8
45	7,76E+06	(58)	1,20E+06	(9)	9	222 144	117.8	59.1	271.5
46	1,30E+07	(97)	1,74E+06	(13)	9	320 175	136.8	77.5	266.5
47	1,23E+07	(164)	1,51E+06	(20)	16	277 123	150.7	95.5	253.3
48	7,50E+06	(56)	2,14E+06	(16)	9	394 194	64.8	36.9	121.4
49	1,26E+07	(125)	1,61E+06	(16)	12	296 146	143.5	86.0	258.9
50	1,12E+07	(93)	1,08E+06	(9)	10	200 130	187.7	96.9	422.7
51	1,03E+07	(128)	1,77E+06	(22)	15	325 137	107.4	68.5	177.7
52	8,88E+06	(221)	2,73E+06	(68)	30	503 122	60.2	45.6	79.4
53	1,62E+07	(121)	2,81E+06	(21)	9	518 224	106.4	67.1	178.4
54	1,07E+07	(133)	3,13E+06	(39)	15	577 184	63.4	44.2	93.2
55	7,58E+06	(107)	2,98E+06	(42)	17	548 169	47.4	33.0	69.6
56	7,41E+06	(123)	4,40E+06	(73)	20	810 190	31.5	23.4	42.7
57	6,43E+06	(64)	1,61E+06	(16)	12	296 146	73.9	42.6	137.5
58	1,00E+07	(83)	2,17E+06	(18)	10	399 186	85.2	51.2	151.2
59	7,89E+06	(262)	2,59E+06	(86)	40	477 103	56.5	44.0	72.5
POOLED	9,31E+06	(7812)	2,15E+06	(1804)	1011	396 22	80.5	74.2	87.3

CHI^2 PROBABILITY (%): 0.0

POOLED AGE W/ 68% CONF. INTERVAL(Ma): 80.5, 77.3 -- 83.9 (-3.3 +3.4)
95% CONF. INTERVAL(Ma): 74.2 -- 87.3 (-6.3 +6.8)

CENTRAL AGE W/ 68% CONF. INTERVAL(Ma): 83.9, 77.3 -- 91.0 (-6.6 +7.1)
95% CONF. INTERVAL(Ma): 71.5 -- 98.3 (-12.4 +14.5)
AGE DISPERSION (%): 53.5

Merged dataset:
C:\BH2\Jairo\Samples-IRR-6-2015\JG-P4-01\JG-P4-01b.ftz
C:\BH2\Jairo\Samples-IRR-6-2015\JG-P4-01\JG-P4-01.ftz

FIT OPTION: Best-fit peaks using the binomial model of Galbraith and Green

INITIAL GUESS FOR MODEL PARAMETERS (number of peaks to fit = 3)

Peak #.	Peak Age	Theta	Fraction(%)	Count
1.	36.60	0.662	7.5	4.43
2.	80.50	0.812	23.1	13.60
3.	133.10	0.878	20.7	12.23

Total range for grain ages: 29,0 to 321,1 Ma
Number of active grains (Num. used for fit): 59
Number of removed grains: 0
Degrees of freedom for fit: 54
Average of the SE(Z)'s for the grains: 0,25
Estimated width of peaks in PD plot in Z units: 0,29

PARAMETERS FOR BEST-FIT PEAKS

* *Standard error for peak age includes group error*
* *Peak width is for PD plot assuming a kernel factor = 0.60*

#.	Peak Age(Ma)	68%CI	95%CI	W(Z)	Frac(%)	SE,%	Count
1.	38.1	-3,2 ...+3,5	-6,1 ...+7,3	0.18	12.9	6.3	7.6
2.	66.6	-3,8 ...+4,0	-7,3 ...+8,2	0.21	43.5	8.0	25.7
3.	164.2	-10,4 ...+11,0	-19,7 ...+22,3	0.32	43.6	6.9	25.7

Log-likelihood for best fit: -225,268
Chi-squared value for best fit: 59,215
Reduced chi-squared value: 1,097
Probability for F test: 0%
Condition number for COVAR matrix: 7,83
Number of iterations: 12

Merged dataset:
C:\BH2\Jairo\Samples-IRR-6-2015\JG-P4-01\JG-P4-01b.ftz
C:\BH2\Jairo\Samples-IRR-6-2015\JG-P4-01\JG-P4-01.ftz

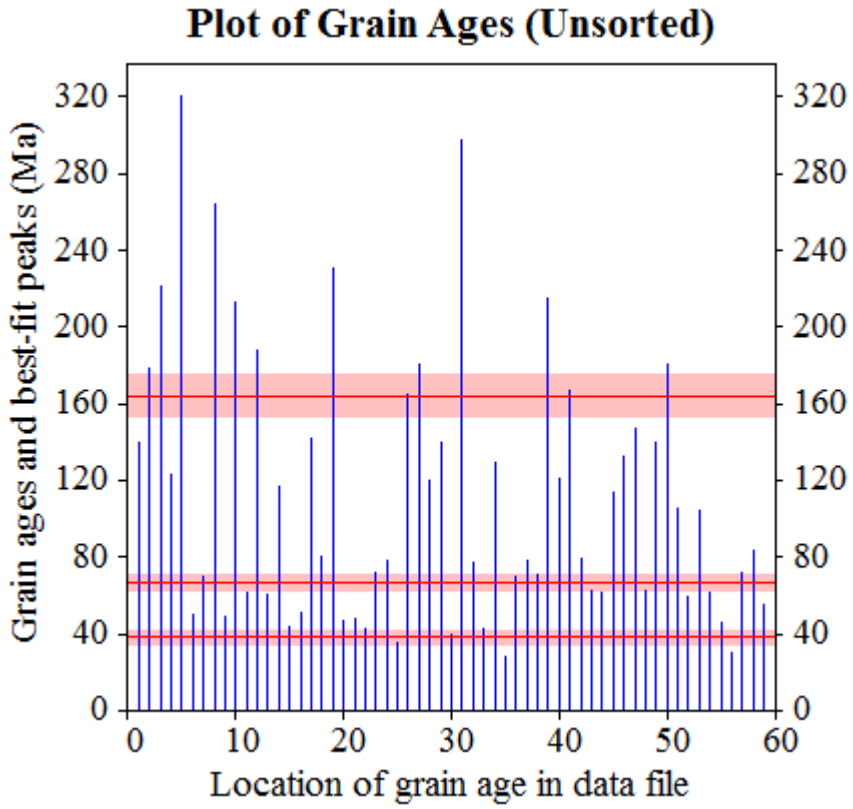

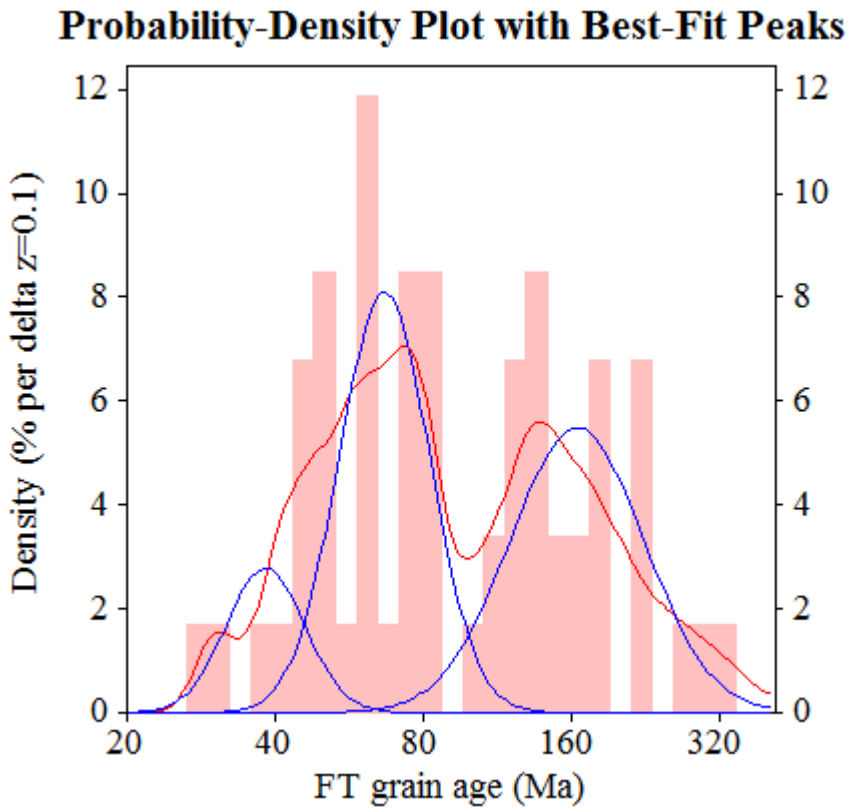

Merged dataset:
C:\BH2\Jairo\Samples-IRR-6-2015\JG-P4-01\JG-P4-01b.ftz
C:\BH2\Jairo\Samples-IRR-6-2015\JG-P4-01\JG-P4-01.ftz

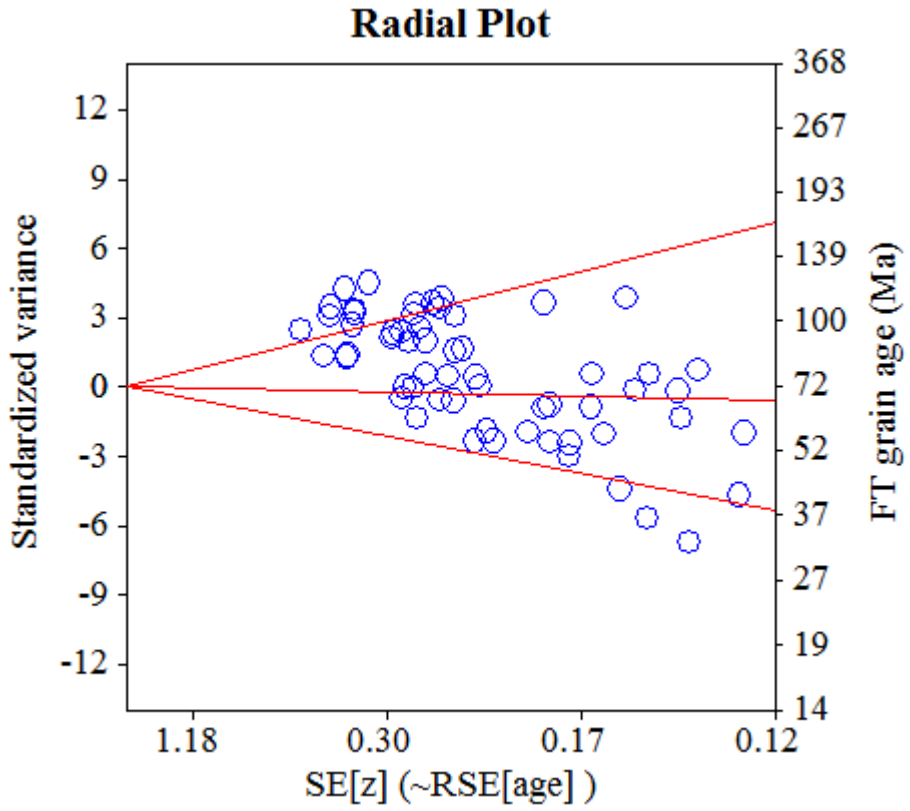

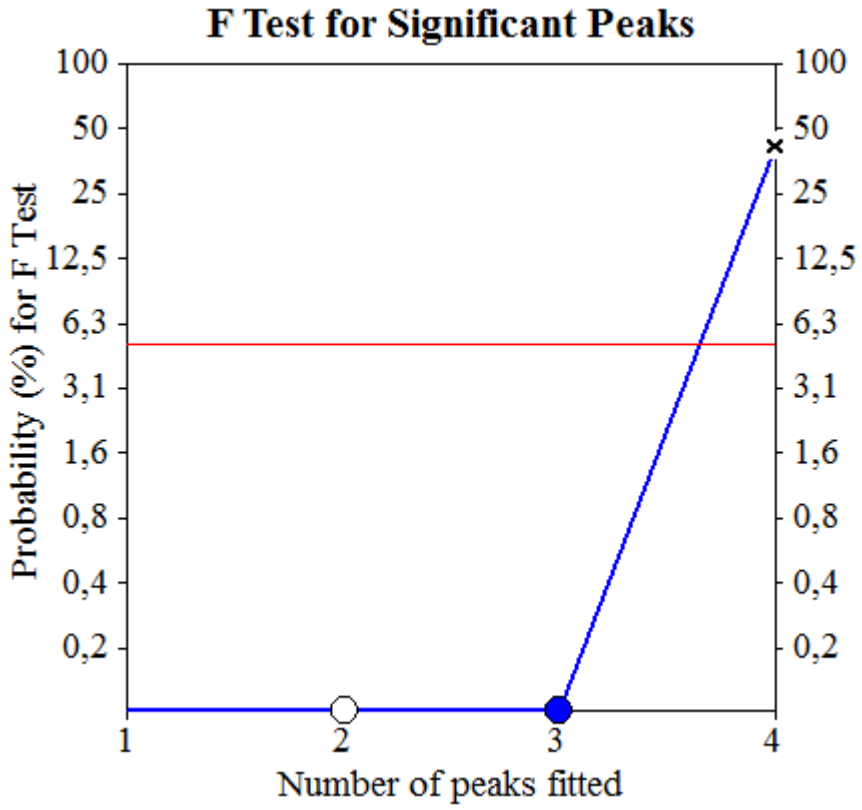

Merged dataset:
C:\BH2\Jairo\Samples-IRR-6-2015\JG-P4-13\JG-P4-13a.ftz
C:\BH2\Jairo\Samples-IRR-6-2015\JG-P4-13\JG-P4-13.ftz

NEW PARAMETERS - ZETA METHOD

EFFECTIVE TRACK DENSITY FOR FLUENCE MONITOR (tracks/cm^2): 2,71E+05
RELATIVE ERROR (%): 1,52
EFFECTIVE URANIUM CONTENT OF MONITOR (ppm): 50,00
ZETA FACTOR AND STANDARD ERROR (yr cm^2): 137,95 4,04
SIZE OF COUNTER SQUARE (cm^2): 8,30E-07

GRAIN AGES IN ORIGINAL ORDER

Grain no.	RhoS (cm^-2)	(Ns)	RhoI (cm^-2)	(Ni)	Squares	U+/-2s	Grain Age (Ma) Age	--95% CI--	
1	7,75E+06	(90)	2,07E+06	(24)	14	382 155	69.3	44.0	114.0
2	5,51E+06	(128)	5,59E+05	(13)	28	103 56	179.2	102.8	345.4
3	8,03E+06	(400)	9,04E+05	(45)	60	167 50	163.3	120.4	227.4
4	4,06E+06	(118)	8,95E+05	(26)	35	165 64	83.7	54.7	133.7
5	8,80E+06	(146)	1,08E+06	(18)	20	200 93	148.5	91.7	257.6
6	7,43E+06	(148)	1,10E+06	(22)	24	204 86	123.6	79.3	203.4
7	6,19E+06	(149)	2,49E+06	(60)	29	461 119	46.1	34.0	63.4
8	5,54E+06	(115)	3,86E+05	(8)	25	71 49	258.1	130.3	607.2
9	4,34E+06	(180)	6,99E+05	(29)	50	129 48	114.3	77.4	175.7
10	9,47E+06	(220)	7,75E+05	(18)	28	143 67	222.3	139.3	381.0
11	1,02E+07	(246)	6,65E+05	(16)	29	123 61	278.1	170.7	491.2
12	7,14E+06	(237)	7,23E+05	(24)	40	134 54	180.6	119.6	287.2
13	5,88E+06	(122)	1,11E+06	(23)	25	205 85	97.7	62.7	160.2
14	6,59E+06	(268)	8,36E+05	(34)	49	154 53	144.9	101.8	213.6
15	8,73E+06	(290)	9,04E+05	(30)	40	167 61	177.1	122.3	267.0
16	6,92E+06	(178)	9,72E+05	(25)	31	180 71	130.8	86.4	207.7
17	7,98E+06	(106)	1,51E+06	(20)	16	278 123	97.5	60.6	166.5
18	6,25E+06	(140)	8,03E+05	(18)	27	148 69	142.4	87.9	247.5
19	1,23E+07	(316)	1,09E+06	(28)	31	201 76	206.2	141.2	314.7
20	7,86E+06	(411)	7,08E+05	(37)	63	131 43	203.2	146.0	292.3
21	5,08E+06	(118)	4,73E+05	(11)	28	87 52	194.6	106.9	399.7
22	8,92E+06	(296)	1,05E+06	(35)	40	195 66	155.3	109.9	227.2
23	9,38E+06	(109)	1,89E+06	(22)	14	350 148	91.3	57.8	152.0
24	4,14E+06	(55)	1,81E+06	(24)	16	334 135	42.5	26.0	71.9
25	8,03E+06	(400)	1,12E+06	(56)	60	208 56	130.8	98.5	173.5
26	8,73E+06	(116)	2,11E+06	(28)	16	390 146	76.5	50.6	120.4
27	9,39E+06	(187)	1,61E+06	(32)	24	297 105	107.7	74.1	162.2
28	7,99E+06	(199)	1,41E+06	(35)	30	260 88	104.9	73.3	155.0
29	9,16E+06	(190)	1,06E+06	(22)	25	196 83	158.2	102.5	258.4
30	7,34E+06	(341)	1,46E+06	(68)	56	270 66	92.3	70.7	120.3
31	9,79E+06	(650)	1,11E+06	(74)	80	206 48	160.8	125.8	205.5
32	1,03E+07	(512)	4,10E+06	(204)	60	757 108	46.6	39.1	55.4
33	6,27E+06	(78)	1,12E+06	(14)	15	208 109	102.2	58.1	196.1
34	8,84E+06	(264)	1,91E+06	(57)	36	352 94	85.1	63.7	113.8
35	8,88E+06	(737)	7,83E+05	(65)	100	145 36	206.7	159.8	267.0
36	8,58E+06	(285)	1,05E+06	(35)	40	195 66	149.6	105.7	219.1
37	7,76E+06	(174)	1,61E+06	(36)	27	297 99	89.3	62.3	131.8
38	1,33E+07	(110)	2,29E+06	(19)	10	423 192	106.4	65.6	183.8
39	9,04E+06	(180)	1,51E+06	(30)	24	278 101	110.5	75.2	168.8
40	7,18E+06	(143)	1,05E+06	(21)	24	195 84	125.0	79.5	208.4
41	1,08E+07	(359)	1,14E+06	(38)	40	211 68	173.3	124.6	248.8
42	1,02E+07	(346)	2,88E+06	(98)	41	532 108	65.2	51.7	82.2
43	1,23E+07	(204)	1,27E+06	(21)	20	234 101	177.6	114.3	292.8
44	6,99E+06	(290)	1,93E+06	(80)	50	356 80	66.9	51.9	86.2
45	8,19E+06	(170)	1,73E+06	(36)	25	321 107	87.2	60.8	128.9
46	1,01E+07	(504)	9,64E+05	(48)	60	178 51	192.5	143.7	264.2
47	3,86E+06	(192)	3,21E+05	(16)	60	59 29	218.1	132.9	388.2
48	9,17E+06	(213)	3,44E+06	(80)	28	636 143	49.2	37.8	64.0
49	5,82E+06	(145)	1,37E+06	(34)	30	252 86	78.8	54.2	118.4
50	8,35E+06	(194)	2,24E+06	(52)	28	413 115	69.1	50.8	95.9
51	9,34E+06	(186)	1,31E+06	(26)	24	241 94	131.4	87.6	206.7
52	1,00E+07	(748)	7,63E+05	(57)	90	141 37	238.4	181.7	312.3

Merged dataset:
C:\BH2\Jairo\Samples-IRR-6-2015\JG-P4-13\JG-P4-13a.ftz
C:\BH2\Jairo\Samples-IRR-6-2015\JG-P4-13\JG-P4-13.ftz

Grain no.	RhoS (cm^-2)	(Ns)	RhoI (cm^-2)	(Ni)	Squares	U+/-2s	Grain Age (Ma) Age	--95% CI--	
53	6,02E+06	(210)	1,43E+06	(50)	42	265 75	77.7	57.0	108.2
54	9,86E+06	(262)	2,52E+06	(67)	32	466 114	72.1	54.8	94.7
55	8,00E+06	(332)	1,90E+06	(79)	50	352 80	77.5	60.2	99.6
56	6,35E+06	(527)	7,11E+05	(59)	100	131 34	163.2	124.3	214.2
57	6,83E+06	(68)	2,41E+06	(24)	12	445 180	52.4	32.7	87.6
58	8,37E+06	(139)	1,87E+06	(31)	20	345 123	82.8	56.1	126.7
59	9,00E+06	(448)	1,89E+06	(94)	60	349 73	87.9	69.9	110.5
60	8,84E+06	(220)	1,73E+06	(43)	30	319 97	94.5	68.1	134.5
61	1,33E+07	(364)	2,01E+06	(55)	33	371 100	121.3	91.0	161.5
62	1,00E+07	(208)	1,01E+06	(21)	25	187 81	181.0	116.6	298.3
63	1,22E+07	(707)	1,33E+06	(77)	70	245 56	168.1	132.1	213.6
64	9,71E+06	(145)	1,34E+06	(20)	18	247 110	133.0	83.8	224.4
65	1,44E+07	(143)	4,82E+06	(48)	12	890 257	55.2	39.7	78.4
66	6,53E+06	(130)	2,16E+06	(43)	24	399 122	56.0	39.5	81.2
67	1,05E+07	(314)	1,07E+06	(32)	36	198 70	179.8	125.7	267.1
68	9,88E+06	(246)	9,64E+05	(24)	30	178 72	187.4	124.2	297.7
69	8,91E+06	(207)	2,32E+06	(54)	28	429 117	71.0	52.5	97.8
70	1,08E+07	(162)	2,28E+06	(34)	18	421 144	88.0	60.8	131.6
71	8,77E+06	(284)	1,58E+06	(51)	39	291 82	102.8	76.3	141.6
72	1,20E+07	(279)	1,08E+06	(25)	28	199 79	203.8	136.5	319.7
73	6,87E+06	(291)	4,72E+05	(20)	51	87 39	264.0	170.1	436.5
74	9,44E+06	(188)	1,00E+06	(20)	24	186 82	171.8	109.4	287.6

Merged dataset:
C:\BH2\Jairo\Samples-IRR-6-2015\JG-P4-13\JG-P4-13a.ftz
C:\BH2\Jairo\Samples-IRR-6-2015\JG-P4-13\JG-P4-13.ftz

NEW PARAMETERS - ZETA METHOD

EFFECTIVE TRACK DENSITY FOR FLUENCE MONITOR (tracks/cm^2): 2,71E+05
RELATIVE ERROR (%): 1,49
EFFECTIVE URANIUM CONTENT OF MONITOR (ppm): 50,00
ZETA FACTOR AND STANDARD ERROR (yr cm^2): 137,95 4,04
SIZE OF COUNTER SQUARE (cm^2): 8,30E-07

Grain no.	RhoS (cm^-2)	(Ns)	RhoI (cm^-2)	(Ni)	Squares	U+/-2s	Grain Age (Ma) Age	--95% CI--	
75	4,14E+06	(110)	1,13E+06	(30)	32	209 76	67.9	45.2	105.5
76	9,70E+06	(338)	3,79E+06	(132)	42	699 123	47.5	38.5	58.6
77	7,98E+06	(212)	1,17E+06	(31)	32	216 77	125.9	86.6	190.1
78	4,72E+06	(47)	7,03E+05	(7)	12	130 95	121.8	56.0	320.9
79	6,21E+06	(134)	1,25E+06	(27)	26	231 88	91.6	60.6	144.4
80	1,11E+07	(147)	9,79E+05	(13)	16	181 99	205.5	118.5	394.1
81	5,35E+06	(142)	8,28E+05	(22)	32	153 65	118.7	76.1	195.7
82	1,31E+07	(152)	1,46E+06	(17)	14	270 129	163.5	100.0	287.9
83	1,13E+07	(207)	1,26E+06	(23)	22	233 96	164.9	108.0	265.8
84	6,99E+06	(87)	1,77E+06	(22)	15	326 138	73.0	45.6	122.8
85	8,63E+06	(258)	1,91E+06	(57)	36	352 93	83.3	62.2	111.4
86	6,22E+06	(155)	8,43E+05	(21)	30	156 67	135.5	86.4	225.3
87	9,49E+06	(315)	9,94E+05	(33)	40	184 64	175.1	123.0	258.6
88	9,72E+06	(807)	8,31E+05	(69)	100	153 37	213.3	166.2	273.5
89	4,58E+06	(152)	5,12E+05	(17)	40	95 45	163.5	100.0	287.9
90	4,15E+06	(155)	4,55E+05	(17)	45	84 40	166.7	102.1	293.3
91	1,03E+07	(128)	8,03E+05	(10)	15	148 92	231.3	124.5	491.6
92	3,54E+06	(94)	6,02E+05	(16)	32	111 55	107.9	63.8	196.9
93	7,54E+06	(169)	1,16E+06	(26)	27	214 83	119.6	79.4	188.6
94	6,71E+06	(156)	1,59E+06	(37)	28	294 96	78.0	54.4	115.1
POOLED	8,22E+06	(22542)	1,31E+06	(3590)	3303	242 11	116.1	108.0	124.9

CHI^2 PROBABILITY (%): 0.0

POOLED AGE W/ 68% CONF. INTERVAL(Ma): 116.1, 111.9 -- 120.5 (-4.2 +4.4)
95% CONF. INTERVAL(Ma): 108.0 -- 124.9 (-8.2 +8.8)

CENTRAL AGE W/ 68% CONF. INTERVAL(Ma): 111.5, 105.2 -- 118.3 (-6.4 +6.8)
95% CONF. INTERVAL(Ma): 99.4 -- 125.2 (-12.1 +13.6)
AGE DISPERSION (%): 43.7

Merged dataset:
C:\BH2\Jairo\Samples-IRR-6-2015\JG-P4-13\JG-P4-13a.ftz
C:\BH2\Jairo\Samples-IRR-6-2015\JG-P4-13\JG-P4-13.ftz

FIT OPTION: Best-fit peaks using the binomial model of Galbraith and Green

INITIAL GUESS FOR MODEL PARAMETERS (number of peaks to fit = 3)

Peak #.	Peak Age	Theta	Fraction(%)	Count
1.	54.40	0.745	6.9	6.45
2.	87.80	0.826	27.7	26.00
3.	116.10	0.863	22.7	21.34

Total range for grain ages: 42,1 to 273,0 Ma
Number of active grains (Num. used for fit): 94
Number of removed grains: 0
Degrees of freedom for fit: 89
Average of the SE(Z)'s for the grains: 0,21
Estimated width of peaks in PD plot in Z units: 0,24

PARAMETERS FOR BEST-FIT PEAKS

* *Standard error for peak age includes group error*
* *Peak width is for PD plot assuming a kernel factor = 0.60*

#.	Peak Age(Ma)	68%CI	95%CI	W(Z)	Frac(%)	SE,%	Count
1.	49.1	-3,2 ...+3,4	-6,0 ...+6,9	0.15	7.9	3.2	7.4
2.	85.4	-4,3 ...+4,5	-8,2 ...+9,1	0.20	39.2	5.9	36.8
3.	173.9	-7,7 ...+8,0	-14,8 ...+16,1	0.22	52.9	6.0	49.8

Log-likelihood for best fit: -364,825
Chi-squared value for best fit: 88,257
Reduced chi-squared value: 0,992
Probability for F test: 0%
Condition number for COVAR matrix: 5,09
Number of iterations: 8

Merged dataset:
C:\BH2\Jairo\Samples-IRR-6-2015\JG-P4-13\JG-P4-13a.ftz
C:\BH2\Jairo\Samples-IRR-6-2015\JG-P4-13\JG-P4-13.ftz

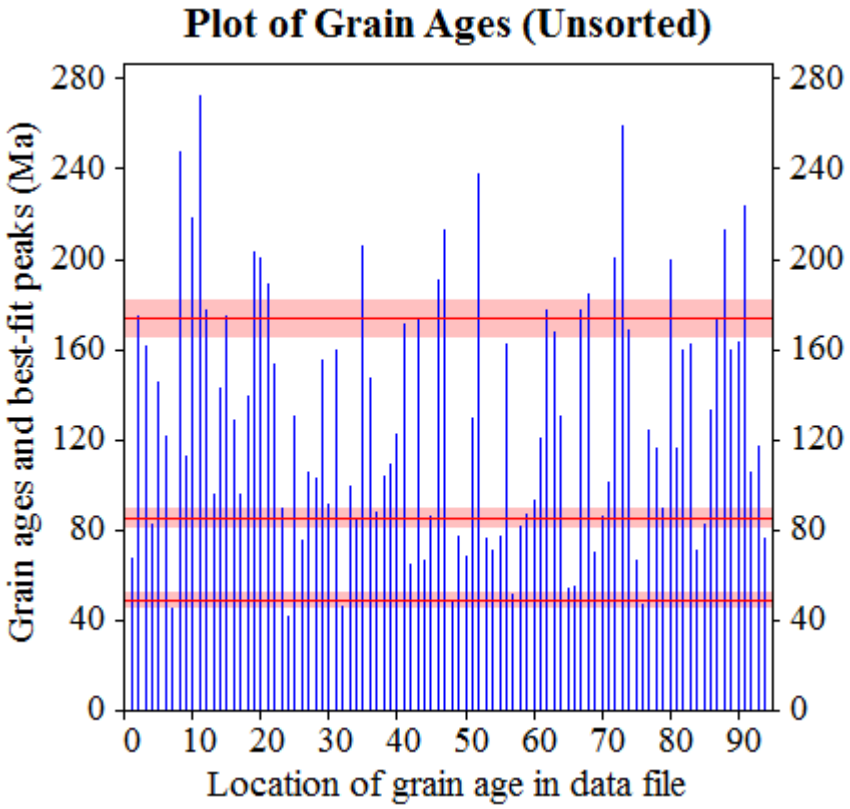

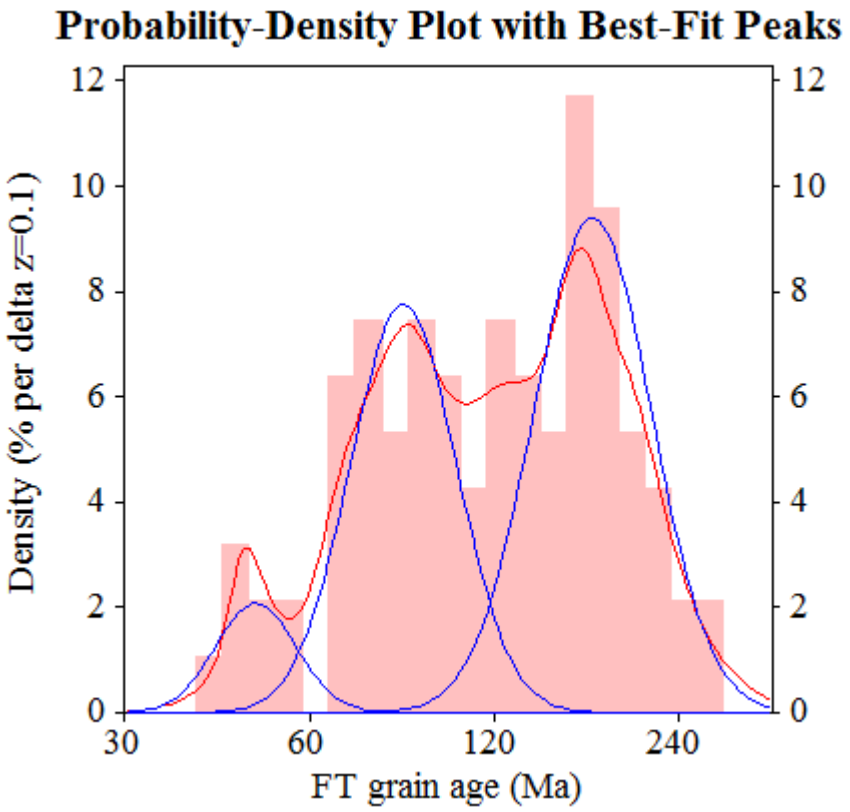

Merged dataset:
C:\BH2\Jairo\Samples-IRR-6-2015\JG-P4-13\JG-P4-13a.ftz
C:\BH2\Jairo\Samples-IRR-6-2015\JG-P4-13\JG-P4-13.ftz

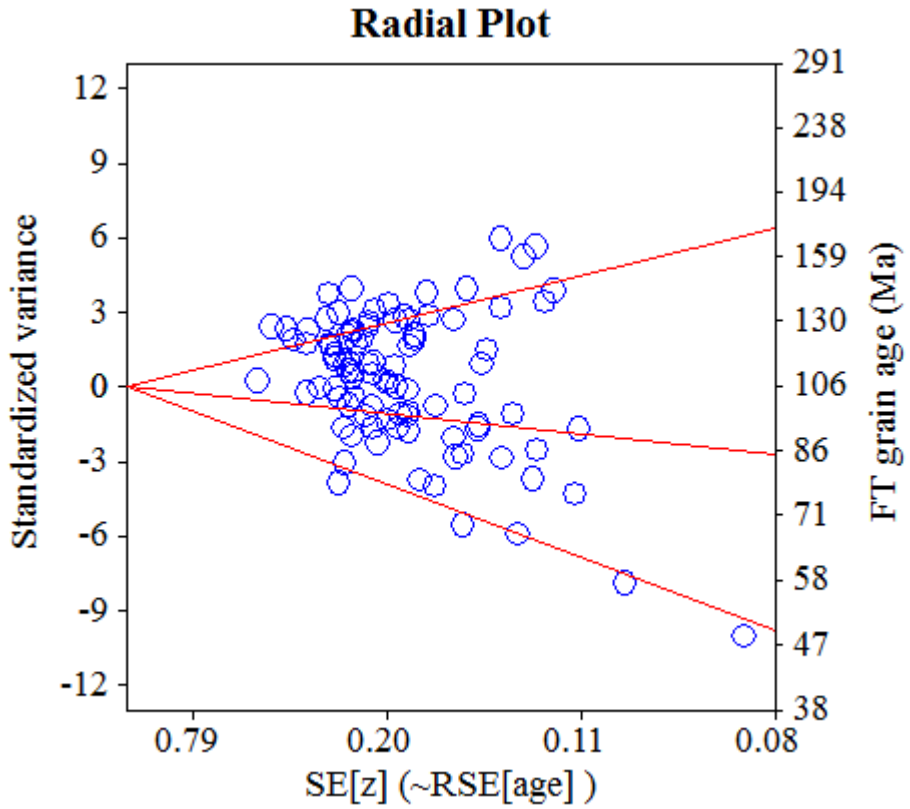

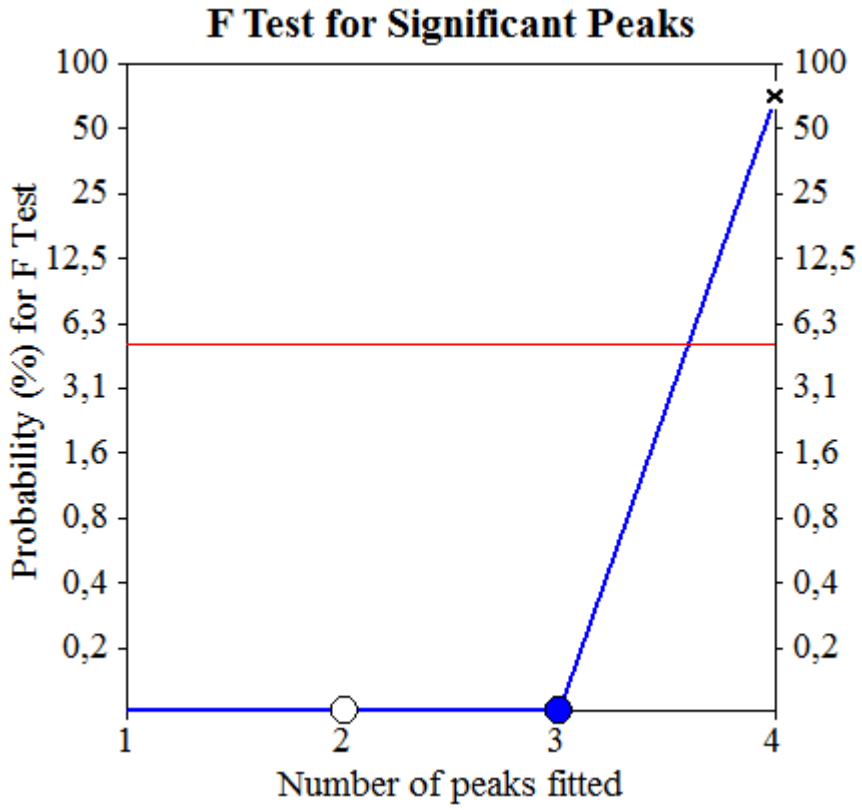

Datafile: C:\BH2\Jairo\Echantillon-IRR082015\JG-P4-02Paila\JG-P4-02-Ap.fta
Title: JG-P4-02 Irr 8-2015-21

NEW PARAMETERS - ZETA METHOD

EFFECTIVE TRACK DENSITY FOR FLUENCE MONITOR (tracks/cm^2): 1,31E+06
RELATIVE ERROR (%): 1,28
EFFECTIVE URANIUM CONTENT OF MONITOR (ppm): 15,00
ZETA FACTOR AND STANDARD ERROR (yr cm^2): 282,02 6,88
SIZE OF COUNTER SQUARE (cm^2): 6,39E-07

GRAIN AGES IN ORIGINAL ORDER

Grain no.	RhoS (cm^-2)	(Ns)	RhoI (cm^-2)	(Ni)	Squares	U+/-2s		Grain Age (Ma) Age	--95% CI--	
1	5,22E+04	(3)	6,94E+06	(399)	90	80	8	1.5	0.3	4.1
2	1,15E+05	(5)	7,32E+06	(318)	68	84	10	3.0	0.9	6.8
3	7,82E+04	(3)	8,56E+06	(328)	60	98	11	1.8	0.3	5.0
4	1,36E+05	(4)	6,43E+06	(189)	46	74	11	4.0	1.1	10.1
5	7,96E+04	(3)	6,13E+06	(231)	59	70	9	2.5	0.5	7.1
6	3,23E+04	(2)	5,49E+06	(340)	97	63	7	1.2	0.1	3.9
7	6,26E+04	(4)	8,14E+06	(520)	100	94	9	1.5	0.4	3.6
POOLED	7,22E+04	(24)	7,00E+06	(2325)	520	80	4	1.9	1.2	2.8

CHI^2 PROBABILITY (%): 61.1
>>> Beware: possible upward bias in Chi^2 probability due to low counts <<<

POOLED AGE W/ 68% CONF. INTERVAL(Ma): 1.9, 1.5 -- 2.4 (-0.4 +0.5)
95% CONF. INTERVAL(Ma): 1.2 -- 2.8 (-0.7 +0.9)

CENTRAL AGE W/ 68% CONF. INTERVAL(Ma): 1.9, 1.5 -- 2.3 (-0.4 +0.4)
95% CONF. INTERVAL(Ma): 1.3 -- 2.8 (-0.6 +1.0)
AGE DISPERSION (%): 0.2

FIT OPTION: Best-fit peaks using the binomial model of Galbraith and Green

INITIAL GUESS FOR MODEL PARAMETERS (number of peaks to fit = 1)

Peak #.	Peak Age	Theta	Fraction(%)	Count
1.	1.90	0.010	26.9	1.88

Total range for grain ages:	1,4 to 4,4 Ma
Number of active grains (Num. used for fit):	7
Number of removed grains:	0
Degrees of freedom for fit:	6
Average of the SE(Z)'s for the grains:	0,52
Estimated width of peaks in PD plot in Z units:	0,61

PARAMETERS FOR BEST-FIT PEAKS

* *Standard error for peak age includes group error*
* *Peak width is for PD plot assuming a kernel factor = 0.60*

#.	Peak Age(Ma)	68%CI	95%CI	W(Z)	Frac(%)	SE,%	Count
1.	1.9	-0,4 ...+0,4	-0,6 ...+1,0	0.63	100.0	0.0	7.0

Log-likelihood for best fit:	-12,788
Chi-squared value for best fit:	4,485
Reduced chi-squared value:	0,748
Probability for F test:	0%
Condition number for COVAR matrix:	1,00
Number of iterations:	5

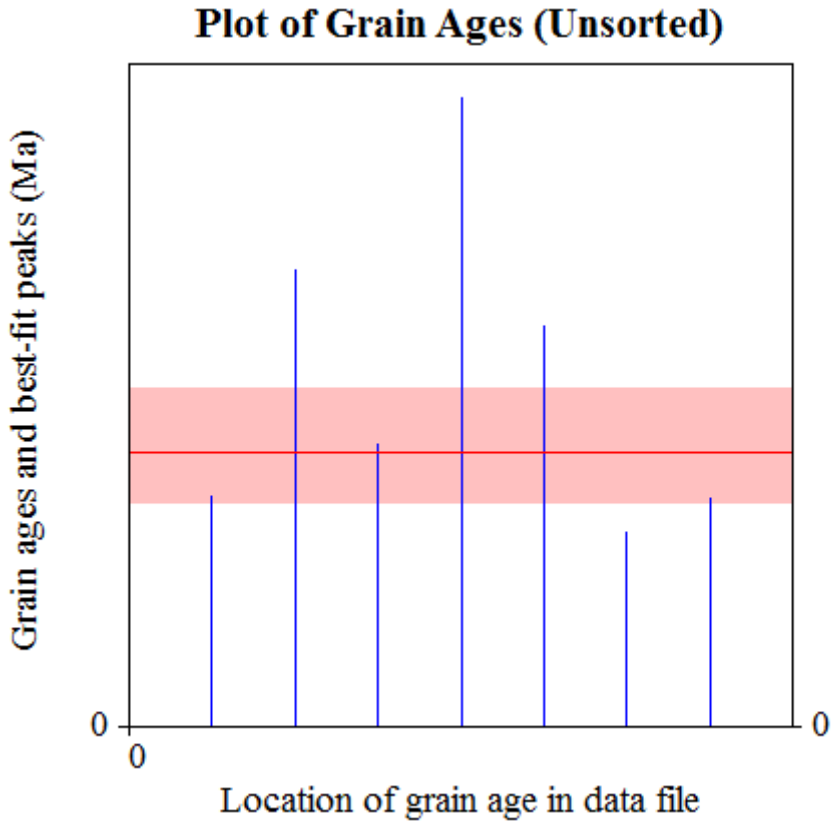
Plot of Grain Ages (Unsorted)
Grain ages and best-fit peaks (Ma)
0
0
0
Location of grain age in data file

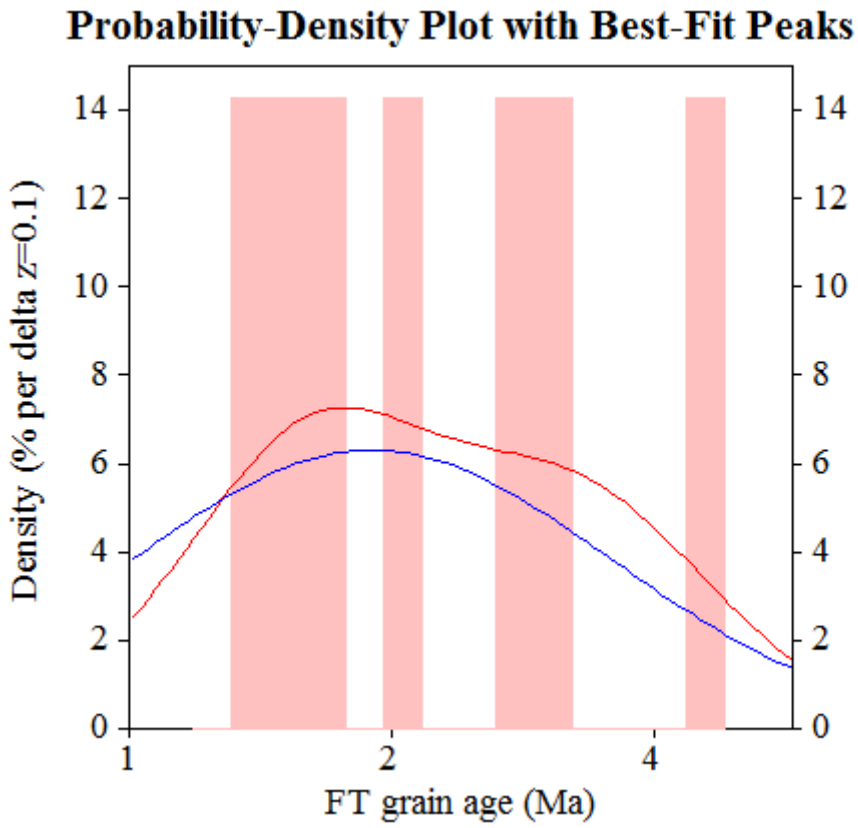
Probability-Density Plot with Best-Fit Peaks
Density (% per delta z=0.1)
14
12
10
8
6
4
2
0
1
2
4
FT grain age (Ma)

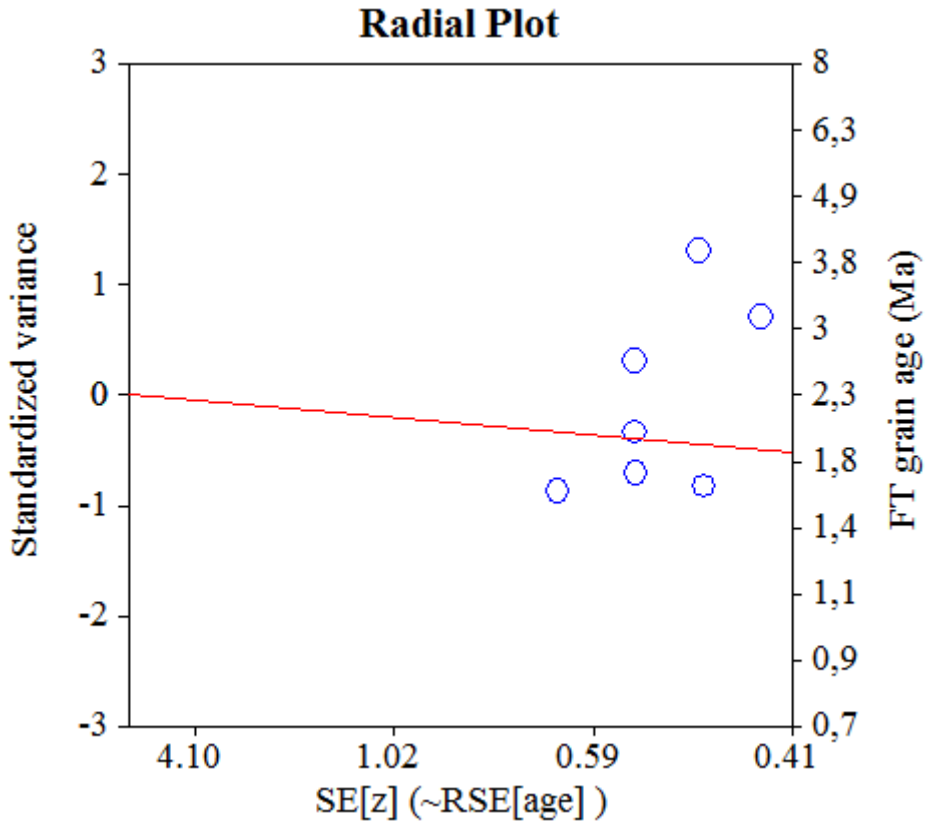
Radial Plot
Standardized variance
FT grain age (Ma)
SE[z] (~RSE[age])
4.10
1.02
0.59
0.41
3
2
1
0
-1
-2
-3
8
6,3
4,9
3,8
3
2,3
1,8
1,4
1,1
0,9
0,7

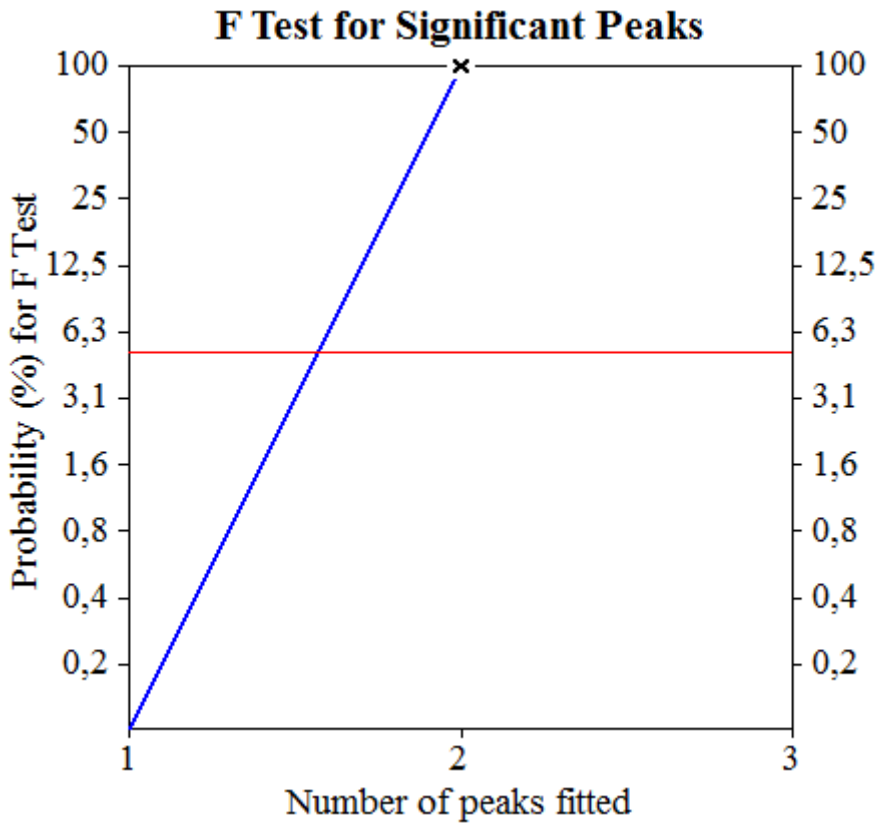
F Test for Significant Peaks
Probability (%) for F Test
Number of peaks fitted
100
50
25
12,5
6,3
3,1
1,6
0,8
0,4
0,2
1
2
3

Datafile: C:\BH2\Jairo\Echantillon-IRR082015\JG-P4-06\JG-P4-06-Ap.fta
Title: JG-P4-06 Irr 8-2015-23

NEW PARAMETERS - ZETA METHOD

EFFECTIVE TRACK DENSITY FOR FLUENCE MONITOR (tracks/cm^2): 1,31E+06
RELATIVE ERROR (%): 1,37
EFFECTIVE URANIUM CONTENT OF MONITOR (ppm): 15,00
ZETA FACTOR AND STANDARD ERROR (yr cm^2): 282,02 6,88
SIZE OF COUNTER SQUARE (cm^2): 6,39E-07

GRAIN AGES IN ORIGINAL ORDER

Grain no.	RhoS (cm^-2)	(Ns)	RhoI (cm^-2)	(Ni)	Squares	U+/-2s		Grain Age (Ma) Age	--95% CI--	
1	2,74E+05	(7)	6,34E+06	(162)	40	72	12	8.2	3.2	16.9
2	1,17E+05	(5)	9,30E+06	(398)	67	106	11	2.4	0.8	5.5
3	1,02E+05	(6)	1,05E+07	(619)	92	120	10	1.8	0.7	3.9
4	1,30E+05	(5)	8,79E+06	(337)	60	100	11	2.8	0.9	6.5
5	2,35E+05	(6)	1,26E+07	(321)	40	143	16	3.6	1.3	7.6
6	1,04E+05	(4)	3,78E+06	(145)	60	43	7	5.3	1.4	13.4
7	1,22E+05	(7)	1,01E+07	(579)	90	115	10	2.3	0.9	4.6
8	9,39E+04	(3)	8,92E+06	(285)	50	102	12	2.1	0.4	5.8
9	6,39E+04	(4)	6,45E+06	(404)	98	74	8	1.9	0.5	4.7
10	1,22E+05	(5)	6,70E+06	(274)	64	77	9	3.5	1.1	8.0
11	1,34E+05	(6)	8,54E+06	(382)	70	98	10	3.0	1.1	6.4
12	1,36E+05	(6)	6,62E+06	(292)	69	76	9	3.9	1.4	8.4
13	1,79E+05	(8)	8,52E+06	(381)	70	97	10	4.0	1.7	7.7
14	2,28E+05	(7)	1,23E+07	(376)	48	140	15	3.5	1.4	7.2
15	1,04E+05	(4)	8,97E+06	(344)	60	103	11	2.2	0.6	5.6
16	1,27E+05	(6)	8,08E+06	(382)	74	92	10	3.0	1.1	6.4
17	1,30E+05	(5)	4,43E+06	(170)	60	51	8	5.6	1.7	13.0
POOLED	1,32E+05	(94)	8,23E+06	(5851)	1112	94	4	3.0	2.4	3.7

CHI^2 PROBABILITY (%): 47.0
>>> Beware: possible upward bias in Chi^2 probability due to low counts <<<

POOLED AGE W/ 68% CONF. INTERVAL(Ma): 3.0, 2.7 -- 3.3 (-0.3 +0.3)
95% CONF. INTERVAL(Ma): 2.4 -- 3.7 (-0.6 +0.7)

CENTRAL AGE W/ 68% CONF. INTERVAL(Ma): 3.0, 2.7 -- 3.3 (-0.3 +0.3)
95% CONF. INTERVAL(Ma): 2.4 -- 3.7 (-0.6 +0.7)
AGE DISPERSION (%): 0.5

FIT OPTION: Best-fit peaks using the binomial model of Galbraith and Green

INITIAL GUESS FOR MODEL PARAMETERS (number of peaks to fit = 1)

Peak #.	Peak Age	Theta	Fraction(%)	Count
1.	3.00	0.016	32.6	5.54

Total range for grain ages: 1,9 to 8,5 Ma
Number of active grains (Num. used for fit): 17
Number of removed grains: 0
Degrees of freedom for fit: 16
Average of the SE(Z)'s for the grains: 0,42
Estimated width of peaks in PD plot in Z units: 0,49

PARAMETERS FOR BEST-FIT PEAKS

* *Standard error for peak age includes group error*
* *Peak width is for PD plot assuming a kernel factor = 0.60*

#.	Peak Age(Ma)	68%CI	95%CI	W(Z)	Frac(%)	SE,%	Count
1.	3.0	-0,3 ...+0,3	-0,6 ...+0,7	0.50	100.0	0.0	17.0

Log-likelihood for best fit: -36,788
Chi-squared value for best fit: 15,758
Reduced chi-squared value: 0,985
Probability for F test: 0%
Condition number for COVAR matrix: 1,00
Number of iterations: 5

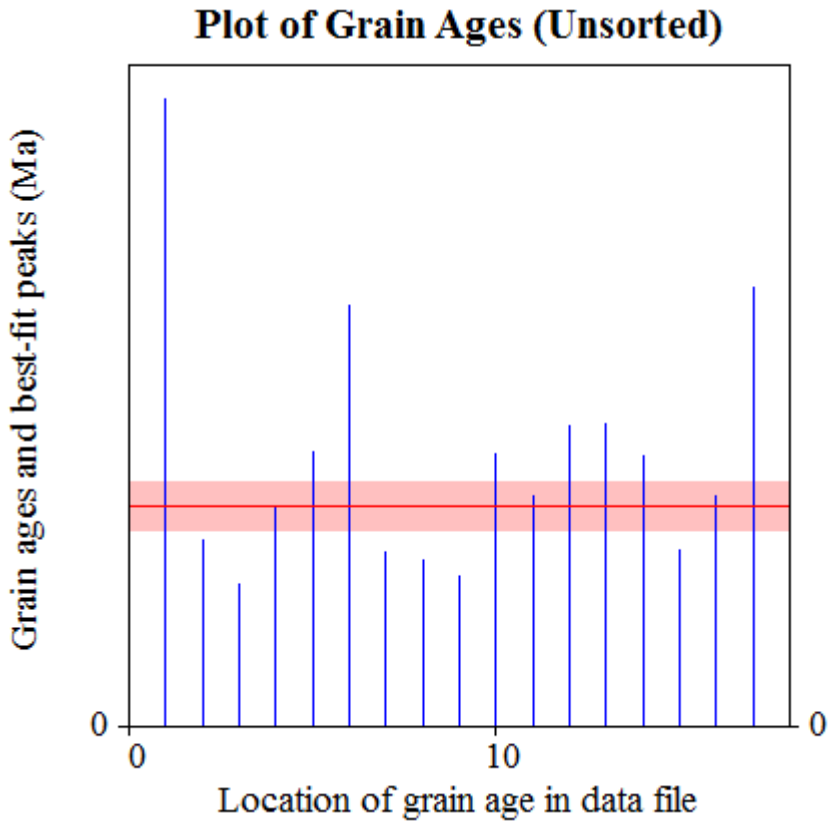
Plot of Grain Ages (Unsorted)
Grain ages and best-fit peaks (Ma)
0
0
10
0
Location of grain age in data file

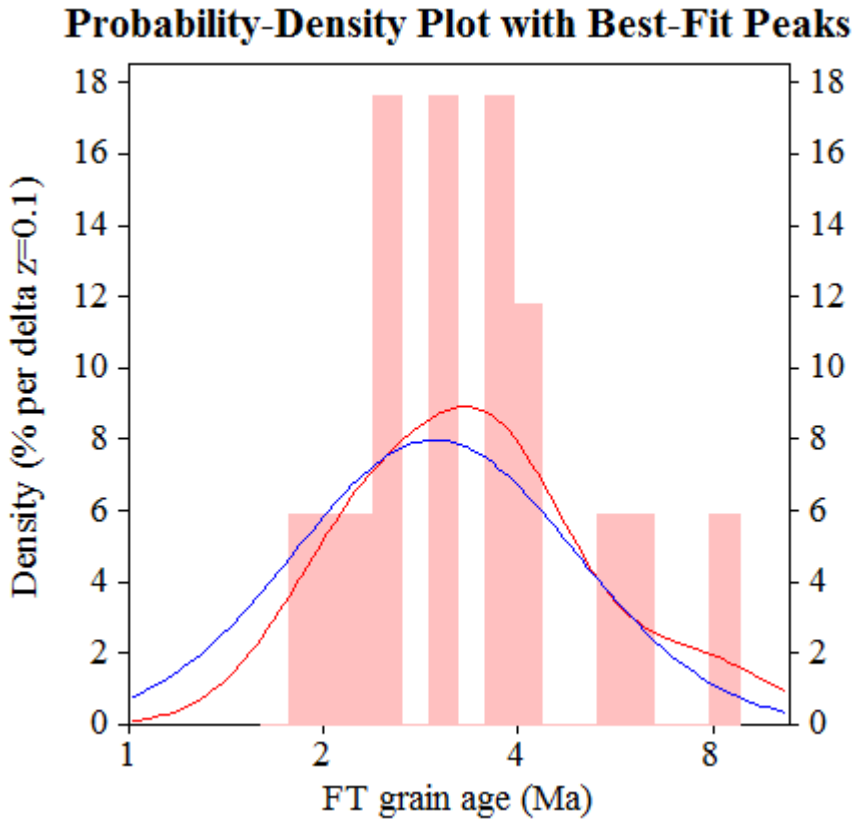
Probability-Density Plot with Best-Fit Peaks
Density (% per delta z=0.1)
18
16
14
12
10
8
6
4
2
0
1
2
4
8
FT grain age (Ma)

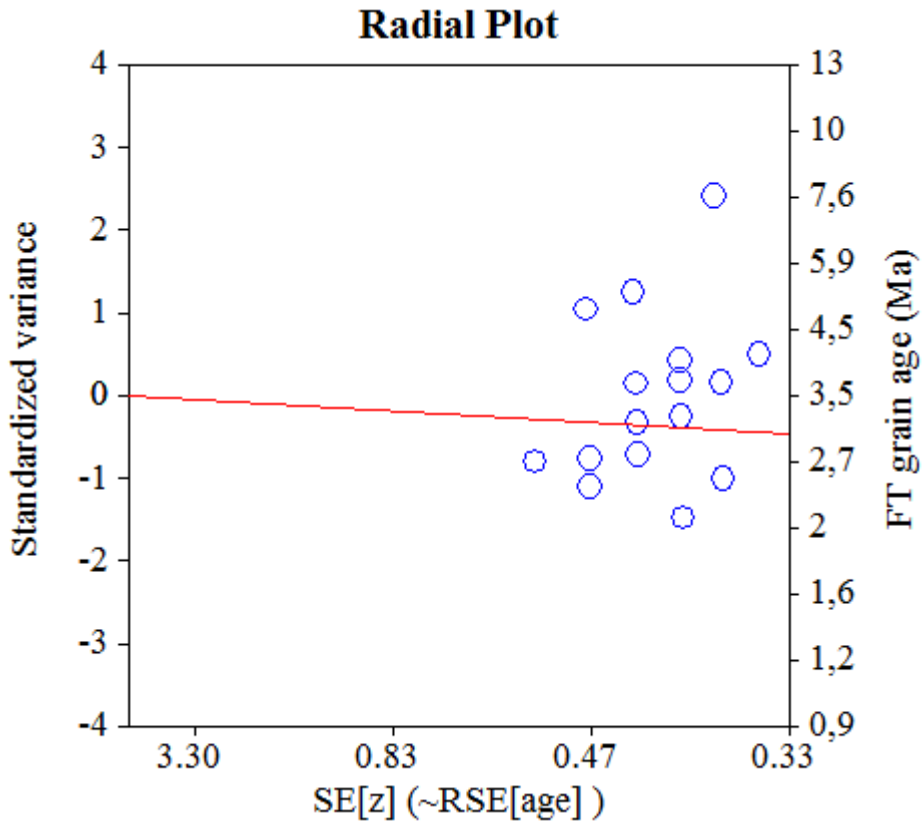
Radial Plot
Standardized variance
4
3
2
1
0
-1
-2
-3
-4
3.30
0.83
0.47
0.33
SE[z] (~RSE[age])
13
10
7,6
5,9
4,5
3,5
2,7
2
1,6
1,2
0,9
FT grain age (Ma)

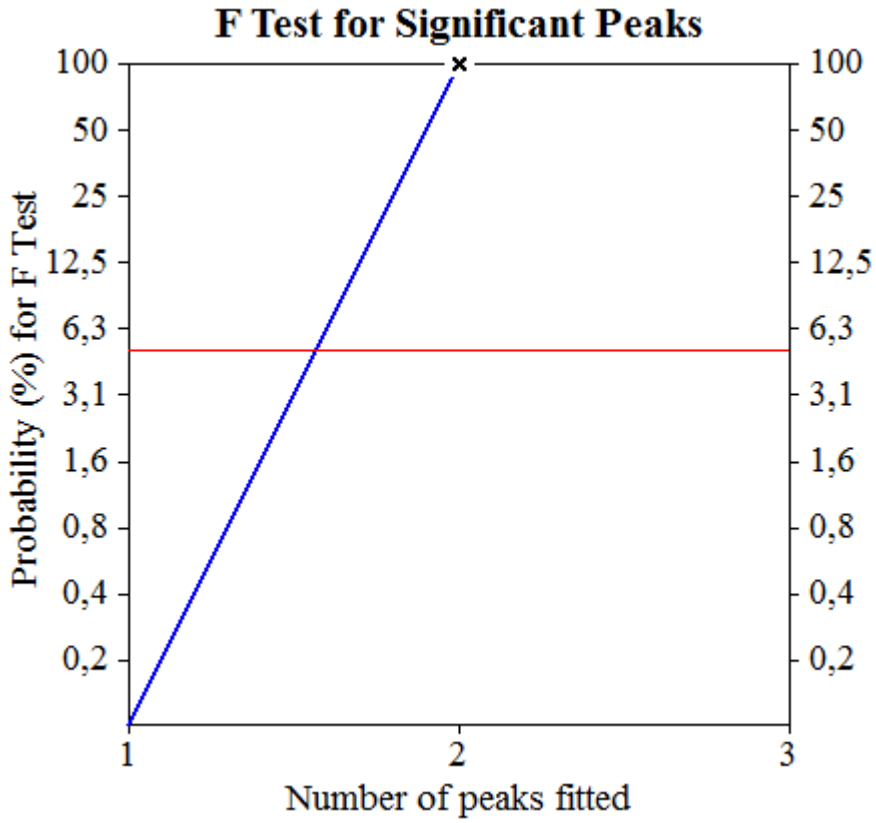
F Test for Significant Peaks
Probability (%) for F Test
100
50
25
12,5
6,3
3,1
1,6
0,8
0,4
0,2
1
2
3
Number of peaks fitted

Datafile: C:\BH2\Jairo\Echantillon-IRR082015\JG-P4-10\JG-P4-10-Ap.fta
Title: JG-P4-10 Irr 8-2015-24

NEW PARAMETERS - ZETA METHOD

EFFECTIVE TRACK DENSITY FOR FLUENCE MONITOR (tracks/cm^2): 1,32E+06
RELATIVE ERROR (%): 1,42
EFFECTIVE URANIUM CONTENT OF MONITOR (ppm): 15,00
ZETA FACTOR AND STANDARD ERROR (yr cm^2): 282,02 6,88
SIZE OF COUNTER SQUARE (cm^2): 6,39E-07

GRAIN AGES IN ORIGINAL ORDER

Grain no.	RhoS (cm^-2)	(Ns)	RhoI (cm^-2)	(Ni)	Squares	U+/-2s		Grain Age (Ma) Age	--95% CI--	
1	9,39E+04	(6)	9,94E+06	(635)	100	113	10	1.8	0.6	3.8
2	2,24E+05	(10)	1,16E+07	(520)	70	132	12	3.6	1.7	6.6
3	6,26E+04	(4)	7,43E+06	(475)	100	85	8	1.6	0.4	4.0
4	1,56E+04	(1)	1,19E+06	(76)	100	14	3	2.8	0.1	14.0
5	2,30E+04	(1)	4,83E+05	(21)	68	6	2	10.1	0.2	54.8
6	2,37E+04	(1)	3,32E+05	(14)	66	4	2	15.0	0.3	86.6
7	4,60E+04	(2)	8,05E+05	(35)	68	9	3	11.4	1.2	41.2
8	1,56E+04	(1)	5,48E+05	(35)	100	6	2	6.1	0.1	31.5
9	3,13E+04	(2)	3,13E+05	(20)	100	4	2	19.8	2.1	76.0
POOLED	5,68E+04	(28)	3,71E+06	(1831)	772	42	2	2.9	1.9	4.1

CHI^2 PROBABILITY (%): 1.0
>>> Beware: possible upward bias in Chi^2 probability due to low counts <<<

POOLED AGE W/ 68% CONF. INTERVAL(Ma): 2.9, 2.3 -- 3.5 (-0.6 +0.6)
95% CONF. INTERVAL(Ma): 1.9 -- 4.1 (-1.0 +1.3)

CENTRAL AGE W/ 68% CONF. INTERVAL(Ma): 3.1, 2.5 -- 3.9 (-0.6 +0.8)
95% CONF. INTERVAL(Ma): 2.0 -- 4.9 (-1.1 +1.7)
AGE DISPERSION (%): 26.2

FIT OPTION: Best-fit peaks using the binomial model of Galbraith and Green

INITIAL GUESS FOR MODEL PARAMETERS (number of peaks to fit = 1)

Peak #.	Peak Age	Theta	Fraction(%)	Count
1.	2.90	0.015	9.5	0.86

Total range for grain ages: 1,8 to 22,6 Ma
Number of active grains (Num. used for fit): 9
Number of removed grains: 0
Degrees of freedom for fit: 8
Average of the SE(Z)'s for the grains: 0,68
Estimated width of peaks in PD plot in Z units: 0,79

PARAMETERS FOR BEST-FIT PEAKS

* *Standard error for peak age includes group error*
* *Peak width is for PD plot assuming a kernel factor = 0.60*

#.	Peak Age(Ma)	68%CI	95%CI	W(Z)	Frac(%)	SE,%	Count
1.	2.8	-0,5 ...+0,6	-0,9 ...+1,3	0.67	100.0	0.0	9.0

Log-likelihood for best fit: -18,384
Chi-squared value for best fit: 20,177
Reduced chi-squared value: 2,522
Probability for F test: 0%
Condition number for COVAR matrix: 1,00
Number of iterations: 5

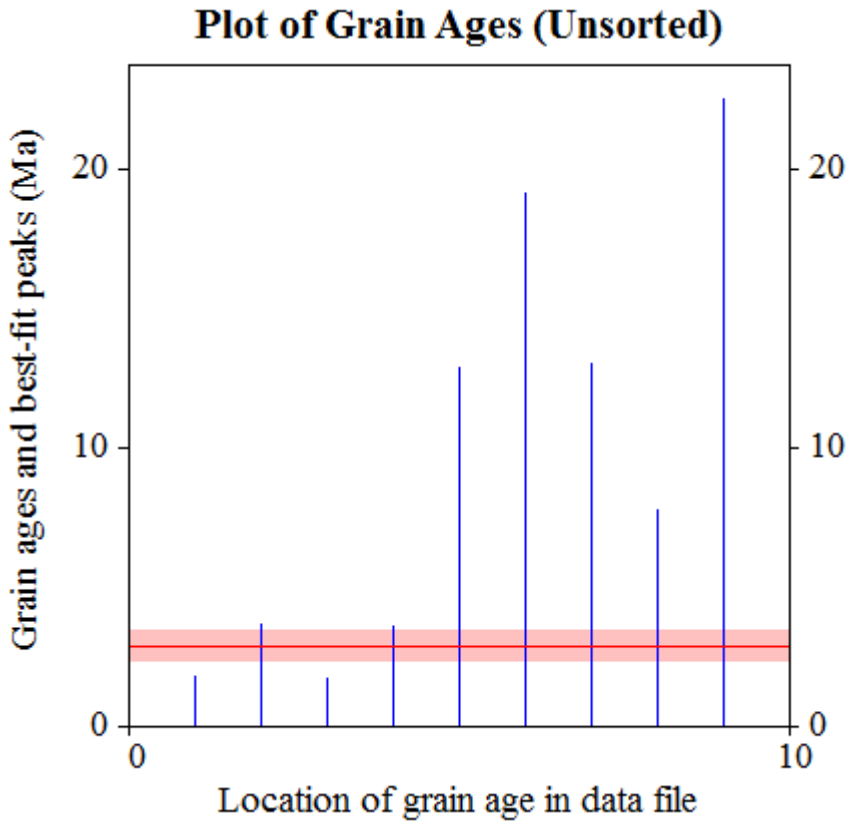
Plot of Grain Ages (Unsorted)
Grain ages and best-fit peaks (Ma)
20
10
0
0
10
Location of grain age in data file

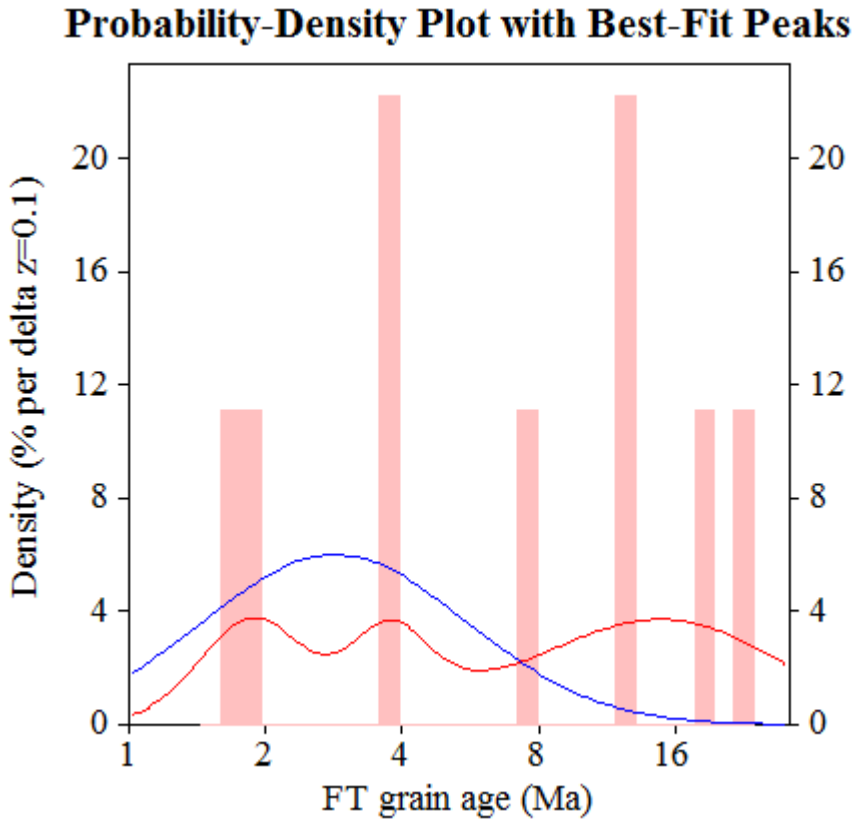
Probability-Density Plot with Best-Fit Peaks
Density (% per delta z=0.1)
20
16
12
8
4
0
1
2
4
8
16
FT grain age (Ma)

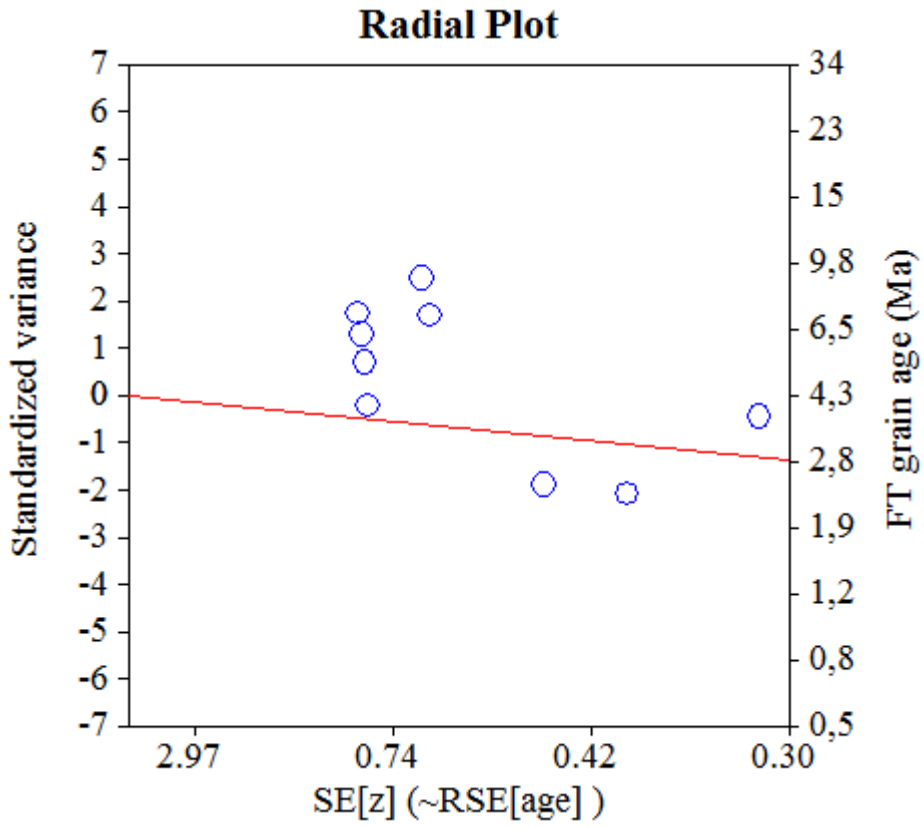
Radial Plot
Standardized variance
FT grain age (Ma)
7
6
5
4
3
2
1
0
-1
-2
-3
-4
-5
-6
-7
34
23
15
9,8
6,5
4,3
2,8
1,9
1,2
0,8
0,5
2.97
0.74
0.42
0.30
SE[z] (~RSE[age])

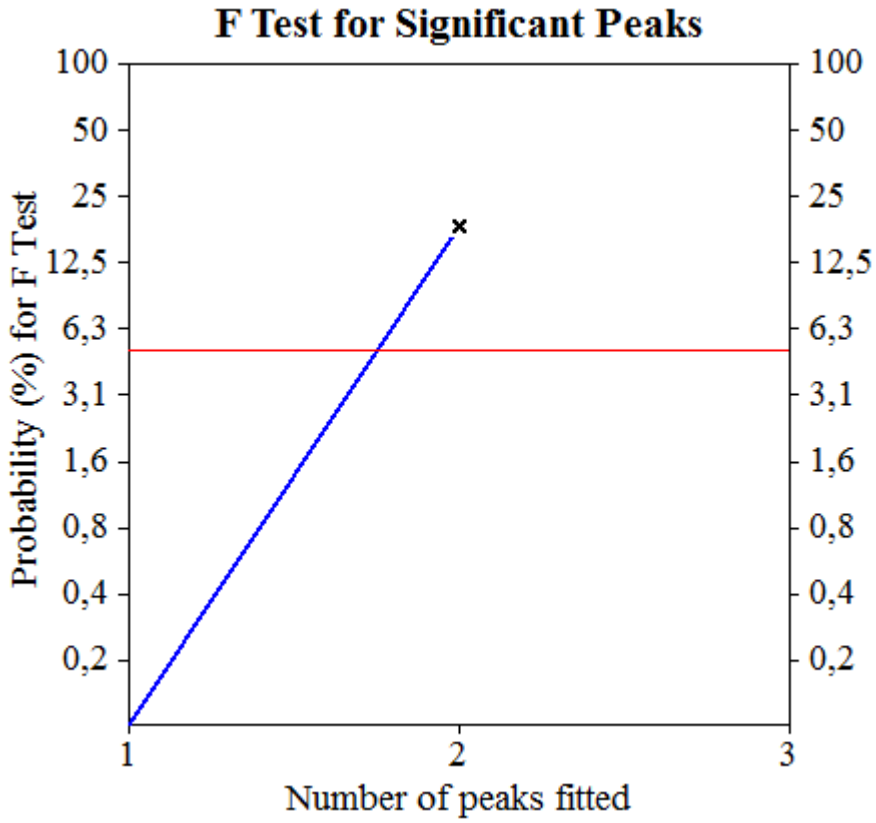
F Test for Significant Peaks
Probability (%) for F Test
100
50
25
12,5
6,3
3,1
1,6
0,8
0,4
0,2
1
2
3
Number of peaks fitted

Datafile: C:\BH2\Jairo\Echantillon-IRR052015\JG-P4-13\JG-P4-13-Ap2.fta
Title: JG-P4-13 Irr 5-2015-22

NEW PARAMETERS - ZETA METHOD

EFFECTIVE TRACK DENSITY FOR FLUENCE MONITOR (tracks/cm^2): 1,23E+06
RELATIVE ERROR (%): 1,31
EFFECTIVE URANIUM CONTENT OF MONITOR (ppm): 15,00
ZETA FACTOR AND STANDARD ERROR (yr cm^2): 282,02 6,88
SIZE OF COUNTER SQUARE (cm^2): 6,39E-07

GRAIN AGES IN ORIGINAL ORDER

Grain no.	RhoS (cm^-2)	(Ns)	RhoI (cm^-2)	(Ni)	Squares	U+/-2s		Grain Age (Ma) Age	--95% CI--	
1	4,69E+04	(3)	1,61E+06	(103)	100	20	4	5.3	1.0	15.1
2	1,30E+05	(1)	4,17E+06	(32)	12	51	18	6.2	0.1	32.3
3	3,13E+04	(2)	3,63E+06	(232)	100	44	6	1.6	0.2	5.5
4	1,56E+04	(1)	4,69E+05	(30)	100	6	2	6.6	0.1	34.6
5	2,03E+05	(13)	1,09E+07	(698)	100	133	11	3.3	1.7	5.6
6	1,22E+05	(5)	9,78E+05	(40)	64	12	4	22.2	6.7	54.6
7	1,28E+05	(8)	4,34E+06	(272)	98	53	7	5.2	2.2	10.2
8	1,25E+05	(8)	1,27E+06	(81)	100	15	3	17.4	7.1	35.3
9	4,35E+04	(2)	2,24E+06	(103)	72	27	5	3.6	0.4	12.5
10	1,56E+04	(1)	3,29E+05	(21)	100	4	2	9.4	0.2	51.1
11	2,50E+05	(4)	2,50E+06	(40)	25	31	10	17.9	4.5	47.8
12	1,29E+05	(8)	6,45E+06	(400)	97	79	8	3.5	1.5	6.9
13	1,14E+05	(7)	3,18E+06	(195)	96	39	6	6.4	2.5	13.0
14	6,26E+04	(4)	1,64E+06	(105)	100	20	4	6.8	1.8	17.4
15	6,26E+04	(4)	1,28E+06	(82)	100	16	3	8.8	2.2	22.4
16	3,48E+04	(2)	2,96E+05	(17)	90	4	2	21.7	2.3	85.3
17	3,48E+04	(2)	5,91E+05	(34)	90	7	2	10.9	1.2	39.6
18	3,13E+04	(2)	1,08E+06	(69)	100	13	3	5.4	0.6	18.8
19	2,52E+04	(1)	8,58E+05	(34)	62	10	4	5.8	0.1	30.3
20	3,29E+05	(20)	9,95E+06	(604)	95	122	10	5.8	3.5	8.9
21	1,37E+05	(7)	8,90E+06	(455)	80	109	11	2.7	1.1	5.5
22	6,26E+04	(4)	1,00E+06	(64)	100	12	3	11.2	2.9	29.0
23	3,16E+04	(2)	2,07E+06	(131)	99	25	4	2.8	0.3	9.7
24	3,13E+04	(2)	5,48E+05	(35)	100	7	2	10.6	1.2	38.4
25	7,82E+04	(5)	1,49E+06	(95)	100	18	4	9.4	2.9	22.0
26	4,69E+04	(3)	3,91E+05	(25)	100	5	2	21.7	4.0	67.8
27	9,88E+04	(6)	5,50E+06	(334)	95	67	8	3.2	1.1	6.8
28	7,20E+04	(4)	7,43E+06	(413)	87	91	9	1.7	0.5	4.3
29	5,80E+04	(3)	8,50E+05	(44)	81	10	3	12.4	2.3	36.7
30	2,41E+05	(8)	1,04E+07	(347)	52	128	14	4.1	1.7	8.0
31	1,41E+05	(9)	6,12E+06	(391)	100	75	8	4.1	1.8	7.6
32	3,16E+04	(2)	4,43E+05	(28)	99	5	2	13.2	1.4	48.9
33	3,19E+04	(2)	5,43E+05	(34)	98	7	2	10.9	1.2	39.6
34	1,56E+04	(1)	9,23E+05	(59)	100	11	3	3.4	0.1	17.0
35	3,13E+04	(2)	9,70E+05	(62)	100	12	3	6.0	0.7	21.0
36	3,13E+04	(2)	3,15E+06	(201)	100	38	6	1.9	0.2	6.3
37	9,68E+04	(6)	5,89E+06	(365)	97	72	8	2.9	1.0	6.3
38	9,78E+04	(6)	2,72E+06	(167)	96	33	5	6.4	2.2	13.8
39	1,56E+04	(1)	9,70E+05	(62)	100	12	3	3.2	0.1	16.1
POOLED	7,77E+04	(173)	2,92E+06	(6504)	3485	36	1	4.6	3.9	5.4

CHI^2 PROBABILITY (%): 0.0
>>> Beware: possible upward bias in Chi^2 probability due to low counts <<<

POOLED AGE W/ 68% CONF. INTERVAL(Ma): 4.6, 4.2 -- 5.0 (-0.4 +0.4)
95% CONF. INTERVAL(Ma): 3.9 -- 5.4 (-0.7 +0.8)

CENTRAL AGE W/ 68% CONF. INTERVAL(Ma): 5.4, 4.8 -- 6.0 (-0.6 +0.6)
95% CONF. INTERVAL(Ma): 4.3 -- 6.7 (-1.0 +1.3)
AGE DISPERSION (%): 39.2

FIT OPTION: Best-fit peaks using the binomial model of Galbraith and Green

INITIAL GUESS FOR MODEL PARAMETERS (number of peaks to fit = 2)

Peak #.	Peak Age	Theta	Fraction(%)	Count
1.	4.60	0.026	16.5	6.42
2.	5.90	0.033	18.4	7.18

Total range for grain ages:	1,9 to 24,7 Ma
Number of active grains (Num. used for fit):	39
Number of removed grains:	0
Degrees of freedom for fit:	36
Average of the SE(Z)'s for the grains:	0,57
Estimated width of peaks in PD plot in Z units:	0,67

PARAMETERS FOR BEST-FIT PEAKS

* *Standard error for peak age includes group error*
* *Peak width is for PD plot assuming a kernel factor = 0.60*

#.	Peak Age(Ma)	68%CI	95%CI	W(Z)	Frac(%)	SE,%	Count
1.	4.1	-0,4 ...+0,4	-0,7 ...+0,9	0.55	79.9	12.9	31.1
2.	13.0	-3,7 ...+5,2	-6,3 ...+12,3	0.62	20.1	12.9	7.9

Log-likelihood for best fit:	-87,305
Chi-squared value for best fit:	33,299
Reduced chi-squared value:	0,925
Probability for F test:	0%
Condition number for COVAR matrix:	18,79
Number of iterations:	45

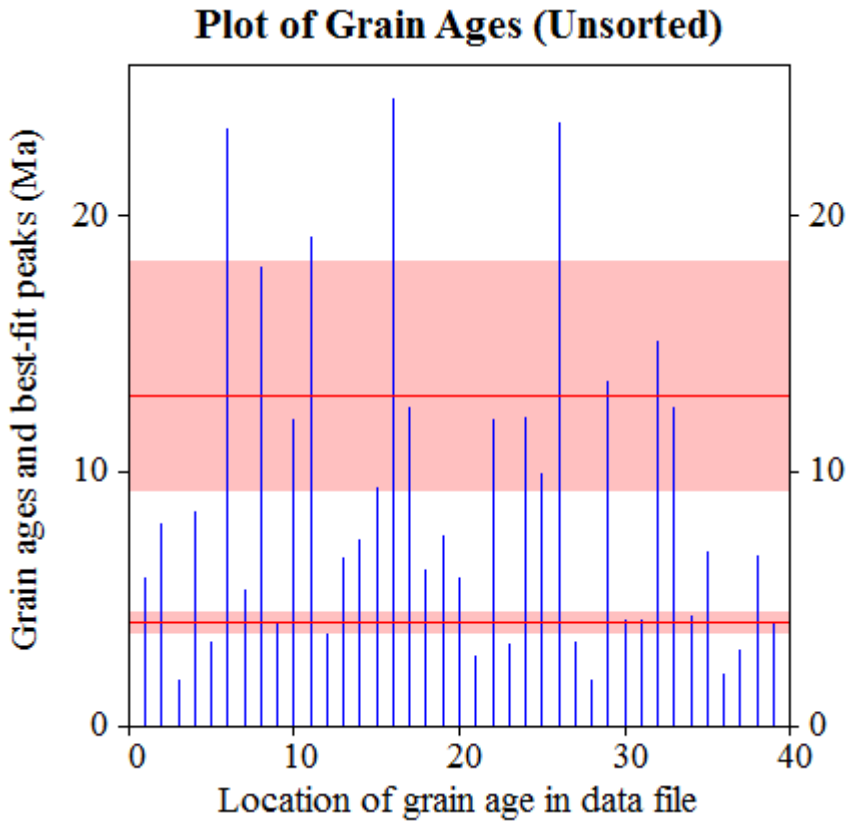
Plot of Grain Ages (Unsorted)
Grain ages and best-fit peaks (Ma)
0
10
20
0
10
20
30
40
Location of grain age in data file

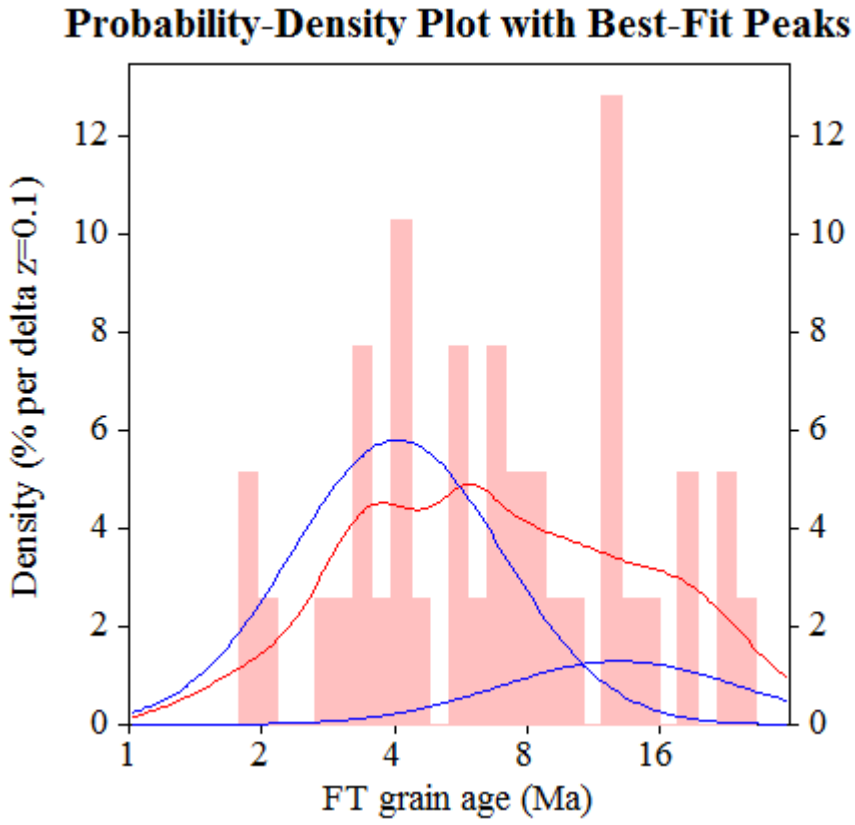
Probability-Density Plot with Best-Fit Peaks
Density (% per delta z=0.1)
0
2
4
6
8
10
12
1
2
4
8
16
FT grain age (Ma)

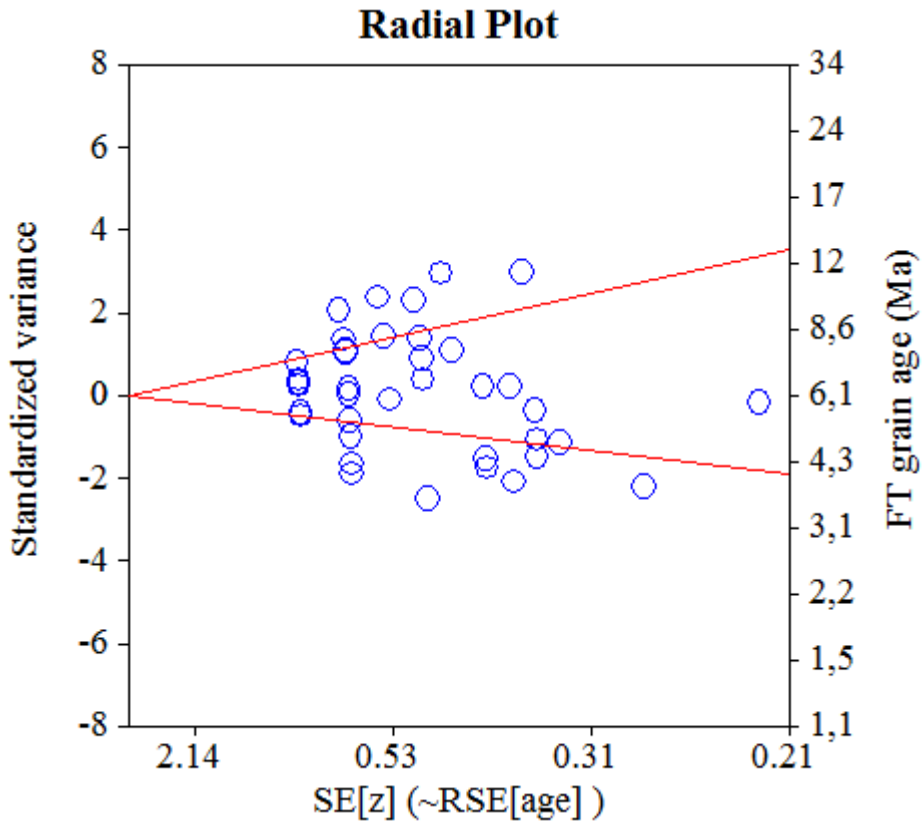
Radial Plot
Standardized variance
8
6
4
2
0
-2
-4
-6
-8
34
24
17
12
8,6
6,1
4,3
3,1
2,2
1,5
1,1
FT grain age (Ma)
2.14
0.53
0.31
0.21
SE[z] (~RSE[age])

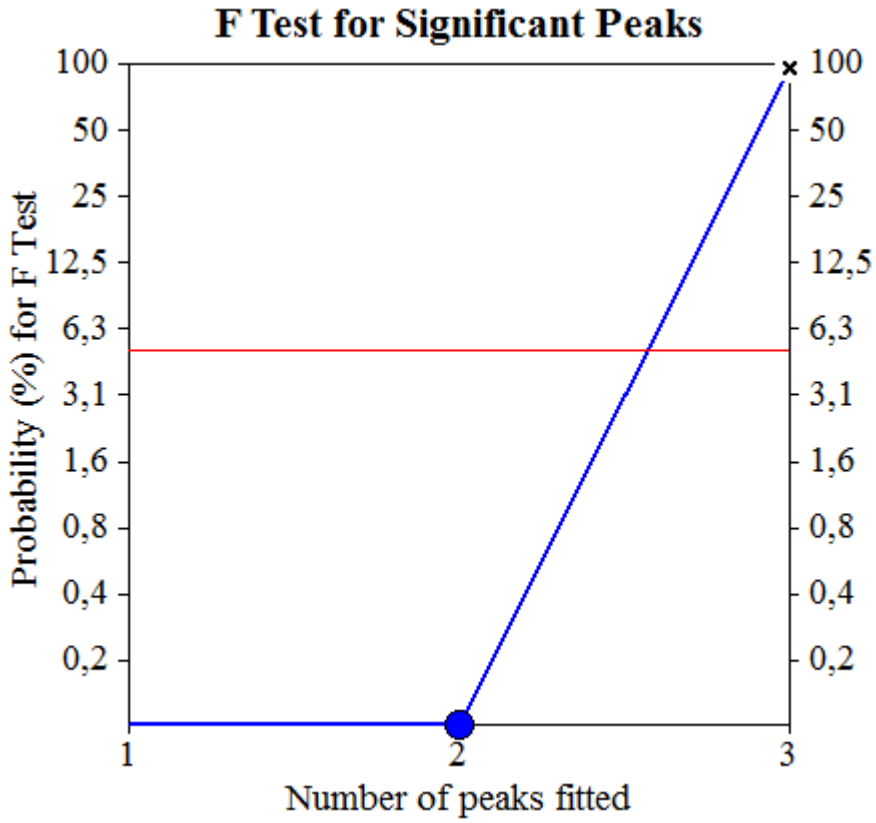
F Test for Significant Peaks
Probability (%) for F Test
100
50
25
12,5
6,3
3,1
1,6
0,8
0,4
0,2
1
2
3
Number of peaks fitted